BRITISH JOURNAL OF APPLIED PHYSICS

933

EDITOR

H. R. LANG

A.R.C.S., PH.D., F.INST.P.

Secretary of The Institute of Physics

VOLUME 8

Supplement No. 6 was not distributed automatically with the "Journal" but may be included in the Volume if required

EASTMAN KODAK CO.
RESEARCH LIBRARY
KODAK PARK

THE INSTITUTE OF PHYSICS

BRITISH JOURNAL OF APPLIED PHYSICS

ADVISORY COMMITTEE

for year ending 30 September, 1957

R. W. SILLARS, B.A., D.PHIL., M.I.E.E., F.INST.P., *Chairman*

C. B. ALLSOPP, PH.D., D.SC., F.INST.P., *Representing the British Institute of Radiology*

H. BARRELL, A.R.C.S., D.SC., F.INST.P.

W. BETTERIDGE, B.SC., PH.D., F.INST.P.

R. L. BROWN, M.A., F.INST.P.

A. B. D. CASSIE, M.A., PH.D., D.SC., F.INST.P.

W. H. J. CHILDS, PH.D., D.SC., F.INST.P., F.R.S.E., *Representing the Scottish Branch*

W. D. CORNER, B.SC., PH.D., F.INST.P., *Representing the North Eastern Branch*

Miss T. J. DILLON, M.SC., F.INST.P., *Representing the Education Group*

M. E. HAINE, D.SC., F.INST.P., *Representing the Electron Microscopy Group*

S. T. HENDERSON, M.A., PH.D., F.INST.P.

O. W. HUMPHREYS, C.B.E., B.SC., M.I.E.E., F.INST.P., *President, The Institute of Physics*

R. KING, B.SC., A.INST.P.

J. M. A. LENIHAN, M.SC., PH.D., F.INST.P.

H. LIPSON, M.A., D.SC., F.INST.P.

M. MCCAIG, M.SC., PH.D., F.INST.P., *Representing the Yorkshire Branch*

R. MEREDITH, D.SC., F.INST.P., *Representing the Manchester and District Branch*

E. A. OWEN, M.A., M.SC., SC.D., D.SC., F.INST.P., *Representing the Liverpool and North Wales Branch*

H. O. PULS, B.SC., PH.D., F.INST.P., *Representing the South Wales Branch*

T. LL. RICHARDS, B.SC., PH.D., F.I.M., F.INST.P., *Representing the Midland Branch*

G. D. ROBINSON, B.SC., PH.D., F.INST.P., *Representing the Royal Meteorological Society*

L. ROTHERHAM, M.SC., F.I.M., F.INST.P.

W. E. SCHALL, B.SC., F.INST.P., *Representing the Non-Destructive Testing Group*

H. SPOONER, B.SC., F.INST.P., *Representing the Stress-Analysis Group*

E. G. STANFORD, M.SC., PH.D., F.INST.P.

J. R. STANSFIELD, M.A., F.INST.P., *Representing the Industrial Spectroscopy Group*

E. G. STEWARD, B.SC., PH.D., A.INST.P., *Representing the X-ray Analysis Group*

E. C. STONER, B.A., PH.D., SC.D., F.INST.P., F.R.S.

A. M. TAYLOR, M.A., PH.D., F.INST.P., *Representing the London and Home Counties Branch*

J. TAYLOR, M.B.E., PH.D., D.SC., F.R.I.C., F.INST.P., *Honorary Treasurer, The Institute of Physics*

S. TOLANSKY, PH.D., D.SC., F.INST.P., F.R.S., *Representing the Physical Society*

F. A. VICK, O.B.E., B.SC., PH.D., A.M.I.E.E., F.INST.P., *Honorary Secretary, The Institute of Physics*

R. G. WOOD, M.SC., A.M.I.E.E., F.INST.P.

D. A. WRIGHT, D.SC., F.INST.P., *Representing the Electronics Group and the Physical Society*

ACCESSION No. C 979

CONTENTS OF VOLUME 8

PAGE

JANUARY 1957

CONFERENCE REPORT

Summarized proceedings of a conference on the electron microscopy of fibres—Leeds, January 1956. By C. E. CHALLICE and J. SIKORSKI 1

ORIGINAL CONTRIBUTIONS

The determination of linear distortion in nuclear emulsions. By A. J. APOSTOLAKIS and J. V. MAJOR 9
The X-ray and γ-ray absorption coefficients of a number of glasses. By D. A. RICHARDSON 11
The flow of gas through composite systems at very low pressures. By C. W. OATLEY 15
An electrical analogue of magnetic domains. By P. F. DAVIS 19
The nature of the emitting surface of barium dispenser cathodes. By I. BRODIE and R. O. JENKINS . . . 27
A tilting stage method for three-dimensional photoelastic investigations. By H. T. JESSOP 30
The triple point of carbon dioxide as a thermometric fixed point. By D. AMBROSE 32
The measurement of the thickness of thin carbon films. By A. W. AGAR 35
The breakdown mechanism of certain triggered spark gaps. By T. E. BROADBENT 37
Barium getters and oxygen. By R. N. BLOOMER . . 40

NOTES AND NEWS

Correspondence:

Scaling of space-charge limited electron-optical systems. From M. E. HAINE 44
Measurements on alloy-type transistors with varying collector voltage. From D. M. EVANS 44

New books 45

Notes and comments 48

FEBRUARY 1957

SPECIAL ARTICLE

Some applications of physics to wood. By R. F. S. HEARMON 49

ORIGINAL CONTRIBUTIONS

The standardization of X-ray output in industrial radiology. By R. S. MORGAN, R. HALMSHAW and B. J. RATCLIFFE 59
A millisecond relaxation process in the reverse current of germanium point-contact diodes. By R. E. BURGESS . 62
The fundamental modes of vibration of uniform beams for medium wavelengths. By G. J. KYNCH . . . 64
Pre-breakdown conduction between electrodes in continuously-pumped vacuum systems. By W. K. MANSFIELD and R. L. FORTESCUE 73
Application of a microfocus Laue technique to the study of deformation in aluminium single crystals. By R. A. COYLE, A. M. MARSHALL, J. H. AULD and N. A. MCKINNON 79
The lives of electron microscope filaments. By R. N. BLOOMER 83

PAGE

NOTES AND NEWS

New books 86

Notes and comments 88

MARCH 1957

SPECIAL ARTICLE

Some recent developments in the physics of fuel combustion. By M. W. THRING 89

CONFERENCE REPORT

Summarized proceedings of a symposium on thin films—Reading, September, 1956. By T. B. RYMER . . . 97

ORIGINAL CONTRIBUTIONS

The measurement of peak voltage using a cathode-ray tube. By E. S. FAIRLEY 101
A method of measuring the shear modulus of thin xylonite sheet. By J. CLARKSON 103
Short duration discharges between separating contacts in a 6 V circuit. By J. RIDDLESTONE 105
An extraction replica method for large precipitates and non-metallic inclusions in steels. By G. R. BOOKER and J. NORBURY 109
Highly-conducting gold films prepared by vacuum evaporation. By A. E. ENNOS 113
The dust-free space surrounding hot bodies. By W. ZERNIK 117
Contact electrification across metal-dielectric and dielectric-dielectric interfaces. By G. S. ROSE and S. G. WARD 121
Properties of two-aperture electron lenses. By G. D. ARCHARD 127

NOTES AND NEWS

Correspondence:

A simple graphical method of calculating the density of current carriers in a semi-conductor from the Hall coefficient. From T. S. ROBINSON, M. SMOLLETT and R. G. PRATT 130

New books 131

APRIL 1957

SPECIAL ARTICLE

The analysis of finite-length records of fluctuating signals. By M. J. TUCKER 137

ORIGINAL CONTRIBUTIONS

Variations in tension of an unwinding thread. By K. H. V. BOOTH 142
Transverse vibrations of power transmission chains. By S. MAHALINGAM 145
The effect of sulphur and oxygen on the electrical properties of oxide-coated cathodes. By G. S. HIGGINSON 148
Some carbon replica techniques for the electron microscopy of small specimens and fibres. By D. E. BRADLEY 150

PAGE

X-ray diffraction studies on precipitates and inclusions in steels using an extraction replica technique. By G. R. BOOKER, J. NORBURY and A. L. SUTTON . . . 155
On the mathematical theory of zone-melting. By I. BRAUN and S. MARSHALL 157
A method for the measurement of heat generation in powdered coal. By P. C. NEWMAN 162
A study of aircraft response to sudden and graded wind gusts by means of a differential analyser. By W. R. BLUNDEN, F. H. HOOKE and H. K. MESSERLE . . . 167

NOTES AND NEWS

Correspondence:

Comments on the A.S.T.M. Powder Data File. From J. W. HUGHES, ISABEL E. LEWIS and A. J. C. WILSON 173

New books 174

Notes and comments 178

MAY 1957

SPECIAL ARTICLE

The effect of radiation damage on the electronic properties of solids. By E. W. J. MITCHELL 179

ORIGINAL CONTRIBUTIONS

The light output of some phosphors excited with electrons of high current density. By P. A. EINSTEIN . . . 190
Dynamic shear properties of some rubber-like materials. By W. P. FLETCHER and A. N. GENT 194
Secondary electron emission from barium dispenser cathodes. By I. BRODIE and R. O. JENKINS . . . 202
Vacuum-deposited films of nickel–chromium alloy. By R. H. ALDERSON and F. ASHWORTH 205
The conductance of a column of vapour for gases at low pressures. By D. S. STARK 210

NOTES AND NEWS

New books 214

Notes and comments 218

JUNE 1957

SPECIAL ARTICLE

Physics below 1° K. By E. MENDOZA 219

ORIGINAL CONTRIBUTIONS

The measurement of surface residual stress by X-rays. By G. A. HAWKES 229
The heating of fluorescent screens bombarded by electrons. By G. D. ARCHARD and P. A. EINSTEIN 232
The penetration of irregularly-shaped particles through an airborne-dust elutriator. By J. G. DAWES, G. K. GREENOUGH and J. S. SEAGER 236
Electron microscope and diffraction studies of 7% chromium–molybdenum steels. By BETTY E. WILLIAMS . 241
The movement of the second crossover potential of insulators. By A. B. MCFARLANE 248

NOTES AND NEWS

New books 253

Notes and comments 258

PAGE

JULY 1957

CONFERENCE REPORT

Summarized proceedings of a conference on electron microscopy—Reading, July, 1956. By C. E. CHALLICE 259

ORIGINAL CONTRIBUTIONS

Some considerations of the magnetostrictive composite oscillator method for the measurement of elastic moduli. By N. B. TERRY 270
The frequency dependence of noise temperature ratio in microwave mixer crystals. By M. E. SPRINKS, G. T. G. ROBINSON and B. G. BOSCH 275
The impedance of the oxide-coated cathode at ultra-high frequencies. By L. J. HERBST 277
Fluoroscopy with an enlarged image. By R. HALMSHAW and C. HUNT 282
The ultrasonic degradation of polystyrene at a frequency of 1 Mc/s. By N. H. LANGTON and P. VAUGHAN . 289
Size of the focal spot in a betatron. By D. GREENE . 293
The preparation of electron microscope replicas from rough porous surfaces. By D. M. HALL 295
The time-dependence of the recording properties of G5 nuclear emulsion. By W. C. BARRON and A. W. WOLFENDALE 297

NOTES AND NEWS

Correspondence:

The electrical conductivity and permittivity of mixtures. From D. A. DE VRIES and C. A. R. PEARCE . . 301
The depth of surface damage produced by lapping germanium monocrystals. From D. BAKER and H. YEMM 302

New books 304

Notes and comments 306

AUGUST 1957

CONFERENCE REPORT

Summarized proceedings of a conference on stress analysis—Cranfield, September 1956 By H. FESSLER . 307

SPECIAL ARTICLE

On the elementary theory of thermoelectric phenomena. By R. STRATTON 315

ORIGINAL CONTRIBUTIONS

The oxidation of evaporated barium films (getters). By R. N. BLOOMER 321
Measurements of the impedance parameters of junction transistors. By E. E. WARD 329
The emission from oxide cathodes in low pressure discharges. By M. A. CAYLESS 331
The spectral reflectivity of back-surface and front-surface aluminized mirrors. By G. G. TWIDLE . . . 337
Determination of the impurity concentrations in a semiconductor from Hall coefficient measurements. By P. A. LEE 340

NOTES AND NEWS

Correspondence:

Action and viscous flow. From A. D. MAUDE and T. V. STARKEY 343

New books 345

Notes and comments 346

SEPTEMBER 1957

PAGE

ORIGINAL CONTRIBUTIONS

Electron micrographs from thick oxide layers on aluminium. By C. J. L. Booker, J. L. Wood and A. Walsh 347
Barium getters and carbon monoxide. By R. N. Bloomer 352
A system for recording transmission errors in universal joints. By A. J. Bartley and R. W. Gregory 355
The effect of oxygen and sulphur on the thermionic emission from matrix cathodes. By J. F. Richardson 361
The ageing of gas-filled standard lamps on a.c. and d.c. By W. Barnett, R. G. Berry and J. S. Preston 363
The use of low-inertia integrating motors. By R. F. Farr 366
An iterative analogue computer for use with resistance network analogues. By I. C. Hutcheon 370
The optical density and thickness of evaporated carbon films. By Anna Cosslett and V. E. Cosslett 374
On the mechanism of the production of dark-current pulses in photomultipliers. By Zs. Náray and P. Varga 377

NOTES AND NEWS

Correspondence:

The diffusion of barium in discharge tubes. From M. A. Cayless and A. D. Forster-Brown 380
The deterioration of nitro-cellulose films used for electron microscopy. From D. M. Hall 380
The mechanism of particle acceleration in high current spark discharges. From Shigeo Nagao 380

New books 382

OCTOBER 1957

ORIGINAL CONTRIBUTIONS

Papers:

Contact stresses in toroids under radial loads. By H. Fessler and E. Ollerton 387
The application of a transient method to the measurement of the thermal conductivity of rocks and building materials. By G. Gafner 393
The measurement of Meyer hardness and Young's modulus on the Rockwell test machine. By D. K. Mackenzie and T. P. Newcomb 398
High-temperature tensometry and its application to amorphous polyethylene terephthalate. By E. L. Foster and H. Heap 400
A method of measuring the thermal constants of granular materials. By T. S. E. Thomas 403
Measurement of the diffusion rate of hydrogen in nickel. By A. G. Edwards 406
On the screen brightness required for high resolution operation of the electron microscope. By A. W. Agar 410
Non-linear forced vibration of a stretched string. By E. W. Lee 411
High vacuum shaft seals, flanged joints and the gassing and the permeability of rubber-like materials. By R. H. V. M. Dawton 414

NOTES AND NEWS

Correspondence:

The γ-ray scintillation spectrometer. From D. H. Pierson and P. Iredale 422
Scaling laws for space charge dynamics. From E. R. Harrison 422

New books 423

Notes and comments 426

NOVEMBER 1957

PAGE

CONFERENCE REPORTS

Summarized proceedings of a conference on X-ray analysis—Cardiff, April, 1957. By P. Gay and P. J. Wheatley 427
Summarized proceedings of a meeting on low temperature distillation—London, March, 1957. By F. Din 436

ORIGINAL CONTRIBUTIONS

Viscous flow between rotating cylinders and a sheet moving between them. By M. R. Hopkins 442
Arc motion with magnetized electrodes. By A. E. Guile, T. J. Lewis and S. F. Mehta 444
A simple calibration technique for improving the accuracy of a Smith resistance thermometry bridge. By G. C. Lowenthal 449
The damping effect of surrounding gases on a cylinder in longitudinal oscillation. By M. T. Browne and J. R. Pattison 452
On the ultimate concentration distribution in zone-melting. By I. Braun 457

NOTES AND NEWS

New books 462

Notes and comments 466

DECEMBER 1957

CONFERENCE REPORT

Summarized proceedings of the eleventh annual conference of the Stress Analysis Group—Leicester, April, 1957. By A. F. C. Brown 467

ORIGINAL CONTRIBUTIONS

The effects of dust and force upon certain very light electrical contacts. By A. J. Maddock, C. C. Fielding, J. H. Batchelor and A. H. Jiggins 471
The breakdown of liquid dielectrics and its dependence on oxidation of the electrodes. By R. Hancox 476
Spectral response and linearity of photomultipliers. By H. Edels and W. A. Gambling 481
Valve instability with cathode standing waves of cylindrical symmetry. By W. W. H. Clarke 486
Spectral sensitivity of neon discharge tubes. By T. J. Dillon 490

NOTES AND NEWS

Correspondence:

Some carbon replica techniques for the electron microscopy of small specimens and fibres. From B. J. Spit; D. E. Bradley 493
The application of the centripetal effect in air to the design of a pump. From B. Popper and M. Reiner 493
The flow of gas at very low pressure. From W. Steckelmacher and C. W. Oatley 494

New books 496

Notes and comments 502

SUBJECT INDEX TO VOLUME 8 503

AUTHOR INDEX TO VOLUME 8 508

INDEX TO VOLUME 8

SUBJECT INDEX

Action and viscous flow 343
Ageing of gas-filled standard lamps on a.c. and d.c., The 363
Air, The application of the centripetal effect in, to the design of a pump 493
Airborne-dust elutriator, The penetration of irregularly-shaped particles through an 236
Aircraft response to sudden and graded wind gusts by means of a differential analyser, A study of 167
Aluminium, Electron micrographs from thick oxide layers on 347
Aluminium single crystals, deformation in, Application of a microfocus Laue technique to the study of 79
Analogue, An electrical, of magnetic domains 19
Analogue computer for use with resistance network analogues, An iterative 370
Analyser, differential, A study of aircraft response to sudden and graded wind gusts by means of a 167
Arc motion with magnetized electrodes 444
A.S.T.M. powder data file, Comments on the 173
Atomic Energy Authority, Bibliographies and reading lists from the 48
Atomic energy, Conference on peaceful uses of 426
Automation and computation, British conference on 258

Barium
dispenser cathodes, Secondary electron emission from 202
dispenser cathodes, The nature of the emitting surface of 27
films (getters), The oxidation of evaporated 321
getters and carbon monoxide 352
getters and oxygen 40
in discharge tubes, The diffusion of 380
Beams, The fundamental modes of vibration of uniform, for medium wavelengths 64
Betatron, Size of the focal spot in a 293
Bibliographies and reading lists from the Atomic Energy Authority 48

Books, New
Advances in electronics and electron physics. Vol. 8 382
American Institute of Physics handbook 496
Analysis of deformation, Vol. 3. *Fluidity* 497
Anleitung zum praktischen Gebrauch der Laplace-transformation 497
Astronomical optics and related subjects 216
Atomic nucleus, The 498
Atomkraft 465
Automatic digital calculators 134
Barker index of crystals, a method for the identification of crystalline substances, The, Vol. II, *Crystals of the monoclinic system*. Part 1, *Introduction and tables*; Part 2, *Crystal descriptions M.* 1 *to M.* 1800; Part 3, *Crystal descriptions M.* 1801 to *M.* 3572 464
Beitrage zur Theorie des Ferromagnetismus und der Magnetiserungsburne 136
Calculation of atomic structures, The 501
Cambridge aeronautical series, Vol. 2, *Wing theory* 253
Cavitation in hydrodynamics 131
Changes of state 305
Chemical engineering practice, Vol. 1, *General*; Vol. 2, *Solid state* 177; Vol. 3, *Solid systems* 425
Chemical processing and equipment 382
Constitutional diagrams of alloys, The (A bibliography) 47
Defects in crystalline solids 305
Detection and measurement of infra-red radiation, The 501
Die Massysteme in Physik and Technik 382
Einfiihrung in die höhere Mathematik, Band I, *Grundlagen* 135

Books, New (*continued*)
Electrical production of music, The 500
Electromagnetically-enriched isotopes and mass spectrometry 47
Elements of pulse circuits 497
Elsevier's dictionary of cinema sound and music 382
Encyclopaedia of chemistry, The 304
Encyclopaedia of physics, Vol. 33, *Kopuskularoptik* 134
Engineering dynamics, Vol. 2 253
Fibres, plastics and rubbers 465
Frequency modulation 256
Frequency modulation engineering 214
Further handbook of industrial radiology, A 257
Gaseous nebulae 132
Glass 136
Grundzuge der Tensorrechnung in analytischer Darstellung; III Teil, *Anwendungen in Physik und Technik* 255
Handbuch der Physik, Band 17, *Dielectrica* 176
Heat transfer and fluid mechanics institute 1956 345
High-energy accelerators 87
High speed aerodynamics and jet propulsion, Vol. 2, *Combustion processes* 216
Hypercircle in mathematical physics, The 501
Hygrometry 465
Information theory 132
Introduction to electrostatic precipitation in theory and practice, An 254
Introduction to junction transistor theory, An 496
Introduction to numerical analysis 87
Irradiation colours and luminescence 214
Jets, wakes and cavities 499
Kernmomente 383
Laboratory administration 383
Laboratory and workshop notes 1953–55 257
Lectures on rock magnetism 177
Light-scattering in physical chemistry 305
Lubrication of bearings 254
Mass spectrometer researches 304
Matrix calculus 255
Mechanism of phase transformations in metals, The 462
Metallurgical analysis by means of the Spekker photoelectric absorptiometer 384
Moderne Messmethoden der Physik, Band 2 462
Molecular flow of gases 135
Molybdenum, Metallurgy of the rarer metals 176
Momentum transfer in fluids 424
Nachrichtentechnische Fachberichte, Band 4, *Elektronische rechenmaschinen und informationsverarbeitung* 176
Neutron cross-sections 86
Neutron transport theory 465
Niederfrequenz- und Mittelfrequenz-Messtechnik für das Nachrichtengebeit 256
Notes on applied science No. 17, *High voltage impulse testing* 254
Order-disorder phenomena 176
Peaceful uses of atomic energy
Vol. 2. *Physics: research reactors* 45
Vol. 3. *Power reactors* 46
Vol. 4. *Cross sections important to reactor design* 46
Vol. 5. *Physics of reactor design* 46
Vol. 7. *Nuclear chemistry and the effects of irradiation* 174
Vol. 8. *Production technology of the materials used for nuclear energy* 384
Vol. 9. *Reactor technology and chemical processing* 174
Vol. 10. *Radioactive isotopes and nuclear radiations in medicine* 174

Books, New (*continued*)
Peaceful uses of atomic energy (continued)
Vol. 11. *Biological effects of radiation* 175
Vol. 12. *Radioactive isotopes and ionizing radiations in agriculture, physiology and biochemistry* 175
Vol. 14. *General aspects of the use of radioactive isotopes: dosimetry* 304
Vol. 15. *Applications of radioactive isotopes and fission products in research and industry* 175
Photoconductivity conference 385
Physical aspects of absorptiometric analysis 133
Physical properties of crystals 462
Physical properties of solid materials 304
Physical techniques in biological research, Vol. 2, *Physical chemical techniques* 424
Physics of flow through porous media, The 462
Physics of non-destructive testing 257
Plant and process dynamic characteristics 499
Pressure measurement in vacuum systems 462
Principles and techniques of applied mathematics 254
Proceedings of the CERN symposium 1956, Vol. 1, *High energy accelerators* 384
Vol. 2, *Pion physics* 385
Proceedings of the Eleventh General Assembly of the International Scientific Radio Union, Vol. 10 135
Proceedings of the international conference on electron transport in metals and solids 425
Production of heavy water 86
Progress in biophysics and biophysical chemistry, Vol. 7 500
Progress in cosmic ray physics, Vol. 3 132
Progress in low temperature physics, Vol. 2 463
Progress in metal physics, Vol. 6 255
Progress in nuclear energy, Series II, *Reactors*, Vol. 1 131
Progress in nuclear physics, Vol. 5 464
Quantum chemistry: an introduction 498
Raum und Bauakustik für Architekten 253
Reactor handbook: Engineering 47
Reactor handbook: Physics 86
Recent advances in science: Physics and applied mathematics 345
Records and research in engineering and industrial science 256
Rectangular-polar conversion tables 87
Relaxation methods in theoretical physics, Vol. 2 385
Reports on progress in physics, Vol. 19 133
Rheology: theory and applications, Vol. 1 386
Rubber in engineering 500
Science and information theory 133
Selected combustion problems, Vol. 2 256
Solid state physics. Advances in research and applications, Vol. 2 214; Vol. 3 425
Spheroidal wave functions 500
Static and dynamic electron optics 216
Statistical mechanics 423
Steric effects in organic chemistry 217
Structure of turbulent shear flow, The 135
Structure reports for 1940–1941, Vol. 8 425
Switchgear principles 500
Synthetic polypeptides. Preparation, structure and properties 386
Table of the Fresnel integral to six decimal places 424
Technical aspects of sound, Vol. 2 463
Théorie et technique de la radiocrystallographie 497
Theories of nuclear moments 501
Theory of networks in electrical communication and other fields, The 499
Thermodynamic functions of gases, Vols. 1 and 2 423
Thermodynamic tables and other data 345
Vacuum deposition of thin films 217
Voltage stabilized supplies 499
Breakdown mechanism of certain triggered spark gaps, The 37
Breakdown of liquid dielectrics and its dependence on oxidation of the electrodes, The 476
British Computer Society 346
British conference on automation and computation 258
British Standards Institution, Publications of the 502
British Standards Institution Yearbook, 1957 218
Building materials, The application of a transient method to the measurement of the thermal conductivity of rocks and 393
Carbon
dioxide, The triple point of, as a thermometric fixed point 32
films, The measurement of the thickness of thin 35
films, The optical density and thickness of evaporated 374
monoxide, Barium getters and 352
replica techniques for the electron microscopy of small specimens and fibres, Some 150, 493
Cathode
, oxide-coated, The impedance of the, at ultra-high frequencies 277
-ray tube, The measurement of peak voltage using a 101
standing waves of cylindrical symmetry, Valve instability with 486
Cathodes,
barium dispenser, Secondary electron emission from 202
barium dispenser, The nature of the emitting surface of 27
matrix, The effect of oxygen and sulphur on the thermionic emission from 361
oxide-coated, The effect of sulphur and oxygen on the electrical properties of 148
oxide, The emission from, in low pressure discharges 331
Centripetal effect in air, The application of the, to the design of a pump 493
Chains, power transmission, Transverse vibrations of 145
Chromium-molybdenum steels, 7%, Electron microscope and diffraction studies of 241
Coal, powdered, A method for the measurement of heat generated in 162
Combustion and flame 218
Combustion engineering association, The 466
Combustion, fuel, Some recent developments in the physics of 89
Computation, British conference on automation and 258
Computer, iterative analogue, for use with resistance network analogues, An 370
Computer Society, British 346
Concentration distribution in zone-melting, On the ultimate 457
Conductance of a column of vapour for gases at low pressures, The 210
Conduction between electrodes in continuously-pumped vacuum systems, Pre-breakdown 73
Conductivity and permittivity of mixtures, The electrical 301
Conductivity, thermal, of rocks and building materials, The application of a transient method to the measurement of the 393
Conference
see also Symposium and Meeting
, British, on automation and computation 258
of the stress analysis group, Summarized proceedings of the eleventh annual—Leicester, April 1957 467
on electron microscopy—Reading, July 1956, Summarized proceedings of a 259
on electron microscopy of fibres, Summarized proceedings of a—Leeds, January 1956 1 (*erratum*) 218
on magnetism and magnetic materials 306
on peaceful uses of atomic energy 426
on stress analysis, Summarized proceedings of a—Cranfield, September, 1956 307
on X-ray analysis, Summarized proceedings of a—Cardiff, April, 1957 427
Contact electrification across metal-dielectric and dielectric-dielectric interfaces 121
Contact stresses in toroids under radial loads 387
Contacts, electrical, The effects of dust and force upon certain very light 471
Contacts, separating, Short duration discharges between, in a 6 V circuit 105
Conversion factors for specific energy, energy and pressure 178
Crystallographers, World directory of 178

Crystal(s), Single, *see* Single crystal(s)
Crystals, microwave mixer, The frequency dependence of noise-temperature ratio in 275
Current-carriers in a semi-conductor, a simple graphical method of calculating the density of, from the Hall coefficient 130
Cylinder in longitudinal oscillation, The damping effect of surrounding gases on a 452

Damage, radiation, The effect of, on the electronic properties of solids 179
Damping effect of surrounding gases on a cylinder in longitudinal oscillation, The 452
Dark-current pulses in photomultipliers, On the mechanism of the production of 377
Data-processing section, Formation of (The Society of Instrument Technology) 466
Deformation in aluminium single crystals, Application of a micro-focus Laue technique to the study of 79
Degradation, ultrasonic, of polystyrene at a frequency of 1 Mc/s, The 289
Density, optical, and thickness of evaporated carbon films, The 374
Deterioration of nitro-cellulose films used for electron microscopy, The 380
Dielectric-dielectric interfaces, Contact electrification across metal-dielectric and 121
Dielectrics, liquid, The breakdown of, and its dependence on oxidation of the electrodes 476
Differential analyser, A study of aircraft response to sudden and graded wind gusts by means of a 167
Diffraction studies of 7% chromium-molybdenum steels, Electron microscope and 241
Diffusion of barium in discharge tubes, The 380
Diffusion rate of hydrogen in nickel, Measurement of the 406
Diodes, germanium point-contact, A millisecond relaxation process in the reverse current of 62
Directory, World, of crystallographers 178
Discharges, low pressure, The emission from oxide cathodes in 331
Discharges, short duration, between separating contacts in a 6 V circuit 105
Discharge tubes, neon, Spectral sensitivity of 490
Discharge tubes, The diffusion of barium in 380
Distillation, low temperature, Summarized proceedings of a meeting on—London, March, 1957 436
Distortion in nuclear emulsions, The determination of linear 9
Dust and force, The effects of, upon certain very light electrical contacts 471
Dust-free space surrounding hot bodies, The 117
Dynamic shear properties of some rubber-like materials 194

Education of Physicists in Universities and Colleges of Technology, The 346
Elastic moduli, Some considerations of the magnetostrictive composite oscillator method for the measurement of 270
Elastometers, Rheology of 48
Electrical analogue of magnetic domains, An 19
Electrical, properties of oxide-coated cathodes, The effect of sulphur and oxygen on the 148
Electrification, Contact, across metal-dielectric and dielectric-dielectric interfaces 121
Electrodes
  in continuously pumped vacuum systems, Pre-breakdown conduction between 73
  , magnetized, Arc motion with 444
  , oxidation of the, The breakdown of liquid dielectrics and its dependence on 476
Electronic properties of solids, The effect of radiation damage on the 179
Electron
  emission, Secondary, from barium dispenser cathodes 202
  lenses, Properties of two-aperture 127
Electron (*continued*)
  micrographs from thick oxide layers on aluminium 347
  microscope and diffraction studies of 7% chromium–molybdenum steels 241
  microscope filaments, The lives of 83
  microscope, On the screen brightness required for high resolution operation of the 410
  microscope replicas from rough porous surfaces, The preparation of 295
  microscopy of fibres, Summarized proceedings of a conference on the—Leeds, January, 1956 1 *erratum* 218
  microscopy of small specimens and fibres, Some carbon replica techniques for the 150, 493
  microscopy, Summarized proceedings of a conference on—Reading, July, 1956 259
  microscopy, The deterioration of nitro-cellulose films used for 380
  -optical systems, Scaling of space-charge-limited 44
Electrons of high current density, The light output of some phosphors excited with 190
Electrons, The heating of fluorescent screens bombarded by 232
Elutriator, The penetration of irregularly-shaped particles through an airborne-dust 236
Emission from oxide cathodes in low pressure discharges, The 331
Emission, thermionic, from matrix cathodes, The effect of oxygen and sulphur on the 361
Energy, specific, energy and pressure, Conversion factors for 178
Errors, transmission, in universal joints, A system for recording 355
Exhibition of scientific instruments and apparatus, The Physical Society's 88
Extraction replica method for large precipitates and non-metallic inclusions in steels, An 109
Extraction replica technique, X-ray diffraction studies on precipitates and inclusions in steels using an 155

Fibres, Some carbon replica techniques for the electron microscopy of small specimens and 150, 493
Fibres, Summarized proceedings of a conference on electron microscopy of—Leeds, January, 1956 1 *erratum* 218
Filaments, electron microscopy, The lives of 83
Films,
  see also Layers
  carbon, evaporated, The optical density and thickness of 374
  gold, highly conducting, prepared by vacuum evaporation 113
  nitro-cellulose, The deterioration of, used for electron microscopy 380
  The oxidation of evaporated barium (getters) 321
  thin carbon, The measurement of the thickness of 35
  thin, Summarized proceedings of a symposium on—Reading, September, 1956 97
  Vacuum-deposited, of nickel–chromium alloy 205
Flow
  of gas at very low pressure, The 494
  of gas through composite systems at very low pressures, The 15
  , viscous, Action and 343
  , Viscous, between rotating cylinders and a sheet moving between them 442
Fluorescent screens bombarded by electrons, The heating of 232
Fluoroscopy with an enlarged image 282
Focal spot in a betatron, Size of the 293
Force, dust and, The effects of, upon certain very light electrical contacts 471
Forced vibration of a stretched string, Non-linear 411
Frequencies, ultra-high, The impedance of the oxide-coated cathode at 277
Frequency dependence of noise-temperature ratio in microwave mixer crystals 275
Fuel combustion, Some recent developments in the physics of 89

Gamma-ray absorption coefficients of a number of glasses, The X-ray and 11

Gamma-ray scintillation spectrometer, The 422
Gas at very low pressure, The flow of 494
Gas, The flow of, through composite systems at very low pressures 15
Gases at low pressures, The conductance of a column of vapour for 210
Gases, surrounding, The damping effect of, on a cylinder in longitudinal oscillation 452
Gassing and the permeability of rubber-like materials, High vacuum shaft seals, flanged joints and the 414
Germanium monocrystals, The depth of surface damage produced by lapping 302
Germanium point-contact diodes, A millisecond relaxation process in the reverse current of 62
Getters,
  Barium, and carbon monoxide 352
  Barium, and oxygen 40
  The oxidation of evaporated barium films 321
Glasses, The X-ray and γ-ray absorption coefficients of a number of 11
Gold films, Highly conducting, prepared by vacuum evaporation 113
Grants, Paul instrument fund 466
Granular materials, A method of measuring the thermal constants of 403

Hall coefficient, A simple graphical method of calculating the density of current carriers in a semi-conductor from the 130
Hall coefficient measurements, Determination of the impurity concentrations in a semiconductor from 340
Hardness, Meyer, The measurement of, and Young's modulus, on the Rockwell test machine 398
Heat generation in powdered coal, A method for the measurement of 162
High resolution operation of the electron microscope, On the screen brightness required for 410
Hot bodies, The dust-free space surrounding 117
Hydrogen in nickel, Measurement of the diffusion rate of 406

Image, Fluoroscopy with an enlarged 282
Impedance of the oxide-coated cathode at ultra-high frequencies, The 277
Impedance parameters of junction transistors, Measurements of the 329
Impurity concentrations in a semiconductor, Determination of the, from Hall coefficient measurements 340
Industrial radiology, *see* Radiology, Industrial
Institute of Physics, Elections to The 48, 218, 306, 426
Insulators, The movement of the second crossover potential of 248
Integrating motors, The use of low-inertia 366
Interfaces, Contact electrification across metal-dielectric and dielectric-dielectric 121
International Journal of Applied Radiation and Isotopes, The 48

Joints, flanged, and the gassing and the permeability of rubber-like materials, High vacuum shaft seals 414
Joints, universal, A system for recording transmission errors in 355
Journal of Ultrastructure Research 346

Lamps, gas-filled standard, The ageing of, on a.c. and d.c. 363
Laue technique, microfocus, The application of, to the study of deformation in aluminium single crystals 79
Layers, oxide, on aluminium, Electron micrographs from thick 347
Lenses, electron, Properties of two-aperture 127
Light output of some phosphors excited with electrons of high current density 190
Liquid dielectrics, The breakdown of, and its dependence on oxidation of the electrodes 476
Loads, radial, Contact stresses in toroids under 387
Low pressure, *see* Pressure, Low
Low-temperature distillation, Summarized proceedings of a meeting on—London, March, 1957 436
Low-temperature physics 219

Magnetic domains, An electrical analogue of 19
Magnetism and magnetic materials, Conference on 306
Magnetized electrodes, Arc motion with 444
Magnetostrictive composite oscillator method for the measurement of elastic moduli, Some considerations of the 270
Mathematical theory of zone-melting, On the 157
Meeting on low-temperature distillation, Summarized proceedings of a—London, March, 1957 436
Melting, Zone-, *see* Zone-melting
Metal-dielectric and dielectric-dielectric interfaces, Contact electrification across 121
Meyer hardness and Young's modulus on the Rockwell test machine, The measurement of 398
Micrographs, Electron, from thick oxide layers on aluminium 347
Microscope, Electron, *see* Electron microscope
Microwave mixer crystals, The frequency dependence of noise-temperature ratio in 275
Mirrors, aluminized, The spectral reflectivity of back-surface and front-surface 337
Monocrystals, germanium, The depth of surface damage produced by lapping 302
Motors, low-inertia integrating, The use of 366

Neon discharge tubes, Spectral sensitivity of 490
Nickel-chromium alloy, Vacuum-deposited films of 205
Nickel, Measurement of the diffusion rate of hydrogen in 406
Nitro-cellulose films used for electron microscopy, The deterioration of 380
Noise-temperature ratio in microwave mixer crystals, The frequency dependence of 275
Nuclear emulsion, G5, The time-dependence of the recording properties of 297
Nuclear emulsions, The determination of linear distortion in 9

Optical density and thickness of evaporated carbon films, The 374
Oscillation longitudinal, The damping effect of surrounding gases on a cylinder in 452
Oscillator method for the measurement of elastic moduli, Some considerations of the magnetostrictive composite 270
Oxidation of evaporated barium films (getters), The 321
Oxide layers on aluminium, Electron micrographs from thick 347
Oxygen
  and sulphur, The effect of, on the thermionic emission from matrix cathodes 361
  , Barium getters and 40
  , The effect of sulphur and, on the electrical properties of oxide-coated cathodes 148

Particle acceleration in high current spark discharges, The mechanism of 380
Particles through an airborne-dust elutriator, The penetration of irregularly-shaped 236
Paul instrument fund grants 466
Peak voltage, The measurement of, using a cathode-ray tube 101
Permeability of rubber-like materials, High vacuum shaft seals, flanged joints and the gassing and the 414
Permittivity of mixtures, The electrical conductivity and 301
Phosphors excited with electrons of high current density, The light output of some 190
Photoelastic investigations, A tilting stage method for three-dimensional 30
Photomultipliers, On the mechanism of the production of dark-current pulses in 377
Photomultipliers, Spectral response and linearity of 481

Physical Society's annual exhibition of scientific instruments and apparatus, The 88
Physics below 1° K 219
Physics of Fluids, The 502
Physics of fuel combustion, Some recent developments in the 89
Physics, Some applications of, to wood 49
Platinum Metals Review 88
Polyethylene terephthalate, amorphous, High-temperature tensometry and its application to 400
Polystyrene, The ultrasonic degradation of, at a frequency of 1 Mc/s 289
Potential, second crossover, The movement of the, of insulators 248
Powder data file, A.S.T.M., Comments on the 173
Power transmission chains, Transverse vibrations of 145
Pressure,
  Conversion factors for specific energy, energy and 178
  low, discharges, The emission from oxide cathodes in 331
  very low, The flow of gas at 494
Pressures, low, The conductance of a column of vapour for gases at 210
Pressures, very low, The flow of gas through composite systems at 15
Process plants, Automatic measurement of quality in 178
Publications of the British Standards Institution 502
Pulses dark-current, On the mechanism of the production of, in photomultipliers 377
Pump, The application of the centripetal effect in air to the design of a 493

Quality in process plants, Automatic measurement of 178

Radiation damage, The effect of, on the electronic properties of solids 179
Radiofrequency spectroscopy symposium 258
Radiological units and measurements, Report of the International Commission on 306
Radiology, industrial, The standardization of X-ray output in 59
Recording properties of G5 nuclear emulsion, The time-dependence of the 297
Records of fluctuating signals, The analysis of finite-length 137
Reflectivity of back-surface and front-surface aluminized mirrors, The spectral 337
Register of British manufacturers 88
Relaxation process, A millisecond, in the reverse current of germanium point-contact diodes 62
Replica
  method, An extraction, for large precipitates and non-metallic inclusions in steels 109
  technique, extraction, X-ray diffraction studies on precipitates and inclusions in steels using an 155
  techniques for the electron microscopy of small specimens and fibres, Some carbon 150, 493
Replicas, The preparation of electron microscope, from rough porous surfaces 295
Report of the International Commission on radiological units and measurements 306
Resistance network analogues, An iterative analogue computer for use with 370
Resistance thermometry bridge, Smith, A simple calibration technique for improving the accuracy of a 449
Rheology of elastometers 48
Rocks and building materials, The application of a transient method to the measurement of the thermal conductivity of 393
Rockwell test machine, The measurement of Meyer hardness and Young's modulus on the 398
Rotating cylinders, Viscous flow between, and a sheet moving between them 442
Rubber-like materials, Dynamic shear properties of some 194
Rubber-like materials, High vacuum shaft seals, flanged joints and the gassing and the permeability of 414
Russian journals, Translation of 502

Scaling laws for space charge dynamics 422
Scaling of space-charge limited electron-optical systems 44
Scintillation spectrometer, The gamma-ray 422
Screen brightness required for high resolution operation of the electron microscope, On the 410
Screens, fluorescent, bombarded by electrons, The heating of 232
Seals, High-vacuum shaft, flanged joints and the gassing and the permeability of rubber-like materials 414
Semi-conductor, A simple graphical method of calculating the density of current carriers in a, from the Hall coefficient 130
Semiconductor, Determination of the impurity concentrations in a, from Hall coefficient measurements 340
Semiconductor Electronics 502
Sensitivity, Spectral, of neon discharge tubes 490
Shear, Dynamic, properties of some rubber-like materials 194
Shear modulus of thin xylonite sheet, A method of measuring 103
Sheet, thin xylonite, A method of measuring the shear modulus of 103
Signals, fluctuating, The analysis of finite-length records of 137
Single crystals, aluminium, Application of a microfocus Laue technique to the study of deformation in 79
Smith resistance thermometry bridge, A simple calibration technique for improving the accuracy of 449
Society of Instrument Technology, formation of data-processing section, The 466
Solids, electronic properties of, The effect of radiation damage on the 179
Space
  -charge dynamics, Scaling laws for 422
  -charge limited electron-optical systems, Scaling of 44
  surrounding hot bodies, The dust-free 117
Spark discharges, high current, The mechanism of particle acceleration in 380
Spark gaps, triggered, The breakdown of certain 37
Spectral response and linearity of photomultipliers 481
Spectral sensitivity of neon discharge tubes 490
Spectrometer, The gamma-ray scintillation 422
Spectroscopy symposium, Radiofrequency 258
Standardization of X-ray output in industrial radiology, The 59
Steels,
  An extraction replica method for large precipitates and non-metallic inclusions in 109
  7% chromium–molybdenum, Electron microscope and diffraction studies of 241
  X-ray diffraction studies on precipitates and inclusions in, using an extraction replica technique 155
Stress
  Analysis Group, Summarized proceedings of the eleventh annual conference of the—Leicester, April, 1957 467
  analysis, Summarized proceedings of a conference on—Cranfield, September, 1956 307
  , surface residual, The measurement of, by X-rays 229
Stresses, Contact, in toroids under radial loads 387
String, stretched, Non-linear forced vibration of a 411
Sulphur and oxygen, The effect of, on the electrical properties of oxide-coated cathodes 148
Sulphur, The effect of oxygen and, on the thermionic emission from matrix cathodes 361
Surface
  damage produced by lapping germanium monocrystals, The depth of 302
  , emitting, The nature of, of barium dispenser cathodes 27
  residual stress by X-rays, The measurement of 229
Surfaces, rough porous, The preparation of electron microscope replicas from 295
Symposium on thin films, Summarized proceedings of a—Reading, September, 1956 97

Teaching aids 466
Temperature, Low, *see* Low temperature
Tension, Variations in, of an unwinding thread 142

Tensometry, High-temperature, and its application to amorphous polyethylene terephthalate 400
Thermal conductivity of rocks and building materials, The application of a transient method to the measurement of the 393
Thermal constants of granular materials, A method of measuring the 403
Thermionic emission from matrix cathodes, The effect of oxygen and sulphur on the 361
Thermoelectric phenomena, On the elementary theory of 315
Thermometric fixed point, The triple point of carbon dioxide as a 32
Thermometry bridge, A simple calibration technique for improving the accuracy of a Smith resistance 449
Thickness of evaporated carbon films, The optical density and 374
Thickness of thin carbon films, The measurement of the 35
Thread, Variations in the tension of an unwinding 142
Tilting stage method for three-dimensional photoelastic investigations, A 30
Time-dependence of the recording properties of G5 nuclear emulsions, The 297
Toroids under radial loads, Contact stresses in 387
Transient method, The application of the, to the measurement of the thermal conductivity of rocks and building materials 393
Transistors, alloy-type, Measurements on, with varying collector voltage 44
Transistors, junction, Measurements of the impedance parameters of 329
Translation of Russian journals 502
Transmission errors in universal joints, A system for recording 355
Triple point of carbon dioxide as a thermometric fixed point, The 32

Ultrasonic degradation of polystyrene at a frequency of 1 Mc/s 289
Universal joints, A system for recording transmission errors in 355

Vacuum
-deposited films of nickel–chromium alloy 205
evaporation, Highly conducting gold films prepared by 113
, high, shaft seals, flanged joints and the gassing and the permeability of rubber-like materials 414
Vacuum (*continued*)
systems, continuously-pumped, Pre-breakdown conduction between electrodes in 73
Valve instability with cathode standing waves of cylindrical symmetry 486
Vapour, The conductance of a column of, for gases at low pressures 210
Vibration, Non-linear forced, of a stretched string 411
Vibration of uniform beams for medium wavelengths, The fundamental modes of 64
Vibrations, transverse, of power transmission chains 145
Viscous flow, Action and 343
Viscous flow between rotating cylinders and a sheet moving between them 442
Voltage, varying collector, Measurements on alloy-type transistors with 44

Wind gusts, A study of aircraft response to sudden and graded, by means of a differential analyser 167
Wood, Some applications of physics to 49

X-ray
analysis, Summarized proceedings of a conference on—Cardiff, April, 1957 427
and γ-ray absorption coefficients of a number of glasses, The 11
diffraction studies on precipitates and inclusions in steels using an extraction replica technique 155
output in industrial radiology, The standardization of 59
X-rays, The measurement of surface residual stress by 229
Xylonite sheet, thin, A method of measuring the shear modulus of 103

Young's modulus, The measurement of Meyer hardness and, on the Rockwell test machine 398

Zeitschrift für Instrumentendenkunde 178
Zone-melting, On the mathematical theory of 157
Zone-melting, On the ultimate concentration distribution in 457

AUTHOR INDEX

Agar, A. W., The measurement of the thickness of thin carbon films 35
On the screen brightness required for high resolution operation of the electron microscope 410
Alderson, R. H., and F. Ashworth, Vacuum deposited films of nickel–chromium alloy 205
Ambrose, D., The triple point of carbon dioxide as a thermometric fixed point 32
Apostolakis, A. J., and J. V. Major, The determination of linear distortion in nuclear emulsions 9
Archard, G. D., Properties of two-aperture electron lenses 127
Archard, G. D., and P. A. Einstein, The heating of fluorescent screens bombarded by electrons 232
Auld, J. H., *see under* Coyle, R. A.

Baker, D., and H. Yemm, The depth of surface damage produced by lapping germanium monocrystals 302
Barnett, W., R. G. Berry and J. S. Preston, The ageing of gas-filled standard lamps on a.c. and d.c. 363
Barron, W. C., and A. W. Wolfendale, The time-dependence of the recording properties of G5 nuclear emulsion 297
Bartley, A. J., and R. W. Gregory, A system for recording transmission errors in universal joints 355
Batchelor, J. H., *see under* Maddock, A. J.
Berry, R. G., *see under* Barnett, W.
Bloomer, R. N., Barium getters and oxygen 40
The lives of electron microscope filaments 83
The oxidation of evaporated barium films (getters) 321
Barium getters and carbon monoxide 352
Blunden, W. R., F. H. Hooke and H. K. Messerle, A study of aircraft response to sudden and graded wind gusts by means of a differential analyser 167
Booker, C. J. L., J. L. Wood and A. Walsh, Electron micrographs from thick oxide layers on aluminium 347
Booker, G. R., and J. Norbury, An extraction replica method for large precipitates and non-metallic inclusions in steels 109
Booker, G. R., J. Norbury and A. L. Sutton, X-ray diffraction studies on precipitates and inclusions in steels using an extraction replica technique 155
Booth, K. H. V., Variations in tension of an unwinding thread 142
Bosch, B. G., *see under* Sprinks, M. E.
Bradley, D. E., Some carbon replica techniques for the electron microscopy of small specimens and fibres 150, 493
Braun, I., and S. Marshall, On the mathematical theory of zone-melting 157
Braun, I., On the ultimate concentration distribution in zone-melting 457
Broadbent, T. E., The breakdown mechanism of certain triggered spark gaps 37

Brodie, I., and R. O. Jenkins, The nature of the emitting surface of barium dispenser cathodes 27
Secondary electron emission from barium dispenser cathodes 202
Brown, A. F. C., Summarized proceedings of the eleventh annual conference of the Stress Analysis Group—Leicester, April, 1957 467
Browne, M. T., and J. R. Pattison, The damping effect of surrounding gases on a cylinder in longitudinal oscillation 452
Burgess, R. E., A millisecond relaxation process in the reverse current of germanium point-contact diodes 62

Cayless, M. A., The emission from oxide cathodes in low pressure discharges 331
Cayless, M. A., and A. D. Forster-Brown, The diffusion of barium in discharge tubes 380
Challice, C. E., Summarized proceedings of a Conference on electron microscopy—Reading, July, 1956 259
Challice, C. E., and J. Sikorski, Summarized proceedings of a conference on the electron microscopy of fibres—Leeds, January 1956 1
Clarke, W. W. H., Valve instability with cathode standing waves of cylindrical symmetry 486
Clarkson, J., A method of measuring the shear modulus of thin xylonite sheet 103
Cosslett, Anna, and V. E. Cosslett, The optical density and thickness of evaporated carbon films 374
Cosslett, V. E., *see under* Cosslett, Anna
Coyle, R. A., A. M. Marshall, J. H. Auld and N. A. McKinnon, Application of a microfocus Laue technique to the study of deformation in aluminium single crystals 79

Davis, P. F., An electrical analogue of magnetic domains 19
Dawes, J. G., G. K. Greenough and J. S. Seager, The penetration of irregularly-shaped particles through an airborne-dust elutriator 236
Dawton, R. H. V. M., High vacuum shaft seals flanged joints and the gassing and the permeability of rubber-like materials 414
de Vries, D. A., and C. A. R. Pearce, The electrical conductivity and permittivity of mixtures 301
Dillon, T. J., Spectral sensitivity of neon discharge tubes 490
Din, F., Summarized proceedings of a meeting on low temperature distillation—London, March, 1957 436

Edels, H., and W. A. Gambling, Spectral response and linearity of photomultipliers 481
Edwards, A. G., Measurement of the diffusion rate of hydrogen in nickel 406
Einstein, P. A., The light output of some phosphors excited with electrons of high current density 190
Einstein, P. A. *See under* Archard, G. D.
Ennos, A. E., Highly-conducting gold films prepared by vacuum evaporation 113
Evans, D. M., Measurements on alloy-type transistors with varying collector voltage 44

Fairley, E. S., The measurement of peak voltage using a cathode-ray tube 101
Farr, R. F., The use of low-inertia integrating motors 366
Fessler, H., Summarized proceedings of a conference on stress analysis—Cranfield, September, 1956 307
Fessler, H., and E. Ollerton, Contact stresses in toroids under radial loads 387
Fielding, C. C., *see under* Maddock, A. J.
Fletcher, W. P., and A. N. Gent, Dynamic shear properties of some rubber-like materials 194
Forster-Brown, A. D., *see under* Cayless, M. A.
Fortescue, R. L., *see under* Mansfield, W. K.
Foster, E. L., and H. Heap, High-temperature tensometry and its application to amorphous polyethylene terephthalate 400

Gafner, G., The application of a transient method to the measurement of the thermal conductivity of rocks and building materials 393
Gambling, W. A., *see under* Edels, H.
Gay, P., and P. J. Wheatley, Summarized proceedings of a conference on X-ray analysis—Cardiff, April, 1957 427
Gent, A. N., *see under* Fletcher, W. P.
Greene, D., Size of the focal spot in a betatron 293
Greenough, G. K., *see under* Dawes, J. G.
Gregory, R. W., *see under* Bartley, A. J.
Guile, A. E., T. J. Lewis and S. F. Mehta, Arc motion with magnetized electrodes 444

Haine, M. E., Scaling of space-charge limited electron-optical systems 44
Hall, D. M., The preparation of electron microscope replicas from rough porous surfaces 295
The deterioration of nitrocellulose films used for electron microscopy 380
Halmshaw, R., and C. Hunt, Fluoroscopy with an enlarged image 282
Halmshaw, R., *see under* Morgan, R. S.
Hancox, R., The breakdown of liquid dielectrics and its dependence on oxidation of the electrodes 476
Harrison, E. R., Scaling laws for space charge dynamics 422
Hawkes, G. A., The measurement of surface residual stress by X-rays 229
Heap, H., *see under* Foster, E. L.
Hearmon, R. F. S., Some applications of physics to wood 49
Herbst, L. J., The impedance of the oxide-coated cathode at ultra-high frequencies 277
Higginson, G. S., The effect of sulphur and oxygen on the electrical properties of oxide-coated cathodes 148
Hooke, F. H., *see under* Blunden, W. R.
Hopkins, M. R., Viscous flow between rotating cylinders and a sheet moving between them 442
Hughes, J. W., Isabel E. Lewis and A. J. C. Wilson, Comments on the A.S.T.M. Powder Data File 173
Hunt, C., *see under* Halmshaw, R.
Hutcheon, I. C., An iterative analogue computer for use with resistance network analogues 370

Iredale, P., *see under* Peirson, D. H.

Jenkins, R. O., *see under* Brodie, I.
Jessop, H. T., A tilting stage method for three-dimensional photoelastic investigations 30
Jiggins, A. H., *see under* Maddock, A. J.

Kynch, G. J., The fundamental modes of vibration of uniform beams for medium wavelengths 64

Langton, N. H., and P. Vaughan, The ultrasonic degradation of polystyrene at a frequency of 1 Mc/s 289
Lee, E. W., Non-linear forced vibration of a stretched string 411
Lee, P. A., Determination of the impurity concentrations in a semiconductor from Hall coefficient measurements 340
Lewis, Isabel E., *see under* Hughes, J. W.
Lewis, T. J., *see under* Guile, A. E.
Lowenthal, G. C., A simple calibration technique for improving the accuracy of a Smith resistance thermometry bridge 449

Mackenzie, D. K., and T. P. Newcomb, The measurement of Meyer hardness and Young's modulus on the Rockwell test machine 398
Maddock, A. J., C. C. Fielding, J. H. Batchelor and A. H. Jiggins, The effects of dust and force upon certain very light electrical contacts 471

Mahalingam, S., Transverse vibrations of power transmission chains 145
Major, J. V., *see under* Apostolakis, A. J.
Mansfield, W. K., and R. L. Fortescue, Pre-breakdown conduction between electrodes in continuously-pumped vacuum systems 73
Marshall, A. M., *see under* Coyle, R. A.
Marshall, S., *see under* Braun, I.
Maude, A. D., and T. V. Starkey, Action and viscous flow 343
McFarlane, A. B., The movement of the second crossover potential of insulators 248
McKinnon, N. A., *see under* Coyle, R. A.
Mehta, S. F., *see under* Guile, A. E.
Mendoza, E., Physics below 1° K 219
Messerle, H. K., *see under* Blunden, W. R.
Mitchell, E. W. J., The effect of radiation damage on the electronic properties of solids 179
Morgan, R. S., R. Halmshaw and B. J. Ratcliffe, The standardization of X-ray output in industrial radiology 59

Nagao, Shigeo, The mechanism of particle acceleration in high current spark discharges 380
Náray, Zs., and P. Varga, On the mechanism of the production of dark-current pulses in photomultipliers 377
Newcomb, T. P., *see under* Mackenzie, D. K.
Newman, P. C., A method for the measurement of heat generation in powdered coal 162
Norbury, J., *see under* Booker, G. R.

Oatley, C. W., The flow of gas through composite systems at very low pressures 15
Oatley, C. W., *see under* Steckelmacher, W.
Ollerton, E., *see under* Fessler, H.

Pattison, J. R., *see under* Browne, M. T.
Pearce, C. A. R., *see under* de Vries, D. A.
Peirson, D. H., and P. Iredale, The γ-ray scintillation spectrometer 422
Popper, B., and M. Reiner, The application of the centripetal effect in air to the design of a pump 493
Pratt, R. G., *see under* Robinson, T. S.
Preston, J. S., *see under* Barnett, W.

Ratcliffe, B. J., *see under* Morgan, R. S.
Reiner, M., *see under* Popper, B.
Richardson, D. A., The X-ray and γ-ray absorption coefficients of a number of glasses 11
Richardson, J. F., The effect of oxygen and sulphur on the thermionic emission from matrix cathodes 361
Riddlestone, J., Short duration discharges between separating contacts in a 6 V circuit 105
Robinson, G. T. G., *see under* Sprinks, M. E.
Robinson, T. S., M. Smollett and R. G. Pratt, A simple graphical method of calculating the density of current carriers in a semiconductor from the Hall coefficient 130
Rose, G. S., and S. G. Ward, Contact electrification across metal–dielectric and dielectric–dielectric interfaces 121
Rymer, T. B., Summarized proceedings of a symposium on thin films—Reading, September, 1956 97

Seager, J. S., *see under* Dawes, J. G.
Sikorski, J., *see under* Challice, C. E.
Smollett, M., *see under* Robinson, T. S.
Spit, B. J., Some carbon replicas techniques for the electron microscopy of small specimens and fibres 493
Sprinks, M. E., G. T. G. Robinson and B. G. Bosch, The frequency of dependence of noise temperature ratio in microwave mixer crystals 275
Stark, D. S., The conductance of a column of vapour for gases at low pressures 210
Starkey, T. V., *see under* Maude, A. D.
Steckelmacher, W., and C. W. Oatley, The flow of gas at very low pressure 494
Stratton, R., On the elementary theory of thermoelectric phenomena 315
Sutton, A. L., *see under* Booker, G. R.

Terry, N. B., Some considerations of the magnetostrictive composite oscillator method for the measurement of elastic moduli 270
Thomas, T. S. E., A method of measuring the thermal constants of granular materials 403
Thring, M. W., Some recent developments in the physics of fuel combustion 89
Tucker, M. J., The analysis of finite-length records of fluctuating signals 137
Twidle, G. G., The spectral reflectivity of back-surface and front-surface aluminized mirrors 337

Varga, P., *see under* Náray, Zs.
Vaughan, P., *see under* Langton, N. H.

Walsh, A., *see under* Booker, C. J. L.
Ward, E. E., Measurements of the impedance parameters of junction transistors 329
Ward, S. G., *see under* Rose, G. S.
Wheatley, P. J., *see under* Gay, P.
Williams, Betty E., Electron microscope and diffraction studies of 7% chromium–molybdenum steels 241
Wilson, A. J. C., *see under* Hughes, J. W.
Wolfendale, A. W., *see under* Barron, W. C.
Wood, J. L., *see under* Booker, C. J. L.

Yemm, H., *see under* Baker, D.

Zernik, W., The dust-free space surrounding hot bodies 117

PRINTED IN GREAT BRITAIN BY UNWIN BROTHERS LIMITED, WOKING AND LONDON

Summarized proceedings of a conference on the electron microscopy of fibres—Leeds, January 1956

A conference on the electron microscopy of textile and other industrial fibres was held on 3 and 4 January, 1956, in the Department of Textile Industries, University of Leeds. The conference was organized by the Textile Physics Laboratory, under the auspices of The Institute of Physics. Seventeen of the eighteen papers are summarized. Many of the papers evoked stimulating informal discussion.

TECHNIQUES IN THE STUDY OF SURFACES

The first paper was read by Mr. O. C. WELLS (Department of Engineering, University of Cambridge) on the examination of fibres in the scanning electron microscope. This method is particularly useful in cases where the high resolution of the transmission electron microscope, used in conjunction with replicas, is not essential, or where the foreshortening and the presence of "long" shadows, involved in the reflexion electron microscope, may be of some disadvantage. A selected area of the specimen is scanned by a narrow electron beam and the electrons leaving the specimen are collected into an electronic multiplier, amplified and fed into a cathode-ray tube so that an image of the surface is produced "looking at" the specimen, along with the incident illumination (Fig. 1, p. 21). Since the electrons do not have to be focused after they leave the specimen, it becomes possible to examine solid surfaces with low values of foreshortening, of the order of only 2·5 to 1. The conditions of illumination compare very favourably with those used in the other methods of electron microscopy. Thus the average values of the electron intensities are lower than in the reflexion method, although the intensity in the spot itself is relatively high; furthermore, because the illumination is confined to the field of view, any heat damage or contamination of the specimen is immediately apparent. The resolution is determined principally by the spot size and is of the order of 250 Å, with a theoretical limit of about 100 Å. The accelerating potential is kept down to 15–20 kV to reduce penetration of the incident beam into the specimen. Magnifications of twenty thousand times are possible. Contrast is provided mainly by variations in surface topography rather than by variations in structural components of the specimen. When examining visually a scan repetition rate of twice a second is used, but when taking photographs a four-minute scan is used for the highest resolution. In general, the only specimen preparation needed is the evaporation on the surface of a thin layer of metal to prevent charge effects; this simplicity is an advantage in many cases, for example in the examination of small particles on the surface of fibres or fine fibrillation such as occurs during wet abrasion (Fig. 2, p. 21). In some specimens a pronounced "three-dimensional" effect is noticeable, and this can be accentuated by taking a stereoscopic pair of photographs. Undoubtedly the most attractive feature of the scanning method lies in the possibility of the manipulation of specimens while they are under examination, a technique that has been used at Cambridge during an investigation into the properties of germanium;[1] thus it should be possible to follow the processes of twisting, bending, extension or abrasion of fibres and to take photographs of these events as they occur.

Dr. J. A. CHAPMAN (Department of Physical Chemistry, University of Cambridge) then described the application of the reflexion technique (grazing incidence) to the study of abraded Nylon fibres. Previous work[2,3] has demonstrated the usefulness of the reflexion technique in the direct examination of textile fibres. The image is obtained by tilting so that the beam falls at a small angle of incidence on the specimen and the scattered electrons are then focused by the objective lens in the usual way. Fibre specimens are mounted on a metal surface and the specimen is coated with a thin film of silver to prevent accumulation of charge on the surface. Nylon monofilaments rubbed once by a flat slider under a heavy load have been examined by this technique. Deformation of the whole fibre occurs and, above a critical load, tearing can be observed in the centre of the track. This tearing is found whenever the frictional shear stress at the surface exceeds about 1·5 kg/mm^2. The deformation is usually concave in shape and probably due to the material in the central region of the track being stretched beyond the elastic limit; at the edges of the track, however, little longitudinal deformation occurs and full elastic recovery in a transverse direction can take place. The effect of prolonged but light abrasion of drawn Nylon fibre has been studied, and Fig. 2 shows a series of three micrographs of a single Nylon filament extracted from fabric knitted with thirty denier (ten filaments) yarn which had been abraded in a washing machine for one hundred hours. The bulk deformation of the fibre has not occurred and the damage is confined to the surface layers, taking the form of thin fibrillar material peeled off from the surface. Regions of damage occur at regular distances along the filament, corresponding to repeat in the knitted structure and exposure to the fabric surface. A similar type of fibrillar disintegration of the surface layers occurs on larger diameter Nylon monofilaments, but is less pronounced. It seems likely that this type of disintegration is associated with fatigue of the outermost layers of the fibre. The advantages of the reflexion electron microscope technique in this type of problem are its simplicity and the high depth of focus, enabling shape and surface structure to be viewed simultaneously. Nylon is unaffected by a low intensity electron beam but the ease with which most fibres are degraded by electron bombardment is a serious difficulty. It may be overcome by taking a positive metal replica of the complete fibre, as shown by Bradley,[3] but it may be difficult to replicate fibrillar material such as that shown in Fig. 2. The foreshortening is inherent in the reflexion method; it can be avoided by using the more complicated scanning method described in the previous paper although, in some problems, the small viewing angle may be an advantage.

Dr. D. G. DRUMMOND (British Cotton Industry Research Association, Didsbury, Manchester) described some of his experiences with fibre replication techniques and listed the following requirements of an ideal replica: (i) accuracy of

reproduction of detail; (ii) applicability to selected portions of individual fibres; (iii) applicability to all types of fibres; (iv) manipulative simplicity; (v) rapidity of working. He went on to examine existing replica methods, with these criteria in mind, and pointed out that the light microscope, within its own limitations of resolving power, fulfils all these requirements. The single-stage polymer replica method, though simple in concept, has been found manipulatively difficult, and gives a specimen which is thin enough for observations only near the centre of the fibre impression. The two-stage, polystyrene–silica method gives satisfactory pictures but is too slow to sustain interest in a technological programme; an analogous method, using butyl methacrylate and carbon, is much faster and is preferable for thermoplastic fibres, because the first impression is made at lower temperature; the carbon films tend to break up, however, if removal of the butyl methacrylate is delayed. Damage to the final film frequently occurs during removal of the first-stage polymer, and various procedures at this point were discussed; laying the composite film over a grid on a wad of filter paper, and allowing solvent to soak up from below, was recommended as being the least hazardous and requiring least apparatus, while permitting prelocation of interesting regions over the centre of the grid. A replica made by direct evaporation on the fibre should reproduce detail more faithfully than one involving a polymer impression, and Ramanathan, Sikorski and Woods[4] have developed successful direct methods for wool and some other fibres, but unfortunately, in Dr. Drummond's experience, these do not work well with viscose rayon. The difficulty lies partly in controlling the depth to which the fibre is embedded in a polymer support, while leaving its upper surface exposed, and some tentative ideas for dealing with this problem were put forward. Fig. 3 (p. 21) shows a single-stage carbon replica of Fibro filament, which is dissolved in sulphuric acid after evaporation of carbon. However, the method has too low an expectation of success for regular use. In the discussion, Dr. P. Kassenbeck (l'Institut Textile de France, Paris) said he had found that the accuracy of reproduction of polystyrene replicas could be improved by working *in vacuo*.

Mr. L. Oster, Dr. J. Sikorski and Mr. H. J. Woods (Department of Textile Industries, University of Leeds) described some recent work in the replication of surfaces of fibres. In spite of recent advances in the application of scanning and reflexion microscopy to the study of the surface structure of fibres, superior results in the range of high resolution are obtained with the transmission type electron microscope used in conjunction with the replicas of surfaces. Materials of low molecular weight should be used, not only for preparation of the final positive replicas, but throughout the replication procedure and the superiority of such a method has been clearly established;[4] although this advantage is somewhat offset by the difficulties of the preparation of replicas, particularly their dry stripping. The embedding technique of Ramanathan, Sikorski and Woods[4] gives a fair percentage of success and provides means for an adequate control of the reproducibility and the incidence of artifacts. The difficulty of obtaining uniform embedding, which some workers stressed as a disadvantage, has not been found important in the work involving high resolution; although when embedding is uniform the chances of successful stripping are greater and, therefore, it may be desirable to control this operation. In order to deal with this problem Długosz[5] introduced recently a preliminary step which consists of the partial embedding of fibres in the gelatine coating of a photographic plate, followed by complete flooding with a suitable monomer which, when polymerized, forms a strong backing layer; after stripping this layer, together with the embedded fibres, the Leeds method is then followed throughout. Still greater success is obtained using a new method of dry stripping of replicas, which are now backed by a thick layer of gum arabic (compare Ref. 6). This material is capable of making contact with the entire surface of the replica even in the regions where adhesive tape cannot, namely, near the points of entry of the curved fibres into the embedding medium. A further advantage of this technique is that replicas so backed can, after stripping, be attached to a moist slide and, when dried, will remain perfectly flat during the preparation of positive replicas. The Leeds workers have stressed that their earlier results were obtained using mainly Lincoln wool and that the extension of their conclusions, to other animal hair and wools, must be made with great caution. This point of view is now confirmed by some recent work on Australian merino wool and it appears that long-term work will be necessary before an adequate interpretation of various features can be given. Results indicate some significant differences in the scale texture of Australian merino and Lincoln wools, namely, that the corrugations on the surfaces of the individual cells in the former have a smaller (but more uniform) wavelength, and a smaller (but again more uniform) amplitude than in the latter. Some observations were made also on the effect of cold drawing—in glycerine—of 6 : 6 Nylon, and it was possible to follow the development of interesting cross-striations on the surface (Fig. 4, p. 22). Furthermore it was possible to observe a qualitative correlation between the degree of extension and surface roughness.[7] In the discussion, Mr. Kidd (British Brush Manufacturers Research Association, Leeds) suggested that it may be of some interest to examine a possible relationship between the intersecting lines on the surface of 6 : 6 Nylon monofilaments (described by Oster, Sikorski and Woods) and an effect which his laboratory had observed some time ago in the same type of Nylon. A Nylon monofilament from an industrial brush, which had been subjected to severe bending, showed the pattern of cracks in the interior of the filament, when mounted in Canada balsam. A similar criss-cross pattern may be produced in some polystyrene monofilaments used for brush-making.

ULTRA-THIN SECTIONING

Mr. A. O. T. Charles and Dr. J. Sikorski (Department of Biomolecular Structure and Department of Textile Industries, University of Leeds) described some practical aspects of ultra-violet polymerization of embedding materials for sectioning. A simple and reliable method was described of polymerizing embedding monomers (methyl, ethyl, n-butyl and isobutyl esters of methacrylic acid) using ultra-violet radiation. Various difficulties encountered in developing the method—removal of inhibitor, use of catalyst, etc.—were mentioned and its advantages and drawbacks summarized.[8]

Dr. P. Chippindale (Tootal, Broadhurst Lee Co. Ltd., Manchester) discussed the sectioning of textile fibres for electron microscopy. Producing sections of textile fibres 200–400 Å in thickness, for examination in the electron microscope, presents several serious difficulties, in addition to those normally encountered in sectioning biological specimens. Fibres are tougher and form a relatively compact mass, preventing the infiltration of the embedding medium into the specimen, which is possible with many biological samples. Perhaps the greatest problem is producing sufficient

adhesion between fibre surface and embedding medium (e.g. polymethacrylate), because if this is insufficient, the sections are ripped from the embedding medium during cutting and subsequently lost. The fibre-section is a disk of diameter 500–1000 times its thickness and therefore has relatively little of its surface in contact with the embedding medium. Apart from its lack of appreciable penetration into the fibre, the methacrylate tends to shrink away from the fibre surface on polymerizing. The following embedding procedure has been designed to achieve maximum possible penetration of the fibres by the methacrylate. After degreasing, the fibres were swollen in water to open their capillary spaces, but since methacrylate monomer is immiscible with water, the fibre must then be dehydrated and transferred to the monomer without collapsing the capillary spaces. The fibres were, therefore, taken through a water/alcohol series to absolute alcohol, then through mixtures of alcohol and methacrylate monomer and finally transferred to monomer in gelatine capsules. The monomers used were 90/10 or 80/20 mixtures of n-butyl and methyl methacrylates polymerized with 2 : 4 dichlorobenzoyl peroxide at 45° C for 24 h. A commercial Porter–Blum microtome with the unit advance set at 250 Å and fitted with a glass-knife was employed. Sections were collected on Formvar-covered grids from a conventional liquid trough. The embedding medium was removed by dipping the mounted sections in xylene for thirty seconds; they were then shadowed with gold–palladium. In this way it is possible to produce fibre sections (e.g. viscose rayon, Nylon, wool) sufficiently thin as to be undamaged by the electron beam. Sections of viscose rayon fibres revealed the existence of the "skin" layer of varying thickness, for example, approximately 1 μ in a fibre about 10 μ in diameter (Fig. 5, p. 22) and much denser than the core. The fine-grained appearance of the latter may correspond to the distribution of fibril bundles. It was found easier to obtain undamaged and flat sections of wool than of other fibres, perhaps on account of its relatively rough surface promoting better adhesion between fibre and embedding medium. Fig. 6 (p. 22) shows a cross-section of 64's Australian merino fibre (about 20 μ in diameter); the over-lapping of the scales (of thickness up to 1 μ) round the cortex is clearly visible, but separate layers of the cuticle are not resolvable with any certainty. Some structure also appears in the cortex and this can be interpreted as the outlines of cortical cells; possibly part of the membranes which, it is suggested, surround these cells.

Mr. G. E. Rogers (Anatomy School, University of Cambridge) discussed some observations made on ultra-thin sections of keratin fibres. Ultra-thin sectioning techniques for electron microscopy have been applied to medullated rabbit hair and wool, and to the hair follicles of the human, guinea-pig and mouse. Following methacrylate embedding, hair follicles were fixed in buffered osmic acid for periods varying from 1 to 5 h; untreated, mature hairs, however, do not require fixation. So far the yield of satisfactory sections from mature fibres was not high and their thickness too great to obtain high resolution, though useful results have been obtained at lower magnifications. Thus cross-sections of untreated rabbit hairs revealed cortical cell outlines, adjacent cells were separated by a less dense gap of about 600 Å; in the centre of this gap a dense membrane profile 150–200 Å wide, derived from the cortical cell membranes, appeared to form a continuous boundary throughout the cortex and between the scale and cortex junction. Variations were shown in the electron density of the cortex and the presence of macrofibrils was observed without prior chemical treatment. Attempts to cut sections of untreated wool have not been rewarding but were successful following oxidation with peracetic acid. Cross-sections from fibres thus treated showed reversal of electron density, the cortical cell membranes and nuclear remnants being denser than the keratin. Cortical cells were intact in the paracortex, whereas macrofibrils were apparent in the orthocortex; the component layers of the cuticle were also revealed in treated material, the epicuticle shown as a dense line overlying a less-dense exocuticle, and the innermost layer, the endocuticle, as denser than the exocuticle. More information about the fine structure of the cuticle and the cortex has been obtained from sections of hair follicles. The keratin of the overlapping scale cells appears to develop in their cytoplasm as dense granules 250–400 Å in diameter, larger than the granules of the ground cytoplasm. Fig. 7 (p. 22). At higher levels in the follicle they aggregate to produce larger masses which form up beneath the outer cell membrane of each scale cell and constitute the exocuticle, Fig. 8 (p. 23); the single cell membrane of the outer scale forms the epicuticle in the mature hair. The exocuticle granules also accumulate in the scale tips, in accordance with the conclusions of Lagermalm,[9] and also of Fraser and Rogers,[10] that the thickened tips of scales remaining after chemical extraction of hairs were due to exocuticle. The endocuticle appears to develop later than the exocuticle and is derived from much smaller granules, which gradually coalesce, in a similar way to the exocuticle, to form a homogeneous layer. In conclusion Mr. Rogers considered that the fibrous nature of the cuticle has been established. The evidence provided by the above experiments suggests that there is no reason to believe in the presence of a morphologically distinct "subcuticle."[11] Mr. Rogers considered that the information already obtained from thin sections has indicated that its pursuit will be rewarding despite the technical difficulties.

In the discussion Dr. P. Kassenbeck asked if it had been possible to distinguish in the sections a difference in submicroscopical structure between what is called "the orthocortex and the paracortex" of the wool fibre. He expressed the view that certain micrographs showed a difference of electron density between those two regions. The mean diameter of the cortical cells seemed equally distinctly different in those two zones. Regarding embedding techniques he said that his experience showed that good sections can be obtained with biological substances, like wool or cotton, but that it is much more difficult to obtain good sections of synthetic or regenerated fibres. His laboratory has worked out an embedding procedure for viscose rayon which gives good results and which can eventually be applied to other fibres. This method involves embedding fibres in paraffin and cutting their cross-sections 50–100 μ in thickness; after dissolution of the paraffin the sections are subsequently re-embedded in butylmethacrylate. The orientation of the sections parallel to the axis of the embedding cylinder is obtained by application of an alternating field (less than 3·5 e.s.u.) during polymerization.

PROTEINS

Prof. D. Burton, Dr. R. Reed and Miss M. J. Wood (Department of Leather Industries, University of Leeds) opened the session on protein fibres with a discussion of the thermal shrinkage of leather. The structural changes following the action of hot water on tanned collagen fibrils were

described. Hydrothermal shrinkage involves a swelling and flattening; the bands become thinner and much closer together, whilst the fibrils assume an interesting helical form, Fig. 9 (p. 23). On continued heating, the fibrils break across cleanly into short, stubby units; the latter are ultimately reduced to glue-like material of ill-defined morphology. These hydrothermal changes are not shown simultaneously by all the tanned fibrils obtained from one particular sample of leather. Some shrink, shorten, and form glue-like material at fairly low temperatures, whilst others withstand much higher temperatures for longer periods without showing any apparent changes. Similar helical structures, which may be either left- or right-handed in direction, are also observed when native collagen fibrils are heated at 37° C with various chemical reagents, covering a wide range of pH value.[12] On the basis of these helical structures from both tanned and native collagen it was considered that the fibril of collagen consists of a cross-helical system of polypeptide chains. Furthermore, it was suggested that certain bundles of chains in this cross-helical system were different in chemical composition from the other chain bundles. In particular, it was suggested that these were rich in hydroxyproline and hence might be expected to be more sensitive towards heating than the other chain bundles. Loosening of the hydroxyproline-rich chain bundles was thought to account for the helical structures illustrated in the paper. Tanning apparently builds cross-linkages between the cross-helical systems of polypeptide chains, whilst shrinkage and swelling involve the relative movement of the cross-helical structures. In answer to a question, Dr. Reed said they found that once swelling sets in and the leather fibrils assume the spiral form, then it is impossible to get back their original unshrunken state. Mr. D. H. Page (British Paper and Board Research Association, Kenley, Surrey) asked whether it was statistically true that there were as many spirals in the one direction as in the other. Dr. Reed replied that he intended to convey simply that there were spirals in both directions.

Mr. M. S. C. Birbeck and Dr. E. H. Mercer (Chester Beatty Institute, London) described the structure and formation of the cuticle in hair. The cuticle of hair is a tube of flattened overlapping cells which ensheath the bundle of long fibrous cells forming the hair cortex. A number of electron microscopical techniques have provided information concerning its structure: (i) surface replicas; (ii) disintegration by various means, followed by an examination of the fragments whole; (iii) thin sectioning of hair or fragments; (iv) thin sectioning of the developing hair in the follicle. The results of these methods are in good agreement and show that the flattened cells possess a lamellar structure. Proceeding from the outer surface inwards one encounters, Fig. 10(*a*): (i) the epicuticle *E*, a modified cell membrane, which being resistant to most chemical and enzymes, is isolated as thin sheet when the rest of the fibre is disintegrated; (ii) the exocuticle *K*, a non-fibrous, heavily keratinized layer closely adhering to the epicuticle; (iii) the endocuticle *R*, a layer containing protein digestible by enzymes but not stabilized by disulphide bonds, i.e. not a keratin, and therefore resistant to keratinolytic solvents; (iv) an inner unspecialized cell membrane *M*. The electron micrographs of thin sections of treated cuticle, shown in Fig. 10 (p. 23), illustrate these features. A fragment of cuticle cell after trypsic digestion is shown in Fig. 10(*b*). The endocuticle *R* has been removed, the epicuticle *E* and exocuticle (resistant keratin) remain. The reverse effect is shown in Fig. 10(*c*), where the keratin *K* has been removed by oxidation and alkaline extraction leaving the endocuticle *R* (non-keratin), the epicuticle and other cell membranes. More detailed information has been obtained from a study of thin sections of the growing hair. Six streams of cells leave the papillary surface and, moving towards the skin surface, differentiate into the several layers of the hair and its enveloping sheaths. All the cells of the germinal layer appear identical but, two or three cell diameters higher, differentiation is revealed by differences in the fine structure. The presumptive cuticular cells are the first to be clearly defined. Above the germinal layer the cells are linked by curious localized cell contacts marked by an increased density of the opposed cell membranes, which give rise to the "cell bridges" visible in the light microscope. The membranes of the presumptive cuticular cells become denser and appear to establish permanent contact over a larger area than those of other cells. Mr. Birbeck and Dr. Mercer suspect that this is an early manifestation with important consequences, since such thickened membranes of lowered activity could conceivably reduce the uptake of nutrient and thus account for the observed slower rate of protein synthesis and the heavily keratinized character of the protein. The cuticular cell stream, strongly integrated by the fused cell membranes, is subsequently flattened and sheared mechanically by the contiguous cell streams. As this proceeds, protein appears as droplets (Fig. 11, p. 23, shows two stages) which condense against the outer cell membranes to form the layer *K*. The layer *R* consists of the cytoplasmic material remaining over when synthesis ceases and the cell dries out. The events contrast with those in the presumptive cortical cells where cell membranes are thinner and there is easy access to the papillary food supply. Protein synthesis is here more rapid and the product consists of thin fibrils (less than 100 Å in diameter) which appear in bundles and condense to form the macrofibrils visible in the light microscope.

Mr. G. E. Rogers (Anatomy School, University of Cambridge) described the electron microscopy of ultra-thin sections of hair follicles. The examination of thin sections of hair follicles in the electron microscope (Siemens, Elmiskop) has yielded information on the synthesis and structure of cortical keratin and other follicle components. According to Mr. Rogers presumptive cortical cells arise by cell division and differentiate from the hair matrix which surrounds the dermal papilla. In pigmented follicles they are closely associated with active melanocytes. Fine cytoplasmic filaments of keratin (protofibrils) less than 100 Å wide and several microns long have been found to develop in close proximity to the nuclear membrane. These observations confirmed conclusions drawn from investigations on chemically disintegrated mature wool fibres.[13,14] Mitochondria in human follicles are small structures, about 0·1 μ wide, and in young mouse follicles they are slightly larger, about 0·2 to 0·4 μ wide. Both types have the typical cristae mitochodriales described for other cells. At a higher level the protofibrils aggregate to the macrofibril stage, and are seen in Fig. 12 (p. 23). The macrofibrils tend to line up along the cortical cell boundaries and around the nucleus, otherwise they are uniformly distributed in the cell cytoplasm. The component protofibrils can be recognized in each macrofibril. It is well known that hair follicles possess a high concentration of sulphydryl groups in cortical cell cytoplasm at the macrofibril stage (fibrillation zone). Furthermore, Bern, Harkness and Blair[15] have shown that cystine is metabolically incorporated into this same zone. These extensive biochemical changes, which include continued fibrillogenesis, proceed in the presence of very few mitochondria, a fact revealed only by the electron microscope. A further observation is that

free protofibrils are not found in the cytoplasm when macrofibrils have developed, therefore it seems likely that after an initial period of protofibril production and lateral aggregation, further keratin is directly synthesized on to the macrofibrils already formed. In similar fashion, fine cytoplasmic filaments of keratin, morphologically identical with those in hair, have been studied in the stratum germinativum cells of young mouse epidermis. The changes which the filaments undergo have been traced, and they can be individually recognized even in the cornified cells of the outer keratinized layer. All three cell layers of the inner root sheath (i.r.s.) synthesize and fill their cytoplasm with filaments morphologically similar to those in the cortex, these are about 70–80 Å wide, several microns long, and are orientated parallel to the direction of fibre growth. In contrast to the cortex they are associated with very large homogeneous dense granules and do not aggregate to form intermediate macrofibrils. The i.r.s. keratin (trichohyalin) differs chemically in that it is probably lacking in disulphide bonds and has a high affinity for heavy metals. The electron microscope shows that the keratin of the medulla cells develops in the form of round masses of variable size and is homogeneous except for a dense periphery. A similar picture is obtained when they are observed after isolation from mature fibres. In young mouse follicles a basement membrane of condensed homogeneous material 300–400 Å thick is situated between the epidermal cells of the hair matrix and the fibrocytes of the dermal papilla. It is spaced about 200 Å from the hair matrix boundary, Fig. 13 (p. 24), and it is continuous with the basement membrane (glassy layer) of the follicle outside the papilla. In the papilla of the adult guinea pig the membrane is made up of fibrils showing periodicity along their length. These fibrils are abundant in the intercellular spaces of the papilla. In the same animal the glassy layer of the follicle, which is an argyrophyllic layer of reticular nature, has been found to consist of a double layer of collageneous fibrils 400 Å in diameter. Proximal to the outer root sheath the closely packed fibrils are orientated parallel to the follicle length, whereas the outer layer is composed of fibrils running at right angles to the former. The glassy layer develops in young animals in the space formed between the outer root sheath and a network of closely united fibrocytes surrounding the follicle primordium. The development of the several morphologically and chemically different keratins and the concomitant submicroscopic events, described by Mr. Rogers, combine to give a static picture of keratin synthesis which is useful as an adjunct to biochemical and histochemical studies of the process.

Dr. J. Sikorski and Mr. H. J. Woods (Department of Textile Industries, University of Leeds) discussed some problems in the electron microscopy of keratin fibres. They described the results obtained by Rogers and others, using the ultra-thin sectioning technique for studying the fine structure of keratin, as most useful when the softer pre-keratinized material in the follicle had been under examination. One of the principal features of their micrographs is the occurrence of microfibrils (approximately 200 Å across) which aggregate into well-defined macrofibrils 2000 Å or more in diameter. Between these macrofibrils there occurs a matrix, which appears to be of an amorphous character, as little structural detail can be seen in it. Sections of more mature fibres do not show these features; this may, of course, be simply a consequence of the difficulty of cutting satisfactory sections of the fully keratinized material, but it is at any rate clear that, after keratinization is complete, the fibre has an altogether firmer and more closely knit texture, suggesting that hardening has a pronounced effect on the matrix itself; perhaps an even greater one than on the fibrils observed in the pre-keratinization zone. It is, in fact, extremely difficult to produce satisfactory fibrillation of the mature fibres without subjecting them to drastic chemical attack. The Leeds laboratory has studied this problem in considerable detail,[16] and has come to the conclusion that when suitable degradation techniques are employed, the microfibrillar texture of the bulk of the cortical cell can be made evident. Furthermore, there appears the strong tendency for the cell to disintegrate into sheet-like aggregates of the microfibrils, sometimes more than a micron across and only a few hundred Ångstrom thick, Fig. 14 (p. 24). It is difficult to reconcile this feature of the disintegration experiments with the idea that the macrofibrillar texture persists in the mature fibre. The dilemma might, perhaps, be resolved if keratinization were to involve a stabilization of microfibrils which are present, but not yet clearly evident, in the matrix of regions of the cell in the follicle, coupled with a uniplanar type of linking between these and the other aggregated microfibrils. Some progress might be expected when sectioning can be extended in a more systematic manner to the examination of chemically treated fibres. In the studies of the disintegration products of keratin in which S–S bonds have been attacked, a clearly marked difference between the effects of oxidizing and reducing agents is believed to have been observed. The former act more specifically on the linkages between the microfibrils, the latter attack the microfibrils (tending to break them into short fragments) before separation is complete. This suggests that there is a distribution of S–S bonds of different reactivity between and within the microfibrils. In oxidation experiments intrafibrillar breakdown is deferred until more than 90% of the sulphur has been oxidized, and this has been interpreted as meaning that the bulk of the sulphur is interfibrillar in location. If this is so, the idea that keratinization has a particularly important effect in linking the microfibrils together laterally would appear to be reasonable.

Dr. K. M. Rudall (Department of Biomolecular Structure, University of Leeds) described some work on the protein ribbons obtained from the egg-case of the praying mantis. The ribbon-like units are approximately 50 μ long, 1–2 μ wide and 100–200 Å thick (Fig. 15, p. 24). The ribbons represent the most crystalline form of naturally occurring α-protein. The polypetide chains are parallel to the ribbon length with lateral axes respectively parallel and perpendicular to the flat face of the ribbons. The electron micrographs show striations inclined to the length of the ribbon at an angle of approximately 22°.

Dr. A. B. Meggy and Dr. J. Sikorski (Textile Chemistry and Textile Physics Laboratories, University of Leeds) described observations on two crystal forms of polyglycine. Polyglycine I was obtained by heating diketopiperazine or glycine with water at 140° C, and is characterized by X-ray diffraction spacings at 3·40 Å and 4·35 Å. Polyglycine II was obtained by dissolving polyglycine I in saturated calcium chloride or lithium bromide solution, and precipitating at room temperature; characteristic X-ray spacing at 4·15 Å. Products precipitated at 100° C contain polyglycine I, and those precipitated at intermediate temperatures showed diffraction patterns intermediate between I and II. Polyglycine I precipitated at 100° C showed, under the electron microscope, cleavage planes, intersecting at about 70°, but without macrocrystalline structure. Polyglycine II, fractionally precipitated from calcium chloride solution, showed well-defined hexagonal laminae with growth steps. The D.P. of

the polymer was about twelve, and the height of the growth steps was less than this; about thirty to forty steps could be counted on each crystal.[17]

CELLULOSE

Prof. R. D. Preston and Dr. Eva Frei (Botany Department, University of Leeds) described work on the electron microscope sections of fibrous cells. The methods of X-ray analysis and of polarization microscopy have, during the past twenty years, together made possible a rather complete elucidation of submicroscopic structure in fibrous plant cells, and particularly in conifer tracheids. From work of this kind, the secondary walls of these elongated cells are now conceived as being on the whole three-layered; within each layer the molecular chains of cellulose lie oriented in a spiral, the spiral in the inner and outer layers being rather flat, and in the central layer rather steep.[18] All three layers vary in structure with the dimensions of the cell in such a way that the constituent spirals are steeper in longer cells, so that it is not possible to make an exact model of any cell type, but rather a general model to which the cells conform. The methods used in elucidating this structure have been indirect in the sense that a conscious mental process intervenes between the observation of the object and the delineation of the image. Prof. Preston and Dr. Frei dealt with a verification of the model by the direct method presented by electron microscopy. The relevant observations were made on thin sections, since only in this way can the spatial relationship of the various layers be ascertained with any surety. In general the observations fully confirmed the structure already described above, namely the presence of inner and outer rather flat spirals and a central steep spiral. In all three layers, cellulose is organized into microfibrils of the order of 150 Å in diameter. The observations, however, add something unexpected. Fig. 16 (p. 24) shows the outer layer as seen in almost longitudinal section, the edge of the cell being visible on the left hand. It is clear that here the orientation of the microfibrils lies in flat spirals, but there are undoubtedly two spirals of opposite sign with the same angle to the transverse of about 25°. It will be noticed, too, that here and there are present microfibrils arranged almost longitudinally. This outer layer is, therefore, more complex than was anticipated. The central layer shows microfibrils running in steep spirals. In Fig. 17 (p. 25), representing a transverse section of tracheid in which the lamellae within the central layer have apparently fallen over, it is obvious that these spirals are steep. It is also clear that the spiral direction varies from lamella to lamella, unless this is due to an artefact involved in the way in which the lamellae have fallen over. Other transverse sections, not illustrated, fully confirm both steep spiral in the central layer and the flatter spiral in the inner and outer layers. It is, however, interesting to note that the walls of ray parenchyma in conifer wood are much more complex than had been imagined. Fig. 18 (p. 25), which represents the section passing almost longitudinally through the wall but lying sufficiently obliquely to cut across the lamella in the wall, shows that the microfibrils vary in direction rapidly from one lamella to the next. All these observations were made on material slightly delignified in order to render the microfibrils more easily visible. The same type of structure was equally visible without the delignification but not so clearly as to be reproducible satisfactorily. The general structure of these fibrous cells was thus confirmed. In answer to Mr. H. J. Woods, Prof. Preston agreed that the microfibrils are presumably embedded in lignin. There is no evidence, however, concerning any chemical association between lignin and cellulose. Large amorphous plates are often seen in material of wood ground in Waring blendor and these could be taken as lignin. If this interpretation is correct then the bulk of the lignin lies in sheets between the microfibrils, possibly in tangential longitudinal sheets, with no firm connexion with them. Mr. Emerton (British Paper and Board Research Association, Kenley, Surrey) asked whether Prof. Preston could enlarge his earlier statement about evidence of a twist in the microfibrils. In reply, Prof. Preston said that twisting of cellulose microfibrils around each other can always be observed in natural cellulosic materials, however carefully prepared. A notable example is given by the individual lamellae in the wall of the green alga *Valonia*, in which the cellulose microfibrils run beautifully parallel to each other except for occasional twists around each other which cannot therefore be artefacts.

Dr. R. H. Marchessault and Dr. B. G. Rånby (Institute of Physical Chemistry, University of Uppsala) presented results of some more detailed work on the correlation between the properties of cotton hydrocellulose and the conditions of hydrolysis. They believe that the application of electron microscopy to the preparation of disintegrated cellulose fibres allows direct observation of the elongated "crystallites," the presence of which was first postulated from X-ray evidence. The general procedure for the preparation of such particles has been to expose the fibrous material to some degradation, for example partial hydrolysis, followed in some cases by mechanical treatment of an aqueous dispersion of the residue. Invariably, after such a treatment, the particles of a colloidal size remain in suspension and can be observed in the electron microscope. From the results of some earlier workers, the following deductions can be made: (i) particles vary in length and width according to method of preparation; (ii) hydrolysis conditions and/or method of sample preparation can influence the size of the observed "crystallites"; (iii) sulphuric acid hydrolysis produces peptization of the material without mechanical treatment; hydrochloric acid alone does not produce peptization. To check the validity of the second deduction, samples, taken from the same cotton pulp preparation, were hydrolyzed using one of the following methods: (i) hydrochloric acid, 2·5 N at 104° C;[20,21] (ii) constant boiling point hydrochloric acid, at 108·5° C;[23] (iii) sulphuric acid, 2·5 N at 101° C;[22] and (iv) sulphuric acid, 950 g/l. at 40° C.[19] After neutralization, aqueous dispersions of each of the samples were treated with ultrasonic waves (22 kc/s and about 1 W/cm^2) for forty minutes and a drop of suspension was then freeze-dried directly on a specimen grid. It is clear, from Figs. 19 and 20, that hydrolysis conditions affect the appearance of hydrolysates, thus seriously impairing the reliability of the particle size measurements. The hydrolysis in constant boiling point hydrochloric acid produces the poorest dispersion, probably due to the fact that under these conditions swelling is somewhat limited (Fig. 19, p. 25). A sulphuric acid medium promotes peptization which can be attributed to sulphation at the surface of the particles. The hydrocellulose from concentrated sulphuric acid contains relatively few aggregates and, according to Woods and his collaborators,[19] the ultimate particles take the form of elongated tabular-shaped units (Fig. 20, p. 25). Mild hydrolysis in 2·5 N hydrochloric acid gives relatively coarse, large particles which are difficult to resolve, hence their observed average length may be somewhat high. On the assumption that cellulose chains, without break in their continuity, may pass through the "crystallites," the chain

lengths calculated from the number average degree of polymerization should be equal to the observed average particle lengths.

It is noteworthy that the value of the degree of polymerization $\overline{DP}_n$, obtained from osmotic measurements, varies inversely as the average particle length, and closest agreement between the calculated and measured chain length was obtained for polarization studies or from examination of grossly swollen fibres, in each case using the light microscope. The transmission electron microscope could be expected to give information only after surface replication which had not yet yielded satisfactory results or after severe disintegration when it was difficult to relate fragments to the tracheids as a whole. The present results were obtained with the reflexion

Results of measurements on hydrocelluloses

Hydrolysis medium	*Temperature* (°C)	*Time* (*h*)	$[\eta]$*	$\overline{DP}_n$	*Calculated chain length* (5·15 $A_{\,n}\overline{DP}_n$) *Å*	*Average particle length*† *Å*
(i) 2·5 N HCl	104	0·25	1·50	82	422	1500
(ii) constant boiling point HCl	108·5	2·5	1·37	80	410	—‡
(iii) 2·5 N H_2SO_4	101	4	1·63	90	464	1200
(iv) 950 g/l. H_2SO_4	40	24	1·76	120	618	1100

* Measured on nitrated hydrocellulose (13·6% N) in butyl acetate.
† Average of seventy independent observations for each method of hydrolysis.
‡ No measurements made because of the high degree of aggregation.

the hydrolysate which showed the best dispersion into single particles.[19] The length measurements on the original electron micrographs showed an exponential distribution of the single particle length.

Dr. SAARA ASUNMAA (Swedish Products Research Laboratory, Stockholm) described a study of laboratory pulps. The ultra-thin sectioning makes it possible to investigate morphological changes in the cell wall of cellulose fibres caused by different chemical treatments. In this study water-swollen fibres were treated with osmic acid and, after drying, they were embedded in methacrylate. The electron micrographs of this material showed the distribution of absorbed heavy atoms, thus making it possible to obtain some information about the accessibility of the water-swollen fibres. The study of the reactivity of carbohydrate components of wood is usually made on a model pulp—holocellulose—prepared by an effective but not drastic removal of lignin, in order to eliminate the effect of the latter. In this investigation the holocellulose was prepared from Swedish spruce and an alkali-treated sample compared with acid and alkali-acid-treated samples.

The electron micrographs of thallated holocellulose[24] showed, according to Dr. Asunmaa, a compact structure, whereas staining with osmic acid demonstrated the different morphological components of the fibre wall, particularly the fine structure of the secondary wall. The fibres treated in hot alkali revealed a high osmium absorption and stained bands, running in the direction of the fibre axis, with periodicity of 0·05 to 0·1 μ. These bands do not run through the whole fibre, but are separated by some material, less accessible to osmic acid. The outermost secondary wall S_0, rich in mannan,[25] appears as a dense but poorly stained structure. In the standard holocellulose the wall S_0 shows uniform thickness, but samples treated in hot alkali are characterized by periodicity in their structure (Figs. 21 and 22, p. 26). The wall S_0 is normally attached to the secondary wall; in the hydrolyzed samples, however, the wall S_0 is often almost separated from the rest of the fibre and could thus indicate the degree of damage involved.

The relationship of the outer secondary wall (S_1) to the other layers of softwood tracheids was examined by Mr. H. W. EMERTON (British Paper and Board Research Association, Kenley, Surrey), who discussed its technological significance in the manufacture of paper and cellulose derivatives. Most information to date has come from (grazing incidence) electron microscope, supplemented with some of the techniques of light microscopy. After emphasizing that the specimens he would show were taken from commercial pulps which had been cooked by processes which are very drastic compared with maceration techniques, Mr. Emerton showed two pictures in which apparently an outer layer was unwinding from its parent tracheid. In each case, however, it had been shown that the "outer layer" was in fact an immature cell wrapped around another. A series of reflexion electron micrographs (taken by Messrs. D. H. Page and J. Watts) was shown in which comparatively thick, more or less transverse fibrils were plainly evident. Amongst these was a micrograph photographed at an angle of viewing (θ_2) of 24°. It is believed to be the first picture of a biological specimen photographed with θ_2 exceeding 12° and, although the resolution had suffered, the transverse fibrils of S_1 were clearly visible (Fig. 23, p. 26). The reflexion electron microscope is not a particularly convenient instrument to use and it was emphasized that one special advantage is its ability to reveal features which can be sought for in the light microscope. A series of photomicrographs was then shown in which effects similar to those described earlier were evident. Included amongst these was a picture of a pine tracheid in which a length of S_1 had been fortuitously ruptured and folded back from the cell, to which it was still attached, and had finally dried flat on the substrate. The structure in this case was particularly clear. The last series of micrographs showed the fibrils of S_1 teased out from the side of the tracheid (Fig. 24, p. 26). These results were summarized as follows: evidence had been shown of the existence of an outer layer of comparatively thick fibrils oriented almost transversely. Although they are often close together, 1 to 5 μ between centres, the spacing is sometimes much greater, in some cases exceeding 20 μ. The strikingly characteristic property, even of the widely spaced fibrils, is the uniformity of their spacing. Gatherings of S_1 are often observed at fairly regular intervals along the length of sulphite fibres but a few widely spaced, transverse fibrils are still evident between these gatherings. When teased out, parts of the wall S_1 have a tape-like structure if the fibrils are fairly close together (not more than 5 μ apart), but, if the fibrils are widely spaced, no connecting membrane is visible. In explanation of these findings, it was suggested that S_1 had the general form proposed by Dolmetsch, Franz and Correns,[26] namely, prominent parallel fibrils joined by a membrane. In the pristine state,

the fibrils are not more than 1 or 2 μ apart, but sulphite digestion caused them to swell in the form of the well-known balloons which they exhibit in certain swelling agents. This caused gatherings of S_1 at fairly uniform intervals and a general separation of the rest of the S_1 fibrils surrounding the distended wall. This was sometimes sufficiently great to rupture the connecting membrane but, even then, a local uniformity of spacing was usually preserved. The pitch of the helix had been found to be about 70–80° in the sinistral sense. Mr. Emerton had recently shown[27] that, in these tracheids, the bulk of the cellulose, situated in the middle secondary wall, spiralled in the opposite sense so that the fibrils of the two layers were almost orthogonal. He had shown some evidence of a crossed fibrillar structure in S_1 but in such cases the sinistral fibrils predominated.

Dr. P. Kassenbeck of the Arte Institut Textil de France, Paris, contributed a paper at this session on the fine structure of regenerated cellulose fibres. Unfortunately it has not been possible to obtain a summary of the paper for inclusion here.

In discussion Prof. A. H. Nissan (Textile Industries Department, University of Leeds) asked whether the crossed fibrillar structure of S_1 which had been shown could be due to the fibrils of S_1 crossing those of the middle secondary wall S_2. Mr. Emerton replied that there was no question of this occurring. The crossed fibrils of S_1 were both nearly transverse, whereas those of S_2 were nearly longitudinal. In most cases the S_2 fibrils could be seen in addition to the crossed fibrils of S_1. A discrepancy was pointed out between the results of Dr. Frei and Prof. Preston, who in their mildly treated material obtained fine microfibrils, and Mr. Emerton's observations of gross macrofibrils in commercial, severely treated pulp. Mr. J. Watts (British Paper and Board Research Association, Kenley, Surrey) suggested that the embedding medium kept the microfibrils apart in the former experiments but that in the latter the structure had been compacted by surface tension during drying.

C. E. Challice
J. Sikorski

REFERENCES

(1) Smith, K. C. A. Annual Conference of the Electron Microscopy Group of The Institute of Physics, Glasgow, 1955; see Challice, C. E. *Brit. J. Appl. Phys.*, **7**, p. 89 (1956).

(2) Chapman, J. A., and Menter, J. W. *Proc. Roy. Soc. A*, **226**, p. 400 (1954).

(3) Bradley, D. E. *Brit. J. Appl. Phys.*, **6**, p. 191 (1955).

(4) Ramanathan, N., Sikorski, J., and Woods, H. J. *Biochim. Biophys. Acta*, **18**, p. 323 (1955).

(5) Długosz, J. *Symposium on Fibre Microscopy* (London: The Royal Microscopical Society, 1955).

(6) Harris, P. H., and Honey, I. M. Annual Conference of the Electron Microscopy Group of The Institute of Physics, Glasgow, 1955; see Challice, C. E. *Brit. J. Appl. Phys.*, **7**, p. 89 (1956).

(7) Woods, H. J. *J. Text. Inst. Manchr*, **46**, p. T629 (1955).

(8) Charles, A. O. T., and Sikorski, J. *Brit. J. Appl. Phys.*, **7**, p. 152 (1956).

(9) Lagermalm, G. *Text. Res. J.*, **24**, p. 17 (1954).

(10) Fraser, R. D. B., and Rogers, G. E. *Text. Res. J.*, **25**, p. 235 (1955).

(11) Alexander, P., and Hudson, R. F. *Wool, its chemistry and physics* (London: Chapman and Hall Ltd., 1954).

(12) Keech, M. K., Reed, R., and Wood, M. J. Annual Conference of the Electron Microscopy Group of The Institute of Physics, Glasgow, 1955; see Challice, C. E. *Brit. J. Appl. Phys.*, **7**, p. 89 (1956).

(13) Farrant, J. L., Rees, A. L. G., and Mercer, E. H. *Nature* [*London*], **159**, p. 535 (1947).

(14) Jeffrey, G. M., Sikorski, J., and Woods, H. J. *Text. Res. J.*, **25**, p. 714 (1955).

(15) Bern, H. A., Harkness, D. R., and Blair, S. M. *Proc. Nat. Acad. Sci., U.S.A.*, **41**, p. 55 (1955).

(16) Jeffrey, G. M., Sikorski, J., and Woods, H. J. *Proceedings of the International Wool Textile Research Conference*, Australia, 1955. To be published.

(17) Meggy, A. B., and Sikorski, J. *Nature* [*London*], **177**, p. 326 (1956).

(18) Preston, R. D. *The molecular architecture of plant cell walls* (London: Chapman and Hall Ltd., 1952).

(19) Mukherjee, S. M., Sikorski, J., and Woods, H. J. *Nature* [*London*], **167**, p. 821 (1951); *J. Text. Inst. Manchr*, **43**, p. T196 (1952); Mukherjee, S. M., and Woods, H. J. *Biochim. Biophys. Acta*, **10**, p. 499 (1953).

(20) Hock, C. W. *Text. Res. J.*, **20**, p. 141 (1950).

(21) Morehead, F. F. *Text. Res. J.*, **20**, p. 549 (1950).

(22) Rånby, B. G., and Ribi, E. *Experientia*, **6**, p. 12 (1950).

(23) Rånby, B. G., and Immergut, E. *Industr. Engng Chem.* To be published.

(24) Asunmaa, S. *Svensk Papperstidn.*, **57**, p. 367 (1954).

(25) Rollinson, R. R., and Wise, L. E. *Tappi*, **35**, p. 139*A* (1952).

(26) Dolmetsch, H., Franz, E., and Correns, E. *Kolloid Z.*, **106**, p. 176 (1944).

(27) Emerton, H. W. *Proc. Techn. Sect., Brit. Paper and Board Makers' Assoc.*, **36**, p. 595 (1955).

The determination of linear distortion in nuclear emulsions

By A. J. Apostolakis, B.Sc., and J. V. Major, B.Sc., Department of Physics,
Durham Colleges in the University of Durham

[*Paper first received* 23 *February, and in final form* 23 *May*, 1956]

The ratio of the linear distortion vector to the curvature distortion vector is found to be (2·03 ± 0·03) within the temperature range (for hot-stage development), of 15–24° C. The vectors are found to be in opposite directions. Some consequences of distortion are considered.

INTRODUCTION

During the processing of glass-backed, nuclear emulsions, stresses are set up or released which give rise to movements of the emulsion relative to the glass plate. The displacement of the emulsion varies from zero at the glass-emulsion interface to a maximum value at the free surface and results in the distortion of the emulsion. The horizontal displacement Δ, of a point at height z in a processed emulsion of thickness d, may be represented by the series,

$$\Delta = \bar{K}_1(z/d) + \bar{K}_2(z/d)^2 + \qquad (1)$$

The first term, $\bar{K}_1(z/d)$ represents a linear displacement which is zero at the glass-emulsion interface and has the value $\bar{K}_1$ at the surface. This distortion is called K_1, or linear distortion. The second term, $\bar{K}_2(z/d)^2$, represents the K_2, or curvature distortion. Several methods[1–4] have been described for the measurement of curvature distortion.

THE MEASUREMENT OF LINEAR DISTORTION

Yngve[5] has pointed out that there can be no shear stresses in the emulsion layers at the free surface. This means that the direction of a track at the free surface must be the same as the original direction of the particle and also that the rate of change of distortion approaches zero at the surface. In Fig. 1 the vertical section of an emulsion is represented.

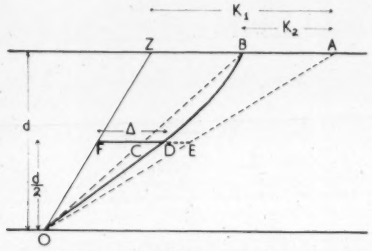

Fig. 1. Vertical section of a processed emulsion showing two types of distortion

Let OZ represent an undistorted track, OA the position of OZ after linear distortion and OB the final observed track after linear and curvature distortion. It is possible to find a relationship between the vectors $\bar{K}_1$ and $\bar{K}_2$.[6] Assuming that higher orders of distortion are negligible then $\bar{K}_1$ and $\bar{K}_2$ are in the same direction and the rate of change of displacement with z is,

$$\frac{d\Delta}{dz} = \frac{\bar{K}_1}{d} + \frac{2\bar{K}_2}{d^2}z$$

This rate of change is zero at the free surface, i.e. $\left(\frac{d\Delta}{dz}\right)_{z=d} = 0$

Therefore $$\bar{K}_1 = -2\bar{K}_2 \qquad (2)$$

In Fig. 1, ZA represents $\bar{K}_1$ and AB represents $\bar{K}_2$. Methods of determining $\bar{K}_2$, thus determine $\bar{K}_1$. Also,[2] if $ZB = \frac{1}{2}ZA$, then at $z = \frac{1}{2}d$, where $CD = DE = \frac{1}{4}\bar{K}_2$, $DF = \frac{3}{4}\bar{K}_2$.

EXPERIMENTAL DETERMINATION OF THE RELATION BETWEEN $\bar{K}_1$ AND $\bar{K}_2$

The relation between $\bar{K}_1$ and $\bar{K}_2$ can be found if the original direction of the track is known. The method adopted to determine the directions of particles in the emulsion was to use two emulsions, one on each side of a thin sheet of glass and to note the points where the particle entered or left the glass (O, O' in Fig. 2). These points remain fixed during processing and their positions can be determined to $\pm 2\,\mu$.

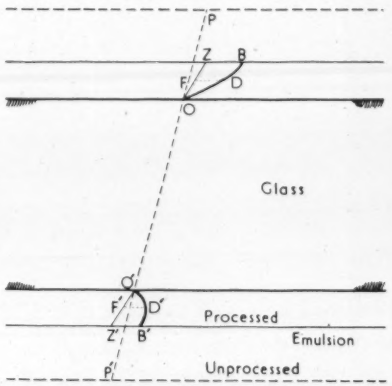

Fig. 2. Schematic drawing of a "sandwich" plate. The original direction of the track PP' is determined by O, O', the points which remained fixed during processing

The sandwich plates were made from glass sheets, about 850 μ thick, with 400 μ thick emulsions on each side. The emulsions were attached by the normal "sticking down" technique. Exposure was made to protons (of average energy 950 MeV), from the Birmingham synchrotron. The processing was by the temperature-cycle method and no attempt was made to keep the distortion small. The density of tracks was small enough to ensure that pairs of tracks were correctly partnered. The thicknesses of the glass sheets

were measured with a micrometer screw gauge. The thicknesses of the unprocessed emulsions were determined in the following way. Long tracks (where the errors due to distortion were relatively small), were traced between pairs of emulsions, whence the ratios of the projected lengths in emulsions and glass were the same as the ratios of the thicknesses of the emulsions and the glass. Knowing the thickness of the glass, the thicknesses of the emulsions were easily found. (This method can also be used to determine the shrinkage factor by measuring the thickness of the processed emulsion directly and the thickness of the unprocessed emulsion as described above.)

The plates were exposed to the proton beam with a small angle of incidence to the plane of the emulsions to obtain short, steep tracks suitable for distortion measurements. A second exposure at a large angle of incidence was made to obtain the longer tracks necessary for the determination of the thicknesses of the unprocessed emulsions.

For each pair of tracks, the xy co-ordinates of ODB and $O'D'B'$ were measured, i.e. the top, mid and bottom points of the tracks in the two processed emulsions (Figs. 2 and 3). From the co-ordinates of the points of contact of the tracks with the glass, i.e. OO' and the thicknesses of the emulsions and glass, the co-ordinates of the positions of the original track, on entering the leaving the sandwich plate, were calculated. These were the points, P, P' which on shrinkage became the points Z, Z'. Similarly the co-ordinates of the midpoints F, F' were calculated. Whence were found,

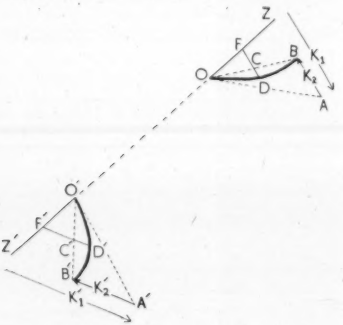

Fig. 3. The distorted tracks as seen through the microscope

$K_1 = 2ZB$, $K_1' = 2Z'B'$ and $K_2 = \frac{4}{3}DF$, $K_2' = \frac{4}{3}D'F'$ where K_1' and K_2' refer to the second emulsion. Fig. 4 shows values of $2ZB$ or $2Z'B'$ against $\frac{4}{3}DF$ or $\frac{4}{3}D'F'$ measured by two observers, for three pairs of plates developed at 15°, 19° and 24° C.

During the measurement of the co-ordinates B to B', the microscope moved vertically through about 1200 μ. Any deviations from the vertical movement would be superimposed on the co-ordinate readings. The vertical motions of the two microscopes used had, however, been calibrated, and each moved linearly at a small inclination to the perpendicular to the plate. This movement introduced only slight errors into the readings.

The mean value obtained experimentally for the ratio $2ZB$ to $\frac{4}{3}DF$ is $(2{\cdot}03 \pm 0{\cdot}03)$. The corresponding mean values for the ratios at the temperatures 15°, 19° and 24° C are $(2{\cdot}06 \pm 0{\cdot}04)$, $(1{\cdot}99 \pm 0{\cdot}06)$ and $(2{\cdot}04 \pm 0{\cdot}03)$. The expected value for this ratio, from Equation 2 is 2·0, in good agreement with the experimental results. Thus the initial assumption is correct that the predominant distortions are first and second order, and that if $\bar{K}_2$ is measured, $\bar{K}_1$ is known.

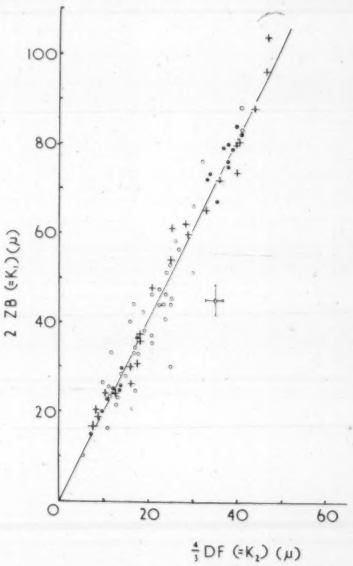

Fig. 4. Graph of the observed values of $2ZB$ against $\frac{4}{3}DF$. The line has been drawn with slope 2·0. Typical errors are shown on one point

+ = 15° C. ○ = 19° C. • = 24° C.

CORRECTIONS FOR DISTORTION

Distortion can produce curvature in a track, and can change the length and orientation of a track.

Following tracks through emulsion strips. Distortion makes the following of a track through emulsion strips difficult because of the change in appearance of the track and its length. It is not necessary to determine the distortion vectors; it is sufficient to note that the tangents to the track at the free surfaces of all the emulsion layers are the same.

Lengths of tracks. An error on the horizontally-projected length of a track is introduced by distortion. For steep tracks the error is K_2 and for tracks at large angles of incidence the r.m.s. error is $K_2/\sqrt{2}$. In the case of a track passing through N emulsions the r.m.s. error on the total horizontally projected length is NK_2 for steep tracks and $K_2\sqrt{\frac{1}{2}N}$ for long tracks. Since the horizontally projected length is combined with the vertical length to give the total length the error is, in general, small even for vertical tracks. In plates of thickness 400 μ a typical value of $\bar{K}_2$, is 20 μ, which results in an increase in length of only 0·5 μ for a vertical track.

Orientation of tracks. A knowledge of the K_1- and K_2-vectors enables a correction to be made to the observed orientation of a track. The correction is important only for steep tracks.

ACKNOWLEDGEMENTS

We should like to thank Professor G. D. Rochester for the facilities provided and Professor P. B. Moon for permission to make an exposure at the synchrotron.

REFERENCES

(1) COSYNS, M., and VANDERHAEGE, G. *Bull. Cent. Phys. Nucléaire Bruxelles* No. 15 (1950).
(2) MAJOR, J. V. *Brit. J. Appl. Phys.*, **3**, p. 309 (1952).
(3) HOPPER, V. D., LIM, Y. K., and WALTERS, M. C. *Austral. J. Phys.*, **7**, p. 288 (1954).
(4) CAULTON, M. *Rev. Sci. Instrum.*, **24**, p. 569 (1953).
(5) YNGVE, V. H. *Phys. Rev.*, **92**, p. 428 (1953).
(6) GOLDSACK, S. J. Private communication.

The X-ray and γ-ray absorption coefficients of a number of glasses

By D. A. RICHARDSON, B.Sc., A.Inst.P., Pilkington Bros. Ltd., St. Helens, Lancashire

[*Paper received* 3 *June*, 1956]

From published data, the X-ray absorption coefficients of a number of glasses have been computed over a wavelength range of 0·01–1·0 Å. The glasses are clear white plate, ceria stabilized plate, 1060 CRT glass, light barium crown 541595, lead plate glass and double extra dense flint glass 927210.

The mass absorption coefficients for most oxides used in glassmaking are plotted as a function of wavelength, and a method of calculating the absorption coefficient of any glass from its composition and this graph is presented.

Lead equivalents for the γ-ray region of some glasses are given as a function of glass density. The glasses considered are ceria stabilized plate; the barium series 541595, 572577, 612585 and 623603; and the lead series 653335, 700303, 748278, 801255, 927210 and lead plate glass. (The numbers given are the type reference numbers given in the catalogue of Chance optical glass.)

The general law governing the absorption of radiation in an homogeneous substance may be expressed as follows:

$$I = I_0 \exp(-\mu t) \qquad \text{(Lambert's law)}$$

i.e. the intensity of the radiation I at any point falls off exponentially from the original intensity I_0 by an amount depending on the absorption coefficient μ of the material and the distance t from the point where the intensity is I_0 to that where it is I. A more fundamental quantity than μ is the mass absorption coefficient W which is equal to μ/ρ, where ρ is the density of the substance. The mass absorption coefficient possesses the useful characteristic of being independent of the physical state of the absorbing matter. Thus, although ice, water and steam would have different values of μ, all would have the same value of W. Further, W is independent of the state of chemical combination since the absorption of X-rays is dependent on the number of atoms and the atomic mass of the chemical elements contained in the absorbing material.

For any substance the mass absorption coefficient of the whole is the summation of the coefficients for the individual elements multiplied by their appropriate weight fraction. Hence, in the case of an oxide RO where R represents the cation, the mass absorption coefficient is given by:

$$W_{RO} = f_R W_R + f_O W_O$$

where f_R and f_O are the respective weight fractions of the cation R and the oxygen O, and W_R and W_O are the respective mass absorption coefficients. The absorption coefficient μ_{RO} of the compound is given by multiplying the resulting mass absorption coefficient W_{RO} by the density of the compound.

The above coefficients must be used at a single wavelength since both W and μ are dependent upon the wavelength of the X-rays and, in general, they increase with increase in wavelength. The variation of the absorption coefficient with wavelength is not a continuous function but contains discontinuities, known as "absorption edges," which occur at shorter wavelengths the greater the atomic number of the element. Fig. 1 shows the variation in mass absorption coefficient of a number of elements of interest to glassmakers, over a wavelength range of 0·01 to 1·0 Å. There barium and lead show absorption edges within this range, whereas

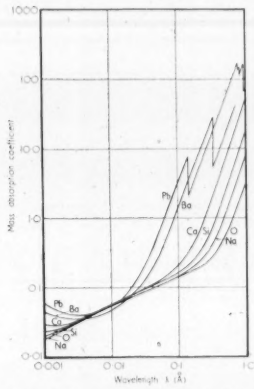

Fig. 1. Mass absorption coefficients of some elements against wavelength

calcium, silicon, sodium and oxygen do not; the first absorption edge (the K absorption edge), for example, for silicon occurs at 6·73 Å.

Victoreen[1,2] has published a method of calculating empirically the mass absorption coefficients of elements 1–96 from short wavelengths to their characteristic K absorption edges. Fig. 1 has been prepared from his data and from

values compiled by S. J. M. Allen[3] for the extension of the barium and lead curves beyond their K edges. Sun and Sun[4] and Brewster[5] have calculated the mass absorption coefficients of a number of oxides from Victoreen's results and their data has been used in producing Fig. 2 which is a graph of mass absorption coefficients of most of the oxides used in glassmaking over the wavelength range of 0·01 to 1·0 Å. The extension for the heavier oxides, beyond their characteristic K edges, has been accomplished by using Allen's data[3] in the case of PbO and data by Henry, Lipson and Wooster[6] for BaO, Sb_2O_3 and Ce_2O_3.

The mass absorption coefficient of a glass (*W* glass) is calculated from the analysis of the glass in terms of weight fractions of the various oxide components and the individual mass absorption coefficients of those oxides as follows:

$$W \text{ glass} = \Sigma(f_{RO}\, W_{RO})$$

where f_{RO} is the weight fraction of the oxide *RO*, W_{RO} is the mass absorption coefficient of the corresponding oxide *RO*, and the summation must cover all the oxides present in the glass.

The absorption coefficient of the glass (μ glass) is then obtained by multiplying the calculated mass absorption coefficient by the density of the glass. This coefficient can be applied, in Lambert's law of absorption, to obtain the intensities on both sides of a sample, or it can be used to obtain the lead equivalent of the glass, which is the thickness of metallic lead equivalent in absorbing power to unit thickness of the glass, i.e.

$$\text{Pb equivalent} = \mu \text{ glass}/\mu_{Pb}$$

where μ_{Pb} is the absorption coefficient of lead.

Two examples of the calculation of the absorption coefficients of glasses are given below. In one case, clear white plate is considered, none of whose components has an absorption edge within the wavelength range chosen, while in the other case, lead plate glass, more than one absorption edge occurs. The examples are given in Tables 1 and 2.

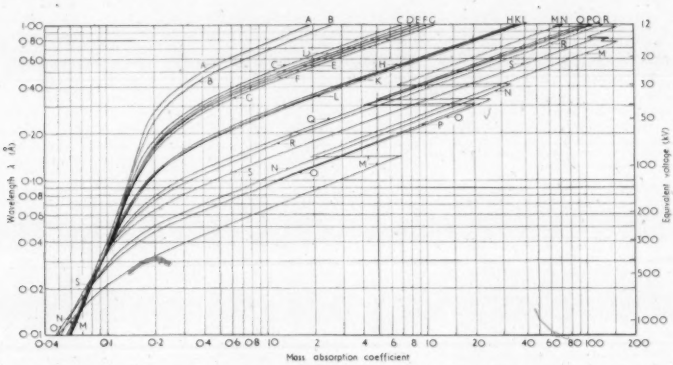

Fig. 2. Mass absorption coefficients of oxides used in glassmaking against wavelength

A, Li_2O; *B*, B_2O_3; *C*, Na_2O; *D*, MgO; *E*, Al_2O_3; *F*, S_iO_2; *G*, P_2O_5; *H*, K_2O; *K*, CaO; *L*, TiO_2; *M*, PbO; *N*, Sb_2O_3; *O*, BaO; *P*, Ce_2O_3; *Q*, ZnO and GeO_2; *R*, As_2O_3; *S*, Rb_2O

In Table 2, the wavelength 0·142 Å is included because the K edge of lead occurs at that wavelength. The two values given for the mass absorption coefficient of PbO at that wavelength are those on both sides of the edge and therefore indicate the discontinuity in the curve. Similarly the K edge for barium appears at 0·33 Å, and another discontinuity occurs. A further absorption edge appears at 0·406 Å for antimony but, because the quantity of Sb_2O_3 is small, the discontinuity is not obtrusive.

Similar computations have been carried out on several other glasses, the compositions of which are given in Table 3, and the results are plotted in Fig. 3. Also included on this graph is the absorption coefficient of metallic lead over the range of wavelengths considered.

Table 1. *Calculation of absorption coefficient of clear white plate*

Wavelength λ =	0·012 Å		0·03 Å		0·06 Å		0·12 Å		0·25 Å		0·6 Å		1·0 Å	
Composition (weight)	W_{RO}	$f_{RO}W_{RO}$	W_{RO}	$f_{RO}W_{RO}$	W_{RO}	$f_{RO}W_{RO}$	W_{RO}	$f_{RO}W_{RO}$	W_{RO}	$f_{RO}W_{RO}$	W_{RO}	$f_{RO}W_{RO}$	W_{RO}	$f_{RO}W_{RO}$
SiO_2 72·7%	0·0624	0·0454	0·0944	0·0686	0·1234	0·0897	0·165	0·1200	0·328	0·238	2·343	1·705	9·942	7·23
Na_2O 13·2%	0·0604	0·0080	0·0913	0·0120	0·1190	0·0157	0·155	0·0205	0·275	0·036	1·687	0·223	7·05	0·931
CaO 9·3%	0·0624	0·0058	0·0952	0·0089	0·1304	0·0121	0·221	0·0206	0·824	0·077	8·809	0·819	37·85	3·52
MgO 3·1%	0·0620	0·0019	0·0937	0·0029	0·1221	0·0038	0·160	0·0050	0·296	0·009	1·920	0·060	8·073	0·25
Al_2O_3 1·2%	0·0613	0·0007	0·0926	0·0011	0·1210	0·0015	0·161	0·0019	0·309	0·004	2·114	0·025	8·937	0·107
W glass		0·0618		0·0935		0·1228		0·1680		0·364		2·832		12·038
Density of glass		2·5		2·5		2·5		2·5		2·5		2·5		2·5
μ glass		0·155		0·234		0·307		0·42		0·91		7·08		30·1

Table 2. *Calculation of absorption coefficient of lead plate glass*

Wavelength λ =		0·012 Å		0·03 Å		0·06 Å		0·12 Å	
Composition (weight)		W_{RO}	$f_{RO}W_{RO}$	W_{RO}	$f_{RO}W_{RO}$	W_{RO}	$f_{RO}W_{RO}$	W_{RO}	$f_{RO}W_{RO}$
SiO_2	32·0%	0·0624	0·0200	0·0944	0·0302	0·1234	0·0395	0·165	0·0528
PbO	45·0%	0·0567	0·0255	0·1719	0·0744	0·7985	0·3595	4·662	2·0979
BaO	14·7%	0·0542	0·0080	0·1094	0·0161	0·338	0·0497	1·876	0·2758
Na_2O	4·0%	0·0604	0·0024	0·0913	0·0036	0·1190	0·0048	0·155	0·0062
Al_2O_3	2·8%	0·0613	0·0017	0·0926	0·0026	0·1210	0·0034	0·161	0·0045
CaO	0·3%	0·0624	0·0002	0·0952	0·0003	0·1304	0·0004	0·221	0·0007
Sb_2O_3	0·7%	0·0555	0·0004	0·1032	0·0007	0·2748	0·0019	1·403	0·0098
W glass			0·0582		0·1279		0·4592		2·4477
Density			4·3		4·3		4·3		4·3
μ glass			0·25		0·55		1·975		10·53

Wavelength λ =		0·142 Å		0·25 Å		0·33 Å		0·6 Å	
Composition (weight)		W_{RO}	$f_{RO}W_{RO}$	W_{RO}	$f_{RO}W_{RO}$	W_{RO}	$f_{RO}W_{RO}$	W_{RO}	$f_{RO}W_{RO}$
SiO_2	32·0%	0·183	0·0585	0·328	0·105	0·55	0·176	2·343	0·750
PbO	45·0%	1·865	0·8385	7·8	3·510	16·3	7·33	80·06	36·0
		6·9	3·105						
BaO	14·7%	3·0	0·4408	13·22	1·944	4·87	0·716	25·59	3·76
						25·13	3·695		
Na_2O	4·0%	0·168	0·0067	0·275	0·011	0·425	0·017	1·687	0·068
Al_2O_3	2·8%	0·175	0·0049	0·309	0·009	0·5	0·015	2·114	0·059
CaO	0·3%	0·277	0·0008	0·824	0·002	1·65	0·005	8·809	0·026
Sb_2O_3	0·7%	2·15	0·0151	10·08	0·071	19·98	0·140	18·5	0·130
W glass			1·365		5·652		8·399		40·793
			3·632				11·378		
Density			4·3		4·3		4·3		4·3
μ glass			5·87		24·3		36·1		175·5
			15·62				49·0		

Using the data for the elements compiled by G. Allen,[7] the mass absorption coefficients of a number of oxides have been calculated for the range of energies 2 to 20 MeV, i.e. wavelengths ranging from 0·006 Å to 0·0006 Å. (It is more usual to classify γ-radiation according to energy rather than wavelength.) These coefficients are given in Table 4 and a selection is plotted in Fig. 4 to show the variation of the mass absorption coefficient with wavelength and molecular weight

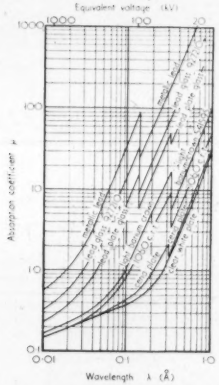

Fig. 3. Absorption coefficients of some commercial glasses against wavelength

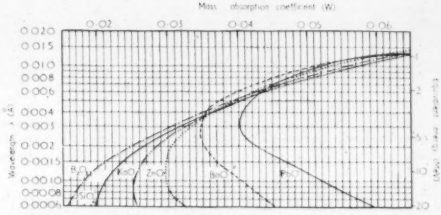

Fig. 4. Mass absorption coefficients of some oxides used in glassmaking against wavelength in the γ-ray region

of the oxides. Table 5 gives for comparison the mass absorption coefficients and absorption coefficients for metallic lead over the same range of energies.

From the values given in Table 4, the absorption coefficients of a number of glasses in the γ-ray region have been calculated. The glasses considered cover a range of densities from that of the ceria stabilized plate glass, with a density

***

Table 3. *Typical percentage compositions of the glasses whose absorption coefficients have been calculated*

Glass number	Clear white plate	Ceria stabilized plate	CRT 1060	Lead plate	Barium series 541595	572577	612585	623603	Lead Series 653335	700303	748278	801255	927210
Oxide													
Li_2O	—	—	0·6	—	—	—	—	—	—	—	—	—	—
B_2O_3	—	—	—	—	2·6	9·7	10·3	15·0	—	—	—	—	—
Na_2O	13·2	13·7	7·0	4·0	2·9	3·3	—	—	1·8	—	—	—	—
MgO	3·1	2·7	—	—	—	—	—	—	—	—	—	—	—
Al_2O_3	1·2	1·8	4·8	2·8	—	0·5	4·6	0·1	—	—	—	—	—
SiO_2	72·7	72·6	67·5	32·0	60·5	46·9	35·2	32·0	40·5	34·8	31·7	27·7	20·2
K_2O	—	—	7·0	—	8·8	4·1	—	—	5·2	5·0	1·9	1·2	—
CaO	9·3	7·5	0·3	0·3	—	—	—	—	—	—	—	—	—
ZnO	—	—	—	—	4·9	10·0	—	—	—	—	—	—	—
As_2O_3	—	—	—	—	0·2	0·6	—	0·4	0·4	0·4	0·2	0·2	—
Sb_2O_3	—	—	0·4	0·7	—	0·5	1·0	—	—	—	—	—	—
BaO	—	—	12·0	14·7	20·0	23·0	48·9	52·5	—	—	—	—	—
Ce_2O_3	—	1·7	—	—	—	—	—	—	—	—	—	—	—
PbO	—	—	—	45·0	—	1·6	—	—	52·5	59·8	66·2	70·9	79·8
Density (g/cm³)	2·5	2·5	2·6	4·3	2·87	3·14	3·56	3·64	3·9	4·33	4·76	5·18	6·11

of 2·5 g/cm³, to that of the special optical glass, double extra dense flint, with a density of 6·11 g/cm.³ The compositions of these glasses are shown in Table 3.

Table 4. *Mass absorption coefficients of some oxides*

Oxide \ Energy	2 MeV	5 MeV	10 MeV	20 MeV
Li_2O	0·0415	0·0252	0·0180	0·0140
B_2O_3	0·0434	0·0266	0·0195	0·0158
Na_2O	0·0432	0·0274	0·0213	0·0186
MgO	0·0443	0·0281	0·0219	0·0192
Al_2O_3	0·0437	0·0278	0·0218	0·0192
SiO_2	0·0446	0·0285	0·0223	0·0198
P_2O_5	0·0441	0·0282	0·0222	0·0197
K_2O	0·0439	0·0298	0·0257	0·0255
CaO	0·0449	0·0304	0·0260	0·0255
ZnO	0·0426	0·0312	0·0296	0·0320
GeO_2	0·0418	0·0302	0·0283	0·0302
As_2O_3	0·0415	0·0307	0·0294	0·0320
Rb_2O	0·0416	0·0319	0·0329	0·0378
Sb_2O_3	0·0410	0·0338	0·0362	0·0412
BaO	0·0404	0·0347	0·0385	0·0449
La_2O_3	0·0404	0·0344	0·0381	0·0441
PbO	0·0441	0·0412	0·0496	0·0586
Bi_2O_3	0·0445	0·0411	0·0490	0·0580

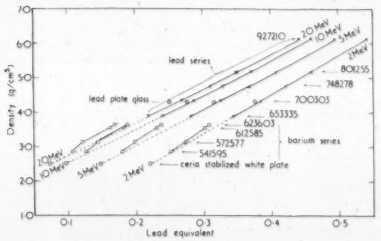

Fig. 5. Lead equivalents of glasses against density in the γ-ray region

The lead equivalents of these glasses have been derived from the absorption coefficients and they are plotted in Fig. 5 against the glass density for the four different conditions of γ-ray equivalent energy. This graph indicates the preponderant effect of density upon absorption for any given wavelength since all the points lie approximately on straight lines. The barium series deviates slightly from the other series, as does the lead plate glass which also contains barium, but they show the comparatively small effect which variations in mass absorption coefficient have as compared with the density effect at these very short wavelengths.

Table 5. *Mass absorption coefficients and absorption coefficients of metallic lead, density 11·3 g/cm³*

	2 MeV	5 MeV	10 MeV	20 MeV
Mass absorption coefficient, W_{Pb}	0·0441	0·0422	0·0518	0·0619
Absorption coefficient, μ_{Pb}	0·498	0·477	0·585	0·700

ACKNOWLEDGEMENTS

The author thanks the Directors of Pilkington Bros. Ltd. for permission to publish this paper and Chance Bros. Ltd. for supplying the compositions of their glasses.

REFERENCES

(1) VICTOREEN, J. A. *J. Appl. Phys.*, **14**, p. 95 (1943).

(2) VICTOREEN, J. A. *J. Appl. Phys.*, **20**, p. 1141 (1949).

(3) ALLEN, S. J. M. *Handbook of Chemistry and Physics*, 34th ed., p. 2235 (Cleveland, Ohio: Chemical Rubber Publishing Co., 1952/53).

(4) SUN, L. L., and SUN, K. H. *Glass Industry*, **29**, pp. 686, 714, 716 (1948).

(5) BREWSTER, G. F. *J. Amer. Ceram. Soc.*, **35**, p. 194 (1952).

(6) HENRY, N. F. M., LIPSON, H., and WOOSTER, W. A. *The Interpretation of X-ray Diffraction Photographs*, Table 3, p. 236 (London: Macmillan and Co. Ltd., 1951).

(7) ALLEN, G. *Handbook of Chemistry and Physics*, p. 2241 (Chemical Rubber Publishing Co., 1952/53).

The flow of gas through composite systems at very low pressures

By C. W. Oatley, M.A., M.Sc., Engineering Laboratory, Cambridge

[*Paper received* 16 *August*, 1956]

It is shown that the conventional method of calculating the flow of gas at very low pressure through composite systems is based on an untenable assumption and leads to incorrect results. An improved method of calculation is given which, though not exact, is unlikely to lead to errors exceeding a few per cent. The physical basis of this method is discussed and its application to various problems of practical importance is considered.

1. Introduction

At very low pressures, where the mean free path of a gas is large compared with the dimensions of the containing vessel and where collisions between molecules can thus be neglected, the precise calculation of the rate of flow of gas through any system presents considerable difficulties. Following the pioneer work of von Smoluchowski and of Knudsen, the flow through circular tubes of finite length was investigated by Clausing[1] who solved this problem subject to certain approximations. Some preliminary calculations made by the present author confirm that Clausing's results can be relied upon to within about 1%.

If a tube connects two vessels A and B where the pressures are p_A and p_B respectively, there will be an interchange of molecules between the two vessels. At the low pressures with which we are now concerned, the flow of gas from A to B will take place quite independently of the flow from B to A, and there will be no loss of generality if we make the latter flow zero by putting $p_B = 0$. This simplification will be made throughout.

Suppose, then, that one end of a tube is connected to a large reservoir of gas at pressure p, while the pressure at the other end is kept negligibly small. If there are n molecules per unit volume in the reservoir and if $\bar{c}$ is their average velocity, the number N entering the tube per second will be given by

$$N = \tfrac{1}{4}n\bar{c}S \tag{1}$$

where $S = \pi r^2$ is the area of cross-section of the tube of radius r. Of these N molecules a fraction αN will pass right through the tube, while the remainder $(1 - \alpha)N$ will, as a result of collisions with the walls of the tube, be returned to the reservoir from which they came. α proves to be a function of L/r only, where L is the length of the tube, and values of α have been tabulated by Clausing.

It follows from equation (1) that the volume of gas, measured at the pressure p in the reservoir, which flows through the tube per second is given by

$$F = \tfrac{1}{4}\bar{c}S\alpha \tag{2}$$

F is independent of p and has the dimensions of vol./s; it is sometimes known as the *conductance* of the tube. For air at room temperature, insertion of numerical values gives

$$F = 11{\cdot}7\,S\alpha \text{ l./s} \tag{3}$$

when S is in cm^2.

2. Two tubes of equal radii in series

Since vacuum systems usually consist of a number of tubes and other components connected together, we need some method of calculating the conductance of a composite system. The method which has generally been used is to work by analogy with electric circuits and to write for tubes in parallel

$$F = F_1 + F_2 + \ldots \tag{4}$$

and for tubes in series

$$\frac{1}{F} = \frac{1}{F_1} + \frac{1}{F_2} + \ldots \tag{5}$$

The validity of equation (4) follows at once from the definition of F and does not call for further comment, but equation (5) is less straightforward.

For the circuit analogy to hold, two conditions must be fulfilled; the rate of flow of gas through a single tube must be proportional to the pressure difference between the ends, and the conductivity of a tube must be independent of the components to which its ends are connected. The first of these is always satisfied while the second, in general, is not. To investigate this point further, we proceed as follows.

From equations (3) and (5), if α_1 and α_2 are the Clausing coefficients for two tubes of the same radius r and of lengths L_1 and L_2 respectively, the coefficient α for a tube of length $L_1 + L_2$ and radius r should be given by

$$\frac{1}{\alpha} = \frac{1}{\alpha_1} + \frac{1}{\alpha_2} \tag{6}$$

The results of calculations of this kind for a number of pairs of tubes are shown in Table 1. The values of α calculated from equation (6), using Clausing's values for α_1 and α_2 are tabulated in column (6) for comparison with Clausing's values in column (5). The percentage differences (column 8) are large and it is to be concluded that equation (6), and therefore equation (5) also, is a very poor approximation to the truth. A better method of calculating α is therefore required.

In Fig. 1, let the two tubes A and B, joined end to end, have coefficients α_1 and α_2 respectively and let N molecules from

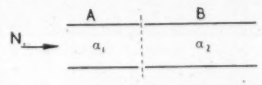

Fig. 1. Two tubes of the same radius

a reservoir enter the left-hand end of A. These molecules have their directions of motion distributed at random when they enter A. We assume, and the assumption will be discussed later, that the molecules which pass from A to B have an equal randomness of direction. Then the behaviour of these molecules within B will be the same as if they had come from a reservoir.

Of the N molecules entering A, $N\alpha_1$ pass into B and $N(1 - \alpha_1)$ are turned back to the reservoir from which they came. Of the $N\alpha_1$ entering B, $N\alpha_1\alpha_2$ emerge from the right-hand end of B while $N\alpha_1(1 - \alpha_2)$ return to A. Of these

$N\alpha_1(1-\alpha_2)(1-\alpha_1)$ enter B once again and $N\alpha_1\alpha_2(1-\alpha_1)(1-\alpha_2)$ emerge from the right-hand end of B. Proceeding in this way, we see that the total number of molecules passing right through the tube from left to right is given by the infinite series

$$N\alpha = N\alpha_1\alpha_2[1+(1-\alpha_1)(1-\alpha_2)+(1-\alpha_1)^2(1-\alpha_2)^2+\ldots]$$

$$= \frac{N\alpha_1\alpha_2}{\alpha_1+\alpha_2-\alpha_1\alpha_2}.$$

Whence

$$\frac{1}{\alpha} = \frac{1}{\alpha_1}+\frac{1}{\alpha_2}-1 \qquad (7)$$

Values of α calculated from equation (7) are recorded in column (7) of Table 1 and the agreement with column (5) is now quite satisfactory. The error, given in column (9), does not exceed 6% for any pair of tubes considered.

Table 1. *Comparison of calculated values of* α

(L_1/r)	(L_2/r)	Values from Clausing's paper α_1	α_2	α	α calculated Eq. (6)	Eq. (7)	Percentage error Eq. (6)	Eq. (7)
(1)	(2)	(3)	(4)	(5)	(6)	(7)	(8)	(9)
0·5	0·5	0·801	0·801	0·672	0·401	0·669	40·3	0·5
1	1	0·672	0·672	0·514	0·336	0·507	34·6	1·4
2	2	0·514	0·514	0·359	0·257	0·346	28·4	3·6
3	3	0·421	0·421	0·281	0·211	0·266	24·9	5·3
4	4	0·359	0·359	0·232	0·180	0·219	22·4	5·6
6	6	0·281	0·281	0·172	0·141	0·164	18·0	4·9
8	8	0·232	0·232	0·137	0·116	0·131	15·3	4·4
10	10	0·197	0·197	0·114	0·099	0·110	13·1	3·5
20	20	0·114	0·114	0·061	0·057	0·060	6·6	1·7
4	1	0·359	0·672	0·315	0·234	0·305	25·7	3·2
4	2	0·359	0·514	0·281	0·211	0·268	24·9	4·6
4	4	0·359	0·359	0·232	0·179	0·219	22·8	5·6
4	6	0·359	0·281	0·197	0·158	0·187	19·8	5·1
4	8	0·359	0·232	0·172	0·141	0·164	18·0	4·6
4	10	0·359	0·197	0·152	0·127	0·146	16·4	4·0
4	16	0·359	0·137	0·114	0·099	0·110	12·7	3·1

3. PHYSICAL CONSIDERATIONS

Although the analogy with an electric circuit is an attractive one, a little thought suffices to show that it rests on very insecure foundations. At higher pressures, where the mean free path is small compared with the dimensions of the apparatus, there is random motion of the molecules: but once a molecule has entered one end of a tube, it will be carried along by the stream and will almost certainly emerge at the other end in due course. In such a case there is a true flow of gas which can properly be compared with the flow of an electric current.

In the present case, however, the motion of each molecule is entirely independent of all the other molecules. Furthermore, in Fig. 1, the fact that a molecule has entered A, or even that it has passed from A to B, gives no certainty that it will ever leave the right-hand end of B. A *flow* of gas, in the usual sense of this word, does not exist.

The real reason for the failure of equation (6) becomes apparent when we consider its derivation in terms of α_1, α_2 and N (Fig. 1). At the left-hand end of A the pressure p is such that N molecules fall per second on this opening, and at the right-hand end of B the pressure is zero. At the junction between the two tubes let the pressure have some intermediate value such that N' molecules fall per second on the right-hand end of A and on the left-hand end of B. Then, from the definitions of α, α_1 and α_2

$$(N-N')\alpha_1 = N'\alpha_2 = N\alpha$$

From these relations equation (6) follows immediately.

The fallacy in this argument lies in the assumption that it is possible to specify a pressure at the junction of the two tubes. If a gas is in a state of equilibrium we can properly speak of its pressure, no matter how low this may be. For a gas which is not in equilibrium, it is still possible to speak of the pressure at a point provided the mean free path is small compared with the dimensions of the containing vessel and any drift velocity of the gas as a whole is small compared with the mean molecular velocity. Under these conditions, inter-molecular collisions will ensure that the molecules in a small volume surrounding the point have a distribution which is very nearly Maxwellian. When, however, the pressure is low and the mean free path is much larger than the dimensions of the containing vessel, the number of molecules crossing the junction from left to right is quite different from the number crossing from right to left. The effective pressure at the junction is therefore a function of direction and has no unique value. Of course, the difference in the numbers of molecules moving in the two directions exists even at high pressures, but it is then an insignificant fraction of the total number of molecules in the vicinity of the junction.

The above line of argument leads to an interesting paradox. Suppose the two tubes A and B in Fig. 1 were separated by a large vessel. If the lateral dimensions of this vessel were great enough it would, according to classical ideas, add no resistance to the flow of gas through the tubes. However, the molecules entering and leaving the vessel *via* the tubes would now have very little effect on the equilibrium of the gas in the vessel and it would be possible to assign a pressure to this gas. Under these circumstances the flow of gas through the whole system should be governed by equation (6) rather than by equation (7). It will be shown in the next section that this result is confirmed by a correct application of equation (7) to the whole system.

While it is obvious that equation (6) is, for most systems, based on a fallacy, it is perhaps less easy to understand why equation (7) leads to results which are a good approximation to the truth. This equation is, after all, based on the assumption that molecules moving in one direction across a junction between two components have their directions of motion distributed at random. In a case such as that of the two tubes in Fig. 1 we feel instinctively that this cannot be true; the molecules leaving A must have been formed into a beam and will therefore enter B with velocities chiefly in a forward direction. This effect is certainly present but the following considerations show that it is unlikely to be very important.

Unless the ratio of length to radius for tube A is relatively large, say greater than 10, we should not expect "beaming" to be very pronounced. Thus the effect will only be important if α_1 is less than about 0·2. Suppose next that tube B is relatively short, so that α_2 is three or four times as great as α_1. Then equation (7) shows that the value of α will depend far more on α_1 than on α_2 and errors in the latter resulting from "beaming" will be less serious than might be expected. These errors will be reduced still further by another effect, now to be considered, which is primarily of importance when α_2 is small but has some influence in other cases also.

From the above arguments it appears that "beaming" will be most serious when both tubes are long in comparison with their radii; i.e. when α_1 and α_2 are both small. Under these circumstances most of the molecules will cross the junction

several times before they emerge from either open end. Thus the molecules crossing from A to B at any time only a small proportion have not previously been in B and it is only this small proportion that we should expect to be formed into a beam by A. That this is so can be seen as follows.

Suppose a long tube PQ to be suspended in a large reservoir of gas at low pressure and consider the conditions at a point T just outside the end Q. In equilibrium, the velocities of the molecules in the vicinity of T must have the same distribution as if the tube had not been there. But, if T is very close to the end of the tube, nearly half of these molecules will have come from the tube and we therefore conclude that the directions of motion of molecules leaving the tube are distributed at random. Of these molecules, some entered the tube through P and these we should expect to be "beamed." With a long tube, however, the majority will have entered through Q and been turned back in due course. Thus the directions of motion of this latter fraction must be such as to balance the tendency towards "beaming" of the molecules which entered *via* P. In the system of Fig. 1, the gas is not in equilibrium so compensation will not be perfect; nevertheless the effects of "beaming" will be much less than they would be if molecules crossed the junction only once.

Summing up, we see that whenever two tubes of equal radii are joined coaxially, "beaming" is unlikely to be serious and it need cause no surprise that equation (7) gives results which are accurate to within about 6% even in the worst case. If two tubes were joined at an angle to each other the effects of "beaming" should be less still.

4. MORE COMPLICATED SYSTEMS

Consider any component of a vacuum system which has two openings of area S_1 and S_2 respectively, and let the corresponding values of α for these openings be α_1 and α_2. If the component were connected to two reservoirs of gas at the same low pressure and the same temperature, the numbers of molecules passing through the component in the two directions would be equal since otherwise the pressure would increase in one reservoir and decrease in the other. Therefore

$$\alpha_1 S_1 = \alpha_2 S_2 \tag{8}$$

We are now in a position to deal with the system shown in Fig. 2(*a*), where a tube of radius r has a flange at one end by means of which it is joined to a second tube of radius R. Suppose the first tube by itself to have a Clausing coefficient α_1 and the second tube (without the flange) a coefficient α_2. Although the determination of α for the complete system by the method of Section 2 is quite straightforward, it is somewhat simpler to re-draw the system as in Fig. 2(*b*) where the two components have been brought to a common radius R by the addition of a second flange and two very short lengths of tube of radius R. If $f = R^2/r^2$ is the ratio of the areas of cross-section of the two tubes, the new coefficient for the first component will be α_1/f. Substitution in equation (7) gives for α_R, the coefficient for the whole system considered as of radius R,

$$\frac{1}{\alpha_R} = \frac{f}{\alpha_1} + \frac{1}{\alpha_2} - 1 \tag{9}$$

Reverting to Fig. 2(*a*) and considering the inlet as of radius r,

$$\frac{1}{\alpha_r} = \frac{1}{\alpha_1} + \frac{1}{f\alpha_2} - \frac{1}{f} \tag{10}$$

Consider next the case discussed in Section 3, where two tubes of the same radius, having coefficients α_1 and α_2 respectively, are separated by a large vessel. We may draw the system as in Fig. 3 where the large vessel is represented

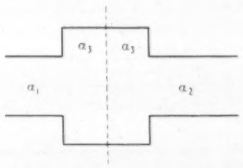

Fig. 3. Two tubes of the same radius separated by a large reservoir

by two equal lengths of tube each having coefficient α_3. With the previous notation, equation (9) shows that the total coefficients for the portions on the two sides of the dotted line are given respectively by

$$\frac{1}{\alpha'_R} = \frac{f}{\alpha_1} + \frac{1}{\alpha_3} - 1$$

and

$$\frac{1}{\alpha''_R} = \frac{f}{\alpha_2} + \frac{1}{\alpha_3} - 1$$

For the whole system, therefore, equation (7) gives

$$\frac{1}{\alpha_R} = \frac{1}{\alpha'_R} + \frac{1}{\alpha''_R} - 1 = \frac{f}{\alpha_1} + \frac{f}{\alpha_2} + \frac{2}{\alpha_3} - 3 \tag{11}$$

If the distance between the two outer tubes is fixed and the radius of the central reservoir tube is made very large, α_3 will tend towards unity and f will become very large compared with unity. Thus equation (11) will become approximately

$$\frac{1}{\alpha_R} = \frac{f}{\alpha_1} + \frac{f}{\alpha_2}$$

or, considering an inlet of radius r,

$$\frac{1}{\alpha_r} = \frac{1}{\alpha_1} + \frac{1}{\alpha_2} \tag{12}$$

in agreement with the result obtained in Section 2.

Another method of deriving this result is instructive. The central reservoir can be regarded as a large vessel with two holes, each of radius r in its walls. If the vessel is large enough, the chance of any molecule entering by one hole and passing straight through the other without first colliding with a wall is negligible. But once a molecule has collided with a wall its direction of motion becomes random and it is as likely to leave by one hole as the other. Thus the coefficient α has the value $\frac{1}{2}$. Applying equation (7) first to

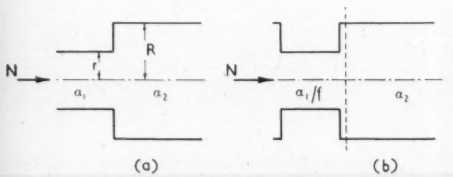

Fig. 2. Two tubes of different radii

the left-hand tube and the reservoir, and then to this combination and the right-hand tube gives

$$\frac{1}{\alpha_r} = \frac{1}{\alpha_1} + \frac{1}{\frac{1}{2}} - 1 + \frac{1}{\alpha_2} - 1 = \frac{1}{\alpha_1} + \frac{1}{\alpha_2}$$

in agreement with equation (12).

As an example of a rather extreme case to which the above methods of calculation can be applied, consider the vapour trap shown in Fig. 4, in which three semi-circular baffles are inserted into a short length of cylindrical tube. The baffles are fixed to an axial rod of small diameter, whose resistance to the flow of gas will be ignored.

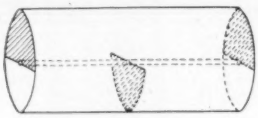

Fig. 4. Vapour trap

Let the Clausing coefficient for each half-length of the tube be α_1 in the absence of all baffles. One might be tempted to think that the result of adding a single semi-circular baffle to one end of such a half-length would be to reduce the coefficient to $\frac{1}{2}\alpha_1$, but this is not the case. Suppose the baffle to be inserted at the end through which molecules enter the system. Of the molecules which fall within the circular perimeter of the tube, one-half will be stopped by the baffle. But of those which are not stopped, some will strike the wall of the tube and be turned back towards the entrance, and of these some will hit the baffle and thus get a second chance of passing through the tube. The overall effect of adding the baffle must thus be calculated from equation (7) putting $\alpha = \frac{1}{2}$ for the baffle. The vapour trap must therefore be taken to consist of five components—two half-tubes and three baffles. Thus, for the whole system,

$$\frac{1}{\alpha} = \left(\frac{1}{\frac{1}{2}} + \frac{1}{\alpha_1} - 1\right) + \left(\frac{1}{\frac{1}{2}} - 1\right) + \left(\frac{1}{\alpha_1} - 1\right) + \left(\frac{1}{\frac{1}{2}} - 1\right)$$

where the first bracket on the right-hand side contains the calculation for the first two components and each succeeding bracket allows for the effect of adding another component. From this equation we get

$$\alpha = \alpha_1/(2\alpha_1 + 2) \qquad (13)$$

Equation (13) should give a reasonable approximation to the truth if the length of the trap is large compared with its radius. For very short traps, however, the gas will not have room to distribute itself uniformly over the cross-section of the tube between one component of the system and the next, and the assumption on which equation (7) is based will not be justified. In particular, as the length of the trap becomes shorter and shorter, α_1 will tend to unity and equation (13) would suggest 0·25 as a limiting value for α. In fact, of course, the baffles would fit together to give a value of zero for α.

In a previous paper[2] the author has shown how experimental measurements of α for such a system can be made, and it is interesting to compare such measurements with calculations from equation (13). For a trap length equal to four times the radius, equation (13) gives 0·169 and the measured value was 0·157, so the agreement is quite good. For a trap length of twice the radius, equation (13) gives 0·20 whereas the measured value was only 0·13*; the theory clearly does not apply satisfactorily to this case.

5. CALCULATIONS INVOLVING DIFFUSION PUMPS

The objections raised in Section 1 to the classical method of calculating the rate of flow of gas through composite systems, apply with equal force to calculations of the effect of a connecting tube on the speed of a pump. The alternative method described in this paper can, however, be applied without difficulty.

A molecule which enters the throat of a pump will have a probability α_1 of passing through the pump and a probability $(1 - \alpha_1)$ of being turned back whence it came. If, therefore, the pump is connected to other apparatus by a system whose overall coefficient is α_2, the probability that a molecule entering the system at the end remote from the pump will eventually pass through the pump, will be given by equation (7). To avoid complication we will assume that the cross-sectional area S cm^2 of the end of the system remote from the pump is equal to that of the throat of the pump, where this is not the case, the calculations must be modified as indicated in Section 4. Then, if F_1 is the speed of the pump in l./s, F is the effective speed at the other end of the system, F_2 is the conductance of the connecting system and we are dealing with air at room temperature,

$$F_1 = 11{\cdot}7\,S\alpha_1$$

$$F_2 = 11{\cdot}7\,S\alpha_2$$

$$F = 11{\cdot}7\,S\alpha$$

so that

$$\frac{1}{F} = \frac{1}{F_1} + \frac{1}{F_2} - \frac{1}{11{\cdot}7S} \qquad (14)$$

An examination of data supplied by manufacturers suggests that α_1 might be about 0·3 for an unbaffled oil diffusion pump. Thus the effective speed calculated from equation (14) may easily differ by as much as 20% from the value calculated by the conventional method. This difference might be particularly important in measurements of the speed of a pump.

6. VALUES OF α FOR TUBES OF NON-CIRCULAR CROSS-SECTION

Only for tubes of circular cross-section do we possess a comprehensive set of values of α; for other shapes we must

Table 2. *Values of α for the annular space between concentric cylinders*

Length / *External radius*	*Ratio of external to internal radius* 3·02	2·4	2·0	1·71	1·5
1	0·59	0·56	0·54	0·51	0·47
2	0·42	0·39	0·37	0·34	0·31
4	0·26	0·24	0·23	0·20	0·18
6	0·19	0·18	0·16	0·15	0·13
8	0·15	0·14	0·13	0·11	0·10
10	0·12	0·11	0·10	0·09	0·08

* In the earlier paper the results were unfortunately given incorrectly. The measured values were those given above and they refer to the whole cross-section of the tube; that is to say, molecules are assumed to fall on the whole circular cross-section of the end, and the effects of the entrance baffle are allowed for in the values of α quoted. If we require α for the open semi-circular aperture of the tube, the above values must be doubled whereas, in the previous paper, they were inadvertently halved.

rely on experimental measurements. If, however, such a measurement has been made for one length of a tube of any particular cross-section, equation (7) can be used to obtain values of α for tubes of the same cross-section of half or double the length measured. The process can then be continued indefinitely to obtain as many new values of α as we require. Nevertheless, since equation (7) is not exact, it would be unwise to carry the extrapolation too far.

In a previous paper[2] the author has described a method by which α for short lengths of tube can be measured and has given values for tubes of rectangular cross-section and for the annular space between concentric cylinders. For rectangular tubes α was found to have nearly the same values as for circular tubes of the same cross-sectional areas and lengths and it is probably as accurate to use these latter values as to attempt to extrapolate the measured results. For concentric cylinders, however, extrapolation is useful and the values given in Table 2 have been derived from the experimental results.

7. REFERENCES

(1) CLAUSING, P. *Ann. Phys.* [*Leipzig*], **12**, p. 961 (1932).
(2) OATLEY, C. W. *Brit. J. Appl. Phys.*, **5**, p. 358 (1954).

An electrical analogue of magnetic domains

By P. F. DAVIS, B.Sc., University of Nottingham

[*Paper first received* 17 *September, and in final form* 12 *October*, 1956]

An electrical analogue which may be used for finding either the magnetic energy or the field associated with a domain structure consists of a square mesh network of resistance wires composed of different gauges of wire running in different directions; the wires having the highest resistance per unit length run in the direction analogous to the direction of magnetization of the domain. (A three-dimensional form might consist of parallel plates of resistive material immersed in an electrolytic tank.)

In 1944 Lifshitz[1] showed that if a small field was applied, for instance to a domain magnetized in the x direction, the relations between field and induction could be written as follows:

$$B_x = H_x + 4\pi I_s$$

$$B_y = \left(1 + 4\pi\frac{I_s^2}{2K}\right)H_y$$

$$B_z = \left(1 + 4\pi\frac{I_s^2}{2K}\right)H_z$$

where I_s is the intrinsic magnetization and K is the anisotropy constant. The effective permeability of the domain in the y and z directions was termed μ^* by Williams, Bozorth and Shockley,[2] in order to distinguish it from the ordinary permeability of the ferromagnetic material; it is given by

$$\mu^* = 1 + \frac{4\pi I_s^2}{2K}$$

The change in the intrinsic magnetization of the domain on applying the field H_x may be neglected, and the increase ΔB_x in B_x in the domain due to H_x is given by

$$\Delta B_x = H_x$$

This corresponds to an incremental permeability of unity in the x direction. The domain may thus be considered to have an incremental permeability with components (1, μ^*, μ^*).

It can be shown that the current and potential gradient in a conducting medium are analogous to the induction and field in a magnetic material, respectively. Let i be the current in the conductor, E the electric field in the conductor, and σ the conductivity of the conductor. The following equations are satisfied by the current and electric field in the conductor,

$$\text{div } i = 0 \qquad \text{curl } E = 0$$
$$i = \sigma E$$

These equations are analogous to Maxwell's equations for a magnetic medium in which no current is flowing,

$$\text{div } B = 0 \qquad \text{curl } H = 0$$
$$B = \mu H$$

But as ordinary conducting materials are isotropic it is necessary to find an analogue to an anisotropic ferromagnetic material. An approximation to a continuous medium may be made in the form of a network of resistance wires, the closeness of the approximation depending on the size of the mesh. An analogue to a domain magnetized in the x direction can be constructed with a square mesh network of resistance wires, in which the ratio of the resistance per unit length of a wire in the x direction ρ_x to the resistance per unit length ρ_y of a wire running in the y direction, is μ^* to 1, i.e.

$$\rho_x/\rho_y = \mu^*/1$$

The magnetic energy of a domain structure may be found by measuring the power dissipated in the electrical analogue of the structure. In some cases it would be possible to find the equilibrium size of a domain if the magnetic energy of the domain were plotted against domain size.

The field in a thick picture frame specimen of iron consisting of four domains, such as is produced when a long straight wire carrying a current passes through the centre of the picture frame, has been found by means of the two-

dimensional wire mesh shown in Fig. 1. To satisfy approximately the boundary conditions a considerable portion of the mesh represents the air surrounding the frame. At a great distance from the picture frame the field would tend to a circular form, and in order to get an approximation to

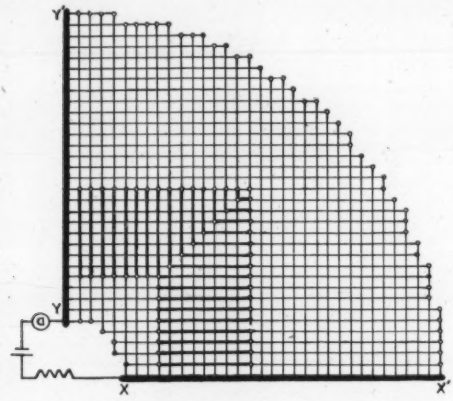

Fig. 1. The electrical analogue of a picture frame specimen in air

the boundary of an infinite volume of air, the analogue was given a circular boundary at some distance from the edge of the portion representing the picture frame. The inner boundary of the region which can be treated by the analogue is the surface of the magnetizing wire. The current density in the analogue increases towards the corner of the analogue, and the inner boundary of the analogue was chosen at a suitable distance from the corner to limit the current to safe values. The field distribution found with the mesh is shown in Fig. 2. The field strength and direction at chosen points are indicated by the length and direction of the arrows, respectively. It is only necessary to represent a quarter of the rectangular picture frame *ABCDEF* because of symmetry. It may be seen that the field decreases almost to zero strength at the corners of the frame. In an actual specimen of iron this effect would be due to a divergence of the intensity of magnetization near the corners of the specimen caused by the rotation of the magnetization vectors of the domains by the field near the internal portions of the corners.

The thin lines in Fig. 1 represent 42 s.w.g. Eureka wires in the mesh, and the thicker lines represent 22 and 32 s.w.g. Eureka wires in parallel. The region representing the air surrounding the analogue was composed of 42 s.w.g. Eureka wires only. XX' and YY' are equipotentials and are made of thick brass strips in the analogue.

If the co-ordinates of the point of intersection of two wires of the lattice are represented by two integers x and y, then the x component of the field at the point (x, y) is found by measuring the potential difference between the intersections $(x-1, y)$ and $(x+1, y)$; and the y component of the field is found by measuring the potential difference between the points $(x, y-1)$ and $(x, y+1)$. The resultant field is found by adding the two components vectorially.

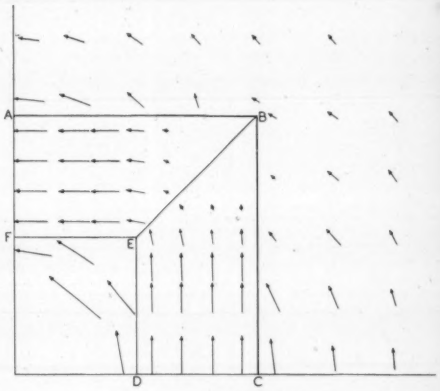

Fig. 2. The field distribution found by means of the electrical analogue

The above two-dimensional analogue was not unduly laborious to construct, but for a three-dimensional problem it might be more practical to use parallel plates of resistive material immersed in an electrolytic tank, orientated with the normals to the plates in the direction analogous to the direction of magnetization. This combination would have a different resistivity perpendicular to the plates from its resistivity parallel to the plates.

ACKNOWLEDGEMENTS

My thanks are due to Prof. L. F. Bates for supervising this work and to Mr. P. M. Griffiths who assisted in the measurements; thanks are also due to Dr. N. Davy for advice on magnetic field problems. I am indebted to the Director of the Electrical and Allied Instruments Research Association for permission to publish the work.

REFERENCES

(1) LIFSHITZ, E. *J. Phys. U.S.S.R.*, **8**, p. 337 (1944).
(2) WILLIAMS, H. J., BOZORTH, R. M., and SHOCKLEY, W. *Phys. Rev.*, **75**, p. 155 (1949).

Summarized proceedings of a conference on the electron microscopy of fibres—Leeds, January 1956

By C. E. CHALLICE and J. SIKORSKI

See pages 1–8

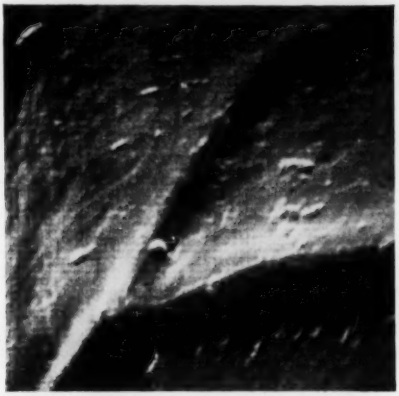

Fig. 1. Wool fibre; scanning electron micrograph. Viewing angle, along the fibre axis, 25°. Horizontal magnification ×11 000

Fig. 2. Nylon filament, after prolonged light abrasion; a composite picture from three reflexion electron micrographs. Angle of viewing 25°. Diameter of filament 15 μ

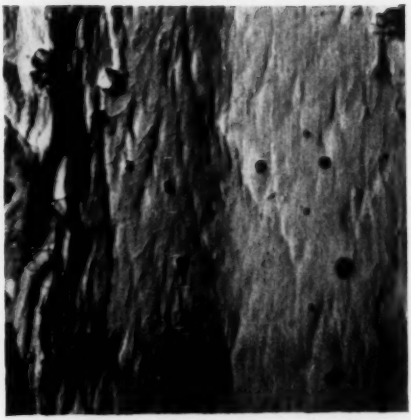

Fig. 3. Fibro filament; direct carbon replica. ×23 500

****

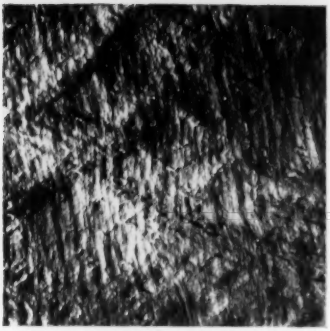

Fig. 4. Nylon monofilament, cold drawn (in glycerine); two-stage Ag/SiO replica. Photographic print from original micrograph. ×3500

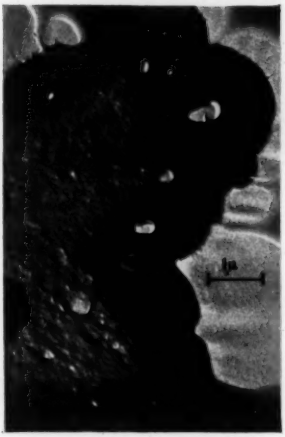

Fig. 5. Viscose rayon filament; part of cross-section. ×10000

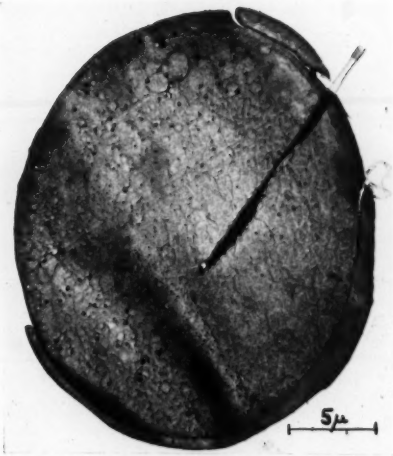

Fig. 6. Australian merino, 64′ s; cross-section. ×3400

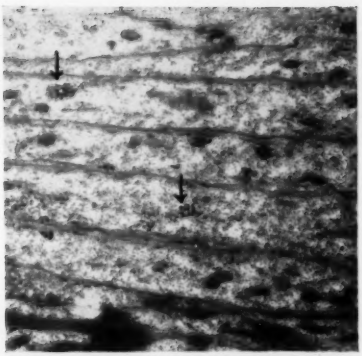

Fig. 7. Human hair cuticle, early stage of development; longitudinal section. Note granules shown by arrows forming in the cytoplasm of individual scale cells. ×20000

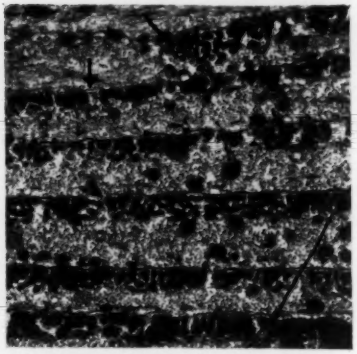

Fig. 8. Cuticle, at a later stage of development than in Fig. 7; longitudinal section. Note exocuticle in each scale cell, the scale tips and epicuticle shown by arrows. ×20000

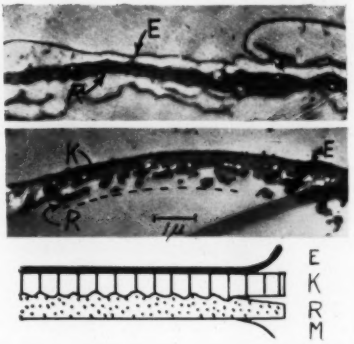

Fig. 10. Cuticle of hair. (*a*) Cross-section, schematic; (*b*) Cuticle cell, after trypsic digestion, cross-section; (*c*) Cuticle cell after oxidation and alkaline extraction; note removal of the exocuticle resistant keratin, *K*. ×8000

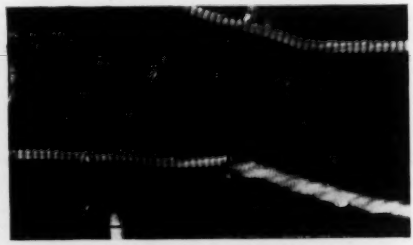

Fig. 9. Collagen fibril, chrome tanned; after heating for one minute at 90° C in water. Note reduced band spacing in the swollen spiral region. ×15000

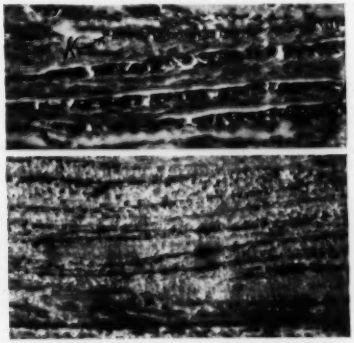

Fig. 11. Cross-sections of two stages of growth of hair cuticle (compare Figs. 7 and 8)

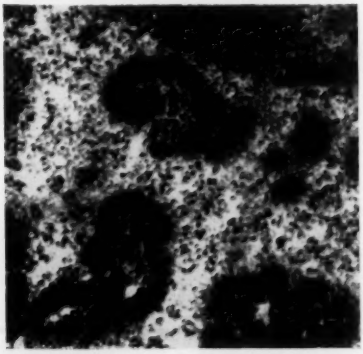

Fig. 12. Human hair follicle, thin section showing the macrofibrils with their component protofibrils. Note the nucleus *n*. ×90000

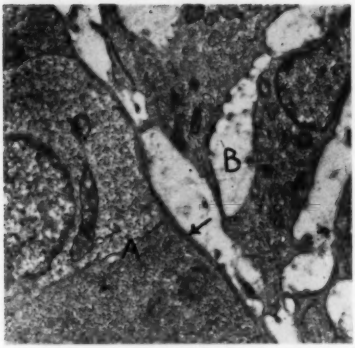

Fig. 13. Hair papilla of a young mouse; longitudinal section. The basement membrane is indicated by arrow, hair matrix *A* and dermal papilla *B*. ×21 500

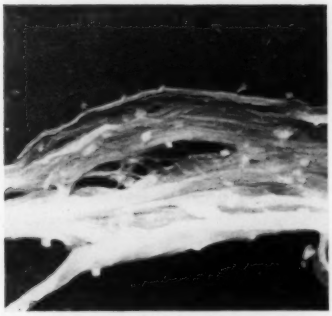

Fig. 14. Lincoln wool, oxidized. ×19 000

Fig. 15. Protein ribbons from the egg-case of the praying mantis. ×8500

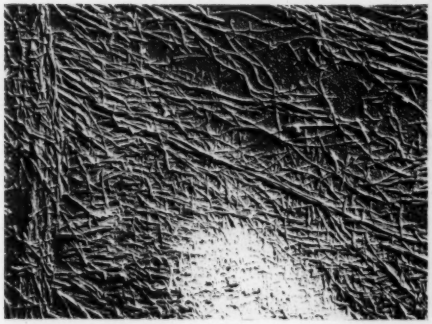

Fig. 16. Conifer wood tracheid, secondary wall; cross-section of the outer layer (flat spiral). ×15 000

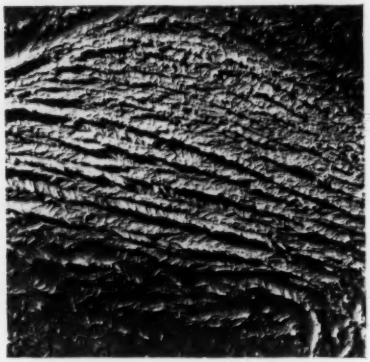

Fig. 17. Conifer wood tracheid, secondary wall; cross-section of the central layer (steep spiral). ×9400

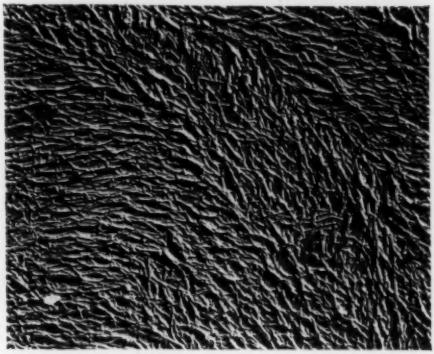

Fig. 18. Conifer wood tracheid, secondary wall; near longitudinal section. Note the change in direction of the microfibrils in neighbouring lamellae. ×16000

Fig. 19. Hydrocellulose from constant boiling point hydrochloric acid. ×25000

Fig. 20. Hydrocellulose from concentrated sulphuric acid. ×25000

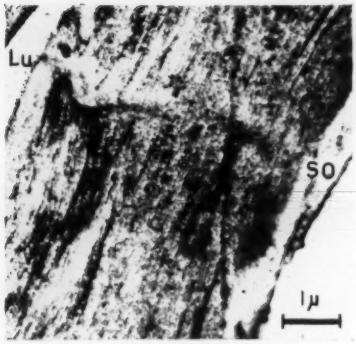

Fig. 21. Holocellulose treated in hot alkali; thin longitudinal section, osmic acid staining. Lu-lumen, S_0-outer secondary wall. ×11 000

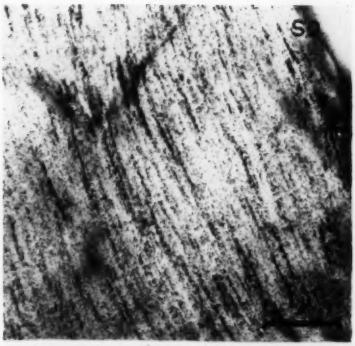

Fig. 22. Holocellulose treated in hot alkali; an ultrathin longitudinal section, osmic acid staining. ×14 000

Figs. 23 and 24. Prominent transverse fibrils of outer secondary wall S_1 of soft wood tracheids; reflexion electron micrographs of sulphite fibres

Fig. 24.

The nature of the emitting surface of barium dispenser cathodes*

By I. Brodie, M.Sc., A.Inst.P., and R. O. Jenkins, A.R.C.S., Ph.D., F.Inst.P., Research Laboratories, The General Electric Co. Ltd., Wembley, Middlesex

[*Paper received* 21 *September*, 1956]

Data concerning the thermionic emission and evaporation characteristics of various barium dispenser cathodes are examined. It is deduced that the tungsten surface of an "L"-type cathode must be covered with a layer of oxygen on which the barium is adsorbed. The thermionic emission from cathodes impregnated with barium aluminate results from a similar layer on the tungsten, the emission from the impregnant at the ends of the pores contributing relatively little. When the impregnant is barium–calcium–aluminate, however, the considerable increase in emission is mainly due to enhancement of the emission from the impregnant and not to an increase in that from the activated tungsten. It is postulated that the emitting surface of the impregnant may be a thin layer of calcium oxide activated by barium.

The various forms of barium dispenser cathode depend for the maintenance of their thermionic emission on the production of free barium. This barium is liberated by chemical reactions taking place either behind or within a porous tungsten body, the outer surface of which forms the emitting area. The continuous supply of barium replaces that evaporating from the surface and thus maintains an active layer which lowers the work function of the tungsten.

The two main forms of dispenser cathode are the "L"-type,[1] in which the barium is produced at the rear face of the tungsten and passes through the pores to the outer emitting face,[2] and the impregnated type,[3–6] in which the pores are filled with barium compounds (usually the aluminates or silicates) which react and form free barium within the body of the cathode, the barium again diffusing to and over the surface. The main difference in the outer surface of these types of cathode is that in the "L"-type it is of activated tungsten only, but in the impregnated type it also contains patches of barium compounds at the pore ends.

Du Pré and Rittner[7] have suggested that the emission from an "L"-type cathode is due to an adsorbed layer of barium and oxygen on tungsten. Adsorbed layers of oxygen always exist on tungsten prepared in the normal way and, owing to the large adsorption energy of oxygen on tungsten, can only be removed quickly by heating to temperatures above 2000° C. On the other hand, Schaefer and White[8] have suggested that the emission comes from barium adsorbed on a clean tungsten surface because the adsorbed oxygen is removed fairly rapidly by the evaporating barium.

In the case of the impregnated cathode, it has been noted that the addition of calcium oxide to the impregnant enhances the emission.[4, 5] The cause of this improvement has not been previously discussed and was the main reason for the inception of this investigation.

THE "L"-TYPE CATHODE

The results of Ryde and Harris,[9] on the thermionic emission from tungsten covered by monolayers of barium and barium and oxygen, show that the emission densities from these two surfaces are not very different at the temperature at which L-cathodes are operated, and the work functions, 1·56 eV and 1·34–1·44 eV, are not sufficiently far apart from emission measurements on L-cathodes to be conclusive in deciding between the two mechanisms, particularly as the coverage of the L-cathode may not be uniform. However, some recent experiments of Moore and Allison[10] on the evaporation of barium monolayers from clean tungsten, together with measurements on the evaporation of barium from L-cathodes by Brodie and Jenkins[2] seem to prove conclusively that the surface cannot be barium on clean tungsten. Moore and Allison's results give the surface coverage of tungsten by barium, plotted against the time of evaporation at 1000 and 1100° K respectively. The evaporation rates of barium at these two temperatures for layers whose surface coverage, in fractions of a monolayer, are 1 and 0·5 respectively, can be derived and are tabulated in Table 1.

Table 1. *Barium evaporation rates*

Temperature (° K)	*Surface coverage* (*fraction of monolayer*)	*Evaporation rate* (*monolayers*/*s*)	*Evaporation rate* (g cm^{-2} s^{-1})
1000	1	$2{\cdot}84 \times 10^{-5}$	$6{\cdot}5 \times 10^{-13}$
1100	1	$1{\cdot}39 \times 10^{-3}$	$3{\cdot}2 \times 10^{-11}$
1000	0·5	$2{\cdot}67 \times 10^{-6}$	$6{\cdot}1 \times 10^{-14}$
1100	0·5	$1{\cdot}31 \times 10^{-4}$	$3{\cdot}0 \times 10^{-12}$

These results have been extrapolated to give evaporation rates from monolayers at the temperatures at which L-cathodes are normally operated by assuming the usual exponential law, $E = A \exp(\phi/kT)$, where E is the evaporation rate, A is a constant, and ϕ is the activation energy for evaporation. The resulting data are shown in Fig. 1, together with some typical measured evaporation rates from L-cathodes. It is seen from Fig. 1 that the amount of barium available, even from the cathode which evaporates more, is inadequate to maintain even half a monolayer of barium on the cathode surface. The thermionic emission from a tungsten surface with a coverage $\theta = 0{\cdot}5$ is about two orders of magnitude[11] below that from a full coverage. Since the emission from an L-cathode is of the same order as that from a full monolayer, it would appear that the emission from an L-cathode cannot be due to barium on clean tungsten. On the other hand, Benjamin and Jenkins,[12] using a field emission electron microscope, have shown that the presence of oxygen considerably increases the temperature required to remove barium from the surface of tungsten. One experiment showed that an appreciable proportion of oxygen adsorbed with the barium increased the temperature required for comparable evaporation rates from 1200° K for a clean surface to 1700° K when oxygen was present. This results in an evaporation plot approximating to the dotted line in Fig. 1. Thus with oxygen present the rate of supply of barium from the L-cathode with the lowest evaporation rate would be quite adequate to maintain a full layer of barium with oxygen. This is confirmed by the fact that under pulse conditions,

* G.E.C. Communication No. 708.

where evaporation is the only significant mechanism for barium removal from the cathode surface, the emission from L-cathodes is not critically dependent on the rate at which barium is being supplied.[13] After the initial activation, both the emission and the evaporation usually remain constant till the supply of barium is exhausted, showing that oxygen must be always present in the layer during the life of the cathode.

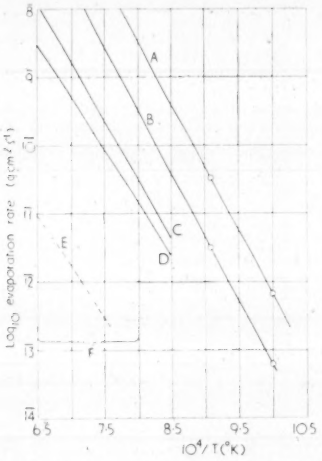

Fig. 1. Evaporation of barium from L-cathodes compared with evaporation from layers on clean tungsten

Curve *A*, evaporation rate to maintain $\theta = 1{\cdot}0$; curve *B*, evaporation rate to maintain $\theta = 0{\cdot}5$; curves *C*, *D* evaporation rates from two typical L-cathodes; curve *E*, approximate evaporation rate to maintain an oxygenated layer; *F*, temperature range over which L-cathodes are used.

○ — Moore and Allison's measurements.

THE IMPREGNATED CATHODE

Two forms of impregnated cathode will be considered, one in which the impregnant consists of barium aluminates only[3,5,6] and the other which contains barium aluminates and calcium oxide.[4,5,6]

In Table 2 pulse emissions for the various forms of cathode are given at two different temperatures. The fraction of the surface occupied by the impregnant has been calculated approximately from the bulk density of the porous tungsten, which differs according to the method of manufacture. It will be seen that even the best reported emissions for impregnated cathodes containing barium aluminates only are inferior to the L-cathode, whilst the best results on the cathode containing calcium oxide show a very significant improvement on the L-cathode.

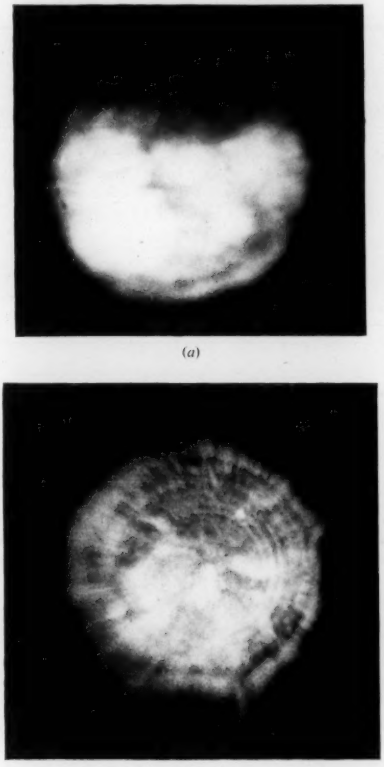

(*a*)

(*b*)

Fig. 2. Cathode images from a partially impregnated cathode. (Barium calcium aluminate)

(*a*) Before activation.
(*b*) After activation and aging.

Table 2. *Pulsed emissions from dispenser cathodes*

Cathode	*Pulse emission at* 1020° C (*A*/cm²)	*Pulse emission at* 1130° C (*A*/cm²)	*Fraction of surface occupied by impregnant*	*Reference*
(1) L-cathode	3·0	10·0	0	1,13
(2) Impregnated cathode pure barium aluminate	1·5–2·3	5·2	0·25	6
(3) Impregnated cathode pure barium aluminate	0·25	1·0	0·45	5
(4) Impregnated cathode barium calcium aluminate	—	10·2	0·25	6
(5) Impregnated cathode barium calcium aluminate	8·0	20·0	0·45	Fig. 2(*b*)

There are two possible mechanisms for the improvement obtained by the addition of calcium oxide. The first concerns the improvement due to a mixed monolayer of barium and calcium on tungsten. This appears to be quite possible as about 10% (molar proportion) of the evaporation products from these cathodes is calcium. Measurements on mixed monolayers of barium and calcium on clean tungsten, which have been reported elsewhere,[14] indicate that a monolayer of which 10% was calcium could account for an improvement of up to 2 : 1 over a monolayer which was barium only. The second possibility is the contribution of the barium compounds at the pore ends. The emission results in Table 1 tend to confirm the second suggestion. If the pure barium aluminate compounds contribute very little to the emission, the effective emitting area is reduced compared with that of an L-cathode. Hence it might be expected that the emission from such impregnated cathodes would decrease as the fraction of surface occupied by the impregnant increased. Cathodes (2) and (3) in Table 2 show that this trend appears to exist. On the other hand, if the emission of the aluminate compounds is considerably enhanced by the calcium oxide, the emission of the impregnant must contribute more to the emission than the surrounding activated tungsten to account for the large improvement in the emission over the L-cathode. In this case improvement would be expected if the fraction of the surface occupied by the impregnant is increased. Cathodes (4) and (5) show this to be true also.

In order to decide whether the presence of calcium in the monolayer was having significant effect on emission, a cathode was made in which an impregnated tungsten disk containing barium calcium aluminate was covered with a plain porous tungsten disk. The fact that the emission from this cathode corresponded to the normal L-cathode value, even after many hundreds of hours aging at a temperature of 1230° C, indicates that the improvement due to mixed monolayer emission is not significant at normal operating temperatures of L-cathodes. Further evidence that the improved emission arises from the pore ends is to be found in Fig. 2. This shows the cathode image of a cathode which has been partially impregnated with barium–calcium aluminates. It will be seen that the part which is not impregnated does emit strongly after aging, but does not reach the emission density from the impregnated part. As final evidence, Fig. 3 compares the d.c. and pulse emission from an impregnated cathode containing calcium oxide and an L-cathode. It will be seen that the pulse and d.c. emissions from the L-cathode are identical at the lower values and only diverge at high values when poisoning due to gas or ion bombardment is taking place, and the same is true for cathodes impregnated with barium aluminate. On the other hand, the pulse emission of the cathode impregnated with barium calcium aluminate is always above that of the d.c. value and this is more typical of semiconductor emission than of monolayer emission.

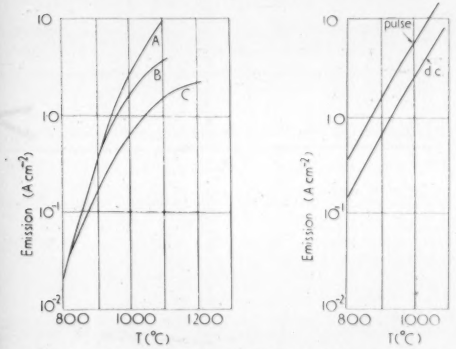

Fig. 3. Direct current and pulse emission from dispenser cathodes

(*a*) L-cathode. Curve *A*, L-cathodes (1) and (2) on pulse; curve *B*, L-cathode (1) on d.c.; curve *C*, L-cathode (2) on d.c. (*b*) Impregnated cathode (3 BaO . Al_2O_3 + ½ Ca . O).

CONCLUSIONS

On the evidence presented here it seems that the emitting surface of an L-cathode must be a monolayer of barium and oxygen on tungsten. At the normal operating temperatures of L-cathodes, oxygen remains permanently in the emitting layer and the barium evaporated from the surface is replaced at a more than adequate rate by the dispensing mechanism.

In the case of the impregnated cathode, the patches of barium compounds at the pore ends can also contribute very significantly to the emission if the impregnant contains calcium oxide, but probably form rather poorly emitting patches if the impregnant does not contain calcium oxide. The reason why the addition of calcium oxide to the barium aluminates causes such a large increase in the contribution of the impregnant is being investigated. It seems possible that during aging a thin film of calcium oxide is left at the end of the pores and is activated by the free barium. The vapour pressure of calcium oxide at the operating temperature is so low that it is unlikely to evaporate subsequently.

ACKNOWLEDGEMENT

The authors wish to thank the Director of Physical Research, Admiralty, for permission to publish this paper.

REFERENCES

(1) LEMMENS, H. J., JANSEN, M. J., and LOOSJES, R. *Phillips Tech. Rev.*, **11**, p. 341 (1950).
(2) BRODIE, I., and JENKINS, R. O. *J. Electronics*, **2**, p. 33 (1956).
(3) LEVI, R. *J. Appl. Phys.*, **24**, p. 223 (1953).
(4) LEVI, R. *J. Appl. Phys.*, **20**, p. 639 (1955).
(5) BRODIE, I., and JENKINS, R. O. *J. Appl. Phys.*, **27**, p. 417 (1956).
(6) COPPOLA, P. P., and HUGHES, R. C. *Proc. Inst. Radio Engrs*, **44**, p. 351 (1956).
(7) DU PRÉ, F. K., and RITTNER, E. S. *Phys. Rev.*, **82**, p. 574 (1951).
(8) SCHAEFER, D. L., and WHITE, J. E. *J. Appl. Phys.*, **23**, p. 669 (1952).
(9) RYDE, J. W., and HARRIS, N. L. Quoted by A. L. REIMANN: *Thermionic Emission* (London: Chapman and Hall, Ltd., 1934).
(10) MOORE, G. G., and ALLISON, H. W. *J. Chem. Phys.*, **23**, p. 1609 (1955).
(11) BECKER, J. A. *Trans Amer. Electrochem. Soc.*, **55**, p. 153 (1929).
(12) BENJAMIN, M., and JENKINS, R. O. *Proc. Roy. Soc. A*, **180**, p. 225 (1942).
(13) BRODIE, I. *Proc. Phys. Soc.* [*London*] *B*, **68**, p. 1146 (1955).
(14) BRODIE, I., and JENKINS, R. O. *Proc. Phys. Soc.* [*London*] *B*. To be published.

A tilting stage method for three-dimensional photoelastic investigations

By H. T. Jessop, M.Sc., A.F.R.Ae.S., F.Inst.P., University College London, W.C.1

[*Paper received 6 September*, 1956]

A method of finding the directions of the principal axes of stress at any point of a "frozen" photoelastic model by the use of a simplified form of universal tilting stage is described. This results in more direct and more accurate measurement of the principal stress-differences at the point.

The most troublesome problem in photoelasticity is that of determining the principal stresses at a point of a three-dimensional model at which no information is directly available as to the directions of the stresses.

In the great majority of cases the critical stresses from the point of view of the failure of a component occur on an unloaded boundary, while the most important internal stresses frequently occur at points lying in a plane of symmetry. In both of these regions the direction of one principal stress is known and it is a comparatively simple matter to find the principal stress differences. There still occur, however, problems in which important stresses occur at a loaded boundary or at internal points where no considerations of symmetry apply.

Even the determination of the principal shear stresses in such cases by direct photoelastic measurements is a long and cumbersome business involving the measurement of three secondary principal stress differences and three isoclinic angles, the calculation from these of the shear-stresses and the normal stress differences referred to three mutually perpendicular axes, and, finally, the solution of a cubic equation.

If, however, one can first determine the directions of the principal stresses at a point, the problem is no more complicated than that of a point in a plane of symmetry.

The separation of the principal stresses, of course, can only be achieved by an integration process, and Frocht's extension to three dimensions of the shear-difference method[1] has to be used for this, whatever the method adopted for finding the stress-differences.

A method of finding the directions of the principal stresses by the use of the von Fedorov type tilting stage has already been described,[2] but this method, besides requiring somewhat expensive apparatus, requires a certain amount of experience for its successful operation. The new method here described requires a tilting stage of much simpler construction, and its operation involves none of the difficulties of the former method. The basis of the new method was suggested by Kammerer,[3] but he did not indicate any means by which it could be employed in practice.

THEORY OF THE METHOD

Let $ABA'B'$, Fig. 1, represent the Fresnel's ellipsoid at the point O at which measurements are required, OA, OB, OC being principal axes. If now the ellipsoid be rotated about any fixed diameter XOX', then the three principal axes will, in turn, be brought into any chosen plane through XOX'. When one principal axis lies in this plane it will, of course, be the principal axis of the section of the ellipsoid by the plane. If then a slice from a frozen stress model is placed in a plane polariscope and rotated about any axis in the plane of the wave-front passing through the chosen point O in the slice, the three principal stress axes at O will be brought in succession into the plane of the wave-front. If this rotation is carried out in short steps one can, at the end of each step, find the directions of the secondary principal axes in the plane by observing the isoclinic fringe through O. These

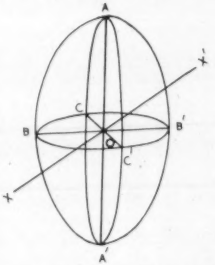

Fig. 1. Fresnel's ellipsoid for point O in a stressed model

axes may be tested in turn to ascertain whether either is a principal axis of the ellipsoid. To test any axis, the effect upon the isoclinic fringe of rotating the slice about that axis is observed. If such rotation leaves the isoclinic still passing through O, the axis is a principal axis.

APPARATUS AND METHOD

Fig. 2 shows a photograph of the tilting stage designed for this method. The central glass platform is provided with spring clips to hold the model in place, with scribed cross-lines indicating the intersection of the rotation axes. This platform is rotatable about the axis XOX' which lies 0·02 in. in front of its surface, and therefore will pass approximately through the mid-plane of any slice of between 0·03 and 0·05 in. thickness. The angle of rotation of the platform about this axis is observed by graduations on the mushroom head. The graduated ring R in which the axis XOX' is mounted rests in a groove in the semi-circular stand S, allowing of rotation about an axis normal to its plane. The stand S itself may be rotated on the base about the vertical axis OV. The upper quadrant Q which carries the index for the graduated circle is hinged to allow the ring R to be removed for adjustments to the model.

In operation the stage stands in a glass tank of immersion fluid (α bromonaphthalene and liquid paraffin) in a plane polariscope, with the plane of the ring R normal to the light beam, and the Polaroids are kept crossed with their vibration axes vertical and horizontal. The model may be viewed through a simple low-powered microscope, or observations may be made on a projected image on a screen.

The sequence of operations is as follows:

(1) Starting with the plane of the platform normal to the incident light, rotate ring R in its own plane until an isoclinic fringe passes through the point O, where the point under investigation coincides with the intersection of the axes.

One of the secondary principal axes in the plane of the wave-front is now vertical. Test this axis by turning the stage about the axis OV.

(2) If the test rotation displaces the isoclinic from O, bring ring R back to its original orientation normal to the light beam and give the platform a small rotation about the axis OX. This will, in general, displace the isoclinic from O.

(3) Rotate ring R in its own plane to bring the isoclinic back to O, and test the new vertical axis as in step (1).

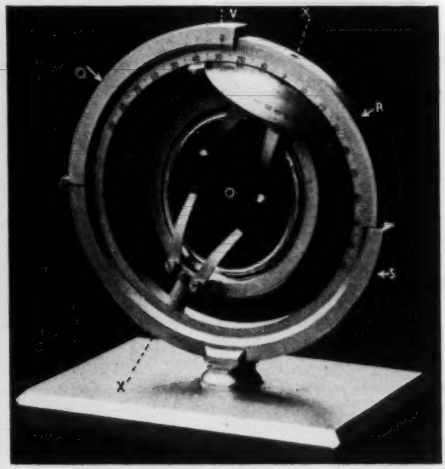

Fig. 2. The tilting stage

Steps (2) and (3) are repeated with progressively increasing tilt of the platform about OX up to about 50°, beyond which the observations usually begin to be unreliable.

The above sequence may now be repeated, but with the rotations of R [steps (1) and (3)] in the opposite direction. This results in the testing of the other secondary principal axes of the same sections of the ellipsoid.

In most cases these tests will result in the identification of two of the principal axes. In the exceptional case in which only one principal axis is found, it will be necessary to re-set the slice on the platform, turning it through 90° from its original position, and to repeat the observations.

In this way the directions of two of the principal axes can generally be found, the exceptions being in cases in which two of the principal stresses are so nearly equal that one principal section of the Fresnel ellipsoid is almost circular. It may be noted that, unlike the von Fedorov method which involves two independent arbitrary small rotations, this method has only one independent variable—the successive small rotations about OX. It is therefore a simple matter to retrace one's steps if the required setting has been overshot, a condition which is revealed by a reversal of the direction of movement of the isoclinic on giving a test rotation about OV.

PLOTTING THE OBSERVATIONS

The directions of the axes are plotted on a stereographic projection with the help of a net which serves as a three-dimensional protractor.[2]

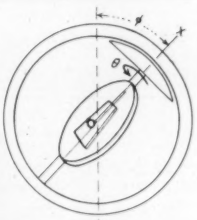

Fig. 3. Diagram of setting of stage which makes one principal axis at O vertical

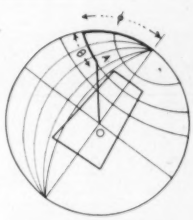

Fig. 4. Stereographic projection showing the principal axis OA obtained from the setting of Fig. 3

If in a setting which makes one principal axis vertical the axis OX is inclined at $\phi°$ to the vertical while the platform has been turned through an angle $\theta°$ as indicated in Fig. 3, the direction of that principal axis relative to the slice is given by OA on the projection (Fig. 4), and may be plotted on a sheet of tracing paper placed on the net. When two such axes are found the traces of the principal planes normal to them may be plotted, and the intersection of these gives the third axis.

If for any reason only one axis can be found by the above method, it is still possible to find the other two. If the axis found is inclined to the normal to the slice at an angle not exceeding about 50°, the slice on its platform may be adjusted so that this principal axis is normal to the plane of the wave-front. Observation of the settings of ring R which then produce an isoclinic fringe through O will give the directions of the other two axes. If the inclination to the normal of the one axis found exceeds the permissible angle of tilt, the only procedure possible is to use a new model and to cut from it a slice more nearly normal to this axis.

MEASURING THE PRINCIPAL STRESS-DIFFERENCES

The ideal way of obtaining the differences of the principal stresses is to measure directly the relative retardations when light passes through the slice normal to each of two principal planes. In practice, however, it may be that these conditions are impossible to achieve with the one slice without exceeding the permissible angle of tilt. If, for example, the three axes were disposed as in the stereographic projection of Fig. 5(*a*), the plane POR could be brought into the plane of the wave-front by a small tilt α and the value of $(\sigma_p - \sigma_r)$ could then be measured directly, but the other two planes would require too great a tilt. In such a case a suitable method would be to tilt in such a way that one axis (say OP) is brought into the plane of the wave-front while the other two are equally inclined to that plane, as in Fig. 5(*b*). The relative retardation with this setting gives the value of $\sigma_p - \frac{1}{2}(\sigma_q + \sigma_r)$, and this

combined with the value of $\sigma_p - \sigma_r$ gives the second stress-difference.

It may be noted that this direct knowledge of the directions and the differences of the principal stresses leads to an equally simple solution for the separate stresses. The shear-difference integration yields the value of the normal stress σs in some direction OS which can be plotted on the projection. By using the stereographic net the angles which OS makes with the principal axes are very simply found, and the relation

$$\sigma_s = l^2\sigma_p + m^2\sigma_q + n^2\sigma_r$$

or $$\sigma_s = l^2(\sigma_p - \sigma_r) + m^2(\sigma_q - \sigma_r) + \sigma_r$$

then leads immediately to the value of σ_r

The method can, of course, be applied even more simply in the determination of free-boundary stresses, in which case it sometimes affords some advantage over the oblique incidence method advanced by Hickson.[4]

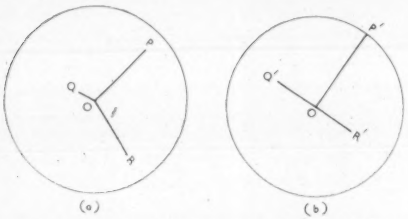

Fig. 5. (*a*) Disposition of principal axes relative to plane of slice. (*b*) Disposition relative to plane of wave-front when slice is tilted for direct measurement of $\sigma_p - \frac{1}{2}(\sigma_q + \sigma_r)$

REFERENCES

(1) Frocht, M. M., and Guernsey, R., Jr. *J. Appl. Mech. Trans A.S.M.E.*, **22**, No. 2 (1955).
(2) Jessop, H. T., and Wells, M. K. *Brit. J. Appl. Phys.*, **1**, p. 184 (1950).
(3) Kammerer, A. *Recherches sur la photoelasticimetrie* (Paris: Hermann et Cie, 1944).
(4) Hickson, V. M. *Brit. J. Appl. Phys.*, **2**, p. 261 (1951).

The triple point of carbon dioxide as a thermometric fixed point

By D. Ambrose, B.Sc., Ph.D., Chemical Research Laboratory, Teddington, Middlesex

[*Paper received* 2 *August*, 1956]

In the technique described, a cell provided with a thermometer pocket was filled with purified carbon dioxide and cooled in a stirred-liquid bath to $-56{\cdot}6^\circ$ C. The three-phase equilibrium was then established and the temperature of a thermometer inserted in the cell remained constant, provided that the temperature of the bath was maintained at $-56{\cdot}6 + 0{\cdot}5^\circ$ C. The value found for the triple-point temperature was $-56{\cdot}603^\circ$ C with a reproducibility of $\pm 0{\cdot}002^\circ$ C.

Over the temperature range -183 to 444° C the International Temperature Scale of 1948[1] is completely defined by a platinum resistance thermometer calibrated at the ice, steam, sulphur and oxygen points, but the use of additional secondary fixed points is a valuable alternative method of defining temperatures, particularly for the calibration of thermocouples in laboratories where no platinum thermometer is available.[2] The use of the sublimation point of carbon dioxide, which would be an obvious choice for such a fixed point in the region between -100 and 0° C, has been discussed[3,4] but it cannot be realized with less uncertainty than $\pm 0{\cdot}01^\circ$, and the triple point ($-56{\cdot}6^\circ$ C) appeared a more promising alternative. Michels, Blaisse and Koens[4] have described an apparatus for the realization of this point within $\pm 0{\cdot}0002^\circ$ C, but it is complicated and inconvenient for general use, and they did not give a value for the temperature. The object, therefore, in the work now described was to make a further determination and produce a simple apparatus which would be more generally available; in achievement of this aim it was found that the triple point could be reproduced to $\pm 0{\cdot}002^\circ$ C in a permanently filled cell when used with a technique similar to that recommended for water triple-point cells.[5]

Maintenance of the three-phase solid-liquid-vapour equilibrium requires good thermal isolation of the system, a condition easily achieved with water by immersing the triple-point cell in a bath of melting ice; heat flux due to the temperature differential of $0{\cdot}01^\circ$ C thus set up is negligible, and the equilibrium with consequent constancy of temperature can be maintained for several days. For carbon dioxide, however, although the maintenance of a constant temperature around -56° C presents no particular difficulties, there is no such simple way of ensuring that that temperature is the correct one. After preliminary experiments carried out in a cryostat of the Scott and Brickwedde type,[6] it appeared that, in fact, for the precision attainable with the thermometer in use there was no need for the temperature of the surroundings to be exactly controlled and a simple stirred bath, maintained manually within $\pm 1^\circ$ C of the triple-point temperature, was adequate.

DESCRIPTION AND FILLING OF CELLS

The vapour pressure of carbon dioxide at the triple point is 3885 mm of mercury,[7] so that any apparatus used for the realization of this equilibrium must withstand a pressure of at least 5 atm. With heavy-walled glass tubing this requirement presents no problem, but a glass cell can only be stored at a temperature in the region of the triple point or below on account of the high pressure developed when the cell warms

up; and a permanently filled, transportable cell must therefore be made of a metal suitable for use at low temperatures. Fig. 1 shows the dimensions of the glass cell in which exploratory experiments were made and of the two stainless steel cells which were filled for permanent storage; the central tubes were approximately $\frac{9}{32}$ in. internal diameter, a close fit on the platinum thermometer.

Commerical solid carbon dioxide, containing traces only of air, water and oil, is of high purity, and was used as the source of the material to fill the cells after it had been dried and sublimed in a vacuum. The filling was done in an apparatus made for the general handling of gases of which

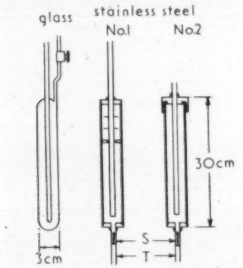

Fig. 1. Design of triple-point cells

the relevant section is shown in Fig. 2. The cells were attached in turn at *A* (a glass-to-copper seal provided with a stopcock was first attached to each of the metal cells) and could be evacuated through *H*. Carbon dioxide was sublimed from flask *B* into trap *D* through the drying tube *C* which was filled with magnesium perchlorate. The tap *G*, beyond which connexions were made with rubber tubing, was shut

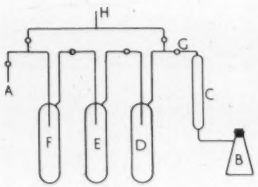

Fig. 2. Filling apparatus

and the gas sublimed into *E* with continuous connexion to the high-vacuum pumps; trap *F* was also kept cold as a guard but despite this there was always a 10–20% loss on the whole process. The carbon dioxide was then transferred by sublimation to the triple-point cell which was given a final evacuation before being closed. The condensing agent used for all operations was liquid nitrogen. The purity of carbon dioxide prepared in this way has been checked by absorbing it in aqueous potassium hydroxide solution; in the test sample less than 1 part in 15000 v/v remained unabsorbed.

The glass cell was closed by means of a polythene diaphragm valve (by Metropolitan Vickers Electrical Co., Ltd.), fixed with Araldite; where a permanent vacuum system exists which can be used whenever required for filling, such a glass cell might be a convenient alternative to metal ones. When carbon dioxide is condensed in a glass vessel with liquid nitrogen, care must be taken to avoid the formation of a solid plug which will shatter the glass through its expansion on warming; the risk of this may be lessened in the filling system by using large traps, but such an accident is especially liable to happen with the triple-point cell because the amount of material required to give an adequate depth of liquid is large for the volume of the cell. The warming process must be allowed to take place slowly, e.g. by inserting the cell into an empty Dewar vessel which has also been cooled with liquid nitrogen. Subsequent freezing of the liquid and cooling to −78° C has caused no trouble.

The stainless-steel cells were designed according to British Standard 1736 : 1951 which specifies a working pressure of 1800 lb/in.^{2} and a filling ratio of 0·75 for containers for carbon dioxide. (The filling ratio is defined as the ratio of the weight of liquefiable gas passed into a container to the water capacity of the container, the water capacity being the weight of water required to fill the container at 15° C.) It works out conveniently that such an amount (80 g) in a cell of the dimensions used gives a liquid depth at the triple point of 18 cm and provides adequate immersion of the thermometer (the same amount was put in the glass cell). Cell 1 (Fig. 1) was provided with the radiation shields and thermal dam shown, as it was intended that the upper end of the cell would emerge above the liquid level in the bath, but in the event the cell was completely immersed and these were omitted from cell 2. Closure of the metal cells was achieved by pinching the copper filling tube *T* (Fig. 1) where it was plugged with the solder *S* which was drilled with a hole $\frac{1}{16}$ in. diameter for evacuating and filling. After the carbon dioxide had been condensed in the cell it was allowed to warm until the pressure reached atmospheric before being detached from the vacuum system, and the excess of carbon dioxide was allowed to blow off until the gross weight corresponded to the correct filling. Permanent closure was effected by nipping the copper tubing and plug in a vice between parallel V-shaped jaws; a satisfactory seal was obtained by three nips, the first two about 8 mm apart to trap the solder, and the last midway between them. Tube *T* beyond the seal was then cut off.

METHOD OF USE

To minimize the effect of any impurities and assist in the maintenance of thermal equilibrium it is desirable to establish the triple point with a minimum of solid carbon dioxide present. This was achieved by the following procedure. One of the metal cells was immersed in a stirred bath of light petroleum contained in a silvered Dewar vessel (100 × 500 mm); the stirrer was a larger version of that used in the cryostat. The temperature of the bath was lowered by the addition of solid carbon dioxide until it was just below the triple-point temperature, previously determined approximately from a melting curve. When the contents of the cell had fallen to the same temperature (measured by means of a copper-constantan couple and potentiometer sensitive to 0·05° C) a sheath of solid carbon dioxide was formed around the thermometer well by the temporary insertion of a brass rod chilled in liquid nitrogen before the platinum resistance thermometer was placed in position; the thermometer well contained a small amount of light petroleum, this is essential for the formation of an even sheath. The bath temperature was then maintained manually by the occasional addition of pieces of solid carbon dioxide. Once it had been found

that the temperature of the resistance thermometer remained constant no particular effort was made to ensure constancy in the bath temperature; generally it was cooled about 0·5 to 1·0° C below the triple-point temperature and allowed to warm to about 0·5° C above it before any further addition of solid carbon dioxide was made. The rate of warming of the bath was 0·05° C/min.

After filling, the glass cell was stored at −78° C and it was therefore necessary to start experiments with this from a temperature below that of the triple point, and to allow the solid to melt before the sheath round the thermometer pocket was formed. This was a tedious process, completion of which would have occupied most of a working day and, in fact, the solid never was completely melted before the formation of the sheath. Observation of this cell showed that one or two insertions of the rod chilled in liquid nitrogen gave a satisfactory sheath together with a crust of solid covering the top of the liquid. No attempt was made to continue with the technique recommended for water triple-point cells,[5] i.e. of freeing the sheath, since solid carbon dioxide is more dense than the liquid and the sheath would sink away from the well, thus nullifying any purification which might be achieved.

For measurement of the cell temperature the platinum resistance thermometer was used in conjunction with a Mueller bridge (by Leeds and Northrup). The reading obtained for the triple point of water was regularly checked.

RESULTS

At intervals during six months, eight determinations were made with the metal cells, in five of which readings were taken over periods of one hour, and in the remaining three of half an hour. There was never a change of more than 0·001° C during any series of readings and a range of 0·002° C covered all the determinations, but slightly higher and more erratic results, for which no reason was apparent, were obtained with the glass cell. With these included, all the values obtained fell within a range of 0·005° C, giving a mean of −56·603° C with a reproducibility of ±0·002° C which may be compared with the value −56·602 ± 0·005° C given by Meyers and van Dusen.[7]

There appeared to be no reason why the constancy of temperature should not have been maintained indefinitely if the temperature of the bath had been controlled automatically.

DISCUSSION

Given adequate immersion of the thermometer the temperatures obtained in these cells will depend on (1) the extent to which the equilibrium is disturbed by heat flux, (2) the pressure in the cells, and (3) the purity of the carbon dioxide.

(1) In dynamic melting-point experiments, in which the bath was allowed to warm up at its natural rate, the triple-point temperature could not be defined within 0·25° C, but the effect of any heat flux in the procedure described above may be ignored since there was no change in the resistance of the platinum thermometer, provided the temperature of the bath was within the limits stated on either side of the triple-point value.

(2) Triple-point conditions are actually only established in the region at the surface of the liquid where all three phases are present, and the temperature of the solid-liquid interface at the bottom of the thermometer pocket where measurements are made will be affected by the pressure prevailing at this point. The melting temperature of carbon dioxide is raised by 1° C for an increase in pressure of 50 atm[8] and the depth of liquid carbon dioxide (about 15 cm ≃ 13 mm of mercury) therefore corresponds to a rise of 0·0003° C. In addition, superheating of the top layer of liquid by radiation if the cell were not completely immersed would raise the total pressure in the cell with a consequent rise in the measured temperature. The vapour pressure of carbon dioxide in this region changes by 175 mm of mercury per ° C and a rise of 0·2° C in the top layer of liquid would thus lead to a rise of 0·001° C in the apparent triple-point temperature.

At first an explanation was sought along these lines for the higher result obtained with the glass cell, but the presence throughout the experiments of the crust of solid over the surface of the liquid rendered it improbable. The effect of radiation on cell 2 was studied by lifting it so that the upper 10 cm were above the level of the liquid in the bath; a rise of less than 0·002° C was detectable and the temperature fell to its original value when the cell was again immersed.

These factors do not seem to be of importance for the present measurements but would require consideration if a higher accuracy were sought.

(3) The melting point is lowered by the presence of soluble impurity but it appears improbable that liquid carbon dioxide exerts much solvent power at such a low temperature for anything which might be present. Cell 2 was, in fact, designed with a screw cap closure (sealing on a copper washer) so that it might be cleaned before filling to ensure that the difference between the glass and metal cells was not due to contamination, e.g. by the flux for the Easiflo solder used in assembly.

ACKNOWLEDGEMENTS

I wish to acknowledge the benefit of discussions with Mr. C. R. Barber of the National Physical Laboratory and thank colleagues of the Chemical Research Laboratory for the construction of the cells. The two metal cells may be borrowed and applications for their loan should be addressed to the Director, Chemical Research Laboratory, Teddington, by whose permission this paper is published.

REFERENCES

(1) National Physical Laboratory, *The International Temperature Scale of 1948* (London: H.M. Stationery Office, 1950).

(2) Smit, W. M. *Chem. Weekbl.*, **51**, pp. 319, 772, 901 (1955): **52**, p. 360 (1956).

(3) Scott, R. B. *Temperature* (American Institute of Physics), p. 206 (New York: Reinhold Publishing Corp., 1941).

(4) Michels, A., Blaisse, B., and Koens, G. *Physica*, **9**, p. 356 (1942).

(5) Barber, C. R., Handley, R., and Herington, E. F. G. *Brit. J. Appl. Phys.*, **5**, p. 41 (1954).

(6) Scott, R. B., and Brickwedde, F. G. *J. Res. Nat. Bur. Stand.*, **6**, p. 401 (1931).

(7) Meyers, C. H., and van Dusen, M. S. *J. Res. Nat. Bur. Stand.*, **10**, p. 381 (1933).

(8) Quinn, E. L., and Jones, C. L. *Carbon Dioxide* (American Chemical Society Monograph), p. 60 (New York: Reinhold Publishing Corp., 1936).

The measurement of the thickness of thin carbon films

By A. W. AGAR, B.Sc., A.Inst.P., Associated Electrical Industries Ltd., Aldermaston, Berks

[*Paper received* 30 *August*, 1956]

A nearly linear relationship has been found to exist between the optical density and the thickness of evaporated carbon films. The determination of film thickness by density measurements is shown to have a number of advantages over measurement by interferometry, particularly for very thin films.

Evaporated carbon films prepared by the method of Bradley[1] are now widely used in electron microscopy. For the purpose of some work in progress in this Laboratory, it was necessary to know the thickness of the films used, to an accuracy of 10% or better.

The standard method for measuring the thickness of thin films developed by Tolansky[2] involves the production of a sharp, straight edge to the film, the coating of the surface with evaporated silver, the preparation of a reference flat with the correct thickness of silver, the correct alinement of the illuminating system, and, for very thin films, the photography of the fringe system, if reasonably accurate results are to be obtained. This procedure is far too lengthy for use in routine work. The measurements are somewhat easier with a shearing interferometer such as the one designed by Dyson.[3] This requires no accurately silvered reference flat and no photographic recording is involved. However, the film must still have an abrupt edge (not necessarily straight), and must be silvered before it can be measured.

As has been pointed out by Bradley, even very thin carbon films are readily visible, and a rough test of suitable thickness is given by watching the coloration of a porcelain indicator during the evaporation process. These properties suggested that the light absorption of the films might be utilized to measure their thickness. A convenient apparatus for doing this is a densitometer as used for measurement of photographic plate densities.

EXPERIMENTAL METHOD

Carbon films of differing thickness were evaporated on to clean microscope slides. Part of each film was removed by flotation or with cellulose tape. The slides were then placed on the table of a densitometer as shown schematically in Fig. 1. The defining aperture used was 1 cm diameter, and this was also the area of film illuminated. (For some of the readings, the spot size was reduced by an optical system, shown dotted, to 1 mm diameter.) The light was first passed through the clear part of the glass slide and fell on to a photomultiplier (Mazda type 27M1) the output of which was measured on a sensitive microammeter. The slide was then moved so that the light passed through the carbon film, and the new output of the photomultiplier measured. (This value was taken as the mean of about six readings from a region of the film close to the edge where it was later to be measured interferometrically.)

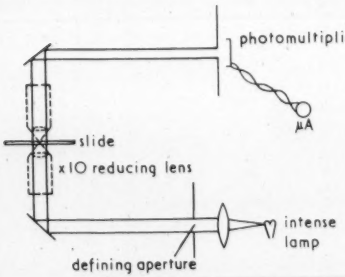

Fig. 1. Schematic diagram of densitometer

The slides were then coated with evaporated silver, and the thickness of the carbon films measured by Tolansky's method and (for the thinner films) by Dyson's shearing interferometer microscope.

RESULTS

If the output of the photomultiplier for light reaching it through the glass of a microscope slide be I_{glass} and for light coming through glass and carbon film be I_{film}, the optical density D of the carbon film is:

$$D = \log_{10}(I_{glass}/I_{film})$$

If, for each carbon film, D be plotted against the measured thickness d, the graph of Fig. 2 is obtained, showing a nearly linear relationship between them. In over fifty films measured, over a period of months, the measured thickness has, with only two or three exceptions, fallen within $\pm 10\%$ of the

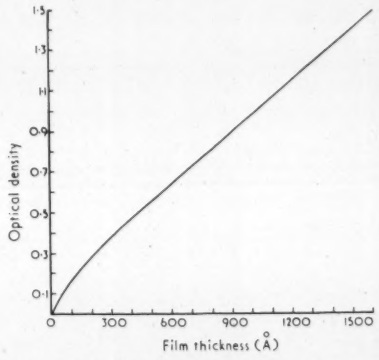

Fig. 2. Relationship of carbon film thickness with optical density

value predicted by this curve. The greater errors are apparent in the measurement of one or two of the very thin films, and this error quite probably resides mainly in the interferometer measurements which are very difficult at these thicknesses. Most of the results have been much more accurate; the standard deviation of results from those predicted from the curve is only 2%.

DISCUSSION

A number of factors which might influence the accuracy of the results were investigated.

(1) *Illuminated area.* This should be kept large in comparison with possible blemishes of the film or glass, scratches, dust particles, etc., which could affect significantly the light transmitted. However, a reduction in illuminated area from a spot of 1 cm diameter to one of 50 μ diameter did not impair the accuracy of the method. An even smaller spot size could be used if a number of readings were taken to expose errors due to blemishes such as those mentioned above.

(2) *Working range of photomultiplier.* The photomultiplier used had a maximum rated output of 1 mA. When tested with a range of neutral density filters using this output for I_{glass}, the response was found to be non-linear. No attempt was made to determine the upper limit of output which could be used, but the response was found to be accurate for outputs below 500 μA. It is inconvenient to use very small currents because of the need to use a sensitive meter, and in these experiments, a maximum output of 250 μA (for I_{glass}) was used, corresponding to the full-scale deflexion of the microammeter. Small adjustments were made to the high tension applied to the photomultiplier to obtain this output for each glass slide examined. (As the measurement on each film is only comparative, and is carried out within seconds of the reference measurement of transmission through the glass on which it is mounted, it is only necessary to keep within the wide operating range quoted above to maintain the desired accuracy.)

(3) *Photomultiplier response to colour.* For a given light intensity, the photomultiplier response varies rather quickly with the wavelength of the light used.

Hence, a differential wavelength absorption by the carbon film could lead to irregularities in the curve if a white-light source were used. However, a comparison with the results obtained with monochromatic (mercury green) illumination showed no difference in the form of the curve, though the optical densities of the carbon films were about 8% higher when measured with white rather than the monochromatic illumination. This indicates that evaporated carbon films are not far removed from being neutral density filters. They appear slightly yellow-brown in comparison with such filters.

The effect of voltage variations on the colour of the white-light source was also investigated. A 25% reduction in voltage caused only a 5% change in the value of optical density measured for a given film, and the effect would be insignificant for normal voltage variations.

It would clearly be desirable, if higher accuracy were sought from the measurements, to use monochromatic illumination.

(4) *Range of thickness measurable.* Since the density scale is logarithmic, the current measurements are most sensitive for very low optical densities, which is the region where they are most valuable. A film only 20 Å thick gives an easily measurable response (about 230 μA output, compared with 250 μA through the clear glass). The photomultiplier response becomes rather insensitive for film thicknesses greater than about 1 500 Å, but, in any case, these are seldom used and can without difficulty be measured by other methods.

CONCLUSIONS

The measurement of carbon film thicknesses by this method offers several advantages over the conventional methods. It is extremely simple, as no silvering of the film is necessary, and the film can be measured at any point, not merely at a prepared edge as with interferometric methods. It can be used to survey the thickness variations over a considerable area of film with great ease. Conversely, a thickness measurement from a tiny fragment of film can be obtained if a small illuminating spot is used. It is also valuable in that it is non-destructive and the film can be used after the measurement has been made. It is most sensitive in measuring very thin films, and these can be measured only with difficulty by other methods.

If the light transmitted through the clear glass is arranged to give a standard output from the photomultiplier, then the current readings for transmission through the carbon can be calibrated to give the thickness measurement directly, without calculation of the optical density.

A simple densitometer could easily be arranged with the mirror system in the vacuum of an evaporation plant. This would enable the density of a carbon film to be measured as the evaporation was proceeding, and thus control the thickness deposited.

Preliminary tests indicate that this method for measuring thickness might be applied to other thin evaporated films which show some optical absorption. The relationship between optical density and thickness appears to be roughly linear, the slope of the line varying with the material used.

ACKNOWLEDGEMENTS

The author wishes to acknowledge the help of Mr. G. Rickards in the experimental work, and the valuable criticisms of Mr. T. Mulvey and to thank Dr. T. E. Allibone for permission to publish this paper.

REFERENCES

(1) BRADLEY, D. E. *Brit. J. Appl. Phys.*, **5**, p. 65 (1954).
(2) TOLANSKY, S. *Multiple Beam Interferometry of Surfaces and Films* (Oxford: Clarendon Press, 1948).
(3) DYSON, J. Private communication.

The breakdown mechanism of certain triggered spark gaps

By T. E. Broadbent, M.Sc., Ph.D.,* Electrical Engineering Department, University of Manchester

[*Paper first received* 28 *May, and in final form,* 25 *July,* 1956]

Experiments designed to investigate the breakdown mechanism of certain triggered spark gaps in air are described. Possible theories of the breakdown mechanism of the trigatron and the thermally triggered spark gap are put forward, based on experimental voltage and time lag to breakdown characteristics, corona measurements, and on optical studies using a photomultiplier. It is shown that the mechanism of breakdown for the two forms of triggered spark gap may be similar and depend, with positive charging polarities, on the movement of positive ions followed by a streamer process, and, in the case of negative charging polarities, on a streamer process only.

The breakdown of a spark gap may be initiated by the passage of a spark between one of the electrodes and an auxiliary electrode which projects into a small hole in the sparking surface of the main electrode. The breakdown voltage of the main gap is thereby considerably reduced. The arrangement is called a trigatron[1] gap and although it is used extensively in high-voltage equipment there appears to be little known about its mode of operation. During a recent investigation[2] it was observed that the presence of a hot wire near the surface of one electrode of a spark gap reduced considerably the breakdown voltage and in many ways the operation of this "thermally triggered" gap resembled that of the trigatron. In this paper an investigation is described of the performance of both types of triggered gap and a theory is proposed of their behaviour.

EXPERIMENTAL METHODS

Both types of gap were investigated by the following methods:

(*a*) Measurements of the change in breakdown voltage caused by triggering action, for both polarities of the main electrode.

(*b*) Time lag measurements, as described later.

Voltage was measured to within $\pm 2\%$, and time to within 0·05 μs using a cathode-ray oscillograph of a type previously described.[3] Triggering pulses for the trigatron gap had a rise time of 0·1 μs and a tail of 14 000 μs. Besides these conventional measurements the development of luminosity in the spark gaps was investigated, using a photomultiplier in the manner described by Meek and Craggs.[4] Gap current during the initiation process was also measured. All experiments were carried out in air at atmospheric pressure using 15 cm diameter spheres as the electrodes of the main gap. The separation of the spheres was varied between 2 and 12 cm. The diameter of the hole in the sparking surface of each type of gap was 0·8 cm and in the trigatron the diameter of the trigger rod was 0·25 cm. The end of the rod was level with the sparking surface. The term "direct breakdown voltage" is used to denote the breakdown voltage of a gap when the triggering mechanism is not in operation.

RESULTS WITH THE TRIGATRON

At the outset it seemed that the lowering in breakdown voltage (amounting to up to 50%) might be due to distortion of field in the main gap caused by the trigger voltage, or to irradiation of the main gap by the light emitted from the spark passing from the trigger to one of the main electrodes. If the first mechanism is operative it is to be expected that:

(*a*) Lowering in breakdown voltage of the main gap depends on the voltage applied to the trigger electrode.

(*b*) Breakdown of the main gap must precede breakdown of the trigger gap.

(*c*) It should not be necessary to break down the trigger gap provided field distortion is present.

These points were investigated with the following results:

(i) The voltage lowering was only slightly dependent on trigger pulse amplitude. It was almost entirely dependent on the gap length and the polarity of the high-voltage electrode.

(ii) Except at gap voltages within about 4% of the direct breakdown voltage, a spark always occurred in the trigger gap, due to the trigger pulse, before the main gap broke down.

(iii) Field distortion without a trigger spark (using a reduced trigger voltage) would not initiate breakdown in the main gap.

The above experiments eliminate field distortion (from the trigger voltage) as a possible breakdown mechanism and support the view that irradiation from the trigger spark is the important factor.

Voltage measurements. Typical curves showing the voltage lowering as a percentage of the direct breakdown voltage are given in Fig. 1. These show that a greater percentage

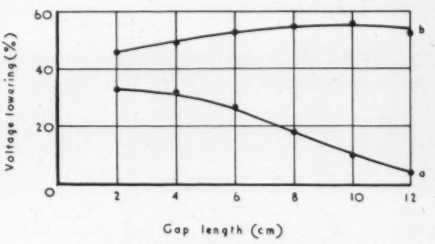

Fig. 1. Gap length-voltage lowering curves for the trigatron. 9 kV trigger pulse

(*a*) High-voltage electrode positive.
(*b*) High-voltage electrode negative.

voltage lowering is obtained with a negative than with a positive high-voltage electrode, and that this lowering decreases with increasing gap length only when the high-voltage electrode is positive.

Time lag measurements. A typical time lag oscillogram is shown in Fig. 2. During measurements the time delay between the application of a voltage pulse to the trigger gap and the breakdown of this gap was made less than 0·1 μs. It was arranged to be as long as 2 μs in the oscillogram solely for the purpose of illustration. The time lag between the application of the trigger pulse and breakdown of the main gap

* Now at Ferranti Ltd., Wythenshawe, Manchester.

was dependent on the main gap length and on the polarity of the high-voltage electrode. With this electrode negative the time lags were random, with large scatter. At given voltages the scatter in time lag was as great as 100 : 1 over a range of gap lengths from 2–12 cm. The arithmetic mean time lag decreased with increasing voltage at constant gap length.

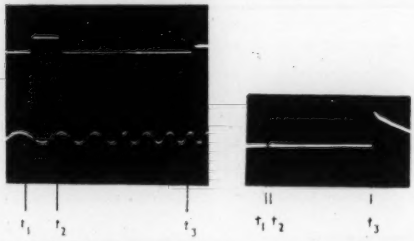

Fig. 2. Time lag oscillogram for the trigatron
t_1 = rise of voltage on trigger gap.
t_2 = collapse of voltage on trigger gap.
t_3 = collapse of voltage on main gap.
200 kc/s calibration trace also shown.

Fig. 4. Oscillogram of corona pulse and main discharge in the trigatron
t_1t_2 = corona pulse.
t_3 = main discharge.
t_1t_2 = 0·05 μs (approx.).
t_2t_3 = 20 μs.

With the high-voltage electrode positive, long regular time lags of the order of tens of microseconds were observed. The time lags decreased with increasing voltage but, at any given voltage, the scatter from maximum to minimum time lag was less than about 2·5 : 1.[5] A typical time lag distribution diagram is shown in Fig. 3, where the arithmetic mean time lag and the time at peak distribution are both 16 μs.

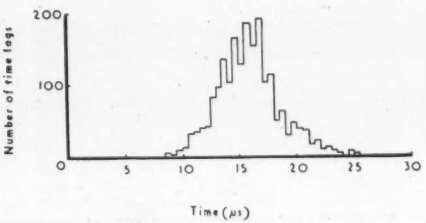

Fig. 3. Time lag distribution diagram for the trigatron. Positive charging voltage

6 cm main gap. 2000 time lag measurements. Gap voltage = 133·7 kV = 90·5% of the direct breakdown voltage.

From the regularity in time lags it seemed that these lags were formative rather than statistical. Calculations showed that, in general, the time required for a positive ion to cross about 10–40% of the gap was approximately the same as the experimentally observed time lag at a given voltage and gap length.

Measurements were carried out with steep-fronted long-tailed impulse voltages applied to the main electrode of the trigatron, instead of having the normal direct voltage on this electrode. This was done to determine whether the absence of approach voltage[6] had any effect on the time lag to breakdown. The trigger pulse and high-voltage impulse were applied simultaneously. With positive impulses long time lags with small scatter occurred. The time lags were the same as those obtained using direct voltages. When negative impulse voltages were applied to the main electrode, with the trigger spark in operation, time lags were random and mostly short, as in experiments with direct voltages on this electrode. With both positive and negative impulses, the voltage lowering was of the same order as that obtained using direct voltages.

Optical studies. With a negative direct voltage on the main electrode no discharge occurred across the gap during the time interval between the breakdown of the trigger gap and that of the main gap. With positive voltages, however, a visible transient discharge occurred when the trigger pulse was applied, reaching out from the cathode towards the anode. The discharge was in the nature of a burst of corona rising to a maximum value in 0·05–0·1 μs and falling to a low value in about 0·5–1·0 μs. With a sufficiently high voltage on the main gap the corona pulse was followed after a time delay by a sudden increase in light intensity corresponding to breakdown of the main gap. A typical oscillogram showing the light output from the transient discharges is given in Fig. 4. The intensity of the light output from the corona pulse fell steadily with increasing distance from the cathode, to zero at about 20–30% across the gap.

Current measurements. With the high-voltage electrode negative no detectable current flowed in the time interval between the breakdown of the trigger and main gaps. With this electrode positive, however, a current pulse of the order of tens of microamps was found to pass.

RESULTS WITH THE THERMALLY TRIGGERED SPARK GAP

Since no trigger voltage is involved, the initiation mechanism must depend either on thermal effects due to the hot wire itself or on space charge formation caused by thermionic emission from the wire. A voltage lowering of 20% was obtained with wire temperatures of only 300–400° C and it therefore appeared that thermionic emission was not responsible for the voltage lowering effect unless such emission was produced by surface layers on the wire.

Voltage measurements. The percentage voltage lowering was dependent on the polarity of the high-voltage electrode and decreased with increasing gap length.[2] A greater percentage lowering was obtained with a negative than with a positive high-voltage electrode, the difference being of the same order as that observed in the trigatron.[5]

Corona measurements. With positive charging voltages less than those required to produce breakdown and with wire temperatures greater than about 700° C a corona discharge occurred at the cathode, reaching out into the main gap. The visible length of the discharge increased with voltage up to about 20–30% of the gap length just below the breakdown potential. With the high-voltage electrode negative no discharge preceded breakdown. The corona current occurring with positive polarities consisted of a series of pulses similar to those observed by Trichel[7] and others[8] with point-plane gaps. The time delays between the peaks of the current pulses were of the same order as the time lags to breakdown of the trigatron under the same conditions of voltage and gap length,[5] and scatter in the times between successive peaks about the same as the scatter in time lags to breakdown of the trigatron.

Time lag measurements. Impulse voltages were applied to the main electrode, their waveshape being the same as in the corresponding tests on the trigatron. With the wire heated the time lag was measured from the application of the impulse to the breakdown of the gap. With positive impulses long time lags with small scatter occurred. Fig. 5 shows

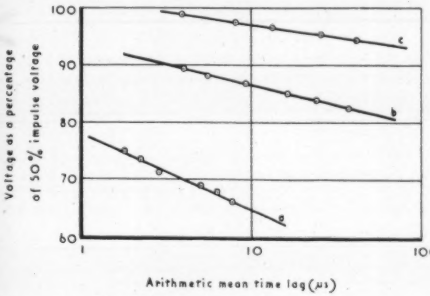

Fig. 5. Voltage-time lag to breakdown curves for the thermally triggered gap. Positive impulse voltages applied to main electrode

(*a*) 2 cm gap. (*b*) 6 cm gap. (*c*) 8 cm gap.

typical curves relating mean time lag with gap voltage. Voltages are expressed as a percentage of the 50% positive impulse breakdown voltage with the wire cold; this corresponds approximately to the direct breakdown voltage when direct voltages are applied to the main electrode. These curves are identical with curves obtained with the trigatron under the same conditions of gap length and voltage.[5]

With negative impulse voltages applied to the main electrode time lags were mainly short, of the order of 1 or 2 μs or less, with large scatter. Similar results were obtained with the trigatron, using both direct and impulse voltages. The lowering in 50% impulse voltage obtained by heating the wire was greater with negative than with positive impulses.

MECHANISM OF BREAKDOWN

The results given in this paper seem to indicate that the breakdown mechanism of the thermally triggered gap is as follows:

The air in the vicinity of the hot wire is heated, consequently the dielectric strength decreases and a small electron avalanche is initiated in this region, either by random ionization or by thermionic emission from surface layers on the hot wire. A small charged volume is thus produced in the space near the earthed main electrode and the increased field immediately round this volume either promotes or inhibits further discharges, depending on the polarity of the high-voltage electrode.

With the high-voltage electrode positive, electron avalanches near the hot wire produce a positive ion space charge which increases the electric field near the cathode and reduces it further towards the anode. At a certain distance from the hot wire the field strength is reduced by the space charge field to a value too low to promote further electron avalanches. The electrons lose energy rapidly and form negative ions by attachment or proceed to the anode without causing further ionization. Since avalanches are not produced further out into the gap the breakdown process is convergent, corona being observed at voltages insufficiently high to cause complete breakdown. The positive ions then move into the cathode and the current pulse is formed. By the time the last few positive ions are approaching the hot wire, the field will have risen again and the cycle is repeated. The experimentally observed time delays between the current pulses (about 30–300 μs) are of the order of time taken for a positive ion to cross a part of the gap under the same conditions of gap length and voltage. With an increased field, electrons in the region of low field strength will have sufficient energy to produce further ionization by collision and a negative streamer develops. The method of propagation of the streamer is well known.[9]

With the high-voltage electrode negative an electron avalanche near the hot wire will leave a positive ion space charge in this region and photoionization will cause further electrons to be produced further out in the gap. These will then be drawn towards the positive ion space charge, causing a positive streamer to be propagated across the gap. The breakdown process is thus divergent since, once started, it continues across the whole gap and corona does not occur at voltages lower than the breakdown voltage.

The above theory for the thermally triggered gap explains the fact that breakdown potentials with negative charging voltages are lower than with positive. This follows since, at a given voltage, the divergent breakdown process with a negative high-voltage electrode will enable complete breakdown to occur, whereas with this electrode positive the breakdown mechanism is convergent, giving partial breakdown in the form of corona. The theory would also explain why the percentage voltage lowering using negative charging is substantially independent of gap length, since the breakdown process, once started, continues. With positive voltages, however, the likelihood of complete breakdown occurring will decrease with increasing gap length, since the breakdown mechanism is convergent. At the higher gap lengths a relatively high voltage will be required in order to raise the field at the head of the corona to a sufficiently high value for a streamer to be propagated across the whole gap, giving complete breakdown.

In the case of the trigatron the experimental results described eliminate field distortion (from the trigger voltage) as a possible breakdown mechanism and support the view that the breakdown mechanism is as follows:

Consider first the case when the high-voltage electrode is positive. A voltage is applied to the trigger electrode and a spark occurs in the annular gap. Electrons are thus produced at the cathode, and electron avalanches occur. At a certain distance from the cathode the field strength, which is distorted by the space charge field, is insufficient to promote further avalanches and the electrons form negative ions by attachment or proceed to the anode without further ionization. Recombination of positive ions and electrons will give rise to a light pulse; the visible corona pulse therefore corresponds to the electron avalanche. The positive ions are then swept towards the cathode. As the last few positive ions approach the cathode, the field may have risen sufficiently for the process to be repeated. Further electrons may be produced, either by the Townsend γ-mechanism or by some other process, so that more electron avalanches occur than in the first cycle. Certain electrons may then have sufficient energy to enable avalanches to traverse the regions of weaker field strength in the gap and a negative streamer will be propagated, leading to complete breakdown. The process thus consists of an electron avalanche followed after a long time delay

by a further avalanche developing rapidly into an anode-directed streamer. The above theory closely resembles that put forward for the thermally triggered gap.

When the high-voltage electrode is negative, electrons are liberated in the region of the anode, electron avalanches are produced in this region, and a cathode-directed streamer is propagated, causing breakdown. The process takes place in a much shorter time than when the high-voltage electrode is positive, since breakdown depends on a streamer mechanism only and not on positive ion movements. The rapidity of the process explains the fact that no visible corona pulse occurs, since this cannot be resolved experimentally from the main discharge. The longer time lags when using negative charging are probably statistical. This would also account for the random nature of these lags.

Measurements on the trigatron in the time interval between the breakdown of the trigger and main gaps (with positive high-voltage polarity) showed that a current flowed in the gap. This is in agreement with the theory suggested above, in which positive ions move towards the cathode during this period. The fact that no current was observed when using negative charging polarities supports the view that with this polarity the time lags are statistical.

A quantitative analysis of the theories of breakdown put forward has not been given in this paper. Several quantities such as initial ion density and rate of electron emission from the triggering source are unknown, and the assumptions thus necessary render any calculations of doubtful value.

ACKNOWLEDGEMENTS

The author wishes to thank Dr. R. Cooper and Dr. D. R. Hardy for their interest in this work.

REFERENCES

(1) Craggs, J. D., Haine, M. E., and Meek, J. M. *J. Instn Elect. Engrs., IIIA*, **93**, p. 963 (1946).
(2) Broadbent, T. E., and Wood, J. K. *Brit. J. Appl. Phys.*, **6**, p. 368 (1955).
(3) Hardy, D. R. *J. Sci. Instrum.*, **29**, p. 241 (1952).
(4) Meek, J. M., and Craggs, J. D. *Nature* [*London*], **152**, p. 538 (1943).
(5) Broadbent, T. E. Ph.D. Thesis (University of Manchester, 1955).
(6) Hardy, D. R., and Wroe, H. *Brit. J. Appl. Phys.*, **5**, p. 335 (1954).
(7) Trichel, G. W. *Phys. Rev.*, **54**, p. 1078 (1938).
(8) Loeb, L. B., Kip, A. F., Hudson, G. C., and Bennett, W. H. *Phys. Rev.*, **60**, p. 714 (1941).
(9) Meek, J. M. *Phys. Rev.*, **57**, p. 722 (1940).

Barium getters and oxygen

By R. N. Bloomer, B.Sc., A.Inst.P., Associated Electrical Industries Ltd., Aldermaston, Berks

[*Paper received* 22 *August*, 1956]

The sorption of oxygen by films of barium evaporated in a vacuum has been studied. The speed of pumping and the capacity were measured. The speed of pumping has been found to be almost independent of the ionizing electron current in the oxygen gas. However, towards the end of the life of a film, it was found that all pumping ceased unless a hot tungsten filament was alight in the gas. Measurements of the variation of speed in the early life of a getter film, and of the influence of evaporation conditions upon pumping, show the importance of nucleation centres at which oxidation starts. The increase of speed and capacity with temperature show that these are limited by diffusion processes within the getter film.

In radio valves and the like, both during manufacture and in service, gases are commonly taken up by chemically active electropositive metals (getters), for example, barium. All the details of the mechanisms of sorption are still not understood.

Reimann[1] distinguished between two principal ways in which gases might be taken up by getters: firstly, by chemical reactions between gas molecules and the getter metal ("contact gettering"); and secondly, by reactions between the metal and gas which has been made more active by the passage of an ionizing electron current ("electric discharge gettering"). Reimann[1, 2] studied the gettering of various gases, by magnesium chiefly. He found that gases combined chemically with getter films, but that the speed of pumping was more rapid when an ionizing electron current was being passed in the gas.

Wagener[3] showed that the speed of pumping of oxygen and nitrogen by barium increased with electron current. Later, however, the same author[4] reported that the speed of pumping of gases (e.g. oxygen) was the same whether or not an ionizing electron current was running nearby. The earlier paper suggests that an electron current is necessary for high speeds of pumping to be obtained: the later note suggests that an ionizing electron current is not necessary. The present paper reports measurements made in an attempt to set at one these contrary findings.

POSSIBLE SIMILARITY BETWEEN GETTERING AND THE CLEANING UP OF GASES BY ELECTRON DISCHARGES ALONE

Wagener[3] deduced the relation

$$G = 176\, N_{RA} I_A \qquad (1)$$

between the pumping speed G (cm^3/s) of a getter and the electron current I_A (mA) in a nearby discharge, where N_{RA} is the number of gas particles made active by each electron. Wagener measured the speed of pumping of getters for

different values of electron current and, for oxygen, obtained these values:

I_A (mA)	5	10	20
G (cm^3/s)	970	1080	1300

(see Table 6 of Ref. 3). These results clearly did not fit the simple relation (1) above. In fact they accurately fit the expression:

$$G = 860 + 22I_A \qquad (2)$$

which suggests that only a part of the speed of the getter is dependent on the electron current. The disagreement between Wagener's results and the simple formula (1) is illustrated in Fig. 1. Curve (*a*) is for the measured speeds for oxygen at different electron currents, extrapolated to zero current: curve (*b*) has the form predicted by formula (1).

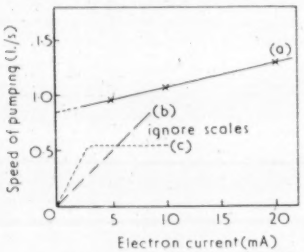

Fig. 1. (*a*) Speed of pumping of oxygen by a barium getter film, after Wagener.[3] (*b*) Form of curve according to Wagener's hypothesis.[3] (*c*) Experimental form of curve for clean-up of gases by electron discharge alone, after Bloomer and Haine[5]

Bloomer and Haine[5] have measured the rate of cleaning up of residual gases in sealed-off ionization gauges. These had no getters. (Evaporated metal films influence the rate of cleaning up of residual gases in sealed-off ionization gauges. For example, Vanerin and Carmichael[6] have shown that the rates for helium increase with the amount of nickel evaporated. In the work of Bloomer and Haine the rates of cleaning-up increased rapidly with the temperature of an evaporating molybdenum filament, fitted in some tubes. But, ordinarily, tungsten filaments were used, and care was taken not to evaporate any metal during the processing of the tube. In these cases the subsequent clean-up rates were low and the same in all gauges.) In that work, in the lower pressure region below 10^{-6}–10^{-7} mm of mercury, it was found that the speed of pumping varied with electron current in the manner shown in curve (*c*) of Fig. 1. The knee of this curve is at a few tens of microamperes of electron current, and below this the speed of pumping is proportional to the electron current, as in the simple formula (1). If getters behave similarly, Wagener's observations at higher currents would not be incompatible with the simple formula. It was decided to test this idea by measuring gettering speeds at very small and zero electron currents.

APPARATUS AND MEASUREMENTS

The apparatus, Fig. 2, is similar to that described by Wagener,[7] except that a Pirani gauge has been added so that pressure measurements can be made without using an ionizing electron current. Commercial getters (e.g. Kemet KlC stirrup by Kemet Products Co., and Barex strip types by King Laboratories Inc.) of 20 mg size with non-magnetic mountings, as in cathode-ray tubes, have been used. In the experiments the getters have been set up so that the

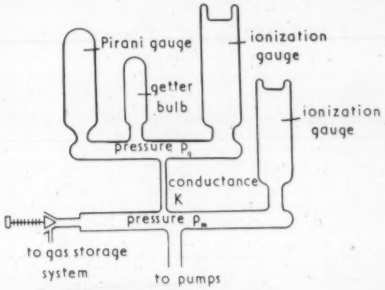

Fig. 2. Schematic diagram of arrangement of experimental tubes in getter studies

wire or strip could be heated from a low voltage mains transformer. When necessary, tubes containing additional devices such as diodes and filaments are added above the capillary tube. Pressures within the manifold are controlled by a needle valve which is connected to a gas storage system.

The Pirani gauge is similar to that described by Reimann.[1] It is connected in a simple Wheatstone bridge circuit (arm resistances each about 30 Ω) which is supplied from a 2 V accumulator. The ionization gauges are of the anti-X-ray type described by Bayard and Alpert,[8] and are made so that they are easy to outgas by electric current heating. Thus the ion collector and electron emitter hairpin filaments are identical (0·005 in. tungsten) and the electron collector is a continuous wire zig-zag (of 0·015 in. molybdenum) formed to enclose a cylindrical space. At high temperatures this arrangement retains its shape better than a simple helix. The whole of the glass part of the pumping system is exhausted through a glass-to-metal seal by a vapour pump charged with either hydrocarbon or silicone oil (Apiezon C by Metropolitan-Vickers Electrical Co. Ltd., or D. C. 703 by Don Corning Corp.).

The vacuum system is mounted off the front of a standard Post Office rack, and the oven is slung from a hoist fixed on top of the rack. The electronic control and measuring panels are so mounted on the back of the rack that the meters can be read from the front. Between the oven and the panels is a gap, defined by the side channels of the rack. Heating is convected away up this during the bake, and hence the electronic gear is unharmed.

As a start, in each run the glassware and the needle valve are baked at about 300–400° C, overnight for convenience. Electric heating tapes are used for the glass pumping pipe and the needle valve outside the oven. Then the electrodes of the gauges are raised to at least an orange heat for a quarter of an hour or so, and the getters are degassed at just below their firing temperature. As a routine, pressures lower than 1 or 2×10^{-7} mm of mercury are obtained on both sides of the capillary pipe. Next, the gas being studied is made to enter fast enough to keep a pressure of about 10^{-5} mm of mercury in the manifold.

The pumping speed S of the getter can be found from the ratio of the pressure in the manifold to that near the getter, p_m/p_g, and the conductance K of the capillary pipe, by using the formula:

$$S = K(p_m/p_g - 1) \quad (3)$$

In the present experiments $K = 0{\cdot}1$ l./s for oxygen at room temperature, calculated from the dimensions of the pipe. There are two experimental causes of error in such calculations, which become more influential as the speed of the getter and the ratio p_m/p_g decrease: firstly, the pair of ionization gauges may not have the same sensitivity; secondly, the pumping action of the gauge above the capillary pipe may not be negligible compared with that of a getter the speed of which has become low. The first error can be detected by letting in argon and measuring the pressure with both gauges, for argon is not taken up by the getter. Acceptable pairs of ionization gauges, with sensitivities agreeing within a few per cent, have been constructed easily. The second error can be measured by letting in the gas under study in the absence of any getter. It was confirmed that the speed of pumping of oxygen by the filament of the ionization gauge, see Langmuir,[9] is $0{\cdot}1$ l./s or so, as has been found by Riddiford.[10] In the present experiments with getters and oxygen, the majority of the measurements have been stopped when the pumping speed has fallen below about $0{\cdot}3$ l./s.

The throughput of gas to the getter at any instant is $Q = K(p_m - p_g)$. The total quantity of gas taken up by the getter, its capacity, can be found by multiplying by K the area under the $(p_m - p_g)$ *versus* time curve. The capacity can be converted to an equivalent number of monolayers upon the apparent surface of the getter film, if two assumptions are made: firstly, that the deposit is smooth down to atomic dimensions, and secondly, that the gas molecules which are sorbed are packed as closely as possible. Errors in these two assumptions will have contrary influences upon the results of a conversion calculation.

RESULTS

The speed of pumping of a getter film for oxygen varies with time, as has been reported by Wagener,[3] and with temperature. Typical plots of speed *versus* time, obtained in the present work, are shown in Fig. 3. In the first, steady or rising speed, period the speed of pumping is unaltered when a nearby ionizing electron beam, or an incandescent filament, is switched on and off: in the second, falling speed, period a nearby filament must be kept hot for the getter film to have any speed. An ionizing electron beam is not necessary.

The speed of pumping of oxygen by a getter film in the first period has been found to be almost independent of the electron current in a nearby ionization gauge. Fig. 4 is a plot of typical results. It has, of course, been checked that the ratio of positive ion current to electron current in the gauge is independent of electron current, in the range 1 to $0{\cdot}001$ mA. In another type of experiment, not using ionization gauges, it was found that the suppression of an ionizing electron current of a few tens of microamperes (accelerating potential 100 V) did not influence the pressure near the getter measured with a Pirani gauge. For such runs the pressure in the manifold was kept constant at some value of the order 10^{-5} mm of mercury.

The amount of gas taken up by the getter (the capacity) was found to increase with temperature. At room temperature the capacity was the same for films of different thicknesses but the same area. At higher temperatures the capacity increased with the thickness of the film. (A convenient way of varying the thickness of the evaporated film

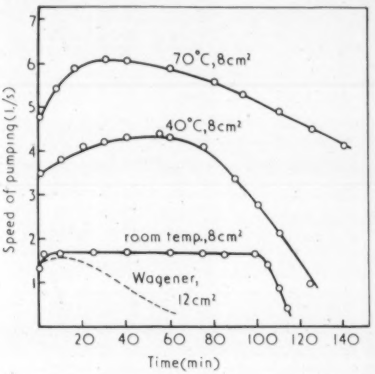

Fig. 3. The variation with time and temperature of the speed of pumping of oxygen by barium (manifold pressure 2×10^{-5} mm of mercury)

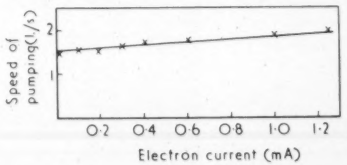

Fig. 4. The speed of pumping of oxygen by a barium getter film for a range of low electron currents

was to vary the time for which a particular heating current was passed through the getter wire.) Typical results are summarized in the table, in which capacities are given both in litre-microns and the equivalent number of monolayers.

Capacities for different temperatures and film thicknesses

Time for which 10 A firing current passed (min)	*Temperature of getter film*	*Area of getter film (cm²)*	*Quantity of oxygen taken up (l.μ.)*	*Number of monolayers*
1	room	4	2·7	23
2	room	5	3·0	20
5	room	4	2·2	19
6	room	5	2·8	19
2	205° C	4	4·5	38
2	220° C	4	10	85
7	200° C	4	23·5	200

The appearance of getter films did not change during the room temperature runs. During high temperature runs the getter films became translucent, with a play of interference colours, at the edges at least. The whole of a getter film was made translucent by keeping it hot after the end of the period

of high-speed pumping, in a pressure of about 10^{-5} mm of mercury of oxygen. Getter films which had ceased to pump oxygen, at room temperature, did so again when heated to 200° C.

In the second period of a speed *versus* time curve, when the speed was falling rapidly, all pumping ceased when the last of several nearby incandescent tungsten filaments was switched off. However, the speed of pumping was not increased, either by switching on further filaments after the first, or by drawing an ionizing electron current from any of them. In these experiments the area of each of the filaments was about 0·1 cm^2. By using a Pirani gauge for measuring the pressure changes at the getter film it was found that a tungsten filament became effective when its temperature was raised above about 1800° K (calculated from the heating current and diameter, using the data of Jones and Langmuir).[11] An increase of temperature, to 2100° K, did not further increase the speed of pumping. A hot filament caused a film to pump even when it was several centimetres away round a bend or two in 25 mm bore glass tubing. But a hot tungsten filament in the manifold, below the capillary pipe, had an effect which was only just detectable. It was checked that the light from a filament was not involved.

In a few of the experimental runs a freshly deposited getter film did not start to take up oxygen immediately the gas was let into the apparatus. In such experiments, upon raising the oxygen pressure further, to the order of 10^{-4} mm of mercury for a few minutes, or after waiting for up to a quarter of an hour or so at lower pressures of the order 10^{-5} mm of mercury, the pumping action began, and in a few minutes increased to a speed of about 1 l./s. Thereafter the speed *versus* time behaviour was normal, like that shown in Fig. 3, even when the manifold pressure was reduced to less than 1×10^{-5} mm of mercury. Initially inert films like this were only, and always, obtained when the getters were outgassed and evaporated so slowly that the pressure near them never rose above about 1×10^{-6} mm of mercury immediately before and during the evaporation.

COMMENTARY

Since the speed of pumping of oxygen by barium was found to be changed very little when the current in a nearby discharge was varied, it is confirmed that the Wagener[3] hypothesis—that the speed of pumping is proportional to the current—is untenable. Thus the taking-up of oxygen by barium follows laws different from those for the cleaning-up of residual gases by low current electric discharges alone. It is true that the speed of pumping of oxygen by barium does increase slightly, and linearly, with electron current, see, for example, Table 6 of Wagener[3] and Fig. 4 of this paper. Thus in addition to, and independently of, ordinary molecular oxygen, some product of the ionizing discharge is taken up by barium.

In the first period of the speed *versus* time curves like Fig. 3, it is probable that molecular oxygen is taken up by the barium, although, of course, the molecules may be split into atoms before being sorbed. If so, the surface itself does this. In the second, falling speed, period the surface is unable to take up oxygen directly. Some of the gas must first have been in contact with a hot tungsten filament before reaching the barium film. However, only a very small fraction need have done so; for increasing the area of heated filament does not increase the speed of pumping, although a small area of hot filament—in the case of the present experiments about 1/100th of the area of the getter film—is necessary. It is probable that a hot tungsten filament is effective because it dissociates some of the incident molecules.[12, 13]

There is some further evidence for the need for traces of catalytic material, this time in the early life of a getter film, because films that are deposited at relatively low pressures (less than 10^{-6} mm of mercury) always fail to take up molecular oxygen immediately. Haase,[14] who worked at such low pressures, and Arizumi and Kotani,[15] have reported similar results. Strictly this is evidence of nucleation, familiar in crystal growth studies, rather than of catalysis.

So much for surface phenomena: now consider a bulk property of barium getter films. Since the speed of pumping increases with temperature, it is clear that diffusion of oxygen, or of the barium/oxygen compound, is the process which limits the speed of pumping of the gas. Also, since the capacity increases with temperature—films go translucent at higher temperatures, but not at room temperature—the low rate of diffusion at room temperature is responsible for the incomplete using up of barium getter deposits in oxygen.

CONCLUSIONS

(i) Barium getter films take up oxygen at all times without the agency of an ionizing electron discharge.

(ii) When the speed of pumping begins to fall, oxygen is still taken up if some of it comes first into contact with a nearby incandescent tungsten filament.

(iii) The speed and capacity are limited by diffusion rates in the barium, and hence increase with temperature.

(iv) Getter films deposited under very good vacuum conditions are initially inert towards oxygen, even in the presence of an ionizing electron discharge or of incandescent filaments.

These last two conclusions are relevant to the design of radio valves and the like, and to their pumping schedules.

ACKNOWLEDGEMENTS

It is a pleasure to thank Mr. K. Sumpter who has made the experimental tubes, Mr. B. M. Cox who has carried out much of the experimental work, Mr. M. E. Haine for helpful discussions, and Dr. T. E. Allibone, Director of this Laboratory, for permission to publish this paper.

REFERENCES

(1) Reimann, A. L. *Phil. Mag.*, **16**, p. 673 (1933).
(2) Reimann, A. L. *Phil. Mag.*, **18**, p. 1117 (1934).
(3) Wagener, S. *Brit. J. Appl. Phys.*, **2**, p. 132 (1951).
(4) Wagener, S. *Nature* [*London*], **173**, p. 684 (1954).
(5) Bloomer, R. N., and Haine, M. E. *Vacuum*, **3**, p. 128 (1953).
(6) Varnerin, L. J., and Carmichael, J. H. *J. Appl. Phys.*, **26**, p. 782 (1955).
(7) Wagener, S. *Brit. J. Appl. Phys.*, **1**, p. 225 (1950).
(8) Bayard, R. T., and Alpert, D. *Rev. Sci. Instrum.*, **21**, p. 571 (1950).
(9) Langmuir, I. *J. Amer. Chem. Soc.*, **35**, p. 105 (1913).
(10) Riddiford, L. *J. Sci. Instrum.*, **28**, p. 375 (1951).
(11) Jones, H. A., and Langmuir, I. *Gen. Elect. Rev.*, **30**, p. 310 (1927).
(12) Langmuir, I. *J. Amer. Chem. Soc.*, **37**, p. 1139 (1915).
(13) Langmuir, I., and Villars, D. S. *J. Amer. Chem. Soc.*, **53**, p. 486 (1931).
(14) Haase, G. *Z. Angew. Phys.*, **11**, p. 188 (1950).
(15) Arizumi, T., and Kotani, S. *J. Phys. Soc. Japan*, **7**, p. 300 (1952).

Correspondence

Scaling of space-charge limited electron-optical systems

It is well known that a purely electrostatic system in electron optics can, in absence of space-charge effects and neglecting electron emission velocities, be scaled in size without altering the shapes of electron trajectories. That is, the radius of curvature of the trajectories at every point scale linearly with the electrodes.

In the case of a system in which electronic space charge has significant effect, this simple scaling law ceases to apply. Nevertheless, it is often desirable to be able to scale a system, either for the purposes of design modification or because of the convenience of carrying out experimental studies on a system bigger or smaller than that finally required. As far as the writer has been able to ascertain, no description of the scaling laws for this case have been previously described. This note derives the relevant laws.

Consider any arbitrary system such as shown in the figure; P is a cathode emitting under space charge limited conditions, and Q is a positively charged electrode. Now consider a

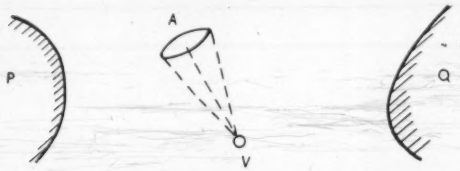

small volume V containing a charge q from the electron beam. If A is an element of area lying perpendicular to AV distant r from V, the number of lines of force traversing A and originating from V will be proportional to the charge within V and the solid angle A/r^2.

Suppose the system can be scaled in size n times while the current is scaled n^x times and the voltage n^y times, so that all electron trajectories follow exactly the same paths relative to the electrodes as before. To achieve the latter aim the radius of curvature at each point in every trajectory must clearly scale n times.

Since the current scales n^x times and areas n^2, the current density will scale as $n^x/n^2 = n^{x-2}$. The charge density depends upon the quotient of current density and velocity which will scale with the square root of potential or as $n^{y/2}$. Hence charge density scales as $n^{x-2}/n^{y/2} = n^{(x-2-y/2)}$.

The charge within a volume V will scale as $n^{(x-2-y/2)}xn^3 = n^{(1+x-y/2)}$.

The total number of lines of force radiated from this volume and the number crossing the arc A will similarly scale, the solid angle A/r^2 remaining constant. The area will scale as n^2. The field due to the charge therefore will scale as $n^{(1+x-y/2)}/n^2 = n^{(x-1-y/2)}$. The Laplacian field will scale as $n^y/n = n^{y-1}$.

For the trajectories to be uncharged the field due to the space charge must scale as the Laplacian field, hence:

$$n^{(x-1-y/2)} = n^{y-1}$$

or

$$x = 3y/2$$

If the emitted electrons have a finite emission velocity a further restriction results. Since this velocity does not change on scaling, clearly all other velocities must not change, hence $y = 0$, and it follows $x = 0$.

The condition for overall scaling is thus met if the voltage and current are left unchanged. Since the current is controlled by space charge the latter condition is automatically satisfied. For a given geometry and voltage the current is independent of size. It will be seen that this result is confirmed by Child's law* for a plane parallel diode.

In many electron-optical systems the emission velocities play little part in determining the beam shape. In such cases scaling of voltage is permissible and the current will scale as the $\frac{3}{2}$ power of voltage. The above argument shows that trajectories are unaffected by this scaling so that space-charge spreading effects are unchanged. The arguments can, of course, tell us nothing of the effects of changing geometry.

A typical application of the scaling law might be to investigate the beam formation in the triode system of the cathode-ray tube by a ten times scaled-up model. The large size would allow good accuracy of measurement, yet the currents to be dealt with would be unchanged.

The writer wishes to thank Dr. T. E. Allibone, Director of this Laboratory, for permission to publish this note.

Associated Electrical Industries Ltd.,
Aldermaston,
Berkshire.

M. E. HAINE

[16 August, 1956]

* CHILD, O. C. *Phys. Rev.*, **32**, pp. 492–511 (1911).

Measurements on alloy-type transistors with varying collector voltage

The dependence of the effective base width W on the collector voltage V_C for an alloy-type transistor biased normally can be expressed by the equation

$$W = W_0 + M\sqrt{(-V_\phi)} - M\sqrt{(-V_C - V_\phi)} \qquad (1)$$

which is readily derived from junction theory (e.g. Early,[1]) the emitter junction width being ignored, where V_ϕ is the equilibrium barrier potential, W_0 is the effective base width for zero applied collector voltage and M is a constant. Thus, for values of $|V_C|$ large compared with $|V_\phi|$, a plot of W against $\sqrt{(-V_C)}$ should yield a straight line of slope $-M$.

Using the method described in Section 4 of a previous paper[2] the effective diffusion constant D for an emitter current I_E of 1 mA, and also W^2/D, were determined for two commercial p–n–p alloy-type transistors to which the applicability of the Shockley theory had been confirmed. The measurements were made at a temperature of 27° C, using a signal frequency of 5 kc/s; a combination of the results of the two measurements enabled W to be determined as a function of collector voltage. A plot of W against $\sqrt{(-V_C)}$ showed that the points (between 1½ and 10 V for transistor A and between 1½ and 25 V for transistor B) lay quite accurately on a straight line for each transistor, which confirms the assumption [implicit in the derivation of equation (1)] that there is an abrupt transition from the n-type to p-type germanium. It was apparent from the plots that $|V_\phi|$ was small enough (certainly less than the theoretical value of about ½ V) to have a negligible effect on the linearity of the plots for

values of $|V_C|$ greater than about $1\frac{1}{2}$ V. The resistivity of the *n*-type germanium of the base (determined from the experimental values for M of $2{\cdot}28 \times 10^{-4}$ and $2{\cdot}36 \times 10^{-4}$ cm $V^{-\frac{1}{2}}$) was found to be 4·84 and 5·20 Ω cm for transistors *A* and *B* respectively. The intercepts for $V_C = 0$ gave, making a rough allowance for $M\sqrt{(-V_\phi)}$, the values of $8{\cdot}3 \times 10^{-3}$ and $5{\cdot}0 \times 10^{-3}$ cm for W_0, respectively.

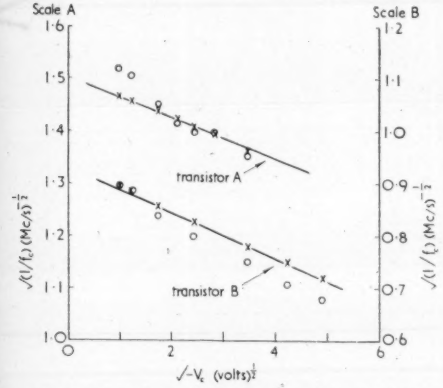

Dependence of α cut-off frequency on collector voltage.
$I_E = 1$ mA; temperature 27° C
○ = direct observed values of f_c.
× = calculated values of f_c (from experimental data at 5 kc/s.

The theoretical expression for the cut-off frequency f_c of the base transport factor β is given by

$$\omega_c = 2\pi f_c = \theta D/W^2 \qquad (2)$$

where θ is a numerical factor which is a slowly varying function of W/L, L being the diffusion length of the minority carriers. From the experimental values of W/L the values of θ were determined to be 2·52 and 2·47 for transistors *A* and *B* respectively (these values being constant to less than $\frac{1}{2}$% for the range of W/L concerned). Substitution of these values of θ and of D/W^2 (obtained from data at 5 kc/s) into equation (2) enabled f_c to be calculated for various values of collector voltage and the results are shown as crosses in the figure in which $1/\sqrt{f_c}$ is plotted against $\sqrt{(-V_C)}$. It can be seen that the crosses lie on straight lines as expected from the equation

$$1/\sqrt{f_c} = -\sqrt{(2\pi M^2/\theta D)}\sqrt{(-V_C)} + W_0\sqrt{(2\pi/\theta D)} \qquad (3)$$

derived from equations (1) and (2), V_ϕ being neglected. The slope of the line for each transistor is consistent with the value of M determined experimentally (above), the value of θ and the value of D used in the determination of W. In addition, f_c was found directly for various collector voltages by measuring the current amplification factor as a function of frequency;[2] these results are shown as circles in the figure. For transistor *A*, the agreement between the experimental points and the calculated points (for the same collector voltage) is good for $|V_C| > 3$ V. For transistor *B*, the agreement is good for $|V_C| < 3$ V. The discrepancy between the two sets of points at low collector voltages for transistor *A* and high collector voltages for transistor *B* must be considered as being due to deviations inherent in the transistors (possibly due to surface effects) from the assumptions that are implicit in the above treatment. For the normal working point of both transistors ($I_E = 1$ mA, $V_C = -6$ volts) the experimental value of f_c is within $1\frac{1}{2}$% for transistor *A* and 7% for transistor *B* of the value calculated from the low frequency data.

Radio Research Station,
Slough, Bucks.

D. M. Evans
[20 January, 1956]

REFERENCES

(1) Early, J. M. *Proc. Inst. Radio Engrs*, **40**, p. 1401 (1952).
(2) Evans, D. M. *J. Electronics*, **1**, p. 461 (1956).

New books

Peaceful uses of atomic energy, Vol. 2. Physics: Research Reactors. (New York: United Nations; London: H.M. Stationery Office, 1956.) Pp. viii + 470. Price 57*s*.

This is the second volume in a series of sixteen reporting the proceedings of the International Conference in Geneva on the Peaceful Uses of Atomic Energy. The volume can be clearly divided into two sections: "Nuclear and fission physics" and "Research reactors."

The first section, concerning neutron physics, contains a variety of papers on neutron scattering, neutron cross-sections for (n, p) and (n, α) reactions and theories of the nucleus. The experimental techniques used by different people are well described, and the papers taken collectively give a good account of some of the more specialized work done with neutron beams from research reactors. The technique used by Groschev and others for measuring the energies and intensities of neutron capture γ-rays in the range 0·5–9 MeV is of particular interest. There are many papers on fission physics, where theoretical analyses of fission processes are reported by Bohr, Wheeler, Geilikman and Huizenga, and experiments to determine many of the fission parameters are also described.

Included in the volume is a verbatim record of each session. These records make the volume much more interesting for many of the questions which spring to one's mind are answered here, and many other ideas and suggestions are promoted.

The second section, "Research reactors," deals with the need for research reactors, experiences in running them and descriptions of both operating and proposed reactors. Three of the four principal high flux reactors in the world are described; MTR-U.S. light water cooled and moderated, RPT–U.S.S.R. graphite and light water moderated, light water cooled, and E.443(DIDO)–U.K. heavy water cooled and moderated; all of which use enriched uranium. It is a pity that a paper on NRU. (Canada, nautral uranium), was not given at the conference, so that powers, fluxes, facilities, versatility, etc., could all be compared. The U.K. and U.S.A. papers deal well with the experimental facilities available in their reactors; and in the high flux reactors, the use of the peaking of the thermal flux in the reflector for irradiation facilities is evident, relatively poor use being made of the intense fast neutron and γ-ray intensities in the core.

Papers are included on homogeneous water boiler reactors

and swimming pool type reactors; the versatility of the latter being well illustrated. Contributions are also included on nearly all the principal graphite moderated, gas cooled research reactors.

With contributions from so many countries it is of interest to compare the various philosophies of design and operation of research reactors, e.g. the feature, in the U.K., of having a high flux reactor housed in a gas-tight containment vessel. In general the section acts as an excellent guide to the world's research reactors, but it would have been improved by the addition of a "Research reactor catalogue" giving a résumé of certain salient features, such as is given in Vol. 3 of this series, on power reactors.

The volume is excellently printed and the diagrams exceptionally clear. The large number of papers (fifty-four), together with the numerous references with each paper, make the volume valuable as a form of specialized reference work on research reactors and the experiments performed using their radiations.

V. S. CROCKER

Peaceful uses of atomic energy. Vol. 3. Power reactors. (New York: United Nations; London: H.M. Stationery Office, 1956.) Pp. 389. Price 54*s*.

This volume covers six sessions of the conference devoted to the production of power from atomic energy, containing the full text of the papers presented and a record of the ensuing discussions. As a result a large part of the available information on power reactors has been collected together in one volume.

The first session is devoted to the economics of various possible fuel cycles and their bearing on reactor design. Initially power-producing programmes will depend on consuming natural or slightly enriched uranium in thermal reactors; but future developments are less clear. Fast ^{239}Pu–U systems or ^{233}U–Th thermal systems will both give breeding gains; but it is still an open question how such reactors can best be integrated into future power programmes.

The other sessions covered in this volume deal with the design and operation of various types of power reactors. The present state of knowledge is reflected in the number of widely differing reactor designs described. Most papers are design studies, though details are given of some half dozen large reactors due to be completed in 1956. Operating experience on power reactors is even more limited and in this respect the papers on the U.S.S.R. power station and the U.S.A. prototype boiling water reactor are both interesting and encouraging.

In a book of this type it is unavoidable that the style of the contributions and the detail of the information given varies greatly from paper to paper. Nevertheless, there is such a large amount of previously unpublished information contained in this volume that for years to come it will remain an essential reference source for information on power reactor design. The volume is produced to a very high standard, the text is well laid out and the standard of the illustrations is particularly high. Altogether the editors and publishers are to be congratulated on making the best use of the unique opportunity afforded them by this historic conference.

R. D. SMITH

Peaceful uses of atomic energy. Vol. 4. Cross sections important to reactor design. (New York: United Nations; London: H.M. Stationery Office, 1956.) Pp. viii + 357. Price 54*s*.

This volume of the Proceedings of the Geneva Conference deals largely with the cross-sections of the fissile nuclides and the techniques employed in their measurement. Until the Conference, most of the data had been in the "classified" category, with the result that many independent measurements of the more important quantities were reported. The general similarity of the techniques used in the various countries and the encouraging overall agreement of the results will impress the reader of this book.

Time-of-flight methods now yield important data over the whole range of neutron energies, and a number of papers deal with developments in this field. The most recent application is to the study of the spectra of inelastically scattered neutrons, where millimicrosecond electronic techniques are employed in conjunction with pulsed neutron sources. An interesting variant on the more conventional "choppers" is the "slowing-down-time spectrometer" described by Russian scientists in which pulses of fast neutrons are injected into a massive lead block containing appropriate detectors.

One of the most impressive papers deals with the measurement of the total cross-section of the radioactive fission product ^{135}Xe as a function of neutron energy, involving the use of samples of many hundreds of curies activity. Other topics include the application of precision mass-spectrometry to the determination of nuclear constants, pile oscillator techniques and the properties of delayed neutrons from fission.

This collection of papers gives an excellent overall picture of the present status of nuclear data relevant to reactors as well as providing a record of several stimulating sessions of the Conference.

J. E. SANDERS

Peaceful uses of atomic energy, Vol. 5. Physics of reactor design. (New York: United Nations; London: H.M. Stationery Office, 1956.) Pp. viii + 545. Price 63*s*.

Volume 5 of the Proceedings of the Geneva Conference deals with the physics of reactor design. It includes papers on the experimental and theoretical aspects of the subject and a verbatim report of the discussion taking place at Geneva immediately after presentation of the papers.

The experimental methods described are all of the integral type, i.e. they aim to measure quantities which are of direct use in reactor design, but which are combinations of the more fundamental nuclear properties of materials. Thus the first section of the book is concerned with the measurement of slowing-down area or neutron-age in various moderators, and of diffusion area. Section 2 includes measurements of resonance escape probability, descriptions of some critical assembly work, of work on the NRX reactor and of integral quantities derived therefrom.

Sections 3 and 4 include descriptions of many zero-energy experiments and show the methods that have been used to derive from such experiments data required in reactor design. The papers presented in the last section of the book are all concerned with the theoretical methods used in reactor design studies. Nuclear reactors are so complex, both in materials and in nuclear processes occurring in them, that the theory usually leads to a result in terms of a combination of several basic nuclear quantities. It is these integral quantities which the experiments are framed to measure directly, the accuracy attainable being discussed in the various papers.

For the specialist with many years of work in the reactor field it is most instructive to study the various approaches that have been made by laboratories hitherto prevented from exchanging their ideas. The book makes this possible. The newcomer to the field may feel he has had to accept a number of recipes for reactor core design. This book contains descriptions of the work on which these various recipes depend and so it is possible to form a better opinion of the

accuracy and range of validity of them. For example in America and the U.S.S.R. the recipe for resonance escape probability in reactors containing ^{238}U has been developed in different forms. Both are dealt with in this book and a detailed comparison of the several papers on the subject would be well worth while.

Among the experimental techniques dealt with in the papers, one finds a great majority are concerned with measurements of the steady state distributions of neutrons in reactor systems using constant sources of neutrons. It is clear that this method has been of great value, but requires quite large quantities of expensive materials. However, the first paper in the book describes work with a pulsed neutron source using smaller amounts of material. With the development of the techniques for measurement of very small time intervals it is conceivable that this alternative technique could dominate the physics pages of the proceedings of the next conference on the peaceful uses of atomic energy. F. W. FENNING

Electromagnetically-enriched isotopes and mass spectrometry. Edited by M. L. SMITH. (London: Butterworths Scientific Publications; New York: Academic Press Inc., 1956.) Pp. xvi + 272. Price 45*s*.

Since the early experiments of Aston on the separation of the isotopes of neon, there has been a continuous interest in techniques of isotope separation and utilization, and in the development of instruments to measure isotope abundance ratios. The discovery of nuclear fission accelerated technological development in this field and lead in 1941–1944 to the building of very large electromagnetic isotope separators. Though other methods are now available for bulk separation, the electromagnetic separator remains the most versatile machine for separating gramme quantities of isotopes for research purposes, since there are very few elements which cannot be separated by it.

There are many problems of considerable technical difficulty, both in the design of machines and in the preparation, ionization, separation and collection of samples. There are analogous and equally difficult problems in the design and operation of the analytical mass spectrometers, and the conference held at Harwell in September 1955, which forms the subject of this book, brought together many of the world's experts in this rather specialized field. The conference was of considerable historic interest because many machines and techniques which had been secret for almost a decade were described for the first time.

In all there were twenty papers on electromagnetic separators, in which problems of materials preparation, ion source design, separation of ion beams and collection of the separated isotopes were discussed. There were four papers on the utilization of stable isotopes for typical researches in physics, but only passing references to applications in chemistry or biology. Finally, five papers dealt with isotopic abundance analysis.

All the papers presented were of a high standard, but it is expected that this book will be read primarily for its factual and practical information on electromagnetic separators. The printing and binding of the book are excellent.

J. BLEARS

The constitutional diagrams of alloys. (A bibliography.) By J. L. HAUGHTON. Second edition compiled by A. PRINCE. (London: The Institute of Metals, 1956.) Pp. 323. Price 35*s*.

The first edition of this book appeared in 1942 and was of the greatest value to those whose work required a knowledge of metallurgical equilibrium diagrams. The convenient arrangement into binary, ternary, and quarternary systems, each with constituent metals in strictly alphabetical order, enables the reader to find work on any system at a glance, and saves much laborious searching of the indexes of abstracts. The printing and arrangement of the book are admirable, and the references to both the original papers and their abstracts in *Metallurgical Abstracts* are most useful, because the entry in the latter will often enable the reader to judge whether the paper is one of which he need consult the original.

As in the earlier edition, papers containing new or revised diagrams are marked with an asterisk to distinguish them from those dealing with physical properties or other matter which may later prove to be of value in constructing the most probable diagram. Here the authors have not always been too successful. Thus the well-known work of Owen and Pickup on the copper–zinc diagram appears without an asterisk, and occasional other examples are found. Some of the entries become very swollen—there are no fewer than 135 references under copper–zinc—and it is to be hoped that in future editions there will be some kind of classification under sub-headings, and some discarding of old work which has been shown to be seriously in error.

The reviewer would also suggest that if any reprinting of the present edition is made, interleaved copies should be sold, because the present book is too closely printed for marginal notes, and it is useful to record new work in the volume which contains the earlier references.

W. HUME-ROTHERY

Reactor handbook; Engineering. U.S. Atomic Energy Commission. (London: McGraw-Hill Publishing Co. Ltd., 1956.) Pp. 1088. Price £5 12*s*. 6*d*.

This large volume of over 1000 pages must of necessity attempt to cover an enormous range of material if it is to justify its title, and in spite of some unevenness a creditable result has been achieved. The preface indicates compilation to a tight schedule of fifteen months and the book bears evidence of this. The editors have taken what to this reviewer seems to be the wise step of including some of the material in discursive form, as many of the aspects in the field are still matters of opinion rather than fact or established practice.

The general approach has been to divide the volume into sections on reactor types, though there are additional chapters on handling and control gear and a catalogue of reactors. There is a considerable variation in the amount of new material and ideas given in the sections, this presumably reflecting the amount of work done on the various types.

There are two great drawbacks to this first unclassified edition, but these should not be allowed to detract unduly from the value of the book—firstly that no data beyond 1953 at the latest and mostly the end of 1952 are included, and secondly, that many of the references given are classified. The first means that the user must refer to the Geneva Conference papers and other sources for more up-to-date information in such a rapidly expanding field (this may be a continuing difficulty for some time in this reactor technology). The second makes the reader not having access to classified information wonder whether this material will become available, and is rather tantalizing.

It is to be hoped that a second edition embodying the vast amount of information recently released can be produced in the not-too-distant future. In the meantime the present edition remains as a most useful (but expensive) collection of information on nuclear engineering. J. SMITH

Notes and comments

Elections to The Institute of Physics

The following elections have been made by the Board of The Institute of Physics:

Fellows: A. H. Anstis, W. D. Bennett, C. E. Challice, A. J. Dyer, G. M. Leak, J. G. Powes, J. R. Stansfield, E. J. W. Whittaker.

Associates: S. A. Ahern, J. R. Bell, A. G. Buswell, K. R. Canfor, F. P. Chappel, A. E. Chester, P. N. Cooper, K. K. Damodaran, J. R. Denholm, E. W. Dickson, G. Duckworth, J. E. Dyson, R. J. Edwards, K. Ellis, P. Fisher, J. J. Gameson, A. M. Godridge, M. J. Goodspeed, D. W. Green, F. Heath, S. Hill, J. N. Hodgson, H. L. W. Jackson, W. L. Jackson, T. O. Jeffries, I. M. L. Jenkins, J. M. Johnston, P. Kalman, R. J. Lamden, I. K. B. Legge, D. Lewis, J. R. H. Lewis, F. M. Lovell, H. A. McCloskey, L. Micco, A. J. Miller, B. A. M. Moon, A. C. T. North, P. H. Oliver, A. E. S. Pengelly, M. Possener, G. Power, R. G. Pratt, M. J. Puttock, C. A. K. Salgado, H. M. Scott, R. E. Shannon, R. H. Slater, R. W. Smith, G. Spurr, P. Swinbank, A. Tarnowski, H. W. Thomas, S. M. A. Tirmizi, G. J. Williams, G. W. Wilson.

Fifty-one Graduates, fifty-seven Students and five Subscribers were also elected.

The International Journal of Applied Radiation and Isotopes

We have received the first issue (Nos. 1 and 2 of Vol. 1, July 1956) of a new periodical entitled *The International Journal of Applied Radiation and Isotopes*. It is intended to provide a forum for the publication and discussion of radioactive and radiation techniques, for the reporting of news of general interest in the field, and for the promotion of international co-operation. This first issue measures $7\frac{3}{8} \times 9\frac{1}{4}$ in. and runs to 144 pages in nicely produced two-column printing. The title of the ten papers in it are: The preparation and maintenance of standards of radioactivity; Radioactive tracer techniques for sand and silt movements under water; A radiochemical technique for determining the specific surface area of aluminium metal surfaces; Liquid scintillators—attributes and applications; Labelled metabolic pools for studying quantitatively the biochemistry of toxic action; Behaviour of ^{14}C- and ^{131}I-labelled plasma proteins in the rat; The production and clinical applications of ^{132}I; A simplified method for quantitation of autoradiography; Gamma-ray vulcanization of rubber; Utilisation d'un discriminateur d'impulsions associé a un detecteur γ à scintillation pour l'analyse par activation. Abstracts are given in English, French, German and Russian. Summaries of the papers presented at a meeting of The Society of Nuclear Medicine held in Salt Lake City, Utah, in June 1956 are included and two pages of news and notes.

The publishers are Pergamon Press of London and New York, and the subscription price is £6 ($17) per volume, or £3 10*s*. ($9.80) if for private use. There is an international editorial advisory board.

Rheology of Elastomers

The British Society of Rheology is organizing a conference on "Rheology of Elastomers" to be held at the Rubber Producers Research Association at Welwyn Garden City on 30 and 31 May, 1957. Contributions are invited for this conference and intending speakers are asked to first write to the Hon. Secretary, 52 Tavistock Road, Edgware, Middlesex.

Bibliographies and reading lists from the Atomic Energy Authority

In accordance with the United Kingdom Atomic Energy Authority's policy of disseminating information on atomic energy, its technical information officers from time to time prepare bibliographies on selected subjects and a list of those already prepared is obtainable from its Chief Press Officer at St. Giles Court, St. Giles High Street, London, W.C.2, together with details saying from where they are obtainable.

Within the limits of available effort the Authority will prepare further bibliographies in answer to requests from industry, learned societies, universities, technical colleges and other research institutions. Priority will naturally be given to subjects for which there is most demand. Requests should be sent to the Librarian, A.E.R.E., Harwell, Berks, or the Chief Librarian, U.K.A.E.A. Industrial Group, Risley, Warrington, Lancs. There is close collaboration between the Groups, and inquiries will be forwarded to the appropriate Library for action.

Journal of Scientific Instruments

Contents of the January issue

SPECIAL ARTICLE

Post-war developments in geophysical instrumentation for oil prospecting. By D. T. Germain-Jones.

ORIGINAL CONTRIBUTIONS

Papers

Contrast arising from elastic and inelastic scattering in the electron microscope. By M. E. Haine.

Two optical instruments used in semiconductor research. By D. G. Avery.

Operation of a diffusion cloud chamber with 23 atm of deuterium. By A. P. Batson, B. B. Culwick, H. B. Klepp and L. Riddiford.

A constant-current device for use in the measurement of transference numbers by the moving-boundary method. By D. T. Hopkins and A. K. Covington.

A bent crystal X-ray spectrograph. By G. B. Deodhar and R. C. Karnatak.

A linear, temperature compensated hot-wire anemometer. By E. L. Deacon and D. R. Samuel.

Measurement of high viscosities by shearing between parallel plates. By F. E. Humphreys and N. Stone.

A portable ionization current comparator. By L. A. W. Kemp and B. J. Banfield.

Laboratory and workshop notes

Curved spectroscopic slits. By D. A. Davies.

Simple voltage change measurement. By B. J. Belcher.

The use of a universal indicating instrument to measure low resistances. By J. C. Cooke.

Fabrication of holes of about 1 μ in diameter used for producing α-particle microbeams. By M. I. Davis, C. L. Smith and P. C. Smethurst.

Wet viewing microscope. By R. C. Moss.

An optical apparatus to measure shrinkage at high temperature. By J. Hutchings and J. P. Roberts.

Spring diaphragms. By D. F. Gibbs.

Gas-cooling device for use with a 19 cm X-ray powder camera. By M. H. Francombe.

NOTES AND NEWS

Correspondence

The eccentric loading of optical flats during grinding. From N. F. Barber; N. J. Rumsey.

Vacuum deposition apparatus. From F. W. Cuckow.

New instruments, materials and tools — New books

Manufacturers' publications — Notes and comments

THIS JOURNAL is produced monthly by The Institute of Physics, in London.

It deals with all branches of applied physics (including theory and technique). All rights reserved. Responsibility for the statements contained herein attaches only to the writers.

EDITORIAL MATTER. Communications concerning editorial matter should be addressed to the Editor, The Institute of Physics, 47 Belgrave Square, London, S.W.1. (*Telephone:* Sloane 9806.) Prospective authors are invited to prepare their scripts in accordance with the *Notes on the preparation of contributions*. (Price 2*s*. 6*d*. including postage.)

REPRODUCTION. The Institute of Physics is a signatory to The Royal Society's Fair Copying Declaration. Details may be obtained upon application from The Royal Society, London, W.1.

ADVERTISEMENTS. Communications concerning advertisements should be addressed to the agents, Messrs. Walter Judd Ltd., 47 Gresham Street, London, E.C.2. (*Telephone:* Monarch 7644.)

CLAIMS FOR MISSING JOURNALS. Claims from regular subscribers to this *Journal* for missing numbers will only be considered if received within 60 days of the date of mailing plus normal outward time of transit and time for lodging the claim. Losses attributable to failure to notify a change of address or to similar omissions will not be considered.

SUBSCRIPTION RATES. A new volume commences each January. The charge is £5 per volume ($14.25 U.S.A.), including index (post paid), payable in advance. Single parts, so far as available, may be purchased at 10*s*. each ($1.50 U.S.A.), post paid cash with order. Orders should be sent to The Institute of Physics, 47 Belgrave Square, London, S.W.1, or to any bookseller.

SPECIAL ARTICLE

Some applications of physics to wood*

By R. F. S. Hearmon, F.Inst.P., Forest Products Research Laboratory, Princes Risborough, Aylesbury, Buckinghamshire

A review is given of some of the more important physical properties of wood, particularly the hygroscopic, thermal, electrical and elastic properties. The vibration behaviour is also considered, with special reference to the effect of shear and rotatory inertia in flexural vibration, and to the connexion between frequency of vibration and elastic stability.

INTRODUCTION: HYGROSCOPIC AND ANISOTROPIC PROPERTIES

From the physical point of view, wood is of interest because it is both hygroscopic and anisotropic. Many natural materials are hygroscopic, in that the amount of moisture they contain depends on the relative humidity of the surrounding atmosphere. If a piece of dry wood is exposed to an atmosphere of constant relative humidity, its weight will increase with time owing to absorption of water vapour and will finally become steady when equilibrium is established. If the humidity is increased, there is a further absorption of water and Fig. 1 shows the equilibrium moisture content, expressed as grams of water per 100 grams of dry wood, plotted against the relative humidity. The moisture content at a given relative humidity depends on whether the equilibrium has been approached from the dry or the wet side, that is to say on whether an adsorption or a desorption process is involved. The adsorption and desorption isothermals of Fig. 1 were measured at a temperature of

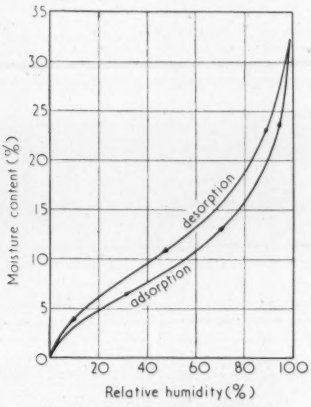

Fig. 1. Sitka spruce isothermal

25° C; at higher temperatures, the amount of water held at a given relative humidity decreases and the hysteresis loop becomes narrower. Fig. 1 refers to Sitka spruce, but the curves are approximately applicable to many other woods; for some species, however, the curves are appreciably different, although still of the same general shape.

As the moisture content increases, the adsorption curve gradually approaches the 100% relative humidity line. It was formerly thought that the intersection of the curve with this line corresponded with a moisture content known as the fibre saturation point, and taken to be the moisture content at which wood contained its maximum amount of adsorbed water but no free water, or alternatively as the moisture content above which certain physical properties no longer change with changes in moisture content. More recently, closer examination has shown that the concept of fibre saturation point is not an exact one, since, for instance, by increasing the accuracy with which the humidity is measured, the estimated moisture content at the apparent point of intersection can be increased considerably. Nevertheless, as an approximate concept, the fibre saturation point is still useful, because at moisture content in the region of 30%, the equilibrium relative humidity approaches 100%, showing that the water in the wood is approaching the free state. Further, many physical properties vary much less rapidly with moisture content at moisture contents above about 30% than at lower ones.

Almost every physical property of wood is affected by change in moisture content. The physical dimensions are an example, because wood swells with an increase and shrinks with a decrease in moisture content and the behaviour of wooden articles in use is determined to a large extent by this property. One of the main objects of seasoning timber is to decrease the moisture content, preferably to the value the timber will reach in service. In this way, dimensional changes of the manufactured article are reduced to a minimum and later troubles such as the sticking of drawers and the warping of doors are largely avoided.

The second important attribute of wood is its anisotropy. In isotropic materials, the physical properties are independent of direction within the material. This is not true of wood, or of certain other materials such as reinforced concrete, paper, and substances in the form of single crystals. The anisotropy of wood with respect to some properties is very marked, and in particular it is possible to show anisotropic elastic effects more clearly on wood than on other substances.

Fig. 2 shows the main structural features on a segment of temperate-zone hardwood. The annual rings, as their name implies, are formed by the wood laid down during the course of the year. The spring wood develops during the period of rapid growth and contains a number of large vessels, which become smaller as the growing season proceeds, so that the summer wood is denser and stronger than the spring wood. The rays, which run from the centre of the tree to the outside, form another prominent structural feature. In the living tree, they serve to store food material.

It is usual in discussing the physical properties of wood to idealize the structure and to assume that the physical behaviour is determined by the existence of three mutually perpendicular

* Based on a lecture given to the Midland Branch of The Institute of Physics on 26 April, 1956.

principal directions, the longitudinal direction, parallel to the axis of the tree; the radial direction, running from the centre of the trunk to the circumference; and the tangential direction, tangential to the growth rings. This assumption is, of course, only a first approximation, but in spite of its obvious shortcomings, it is possible to use such a model to interpret quite satisfactorily many aspects of the physical behaviour of wood.

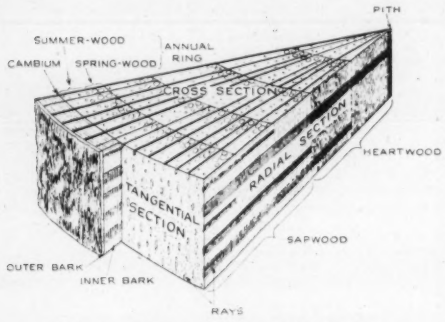

Fig. 2. Diagram of segment of hardwood

In isotropic materials, the physical properties are specified by a limited number of physical constants, for example, by one thermal expansion coefficient, one thermal conduction constant, one dielectric constant and two elastic constants. The properties of an ideal material possessing the three perpendicular symmetry directions require a larger number of constants for their specification, for example, three thermal expansion coefficients, three thermal conduction constants, three dielectric constants, each constant having a definite value for each of the principal directions.

The same number of constants is also needed to specify the shrinkage, and Fig. 3 shows the effect of moisture content on the radial and tangential shrinkage of wood. Above about 20% moisture content, there is considerable hysteresis in the shrinkage curves; longitudinal shrinkage is generally negligible, but may be appreciable in wood formed under abnormal conditions of growth. The shrinkage and swelling of beech are relatively high; among a series of timbers grown in the United States, the highest values were observed on hickory (11% tangential, 7% radial, not very different from beech) and the lowest were observed on a cedar (tangential 5%, radial 2%, less than half the values for beech).

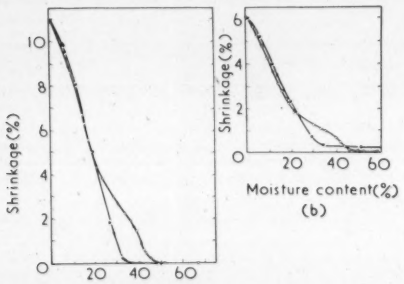

[Reproduced from *Forestry*]

Fig. 3. Relation between shrinkage and moisture content of beech: (*a*) tangential shrinkage; (*b*) radial shrinkage (after W. C. Stevens)

○ desorption ● adsorption

The number of independent constants needed to specify the elastic behaviour completely is nine—three Young's moduli corresponding with extensional stresses in the principal directions, three shear moduli corresponding with shear stresses in the principal planes, and three Poisson's ratios, corresponding with the ratio of lateral to extensional strain in the three principal planes. Naturally, this number of constants considerably complicates both theoretical and experimental work on the elastic properties of wood.

The physical properties so far mentioned are defined in terms of vector or tensor relations. Other properties, of which density and specific heat are examples, are scalar quantities and there is no increase in their number on passing from isotropic to anisotropic materials.

The density of wood is very important in that it provides an index to the magnitude of the physical properties. This is not to say that all physical properties can be inferred from a knowledge of density alone. In any case the moisture content would also have to be known, but some properties, for instance, dielectric constant and thermal conductivity, are very closely related to density; others such as some of the elastic and strength properties show only a broad general relationship; still others such as power factor and the remaining strength and elastic properties show little dependence on density at all. It is important to realize that the physical properties of a single species at a single moisture content may show considerable variability, and for some purposes a measure of the spread such as the standard deviation should be quoted, as well as the mean value. Fig. 4 shows a frequency distribution curve for density of Sitka spruce and indicates that for this set of specimens the density ranges from 0·24 to 0·5 g/cm^3. The mean density of different woods ranges

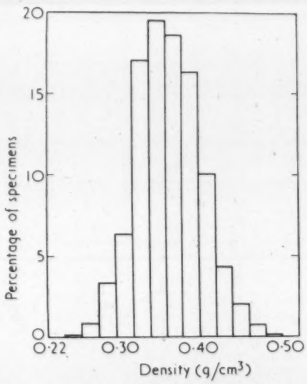

Fig. 4. Frequency distribution of density in Sitka spruce (after F. Kollmann)

from about 0·16 g/cm³ for balsa to 1·3 g/cm³ for lignum vitae.

THERMAL AND ELECTRICAL PROPERTIES

The effects of moisture content, anisotropy and density may be illustrated by considering in turn the thermal, the electrical, and the elastic properties of wood. The properties principally involved in the thermal behaviour are the specific heat and the thermal conductivity; the specific heat determines the amount of heat required to raise wood through a given temperature range, and the thermal conductivity, in conjunction with the specific heat and density, determines the time required to heat up pieces of wood of various shapes in such applications as the steaming and the radio frequency heating of wood. The thermal conductivity is also an important factor in assessing the thermal insulation of wood.

Specific heat is a scalar quantity and is therefore independent of the direction in which it is measured. Fig. 5 shows the

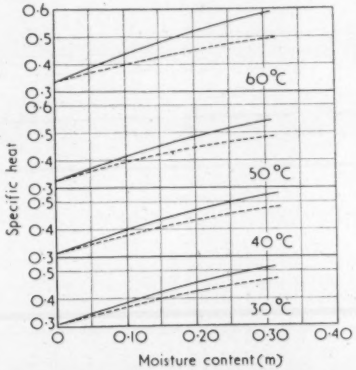

[Reproduced from *Chemistry and Industry*]

Fig. 5. Specific heat of beech flour as affected by temperature and moisture content

dependence of specific heat on the moisture content and temperature. The solid lines represent the variation of observed specific heat with moisture content; the dotted lines are the specific heats calculated from the proportions and specific heats of the components assuming a simple mixture law. At all temperatures, the observed specific heats are higher, and this has sometimes been interpreted as showing that the specific heat of the sorbed water is greater than unity. Actually, the effect can be interpreted thermodynamically, without assuming any abnormality in the specific heat of water. If the sorption of water by wood is regarded as a chemical reaction, then the heat evolved when water is sorbed can be identified with the heat of reaction. A well-known thermochemical equation due to Kirchhoff states that the excess heat capacity of the products of a chemical reaction over the combined heat capacities of the initial components is equal to the variation of heat of reaction with temperature. In Fig. 6, the heat of sorption of water by wood is plotted against temperature at four moisture contents, and from these curves the change in heat of sorption with temperature can be found. Table 1 shows the comparison between the excess of observed over calculated specific heat (Δc), and the change in heat of sorption with temperature. The divisor $(1 + m)$, where m is the moisture content in grammes per 1 g of dry wood, is required because the

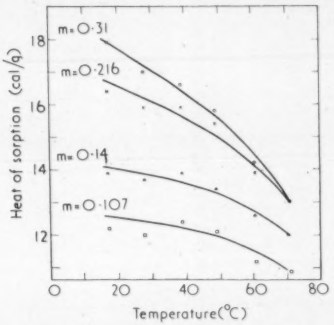

Fig. 6. Heat of sorption of beech flour as affected by moisture content and temperature

Kirchhoff equation refers to heat capacities, and in Table 1 the comparison is with specific heat. The agreement between corresponding figures in the last two columns of Table 1 is good and justifies the application of the Kirchhoff equation.

Table 1. *Thermal properties of wood*

m	T(°C)	Δc	$(\partial \Delta H/\partial T)/(1+m)$
0·107	30	0·02	0·02
	40	0·02	0·02
	50	0·02	0·03
	60	0·04	0·05
0·140	30	0·02	0·02
	40	0·03	0·03
	50	0·03	0·04
	60	0·06	0·05
0·216	30	0·03	0·03
	40	0·04	0·04
	50	0·05	0·06
	60	0·08	0·07
0·310	30	0·04	0·05
	40	0·05	0·06
	50	0·06	0·07
	60	0·09	0·09

This example is of interest as showing that when interpreting the effect of moisture content on physical properties of wood, secondary effects such as the change in heat of sorption with temperature may have to be taken into account. The excess specific heat observed on wood is also found with many other hygroscopic materials, for example gelatin, plastics and dried foods, and the same intepretation probably holds for these materials as well.

In contrast with specific heat, the thermal conductivity of wood is a directional property. The thermal conductivity across the grain is numerically about half the conductivity along the grain. The radial conductivity is usually slightly

higher than the tangential conductivity but as a rule this difference is negligible, and for most purposes wood can be regarded as having two thermal conductivity coefficients only, one transverse and the other longitudinal.

The thermal conductivity, moisture content and density of wood are closely inter-related. This relationship can be exhibited in the form of a nomogram as in Fig. 7. The

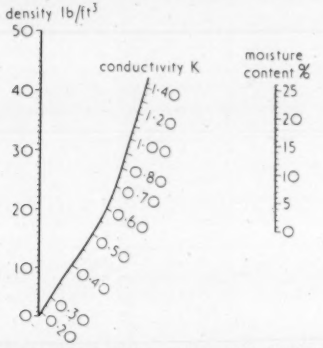

[Reproduced from *Heating, Piping and Air Conditioning*]

Fig. 7. Nomogram for thermal conductivity of wood (after F. Wangaard). Density = lb dry wood per ft³ at time of test. Thermal conductivity K = B.t.u./°F/ft²/in./h. Moisture content = 100 × wt. of water/wt. of dry wood

transverse conductivity is estimated simply by laying a straight edge between the appropriate values of density and moisture content and reading off the value of the conductivity on the middle scale. The nomogram was constructed from results obtained on American timbers, and in Fig. 8 the observed

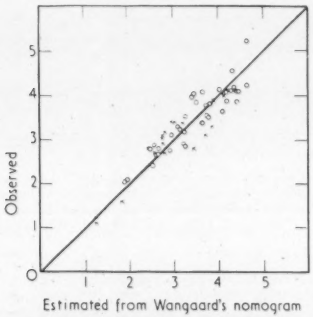

Fig. 8. Comparison of observed and predicted thermal conductivities (× 10^4 c.g.s. units)
× Griffiths and Kaye; van Rest
○ Narayanamurti and Ranganathan

values on Indian timbers (circles) and British timbers (crosses) are compared with those derived from the nomogram. The correspondence is quite close, and the nomogram can therefore be used with considerable confidence to predict the thermal conductivity of timbers for which actual numerical values are not available.

The electrical properties of wood are of interest in connexion with the determination of moisture content by electrical means and with the heating of wood by radio-frequency methods. So far as direct currents are concerned, the only property involved is the resistance, or its inverse, the conductivity. The conductivity in the longitudinal direction is about twice the conductivity in the radial or tangential directions. The outstanding feature of the electrical conductivity of wood, however, is its extraordinarily large variation with moisture content. Fig. 9, in which

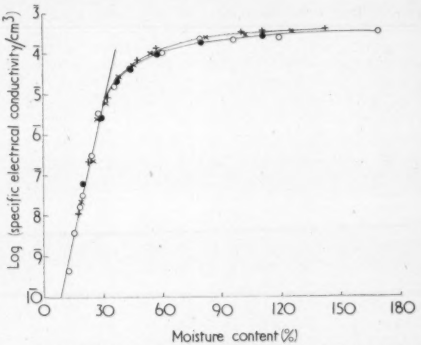

[Reproduced from *Industrial and Engineering Chemistry*]

Fig. 9. Effect of moisture content on the specific electrical conductance of redwood (after A. J. Stamm)
○ green ● same specimen oven-dried and resoaked
× green + same specimen oven-dried and resoaked

conductivity is plotted on a logarithmic basis, shows that the conductivity increases by about a millionfold between 10 and 80% moisture content.

The behaviour of wood with respect to alternating currents is more complex. In radio frequency heating the wood is often placed between two plane parallel electrodes and

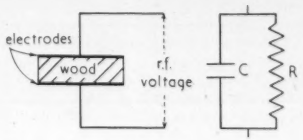

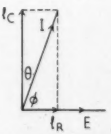

Fig. 10. Radio frequency heating
$P \propto E^2 fK \tan\theta$

therefore forms the dielectric of a condenser as shown in Fig. 10. The behaviour of the wood can be represented by a resistance in parallel with a condenser, and associated with these two circuit components are two quantities, usually taken as dielectric constant or relative permittivity (K) and loss tangent ($\tan\theta$), by means of which the dielectric properties of the material are specified. The power developed in the material is approximately proportional to $E^2fK\tan\theta$ where E is the applied voltage and f is the frequency of the alternating current. In wood, the loss tangent is usually small, and is then negligibly different from the power factor ($\cos\phi$). The permittivity and loss tangent of wood depend on a number of factors such as species, grain direction, moisture content, frequency and temperature; in general, the permittivity and loss tangent measured under given conditions in the longitudinal directions are very roughly one and a half times the transverse values. The radial values are usually a few per cent higher than the transverse ones.

Fig. 11 shows the results of some typical measurements of these quantities. Figs. 11(*a*, *b* and *c*) refer to measurements taken in the radial direction and Fig. 11(*d*) to tangential measurements. The diagrams show that the permittivity changes regularly with changes in moisture content and frequency [Fig. 11(*a*)] and is closely related to density [Fig. 11(*b*)]. There is no such close connexion between loss tangent and density, and Figs. 11(*c*) and (*d*) therefore refer

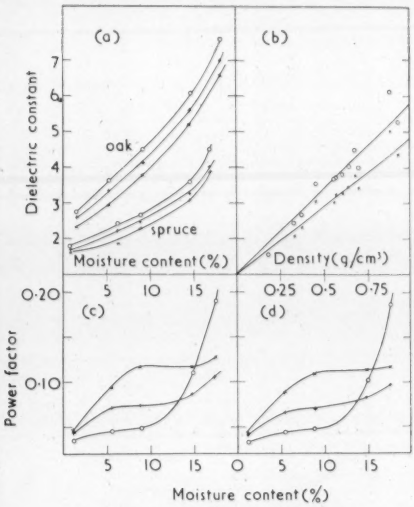

Fig. 11. Dielectric properties of wood
○ 1 Mc/s; + 10 Mc/s; × 100 Mc/s

to loss tangent averaged over twelve species. It will be seen that the shape of the moisture content-loss tangent curve depends very markedly on frequency and at the highest frequency there is some evidence of a maximum at about 10% moisture content, followed by a minimum at about 15% moisture content. More detailed measurements carried out on Scots pine have confirmed that there is a maximum; one implication of its existence is that any method of moisture measurement based on loss tangent at high frequencies would give ambiguous indications, and if loss tangent or any associated quantity is to be used for moisture measurement, the frequency should be kept below about 1 Mc/s.

ELASTIC PROPERTIES

As mentioned earlier, the complete specification of the elastic behaviour of wood requires nine independent elastic constants. Hitherto the elastic constants have mostly been measured on large-scale testing machines and these tests are usually destructive. Furthermore, the constant almost invariably measured is the modulus of elasticity along the grain, and it is not easy to control the conditions of exposure of the specimens when investigating the effect of temperature and moisture content on the elastic constants. For these reasons, some attention has been paid to the development of simple, non-destructive tests for the measurement of elastic constants. One such test is illustrated in Fig. 12. A strip

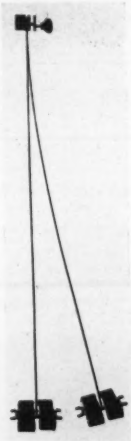

Fig. 12. Vibration method for measuring Young's modulus of wood

of wood, clamped vertically with a weight at the end, is set into flexural vibration and the frequency timed with a stopwatch. The modulus of elasticity is calculated from the frequency of vibration, the dimensions of the strip and the weight attached to the free end. Fig. 12 is a double exposure photograph, one exposure being taken with the strip stationary and the second near the extremity of the swing with the strip in vibration. The method shown in Fig. 12 has been applied to the investigation of the effects of temperature and humidity by suspending a number of strips inside a space, the humidity and temperature of which could be varied as required over wide ranges, and by making measurements of the frequency of vibration at different temperatures and humidities, the effect of these factors on the elastic constants was determined.

Fig. 13 shows some of the results obtained. In these graphs the Young's modulus is plotted against temperature at four relative humidities—30, 60, 80 and 90%. At the

lower humidities, the relationship between Young's modulus and temperature is linear, but at the higher humidities this is not so and the modulus-temperature relationship is noticeably curved. The general effect of moisture content on the

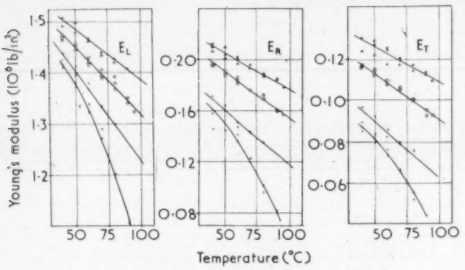

Fig. 13. Effect of temperature and relative humidity on Young's moduli of beech

△ 30% r.h.; ○ 60% r.h.; × 80% r.h.; + 90% r.h.

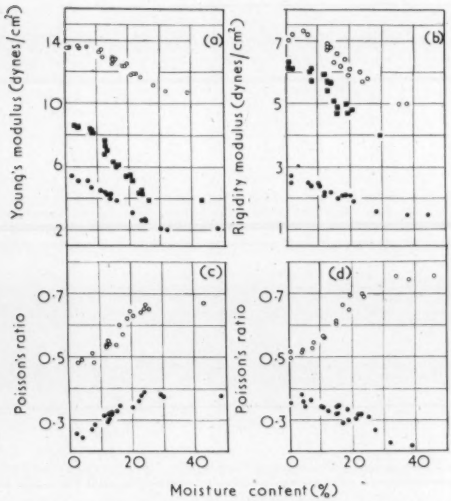

Fig. 14. Effect of moisture content on elastic constants of Sitka spruce (after H. Carrington)

(*a*) ○ $10^{-10}\,E_L$ ■ $10^{-9}\,E_R$ ● $10^{-9}\,E_T$
(*b*) ○ $10^{-9}\,G_{RL}$ ■ $10^{-9}\,G_{TL}$ ● $10^{-8}\,G_{TR}$
(*c*) ○ σ_{RT} ● σ_{TR}
(*d*) ○ σ_{LT} ● σ_{LR}

elastic constants is shown in Fig. 14. The Young's moduli and shear moduli all decrease with increasing moisture content, but some of the Poisson's ratios increase. These curves illustrate a point mentioned previously, that above about 30% moisture content, the physical properties often change very little with moisture content.

The assumption of three perpendicular principal axes places wood in the same category as orthorhombic crystals. The behaviour of such crystals was first investigated theoretically and experimentally nearly a century ago, and equations were derived expressing the variation of elastic constants with orientation relative to the principal directions. Fig. 15 compares the observed values of Young's modulus

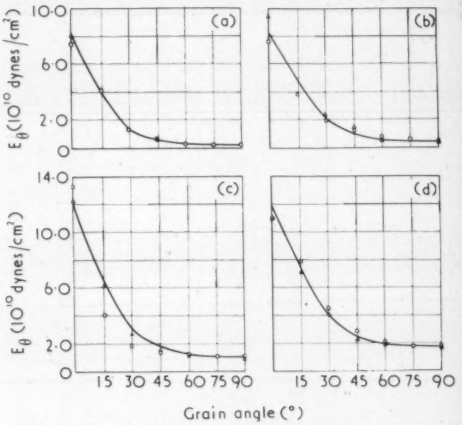

Fig. 15. Effect of grain direction on the Young's moduli of beech and Sitka spruce

(*a*) *E* Sitka spruce TL plane (*b*) *E* Sitka spruce RL plane
(*c*) *E* Beech TL plane (*d*) *E* Beech RL plane
——— theoretical
□ △ } observed

of wood as a function of grain direction with the theoretical values calculated from the equations appropriate to rhombic crystals and shows that the theoretical equations give quite a good representation of the observed values.

The elastic constants encountered in ordinary isotropic theory, Young's modulus, shear modulus, and Poisson's ratio are shown in Fig. 16. There is an additional constant,

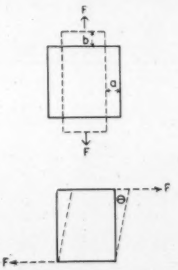

Fig. 16. Elastic constants of an isotropic material

Young's modulus $E = F/b$
Poisson's ratio $\sigma = a/b$
Rigidity modulus $G = F/\theta$

the bulk modulus which is not shown but, in an isotropic material, only two of the elastic constants are independent; there is, for example, the relation

$$G = E/2(1 + \sigma)$$

between shear modulus G, Young's modulus E, and Poisson's ratio σ. In isotropic materials, the effects of extensional and shear stresses are clearly differentiated; an extensional stress produces an extensional strain in the direction of the applied stress, and a perpendicular lateral contraction, whereas a shear stress produces an angular deformation. This differentiation also holds for wood specimens when the stresses act along or perpendicular to the grain, but if the stresses act at any other angle, then an extensional stress, besides producing an extensional strain, also produces a shear strain and *vice versa*. This coupling between shear and extension implies a coupling between torsion and flexure as shown in Fig. 17, which is a photograph of loaded strips

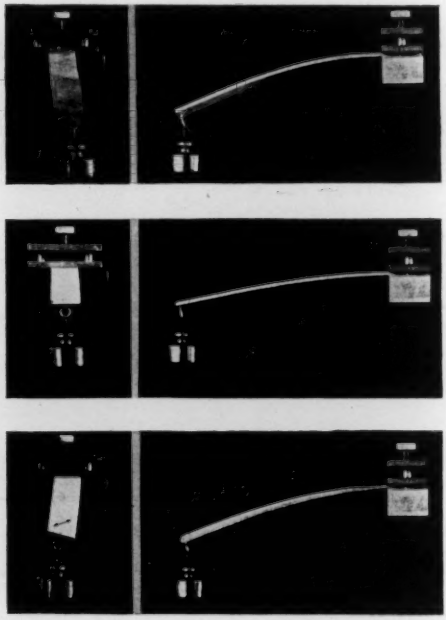

Fig. 17. Coupling between torsion and bending in wood strips

of two-ply. In the upper strip, the grain of both plies is at 45° to the axis of the strip and in the lower strip the grain is also at 45°, but in the complementary direction. The middle strip is made up of two 45° plies with the grain directions crossed at 90°. The twist of the upper and lower strips under the influence of a pure bending stress, and the absence of twist in the middle strip can be clearly seen. It is noticeable, too, that under a given bending stress, the end deflexion of the middle strip is less than that of the other two, so that the crossing of the plies has led to a stiffening of the material.

One of the applications of the elastic constants is to the calculation of the behaviour of wood and particularly plywood plates under load. It is necessary to modify standard elastic theory to allow for the anisotropic nature of the material, but when this is done, equations can be obtained for critical buckling stresses, deflexion under concentrated and uniformly distributed loads, and frequency of vibration of plywood plates.

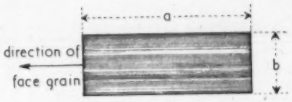

Fig. 18. Frequency of vibration of plywood plates

$$\nu_c = \frac{1{\cdot}04\,h}{a^2\sqrt{\rho}}\left[E_1 + \left(\frac{a}{b}\right)^4 E_2 + \left(\frac{a}{b}\right)^2 (0{\cdot}57E_1\sigma_{21} + 1{\cdot}13G_{12})\right]^{\frac{1}{2}}$$

$$\nu_s = \frac{0{\cdot}456\,h}{a^2\sqrt{\rho}}\left[E_1 + \left(\frac{a}{b}\right)^4 E_2 + \left(\frac{a}{b}\right)^2 (2{\cdot}00E_1\sigma_{21} + 3{\cdot}96G_{12})\right]^{\frac{1}{2}}$$

As a rule the equations obtained by applying exact elastic theory are extremely cumbersome, if obtainable at all, and it is often preferable to derive the results by approximate methods, for example by the Rayleigh or Rayleigh–Ritz procedure. Fig. 18 shows the equations obtained by the Rayleigh method for frequency of transverse vibration of a wooden plate. ν_c is the frequency with all edges clamped,

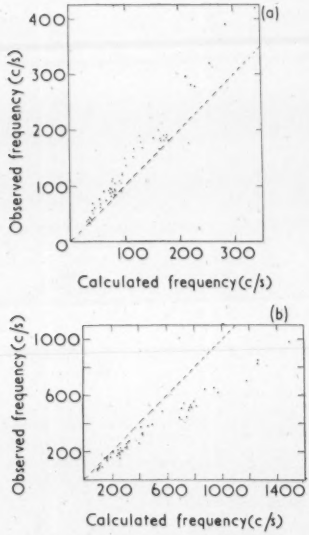

Fig. 19. Comparison of observed and calculated frequencies of vibration of plywood plates

(*a*) supported edges (*b*) clamped edges

v_s is the frequency with all edges supported, E_1 and E_2 are the Young's moduli along and across the face grain, σ_{21} is the Poisson's ratio corresponding to stress in the face grain direction, and G_{12} is the shear modulus corresponding to shear stresses along the edges of the plate.

The comparison between the theoretical and observed frequencies is shown in Fig. 19. For supported edges the observed frequencies are rather higher than the calculated ones and for clamped edges they are rather lower, but the agreement is reasonable on the whole. It is probable that the discrepancies arise not from any inaccuracy in the theory, but from the difficulty of realizing experimentally the mathematical conditions assumed to exist at the edges of the plate, and it appears that in the experiments to which Fig. 19 refers, the actual conditions at the edges of the plates were always intermediate between those assumed for supported and for clamped edges.

The frequencies of vibration were measured with an arrangement illustrated diagrammatically in Fig. 20. This figure actually shows the specimen to be a wooden beam vibrating as a cantilever, but with suitable modification, the apparatus can also be used to measure the frequency of vibration of plates. In Fig. 20, the beam has two iron plates

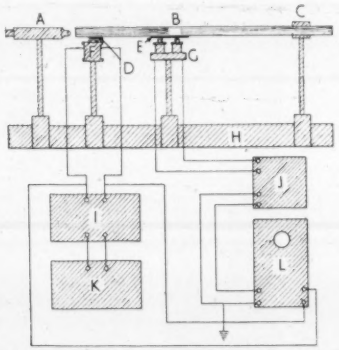

Fig. 20. Apparatus for measuring frequency of vibration

A, microscope; *B*, wood strip; *C*, clamp; *D*, *E*, thin iron plates; *F*, driving coil; *G*, telephone receiver; *H*, optical bench bar; *I*, driving amplifier; *J*, response amplifier; *K*, oscillator; *L*, cathode-ray oscillograph.

attached to it, one above the driving coil and the other above a telephone receiver. The driving coil is fed with amplified current from a variable frequency oscillator, and any response induced in the telephone receiver is amplified and passed to the vertical plates of an oscilloscope. The experiment consists in varying the frequency of the driving current until the response as indicated on the oscilloscope screen is a maximum, and calculating the Young's modulus from the resonant frequency and dimensions of the specimen. It is also possible to measure the damping capacity of the specimen by detuning slightly from the resonant frequency and measuring the corresponding change in response. Methods essentially the same as that illustrated in Fig. 20 have been widely used recently for measuring damping capacity and Young's modulus of wood. However, it is known that the resonant frequency is affected to some extent by the occurrence of shear in the vibrating specimen, and it is therefore of interest to examine the effect of shear more closely. For this purpose, it is convenient to work with free-free specimens suspended by loops of thread at the nodal points, because with this type of suspension, it is possible to realize experimentally end conditions which agree with those assumed in the theoretical development.

The theory of the flexural vibrations of such beams was worked out by Rayleigh who obtained the formula

$$f_r = \frac{im^2}{2\pi l^2}\sqrt{\frac{E}{\rho}}$$

for the frequency of vibration f_r, where i is the radius of gyration of cross section, l the length of the specimen, E the Young's modulus, ρ the density, and m a pure number given in terms of mode number p by $m = 4{\cdot}730$ for $p = 1$ (the fundamental), and to sufficient accuracy for higher values of p by

$$m = (2p + 1)\pi/2.$$

Rayleigh's treatment assumes pure bending, but as the slenderness ratio (the ratio of i to l) increases and as the order of the mode increases, the deformation includes more and more shear. The differential equation for the vibration taking shear and rotatory inertia into account was first thoroughly discussed by Timoshenko in 1922, and since that time many workers have obtained solutions for various end conditions and have used various methods for evaluating and presenting the solution in a form convenient for practical calculation. According to the solution obtained by Goens in 1931, the true frequency f_g for a free-free beam is

$$f_g = f_r/\sqrt{T}.$$

The quantity T is given by

$$T = 1 + \frac{i^2}{l^2}\left[F_1(m) + \frac{sE}{G}F_2(m)\right] - \frac{4\pi^2\rho s i^2 f_0^2}{G}, \qquad (1)$$

where s is a factor depending on the distribution of shear stress over the cross-section and has the value 1·2 when the cross-section is rectangular, f_0 is the observed frequency, G is the shear modulus, $F_1(m)$ and $F_2(m)$ are known functions of m which can be tabulated once and for all. The last term in equation (1) is an approximate correction term which is small in magnitude, and T therefore depends mainly on the slenderness ratio i/l, the ratio of E to G, and the known functions of m.

In order to check the theoretical results, experiments have been carried out on two beams of beech. The length of each beam lay in the longitudinal direction of the wood. In one cross-section *A*, Table 2, the greater dimension coincided with the radial direction of the wood; in the other *B* it coincided with the tangential direction. Each specimen could be vibrated with the plane of vibration parallel either to the larger or the smaller dimension of the cross-section. If in beam *A* the vibrations are parallel to the larger cross-sectional dimension the shear modulus involved is the one in the *RL* plane of the wood; if the vibration is parallel to the smaller cross-sectional dimension, the shear modulus is the one in the *TL* plane of the wood, and *vice versa* for beam *B*.

Table 2 gives some of the results, and shows that the Rayleigh frequency (f_r) is always greater than the observed frequency (f_0). As the mode number p increases, the difference between the two frequencies also increases, and for the highest modes of vibration, f_r may be more than double f_0.

Table 2. *Study of vibration properties of a sample of beech 75 cm long*

E and G in dynes per cm^2; f in cycles/second.

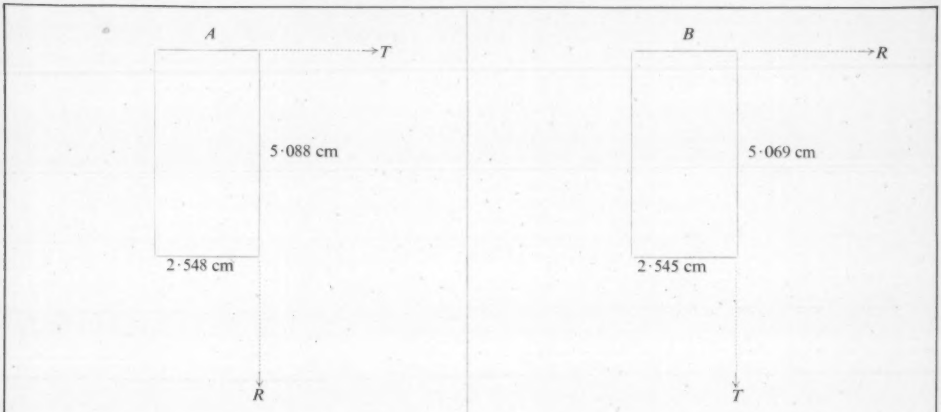

T vibrations

$E = 1{\cdot}414 \times 10^{11}$; $G = 0{\cdot}089 \times 10^{11}$

p	f_r	f_0	f_g
1	214·1	210·3	211·4
2	590·1	567·4	564·1
3	1157	1066	1058
4	1912	1659	1654
5	2857	2336	2323
6	3990	3030	3039
7	5312	3785	3783
8	6823	4544	4543
9	8523	5313	5314
10	10411	6048	6085
11	12488	6860	6854

R vibrations

$E = 1{\cdot}256 \times 10^{11}$; $G = 0{\cdot}169 \times 10^{11}$

p	f_r	f_0	f_g
1	199·6	195·9	198·2
2	550·1	521·0	537·2
3	1078	1036	1027
4	1783	1641	1648
5	2663	2371	2373
6	3720	3156	3188
7	4952	4063	4069
8	6361	4956	5001
9	7945	5914	5974
10	9706	6823	6978

R vibrations

$E = 1{\cdot}401 \times 10^{11}$; $G = 0{\cdot}153 \times 10^{11}$

p	f_r	f_0	f_g
1	425·5	411·6	411·5
2	1173	1065	1058
3	2300	1904	1896
4	3801	2840	2839
5	5679	3839	3832
6	7931	4841	4845

T vibrations

$E = 1{\cdot}258 \times 10^{11}$; $G = 0{\cdot}092 \times 10^{11}$

p	f_r	f_0	f_g
1	397·5	381·0	380·0
2	1096	955	953
3	2148	1676	1663
4	3552	2418	2430
5	5305	3232	3213
6	7410	3976	3995
7	9865	4738	4770
8	12670	5497	5538
9	15830	6271	6301
10	19340	7105	7060

From the observed frequencies and the equation for T, it is possible to derive values of E and G by a least squares procedure. These values are given at the head of the appropriate sections of Table 2. The variation among the values of E shows that the material was neither perfectly homogeneous nor perfectly matched, but nevertheless there is good agreement between the corresponding values of G. If these values of E and G are used to calculate f_g the agreement with f_0 is very close throughout (Table 2), and it appears that the Goen's method, although put forward only as an approxi-

mation, nevertheless represents the results very well up to at least the 10th or 11th mode.

Although this work was carried out with wood as the test material, the results are actually applicable over a much wider field, since the calculation of the vibration frequency of bodies having various shapes, sizes and physical properties is one of the fundamental problems of acoustics, and, moreover, is of general engineering interest.

Another problem of general interest is the connexion between elastic stability and frequency of vibration. It has been suggested that the critical load of a complex structure might be determined non-destructively by subjecting the structure to a series of loads, measuring the natural frequency corresponding to each load, and estimating the critical load by extrapolating the observations to zero frequency. The method illustrated in Fig. 12 lends itself to testing this suggestion. In the photograph, the attached weight is below the point of suspension, the stress in the strip due to the attached weight is always tensile, and the question of elastic instability does not arise. If, however, the weight is above the clamp, the stress is compressive, and at a certain value of the stress, the system will become elastically unstable. Application of Rayleigh's method to the system leads to the equation

$$(\omega/\omega_0)^2 = 1 - Pl^2/2{\cdot}5EI, \qquad (2)$$

where ω is the angular frequency and of vibration under stress P, ω_0 is the frequency in the absence of stress, E is Young's modulus, I is the moment of inertia of cross-section and l is the length of the strip. If $\omega = 0$

$$P = 2{\cdot}5EI/l^2, \qquad (3)$$

compared with the Euler value for the critical load of a fixed-free strip

$$P_{cr} = \pi^2 EI/4l^2 = 2{\cdot}468EI/l^2. \qquad (4)$$

The assumption that the load at zero frequency is the critical load therefore leads to a reasonable theoretical estimate, since the difference between the numerical coefficients in equations (3) and (4) is small and can be attributed to the approximate nature of the Rayleigh analysis.

Equation (2) predicts that the square of the frequency ratio should give a straight line when plotted against P, that the frequency ratio should be 1 at zero stress, and the load at zero frequency should be the Euler load. Fig. 21 shows some experimental results plotted on this basis, and the agreement with theory is very satisfactory. The line is straight, it intersects the vertical axis at 1 and the horizontal axis at a point very close to the Euler load and it would evidently be possible to predict the critical load for this simple well defined system from frequency observations. The question of the applicability of the method to more complicated systems, however, remains an open one, although some American results are quite promising.

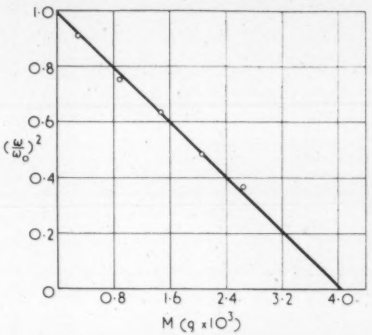

Fig. 21. Frequency of vibration and elastic stability

boxwood : l = 45 cm
intercept = 4050 g
$\pi^2 EI/4l^2 g$ = 4163 g

CONCLUSION

Owing to limitations of space, a number of applications of physics to wood have not been dealt with here. Among these may be mentioned the movement of liquids and gases, particularly water and water vapour, through wood, and the anelastic properties, particularly creep and stress relaxation, topics on which work is being actively pursued in Forest Products and other laboratories in various parts of the world. Only a few applications of the newer physics have been made. These include the use of X-rays and the electron microscope for studying the fine structure of wood and the use of X-rays and supersonics for non-destructive testing. The penetration of liquids has been followed by a radio active tracer technique and electronic methods have been found useful in detecting the presence of insects and metallic objects in wood. Thus, although the older physics has been found the more useful, the newer techniques and equipment have not been neglected, and it is possible that they will find increased application in the not too distant future.

ACKNOWLEDGEMENT

Some of the work described above has been carried out as part of the programme of the Forest Products Research Board, and is published by permission of the Department of Scientific and Industrial Research.

A

The standardization of X-ray output in industrial radiology

By R. S. Morgan, B.Sc., A.Inst.P., R. Halmshaw, B.Sc., A.R.C.S., A.Inst.P., and B. J. Ratcliffe, Armament Research and Development Establishment, Woolwich, London

[*Paper first received* 9 *July, and in final form* 29 *August*, 1956]

Variations in the output of radiation from different X-ray sets, when operated at the same nominal scale voltage, have been shown to be attributable to differences in the effective applied voltage. Such variations of output lead to difficulties in the standardization of radiographic techniques. More accurate calibration of the effective applied voltage has been shown to be required and it is suggested that considerable improvement could be obtained by calibrating the output of X-ray sets in terms of roentgens per minute and specifying exposures in roentgens.

It has frequently been suggested that the quotation of voltage and exposure factor (milliampere-minutes) for specifying X-ray techniques is inadequate because of variations between different X-ray tubes and between the different circuits employed in the high-tension generators. It is certainly true that difficulty has been encountered in transferring techniques from one set to another. Considerable variation in output necessitating appreciable changes in exposure times has been found between different sets of the same type. Errors in calibration may account for certain of these discrepancies, but it is apparent that variations associated with the X-ray apparatus also contribute.

In this investigation six X-ray sets have been compared for the quality and quantity of their output, and the possibility of standardizing X-ray techniques by defining the quality of radiation in terms of "half-value thickness" rather than voltage, and the quantity or output in roentgens rather than exposure factor (milliampere-minutes), has been explored.

APPARATUS

The following X-ray sets were available for comparison:

Set	*Nominal maximum voltage (kVp)*	*Circuit*
A	140	Villard: full-wave rectification.
B	150	Smoothed Villard: full-wave rectification with earthed anode.
C	220	Rectifier valve in transformer primary: half-wave rectification.
D_1	250	
D_2	250	
E	400	Fully rectified: constant potential.

A photoelectric instrument measuring both the quality and the quantity of X-rays, designed by Dr. Herz of Kodak Ltd. primarily for medical radiography, has been kindly lent by him to try on the above X-ray sets.*

EXPERIMENTAL DETERMINATION OF THE QUALITY AND QUANTITY OF TUBE OUTPUT

Quality: comparison of voltage settings and half-value thickness for various sets. Radiographs taken with the same X-ray set of a welded specimen of mild steel plate containing extensive porosity and fine cracks, suggested that a difference of 25 kV is needed to distinguish visually between radiographs taken at different voltages around 200 kV and less than 10 kV at 120 kV. A series of radiographs of the same weld taken at 120 kV nominal with X-ray sets *A*, *B*, *C* and *E* indicated that:

(1) provided the exposure is adjusted to give radiographs of the same density, the variation in the quality of the radiation emitted by the different X-ray sets, when operating at the same nominal voltage, is small and not likely to be significant in practice;
(2) the maximum variation between the sets at 120 kV is equivalent to a change of at least 10 kV.

In order the better to assess the significance of these observations and to provide a quantitative basis for comparison, the quality of the radiation of the six different installations has been measured in terms of the half-value thickness of steel.

A steel step-wedge placed at the centre of a large flat steel plate was radiographed at the same nominal voltage with the six X-ray sets and the exposure factor (milliampere-minutes) adjusted to give a fixed density under the thinnest step of the wedge. From the appropriate film characteristic curve and measurements of the film-density beneath the various steps of the wedge, derived curves of exposure-factor against steel-thickness could be obtained (Fig. 1). The steel thickness chosen was adequate to ensure that the straight line region

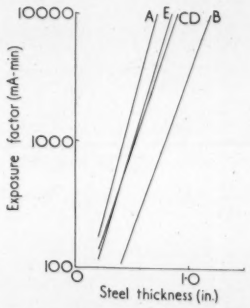

Fig. 1. Variation of exposure-factor with steel thickness for various sets at 120 kV nominal

A, Villard circuit; *B*, smoothed Villard circuit; *C* and *D*, primary half-wave rectification; *E*, constant potential.
Film, Ilford process; lead screens, 0·004 in. front, 0·020 in. back; focus-film-distance, 36 in.; development, D19b, 68° F for 5 min.

* Herz, R. H. *Brit. J. Radiol.*, **15**, p. 110 (1942).

of the exposure-curve was well-defined. The half-value thickness is then obtained from the slope of the straight line. The half-value thicknesses obtained for the different sets at various voltages are tabulated in Table 1.

Table 1. *Comparison of the quality of the radiations in terms of the half-value thickness of steel*

Installation	*Half-value thickness (in.)* 100 kV	120 kV	150 kV	200 kV
A	0·07	0·09	—	—
B	0·106	0·12	—	—
C	0·09	0·11	0·14	0·19
D_1	0·08	—	0·14	0·195
D_2	0·09	0·11	0·14	0·19
E	0·075	0·095	0·12	0·17

These results show definite differences in half-value thickness. At 120 kV the radiation emitted by set *B*, having a smoothed Villard circuit, is harder in quality than that emitted by the other sets. Set *A* with unsmoothed Villard circuit and set *E* with true constant potential emit radiation of practically the same quality, which is softer than that emitted by sets *C* and *D*, having simple half-wave rectification. Sets *C* and *D* do not differ significantly amongst themselves throughout the range of voltage.

The data from these experiments enabled an estimate to be made of the equivalent voltages of the different sets (Fig. 2).

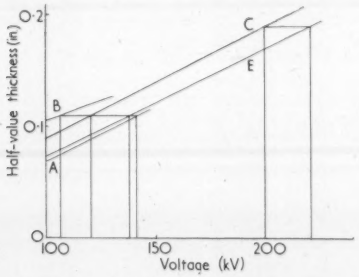

Fig. 2. Variation of half-value thickness with voltage for various sets

A, Villard circuit; *B*, smoothed Villard circuit; *C*, primary half-wave rectification; *E*, constant potential.

If sets *C* and *D* are operated at 120 kV, it is estimated that the same quality of radiation is obtained from set *B* operated at 105 kV nominal and from sets *A* and *E* at about 140 kV. Also, sets *C* and *D* at 200 kV are equivalent to set *E* operating at 220 kV. Radiographs of the welded specimen taken at these equivalent voltages with the exposures adjusted to give a constant film-density were indistinguishable.

While these differences based on careful densitometric measurements may appear large, their significance in relation to practical sensitivity in radiography is probably small. From the visual assessments of film contrast differences, obtained by radiographing the step-wedge at various tube voltages, it was estimated that the minimum detectable contrast difference at 200 kV was associated with a voltage change of 10 kV.

It can be shown that the change in the half-value thickness factor required to give the minimum detectable change in radiographic density for a given quality of radiation, is proportional to the square of the half-value thickness, i.e.

$$\Delta T = KT^2\Delta D \qquad (1)$$

where T is the half-value thickness and ΔD the minimum discernible difference in density.

Consider the absorption relation

$$I = I_0 e^{-\mu t} \qquad (2)$$

where μ is the linear absorption coefficient for the material and t its thickness.

It is easily shown that

$$\mu = 0{\cdot}693/T \qquad (3)$$

where T is the half-value thickness.

By substitution

$$I = I_0 \exp(-0{\cdot}693t/T) \qquad (4)$$

Differentiating with respect to T

$$dI/dT = 0{\cdot}693It/T^2 \qquad (5)$$

For a given film, over the straight line portion of the characteristic curve

$$G \log_{10} I = D + C$$

where G is the film gradient, D the density and C a constant.

Differentiating with respect to D

$$dI/dD = I/0{\cdot}4343G \qquad (6)$$

From equations (5) and (6)

$$dD/dT = 0{\cdot}301Gt/T^2 \qquad (7)$$

For a given thickness of material and over a restricted range of density we may write

$$\Delta T = KT^2\Delta D \qquad (8)$$

The argument assumes a linear relationship between half-value thickness and voltage, which is only approximately true over the extended range 100 to 400 kV. It also assumes the absence of scattered radiation within the specimen, but since the effect of scatter is to reduce contrast, the discernibility would be poorer, that is, larger voltage differences would be required in practice to be distinguished with certainty.

If we consider the voltage equivalents of the half-value figures and their increments and accept the minimum significant value of 10 kV at 200 kV, the calculated value at 100 kV is 2 kV and at 400 kV is 60 kV. The surprisingly high value at 400 kV has been checked experimentally. Fig. 3 shows the variation of film density against the thickness of steel for radiographs taken at 340, 360 and 400 kV.

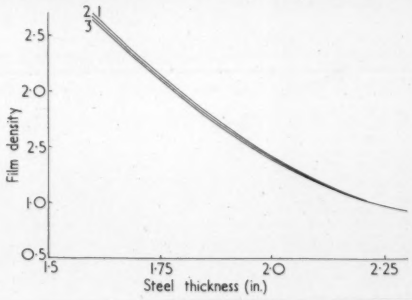

Fig. 3. Variation of film density with steel thickness

(1) 340 kV; (2) 360 kV; (3) 400 kV. Installation, 400 kV (constant potential).

The investigation of the quality of the output of six installations, at least at voltages between 100 and 250 kV, has shown that the differences in quality as measured with the step-wedge, even though greater than the minimum discernible difference, are not very significant in practice. Provided the exposure factors are adjusted to give radiographs of similar density from the different sets, the differences in radiographic contrast induced by operating the sets at the same nominal voltage are not sufficient to impair the quality of the radiographs.

Quantity: comparison of mA min ratings and roentgen output for various sets. The comparison of the output (quantity) of various sets from the relative exposure factors required to produce a given film density is open to considerable errors, arising from variables associated with the processing of X-ray films and from fluctuations of the applied voltage and tube current during long exposures. In order to obviate these difficulties the output of the various sets has been measured by means of an ionization chamber placed at a constant distance from the focus of the tube. A large flat plate of aluminium, 1 in. thick, was interposed between the tube and the ionization chamber close to the ionization chamber to represent a specimen, and to reduce differences due to different inherent filtrations. The results obtained are plotted in Fig. 4.

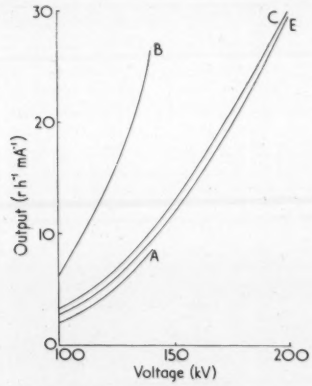

Fig. 4. Variation of quantity of radiation with nominal voltage for various sets

A, Villard circuit; *B*, smoothed Villard circuit; *C*, primary half-wave rectification; *E*, constant potential.
Filtration, 1 in. aluminium; anode-to-chamber distance, 36 in.

A single measurement obtained for comparison on a 400 kV set with a half-wave generator, gave a value of 86 r $mA^{-1}\,h^{-1}$ for the output at 400 kV (nominal).

These results show a large difference in the relative output between the different sets at 120 kV nominal, the difference being most marked in set *B* with the smoothed Villard circuit, which has a considerably greater output than any of the other sets. At this nominal voltage, the output of set *E* is very little different from that of set *C*. When the voltage is adjusted so that the same quality of radiation (equal half-value thicknesses) is obtained from the different sets, however, the position is changed. The corrected outputs derived from Fig. 4 are given in Table 2.

Table 2. *Comparison of output (quantity) at equivalent voltages*

Installation	*Equivalent voltage (kV nominal)*	*Output (r $mA^{-1}\,h^{-1}$)*
A	140	8·6
B	105	8·0
C	120	6·0
E	135	8·2

(Sets D_1 and D_2 do not differ significantly from each other or from set *C* either in the quality or quantity of their emission.)

It is apparent from the graphs that the variation of output (quantity) with voltage is the same for sets *A*, *C* and *E* at voltages to 200 kV (140 kV for set *A*); the respective graphs are parallel. The output of set *B*, however, increases much more rapidly with voltage. The output of set *E* increases more rapidly with voltage at voltages above 200 kV (not shown in Fig. 4).

These observations have been confirmed by measurements using an instrument incorporating a fluorescent screen and photocell circuit designed and lent by Dr. R. H. Herz. This instrument was designed to provide simultaneous measurement of both the quality and quantity of radiation but the sensitivity of quality measurement was not sufficient to determine consistently the variations discussed in the section dealing with the quality of the radiations. This is probably due to the fact that this instrument was designed for a range of kilovoltage considerably lower than that with which this work is mainly concerned.

DISCUSSION

The step-wedge exposures have demonstrated that there are measurable differences in the quality of radiation from different X-ray sets operated at the same nominal voltage. These differences have been measured in terms of half-value thicknesses, but expressed in equivalent voltage changes the maximum difference between the sets used is of the order of 35 kV at 120 kV and 20 kV at 200 kV. From step-wedge measurements it was estimated that minimum differences of 2 kV at 100 kV, 10 kV at 200 kV and 60 kV at 400 kV can be detected. These differences are based on contrast differences obtained with step-wedges, but in the radiography of specimens containing fine flaws such as cracks, the minimum detectable differences are much higher, and, with the specimen used in this work, were assessed as 25 kV at 200 kV and 10 kV at 120 kV, and, in fact, provided the radiographs are exposed to the same density it is difficult to discriminate between the radiographs from different sets.

The actual measured values of the half-value thickness appear anomalous in relation to the nominal voltage and the circuit involved and suggest discrepancies between the nominal scale voltage and the effective applied peak or constant potential. Table 3, in which set *A* is taken as the standard, illustrates this point.

Table 3. *Comparison of the quality of different sets operating at the same nominal voltage*

Set	*Circuit*	*Nominal voltage (kV)*	*Quality of radiation measured in terms of voltage on set A to give same h.v. thickness (kV)*
A	Villard: full-wave rectification	120	120
B	Smoothed Villard	120	153
C	Primary half-wave rectification	120	140
E	Constant potential	120	125

While the experimental radiographs of steel specimens indicate that the differences in quality may not, in general, lead to practical difficulties, the magnitude of these differences in equivalent voltages suggests that a better calibration of the effective applied voltage would be useful. This would be preferable to the measurement of half-value thicknesses, for although the latter are measurable, reliable and accurate measurements are tedious and time-consuming when film is used as the measuring medium.

The most significant source of variation between the various sets examined appears to be in the effective quantity of radiation emitted per milliampere, particularly when the sets are operated at the same nominal scale voltage. With the exception of the sets based on primary half-wave rectification circuits, the differences in output are less marked when the sets are operated at voltages which give the same quality of radiation, as determined by half-value thicknesses. Thus although our observations suggest that the differences in effective applied voltage and the consequent differences in quality of radiation are not significant in terms of radiographic quality, the rapid rise of roentgen output with increase in applied voltage means that the variations in applied voltage are the primary cause of the large variations in roentgen output. From this point of view more accurate calibration of the effective applied voltage is important.

Despite this argument, a considerable improvement in attaining consistency of technique with various sets could be attained by the practical expedient of specifying exposure in roentgens instead of milliampere-minutes or by calibrating sets in terms of roentgens per milliampere. It should not be difficult to provide suitable monitoring equipments which would enable this to be done.

ACKNOWLEDGEMENTS

The authors wish to express their thanks to Mr. B. D. Burns, under whose direction the work was undertaken, for valuable discussions. Crown copyright is reserved; this paper is reproduced with the permission of the Controller, H.M. Stationery Office.

A millisecond relaxation process in the reverse current of germanium point-contact diodes

By Prof. R. E. BURGESS, B.Sc.,* Radio Research Station, Slough, Bucks

[*Paper first received* 29 *March, and in final form* 4 *October*, 1956]

When a reverse voltage is suddenly applied to a germanium point-contact diode initially having zero bias it has been found that there is usually a decrease of current to the final steady value with a relaxation time of about 1 ms. Possible mechanisms for this process are discussed, and it is suggested that redistribution of surface charge is the most likely cause.

It is well known that if a reverse voltage is suddenly applied to a germanium point-contact rectifier which is initially biased in the forward direction there is a relatively large reverse current which decays in a time of the order of 0·1–10 μs to a steady value. The "reverse recovery effect" as it is sometimes termed is attributed to the removal by the reverse bias of the minority carriers injected into the germanium during the preceding forward current flow and the time constant of the process is closely related to the lifetime of the excess minority carriers, and always of the order of microseconds. The effect to be described is, however, appreciably slower and arises from a different physical mechanism.

OBSERVATIONS

In the observations of the reverse bias transient response the initial condition was chosen as that of zero bias in order to provide a well-defined equilibrium condition in which the electron and hole distributions conform to a uniform Fermi level.

Constant voltage pulses (from 0–20 V) with equal on and off periods were applied to the diode in the reverse direction at various recurrence frequencies ranging from 50–500 per second. The diode was connected as one arm in a bridge circuit with two resistive arms P and Q while the remaining arm consisted of a variable resistor S_2 in series with a shunt combination of a variable capacitor C and a variable resistor S_1. The bridge ratio P/Q was usually 200 and consequently nearly the full pulse voltage was applied to the diode. The bridge output was connected through a differential amplifier to an oscilloscope whose time base was synchronized with the pulse recurrence frequency. The amplifier had wide overload limits so that the initial short but intense spike due to the "reverse recovery effect" did not cause spurious effects during the pulse period.

The technique of observation consisted of adjusting S_2 so that there was zero bridge unbalance at the beginning of the pulse and then adjusting S_1 and C so that the magnitude and time constant of the decay of diode conductance were matched by those of the network CS_1S_2, resulting in null output during the pulse. The closeness with which a null could be achieved was a measure of the validity of the assumption that the diode conductance decayed with a single relaxation time.

If G_0 and G_s are the initial and steady-state values of the diode conductance then

$$G_0 = Q/PS_1 \quad \text{and} \quad G_s = Q/P(S_1 + S_2)$$

while the relaxation time is given by

$$T = CS_1S_2/(S_1 + S_2)$$

Thus if the instantaneous conductance $G(t)$ of the diode at time t after the application of the reverse bias had the form

$$G(t) = G_s + (G_0 - G_s)\exp(-t/T)$$

it could be perfectly balanced in the bridge described.

In order that the decay process be completed during a pulse period and yet be accurately observable the recurrence frequency was chosen to be about $1/10T$.

All the measurements were carried out at room temperature and the diodes were all of commercial manufacture and of various makers and types. Their turnover voltages were in the range 50–200 V and the reverse conductance at the

* Now at Dept. of Physics, University of British Columbia, Vancouver, Canada.

applied reverse pulse biases used in the tests lay between 0·5–20 micromho.

Of the units studied the majority showed a decreasing conductance after the application of reverse bias, the fractional decreases ranging from about 1–50% for voltages above 1 V but usually negligible for smaller voltages. The relaxation times lay between 0·3–2 ms. The effect was clearly a reversible one since the same recurrent pattern of conductance decay could be obtained for indefinite periods of observation, i.e. for many tens of thousands of pulses. During the process of conductance decay the current noise generated by the diode appeared to be substantially constant.

DISCUSSION

The diodes examined had electrically formed contacts to *n*-type germanium. As Waltz[1] has shown, the effect of forming is to produce thermal and/or impurity conversion of the *n*–Ge under the whisker to *p*-type and the resulting rectification properties reside primarily in the *p*–*n* transition since the metal to *p*-type contact is relatively non-rectifying.

Since the reverse currents of the diodes are increasing functions of temperature under the conditions of the experiments, the possibility of a thermal origin for the decreasing conductance seems to be excluded. Furthermore the power expended in the diode during the pulse never exceeded 10 milliwatts and was often of the order of 0·1 mW so that the rise in contact temperature would therefore be an insignificant factor.

The time scale of the conductance decay is too long for extraction by the reverse bias of mobile carriers in the region of the rather crude *p*–*n* junction produced by forming since this is known to be of order of 0·1–10 μs. On the other hand the millisecond effect is far too rapid to be attributable to the motion of ions in the bulk germanium.

Accordingly explanation is sought in terms either of the effect of a change of electronic occupancy of bound levels (in the bulk or on the surface) when the reverse bias is applied or to the motion of ions over the surface of the germanium. Broadly speaking the time variation of diode current could be due to one of two types of mechanism: either a removal of charge (which will equal the integrated value of the excess current) or to a true modulation conductance of the diode, e.g. by changes of potential distribution. The suggested possibilities will now be considered separately:

(*a*) *Charge flow to and from traps.* If bound levels in the semiconductor change their state of electronic occupancy on the application of bias there will be a flow of charge (i.e. electrons and holes entering or leaving the traps) which will last for a time of the order of reciprocal of the capture or ionization probability of the traps involved. If the apparent conductance decays from G_0 to G_s with a relaxation time T at diode voltage V the charge removed is

$$Ne = V(G_0 - G_s)T$$

In a typical case $V = 10$ V, $G_0 - G_s = 1$ micromho and $T = 1$ ms, corresponding to the removal of 6×10^{10} electrons. Now the volume from which this trapped charge was removed would at the most be of the order of that of a hemisphere of radius equal to the hole diffusion length in the *n*-type germanium. With a hole lifetime of 10 μs this volume would be $1{\cdot}7 \times 10^{-5}$ cm^3 and thus a mean density of electronic charge removal of 4×10^{15} cm^{-3} is required. Since not all traps will change their state of occupancy throughout this volume it is seen that the trap density must probably be at least 10^{16} cm^{-3} to account for the observed effect. Now in 5 ohm cm *n*-type germanium at 300° K the electron density is 3×10^{14} cm^{-3} and the hole density is 2×10^{12} cm^{-3} and it is impossible to postulate a consistent model with such a high density of suitable traps.

(*b*) *Current flow over the surface.* Law[2] showed that the very marked effect of adsorbed water on the reverse current of *p*–*n* junctions could be attributed to ionic conduction over the surface of the germanium. Thus it is possible that the transient excess conductance arises from the motion of adsorbed ions over the surface when the field due to the reverse bias is operative.

On applying a reverse bias to the whisker, the upper limit to the initial ionic conductance will be determined by the density distribution and mobility of the ions. The density has a maximum value of 10^{15} cm^{-2} for a monolayer and it is found that to account for an initial excess conductance of 1 micromho a mobility greater than 10^{-3} cm^2 V^{-1} s^{-1} would be required. The relaxation time for this conductance would be set by the approach to balance of the opposed effects of the electric field and of diffusion and electrostatic interaction. This is difficult to estimate although the overall charge displacement involved in the excess current pulse may be roughly deduced. If an initial uniform ion density n_0 over a surface area A is compressed into the limiting monolayer density the effective charge displacement is somewhat less than en_0A. Reasonable values of n_0 (e.g. 10^{14} cm^{-2}) and A (e.g. 10^{-3} cm^2) could therefore account for the charge displacements observed in practice.

One difficulty with the ionic hypothesis is the assumption that mobile positive and negative ions can exist stably on the germanium surface and can move in a reversible fashion under the applied field and yet not result in evolution of gas or in firm binding to the surface atoms.[3] An alternative hypothesis to ionic motion is one which is phenomenologically similar, namely the motion of electrons from one surface atom to the next; if the potential wells are not too deep (e.g. about 0·1 eV) this would appear like ionic motion with a charge mobility of the order of that inferred above.

(*c*) *Channel conductance.* An alternative surface leakage mechanism is the flow of carriers along a surface channel and this may occur on both *n*- and *p*-type germanium. Although carrier mobility will be lower in the channel than in the bulk when the channel width is small compared with the mean free path[4] it seems that this reduction would not be sufficient to account for a millisecond relaxation time. However, the surface levels (due, for instance, to oxidation) will relatively slowly change their charged state when reverse bias is applied, and this in turn will modify the channel characteristics and so modulate the surface conductance. In other words if it is a slow change of the surface leakage component of the reverse bias which we observe the ability of the surface states governing the leakage to receive and give up electrons determines the rate and magnitude of the process.

ACKNOWLEDGEMENTS

The work described above was carried out as part of the programme of the Radio Research Board. This paper is published by permission of the Director of Radio Research of the Department of Scientific and Industrial Research.

REFERENCES

(1) WALTZ, M. C. *Proc. Inst. Radio Engrs*, **40**, p. 1483 (1952).
(2) LAW, J. T. *Proc. Inst. Radio Engrs*, **42**, p. 1367 (1954).
(3) KINGSTON, R. H. *J. Appl. Phys.*, **27**, p. 101 (1956).
(4) SCHRIEFFER, J. R. *Phys. Rev.*, **97**, p. 641 (1955).

The fundamental modes of vibration of uniform beams for medium wavelengths

By G. J. KYNCH, Ph.D., D.I.C., Department of Applied Mathematics, University College of Wales, Aberystwyth

[*Paper first received* 8 *August, and in final form* 17 *September*, 1956]

The Rayleigh–Ritz method is used to determine approximate forms for the dispersion curves of a vibrating infinite beam of arbitrary shape, using the exact elasticity equations. The method is also used to investigate the relations between the different types of vibration. The results for flexural vibrations confirm the Timoshenko equation for most beams and include corrections for thin strips. Dispersion curves are obtained for longitudinal-type vibration which shows the variation with shape and the change in classification of the modes when the symmetry of the cross-section is altered. When the wavelength is of the order of magnitude of the perimeter, the usual longitudinal mode is replaced as the fundamental mode by a new mode.

1. INTRODUCTION

The purpose of this paper is to show that the Rayleigh–Ritz method can be applied to obtain very useful, though not always exact information about the frequencies of vibration and the corresponding dispersion curves of infinite beams. In particular the method is used to find the modes of importance when the wavelength is of the order of the perimeter of the beam.

The theory of the vibrations of beams is mainly restricted to the solution of important engineering problems on the frequencies and modes of vibration of beams, when the wavelength is considerably greater than the perimeter. Under this restriction a perfectly adequate elementary theory of the propagation of waves has been constructed which is quite consistent with the theory of elasticity. There are three fundamental modes which we describe as torsional, longitudinal and flexural.

Many years ago corrections were derived by Chree[1] and Rayleigh[2] to allow for the finite cross-section of the beam in longitudinal oscillation and corrections were also obtained for flexural oscillations by Timoshenko,[3] where they are likely to be of greater importance owing to the strong dependence of phase velocity on wavelength. More recently interest has revived in the propagation of stress waves along beams and experimental techniques have greatly improved. Excellent summaries of the experimental and theoretical results up to the time when they were written have already been made by Kolsky[4] and Davies[5] so we shall not refer to all papers on these matters. It is sufficient to say that the interpretation of the results requires a knowledge of the dispersion curves over the whole range of wavelengths, whereas our present knowledge of those curves is very incomplete.

Vibrations of a circular beam have already been calculated exactly for the three fundamental modes already mentioned and for certain higher modes of the longitudinal type, but the boundary conditions to be imposed on the solutions of the elasticity equations cause such difficulties that the number of attempts of this kind with other shapes of beam is severely limited. This is the reason for the number of approximate methods which have been suggested. We have mentioned that of Timoshenko for flexural oscillations, which gives very good agreement with the exact theory for a circular beam over the whole range of frequencies. Of the methods devised for longitudinal oscillations, that of Mindlin and Hermann[6] is the most satisfactory. When the wavelengths are very short it is likely, though not certain, that all stress waves tend to become surface waves of the type discovered by Rayleigh.[2]

It is clear from this brief discussion that our knowledge of the modes of vibration of beams of simple shapes is small except for small frequencies and large wavelengths. This ignorance is in part due to the lack of a general procedure to obtain solutions of the elasticity equations or to obtain approximate solutions. Without such a procedure we are not in a position to answer most of the interesting questions about the various modes. For a given wavelength, an infinite beam of a given cross-section and material has a spectrum of frequencies. We should like to know how this spectrum varies with wavelength; so that we can draw dispersion curves, how it varies with the elastic constants, how it varies with the shape of the beam, and the fundamental modes for various wavelengths, since they need not be the same as for long waves. We can also ask whether the modes are the same for beams of different sections whose symmetry is different. For example, a rectangular beam, a square beam and a beam in the form of a regular hexagon have, respectively, two, four and six planes of symmetry through the axis, and it is by no means obvious that their modes should be classified in the same way, or that they should be classified in the same way as those of a circular cylinder. The last two questions about the fundamental modes and the classification of the modes have not yet, to my knowledge, ever been discussed in the literature, yet they are surely important before we can begin to discuss the modes of oscillation of beams with complicated sections, such as an H-section, at any but the lowest frequencies.[7]

In this paper we show that the Rayleigh–Ritz method seems to be very satisfactory for both the specific and general problems mentioned in the previous paragraph. In this method we use approximate instead of accurate forms for the displacements to calculate the time averages of the kinetic and elastic energies, and deduce the frequency of a normal oscillation by equating the two time averages. A variation principle is established by showing that the ratio which determines the frequency is stationary with respect to arbitrary variations of the amplitudes of the displacements from their true values. It yields good results in many standard problems and we include as an illustration, in Section 3, a determination of the fundamental frequency of the radial vibrations of a uniform sphere.

In the proof of the validity of the method for problems in elasticity theory, given in Section 2, it appears that the approximate forms for the displacements need not necessarily satisfy the boundary conditions on the stress components. We interpret this result to mean that failure to satisfy these conditions does not lead to serious errors in the frequencies, although the displacements and the stresses calculated from

their derivatives may be wrong. Since the boundary conditions have caused more difficulty in elasticity theory than any other single factor, we have taken advantage of this result, for two reasons. The first reason is that at this stage it is important to obtain a set of results which are qualitatively correct. These results can then be improved by using better approximations, and they can be checked, once known, by exact calculations or by experiment. The second reason is that the expressions used for the displacements are very elementary and contain only a few parameters. It is not known beforehand which is better, the set of values of these parameters obtained by imposing the boundary conditions or the values obtained by applying a variation method without boundary conditions. If the Rayleigh–Ritz method is associated with a minimal principle, which is likely for the fundamental modes, it is better not to apply the boundary conditions.

Calculations were made for wavelengths of the order of the perimeter of the beam or longer. In the absence of any useful guidance as to the forms to be used for the displacements in this range we assume trial functions consisting of one or more terms of a Maclaurin expansion in the coordinates across a section an expansion similar to but not identical with, an expansion in powers of the reciprocal wavelength. This facilitates a comparison with the elementary theory for long wavelengths: moreover, later terms of a given order in the expansion, taken by themselves, correspond to displacements with more nodal planes through the axis, so that we know the type of oscillation which is introduced by the inclusion of a new set of terms.

In this way, our primary aim has been achieved, to obtain dispersion curves for longitudinal and flexural oscillations of beams of simple shapes. From an elementary approximation a dispersion curve is obtained for the longitudinal oscillations of a circular beam, as accurate as that of Mindlin and Herman. The modes of vibration of a circular beam are compared with those of square, elliptical and rectangular beams, and an attempt is made to relate them to those of a flat strip. For flexural oscillations we obtain at once the dispersion curves found by other approximate methods and are able to suggest modifications to be used when the beam is flat.

The second aim of this work was to find the fundamental modes, and this has been partially realized since our approximate calculations show that a square or circular beam, or any whose section has four-fold symmetry, has a mode of oscillation whose dispersion curve intersects that of the longitudinal mode when the wavelength is of the order of the perimeter. This suggestion, which has been verified using the exact equations[8] means that the mode becomes the fundamental in this range of wavelengths. This new mode has been called the screw mode.[9] When the section is less symmetrical, as for an elliptical beam, the eccentricity acts as a coupling parameter between the two modes so that the cross-over is eliminated, as in any similar mechanical system. The same phenomenon exists when there is a change of shape from square to rectangular, and it explains the experimental results of Morse.[10] We are also able to explain another result obtained by Morse, that the dispersion curves for different beams of the same thickness intersects in a common point, and to predict similar points in other circumstances.

The Rayleigh–Ritz method with trial displacements which are linear functions of the parameters is equivalent to a perturbation theory and for each wavelength a spectrum of frequencies is obtained by finding the latent roots of a determinant. These roots are identified by the long wavelength limit or some other way. Now it is known that this method is unlikely to give the magnitude or even the order of higher modes with any accuracy, and it is possible that spurious roots are introduced. For this reason we only discuss the smallest roots which persist in succession to approximations. In the conclusion we discuss briefly the regular appearance of the phase velocity $(2\mu/\rho)^{\frac{1}{2}}$ as an important value for vibrations with wavelengths roughly equal to the perimeter. The solutions corresponding to this velocity could form a good starting point for approximate displacements in this range.

The approximations which we have used are the simplest possible and better ones are badly needed for still shorter wavelengths. When the wavelength is less than the perimeter of the beam there are many modes with phase velocities of the order of the shear wave velocity and the vibration spectrum may become exceedingly complex, the number of nodal surfaces increases and fairly accurate displacements are needed to give an accurate account of these changes.[11]

2. GENERAL PRINCIPLES

The purpose of this section is to establish that the frequencies of the free elastic vibrations of a body are determined by equating the potential and kinetic energies, and that a variation method can be used to obtain approximate values.

The strain and stress components at any point x_β, i.e. (x, y, z), are obtained from the Cartesian components of the displacement v_α, i.e. (u, v, w), by the equations

$$e_{\alpha\beta} = \tfrac{1}{2}(\partial v_\alpha/\partial x_\beta + \partial v_\beta/\partial x_\alpha) \quad \Delta = \Sigma e_{\alpha\alpha} \tag{1}$$

$$p_{\alpha\beta} = \lambda\Delta\delta_{\alpha\beta} + 2\mu e_{\alpha\beta} \tag{2}$$

For a normal oscillation of period $2\pi/\omega$ the equations of motion become

$$\Sigma_\beta \partial p_{\beta\alpha}/\partial x_\beta = \rho(\partial^2 v_\alpha/\partial t^2) = -\rho\omega^2 v_\alpha \tag{3}$$

Body forces have been neglected. We multiply by v_α, smu over α, and integrate over the volume of the body

$$\tfrac{1}{2}\int \rho\omega^2 v_\alpha^2 d\tau = -\tfrac{1}{2}\int v_\alpha(\partial p_{\beta\alpha}/\partial x_\beta)d\tau$$

Integrate by parts and introduce the components F_α of the stresses applied across the boundary

$$\tfrac{1}{2}\int \rho\omega^2 v_\alpha^2 d\tau = \tfrac{1}{2}\int p_{\alpha\beta}e_{\alpha\beta}d\tau - \tfrac{1}{2}\int v_\alpha F_\alpha dS \tag{4}$$

The surface integral involving the applied stresses vanishes when the body is oscillating freely, or oscillating steadily with no energy loss by radiation.

Averaged with respect to time, the l.h.s. of this equation is the kinetic energy and the r.h.s. is the potential elastic energy. We find, therefore,

$$\omega^2 = W_0/N_0$$

$$W_0 = \tfrac{1}{2}\int p_{\alpha\beta}e_{\alpha\beta}d\tau - \tfrac{1}{2}\int v_\alpha F_\alpha dS, \qquad N_0 = \tfrac{1}{2}\int \rho v_\alpha^2 d\tau \tag{5}$$

This proves our first result, which we refer to as the energy equality.

In the previous equation the displacements v_α are the correct solutions of the problem. Let $W = W_0 + \delta W$, $N = N_0 + \delta N$ be the corresponding integrals calculated with an incorrect solution $v_\alpha + \delta v_\alpha$ and the stresses obtained from

equation (2) using these displacements. To first order, the change in W/N is

$$(W/N) = (N_0\delta W - W_0\delta N)/N_0(N_0 + \delta N) = \\ = (\delta W - \omega^2\delta N)/(N_0 + \delta N)$$

Now, to first order in δv_α

$$\delta W - \omega^2\delta N = \int \delta v_\alpha(-\partial p_{\beta\alpha}/\partial x_\beta - \rho\omega^2 v_\alpha)d\tau - \\ - \int \delta v_\alpha(F_\alpha - n_\beta p_{\beta\alpha})dS \quad (6)$$

Since the equations of motion and the boundary conditions are satisfied by the correct solution, both these terms are zero, and we deduce the variation equation

$$\delta W - \omega^2\delta N = 0 \quad (7)$$

for arbitrary small variations in the displacements. Alternatively

$$\delta(W/N) = 0 \quad (8)$$

so that W/N is stationary for small arbitrary variations of the displacements. It is to be emphasized that this proof shows that the trial solution, i.e. the correct solution together with variations, need not satisfy the boundary conditions of the problem.

Thus, when W and N are calculated from displacements which differ only slightly from their true values, the ratio W/N is a good approximation to ω^2. Alternatively we can devise a variation method based on either equation (7) or equation (8); assuming forms for the displacements containing parameters, appropriate to the vibration under examination, we calculate the stationary values of W/N.

The integrals can be simplified for waves travelling in one direction, say, along the z-axis. The displacements of a progressive wave are proportional to either $\sin(kz - \omega t)$ or $\cos(kz - \omega t)$, where the wavelength is $2\pi/k$, the phase velocity being $c = \omega/k$. By taking a time average, or integrating along the beam over an integral number of wavelengths, the volume integration reduces to an integration over a normal cross-section. We shall write $\rho\omega^2 = W/N$, where W is now twice the mean elastic energy density, and N the mean square displacement per unit volume.

$$\left.\begin{aligned} W &= (1/S)\int (\lambda\Delta^2 + 2\mu e_{\alpha\beta}e_{\alpha\beta})dxdy \\ N &= (1/S)\int v_\alpha^2 dxdy \end{aligned}\right\} \quad (9)$$

where S is the area of the section. Only in Sections 3 and 8 do we use the more general definition of W and N.

If the displacements are assumed to be functions of parameters $A_1, A_2, A_3, \ldots A_k$, then the variational equations are

$$\frac{\partial W}{\partial A_i} - \omega^2\frac{\partial N}{\partial A_i} = 0 \quad (i = 1, 2, \ldots k) \quad (10)$$

3. RADIAL VIBRATION OF A SPHERE

As a simple illustration of the method described in the last section and the need to apply boundary conditions, let us calculate the frequency of the simplest radial oscillation of a free uniform sphere of radius a. (An extension to a non-uniform sphere is easy.) As a trial function for the radial displacement we assume

$$u = Aa^2r - Br^3 \quad (11)$$

so that the principal strains are

$$e_{rr} = \partial u/\partial r = Aa^2 - 3Br^2, \quad e_{\theta\theta} = e_{\phi\phi} = (u/r) = Aa^2 - Br^2$$

First we calculate the frequency assuming the boundary condition $p_{rr} = 0$ at $r = a$, so that $(3\lambda + 2\mu)A = (5\lambda + 6\mu)B$. Equating the kinetic and strain energies as in equation (4) we obtain

$$x = \rho\omega^2a^2/\mu = \frac{(3\lambda + 2\mu)}{\mu}\cdot\frac{10\lambda^2 + 36\mu\lambda + 32\mu^2}{3\lambda^2 + 12\tfrac{1}{3}\mu\lambda + 7\tfrac{1}{3}\tfrac{7}{3}\mu^2}$$

When $\lambda = u$, this gives $\rho\omega a^2/\mu = 19{\cdot}78$, which is very close to the correct value of $19{\cdot}71$.

We now apply the variation method without using the boundary condition on the stress, so that the ratio A/B is a parameter. To find the stationary values of W/N, we write down the conditions that $\delta(W - \omega^2N) = 0$, namely

$$(3\lambda + 2\mu - \tfrac{4}{3}x)A - (3\lambda + 2\mu - \tfrac{4}{3}x)B = 0$$

$$-(3\lambda + 2\mu - \tfrac{4}{3}x)A + [(25\lambda + 22\lambda)/7 - x/9]B = 0$$

The consistency of these equations gives a quadratic equation for x, with a smaller root of $19{\cdot}75$, when $\lambda = \mu$, which is a little closer than that obtained before. This value of x gives $B/A = 0{\cdot}482$, compared with the value $0{\cdot}455$ when the boundary condition is satisfied. Although the stress calculated from the approximate displacement is not zero at the boundary, the value of x is slightly improved.

The other root of the quadratic equation is $x = 239$ which lies midway between the correct values for the next two modes. If a term in r^5 is introduced into the displacements, this root is lowered considerably.

4. LONGITUDINAL MODES

Many attempts have been made to obtain approximate dispersion curves for the longitudinal mode of vibration, with varying degrees of success. Almost all the results which can be expressed in a simple form appear amongst the first formulae given by the Rayleigh–Ritz method.

The first attempts were made by Lord Rayleigh[2] and Chree[1] who obtained the correction to the elementary value of the phase velocity $c_0 = (E/\rho)^{\frac{1}{2}}$ due to the Poisson contraction when the beam is not infinitesimally thin. Subsequently Love[12] obtained a formula which reduced to their formulae for long wavelengths, by assuming a simple Poisson contraction to derive an approximate Lagrangian of the motion. The value of this formula given in equation (13) is diminished by the fact that the phase velocity decreases steadily to zero with decreasing wavelength.

Amongst the more recent attempts we mention those of Mindlin and Hermann[6] and Bishop.[13] Mindlin and Hermann obtained a dispersion curve of the right shape for a circular cylinder which is more accurate than that obtained by any other approximate method, by assuming that the longitudinal motion along the axis of the beam is coupled to a radial motion. This assumption is discussed later. Bishop integrated the equations of motion to obtain approximate stresses which satisfy the boundary conditions. He first derived a formula given below, equation (16), and then improved this by using better forms for the displacements.

In Fig. 1 we have drawn graphs to compare these approximations, for a circular cylinder when $\sigma = 0{\cdot}30$. Exact values are plotted for $\sigma = 0{\cdot}29$ rather than $0{\cdot}30$, as they were available[14] and the difference would not show on the graph.

Elementary theory. This assumes that there is a periodic stress along the axis, $p_{zz} = -EAk\sin(kz - \omega t)$. Neglecting the Poisson contraction, this corresponds to an axial strain, with displacements $u = v = 0$, $w = A\cos(kz - \omega t)$. From

the equation of motion of the beam, $\rho\ddot{w} = \partial p_{zz}/\partial z$, we deduce that the velocity of the wave is $c = (E/\rho)^{\frac{1}{2}}$. The same result is given by the energy equality [see equation (4)].

Poisson contraction. When allowance is made for contraction in the normal cross-section, the displacements in the section become

$$u = \sigma' Akx \sin(kz - \omega t) \quad v = \sigma' Aky \sin(kz - \omega t) \quad (12)$$

where σ' is the contraction ratio. To obtain the same stress function as in the elementary theory it is necessary to put $\sigma' = \sigma$, where σ is Poisson's ratio. With this assumption, Love[12] derived a Lagrangian for the motion of the beam and deduced the dispersion formula

$$c^2(1 + \sigma^2 k^2 K^2) = c_0^2 \quad (13)$$

where K^2 is the square of the radius of gyration of the cross-section of the beam about the z-axis. For small values of k this formula reduces to the formula $c = c_0(1 - \frac{1}{2}\sigma^2 k^2 K^2)$ obtained by Rayleigh and Chree.

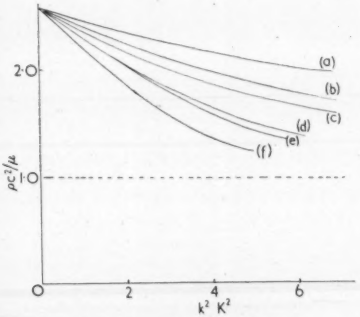

Fig. 1. Longitudinal oscillations

(*a*) Energy equation (equation 16). (*b*) Energy (dynamic contraction) (equation 18). (*c*) Love.[12] (*d*) Mindlin and Herman.[6] (*e*) Circular beam (equation 30). (*f*) Circular beam (exact).

We can use these displacements to calculate the kinetic and potential energies of the beam and apply the energy equality. This allows partially for the shear strain.

$$\rho c^2(1 + \sigma^2 k^2 K^2) = \lambda(1 - 2\sigma)^2 + 2\mu(1 + 2\sigma^2) + \mu\sigma^2 k^2 K^2 \quad (14)$$

Using the usual relationships between the elastic constants,

$$E\sigma = 2\mu\sigma(1 + \sigma) = \lambda(1 - 2\sigma)(1 + \sigma) \quad (15)$$

this formula can be recast in the form

$$c^2(1 + \sigma^2 k^2 K^2) = c_0^2 + c_s^2 \sigma^2 k^2 K^2 \quad (16)$$

Dynamic contraction. Although the contraction ratio may have the value σ for very long waves, there is no obvious reason why it should do so for other wavelengths. The last formula ought therefore to be improved by assuming that this ratio has a dynamic value depending on wavelength of frequency. We substitute σ' for σ in equation (14) and determine σ' as a function of wavelength, by the variation method, i.e. we regard it as a parameter to be chosen so that ω, or c, is stationary with respect to its variation. Using this method we find that $\sigma' = s$, where s is a function of the velocity defined in the following way:

$$\rho c^2 = \lambda(1 - 2s) + 2\mu = \tfrac{1}{2}\lambda(1 - 4\sigma s) + \mu = E + 2\lambda(\sigma - s) \quad (17)$$

These alternative expressions are given to show the variation of s with velocity. Its maximum value is $(1 - \sigma)/2\sigma$ when $c = 0$.

The equation for the dispersion curve is now

$$c^2(1 + \sigma s k^2 K^2) = c_0^2 + c_s^2 \sigma s k^2 K^2 \quad (18)$$

This is a quadratic equation for c^2: the smaller root corresponds to the main longitudinal oscillation (L branch) and $\rho c^2 \to \mu$ for short waves. The other root presumably corresponds to a higher mode (E branch) where $\rho c^2 \to (\lambda + 2\mu)$ for short waves.

The behaviour of the wave-number as the frequency varies can be easily obtained by writing equation (18) in the form

$$P \equiv \tfrac{1}{4}k^2 K^2(\rho c^2/\mu - 1) = (s - \sigma)/s(1 - 2\sigma) \quad (19)$$

and remembering that $k^2 c^2 = \omega^2$. P is always positive and on the main branch increases with frequency from 0 to a maximum value of $(1 + 2\sigma)$ as s increases from σ to $(1/4\sigma)$. On the higher mode, according to equation (19), P increases from $1/(1 - 2\sigma)$ to ∞, as s increases from $-\infty$ to 0, so that for long wavelengths we derive the approximation $\rho\omega^2 = \mu k^2 + 4\mu/K^2(1 - 2\sigma)$. In other words there is a minimum frequency of excitation $\omega_0^2 = 4\mu/\rho K^2(1 - 2\sigma)$.

Comparison of formulae. The formulae obtained in this section are derived using such elementary displacements that great accuracy cannot be expected. Nevertheless we discuss them in detail because qualitatively they agree with the more accurate results obtained in Section 6. None are as good as that of Love except in one respect, that the phase velocity tends to a limit c_s for high frequencies which is close to the true Rayleigh surface wave velocity. Equation (13) was obtained by Bishop[13] using a more complicated method.

The assumption that the contraction ratio σ' varies with wavelength has also been made by Mindlin and Hermann,[6] although they prefer to regard this ratio as a coupling constant between longitudinal and radial oscillations, an interpretation which we reject for reasons discussed in the conclusion. We have found that σ' increases from σ at long wavelengths to the value $\sigma' = \frac{1}{2}$ when $c^2 = 2\mu/\rho$ and then increases still further to the value $1/4\sigma$,along the main branch. As we see later, the deduction that there is zero dilatation, corresponding to $\sigma' = \frac{1}{2}$, when $\rho c^2 = 2\mu$, is correct for a rectangular beam, and this suggests a possible reason for the frequent appearance of the velocity $(2\mu/\rho)^{\frac{1}{2}}$ in our discussions. The interpretation of values of σ' greater than $\frac{1}{2}$ is not clear, but the way in which it arises in our equations suggests that at high frequencies the material prefers to move sideways rather than longitudinally, owing to inertia.

5. ELLIPTICAL AND RECTANGULAR BARS

In this section we use the same crude approximations for the displacements to discover any features which may appear due to lack of axial symmetry of the beams. For beams with rectangular or elliptical sections, it is unrealistic to assume that the contraction normal to the axis is the same in all directions. More suitable displacements are

$$u = (\alpha x + \beta y)\sigma k \sin(kz - \omega t),$$

$$v = (\gamma x + \delta y)\sigma k \sin(kz - \omega t), \; w = A \cos(kz - \omega t)$$

The energy functions are

$$\left.\begin{aligned}(W/k^2) &= \lambda(A-\sigma\alpha-\sigma\beta)^2+2\mu(A^2+\sigma^2\alpha^2+\sigma^2\delta^2)+\\ &+\mu\sigma^2[(\beta+\gamma)^2+k^2(\alpha^2\overline{x^2}+2\alpha\beta\overline{xy}+\beta^2\overline{y^2})+\\ &+k^2(\gamma^2\overline{x^2}+\sigma^2\gamma\delta\overline{xy}+\delta^2\overline{y^2})]\\ N &= A^2+\sigma^2k^2[(\alpha^2+\gamma^2)\overline{x^2}+\\ &+2(\alpha\beta+\gamma\delta)\overline{xy}+(\beta^2+\delta^2)\overline{y^2}]\end{aligned}\right\}\quad(21)$$

(A bar denotes an average over the normal section.)

We can make $\overline{xy}=0$ by choosing the co-ordinate axes along the principal axes of the section. If $\overline{x^2}=a^2$ and $\overline{y^2}=b^2$, then a and b are the radii of gyration about the principal axes, and we choose the x-axis so that $a>b$.

Since there are five parameters, application of the variation method leads to five equations of the form

$$(\partial W/\partial A-\rho\omega^2\partial N/\partial A)=0$$

and therefore to five dispersion curves. However, since both W and N separate into two groups of terms, those containing A, α and δ and those containing β and γ, the solutions separate into one group where $A=\alpha=\delta=0$ and another group of three where $\beta=\gamma=0$.*

The first group has two solutions

(i) $\beta=-\gamma\quad c^2=\mu/\rho$.

(ii) $\beta=Ca^2\quad\gamma=Cb^2\quad\rho\omega^2/\mu=k^2+(1/a^2)+(1/b^2)$.

The first of these is clearly a torsional oscillation and does not concern us. The second is of a rather different type, corresponding to a dispersion curve which we call the S_2 or screw branch. According to the formulae just given the displacements correspond to a shearing motion, where the rod is squeezed first one way and then at right angles, along directions bisecting the angles between the principal axes. It is not a higher torsional mode.

For a circular beam and therefore for other beams we should expect another mode S_1 of the same type, where the squeezing is along the principal axes. Such a mode does, in fact, occur in the second group of solutions obtained by varying A, α and δ and putting $\beta=\gamma=0$. The equations for these can be reduced to

$$\left.\begin{aligned}&\frac{\alpha}{A}[1-\tfrac{1}{2}k^2a^2(\rho c^2/\mu-1)]=\\ &\quad=\frac{\delta}{A}[1-\tfrac{1}{2}\rho k^2b^2(\rho c^2/\mu-1)]=\frac{1-2s}{1-2\sigma}\\ &\text{and}\\ &\frac{\alpha+\delta}{2A}=\frac{s}{\sigma}\end{aligned}\right\}\quad(22)$$

They give the contraction ratios $\sigma_x=\alpha\sigma/A$ and $\sigma_y=\delta\sigma/A$ in the x- and y-directions. We note that the mean contraction ratio is $\frac{1}{2}(\sigma_x+\sigma_y)=s$, which is the same function of the velocity as we obtained in the previous section.

To compare the results with those of the last section, we now consider square or circular beams for which $a=b$. The equations separate into two parts.

$$\left.\begin{aligned}&L\text{ and }E\text{ branches:}\\ &\quad\alpha=\delta=sA/\sigma\quad\tfrac{1}{4}k^2K^2(\rho c^2/\mu-1)=(s-\sigma)/s(1-2\sigma);\\ &S_1\text{ branch:}\\ &\quad\alpha=-\delta,\ A=0\quad\tfrac{1}{4}k^2K^2(\rho c^2/\mu-1)=1\end{aligned}\right\}\quad(23)$$

* In this section, and later, we usually omit the variation equations to save space.

The identification is simple. The equation for the L and E branches is the same as equation (19) and that for the S_1 branch is identical with equation (21) when $a=b$. From equations (23) the L and S_1 branches interesect at the common point $s=\frac{1}{2}$, or $\rho c^2=2\mu$, when the wavelength is such that $k^2K^2=4$.

When a and b are not equal the L and S branches are coupled. By the introduction of K and ϵ, where $a^2=\frac{1}{2}K^2(1+\epsilon)$ and $b^2=\frac{1}{2}K^2(1-\epsilon)$, and the function $P=\frac{1}{4}k^2K^2(\rho c^2/\mu-1)$, as in the previous section, equations (22) can be reduced to a single equation by the elimination of α and β, and this equation is

$$\frac{\sigma(1-2s)}{s(1-2\sigma)}=\frac{(1-P)^2-P^2\epsilon^2}{1-P}\quad(24)$$

A particular solution is shown in Fig. 2.

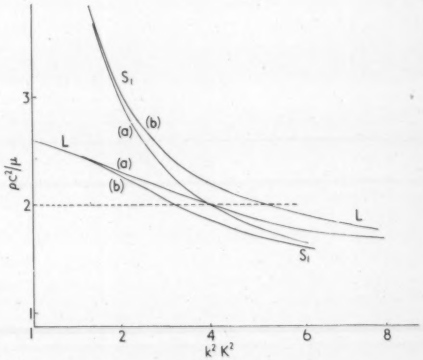

Fig. 2. Longitudinal and screw oscillations. Equation (24), $\sigma=0{\cdot}3$

(*a*) Circular beam, $\epsilon=0$. (*b*) Elliptical beam, $\epsilon=\frac{1}{4}$.

These curves are interpreted in the following way. The shape factor ϵ acts as a coupling parameter between the S_1 and L branches. When it is zero the two branches intersect at $\rho c^2=2\mu$: when it is not zero they are shifted and the cross-over is eliminated. This is an effect which is well known in other mechanical systems; when two normal vibrations of the same frequency are coupled, the perturbation gives rise to beats and the two vibration frequencies separate. In our problem, there are two screw vibrations to interfere with the longitudinal vibrations, but only one has the right symmetry to do so (the other mixes with the torsional oscillation).

From the diagram it appears that the main branch, in the limit $\epsilon=0$, goes over into the L branch when $\rho c^2<2\mu$, and into the S branch when $\rho c^2>2\mu$, so that it is mainly a longitudinal vibration at low frequencies and a screw vibration at high frequencies. The other subsidiary branch which results from the mixing goes over to the S branch for low frequencies and the L vibration for high frequencies.

Our last equation shows that, for a given velocity, the change in the wavelength due to a small eccentricity ϵ is in general of order ϵ^2, except near the cross-over point where

the change is much larger and of order ϵ. In fact we find, from equations (23) or (22), that:

$$\left.\begin{aligned} &\rho c^2 = 2\mu(s = \tfrac{1}{2}) \quad \text{Main branch} \\ &\qquad k^2K^2(1+\epsilon) = 2k^2a^2 = 4, \quad \beta = 0 \\ &\qquad \text{Subsidiary branch} \\ &\qquad k^2K^2(1-\epsilon) = 2k^2b^2 = 4, \quad \alpha = 0 \end{aligned}\right\} \quad (25)$$

In other words, all beams with the same larger principal moment of inertia a^2 have main branches passing through a common point where $c^2 = 2\mu/\rho$ and $k^2a^2 = 2$, the reason being that there is no motion then in the y-direction, so that the dimension in that direction only appears as a constant factor in the kinetic and potential energies. Similarly, all subsidiary branches of beams with the same smaller principal moment of inertia b^2 pass through a common point, the reason being that there is then no motion in the x-direction. Our analysis suggests that this result is of much wider application, and enables a comparison to be made between beams of different sections, for the main branch as well as for the subsidiary branch.

We now verify that the motion on the main branch is of *S* nature for short waves. In this region ρ is nearly equal to unity, and equations (22) become approximately

$$-\alpha\epsilon = \delta\epsilon = (1 - 2s)A/(1 - 2\sigma) \quad (26)$$

Thus the motion along the axis, measured by A, is small when ϵ is small, whereas the transverse motion is of *S*-form, a contraction along the x-axis being accompanied by an expansion along the y-axis.

Finally we make a few comments on the motion of a flat rectangular beam, where $b \ll a$ and $\epsilon \to 1$. Approximate equations can now be obtained for the main and subsidiary branches from equations (22). For the main branch, when $kb \ll 1$, these equations show that

$$\delta/A = (1 - 2s)/(1 - 2\sigma) : 1 - \tfrac{1}{2}k^2a^2(\rho c^2/\mu - 1) = \doteq (1 - 2\sigma)/[2s(1 - \sigma) - \sigma]$$

where $s \to 0$ as $k \to 0$.

The subsidiary branch for wavelengths $kb \simeq 1, ka \gg 1$ gives

$$|\alpha/A| \ll (1 - 2s)/(1 - 2\sigma) : 1 - \tfrac{1}{2}k^2b^2(\rho c^2/\mu - 1) \simeq \sigma(1 - 2s)/2s(1 - 2\sigma)$$

This equation is not valid for longer wavelengths ($\rho c^2 \to \infty$ as $k \to 0$ and α is not small), but by taking the formal limit $a \to \infty$, then $\alpha \to 0$, and the equation for the velocity gives $c^2 \to c_p^2 = 2\mu/\rho(1 - \sigma)$. Alternatively the original equation (22) has only one solution for $c = c_p$ namely

$$k^2 = \frac{1 - \sigma}{1 + \sigma} \cdot \frac{2}{ab} \quad (27)$$

which tends to zero in the limit of a flat plate.

Let us now interpret these results, comparing them with experimental and other theoretical results. The reality of the branches *S* is no longer in doubt. In the first place calculations have been made here using the Pockhammer equations for a circular cylinder and it has been verified that the *S* branch cuts the *L*-branch near $\rho c^2 = 2\mu$. Secondly, we suggest that the cross-over is eliminated for rectangular plates, and that the two dispersion curves which result, called here the main and subsidiary branches, have a special property: that the main branches have a common point for beams of the same width $2a$ but different thicknesses b, and that the subsidiary branches have a common point for plates of the same thickness b but different width $2a(>2b)$. The experiments of Morse on beams of different widths agree with this suggestion, provided the identification of the vibrations is correct. The evidence for this is that Morse tried to excite longitudinal vibrations but found it easier to obtain the second higher branch at high frequencies, and that he obtained a common point where $\rho c^2 \simeq 2\mu$. Finally it can be shown from the exact equations that this point exists for rectangular beams.

Our final remarks on the vibrations of plates also correspond to known calculations. It has been shown by Love assuming plane stress, that a branch exists where the velocity tends to c_p for long-wavelengths and by Bishop[15] assuming plane strain, that there is a branch corresponding to equation (27). Moreover the *S*-branch exhibits the general features of plane strain when the wavelength is long. Thus we feel that it is reasonable to suggest that the plane-stress and plane-strain branches correspond to our main and subsidiary branches or the *L* and *S* branches of a circular beam.

We have given the name *screw vibrations* to the S_1 and S_2 branches. A name seems to be required since they are elementary in form, and become a fundamental mode when the wavelength is less than the perimeter. Our analysis is very approximate and the name was given because it seems that the nodes of a stationary wave lie on a helix.

6. SECOND APPROXIMATION FOR LONGITUDINAL VIBRATIONS

The lengthy discussion of the two previous paragraphs does not mean that the numerical results are very accurate. The discussion was qualitative in form, and the dispersion curve for the longitudinal vibrations, which is likely to be more accurate than the others, leads to values for the phase velocity which do not decrease sufficiently rapidly with increasing frequency, the value $\rho c^2 = 2\mu$ being reached when $k^2a^2 = 2$, whereas the exact value is nearer 1. This discrepancy also occurs in all other approximations, except that of Love. In this section, therefore, we carry through an analysis using the Rayleigh–Ritz method with a correction term in the axial displacement term. Even better results could be obtained using further corrections to the other displacements. As in the previous section, we do not assume solutions corresponding specifically to longitudinal vibrations, which would contain far fewer parameters, but, wisely or unwisely, try to obtain a fairly complete vibration spectrum for each wavelength.

The improved displacements to be used are

$$\left.\begin{aligned} w &= A + \sigma k^2[F(a^2 - x^2) - 2Hxy + \\ &\qquad + G(b^2 - y^2)] \cos(kz - \omega t) \\ u &= (\alpha x + \beta y)\sigma k \sin(kz - \omega t), \\ v &= (\gamma x + \delta y)\sigma k \sin(kz - \omega t) \end{aligned}\right\} \quad (28)$$

Thus A is the mean axial displacement over any section. The energy functions are

$$\left.\begin{aligned} W/k^2 &= \lambda[(A - \sigma\alpha - \sigma\beta)^2 + \sigma^2k^4D^2] + \\ &\quad + 2\mu\sigma^2(\alpha^2 + \delta^2 + k^2D^2) + 2\mu A^2 + \\ &\quad + \mu\sigma^2\{(\beta + \gamma)^2 + k^2a^2[(\alpha - 2F)^2 + (\gamma - 2H)^2] + \\ &\quad + k^2b^2[(\beta - 2H)^2 + (\delta - 2G)^2]\} \\ N &= A^2 + \sigma^2k^2a^2(\alpha^2 + \gamma^2) + \\ &\qquad + \sigma^2k^2b^2(\beta^2 + \delta^2) + \sigma^2k^4D^2 \end{aligned}\right\} \quad (29)$$

where

$$D^2 = fF^2a^4 + gG^2b^4 + 2hFGa^2b^2 + 4(h+1)H^2a^2b^2 = \\ = F^2(\overline{x^4} - a^4) + G^2(\overline{y^4} - b^4) + \\ + 2FG(\overline{x^2y^2} - a^2b^2) + 4H^2\overline{x^2y^2}$$

(We assume that the beam is symmetrical about one principal axis, $\overline{xy^3} = \overline{x^3y} = 0$.) The last equality defines the shape parameters f, g and h. The introduction of new parameters introduce new branches and algebraic complications.

Variation of all parameters leads, as before, to two groups of solution. The first group, where only β, γ and H are not zero, includes the torsional oscillation and one screw vibration. These two are now mixed for a section which is not axially symmetric, a result to be discussed elsewhere.

The second group is the solutions of five equations

$$\left.\begin{aligned} \sigma(\alpha+\delta) &= 2sA \\ \alpha[1 - k^2a^2(\rho c^2/\mu - 1)] - 2k^2a^2F &= A(1-2s)/(1-2\sigma) \\ \delta[1 - k^2b^2(\rho c^2/\mu - 1)] - 2k^2b^2G &= A(1-2s)/(1-2\sigma) \\ (2\mu + \lambda - \rho c^2)(fk^2a^2F + hk^2b^2G) &= 2\mu(\alpha - 2F) \\ (2\mu + \lambda - \rho c^2)(hk^2a^2F + gk^2b^2G) &= 2\mu(\delta - 2G) \end{aligned}\right\} \quad (30)$$

For a circle or ellipse, $f = g = 1$, $h = -\frac{1}{3}$; for a square or rectangle, $f = g = \frac{4}{3}$, $h = 0$.

For the rectangular type of beam the fact that $h = 0$ means that F can be expressed in terms of α alone and G in terms of β, which simplifies calculations. For a square beam, there are the two branches where $\alpha = \delta$, $A = 0$, and three branches where $\alpha = \delta = sA/\sigma$. The former includes the screw vibration, and the latter the longitudinal vibration, these two intersecting where $\rho c^2 = 2\mu$. For certain values of Poisson's ratio they have minima, where the velocity is less than c_s, but this agreement with the exact theory[16] is fortuitous, since the position and existence of the minimum is sensitive to the nature of the approximation for such short waves.

For a rectangular beam the intersecting branches separate as before. The feature of common points still remains, at the same velocity $\rho c^2 = 2\mu$. The wavelengths can easily be obtained from our equations by putting $h = \alpha = 0$ for the subsidiary branch and $h = \delta = 0$ for the main branch. On the subsidiary branch the point is common to all rectangular beams with the same width a and on the main branch the point is common to all with the same thickness $b < a$.

For a circular or elliptical beam, the value of h is not zero, but negative. The result of this for a circular beam is that the equation for its longitudinal branch is the same as that for a square with $(f + h)$ instead of f, and the equation for the screw branch is the same with $(f - h)$ instead of f. The point of intersection of these two branches is, according to our approximation, at a lower phase velocity than before, as seen in Fig. 3. For a certain range of small values of Poisson's ratio these branches intersect, again at very high frequencies, owing to the negative value of h, but this may be due to our use of an approximate solution. A comparison with exact calculations is not possible as these have not been made for small σ. For an elliptical beam as for rectangular beams, the branches separate and beams with the same major axis, but different minor axes, have $\rho c^2 = 2\mu$ on the main branch for slightly different, but not very different, wavelengths. In fact, at this velocity, the value of k^2a^2 on the main branch, and the value of k^2b^2 on the subsidiary branch, lie between the values of k^2K^2 for these branches for a circular beam with the same value of $K^2 = a^2 + b^2$.

The main curve for a circle is also plotted in Fig. 1. It is rather better than the other approximations given. For a given velocity, the error in the wavelength is usually of the order of 15%.

In conclusion, our various calculations on longitudinal vibrations show that each improvement in the assumed displacements brings out new features of the dispersion curves, and refines the description of the earlier features, so that the effect of a symmetry in the beam can be understood.

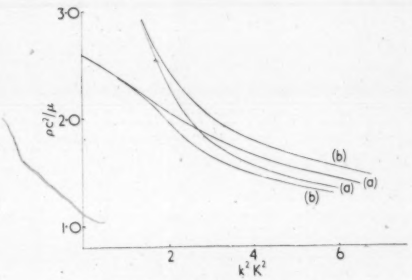

Fig. 3. Longitudinal and screw oscillations. Equation (30), $\sigma = 0{\cdot}3$
(*a*) Circular beam, $\epsilon = 0$. (*b*) Elliptical beam, $\epsilon = \frac{1}{4}$.

7. FLEXURAL OSCILLATIONS

In flexural oscillations the central z-axis of the beam oscillates in a plane in the direction of the x-axis. The beam bends about the y-axis. There are several approximations for the velocity of such oscillations.

Elementary;
$$c^2 = k^2a^2c_0^2$$
Rotational correction:
$$c^2 = k^2a^2(c_0^2 - c^2)^{(2)}$$
Energy correction;
$$c^2 = k^2a^2[c_0^2 - c^2 + c^2\sigma^2(1 - b^2/a^2)]^{(12)} \quad (31)$$

Corrected stresses;
$$c^2 = k^2a^2(c_0^2 - c^2)(1 - c^2/c_s^2)^{(17)} \quad (32)$$

Rotation and shear;
$$c^2 = k^2a^2(c_0^2 - c^2)(1 - c^2/Kc_s^2)^{(3)} \quad (33)$$

Internal constraints;
$$c^2 = k^2a^2(\alpha c_0^2 - c^2)(1 - c^2/c_s^2)^{(18)} \quad (34)$$

The variation method yields an equation similar to equation (34). In these equations $a^2 = \overline{x^2}$, so that a is the radius of gyration of the normal cross-section about the axis of bending. Equation (33) is surprisingly successful; the value $K = 0{\cdot}9$ assumed by Davies, or the value $K = 0{\cdot}85$ calculated by Mindlin,[6] correct the velocity for short waves. The equation of Prescott[17] is obtained from equation (33), by putting $K = 1$. Equation (34) is derived by Volterra[18] with a value of α so that $\alpha E = \lambda + 2\mu$, which gives incorrect values for long wavelengths. Using the energy and variation method, we are led to equation (34) with a value of α different from that of Volterra which does not suffer from that defect. To force agreement at the high frequency end we can insert a factor K in the last bracket. Curves obtained with this

expression, with $K = 1$, are shown in Fig. 4. Of course, equations (32–34) all lead to higher branches as well as the main flexural branch, and equation (34) has several because α is a function of c. If they correspond to real solutions, these are in no way flexural oscillations in the usual sense.[7]

With the choice of axes mentioned above, motion in the x-direction produces contraction and expansion along the z-axis, and this, in turn, results in correction terms to the displacements normal to the axis. This leads us to consider displacements of the form

$$\left.\begin{aligned} u &= \left\{A + \tfrac{1}{2}\sigma_1 k^2 B[a^2 - x^2 - (b^2 - y^2)]\right\} \sin(kz - \omega t) \\ v &= -\sigma_2 k^2 Bxy \sin(kz - \omega t) \\ w &= -kBx \cos(kz - \omega t) \end{aligned}\right\} \quad (35)$$

The constants in the first of these are adjusted so that A is the mean value over the cross-section.

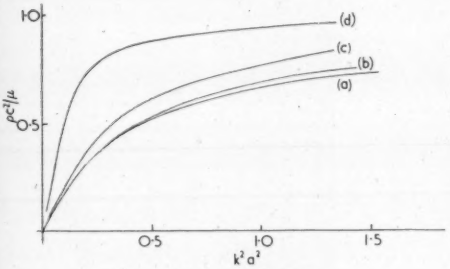

Fig. 4. Flexural oscillations

(*a*) Square (Prescott) and equation (38) when $b \leq a$. (*b*) Rectangle $b = 2a$ (equation 38). (*c*) Rectangle $b = 4a$ (equation 38). (*d*) Rectangle $b = 10a$ (equation 38).

When $\sigma_1 = \sigma_2 = \sigma$, and $A = B$, these are the usual displacements[12] assumed for flexural oscillations at low frequencies. Direct use of the energy equality, without variation as there are no parameters, leads to an equation similar to equation (34) of Love, with an extra term giving the limit $c = c_s$ for high frequencies.

If we assume that $\sigma_1 = \sigma_2 = \sigma$, and $A \neq B$, so that the displacement along the axis of the beam is not always the same fraction of the sideways displacement for all frequencies, the variation method leads to equation (31) with

$$\left.\begin{aligned} \alpha E &= E + \epsilon\sigma^2 k^2 a^2(\mu - \rho c^2) \\ \text{where} \quad 4\epsilon a^4 &= 4a^2 b^2 + fa^4 + 2ha^2 b^2 + gb^4 \end{aligned}\right\} \quad (36)$$

using the notation of the previous section. Hence the equation is identical with equation (32) of Prescott if the term in ϵ is zero. To estimate the correction, we note that, from equation (34), the factor $k^2 a^2(1 - c^2/c_s^2)$ is less than its value when $\epsilon = 0$ and tends to a limit as c increases to c_s which is less than $\rho c_s^2/(E - \rho c_s^2) = 1/(1 + 2\sigma)$

therefore $\alpha < 1 + \epsilon\sigma^2\mu/E(1 + 2\sigma)$

i.e. $1 + \epsilon\sigma^2/2(1 + \sigma)(1 + 2\sigma) < 1 + \epsilon/24$

Thus the correction is quite small, except for beams bending about their major axis, where $b > a$ and ϵ is large. The ratio B/A is $1 - c^2/c_s^2$.

We now consider the results using the displacements given in equation (35) without any simplification. It might be expected that σ_1 and σ_2 would not be equal, even for a circular or square beam, since the motion is not symmetrical about the z-axis. In fact, it seems that the difference between them is much smaller than either over the whole range of frequencies along the main branch, as long as $b < a$ and ϵ is small. The actual changes to be made are the following: the ratio B/A is unaffected by the change, but now

$$\alpha E = E + \tfrac{1}{2}\epsilon''\sigma(\sigma_1 + \sigma_2)k^2 a^2(\mu - \rho c^2) \quad (37)$$

so that $\epsilon\sigma$ is replaced by $\frac{1}{2}\epsilon''(\sigma_1 + \sigma_2)$, ϵ'' being defined later. The mean contraction ratio is

$$\sigma' = \tfrac{1}{2}(\sigma_1 + \sigma_2) = \sigma/[1 + \epsilon'' P(1 - 2\sigma)] \quad (38)$$

where $P = \frac{1}{4}k^2 a^2(1 - c^2/c_s^2)$. Since $P < 1/4(1 + 2\sigma)$ it follows that σ' is not appreciably different from σ unless ϵ'' is large. Moreover αE can at most only vary between E and $2\lambda + \mu$.

The difference of the contraction ratios is determined by

$$\kappa = (\sigma_1 - \sigma_2)/(\sigma_1 + \sigma_2) = \frac{P\epsilon'}{1 + P\epsilon + (b^2/a^2)} \quad (39)$$

involving a new shape factor $\epsilon' = \epsilon - 2(h + 1)b^2/a^2$.

Finally the definition of ϵ'' is

$$\epsilon'' = \epsilon - \kappa\epsilon' \quad (40)$$

Using these equations it can be shown that κ is small for beams with $b < a$ bending about the smaller axis, is less than for a square or circular beam $b = a$, and even for such beams is never greater than 5%. Consequently for such vibrations there is no significant difference between ϵ'' and ϵ.

For the same beam vibrating about the other axis, where $b > a$, this is no longer true, and both ϵ' and ϵ'' can be large. In this case it is difficult to give a general discussion, but the reader can examine the curves given in Fig. 4 using these equations.

8. NON-UNIFORM BEAMS

The equations given in the earlier sections can readily be generalized to include beams whose cross-sections vary along their length, if the principal axes have fixed directions. The assumption to be made is, that the displacements are proportional to some function of z and a periodic function of the time.

As a simple example of the method, let us derive the equation for longitudinal oscillations, assuming that the displacements are of the form

$$u = \sigma x g(z) \sin \omega t \quad v = \sigma y g(z) \sin \omega t \quad w = f(z) \sin \omega t \quad (41)$$

so that the time averages of the energy integrals are

$$\left.\begin{aligned} W &= \int [\lambda(f' + 2\sigma g)^2 + 2\mu(f^2 + 2\sigma^2 g^2) + \\ &\qquad + \mu\sigma^2(a^2 + b^2)g'^2]dz \\ N &= \int [f^2 + \sigma^2(a^2 + b^2)g^2]dz \end{aligned}\right\} \quad (42)$$

The variation equations are

$$\left.\begin{aligned} &(\lambda + 2\mu)d^2 f/dz^2 + \rho\omega^2 f + 2\sigma\lambda dg/dz = 0 \\ &2\sigma\lambda df/dz + 4\sigma^2(\lambda + \mu)g + \\ &\qquad + (\rho\omega^2 - \mu)\sigma^2 d[(a^2 + b^2)dg/dz]/dz = 0 \end{aligned}\right\} \quad (43)$$

These equations reduce to equations (13) when we assume that $(a^2 + b^2)$ is constant, and that $f(z)$ and $g(z)$ are periodic functions. Apart from the order of certain factors, the rule

is simply to replace the symbol k by the operator $(\partial/\partial z)$ and if it is desired, ω by $(\partial/\partial t)$.

Similar equations to these have been derived by Mindlin and Hermann[6] using the equations of motion. The differences are due to their use of the boundary conditions, and their introduction of two arbitrary parameters.

9. CONCLUSION

From the calculations of the previous sections it appears that the Rayleigh–Ritz method, without special assumptions as to the form of the displacements, yields useful information about the dispersion curves and the modes of vibration of beams. Section (5) contains a number of suggestions, the result of elementary calculations, which have been verified where this has been possible. At the moment in this field it is as important to discover possible relations as it is to verify them, and the attitude adopted here is that the Rayleigh–Ritz method forms a useful basis for further work. The exact elasticity equations are so complicated that it is possible to overlook the existence of such modes as the screw vibration without some general approximate method. Here, the interaction of the screw and longitudinal modes has been discussed but calculations have still to be made on the interaction of the second screw mode and the torsional mode for non-circular beams, and it would also be interesting to examine the vibrations of a beam with a suitable screw thread cut on it, since complicated motions might ensue when the wavelength equals the pitch of the thread.

We have made no attempt to discuss accurately the dispersion curves when the wavelength is much shorter than the perimeter of the beam. In this range it would be necessary to use, for the displacements, functions which allowed for the radial nodes and resembled the exact solutions for some wavelengths.

In this connexion, we have looked for simple solutions of the equations of motion when the phase velocity has the value $c^2 = (2\mu/\rho)$, a value which seems to have a special significance in our approximations. It was found that the boundary conditions do simplify for this value of the phase velocity, but not sufficiently to suggest an easy method of obtaining exact solutions. Apart from higher modes of torsional oscillations which all have this phase velocity for very short wavelengths[12] and a flexural oscillation mentioned below, we were only able to obtain simple solutions when the dilatation was zero. This was quite satisfactory, since it implies that the solutions depend on the value of μ, but not on the value of Poisson's ratio. Moreover the simple solutions which were obtained all involved transverse displacements in the same direction at all points of the beam. Hence the cartesian displacements (u, v, w) satisfied the equations, $v = 0$, $kw = -(\partial u/\partial x)$.

For the rectangular beam bounded by $x = a$, $y = b$, we found the solutions

$$u = A \sin kx \qquad \text{where } \cos ka = 0;$$
$$u = A \cos kx \qquad \text{where } \sin ka = 0.$$

The lowest value of k obtained from these equations is $k_0 = (\pi/2a)$ corresponding to a wavelength of $4a$. There are other solutions where the displacements are in the y-direction, of course, with a smallest wavelength $4b$. These correspond to the common point of the dispersion curves mentioned in Sections 5 and 6.

For a circular beam of radius a, we obtained a solution

$$u = AJ_0(kr)\cos(kz - \omega t) \qquad \text{where } J_0'(ka) = 0$$

This is a solution of the Pochammer equation for flexural oscillations, and lies on an harmonic of the usual curve for such vibrations. This shows that there is an error in the conclusion drawn by Hudson, and widely quoted in the literature of stress waves, that the flexural vibrations have no higher modes. In addition, we found the longitudinal vibration, and the various torsional modes. For this phase velocity, the screw vibration of a circular cylinder does not correspond to a simple solution, so we did not find it.

We conclude with a few words on coupling constants. The normal modes depend on various parameters, and for certain values of these parameters the spectrum of frequencies may be very simple and the various types of vibration clearly separated. Changes in the values of the parameters from these special values can then be regarded as coupling constants between modes of vibration. Thus it has been suggested by Mindlin and Hermann that the longitudinal mode can be regarded as the result of coupling between a purely longitudinal motion and a radial expansion and contraction. The coupling constant is Poisson's ratio and it is possible to imagine an ideal material for which this is zero. The vibrations of a real beam should then be expressed as a combination of the various modes of a similar beam made of this ideal substance. In this paper we have assumed the known elastic constants and introduced coupling parameters depending on the geometry. In Section 4 the variation of σ' from σ is attributed to the finite size of the cross-section and in later sections the coupling constants ϵ are shape factors.

It is advisable to distinguish between these two types of coupling, which lead to quite different lines of approach to the problem. In the first we have an ideal material and the proper development of the method would take the form of an examination of the vibrations of bodies of all shapes made from this ideal material. In the second there is an ideal shape, which may be a circular or square beam, or a flat plate, whichever is found to be best. We have chosen the second approach because we are concerned with the effect of the shape of the cross-section on the dispersion curves.

Different views on this matter also lead to different opinions on nomenclature on vibrations. It must be clear by now to the reader that names given to the elementary vibrations of low frequency are not suitable for higher frequencies. The absence of suitable constants of the motion and the vector nature of the displacements have the almost inevitable result that the modes are described as combinations of vibrations of ideal beams, with limitations imposed by the symmetry of the section. So far this question has been ignored, but a systematic description of the modes will become necessary when frequencies are so high that many vibrations are equally fundamental, even though we choose to dismiss all other types of vibration as higher modes.

REFERENCES

(1) CHREE, C. *Trans Camb. Phil. Soc.*, **14**, p. 250 (1889).
(2) RAYLEIGH. *Collected Papers, Vol. II* (Cambridge: University Press, 1900).
(3) TIMOSHENKO, S. P. *Phil. Mag.* (*series* 6), **41**, p. 744 (1921).
(4) KOLSKY, H. *Stress Waves in Solids* (London: Oxford University Press, 1953).
(5) DAVIES, R. M. *Appl. Mech. Rev.*, **6**, p. 1 (1953).
(6) MINDLIN, R. D., and HERMANN, G. *Appl. Mech. Rev.*, **5**, p. 1308 (1951).
(7) KYNCH, G. J., and GREEN, W. A. *Quart. J. Mech. Appl. Maths.* (To be published.)

(8) GREEN, W. A. *Quart. J. Mech. Appl. Maths.* (To be published.)
(9) KYNCH, G. J. *Nature* [*London*], **175**, p. 559 (1955).
(10) MORSE, R. W. *J. Acoust. Soc. Amer.*, **20**, p. 833 (1948).
(11) MCSKIMIN, H. J. *J. Acoust. Soc. Amer.*, **28**, p. 469 (1956).
(12) LOVE, A. E. H. *Theory of Elasticity* (*4th Ed.* New York: Dover Publications, 1944).
(13) BISHOP, R. E. D. *Aero. Quart.*, **3**, p. 280 (1952).
(14) DAVIES, R. M. *Phil. Trans A*, p. 375 (1948).
(15) BISHOP, R. E. D. *Quart. J. Mech. Appl. Maths.*, **6**, p. 250 (1953).
(16) BANCROFT, D. *Phys. Rev.*, **59**, p. 588 (1941).
(17) PRESCOTT. *Phil. Mag.*, **33**, p. 703 (1942).
(18) VOLTERRA, E. *Ing. Archiv.*, **23**, p. 410 (1955).

Pre-breakdown conduction between electrodes in continuously-pumped vacuum systems

By W. K. MANSFIELD, B.Sc., A.Inst.P., and R. L. FORTESCUE, M.A., A.M.I.E.E., Nuclear Particle Laboratory, Queen Mary College, University of London

[*Paper received* 30 *July*, 1956]

Electron loading in electrostatic generator accelerator tubes due to the passage of pulses of current of millisecond duration has been investigated. The characteristics of pulse discharge conduction are described and a theory of its origin proposed. This theory envisages an exchange of positive and negative ions of hydrogen between the electrodes in a regenerative reaction, the source of the ions being a chemi-sorbed layer of hydro-carbon on the electrode surfaces. Measurements of the secondary emission coefficients and other experimental evidence appear to be consistent with such a hypothesis. Methods of suppression of this pulse discharge conduction are discussed.

Electron loading in continuously-pumped accelerator tubes for electrostatic generators has been reported by several workers.[1–6] Current flows in the tube with electric fields considerably less than those which give rise to field emission. This current may seriously limit the performance of the generator as it acts as a direct current load which reduces the available useful output. The effect is much increased because such currents produce X-rays which give rise to ionization of the gaseous insulating medium. This leads to insulation leakage from the high voltage terminal of the generator which greatly increases the total loading. Similar pre-breakdown currents have been reported by users of electron-microscopes with electrostatic lenses[7] and they appear to be the general rule in continuously-pumped vacuum systems subject to high voltage. To distinguish this form of conduction it will be referred to as pulse discharge conduction.

The nature of the processes giving rise to pulse discharge conduction has been studied in this laboratory by D. S. Clifford, D. J. Harris, D. G. Stevenson, A. W. Hough-Grassby and the authors. Results of these studies, some of which have already been the subject of Ph.D. theses at the University of London[8–11] are here summarized and a physical mechanism of conduction in accordance with these results is discussed.

The investigations can be divided into two types of experiments. The first dealing with conduction between two electrodes in continuously-pumped glass vacuum chambers, and the second with conduction in an accelerator tube installed in a 1 MV pressurized electrostatic generator. Pulse discharge conduction in the two systems was fundamentally similar.

The results of these investigations are described in detail in the next section, but may here be summarized to emphasize the distinctive characteristics of pulse discharge conduction:

(1) The current flows as self-extinguishing pulses of millisecond duration.
(2) The initiation is dependent upon voltage, though the field strength is also relevant.
(3) There is a pronounced conditioning effect, and electrodes may be super-conditioned to withstand a voltage in excess of the normal pulse discharge value for short periods.
(4) An increase of residual gas pressure in the vacuum system raises the voltage required to produce pulse discharges.
(5) The discharge is diffuse, not filamentary.
(6) The discharge is dependent upon electrode surface nature. It is characteristic of continuously-pumped systems and is inhibited by electrode out-gassing.

EXPERIMENTAL OBSERVATIONS

The apparatus used to study pre-breakdown conduction *in vacuo* is shown in Figs. 1, 2 and 3. Fig. 1 shows the apparatus used by Clifford in which parallel plane electrodes of 6 cm diameter and shaped to a Bruce[12] profile are placed in an evacuated bell-jar. D.c. voltages up to 150 kV derived from a conventional Cockcroft–Walton doubling circuit can be applied to the electrodes. The lower electrode is connected to the earth side of the voltage supply *via* a resistance and a microammeter, and the voltage developed across this resistance is monitored by a cathode-ray oscilloscope. The lower electrode is fitted to a rod passing through a Wilson seal permitting the electrode separation to be adjusted; for most of the measurements the gap was less than 1 cm. Stevenson's apparatus, Fig. 2, resembles Clifford's in using profiled copper electrodes in a glass bell-jar, but in his case a mercury diffusion pump is used to reduce oil vapour contamination of the electrodes. Apart from the electrodes and their supports the vacuum system is made entirely of glass. Fig. 3 shows the small pressurized electrostatic generator (1 MV) used by Harris and Hough-Grassby to examine conduction

of this kind. The accelerator tube was made by Messrs. General Electric Co. Ltd., and is of a sandwich construction, copper disks being sealed to glass cylinders, with a pitch of $\frac{1}{4}$ in. The tube is 15 in. long and has an aperture of 4 in.

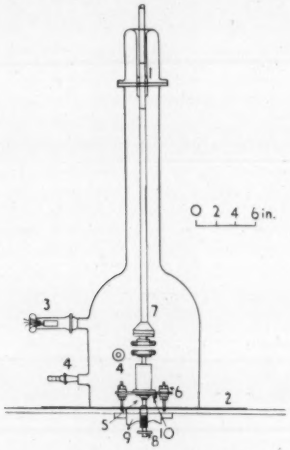

Fig. 1. Vacuum chamber and electrode supports used by D. S. Clifford

(1), metal-to-glass seal; (2), rubber gasket; (3), ionization gauge (fitted with B. 45 cone); (4), B. 14 cone outlets; (5), micrometer (0–1·5 cm); (6) Perspex insulators; (7) ball joint; (8), flexible coupling to glass control rod; (9), outlet to pumps; (10), insulated connexion.

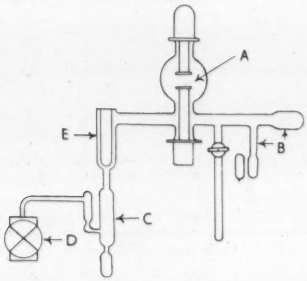

Fig. 2. All-glass vacuum system used by D. G. Stevenson

A, test gap; *B*, gauges; *C*, mercury diffusion pump; *D*, backing pump; *E*, vapour trap.

diameter. Since the separation of the equipotential plates of the generator is $\frac{3}{4}$ in., every third copper disk is connected to an equipotential plate. The remaining disks, which have sharp edges, are left unconnected and adjust their potentials by corona-discharge.

In the apparatus shown in Fig. 1, a slowly increasing voltage (5 kV/min) is applied to one of the two electrodes with a pressure of 10^{-5} mm of mercury in the vacuum chamber, and the following sequence of conduction effects is observed:

(i) At about 20 kV (for a 0·2 cm gap) a steady current of the order of 1 μA is measured.

(ii) At a slightly higher voltage current transients pass whose peak amplitudes are about 200 μA and duration 50 ms, shown in Fig. 4(*a*). The double peak is produced because the pulse almost extinguishes on the negative excursion of the ripple ($\simeq 1\%$). As the voltage is increased these pulses occur at increasing frequencies.

(iii) At a voltage of about 100 kV a bright filamentary spark passes.

These three conduction states will be referred to as (i), (ii) and (iii). It is found that if the voltage is maintained at the

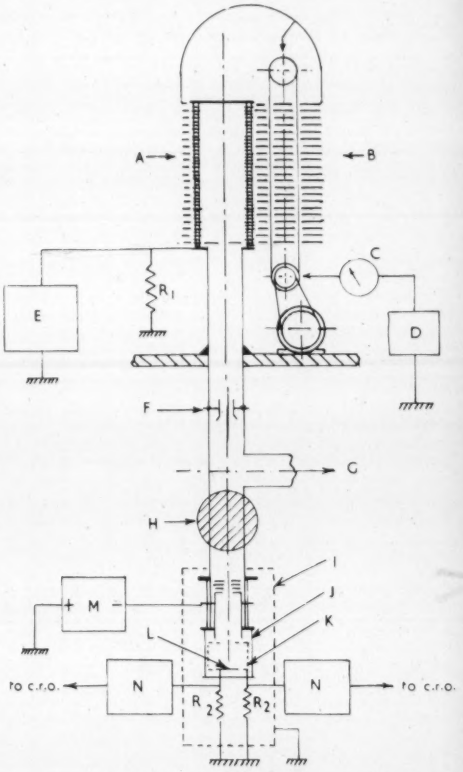

Fig. 3. Accelerator tube, electrostatic generator and apparatus used to measure secondary emission coefficient

A, accelerator tube; *B*, electrostatic generator; *C*, micro-ammeter; *D*, 0–40 kV d.c. supply; *E*, C.R.O. amplifier; *F*, electrostatic deflector plates; *G*, vacuum pumps; *H*, magnetic field; *I*, screening box; *J*, Faraday chamber; *K*, target grid; *L*, target; *M*, 0–2 kV d.c. supply; *N*, amplifiers; R_1, 10 kΩ; R_2, 10 000 Ω or 1 MΩ.

lowest voltage which produces state (i), the steady current dies away and such a steady current can only be produced again either by increasing the applied voltage, or by modifying the electrodes states. This current is reversible with voltage application and it is thus tempting to ascribe conduction in state (i) to some form of field emission from dust particles or minute projections on the electrode surfaces. It should be pointed out, however, that the applied field, 100 kV/cm is remarkably low for field emission to occur.

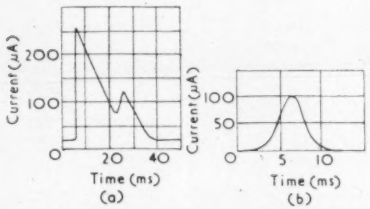

Fig. 4. (*a*) Waveform of pulse occurring between copper electrodes with a 1 cm gap. (*b*) Waveform of pulse for accelerator tube

State (iii) is known as vacuum spark breakdown and is characterized by a low voltage drop in the discharge channel. It is presumed that a vacuum spark leads to a vacuum arc if the impedance of the voltage source is low enough. The three conduction states described above for the parallel plane electrode geometry are also found when voltage is applied to the accelerator tube. The difference is that the third state, a vacuum discharge, occurs along the surface of the glass. Conduction state (ii) is the subject of the present paper and the following characteristics have been observed.

Conditioning effects. The lowest voltage at which the pulse discharge occurred was very variable and two methods of determining the threshold voltage were used. In the first method the bell-jar type of apparatus was used and the voltage was raised slowly until a pulse occurred. A relay was then operated and the voltage was switched off. A recording voltmeter traces this voltage excursion. The voltage was again raised slowly until a second pulse was obtained and again the voltage was switched off. This sequence was repeated until many hundred discharge voltages had been recorded, see Fig. 5. From this record it was possible to postulate a mean threshold voltage, V_{th}, with a standard deviation of around 6%. It is seen that the mean level is not attained immediately, the voltage necessary for the first 20 or so pulses showing a steady increase.

The second method adopted for determining the threshold voltage depends upon the time elapsing between successive pulse discharges. If the voltage is raised by 1 kV steps until a discharge occurs, it is found that, if the voltage is maintained, a few further pulses are observed but with successively increasing time intervals between them until no further pulses occur. The voltage is then increased until pulses are again obtained and then left at this value until there is no further pulsing. By repeating this process a voltage is eventually obtained at which the pulses recur indefinitely at a frequency of 2–3 per min. This voltage is also referred to as the threshold voltage. The difference between the conditioned threshold voltages obtained by the two methods is small and certainly less than the standard deviation.

A super-conditioning effect was also noted by which the threshold voltage could be temporarily increased. This effect is produced by raising the applied voltage above V_{th} and allowing numerous puises of current to pass. If the voltage is then reduced it is found that V_{th} has been increased. V_{th} decreases thereafter with time to its original value which may be reached after 10–60 min, see Fig. 5. A threshold voltage for state (ii) can be determined using the electrostatic generator apparatus by methods similar to those used for the bell-jar equipment, and the conditioning and super-conditioning effect can likewise be demonstrated, see Fig. 6.

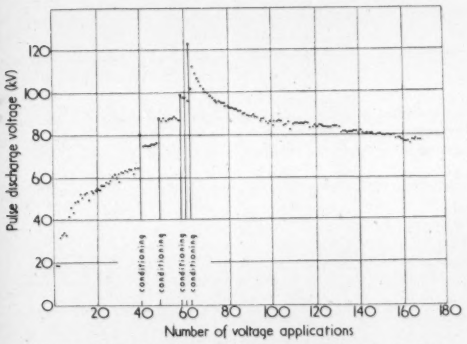

Fig. 5. "Conditioning" and "super-conditioning" effect on pulse discharge voltage for 1·5 cm gap between copper electrodes. (Cathode, 1 in. diameter hemisphere; anode, plane)

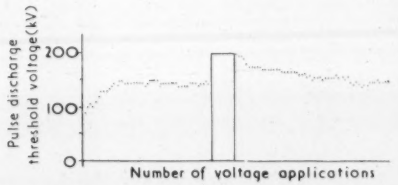

Fig. 6. "Conditioning" and "super-conditioning" effect on pulse discharge threshold voltage for accelerator tube

The pulse in this case has a peak amplitude of about 100 μA and a duration of 5 ms. The wave form is more symmetrical as shown in Fig. 4(*b*).

Threshold voltage—electrode separation dependence. No simple relationship was found between electrode separation and threshold voltage for pulse conduction. Thus for the 6 cm diameter copper electrodes used by Clifford, the variation of V_{th} with gap is as shown in Fig. 7. whilst for the accelerator tube with an effective gap of 38 cm, V_{th} was about 120 kV. It is thus clear that the macroscopic field strength is not the determining factor. Clifford showed that the area of the plane electrodes was significant, the larger the electrodes the lower V_{th}, the strongest geometry being a positive point to plane system. However, it also appears that the field at the positive electrode is important; thus Harris found that shorting out sections of the accelerator tube from the anode end actually increased V_{th} (the field at the anode plate being decreased by the Faraday cage formed by the short-circuited

length of tube). Shorting from the cathode had little effect. The pulse discharges could only be maintained if the voltage is within a few per cent of V_{th}. With good supply voltage regulation, the pulse extinguishes itself, whereas with poor voltage regulation the voltage fall is the main factor in extinguishing the pulse. Insufficient energy density is obtained in individual pulses for them to set up a low voltage discharge.

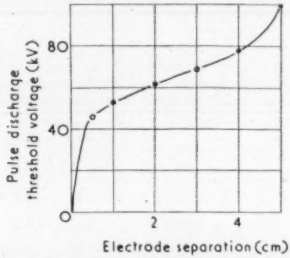

Fig. 7. Variation of pulse discharge threshold voltage with electrode separation

Pressure effects. Whereas the breakdown potential for a vacuum gap is independent of pressure below 10^{-4} mm of mercury, it is found that V_{th} is pressure dependent although more markedly for the long gap in the accelerator tube. Thus for the tube an increase of pressure from 2×10^{-5} to 2×10^{-4} mm of mercury increases V_{th} from 125–450 kV, see Fig. 8, while for the parallel plane gap Clifford observed only a 12–20% increase in V_{th} for a pressure rise from 10^{-5}–10^{-4} mm of mercury. This effect has been observed by several other users of accelerator tubes[2,3,5,6]; thus Turner reports a linear relationship between V_{th} and the mass of gas in the tube.

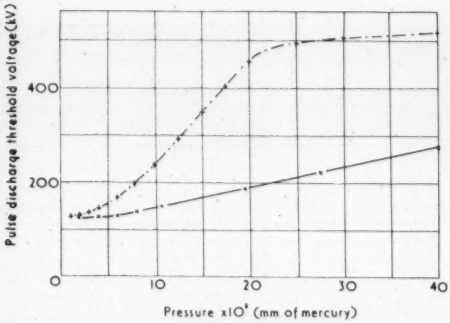

Fig. 8. Effect of pressure on pulse discharge threshold voltage

+ — · — + — · — = admission of air.
× ——— × ——— = admission of hydrogen.

Simultaneously with the pulse discharge, a pressure rise in the vacuum chamber is recorded. Stevenson was able to show that this pressure rise is the effect of the pulse discharge rather than the cause. He observed that the pressure rise is too small and occurs too late to cause conduction and it was found possible to both increase and decrease the magnitude of the pressure rise with no appreciable effect upon the size of the current pulses or the threshold potential.

Discharge channel. By coating the surface of the cathode with a fluorescent powder, Clifford observed that the discharge channel was of a diffuse nature rather than filamentary. Similarly in the accelerator tube the ratio of the current passing through a central hole in either the cathode or anode to the total discharge current in the tube was approximately equal to the ratio of the area of the hole to the cross-sectional area of the accelerator tube; i.e. the current density at the electrodes was uniform.

Effect of electrode material and pumping fluid. The influence of electrode materials was investigated by Clifford who found that the state and material used for both anode and cathode was important. V_{th} for copper electrodes was lower than V_{th} for aluminium electrodes. The influence of diffusion pump fluid was also studied and it appeared that V_{th} was higher for a mercury pumped system, than for systems using oil pumping fluids (Silicone and Apiezon B). By using combinations of copper and aluminium electrodes it was found that aluminium is to be preferred as anode material in both mercury and oil pumped systems, but the effect is not great (20%), and may not be significant.

THEORY OF THE CONDUCTION PROCESS

For pressures less than 10^{-4} mm of mercury the breakdown voltage of parallel plane gaps is independent of pressure. Van Atta *et alii*[1] suggested as a criterion for breakdown that the product AB should be greater than 1 where A is the number of ions ejected from the anode by incident electrons and B is the number of electrons ejected by positive ions incident at the cathode. Measurements of these two coefficients however, give a value of $AB \ll 1$.[13] Alternative theories of vacuum discharge have been put forward by Dyke, Trolan, Martin and Barbour,[14] and Cranberg[15]; the former is based on field emission from fine points and the latter on clumps of charged material detached from the electrodes by electrostatic forces. The fields at the electrodes at which pulse conduction occurs are too small for field emission to be significant and the observed diffuse nature of the discharge is not compatible with the "clump" theory, so that it is worth reconsidering the Trump and Van de Graaff mechanism. For this mechanism to be operative either (1) AB must be considerably larger than the measured values, or (2) some other particles are exchanged between the two electrodes for which the product $A'B'$ is greater than 1 where A' is the number of particles of type "b" ejected by particles of type "a" at the anode, and B' is the number of particles of type "a" ejected by particles of type "b" at the cathode. Considering the former possibility the fact that the discharge is self-extinguishing is significant and it is probable that the product of the coefficients is initially greater than one, but during the pulse the coefficients decrease until the product is less than one when the conduction ceases. During the measurements of A and B it was reported[13] that initial values of A and B were higher than the steady state values, although from the nature of the measurements no reliable figures for the gassy surfaces here considered can be obtained since the surfaces are bombarded continuously by high energy particles.

On the other hand the second possibility is supported by the results of Blewett[16] and Turner[3] who found that the

pulse conduction was not suppressed when secondary electrons were prevented from leaving the cathode. They point out that the magnetic field used to suppress the electrons would not have prevented negative ions from returning down their accelerator tube.

Stevenson found that he could raise the threshold potential of pulse conduction (for copper electrodes in a mercury pumped system), (1) by heating the electrodes *in vacuo* to temperatures in excess of 200° C. (2) by prolonged operation under pulsed conduction conditions, and (3) by bombardment of the electrodes by hydrogen ions produced in a hydrogen discharge at 1 mm of mercury pressure. The increase in the threshold potential thus obtained was not however permanent, and the threshold potential reverted to its original conditioned value in a period of some 5 h if the electrodes were left in the vacuum. This reduction in threshold potential could be more speedily attained by (1) washing the electrodes with commercial solvents such as acetone or toluene, or (2) by exposure to the atmosphere when the humidity was high.

Before discussing the conclusions drawn from these effects it is necessary to point out a further feature of the pulse conduction observed both with plane electrodes in a glass chamber and in accelerator tubes. It is found that the pulse extinguishes either after a fixed amount of charge has been transferred (for plane electrodes $\simeq 4\,\mu C$,[10] and for an accelerator tube $\simeq 10\,\mu C$,[6] or after the voltage has fallen by about 1% due to the regulation of the supply voltage.

These results could be explained by assuming that pulse conduction only occurs when the electrodes are covered by a layer of contaminating material and that during the pulse conduction this layer is either removed or in some way modified so that it can no longer maintain the discharge. The fact that the pulse conduction is little affected by heating to temperatures less than 200° C suggests that the contaminant is a chemi-sorbed monolayer rather than a physically adsorbed layer. Stevenson further suggested that the layer might be a fatty acid with the $-COOH$ radical adhering to the metal surface. Other possibilities are long chain hydrocarbons with acid radicals obtained from the pump oils or vacuum greases. It should be pointed out that the quantities necessary to form a mono-layer are microscopic and it is not inconsistent that the mercury pumped system of Stevenson also showed pulse conduction since small quantities of vacuum grease were present at the cone joints and in any case his backing pump contained oil.

It is pertinent to calculate the effect such a mono-layer will have upon the secondary emission coefficients at the surfaces. Taking as a model the fatty acid stearic acid $C_{17}H_{35}.COOH$, it is found that the dimensions of the molecule are, length 25×10^{-8} cm, cross-sectional area $2{\cdot}5 \times 10^{-15}$ cm^2. A mono-layer will have approximately 4×10^{14} mol./cm^2 and the density of hydrogen atoms will be $5{\cdot}7 \times 10^{22}$ H atoms/cm^3. As far as the fast moving ions are concerned, the fact that the hydrogen atoms are bound chemically to carbon atoms is immaterial and the layer will behave as though hydrogen was present at 1000 atmospheres pressure. Taking an ionization cross-section for 100 keV protons in hydrogen of 10^{-16} cm^2,[17] the probability of ionization is $10^{-16} \times 5{\cdot}7 \times 10^{22} \times 25 \times 10^{-8} = 1{\cdot}4$.

The calculation for negative hydrogen ions should give a similar result, whence one would except that a negative ion should yield at least one positive ion at the anode. The ionization cross-section for electrons is several orders of magnitude less than that for positive ions with the same energy so that one would expect few positive ions to be released by electrons.

It is not possible to estimate the number of negative ions released by a positive ion in the layer. Fogel[18] gives a cross-section of $\simeq 10^{-18}$ cm^2 for the reaction $H_1^+ + H_2 = H_1^- + H_1^+ + H_1^+$ for 30 keV protons. It is conceivable that either the reaction $H_1^+ + [C-H] = H_1^- + H_1^+ + [C-]^+$ occurs, or sputtered neutral hydrogen atoms pick up electrons produced by the ionization processes going on in the layer.

To investigate the nature of the particles exchanged between the two electrodes the small pressurized electrostatic generator was used (Fig. 3). A slit was cut in a blanking-off plate at the lower end of the accelerator tube and the particles produced in the discharge were magnetically analysed after they had passed through this slit. This analysis[9] showed that particles of mass numbers 1, 2 and between 8–12 were found with positive charges. In addition high-energy neutral particles were observed. On the opposite polarity negatively charged particles of mass numbers 1 and 12 were observed also in company with high-speed neutral particles. It is not possible to say to what extent these neutral particles arise due to charge exchange reactions in the accelerator tube or are produced by collisions of positive and negative ions with the collimating slits.

By means of electrostatic and magnetic deflexion, the collimated beam could be split so that (1) only neutral particles, (2) neutral particles and heavy ions, or (3) the whole beam continued undeflected on to a target placed in a Faraday chamber, see Fig. 3. By surrounding the target with a grid and measuring the currents to the target, grid and Faraday chamber, suitable bias voltages being applied to these electrodes, it was possible to estimate some of the secondary emission coefficients together with the magnitudes of each component of the beam.[19]

The ratio of electrons to negative ions in the negative beam was 25 : 1. The ratio of the negative beam to the positive ion beam was 12·5 : 1. The ratio of secondary-emitted negative current from the target to the incident positive ion beam was 12·5 : 1. The measurement of the other secondary emission coefficients was complicated by two difficulties, firstly the reflexion coefficient for 250 keV electrons was so large that a determination of the secondary emission coefficient of positive ions under electron bombardment was impossible, and secondly the secondary emission coefficient of negative particles under positive ion bombardment was determined only for electrons and negative ions together. If it is assumed that the ratio electrons to negative ions is maintained in the ratio of 25 : 1 for this secondary-emitted negative current then the secondary-emission coefficient for negative ions under positive ion bombardment is 0·5. The neutrals associated with the positive ion beam also released negative particles, the ratio of the negative beam released by positive ions to those released by the neutrals being 2·5 : 1. For the negative ion beam the ratio of positive ions emitted by negative ions was 0·7.

Ignoring for the moment the contribution of the neutrals, the reaction, positive ion produces negative ion produces positive ion, has a reproduction constant $A'B' = 0{\cdot}5 \times 0{\cdot}7 = 0{\cdot}35$. It is seen that although $A'B'$ is still < 1 it approaches unity more nearly than the product AB for electrons and positive ions.

Another hypothesis for the discharge mechanism has been put forward by Harris in which he postulates a reaction involving positive ions and neutrals. It is impossible, with the apparatus used, to measure the coefficients for neutral particles under positive ion bombardment and for positive ions produced by neutral particles; although it was found that neutral particles were able to release electrons and positive

ions. In support of his hypothesis Harris puts forward two pieces of experimental evidence; (1) on shorting out sections of the accelerator tube an increase in threshold potential was obtained if the shorting was carried out from the anode end, whilst the threshold potential remained constant when shorted out from the cathode end, and (2) by applying a retarding field at the cathode a 10% increase in threshold potential occurred whereas with the same retarding field applied at the anode the improvement was 75%.

Hough-Grassby has repeated the latter experiment and by applying a greater retarding field at the ends of the tube he found that he could completely suppress pulse discharge conduction on both polarities. He concluded that the exchange mechanism must involve particles of both signs.

It is still necessary to account for the asymmetrical effects of shorting-out the tube. If the positive ion per negative ion coefficient A' were field dependent in such a manner that a reduction of field also reduced A', then the action of shorting-out the tube from the anode would be to reduce the field at the anode and hence A', accounting for the increase in threshold potential. If this were the case the measured value of $A'B'$ would be low since A' is measured in a low field region in the Faraday cage. There is other evidence to suggest that the A' coefficient determined is too small. If it is assumed that most of the positive ions are produced by negative ions and vice versa, the ratio of the positive ion current to the negative ion current should be equal to the A' coefficient which gives A' as 2·0 and B' as 0·5.

One final point concerning the measured value of $A'B'$ must be made and that is that the secondary emission coefficients are not the initial values but are values obtained when the pulse current reaches its peak. It is reasonable to suppose that the value of the coefficients decrease with time as the surface is bombarded so that, although the measured value of $A'B'$ is < 1, the initial value might be $\geqslant 1$. The effects of gas pressure on the threshold potential is thought to be due to the scattering of the positive ions (H^+) and negative ions (H^-) by the gas molecules. The most probable scattering process is that of charge exchange for which the peak cross-section is 10^{-15} cm^2[17,18] at about 10 keV. The chance of a proton making a collision at a pressure of 10^{-4} mm of mercury is then

$$\frac{6{\cdot}0 \times 10^{23}}{22\,400} \times \frac{10^{-4}}{760} \times 10^{-15} \times 37{\cdot}5 = 0{\cdot}13$$

The calculation gives only the order of magnitude, but it is seen that gas pressure is likely to have an effect on the proposed mechanism.

CONCLUSIONS

In conclusion it is proposed that the operative mechanism in pulse discharge conduction is the production of positive ions in the gap or at the electrodes by some process such as the ejection of a positive ion by an electron. Then provided that the surfaces of the electrodes are covered by a suitable contaminating layer of hydro-carbons this positive ion will more than regenerate itself by the production of negative ions at the anode which release further positive ions at the cathode. The conditioning process is envisaged as a reduction of a grossly contaminated surface to a surface contaminated with a chemi-sorbed monolayer. Super-conditioning of the surface removes this layer which reforms only slowly. During conduction the contaminating layer is modified so that $A'B' < 1$ and the discharge quenches. The modification to the layer is not so extensive as in the case of super-conditioning and it reverts to its initial form more rapidly.

Pulse discharges can be suppressed by preventing hydrocarbon contamination of the surfaces in the high voltage region. This is not easy in practice since the accelerator tube vacuum system uses greased O-rings for vacuum seals and rotary backing pumps containing oil. It is clear that a minimum of grease should be used on such seals and that the seals should be broken as infrequently as possible. Similarly the back-streaming of oil from an oil vapour diffusion pump should be minimized and the vacuum system should be fitted with an isolating valve judiciously placed between the pumps and the accelerator. Continuous refrigeration of the vapour traps is likewise to be desired.

An alternative approach to the suppression of pulse discharges is to use reverse fields at both ends of the accelerator tube to prevent the charged ions from leaving the end surfaces. In essence this method of suppression uses the area effect described above since it reduces the area of the effective electrodes. This method of suppression also has its limitations as it makes the extraction and focusing of the ion beam very difficult. However, improvement in performance is obtained if it is used at one end of the tube only.

REFERENCES

(1) Van Atta, L. C., Northrup, D. L., and Van de Graaff, R. J. *Phys. Rev.* **49**, p. 761 (1936).

(2) Chick, D. R., and Miranda, F. J. *J. Sci. Instrum.* **27**, p. 337 (1950).
Chick, D. R., and Petrie, D. P. R. *Proc. Instn Elect. Engrs, B*, **103**, p. 132 (1956).

(3) Turner, C. M. *Phys. Rev.* **81**, p. 305 (1951).

(4) McKibben, J. L., and Boyer, K. *Phys. Rev.* **82**, p. 317 (1951).

(5) Heard, H. G., and Lauer, E. J. *University of California Radiation Laboratory, U.C.R.L.*, 1622 (1952).

(6) Bruck, H., Prevot, F., and McMinn, W. O. *Commissariat à l'Energie Atomique, Rapport* 189 (1953).

(7) Arnal, R. *C.R. Acad. Sci. (Paris)*, **237**, p. 308 (1953).
C.R. Acad. Sci. (Paris), **238**, p. 2061 (1954).
C.R. Acad. Sci. (Paris), **238**, p. 2402 (1954).

(8) Clifford, D. S. *Ph.D. Thesis* (University of London, 1952).

(9) Harris, D. J. *Ph.D. Thesis* (University of London, 1953).

(10) Stevenson, D. G. *Ph.D. Thesis* (University of London, 1954).

(11) Hough-Grassby, A. W. *Ph.D. Thesis* (University of London, 1956).

(12) Bruce, F. M. *J. Instn Elect. Engrs*, **94**, p. 138 (1947).

(13) Webster, E. W., Van de Graaff, R. J., and Trump, J. G. *J. Appl. Phys.*, **23**, p. 264 (1952).

(14) Dyke, W. P., Trolan, J. K., Martin, E. E., and Barbour, J. P. *Phys. Rev.*, **91**, p. 1043 (1953).

(15) Cranberg, L. *J. Appl. Phys.*, **23**, p. 518 (1952).

(16) Blewett, J. P. *Phys. Rev.*, **81**, p. 305 (1951).

(17) Keene, J. P. *Phil. Mag.*, **40**, p. 369 (1949).

(18) Fogel, I. M., Krupnik, L. I., and Safronov, B. G. *J. Exper. Theor. Phys.*, **28**, p. 589 (1955).

(19) Hough-Grassby, A. W., and Mansfield, W. K. (to be published).

Application of a microfocus Laue technique to the study of deformation in aluminium single crystals

By R. A. Coyle, F.M.T.C., A. M. Marshall, M.Sc., Grad.Inst.P., J. H. Auld, M.Met., and N. A. McKinnon, M.Sc., Aeronautical Research Laboratories, Department of Supply, Commonwealth of Australia, Melbourne

[*Paper received* 8 *August*, 1956]

A microfocus Laue technique is applied to deformed single crystals; the criterion for resolution is discussed and a description is given of an indexing net and a method of measuring image distortions and magnifications. Images of kink bands and bands of secondary slip are shown and the formation of kink bands by rotation about a [211] axis is confirmed. Kink band images are shown to be caused by over-lapping images and not extinction effects at the low amounts of strain (1%) used.

Berg[1, 2] in 1931 suggested two ways of obtaining X-ray images of crystal surfaces. The first of these made use of a parallel beam of monochromatic rays from a line source, and this method as developed by Barrett[3] and Honeycombe[4, 5] has proved extremely useful in studying inhomogeneities in deformed metal crystals. The second method employing a divergent beam of polychromatic rays from a point source has been used by Guinier and Tennevin[6] in conjunction with their focusing technique on transmission specimens, but apart from this it has been neglected until recently applied by Schulz[7] to the examination of defects in metal and ionic crystals. Subsequently Kelly and Wei[8] reported its use to detect imperfections in as-grown single crystals of aluminium. Holmes[9] also in effect used this method to study the perfection of semi-conductors. We have been using this method for a similar purpose in connexion with the study of deformed single crystals of aluminium and some of its alloys, and it is thought that some of the techniques developed may be of interest to other workers in this field.

EXPERIMENTAL TECHNIQUE

Apparatus and specimens. A divergent beam of white radiation is obtained from a microfocus X-ray tube of focal spot size approximately 50 μ, a copper target being used in preference to tungsten to avoid the unwanted L spectra from the latter. The beam is allowed to fall on the flat surface of the specimen AB (Fig. 1) at a selected angle between 20° and 45°, and the different families of crystallographic planes form enlarged Laue spots on a film F_1 placed parallel to the specimen surface. Fig. 2 shows a typical pattern of Laue images from an undeformed aluminium crystal.

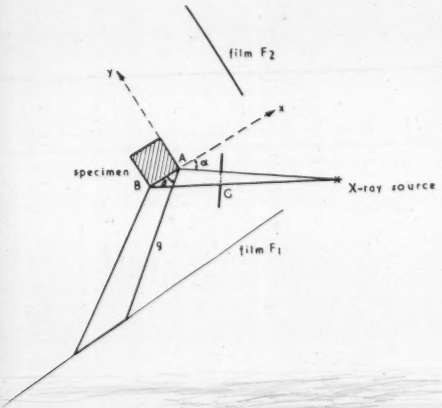

Fig. 1. Diagram showing arrangement of crystal in beam

Single crystals of aluminium (99·99 + %) were grown by the strain-anneal method and electropolished in a 5% perchloric acid 95% glacial acetic acid bath prior to straining. The work described here was done on flat specimens in the shape of a standard test piece of section 0·3 × 0·1 in. and gauge length 2·3 in. Images from the side faces of these specimens are too narrow to give much information at the higher extensions and in order to overcome this difficulty crystals are being grown with a $\frac{1}{4}$ in. square section. These square crystals can be set up as in Fig. 1 so that simultaneous photographs are obtained from two perpendicular faces with the beam striking both at 45°.

Indexing of reflexions. In order to interpret effects seen in the images from different sets of planes it is necessary to index the main reflexions. A rapid method of indexing has been devised, using a transparent net laid over the film (Fig. 2). This net gives the horizontal and vertical components of the angle between the surface and the reflecting plane; co-ordinates of points on the net at which images occur are plotted directly on to a stereogram where they represent normals to the reflecting planes, the centre (zero) point of the stereogram being the normal to the crystal surface. The lower left-hand corner of each image is used as a reference point, the corresponding point on the specimen being set in the beam so that the ray at this point is perpendicular to the vertical line of the specimen and makes the selected horizontal angle with the specimen surface. (The net in Fig. 2 is constructed for a camera angle of 45°.)

The construction of the net is as follows: the origin of a set of orthogonal axes is taken at a point A where the incident ray meets the surface of the specimen. The direction cosines of the normal to the reflecting plane are $l_1 l_2 l_3$ and those of the X-ray source with respect to this origin are $m_1 m_2 m_3$. Then as the normal to the reflecting plane bisects the angle between incident and reflected rays, the reflected ray is defined by:

$$F = \left[l_1 - \frac{m_1}{2(m_1 l_1 + m_2 l_2 + m_3 l_3)} \right] i + \left[l_2 - \frac{m_2}{2(m_1 l_1 + m_2 l_2 + m_3 l_3)} \right] j + \left[l_3 - \frac{m_3}{2(m_1 l_1 + m_2 l_2 + m_3 l_3)} \right] k$$

By altering $l_1 l_2$ and l_3 points on the net are calculated for every 10° rotation of the reflecting planes about horizontal and vertical axes in the specimen.

The geometry of image formation. Whilst the various images are formed from the different crystallographic planes of the specimen, they are all basically images of its surface layer. Thus each image, irrespective of the reflecting planes, will show the intersection of any lattice misorientation with the surface and its orientation can be determined by measurement of the angles between its trace and the specimen axis on images from two perpendicular faces. However, this angle can only be measured directly when there is no distortion of the image. This is only so when the angle of incidence to the surface α is equal to the angle of reflexion β (Fig. 1), i.e. when the reflecting planes are parallel to the surface. This is a rare occurrence and most of the images have both angular distortion and unequal horizontal and vertical magnifications. Whilst angles, distances and magnifications can be calculated for each image we have found it easier to obtain them experimentally by placing a square wire grid in the incident beam at G (Fig. 1). This superimposes a known pattern on the specimen face which is magnified and distorted on the image [e.g. see Fig. 5(d)]. Depending on their positions, the various images are magnified by 1·5–3·5 times full size and optical magnification to a maximum of 20 times is then possible.

Resolution. The resolution depends largely on the focal spot size and the specimen-source distance, as these conditions define the range of angles over which any point can reflect. Two points on the specimen will then appear separate on the image if the angle subtended by them at the image point on the film is greater than this angular range. Using a specimen-source distance of 10 cm, specimen-film distance 5 cm and a vertical X-ray tube with focal spot size 50 μ, this range is 2′ horizontally and about 20″ vertically because of the foreshortening due to the angle of viewing the target. Approaching the limit of resolution a small circle will appear as a streak owing to this greater vertical resolution. The horizontal resolution at a constant magnification varies as $\sin\beta$ (Fig. 1) and hence is a maximum where the reflected ray is normal to the specimen. The vertical resolution is a maximum at the horizontal axis of the net (Fig. 2) and changes only slightly over the area of the film.

The measurement of misorientations. The use of white radiation ensures that if a region of the matrix is tilted it will continue to reflect in its new position. Its presence is usually detected by either a black region caused by overlapping of the two images or a white region where there is a gap between them.[8, 9] A number of these gaps are indicated by arrows in Fig. 4(a). If the tilt boundary extends to the edge of the image it will in general show as a distortion of this edge. Thus the criterion for resolution of a small angle of tilt is not the complete separation of two images as is used by Holmes,[9] but the resolution of these small overlaps or gaps and the detection of movements of the edge of the image.

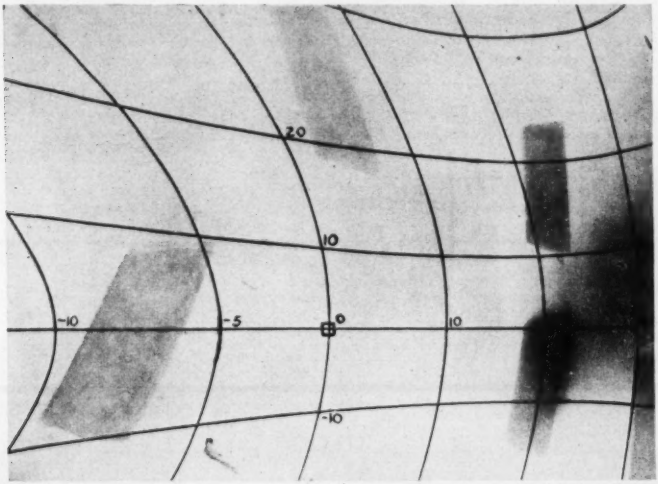

Fig. 2. Half plate X-ray photograph of an undeformed aluminium single crystal, with indexing net superimposed

The amount of movement of an image for an angle of tilt ϕ is given by Schulz[7] as $2\phi g/\sin\alpha$ for a tilt about a horizontal axis and $2\phi g \sin\alpha$ for one about a vertical axis, g being the specimen-image distance and α the angle of incidence to the surface. This means that, with our experimental set-up, the sensitivity to movement about a vertical axis is twice that about a horizontal axis. In addition to this difference in sensitivity we have, as mentioned previously, a difference in resolution in the two directions, which with a vertical X-ray tube tends to accentuate these differences. The use of a horizontal X-ray tube would result in a clearer picture, and this expected improvement has been obtained by placing the film in a horizontal plane. However, this set-up is not used regularly as it requires an awkward specimen mounting. The edges of the image are formed from the X-ray beam divergence

aperture and the edge of the specimen. The specimen edge is usually rounded during electro-polishing so that the edge of the image is rather indistinct and it becomes difficult to detect small tilts or rotations by this method, but a knife edge may be placed in the incident beam to form a reference edge on the image. The grid which was mentioned previously, is equivalent to two sets of knife edges placed vertically and horizontally in the beam, and acts as reference lines over the whole surface irradiated.

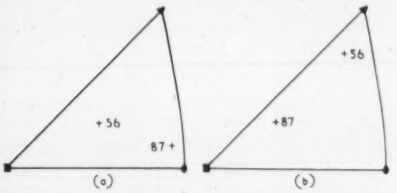

Fig. 3. (*a*) Stereographic projection of the tension axes of crystals 87 and 56. (*b*) Stereographic projection of the normals to faces of crystals 87 and 56

In the best possible case, that of sharp low angle boundaries in undeformed crystals, angles of tilt of the order of 20″ of arc have been detected. (The boundaries in Fig. 4(*a*) represent misorientations of 1–1·5′ of arc.) Where the boundaries between misoriented regions are less sharp, as in deformed crystals, the limit appears to be 1–2′.

Attempting to increase the resolution by increasing the specimen-source distance gives lower magnification and increased exposure time, while decreasing the specimen-film distance gives lower magnification and lower angular sensitivity. The best compromise is to make these distances approximately equal, and in practice a specimen-source distance of 8–10 cm and a specimen-film distance of 5–6 cm is used.

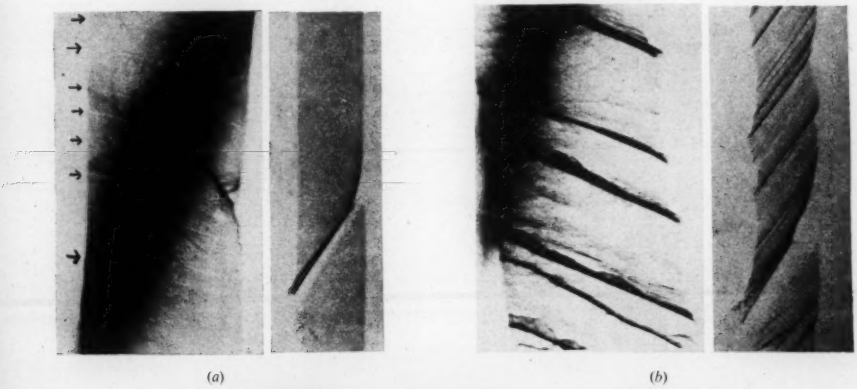

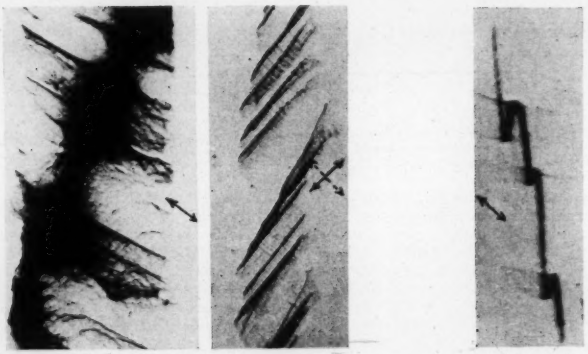

Fig. 4. (*a*, *b*, *c*) X-ray images of two faces of crystal 87 after 1% extension, 2% extension, 3% extension. (*d*) Short exposure of crystal 87 after 2% extension, showing a characteristic wavelength line only

(Solid arrows show direction of kink bands and broken arrows show direction of slip.)

Whilst most of the work has been done using coarse-grained industrial X-ray film with an exposure time of about 30 min, more detail can be obtained on a medium-grained film such as Kodak Crystallex. The very fine-grained films are not justified at the resolutions attainable.

RESULTS AND DISCUSSION

The method shows two major effects in deformed aluminium crystals, (*a*) bands parallel to the (110) plane perpendicular to the primary slip direction, shown here to be the kink bands of Cahn[10] and Honeycombe,[11] and (*b*) lines approximately parallel to the primary slip plane trace on the surface, called slip band indications. Both these effects are shown prominently in Fig. 5(*a*).

(*a*) *Kink bands.* The appearance of kink bands in the X-ray images varies considerably, depending on firstly, the orientation of the lattice with respect to the specimen axes, and secondly, the geometrical relationship between the reflecting planes and the lattice distortions caused by deformation. Due to the second effect different images on the one film, arising from different crystallographic planes, show different effects.

Specimens 87 and 56 whose orientations are shown in Fig. 3 are used to illustrate these effects. Figs. 4(*a*), (*b*) and (*c*) are images obtained from the front and side faces of crystal 87 after 1%, 2% and 3% strain respectively. Before deformation this particular specimen contained sub-boundaries which appear as roughly horizontal white lines[12] and persist up to at least 2% strain without appearing to affect the deformation. In these photographs the single broad black band is due to the characteristic radiation from the anode.

Fig. 4(*a*) shows a kink band which started from a small included grain at the right-hand edge. A few other kink bands also appeared near the shoulders of the crystal at 1% strain. On further elongation other kink bands developed and measurements on two perpendicular sides of the crystal showed that they were in the (110) plane perpendicular to the primary slip direction. The side face image in Fig. 4(*c*) also shows the slip band indications (discussed later) approximately perpendicular to the kink bands. The reason why they are not seen on the front face of the crystal is probably related to the fact that their trace is almost parallel to the trace of the kink band plane on this face; however, they may be contributing to the detail seen between the kink bands in this image [Fig. 4(*c*)].

The impression that the blackening at a kink band in these images is due to a fold in the image is well confirmed by Fig. 4(*d*) which was obtained from specimen 87 after 2% elongation, with an exposure time sufficient to give only an image from the characteristic wavelength.

The variation in the appearance of kink bands on the different crystallographic planes is illustrated in Fig. 5 which shows the images from three planes of specimen 56 after 1% strain. In the 111 reflexion the kink bands appear as black lines and also the relative orientation change across the kink bands is shown by the bending of the edge of the image. In the 110 reflexion, blackening no longer appears because in this case the reflexions from various parts of the kink band no longer overlap. The fact that no blackening at all is visible indicates that there is no real increase in the intensity of the diffracted rays at these bands and hence that extinction does not play any significant part in the black appearance of kink band images. This probably is also the case in the photographs obtained by Honeycombe.[4]

The 211 reflexion is very interesting in that nearly all evidence of kink bands has disappeared; i.e. there is practically no overlap, no bending of the image or of the slip band indications. This indicates that any misorientation must be confined to a rotation about the [211] axis which is the normal to the plane giving this reflexion. This is consistent with the work of Cahn[10] who found the kink bands to be formed by a rotation about the [211] axis which is the intersection of the primary slip plane and the kink band plane. Portions of reflexions from other planes near the {211} planes appearing at each end of the 211 image [Fig. 5(*c*)] show distinct traces of kink bands.

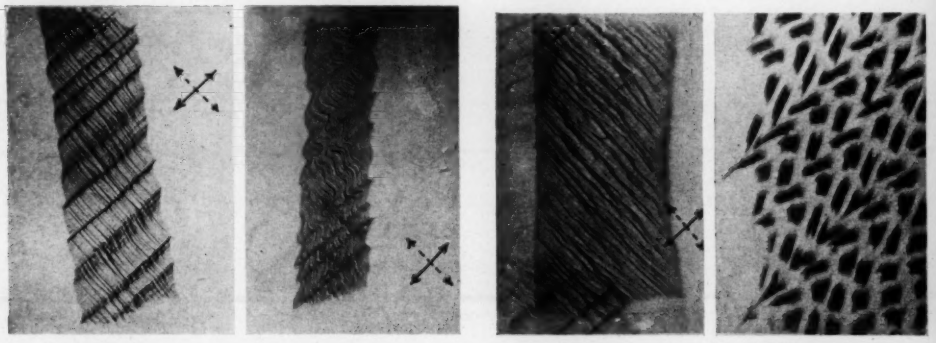

(*a*) (*b*) (*c*) (*d*)

Fig. 5. Different reflexions from one face of crystal 56 after 1% extension

(Solid arrows show direction of kink bands and broken arrows show direction of slip.)

(*a*) The 111 reflexion. (*b*) The 110 reflexion. (*c*) The 211 reflexion. (*d*) Part of the 110 reflexion with a square wire grid placed in the incident beam.

(*b*) *Slip band indications.* Frequently, in addition to kink bands, lines occur which are closely parallel to the primary slip plane. Generally these have the appearance of dark lines bordered by light edges [Fig. 5(*a*)]. Many of these light edges have been measured by using a micro-photometer and found to be of the same intensity as the general background of the film, while some of the dark bands are slightly more than twice as intense as the undistorted image. This indicates that a narrow discrete portion of the lattice parallel to the slip planes has altered its orientation relative to its neighbours. However, in this case there may be a slight additional effect due to extinction but it has not been possible to isolate it.

Optical examination of specimens giving the slip band indications in X-ray images showed bands of secondary slip; counts of both the lines in the X-ray image and the bands of secondary slip showed they were approximately equal in number. Thus it is probable that the above orientation change arises from the operation, within a band, of a second slip system. However, a rotation parallel to the slip planes as suggested by Wilman[13] could produce a similar effect.

CONCLUSION

The examination of deformed aluminium single crystals by the X-ray microfocus method has shown features of the deformation which are not revealed when the monochromatic radiation method as developed by Honeycombe is used. This latter method, however, enables higher magnifications to be obtained, but this drawback of the present technique could in theory be overcome by the use of a sufficiently fine focal spot. In addition a great advantage of this technique is the extreme simplicity of set-up lending itself especially to a rapid determination of the state of the specimen before proceeding to a microscopic examination. A large area of crystal is irradiated and in a normal exposure of half an hour many images from different sets of crystallographic planes are obtained which, when compared with one another, give further information.

Finally, accurate measures of changes in orientation within a crystal are obtained from the relative displacement of parts of the one image instead of requiring a number of photographs to be taken at accurately controlled angles.

ACKNOWLEDGEMENTS

The authors wish to thank Dr. R. I. Garrod for his encouragement during the course of this work and the Chief Scientist, Department of Supply, Australia, for permission to publish this paper.

REFERENCES

(1) Berg, W. F. *Naturwissenschaften*, **19**, p. 391 (1931).
(2) Berg, W. F. *Z. Krist.*, **89**, p. 286 (1934).
(3) Barrett, C. S. *Trans Amer. Inst. Min. Metall. Engrs*, **161**, p. 15 (1945).
(4) Honeycombe, R. W. K. *J. Inst. Metals*, **80**, p. 39 (1951).
(5) Honeycombe, R. W. K. *J. Inst. Metals*, **80**, p. 45 (1951).
(6) Guinier, A., and Tennevin, J. *Acta Cryst.*, **2**, p. 133 (1949).
(7) Schulz, L. G. *J. Metals*, **6**, p. 1082 (1954).
(8) Kelly, A., and Wei, C. T. *J. Metals*, **7**, p. 1041 (1955).
(9) Holmes, P. J. *Brit. J. Appl. Phys.*, **6**, p. 180 (1955).
(10) Cahn, R. W. *J. Inst. Metals*, **79**, p. 129 (1951).
(11) Honeycombe, R. W. K. *Trans Amer. Inst. Min. Metall. Engrs*, **188**, p. 1039 (1950).
(12) Auld, J. H., Coyle, R. A., Marshall, A. M., and McKinnon, N. A. *X-ray Microscopy of As-Grown and Deformed Single Crystals of Aluminium* (to be published).
(13) Wilman, H. *Proc. Phys. Soc. A*, **64**, p. 329 (1951).

The lives of electron microscope filaments

By R. N. Bloomer, B.Sc., A.Inst.P., Associated Electrical Industries Ltd., Aldermaston, Berks

[*Paper received* 20 *August*, 1956]

The lives of the tungsten filaments used in electron microscopes can be limited by the thermal evaporation of the metal, or by chemical attack, in inferior vacua. The lives to be expected when either cause is dominant are calculated for a variety of operating conditions. Comparison of these calculated values with measured lives shows that thermal evaporation limits lives in microscopes used at high magnifications. The life limited by evaporation decreases as the temperature and thermionic emission increase, and so corresponding values of filament life and ideal gun output brightness (thermionic emission density per unit solid angle) have been calculated for normal working temperatures, in order that a compromise may be made.

The tungsten filaments of the high-voltage electron guns used in electron microscopes are run at very high temperatures in order to obtain adequate output brightness (thermionic emission density per unit solid angle). Evaporation of the metal, which, like thermionic emission, increases rapidly with temperature, can limit filament lives to a few hours only. Hence, corresponding values of evaporation rate and thermionic emission must be known, and the filament temperature controlled accurately if the best compromise is to be made. In this paper it is confirmed that filament temperatures can be found accurately from the heating current and wire diameter. Another possible cause of short lives is gas attack upon the tungsten in inferior vacua. Since vacua, but not evaporation rates, can be improved for any given output brightness, it is necessary to be able to distinguish between these two causes.

Filaments which have been burnt out by gas attack look different from those burnt out through evaporation. Chemically attacked filaments are thinned uniformly over the incandescent region, usually to a half or less of their original diameter, because the rate of reaction of gases with hot tungsten does not change very rapidly with temperature. Filaments burnt out through evaporation are thinned noticeably only near the break, because evaporation rate varies rapidly with temperature. Under gas attack, the break may be anywhere: with evaporation, it is always at the hottest place—a little aside from the tip in the hairpin filaments of electron microscopes.

In the following section, the limitation of filament lives by residual gas attack is described. The remainder of this paper is concerned with the limitation of lives by evaporation.

LIVES LIMITED BY GAS ATTACK

The two abundant, harmful, residual gases in demountable vacuum systems are water vapour desorbed from the walls[1] and oxygen. In the present experiments, water vapour at the same pressure has been found to be a fifth as corrosive as oxygen. Using the data of Langmuir[2] for oxygen (allowing for the change in temperature scale reported by Jones, Langmuir and Mackay[3]), and the measured values for water vapour, calculations have been made of the lives to be expected with tungsten filaments run at a temperature of 2900° K in air or water vapour as a function of pressure. It has been assumed that life ends after one-third of the wire has been eroded—if anything, an underestimation. The results are plotted in Fig. 1 for air and water vapour, which are about equally destructive.

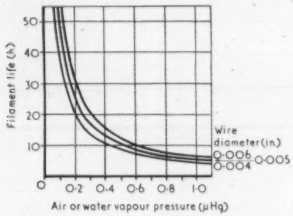

Fig. 1. Filament life, at 2900° K, *versus* eroding gas pressure, neglecting evaporation

For other temperatures, the lives plotted in Fig. 1 should be multiplied by the following factors:

temperature (°K)	2500	2600	2700	2800	3000
factor	1·36	1·25	1·15	1·04	0·92

The information in Fig. 1 is also displayed in another way in Fig. 4, for the sake of completeness.

LIVES LIMITED BY EVAPORATION

Outline of the calculations. Jones and Langmuir[4] have reported current $\times$(diameter)$^{-3/2}$ *versus* temperature data. Reimann[5] has measured the evaporation rates corresponding with temperatures found from current $\times$(diameter)$^{-3/2}$ values. From this principal data, the life *versus* initial temperature curves of Fig. 2 have been prepared, for 0·55 in. long hairpin filaments of initial diameters 0·005 in. and 0·0048 in. supplied at constant current. Allowances have been made for the heat lost to the ends by conduction, following the simple theory of Worthing.[6]

The lives of filaments are influenced by the type of electrical supply used for heating. Thus, filaments run at constant voltage become cooler, but, at constant current, become hotter as they thin. Both types of supply are used in practice, and hence lives have been calculated for each, and for intermediate cases. Fig. 3 is a plot of lives calculated for different ratios of electrical supply source to load impedance in a typical case. This shows that the sum of the source and cable impedances must be reduced to a small fraction of the filament impedance before the lengthening in filament life becomes valuable.

Measurements. The lives of 0·005 in. and 0·0048 in. diameter long filaments (2·0 in.) for the central regions of

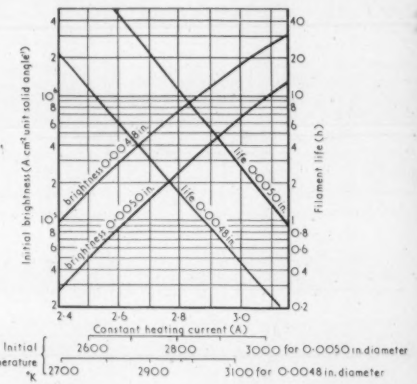

Fig. 2. Initial gun output brightness and evaporation limited life *versus* equivalent heating current and initial temperature, for 0·55 in. long filaments of 0·0048 and 0·0050 in. diameter

which end conduction losses are negligible, and of short (0·55 in.) hairpin filaments, have been measured in the temperature range 2700–3000° K for d.c. and a.c. heating sources of constant voltage and current types. For all filaments, the measured and calculated lives agreed, if they were assumed to end after 6% thinning,[7] rather than after 10% thinning.[8] (The curves in Fig. 2 are for lives ending after 6% thinning; the difference between 6% and 10% lives

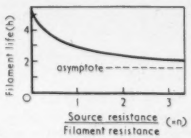

Fig. 3. Variation of evaporation limited life with change from constant voltage ($n = 0$) to constant current ($n = \infty$) supply, for initial current 3·0 A in 0·0050 in. diameter wire

for a constant current case is very small.) The agreement for long wires confirms that the basic data for evaporation rate and heating current at different temperatures is accurate. The agreement for the short filaments shows that the end losses are correctly predicted by the simple theory[6] in the temperature range of the measurements.

Lives obtained in demountable electron guns after an initial pumping of a quarter of an hour or longer have been as great as in well-baked glass vacuum systems, confirming

that, at high operating temperatures, the gas attack rates are negligible compared with the evaporation rates.

DISCUSSION

It has been shown by Haine and Einstein[9] that an electron gun gives the theoretical output brightness, when worked at optimum bias. This theoretical output brightness (β) is expressed by the Langmuir[10] formula:

$$\beta = I_e V_A e/\pi k T$$

where I_e = the thermionic emission density
V_A = the electron accelerating voltage
e = the charge on the electron
k = Boltzmann's constant
T = the filament temperature (absolute)

In Fig. 4 (full curve), the corresponding filament lives are plotted against this theoretical output brightness, for an operating voltage of 50 kV. It is seen clearly that brevity of lives restricts the brightness which can be used in service.

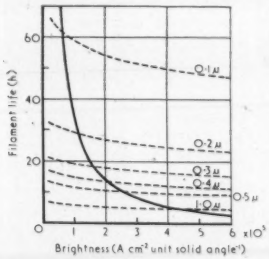

Fig. 4. Life, of 0·0050 in. diameter filament *versus* 50 kV gun output brightness, limited by evaporation (full curve) and gas attack (dotted curves) at indicated pressures (microns of mercury)

At very high temperatures, the tip of a short hairpin filament is about 1% cooler than the neighbouring parts. In high voltage guns, the thermionic emission current is drawn from only a small area, at the tip.[9] Thus, the filament lives that can be obtained at a given gun output brightness are less than they would be if the tip was as hot as nearby parts. However, in preparing Figs. 2 and 4, this complication has been ignored.

The filament lives obtained in service in microscopes worked always at a gun output brightness of 1×10^5 A cm^{-2} unit solid angle^{-1} (Haine and Mulvey[11]) have been between six and eight hours. Thus, actual electron gun output brightness is only one-quarter to one-third of ideal for this life.

Haine and Einstein[9] found that the measured brightnesses fell increasingly below the theoretical values, calculated from the Langmuir[10] formula, when the temperature of the gun filament was raised above about 2700° K. If the curve shown in Fig. 5(*b*) of the Haine and Einstein[9] paper is extrapolated to a temperature of 2950° K, the ratio measured brightness/theoretical brightness is a third or less. Furthermore, it is well known that the output brightness of electron microscope guns does not increase throughout the life of filaments which are supplied at constant current. Such filaments become thinner and hotter as time goes on. Thus the gun output brightness would increase if it was proportional to the temperature limited thermionic emission from the filament.

CONCLUSIONS

Tungsten filament temperatures can be accurately predicted from heating current measurements, provided the wire diameter is known.

It is concluded that filament lives cannot be limited by gas attack alone to less than about twenty hours, since normal working pressures are too low (see Fig. 1).

If electron microscope filaments are used at low temperatures (say below 2700° K), their lives may be limited by gas attack to values which are tolerably long, but which are less than if they were limited by evaporation at these temperatures. In such cases, lives can be lengthened by reducing the water vapour pressure near the filament; for example, by keeping short the times of standing at atmospheric pressure.

In electron microscopes used at high magnifications, for which high filament temperatures (2900–3000° K) are required, filament lives are limited by evaporation. For a 0·55 in. long × 0·005 in. initial diameter filament to have a life of ten hours, the maximum obtainable gun brightness at 50 kV is 250 000 A cm^{-2} unit solid angle^{-1}.

ACKNOWLEDGEMENT

It is a pleasure to thank both Mr. M. E. Haine, for advice and encouragement, and Mr. B. M. Cox, for much help with the experiments. Thanks are also due to Dr. T. E. Allibone, Director of the Laboratory, for permission to publish this paper.

REFERENCES

(1) BLEARS, J. *J. Sci. Instrum.*, **28**, *Suppl. No.* 1, p. 36 (1950).
(2) LANGMUIR, I. *J. Amer. Chem. Soc.*, **37**, p. 1139 (1915).
(3) JONES, H. A., LANGMUIR, I., and MACKAY, G. M. J. *Phys. Rev.*, **30**, p. 201 (1927).
(4) JONES, H. A., and LANGMUIR, I. *Gen. Elect. Rev.*, **30**, p. 310 (1927).
(5) REIMANN, A. L. *Phil. Mag.*, **25**, p. 834 (1938).
(6) WORTHING, A. G. *Phys. Rev.*, **4**, p. 524 (1914).
(7) BAS-TAYMAZ, E. *Z. Angew. Phys.*, **2**, p. 374 (1950).
(8) DUSHMAN, S. *Gen. Elect. Rev.*, **18**, p. 156 (1915).
(9) HAINE, M. E., and EINSTEIN, P. A. *Brit. J. Appl. Phys.*, 3, p. 40 (1952).
(10) LANGMUIR, D. B. *Proc. Inst. Radio Engrs*, **25**, p. 977 (1937).
(11) HAINE, M. E., and MULVEY, T. *J. Sci. Instrum.*, **31**, p. 326 (1954).

New books

Production of heavy water. Edited by G. M. MURPHY. (London: McGraw-Hill Publishing Co. Ltd., 1955.) Pp. xvii + 394. Price 39*s*. 6*d*.

This volume is one of a series in course of publication recording the work carried out in the U.S.A. during the war under the Manhattan Project and the Atomic Energy Commission. It is therefore concerned exclusively with American activities. The complete series will comprise about sixty volumes, covering eight divisions and it will thus provide a fitting monument to the most massive and highly-co-ordinated chemical engineering achievement that has yet been accomplished. The speed with which the project was brought to fruition still appears miraculous and was realized only by simultaneous concentration on all technical possibilities which might contribute to the main structure. Many of the building blocks were rough-hewn and rejected, and the final structure, though massive, was unpolished. This is the impression given by the present volume which covers the work on heavy water production. The architects were many; this book alone has three editors and eight authors and its material is drawn from several hundred reports which have only been made public ten years after the work has been completed. It must therefore be judged as an historical record rather than as an up-to-date scientific work. The editors have taken pains to emphasize this point and they admit to a certain amount of duplication and many discrepancies. They also explain that the authors have been too preoccupied to review their work adequately before publication. However much we regret this lack of polish we are grateful that the record has now been made available and our admiration of the achievement remains undiminished.

The book is in two main parts; the first describes the commercial production of heavy water and the second gives details of some of the laboratory studies which led to the technical design. Two methods were actually used on the large scale, catalytic exchange-electrolysis and distillation of water. Fractional distillation of hydrogen was considered as a third possibility but rejected on account of its technical uncertainties although calculations suggest that, as a future development, it might prove to be the cheapest and most efficient of all. The catalytic exchange-electrolysis method depends on a source of electrolytic hydrogen in large quantities and was therefore linked with the electrolysis plant of the Consolidated Mining and Smelting Co. at Trail, B.C. Water distillation plants were set up at three separate locations in the U.S.A. The Trail plant had an output of 0·55 tons a month of heavy water and the distillation plants produced altogether 1·2 tons a month. A total of 32 tons of heavy water had been produced when operations were suspended in October 1945. (The reader should remember that the American ton is 2000 lb.)

The technical details of the processes are well described and will be of interest to chemical engineers. A statement of production costs is given, but this is of little value in view of changed conditions and lack of detail to permit adjustment. It may be judged, however, that the cost of producing heavy water by present methods is not likely to fall below three to four dollars an ounce.

The studies described in Part II are somewhat unbalanced. The production of catalysts for the exchange reaction is described in detail and a number of rejected methods of heavy water recovery are briefly discussed. Some of these are remarkable as evidence of the American determination to leave no stone unhewn. Further information concerning laboratory technique would have been more useful; for instance, methods of analysis of heavy water mixtures receive very scanty treatment.

In considering the work as a whole one is impressed with the magnitude of the achievement but also with the remarkable inefficiency of the processes used. It is perhaps inevitable that separation of a component which has an abundance of only one part in seven thousand of raw material will be difficult, but a thermodynamic efficiency of the order of 1 : 100 000, which calculation indicates for the processes employed, represents an alarming waste of energy. Many physico-chemical methods may be conducted in a manner approaching thermodynamic reversibility. For example, the separation of heavy water by distillation would appear to be an ideal case for the technique of vapour recompression as a means of evaporation and condensation, but only single-effect evaporation has been practised. A more leisurely scientific approach than was possible under the circumstances might have led to greater efficiency and economy.

The book is well produced and errors and misprints are few. It is surprising, however, to find on p. 7 that steel is listed, without qualification, as the material of construction for hydrogen distillation plant operating at a temperature of 20° K. The flow diagram of Fig. 5.1 has an arrow pointing in the wrong direction which makes understanding difficult.

A. M. CLARK

Neutron cross-sections. By D. HUGHES and J. HARVEY. U.S. Atomic Energy Commission. (London: McGraw-Hill Publishing Co. Ltd., 1955.) Pp. 363. Price 90*s*.

This up-to-date compilation of neutron cross-section data will prove indispensable to nuclear and reactor physicists. Most of the book consists of graphical presentations of total and reaction cross-sections as a function of neutron energy from thermal up to several million electron volts. Comparison of these with the original version (AECU-2040) indicates strikingly the advances made in neutron spectroscopy in the past few years, due largely to the availability of velocity selectors at high flux reactors. Tables of thermal cross-sections, resonance parameters and angular distribution functions for neutron scattering are also included. It is a pity that the supplement issued at the Geneva Conference was omitted from the present edition, since it contained valuable data on the cross-sections of the fissile nuclides. This is the reviewer's one adverse criticism of an otherwise admirable volume which is a great credit to the authors and their compilation group at the Brookhaven Laboratory.

J. E. SANDERS

Reactor handbook: Physics. Editors: J. F. HOGERTON and R. C. GRASS, U.S. Atomic Energy Commission. (London: McGraw-Hill Publishing Co. Ltd., 1955.) Pp. 804. Price 90*s*.

This volume contains a vast amount of data relevant to reactor design problems. The first and larger section is

devoted to basic reactor physics and includes chapters on experimental techniques, nuclear physics, kinetic theory of neutrons and reactor statics and dynamics. The second section deals with nuclear radiation shielding. Brief discussions of theory precede the tables and graphs of data, most of which are taken from U.S.A.E.C. reports. The speed with which the handbook was compiled from numerous sources no doubt accounts for its lack of unity and balance. No data later than December 1952 is included, and the book should be used in conjunction with more recent sources of information (such as the book *Neutron cross-sections* from the same publisher which is reviewed above). Consulted critically, however, the handbook should prove a valuable addition to the reactor physicist's library. J. E. SANDERS

Introduction to numerical analysis. By F. B. HILDEBRAND. (London: McGraw-Hill Publishing Co. Ltd., 1956.) Pp. x + 511. Price 64*s*.

In spite of the development of high-speed computing devices, desk calculating machines are likely to continue to be used for many purposes, particularly in some of those branches of numerical analysis in which in recent years there have been significant advances and a widening field of applications. This is affecting, and will increasingly modify, the teaching of mathematics in our universities and technical colleges.

The new volume by Prof. Hildebrand in the International series in pure and applied mathematics is based on an introductory course in numerical analysis given at the Massachusetts Institute of Technology. The aim of the course, and of the book, is to provide "a fairly substantial grounding in the basic operations of computation, approximation, interpolation, numerical differentiation and integration, and the numerical solution of equations . . ." All this is excellently done.

There is a useful introductory chapter on errors and approximations, followed by four chapters on finite differences and various methods of interpolation. Then there are successive chapters on the numerical solution of ordinary differential equations, the determination of polynomial approximations by the method of least squares, Gaussian and other types of quadrature, various kinds of approximations including Fourier series, series of exponentials and continued fractions, and finally a chapter summarizing a number of methods available for the numerical solution of sets of equations, linear and non-linear. Collections of problems are provided at the end of each chapter.

The author has admirably fulfilled his aims, and has written an attractive book which can be strongly recommended. It is likely to become a useful companion to other recent books on the subject. J. TOPPING

Rectangular-polar conversion tables. By E. H. NEVILLE. (London: Cambridge University Press, 1956.) Pp. xxxii + 109. Price 30*s*.

This is the second volume in the Royal Society Mathematical Tables series, the successor to the British Association Mathematical Tables. It gives values of $r = \sqrt{(x^2 + y^2)}$ and $\theta = \tan^{-1}(y/x)$ in degrees to thirteen decimal places, and also of ln r and θ in radians to fifteen decimal places. The ranges covered are $x = 1(1)105$, $y = 1(1)x$. The volume is carefully arranged and beautifully printed.

The tables are designed "primarily for the use of table-makers, and for others who can often choose arguments so that interpolation is infrequent." Interpolation is possible, however, and the author describes and illustrates by examples methods based on the use of the binomial and Gregory's series once the nearest entries in the table have been located, a matter which requires some ingenuity.

The usefulness of the tables must be questioned. To a rapidly increasing extent new tables are being prepared entirely by calculation on high-speed automatic computers and fundamental tables of this kind are not needed. Moreover, table-makers using desk machines cannot always avoid interpolation. Many tables may be used, the entries in some of which form the arguments of others. Should non-pivotal values be required in the present table, most users will find it simpler and quicker not to interpolate by the methods suggested but to calculate r directly on a desk-calculating machine and θ by interpolation in a table of inverse tangents; twelve decimals (radian measure) can be obtained from existing tables.* It seems a pity that much labour and care has been lavished on the present tables for which alternatives exist, when there are so many higher transcendental functions in need of tabulation.

F. W. J. OLVER

* National Bureau of Standards. *Table of* arctan x. (Washington: Government Printing Office, 1942.)

High-energy accelerators. By M. S. LIVINGSTON. (New York: Interscience Publishers, Inc., 1956.) Pp. viii + 157. Prices $1.75 (paper cover), $3.50 (hard cover).

Dr. Livingston has written an eminently readable account of the fundamental principles of high-energy accelerators. His personal contributions in this field extend over the past twenty years from the early development of continuous wave cyclotrons to the design of the Cosmotron at Brookhaven and still more recently, in collaboration with Courant and Snyder, to the discovery of the alternating gradient synchrotron. His object has been to describe the elementary physics of orbital stability, phase stability and particle acceleration and their applications to the various high-energy accelerators now in existence. Separate chapters are devoted to the electron synchrotron, synchrocyclotron and linear accelerator, proton synchrotrons and alternating gradient synchrotrons. Typical machines in each class are described in some detail. This monograph, written two years ago, provides a useful introduction to the study of particle accelerators, the development of which shows no sign of slackening. The last chapter on alternating gradient synchrotrons is described by the author as being openly speculative. This is no longer so. Major advances in our understanding of these machines have been made in the intervening years whilst exciting new proposals for even higher energy and higher intensity machines are now being studied. W. WALKINSHAW

Notes and comments

The Physical Society's annual exhibition of scientific instruments and apparatus

The Physical Society announces that its forty-first annual exhibition will be held at the Royal Horticultural Society's Old and New Halls, Westminster, London, S.W.1, from 25–28 March, 1957 (inclusive).

Entrance to the exhibition is by ticket only and these may be obtained, free of charge, from the offices of the Society, 1 Lowther Gardens, Prince Consort Road, London, S.W.7. Members of The Institute of Physics may obtain tickets from the Institute's office. The handbook of scientific instruments and apparatus published in connexion with the exhibition will be available at the beginning of March, price 6s.; by post 7s. 6d.

Register of British manufacturers

The twenty-ninth edition (1957) of the F.B.I. register of British manufacturers classifies the products and services of over 7000 firms who are members of the Federation of British Industries. The headings used are: products and services, addresses, trade associations, brands and trade names, trade marks. In addition there are language glossaries in French, German and Spanish.

The register is published by Kelly's Directories Ltd., and Iliffe and Sons, Ltd., Dorset House, Stamford Street, London, S.E.1. The price is 42*s*.

Platinum Metals Review

A new quarterly Journal entitled *Platinum Metals Review* has just been established to provide a survey of research on the platinum metals and of developments in their applications in industry. The first issue contains eight articles under the following headings: Platinum mining in the Transvaal; The protection of chemical process equipment; Electrodeposited rhodium in co-axial radio-frequency circuits; Electrodeposition of ruthenium; A thermocouple for high temperatures; Creep properties of platinum metals and alloys; The platinum metals in catalysis; Cathodic protection of naval vessels.

The Journal is well produced and is printed on art paper throughout in a two colour process. It contains many illustrations and also a section devoted to abstracts of current literature on the platinum metals and their alloys.

The Journal which is published by Johnson, Matthey & Co., Ltd., of 78 Hatton Gardens, London, E.C.1, is obtainable from the publishers at any one of their offices or associated companies free of charge.

Erratum

In equation (10) on page 451 of the December 1956 issue of this Journal, the terms in the square bracket should be multiplied by the length *l*.

British Journal of Applied Physics

Original Contributions accepted for publication in future issues of this Journal

A study of aircraft response to sudden and graded wind gusts by means of a differential analyser. By W. R. Blunden, F. H. Hooke and H. K. Messerle.
Heat transfer with non-uniform heat generation. By P. C. Newman.
An extraction replica method for large precipitates and non-metallic inclusions in steel. By G. R. Booker and J. Norbury.
X-ray diffraction studies on precipitates and inclusions in steel using an extraction replica technique. By G. R. Booker, J. Norbury and A. L. Sutton.
The penetration of irregularly-shaped particles through an air-borne dust elutriator. By J. G. Dawes, G. K. Greenbugh and J. S. Seager.
Transverse vibrations of power transmission chains. By S. Mahalingam.
Variations in tension of an unwinding thread. By K. H. V. Booth.
A method of measuring the shear modulus of thin xylonite sheets. By J. Clarkson.
An improved spray droplet technique for quantitative electron microscopy. By H. L. Nixon and H. L. Fisher.
Highly-conducting gold films prepared by vacuum evaporation. By A. E. Ennos.
Vacuum deposited films of nickel-chromium alloy. By R. H. Alderson and F. Ashworth.
Short duration discharges between separating contacts in a 6-volt circuit. By J. Riddlestone.
Contact electrification across metal: dielectric and dielectric: dielectric interfaces. By G. S. Rose and S. G. Ward.
The dust-free space surrounding hot bodies. By W. Zernik.
On the mathematical theory of zone-melting. By I. Braun and S. Marshall.
The effect of sulphur and oxygen on the electrical properties of oxide-coated cathodes. By G. S. Higginson.
The movement of the second crossover potential of insulators. By A. B. McFarlane.
The measurement of surface residual stress by X-rays. By G. K. Hawkes.
Mercury-in-quartz thermometers for very high accuracy. By J. A. Hall and Vera M. Leaver.

Journal of Scientific Instruments

Contents of the February issue

SPECIAL ARTICLE

An introduction to the study of non-linear control systems. By J. F. Coales.

ORIGINAL CONTRIBUTIONS

Papers

A sensitive photoelectric polarimeter. By B. R. Malcolm and A. Elliott.
A precision paramagnetic resonance spectrometer. By K. D. Bowers, R. A. Kamper and R. B. D. Knight.
A variable structure-factor graph for use in crystal-structure determination. By K. A. Morley and C. A. Taylor.
A thermistor device as automatic gain control in lamp-photocell transducer systems. By A. M. Hamble.
A small vacuum induction furnace. By J. C. Matthews.
An improved inductance method for measuring susceptibilities of small paramagnetic specimens at low temperatures. By F. R. McKim and W. P. Wolf.
A 100 kV compressed-gas standard capacitor. By T. R. Foord.

Laboratory and workshop notes

A microscope stage fibre extensometer. By E. H. Andrews.
A technique for sealing aluminium-silicon foils to glass X-ray cameras. By P. J. C. Kent.
Simple double-path densitometer for controlling thickness of evaporated films. By N. A. Slark.
A centrifugal magnetic circulating pump for a totally enclosed diffusion cell. By F. Bond.
On the high residual pressure obtained during the activation of valves containing oxide-coated cathodes. By H. J. Curnow.
Preparation of seed crystals. By G. W. Green.

NOTES AND NEWS

Correspondence

Control of the distribution of a spray projected to an area. From D. J. Rasbash and G. W. V. Stark.
A water-driven device for filling, aerating and agitating baths. From A. L. Sims.

Manufacturers' publications

New instruments, materials and tools

Notes and comments

THIS JOURNAL is produced monthly by The Institute of Physics, in London. It deals with all branches of applied physics (including theory and technique).
All rights reserved. Responsibility for the statements contained herein attaches only to the writers.
EDITORIAL MATTER. Communications concerning editorial matter should be addressed to the Editor, The Institute of Physics, 47 Belgrave Square, London, S.W.1. (*Telephone:* Sloane 9806.) Prospective authors are invited to prepare their scripts in accordance with the *Notes on the preparation of contributions*. (Price 2*s*. 6*d*. including postage.)
REPRODUCTION. The Institute of Physics is a signatory to The Royal Society's Fair Copying Declaration. Details may be obtained upon application from The Royal Society, London, W.1.
ADVERTISEMENTS. Communications concerning advertisements should be addressed to the agents, Messrs. Walter Judd Ltd., 47 Gresham Street, London, E.C.2. (*Telephone:* Monarch 7644.)
CLAIMS FOR MISSING JOURNALS. Claims from regular subscribers to this *Journal* for missing numbers will only be considered if received within 60 days of the date of mailing plus normal outward time of transit and time for lodging the claim. Losses attributable to failure to notify a change of address or to similar omissions will not be considered.
SUBSCRIPTION RATES. A new volume commences each January. The charge is £5 per volume ($14.25 U.S.A.), including index (post paid), payable in advance. Single parts, so far as available, may be purchased at 10*s*. each ($1.50 U.S.A.), post paid, cash with order. Orders should be sent to The Institute of Physics, 47 Belgrave Square, London, S.W.1, or to any bookseller.

Some recent developments in the physics of fuel combustion*

By Prof. M. W. THRING, F.Inst.F., F.Inst.P., M.I.Chem.E., University of Sheffield

The main factors limiting combustion intensity in practical solid or liquid fuel systems are macro and micro mixing of fuel and air, heating the incoming fuel and heat loss from the flame. Micro mixing leads to a combustion time proportional to the square of the initial particle or droplet diameter so that fineness of grinding or "atomization" is the prime essential. In grate firing the high relative velocity of gas and particle can give a much greater rate of micro mixing and the particles remain in the combustion chamber until they are consumed. Macro mixing can be predicted from isothermal models in the three cases of the high velocity fuel jet, the large preheated gaseous fuel jet and the low Reynolds number heating flue—the geometrical distortion to allow for the density change on combustion is different in the three cases. The first case which corresponds to the liquid fuel fired open hearth steel-melting flame has been extensively studied to throw considerable light on the optimum design. Models can also be used for predicting the erosion of walls, the distribution of fuel residence times and the effect of buoyancy. A method of calculating the heat transfer rate from various flames in the open hearth furnace is providing a link between the model work, and flame radiation measurements and practical operation.

INTRODUCTION

The satisfactory combustion of any fuel requires:

(1) stability of the flame.
(2) completion of the heat releasing reactions in a chosen volume of the combustion chamber.
(3) maximum heat transfer rate from the flame to the object to be heated.

All methods of ensuring stability of the flame require the heating of a fuel-air mixture up above a critical ignition temperature; the classical method was to have so low a velocity of the incoming fuel-air stream that the conduction of heat against the incoming premixed stream was sufficient as in the Bunsen burner. The use of the work of compression to raise the temperature is a second method which is applied in the Diesel engine. The oil fired open hearth furnace or the pulverized coal fired boiler rely on radiation from the later flame, direct and indirect via refractory walls, to heat up the incoming fuel so that it ignites in a region where the edges of the stream have already entrained some of the surrounding combustion air. Finally the use of recirculated combustion products re-entrained by the incoming fuel or fuel-air mixture is the method which enables flames to be stabilized at velocities of the order of hundreds of feet per second in the gas turbine combustion chamber.

This paper deals, however, mainly with experiments concerned with the attempt to throw light on the second and third of the requirements.

THE PHYSICS OF COMBUSTION

Longwell[1] has recently injected a premixed fuel-air stream radially at very high velocity through a number of small holes in a small sphere at the centre of a large refractory lined sphere, the combustion products leaving through holes in the outer sphere which are not in line with those in the inner sphere. Thus he obtains almost homogeneous mixing of the combustion products and the incoming fuel-air mixture. This has shown that heat release rates of the order of 10^8 C.H.U./ft^3 h are obtainable when the physical processes are sufficiently rapid. It thus proves that the chemical reaction rate is so fast at the temperatures prevailing in practical flames at normal pressures that the factors limiting actual combustion rates are entirely the physical ones of mixing and heat loss from the flame.

The combustion intensity in a pulverized coal fired boiler is of the order of 3×10^4 C.H.U./ft^3 h and if the firing rate is pushed above this value unburnt carbon appears in the gases leaving the combustion chamber. The fraction of the volume of the combustion chamber used for igniting the fuel stream is relatively small so we can say that the main problem is the physical one of macro- and micro-mixing, that is bringing the oxygen first between the coal particles and then to their surface.

The micro-mixing process for burning of liquid fuel droplets and solid fuel particles can be studied by suspending single droplets or particles on a silica thread in an atmosphere of air and igniting them either by an instantaneous passage of a flame[2] or by surrounding them with a source of radiation and convected warm air.[3] Simpson[4] at the Massachusetts Institute of Technology has used the more difficult technique of throwing droplets of a known size through a hot furnace for a known time and then catching them and weighing them. The results of such studies can be summarized as in Fig. 1. They lead to the conclusions that:

(i) The lighter liquid fuels burn by evaporating under the action of heat conduction to the droplet from the flame of vapour burning around it.

(ii) Heavier hydrocarbons burn partially in this way and then form a residual coke particle which burns much more slowly than the volatile component. Fig. 2 shows such a heavier hydrocarbon before and during burning.[5]

(iii) When either a liquid droplet or a solid fuel particle is burning by one mechanism alone the rate of loss of mass is approximately proportional to the first power of the diameter so that the total time of combustion of a particle is approximately proportional to the square of its initial diameter. This is, of course, why in burning pulverized coal it is the fraction of coarsely ground coal which gives the most trouble and similarly in burning "atomized" fuel oil it is the fraction of coarse droplets which are liable to land on surfaces before they are burnt out.

This brings us to the problem of atomization of liquid fuels. When steam or high pressure compressed air is used for atomization there is plenty of energy available and it is not necessary to impinge the gas at high velocity past the emerging liquid to obtain fine droplets; indeed a simple system in which the oil leaks out into the gas just before the latter is expanded to high velocity gives as good atomization

* Based on a lecture delivered to Section A of the British Association at Sheffield, 1956.

as the systems which destroy a considerable fraction of the energy of the gas solely for this purpose. Recent work by Fraser[6] has shown that even with pressure jet atomization the surrounding atmosphere plays a big role in breaking the sheet of fluid up into fine droplets so that the droplets suddenly become much coarser if the atmospheric pressure is reduced.

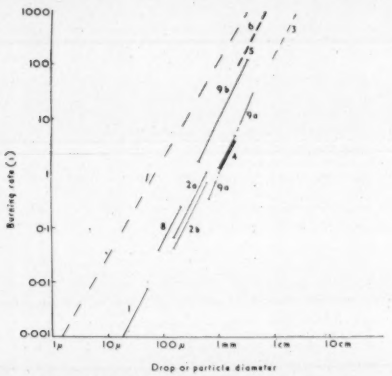

Fig. 1. Measurement of the burning time of single particles and droplets (t_c against $k \cdot d_0^n$)

t_c = burning time (s).
d_0 = initial diameter (cm).
k, n = constants.

Numbers on graphs refer to investigations carried out as follows:

		Investigator	*Fuel*
Liquid fuels	(1)	Burgoyne and Cohen	Tetralin drops in flame
	(2*a*)	Hall and Diederichsen	Kerosine
	(2*b*)	Hall and Diederichsen	Tetralin
	(3)	Spalding	Kerosine on 1 in. sphere
	(4)	Godsave	Various fuels
Solid carbon	(5)	Spalding	Predicted
	(6)	Godsave	Predicted
Pulverized coal	(7)	Rosin equation	Particles in flame
	(8)	Orning, Griffin, Adams and Smith	Single particles
	(9*a*)	Essenhigh	Captive particles (volatiles)
	(9*b*)	Essenhigh	Captive particles (residue)

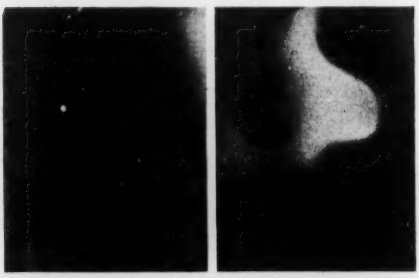

Fig. 2. Droplet of heavy fuel oil (*a*) before burning, and (*b*) burning

There are two aspects of the combustion of solid coke on a grate which involve physics. When oxygen is being consumed in a fuel bed the temperatures rise to values at which the surface chemical reaction rate is so fast that the rate determining process is the transfer of oxygen to the surface. It has been shown[7] that this rate can be predicted quite accurately using the known heat transfer rates in packed beds and the heat transfer/mass transfer analogy. In the case of the carbon dioxide reduction reaction which occurs later in the bed, the temperatures are falling and the mass transfer and chemical reaction rate are liable to compete as rate determining processes. Hornsby Smith[8] is measuring the overall reaction rate and the heat transfer rate in the same packed bed in the endeavour to separate the two resistances at various temperatures.

The other physical process is the radial transfer of heat to water cooled walls in burning a bed of coke at very low combustion rates as in a domestic boiler banked at night. It is common experience that if one tries to run such a boiler on hard coke at less than about 1 lb/h burning rate it is liable to go out, but work by Moles[9] is indicating that with controlled forced draught the radial heat flow does not quench combustion on the axis of the fuel bed at much lower combustion rates.

AERODYNAMICS OF COMBUSTION

In the gas turbine combustion chamber where mixing is very good it is likely that the burning time of individual fuel droplets is a major factor determining the maximum combustion intensity, but in the turbulent jet diffusion flame such as occurs in the open hearth furnace the entrainment of air is the primary factor. Hence aerodynamic studies are of great importance for deciding the best flame conditions. The most obvious method for making such studies is to use small scale isothermal models such as shown in Fig. 3.

Similarity in isothermal models. In general it is not possible to construct an isothermal model which gives a flow throughout which is completely similar to that in a system in which heat is being released by combustion. However, there are three cases in which suitable assumptions allow a flow pattern to be achieved which is correct in the vital part of the system, namely that where the fuel stream entrains the stoichiometric proportion of air.

(*a*) The fully turbulent system with a very small nozzle discharging a high energy fuel stream into a large chamber with slowly moving air (open hearth flame with steam or compressed air atomization). In this case one can assume that (i) all the energy of mixing comes from the fuel stream, (ii) the jet behaves like a free jet until a point where the temperature of the flame is close to the maximum value so that its momentum is conserved and it entrains air at a mass rate per unit distance proportional to the square root of the product of the jet momentum and the density on the axis, and (iii) the angle of this free jet is unaffected by the temperature rise. This leads to the similarity condition that the model is geometrically similar to the full size furnace, but operated with that jet nozzle diameter which would give the correct mass flow rate of fuel with the correct jet momentum, but with the density of the hot flame. In this case, therefore, the nozzle is distorted to a proportionately larger size than in the non-isothermal original.

(*b*) In the case where the volume flows of both the entering air and fuel streams are of the same order and the linear dimension of the fuel nozzle is comparable to the width of the furnace so that the whole flame is the transition region from the nozzle flame to the free jet flow, it is usual to assume that mixing occurs primarily as a result of turbulent flow in the main furnace impingement on the bath. For a free jet with infinite air available the distance to reach the stoichiometric mixture (mass concentration of nozzle fluid C_T) on the axis is given approximately by the formula

$$l_T = 5{\cdot}0\,.\,(d_0'/C_T)$$

where d_0' is the equivalent nozzle diameter as defined above

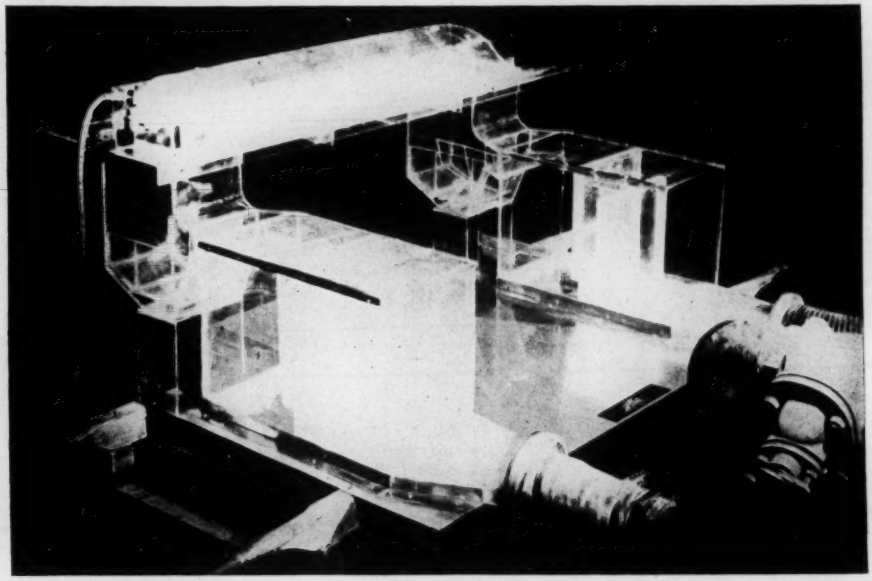

Fig. 3. Open hearth aerodynamic model

structure and to make the air and fuel entry ports geometrically similar in the model to the original. Since the case here is usually that of producer gas firing where both gas and air are preheated to over 1000° C before entering the furnace while the maximum flame temperature is about 1700–1800° C, the density change is not too great and the simple approximation of ignoring it gives reasonably valid results.

(*c*) The third case arises when the flow is on the borderline of streamline and turbulent as in the firing of individual flues of a coke oven.[11] Here it is necessary to have the correct Reynolds number both in the entry ports and in the combustion chamber which means that in the isothermal model the entry ports for the light coke oven gas is proportionately much smaller than the main flue while the air entry port has to be very slightly proportionately smaller.

Mixing. The length of the steam atomized oil flame in the open hearth furnace has been largely explained by applying the conception of the free jet mixing system with the assumption that combustion does not change the angle of the jet, and then superimposing the effect of the walls and the flame for similarity of this type of system; d_0' can be shown to be given by

$$d_0' = 2(m_0 + m_s)/\sqrt{\pi \rho_f G}\ \text{cm}$$

where m_0 = mass flow of oil
m_s = mass flow of steam (g/s)
ρ_f = density of hot flame gases (g/cm^3)
G = jet momentum (dyn).

The concept of the equivalent nozzle diameter has been shown[10] to give a good account of hot jets mixing in cold air (Fig. 4), but not to account fully for the effect of nozzle pressure. The agreement for an actual horizontal Town's gas flame jet (Fig. 5) is not perfect but shows that combustion does not produce a large change in the jet angle. Fig. 6 shows that the initial density of the jet does not change the visual jet angle.

The next step in bringing the studies of mixing towards useful application is the case of the jet flowing down the axis of a long channel of square cross-section. Such enclosed jets mix at first like free jets, but then the jet entrains all the available combustion air and so its further requirements of entrainable fluid must be made up by fluid recirculated from later in the stream. Hence the initial rate of mixing falls off

and eventually the final mixture corresponds to the fuel-air ratio inserted into the system. At first sight one might think that there are two independent parameters to provide families of curves for the mixing process, namely the ratio of the nozzle diameter to the enclosing tube diameter, or furnace dimension and the fuel air supply mass ratio. However,

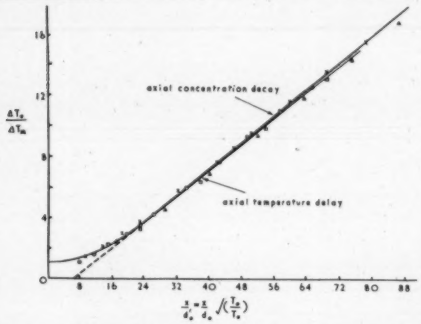

Fig. 4. Hot jets mixing in cold air. Axial decay of temperature plotted in terms of equivalent nozzle diameter [$= d_0\sqrt{(T_a/T_0)}$ in this case] for low nozzle pressure. Experimental points refer to temperature measurements

○ = $\frac{3}{8}$ in. diameter
× = $\frac{5}{16}$ in. diameter.
△ = $\frac{1}{2}$ in. diameter.
□ = $\frac{3}{16}$ in. diameter.

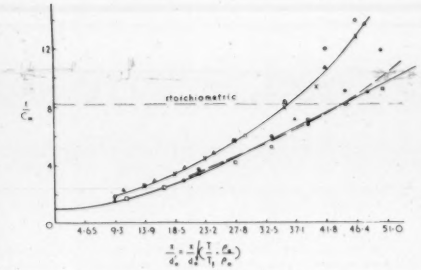

Fig. 5. Axial concentration decay in horizontal unaerated flame

	$\frac{3}{8}$ *in. nozzle diameter*	$\frac{5}{8}$ *in. nozzle diameter*
1st run	× = CO by combustion	• = CO by combustion
2nd run	○ = CO by combustion	□ = CO by absorption
3rd run	△ = CO by absorption	

provided the nozzle is very small compared to the furnace and the air mass flow is large compared to the fuel mass flow, they can be combined into a single family if one plots

$$\frac{1}{C_m}\cdot\frac{r_0}{L} \text{ against } \frac{x}{L} \text{ with } \phi = \frac{1}{C_\infty}\cdot\frac{r_0}{L} \text{ as the parameter,}$$

where

C_m = mass concentration of nozzle fluid on the axis
r_0 = equivalent nozzle radius
L = characteristic dimension of channel, e.g., side of square cross-section
x = distance along the axis from the nozzle
C_∞ = mass concentration of nozzle fluid when the two streams are fully mixed.

This follows because all the free jet mixing lines are the same with this plot and the distance to the point where all the available air has been entrained

$$= \text{const.}\ \frac{r_0}{C_\infty} = \text{const.}\ \phi\ .\ L$$

so that it is the same in terms of L for the same value of the parameter ϕ whatever r_0 is. This point is shown in Fig. 7.

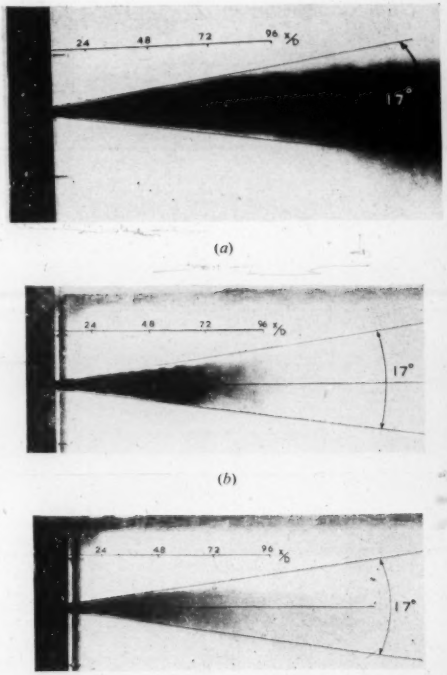

Fig. 6. Jets of magnetite slurry projected into slowly moving stream of water for density ratios of 1·2, 1·5 and 2·0

(*a*) U_0 = 23·4 ft/s; sp. gr. = 1·2; exposures = 16 s.
(*b*) U_0 = 28·1 ft/s; sp. gr. = 1·5.
(*c*) U_0 = 23·1 ft/s; sp. gr. = 2·0.

Fig. 7(*a*) shows the results with three different nozzle sizes in one box (one value of L) plotted against x/d_0' for the same value of C_∞. The free jet lines and the mixing at infinite distance are made to coincide, but the intermediate mixing curves are quite different. Fig. 7(*b*) shows the proposed method of plotting for two values of the parameter ϕ, each curve consisting of results for four different nozzle sizes.

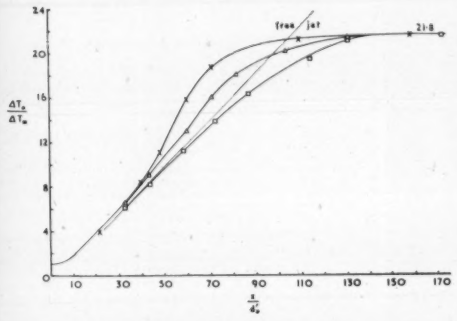

Fig. 7(*a*). Enclosed jet temperature decay as a function of axial distance in equivalent nozzle diameter
× = $\frac{5}{16}$ in.; △ = $\frac{1}{4}$ in.; □ = $\frac{3}{16}$ in. diameter.

As far as mixing is concerned the oil fired open hearth furnace is very similar to the simplified system of the axial enclosed jet except that the air is not introduced quite uniformly over the end and the jet impinges at a small angle on the surface of the molten bath. The former effect makes practically no difference to the axial mixing of the jet, but does effect the recirculation pattern since recirculation is rarely exactly symmetrical. This is probably quite important in determining the rate of heat transfer to the walls of the furnace and hence the maximum fuel input rate possible without melting the walls, but the exact laws of the process are not yet known. The effect of impingement of the jet on the bath is mainly to slow down mixing because it prevents access of air to the underside of the jet.

Mixing and flame length in the producer gas fired open hearth furnace are much more sensitive to the shape of the air inlet ports than in the case of oil firing and the main method of accelerating mixing is to bring the air onto the fuel jet at as great an angle as possible and with as high a velocity as the small pressure head available will permit.

Fig. 8[11] illustrates the method of varying the mixing length in systems of the third type, that is, operating with a Reynolds number in the region of the critical value. It is a water model of the hairpin flue of a coke oven. Here, enlarging both the air and gas ports for given mass flow rates slows down mixing to the point where combustion is still proceeding round the bend of the flue. This enables the evenness of heating up the oven wall to be adjusted.

Although chemical reactions are very fast at combustion temperatures it does not follow that combustion is complete

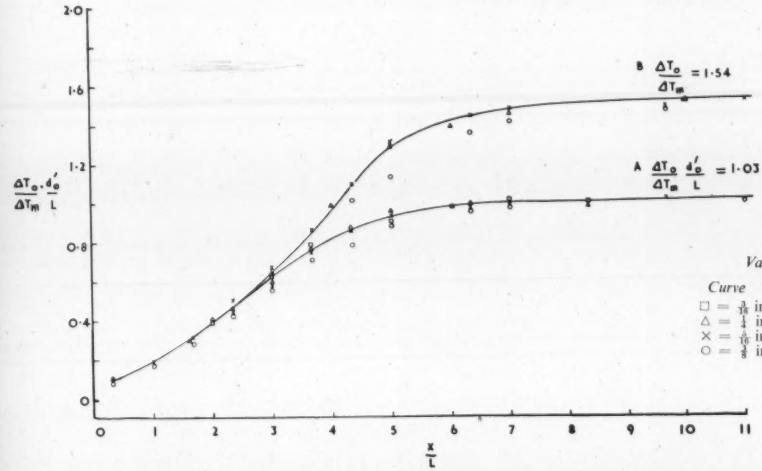
B $\frac{\Delta T_0}{\Delta T_m}$ = 1·54
A $\frac{\Delta T_0}{\Delta T_m} \cdot \frac{d_0'}{L}$ = 1·03
$\frac{\Delta T_0}{\Delta T_m} \cdot \frac{d_0'}{L}$
$\frac{x}{L}$
Values of $\Delta T_0/\Delta T_\infty$
Curve A B
□ = $\frac{3}{16}$ in. 21·8 33·1
△ = $\frac{1}{4}$ in. 16·35 24·8
× = $\frac{5}{16}$ in. 13·1 19·85
○ = $\frac{3}{8}$ in. 10·9 16·5

Fig. 7(*b*). Enclosed jet temperature decay plotted as $\frac{\Delta T_0}{\Delta T_m} \cdot \frac{d_0'}{L}$ against $\frac{x}{L}$

These figures also show that as the parameter ϕ gets larger and the distance to entrain all the available combustion air becomes equal to the distance for the jet to spread to the walls, the enclosed jet actually mixes faster than the free jet because the velocity of the surrounding air stream becomes large enough to superimpose its mixing on that of the jet.

when the time average mixture at a point is stoichiometric because there are random fluctuations in composition in a turbulent jet so that excess fuel and excess air conditions alternate in time. Hottel[12] has shown how one can calculate the magnitude of these fluctuations from the extent to which oxygen and combustibles are found together in a time mean

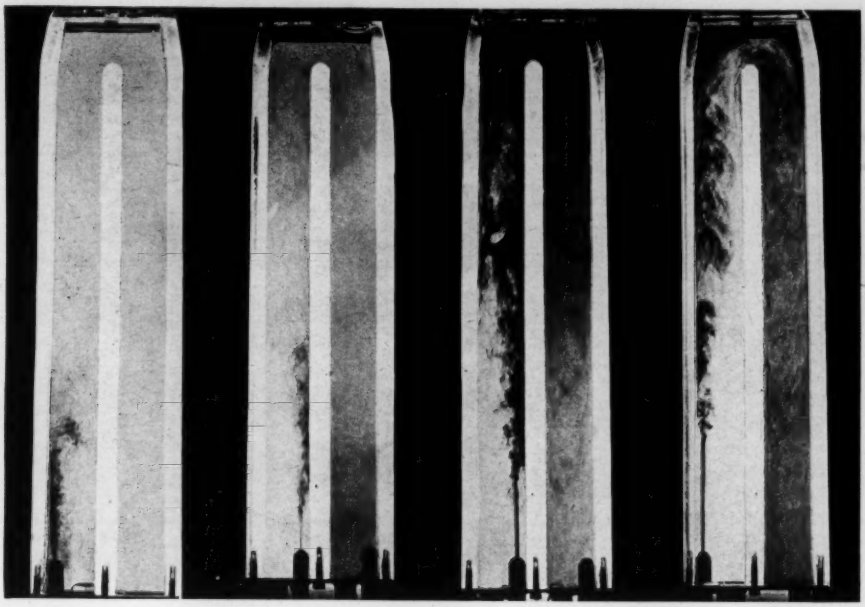

Fig. 8(*a*). Water model of hairpin flue of coke oven

Fig. 8(*b*). Mixing contours for coke oven heating flue flames

——— stoichiometric line.
– – – – lines of equal concentration.

	Model	*Plant*	*Model*	*Plant*
	A		*B*	
Gas nozzle dia. mm.	1·67	50	1·67	50
Airports mm²	7·65	106	13·00	182
Flame length mm. ft	135	4·4	220	7·2
	C		*D*	
Gas nozzle dia. mm	3·14	94	3·14	94
Airports mm²	13·00	182	17·20	240
Flame length mm. ft	300	9·8	Very long	

sample taken from a flame with a reaction quenching probe, but Raper[13] is now developing a gas analysis probe with a hypodermic needle tip so rapid in analysing that the magnitude of these fluctuations can be distinctly observed.

Flow pattern and wear. The air and water model technique have probably been applied to the study of combustion systems for evaluation of problems of flame erosion of walls more than to any other type of problem. In the open hearth furnace the charge has to be tapped at a temperature only 150° C below that at which the roof and wall bricks actually melt, and hence it is vitally important that the flame shall be as close to the charge as possible and as far from the walls as possible. Unfortunately the simplest way to bring the flame close to the charge is to impinge the fuel jet onto the surface of the bath and in a long narrow furnace this means that the flame bounces off the surface and spreads up the side walls to hit the roof. Model tests and flame photographs using the British Iron and Steel Research Association periscope[14] have shown this effect very clearly. An air model technique used to study the aerodynamic effects of the flame on the furnace walls has been the "sticky dust" technique in which the roof of the model is made sticky and the distribution of dust on it is observed after releasing the dust in front of the burner nozzle and is shown in Fig. 9. This technique has given interesting results on the effect of the sloping backwall on the grooving of the roof along the back, but it has been criticized on the grounds that the dust does not indicate the correct effect of flame pick-up of fluxing materials from the bath. United Steels have accordingly used a gaseous tracer emitted through the surface of the model bath and the Royal Dutch Steelworks have used an electrically heated surface to represent the bath and then measured the rise in temperature of the roof due to forced convection by the flowing gases from the bath to the roof. It is probably true to say that models can be used quite satisfactorily now to decide whether one design will suffer more or less than another from this type of erosion

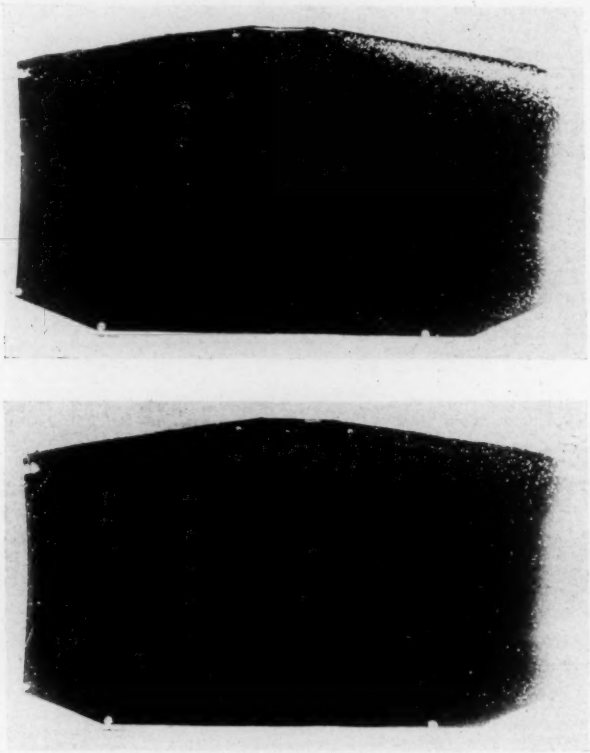

Fig. 9. Distribution of dust on roof of "sticky dust" model.
(*a*) Better distribution. (*b*) Bad distribution.

**

although we cannot yet specify in general terms what are the right design principles.

The cold furnace itself has also been used as a model[15, 16] for studies of the velocity distribution in glass tanks and open hearth furnaces, using Reynolds similarity and equality of jet momentum and obtaining the flow by the use of the induced draft fan and compressed air jets. This technique ensures perfect reproduction of small irregularities of the furnace walls but does not lend itself readily to changes in the geometrical shape of the furnace.

Particle dwell times. With liquid fuel droplets or pulverized coal particles a finite time is required to burn the particle even after all the combustion air is mixed between the particles, and hence the residence time of the fuel in the combustion chamber is of importance. Clearly the best system is one in which all the fuel flows at equal velocity along paths of equal length in the combustion chamber for then its residence time is given by the classical formula

$$t_m = \frac{\text{Volume of chamber } (m^3)}{\text{Volume flow rate of combustion products at flame temperature } (m^3/s)} \text{ seconds}$$

no matter what the path is. However, at the other extreme, there is the case where 99% of the fuel flows down the axis of the chamber in $\frac{1}{10}$ of the total volume and hence with a residence time $\frac{1}{10}t_m$ while the remaining 1% recirculates slowly in the other $\frac{9}{10}$ of the chamber.

Thus, for example, the time for the fuel which flows along the axis of a free jet can be calculated from the hyperbolic velocity function

$$\frac{U}{U_0} = \frac{6{\cdot}4\, d_0'}{x}$$

assuming it heats up rapidly so that d_0' is the equivalent nozzle diameter to be $x^2/12{\cdot}8\, U_0 D_0$. The ratio of this time to the classical mean time t_m for a square box of side D and length $l = nD$ is given by

$$\frac{t_m}{t_1} = \frac{p}{n} \cdot \frac{m_0}{m_0 + m_a} \cdot 12{\cdot}8 \sqrt{\frac{4}{\pi}}$$

where m_0 is the mass flow of the fuel stream, m_a that of the air stream and $p = D/d_0'$. For a steam atomized oil flame $m_0/(m_0 + m_a) = 0{\cdot}09$, p would be of the order of 30, $n = 3$, so that $t_m/t_1 \simeq 15$. I.e. the fuel that travels down the axis leaves the chamber in $\frac{1}{15}$ of the classical mean time. This crude calculation shows that the distribution factor for residence times is as important as the volume of the combustion chamber. Peirce[17] is studying the residence time distribution for actual pulverized coal combustion chambers by means of cold air models using a visual indicator and the interruption of a light beam at entry and exit to give the time distribution. The work already indicates that the practical combustion systems developed empirically although quite different from each other agree in having aerodynamic arrangements which give most of the fuel flow at the mean time.

Buoyancy. High velocity flames are not appreciably deflected from the constant density path by buoyancy effects and there is no need to take account of such effects in using isothermal models. However, in the case of low velocity flames of light fuel gases such as coke oven gas a condition can arise where the flame rises rapidly to the roof of the furnace under the action of buoyancy. A model technique for simulating these effects was used 50 years ago in Russia by Groume Grjimailo[18] but he used streamline flow to represent furnace flow which is almost always turbulent. Rosin[19] used salt briquettes dissolving in water to represent hot combustion gases rising from a fuel bed in an inverted model, but in such a model the final fluid cannot be recycled which involves the use of very large quantities of water if Reynolds similarity is maintained. Hence the use of a magnetite slurry with a density of up to 2 in water had recently been introduced[20] with the further advantage that the "flame" can be seen and photographed, as shown in Fig. 10.

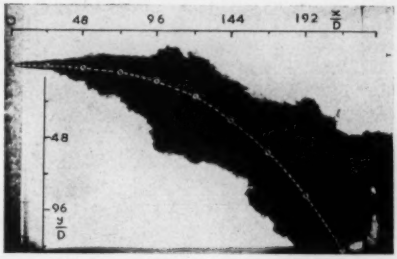

Fig. 10. Horizontal jet of magnetite slurry deflected by gravity in water
$U_0 = 20{\cdot}09$ ft/s; sp. gr. $= 2{\cdot}0$.

This technique has enabled a general formula to be developed for the path of an initially horizontal jet of density different from its surrounding, allowing both for the decay of velocity and the decay of density difference as the jet entrains the surrounding fluid.

HEAT TRANSFER FROM FLAMES

The complete calculation of the rate and distribution of heat transfer from a live flame is impossible both because of the complexity of the radiant interchanges involved and because of lack of knowledge of the differential equations connecting combustion mixing heat release and local flame luminous emissivity. It is for this reason that all practical flame heating systems have evolved more or less empirically and often rival methods quite different in arrangement are equally flourishing. The work of the Flame Radiation Committee in the attempt to fill in the differential equations connecting combustion and flame emissivity was described in a paper to the British Association last year. Here it may be interesting to describe briefly the simplifying assumptions that have been used[21] to develop a practicable method of calculating the heat transfer in one system—the open hearth furnace—using the Flame Radiation Committee results to predict the flame characteristics. These are:

(i) The furnace and flame are divided into six longitudinal sections and it is assumed that net heat flow between sections by radiation and by flame recirculation can be neglected.

(ii) The surface of the bath is assumed to be at a temperature which is uniform along its length and constant at an appropriate mean value (1500° C) throughout the whole time of the charge.

(iii) The aerodynamics of the flame are simplified to bring it to the shape of a flat laminar wedge spreading from a point at the burner tip to half the width of the bath at the outgoing end of the furnace.

(iv) The flame is assumed to release all its heat by com-

bustion uniformly along a certain fraction of the length of the furnace as the air is entrained into the flame.

(v) The emissivity of the flame is assumed to fall linearly from unity at the start to the non-luminous value corresponding to the carbon dioxide/water content of the combustion products (about 0·2).

(vi) All the heat transfer is assumed to be by radiation.

This calculation model enables one to evaluate quantitatively the effect on the flame temperature, the heat transfer rate and the roof temperature of changing the fuel to change the emissivity or changing the steam oil ratio or the fuel input. It tends to give too high a heat transfer rate (too short a calculated melting time) which would appear to indicate that there is no room for appreciable heat transfer by convection, although there is an apparent slight anomaly when the effect of shortening the flame by increasing the steam oil ratio is calculated which might be explained by convection.

CONCLUSIONS

There is much more research to be done in the no-man's-land between industrial combustion systems and the laboratory differential equations before the latter can be used for complete design calculation of the former, but some of the missing steps are being filled in gradually by pilot plant, model and more complicated laboratory measurements. The chemistry of combustion has been more studied in the past than its physics, but this situation is being remedied particularly in view of the needs of rockets and gas turbines.

REFERENCES

(1) LONGWELL, J. P., and WEISS, M. A. *J. Industr. Engng Chem.*, **47**, p. 1634 (1955).

(2) GODSAVE, G. A. E. *Fourth International Symposium on Combustion*, p. 818 (Massachusetts Institute of Technology, September, 1952) (Baltimore: Williams Wilkins Company).

(3) ESSENHIGH, R. H. *Private communication* (1956).

(4) SIMPSON, H. C. *Sc.D. Thesis* (Massachusetts Institute of Technology, 1954).

(5) MIKHAIL, M. I. *Private communication* (1955).

(6) FRASER, R. P., and EISENKLAN, P. *Inst. Chem. Eng.*, **34**, p. 294 (1956).

(7) THRING, M. W. *Fuel*, **31**, p. 355 (1952).

(8) HORNSBY SMITH, M. P. *Private communication* (1956).

(9) MOLES, F. D. *Private communication* (1956).

(10) THRING, M. W., HULSE, C., SUNAVALA, P. D., and HORN, G. *Fuel* (in the press).

(11) JAYARAMAN, V. *Private communication* (1956).

(12) HAWTHORNE, W. R., WEDDELL, D. S., and HOTTEL, H. C. *Third International Symposium on Combustion*, p. 267 (Madison, Wisconsin, September, 1948) (Baltimore: Williams Wilkins Company).

(13) RAPER, A. G. *Private communication* (1956).

(14) BURNS, C. *J. Iron Steel Inst.*, **180**, part 3, p. 241 (1955).

(15) NEWBY, M. P., COLLINS, R. D., and LEYS, J. A. *British Iron and Steel Research Association Document*, P/C 68.

(16) GOODING, E. J., and THRING, M. W. *Trans Soc. Glass Tech.*, **25**, p. 23 (1941).

(17) PEIRCE, T. J. *Private communication* (1956).

(18) GROUME-GRJIMAILO, W. E. *The Flow of Gases in Furnaces* (New York: John Wiley and Sons, 1923).

(19) ROSIN, P. O. *J. Inst. Fuel*, **9**, p. 287 (1936).

(20) HORN, G., and THRING, M. W. *Nature* [*London*], **175**, p. 1081 (1955).

(21) THRING, M. W. *J. Iron Steel Inst.*, **171**, p. 381 (1952).
THRING, M. W., and SMITH, D. *J. Iron Steel Inst.*, **179**, p. 227 (1955).

CONFERENCE REPORT

Summarized proceedings of a symposium on thin films—Reading, September, 1956

The Electronics Group of The Institute of Physics held a symposium on thin films at the University of Reading on 28 and 29 September, 1956. The papers presented are summarized in the report.

The symposium began with a paper by DR. M. BLACKMAN (Imperial College of Science and Technology, London) on the conditions for the occurrence of oriented overgrowth (epitaxy). Early studies of overgrowths deposited from solution led to the general rule that orientation of the deposit did not occur if there was a misfit of 15% or more between the spacings in the contact plane between substrate and deposit. Electron diffraction methods have extended the scope of these investigations to overgrowths produced by vacuum evaporation, chemical attack or electrolytic deposition. They have also enabled very thin layers of deposit to be studied; this is important because orientation may occur only in the initial stages of the deposit. Such studies showed that orientation could occur when the misfit was as much as 38% (nickel on heated rocksalt). They also appeared to indicate that in certain cases (notably zinc oxide on zinc) the basal plane of the overgrowth had the same spacing as the deposit, this so-called "basal plane pseudomorphism" persisting over a fairly thick layer. Frank and Merwe[1] attempted to explain these results by considering the energy of a linear chain in the periodic field of a substrate. They found that the state of lowest energy was where the spacing of the chain was changed to that of the substrate, provided the misfit did not exceed a critical value of 15–20%. For greater values of misfit, orientation should not occur. This theory is, however, at variance with later work of Schulz[2] and Lüdemann.[3] The most striking discrepancy was found in a study of deposits formed by vacuum evaporation of five alkali halides on to a lithium fluoride crystal. The misfits ranged in roughly even steps from 15–75% and orientation occurred in all cases. It has further been shown by Newman[4] and others that the claims of some earlier workers to have established basal plane pseudomorphism are erroneous. It therefore appears that orientation is not determined solely by the degree of misfit, and it is necessary to study the initial stages of orientation in more detail than has been attempted so far. Dr. Blackman suggested that it would be worth devoting more attention to the reasons for

the *absence* of orientation in some cases; this is even more puzzling than its occurrence.

DR. L. E. COLLINS (Atomic Weapons Research Establishment, Aldermaston, Berks) discussed the orientation of single crystal films of nickel, cobalt and iron grown on (100), (110) and (111) faces of a rock-salt substrate. In the case of thin films, there was always a parallel orientation, the (001) planes of nickel and sodium chloride being parallel and the [110] axis of nickel coinciding with the [100] axis of sodium chloride. Although this orientation has a lower misfit than the parallel type, it is unstable in thick films. Most films showed twinning on (111) planes; this plays no part in determining the initial stages of epitaxy, but does provide a strain-releasing mechanism in thick films. In cobalt films, hexagonal and cubic forms co-exist owing to the presence of stacking faults. Films less than 200 Å thick lose their orientation when removed from the substrate and become polycrystalline hexagonal cobalt, thus illustrating the orienting influence of the substrate. The differences between the orientation of body-centred cubic iron on the one hand and face-centred cubic nickel and cobalt on the other can be explained by supposing that in general the orientation assumed in thick films is one in which there is a continuation of the co-ordination across the interface between substrate and deposits. However, the results as a whole show that neither conditions of smallest misfit nor of best co-ordination fit alone determine the orientation of the deposit. Oxidation overgrowths on nickel and cobalt are initially oriented, but thicker films of oxide are polycrystalline with random orientation. On the other hand, even thick oxide layers on iron are oriented and the oxide in the layers next to the metal is strained to fit the iron lattice. Initially FeO is formed, but a transition rapidly takes place to Fe_3O_4. There is a strong tendency for the oxide to grow so that there is a continuation of the metal structure into the oxide. The results are consistent with Frank and Merwe's[1] theory of oriented overgrowths and Cabrera and Mott's[5] theory of oxidation.

DR. H. D. KEITH (University of Bristol) described experiments to study the micro-crystalline texture of thick films (500–2000 Å) of copper and its dependence on temperature and gaseous contamination. A focusing X-ray powder camera was constructed entirely of glass, the X-rays entering and passing out to the photographic film *via* thin glass windows. The camera was pumped and baked and the metal filaments and beads thoroughly outgassed. After sealing off, the system was gettered and the copper film deposited by vacuum evaporation from the filament on to a glass substrate in contact with liquid oxygen. Films deposited and maintained at −183° C had a murky green colour and gave broad diffraction lines corresponding to a particle size of 40 Å. Annealing to room temperature in a vacuum produced a rapid change in colour to that characteristic of bulk copper and an increase in particle size to more than 400 Å. The films showed no preferred orientation either before or after annealing. If oxygen is admitted to a film at −183° C in quantity sufficient to produce a saturated chemisorbed monolayer and the film is subsequently annealed at room temperature, the murky green colour persists and the breadth of the diffraction lines indicates a particle size of 60 Å. These measurements of particle size are in general agreement with those deduced from estimates of the ratio of the real to apparent surface area of such films based on gas adsorption studies.[6] If films are annealed to room temperature in the presence of insufficient oxygen to produce a complete monolayer, the final product is indistinguishable from films annealed in a vacuum. The initial stages of the re-crystallization are almost unaffected, but the later stages are retarded and require days rather than minutes for completion. The predominant mechanism in the re-crystallization appears to be surface self-diffusion. These results show that it is very desirable when studying thin films to use the best vacuum conditions, which are obtained only in baked, sealed-off and gettered glass systems.

The infra-red absorption of thin films was discussed by PROF. G. K. T. CONN (University of Exeter). At such frequencies ($2{\cdot}5 \times 10^{13}$ to 3×10^{14} c/s or 12 to 1 μ wavelength) the penetration into solids showing significant absorption is small, and in the case of metals is of the order of 10^{-6} cm. The nature of the surface is therefore important. Surfaces have been prepared by vacuum evaporation and mechanical polishing of bulk specimens; chemically etched, electrolytically etched and annealed surfaces have all been studied. It is necessary to measure two parameters to describe the surface; these may be either the components of the complex refractive index n–ik or the real and imaginary part (conductivity) of the dielectric constant. Owing to the high absorption, the measurements[7–10] are based on the study of light reflected by the specimen. Since the primary absorption of metals is due to the conduction electrons, the experiments must be designed so that this may be distinguished from selective absorption.[11] Prof. Conn mentioned five reasons for studies of the kind:

(*a*) few measurements exist at wavelengths greater than 5 μ;
(*b*) surface conductivity is a subject of great interest obviously relevant to the "anomalous skin effect";
(*c*) the number of free electrons per atom can be determined;
(*d*) the "relaxation time" or "relaxation wavelength" can be found;
(*e*) the selective absorption can be studied.

In this region of the spectrum, n^2 is not even approximately equal to k and the usual Rubens–Hagen assumption is invalid. Experiments are in progress on metals, semi-metals and semi-conductors, and are yielding information on band structure.

MESSRS. R. W. FRANKLIN and F. C. COWLARD (Plessey Co. Ltd., Towcester) discussed the formation and electrical properties of anodic oxide films, with special reference to the non-porous type of film. The thickness of such oxide coatings reaches a limiting value depending on the formation voltage and temperature and is of the order of 10–20 Å/V. The maximum attainable thickness is determined by electronic breakdown at a voltage dependent on the conditions of ionization. The oxide film grows by migration of ions under the high field existing across it (10^6–10^7 V/cm); this migration of ions constitutes an ionic current i_+ which varies with the field F according to the experimental relation[12]

$$i_+ = Ae^{BF}$$

where A and B are constants. A basically similar relationship was derived by Cabrera and Mott[5] by assuming that the passage of ions through the film is restricted by a potential barrier between the metal and the oxide. Some recent experimental results do not agree with this theory and Dewald[13] had derived a different equation, which fits some of the results, by assuming that space charges in the oxide film affect the rate of growth. A relationship between the *electronic* current through the oxide film and the field has been derived[14] on the assumption that the current is limited by a potential barrier. Vermilyea[15] considered this

assumption unsatisfactory, and derived a different relation by attributing the current limitation to the presence of electron traps in the oxide. When the oxide-coated metal is made cathodic, a much higher current flows than when it is anodically polarized. Most of the theories proposed to account for this rectifying action assume that the oxide behaves as a semi-conductor. Many anodic coatings can be used as dielectrics, though they have rather high losses. Various equivalent circuits have been proposed to simulate their behaviour over a range of frequencies, but none of the simpler ones is satisfactory. Van Geel and Scholte[16] found that their results were in agreement with an equivalent circuit consisting of a number of capacitors in series, each with a resistor in parallel. Young[17] extended this idea by assuming that the resistivity of the oxide varies exponentially with distance through the coating.

MR. E. J. GILLHAM (National Physical Laboratory, Teddington, Middlesex) described experiments on the production of transparent conducting gold films. Such transparent, electrically conducting films are required for coating aircraft windscreens so that heat can be supplied to the windscreen for de-misting and de-icing. Tin oxide films have been used, but there is a demand for higher power ratings, and consequently lower film resistances, than this material can provide. Attention was therefore directed to the use of thin metal films. Calculations based on the bulk electrical and optical properties of metals such as silver and gold indicate that such films should combine an optical transmission factor of 80% with a resistance of only a few ohms per square. In practice, thin films evaporated or sputtered on to a substrate such as glass have much worse characteristics, partly because the material of the film is in a highly disordered state and partly because the film is not uniform but consists of a mist of droplets. Heating anneals the material of the film, but unfortunately also increases the degree of aggregation. Since aggregation is presumably caused by surface tension forces, which will depend on the substrate, the effect of different substrates was investigated. It was found that gold films had greatly improved properties when sputtered on to glass which had previously been sputtered with the oxide of lead, antimony or bismuth. Such films appeared yellow by transmitted light, instead of the usual green, indicating that the optical properties more nearly resembled those of bulk gold, and the electrical resistivity was only about 5 times the bulk value. The films could be heated to about 250° C, with a slight improvement in the optical transmission and a fall in resistivity to about 2·5 times the bulk value. All these results are consistent with the assumption that the metallic oxide film enables the gold to "wet" the surface of the substrate and form a film of uniform thickness. By sandwiching the gold between two layers of oxide the stability was still further improved; the films could then be heated to 350–400° C, with a fall of the resistivity to about 1·5 times the bulk value. Furthermore, by making each oxide film $\frac{1}{4}$ wavelength thick, optical losses could be appreciably reduced. By these means, it was possible to obtain films with a transmission factor of about 80% and a resistance of only 2·5 Ω per square.

DR. K. H. R. WRIGHT (Mechanical Engineering Research Laboratory, Thornton Hall, Glasgow) described some electron emission phenomena observed with freshly disturbed metal surfaces. Kramer, using a point counter as current measuring device, observed electron emission in darkness and considered that the exothermic reaction accompanying phase changes in the metal surface was the source of energy giving rise to the electron emission. Recent experiments of Grunberg and Wright[18] have been concerned with the photoelectric properties of disturbed surfaces. It was found that certain metals, notably aluminium, magnesium, zinc and, to a lesser degree, cadmium, lead and indium, all show after abrasion an enhanced photoelectric sensitivity in the visible range of wavelengths. In every case, there is a strong emission peak at 4700 Å and weaker peaks at 5200 Å and 6000–7000 Å. The photosensitivity diminished with time, the rate of decay being greater in air than in an inert atmosphere. A surface which had decayed in air could be re-activated by removing a thin, inactive outer layer by etching with hydrogen fluoride. In this way, it was found that abrasion produced an active layer of depth of the order of 20 μ, the same order of magnitude as the depth to which oxide fragments become embedded after surface working. Active surfaces can also be prepared by vacuum evaporation and by extension; such surfaces have the same spectral response and decay characteristics as those produced by abrasion. The emission peak at 4700 Å is probably due to absorption of light by F'-centres (oxygen ion vacancies trapping two electrons) within the fragmented oxide particles. The energy of an excited F'-centre not more than 30–40 Å from the surface could be transferred to an electron trapped at a surface level and eject it from the surface. Such surface levels might originate from adsorbed oxygen. Other workers have recently examined the emission effects produced by the crushing, ultra-violet or X-ray irradiation of non-metallic crystals. Many of the thermal emission phenomena of such crystals can be attributed to defect structures of F-centre type. This supports the interpretation, based on the presence of oxide particles, of the emission properties of metal surfaces. Some of the latter experiments showed a striking parallelism between the thermal emission and the luminescent glow curves, indicating a close relation between the two phenomena and suggesting the wide range of application of this new method of investigation.

The preparation and properties of stable films of vacuum-deposited 80 nickel : 20 chromium alloy was the subject of a contribution by DR. F. ASHWORTH (Metropolitan-Vickers Co. Ltd., Manchester). The most important features of their preparation are the source temperature, which must not fall below 1600° C, the degree of vacuum in the system, which must be better than 10^{-4} mm of mercury, and the temperature of the receiving surface during film formation, which should not be less than 350° C. At this temperature a stabilizing period of thirty minutes is necessary to ensure film stability. The film composition is related both to source composition and temperature. An 80 nickel : 20 chromium source at temperatures below 1600° C produces chromium-rich films: at 1500° C, the resultant film is 70 nickel : 30 chromium and at 1420° C it is 60 nickel : 40 chromium. The relationship was shown between film thickness and electrical resistance. At 50 Å thickness the resistance is of the order of 400 Ω per square; at 100 Å it is 120 Ω per square; at 200 Å it is 70 Ω per square. Films of resistance less than 300 Ω per square have a long-term stability within $\frac{1}{4}$%, and are capable of dissipating more than 1 W/in.^{2}, under d.c. and l.f. conditions, at a temperature of 400° C. Those of resistance greater than 400 Ω per square deteriorate in time. The resistivity of the bulk material is 10^{-4} Ω cm; the values for films vary from $1{\cdot}2 \times 10^{-4}$ Ω cm at 700 Å thickness to $1{\cdot}65 \times 10^{-4}$ Ω cm at 50 Å. The temperature coefficient of resistivity also depends on thickness as well as on composition. For 80 nickel : 20 chromium alloy, the coefficient for the bulk metal is 0·04% per °C, but it is only 0·01% per °C for films a few hundred Å thick. Electron micrographs indicate that

stabilized films have a grain size of the same order as their thickness measured interferometrically. Thick films (up to 10 μ) of 80 nickel : 20 chromium may be formed on soda glass, the expansion coefficients being 13 and 12×10^{-6} per °C respectively, but films thicker than a few thousand angstroms deposited on borosilicate glass (expansion coefficient $3{\cdot}6 \times 10^{-6}$ per °C) fly off spontaneously when they cool down from 350° C to room temperature. The pieces of film come off with flakes of glass firmly adhering to them, showing that the bond between alloy and glass is stronger than the tensile strength of the glass itself. The thinner films have neutral density characteristics over the optical range, with an optical density of 1·6 for a thickness of 400 Å. Films of a few hundred ohms per square have been used in microwave attenuators; a typical attenuator can dissipate a few watts at 10 cm wavelength. Breakdown occurs under pulsed conditions at a loading of about 1 W/in.^{2} The breakdown patterns consist of straight lines with random tracks branching from these. The former are due to slight discontinuities of film thickness along polishing sleeks in the glass surface; the latter, which are observed only at higher powers, are due to the field distribution in the film together with slight local variations in film characteristics.

Dr. Ashworth also reviewed the use of field emission microscopy (f.e.m.) for the study of surface structure. Müller, who is the pioneer of f.e.m., has shown that this technique is capable of atomic resolution and magnifications of $\times 10^8$. The method is applicable only to a limited range of surfaces, but nevertheless provides much detailed and fundamental information about surface structures, the adsorption of atoms and molecules arriving at the surface from the vapour phase and the growth of layers of atoms deposited during the all-important initial stages of film formation. Modern developments of the technique include the transition from pure electron field-emission[19] to positive ion emission[20] and the use of two-colour photographic recording. Electron f.e.m. is capable of 10 Å resolution of surface structure. Examples shown included copper films forming on a tungsten substrate and the formation of films of barium, oxygen, aluminium oxide and strontium oxide on different crystal faces of tungsten. The transition from body-centred cubic to hexagonal form in the surface structure when carbon is deposited on tungsten, thus converting the surface layers to W_2C can be clearly seen by f.e.m. Other examples are the epitaxial growth of Cu_2O on the (013) face and of U_2O_3 on the (112) face of a tungsten crystal. The resolution of individual molecules is not always straightforward, but copper phthalocyanine is clearly resolved as a quadrupartite structure. The use of positive ions greatly increases the scope of f.e.m. By reversing the polarity and introducing hydrogen at a pressure of 1 μ, *field desorption* of protons from the specimen surface yields a resolution of 5–10 Å. Further improvements in resolution are possible if helium (which has a lower polarizability than hydrogen) is used as a source of ions and the specimen is cooled to improve the accommodation coefficient. A resolution 1·5 Å is possible using helium gas at between 1 and 10 μ pressure with liquid hydrogen cooling. In this way Müller has obtained field desorption patterns (see figure) of tungsten and rhodium surfaces in which individual atoms in lattice arrays are clearly seen. Surface changes may be recorded by taking two superposed colour photographs—one before and one after the event—using red and green filters. Recent colour photographs (kindly furnished by Prof. E. W. Müller) were exhibited of a tungsten surface, showing field evaporation and condensation of tungsten atoms; individual atoms were clearly resolved.

T. B. Rymer

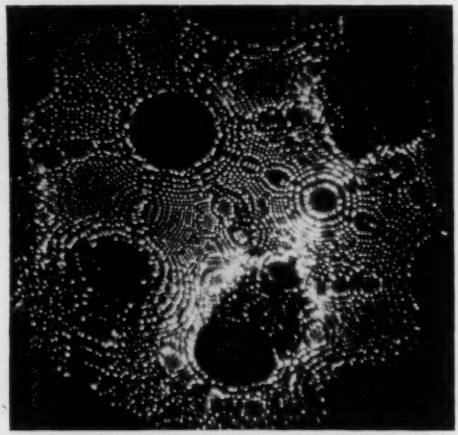

[Reproduced by permission of Prof. E. W. Müller.]

Field desorption micrograph of a rhenium tip radius 800 Å using a potential of 18 kV, helium at 1 μ pressure and liquid hydrogen cooling. Rows of individual atoms are clearly visible

REFERENCES

(1) Frank, F. C., and van der Merwe, J. H. *Proc. Roy. Soc. A*, **198**, p. 216 (1949).
(2) Schulz, L. G. *Acta Cryst.*, **5**, p. 130 (1952).
(3) Lüdemann, H. *Z. Naturforsch.*, **8a**, p. 252 (1954).
(4) Newman, R. C. *Proc. Phys. Soc.* [*London*] *B*, **69**, p. 432 (1956).
(5) Cabrera, N., and Mott, N. F. *Rep. Progr. Phys.*, **12**, p. 163 (1948).
(6) Evans, C. C., and Mitchell, J. W. To be published.
(7) Avery, D. G. *Proc. Phys. Soc.* [*London*] *B*, **64**, p. 1087 (1951); *B*, **65**, p. 425 (1952).
(8) Conn, G. K. T., and Eaton, G. K. *J. Opt. Soc. Amer.*, **44**, pp. 484, 546 (1954).
(9) Beattie, J. R., and Conn, G. K. T. *Phil. Mag.*, **46**, p. 222 (1955).
(10) Beattie, J. R. *Phil. Mag.*, **46**, p. 235 (1955).
(11) Beattie, J. R., and Conn, G. K. T. *Phil. Mag.*, **46**, pp. 989, 1002 (1955).
(12) Güntherschulze, A., and Betz, H. *Elektrolytkondensatoren* (Berlin: H. Cram, 1952).
(13) Dewald, J. F. *J. Electrochem. Soc.*, **102**, p. 1 (1955).
(14) Charlesby, A. *Proc. Phys. Soc.* [*London*] *B*, **66**, p. 533 (1953).
(15) Vermilyea, D. A. *Acta Met.*, **2**, p. 346 (1954).
(16) Van Geel, W. Ch., and Scholte, J. W. A. *Philips Res. Rep.*, **6**, p. 54 (1951); **8**, p. 47 (1953).
(17) Young, L. *Trans Faraday Soc.*, **51**, p. 1250 (1955).
(18) Grunberg, L., and Wright, K. H. R. *Proc. Roy. Soc. A*, **232**, p. 403 (1955).
(19) Ashworth, F. *Advances in Electronics*, **3**, p. 1 (1951).
(20) Müller, E. W. *J. Appl. Phys.*, **27**, p. 474 (1956).

The measurement of peak voltage using a cathode-ray tube

By Eric S. Fairley, Ph.D., A.R.T.C., M.I.E.E., Department of Electrical Engineering, The Royal College of Science and Technology, Glasgow

[*Paper first received* 28 *June, and in final form* 2 *August*, 1956]

The voltage to be measured is applied across the primary of a standard potential transformer and the secondary voltage, at approximately 110 V, is balanced against a direct voltage, using a cathode-ray tube as a null indicator. The direct voltage is measured accurately using a suitable potentiometer and volt-ratio box. Using a cathode-ray tube specially developed for this particular application, an accuracy of better than 0·15% may be readily obtained. An alternative arrangement, in which the potential transformer is replaced by a suitable high voltage resistor divider, is described.

OPERATION

The circuit of the instrument is given in Fig. 1. Only one pair of oscillograph deflector plates are required, the others being connected to the third anode. When the shorting switch is closed the spot will occupy a position on the screen corresponding to zero potential difference between the deflector plates. This position is accurately marked on the screen. With the key open and the voltage to be measured applied to the primary of the potential transformer the direct voltage is adjusted until one end of the trace coincides exactly with the zero position already marked on the screen. Under these conditions the direct voltage is equal to the peak value of the secondary voltage of the potential transformer. The direct voltage is measured accurately using standard potentiometer methods. The peak value of the primary voltage can be found if the nominal ratio and the ratio error of the potential transformer are known. It should be noted that, although the deflecting voltage is asymmetric, no defocusing of the spot occurs at the critical part of its travel near the zero position, as the potential difference between the deflector plates is practically zero at this point.

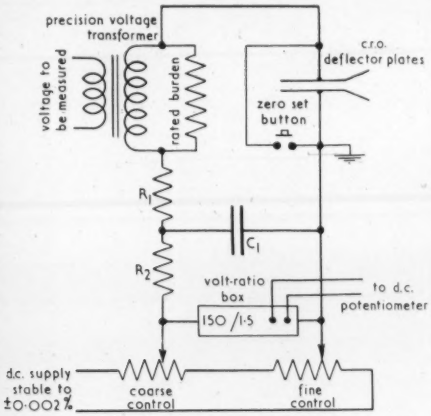

Fig. 1. Circuit for the measurement of peak voltage using a cathode-ray tube

R_1, R_2 = 25 kΩ w.w.
C_1 = 16 μF paper capacitor.

SENSITIVITY

The sensitivity is controlled by three factors:

(*a*) the value of the secondary voltage of the potential transformer,
(*b*) the deflexion sensitivity of the tube,
(*c*) the precision with which the end of the trace can be set to the zero position.

Although sensitivity could be increased by using a range of potential transformers designed for considerably higher secondary voltages, much is to be gained by operating at 110 V and thus enabling a standard transformer to be used.

The deflexion sensitivity of the tube is dependent on the gun voltage and on the length and spacing of the deflector plates. When the gun voltage is reduced the sensitivity increases but at the expense of writing speed and focus. Using a standard type ECR 60 tube the minimum gun voltage at which operation is practicable is 200 and the corresponding deflexion sensitivity is 3 mm/V. Under these conditions, which represent the best compromise, the focus is poor and setting the end of the trace to the zero position is difficult. The estimated sensitivity is 0·5%.

ACCURACY

Unless both the alternating voltage under test and the direct voltage used for backing off the trace are very stable, random errors will be introduced. This matter is dealt with later, and meantime both supplies will be assumed to be stable. Errors in the d.c. potentiometer measurement can readily be made less than 0·01%, which is negligibly small for present purposes. If class AL potential transformers are used then the ratio error may be measured or certified by N.P.L. to better than 0·1%. The difference between the primary and secondary voltage waveforms is insignificant if the secondary is loaded with its rated burden. No systematic error is introduced by the cathode-ray tube, and the accuracy will be limited only by the sensitivity.

SPECIAL CATHODE-RAY TUBE

It is obvious that the normal design of cathode-ray tube is not suited to this application, and the Mullard Radio Valve Co. Ltd. agreed to build an experimental tube to the special

requirements. This is given the type number 8CDD41/1. Only one pair of deflector plates are provided, and they extend from the final anode to near the screen. The spacing is as close as is practicable, being limited by the difficulty of lining up the electrode structure. The final anode is earthed and the cathode is operated at -500 V. In order to increase the intensity of the trace, one post-deflexion accelerator electrode is provided. In practice, it has not proved necessary to use this, and the accelerator electrode is connected to the final anode. The deflexion sensitivity obtained is 11·5 mm/V and the maximum trace length is 8 mm. This limited trace length is inevitable, but is not a serious operational disadvantage. The tube is enclosed by a mu-metal shield 3 in. in diameter and 9½ in. long. This is necessary, as even a weak extraneous electrostatic or a magnetic field may deflect the beam sufficiently to make it strike the long deflector plates.

It is preferable to supply heater and anode voltages from batteries, and when this is done, a sharp focus is obtained which makes an accurate balance easy. When using standard potential transformers with 110 V secondaries, balance can be obtained to better than 0·05%.

A.C. AND D.C. SUPPLIES

A total random fluctuation of ±0·3% between the peak value of the alternating voltage being measured and the direct voltage used to back off the trace, will be sufficient to deflect the end of the trace beyond the working area of the screen. In any case, the combined stability figure for both a.c. and d.c. supplies should be better than the sensitivity of the measuring instrument. The technique of stabilizing the direct voltage is standard and need not be discussed here. The performance is such that the short time random fluctuation of the d.c. supply is within ±0·002%.

The a.c. supply used is obtained from a synchronous generator driven by a 20 h.p. d.c. motor which is fed from a 250 V, 100 A stabilized d.c. supply. The speed of the set is controlled automatically from a quartz crystal clock. The alternator field is supplied from a 12 V, 500 Ah lead-acid battery through silver slip rings and silver-morganite brushes, The rapid fluctuation in voltage due to variation in brush contact resistance is less than ±0·01%. The automatic frequency control holds the frequency within ±0·05%, and only a very slow drift occurs within these limits. This variation in frequency produces a corresponding slow variation in the generator voltage within the same limits.

USE WITH RESISTANCE DIVIDER

If a suitable precision high voltage resistor is available it can be used in place of the instrument transformer and the balance can be carried out at a voltage considerably greater than 110, and with a corresponding improvement in sensitivity. The limit will be set by either the writing speed or flash-over between the tube electrodes. The current rating must be sufficiently high to render negligible the capacitance current to the deflector plate circuit. In this case it is preferable to earth the point in the circuit common to both a.c. and d.c. supplies, and to operate the entire tube system above or below earth potential by the value of the d.c. supply. Such an arrangement is shown in Fig. 2 and was used on a series of breakdown voltage measurements on uniform field gaps. The potential divider comprises forty-three 50 000 Ω vitreous enamel resistors wound with nickel chromium wire and each continuously rated at 90 W. The resistors are assembled in an open *W* formation on a simple Bakelite frame measuring approximately 5 × 4 ft. Suitable corona shields are provided at the apices where necessary. When in use the divider is suspended from the high voltage busbar and care is taken to ensure that it is well clear of all other equipment whether earthed or not. Under these conditions the maximum capacitance current will be negligible and the voltage-ratio can be measured on direct current.

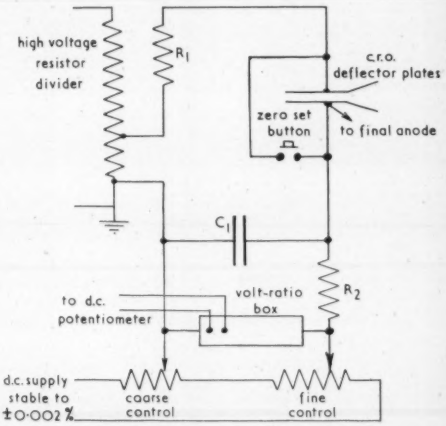

Fig. 2. Alternative arrangement of circuit replacing the potential transformer by a high voltage resistor divider

R_1, R_2 = 25 k Ω w.w.
C_1 = 16 μF paper capacitor.

The cathode-ray tube must be situated at a point where the electrostatic field due to the high voltage equipment is negligible and connected to the lower end of the divider by screened cable. Such a divider will operate satisfactorily up to 70 kV peak and if the fraction of the test voltage applied to the tube is of the order of 700 V then the only significant error will be that introduced by assuming that the ratio of the potential divider measured on a relatively low value of direct voltage, will hold when the divider is operating on high alternating voltage. The overall accuracy is estimated to be within ±0·1%.

ACKNOWLEDGEMENT

We are greatly indebted to the Cathode-ray Tube Development Division of the Mullard Radio Valve Co. Ltd. for undertaking to build the special tube desirable for this method of measurement.

A method of measuring the shear modulus of thin xylonite sheet

By J. CLARKSON, B.Sc., Naval Construction Research Establishment, Dunfermline, Fife

[*Paper received* 1 *October*, 1956]

A torsion balance is described, in which a common torque is applied to narrow strips of steel and xylonite connected end to end, and the twist of each specimen is measured. Knowing the shear modulus of steel, its twist gives a measure of the torque, and the shear modulus of the xylonite may then be calculated from its rotation. The measurements throughout are very easily made, and they do not depend in any way on frictional forces, nor are any forces applied to the specimens apart from the end forces producing the torque. These features are particularly important for thin xylonite which has very small torsional and bending stiffness.

One of the disadvantages of the cellulose nitrate plastic, xylonite, which is frequently used for making model structures, is that its material properties, Young's modulus and shear modulus, vary from sheet to sheet and need to be determined for each sheet, unless rough average values are acceptable. This leads to the requirement for simple routine tests to determine these moduli.

Young's modulus may be determined without difficulty by a tension test, but the shear modulus is more difficult to measure. Possible methods, by measuring the transverse strain in a tension test (giving Poisson's ratio), or the distortion in pure shear, involve the use of either electrical wire resistance strain gauges with the attendant sticking difficulties, or mechanical strain gauges which would be too heavy to attach to the thinner xylonite often used in models, of the order of 0·02 in. thickness. In addition, the condition of pure shear is very difficult to obtain, experimentally.

An indirect method of obtaining the shear modulus is by twisting a narrow leaf strip held rigidly at each end, and measuring the torsional stiffness: the shear modulus may be calculated, assuming the material to be isotropic and homogeneous through its thickness. Unfortunately, there is some evidence, from the variation of the mechanical properties of xylonite with age and sheet thickness, to suggest that it is not homogeneous. Since, in a leaf torsion specimen, the shear stress varies from a maximum at the surfaces to zero at the centre, this lack of homogeneity would lead to some error in the average value of shear modulus for the complete plate thickness. However, this theoretical drawback is probably preferable to the experimental difficulties of other methods.

For xylonite of thicknesses in the range 0·01 to 0·05 in. the stiffness of a leaf strip in torsion is very small. Thus, to twist a specimen 0·04 × 0·4 × 10 in. long through an angle of 10° over its length would require a moment of only 0·016 lb in., assuming a shear modulus of $11{\cdot}5 \times 10^4$ lb/in.^{2} For torques of this order, friction at bearings is a serious problem, and the type of apparatus using weights hung from a string over a pulley is not at all suitable. To avoid errors due to friction, the torsion balance, described below, was designed. In this apparatus, a common torque is applied to steel and xylonite specimens connected end to end, and the rotation of each is measured: the twist of the steel gives a measure of the torque, and one has the following relations from which to calculate the shear modulus of the xylonite:

$$\text{torque} = G_x k b_x t_x^3 \theta_x / L_x = G_s k b_s t_s^3 \theta_s / L_s \qquad (1)$$

assuming that the cross-sections of the steel and xylonite specimens are geometrically similar (same b/t), where L = length of specimen; b = breadth of cross-section; t = thickness of cross-section; θ = total twist of length L; G = shear modulus; k is a constant depending on b/t; and the suffices x and s refer to xylonite and steel, respectively.

The shear modulus of the steel is determined very simply in a separate experiment, by measuring the period of torsional vibration, attaching an inertia bar to the specimen to increase the period to about 0·5 s for easy observation. (It should be noted that a direct measurement of the shear modulus of xylonite by torsional vibration would not be suitable, owing to its creep characteristics.)

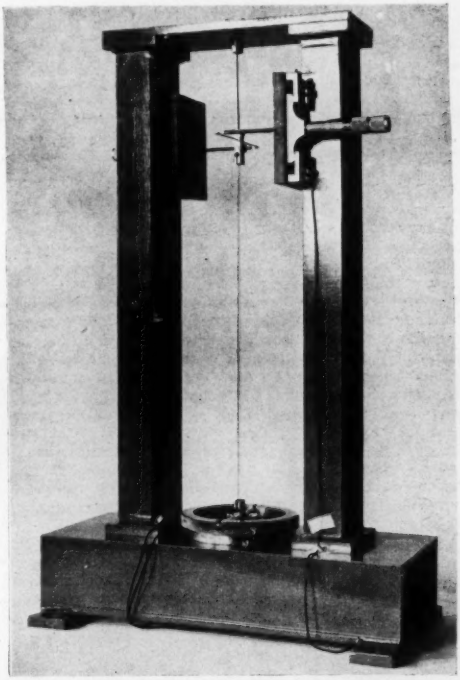

Fig. 1. The xylonite torsion balance

The torsion balance is shown in Fig. 1. The apparatus is mounted in a rigid portal frame, and the top of the steel strip is clamped rigidly to the top member of the portal. The steel used (1% carbon, 0·5% chromium, quenched and

***

tempered) has a large elastic range and does not show any hysteresis. The lower end of the steel strip 3 in. long is attached to the top end of the xylonite strip, and the connexion fitting carries two diametrically opposite pointers of radius 2·35 in. The lower end of the 13 in. long xylonite strip is connected to a horizontal rod resting in vertical grooves in a setting ring, which is accurately engraved round the outside in 5° graduations and positioned outside a disk centred through the axis of the specimens. The weight of the rod serves to keep the specimen straight, and the depth of the grooves allows for slight variations in the overall length of the specimens. The setting ring may be rotated to any desired angle indicated against a fixed scribed line on the base of the apparatus, and it is held in position by a locking screw: this prescribes the total rotation, $\theta_x + \theta_s$.

Typical cross-sectional dimensions for the steel and xylonite are 0·0179 × 0·145 in. and 0·04 × 0·325 in. respectively, and these sizes lead to a ratio of $\theta_s : \theta_x$ of about 1 : 15. This ratio is kept very roughly 1 : 15 for other thicknesses of xylonite by using a number of interchangeable steel strips of different thicknesses. Thus, when the setting ring is rotated through 90°, the steel rotates through about 5½°, with a corresponding sideways movement at the ends of the pointer of about 0·23 in. The ends of the pointer are bent at right angles, and the sideways movement is measured by depth micrometers. To prevent the micrometer from pushing on the pointer and falsifying the readings, contact is detected electrically. The micrometers are mounted on the sides of the portal but are insulated from it, and the portal and micrometers are connected to an oscillating unit, providing a 2–3 V supply at about 2000 c/s, and a loudspeaker. When contact between a depth micrometer and the pointer is made, the circuit is connected and a buzz is heard: the readings are repeatable to within 0·0002 in., and are not affected by the magnitude of the voltage for supplies of up to 8 V, even for the thinnest specimens (0·01 in. thick xylonite). The apparatus is alined so that in the initial position the pointer lies about 2½° to one side of the direction normal to the micrometer spindles: then, after rotating the base setting ring through 90°, which is the order of the maximum strain, the pointer lies about 2½° to the other side of the normal through the micrometer spindles. For angles within 2½°, the small angle approximation, $\theta_s = d/2{\cdot}35$ where d equals the movement of micrometer, applies to within 0·1%. The two diametrically opposite pointers with micrometers are incorporated, since slight initial bends in the specimens may induce further bends during twisting, and by using the average of the two micrometer readings, the true rotation θ_s is obtained:

$$\theta_s = (d_A + d_B)/4{\cdot}70 \qquad (2)$$

To check that initial bends of the magnitude experienced in practice do not influence the results, larger bends have been purposely induced and the readings have shown no measurable change.

An experiment to determine the shear modulus of a xylonite specimen of nominal thickness 0·04 in. is now described. Owing to the creep of xylonite, its elastic properties vary with time, and, in the torsion balance, the twist of the steel strip θ_s, giving a measure of the torque, varies with time, although the total rotation $\theta_x + \theta_s$ is kept constant. In the experiment described here, the shear modulus is determined ten minutes after application of the load. The widths and thicknesses of the steel and xylonite specimens, measured with a micrometer, gave the following average values:

$t_s = 0{\cdot}0179$ in. $\quad b_s = 0{\cdot}146$ in.
$t_x = 0{\cdot}0401$ in. $\quad b_x = 0{\cdot}327$ in.

The shear modulus of the steel, determined by a torsional vibration experiment, was $11{\cdot}4 \times 10^6$ lb/in.^{2} Introducing these values and also $L_s = 3$ in, $L_x = 13$ in. into equation (1), we obtain

$$G_x = 0{\cdot}172\,(\theta_s/\theta_x)\,G_s = 1{\cdot}96 \times 10^6\,(\theta_s/\theta_x) \text{ lb/in.}^2$$

After fitting the specimens in the apparatus, a number of cycles of loading to the maximum strain, in this instance $\theta_x + \theta_s = 120°$, were carried out, to condition the material and check that the readings were repeating: in each cycle the micrometer readings were taken immediately before application of strain and ten minutes after application, and an interval of twenty minutes was allowed for recovery after returning to the zero position. Then three equal increments of strain, $\theta_x + \theta_s = 40°$, were applied at ten minute intervals and the readings of the micrometers were taken ten minutes after application of each increment. The readings converted into radians [using equation (2)] are plotted in Fig. 2. The

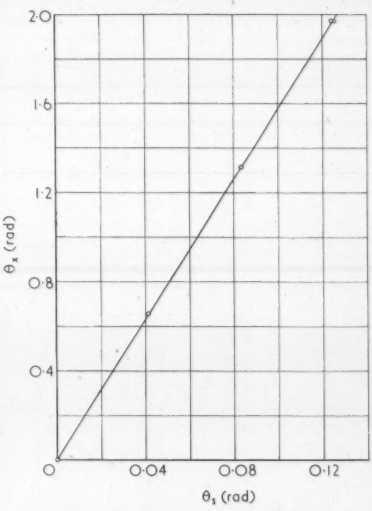

Fig. 2. Typical experimental results

slope is $\theta_s/\theta_x = 0{\cdot}0635$, giving G_x (10 min) $= 12{\cdot}5 \times 10^4$ lb/in.^{2} The maximum strain, $\theta_x + \theta_s = 120°$, corresponds to maximum stresses in the xylonite and steel of approximately 770 lb/in.^{2} and 8500 lb/in.^{2} respectively, which are well below the elastic limits.

ACKNOWLEDGEMENTS

The author wishes to thank Mr. J. B. Hewitt and Mr. G. Wallace for their assistance in the design and development of the apparatus. This article is published with the permission of the Admiralty, but the author is responsible for statements of fact or opinion.

Short duration discharges between separating contacts in a 6 V circuit

By J. RIDDLESTONE, B.A., The Electrical Research Association, Leatherhead, Surrey

[*Paper received* 16 *October*, 1956]

Records of arc voltages of very short duration between separating contacts have been obtained with the Electrical Research Association ultra-high-speed oscillograph. The contacts used were of platinum, palladium and silver. The closed circuit currents were 4·5 and 8 A for platinum and 4·5 A for palladium, the circuit inductance ranging from 0·07 to 4·7 μH. Representative records and a tabular analysis of their important characteristics are given. Discharges occur under all conditions covered in the experiments, their durations varying from about 0·01 to 1·0 μs. Voltages are low, in some cases as low as 7 V, but usually lying within the range 10–18 V. It is shown that there is insufficient evidence as yet on which to base a theory of the arc at separation or a relationship between transfer and arc characteristics.

An investigation by the author into the amount and nature of fine transfer between separating platinum contacts[1,2] showed the pronounced effect of small changes in circuit inductance down to an inductance as low as 0·07 μH. It was inferred that the effect was due to some kind of discharge. The existence of such short-duration discharges has now been verified by the use of an ultra-high speed oscillograph. An earlier note[3] is here extended to a description of the technique and an analysis of the voltages and durations of the discharges recorded.

TECHNIQUE

The discharges were produced between the separating contacts of the same relay used for previous work.[2] The contacts were crossed cylinders of 22 s.w.g. wire operated at 50 c/s with an opening speed of about 0·5 cm/s. The test circuit was the same except that the circuit voltage was positive-to-earth and there were two short coaxial cable connexions (about 3 in.) across the contacts, one through suitable damping resistors to the oscillograph plates and the other to the trip unit, which required a negative input signal (see Fig. 1). The records of the voltage between the separating

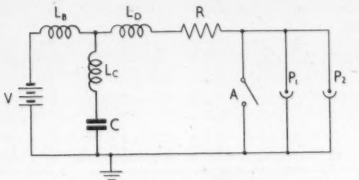

Fig. 1. Circuit diagram

V, 6 V battery; L_B, inductance of battery leads; L_C, self-inductance of capacitance *C*; L_D, inductance of contact circuit; *A*, relay contacts; P_1, P_2, coaxial sockets leading to trip unit and oscillograph plates; *R*, resistor.

contacts were taken with the E.R.A. ultra-high-speed oscillograph fitted with a post-deflexion acceleration tube. The transients were displayed repetitively on the screen and records were taken at random with 1/50 s exposure so that a single transient was recorded at each exposure.

The time-base was triggered by a circuit essentially similar to the high speed trigger circuit, using a secondary emission pentode (type EFP 60), described by Moody, Maclusky and Deighton.[4] A buffer amplifier, inserted between the voltage appearing across the contacts and the input to this circuit, effected an improvement. It is possible to adjust the trigger circuit so that the fast rising output pulse, which is of about 50 V amplitude, is produced only when a certain input voltage is exceeded and that by a very small amount. However, the voltage rise across the opening contacts was so slow (about 1·5 V in several hundred microseconds) that it was difficult to set the circuit to trigger the oscillograph at the required short interval (about 0·1 μs) before the contact voltage rose sharply at the final separation. For most of the records triggering did not occur until this final rise of the voltage at separation so that the delay in the trigger circuit (about 3×10^{-8} s) plus that in the time-base prevented more than the final stages of the discharge transient from being recorded. However, about one-fifth of all exposures produced a useful record.

Another serious difficulty arose because the separating contacts were sometimes observed to close and reopen within the short intervals of time recorded. Since multiple triggering impulses caused erratic variations in time-base speed for sweeps exceeding about 2 μs duration, it was not possible to obtain records long enough to be sure that all the closures, reopenings and succeeding transient discharges were comprised within them. Thus the single transients recorded on higher speed sweeps may or may not have been representative of the majority of opening transients. Nevertheless, those that have been recorded seemed to be of sufficient interest to justify measurement and an attempt at analysis.

ANALYSIS OF RESULTS

Records were taken of voltage transients in a 6 V circuit between separating platinum and palladium contacts with effective circuit inductance *L* between the residual value ($<0·1$ μH) and 4·7 μH, and closed circuit currents of 4·5 A for both metals and 8 A for platinum. Some measurements were also made on silver contacts. Typical records are shown in Figs. 2 and 3. From examination of these records it can be seen that the voltage rises slowly to the boiling voltage, V_B, in the usual manner[1,2] and then more rapidly to some value less than 6 V at which point there is a sudden rise to a relatively steady arc voltage. The apparent time of this last rise is limited to the response time of the oscillograph. The arc voltage is generally less than 20 V and varies erratically for a fraction of a microsecond. This is followed by sudden extinction of the arc and a subsequent oscillation determined by the circuit constants, contact capacitance and the value of the extinction current.

The accuracy of voltage measurement was limited by the

spot size of the oscillograph beam equivalent to about 1 V. Variations in sweep speed, presumably due to slight variations in the triggering impulse, were as much as $\pm 5\%$. The sweep was always calibrated whilst being triggered from the voltage across the relay contacts itself. A large number of records was analysed and the most important results are given in

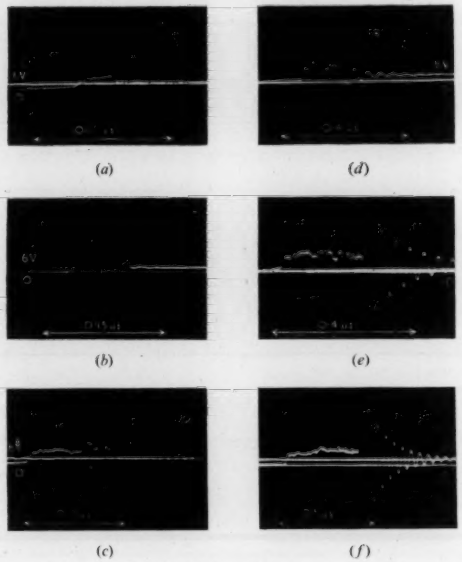

(*a*) (*d*) (*b*) (*e*) (*c*) (*f*)

Fig. 2. Typical oscillograms of single openings (platinum)

Break current and inductance for each: (*a*) 3·3 A, 0·09 μH; (*b*) 3·3 A, 0·16 μH; (*c*) 3·3 A, 0·63 μH; (*d*) 1·8 A, 1·34 μH; (*e*) 3·3 A, 1·34 μH; (*f*) 6·0 A, 1·32 μH.

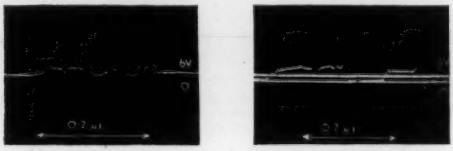

(*a*) (*b*)

Fig. 3. Oscillograms showing reclosures (platinum)

(*a*) break current 6·0 A, inductance 0·07 μH; (*b*) break current 6·0 A, inductance 0·32 μH.

Table 1. The characteristics in all cases are taken only from records showing single opening transients without reclosures. The number of records used is denoted in each case by *n*. The variation of parameters measured is wide and since it is doubtful whether much significance can be attached to recorded means, minimum and maximum values are also given in the table.

The notation used is explained in the table. The theoretical arc durations t_a and t_b are determined on the assumption that the initial current in the arc is equal to the break current—the break current is less than the open-circuit current by the amount V_B/R—that the final current is zero and that the arc voltage is constant. The values t_a and t_b are obtained by considering the equivalent circuit for the arc as shown in Fig. 1(*c*) of reference 2 and are as follows:

$$t_a = \frac{L}{R}\log_e\left(\frac{V_M - V_B}{V_M - E}\right) \qquad t_b = \frac{L}{R}\log_e\left(\frac{V_I - V_B}{V_I - E}\right)$$

where V_I is the mean value of the initial arc voltage (this is also the minimum value) and V_M is the mean value of the maximum arc voltage, both these values being obtained from Table 1.

The frequencies of the final oscillations are consistent with an LC circuit in which the inductance is L and the effective capacitance across the contacts is about 40 pF. The extinction currents cannot easily be deduced from the amplitudes of the final oscillations except for $L \geqslant 0{\cdot}3$ μH, when certain small reactances can be ignored and the calculation is then straightforward. The approximate values covered a wide range for each set of conditions, the minimum values being considerably less than 0·1 A except for $L \geqslant 1$ μH and the maximum values being in the range 0·4–0·7 A. These maximum values are about the same as those given by Holm[5] and those for "normal" contacts given by Atalla.[6] The lower values are about the same as those given by Atalla and by Germer[7] for "activated" contacts. In the present case the contacts were cleaned in trichlorethylene and dried and handled carefully before use but it is possible that some slight residual film of grease might have been present. Direct confirmation of these deduced values is proposed.

DISCUSSION

It is seen from Table 1 that the observed arc durations are generally less than the minimum theoretical value t_b. A possible cause would be the initiation of the arc at a current less than the break current I_B; this could occur if the final rise of voltage across the contacts from V_B to the arc initiation voltage were sufficiently slow but measurement shows that this is not so. The inductance is sufficient to prevent an appreciable change in the current during this short time. Another possible cause would be a high value of arc extinction current but with the values of extinction current actually observed the theoretical minimum arc duration would not be altered appreciably. Thus although the arc durations are approximately proportional to L/R they are less than expected and the reason for this is not clear.

The observed arc voltages are all low, the lowest values occurring at minimum inductance. The values at 8 A for platinum are slightly lower than those at 4·5 A. The values for palladium at 4·5 A are slightly lower than those for platinum at the same current. Table 2 shows values of minimum arc voltages published elsewhere. The results of Holm[5] and of Fink[8] were obtained from arcs drawn out between separating contacts and those of Atalla,[6] Germer[7] and Germer and Boyle[10] from arcs at closing contacts at small separations. In all cases except reference (10) the arc energies and durations were greater than those used here.

It is noteworthy that discharges still occur in platinum for inductances less than 0·2 μH, although this is the region in which it is believed that residual transfer has been demonstrated.[2] At minimum inductance the discharge voltage is

Table. 1. *Characteristics of recorded single arcs between separating contacts in a 6 V circuit*

1 Conditions	2 L (μH)	3 n	4 L/R (μs)	5 t(μs) Min.	5 t(μs) Mean	5 t(μs) Max.	6 t_a (μs)	7 t_b (μs)	8 V_I(V) Min.	8 V_I(V) Mean	8 V_I(V) Max.	9 V_M(V) Min.	9 V_M(V) Mean	9 V_M(V) Max.	10 V_E(V) Min.	10 V_E(V) Mean	10 V_E(V) Max.
Pt	0·09	17	0·07	0·01	0·03	0·05	0·04	0·07	8	8·6	10	10	11·0	12	8·5	10·6	12
3·3 A	0·16	20	0·12	0·01	0·04	0·06	0·06	0·11	7	9·2	11	11	13·2	16	11	12·8	15
	0·22	19	0·17	0·02	0·05	0·10	0·07	0·13	7	9·8	12	11	14·2	17·5	11	13·5	17·5
	0·34	20	0·26	0·04	0·07	0·11	0·10	0·19	9	10·2	13	11	15·9	20	9	15·2	20
	0·63	27	0·47	0·03	0·13	0·19	0·15	0·32	8·5	10·7	13	14·5	17·3	21	14	16·4	21
	1·34	13	1·00	0·22	0·26	0·33	0·32	0·77	9	9·8	11	16	18·4	21	13	15·3	19
	4·7	6	3·5	0·70	0·83	0·97	1·10	1·70	11	13·0	15	17	18·7	22	16	16·6	18
Pt	0·07	8	0·09	0·04	0·05	0·07	0·07	0·10	7·5	8·2	10	8	9·2	11	7·5	9·2	11
5·9 A	0·14	9	0·19	0·06	0·08	0·12	0·11	0·17	8	9·1	11	10	11·3	13	9	10·5	13
	0·20	20	0·27	0·07	0·13	0·18	0·12	0·26	7·5	8·7	10	10	13·0	19	8	11·2	16
	0·32	20	0·43	0·09	0·17	0·22	0·17	0·37	8	9·2	11	12	14·9	17	10	13·2	16
	0·61	15	0·82	0·13	0·23	0·34	0·30	0·77	8	9·0	11	13	16·2	21	10	13·7	21
	1·32	6	1·75	0·17	0·29	0·42	0·63	1·22	10	10·3	11	15	16·3	18	13·5	14·3	15
Pt 1·7 A	1·34	5	0·51	0·08	0·09	0·11	0·15	0·37	10	10·2	11	16	18·7	22	14	16·2	18
Pd	0·09	16	0·07	0·03	0·04	0·05	0·06	0·08	7·5	8·3	9	9	9·7	11	9	9·7	11
3·5 A	0·34	20	0·26	0·06	0·09	0·14	0·12	0·26	8	8·7	10	11	14·4	18	11	13·5	18
	0·63	29	0·47	0·14	0·21	0·32	0·22	0·40	8	9·5	12	11	14·0	16	9	12·0	16
	1·34	6	1·00	0·21	0·25	0·27	0·39	0·74	9	10·3	11	15	16·0	17	12	14·1	15
Ag	0·09	2	0·07	0·06	0·07	0·08	0·06	0·09	7·5	7·9	8	8·5	10·7	13	8	8·3	8·5
4·0 A	0·63	4	0·47	0·08	0·16	0·21	0·12	0·53	7·5	8·5	10	17	23·0	28	17	23·0	28

Key: (1) Conditions: metal and break current; (2) circuit inductance, L; (3) number of arcs, without reclosures, observed and analysed, n; (4) L/R; R = circuit resistance; (5) duration of arc, t; (6) theoretical minimum arc duration, t_a; (7) theoretical maximum arc duration, t_b; (8) initial arc voltage, V_I; (9) maximum arc voltage, V_M; (10) arc voltage at extinction, V_E.

generally low and steady throughout. At a slightly higher inductance the low voltage lasts for a shorter time and then rises to a maximum, which is also the extinction voltage. This change may indicate an arc taking place in high pressure metal vapour evaporated from the anode, the delay being thermal and the final arc being of the "reversed short arc" type postulated previously.[2] Further increase of inductance reduces still further the duration of the initial low voltage stage and increases the number of the subsequent rises and falls in voltage. The falls are not usually to values as low as the initial voltage and the rises are to values which increase with the inductance.

Table 2. *Published values of minimum arc voltages*

Metal	Minimum arc voltage (volts) Holm	Fink	Atalla	Germer	Germer and Boyle
Ag	12	8	11–13	11	
Pt	7·5	13·5	—	15	
Pd	—	—	14–15	14	Cathode 13–18 Anode 9–12

It was noted that the greatest number of reclosures occurred with minimum inductance: Fig. 3(*a*) shows the kind of trace often obtained. Fig. 3(*b*) shows the kind of reclosure observed with higher inductance. It seems reasonable that a partial bridging of the gap by metal being melted from the anode could occur in the initial stages of an arc and that the consequences would be more apparent the more rapidly the car current dropped.

Although the records described are of interest in that they give clear indication of the type of discharge occurring between separating contacts it is not possible to find a close correlation between these records and the transfer measured under

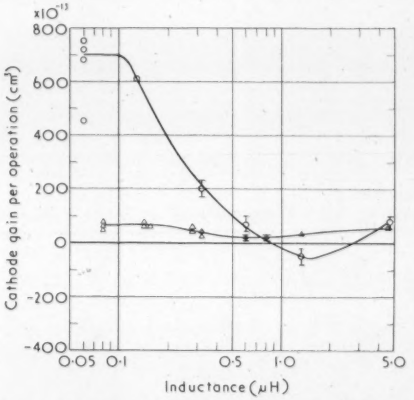

Fig. 4. Variation of transfer with inductance (platinum)
○ = break current 5·9 A. △ = break current 3·3 A.

corresponding conditions. For purposes of comparison, curves of metal transfer for the range of inductance covered in Table 1 are given in Figs. 4, 5 and 6. The data for these

curves are taken from a previous paper[2] and from work done at the E.R.A. as yet unpublished.*

Recent work by Atalla[9] and by Germer and Boyle[10] on short duration, short-distance discharges between slowly closing and stationary contacts gives results which are to some extent comparable with those given in this paper. Comparison of arc durations shown in Table 1 with the direction of transfer shown in Figs. 4, 5 and 6 reveals no simple dependence of direction of transfer on arc duration as found by Atalla. However, it is likely that the experimental conditions in the present work give rise to more complicated phenomena than in the experiments at the Bell Telephone Laboratories.

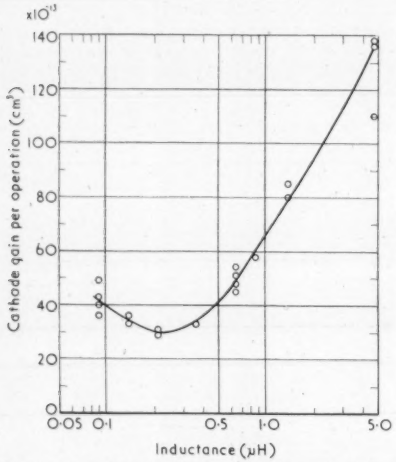

Fig. 5. Variation of transfer with inductance (palladium)
Break current 3·3 A.

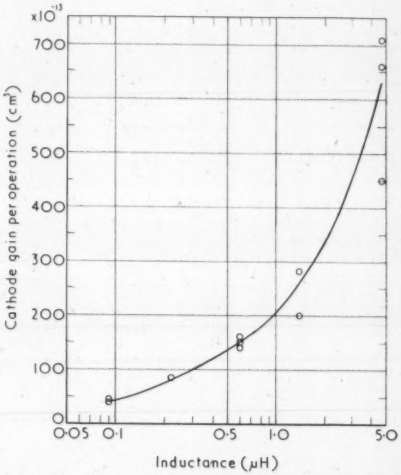

Fig. 6. Variation of transfer with inductance (silver)
Break current 3·7 A.

CONCLUSIONS

Although the work requires extension before firm conclusions can be drawn the following preliminary generalizations may be advanced:

(1) Low voltage discharges occur between separating contacts over the complete range of inductances and currents investigated ($L = 0{\cdot}07$–$4{\cdot}7\ \mu$H, $I = 4{\cdot}5$ and 8 A).

(2) The arc durations are approximately proportional to L/R and vary from about 0·01–1·0 μs.

(3) The initial arc voltages are low, 8–11 V, but increase after about 0·05 μs; the maximum values attained do not exceed about 20 V.

(4) The extinction currents cover a wide range from 0·6 A down to less than 0·1 A. The low values may be due to activation.

* The current values for these curves have been increased by about 10% due to an error in the measurements discovered since the previous publication.

ACKNOWLEDGEMENTS

The author wishes to thank the British Electrical and Allied Industries Research Association for permission to publish this paper and to acknowledge the interest shown in the work by Mr. W. Nethercot and the advice and assistance given by Mr. H. G. Riddlestone in the initial stages of the experimental work.

REFERENCES

(1) Warham, J. *Proc. Instn Elect. Engrs I*, **100**, p. 163 (1953).

(2) Riddlestone, J. *Proc. Instn Elect. Engrs C*, **102**, p. 29 (1955).

(3) Riddlestone, J. *Nature* [*London*], **175**, p. 909 (1955).

(4) Moody, N. F., Maclusky, G. J. R., and Deighton, M. O. *Electronic Engng*, **24**, p. 214 (1952).

(5) Holm, R. *Electric Contacts* (Stockholm: H. Gebers Forlag, 1946).

(6) Atalla, M. M. *Bell Syst. Tech. J.*, **32**, p. 1493 (1953).

(7) Germer, L. H. *J. Appl. Phys.*, **22**, p. 955 (1951).

(8) Fink, H. P. *Wiss Veroff. aus d. Siemens Werken*, **17**, Heft III, p. 45 (1938).

(9) Atalla, M. M. *Bell Syst. Tech. J.*, **34**, p. 1081 (1955).

(10) Germer, L. H., and Boyle, W. S. *J. Appl. Phys.*, **27**, p. 32 (1956).

An extraction replica method for large precipitates and non-metallic inclusions in steels

By G. R. Booker, B.Sc., A.Inst.P., and J. Norbury, B.Sc., Ph.D., F.Inst.P., A.R.T.C.S., Research Laboratories, Richard Thomas and Baldwins Ltd. and Steel Co. of Wales Ltd., Whitchurch, Bucks.

[*Paper first received* 5 *June, and in final form* 5 *October*, 1956]

A replica method is described which enables large (up to 10 μ or so) precipitates and inclusions to be extracted from steels. There is no etching through the replica, and consequently weakening and staining of the film are avoided. In addition to more stable constituents, included material normally dissolved by bulk extraction methods has been successfully extracted. Examples of the extraction of iron nitride, iron carbide, and non-metallic inclusions are given.

The methods of examination and identification of precipitates and inclusions in metals can be divided into two groups, namely: (*a*) those in which the material is examined whilst still embedded in the metal, and (*b*) those in which the material is extracted from the surface before examination.

The use of the metallurgical microscope for the examination of included materials in metals, and the application of etching tests such as those proposed by Campbell and Comstock[1] for non-metallic inclusions, can yield sufficient evidence to identify the included material, but the results are often conflicting or inconclusive. Other methods of studying included material in the matrix have been used. Crystal structure may be deduced by reflexion electron diffraction[2] or micro-beam X-ray techniques, whilst chemical composition may be determined by X-ray fluorescence analysis[3] or by electron probe methods.[4,5]

Several methods of extracting included material in amounts sufficient to allow identification by micro-analytical, X-ray or other methods are available. These methods, in which the matrix is usually dissolved either chemically[6,7] or electrolytically,[8] require careful experimental control to minimize modification of the less stable constituents. Thus, with chemical methods, silica, alumina, iron oxides, manganese oxides, silicates, and aluminates may be successfully extracted, whilst carbides, sulphides, and nitrides are modified or decomposed. With electrolytic methods, oxides, sulphides, and some of the more stable carbides may be successfully extracted, in addition to the more stable constituents.

THE EXTRACTION REPLICA METHOD

The extraction replica method used by Fisher[9] [Fig. 1(*a*)] is a notable advance in the isolation and identification of included material. The short extraction time reduces modification to a minimum, the extracted material retains the same configuration in the replica that it possessed in the metal, and individual constituents can be examined, and identified by electron diffraction. In addition, grain boundaries, material not extracted, marked areas, etc., make imprints in the replica, facilitating the selection for examination of specific areas of the replica, corresponding to areas of interest in the polished section.

Fisher has used the technique to study carbides in the form of pearlite, bainite, martensite and tempered martensite from eutectoid carbon steel. The extracted material was always considerably thinner than 1 μ, and often merely a few 100 Å thick. Consequently a light second etch through the film proved adequate for extraction, and the extracted material was in a form ideally suited to give good electron diffraction effects.

EXTRACTION REPLICAS APPLIED TO LARGE INCLUDED MATERIAL

The present writers have found that when Fisher's technique is applied to large inclusions and precipitates (the order of 10 μ in size) difficulties arise. To free these large inclusions from the matrix, severe etching (of the order of 3 min in 10% nital) through the film is necessary, and this causes a marked staining of the film, which gives rise to spurious electron diffraction effects. Furthermore, the prolonged etch weakens the plastic film so severely that the dry stripping method used by Fisher is unsatisfactory.

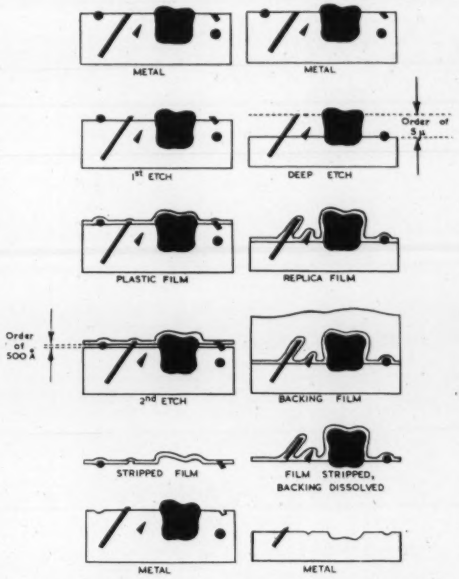

Fig. 1. A comparison of the double and single etch methods. Note the light etch in (*a*) (*left*) the Fisher double etch method and the severe etch in (*b*) (*right*) the single etch method

An improved method of extraction suitable for large

included material has, therefore, been developed, and has given good results over a wide range of application. In this method the polished metal surface is initially given a prolonged etch, which is sufficient to enable the included material to be subsequently removed simply by coating the surface with a plastic film and dry stripping.

EXPERIMENTAL

The surface to be studied is polished in the usual manner, and, where necessary, given a light etch (e.g. of the order of 5 s in 3% nital) to reveal the included material [Fig. 1(*b*)]. Using 10% nital, the surface is then repeatedly etched (e.g. for ½, 1, 2, 3 . . . min total etch time respectively) and the surface inspected in the optical microscope after each etch. This enables the effectiveness of the etching treatment to be assessed, and allows any changes in the appearance of the included material to be observed during the etch. The etching series is normally terminated when the optimum etch (see below) has been given.

For a specimen which has not been examined previously by this method, an extraction replica may be made after each increment in etch time, and examination of these will show the optimum etch time to secure good extraction. After some experience, the time can usually be decided by the examination of the metal surface with the optical microscope after each etch. Once the optimum etch time has been determined, it can be applied in one stage whenever further extraction replicas are required from that specimen.

The preparation of the extraction replica is then as follows:

(1) Immediately after the final etch, the specimen is thoroughly rinsed with alcohol, and dried in a stream of warm air.
(2) The etched metal surface is coated with a thin Formvar film, and then backed with a thick collodion (from 4% collodion in ethyl acetate) film, and allowed to dry in a desiccator.
(3) When completely dry (about 15 min), the composite film is breathed on heavily, carefully loosened at the edges with a razor blade, and dry stripped in one piece with tweezers.
(4) Immediately after stripping, the metal specimen is rinsed in alcohol and dried, to preserve it for possible future examination. The stripped film is allowed to dry (moist from breathing on it) in a desiccator, and is then ready for examination.

For mounted steel specimens the films can be applied so as to cover both the surface of the metal and the mount, and the composite film removed in one piece. The edges of the film can conveniently be attached by adhesive tape to a cardboard or metal slide containing a central hole, so that the film lies flat on the slide with the part of the replica corresponding to the metal surface located over the hole. The replica can then be examined in the optical microscope, and the success of the extraction process ascertained.

For examination in the electron microscope, the backing film can conveniently be removed using a method similar to that described by Bradley.[10] Disks ⅛ in. in diameter are cut from the composite film, and placed collodion side up on an electron microscope grid, which is moistened with a drop of amyl acetate, and rests in a horizontal position on a hollow brass peg. The peg is placed under a burette, and about 10 cm^3 of amyl acetate run slowly but continuously over the film during a period of about 15 min, at the end of which time the collodion backing has completely dissolved. The grid is removed from the peg, allowed to dry, and is then ready for study in the electron microscope.

When particular areas of the replica are required, the same procedure is followed, but some form of positioning device is desirable so that when placing the stripped film on the electron microscope grid, the area of interest is favourably positioned for viewing. A simple device, somewhat similar to that used by Bradley,[11] has been successfully used for this purpose.

The application of the method to iron nitrides in mild steel, iron carbide in a plain carbon steel, and aluminous inclusions in a vacuum cast ingot, is illustrated in Figs. 2, 3 and 4. The micrographs in Fig. 2 are not of the same area, but those of Fig. 4 show the same inclusion during various stages of extraction.

DISCUSSION

The single etch extraction replica method has the merits of Fisher's technique, and has the advantage, when applied to large inclusions and precipitates, that the plastic film is not exposed to the etchant, and is never in contact with the disintegration products. Weakening and staining of the film are therefore obviated.

The extraction process is very much quicker than bulk extraction. The replica film, necessarily thin for electron microscope and electron diffraction studies, has to be backed with a thick strengthening film for satisfactory stripping, and most of the time taken to prepare the replica is required for the drying and subsequent removal of the backing film (about 30 min).

Non-metallic inclusions have been successfully extracted even when they were of such a size that they must have extended further into the matrix than the general depth to which the matrix was etched. There is evidence that the severe etch preferentially attacks the matrix around non-metallic inclusions, loosening many that are deeper than the general level of the etched matrix, and allowing them to be extracted in the replica. With large lamellar precipitates, the extracted lamellae are usually the portions of the precipitate which were exposed during etching and have been detached from the remainder of the precipitate during the dry stripping.

When large and small included material is present in the metal, the severe etch necessary to extract the large material does not preclude the extraction of the small material, since fresh small material is revealed by the deep etch. This is illustrated in Fig. 1(*b*) and Fig. 2(*b*).

When the total etch is given in one single operation there is the possibility that some included material may be lost before the plastic replica is made. This is no disadvantage in many applications, but in those instances where it is essential that most of the included material shall be retained for examination, the technique can be modified. Thus, in the extraction replica shown in Fig. 4, about 50% of the non-metallic inclusions observed in the surface originally were successfully extracted. When the same surface was repolished and extraction replicas made after etching for 2½ min and a further 1½ min in 10% nital respectively, the two replicas together contained about 75% of the inclusions originally present in the polished surface. By increasing the number of extraction replicas to four, and selecting suitable etch times, about 95% of the inclusions were extracted by the replicas.

With specimens such as nitrided steel, pearlitic steel, and cast iron, it has been found possible to make satisfactory extraction replicas repeatedly, without repolishing the surface after each extraction, when general areas only are of interest.

In these studies there has been no significant evidence that

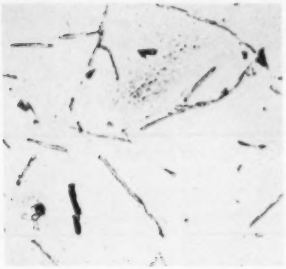

(*a*)

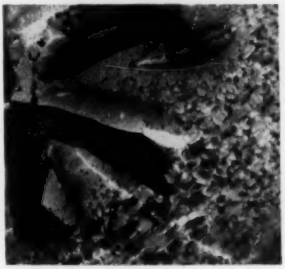

(*b*)

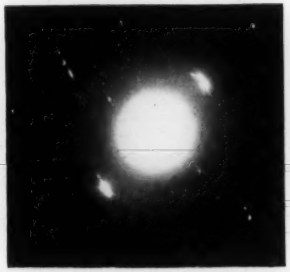

(*c*)

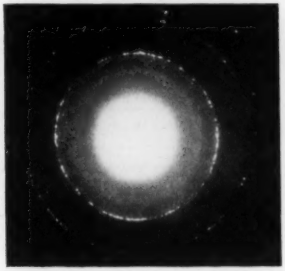

(*d*)

Fig. 2. Mild steel containing iron nitride precipitates

(*a*) Extraction replica made after etching in 10% nital for 3 min. Transmission optical micrograph. ×600.
(*b*) As Fig. 2(*a*). Transmission electron micrograph. ×1500.
(*c*) Electron diffraction pattern from the large type of extracted precipitate.
(*d*) Electron diffraction pattern from the small type of extracted precipitate.

(*a*)

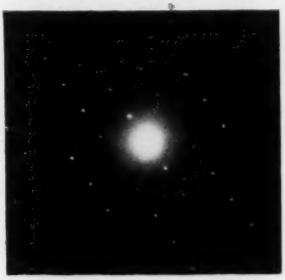

(*b*)

Fig. 3. 0·6% plain carbon steel exhibiting coarse pearlite structure

(*a*) Extraction replica made after etching in 10% nital for 1 min, showing lamellar cementite. Transmission electron micrograph. ×3000.
(*b*) Electron diffraction pattern from extracted material similar to that of Fig. 3(*a*).

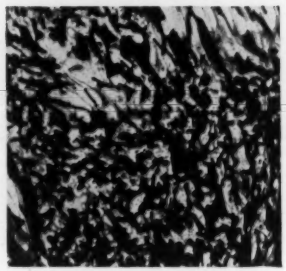

(*c*)

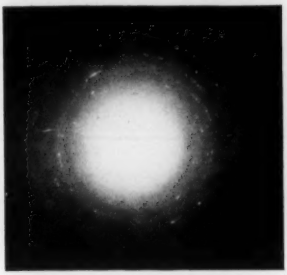

(*d*)

Fig. 3. 0·6% plain carbon steel exhibiting coarse pearlite structure (*continued*)

(*c*) Another area of the extraction replica of Fig. 3(*a*), but showing globular cementite. Transmission electron micrograph. ×3000.

(*d*) Electron diffraction pattern from extracted material similar to that of Fig. 3(*c*).

(*a*)

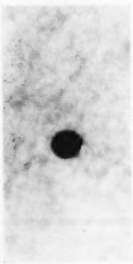

(*b*)

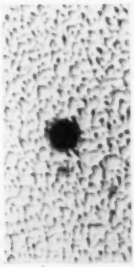

(*c*)

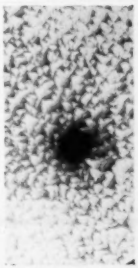

(*d*)

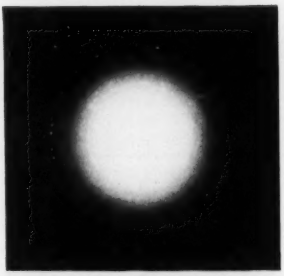

(*e*)

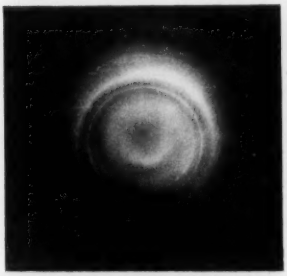

(*f*)

Fig. 4. Vacuum cast ingot containing aluminous inclusions

(*a*) Metal surface unetched. Optical micrograph. ×1000.
(*b*) Metal surface etched in 10% nital for 3 min. Optical micrograph.
(*c*) Extraction replica made after etching in 10% nital for 3 min. Transmission optical micrograph. ×1000.
(*d*) As Fig. 4(*c*). Transmission electron micrograph. ×1000.
(*e*) Electron diffraction pattern from a stringer type of inclusion present in the extraction replica.
(*f*) Electron diffraction pattern from an angular type of inclusion present in the extraction replica.

nital produces appreciable modification of any of the included material, but other etchants, e.g. 5% iodine in methanol, may be employed if attack is suspected. 5% iodine in methanol dissolves the matrix at roughly the same rate as 10% nital, but has the disadvantage that it sometimes produces deep etch pits.

The examination of the extracted material in the replica need not be confined to electron microscopy and electron diffraction. The material is in a form eminently suited for transmission optical microscope studies, using ordinary and polarized light. Such studies may contribute additional information relating to the morphology and crystallographic form. When extraction replicas are only to be examined with the optical microscope, it is not always necessary to have a final thin replica film. Extraction may then be achieved by omitting the Formvar film, and extracting in a thick collodion film alone.

ACKNOWLEDGEMENTS

The authors are indebted to Mr. H. A. Sloman, who kindly provided the deoxidation series ingots, one of which is illustrated in Fig. 4, to Mr. C. A. Stratfull for his assistance in the preparation of the specimens and extraction replicas, and to the Metallurgical Department of these Laboratories for the optical micrographs.

Thanks are also due to Mr. R. A. Hacking, Director of Research, for permission to publish this paper.

REFERENCES

(1) CAMPBELL, W., and COMSTOCK, G. F. *Proc. Amer. Soc. Test Mat.*, **23**, p. 521 (1923).
(2) HEIDENREICH, R. D., STURKEY, L., and WOODS, H. L. *J. Appl. Phys.*, **17**, p. 127 (1946).
(3) American Society for Testing Materials. Symposium on Fluorescent X-ray Spectrographic Analysis *A.S.T.M.* (1954).
(4) CASTAIGN, R. *Analyt. Chem.*, **25** (5), p. 724 (1953).
(5) PHILIBERT, J., and CRUSSADE, C. *J. Iron Steel Inst.*, **183**, p. 42 (1956).
(6) DICKENSON, J. H. S. *J. Iron Steel Inst.*, **113**, p. 177 (1926).
(7) ROONEY, T. H. B.I.S.R.A. Steelmaking Division, Solid Steel Study Group of the Gases and Non-Metallics Sub-Committee, Dec. 1952.
(8) KLINGER, P., and KOCH, W. *Beiträge zur Metallkundlichen Analyse* (Dusseldorf: Stahleisen, 1949).
(9) FISHER, R. M. *A.S.T.M. Special Tech. Publication No. 155*, p. 49 (1953).
(10) BRADLEY, D. E. *J. Inst. Met.*, **83**, p. 35 (1954).
(11) BRADLEY, D. E. *Brit. J. Appl. Phys.*, **6**, p. 430 (1955).

Highly-conducting gold films prepared by vacuum evaporation

By A. E. ENNOS, M.Sc., A.Inst.P., Research Laboratory, Associated Electrical Industries Ltd., Aldermaston, Berks.

[*Paper received* 10 *October*, 1956]

Thin gold films formed by vacuum evaporation on to freshly evaporated layers of certain metallic oxides show high conductivity, in a similar way to layers prepared by cathodic sputtering. The evaporated layers are robust and of high current-carrying capacity down to 30 Å thickness. The conductivity approaches the bulk value for annealed films thicker than 60 Å. The properties of these films are discussed in relation to those of the sputtered layers, with which they compare favourably.

In the technical field there has arisen the need for rendering the surface of glass electrically conducting without greatly impairing its transparency, and attention has recently been focused on the use of thin metal films for the purpose. These films are potentially capable of combining high conductivity with high transparency, but, as prepared by conventional techniques, their electrical resistivity is found to be many times higher than that to be expected from the bulk metal constants. However, Gillham and Preston[1] found that, by sputtering a layer of gold on top of a sputtered layer of bismuth or indium oxide, the adherence, strength and conductivity of the gold could be improved to such a degree as to make the films useful as surface heating elements. Apart from their practical uses, these films are of theoretical interest in studying the mechanism of electrical conduction near the surface of a metal, since, according to the electron theory of metals, the film thicknesses employed are comparable with the mean free path of the conduction electrons in the metal. Thus, one might expect some interaction of these electrons with the boundary surface so as to decrease the conductivity. In a later detailed study of the properties of sputtered gold films on reactively sputtered bismuth oxide, Gillham, Preston and Williams[2] show that variations in conductivity from the bulk metal value cannot be due to this cause, so that the conduction electrons in the film must be almost totally reflected at the film boundaries, rather than inelastically scattered.

There are indications in the Patent literature[3] that highly-conducting metal films may also be made by vacuum-evaporation methods. Films formed in this way might have advantages over sputtered layers since they are less likely to contain occluded gases, which are known to be present in appreciable quantity in sputtered films. Accordingly, the properties of thin gold films evaporated on to a number of different substrates were examined, and, as a result, it was found possible to make thin layers having electrical properties more nearly approaching the bulk metal values than their sputtered counterparts. The following is an account of the methods of preparing these films and some of their properties.

PREPARATION OF FILMS

Vacuum evaporation was used to deposit both substrate material and the metal, and the evaporations were carried out in a standard evaporation plant employing oil pumps and rubber gaskets. No degassing or gas discharge cleaning of the components or of the glass on which the films were deposited was carried out. Microscope slides which were superficially cleaned with detergent solution and dried on a cloth were used for convenience, and these were mounted at

a sufficient distance from the evaporation source (about 20 cm) to give substantially uniform films over their surface. The gold was evaporated from a molybdenum foil strip having a small indent to hold the molten metal, and the substrate material from platinum foil, or from molybdenum foil when it was certain that no chemical reaction would take place between the material and molybdenum. For high conductivity films to be formed, it was found that a good vacuum (5×10^{-5} mm of mercury or better) was essential, and that the gold had to be evaporated immediately after putting down the substrate material, without breaking the vacuum in between. The gold film was condensed at a rate of 10–20 Å/s. The thickness of the substrate material was estimated by observing interference colours on the glass slides themselves or on a monitor slide placed closer to the evaporation source. The thickness of the gold films was controlled by the quantity of gold put in the boat, all of which was

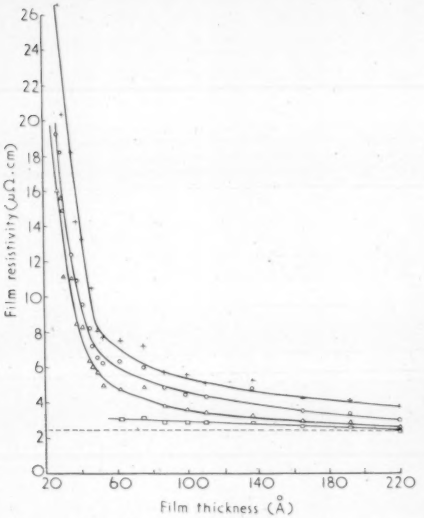

Fig. 1. Resistivity of evaporated gold films on evaporated bismuth oxide

+ = unannealed; ○ = annealed at 150° C; △ = annealed at 250° C; □ = annealed at 350° C; – – – – = bulk resistivity.

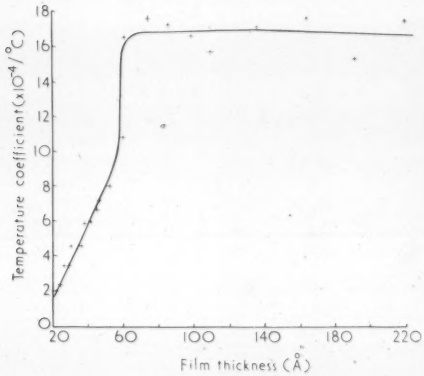

Fig. 2. Temperature coefficients of evaporated gold films on evaporated bismuth oxide

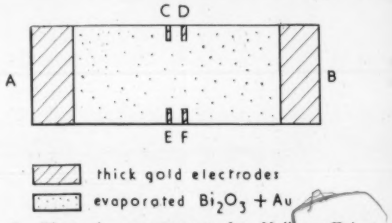

Fig. 3. Electrode arrangement for Hall coefficient measurements

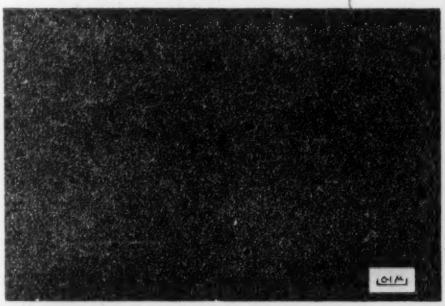

Fig. 4. Direct electron micrograph of evaporated bismuth oxide

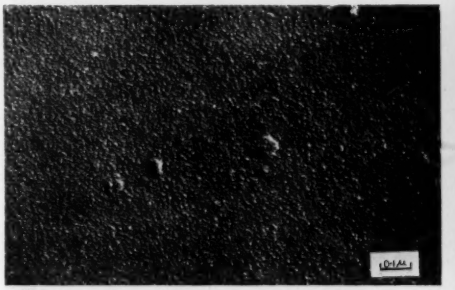

Fig. 5. Carbon replica of bismuth oxide evaporated on glass. Shadowed 2 : 1

evaporated. It was, however, found unreliable to use the weight of gold in the boat, except to give a very rough calibration of the thickness of the resulting deposit, owing to individual variations in the evaporation conditions. Absolute values of the film thickness, or rather the weight per unit area, were measured by chemical determination of the gold content after the physical properties of the films had been measured.

The substrate materials which were found to enhance the conductivity of the overlying gold layer were the oxides of antimony, indium, bismuth and lead. Antimony sulphide acted in the same way to a lesser extent. As an example, a 30 Å layer of gold on antimony oxide had a resistance of 50 Ω per "square" after suitable heat treatment subsequent to deposition, while a similar thickness of gold on antimony sulphide had a resistance of 1800 Ω per "square" after similar heat treatment. Both films were capable of carrying relatively large currents, and, by cooling in oil, the former type of film could dissipate at least 1 W/cm^2 without breakdown. Although these evaporated gold films are robust enough to withstand considerable heating and immersion in oil, etc., further mechanical protection can be afforded them by the evaporation of a second layer of oxide, but usually at the expense of the transparency. However, a multiple film using antimony oxide and 30 Å of gold, as quoted above, had a transparency of 75%.

Evaporation of metallic oxides often results in their partial decomposition into the metal and oxygen, so that thick layers of the evaporated oxide will absorb light appreciably. This was more noticeable for the oxide of bismuth than for the other three. The transparency of this layer can, however, be kept as high as possible by keeping it thin. The lower limit of thickness at which evaporated bismuth oxide gives the highest conductivity in the gold film was found to be about 80 Å. Condensation of the bismuth metal can also be prevented by heating the glass while evaporation of the oxide takes place, but experiments carried out with the glass at 200° C showed only slight improvement in transparency of the oxide layer. Furthermore, it is necessary to allow the glass to cool down before the gold can be evaporated, which makes the whole process unnecessarily long. Experiments also indicated that the increase in transparency, which results from the heat treatment in air which is necessary to obtain the highest conductivity, is partially due to reoxidation of the bismuth metal. The appearance of the evaporated gold on the metal oxide substrates is grey by reflexion, as opposed to the greenish hue of gold evaporated directly on to glass. This is similar to the corresponding films formed by sputtering.

From a practical point of view, a highly-conducting film of reasonable transparency is most easily made by evaporating gold on to a thin substrate of lead oxide, evaporated from a platinum boat. Increased conductivity and stability of the film is then obtained by heat treatment in a similar manner to the sputtered layers of Gillham and Preston. This effect will be dealt with in greater detail below.

ELECTRICAL AND THERMAL PROPERTIES OF EVAPORATED BISMUTH OXIDE-GOLD FILMS

A bismuth oxide substrate was chosen when examining the electrical properties of the evaporated films, so that a direct comparison could be made with the corresponding properties of the sputtered films of Gillham and Preston. To obtain a range of thickness of gold films prepared under identical conditions, the following experimental arrangement was used. Glass slides 3 × ½ in. were mounted on a jig at different distances from the evaporation source, such that they would receive the gold in the proportions of 4 : 5 : 6 : 7 : 8. For this, it was assumed that the inverse square law of propagation and uniform radial evaporation of the gold would hold over the narrow cone subtended by the source at the glass slides. This was justified by subsequent analysis of the gold deposits. Further extension of the range of thicknesses required to establish a thickness-conductivity relationship was obtained by carrying out a number of evaporations using different quantities of gold in the boat, but keeping the other experimental conditions as constant as possible. However, as mentioned before, the variation in film thickness from one evaporation to another is considerable, and absolute thicknesses had always to be measured by chemical determination of the deposits themselves. Thick gold electrodes were subsequently evaporated over the ends of the slides to give good electrical contacts and to define a film area 2 × ½ in. For these films, a fairly thick (200 Å) layer of bismuth oxide was used, and no protective coating was added over the gold.

(a) *Electrical resistivity.* Fig. 1 shows a plot of film resistivities for thicknesses varying from 25 to 220 Å. Films thinner than 25 Å were in general unstable and, when heated, increased in resistance and often became a completely open circuit. It is seen that in the range of thicknesses plotted, the effect of heating the films in air is to reduce the resistance in a consistent manner, depending on the temperature. The thicker films can withstand a higher annealing temperature than thinner ones, but it was found that even for the thicker films a temperature much in excess of 350° C begins to break up the film and gives rise to much greater resistance. These changes in resistance on heating, which are permanent, are similar to the processes which occur on heating the sputtered films, which Gillham, Preston and Williams refer to as "annealing." The complete process of annealing for sputtered films has been followed by Holland and Siddall,[4] who have verified some of the results of the above authors in a review article on methods of preparing transparent conducting films.

There are two main points to note about the curves of Fig. 1. The first is that the fully annealed films (350° C heating) have a resistivity very close to the bulk resistivity of gold (2·44 μΩ cm at 20° C). In fact, at 200 Å, the resistivity is identical, within experimental error, with the bulk value, and, as the films become thinner their resistivity does not rise appreciably until a value of around 50–60 Å is reached. Secondly, at this figure of 50–60 Å, the curves rise abruptly, and, although the experimental points are insufficient and too inexact to determine the precise mechanism in this region, it appears that some sharp change occurs in film characteristics for this thickness.

(b) *Temperature coefficient of resistance.* The temperature coefficient of the fully-annealed films was also measured in the range 20–80° C by mounting them in an enclosed cell immersed in a thermostatically-controlled oil bath. The coefficient was measured by thermally cycling the films to allow for small changes in their electrical characteristics, even after annealing. The results of these measurements, shown in Fig. 2, indicate that for films greater in thickness than about 60 Å, the coefficient is approximately constant at a value of $1{\cdot}7 \times 10^{-3}$ per °C, which is about one-half the bulk-metal value. At 60 Å there is a discontinuity, the coefficient dropping suddenly, and thereafter it falls almost linearly with the thickness. However, the coefficient is still positive for the 25 Å films.

(c) *Hall coefficient.* The Hall coefficient of a conducting material gives a measure of the density of charge carriers in it, and variations of this parameter measured for thin films

may indicate whether the mode of conduction in the film is different from that in the bulk material. These highly-conducting metal films are very suitable for the measurement of Hall coefficient, for the magnitude of the Hall voltage, which is the experimental parameter to be determined, is proportional to the current density flowing longitudinally in the film and to the transverse magnetic field. Current densities of at least half a million amperes per square centimetre cross-section are easily achieved for these films, so that quite small magnetic fields can be used to give a measurable Hall voltage.

Fig. 3 shows the electrode arrangement used for measuring Hall coefficient of the films. Thick gold layers *C*, *D*, *E* and *F* were evaporated on top of the thin gold film to provide the voltage electrodes in addition to the current electrodes *A* and *B*. With a constant current of about 20 mA flowing in the film, and no magnetic field applied, an equipotential across the breadth of the film was found by adjusting potentiometers across *CD* and *EF*. On application of the transverse magnetic field of about 4000 G, the Hall voltage was then measured by a null method.

Only two films were measured, both fully annealed. Values of Hall coefficient of $-4{\cdot}2 \times 10^{-4}$ c.g.s. units for a nominal 25 Å film and $-7{\cdot}0 \times 10^{-4}$ c.g.s. units for a 41 Å film were obtained. These compare with the bulk metal value of $-7{\cdot}04 \times 10^{-4}$ c.g.s. units. Measurements on a wider range of thickness of films would be profitable, but the present results are significant in showing that the magnitude and sign of the Hall coefficient for these thin films is not widely different from the bulk metal value.

COMPARISON OF ELECTRICAL PROPERTIES OF EVAPORATED AND SPUTTERED LAYERS

In comparison with sputtered films of gold on bismuth oxide, the evaporated films described here can be made with a higher conductivity in thinner layers. For example, sputtered films of 200 Å have a resistivity greater than the bulk metal value by a factor of 1·6, while the evaporated films of the same thickness have practically bulk resistivity. Further, the resistivity of sputtered films begins to rise steeply for thicknesses below 100 Å, while for the evaporated films the steep rise occurs at about half this value. Sputtered films, on the other hand, are capable of withstanding a somewhat higher annealing temperature without breakdown of the film.

The difference in temperature-resistance characteristics for the two types of film is quite marked. For sputtered films, the variation of temperature coefficient α_F with film thickness is continuous, and follows the same course as the variation of conductivity σ_F with thickness. (See Holland and Siddall,[4] Fig. 6.) The relation $\alpha o/\alpha_F = \sigma o/\sigma_F$, in fact, holds for all thicknesses of film, and Holland and Siddall quote this in support of the supposition that the resistance of the films can be considered as made up of two components, one temperature-dependent and the other invariant (Mathieson's rule). For the evaporated films, on the other hand, the above relation holds only approximately for the thin films below 60 Å. Obviously the thicker films with near bulk conductivity should have a temperature coefficient approaching the bulk value if the same relation is to apply to them.

STRUCTURE OF EVAPORATED FILMS

Transmission electron diffraction was used to examine the crystal structure of the composite evaporated films. The oxide and a 50 Å layer of gold were evaporated on to a carbon film mounted on a copper mesh, which could be given the appropriate heat treatment. The evaporated bismuth oxide condensed as a polycrystalline layer showing no preferred orientation, with crystal size about 40 Å. This structure was not appreciably modified on heating, and there was no evidence of bismuth metal being present. The gold film, as initially evaporated, was also polycrystalline and non-orientated, having an average crystal dimension in the plane of the film of 200 Å, which, after the annealing process, increased to over 300 Å. These values contrast with the crystal sizes as measured for the sputtered films by Gillham, Preston and Williams, namely, sputtered bismuth oxide amorphous; sputtered gold on the oxide, annealed, 40 Å.

The overall thickness of a bismuth oxide-gold film makes it difficult to observe fine structure when examined in the electron microscope, owing to heavy electron scattering in the film. Furthermore, since the main feature of interest in the films is the topography of the bismuth oxide on which the gold condenses, examination of this layer alone was found to give most information. Fig. 4 is a direct electron micrograph of an evaporated bismuth oxide film, which shows granularity to the extent of 50–100 Å. However, this granularity may not extend to the surface, since it is possible that the contrast in this micrograph is caused by Bragg scattering of electrons outside the cone accepted by the microscope objective aperture, and not to variations in film thickness. Examination by a replica technique was thus attempted. Fig. 5 is a carbon replica, prepared by the method of Bradley,[5] of evaporated bismuth oxide which had been heated in air. The replica has been shadow-cast with gold to show up the surface structure. Apart from occasional large excrescences in the surface, the surface structure shows a roughness of comparable magnitude to that predicted by the direct micrograph, namely, 50–100 Å. The interesting point to note is that the structure size of the surface corresponds roughly to the thickness at which the electrical properties of the films change.

DISCUSSION

To explain the electrical properties of these evaporated films, one can first examine them in the light of the theories of Fuchs[6] and Sondheimer,[7] who predict the effects to be observed if the conduction electrons are limited in their mean free path by inelastic collision with the walls of the film. Interaction with the walls will obviously occur for films of comparable or smaller thickness than the mean free path, which, for electrons in gold, is about 620 Å at room temperature. Since, however, the annealed evaporated films do not rise in resistivity until their thickness becomes less than 200 Å, it is clear that the theory is not obeyed. For smaller thicknesses, the discrepancy between measured resistivity and that predicted theoretically is even greater. Further, the theory predicts that the temperature coefficient should vary with thickness t as:

$$\frac{\alpha_F}{\alpha} = \frac{1}{1 + \log(\lambda/t)}$$

where λ is the mean free path of the electron. (This expression is derived from a simplified theoretical treatment by Lovell,[8] which is a close approximation to the general case treated by Fuchs.) A steady decrease in temperature coefficient with decrease in thickness is indicated instead of the discontinuous relationship as measured. Finally, Sondheimer has shown that the Hall coefficient for thin lamella films should rise as the film thickness decreases. For a 30 Å gold film in which

completely inelastic scattering of the electrons occurs at the film boundaries, the coefficient should be about twice the bulk value. The observed Hall coefficients, albeit on two films only, showed, if anything, a decrease in Hall coefficient. Hall coefficients of films as thin as these have not before been measured, but Bonfiglioli, Coen and Malvano,[9] working with thicker gold films evaporated on glass, have shown the important influence of non-uniformities in the thickness of the film upon the apparent Hall coefficient. In view of this, it is doubtful whether any great significance can be attached to the absolute values of the coefficient for these very thin films.

It appears then that the electrical properties of these films must be ascribed to their internal structure alone. As in the case of the sputtered films, it is evident that the gold deposits in a continuous layer, with lattice misfits between individual grains. These are reduced by the annealing process, giving rise to increased conduction. However, in the case of the sputtered films, part of the annealing is due to release of occluded gas, which will not be present to such an extent in the evaporated films. This is evident from a comparison of the resistivity-thickness curves. For corresponding thicknesses, the unannealed evaporated films undergo less resistance change than the sputtered films when they are heat-treated, indicating that the evaporated films behave more nearly like the bulk metal when first deposited. It seems that these films are capable of retaining a high degree of continuity until their thickness becomes comparable with the roughness of the surface on which they deposit. One can then imagine that "necking" of the film might occur over the rough patches, giving rise to the apparent increased resistivity. The anomalous behaviour of the temperature coefficient is more difficult to explain. Since, for the thicker films, the bulk resistivity is attained, one cannot postulate that this is made up of a temperature-dependent and a temperature-independent part, as for the sputtered films. The only likely explanation of the decreased temperature coefficient is that the differential expansion of the glass, the oxide substrate and the gold, somehow modify the nature of the film.

CONCLUSIONS

It has been shown that it is possible to make highly conducting transparent layers by vacuum evaporation of a thin gold layer on thin layers of various metal oxides. These layers very nearly retain many of the electrical characteristics of the bulk metal down to smaller thicknesses than previously reported, namely, less than 100 Å. The layers, which are conveniently made using standard laboratory equipment, can have a variety of uses as transparent electrodes or surface heating elements.

ACKNOWLEDGEMENTS

Acknowledgements are made to Mr. J. S. Preston for useful discussion and information on sputtered layers, Mr. M. E. Haine for helpful suggestions in the course of this work, and to Miss P. E. Rush for preparing the electron micrographs: also to Dr. T. E. Allibone for permission to publish this paper.

REFERENCES

(1) Gillham, E. J., and Preston, J. S. *Proc. Phys. Soc. [London] B*, **65**, p. 649 (1952).
(2) Gillham, E. J., Preston, J. S., and Williams, B. E. *Phil. Mag.*, **46**, p. 1051 (1955).
(3) Libbey–Owens–Ford Glass Co. British Patent 682 264.
(4) Holland, L., and Siddall, G. *Vacuum*, **3**, p. 375 (1953).
(5) Bradley, D. E. *Brit. J. Appl. Phys.*, **5**, p. 96 (1954).
(6) Fuchs, K. *Proc. Cambridge Phil. Soc.*, **34**, p. 100 (1938).
(7) Sondheimer, H. *Advances in Phys.*, **1**, p. 1 (1952).
(8) Lovell, A. C. B. *Proc. Roy. Soc. A*, **157**, p. 311 (1936).
(9) Bonfiglioli, G., Coen, E., and Malvano, R. *J. Appl. Phys.*, **27**, p. 201 (1956).

The dust-free space surrounding hot bodies

By W. Zernik, B.Sc., Grad.Inst.P.,* Research Department, Simon-Carves Ltd., Stockport

[*Paper received* 7 *November*, 1956]

It is generally accepted that the dust-free space around hot bodies is due to the combined action of a radiometer force and an aerodynamic force caused by convection currents but no attempt has yet been made to derive a quantitative theory. Starting from the published work on the derivation of these forces a method has been evolved for equating them and the theory is worked out quantitatively for a vertical plate and for a horizontal cylinder in terms of temperature difference and the properties of the surrounding medium. The resulting relations are in good agreement with published experimental data.

INTRODUCTION

It has been known since 1884[1,2] that a dust-free space, usually a fraction of a millimetre thick, is formed around a hot body. The effect has been extensively utilized in the construction of thermal precipitators for dust sampling.[3, 4] Little experimental work has been done on the dust-free space as such, but some accurate measurements have been reported by Watson.[5]

It has often been pointed out that the effect is partly the result of the radiometer force that tends to move dust particles down a temperature gradient. The expression for this force has been derived by Epstein[6] and has been experimentally verified by Rosenblatt and LaMer[7] and Saxton and Ranz.[8] Several authors have suggested that the radiometer force must be counteracted to a certain extent by convection currents[5, 7] so as to account for the fact that the dark space has a sharply defined boundary and a size independent of the type of dispersed material. However, no quantitative theory on these lines has hitherto been put forward.

The temperature and velocity distribution associated with free convection from a vertical plate in air has been calculated by Schmidt and Beckmann[9] with results that agree well with experiment in the range of Grashof numbers 10^6 to 10^8 approximately. A recent more general investigation by Ostrach[10] leads to the same differential equations. The corresponding calculations for a horizontal cylinder have

* Now at Yale University, New Haven 11, Connecticut, U.S.A.

been carried out by Hermann.[11] His results agree fairly well with experiment in the range of Grashof numbers 10^5 to 10^7 approximately.

It is shown below that if the expression for the aerodynamic force on a dust particle due to the convection current is equated to the expression for the radiometer force due to the temperature gradient, it is possible to derive an expression for the dust-free space which is in good agreement with Watson's experimental results.[5]

It is assumed that the particles are spherical and that radiative heat transfer can be neglected.

LIST OF SYMBOLS

T_1 = temperature of hot body (°K).
T_0 = ambient temperature (°K).
a = radius of particle.
η = dynamic viscosity of air.
ρ = density of air.
ν = kinematic viscosity of air.
g = gravitational acceleration.
S = Sutherland's viscosity constant.

Other symbols will be defined in the text as required. C.g.s. units are used throughout.

THE AERODYNAMIC AND RADIOMETER FORCES

If the velocity of the convection air current towards the hot surface is v, the aerodynamic force on a particle will be given by:

$$F_A = 6\pi a\eta v \tag{1}$$

since at the edge of the dust-free space v is always small enough for Stokes' law to apply.

The radiometer force is given by Epstein[6] as:

$$F_T = -\frac{9\pi a}{4}\cdot\frac{\eta^2}{\rho}\cdot\frac{C_a}{2C_a + C_i}\cdot\frac{1}{T}\cdot\frac{dT}{dy} \tag{2}$$

where T = absolute temperature at a distance y from the surface,

C_a = thermal conductivity of air,
C_i = thermal conductivity of particle.

This formula was derived on the assumption that the particles remain stationary. In the present case, however, they are in continuous motion so that the time that any particle spends in the narrow region around the hot body where a temperature gradient exists must be comparatively small. Accordingly their temperature can rise little above ambient, i.e. they behave as if $C_i = 0$ so that we can write:

$$F_T = -\frac{9\pi a}{8}\cdot\frac{\eta^2}{\rho}\cdot\frac{1}{T}\cdot\frac{dT}{dy} \tag{3}$$

THE DUST-FREE SPACE AROUND A HOT VERTICAL PLATE

Let y be the perpendicular distance from the plate and x the distance from the lower edge. The width of the plate is assumed to be infinite.

Let a variable C be defined as:

$$C = \left[\frac{g(T_1 - T_0)}{4\nu^2 T_0}\right]^{\frac{1}{4}} \tag{4}$$

and a dimensionless variable ξ as:

$$\xi = Cyx^{-\frac{1}{4}} \tag{5}$$

The air velocity towards the plate v_y can now be written as [Ref. 9, equation (32)]:

$$v_y = -\nu C[3x^{-\frac{1}{4}}\zeta - Cyx^{-\frac{1}{4}}\zeta'] \tag{6}$$

where $\zeta(\xi)$ is a function of ξ which is given later [see equation (17)]

and $$\zeta' = d\zeta/d\xi$$

(The factor 3 is not printed in the reference given.)
Substituting for $Cyx^{-\frac{1}{4}}$ from equation (5)

$$v_y = -\nu C[3x^{-\frac{1}{4}}\zeta - x^{-\frac{1}{4}}\xi\zeta'] \tag{7}$$

and putting this value of velocity in equation (1).

$$F_A = 6\pi a(\eta^2/\rho)Cx^{-\frac{1}{4}}[3\zeta - \xi\zeta'] \tag{8}$$

Let T be the absolute temperature at a distance y from the plate, and let θ be another dimensionless variable such that

$$\theta = (T - T_0)/(T_1 - T_0) \tag{9}$$

then $$\frac{dT}{dy} = \frac{d\theta}{dy}(T_1 - T_0) = \frac{d\theta}{d\xi}\cdot\frac{d\xi}{dy}(T_1 - T_0) \tag{10}$$

At $$\xi = 0,\ d\theta/d\xi = -0{\cdot}508 \simeq -\tfrac{1}{2} \tag{11}$$

(Ref. 9, Table 4) and it can easily be seen that $d\theta/d\xi$ remains effectively constant within the narrow region occupied by the dark space.

Therefore $$dT/dy = -\tfrac{1}{2}(T_1 - T_0)Cx^{-\frac{1}{4}} \tag{12}$$

and $$T = T_1 - \tfrac{1}{2}(T_1 - T_0)Cx^{-\frac{1}{4}}y \tag{13}$$

Substituting equations (12) and (13) in equation (3) we obtain:

$$F_T = \frac{9\pi a}{8}\cdot\frac{\eta^2}{\rho}\cdot\frac{Cx^{-\frac{1}{4}}}{[2T_1/(T_1 - T_0) - Cx^{-\frac{1}{4}}y]} \tag{14}$$

and putting $2T_1/(T_1 - T_0) = T'$ we can write:

$$F_T = \frac{9\pi a}{8}\cdot\frac{\eta^2}{\rho}\cdot\frac{Cx^{-\frac{1}{4}}}{(T' - \xi)} \tag{15}$$

Equating F_A and F_T we obtain:

$$(3\zeta - \xi\zeta')(T' - \xi) = 3/16 \tag{16}$$

$\zeta(\xi)$ is given by (Ref. 9, p. 401):

$$\zeta(\xi) = \frac{\xi^2}{2!}m - \frac{\xi^3}{3!} - \frac{\xi^4}{4!}n + \frac{\xi^5}{5!}m^2 + \ldots \tag{17}$$

where $$m = d^2\zeta/d\xi^2(\xi = 0) = 0{\cdot}675 = 27/40$$
$$n = d\theta/d\xi(\xi = 0) = -0{\cdot}508$$

Within the dust-free space ξ is always less than unity so that the series given in equation (17) converges fairly rapidly. If we take the first two terms only and in the first place put

$$T' - \xi \simeq T' \tag{18}$$

we obtain for an approximate value of ξ, ξ_a:

$$\frac{m}{2!}\cdot\xi_a^2 T' = \frac{3}{16} \tag{19}$$

therefore $$\xi_a = (5/9\,T')^{\frac{1}{2}} \tag{20}$$

If we now correct this formula for the approximation made in equation (18) we obtain for ξ_0, the value of ξ corresponding to the width of the dark space:

$$\xi_0 = \left\{5/[9(T' - \xi_a)]\right\}^{\frac{1}{4}} = f(T') \text{ say} \tag{21}$$

We can now obtain the width of the dark space y_0 from equation (5).

As the temperature drop within the dark space is relatively small we can assume that ν in equation (4) has the value ν_1 at T_1.

Now
$$\nu^2 = \eta^2/\rho^2 \tag{22}$$

and
$$\rho_1 = \rho_0 \cdot \frac{273}{T_1} \tag{23}$$

$$\eta_1 = \eta_0 \cdot \frac{273 + S}{T_1 + S} \cdot \left(\frac{T_1}{273}\right)^{\frac{3}{2}} \tag{24}$$

where ρ_0, η_0 are values at 0° C.

Substituting equations (22), (23) and (24) in equation (4) and then using equations (5) and (21) we finally obtain:

$$y_0 = x^{\frac{1}{4}} F(T_1) f(T') \tag{25}$$

where
$$F(T_1) = \left[\frac{4\eta_0^2}{g\rho_0^2} \cdot \left(\frac{273 + S}{T_1 + S}\right)^2 \cdot \frac{T_1^5}{273^5} \cdot \frac{T_0}{T_1 - T_0}\right]^{\frac{1}{4}} \tag{26}$$

Finally it is necessary to calculate the error introduced by taking the first two terms only of the series in equation (17). If we take account of the third term we obtain instead of equation (19):

$$\left(\frac{m}{2} \cdot \xi^2 + \frac{n}{24}\xi^4\right) T^1 = \frac{3}{16} \tag{27}$$

The percentage change in ξ^2 is given by:

$$\frac{\xi^2 n}{12m} \times 100$$

Therefore if $\xi = 1$ corresponding to a dark space approximately 2 mm wide the change in ξ^2 is 6·2%, i.e. the error in ξ is 3·1%. Therefore for $\xi < 1$ the third and higher terms can be neglected.

THE DUST-FREE SPACE SURROUNDING A HOT HORIZONTAL CYLINDER

The position of any point outside the cylinder is specified by a normal co-ordinate R and an angle x measured anti-clockwise from the downward vertical. The length of the cylinder is assumed to be infinite.

Now introduce the Grashof number defined by

$$G_r = \frac{g(T_1 - T_0)r^3}{\nu^2 T_0} \tag{28}$$

where r is the cylinder radius, and an "azimuth function" $g(x)$ whose values are taken from Table 4 of reference (11). Also define a dimensionless variable q as:

$$q = \frac{R}{r} \cdot G_r^{\frac{1}{4}} \cdot g(x) \tag{29}$$

A function $p(q)$ which has the same form as the function $\zeta(\xi)$ of equation (17) and the dimensionless temperature function $\theta(q)$ of equation (9) are also employed.

The differential equations for the functions p and q can then be shown to have the form [Ref. 11, equation (52)]:

$$p''' + 3pp'' - 2(p')^2 + \theta = 0 \tag{30}$$

$$\theta'' + \frac{3\nu}{\alpha} p\theta' = 0 \tag{31}$$

Where α = thermal conductivity of air and $p' = dp/dq$, etc.

These equations have exactly the same form as the equations for $\zeta(\xi)$ and $\theta(\xi)$ in the case of the vertical plate [Ref. 9, equations (26) (27)].

Thus the two sets of dimensionless functions $\zeta(\xi)$, $\theta(\xi)$ and $p(q)$, $\theta(q)$ are derived from differential equations of identical form. Since equation (16) consists entirely of dimensionless terms it follows that the corresponding equation for the case of the horizontal cylinder must also have exactly the same form.

Therefore
$$(3p - qp')(T' - q) = 3/16 \tag{32}$$

This equation can also be derived in the same way as equation (16) from the basic equations by Hermann.[11]

By analogy with equation (21) q_0 is given by:

$$q_0 = \left[5/9(T' - q_a)\right]^{\frac{1}{4}} = f(T') \tag{33}$$

so that
$$R_0 = q_0 \cdot \frac{rG_r^{-\frac{1}{4}}}{g(x)} \tag{34}$$

but
$$rG_r^{-\frac{1}{4}} = r^{\frac{1}{4}}/C\sqrt{2} \tag{35}$$

therefore
$$R_0 = \frac{r^{\frac{1}{4}}}{\sqrt{2} \cdot g(x)} \cdot F(T_1) \cdot f(T') \tag{36}$$

For constructing the theoretical curves shown in Figs. 1 and 2 the following values for air at 76 cm of mercury were used

$T_0 = 300°$ $\qquad$ $\rho_0 = 1{\cdot}293 \times 10^{-3}$

$\eta_0 = 1{\cdot}718 \times 10^{-4}$ $\qquad$ $S = 117$

COMPARISONS WITH EXPERIMENTAL RESULTS

The only exact experimental results published are those obtained by Watson.[5] Watson states that the width of the dark space is uniform opposite a plate. The theory given above predicts that the width of the dark space opposite a plate should vary according to the fourth root of the distance from the lower edge, whilst that around a cylinder should vary according to the inverse of the azimuth function $g(x)$.

In comparing the theory with Watson's results, account is taken of the fact that the microscope readings were taken half-way up the plates and at the end of the horizontal diameters of the cylinders.

Watson[12] found that for the rods R_0 was smaller at $x = 0$ than at $x = \pi/2$ as predicted by the theory.

The theoretical values for the plates and cylinders are compared with the experimental values in Figs. 1 and 2. It will be seen that the agreement is as good as can be expected considering the approximate nature of the convection theory.

The comparison of theory and experiment is subject to an important difficulty not previously mentioned. Schmidt and Beckmann's[9] and Hermann's[11] experiments were carried out in the range of Grashof number $10^5 - 10^9$ approximately, where the Grashof number for the vertical plate is defined as in equation (27) with r replaced by the height of the plate. According to Hermann[11] if Grashof numbers larger than this are used the flow becomes turbulent whilst for Grashof

numbers smaller than about 10^4 the layer of air in which heat exchange takes place can no longer be considered small in comparison with the size of the hot body so that the assumptions of boundary layer theory, which are used in

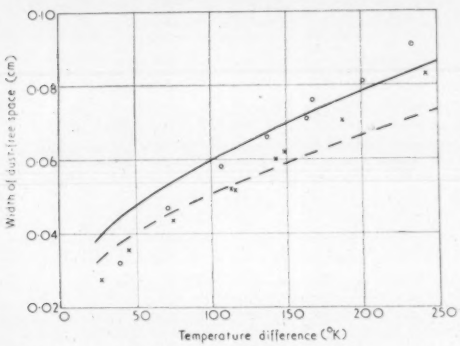

Fig. 1. Variation of dust-free space with temperature for vertical plates

Plate 6 cm high
Theory
Experiment
Plate 3·1 cm high
Theory
Experiment

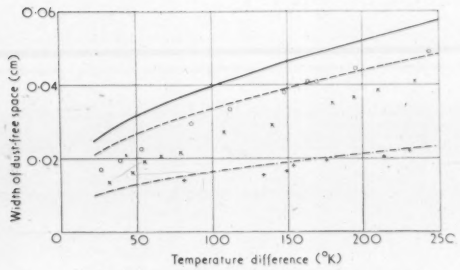

Fig. 2. Variation of dust-free space with temperature for horizontal cylinders

Cylinder 0·45 cm radius
Theory
Experiment
Cylinder 0·23 cm radius
Theory
Experiment
Cylinder 0·0127 cm radius
Theory
Experiment

deriving the convection equations quoted in this paper are no longer valid.

The Grashof numbers used in Watson's experiments range from about 5×10^{-2} to about 5×10^4 so that it might appear that most of his results should not be amenable to the theoretical treatment given in this paper. However, this does not appear to be the case, for even in the case of a wire of diameter 0·0254 cm ($G_r \simeq 5 \times 10^{-2}$) the agreement with theory is good, in fact rather better than for the results at higher Grashof numbers.

It must be concluded that even though the convection equations used in this paper may not be valid throughout the entire width of the heat-transfer layer they are, nevertheless, true to a good approximation within the dust-free space which usually has only a small fraction of the width of the heat transfer layer. However, it must be admitted that this is a point that requires further elucidation.

It remains to discuss the approximation involved in putting $C_i = 0$ [equation (3)]. This cannot be large since Watson[5] has shown that the size of the dark space is substantially the same for various dispersed materials including carbon black ($C_i = 6{\cdot}5 \times 10^{-4}$ W/cm° C) and magnesium oxide ($Ci = 126 \times 10^{-4}$ W/cm° C). Watson has been kind enough to point out[12] to the author that taking account of C_i would lower the theoretical values, the effect being larger at the lower temperature differences when the convection currents are slower, and smaller for smaller hot surfaces.

ACKNOWLEDGEMENTS

The author is greatly indebted to Mr. W. Bostock and Mr. J. K. Donoghue, Simon-Carves Ltd., for their advice and encouragement, and Mr. H. H. Watson, Suffield Experimental Station, Ralson, Alberta, for reviewing the draft of this paper and offering valuable comments.

The author is grateful to the Management Board, Simon-Carves Ltd., for their interest and permission to publish this work.

REFERENCES

(1) AITKEN, J. *Trans Roy. Soc. Edinburgh*, **32**, p. 239 (1884).

(2) LODGE, O. J., and CLARK, J. W. *Phil. Mag.*, **17**, p. 214 (1884).

(3) GREEN, H. L., and WATSON, H. H. *Medic. Res. Counc. Spec. Report*, No. 199 (London: H.M. Stationery Office, 1935).

(4) BREDL, T., and GRIEVE, T. W. *J. Sci. Instrum.*, **28**, p. 21 (1951).

(5) WATSON, H. H. *Trans Faraday Soc.*, **32**, p. 1073 (1936).

(6) EPSTEIN, P. S. *Z. Phys.*, **54**, p. 537 (1929).

(7) ROSENBLATT, P., and LAMER, V. K. *Phys. Rev.*, **70**, p. 385 (1946).

(8) SAXTON, R. L., and RANZ, W. E. *J. Appl. Phys.*, **23**, p. 917 (1952).

(9) SCHMIDT, E., and BECKMANN, W. *Tech. Mech. u. Thermodynamik.*, **1**, pp. 341, 391 (1930).

(10) OSTRACH, S. *Nat. Advis. Comm. Aeronaut. (U.S.A.), Report*, IV (Washington: Government Printing Office, 1927).

(11) HERMANN, R. *Forschungsheft* 379 (Dusseldorf: Deutscher Inginieur Verlag, 1936).

(12) WATSON, H. H. Personal Communication.

Contact electrification across metal-dielectric and dielectric-dielectric interfaces

By G. S. Rose, Ph.D., B.Sc., A.Inst.P., and Prof. S. G. Ward, Ph.D., Department of Mining, University of Birmingham

[*Paper first received* 1 *August, and in final form* 2 *November*, 1956]

An apparatus is described by means of which a spherical dielectric surface can be compressed under various loads against either a plane metal disk or a plane dielectric disk. A transfer of electric charge across the interface is recorded when the surfaces are separated. The polarity of charging between any two materials depends upon the relative positions of those materials in an electrostatic series; a metal surface does not always assume a positive charge as found for impact electrification. For two given materials the amount of charge is proportional to the contact area between the surfaces and provided that one of the surfaces has a resistivity above a critical value ($5 \times 10^{11}\ \Omega$ cm) then the charge density for various combinations of materials is approximately proportional to the lower dielectric constant in each combination. This result suggests that the charging may be limited by electrical back-discharge between the separating surfaces. It is considered to be unlikely that the electrification originates from a difference in the contact potentials of the two surfaces involved.

The generation of static electrification between two solid materials is a surface phenomenon. The amount and polarity of the charge generated is therefore dependent on the nature and condition of the surfaces in question and on the type of contact between them. This statement is adequately supported by the results of Shaw[1] and his co-workers[2, 3] who found that the charge transfer produced by contact between two given materials varied in sign as well as magnitude. The capricious nature of the experimental results obtained in this field is summarized by Loeb[4] who suggests that several independent mechanisms are simultaneously contributing to the final charge.

In order to control more accurately the type of contact between the surfaces and to determine the actual contact areas, Richards,[5] Hess[6] and more recently Knowles[7] employed one plane and one spherical surface. Richards and Knowles allowed a spherical insulating surface to impinge normally upon an insulated plane metal surface. The metal always assumed a positive charge and for two given surfaces the charge per unit contact area was constant. Hess, on the other hand, compressed two dielectric surfaces together with loads up to 100 g; he claims that his results support Coehn's law. Coehn[8] established that after contact between a poorly conducting liquid and an insulator, the one of higher dielectric constant assumed a positive charge and that the charge density was proportional to the difference in dielectric constants.

However, an examination of the experimental data given in Hess's paper suggests that his conclusions are somewhat unfounded; it is not a convincing verification of Coehn's law. Further suspicion is thrown upon the subject by the work of Richards.[9] He assumed Coehn's law to be valid for charging between two solid surfaces and hence concluded that all metals must possess dielectric constants between 3·0 and 4·0. The following experiments were designed to investigate the validity of Coehn's law and to extend the work of Hess to include metal-dielectric contacts.

APPARATUS

The apparatus was so designed that a spherical dielectric surface could be compressed normally against a plane surface by applying loads up to 25 kg. A line drawing of the apparatus is shown in Fig. 1. The spherical dielectric specimen is held in a brass retaining cup of appropriate size which in turn is mounted on the screw thread adjustment *m*, along the axis of the aluminium carrier *c*. By operation of the control wheel *l* the spindle *r* can be raised vertically to lift the main spring *s* and the aluminium carrier. The latter rises until the spherical surface makes contact with the plane

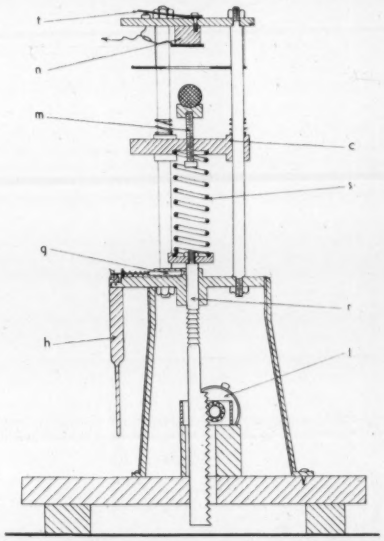

Fig. 1. Line drawing of static compression apparatus

metal disk on the bottom of the Perspex cylinder *n*. Further elevation of the spindle compresses the main spring and causes a pressure to be applied between the two surfaces. This pressure can be released by depressing the lever *h* and withdrawing the spring-loaded pin *g* from one of the notches in the spindle *r*.

The main spring is calibrated and for a given setting of the adjustment *m* (to give a standard height of the spherical

surface above the aluminium carrier) the loads corresponding to all notches are known. The carrier and guide rods, machined to 0·001 in. tolerance, prevent any lateral motion of the dielectric surface, while the seating of the guide rods in the top plate ensures that the load is applied in a direction normal to the plane surface. Friction between the two surfaces is thereby reduced to a minimum. Frictional effects are also reduced by means of the side springs, one on each guide rod, which ensure a rapid separation of the surfaces with a minimum amount of sticking.

In a series of experiments described elsewhere[10] a controlled amount of friction was deliberately introduced between the surfaces in contact. The mounting of the dielectric specimen on the aluminium carrier was modified so that the plastic surface could be simultaneously compressed against the metal disk and rotated about the axis of symmetry normal to the disk. The charge transfer measured upon separation was of the same order as that recorded after static compression but the reproducibility of both magnitude and sign was much less. Examination of the surfaces after compression revealed several small metallic particles embedded in the dielectric surface. The plastic material had apparently melted (this occurred even on light loads and small—1 rev/min—speeds of rotation) and the surface was noticeably deformed over the area of contact. Such a transfer of material from one surface to another was never observed after static compression and the polarity of charge transfer between two given surfaces was always consistent. It is therefore concluded that in the present apparatus friction is reduced to a satisfactory minimum, i.e. any frictional effects are less than the experimental error.

As shown in Fig. 1 the plane metal electrode is supported by a Perspex insulating cylinder *n*. The electrode is connected *via* a 100 000 MΩ resistor to the input of a Farmer–Baldwin electrometer, biased with a 200 V d.c. supply in order to measure both positive and negative voltages. The high resistor prevents instantaneous voltages being applied directly to the grid of the electrometer valve, i.e. precludes grid current when recording increases in voltage.

Fig. 2 shows a modified version of the apparatus in which the metal electrode is replaced by a Faraday cage arrangement. This was used for experiments on dielectric-dielectric

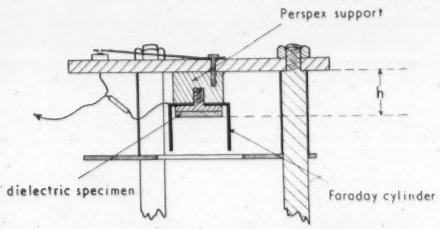

Fig. 2. Diagram of Faraday cage arrangement

compressions. The cage is mounted on an insulating Perspex cylinder and connected to the electrometer in the manner described above. A plane dielectric specimen is screwed to a brass disk in the base of the cylinder; the charge transfer in this case is measured by induction. In order to ensure a standard load calibration, all dielectric specimens were ground to the same thickness so that the height *h* was kept constant.

Cellulose nitrate, ethyl cellulose, cellulose acetate, casein, ebonite, Perspex, polystyrene, Tufnol, polytetrafluoroethylene (Teflon) and polythene were used. From the majority of these materials spherical specimens were produced by turning in a lathe and then grinding with carborundum powder using a linen-lined brass cup of the correct curvature as a former. Plane dielectric surfaces were made by turning a disk of the material from 1 in. diameter rod and grinding one surface on a sheet of plate glass. All dielectric specimens were carefully washed in distilled water and a final mirror-like surface was obtained using Silvo metal polish. The diameters of the spheres were between $\frac{1}{2}$ and 1 in. For each sphere the diameter was measured using a micrometer screw gauge; a mean of ten readings was taken. All readings lay within $\pm 1\%$ of the mean.

Plane metal surfaces of copper, zinc, brass, iron, bismuth and aluminium were prepared in a similar manner, by turning on a lathe and grinding on successively finer grades of emery paper before the final polishing with Silvo. All the metals, with the exception of brass, were at least 99·95% pure.

EXPERIMENTAL

Before taking a reading both surfaces in question were polished with cotton wool and cleaned with some suitable organic solvent (e.g. ethyl alcohol, benzene or ether which did not attack the particular dielectric material) to remove grease and other superficial surface contamination. The electrometer input was brought to earth potential by depressing the earthing key *t* (see Fig. 1) and all spurious surface charges were removed from the dielectric specimens by playing a small, luminous coal-gas flame at a distance of about 10 cm from the surface for about 5 s. A radioactive source, namely 15 mc of thallium 204, was also used for removing the electrostatic charge. This method, however, was not very satisfactory; the rate of loss of charge was slow, presumably on account of the low penetrating power of the β-rays emitted.

The two surfaces were compressed and upon separation the change in voltage of the insulated plane surface was recorded on the electrometer. For purposes of calibration this voltage was converted into charge; the capacity of the particular electrode arrangement was determined by the method of charge sharing with a standard condenser.

From the theory developed by Hertz,[11] it is clear that when one spherical surface and one plane surface are compressed together, each will be elastically deformed and produce an area of contact common to both bodies. These contact areas were determined experimentally by coating the plane surface with a very thin layer of soot. The spherical surface was then compressed against the plane one with a known load. Upon separation, it was found that the original layer of soot was intact except for the portion which had been in contact with the spherical surface, while a circle of soot had adhered to the sphere over the same area of contact. The diameter of the circle on the spherical surface was measured in two directions at right-angles using a travelling microscope and the contact area was then calculated. This procedure was repeated with several metal-dielectric and dielectric-dielectric combinations. Very good agreement was found between the observed values and those calculated from Hertz's theory.

RESULTS

Polarity of charging. Compression between a dielectric sphere and a metal plate produced a charge transfer, the

direction of which was independent of the nature of the metal forming the plate; it depended solely upon the nature of the dielectric material used. Using two dielectric specimens, however, the direction of charge transfer was found to depend upon the nature of both materials used. It is possible to arrange all the materials used in such an order that any one material assumes a negative charge when compressed with another material above it in the order, and a positive charge after compression against any material below it. The order found is as follows:

positive	ethyl cellulose
	casein
	Perspex
	Tufnol
	ebonite
	cellulose acetate
	glass
	all metals
	polystyrene
	polyethylene
	Teflon
negative	cellulose nitrate

Such an order is somewhat analogous to the electromotive series for metals and may be called an electrostatic series. Owing to the rather capricious nature of results obtained by previous workers on problems similar to the above, the process was repeated on two occasions after intervals of approximately one week. The results were almost identical; the charges varied slightly in size but never in sign.

Bearing in mind the existence of such a series, compression of two surfaces of the same material would be expected to yield zero charging. The voltages recorded on a cellulose nitrate sphere are presented graphically in Fig. 3 in the order

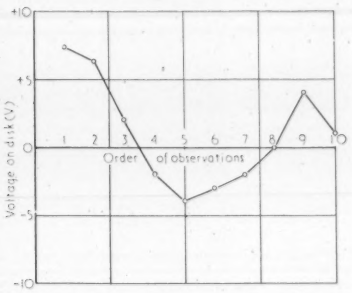

Fig. 3. Electrification between two cellulose nitrate surfaces

observed experimentally. It is seen that the charge transfer exhibits no predominant polarity and that the average of ten successive readings is sensibly zero.

Amount of charging. For all combinations of materials on all loads the amount of charging was independent of the time of contact of the two surfaces. The quantity of charge produced after compression of a dielectric sphere against a plane metal disk was also found to be independent of the type of metal forming the disk. Thus, using a plane brass disk as a standard metal surface, the charge produced after compression against any spherical dielectric surface was proportional to the area of contact common to both bodies. This is represented graphically in Fig. 4 for ethyl cellulose and ebonite; each point is the mean value of four experimental readings. The contact areas obtained with the materials and loads used were of the order of 3×10^{-2} cm^2.

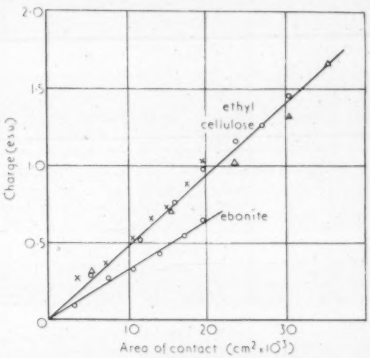

Fig. 4. Variation of charge with contact area for two metal-dielectric compressions

X, ½ in. diameter; *O*, 1 in. diameter; △, 2 in. diameter.

Similar linear relationships between charge and contact area were obtained for other dielectric materials. Table 1 gives the values of charge density (charge per unit contact area) acquired by the various dielectric materials after compression against a metal surface. The accuracy of these values, estimated from the spread of the experimental results, is approximately ±3%.

Table 1. *Charge densities obtained by compression of dielectric surfaces against a plane metal disk*

Dielectric materia	*Charge density (e.s.u./cm²)*
Cellulose nitrate	79
Polytetrafluoroethylene	27
Polystyrene	35
Ethyl cellulose	47
Cellulose acetate	46
Ebonite	34
Tufnol	12
Casein	22
Perspex	16

Continuing these experiments to include compression of two dielectric surfaces, it was again found that the charge per unit contact area was constant for two given materials. One plane and one spherical surface were prepared from each of the seven materials: ethyl cellulose, cellulose acetate, ebonite, casein, Tufnol, cellulose nitrate and polystyrene. A linear relationship was obtained between charge and contact area for each of the twenty-one combinations of two materials. Four of these are shown in Fig. 5 and Table 2 gives a complete list of the charge densities for all combinations. The accuracy is about ±5%. These values have all been corrected to allow for the fact that the Faraday cage does not surround the charge surface by a solid angle of 4 π.

Influence of resistivity. Fig. 6 shows the variation of charge density with the lower dielectric constant of each combination. A linear relationship appears to hold for most materials, both

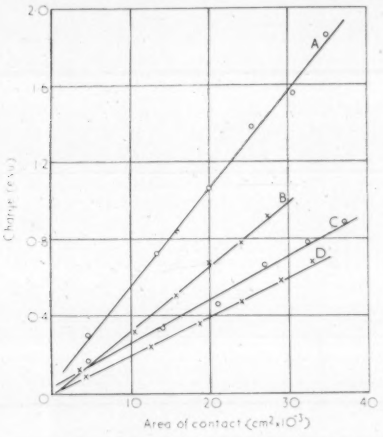

Fig. 5. Variation of charge with contact area for four dielectric-dielectric compressions

A, casein–cellulose nitrate; *B*, Tufnol–ethyl cellulose; *C*, cellulose acetate–ebonite; *D*, ethyl cellulose–polystyrene.

Table 2. *Charge densities obtained by compression of two dielectric surfaces*

Dielectric combination	*Charge density (e.s.u./cm²)*
Cellulose nitrate–ebonite	29
Cellulose acetate–ebonite	24
Polystyrene–ebonite	24
Ethyl cellulose–ebonite	28
Ethyl cellulose–polystyrene	20
Cellulose nitrate–ethyl cellulose	36
Cellulose nitrate–cellulose acetate	35
Cellulose nitrate–polystyrene	22
Cellulose acetate–polystyrene	20
Cellulose acetate–ethyl cellulose	34
Casein–cellulose nitrate	53
Casein–cellulose acetate	37
Casein–polystyrene	22
Casein–ebonite	25
Casein–ethyl cellulose	37
Tufnol–cellulose nitrate	54
Tufnol–ethyl cellulose	33
Tufnol–ebonite	27
Tufnol–polystyrene	23
Tufnol–cellulose acetate	32
Tufnol–casein	21

for metal-dielectric and dielectric-dielectric combinations. There are, however, some noticeable exceptions to this rule, namely, Perspex, casein and Tufnol for metal-dielectric compression and the dielectric-dielectric combination of casein–Tufnol.

The variation of the charging produced across a metal-dielectric interface with the resistivity of the dielectric material

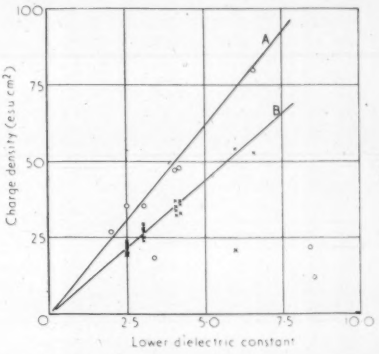

Fig. 6. Variation of charge density with lower dielectric constant

A, metal-dielectric compression; *B*, dielectric-dielectric compression.

is shown in Fig. 7. Resistivity is plotted against the factor charge density per unit dielectric constant for each material. In this way, those materials which conform with the linear relation between charge density and dielectric constant in Fig. 6 possess the same ordinate in Fig. 7. They have a resistivity above a critical value of $5 \times 10^{11}\ \Omega$ cm. For

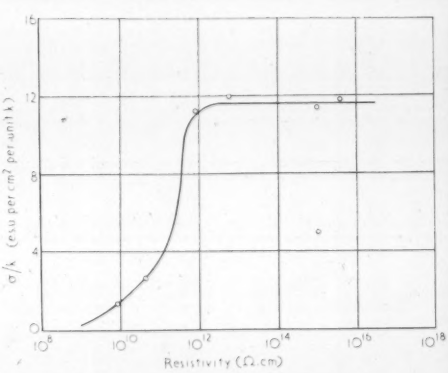

Fig. 7. Variation of charging with resistivity for metal-dielectric compressions

materials having resistivities below this critical value, e.g. casein, Tufnol, the charging falls rapidly. Perspex, however, is a most noticeable exception to this rule; its resistivity ($9 \times 10^{14}\ \Omega$ cm) is well above the critical value yet very little charging is observed.

The resistivities of the insulating materials used were measured by allowing a known capacitance to discharge through a high resistance. The latter consisted of a parallel-sided disk of the material in question; electrical contact was made by coating the opposite sides with a suspension of conducting graphite in water and allowing to dry.

ACCURACY OF RESULTS

Four separate combinations were chosen, two metal-dielectric and two dielectric-dielectric, namely brass–cellulose nitrate, brass–ethyl cellulose, polystyrene–ebonite and casein–cellulose acetate. For each combination thirty voltage readings were taken on each of the six values of applied load. It was necessary to clean each surface with an appropriate solvent at intervals of 15 min (every fifty compressions) throughout the experiments. The harder material of each dielectric-dielectric combination (casein and polystyrene) was used for the plane surface, since continual compression of a hard sphere against the same spot on a soft plane was found to cause considerable permanent set of the latter.

For a given load the set of thirty readings was divided into three individual groups comprising:

(*a*) the first four readings,
(*b*) the first ten readings,
(*c*) the whole thirty readings.

For each of these groups the average voltage was found and the standard deviation of the results was calculated using the formula:

$$\text{Standard deviation} = \sqrt{[(v - \bar{v})^2/(n - 1)]}$$

where v = voltage reading
$\bar{v}$ = mean voltage
n = number of observations.

For a given group of results and a given combination the standard deviation exhibited no systematic variation with the load between the surfaces, thereby indicating that the accuracy of the apparatus does not vary to any significant degree over the range of loads used ($1 \times 10^6 - 15 \times 10^6$ dyn). The values of standard deviation were therefore averaged for the six loads; the results for all combinations are shown in Table 3.

Table 3. *Standard deviations for all combinations*

Combination	*First 4 readings*	*First 10 readings*	*30 readings*	*Average*
Brass–ethyl cellulose	0·99	0·90	0·90	0·93
Brass–cellulose nitrate	1·37	1·28	1·31	1·32
Polystyrene–ebonite	1·24	1·37	1·55	1·39
Casein–cellulose acetate	2·37	2·53	2·53	2·48

It appears that in general the accuracy of the results is not increased by any significant amount by taking thirty voltage readings instead of the usual four. Table 3 also shows that the spread of experimental results is less for metal-dielectric than for dielectric-dielectric combinations. This is in agreement with the experimental accuracies given previously and is ascribed to the fact that contact areas can be determined more accurately for a metal-dielectric interface. The theoretical calculations of contact area were made assuming the area to be a plane circle. This is not strictly true, as, due to the deformation of both surfaces, the contact area is actually a section of the surface of a sphere (i.e. a spherical cap). For metal-dielectric contacts, however, when the elastic modulus of the metal disk is of the order of fifty times that of the dielectric sphere, the deformation takes place almost entirely in the sphere and the contact area approaches very closely to a plane circle.

DISCUSSION

When two dielectric surfaces or one dielectric surface and one metal surface are compressed together, a finite amount of electric charge is transferred across the interface. Richards[5] and Knowles,[7] investigated electrification produced by the impact of a dielectric sphere upon a metal disk and found that the metal always assumed a positive charge. This, however, is not true for electrification by compression as brass, copper, aluminium, iron, bismuth and zinc all occupy one position, mid-way down the electrostatic series. The positions of all materials in this series were found to be very consistent but the results give no support whatsoever to Coehn's law. They are, however, similar to those obtained by Richards[9] and Henry[12] who both found certain metals to occupy positions between various insulating materials in an electrostatic series.

The quantitative results of the experiments described above support the findings of Hess, Richards and Knowles in as much as a constant charge density was recorded after contact between two given materials. It is suggested, therefore, that the amount of charge transfer per unit area of contact is dependent upon some intrinsic property of the materials involved. There is a noticeable analogy between this charging and the formation of an electric double layer of charge at the interface between two metals, as postulated by the Volta–Helmholtz hypothesis,[13] although electron transfer either into or out of an insulator is not predicted by classical electrostatics.

However, according to Skinner,[14] at a metal-insulator contact electrons can transfer directly from the Fermi level of the metal to the conduction band of the insulator. The potential barrier is equal to $\phi - \chi$, where ϕ = work function of the metal and χ = depth of conduction band in the insulator. Mott and Gurney[15] give examples of inorganic crystals for which this energy gap is so small that considerable charge transfer can occur. Skinner suggests that such a charge transfer reaches a dynamic equilibrium and results in a spatial distribution of charge (or volume charge) inside the insulator. Experimental evidence of the existence of a volume charge distribution in an insulator is furnished by Skinner, Gaynor and Sohl[16] who observed the transient potential of a plastic adhesive immediately after separation from a metal surface. However, if the mechanism suggested by Skinner produces the charge transfer recorded in the above experiments then it is very surprising that:

(i) the charge transfer across a metal-dielectric interface is independent of the nature of the metal, be it copper or aluminium whose contact potentials with respect to platinum differ as much as 1 V; and

(ii) the charge densities between various materials in the electrostatic series are not additive, i.e. $\sigma_{AB} \neq \sigma_{AC} + \sigma_{CB}$ where σ_{AB} is the charge density produced by compression between surfaces A and B, as measured on A.

Tamm,[17] on the other hand, postulated the existence of surface electron levels on insulators which might be instru-

mental in the charging of insulators by contact with another insulator or with a metal. According to Shockley,[18] such surface levels can theoretically exist on the surface of a crystal lattice with energies in the forbidden region, i.e. between the filled band and conduction band. Their number is equal to the number of surface atoms (about 10^{15} per cm^2) and in a neutral crystal they are half-filled with electrons. Bardeen[19] has shown how a relatively high density of surface states (10^{12} per cm^2) can give rise to a double layer of electric charge on a free surface of a semi-conductor. In an insulator very few electrons are mobile but it is possible, however, that even at low temperatures sufficient surface states may be filled to give charge densities of the order of those measured above. It can therefore happen that the amount of charge transferred across a metal-insulator contact will be independent of the nature of the metal. This mechanism also explains why charge densities between various materials in the electrostatic series are not additive. However, if the charging observed above is due to the presence of Tamm levels on the insulator surface then one would expect the magnitude and probably the polarity to be greatly influenced by the condition of the surfaces in question and by the method of cleaning employed. This is not so and it appears, therefore, that this charging of insulators does not originate from a difference of contact potential.

Harper[20] found that certain insulators, e.g. polystyrene, Perspex, polyethylene and Teflon, give no electrification after light contact with metals although he recorded charges of the order of 10^{-3} e.s.u. with glass, magnesium oxide and silica. In contrast, charges as high as 1 e.s.u. were not uncommon in the experiments now described. These results and those of Harper are not incompatible particularly as contact areas of approximately 10^{-2} cm^2 were used above, compared with the point contact with spheres in Harper's experiments; the significant point, however, is that Harper did not detect any electrification with insulators such as polystyrene and Teflon. Both of these materials were readily charged by compression. This fact suggests that the charging recorded in the above experiments may be due to the compression and subsequent elastic deformation of the two surfaces in question and not to a difference between their contact potentials. The significance of mechanical stress upon the surfaces involved is emphasized by Jamieson[21] who correlated the charge produced between two celluloid sheets with the strains at their surfaces. Nevertheless, this hypothesis is rather speculative and awaits further investigation.

Knowles[7] investigated electrification by impact and found a linear relationship between charge density and dielectric constant, similar to that of Fig. 6. In an attempt to explain this he suggests that if the charging across a metal-dielectric interface is limited by back-discharge, as claimed by Medley,[22] then all surfaces will separate, in air, with the same potential difference. Knowles postulates that the charge producing such a potential on a dielectric surface may be dependent upon the resultant polarization within the dielectric, and that the amount of polarization is proportional to the dielectric constant of the material. Thus, it would be expected that the charge itself would be proportional to the dielectric constant.

Extending this theory to the separation of two dielectric surfaces, it is seen that the surface having the lower dielectric constant will control the amount of separation charge, as this surface assumes the limiting value of potential for a smaller charge transfer. On this basis, all additional charging will be limited by back-discharge and the final charge density will therefore be proportional to the lower dielectric constant of each combination. If this is indeed the case then it explains why the charge densities between various combinations are not additive and also why the charge densities for metal-dielectric compressions are independent of the nature of the metal.

The amount of electrification across a metal-dielectric interface appears to be uninfluenced by the resistivity of the dielectric material provided it is above the critical value of 5×10^{11} Ω cm. This result agrees very well with the findings of Medley.[23] During separation of the two surfaces, if the resistivities of both surfaces is less than the critical value then the charges have time to flow along the surfaces and neutralize each other at the last point of contact.

Perspex, however, is a noticeable exception to this rule; it has a resistivity of 9×10^{14} Ω cm yet it exhibits very little charging. As yet, no explanation of its behaviour can be given.

REFERENCES

(1) Shaw, P. E. *Proc. Roy. Soc.*, **94**, p. 16 (1918).

(2) Shaw, P. E., and Jex, C. S. *Proc. Roy. Soc.*, **111**, p. 339 (1926); **118**, pp. 97, 108 (1928).

(3) Shaw, P. E., and Leavey, E. W. L. *Proc. Roy. Soc.*, **138**, p. 502 (1932).

(4) Loeb, L. B. *Science*, **102**, p. 573 (1945).

(5) Richards, H. F. *Phys. Rev.*, **16**, p. 290 (1920).

(6) Hess, E. *Zeit. f. Phys.*, **78**, p. 430 (1932).

(7) Knowles, B. G. *Ph.D. Thesis* (University of Birmingham, 1952).

(8) Coehn, A. *Weid. Ann.*, **64**, p. 217 (1898); *Ann. der Phys.*, **30**, p. 777 (1909); *Ann. der Phys.*, **43**, p. 1048 (1914).

(9) Richards, H. F. *Phys. Rev.*, **22**, p. 122 (1923).

(10) Rose, G. S. *Ph.D. Thesis* (University of Birmingham, 1954).

(11) Hertz, H. *J. reine angew, Math.*, **92**, p. 156 (1882).

(12) Henry, P. S. H. *Brit. J. Appl. Phys. Suppl.* 2, **4**, p. S 31 (1953).

(13) Helmholtz, H. *Wissenschaftliche Abhandlungen, Erster Band*, p. 860. (Leipzig: Barth, 1882.)

(14) Skinner, S. M. *J. Appl. Phys.*, **26**, p. 498 (1955).

(15) Mott, N. F., and Gurney, R. W. *Electronic Processes in Ionic Crystals*, p. 168 (Oxford: Clarendon Press, 1940).

(16) Skinner, S. M., Gaynor, J., and Sohl, G. W. *Modern Plastics*, p. 127 (Feb. 1956).

(17) Tamm, I. *Phys. Z. Sowjet.*, **1**, p. 733 (1932).

(18) Shockley, W. *Phys. Rev.*, **56**, p. 317 (1939).

(19) Bardeen, J. *Phys. Rev.*, **71**, p. 177 (1947).

(20) Harper, W. R. *Proc. Roy. Soc.*, **218**, p. 111 (1953).

(21) Jamieson, W. *Nature* [*London*], **83**, p. 189 (1910).

(22) Medley, J. A. *Nature* [*London*], **166**, p. 524 (1950).

(23) Medley, J. A. *Brit. J. Appl. Phys. Suppl.* 2, **4**, p. S 23 (1953).

Properties of two-aperture electron lenses

By G. D. Archard, A.Inst.P., Associated Electrical Industries Ltd., Aldermaston, Berks.

[*Paper received* 6 *September*, 1956]

Spherical and chromatic aberrations and focal properties of two-aperture ("immersion") electron lenses are investigated theoretically, and the results are presented graphically as functions of lens geometry and voltage ratio.

The properties of three-aperture electron lenses have been thoroughly studied, notably in theoretical work of Regenstreif,[1] but consideration of two-aperture ("immersion") lenses seems rather more scattered. These lenses consist of two thin plane electrodes containing circular apertures and bearing different potentials, so that an electron traversing both suffers a net change in axial velocity. An approximate analytical calculation of the focal properties of a particular case is given by Zworykin and others (Ref. 2, p. 447), but agreement with numerical ray-tracing is poor. Cosslett (Ref. 3, p. 61) gives another approximation, based on a combination of the weak lens formulae of two single aperture lenses. This agrees in order of magnitude with experimental work of Polotovski (quoted without reference by Cosslett). Glaser and Robl[4] give an analytic solution for a potential distribution of the same general form as that produced by two apertures; the form of the results is complicated and does not allow a clear representation of the spacing between electrodes; it is more appropriate to two-cylinder lenses where the gap is nearly zero.

The technique of Regenstreif[1] seems to be best for the general treatment of the two-aperture lens, and the results are given in the following sections.

METHOD OF CALCULATION

The axial potential distribution of an isolated thin plane electrode containing a circular aperture has the form:

$$\Phi(z) = a + bz + z\tan^{-1}(z/R) \qquad (1)$$

where R is the radius of the aperture (Zworykin and others[2]). Regenstreif based his (experimentally justified) theory of the three-aperture lens on the assumption that three such distributions, corresponding to the three electrodes, could be superimposed, and the result approximated by arcs selected from three parabolas. In the present case, it will be assumed that two such distributions, corresponding to the two electrodes of the immersion lens shown in Fig. 1, may be superimposed and replaced by two parabolas, so arranged as to give the correct potentials at the most vital (i.e. most refracting) points, the centres of the apertures. [As a check Zworykin's formulae (Ref. 2, p. 385) show that the contribution of one aperture to the potential at the centre of the other varies from the value which would obtain if the diameter of the former were zero by 1% for $S/D = 1$ and 4% for $S/D = \frac{1}{2}$.]

The parabolas are:

$$\Phi(z) = \Phi(\pm S/2) + n_{\pm}(z \mp S/2)^2, (z \gtrless 0) \qquad (2)$$

where
$$n_- = -n_+ = \frac{V_2 - V_1}{\pi(S/2)^2}\tan^{-1}\left(\frac{2S}{D}\right) \qquad (3)$$

and
$$\Phi\left(\pm\frac{S}{2}\right) = \frac{V_1 + V_2}{2} \pm \frac{V_2 - V_1}{\pi}\tan^{-1}\left(\frac{2S}{D}\right) \qquad (4)$$

the voltages V_1, V_2 and dimensions S, D, being as shown in Fig. 1. The arcs in question occupy the ranges $0 < z < S/2$, $-S/2 < z < 0$ respectively.

When these expressions are put into the general ray equation, an exact solution results. In the two ranges this has the form:

$$r = A\cos\left\{\frac{1}{\sqrt{2}}\sinh^{-1}[\gamma_-(z + z_0)] - \xi_-\right\}(z < 0) \qquad (5)$$

$$r = B\frac{\cosh}{\sinh}\left\{\frac{1}{\sqrt{2}}\sin^{-1}[\gamma_+(z + z_0)] - \xi_+\right\}(z > 0) \qquad (6)$$

wherein:

$$\left.\begin{aligned}\gamma_-^2 &= 2\alpha^2/(2 - \alpha^2A^2)\\ \gamma_+^2 &= 2\beta^2/(2 \pm \beta^2B^2)\\ \alpha^2 &= n_-/\Phi(-S/2)\\ \beta^2 &= n_+/\Phi(S/2)\end{aligned}\right\} \qquad (7)$$

In these equations the height r_0 of an electron, supposed incident parallel to the axis from the direction of negative z, implicitly occurs squared in the γ's (A and B being proportional to r_0). If attention is confined to paraxial conditions,

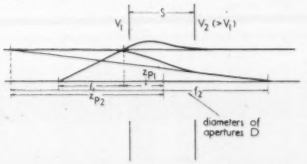

Fig. 1. Schematic representation of two-aperture electron lens

terms in r_0^2 may be neglected. In the present case, it is desired to include third order spherical aberration, and accordingly expressions such as $(2 - \alpha^2A^2)^{-\frac{1}{2}}$ are expanded by the binomial theorem, terms in A^4 and higher powers being omitted. The right-hand sides of equations (5) and (6) are thus split up into first and third order terms, giving respectively focal properties and spherical aberration. The value of r at the paraxial focus, divided by r_0^3, gives C_s/f^3. The paraxial calculations are quite standard and closely resemble those of Regenstreif; the third order calculations are elementary but tedious; only the final expressions will be given in the succeeding sections.

Chromatic aberration is directly given by

$$C_c = \frac{3}{8}f^2\frac{V_1 + V_2}{2}\int(\Phi'^2/\Phi^3)dz \qquad (8)$$

(c.f. Glaser Ref. 5, p. 257). This relates C_c to variations in the mean accelerating potential $(V_1 + V_2)/2$.

All the lens properties may be expressed in terms of the basic parameter:

$$y = \frac{(V_2/V_1 - 1)\tan^{-1}(2S/D)}{(\pi/2)(V_2/V_1 + 1)} \tag{9}$$

This represents the ratio:

p.d. between lens centre and centre of either aperture
÷ mean potential

It is in some ways analogous to Regenstreif's parameter x, save that small x corresponded to strong lenses, where small y corresponds to weak lenses.

FOCAL LENGTHS

The focal length corresponding to a ray entering the lens parallel to the axis from the high voltage side (f_1) will be termed the first focal length, and that corresponding to a ray entering the lens parallel to the axis from the low voltage side (f_2) will be termed the second focal length (Fig. 1).

The expressions for f_1 and f_2 are:

$$P(f_1/S) = -Q(f_2/S) = (1/\sqrt{2})(\sinh\beta_0\cos\alpha_0 - \cosh\beta_0\sin\alpha_0)^{-1} \tag{10}$$

where

$$\left.\begin{aligned}\alpha_0 &= (1/\sqrt{2})\sinh^{-1}P\\ \beta_0 &= (1/\sqrt{2})\sin^{-1}Q\\ P &= \sqrt{[y/(1-y)]}\\ Q &= \sqrt{[y/(1+y)]}\end{aligned}\right\} \tag{11}$$

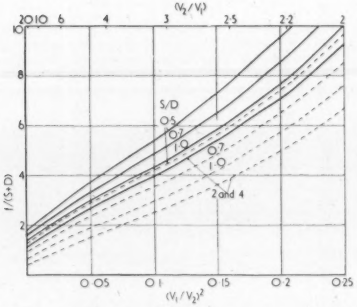

Fig. 2. Relative focal lengths of two-aperture lens
——— $f_2(S + D)$ (high voltage side).
– – – – – $f_1(S + D)$ (low voltage side).

A weak lens approximation, 10% accurate in the range $0 \leqslant y \leqslant 0{\cdot}5$ (this means, for $S/D = 4$ $V_2/V_1 \leqslant 4$; for $S/D = 2$ $V_2/V_1 \leqslant 5$; for $S/D = 1$ $V_2/V_1 \leqslant 8$; for $S/D = 0{\cdot}5$ $V_2/V_1 \leqslant 30$) is:

$$\frac{f_2}{S} = -\left(\frac{P}{Q}\right)\left(\frac{f_1}{S}\right) = \frac{(4/3)(y^2-1)}{y^2} \tag{12}$$

The focal lengths are plotted as functions of $(V_1/V_2)^2$ for various values of S/D in Fig. 2.

The expression for f_2/S agrees within 15% with the results of numerical ray-tracing given by Zworykin and others (Ref. 2, p. 449) for a particular case. This agreement is very much better than that of the Gans approximation which they quote.

PRINCIPAL FOCI AND PRINCIPAL PLANES

The position of the second principal focus is given by:

$$\frac{z_{F_2}}{S} = \frac{1}{2} + (1/\sqrt{2}\cdot Q)\frac{\coth}{\tanh}\xi_0 \tag{13}$$

where

$$\xi_0 = \frac{\tanh^{-1}}{\coth^{-1}}(\tan\alpha_0) - \beta_0 \tag{14}$$

the upper symbols being taken when $\alpha_0 < \pi/4$ and the lower when $\alpha > \pi/4$. The position of the corresponding principal plane (z_{P_2}) is found by subtracting f_2 from z_{F_2}.

The position of the first principal focus is given by:

$$-z_{F_1}/S = \tfrac{1}{2} + (1/\sqrt{2}\,.\,P)\cot\bar{\xi}_0 \tag{15}$$

where

$$\bar{\xi}_0 = \alpha_0 - \tan^{-1}(\tanh\beta_0) \tag{16}$$

The position of the corresponding principal plane (z_{P_1}) is found by subtracting f_1 from z_{F_1}, with due care regarding signs (see Fig. 1).

The values of $z_{P_1}/(S + D)$ and $z_{P_2}/(S + D)$ are plotted as functions of $(V_1/V_2)^2$ for various values of S/D, in Fig. 3. For the particular case given by Zworykin and others (Ref. 2, p. 449) the values of z_{F_2}/S deduced from equation (13) agree almost exactly with the results of numerical ray-tracing.

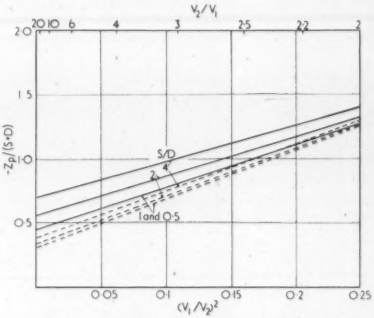

Fig. 3. Relative positions of principal planes of two-aperture lens
——— $-z_{P_2}/(S + D)$ (focus on high voltage side).
– – – – – $-z_{P_2}/(S + D)$ (focus on low voltage side).

SPHERICAL ABERRATION

The spherical aberration constant C_s of electron lenses is normally "referred to the object plane," so that the radius of the disk of confusion formed at the object by rays approaching the lens parallel to the axis from the image side is $C_s\theta^3$, where θ is the angular semi-aperture of the beam in object-space. This is unambiguous in the case of sym-

metrical lenses, but in the case of immersion lenses it is appropriate to speak of C_{s2} and C_{s1}, depending upon whether the object is on the high or low voltage side respectively. For weak lenses, or for a single discontinuous refraction such as obtains in glass optics, the following relation holds:

$$C_{s1}/f_1 = C_{s2}/f_2 \tag{17}$$

but deviations arise in the case of strong electron lenses. For C_{s2}

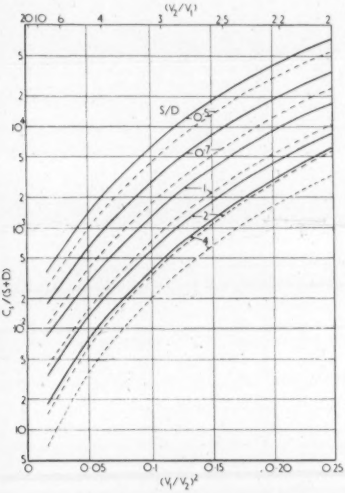

Fig. 4. Ratio of spherical aberration constant to parameter $(S + D)$ of two-aperture lens

——— $C_{s2}/(S + D)$ (object on high voltage side).
– – – – – $C_{s1}/(S + D)$ (object on low voltage side).

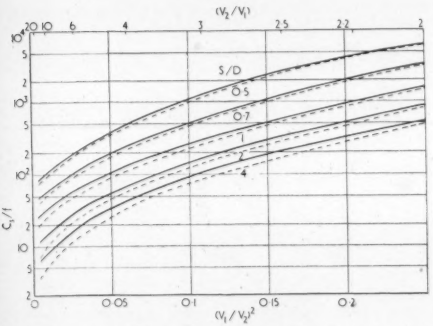

Fig. 5. Ratio of spherical aberration constant to focal length of two-aperture lens

——— C_{s2}/f_2 (object on high voltage side).
– – – – – C_{s1}/f_1 (object on low voltage side).

(a) if the paraxial ray cuts the axis outside the lens (i.e. where $z > S/2$):

$$\frac{C_{s2}}{S} = 4(f_2/S)^3 N\left(\tfrac{1}{4}Q^2N^2\frac{\cosh}{\sinh}\xi_0 - L\frac{\text{cosech}}{\text{sech}}\xi_0\right) \tag{18}$$

(b) if the paraxial ray cuts the axis inside the lens (i.e. between the electrodes):

$$C_{s2}/S = 4(f_2/S)^3 N[(1/4\sqrt{2})Q^2N^2\tan(\xi_0\sqrt{2}) - L] \tag{19}$$

where

$$\left.\begin{aligned} N^2 &= \pm\cos 2\alpha_0 \\ L &= (\tfrac{1}{4}J\sin 2\alpha_0 - K)\sec 2\alpha_0 \\ &\quad \pm Q^3N^2/4\sqrt{2}\sqrt{(1-Q^2)} \\ K &= P^3/4\sqrt{2}\sqrt{(1+P^2)} \\ J &= P^2\cos^2\alpha_0/(1+P^2) \end{aligned}\right\} \tag{20}$$

For C_{s1}, the rays involved in the calculation will not cut the axis inside the lens except for impracticably strong lenses, and the only useful expression is:

$$C_{s1}/S = 4(f_1/S)^3 M(\tfrac{1}{4}P^2M^2\cos\bar{\xi}_0 + G\,\text{cosec}\,\bar{\xi}_0) \tag{21}$$

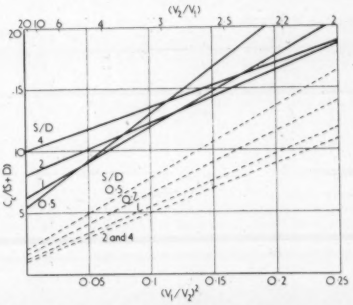

Fig. 6. Relative chromatic aberration constant of two-aperture lens

——— $C_{c2}/(S + D)$ (object on high voltage side).
– – – – – $C_{c1}/(S + D)$ (object on low voltage side).

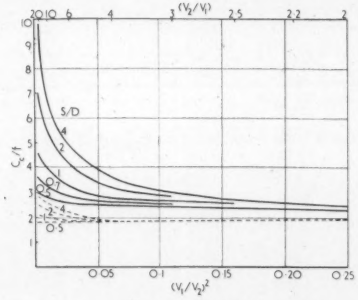

Fig. 7. Ratio of chromatic aberration constant to focal length of two-aperture lens

——— C_{c2}/f_2 (object on high voltage side).
– – – – – C_{c1}/f_1 (object on low voltage side).

where

$$\left.\begin{aligned} M^2 &= \cosh 2\beta_0 \\ G &= -(\tfrac{1}{4}H\sinh 2\beta_0 + F)\operatorname{sech} 2\beta_0 \\ &\quad + P^3M^2/4\sqrt{2}\sqrt{(1+P^2)} \\ F &= -Q^3/4\sqrt{2}\sqrt{(1-Q^2)} \\ H &= -Q^2\cosh^2\beta_0/(1-Q^2) \end{aligned}\right\} \quad (22)$$

Weak lens approximations, 30% accurate in the range $0 \leqslant y \leqslant 0{\cdot}5$, are:

$$C_{s2}/S = 4(f_2/S)^3 \quad (23)$$

$$C_{s1}/S = 6(f_1/S)^3 \quad (24)$$

The glass-optical formula:

$$C_{s1}/f_1 = C_{s2}/f_2 \quad (25)$$

holds to an accuracy of 20% in the range $0 \leqslant y \leqslant 0{\cdot}6$.

The spherical aberration constants are plotted as functions of $(V_1/V_2)^2$ for various values of S/D in Figs. 4 and 5, which give $C_s/(S+D)$ and C_s/f respectively.

CHROMATIC ABERRATION

When the potential distribution of equation (2) is put into equation (8), elementary integration gives:

$$\frac{-C_{c1}/S}{(f_1/S)^2} = \frac{C_{c2}/S}{(f_2/S)^2} = 3\left\{\frac{P}{1-y}\left[\frac{1}{8}\tan^{-1}P + \frac{1}{8}\frac{P}{1+P^2} - \frac{1}{4}\frac{P}{(1+P^2)^2}\right] - \frac{Q}{1+y}\left[\frac{1}{8}\tanh^{-1}Q + \frac{1}{8}\frac{Q}{1-Q^2} - \frac{1}{4}\frac{Q}{(1-Q^2)^2}\right]\right\} \quad (26)$$

A weak lens approximation, 30% accurate in the range $0 \leqslant y \leqslant 0{\cdot}5$, is:

$$C_{c1}/f_1 = C_{c2}/f_2 = 2 \quad (27)$$

The chromatic aberration constants are plotted as functions of $(V_1/V_2)^2$ for various values of S/D in Figs. 6 and 7 which give $C_c/(S+D)$ and C_c/f respectively.

ACKNOWLEDGEMENTS

The author wishes to thank Mr. M. E. Haine, the late Dr. G. Liebmann and Mr. T. Mulvey for helpful comment, and Dr. T. E. Allibone, Director of this Laboratory, for permission to publish this note.

REFERENCES

(1) REGENSTREIF, E. *Ann. Radioeléctricité*, **6**, pp. 51 and 114 (1951).

(2) ZWORYKIN, V. K., and others. *Electron Optics and the Electron Microscope* (New York: J. Wiley and Sons Inc., 1945).

(3) COSSLETT, V. E. *Introduction to Electron Optics* (Oxford: University Press, 1946).

(4) GLASER, W., and ROBL, H. *Z. Angew. Math. Phys.*, **2**, p. 444 (1951).

(5) GLASER, W. *Grundlagen der Elektronenoptik* (Vienna: Springer, 1952).

NOTES AND NEWS

Correspondence

A simple graphical method of calculating the density of current carriers in a semi-conductor from the Hall coefficient

The equations* usually used to obtain the density of current carriers in a semi-conductor from measurements of the Hall effect are

$$R = \frac{3\pi}{8e}\frac{(p - nb^2)}{(p + nb)^2} \quad (1)$$

and

$$np = n_i^2 \quad (2)$$

where R is the Hall coefficient in cm^3/C, e is the electronic charge in coulombs, p is the number of holes per cubic centimetre, n is the number of electrons per cubic centimetre, b is the ratio of electron to hole mobility and n_i is the intrinsic number of carriers per cubic centimetre. If equations (1) and (2) are combined, a quartic equation is obtained which is not easy to solve directly. The equation gives four sets of values of n and p of which two sets are negative and two positive. The following analysis leads to a graphical method of calculating the positive values from a single measurement of R if n_i and b are known.

From equation (1) writing $\alpha = 3\pi/8e$ and solving for p

$$p = \frac{\alpha}{2}\left\{\frac{1}{R} - \frac{2bn}{\alpha} \pm \left[\frac{1}{R^2} - \frac{4bn(1+b)}{R\alpha}\right]^{\frac{1}{2}}\right\} \quad (3)$$

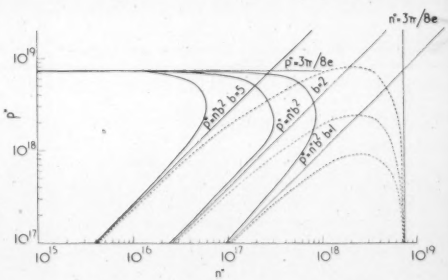

Relation between n^* and p^* given by equation (4) for $b = 5$, 2 and 1. Continuous curves are for positive values of R and dashed curves are for negative values of R

* SHOCKLEY, W. *Electrons and Holes in Semiconductors*, p. 217 (New York: D. Van Nostrand Co. Inc., 1950).

If we multiply this equation by R and write n^* and p^* for nR and pR respectively, we obtain

$$p^* = \frac{\alpha}{2}\left\{1 - \frac{2bn^*}{\alpha} \pm \left[1 - \frac{4bn^*(1+b)}{\alpha}\right]^{\frac{1}{2}}\right\} \quad (4)$$

Thus, for given b, p^* is a function of n^* only and a plot of equation (4) will give a curve which is valid for all values of R.

In the figure, p^* is plotted on a logarithmic scale against n^* using the relation in equation (4) and values of $b = 5$, 2 and 1. The continuous curves represent the values of n^* and p^* for positive values of R and the dashed curves represent the modulus of the values for negative R. The positive curves tend to the straight line $p^* = \alpha$ and the negative curves to the straight line $n^* = \alpha$. Each curve tends to the line $p^* = n^*b^2$ corresponding to its particular value of b.

Equation (2) may be rewritten

$$n^*p^* = n_i^2R^2 \quad (5)$$

This curve is a hyperbola which transforms to a straight line on the logarithmic scale used. It intersects in two points every curve given by equation (4). Each of these points corresponds to a pair of values of n^* and p^*. Using these values together with the measured value of the conductivity, the corresponding values of the mobilities may be calculated. Often one pair of values of n^* and p^* can be rejected as it leads to absurd values of the mobilities.

The curves have been found to be most useful when investigating a large number of specimens of the same material, since it is only necessary to make one determination of b and n_i for the material and then a single measurement of R (at the same temperature) on each specimen.

The authors wish to thank the Manager of Mullard Research Laboratories and the Directors of Mullards Ltd., for permission to publish this note.

Mullard Research Laboratories,
Salfords,
Nr. Redhill, Surrey.

T. S. Robinson†
M. Smollett
R. G. Pratt

(5 November, 1956)

† Now at Kungl. Tekniska Högskolan, Stockholm, Sweden.

New books

Cavitation in hydrodynamics. (London: H.M. Stationery Office, 1956.) Pp. 488. Price 30*s*.

In September 1955, the first International Symposium on Cavitation in Hydrodynamics was held at the National Physical Laboratory and attracted 140 delegates from fifteen countries. The volume under review, the Proceedings of this Symposium, contains the twenty-six papers presented and a record of the discussions.

The first paper, "A critical review of recent progress in cavitation research," was given by P. Eisenberg of the U.S. Office of Naval Research. The field covered is reflected by the subject headings of the subsequent sessions so that the paper was, in fact as well as in intention, a "keynote" address. Session 2 dealt with factors governing cavitation inception—the tensile strength of liquids, the existence of nuclei, turbulence and boundary layer effects. Session 3 considered experimental techniques. Instruments for measuring steady and transient forces, pressures and velocities were described and an account given of one water tunnel. A. T. Ellis of the California Institute of Technology described some high-speed photographic techniques; it is a pity, though inevitable, that the method of reproduction of this volume cannot do justice to some truly remarkable photographs he exhibited. In Session 4, on scale effect factors, results were given of tests on turbines and propellers and a theory of air entrainment at the rear of a steady cavity was developed and check experimental results given. Effects on hydrodynamic performance (Session 5) included hydrofoils, both in the surface and fully submerged, and supercavitating foils and struts. Session 6, on cavitation damage, considered erosion and other forms of damage in various types of cavitating flow. Finally, a session on ultrasonic cavitation, organized as an independent meeting, produced four short papers.

Pre-publication of the papers ensured that any deficiencies (and not all papers reached the same standard) were brought to light in the discussion. It also allowed any controversial points to be thoroughly thrashed out. For example, the proponents of mechanical, mechanochemical, electrochemical and other theories of damage all had their say and the case for and against resorbers in water tunnels was argued.

The N.P.L. is to be congratulated on assembling such a representative set of papers (from eight countries), giving the reader an accurate picture of the present state of the subject. The volume, as is the standard practice for N.P.L. Symposia, is reproduced from typescript, and is $10\frac{3}{4} \times 8\frac{1}{2}$ in. While not free from misprints it is easy to read and there is no doubt that this format is admirable for this type of publication.

J. L. King

Progress in nuclear energy: Series II. Reactors. Vol. 1. Edited by R. A. Charpie, D. J. Hughes, D. J. Littler and M. Trocheris. (London: Pergamon Press Ltd., 1956.) Pp. ix + 492. Price 100*s*.

The merit of this book is that it collects together in one volume the important information which has been published about the many reactors now in operation or being designed. The first half of the book deals with research reactors, while the second half discusses the most important types of power reactors. In addition, at the end of the book, besides an adequate index, there is a catalogue of nuclear reactors, which is very useful for quick reference to obtain the main features of a particular reactor, and to find out what the many combinations of initials now in use stand for. The discussion of research reactors is divided up into five chapters, one each on Canadian, United States, Soviet, and United Kingdom research reactors, and one chapter on research reactors in the rest of Europe. In a subject like this, where development has reached a different stage in different countries, it is impossible to give a uniform treatment, but in this volume there are sufficient details of the general constructional details of the different types of research reactors to enable the reader to obtain a good picture of the capabilities of each system. The treatment of the physics of the N.R.X. research reactor in Canada is particularly extensive, but in

the case of the other reactors the basic physics information on critical sizes and neutron fluxes is given in adequate detail. The experimental facilities available in these research reactors are discussed and it can be seen that while they differ in detail, the same general principles are repeated in each case.

There are three main types of research reactor, graphite-moderated, heavy-water moderated, and ordinary-water moderated, and there are examples of each type in this volume. The ordinary-water moderated system has the advantage of giving the highest fast neutron fluxes for a given heat output, but the graphite- and heavy-water moderated systems in general have more space available for experimental facilities.

In the second half of the book there are descriptions of six types of power reactors which are in various stages of development. One of them, the graphite-moderated, gas-cooled Calder Hall pile has now commenced operation, and considerably more information has recently been published about it. Another one, the pressurized water reactor, at Shippingport, is due to be in operation in 1957. The remaining types—a boiling water, an aqueous homogeneous, a sodium-cooled graphite-moderated, and a fast power reactor—are not as far advanced in development, but the reasons for considering them as possible nuclear power stations are discussed. The engineering problems of the pressurized water reactor and the sodium-cooled graphite-moderated reactor and the homogeneous aqueous power reactor are discussed in more detail than the other systems, and in the case of the first two, the problem of the fuel element design is given the importance it deserves. The homogeneous aqueous system, of course, does not have the same problems of fuel element design, but in its stead there are serious corrosion problems to be solved.

This book is a worthy companion to the other volumes in the series, and provides a very good summary of the position on research and power reactors as it was in 1956.

C. A. RENNIE

Gaseous nebulae. By L. H. ALLER. (London: Chapman and Hall Ltd., 1956.) Pp. xi + 322. Price 63*s*.

Advances in our knowledge of the gaseous nebulae have been so rapid in recent years as to render all existing textbook treatments out of date, and so extensive as to require a separate volume devoted to the subject. Astrophysicists will be greatly indebted to Professor Aller, himself one of the foremost workers in this field, for this comprehensive and authoritative survey. It is far more than a mere compilation of the established results, including as it does a critical review of much theoretical work and some hitherto unpublished results.

The physicist, even though his knowledge of astronomy may be elementary, will find much to interest him. On the experimental side, for example, there are descriptions of applications of the Fabry–Perot etalon and of narrow band-pass optical filters to the study of the structures and motions of gaseous nebulae: there are also accounts of ingenious modifications of spectrographs and spectrophotometers which might well find applications in laboratory investigations. The theoretician will appreciate the exceptionally full treatment of forbidden line radiation, and may well be stimulated to follow up some of the fascinating problems which are here presented, especially perhaps those relating to the origin and consequences of the magnetic fields which apparently pervade vast regions of space, and also those resulting from the application of the principles of hydrodynamics to the motions of interstellar matter, which when excited to luminosity by radiation from neighbouring stars, is observable as diffuse gaseous nebulae.

The production is excellent, there are many beautiful photographs and the bibliography is very full, containing some 500 references. In the next edition the spelling of "fiducial" ("fudicial" in Figs. II 14 and VII 17) will no doubt be corrected, unless indeed this is an Americanism with which the reviewer is unfamiliar.

W. E. CURTIS

Progress in cosmic ray physics. Vol. 3. Edited by J. G. WILSON. (Amsterdam: North-Holland Publishing Co., 1956.) Pp. xii + 420. Price 76*s*.

The third volume in the series *Progress in cosmic ray physics* will be of great value to workers in the field of cosmic rays and elementary particles. The new volume contains three long reviews and one shorter article, all of which are effectively dated "early 1955" although some later papers are included. The book has been well edited and is provided with extensive references and a useful index.

The first review, by Professor K. Greisen, is concerned with the properties of extensive air showers. It is the only up-to-date account of this subject which is now generally available. The treatment is lucid and free from unnecessary mathematical details. It covers all important aspects of the subject including the nuclear and meson components, time variations and the primary spectrum as well as the angular and lateral distributions of the electron component.

The second and third reviews deal with the properties of new unstable particles. In his preface the editor points out that these articles treat comprehensively the cosmic ray work in this field; they do not claim to deal exhaustively with artificially produced particles. This means that many of the exciting results obtained using the Berkeley and Brookhaven machines are not included. In the second article Dr. H. S. Bridge describes the properties of charged K-mesons and hyperons, while Professor R. W. Thompson gives a detailed account of the neutral particles in the third article. Both articles are excellent and will remain valuable for some years because they deal completely with the first phase of research on the strange particles, the phase in which cosmic rays were used as the source of high energy particles.

In the last chapter Professor G. Puppi discusses the fate of the cosmic ray flux of energy falling on the atmosphere at a latitude of 50° N. The μ-meson, the photoelectron and the nucleonic components are considered in detail and finally an approximate energy balance between the components is established.

It is a pleasure to note that the publishers have announced their intention of continuing the present series under an expanded title of *Progress in elementary particles and cosmic ray physics*. It is hoped to publish annually and with greater regularity than in the past. Professor S. A. Wouthuysen of Amsterdam University will join Professor Wilson as editor of the new series.

C. C. BUTLER

Information theory. Edited by C. CHERRY. (London: Butterworth's Scientific Publications, 1956.) Pp. xii + 401. Price 70*s*.

This could well be described as an account of the struggle to sharpen the definitions of concepts such as information, meaning and knowledge till they become amenable to precise and quantitative study, and then to analyse their modes of transmission and reception. The book embodies the papers presented at the third Symposium on Information Theory to be held in London within the last six years. Of the forty

papers read at the Symposium, thirty-six are reproduced here in slightly shortened form, together with a generous selection of contributions to the discussion. Short summaries of the remaining four papers are given. The papers are arranged in five sections of closely-related material under the general headings: Fundamentals; Coding, taxonomy, etc.; Language analysis and mechanical translation; Meaning and the human senses; Behaviour and its mechanism. As is to be expected from such a symposium we have here a cross-section of outstanding recent developments with emphasis on the work upon coding, upon neuro-physiological models, upon mechanical translation and upon the theory of hearing. There is, too, an interesting insight into the extent to which information theory has been assimilated by other scientific studies, such as linguistics, experimental psychology and physics.

The authors are drawn from many different schools and countries, and while this is one of the essential ingredients of a successful symposium it almost inevitably means that the standard of the published papers will be highly variable, not only on account of the work they report but of the clarity of writing, remembering, of course, the hazards of translation. Some authors have presented enough introductory background to render their papers intelligible. Others demand either specialist knowledge or wide reading before the significance of their papers is clear. Altogether, however, this is a praiseworthy attempt by the authors, editor and publishers combined to produce a wide and up-to-date view of a rapidly developing subject. That they have accomplished this so soon after the Symposium is a matter for congratulation. The absence of an index of any sort seems a curious omission from a book containing at least one paper on information retrieval, but, this apart, the book is well produced and, considering the specialist nature of much of the printing, the price is not unduly high. J. CRANK

Reports on progress in physics, Vol. 19. Edited by A. C. STICKLAND. (London: The Physical Society, 1956.) Pp. 367. Price 50*s*.

This volume contains several highly-developed mathematical discussions; one deals with uniform and non-uniform systems of monatomic liquids, another with irreversible thermodynamics, and a third with some phenomena called thermoacoustics, a subject known to many physicists only because of the "flame organ" or of Rayleigh's explanation of Rijke's singing pipes, but of importance today because of the power dissipated as noise from jet engines. There is an account of infra-red absorption in semi-conductors and another on neutron diffusion. The physicist lacking prior knowledge in any of these fields is unlikely to find these sections easy reading. One of the reports has a beautiful and exhaustive treatment, necessarily mathematical, of diffraction resulting from amplitude or phase modulation of a wave-front, takes account of incoherence and considers the application of correlation methods to the analysis of diffraction from sources of "white noise"; the results are applied to the ionosphere and to radio-astronomy. Another report describes radioactive methods of finding geological age, and an interesting table shows the comparison between estimates of the ages of minerals, the earth, meteorites and the universe. Another consists of a readable discussion of the dynamics of operation and phase stability of proton synchrotrons, already built and others under construction, with special reference to alternating gradient machines; finally, there is a simple and intelligible account of new lens systems developed for various purposes.

To read early volumes of the *Reports on progress in physics* was heartening and inspiring; even ten years ago a great breadth of information could be acquired quickly and comparatively easily; today the reader may be bewildered and repelled. Doubtless this is partly the inevitable result of the fantastic growth of every section of knowledge, but if the aim of the Reports is to enable physicists to survey the scene of scientific advance, contributors to future volumes should address themselves not to the specialist, but to the general student of physics. A. M. TAYLOR

Physical aspects of absorptiometric analysis. (London: The Iron and Steel Institute, 1956.) Pp. 37. Price 25*s*.

This report has been compiled by a Study Group appointed by the British Iron and Steel Research Association and deals with the factors affecting the performance of the Hilger photoelectric absorptiometer (Spekker). It should be appreciated that this instrument is used almost entirely by analytical chemists, most of whom must be unfamiliar with the properties of the components of such instruments. These are explained in sufficient detail supported by the necessary theory.

The Group, composed of experienced users, is to be congratulated on the thoroughness with which they have investigated every component without becoming unnecessarily involved in theory *per se*.

Their report will undoubtedly be of great help to the many users of this type of instrument. R. A. C. ISBELL

Science and information theory. By LEON BRILLOUIN. (New York: Academic Press Inc., 1956.) Pp. xvii + 320. Price $6.80.

Ever since Shannon published his original work on the mathematical theory of communication,[1] people have been talking and writing about "information theory." What started as an elegant and self-contained mathematical theory of codes has proved to be of interest, if not always of value, to all manner of scientists. Communication engineers were the first to be interested, and physicists the first to be disappointed. The quantity which turned out to be fundamental in communication theory, Shannon's H, was already well known in statistical thermodynamics as the expression for entropy; yet communication theory, being largely concerned with abstract problems of coding which do not arise in statistical thermodynamics, had little to add to that imposing subject. All it did was to reinforce the interpretation of entropy in physics as missing information about a system. (It is unfortunate for physicists that Shannon chose the symbol H and not S for entropy, since Boltzmann used H for a quantity which is effectively negative entropy.[2])

The aim of *Science and information theory* is to show that the connexion between information theory and thermodynamics is so close that "consistency requires a physical theory of information." The heart of the book is concerned with proving, by means of some very interesting examples, that when the entropy of a physical system is reduced, or *in other words* more information is obtained about it, the entropy of something else in the laboratory must increase by at least an equal amount. Once the interpretation of entropy as missing information is accepted, the law itself is surely acceptable without further ado. Chapter 12, where the law is first propounded, is the most obscure in the book. The reviewer has seldom encountered a more confused scientific exposition. Fortunately it is possible, after studying the examples in later chapters, to see what was meant, but one

hopes that the chapter will be re-written in future editions. Lack of clarity is to be found elsewhere, too. Although one again sees what the author means, is it really fair to say that hot radiation put into a cold gas pours *negative* entropy into the gas, when in fact the usual result is a rise in the temperature of the gas and a corresponding *increase* in its entropy? And it is certainly quite wrong (Chapter 12 again) to say that Shannon "defined entropy with a sign just opposite to that of the standard thermodynamical definition," in spite of his unfortunate choice of a symbol. This may be conclusively verified by comparing Section 6 of Shannon (*loc. cit*) with, say, the chapter by Slater.[3] An irreversible filter, contrary to what is stated in the book, does indeed reduce the entropy of signals—completely to zero if the filter is opaque, for the number of complexions of a zero output is exactly one. The point which has been missed is that communication theory, unlike thermodynamics, is not concerned with the heat dissipated by the filter.

In spite of the adverse criticisms which sincerity demands, the book as a whole is attractive. Its twenty chapters cover, in short sections, a variety of subjects from Maxwell's Demon to computing, from the well-informed heat engine to "Dead information, and how to bring it back to life."

P. M. WOODWARD

(1) SHANNON, C. E., and WEAVER, W. *The Mathematical Theory of Communication* (Urbana: Illinois University Press, 1949).
(2) TOLMAN, R. C. *The Principles of Statistical Mechanics*, Chapter 13 (London: Oxford University Press, 1938.)
(3) SLATER, J. C. *Introduction to Chemical Physics*, Chapter 3. (New York: McGraw-Hill Book Co. Inc., 1939.)

Automatic digital calculators. 2nd Ed. By A. D. BOOTH and K. H. V. BOOTH. (London: Butterworth's Scientific Publications, 1956.) Pp. ix + 261. Price 32*s*.

This book is intended to introduce new workers to the design, construction and use of automatic digital computing machines. The first three chapters provide a historical summary of the development of these machines, whilst the next nine chapters are devoted to their design and construction. The field is covered thoroughly and the book serves to give a good overall picture. Certain of the topics, however, are treated rather briefly, and whilst the second edition has been extended to include a description of new devices such as magnetic cores and transistors, the treatment of the latter, in particular, is scanty.

The last five chapters deal with user aspects. These include the choice of the basic instructions from which are built up the "routines" (sequences of instructions) for carrying out more complex requirements such as interpolation and the calculation of square roots. The assembly of "routines" to form a complete "programme" is briefly mentioned. A final chapter deals with applications. In order to exhibit the scope of digital calculators only one problem of a directly mathematical nature is described, but this is supplemented by an account of various non-numerical applications. The most interesting of these is the use of the machine to translate from some foreign language into English, or *vice versa*. Here we were surprised to find that nothing had been added to the original account, although Dr. A. D. Booth has himself made considerable contributions in this field.

Two new topics have been included in the second edition, namely, the generation of pseudo random numbers and techniques designed to simplify the preparation of programmes for machines.

Finally it should be added that the classified bibliography has also been revised and brought up to date, and now contains over twice as many references as the original.

R. A. BROOKER
R. L. GRIMSDALE

Encyclopaedia of physics. Vol. 33. Kopuskularoptik. Edited by S. FLUGGE. (Berlin: Springer-Verlag, 1956.) Pp. vi + 702. Price £10 8*s*. 6*d*.

This volume, as the title suggests, deals with electron and ion optics. It comprises five comprehensive review papers: "Electron and ion sources," by Detlef Kamke; "Electron optics," by W. Glaser; "The electron microscope," by Siegfried Leisegang; "Mass spectroscopic apparatus," by Heinz Ewald; and "Beta-ray spectroscopes," by Tor Ragnar Gerholm. The first four are in German and the last in English. The volume contains nearly 700 pages and 492 figures.

All five reviews are comprehensive, and have obviously been prepared with meticulous care. They are, on the other hand, almost entirely non-critical. They contain a mass of information very largely abstracted directly from the original papers.

D. Kamke gives a well-balanced account of electron and ion sources, and the means by which the particles are extracted and focused. A sufficiency of numerical data is included together with a good account of practical applications.

W. Glaser treats electron and ion optics both from the optical and wave-mechanical points of view. This includes a considerable amount of work based on the well-known "bell-shaped" field, both for electrostatic and magnetic lenses, together with an extensive and mathematically thorough account of third-order aberrations (all this is rather similar to Glaser's own book *Grundlagen der Elektronenoptik*). Other limiting features such as first-order astigmatism and chromatic aberration are also adequately described. Further sections deal with focusing in systems of four-fold symmetry (strong focusing), and with deflexion systems and their aberrations.

The section is highly mathematical. It is perhaps more a review of the mathematics of electron optics; the very important practical aspects of the subject are not considered, and much of the analysis is more rigorous than useful to the practising electron optician. A good deal of important modern work even on the analytic side of electron optics is not included in the discussion.

S. Leisegang's account of the electron microscope overlaps Glaser's contribution to a certain extent in its description of lenses and their aberrations, though his description of these is less mathematical and easier to follow. The practical design aspects and the factors affecting performance are dealt with in detail, and some of the variants of the electron microscope method discussed.

H. Ewald discusses mass spectrometer instrumentation widely and competently. The factors affecting performance are dealt with, and the various special types of instruments which have been developed in the last few years are described.

T. R. Gerholm gives a thorough treatment of β-ray spectrometers. The basic mathematics is briefly sketched, and considerable practical detail including some useful tables is given.

The volume comprises a comprehensive reference book containing a large mass of information, theoretical and practical. The diagrams and printing are of a high standard throughout.

M. E. HAINE

The structure of turbulent shear flow. By Dr. A. A. TOWNSEND. (London: Cambridge University Press, 1956. Pp. 315. Price 40*s*.

This is a book concerned with the anatomy of turbulent shear flows. The specialist will know, but it is perhaps only fair to warn the less initiated, that anatomy is the right word and that the time is not yet ripe for the living man or the overall working model to emerge. The time is, however, ripe for this detailed examination of the structure of a number of fundamental turbulent shear flows, and Dr. Townsend is to be congratulated on showing so clearly how many of the constituent parts function.

This book makes available in one connected account a vast amount of experimental information which the author has amassed, much of it first-hand information. The book is, however, far from being a mere compilation of these data, valuable as that would be, for the author has examined the data piece by piece in the light of theoretical developments, and research workers, both experimental and theoretical, are provided with new starting points. With these as the outcome one feels that there is much to be said for this reversal, if only for a time, of the author's normal role (to draw from his light-hearted introduction to the preface) in now providing targets for criticism rather than maintaining the flow of ammunition.

After an introduction comprising the fundamental ideas of the subject, the account proceeds through a chapter on the equations of shear flow to a discussion of isotropic turbulence and its distortion in a duct whose sectional area varies with the distance along it. This type of distortion is particularly important because of the existence of a theoretical solution when the rate of distortion is large enough. The main body of the book then unfolds in analyses of flow in jets, wakes, pipes, channels and between rotating cylinders and in boundary layers with and without pressure gradients. Each of the flows is subject to a searching examination and the importance, relevance and incidence of such ideas as self-preservation, Reynolds number similarity and the logarithmic velocity distribution are delineated.

The author should be congratulated on producing such a readable as well as valuable account of this rapidly growing subject.

L. HOWARTH

Proceedings of the Eleventh General Assembly of the International Scientific Radio Union. Vol. 10. Part 7 "On radioelectronics." (Union Radio-Scientifique Internationale, 42 Rue des Minimes, Brussels, Belgium.) Pp. 140. Price 21*s*. 6*d*.

This publication reports on the formal business meetings of Commission 7 of U.R.S.I., which took place at The Hague in September 1954. In addition there is useful general information embodied in summaries of the progress in radio-electronics made in the various member countries during the period preceding the meeting.

These summaries are, in some cases, very brief; but the reader may be interested to know that extensive lists of references to published work are also provided.

J. SAYERS

Einführung in die höhere Mathematik. Band I: Grundlagen. By K. STRUBECKER. (Munich: R. Oldenbourg Verlag, 1956.) Pp. xv + 819. Price DM 36.

This book is the first of three volumes. It is based on lectures given by the author to students of physics, chemistry, biology and technology, as well as mathematics, at the Technische Hochschule of Vienna and Karlsruhe and at the universities of Vienna and Strasbourg. A subtitle states that special consideration is given to applications to the sciences. The aims of the author are to provide a firm basis of pure mathematics, to give an adequate treatment of the numerical, graphical and instrumental procedures of mathematical practice and to discuss numerous illustrative examples of scientific applications. These three themes are interwoven throughout the book. To select some examples from the first chapter, on numbers and numerical calculation, one finds for instance, Peano's axioms, the completeness postulate for the real number system and even a mention of Gödel's theorem on the consistency of the axioms of pure mathematics. There is a description of hand and electrical desk calculating machines (with pictures) and a brief note on digital computers such as the ENIAC and EDSAC. As an application of continued fractions to a physical problem there is the calculation of the formula for the wave numbers of the lines of the Balmer series.

The book is a substantial work, containing in all, 197 numbered sections. These fall into four main divisions, with the titles: I Numbers and numerical calculation; II Elementary algebraic functions; III Limits. Infinite series; IV Elementary transcendental functons. Continuous functions. Inverse functions. The longest of these is part II, containing seven chapters entitled: Linear and quadratic functions, complex numbers; Geometrical applications; Plane vector calculus; Polynomials and algebraic equations; Interpolation; Rational and algebraic functions; Affine and projective geometry of the plane.

Some of the worked examples are very elementary, while others require more advanced ideas. They are all, however, explained with the same care and attention to detail. This volume should be of considerable interest to anyone who teaches mathematics to science students, if only because of the way in which it cuts across the traditional ideas of what is elementary and what is advanced. The idea of a group is introduced quite early, and later, in the chapter on the exponential, circular and hyperbolic functions, there is a section on the group of Lorentz transformations. After reading about uniform convergence one comes later to a chapter on the theory and use of the slide rule. The general treatment reminds one of Klein's well-known book *Elementary mathematics from an advanced standpoint*. Two pleasing features deserve special mention—the excellent quality of the diagrams and the interest and relevance of the historical notes which form part of the exposition.

M. R. HOPKINS

Molecular flow of gases. By G. N. PATTERSON. (London: Chapman and Hall Ltd., 1956.) Pp. x + 217. Price 60*s*.

For many purposes the flow of a gas may be regarded as the flow of a continuous medium. But there are at least two very important phenomena for which this approximation is invalid. They concern shock waves and slip flow in a rarefied gas. In a shock wave the pressure and temperature change so fast that relaxation times for the absorption and emission of energy are important: in a rarefied gas molecular collisions are infrequent.

It is the purpose of this book to introduce the reader to the molecular view-point which is necessary in these modern aerodynamic problems. Its concern is with the distribution function for molecular velocities, its rate of change in collisions

and the application of this to shock waves and boundary layer flow and flow round corners and edges. Much of the book concerns frictionless compressible (isentropic) flow, but slightly non-isentropic flow is also considered. The treatment is extremely clear, even though the complete absence (till p. 92) of any vector formulation makes the sets of equations look sometimes more terrifying than they actually are. The relation of theory and experiment is excellently discussed, and the mathematics is everywhere kept as simple as possible. Unlike any other book of this kind that I know, it can be read by a final honours year student in mathematics or physics without help from other people. Only occasionally, as when on p. 2 the author speaks as if no long-range attractive force exists between atoms, is there anything to which scientific exception could be taken.

Yet somehow the subject is still only half-way to its true stature. The very use of a distribution function is a denial of the uncertainty principle, and our almost complete ignorance of the details of all real molecular collisions points to a further progress into molecular physics which is needed before we can fully discuss the flow of gases. This is an essentially quantum problem, and no one has any right to blame Professor Patterson that he says so little about it here.

C. A. COULSON

Glass. By G. O. JONES. (London: Methuen and Co. Ltd., 1956.) Pp. 119. Price 8*s*. 6*d*.

This is an excellent little book, but it is not, as suggested by the announcement on the dust-cover, a "most useful starting point for anyone who wishes to use or study glass." No more justified is the author's own claim—"while the book is in no sense a handbook of glass technology, a judicious use of the index will help the reader to find answers to many practical questions about the manufacture and uses of glass."

The book can stand on its own merits as a very clear and concise summary of the physics of glasses. After the glassy state has been defined there is a statement of the available information on the structure of glasses as deduced from X-ray diffraction patterns. The crystallization and stability of glasses are next discussed, then follows a chapter called "The transformation temperature" but, as is pointed out in the first paragraph, this chapter should be called the "Transformation range." This chapter and the next, on the behaviour of glass under stress, deal with fields to which the author has made major contributions; it is all very good; the last chapter is a little scrappy in comparison with the others.

This book is a valuable contribution of the very high standard which one would expect from the author.

R. W. DOUGLAS

Beitrage zur Theorie des Ferromagnetismus und der Magnetiserungsburne. By W. KÖSTER. (Berlin: Springer-Verlag, 1956.) Pp. ix + 189. Price DM 24.

This collection, reminiscent of the *Probleme der technischen Magnetisierungskurve* edited by R. Becker about twenty years ago, continues that policy of assembling critical summaries and developments of hitherto unpublished or little known papers in that same field of physics. In all, six authors contribute and the principal work deals with the independence of the magnetic saturation intensities in the transition metals and their crystal structure. After a consideration of the shortcomings of the existing theories of the electronic structure of the ferromagnetics, a new semi-empirical view due to Bader is discussed by the author, together with an account of an attempt by Ganzhorn to provide a satisfactory energy band picture that covers the whole of the relevant experimental data. The second section deals with investigations, largely due to Kneller, on various magnetic properties of nickel relating to the magnetization curve, which cover a range of temperature from that of liquid air to the Curie temperature. The author attaches importance to the use of the same specimens throughout these determinations. Among the later short chapters is one dealing with the investigation of internal strain by magnetic and X-ray methods. Prof. Köster's collection will be of interest to all those whose work lies in theoretical and experimental ferromagnetism.

W. SUCKSMITH

Journal of Scientific Instruments

Contents of the March issue

SPECIAL ARTICLE

A survey of image storage tubes. By H. G. Lubszynski.

ORIGINAL CONTRIBUTIONS

Accessories for measuring circular dichroism and rotatory dispersion with a spectrophotometer. By S. Mitchell.
The calibration and use of an air-driven ultracentrifuge. By P. Johnson.
An improved micro-electrophoresis electrode assembly for use in micro-biological investigations. By D. E. E. Loveday and A. M. James.
Experimental investigations of the dead time of univibrators. By D. Kiss and I. Szivek.
An improved technique for the measurement of contact potential differences. By K. A. Macfadyen and T. A. Holbeche.
Improving the linearity of barrier-layer photocells. By D. G. Wyatt.
A soft valve scaler for intermittent fast counting. By G. W. Hutchinson.
An apparatus for investigating the low-pressure oxidation kinetics of hot metals. By L. G. Carpenter and W. N. Mair.
An extensometer microscope stage for photoelastic studies in rubber. By E. H. Andrews.
A system for controlled linear of laboratory furnaces. By T. W. Lomas and L. G. Finch.

Laboratory and workshop notes

Bakeable high vacuum seals. By N. W. Robinson.
A direct-vision crystal growth furnace. By D. F. Gibbs, H. F. Kay and M. A. Short.
An automatic vacuum isolation valve. By A. Franks.
A technique for hardening beryllium copper. By R. A. Cox.
Indium seals for dismountable vacuum systems. By H. A. Adams, S. Kaufman and B. S. Liley.
A sealing compound for glass-to-metal joints of optical instruments. By K. Hillman.

NOTES AND NEWS

Correspondence

Water failure guard for use with gas-heated pumps. From C. Steel, R. F. Smith and B. Sunners.
A method for comparing ultrasonic velocities in solids and liquids using a spectrometer. From E. Hayess; G. M. Sreekantath and A. O. Mathai.
A trigonometric analogous computer using linear elements. From M. S. M. Abou-Hussein.

Manufacturers' publications
Notes and comments

THIS JOURNAL is produced monthly by The Institute of Physics, in London. It deals with all branches of applied physics (including theory and technique).

All rights reserved. Responsibility for the statements contained herein attaches only to the writers.

EDITORIAL MATTER. Communications concerning editorial matter should be addressed to the Editor, The Institute of Physics, 47 Belgrave Square, London, S.W.1. (*Telephone:* Sloane 9806.) Prospective authors are invited to prepare their scripts in accordance with the *Notes on the preparation of contributions*. (Price 2*s*. 6*d*. including postage.)

REPRODUCTION. The Institute of Physics is a signatory to The Royal Society's Fair Copying Declaration. Details may be obtained upon application from The Royal Society, London, W.1.

ADVERTISEMENTS. Communications concerning advertisements should be addressed to the agents, Messrs. Walter Judd Ltd., 47 Gresham Street, London, E.C.2. (*Telephone:* Monarch 7644.)

CLAIMS FOR MISSING JOURNALS. Claims from regular subscribers to this *Journal* for missing numbers will only be considered if received within 60 days of the date of mailing plus normal outward time of transit and time for lodging the claim. Losses attributable to failure to notify a change of address or to similar omissions will not be considered.

SUBSCRIPTION RATES. A new volume commences each January. The charge is £5 per volume ($14.25 U.S.A.), including index (post paid), payable in advance. Single parts, so far as available, may be purchased at 10*s*. each ($1.50 U.S.A.), post paid, cash with order. Orders should be sent to The Institute of Physics, 47 Belgrave Square, London, S.W.1, or to any bookseller.

SPECIAL ARTICLE

The analysis of finite-length records of fluctuating signals

By M. J. TUCKER, B.Sc., A.Inst.P., National Institute of Oceanography, Wormley, Surrey

The problem discussed is that of estimating the characteristics of a signal from a record of finite length by Fourier-type analysis or by direct measurement. The paper is an attempt to present the fundamentals of the problem in a coherent form and with the simplest possible mathematics: the results given are not new. The main discussion is of the accuracy of estimates of the power spectra and r.m.s. amplitudes of stationary random Gaussian processes: these have the characteristics of filtered random noise and include a class of signals of great practical importance. The arguments also apply to the problem of estimating the maximum speed with which a signal can be measured and analysed directly.

1. INTRODUCTION

The author has for some years been concerned with the analysis of recorded fluctuating signals. For both instrumental and more fundamental reasons the length of record that could be analysed has been limited, and it was important to know what limitations this placed on the accuracy of the results. The relevant information is mostly available in the literature, but it is scattered and often accompanied by mathematics which is rather frightening to the average practical physicist or electrical engineer. The present paper is an attempt to present the fundamentals of the problem in a coherent form and with the simplest possible mathematics. No previous knowledge of statistics is assumed. Correlation-type analysis will not be considered.

The discussion below applies to records which contain several cycles (in practice more than about five) of the lowest frequency present in the original signal. Only in special circumstances will the results apply when the record is shorter than this. Signals will be considered as fluctuating with time, but the theory applies equally well to fluctuations with displacement in space.

2. REPRESENTATION OF A FINITE RECORD BY DISCRETE FREQUENCY COMPONENTS

Consider a record extending in time from $t = 0$ to $t = T$ (Fig. 1). If this record is copied many times and the copies are joined end-to-end, the result will be a periodically repeating waveform with a fundamental frequency $F = 1/T$. This repeating waveform can be represented as the sum of a number of harmonic components each of which has an exact number of periods in the length of the record, so that the n^{th} harmonic has an instantaneous amplitude of $a_n \cos [(2\pi nt/T) + \theta_n]$. The record may thus be represented by

$$v = \sum_{n=0}^{\infty} a_n \cos [(2\pi nt/T) + \theta_n] \qquad (1)$$

This is, of course, the familiar Fourier-series representation. It represents the original signal in the interval 0 to T only and cannot be used to predict the values of v outside this interval: if such a prediction is attempted, all that is predicted is a repetition of the signal in the interval 0 to T.

The values of a_n and θ_n carry all the information contained in the original record, since from a knowledge of them the record can be reconstructed exactly.

From equation (1) the mean square amplitude $\overline{v^2}$ is given by

$$\overline{v^2} = \frac{1}{T}\int_0^T v^2 dt = \frac{1}{T}\int_0^T \left\{ \sum_{n=0}^{\infty} a_n \cos [(2\pi nt/T) + \theta_n] \right\}^2 dt$$

When the series inside the bracket is squared, square and cross product terms are produced. The cross-product terms may be resolved into sum- and difference-frequency components, each of which has an integral number of periods in the record and which therefore disappear when averaged over the length of the record. The square terms, however, contain "d.c." components which do not disappear, so that

$$\overline{v^2} = \sum_{n=0}^{\infty} a_n^2/2 \qquad (2)$$

which shows that the mean square amplitude of a record is the sum of the mean square amplitudes of its harmonic components.

$\overline{v^2}$ is a measure of the mean energy per unit time, that is, of the power of the record, and the reasoning can be extended to show that the power contained in a range of harmonics from the N^{th} to the M^{th} is $\sum_{n=N}^{M} a_n^2/2$. If the spectrum is split up into a number of such bands, the total power is the sum of the powers in each band. The amplitudes, because of differing phase angles, are not additive in this way, and it is therefore usual to work with the power spectrum (sometimes called the energy spectrum).

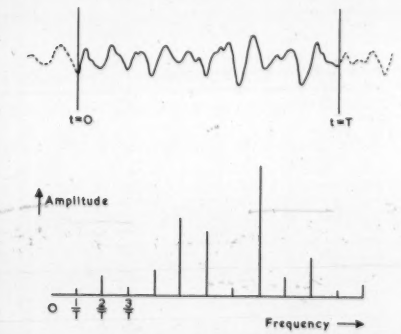

Fig. 1. A finite record and its frequency spectrum (diagrammatic)

3. SINUSOIDAL SIGNALS

If the original signal consisted of a pure sinusoidal wave of frequency f_s which is not a harmonic of the record length, what will happen when the record is analysed? The energy must split itself amongst the adjacent harmonics, and the way it does this is indicated in Fig. 2. A curve with the equation shown is drawn and the values of a at values of Δf corresponding to the harmonic frequencies are the amplitudes

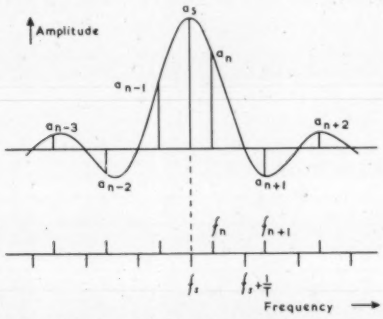

Fig. 2. How the energy from a sine wave of frequency f_s and amplitude a_s splits itself amongst the adjacent harmonics. The equation of the curve is

$$a = a_s (\sin \pi T \Delta f)/\pi T \Delta f$$

where $\Delta f = f - f_s$

of the harmonics. (This equation neglects a term which becomes smaller as the number of wavelengths in the record increases. For most purposes, only five waves are required before the errors become negligible.) The phases of the harmonic components are related to the phase of the sinusoidal signal, but phases are not usually important.

4. STATIONARY RANDOM GAUSSIAN PROCESSES

A typical stationary random Gaussian process is thermal noise which has passed through a filter with linear amplitude response but with any frequency characteristics. The process is stationary in the statistical sense, that is, there is no change with time in the probability that the signal will fall within a particular small range of values, or in the joint probability that it will fall within a given small range at one instant and in any other small range at any given interval after that instant. The signal is the sum of the effects of a large number of individual generators with random phases, and it can be shown that such a random superposition results in a probability distribution of the output which is "normal" or "Gaussian." This means that if a large number of instantaneous values of the signal are measured, the proportion which will fall in the range v to $v + \delta v$ is given by

$$[\delta v / V\sqrt{(2\pi)}] \exp -\tfrac{1}{2}(v/V)^2$$

where V is the r.m.s. amplitude of the signal.

It is convenient to use the "distribution function" $P(v)$ such that $P(v)dv$ is the probability that the output will fall between v and $v + dv$ as $dv \to 0$. In the present case it will be seen that

$$P(v) = [1/V\sqrt{(2\pi)}] \exp -\tfrac{1}{2}(v/V)^2$$

5. STATISTICAL FLUCTUATIONS IN THE AMPLITUDE OF A HARMONIC COMPONENT

In a random process the spectrum is continuous, that is, the signal considered over a long period may be regarded as consisting of a large number of components closely spaced in frequency and with random phases. If a short record is now taken, each of these components splits itself amongst the adjacent harmonics in the manner described in Section 3, so that each harmonic is the vector sum of a large number of contributions which are random in phase. Thus, the amplitude of a particular harmonic is to some extent random, and if many records of the same signal are analysed the amplitude of the harmonic will fluctuate from analysis to analysis (Fig. 3).

This problem has been considered by Lord Rayleigh.[1] Applying his result to the present case, the probability that the amplitude of the n^{th} harmonic will lie between a_n and $a_n + \delta a_n$ is

$$\delta a_n (2a_n/A_n^2) \exp -(a_n/A_n)^2 = P(a_n)\delta a_n \text{ by definition} \quad (3)$$

where A_n^2 is the average value of a_n^2 derived from many analyses of independent records of the same signal (called the ensemble average). This is sometimes known as the "random walk" or as the "target" distribution, and is the equivalent

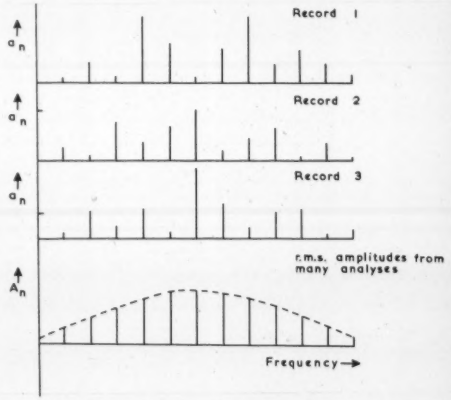

Fig. 3. The first three of a large number of analyses of independent records of the same length from the same signal, and their r.m.s. averages

of the normal distribution for a quantity which can vary in two dimensions: in the present case the two dimensions are the sine and cosine components which may be considered as being plotted on a vector diagram. The amplitudes of the harmonics are distributed independently of one another: that is, the probability that a particular harmonic will have a particular amplitude is not affected by the amplitudes of the nearby harmonics.

Consider Fig. 3, in which it has been assumed that a large number of independent records of the signal are available for analysis. The root mean square amplitude A_n of the n^{th} harmonic from all the analyses is truly characteristic of the original signal, and the amplitude spectrum of the signal may be defined as the envelope of these (the dotted line in Fig. 3). A rigorous definition would be more complicated than this,

but will not be discussed here since the amplitude spectrum is rarely used. For reasons discussed in Section 2, it is usual to work with the power spectrum and a similar diagram could be drawn plotting a_n^2 and A_n^2. If the spectral density changes slowly compared with the interval δf between harmonics, A_n^2 is the component of the power of the original signal contained in this interval, and if $E(f)$ is the power spectrum of the original signal

$$A_n^2 = E(f)\delta f = E(f)/T$$

In practice only one, or perhaps a small number of records is available, and the problem is to determine A_n^2, and hence $E(f)$, as accurately as possible from these.

Lord Rayleigh also showed that the phases θ_n of the components are random, and they therefore carry no information about the original signal. The relative phases between components in two related records can be of importance in some problems, but this will not be discussed here.

To avoid confusion, let $a_n^2 = s_n$, which will be termed the power of the n^{th} harmonic with an average over many analyses of $A_n^2 = S_n$ (strictly speaking this is not the power since it has not the correct dimensions, but it is proportional to it in a given system). Equation (3) gives the proportion of a large number of independent measurements of the amplitude of the n^{th} harmonic that will fall between a_n and $a_n + \delta a_n$. This is therefore the proportion that will fall between $s_n = a_n^2$ and $s_n + \delta s_n = (a_n + \delta a_n)^2 \simeq s_n + 2a_n\delta a_n$ so that by definition the distribution function $P(s_n)$ of s_n is given by

$$P(s_n)\delta s_n = \delta a_n(2a_n/A_n^2)\exp -(a_n/A_n)^2 = \\ = (\delta s_n/S_n)\exp -(s_n/S_n) \quad (4)$$

This distribution is plotted in Fig. 4. It is clear that s_n is a very bad estimate of S_n: there is, for example, a 39% probability that $s_n < 0{\cdot}5\,S_n$ and a 14% probability that $s_n > 2\,S_n$.

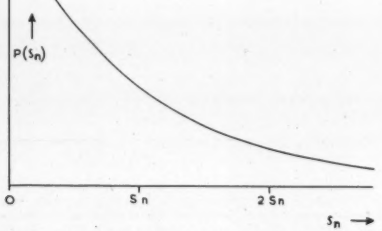

Fig. 4. The distribution function of the square of the amplitude of the n^{th} harmonic $s_n = a_n^2$. The probability that the (amplitude)^2 will lie between s_n and $s_n + \delta s_n$ is $P(s_n)\delta s_n$. The equation of the curve is

$$P(s_n) = (1/S_n)\exp(-s_n/S_n)$$

It is usual to specify the statistical error of an estimate in terms of the standard error σ which may be described as the r.m.s. error and is defined in the present case by σ_n^2 = mean value of $(s_n - S_n)^2$ averaged over many independent measurements of s_n from the same signal (that is, averaged vertically in Fig. 3). σ_n may be calculated from equation (4), giving

$$\sigma_n = S_n \quad (5)$$

that is, the proportional standard error is 100%!

It is apparent that little meaning can be attached to the amplitude of a particular harmonic of an analysis, and it is necessary to average many harmonics either of the same order from analyses of independent records, or adjacent harmonics from the same analysis, Since the average power is usually required, values of $s_n = a_n^2$ should be averaged.

6. REDUCTION OF THE STATISTICAL ERROR BY AVERAGING

In the analysis of a record, the measured values of the powers of the harmonic components are $s_1, s_2 \ldots s_n \ldots$ If it were possible to take averages over many analyses of independent records of the same signal, the values obtained would be $S_1, S_2 \ldots S_n \ldots$ which are truly characteristic of the original signal.

The average from the m^{th} to the $(m + N - 1)^{th}$ harmonic is $(s_m + s_{m+1} \ldots + s_{m+N-1})/N$ and the error is the amount this differs from $(S_m + S_{m+1} \ldots + S_{m+N-1})/N$. The square of the error is

$$[(s_m - S_n) + (s_{m+1} - S_{m+1}) \ldots + \\ + (s_{m+N-1} - S_{m+N-1})]^2/N^2 = \\ = \left[\sum_{n=m}^{m+N-1}(s_n - S_n)^2 + \sum_{n\neq l}(s_n - S_n)(s_l - S_l)\right]\Big/N^2$$

The average value of this over many analyses is (by definition) the square of the standard error σ_{mN}.

The values of $(s_n - S_n)$ and $(s_l - S_l)$ are unrelated, and it follows that their product averaged over many analyses tends to zero. [If from a large number of analyses all those terms with values of $(s_n - S_n)$ in a particular small range are selected, the corresponding values of $(s_l - S_l)$ will be randomly positive and negative and the mean product will be zero.]

Thus

$$\sigma_{mN}^2 = \sum_{n=m}^{m+N-1}\overline{(s_n - S_n)^2}/N^2 \\ = \sum_{n=m}^{m+N-1}\sigma_n^2/N^2 \quad (6)$$

If the true power spectrum is uniform over the interval under consideration, that is, if all values of S_n are equal, all the values of σ_n are equal and $\sigma_{mN}^2 = \sigma^2/N = S_n^2/N$ from equation (5). Thus, the proportional standard error $\sigma_{mN}/S_n = 1/\sqrt{N}$.

This result holds equally if the averaging is over the same order harmonic from different analyses.

To appreciate the significance of this result, consider the analysis of a record using a filter with a bandwidth equivalent to 4 c/s. If a 5% standard error is required, then there must be 400 harmonics in the pass band of the filter, that is, the record must be 100 s long. If a 1% standard error is required, then the record must be 2500 s, or nearly three-quarters of an hour long!

This reasoning can be extended to cover the case of the analysis of a signal directly without intermediate recording. A commonly used commercial wave analyser has this pass band of 4 c/s, and it is apparent that when random Gaussian signals are being analysed, the analysis must take place very slowly indeed if high accuracy is required.

The statistical errors in estimating power spectra are often spoken of in terms of the "number of degrees of freedom" of each value obtained. This parameter, usually denoted by the symbol ν, arises in the derivation of the "chi-squared

distribution," which is discussed in standard text-books of statistics, and which is the statistical distribution function of the estimate of spectral density. In the present case the number of degrees of freedom $\nu = 2N$, the factor 2 arising because each value of a^2 is itself the sum of the squares of the sine and cosine components of the harmonic, and these can be shown to be independent and "normally" distributed.

When N is large, there is a 95% chance that the true value of the spectral density will be within $\pm 2\sigma_{mN}$ of the measured value, and these are termed the 95% confidence limits. If N is small, these limits are not symmetrical about the measured value, but can be looked-up in tables contained in most standard text-books of statistics.

7. THE RESOLVING POWER OF AN ANALYSIS

The most obvious limitation on the resolving power of an analysis is the width of the curve shown in Fig. 2, which shows that a particular harmonic receives contributions from a range of frequencies that may be considered as $2/T$, and that the half-power bandwidth is just under $1/T$. However, the statistical scatter in the amplitudes of the harmonics will mask most rapid changes in the power spectrum, and the only case where the full resolution gives useful information is when a sudden change is extremely large. Suppose, for example, that the signal had come through an almost ideal low-pass filter. Below the cut-off the harmonics would be scattered but on the whole fairly large, with very little chance of being too small to appear: above cut-off the harmonics would decrease rapidly to negligible amplitude and the cut-off frequency could be specified within one, or perhaps two, harmonics.

In most cases, however, the limiting factor is the statistical variation, and it is not possible to specify a fixed resolving power. When an average has been taken over N harmonics, it is possible to state the "confidence limits" of the average value: as has been stated the usual criterion is that there is only one chance in twenty of the true value lying outside these limits, and as N becomes large these limits tend to $\pm$ twice the standard error. If two adjacent values differ by more than the confidence limits, there has probably been a significant change in the power level between them. Thus, the resolving power is better for large changes than for small changes.

There is obviously a compromise between high accuracy in the measurement of power and blurring the spectrum frequency-wise. This problem has been investigated by Chang,[2] who has shown that a simple average over a number of adjacent harmonics does not give the best results. He has shown that if the analysis is performed using a filter passing several harmonics and followed by a power-law detector, there is an optimum shape for the filter characteristic which can be approximated reasonably closely using two, or preferably three, isolated tuned circuits with different Q values in cascade. A single resonant circuit is a very bad filter in this respect.

8. ESTIMATING THE R.M.S. AMPLITUDE OF THE SIGNAL

If $s/2$ is defined as the mean square amplitude of the record, it follows from equation (2) that:

$$s = 2\overline{v^2} = \sum_{n=0}^{\infty} a_n^2 = \sum_{n=0}^{\infty} s_n$$

If the analysis in Section 6 is repeated using sums instead of averages and the sum is taken over the whole spectrum, then the equivalent of equation (6) shows that if the standard error of s about its ensemble average S (that is, the average over many independent records) is $\sigma_{(s)}$, then from equation (5)

$$\sigma_{(s)}^2 = \sum_{n=0}^{\infty} \sigma_n^2 = \sum_{n=0}^{\infty} S_n^2 \tag{7}$$

If the power spectrum $E(f)$ changes slowly compared with the interval $\delta f = 1/T$ between harmonics,

$$S_n \simeq E(f_n)\delta f$$

and

$$\sigma_{(s)}^2 \simeq \sum_{n=0}^{\infty} E^2(f_n)(\delta f)^2$$

$$= \frac{1}{T}\sum_{n=0}^{\infty} E^2(f_n)\delta f$$

$$\to \frac{1}{T}\int_0^{\infty} E^2(f)df$$

or the proportional standard error

$$\frac{\sigma_{(s)}}{S} = \frac{1}{\sqrt{T}} \frac{\sqrt{\left[\int_0^{\infty} E^2(f)df\right]}}{S} =$$

$$= \frac{1}{\sqrt{T}} \frac{\sqrt{\left[\int_0^{\infty} E^2(f)df\right]}}{\int_0^{\infty} E(f)df} \tag{8}$$

This expression shows that the narrower the spectrum, the greater is the proportional error. For example, if the spectrum is uniform over a range of frequencies W and is zero elsewhere,

$$\sigma_{(s)}/S = 1/\sqrt{(TW)}$$

In some cases, for example, when a "white" noise has passed through a filter of known shape, the shape of the spectrum will be known. In general, however, this will not be so, and the only information available will be that contained in the record itself. From the known probability distribution of s_n it can be shown that the average of s_n^2 over many independent analyses $= 2S_n^2$; and inserting this in equation (7)

$$\sigma_{(s)}^2 \simeq \tfrac{1}{2}\sum_{n=0}^{\infty} s_n^2$$

$$\frac{\sigma_{(s)}}{S} \simeq \frac{1}{\sqrt{2}} \frac{\sqrt{(\Sigma s_n^2)}}{\Sigma s_n} \tag{9}$$

This estimate of σ_s/S is itself now subject to statistical error, but it is an error in the estimate of the error, and as such is a second order effect which can usually be neglected. It enables the proportional standard error in the r.m.s. amplitude to be estimated from the actual record in hand.

It may appear curious at first sight that equation (9) does not include T, the length of the record, but it is included indirectly because if T is increased, the number of harmonics is increased and the numerator is increased in proportion to $\sqrt{T}$ whereas the denominator is increased in proportion to T. In other words, if records of lengths T_1 and T_2 are analysed, the standard errors will be in the proportion $\sqrt{(T_2/T_1)}$.

In practice, the main requirement will probably be to estimate the length of recording time required to measure the r.m.s. amplitude to a given accuracy, and equation (8) will

be used with an approximate knowledge of the spectrum and a factor of safety then applied.

Equations (8) and (9) refer to the proportional errors in mean square amplitude. It is apparent that the proportional errors in r.m.s. amplitude will be approximately half these. In this connexion the author has discovered a curious feature which he has not been able to explain. When first attempting to check these results experimentally, he recorded mean rectified amplitude and assumed that this would fluctuate in the same way as r.m.s. amplitude. The measurements gave fluctuations approximately 1·4 (possible $\sqrt{2}$?) times larger than the theoretical values. When the theory was checked using square-law rectifiers, the agreement was good (see below).

9. EXPERIMENTAL CONFIRMATION

The theory has been checked using ocean waves. This is a particularly important problem to the oceanographer, since the state of the sea is continually changing and there has to be a compromise between measuring the characteristics accurately and blurring changes.

The output of the wave recorder was fed to an indirectly-heated vacuo thermo-junction whose output was in turn amplified, slightly smoothed, and recorded. The mean square wave-height over 10 min intervals was obtained using a planimeter to integrate the records. The plotted results are shown in Fig. 5. Means for twenty points were obtained, and the mean square error about these means were computed. Since the measured mean is not the true mean, the measured mean square error has to be multiplied by 20/19 to give the best estimate of the true mean square error.

At suitable intervals during the period of observation, 10 min records were taken in a form suitable for analysis on the National Institute of Oceanography wave analyser.[3] The analyses were measured and the theoretical proportional standard error obtained using equation (9).

Two analyses are shown in Fig. 6. Owing to the characteristics of the analysing instrument the harmonics do not appear as lines, but each gives a resonance curve. The higher harmonics are so close together that the resonances overlap, but it is still possible to measure the amplitudes with sufficient accuracy (they are clearer on the original analyses than in the reproduction shown here).

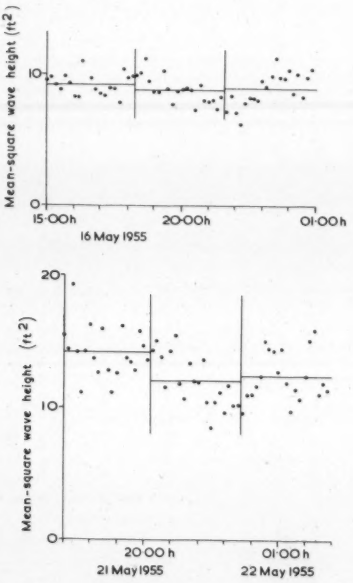

Fig. 5. Values of mean square wave-height averaged over 10 min intervals. The mean value of each group of twenty is shown

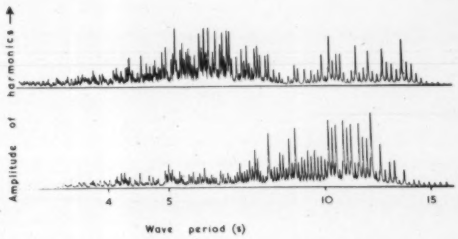

Fig. 6. Analyses of wave records taken during the periods corresponding to Fig. 4. Upper analysis 17·00 h 16.5.55. Lower analysis 18·40 h 21.5.55. Record duration approximately 10 min

Table of comparisons between the proportional root mean square statistical fluctuation in mean square waveheight averaged over 10 min intervals as calculated from the shapes of the frequency spectra using equation (9) with values from spectra such as those shown in Fig. 6, and as calculated from the measurements shown in Fig. 5

16 *May*, 1955	*First* 20 *observations*	*Second* 20 *observations*	*Third* 20 *observations*
σ_s/S calculated from analyses	0·0917	0·1137	0·0913
σ_s/S measured from records	0·0852	0·1154	0·1505
22 *May*, 1955	*First* 20 *observations*	*Second* 20 *observations*	*Third* 20 *observations*
σ_s/S calculated from analyses	0·1419	0·1520	0·1450
σ_s/S measured from records	0·1346	0·1622	0·1514

The calculation of the statistical error of these comparisons has not been carried out exactly, but it is in the region of 25%, so that the results are all within the confidence limits, with the possible exception of the last comparison of the first set. This error may, however, partly be due to a rapid trend of the mean which is apparent from Fig. 5 but which has not been allowed for.

It should be noted that the wider spectrum on the 16 May has resulted in a smaller random error in the measurement

of the mean square amplitude when compared with the 22 May.

ACKNOWLEDGEMENT

The author would like to thank his colleagues Mr. D. E. Cartwright, who took the records used in Section 9, and Mrs. Pamela Edwards who analysed them.

REFERENCES

(1) RAYLEIGH, LORD. *Phil. Mag.*, **10**, p. 73 (1880).
(2) CHANG, S. S. L. *Proc. Inst. Radio Engrs*, **42**, p. 1278 (1954).
(3) DARBYSHIRE, J., and TUCKER, M. J. *J. Sci. Instrum.*, **30**, p. 212 (1953).

ORIGINAL CONTRIBUTIONS

Variations in tension of an unwinding thread

By K. H. V. BOOTH, Ph.D., Birkbeck College Computational Laboratory, University of London

[*Paper received* 26 *September*, 1956]

The variations in tension occurring as a thread is pulled with uniform speed from a cylindrical spool are considered. For simplicity the steady state case when the thread follows a curve of constant shape on the surface of the spool is taken. It is shown that there is a limiting value, depending on the tension of winding and speed of the thread, for the angle with which the thread leaves the spool. Curves are given from which it is possible to estimate the variations in tension as the point of unwinding moves up the spool surface.

1. INTRODUCTION

In various textile processes the situation occurs in which thread is pulled with uniform and often high speed from a spool or bobbin, and then passed through a tensioning device. It is found that variations in tension occur, and as these are magnified by the tensioning device they can be troublesome. Moreover, these variations are, in general, periodic in nature, and they may excite resonant oscillation in other parts of the system.

One possible cause is that, as the thread unwinds, it is pulled across the spool surface, and variation in the length and shape of the curve which it follows will cause variation in tension. Little work appears to have been done on this problem and this paper describes a mathematical investigation into a particular case of this type.

The case considered is that in which the spool is in the form of a right circular cylinder, and the windings are approximately perpendicular to the axis of the spool. The general situation is shown in Fig. 1.

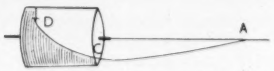

Fig. 1. Thread unwinding from a spool

Thread is pulled at uniform velocity V from the spool, and then passes through a guide A on the axis of the spool. The tension with which the thread leaves the spool at C will vary, being least when the thread is unwinding from the end nearest to A, and greatest when unwinding from the other end. It has been assumed that A is at a great distance compared with the spool length, and that there are, therefore, no special frictional forces at C. Also, although frictional forces between the thread and spool surface have been included, yarn "adherence" has been neglected since this is an intermittent force, and it is difficult to see how it can be included at this stage.

A complete mathematical description of this problem would have to take into account the variation of the size and shape of the curve CD (D being the point which is just about to move) with time, and this involves the solution of simultaneous, second order, non-linear equations. Even when several simplifications were introduced, these proved somewhat intractable, and it was therefore decided to investigate the "steady state" case in which D remains at the same level on the axis, i.e. the curve CD is constant in shape and length, and moves round the surface of the spool, which is assumed to be fully wound with thread, at a constant rate. The introduction of moving axes then enables the equations of motion to be written in a simpler form, admitting of exact solution. By comparing solutions for different positions of D, it is then possible to obtain an estimate of the variations of tension occurring in the real case.

2. THE EQUATIONS OF MOTION

Consider the steady state case in which inextensible thread is pulled with constant speed V from a spool in the form of a right circular cylinder of radius a and height Z_0 (Fig. 2). The unwound portion of thread CD, which is assumed to be in contact with the spool at all points, lies on a curve of

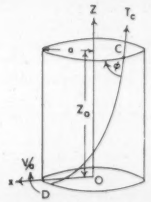

Fig. 2. Diagram of cylindrical spool

constant shape, which moves round the spool with angular velocity V/a. At the same time the thread is moving along the curve DC with velocity V, and the frictional force at any point on curve DC therefore acts in the opposite direction to the resultant of these two velocities.

It is convenient to use cylindrical polar co-ordinates, (r, θ, z), rotating with angular velocity V/a round the axis of the spool, and with the axis Ox, from which θ is measured, passing through D as shown. Then, since $r = a$ at all points, all derivatives of r vanish.

Assuming the frictional force to be μN, where N is the normal reaction of the surface on the thread, and μ is the coefficient of friction, the resolved components of the forces, tensions and accelerations acting on a typical element ds, where s is the distance along CD measured from D, can be shown to be:

	Force	*Tension*	*Acceleration*
Radial:	Nds	$-aT\theta'^2 ds$	$2V\dot{\theta} - a\dot{\theta}^2 - V^2/a$
Circumference:	$\frac{\mu N}{\sqrt{2}}(1 - a\theta')^{1/2} ds$	$(aT'\theta' + aT\theta'')ds$	$Va\dot{\theta}'$
OZ:	$-\frac{\mu N}{\sqrt{2}} Z' \cdot \frac{ds}{(1 - a\theta')^{1/2}}$	$(T'Z' + TZ'')ds$	$V\dot{Z}'$

where T is the tension at the point under consideration and dashes denote differentiation with respect to s, dots with respect to time t.

Since the curve CD is stable, $ds/dt = V$,

and $\dot{\theta} = V\theta' \qquad \dot{\theta}' = V\theta''$

$\dot{Z} = VZ' \qquad \dot{Z}' = VZ''$

The equations of motion can therefore be written:

$$N = a\theta'^2(T - mV^2) + 2mV^2\theta' - (mV^2/a) \tag{1}$$

$$a\theta''(mV^2 - T) = aT'\theta' + (\mu N/\sqrt{2})(1 - a\theta')^{1/2} \tag{2}$$

$$Z''(mV^2 - T) = Z'[T' - (\mu N/\sqrt{2})(1 - a\theta')^{-1/2}] \tag{3}$$

The condition for inextensibility gives:

$$\left.\begin{aligned} Z' &= (1 - a^2\theta'^2)^{1/2} \\ Z'' &= -a^2\theta'\theta''/(1 - a^2\theta'^2)^{1/2} \end{aligned}\right\} \tag{4}$$

Using these conditions and equations (2) and (3) to eliminate Z', Z'' and N we obtain:

$$a\theta''/(1 + a\theta') = T'/(mV^2 - T) \tag{5}$$

Integrating and putting $\theta' = \theta'_0$ when $T = T_0$,

$$1 + a\theta' = c/(mV^2 - T) \text{ where } c = (1 + a\theta'_0)(mV^2 - T_0) \tag{6}$$

Note that since this expression must hold for all t, c is independent of t.

Eliminating N and θ'' from equations (1), (2) and (5):

$$T' = (\mu/\sqrt{2})(1 - a\theta')^{1/2}[a\theta'^2(T - mV^2) + 2mV\theta' - (mV^2/a)] \tag{7}$$

We introduce now the non-dimensional quantity τ defined by:

$$\tau = (T/mV^2) - 1$$

Thus, from equation (6),

$$a\theta' = -\frac{c/mV^2}{\tau} - 1 = \frac{K}{\tau} - 1 \quad \text{where} \quad K = -c/mV^2 \tag{8}$$

and from equations (4) and (7) we obtain finally:

$$dZ = \frac{a\sqrt{(2K)}}{\mu} \cdot \frac{\tau^{1/2} d\tau}{\tau^2 - \tau(2K + 3) + K(K + 2)} = \frac{a\sqrt{(2K)}}{\mu} \cdot \frac{\tau^{1/2} d\tau}{(\tau - \alpha)(\tau - \beta)}$$

where $\alpha = \frac{1}{2}(2K + 3 + \sqrt{(4K + 9)})$

$\beta = \frac{1}{2}[2K + 3 - \sqrt{(4K + 9)}]$

Integrating with limits 0 and Z_0 for Z and τ_D, τ_C for τ we obtain:

$$Z_0 = \frac{a}{\mu}\sqrt{\left(\frac{2K}{4K + 9}\right)}\left[\sqrt{\alpha}\log_e\frac{\tau^{1/2} - \alpha^{1/2}}{\tau^{1/2} + \alpha^{1/2}} - \sqrt{\beta}\log_e\frac{\tau^{1/2} - \beta^{1/2}}{\tau^{1/2} + \beta^{1/2}}\right]_{\tau_D}^{\tau_C} \tag{9}$$

3. THE LIMITS OF INTEGRATION

Suppose, now, that the lower limit of integration in equation (5) is taken at D. Then, since the thread is wound perpendicular to the axis of the spool $\theta'_D = 1/a$. Thus, from equation (8),

$$2\tau_D = K$$

i.e. $\tau_D = K/2$ where τ_D is the value of τ at D. If the thread leaves the cylinder at an angle ϕ with the horizontal, as shown in Fig. 2, $a\theta'_C = \cos\phi$

and $\tau_C = K/(1 + \cos\phi) = 2\tau_D/(1 + \cos\phi)$

The limits of integration in equation (9) can therefore be written as:

$$\tau_D \text{ and } 2\tau_D/(1 + \cos\phi)$$

and equation (9) therefore becomes:

$$Z_0 \cdot \frac{\mu}{a} = \sqrt{\left(\frac{2K}{4K + 9}\right)} \cdot \left\{\sqrt{\alpha}\log_e\left[\frac{\alpha_1 - \sqrt{(1 + \cos\phi)}}{\alpha_1 + \sqrt{(1 + \cos\phi)}} \cdot \frac{\alpha_1 + \sqrt{2}}{\alpha_1 - \sqrt{2}}\right] - \sqrt{\beta}\log_e\left[\frac{\beta_1 - \sqrt{(1 + \cos\phi)}}{\beta_1 + \sqrt{(1 + \cos\phi)}} \cdot \frac{\beta_1 + \sqrt{2}}{\beta_1 - \sqrt{2}}\right]\right\} \tag{10}$$

where $\alpha_1 = (2\tau_D/\alpha)^{1/2}$

$\beta_1 = (2\tau_D/\beta)^{1/2}$

4. THE POSSIBLE RANGE OF SOLUTION

There appears to be little information available on the values of τ occurring in practice, but it is possible to impose certain theoretical limits. Thus, since T/mV^2 is essentially positive, $\tau > -1$ and $K > -2$.

Consider, now, the expression for the normal reaction, N, when θ' is eliminated between equations (1) and (8).

We obtain, $N = (mV^2/a\tau)(\tau - \alpha)(\tau - \beta)$

Now a discontinuity exists at $\tau = 0$ since $N \to \infty$, $\tau_C \to \tau_D$ and $Z_0 \to 0$. Moreover, if $\tau < 0$, $\tau_C < \tau_D$, i.e. the tension at C is less than that at D which is clearly absurd. Solutions of practical interest are therefore confined to values of τ greater than 0. Moreover, since the thread is assumed to be in contact with the cylinder, $N > 0$ and for $\tau > 0$, this implies that $0 < \tau < \beta$ or $\tau > \alpha$. But it can be shown that for $\tau > 0$, $\beta > \tau_D$ and the possible values of τ are therefore limited to the range: $0 < \tau < \beta$. This condition imposes a restriction on the upper limit of integration for a given value of τ_D. Thus we have:

$$2\tau_D/(1 + \cos\phi) < \beta$$

or $\phi < \cos^{-1}\left(\frac{2\tau_D}{\beta} - 1\right) = \cos^{-1}\frac{\sqrt{(4K + 9)} - 3}{2K - 3 - \sqrt{(4K + 9)}}$

We have, therefore, shown that for motion of this type $T_D > mV^2$ and that for a given value of T_D/mV^2, where T_D is the tension of winding on the spool, there exists an upper limit ϕ_{max} to the value of ϕ, the angle at which the thread leaves the spool. Note that as $T_D/mV^2 \to 1$, $\phi_{max} \to \pi/3$, and as $T_D/mV^2 \to \infty$, $\phi_{max} \to \pi/2$.

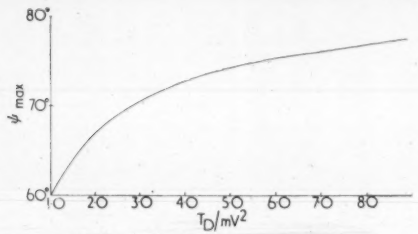

Fig. 3. Variation of ψ_{max} with T_D/mV^2

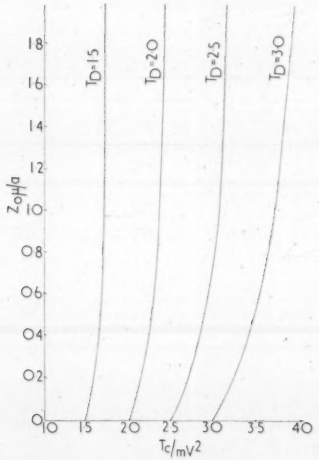

Fig. 4. Variation of T_C/mV^2 with $Z_0\mu/a$ for constant T_D

The variation of ϕ_{max} with T_D/mV^2 is shown in Fig. 3 and Fig. 4 gives the relationship between $Z_0\mu/a$ and T_C/mV^2 for a range of values of T_D/mV^2. Note that as $\phi \to \phi_{max}$, $Z_0 \to +\infty$ since the second term in equation (10) tends to infinity.

5. SUMMARY OF RESULTS

It has been shown that steady-state motion of the form postulated in Section 2 is impossible when the winding tension, T_D, is less than mV^2.

When $T_D > mV^2$, a solution has been obtained giving the relationship between the quantity $Z_0\mu/a$ and T_C, the tension of the thread on leaving the spool. It has also been shown that, for any given value of T_D/mV^2, there exists a limiting value for ϕ, the angle with which the thread leaves the spool.

Curves are given, showing the relationship between $Z_0\mu/a$ and T_C/mV^2 for various values of T_D/mV^2 and from these it is possible to obtain an estimate of the change in tension occurring as the point of unwinding moves from one end of the spool to the other. Thus, for example, for $T_D/mV^2 = 2{\cdot}5$ there is a change in tension of 20% when unwinding from a spool for which $Z_0\mu/a = 0{\cdot}76$.

The table shows the percentage change in tension for $Z_0\mu/a$ for five values of T_D/mV^2. It will be seen that this change *increases* with T_D/mV^2.

Variation in percentage increase in tension with T_D/mV^2

T_D/mV^2	Percentage increase in tension between C and D
1·5	12·7
2·0	18·5
2·5	20·4
3·0	21·7

Finally it may be mentioned that in practice the thread is often pulled off with such speed that "ballooning" occurs; that is, the thread flies outward from the surface of the spool. In this case the results obtained can still be applied to the portion of thread in contact with the spool, but taking the top of the spool to be the point at which the thread leaves the spool surface. The behaviour of the ballooning portion of thread must, of course, be considered separately, and much work has already been done on this problem.*

* HANNAH, M. *J. Text. Inst. Manchr.*, **43** (10), p. 519 (1952).

Transverse vibrations of power transmission chains

By S. MAHALINGAM, B.Sc., Ph.D., Department of Applied Mechanics, University of Sheffield*

[*Paper received* 10 *September*, 1956]

In this paper the natural frequencies of a travelling chain are determined by treating the chain as a uniform string. For a constant chain tension the natural frequencies decrease progressively to zero as the chain speed approaches the velocity of transverse wave propagation. In practice such a condition is not obtained since the chain tension increases with speed owing to centrifugal effects. Formulae are obtained for the amplitude of forced vibration of the chain when excited by a transverse displacement at one end. The effect of damping is considered and exact and approximate methods of determining resonant amplitudes are given.

LIST OF SYMBOLS

m = mass of chain per unit length
T = chain tension
T_s = initial (static) tension of chain
p = pitch of chain
c = damping coefficient
V = speed of chain
L = length of chain
ω_n = circular frequency of free vibration
ω = circular frequency of exciting force

The term "chain," in general, would refer to the free unsupported strand between sprockets.

INTRODUCTION

Transverse vibration of the strand of a chain drive may be excited both by transverse and longitudinal displacements of the ends of the chain. One source of excitation is polygonal action,[1] i.e. the periodic fluctuation of the velocities of the ends of a chain caused by the fact that a chain lying on a sprocket forms a polygon rather than a circle. When sprockets with small numbers of teeth are used, these vibrations are large and may reach resonant conditions. Vibrations may also be excited by external forces, e.g. the torsional vibration of a sprocket, and out-of-balance in the drive, etc. In the case of the torsional vibration of a sprocket, the end of the chain is given a periodical displacement which is largely longitudinal and, to a small extent, transverse. In practice, the most important condition is that of resonance, in which the excitation frequency coincides with one of the natural frequencies of the chain. It is therefore necessary to determine the natural frequencies, taking account of the longitudinal velocity of the chain, and the variation in tension due to centrifugal effects. By assuming a damping force proportional to the transverse velocity, the resonant amplitude of the chain may also be determined.

FREE VIBRATIONS

A chain may be idealized as a light string carrying a number of equal equidistant particles. Although this idealization preserves the finite and discrete nature of each link, it is not very suitable for the study of a travelling chain. In the following analysis the chain will be idealized as a uniform heavy string. Comparison of the critical frequencies of a stationary chain as given by the two idealizations shows that the difference in the fundamental frequency and the first few harmonics is very small provided the number of links in the chain is large. The natural frequencies of a stationary uniform string are well known, but the effect of longitudinal velocity has only recently been considered by Sack.[2]

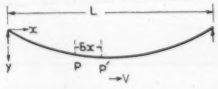

Fig. 1. Displacements of travelling chain

In Fig. 1, let the deflexion at a point P be y. After an interval δt, the point will have moved to the position P' where the deflexion will be:

$$y + \frac{\partial y}{\partial x} \cdot \delta x + \frac{\partial y}{\partial t} \cdot \delta t = y + \left(V \frac{\partial}{\partial x} + \frac{\partial}{\partial t} \right) y \, . \, \delta t$$

Then the transverse velocity of the point is

$$\left(V \frac{\partial}{\partial x} + \frac{\partial}{\partial t} \right) y \tag{1}$$

and the transverse acceleration $= \left(V \frac{\partial}{\partial x} + \frac{\partial}{\partial t} \right)^2 y$

$$= V^2 \frac{\partial^2 y}{\partial x^2} + 2V \frac{\partial^2 y}{\partial x \partial t} + \frac{\partial^2 y}{\partial t^2} \tag{2}$$

The equation of motion is

$$T \frac{\partial^2 y}{\partial x^2} = m \left(V^2 \frac{\partial^2 y}{\partial x^2} + 2V \frac{\partial^2 y}{\partial x \partial t} + \frac{\partial^2 y}{\partial t^2} \right)$$

which may be written

$$V_0^2 \frac{\partial^2 y}{\partial x^2} = V^2 \frac{\partial^2 y}{\partial x^2} + 2V \frac{\partial^2 y}{\partial x \partial t} + \frac{\partial^2 y}{\partial t^2} \tag{3}$$

where $V_0 = \sqrt{(T/m)}$ is the velocity of propagation of transverse waves.

The general solution of this equation for vibrations of circular frequency ω is given by:

$$y = A_1 \cos \left[\omega t + \omega x/(V_0 - V) + \phi_1 \right] + A_2 \cos \left[\omega t - \omega x/(V_0 + V) + \phi_2 \right] \tag{4}$$

Substituting the boundary conditions $y = 0$ at $x = 0$ and $x = L$ in equation (4), we get the natural frequencies

$$\omega_n = (n\pi V_0/L)[1 - (V/V_0)^2] \tag{5}$$

* Now at Department of Mechanical Engineering, University of Ceylon.

and the mode of vibration is given by

$$y = \sin\frac{n\pi x}{L}\sin\left(\omega_n t + \frac{n\pi x}{L}\frac{V}{V_0} + \phi\right) \tag{6}$$

where $n = 1, 2, 3 \ldots$ and ϕ is an arbitrary phase angle. According to equation (5) the natural frequencies decrease to zero as V approaches V_0.

EFFECT OF CENTRIFUGAL TENSION

If the tensions of the tight and slack strands of a stationary chain drive are assumed to be T_s and T_s' respectively then, when the chain is travelling at a speed V, the tensions become $(T_s + mV^2)$ and $(T_s' + mV^2)$ respectively where mV^2 is the centrifugal tension. This has been considered by Stamets[3] and others. The velocity of wave propagation V_0 in the tight strand of the travelling chain is given by

$$V_0^2 = T/m = (T_s + mV^2)/m = (V_s^2 + V^2)$$

where $V_s^2 = T_s/m$. From equation (5) the natural frequencies are given by

$$\omega_n = \frac{n\pi}{L}\frac{V_s^2}{(V_s^2 + V^2)^{\frac{1}{2}}} \tag{7}$$

Equation (7) shows that owing to the presence of centrifugal tension $\omega_n \to 0$ only as $V \to \infty$.

Forced vibrations due to polygonal action reach resonance when the frequency of tooth engagement is equal to the critical frequency of the chain. For this condition,

$$2\pi\frac{V}{p} = \frac{n\pi}{L}\frac{V_s^2}{(V_s^2 + V^2)^{\frac{1}{2}}}$$

where p is the pitch of the chain.

Solving for V,

$$V^2 = \frac{V_s^2}{2}\left\{\sqrt{\left[1 + \left(\frac{np}{L}\right)^2\right]} - 1\right\} \tag{8}$$

FORCED VIBRATION DUE TO TRANSVERSE EXCITATION

When a chain drive runs at constant speed, polygonal action gives both ends of the chain periodic transverse displacements. Considering the fundamental components of these excitations, the boundary conditions for equation (4) may be written

$$\left.\begin{aligned} x &= 0, \quad y = a_1\cos\omega t \\ x &= L, \quad y = a_2\cos(\omega t + \theta) \end{aligned}\right\} \tag{9}$$

where ω = circular frequency of tooth engagement $= 2\pi V/p$

θ = "phase difference" between the two ends of the chain corresponding to the fractional pitch in the tangent length of the chain.

The response at any point on the chain will be the sum of the responses due to the excitations given by:

$$\left.\begin{aligned} x &= 0, \quad y = 0 \\ x &= L, \quad y = a_2\cos(\omega t + \theta) \end{aligned}\right\} \tag{10a}$$

and

$$\left.\begin{aligned} x &= L, \quad y = 0 \\ x &= 0, \quad y = a_1\cos\omega t \end{aligned}\right\} \tag{10b}$$

Substituting equation (10a) into equation (4), we have

$$y_1 = \frac{a_2}{\sin\left[\dfrac{\omega V_0 L}{(V_0^2 - V^2)}\right]}\sin\frac{\omega V_0 x}{V_0^2 - V^2}\cos\left[\omega t - \frac{\omega V(L-x)}{V_0^2 - V^2} + \theta\right] \tag{11}$$

and equation (10b) into equation (4), we have

$$y_2 = \frac{a_1}{\sin\left[\dfrac{\omega V_0 L}{(V_0^2 - V^2)}\right]}\sin\frac{\omega V_0(L-x)}{V_0^2 - V^2}\cos\left(\omega t + \frac{\omega V x}{V_0^2 - V^2}\right) \tag{12}$$

Amplitude of vibration at any point $= y_1 + y_2$.

FORCED VIBRATION DUE TO LONGITUDINAL EXCITATION

When one of the sprockets is subject to torsional vibration, one end of the chain is given a transverse excitation $a\cos 2\omega t$ and a longitudinal excitation $a'\cos\omega t$ where ω is the circular frequency of torsional vibration of the sprocket. The response to the transverse excitation is given by equation (11), while the response to the longitudinal component may be analysed as follows.

Owing to the longitudinal excitation, the tension of the chain at any instant is $(T + \Delta T\cos\omega t)$. The equation of motion (3) then becomes:

$$(V_0^2 + \Delta V_0^2\cos\omega t)\frac{\partial^2 y}{\partial x^2} = V^2\frac{\partial^2 y}{\partial x^2} + 2V\frac{\partial^2 y}{\partial x\partial t} + \frac{\partial^2 y}{\partial t^2} \tag{13}$$

Putting $y = e^{i\mu x}y_0(t)$ and $\omega t = 2z$ we have

$$\ddot{y}_0 + 2iV\mu\dot{y}_0 + [\mu^2(V_0^2 - V^2 + \Delta V_0^2\cos 2z)]y_0 = 0$$

Substituting $y_0 = e^{-iV\mu z}u(z)$ we get

$$\ddot{u} + (\alpha + 2q\cos 2z)u = 0 \tag{14}$$

where $\alpha = \mu^2 V_0^2$

$2q = \mu^2\Delta V_0^2$

Equation (14) is the well-known Mathieu's equation, a brief discussion of which is given by Den Hartog.[4] The response of the chain, in this case, has half the frequency of the excitation.

EFFECT OF SPEED ON THE AMPLITUDES AT RESONANCE

In order to determine the resonant amplitudes of the chain it is necessary to take damping into account. If it is assumed that there is a damping force proportional to the transverse velocity, then the equation of motion may be written:

$$\left(V^2\frac{\partial^2}{\partial x^2} + 2V\frac{\partial^2}{\partial x\partial t} + \frac{\partial^2}{\partial t^2}\right)y + b\left(V\frac{\partial}{\partial x} + \frac{\partial}{\partial t}\right)y = V_0^2\frac{\partial^2 y}{\partial x^2} \tag{15}$$

where $b = c/m$ and c is the damping force coefficient. Let one end of the chain be given a transverse displacement

$a\,e^{i\omega t}$. Then, the real part of the response to this excitation will be that corresponding to a harmonic excitation $a\cos\omega t$.

Putting $y = y_0(x)\,e^{i\omega t}$, equation (15) becomes

$$\left(V^2\frac{d^2}{dx^2} + i2V\omega\frac{d}{dx} - \omega^2\right)y_0(x) + \\ + b\left(V\frac{d}{dx} + i\omega\right)y_0(x) = V_0^2\frac{d^2}{dx^2}y_0(x)$$

Now, let $y_0(x) = e^{i\mu x}$. We then have

$$\mu^2(V_0^2 - V^2) - \mu(2V\omega - ibV) - (\omega^2 - ib\omega) = 0 \quad (16)$$

Let the solution of equation (16) be

$$\mu = \alpha_1 + i\beta_1$$

and

$$\mu = \alpha_2 + i\beta_2$$

Then the general solution of equation (15) is

$$y = R[A_1 e^{i(\omega t + \alpha_1 x + i\beta_1 x)} + A_2 e^{i(\omega t + \alpha_2 x + i\beta_2 x)}]$$

For the boundary condition $x = 0$, $y = 0$ for all t, we get

$$A_1 = -A_2$$

Substituting $A_1 = k\,e^{i\phi}$ where k and ϕ are real constants, we get

$$y = Rk[e^{-\beta_1 x}e^{i(\omega t + \phi + \alpha_1 x)} - e^{-\beta_2 x}e^{i(\omega t + \phi + \alpha_2 x)}]$$
$$= k[(e^{-\beta_1 x}\cos\alpha_1 x - e^{-\beta_2 x}\cos\alpha_2 x)\cos(\omega t + \phi) - \\ - (e^{-\beta_1 x}\sin\alpha_1 x - e^{-\beta_2 x}\sin\alpha_2 x)\sin(\omega t + \phi)]$$
$$= k[e^{-2\beta_1 x} + e^{-2\beta_2 x} - \\ - 2e^{-(\beta_1+\beta_2)x}\cos(\alpha_1 - \alpha_2)x]^{\frac{1}{2}}\cos(\omega t + \theta_x + \phi)$$

where $$\theta_x = \tan^{-1}\frac{e^{-\beta_1 x}\sin\alpha_1 x - e^{-\beta_2 x}\sin\alpha_2 x}{e^{-\beta_1 x}\cos\alpha_1 x - e^{-\beta_2 x}\cos\alpha_2 x}$$

Using the other boundary condition $x = L$, $y = a\cos\omega t$ we get

$$y = a\left[\frac{e^{-2\beta_1 x} + e^{-2\beta_2 x} - 2e^{-(\beta_1+\beta_2)x}\cos(\alpha_1 - \alpha_2)x}{e^{-2\beta_1 L} + e^{-2\beta_2 L} - 2e^{-(\beta_1+\beta_2)L}\cos(\alpha_1 - \alpha_2)L}\right]^{\frac{1}{2}} \\ \cos(\omega t + \theta_x - \theta_L) \quad (17)$$

It will be seen from equation (16) that if b is small and $\omega = \omega_n$ then α_1 and α_2 will be such that $(\alpha_1 - \alpha_2)L \simeq 2\pi$. Substituting in equation (17)

$$\text{resonant amplitude at mid-span} = a\frac{1}{e^{-\beta_1(L/2)} - e^{-\beta_2(L/2)}} \quad (18)$$

A numerical example considering a $\frac{3}{4}$ in. pitch simple roller chain

$$m = 0{\cdot}066 \text{ lb per in./386} \qquad L = 36 \text{ in.} \quad T_s = 50 \text{ lb}$$
$$b = 2{\cdot}5 \text{ sec}^{-1} \text{ units}$$

is given in Fig. 2. Curve I, which represents resonant amplitudes for the fundamental frequency, shows a steady decrease with speed—a trend which has been verified experimentally by the author. The resonant amplitudes for a damping force proportional to $\partial y/\partial t$ is given by curve II. This, however, shows an increase of resonant amplitudes with speed.

The damping force in a vibrating chain is provided by the frictional resistance between the pins and bushes during the articulation of the links, the resistance of the air, etc. It is difficult to make an accurate assessment of these factors but experimental evidence, which indicates a decrease of resonant amplitudes with increase of speed, suggests that a damping force proportional to $\left(V\frac{\partial y}{\partial x} + \frac{\partial y}{\partial t}\right)$ gives a fairly good approximation.

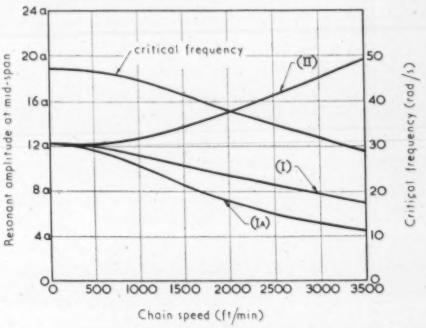

Fig. 2. Effect of speed on the critical fundamental frequency and the resonant amplitude

Resonant amplitudes: curve I, damping force $\propto \left(V\frac{\partial y}{\partial x} + \frac{\partial y}{\partial t}\right)$ (exact); curve IA, damping force $\propto \left(V\frac{\partial y}{\partial x} + \frac{\partial y}{\partial t}\right)$ (approximate) curve II, damping force $\propto (\partial y/\partial t)$ (exact).

An approximate but much simpler expression for resonant amplitudes can be obtained by using the principle of work done. Consider a displacement $y = a\cos\omega_n t$ applied at the end $x = L$. The major component of the response of the chain may be written

$$y = A\sin\frac{\pi x}{L}\sin\left(\omega_n t + \frac{\pi x}{L}\cdot\frac{V}{V_0} - \pi\frac{V}{V_0}\right) \quad (19)$$

where A is the amplitude at mid-span. This represents a vibration of frequency ω_n in the fundamental natural mode, at a phase angle 90° with the applied displacement. In addition, a small component in phase with the excitation will be present. If the damping is small, this component may be neglected.

From equation (19) we have

$$[\partial y/\partial x]_{x=L} = (A\pi/L)\sin\omega_n t$$

The transverse component of the chain tension at $x = L$ is therefore

$$(TA\pi/L)\sin\omega_n t \quad (20)$$

from which the work done per cycle

$$= \int_0^{2\pi/\omega_n}\frac{TA\pi}{L}\sin\omega_n t\frac{d}{dt}(a\cos\omega_n t)dt$$
$$= \frac{TaA\pi^2}{L} \quad (21)$$

Now consider the energy dissipated in damping.

$$\text{Damping force} = bm\left(V\frac{\partial}{\partial x} + \frac{\partial}{\partial t}\right)y$$

Total energy dissipated per cycle

$$= \int_0^L \int_0^{2\pi/\omega_n} bm\left(V\frac{\partial}{\partial x} + \frac{\partial}{\partial t}\right)^2 y\,dx\,dt$$

Substituting for y from equation (19), we have

$$\text{energy lost} = bmA^2\left[\left(\frac{V\pi}{L}\right)^2 \frac{\pi L}{2\omega_n} + \left(\frac{V^2\pi}{V_0 L} + \omega_n\right)^2 \frac{\pi L}{2\omega_n}\right] \quad (22)$$

From equation (5)

$$\omega_n + (V^2\pi/V_0 L) = \pi V_0/L$$

Substituting in equation (21) we get

$$\text{energy lost} = bmA^2(\pi^3/2\omega_n L)(V_0^2 + V^2) \quad (23)$$

Equating equations (21) and (23)

$$A = \frac{Ta}{mb}\frac{2\omega_n}{\pi}\frac{1}{(V_0^2 + V^2)}$$

$$= a \cdot \frac{2V_s^2}{bL}\frac{(V_s^2 + V^2)^{\frac{1}{2}}}{(V_s^2 + 2V^2)} \quad (24)$$

This shows that A decreases with increasing V, and $A \to 0$ as $V \to \infty$. For the numerical example considered earlier, the resonant amplitudes given by equation (24) are represented by curve $1A$ in Fig. 2. Owing to the assumptions made, the curve is necessarily approximate and shows considerable discrepancy at high chain speeds.

ACKNOWLEDGEMENTS

The above paper was part of a research project carried out at this University, and the author wishes to express his indebtedness to Prof. W. A. Tuplin and Dr. R. P. N. Jones for their valuable criticism and advice.

REFERENCES

(1) MORRISON, R. A. *Machine Design*, **24** (9), p. 155 (1952).

(2) SACK, R. A. *Brit. J. Appl. Phys.*, **5**, p. 224 (1954).

(3) STAMETS, W. K. *Trans Amer. Soc. Mech. Engrs*, **73**, p. 655 (1951).

(4) DEN HARTOG, J. P. *Mechanical Vibrations*, 3rd Ed., p. 415 (New York: McGraw-Hill Book Co. Inc., 1947).

The effect of sulphur and oxygen on the electrical properties of oxide-coated cathodes

By G. S. HIGGINSON, B.A., Physics Department, University College of North Staffordshire

[*Paper received* 16 *November*, 1956]

Poisoning and recovery experiments using both oxygen and sulphur substantiate the Loosjes and Vink theory of conduction. Sulphur is found to have a greater poisoning effect than oxygen. A possible reason for this is suggested.

The deleterious effect of oxygen on thermionic emission from oxide-coated cathodes has been subjected to extensive investigation by Metson,[1] Wagener[2] and others. Comparatively little is known about the effect of sulphur, although Stahl[3] has reported that cathodes subjected to atmospheric pollution by sulphur before assembly in a vacuum tube give reduced emission on subsequently undergoing the carbonate-to-oxide conversion.

Measurements have been made of the effect of oxygen and sulphur on barium-strontium oxide cathodes over a wide temperature range. Probe-diodes, of a type described by Shepherd,[4] were employed in order that the behaviour of both the electrical conductivity of the oxide and the thermionic emission could be studied. The experimental procedure described by Shepherd was used: briefly, the temperature was set, the cathode was poisoned by the controlled admission of sulphur vapour or oxygen to the space round it until the thermionic emission was reduced to about 10% of its original value, and then both the emission and electrical conductivity of the cathode were measured during the following ten minutes or so. A tungsten filament coated with barium peroxide was used as a source of oxygen and a similar filament coated with molybdenum sulphide was found to be a suitable source of sulphur. A filament of each type was enclosed in the vacuum tube in order that comparative measurements could be made on the same cathode.

Oxygen and sulphur poisoning and recovery experiments were performed at a number of temperatures between 500 and 1000° K. Fig. 1 shows the behaviour of the emission and conductivity after poisoning in a typical experiment at high temperatures (in this case 900° K). Recovery from both sulphur and oxygen poisoning at this temperature was found to occur but recovery from sulphur poisoning was a somewhat slower process. The emission and conductivity in each case followed similar recovery patterns. This kind of behaviour was always observed at temperatures above 800° K and is consistent with the pore-conduction theory of Loosjes and Vink,[5] according to which conduction in this range of temperature is in the main a thermionic emission process in the interstices of the porous oxide coating.

The behaviour of a cathode after poisoning at a temperature of 550° K is shown in Fig. 2. No recovery of emission was observed at this temperature and the conductivity after an initially rapid decrease during poisoning, continued to diminish during the subsequent ten-minute period. The reduction in conductivity due to poisoning in the temperature range 500–700° K was found to depend upon the temperature; the greater reduction occurring at the higher temperatures.

In every case sulphur was observed to poison the cathode emission and conductivity to a greater extent than oxygen.

Recovery from poisoning in all experiments was facilitated by raising the temperature of the cathode to 1200° K and applying 50 V to the anode. Under these conditions complete recovery of the cathode occurred within an hour or so. The oxygen or sulphur evolved during recovery was taken up by two barium getters enclosed within the vacuum tube. As many as twenty or more poisoning cycles were performed on each of several cathodes without any noticeable permanent effect on the conductivity or emission.

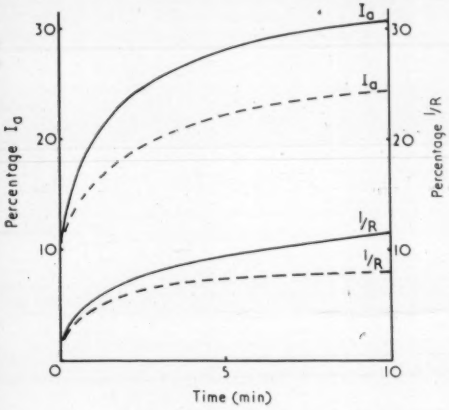

Fig. 1. Conductance (1/R) and emission (I_a) after poisoning
Temperature 900° K
——— = oxygen – – – – – – = sulphur

It was not expected that in general sulphur poisoning would differ to a marked extent from oxygen poisoning. The results reported here, however, confirm that sulphur poisoning is reversible in the range of temperature at which oxide-coated cathodes are normally operated and show that the application of an electric field facilitates recovery, which suggests that the sulphur emitted during recovery is negatively charged. The greater effect of sulphur poisoning of the conductivity, most evident in the low temperature region, may be explained on the basis that sulphur has a smaller electron affinity than oxygen. Consequently, in order that the work function of a cathode may be increased to reduce the emission to 10% of its initial value, a greater quantity of sulphur than of oxygen will be required. Thus in the case of sulphur poisoning a larger concentration of sulphur will exist in the region of the coating than of oxygen in oxygen poisoning and some of it will diminish the low-temperature conductivity to a greater extent, possibly by occupying donor sites in the crystals or on the crystal surfaces. The initially rapid reduction of the conductivity in poisoning experiments at temperatures below 700° K suggests that some form of surface conductivity

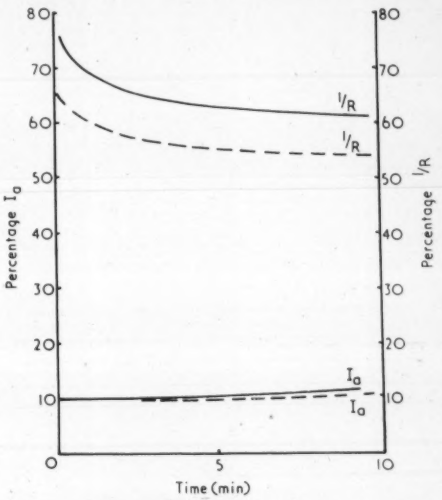

Fig. 2. Conductance ($1/R$) and emission (I_a) after poisoning
Temperature 550° K
——— = oxygen – – – – – – = sulphur

contributes to the conductivity of the oxide-coating in this temperature region. This phenomenon is receiving further attention and will be reported more fully elsewhere.

ACKNOWLEDGEMENTS

The author wishes to acknowledge the facilities made available by Prof. F. A. Vick, under whose general direction the work was carried out.

REFERENCES

(1) METSON, G. H. *Nature* [*London*], **164**, p. 540 (1949).
(2) WAGENER, S. *Proc. Phys. Soc.* [*London*] *B*, **67**, p. 369 (1954).
(3) STAHL, H. A. *Appl. Sci. Res*, *B*, **1**, p. 397 (1950).
(4) SHEPHERD, A. A. *Brit. J. Appl. Phys.*, **4**, p. 70 (1953).
(5) LOOSJES, R., and VINK, H. J. *Philips Res. Rep.*, **4**, p. 449 (1949).

Some carbon replica techniques for the electron microscopy of small specimens and fibres

By D. E. Bradley, Associated Electrical Industries Ltd., Aldermaston, Berks.

[*Paper received* 18 *December*, 1956]

The difficulties encountered in making replicas of fibres and other small specimens are discussed, and three carbon replica methods are described. The first is designed specifically for fibres. The tedious partial embedding techniques which have hitherto been required for such specimens are eliminated. The second method is for small specimens which are difficult to handle and range between about 0·5 and 2·0 mm in size. It has not been possible to use conventional methods with these specimens. The third method is for soft biological specimens such as bacteria. Existing single-stage replica techniques failed with such specimens, largely because of the strong chemical reagents required to dissolve the organic materials. All three methods are illustrated by various applications.

Hitherto, the preparation of replicas of fibres has generally involved the use of elaborate partial embedding processes.[1] These techniques ensure that only a very small part of the circumference of the fibre is replicated, otherwise the replica film invariably fractures. It has been found possible to eliminate embedding by the use of a simple two-stage method.

In addition to fibres, many other specimens are difficult to replicate because they are too small to permit the usual stripping techniques required in two-stage replica methods. Such specimens would include the eyes or antennae of insects, small pieces of metal and perhaps various botanical specimens. These vary in size from about 0·5 to 2 or 3 mm. It is also extremely difficult to remove them from any vacuum deposited replica by solution without breaking up the replicating film. The method which has been devised for such specimens is a two-stage technique of some complexity which has been found to be both practicable and valuable.

The third replica method which is described is for soft biological specimens such as bacteria. It has been found that, in the preparation of replicas of these specimens, the strong chemical reagents required to remove organic material cause the breaking up of the replica. In this process, the difficulty is overcome by mounting a carbon replica on a grid before the solution of the specimen.

A SIMPLE REPLICA TECHNIQUE FOR FIBRES

The method utilizes the fact that Formvar is softened but not dissolved when immersed in acetone. (Bedacryl softened with methylated spirits can be used.)

An electron microscope specimen support grid is slightly bent and placed on the flat top of a $\frac{1}{8}$ in. diameter metal peg; it is then covered with a thick Formvar film. It is essential that this film should be sufficiently thick otherwise it will break later in the process. A film of the correct thickness can be obtained by dipping a microscope slide into a 2–4% solution of Formvar in chloroform and allowing it to drain vertically on to a filter paper until all the solvent has evaporated.

The Formvar is then softened with acetone by placing the grid, still on the peg, about 1 mm below the nozzle of a burette containing acetone and allowing 1–2 ml. of the solvent to flow over the grid at the rate of about 1 ml./min. The grid and peg are then removed from the burette, and, before the acetone evaporates, the fibre is placed across the grid. It is desirable to add one more drop of acetone before the assembly is left to dry under a lamp for at least five minutes. The specimen is next pulled away from the Formvar film in which there now remains a primary impression. This can easily be seen optically under vertical illumination without removing the grid from the peg. If it is found that the fibre has only touched the Formvar in a few places, so that there are only small areas of the primary impression, the fibre can be cut into short lengths before it is placed on the softened plastic. The pieces are removed after drying by carefully brushing the surface of the Formvar film with the edge of a filter paper or paint brush.

The final replica is made by evaporating carbon on to the Formvar.[2] The thickness of the carbon film used depends upon the coarseness of the structure under examination. If the surface of the fibre is very rough, then a film about 150 Å thick is satisfactory; with fine detail, films less than 100 Å are more suitable. The carbon is deposited on to the structure surface of the Formvar without removing the grid from the metal peg. Lastly, the Formvar film is removed by flowing about 1 ml. of chloroform over the grid from a burette, as with the acetone softening. After drying, the replica is ready for examination in the electron microscope. If shadowing is to be used, the metal must be deposited through the grid bars otherwise a "negative" picture of the surface will be obtained.

The method is also applicable to the larger pollen grains, coarse particles, etc. When such specimens are being examined, they may be dispersed in acetone and applied as a suspension on to the softened Formvar film, or, alternatively, if they are larger, they can be handled as a fibre. Another method of mounting such specimens on the Formvar is to place them on the softened film immediately after removing surplus acetone with a filter paper or by drying, and dispersing them over the film by applying further drops of the solvent.

It may be found that the final replica is contaminated by dirt which has been transferred from the original specimen to the Formvar film. This can often be removed by immersing the final carbon replica, mounted on the grid, in a solution of 1·5 g of $KMnO_4$ plus 1·5 g of $K_2Cr_2O_7$ in 15 ml. of concentrated sulphuric acid for a few minutes. The grid is washed in dilute hydrochloric acid and then water. It is desirable that this should be carried out on specimens which have not been shadowed and examined in the electron microscope. Serious contamination of the replica can usually be detected optically.

Results.—Possibly contrary to expectations, this method produces replicas giving good resolution. Fig. 1 shows a replica of the surface of a paper-making fibre in which many fibrils 100–200 Å in size can be seen. The Formvar has softened sufficiently to penetrate deep cavities, and the complex surface has been clearly reproduced.

A completely different kind of surface is shown in Fig. 2

which illustrates a replica of a pollen grain of *Bryonia dioica*. The softened film appears to be sufficiently pliable to reproduce very coarse structures, the deep cavities can be seen without any indication of artefacts.

The only artefact which is likely to be encountered is a wrinkling of the surface of the Formvar which will be reproduced in the replica. In cases where it occurs, it is easily recognizable, and areas free from this distortion can be readily found.

It is clear that the method is exceedingly simple, and can be carried out in a very short time. It should therefore be of considerable value for the examination of large numbers of specimens where a two-stage technique is permitted. It is likely that other suitable combinations of plastics and solvents could be found.

A REPLICA TECHNIQUE FOR VERY SMALL SPECIMENS

The following method has been found useful for preparing replicas of small specimens of about 0·5 to 2·0 mm in size.

An electron microscope specimen support grid is placed on a strip of 0·040 in. thick Celastoid (cellulose acetate) (Fig. 3*a*), and a drop of acetone, a solvent for the plastic, allowed to fall on the grid (Fig. 3*b*). The acetone is allowed to evaporate until the solution formed becomes slightly viscous. The specimen under examination is then placed in the liquid directly over the grid, and the whole assembly allowed to dry (Fig. 3*c*). After about ten minutes, the specimen is pulled away from the plastic with a pair of forceps, or using adhesive tape, leaving a primary impression (Fig. 3*d*). A fairly thick layer of carbon, about 200 Å thick, is now deposited on the impression (Fig. 3*e*). This constitutes the final replica. The next stage in the process is the separation of the carbon film from the Celastoid, a difficult operation since the plastic swells excessively when dissolved. It is therefore necessary to strengthen the carbon by backing it with a plastic before dissolving the Celastoid. The carbon layer is therefore flooded with a 2% solution of Formvar in chloroform, and drained vertically until the solvent has evaporated (Fig. 3*f*). Other backing materials, insoluble in acetone, may be used instead of Formvar. The grid is then cut away from the plastic strip, thus reducing the amount of Celastoid to be removed, and the time taken for its solution and hence the consequent swelling effects. This is most easily carried out using a broken razor blade to cut into the plastic beneath the grid, working round in a small circle. With a little practice, grids can be removed quickly and without damage, with only a small amount of Celastoid remaining on the under-side (Fig. 3*g*). The remaining Celastoid is now removed by placing the grid in an acetone bath for two or three minutes, and then removing it in a pair of forceps; the under-side is wiped on a filter paper, thus removing the bulk of the softened Celastoid. The grid is returned to the acetone bath for a few minutes, then removed and dried. The last traces of the plastic were washed away by flowing several millilitres of acetone over the grid from a burette (Fig. 3*h*). The final stage, the removal of the Formvar, must be carried out very carefully to avoid rupture of the carbon film. The grid is held in a pair of forceps and lowered slowly on to the surface of a chloroform bath. The solvent should just touch the underside of the grid, but on no account must it be allowed to flow over the upper surface. The grid is held thus for about one minute, then removed and dried. This procedure is then repeated twice. The third time, the grid can be totally immersed in the solvent, and is left there for a few minutes before removal. The solution of the last traces of Formvar may be achieved by prolonged immersion in a chloroform bath or by flowing the solvent over the grid from a burette.

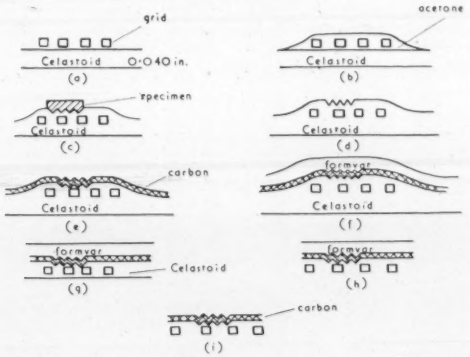

Fig. 3. Diagrammatic representation of a carbon replica method for small specimens

After the removal of the Formvar, the replica is ready for shadowing (it is again necessary to shadow through the grid bars) or examination in the electron microscope (Fig. 3*i*).

It may be found that the carbon film breaks up during the final washing process, but a close examination will show that only the area surrounding the specimen has ruptured, and that the complete grid squares are those which contain the desired replica. The probable reason for this is that the carbon film surrounding the replicated area is relatively structureless and hence less flexible than the structured region. It is thus unable to withstand the forces imposed by the washing processes. This factor has been found useful in locating the replica in the electron microscope, since only the grid squares having a covering of film are those containing the replica.

The washing technique which is used for the removal of the Formvar is also useful for dissolving away other plastics

such as Bedacryl from carbon replicas in cases where the replica is liable to fracture.

Results.—Though this replica technique is complicated, it has been found to be very reliable and has permitted the examination of specimens which could not have been replicated by any other method. In Figs. 4 and 5, the surfaces of the antenna of a honey bee, and the egg of the wheat bulb fly are shown as illustrations of the application of the method.

The antenna of a honey bee, shown in Fig. 4, is extremely smooth and remarkably free from fine structure. The majority of the surface is divided into hexagonal cells, but occasionally one encounters oval regions such as that shown in the micrograph. Here, there is a peculiar "piecrust" structure on the rim, the significance of which is not known.

Some knowledge of the sub-microstructure of the surface of the egg of the wheat bulb fly was required in connexion with a study of the water relationship of the egg. The micropilar structure of the end of the egg was of particular interest, and provided a difficult problem in replication since the egg itself was a cigar-shaped object measuring only $1 \cdot 5 \times 0 \cdot 5$ mm, and the area on the end was only about 80 μ across. However, by using the technique described, no difficulty was encountered in obtaining a good replica. It was found that the surface was very rough and coarsely porous. Such a region is shown in Fig. 5.

Although all the illustrations of the technique are of entomological specimens, the method can be used for many other objects such as thin wires, small crystals, small plant organs, geological specimens, metallurgical specimens, in fact, any specimen which is too small to examine by conventional methods.

A SINGLE-STAGE REPLICA METHOD FOR BIOLOGICAL SPECIMENS

If the single-stage carbon replica technique described by Bradley[3] is used for many soft biological specimens, it will be found that a number of practical difficulties are encountered. In this method, the specimen under examination is dried down from a suspension on to a glass microscope slide. The slide is then coated with carbon and backed with Bedacryl. The combined carbon-Bedacryl film is floated on to water, and then transferred to a bath which dissolves the specimen. It is finally washed in water, then chloroform, leaving the replica. When specimens such as bacteria are under examination, it is impossible to strip the backed carbon film from the slide. Secondly, Bedacryl will not withstand such reagents as chromic acid, which are used to dissolve organic material. If attempts are made to float an unbacked carbon film on chromic acid, it always breaks up. It is clear that some other manipulative procedure is required. A more reliable technique was used by Bradley in the study of yeast bud scars,[4] but this method has since been improved and modified so that it is of more universal application. The process is carried out as follows.

An electron microscope specimen support grid is slightly bent and placed on a $\frac{1}{8}$ in. diameter metal peg. It is then covered with a film of Formvar. A drop of a suspension of the specimen is allowed to dry on the Formvar film, or, alternatively, if the specimen is dry, a little is dusted on to the film. The grid, still on the peg, is transferred to a vacuum plant and coated with a layer of carbon about 150 Å thick. It is now necessary to dissolve the specimen from the carbon film, but, before this can be carried out, it is necessary to remove the Formvar film by washing the grid with a few millilitres of chloroform flowed over the grid from a burette. The organic specimen is finally removed by immersing the grid in a solution of $1 \cdot 5$ g of potassium permanganate and $1 \cdot 5$ g of potassium dichromate in 15 ml. of concentrated sulphuric acid. This solution should be freshly made up as it deteriorates within forty-eight hours even if kept in a stoppered bottle. It is also extremely corrosive and dangerous if it comes into contact with the skin. The acid will not react with the copper of the grid to any significant extent, and the carbon film is completely resistant to attack. The solution of even large specimens such as pollen grains is complete within about five minutes. The grid is then removed from the solution and immersed in water; it should not be released from the forceps, but moved about in the water until all the permanganate is removed from it. It is then transferred to concentrated hydrochloric acid for a few seconds to remove the manganese dioxide produced by the decomposition of the acid solution on mixing with water. It is finally washed in water and shadowed if desired.

It may be found that the carbon film floats off the grid during the washing in the hydrochloric acid or water baths. In this case, the grid is used as a lifter to transfer the film from one bath to another, where it is allowed to float on the surface for a short time in each case.

Results. This method is extremely reliable, and may be used for specimens up to about 80 μ in size. As this size is approached, it is found that most of the particles break up in the acid leaving a hole in the replicating film. Beyond 80 μ, no replicated particles can be found. The method has been used for inorganic specimens such as powders as well as for organic specimens.

An illustration of the method is shown in Fig. 6 which is a replica of spores of *Bacillus polymyxa*. The characteristic ribbing cannot be seen by examining the spore directly. The method has also been used in the study of the smaller pollen grains.

DISCUSSION

An important achievement for electron microscope replica techniques would be the ability to replicate any form of specimen which might be encountered. The methods described here contribute towards this goal and help to increase the scope of the electron microscope.

It is hoped that the method described for fibres will enable investigations involving large numbers of specimens to be carried out. The technique for small specimens is particularly important since such objects are continually being encountered and, hitherto, there has not been any effective way of studying them. Though the method is complicated, it is unlikely that any simple technique could be devised for such objects. The chief advantage of the single stage method for organic specimens is its reliability; in addition, many replicas can be prepared at the same time.

ACKNOWLEDGEMENTS

The author is grateful to Mr. D. B. Long of the Rothamsted Experimental Station for providing specimens of the wheat bulb fly egg, to Miss P. E. Rush of this Laboratory for her valuable help in developing the methods, and to Dr. T. E. Allibone, Director of the Laboratory, for permission to publish this paper.

REFERENCES

(1) DLUGOSZ, J. *Nature* [*London*], **177**, p. 515 (1956).
(2) BRADLEY, D. E. *Brit. J. Appl. Phys.*, **5**, p. 65 (1954).
(3) BRADLEY, D. E. *Brit. J. Appl. Phys.*, **5**, p. 96 (1954).
(4) BRADLEY, D. E. *J. Roy. Micro. Soc.*, **75**, p. 254 (1956).

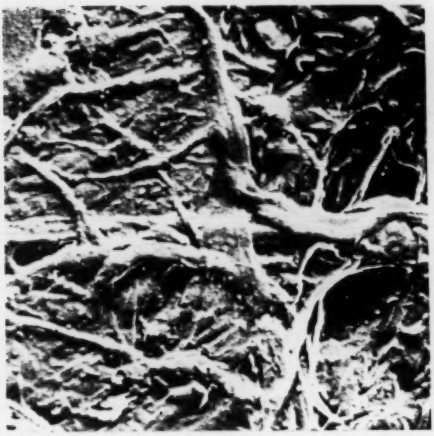

Fig. 1. Carbon replica of a paper-making fibre shadowed with gold palladium. × 27 000

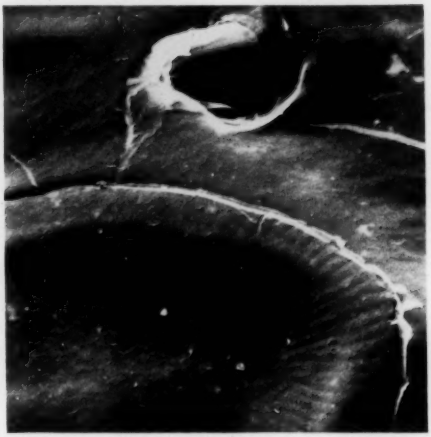

Fig. 4. Carbon replica of the surface of the antenna of a honey bee, shadowed with gold palladium. × 5 000

Fig. 2. Carbon replica of a pollen grain of *Bryonia dioica* shadowed with gold palladium. The network consists of ridges though an optical illusion may cause them to appear as furrows. × 10 000

Fig. 5. Shadowed carbon replica of the micropilar structure on the end of the egg of the wheat bulb fly. × 13 500

Fig. 6. Shadowed carbon replica of spores of *Bacillus polymyxa*.

× 15 000

[Reproduced from *Research*]

X-ray diffraction studies on precipitates and inclusions in steels using an extraction replica technique

By G. R. Booker, B.Sc., A.Inst.P., J. Norbury, B.Sc., Ph.D., F.Inst.P., and A. L. Sutton, M.A., D.Phil.

See pages 155–157

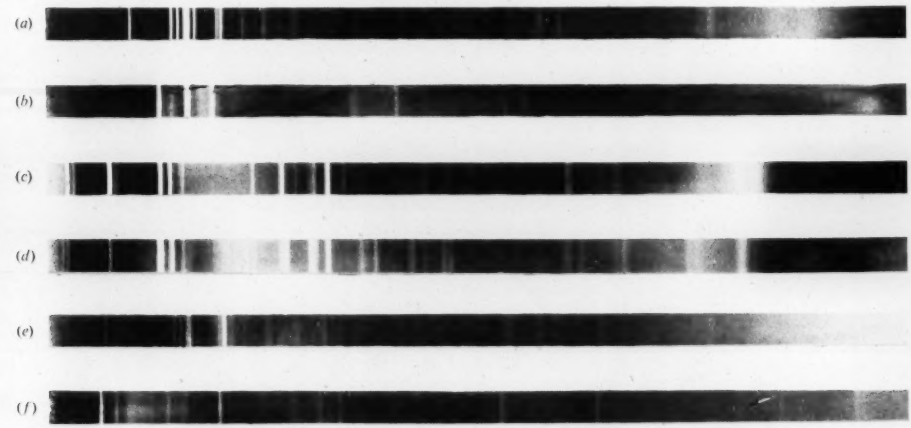

Fig. 2. X-ray powder diffraction patterns from extraction replicas taken from steels containing various types and amounts of included material. 19 cm camera, CoKα radiation

(*a*) 0·6% plain carbon steel containing coarse pearlite. Wt % of included material, 10 (estimated from carbon content). Main constituent, Fe_3C.

(*b*) Pure iron containing iron nitride precipitates. Wt % of included material, 2 (estimated from nitrogen content). Main constituents, Fe_4N and $Fe_{16}N_2$.

(*c*) Vacuum cast deoxidation series ingot containing aluminous inclusions. Wt % of included material 0·4 (estimated from bulk extraction). Main constituents, FeO, Fe_3O_4 and $FeO \cdot Al_2O_3$.

(*d*) Vacuum cast deoxidation series ingot containing siliceous inclusions. Wt % of included material, 0·35 (estimated from bulk extraction). Main constituents, FeO, Fe_3O_4, $2FeO \cdot SiO_2$ and SiO_2.

(*e*) Commercial open hearth steel. Wt % of non-metallic inclusions, 0·08 (estimated from optical microscope survey). Main constituents, Fe_3C, MnS and FeO.

(*f*) Commercial Bessemer steel. Wt % of non-metallic inclusions, 0·08 (estimated from optical microscope survey). Main constituent, MnS.

X-ray diffraction studies on precipitates and inclusions in steels using an extraction replica technique

By G. R. Booker, B.Sc., A.Inst.P., J. Norbury, B.Sc., Ph.D., F.Inst.P., and A. L. Sutton, M.A., D.Phil.,*
Research Laboratories, Richard Thomas and Baldwins Ltd., and Steel Co. of Wales Ltd., Whitchurch, Bucks.

[*Paper first received* 26 *June, and in final form* 5 *October*, 1956]

A simple extraction method is described in which precipitates and inclusions in steels can be isolated for identification by X-ray diffraction. The included material is removed from the metal surface embedded in a thin plastic replica, which is then formed into a small, compact, cylindrical specimen suitable for powder cameras. The scope of the method is discussed, and examples of the application of the method are given. Because the extraction period is only a few minutes, the method has several advantages over bulk extraction methods. In addition to the more stable constituents, iron carbide, iron nitrides and metal sulphides have been successfully extracted.

The difficulties in isolating non-metallic inclusions and precipitates from metals for identification by chemical and X-ray methods are well known. Most of these methods involve the dissolution of the metal matrix, either chemically or electrolytically, and often some of the included material is modified or dissolved during the long time it is in contact with the solvent for the matrix. Furthermore, very small particles may not be recovered from the solvent after the extraction process, and so are not present in the residue analysed.

A method has been developed which is free from these disadvantages, and allows sufficient material to be quickly extracted to give X-ray powder diffraction patterns of sufficient intensity to enable an analysis of the included material to be made. The method of extraction is similar to that described by Booker and Norbury[1] for the extraction of included materials from steels for examination by optical and electron microscopy, and electron diffraction. It is much quicker than bulk extraction techniques, does not require elaborate equipment, and only small amounts of the metal specimen are used.

EXPERIMENTAL

The method is briefly as follows. A polished section of the specimen is prepared, and given a certain optimum etch (of the order of 1–3 min) using 10% nital at room temperature. A thin Formvar film is formed on the surface, and backed with a thick collodion film to give mechanical strength. The composite film is dry-stripped, bringing with it much of the included material from the surface of the specimen, embedded in the Formvar film. The extraction replica is placed collodion side up in a bath of amyl acetate, and the backing film completely dissolved. The resulting thin Formvar film is picked up with a needle point so that the film coalesces, placed on a clean glass slide, and formed into a small cylinder, about 1 mm in diameter and a few millimetres long, whilst being dried in a feeble, warm air stream. A small amount of Canada balsam may be used to assist in binding the material together.

The small cylinder is cemented to the end of a thin glass fibre, mounted in an X-ray powder diffraction camera, and the diffraction pattern recorded in the normal manner. The exposure necessary varies according to the nature and amount of material in the extraction replica, but after some experience the greyness of the X-ray powder specimen affords some indication of the time required. Using CoKα radiation from a Raymax Rotating Anode X-ray set, and a 19 cm powder camera, exposures have varied from 1 h for very dark specimens, to 5 h for light grey specimens. Alcoholic iodine (5% in methanol) at room temperature may be used as an alternative etchant. It has approximately the same etch rate on steels as 10% nital.

SCOPE OF THE METHOD

The success of the method depends on the extraction of sufficient material in the replica to give a measurable X-ray diffraction pattern. With suitable X-radiation, the minimum amount of material necessary is considered to be about 20 μg, if the particles are sufficiently crystalline, not too small ($< 0{\cdot}1\ \mu$), and contain atoms of scattering power somewhat similar to that of iron.

The amount of material in the extraction replica depends on:

(*a*) the percentage by weight of included material in the metal specimen;

(*b*) the surface area of the metal specimen from which the replica is taken; and

(*c*) the extraction efficiency, which is related to both the shape and size distribution of the particles, and to the depth of etch.

Assuming the extraction process to be 100% efficient (i.e. all the particles that were present in the portion of the matrix dissolved by the etchant become entrapped in the plastic), the general depth of etch to be 5 μ (which is roughly correct for mild steel etched for 3 min in 10% nital), and the average specific gravity of the matrix to be eight, the total weight of material extracted by the replicas for various weights per cent of included material in the metal specimen, and for various surface areas of extraction, has been calculated, and is depicted graphically in Fig. 1. The broken line represents the minimum amount of material which is considered to be necessary for successful X-ray powder diffraction.

Hence, it may be predicted (if an extraction efficiency of 100% is assumed) that specimens containing included material in the range 1–10% by weight should give an

* Now at Research Laboratories, General Electric Co. Ltd., Wembley, Middlesex.

abundance of material for X-ray diffraction; material in the range 0·1–1% should be adequate; and material in the range 0·01–0·1% should also be adequate provided a

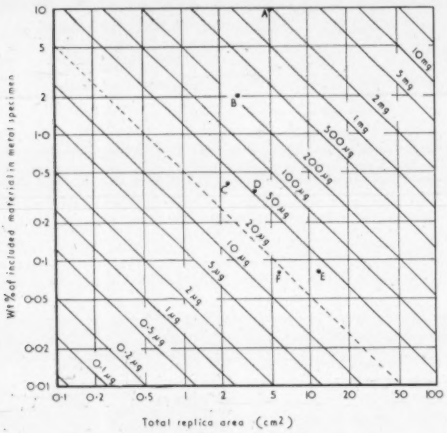

Fig. 1. Graph showing the relationship between the weight percentage of included material in the metal specimen, the replica area, and the weight of included material in the replica, assuming (1) an extraction efficiency of 100%, and (2) a 5 μ depth of etch. Points *A*, *B*, *C*, *D*, *E* and *F* indicate the theoretical amounts of extracted material in the replicas, whose diffraction patterns are shown in Fig. 2

A, pearlite steel; *B*, nitrided pure iron; *C*, aluminium deoxidised ingot; *D*, silicon deoxidised ingot; *E*, open hearth steel; *F*, Bessemer steel.

sufficiently large area of metal specimen is used for extraction. Non-metallic inclusions in commercial steels, reported to be in the range 0·03–0·15%, come within these limits.

The method has been applied to several materials. Details of some of the extraction replicas and diffraction patterns are given in the table and Fig. 2. Figs. 2(*a*) and (*b*) relate to materials containing large amounts of precipitates, Figs. 2(*c*) and (*d*) to materials known to contain only non-metallic inclusions, and Figs. 2(*e*) and (*f*) to commercial steels containing both types of included material.

Points *A* to *F* in Fig. 1 correspond to the extraction replicas from these specimens. The quality of the X-ray diffraction patterns, particularly those from replicas corresponding to points *E* and *F*, which are very near to the minimum amount of material considered necessary to give adequate patterns, indicates that the experimental extraction efficiency attained is high. The graph may therefore be used for estimating the area of replica necessary to give a reasonable diffraction pattern when the weight per cent of included material in the metal is known.

Where constituents of the included material have much the same particle size, the extraction efficiencies are similar, and the relative amounts of each deduced from the X-ray pattern from extraction replicas will be close to the true values. For example, the relative amounts of inclusions in the extraction replicas determined from the X-ray patterns of Figs. 2(*c*) and (*d*) are in good agreement with the results of Sloman and Evans[2,3] for bulk extraction residues.

On the other hand, if the particle size of one of the constituents is much less than the remainder, the optimum etch time for that constituent will not be the same as for the others. A second extraction replica using a shorter etch time may allow that constituent to be isolated and identified.

The very short time, compared with bulk extraction methods, for which the material is in contact with the etchant, enables more types of inclusions to be isolated without modification. Amongst the types of material which have been successfully extracted from steels and identified are iron carbide (Fe_3C), iron nitride (Fe_4N and $Fe_{16}N_2$), ferrous oxide (FeO), magnetite (Fe_3O_4), alumina (Al_2O_3), hercynite ($FeO \cdot Al_2O_3$), silica (SiO_2), fayalite ($2FeO \cdot SiO_2$), manganese oxide (MnO), manganese sulphide (MnS), tephroite ($2MnO \cdot SiO_2$), iron sulphide (FeS) and graphite (C). Some of these substances, e.g. iron carbide, iron nitrides and metal sulphides, are modified or completely dissolved in normal bulk extraction methods.

With suitable choice of etchants, this extraction method could be used to isolate included material and precipitated phases in other metals for examination by X-ray diffraction.

Data concerning the specimens, extraction replicas, and diffraction patterns used to illustrate the method

Figure	Specimen		Extraction replica			Diffraction pattern			
	Type	Wt. % of included mat.	Area cm²	Etchant	Time (min)	Exposure hours	No. of lines measured	No. of constituents identified	No. of lines unidentified
2(*a*)	Pearlite steel	10 (*E*)	5·0	10% nital	2	2¼	34	1	1
2(*b*)	Nitrided pure iron	2 (*E*)	2·8	10% nital	3	3½	19	3	3
2(*c*)	Al deoxidised ingot	0·4 (*B*)	2·3	10% nital	3	4	31	3	4
2(*d*)	Si deoxidised ingot	0·35 (*B*)	3·8	10% nital	3	3	43	4	10
2(*e*)	Commercial open hearth steel	0·08* (*E*)	12	10% nital	3	2½	47	5	8
2(*f*)	Commercial Bessemer steel	0·08* (*E*)	5·8	10% nital	3	5	17	3	4

E, estimated *B*, bulk extraction * disregarding iron carbide

ACKNOWLEDGEMENTS

The authors are indebted to Mr. H. A. Sloman, who kindly provided the deoxidation series illustrated in Figs. 2(*c*) and 2(*d*). They wish to thank Mr. C. A. Stratfull and Mr. P. J. Little for assistance with the experimental work.

Thanks are also due to Mr. R. A. Hacking, Director of Research, for permission to publish this paper.

REFERENCES

(1) BOOKER, G. R., and NORBURY, J. *Brit. J. Appl. Phys.*, **8**, p. 109 (1957).
(2) SLOMAN, H. A., and EVANS, E. L. *J. Iron Steel Inst.*, **165**, p. 81 (1950).
(3) EVANS, E. L., and SLOMAN, H. A. *J. Iron Steel Inst.*, **172**, p. 296 (1952).

On the mathematical theory of zone-melting

By I. BRAUN, and S. MARSHALL, H. H. Wills Physical Laboratory, University of Bristol

[*Paper first received* 13 *November, and in final form* 27 *December*, 1956]

A complete solution is presented of the equations governing the redistribution of solutes in zone-melting processes. The effect of "normal freezing" in the last zone-length of a bar is treated rigorously. The solutions hold for all values of the distribution coefficient k. Numerical calculations have been made of the concentration profiles resulting from repeated zone-melting, and specimen graphs are given.

Since the original paper of Pfann[1] which stated the basic principles of zone-melting, several mathematical treatments of the subject have been published.[2-4] While for most practical purposes these are adequate, none of them is entirely rigorous or of general applicability. It was felt, therefore, that a general solution of the equations of zone-melting for a finite bar, taking into account the effect of normal freezing in the last zone-length, would be of some interest and possibly of practical value.

The elementary principles of zone-melting will not be recapitulated, since they have been given in the literature quoted. For simplicity, the idealized conditions specified by Pfann have been assumed to apply at all stages of the processes. The notation used is as follows:

x, distance along the bar, measured in zone-lengths from the starting end;

p, integration variable, equivalent to x;

N, total length of the bar in zone-lengths;

$C_n^{(N-m)}(x)$, concentration of solute, relative to the original average concentration in the bar, after the nth zone-pass, at the point x, which lies in the $(N-m)$th zone of the bar. (See Fig. 1.) The bar is assumed to be an integral number of zone-lengths long and divided into zones of unit length starting from $x = 0$, each being designated by the co-ordinate of its starting point. The numbering of the zones is thus from 0 to $N-1$. Thus the function $C_n^{(N-m)}(x)$ represents the solute concentration defined only in the range $N-m \leqslant x \leqslant N-m+1$.

Analytical expressions for the solute concentration in a semi-infinite bar, or in those regions of a terminated bar not affected by the termination, for any number of zone-passes, have been given by Lord.[2] The present work takes into account the fact that the theoretical solute distribution in a finite bar differs from that in an infinite bar in the last n zone-lengths, where n is the number of completed zone-passes, since the effect of normal freezing in the last zone is carried back through one zone-length at each pass. Thus Lord's solutions apply up to the point $x = N-n$, beyond which the effect of the termination is felt. The concentration values given by Lord's equations, in the regions to which they apply, will be made use of in the following theory, and denoted by $\bar{C}(x)$.

THEORY

The basic equations of zone-melting will be written for purposes of the present work in the form:

$$C_n(x) = k \exp(-kx)\left\{\int_1^{x+1} C_{n-1}(p) \cdot \exp[k(p-1)] \cdot dp + \int_0^1 C_{n-1}(p) \cdot dp\right\} \qquad 0 \leqslant x \leqslant N-1 \quad (1)$$

$$C_n(x) = (N-x)^{k-1} \cdot C_n(N-1) \qquad N-1 \leqslant x \leqslant N \quad (2)$$

The solute distribution represented by equation (2), which always exists in the last zone to freeze in the bar, will be referred to as the "normal freezing distribution."

Putting $x = N-m$ in equation (1), and combining the result with the original equation for general x by elimination of the second integral, we have:

$$C_n(x) = C_n(N-m) \cdot \exp[-k(x-N+m)] + k \cdot \exp(-kx) \cdot \int_{N-m+1}^{x+1} C_{n-1}(p) \cdot \exp[k(p-1)] \cdot dp \quad (3)$$

If we restrict this equation to the $(N-m)$th zone, it has the form:

$$C_n^{(N-m)}(x) = C_n(N-m) \cdot \exp[-k(x-N+m)] + k \cdot \exp(-kx) \cdot \int_{N-m+1}^{x+1} \bar{C}_{n-1}^{(N-m+1)}(p) \cdot \exp[k(p-1)] \cdot dp \quad (4)$$

This equation shows that the solute distribution in a given zone after n zone-passes [i.e. $C_n^{(N-m)}(x)$] can be calculated exactly, from a knowledge of:

(*a*) the form of the distribution after the previous pass in the next zone along, and

(*b*) the value of the concentration at the beginning of the zone in question.

To use equation (4) it is necessary, then, to calculate the distributions successively with increasing values of n, starting with $C_0(x) = 1$. Each computation must be made progressively zone by zone; the value of the concentration at

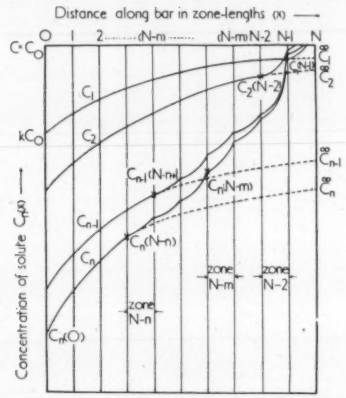

Fig. 1. Concentration profiles after repeated zone-melting. Full lines are for terminated bar of N zones. These curves are schematic, qualitatively correct for the exaggerated form of the discontinuities. Dotted lines are for semi-infinite bar

the last point in any zone provides the starting point for the computation in the next zone. The initial value is obtained in one of the following two ways.

(*a*) If $n \leqslant N$, Lord's equations[1] may be used to calculate $C_n(x)$ from $x = 0$ to $x = N - n$ by the relation:

$$\overset{\infty}{C}_n(x) = C_0\left\{1 - (1-k)\,.\,\exp(-kx)\,.\left[n - \sum_{t=1}^{n-1}\sum_{s=1}^{t} k^{s-1}\,.\,\exp(-sk)\,.\sum_{r=0}^{s-1} f_r(s)\,.\,x^r\,.(r+1-kx)\right]\right\}$$

where

$$f_r(s) = \frac{s^{s-r-2}}{(s-r-1)!\,r!}$$

We denote here by $\overset{\infty}{C}_n(x)$ the concentration distribution of a semi-infinite bar after n zone-passes. The concentration distribution of a finite bar $C_n(x)$ is an analytic function up to $x = N - n$; after this point $C_n(x)$ is a piecewise analytic function with singularities at the end points of every region.

(*b*) If $n > N$, the equations for the semi-infinite bar no longer apply in any region, but the starting point at $x = 0$ can always be computed, according to equation (1), by the integral

$$C_n(0) = k\,.\int_0^1 \overset{0}{C}_{n-1}(p)\,.\,dp \qquad (6)$$

SOLUTIONS FOR THE FIRST THREE PASSES

First pass. The first $(N-1)$ zones have a solute distribution given by equation (5) and the last zone solidifies by normal freezing according to equation (2):

$$C_1^{(N-1)}(x) = \overset{\infty}{C}_1(N-1)\,.\,(N-x)^{k-1} \quad (N-1) \leqslant X \leqslant N \qquad (7)$$

since $C_1(N-1) = \overset{\infty}{C}_1(N-1)$. This value must be computed by equation (5).

Second pass. The function $C_2^{(N-2)}(x)$ must be calculated by integration of $C_1^{(N-1)}(x)$. Substitution of $n = 2$, $m = 2$ in equation (4) and with equation (7) gives:

$$C_2^{(N-2)}(x) = \overset{\infty}{C}_2(N-2)\,.\,\exp\left[-k(x-N+2)\right] + \overset{\infty}{C}_1(N-1)\,.\,k\,.\,\exp(-kx)\,.\int_{N-1}^{x+1}(N-p)^{k-1}\,.\,\exp\left[k(p-1)\right].dp$$

since $C_2(N-2) = \overset{\infty}{C}_2(N-2)$. By changing the variable under the integral of the last equation so that $z = N - p$, we obtain:

$$C_2^{(N-2)}(x) = \overset{\infty}{C}_2(N-2)\,.\,\exp\left[-k(x-N+2)\right] + k\,.\,\overset{\infty}{C}_1(N-1)\,.\,\exp\left[-k(x-N+1)\right]\int_{N-x-1}^{1} p^{k-1}\,.\,\exp(-kp)\,.\,dp$$

and since

$$\int p^{k-1}\,.\,\exp(-kp)\,.\,dp = \exp(-kp)\,.\left[\frac{p^k}{k} + \frac{kp^{k+1}}{k\,.\,(k+1)} + \frac{k^2p^{k+2}}{k\,.\,(k+1)\,.\,(k+2)} + \ldots\right]$$

we get finally

$$C_2^{(N-2)}(x) = \left[\overset{\infty}{C}_2(N-2) + \overset{\infty}{C}_1(N-1)\,.\,k\,.\,F_1(1)\right].\exp\left[-k(x-N+2)\right] - k\,.\,\overset{\infty}{C}_1(N-1)\,.\,F_1(N-x-1) \qquad (N-2) \leqslant x \leqslant (N-1) \qquad (8)$$

with

$$F_1(u) = u^k\,.\sum_{r=0}^{\infty}\frac{(u\,.\,k)^r}{k\,.\,(k+1)\,.\,(k+2)\ldots(k+r)} \qquad (8a)$$

where $u = N - x - 1$ and $F_1(1)$ is the value of $F_1(u)$ for $u = 1$. It is easy to verify that equation (8*a*) can also be written in the form

$$F_1(u) = k\int_0^u F_0(z)\,.\,dz + k^2\int_0^u\int_0^u F_0(z)\,.\,(dz)^2 + k^3\int_0^u\int_0^u\int_0^u F_0(z)\,.\,(dz)^3 + \ldots \qquad (8b)$$

with

$$F_0(z) = \frac{z^{k-1}}{k}$$

Equation (8) together with equation (8*a*) provides the value of $C_2(N-1)$ for $x = N - 1$:

$$C_2^{(N-2)}(N-1) \equiv C_2(N-1) = \left[\overset{\infty}{C}_2(N-2) + \overset{\infty}{C}_1(N-1)\,.\,k\,.\,F_1(1)\right].\exp(-k) \qquad (9)$$

The last zone solidifies according to equation (2):

$$C_2^{(N-1)}(x) = C_2(N-1) \,.\, (N-x)^{k-1} \qquad (10)$$

where $C_2(N-1)$ is given by equation (9). Note that $C_2(N-1) \neq \overset{\infty}{C}_2(N-1)$.

Third pass. The distributions in the zones $(N-3)$, $(N-2)$ and $(N-1)$ are required since in the lower zones Lord's equations (5) can be applied. By starting with the first zone where the effect of the end is felt, we have by substituting in equation (4) $n = 3$, $m = 3$:

$$C_3^{(N-3)}(x) = \overset{\infty}{C}_3(N-3) \,.\, \exp\left[-k(x-N+3)\right] + \\ + k \,.\, \exp(-kx) \,.\, \int_{N-2}^{x+1} C_2^{(N-2)}(p) \,.\, \exp\left[k(p-1)\right] \,.\, dp$$

By substituting equation (8) with equation (8*a*) into the last equation and on integration:

$$C_3^{(N-3)}(x) = \left\{ \overset{\infty}{C}_3(N-3) - \overset{\infty}{C}_1(N-1) \,.\, k \,.\, F_2(1) + \right. \\ + \left[\overset{\infty}{C}_2(N-2) + \overset{\infty}{C}_1(N-1) \,.\, k \,.\, F_1(1) \right] \cdot \\ \left. k \,.\, (x-N+3) \right\} \,.\, \exp\left[-k(x-N+3)\right] + \\ + \overset{\infty}{C}_1(N-1) \,.\, k \,.\, F_2(N-x-2) \\ (N-3) \leqslant x \leqslant (N-2) \qquad (11)$$

where

$$F_2(u) = u^k \,.\, \sum_{r=1}^{\infty} \frac{r \,.\, k^r \,.\, u^r}{k \,.\, (k+1) \,.\, (k+2) \,.\, \ldots \,.\, (k+r)} \qquad (11a)$$

with $u = N - x - 2$. $F_2(u)$ can also be written in the form:

$$F_2(u) = k \,.\, \int_0^u F_1(z) \,.\, dz + k^2 \,.\, \int_0^u \int_0^u F_1(z) \,.\, (dz)^2 + \\ + k^3 \,.\, \int_0^u \int_0^u \int_0^u F_1(z) \,.\, (dz)^3 + \ldots \qquad (11b)$$

where $F_1(z)$ is given by equation (8*a*). $C_3^{(N-2)}(x)$ is deduced analogously to $C_2^{(N-2)}(x)$, the expression obtained is similar to equation (8):

$$C_3^{(N-2)}(x) = \left[C_3(N-2) + \right. \\ \left. + C_2(N-1) \,.\, k \,.\, F_1(1) \right] \,.\, \exp\left[-k(x-N+2)\right] - \\ - C_2(N-1) \,.\, k \,.\, F_1(N-x-1) \\ (N-2) \leqslant x \leqslant (N-1) \qquad (12)$$

Also $C_3^{(N-1)}(x)$ is similar to equation (10) and is given with equation (2) by the expression

$$C_3^{(N-1)}(x) = C_3(N-1) \,.\, (N-x)^{k-1} \qquad (13)$$

where $C_3(N-1)$ is deduced from equation (12) for $x = N-1$.

GENERAL SOLUTION

By continuing as above for $C_4^{(N-4)}(x)$, $C_4^{(N-3)}(x)$, etc., we get by induction general formulae. We shall first give the solution for the $(N-n)$th zone, which is the first in which the distribution differs from that in a semi-infinite bar. By repeated application of equation (4), by starting with the zone $(N-n)$, progressing through one zone-length at each stage, we obtain the general formula for the nth pass in the $(N-n)$th zone:

$$C_n^{(N-n)}(x) = \exp\left[-k(x-N+n)\right] \,.\, \sum_{s=0}^{n-2} \frac{k^s}{s!} \,.\, (x-N+n)^s \,.\, \\ \left[\overset{\infty}{C}_{n-s}(N-n+s) + (-1)^{n-s} \,.\, \overset{\infty}{C}_1(N-1) \,.\, k \,.\, F(1)_{n-s-1} \right] + \\ + (-1)^{n-1} \,.\, \overset{\infty}{C}_1(N-1) \,.\, k \,.\, F_{n-1}(N-x-n+1) \\ (N-n) \leqslant x \leqslant (N-n+1) \qquad (14)$$

where the functions denoted by $F_q(u)$ are given by the recurrence formula:

$$F_q(u) = k \,.\, \int_0^u F_{q-1}(p) \,.\, dp + k^2 \,.\, \int_0^u \int_0^u F_{q-1}(p) \,.\, (dp)^2 + \\ + k^3 \int_0^u \int_0^u \int_0^u F_{q-1}(p) \,.\, (dp)^3 + \ldots$$

or

$$F_q(u) = \sum_{r=1}^{\infty} k^r \,.\, \underbrace{\int_0^u \int_0^u \ldots \int_0^u}_{r} F_{q-1}(p) \,.\, (dp)^r \\ \text{with } u = N-x-n+1 \qquad (15)$$

By starting with

$$F_0(u) = \frac{u^{k-1}}{k} \quad \text{[see equations (8}b\text{) and (11}b\text{)]} \quad 0 \leqslant u \leqslant 1 \qquad (16)$$

we get successively all the $F_q(u)$-functions:

$$F_1(u) = \frac{1}{k} u^k + \frac{k}{k \,.\, (k+1)} u^{k+1} + \\ + \frac{k^2}{k \,.\, (k+1) \,.\, (k+2)} u^{k+2} + \ldots \qquad (16a)$$

in accordance with equation (8*a*)

$$F_2(u) = \frac{k}{k \,.\, (k+1)} u^{k+1} + \frac{2k^2}{k \,.\, (k+1) \,.\, (k+2)} u^{k+2} + \\ + \frac{3k^3}{k \,.\, (k+1) \,.\, (k+2) \,.\, (k+3)} u^{k+3} + \ldots \qquad (16b)$$

in accordance with equation (11*a*), etc., for higher values of q. Every series is of higher order than the preceeding one. Equation (15) together with equation (16) can easily be transformed to the general formula

$$F_q(u) = u^k \,.\, \sum_{r=0}^{\infty} \frac{\binom{q+r-1}{r} \,.\, (k \,.\, u)^{q+r-1}}{k \,.\, (k+1) \,.\, \ldots \,.\, (k+q+r-1)} \\ \text{with } q = 1, 2, 3 \ldots \qquad (17)$$

where

$$\binom{q+r-1}{r} = \frac{(q+r-1)!}{(q-1)!\,r!} \qquad (17a)$$

For a bar of n zone-lengths, in the case of $n \leqslant N$, $n-1$ different $F_q(u)$-functions are needed for the computation of $C_n(x)$; in the case of $n > N$, $N-1$ different $F_q(u)$-functions must be computed, even if n takes increasingly larger values.

Equation (14) gives us for $x = N-n+1$ the starting point for the concentration distribution in the $(N-n+1)$th region. Knowing this value by successive application of

equation (4) we get the distribution in the $(N-n+1)$th region. In general, we get, for the solution distribution after the nth zone-pass at a point in the $(N-m)$th zone, by repeated application of equation (4):

$$C_n^{(N-m)}(x) = \exp\left[-k(x-N+m)\right].\sum_{s=0}^{m-2} a_{n-s}^{m-s}\cdot\frac{k^s}{s!}.(x-N+ +m)^s + (-1)^{m-1}.C_{n-m+1}(N-1).F_{m-1}(N-x-m+1) \quad (N-m) \leqslant x \leqslant (N-m+1) \quad (18)$$

for $m \geqslant 2$ and $n-m+1 > 0$.

where the coefficients a_{n-s}^{m-s} denote the constants already used in earlier stages of the zone-melting process:

$$a_{n-s}^{m-s} = C_{n-s}(N-m+s) + (-1)^{m-s}.\ C_{n-m+1}(N-1).k.F_{m-s-1}(1) \quad (18a)$$

The constants $F_{m-s-1}(1)$ are calculated by equation (15) for $u=1$, the function $F_{m-1}(N-x-m+1)$ is also calculated by equation (15) for $u = N-x-m+1$.

If $n > N$, equation (18) can still be applied, only the starting value of the curve in the lowest region (o) must be calculated by equation (6). Since, in accordance with equation (15), $C_n^0(x)$ is always an integrable function, we get from equation (6) after integration for any n:

$$C_n(0) = -\exp(-k)\sum_{s=0}^{N-2} a_{n-1-s}^{N-2}.\left(1+k+\ldots+\frac{k^s}{s!}\right) - \sum_{s=0}^{N-2} a_{n-1-s}^{N-2} - (-1)^N.k^2.C_{n-N}(N-1\int_0^1 F_{N-1}(p)dp \quad (19)$$

where the constants a_{n-1-s}^{N-s} are given by equation (18a). The integral in the last term in equation (19) is a definite number, since the functions given in equation (17) are convergent power series.

It may be seen that equation (14) is a special form of equation (18) for $m=n$, where $C_{n-s}(N-n+s) = \overset{\infty}{C}_{n-s}$ $(N-n+s)$.

In theory it would be possible to express all the $C_n^{(N-m)}(x)$-functions as functions of k, N, m and n, but the total result would be extremely cumbersome. Therefore the successive computation was used.

The complete theory of the ultimate distribution (if $n \to \infty$) will be published later.

NUMERICAL CALCULATIONS

The foregoing equations for the concentration distributions in the various zones have been used to compute the two cases:

case (i) $N = 10$, $k = 0{\cdot}1$, $n = 1$, 2 and 3; and
case (ii) $N = 5$, $k = 0{\cdot}3$, $n = 1$ to 10.

The results are shown in Figs. 2 and 3. (For details see Appendix.) The following conclusions may be drawn:

Case (i). For a longer bar the concentration curves deviate only in the last three zones sensibly from the concentration curves of a semi-infinite bar. For comparison both curves have been drawn.

Case (ii). The effect of the termination of the bar is felt at the beginning of the bar when $n = 6$, and more strongly for higher values of n.

The slope of the curves as n increases approaches the slope of the renormalized Pfann-distribution denoted by $\overset{\infty}{C}_\infty(x)$. This function was deduced by Pfann[1]:

$$\overset{\infty}{C}_\infty(x) = A.\exp(Bx) \quad \text{where } k = \frac{B}{\exp(B)-1}$$

which represents a distribution of impurity which would be invariant after further zone-passes in a semi-infinite bar.

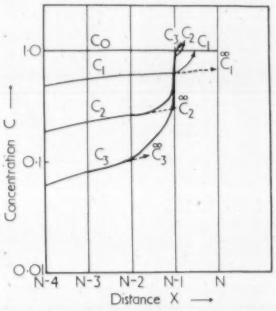

Fig. 2. Concentration profiles in a zone-melted rod $N = 10$, $k = 0{\cdot}1$

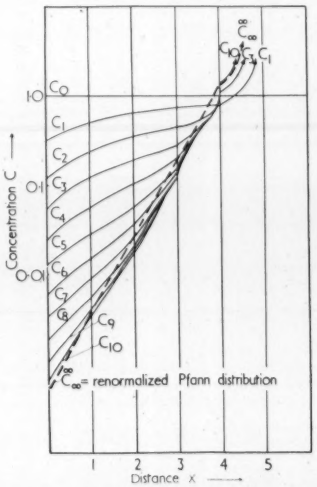

Fig. 3. Concentration profiles in a zone-melted rod $N = 5$, $k = 0{\cdot}3$.

We have modified this function by assuming it to apply up to $x = N-1$, after which the last zone solidifies by normal freezing. The constant A is determined so that the integral of the function over the whole region gives the total impurity concentration. It is seen from Fig. 3 that the curves themselves diverge from this distribution for higher values of x.

It appears that the curves have slight curvatures in each zone, the successive curves being similar in the same region. The curves are very similar to those published by Burris, Stockmann and Dillon,[4] where numerical integration was used throughout.

ACKNOWLEDGEMENTS

The authors are greatly indebted to Prof. F. C. Frank for invaluable discussions throughout the work. One of the authors (I. B.) is indebted to the Technion Society of Great Britain for a grant and the other (S. M.) is indebted for a maintenance grant from the Department of Scientific and Industrial Research.

REFERENCES

(1) Pfann, W. G. *J. Metals, N.Y.*, **4**, p. 747 (1952).
(2) Lord, N. W. *J. Metals, N.Y.*, **5**, p. 1531 (1953).
(3) Reiss, H. *J. Metals, N.Y.*, **6**, p. 1053 (1954).
(4) Burris, L., Stockman, C. H., and Dillon, I. G. *J. Metals, N.Y.*, **7**, p. 1017 (1955).

APPENDIX

To make numerical calculations easier, a detailed example is given. Lord's equation (5) can always be applied for any pass $n < N$ up to the point $x = N - n$, where we still have $C_n(N-n) = \overset{\infty}{C}_n(N-n)$. This point is always the starting point from which the concentration profiles are given by equation (18). In the last $(N-1)$th zone we have the "normal freezing distribution" given by equation (2). The value of $C_n(N-1)$ is given by the end-point of the function $C_n^{(N-2)}(x)$ for $x = N-1$, with $C_n^{(N-2)}(N-1) \equiv C_n(N-1)$.

In general the concentration profiles for different passes n in the same $(N-m)$th zone are similar and are given by the following formulae:

(i) *In the* $(N-2)$*th zone*, i.e. $m = 2$ or $N-2 \leqslant x \leqslant N-1$. We have for

$n = 1$, Lord's equation (5) up to $C_1(N-1) = \overset{\infty}{C}_1(N-1)$

$n = 2$, in accordance with equation (18):

$$C_2^{(N-2)}(x) = a_2^2 \exp(-ku) - k \,.\, \overset{\infty}{C}_1(N-1)\,.\,F_1(1-u)$$

$n = 3$,

$$C_3^{(N-2)}(x) = a_3^2 \exp(-ku) - k \,.\, C_2(N-1)\,.\,F_1(1-u)$$

with $u = x - N + 2$

$n = n$,

$$C_n^{(N-n)}(x) = a_n^2 \exp(-ku) - k \,.\, C_{n-1}(N-1)\,.\,F_1(1-u) \tag{20}$$

where the coefficients are given in accordance with equation (18*a*) by

$$a_2^2 = \overset{\infty}{C}_2(N-2) + k \,.\, \overset{\infty}{C}_1(N-1)\,.\,F_1(1)$$
$$a_3^2 = C_3(N-2) + k \,.\, C_2(N-1)\,.\,F_1(1)$$
$$a_n^2 = C_n(N-2) + k \,.\, C_{n-1}(N-1)\,.\,F_1(1)$$

The concentrations at the point $x = N-1$ or $u = 1$ are given in accordance with equation (20):

$$C_n^{(N-2)}(N-1) = C_n(N-1) = a_n^2 \,.\, \exp(-k)$$

since $F_1(0) = 0$. These values are needed to calculate the concentration profiles in the $(N-1)$th zone.

(ii) *In the* $(N-3)$*th zone*, i.e. $m = 3$ or $N-3 \leqslant x \leqslant N-2$. For

$n = 1$, Lord's equation (5) must be applied as well as for $n = 2$ up to the point $x = N-2$, where we still have $C_2(N-2) = \overset{\infty}{C}_2(N-2)$. For $n > 2$ we get with equation (18) for

$n = 3$,

$$C_3^{(N-3)}(x) = \left[a_3^3 + k \,.\, a_2^2 u\right] . \exp(-ku) + k \,.\, \overset{\infty}{C}_1(N-1)\,.\,F_2(1-u)$$

$n = 4$,

$$C_4^{(N-3)}(x) = \left[a_4^3 + k \,.\, a_3^2 \,.\, u\right] . \exp(-ku) + k \,.\, C_2(N-1)\,.\,F_2(1-u)$$

$n = n$,

$$C_n^{(N-3)}(x) = \left[a_n^3 + k \,.\, a_{n-1}^2 \,.\, u\right] . \exp(-ku) + k \,.\, C_{n-2}(N-1)\,.\,F_2(1-u) \tag{22}$$

with $u = x - N + 3$, where the coefficients are given for any n by:

$$a_n^3 = C_n(N-3) - k \,.\, C_{n-1}(N-1)\,.\,F_2(1) \tag{23}$$

For $x = N-2$, or $u = 1$, we get again the starting points for the concentration profiles in the $(N-2)$th zone.

(iii) *In the* $(N-4)$*th zone*, i.e. $m = 4$ or $N-4 \leqslant x \leqslant N-3$. For any $n < N$ up to the point $C_n(N-4)$, we again use Lord's equation (5). For $n > 3$, equation (18) is applied and we get for any pass n:

$$C_n^{(N-4)}(x) = \left[a_n^4 + k \,.\, a_{n-1}^3 \,.\, u + \frac{k^2}{2!} \,.\, a_{n-2}^2 \,.\, u^2\right] . \exp(-ku) - k \,.\, C_{n-3}(N-1)\,.\,F_3(1-u) \tag{24}$$

with $u = x - N + 4$ and the coefficients given by equation (18*a*).

(iv) *In the* $(N-5)$*th zone*, i.e. $m = 5$ or $N-5 \leqslant x \leqslant N-4$. We get again for $n > 4$:

$$C_n^{(N-5)}(x) = \left[a_n^5 + k \,.\, a_{n-1}^4 \,.\, u + \frac{k^2}{2!} \,.\, a_{n-2}^3 u^2 + \frac{k^3}{3!} \,.\, a_{n-3}^2 \,.\, u^3\right] . \exp(-ku) + k \,.\, C_{n-4}(N-1)\,.\,F_4(1-u) \tag{25}$$

with $u = x - n + 5$, and so on for the lower zones.

As a concrete example let us calculate $C_6(x)$ in the case of $N = 5$ (see Fig. 3), knowing already the whole concentration profiles up to $C_5(x)$. Since $N = 5$, $m_{max} = 4$, we need only the functions $F_1(u)$, $F_2(u)$, $F_3(u)$ and $F_4(u)$ in accordance with equation (20), (22), (24) and (25). The functions $F_1(u)$ and $F_2(u)$ have been calculated and are given by equation (16*a*) and (16*b*). $F_3(u)$ and $F_4(u)$ are calculated by equation (17) with $q = 3$ and $q = 4$ and we get:

$$F_3(u) = \frac{k^2}{k\,.\,(k+1)\,.\,(k+2)} u^{k+2} + \frac{3k^3}{k \ldots (k+3)} u^{k+3} + \frac{6k^4}{k \ldots (k+4)} u^{k+4} + \ldots \tag{26}$$

and

$$F_4(u) = \frac{k^3}{k \ldots (k+3)} u^{k+3} + \frac{4k^4}{k \ldots (k+4)} u^{k+4} + \\ + \frac{10k^5}{k \ldots (k+5)} u^{k+5} + \ldots \quad (27)$$

For the starting point $C_6(0)$ we can no longer apply Lord's equation (5) since $n = 6 > N = 5$. Therefore equation (19) must be applied for $N = 5$, $n = 6$, $m = 5$:

$$C_6(0) = -\exp(-k) \cdot \left[a_5^5 + (1+k) \cdot a_4^4 + \right. \\ \left. + \left(1 + k + \frac{k^2}{2}\right) \cdot a_3^3 + \left(1 + k + \frac{k^2}{2} + \frac{k^3}{3}\right) \cdot a_2^2 \right] + \\ + a_5^5 + a_4^4 + a_3^3 + a_2^2 + k^2 \cdot \overset{\infty}{C_1}(n-1) \cdot \int_0^1 F_4(p) \cdot dp \quad (28)$$

with

$$\int_0^1 F_4(p) \cdot dp = \frac{k^3}{k \ldots (k+4)} + \frac{4k^4}{k \ldots (k+5)} + \\ + \frac{10k^5}{k \ldots (k+6)} + \ldots \quad (29)$$

This same integral is needed for every $C_n(0)$ for $n > N$. The coefficients of equation (28) are all related to the values of the previous curves $C_1(x)$ to $C_5(x)$. Knowing the value of $C_6(0)$ we can calculate $C_6(x)$ in the (0)th zone, i.e. for $0 \leqslant x \leqslant 1$. With equation (25) we get for $N = 5$, $n = 6$ $(m = 5)$:

$$C_6^{(N-5)}(x) = C_6^{(0)}(x) = \left(a_6^5 + k \cdot a_5^4 \cdot x + \frac{k^2}{2!} \cdot a_4^3 \cdot x^2 + \right. \\ \left. + \frac{k^3}{3!} \cdot x^3 \cdot a_3^2 \right) \cdot \exp(-kx) + k \cdot C_2(4) \cdot F_4(1-x) \quad (30)$$

Only the coefficient a_6^5 contains $C_6(0)$, the other coefficients are related to $C_1(x)$ to $C_5(x)$. For $x = 1$ we get $C_6(1)$ from equation (30). This value is needed for the computation of $C_6^{(1)}(x)$ in the first zone. With equation (24) we get for $1 \leqslant x \leqslant 2$:

$$C_6^{(N-4)}(x) = C_6^{(1)} = \left(a_6^4 + k \cdot a_5^3 \cdot u + \right. \\ \left. + \frac{k^2}{2} \cdot a_4^2 \cdot u^2 \right) \cdot \exp(-ku) - k \cdot C_3(4) \cdot F_3(1-u)$$

with $u = x - 1$. For $x = 2$ or $u = 1$ we get from this last equation $C_6(2)$, a value needed for the computation of $C_6^{(N-3)}(x) = C_6^{(2)}(x)$. So progressing zone by zone we get the whole concentration profile of $C_6(x)$.

A method for the measurement of heat generation in powdered coal

By P. C. Newman, M.A., A.Inst.P.,* National Coal Board, Stoke Orchard, Glos.

[*Paper first received* 1 *June, and in final form* 17 *December*, 1956]

A new method is proposed for measuring the generation of heat in coal or other finely divided powders. This method depends only on the thermal constants of the material and not on the heat losses to the surroundings of the calorimeter.

New solutions to the heat flow equation for heat generation in cylindrical and spherical bodies as required for calculating the results are presented, and experimental confirmation of the suitability of the method is obtained. During the course of the work, an interesting result is obtained on the critical sizes of systems which generate heat at a rate which increases linearly with temperature.

1. Introduction

A knowledge of the rate of heat generation in the reaction of coal with oxygen is desirable for several reasons. Apart from any light that such knowledge may be able to shed on the constitutions of the coals used, it is also required for the design of oxidation plant and for consideration of the safety of stored coal. Some of the previous work on this field is described in Refs. 1–4.

This paper describes an apparatus developed to measure the rate of heat generation in powdered coal exposed to gases containing a varying proportion of oxygen at temperatures in the range 15–150° C. As is customary in this type of work, powdered coal was used to obtain a reasonable external specific surface for reaction; even so it was necessary to detect rates of heating as small as 0·03 cal per g of coal per h (i.e. about $6{\cdot}7 \times 10^{-6}$ cal cm^{-3} s^{-1}). This very small rate of heat generation, combined with the low thermal conductivity ($10^{-3} - 10^{-4}$ cal cm^{-1} s^{-1} °C^{-1}) and diffusivity ($10^{-2} - 10^{-3}$ cm^2/s) of powdered coal, control to a very large extent the design of the apparatus.

Previous forms of apparatus have been of three types. The first and simplest[1] consists merely of a furnace to heat a small quantity of coal at a rate of a few degrees per minute. The temperatures of the furnace and the coal are recorded, and the point at which the temperature of the coal is observed to rise continuously above that of the furnace is designated the "ignition point" of the coal in that atmosphere. Secondly, for determining absolute rates of heat generation, adiabatic calorimeters have been developed.[2, 3] In these the temperature of the furnace is made to follow that of coal contained in it, starting from some specified value at which the rate of rise of temperature is very low. The principle behind these methods is that no heat is lost from the coal to its surroundings. This may not always be true;[5] no attempt to verify this assumption by measuring heat losses was made in the cases quoted. Thirdly, if it can reasonably be assumed that a constant quantity of heat is liberated for every gramme

* Now at Mullard Research Laboratories, Salfords, Nr. Redhill, Surrey.

of coal consumed, then small amounts of heat generated may be observed through measurements of small changes in weight. An apparatus for measurements of change in weight has been described;[4] however, the complementary experiment on the dependence of heat generated on weight lost does not appear to have been made.

It can be seen that there are objections to all the above methods of measurement. The adiabatic calorimeter is most suitable provided measurements of heat losses are made: even so there is still the serious objection that at the low rates of heating envisaged the rate of temperature rise will only be of the order of 20° C per week. Even allowing for an exponential increase of heating rate with temperature it still seems probable that coal specimens may be exposed to oxygen for about a week before the desired temperature is reached. This would considerably alter the properties of the specimen.

As an alternative it was decided to develop a method of measuring heat generations in which no attempt was made to work under adiabatic conditions, but in which heat fluxes in the system, which could be correlated with heat generations, were deduced from measurements of temperature difference in the coal itself. This is practicable since powdered coal has such a low thermal conductivity that very small heat fluxes can give rise to readily observable temperature differences. However, if these heat fluxes are produced by the heat of reaction in a specimen, they may take a matter of hours to appear.

2. EXPERIMENTAL METHOD

Practical considerations point to a cylindrical form of apparatus in which radial heat flow is observed, as in such an assembly access to the coal is possible along lines parallel to the axis of the cylinder so that thermocouples and gas ducts do not form thermal short circuits. By making the cylinder long enough radial heat flow may be approximated with a high degree of accuracy over the meridian plane of the cylinder so that the effect of the end plates may be ignored. The apparatus then takes the general form shown in Fig. 1.

In the apparatus described the coal is contained between two coaxial perforated cylinders. The outer one is made of perforated brass sheet rolled to shape and covered with fine mesh gauze to retain the powdered coal; the inner one is made of a Tufnol tube drilled with many fine holes. Thermocouples are arranged just within the surfaces of the coal, both internal and external; there are several in the median plane of the cylinder for the actual measurements used in estimating heat flows, and some in planes on either side of this for checking that temperature gradients parallel to the axis are negligible, so that heat flow can be considered truly radial. On the inner tube is also placed a heating coil with potential tapping points near the median plane.

The complete cylinder is placed in a thermostatically controlled bath. The wires are led out from the cylinder and bath through gas-tight seals, and unions are provided for the inlet and exhaust of the gases. Care must be taken either to reduce any temperature gradients at the seals on the thermocouple wires to negligible amounts if different metal is used for the seals, or to use the same wire throughout. Manipulation of the many wires in the centre tube may be eased by making this tube in four sections as shown, with the thermocouples themselves mounted in the joints. The outer thermocouples may be mounted in Tufnol bolts, which are fixed to the perforated outer cover with standard nuts. Calculations on orders of magnitude, using the thermal constants and minimum rates of heating given above, indicate that the external radius of the cylinder of coal should not have to be more than 10 cm to produce a readily observable temperature differential (say 0·25° C). The function of the constant temperature bath is to bring the coal to the desired temperature; heat transfer between the coal and the bath does not enter directly into the calculation of the heat generated within the coal, which is based on temperature differences observed within the coal.

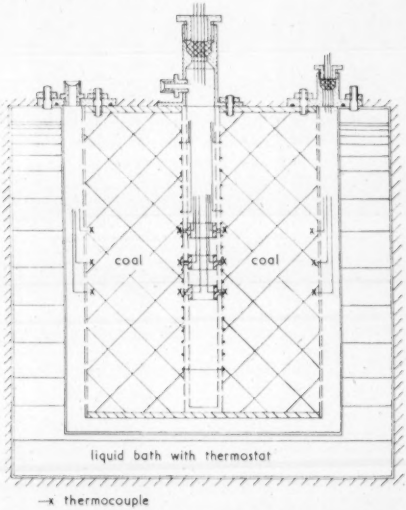

Fig. 1. Apparatus for the measurement of heat generation in powdered coal

There are two simple methods of measuring generation of heat with this apparatus. In either case, the whole cylinder of coal is brought to an even temperature under a flow of inert gas, and an equal flow of the reacting gas is then substituted. The temperature of the coal near the axis of the cylinder then begins to rise relative to that near the outside.

If the rate of heat generation is near the lower limit of detection then the final steady temperature difference is the most sensitive form of measurement. This will take some hours to be reached, but the apparatus may be left to run itself while this is happening. If, however, the rate of heat generation is relatively high, then it may be obtained from the initial rate of rise at the centre of the cylinder. With a recorder of suitable speed and sensitivity, a result can then be obtained in a fraction of one hour, rather than several hours.

In either case, the observed data is in terms of temperature. To convert this to a rate of heat generation, one of the thermal constants of the coal must be measured. The heating coil in the centre of the cylinder is used for this purpose. The coal is again brought to a condition of uniform temperature under a flow of inert gas equal to the flow used in the previous experiments. The heater is then switched on. The initial curve of rise of temperature at the centre provides

information of the volume specific heat, and the final temperature difference between the centre and outside in the steady state provides information of the thermal conductivity. Any effects of the gas flow on the thermal conductivity are minimized by maintaining the flow at a constant rate.

3. THE HEAT TRANSFER EQUATION

To interpret the results obtained in the apparatus, we need solutions to the heat transfer equation

$$\rho c(\partial\theta/\partial t) = \text{div. } (k \text{ grad } \theta) + q(\theta) \tag{1}$$

under certain boundary conditions.

Here θ = temperature
t = time
k = thermal conductivity
ρ = density
c = mass specific heat
$q(\theta)$ = rate of heat generation, as a function of temperature.

The boundary conditions which are applicable to the apparatus are:

(1) A hollow cylinder initially at a uniform temperature which is afterwards maintained at the outer surface. Heat generated in the cylinder. No heat losses from the inner surface of the cylinder.

(2) A hollow cylinder starting from a uniform temperature and heated by a coil at the inner surface. No heat generated in the cylinder.

Heat generation according to the law

$$q(\theta) = Q + R\theta \tag{2}$$

where Q and R are constants is considered here. The special case of $R = 0$ usually leads to a different form of solution.

The general solution to equations (1) and (2) for cylindrical symmetry, which is derived in Appendix 1, is

$$Q + R\theta = (Q + R\Theta_1)J_0\left[\sqrt{\left(\frac{R}{k}\right)}r\right] + (Q + R\Theta_2)Y_0\left[\sqrt{\left(\frac{R}{k}\right)}r\right] + \exp\left[(R/\rho c)t\right]\sum_p \left[a_p J_0(c_p r) + b_p Y_0(c_p r)\right]\exp\left(-\alpha c_p^2 t\right) \tag{4}$$

For $R = 0$, this reduces to

$$\theta = \Theta - K\ln r - \frac{Q}{4k}r^2 + \sum_p \left[a_p J_0(c_p r) + b_p Y_0(c_p r)\right]\exp\left(-\alpha c_p^2 t\right) \tag{5}$$

where $\Theta, \Theta_1, \Theta_2, K, a_p, b_p, c_p$

are constants, and $\alpha = k/\rho c$.

Under the first boundary conditions, only two results are needed; the initial rate of rise of temperature at the inner surface and the steady state difference in the temperatures of the inner and outer surfaces. Physical arguments indicate that the first result should be

$$(\partial\theta/\partial t)_{a,0} = (Q + R\theta_{a,0})/\rho c \tag{6}$$

provided that the inner radius is small compared with the outer.

The validity of this conclusion is checked in Appendix I. The solution for a sphere is used as being more convenient for checking the validity of physical arguments than the solution for a cylinder. The steady state solutions for hollow cylinders and spheres are given in Table 1.

Here a equals radius of internal surface and b equals radius of external surface.

If $\sqrt{(R/k)}(b-a) \lesssim 0{\cdot}7$ then the error in taking equations (7) and (8) for (9) and (10), when $r = a$, is only about 1%.

It may be noted that when $a = 0$, equations (9) and (10) become

$$Q + R\theta = (Q + R\theta_{b,0})\frac{J_0[\sqrt{(R/k)}r]}{J_0[\sqrt{(R/k)}b]}$$

and $$Q + R\theta = (Q + R\theta_{b,0})\frac{\sqrt{(R/k)}b}{\sin\sqrt{(R/k)}b}\cdot\frac{\sin\sqrt{(R/k)}r}{\sqrt{(R/k)}r}$$

When either $J_0[\sqrt{(R/k)}b] = 0$ or $\sin\sqrt{(R/k)}b = 0$, then $\theta_{0,\infty} \to \infty$. Thus there is a critical size to an assembly each part of which generates heat at a rate which increases with temperature. This interesting result is later developed more fully.

Under the second set of boundary conditions, there are again two useful parts of the solution. When $\alpha t/a^2 \ll 1$, for a cylinder,

$$\theta_{a,t} = \theta_{a,0} + \frac{H}{2\pi k}\sqrt{\left(\frac{\alpha t}{\pi a^2}\right)} \tag{11}$$

Table 1. *Solutions to heat transfer equation* (1)

Heat generation function	*Cylinder*	*Sphere*
$q(\theta) = Q$	$\theta = \theta_{b,\infty} - \frac{Q}{2k}a^2\ln b/r + \frac{Q}{4k}(b^2 - r^2)$ (7)	$\theta = \theta_{b,\infty} - \frac{Q}{3k}a^3\left(\frac{1}{r} - \frac{1}{b}\right) + \frac{Q}{6k}(b^2 - r^2)$ (8)
$q(\theta) = Q + R\theta$	$Q + R\theta = (Q + R\theta_{b,\infty})\dfrac{Y_1\left[\sqrt{\left(\frac{R}{k}\right)}a\right]J_0\left[\sqrt{\left(\frac{R}{k}\right)}r\right] - J_1\left[\sqrt{\left(\frac{R}{k}\right)}a\right]Y_0\left[\sqrt{\left(\frac{R}{k}\right)}r\right]}{Y_1\left[\sqrt{\left(\frac{R}{k}\right)}a\right]J_0\left[\sqrt{\left(\frac{R}{k}\right)}b\right] - J_1\left[\sqrt{\left(\frac{R}{k}\right)}a\right]Y_0\left[\sqrt{\left(\frac{R}{k}\right)}b\right]}$ (9)	$Q + R\theta = (Q + R\theta_{b,\infty})\dfrac{b}{r}\cdot\dfrac{\sin\sqrt{\left(\frac{R}{k}\right)}(r-a) + \sqrt{\left(\frac{R}{k}\right)}a\cos\sqrt{\left(\frac{R}{k}\right)}(r-a)}{\sin\sqrt{\left(\frac{R}{k}\right)}(b-a) + \sqrt{\left(\frac{R}{k}\right)}a\cos\sqrt{\left(\frac{R}{k}\right)}(b-a)}$ (10)

when $t \to \infty$

$$\theta_{b,\infty} = \theta_{a,\infty} - \frac{H}{2\pi k} \ln \frac{b}{a} \tag{12}$$

where H = rate of heat supplied per unit length.

From equation (12) a value of k may be obtained; knowing this, equation (11) enables ρc to be determined. These are the two thermal constants required for converting the experimental results into absolute values of rate of heat generation.

4. EXPERIMENTAL RESULTS

An apparatus was built according to the description outlined above and having the dimensions: radius of inner surface, 0·65 cm; radius of outer surface, 7·50 cm; length of cylinder, 60·0 cm.

This size of cylinder should give an equilibrium temperature difference of about $\frac{1}{4}$° C between inner and outer surfaces, for coal of thermal conductivity $3{\cdot}0 \times 10^{-4}$ cal cm^{-1} s^{-1} °C^{-1} generating heat at 7×10^{-6} cal cm^{-3} s^{-1}. A set of results obtained with this apparatus is shown in Fig. 2 and in Table 2.

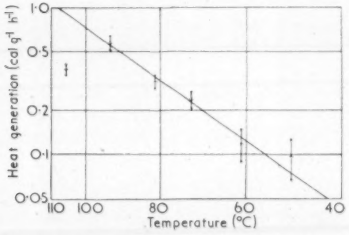

Fig. 2. Heat generation in Betteshanger coal

Table 2. *Experimental results with Betteshanger coal*

Coal	*Betteshanger "H" seam, −30 B.S. mesh. N.C.B. code No. 204*
Volume, specific heat	0·195 cal cm^{-3} °C^{-1}
Thermal conductivity	$2{\cdot}32 \times 10^{-4}$ cal cm^{-1} s^{-1} °C^{-1}
Heat generation at 50° *C*	$2{\cdot}11 \times 10^{-5}$ cal cm^{-3} s^{-1} 0·097 cal g^{-1} h^{-1}
Activation energy 50–95° C	11 150 cal/mol. 0·485 eV/molecule

The apparatus performed satisfactorily and was capable of detecting the lowest rates of heat generation which had to be observed.

5. THERMAL INSTABILITY OF ASSEMBLIES

It has been noted that equations (9) and (10) lead to infinite values of temperature when a certain size of assembly is exceeded. This is a point of industrial importance with regard to the storage of bulk quantities of materials that may generate heat during storage (e.g. powdered coal, damp hay, etc.). To consider the effect in more detail, take the case of a solid sphere in which heat is generated according to the law $q(\theta) = Q + R\theta$, and which starts at a uniform temperature throughout. Let the heat transfer coefficient at the surface be L and $h = L/k$.

The steady state solution is

$$q(\theta) = q(\Theta_1) \frac{\sin \sqrt{(R/k)}r}{\sqrt{(R/k)}r} + q(\Theta_2) \frac{\cos \sqrt{(R/k)}r}{\sqrt{(R/k)}r}$$

From the boundary conditions, $q(\Theta_2) = 0$

$$q(\Theta_1) = \frac{Qhb^2}{kb \cos \sqrt{(R/k)}b - (k - hb)\sqrt{(k/R)} \sin \sqrt{(R/k)}b}$$

Hence, the temperature at the centre of the sphere $\Theta_1 \to \infty$, when

$$\frac{\tan \sqrt{(R/k)}b}{\sqrt{(R/k)}b} = \frac{k}{k - hb} \tag{13}$$

The curves $y = \dfrac{\tan \sqrt{(R/k)}b}{\sqrt{(R/k)}b}$ and $y = 1 \Big/ \left(1 - \dfrac{hb}{k}\right)$

are plotted in Fig. 3, for a few values of $h/\sqrt{kR}$. The value of $\sqrt{(R/k)}(b/\pi)$ for an infinite centre temperature is given by the first positive intersection of the two curves. As h decreases from infinity to zero, the value of $\sqrt{(R/k)}(b/\pi)$ decreases from 1 to 0. Thus when the sphere is greater than a critical size, there will be a continual increase in the temperature at the centre of the sphere under these boundary conditions. That the rate of increase will be significant is shown by the transient solution to the heat flow equation for spherical symmetry as given in Appendix I.

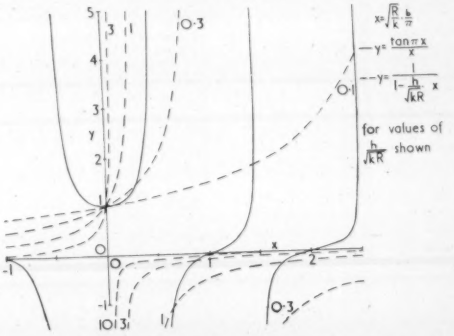

Fig. 3. Graphs for solution of the problem of thermal instability in a spherical assembly

In this solution, there is a positive exponential term in t if $R/\rho c > \alpha c_p^2$.

For very large values of h, $c_p \simeq \pi/b$ so that the condition for an exponentially increasing temperature is $b > \pi\sqrt{(k/R)}$. For smaller values of h the critical value of b is reduced, corresponding to the result found above. Thus, not only will the temperature inside the sphere continue to increase, it will do so at an exponentially increasing rate, so that the system is thermally unstable.

6. CONCLUSIONS

A new method of measuring the rate of heat generation in coal, or other finely divided material, has been proposed.

Experimental confirmation of the suitability of this method has been obtained. The measurements required are simple ones, either the rate of rise of the temperature at a point, or the difference between the temperatures at two points; they may be safely left to a recorder. Provided the condition $\sqrt{(R/k)}(b-a) < 0{\cdot}7$ is fulfilled in the apparatus, a uniform rate of heat generation may be assumed in calculating the results from the measurements of temperature differences. However, with material in which the rate of heat generation increases with temperature, a critical size of assembly exists, beyond which the system is thermally unstable.

ACKNOWLEDGEMENTS

Acknowledgements are made to Dr. A. Z. Keller, who provided one of the solutions to the heat transfer equation, and to the National Coal Board for permission to publish this paper. The views expressed are those of the author and not necessarily those of the Board.

APPENDIX 1

The heat transfer equation

The heat transfer equation (1) reduces to the following forms for cylindrical and spherical symmetry respectively.

$$\rho c\frac{\partial\theta}{\partial t} = k\left(\frac{\partial^2\theta}{\partial r^2} + \frac{1}{r}\frac{\partial\theta}{\partial r}\right) + q(\theta)$$

$$\rho c\frac{\partial\theta}{\partial t} = k\left(\frac{\partial^2\theta}{\partial r^2} + \frac{2}{r}\frac{\partial\theta}{\partial r}\right) + q(\theta)$$

For $q(\theta) = Q + R\theta$

we have
$$\frac{\partial^2\theta}{\partial r^2} + \frac{1}{r}\frac{\partial\theta}{\partial r} + \frac{R}{k}\theta - \frac{1}{\alpha}\frac{\partial\theta}{\partial t} = -\frac{Q}{k}$$

$$\frac{\partial^2\theta}{\partial r^2} + \frac{2}{r}\frac{\partial\theta}{\partial r} + \frac{R}{k}\theta - \frac{1}{\alpha}\frac{\partial\theta}{\partial t} = -\frac{Q}{k}$$

The particular integrals of these two equations are

$$\theta = -\frac{Q}{R} + AJ_0\left[\sqrt{\left(\frac{R}{k}\right)}r\right] + BY_0\left[\sqrt{\left(\frac{R}{k}\right)}r\right]$$

$$\theta = -\frac{Q}{R} + A\frac{\sin\sqrt{(R/k)}r}{\sqrt{(R/k)}r} + B\frac{\cos\sqrt{(R/k)}r}{\sqrt{(R/k)}r}$$

i.e. $$q(\theta) = q(\Theta_1)J_0\left[\sqrt{\left(\frac{R}{k}\right)}r\right] + q(\Theta_2)Y_0\left[\sqrt{\left(\frac{R}{k}\right)}r\right]$$

$$q(\theta) = q(\Theta_1)\frac{\sin\sqrt{(R/k)}r}{\sqrt{(R/k)}r} + q(\Theta_2)\frac{\cos\sqrt{(R/k)}r}{\sqrt{(R/k)}r}$$

These are the steady state solutions; for the transient solutions, which are the complementary functions, we assume that the variables are separable, i.e. $\theta = F(t)\,.\,G(r)$. Then, for the cylinder and sphere respectively,

$$F'(t) + \left(c_p^2 - \frac{R}{k}\right)F(t) = 0,\quad G''(r) + \frac{1}{r}G'(r) + c_p^2G(r) = 0$$

$$F'(t) + \left(c_p^2 - \frac{R}{k}\right)F(t) = 0,\quad G''(r) + \frac{2}{r}G'(r) + c_p^2G(r) = 0$$

where c_p is arbitrary. Hence

$$\theta = \sum_p [a_pJ_0(c_pr) + b_pY_0(c_pr)]\exp[(R/\rho c)t]\exp(-\alpha c_p^2t)$$

$$\theta = \sum_p \frac{1}{r}(a_p\sin c_pr + b_p\cos c_pr)\exp[(R/\rho c)t]\exp(-\alpha c_p^2t)$$

Thus the complete solutions are

$$q(\theta) = q(\Theta_1)J_0\left[\sqrt{\left(\frac{R}{k}\right)}r\right] + q(\Theta_2)Y_0\left[\sqrt{\left(\frac{R}{k}\right)}r\right] + \\ + \exp[(R/\rho c)t]\sum_p [a_pJ_0(c_pr) + b_pY_0(c_pr)]\exp(-\alpha c_p^2t)$$

$$q(\theta) = q(\Theta_1)\frac{\sin\sqrt{(R/k)}r}{\sqrt{(R/k)}r} + q(\Theta_2)\frac{\cos\sqrt{(R/k)}r}{\sqrt{(R/k)}r} + \\ + \frac{\exp[(R/\rho c)t]}{r}\sum_p (a_p\sin c_pr + b_p\cos c_pr)\exp(-\alpha c_p^2t)$$

The values of the constants in these equations have been obtained under the boundary conditions

(*a*) At $t = 0$, $\theta_{r,0} = \theta_{b,0}$ for $0 \leqslant r \leqslant b$
(*b*) For $t > 0$, $\theta_{b,t} = \theta_{b,0}$
(*c*) For $t > 0$, $\theta_{0,t}$ is finite.

Hence $$b_p = 0$$

$$q(\Theta_2) = 0$$

c_p is the pth root of $\begin{cases} J_0(bc_p) = 0 \\ \sin bc_p = 0 \end{cases}$

$$q(\Theta_1) = \frac{q(\theta_{b,0})}{J_0[\sqrt{(R/k)}b]} \text{ for cylinders}$$

$$q(\Theta_1) = q(\theta_{b,0})\frac{\sqrt{(R/k)}b}{\sin\sqrt{(R/k)}b} \text{ for spheres.}$$

By Fourier analysis

$$a_p = \frac{2q(\theta_{b,0})}{bc_pJ_0'(bc_p)}\frac{1}{1 - \dfrac{kc_p^2}{R}} \text{ for cylinders}$$

$$a_p = (-1)^{p+1}\frac{2bq(\theta_{b,0})}{p\pi}\frac{1}{1 - \dfrac{R}{k}\left(\dfrac{p\pi}{b}\right)^2} \text{ for spheres.}$$

Hence

$$q(\theta) = \frac{q(\theta_{b,0})}{J_0\left[\sqrt{\left(\frac{R}{k}\right)}b\right]}J_0\left[\sqrt{\left(\frac{R}{k}\right)}r\right] + \\ + \exp[(R/\rho c)t]\sum_{p=1}^{\infty}\frac{2q(\theta_{b,0})}{bc_pJ_0'(bc_p)}\frac{1}{1 - \dfrac{kc_p^2}{R}}J_0(c_pr)\exp(-\alpha c_p^2t)$$

for cylinders

$$q(\theta) = \frac{q(\theta_{b,0})\sqrt{(R/k)}b}{\sin\sqrt{(R/k)}b}\frac{\sin\sqrt{(R/k)}r}{\sqrt{(R/k)}r} + \\ + \frac{\exp[(R/\rho c)t]}{r}\sum_{p=1}^{\infty}(-1)^{p+1}\frac{2bq(\theta_{b,0})}{p\pi} \\ \frac{1}{1 - \dfrac{k}{R}\left(\dfrac{p\pi}{b}\right)^2}\sin\frac{p\pi r}{b}\exp[-\alpha(p\pi/b)^2t]$$

for spheres.

To show that $\left(\frac{\partial\theta}{\partial t}\right)_{0,0} = \frac{q(\theta_{0,0})}{\rho c}$ take the solution for a sphere.

Then

$$R\frac{\partial\theta}{\partial t} = \frac{\exp\left[(R/\rho c)t\right]}{r}\sum_{p=1}^{\infty}(-1)^{p+1}\frac{2bq(\theta_{b,0})}{p\pi}$$

$$\frac{\frac{R}{\rho c} - \frac{k}{\rho c}\left(\frac{p\pi}{b}\right)^2}{1 - \frac{k}{R}\left(\frac{p\pi}{b}\right)^2}\sin\frac{p\pi r}{b}\exp\left[-\alpha(p\pi/b)^2 t\right]$$

$$= \frac{\exp\left[(R/\rho c)t\right]}{r}\sum_{p=1}^{\infty}(-1)^{p+1}q(\theta_{0,0})\frac{2b}{p\pi}$$

$$\frac{R}{\rho c}\sin\frac{p\pi r}{b}\exp\left[-\alpha(p\pi/b)^2 t\right]$$

since $\theta_{b,0} = \theta_{0,0}$

$$\left(\frac{\partial\theta}{\partial t}\right)_{r,0} = \sum_{p=1}^{\infty}(-1)^{p+1}\frac{2q(\theta_{0,0})}{\rho c}\frac{\sin\frac{p\pi r}{b}}{\frac{p\pi r}{b}}$$

$$= \frac{2q(\theta_{0,0})}{\rho c}\frac{1}{z}\left(\sin z - \frac{\sin 2z}{2} + \frac{\sin 3z}{3} - \ldots\right)$$

where $pz = \frac{p\pi r}{b}$

$$= \frac{2q(\theta_{0,0})}{\rho c}\frac{1}{z}\frac{z}{2}, \text{ for } -\pi < z < \pi$$

$$= \frac{q(\theta_{0,0})}{\rho c} \text{ for all points in the sphere except the surface.}$$

APPENDIX 2

Other methods of measuring heat generation

Since this method of measurement was proposed and the apparatus constructed, van Doornum[6] has described another form of apparatus for measuring heat generation. In this, the coal is contained in holes bored in an aluminium cylinder, the flow of gas in the bores being axial. However, in use, this apparatus is likely to suffer from the same defect as that of Orning, Mallov and Neff,[3,5] that is the appearance of a considerable temperature gradient in a $\frac{1}{2}$ in. diameter cylinder of coal, which must be ignored in calculating the results.

REFERENCES

(1) Parr, S. W., and Coons, C. C. *Industr. Engng Chem.*, **17**, p. 118 (1925).
(2) Davis, J. D., and Byrne, J. F. *Industr. Engng Chem.*, **17**, p. 125 (1925).
(3) Orning, A. A., Mallov, S., and Neff, M. *Industr. Engng Chem.*, **40**, p. 429 (1948).
(4) Oreshko, V. F. *Fact. Lab. Moscow*, **14**, p. 290 (1948).
(5) Newman, P. C. *Fuel*, **35**, p. 295 (1956).
(6) van Doornum, G. A. W. *J. Inst. Fuel*, **27**, p. 482 (1954).

A study of aircraft response to sudden and graded wind gusts by means of a differential analyser

By W. R. Blunden, B.Sc., B.E., A.M.I.E.Aust., A.Inst.P., Australian Military Forces Military Board, Melbourne, F. H. Hooke, B.Sc., B.E., A.M.I.E.Aust., A.F.R.Ae.S., Aeronautical Research Laboratory, Australian Department of Supply, Melbourne, and H. K. Messerle, M.Eng.Sc., B.E.E., A.M.I.E.Aust., Electrical Engineering Department, University of Sydney, Australia

[*Paper first received* 27 *January, and in final form* 9 *October*, 1956]

The solution of the "gust" problem for a range of parameters, sufficient to give results that would be useful to designers, is not practicable without the aid of an automatic computer. This paper describes the assumptions made for a detailed analysis on a mechanical differential analyser and the results obtained are summarized. Some discussion is given on the speed and accuracy of the solutions obtained.

The effect of vertical wind gusts on an aircraft in flight gives rise to two general problems:

(*a*) the determination of the response of an aircraft to a known gust;

(*b*) the derivation of the gust disturbance from known experimentally determined response curves.

In the former case solutions are required to provide aircraft designers with information of the alleviation of load on the aircraft under specific design conditions, while in the latter the data would permit the accurate interpretation of flight data and so assist airworthiness authorities in establishing design conditions in gusty air. Whilst the determination of the response to a known gust is tractable although complex and laborious, the inverse problem does not appear to be amenable to direct solution, though trial and error methods will yield results.

Various authors have investigated problem (*a*), the assumptions and approximations varying in each case. Fisher[1] and Bryant and Jones,[2] for example, assumed the aircraft to be completely rigid and neglected delays in the response to gusts due to inertia effects. Williams and Hanson[3] allowed for flexibility and lift lag effects were introduced later by Pierce[5] and Rhode.[4] The mathematics involved when allowing for lift lag becomes so complex, however, that only specific cases could be analysed, as is also shown by Hooke.[6] Although the use of Laplace transformation has made the

consideration of lag effects feasible,[6] any attempt to allow for flexibility in the wings and to obtain solutions for a sufficient range of aircraft and gust parameters for general use to designers is virtually impossible without recourse to an automatic calculating instrument or machine.

This paper describes the application of the differential analyser of the Commonwealth Scientific and Industrial Research Organization[7] to the solution of the response of rigid and flexible aircraft allowing for lift lag effects. The use of this computer made it possible to investigate the effects of all the most important aircraft parameters on the response and overstress arising during gust loading. As an introduction the simple rigid aircraft is considered first and the lift lag is introduced next. The lift lag functions are represented by exponential expressions as derived from reference (8). Next the aircraft is assumed to be flexible, allowing for one degree of freedom, i.e. considering only the fundamental mode of vibration of the wings. Some typical results are given showing various characteristic features. The purpose of this paper is mainly to discuss the method of analysis that has been used.

THE EQUATION OF MOTION FOR A RIGID AEROPLANE ENTERING VERTICAL GUSTS WITHOUT LAG

The mathematical analysis is fairly simple if an aeroplane is assumed to be rigid and when gust lag effects are neglected. Thus, assuming the forward velocity of the aeroplane to remain constant, as shown in Fig. 1, the basic equation of motion relates the vertical aircraft velocity $u(t)$, which is caused by the vertical gust, with the gust velocity $v_g(t)$, where both are functions of time t. The equation of motion is given by:[6]

$$\frac{W_a}{g}\frac{d}{dt}u(t) + \tfrac{1}{2}\rho USau(t) = \tfrac{1}{2}\rho USav_g(t);$$

where W_a = aeroplane gross weight
ρ = air density
U = horizontal velocity of aircraft (assumed constant)
S = wing area
a = slope of lift curve against incidence in steady flow
g = gravitational acceleration.

This equation can be transformed into

$$\frac{d}{ds}\mu(s) + C\mu(s) = C\vartheta(s) \qquad (1)$$

where $s = 2Ut/c$ = distance travelled in terms of chord length
c = wing chord
$\mu(s) = u(s)/v_{gmax}$ = vertical velocity response ratio
$= \dfrac{\text{vertical velocity of aeroplane in the gust}}{\text{maximum value of gust velocity}}$

$\vartheta(s) = \dfrac{v_g(s)}{v_{gmax}}$ = gust disturbance ratio $= \dfrac{\text{local gust velocity}}{\text{maximum value of gust velocity}}$

$C = \dfrac{\rho agc}{4W_a}$ = aircraft relative density parameter, i.e. a parameter defining the ratio of air density to the weight per cubic foot of the aeroplane.

Equation (1) is a first order differential equation which can be solved by ordinary formal methods if the gust disturbance function $\vartheta(s)$ is of simple form. However, the gust disturbance is usually an arbitrary function of time and then no formal solution exists.

For a general investigation the "sharp edged" gust can be taken as representing the worst possible condition and can be used as a basis for any detailed mathematical analysis.

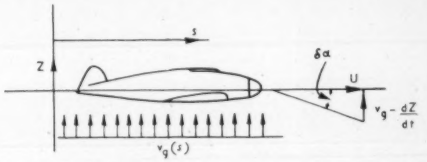

Fig. 1. Rigid aircraft entering gust at $s = 0$

Z, vertical displacement of centre of gravity of fuselage; α, angle of incidence, $dZ/dt = u(t)$.

As shown in Fig. 2, a sharp edged gust simply involves an instantaneous change in the vertical wind velocity from one steady state to another steady state condition.

To allow for less severe conditions, "graded" gusts may be considered. As shown in Fig. 2, linearly graded gusts involve a gradual, linear transition from one steady value of the vertical wind velocity to the final steady value over a distance s_g which is the gust gradient expressed in half wing chords; typical values of this gradient are shown in Fig. 2 as s_{g_1} and

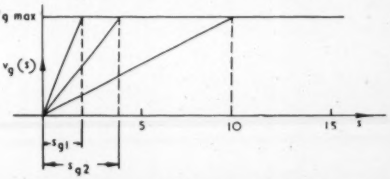

Fig. 2. Sharp-edged and graded wind gusts

s_{g_2}. The overall variation in the vertical velocity is defined as v_{gmax}. Solutions for sharp edged and graded gusts can be derived formally. However, for an arbitrary gust function it is necessary to use an automatic computer or finite difference techniques. A mechanical differential analyser is particularly suitable for this sort of problem if a large number of solutions for various conditions is required, since arbitrary functions can be handled quite easily.

RIGID AEROPLANE ENTERING VERTICAL GUST ALLOWING FOR FLUID INERTIA

Equation of motion. Any change in the gust and relative aircraft velocities cannot produce an instantaneous change in the flow conditions around a wing because of the inertia of the fluid. Allowing for delays due to fluid inertia the fundamental equation of motion becomes as shown in reference (6).

$$\frac{W_a}{g}\frac{d}{dt}u(s) + \tfrac{1}{2}\rho US\int_{\sigma=0}^{s} k_1(s-\sigma)\frac{du(\sigma)}{d\sigma}d\sigma =$$
$$= \tfrac{1}{2}\rho US\int_{\sigma=0}^{s} k_2(s-\sigma)\frac{dv_g(\sigma)}{d\sigma}d\sigma$$

which can be transformed into

$$\frac{d\mu(s)}{ds} + C\int_{\sigma=0}^{s} \frac{k_1(s-\sigma)}{a}\,\frac{d\mu(\sigma)}{d\sigma}d\sigma = C\int_{\sigma=0}^{s} \frac{k_2(s-\sigma)}{a}\,\frac{d\vartheta(\sigma)}{d\sigma}\,d\sigma \qquad (2)$$

where σ = distance from origin $s = 0$ to the point where a change in gust velocity or incidence takes place.

In this equation the first term on the left-hand side is due to the inertia of the aeroplane itself. The second term is due to the lift force caused by the vertical velocity $u(t)$ of the aeroplane delayed by the lift lag function $k_1(s)$. The lift lag functions are defined as follows:

$\frac{k_1(s)}{a}$ = lift lag function appropriate to vertical motion of the aerofoil through initially undisturbed atmosphere, represented approximately by an exponential function as

$$= 1 - b_1\,e^{-\lambda_1 s}$$

$\frac{k_2(s)}{a}$ = lift lag function appropriate to motion from undisturbed atmosphere into a region of air in vertical motion, represented approximately as

$$= 1 - b_2\,e^{-\lambda_2 s} - b_3\,e^{-\lambda_3 s}$$

The magnitude of the constants b_1, b_2, b_3, λ_1, λ_2, λ_3 depends on the wing aspect ratio A and using reference (8) the following values apply for a rectangular wing in translational motion:

Aspect ratio $A = 6$

$b_1 = 0{\cdot}347$	$\lambda_1 = 0{\cdot}28$
$b_2 = 0{\cdot}48$	$\lambda_2 = 0{\cdot}246$
$b_3 = 0{\cdot}52$	$\lambda_3 = 1{\cdot}83$

Aspect ratio $A = \infty$

$b_1 = 0{\cdot}335$	$\lambda_1 = 0{\cdot}32$
$b_2 = 0{\cdot}5$	$\lambda_2 = 0{\cdot}13$
$b_3 = 0{\cdot}5$	$\lambda_3 = 1{\cdot}0$

The lag functions actually employed in the programme of work discussed here are given in Fig. 3 for $A = 6$.

Using these exponential lag functions it becomes possible to transform equation (2) into an ordinary linear differential equation of the form:

$$\frac{d^3\mu(s)}{ds} + [\lambda_1 + C(1-b_1)]\frac{d^2\mu(s)}{ds^2} + \\ + C\lambda_1\frac{d\mu(s)}{ds} = \frac{d^2 f(s)}{ds^2} + \lambda_1\frac{df(s)}{ds} \qquad (3)$$

where

$$f(s) = C\int_0^s [1 - b_2 e^{-\lambda_2(s-\sigma)} - b_3\,e^{-\lambda_3(s-\sigma)}]\frac{d\vartheta(\sigma)}{d\sigma}d\sigma$$

Equation (3) can be solved formally for sharp edged and graded gusts, but for general disturbance functions an automatic computer is necessary. A formal solution of equation (3) is obviously much more tedious than that of equation (1), and if a number of solutions is required the differential analyser should help in speeding up the analysis.

For the differential analyser set-up it was found more suitable to deal with the equation in the original form as given in equation (2). It is possible, then, to deal with the various lag effects independently, as will be shown in the next section. This feature is particularly important when the flexible aircraft is considered and the equation of motion becomes more complex.

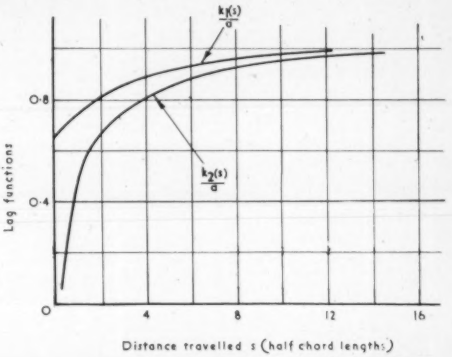

Fig. 3. Lift lag functions $k_1(s)$ and $k_2(s)$ for a wing of aspect ratio, $A = 6$. $k_1(s)$ is lift lag function for a sudden jump in geometrical incidence at $s = 0$. $k_1(s)/a = 1 - 0{\cdot}347\,e^{-0{\cdot}28s}$ (approx.)

$k_2(s)$ is lift lag function for entry into uniform unit upgust from stationary atmosphere at $s = 0$. $k_2(s)/a = 1 - 0{\cdot}48\,e^{-0{\cdot}246s} - 0{\cdot}52\,e^{-0{\cdot}183s}$ (approx.).

Velocity lag and gust lag simulation on the differential analyser. The velocity lag component in equation (2) was

$$W_\mu(s) = \int_{\sigma=0}^{s} \frac{k_1(s-\sigma)}{a}\,\frac{d\mu(\sigma)}{d\sigma}d\sigma$$

$$= \int_{\sigma=0}^{s} [1 - b_1 e^{-\lambda_1(s-\sigma)}]\frac{d\mu(\sigma)}{d\sigma}d\sigma \qquad (4)$$

and the problem is to transform this equation so that it can be programmed directly on a differential analyser. This is done as follows:

Define the function $V_\mu(s)$ by

$$V_\mu(s) = b_1\int_{\sigma=0}^{s} [1 - e^{-\lambda_1(s-\sigma)}]\mu'(\sigma)d\sigma \qquad (5)$$

where $\mu'(\sigma) = d\mu(\sigma)/d\sigma$

Then $$\frac{dV_\mu(s)}{ds} = b_1\int_{\sigma=0}^{s} \lambda_1 e^{-\lambda_1(s-\sigma)}\mu'(\sigma)d\sigma$$

since the integrand of the integral defining $V_\mu(s)$ vanishes at $\sigma = 0$.

Hence $$\frac{1}{\lambda_1}\frac{dV_\mu(s)}{ds} + V_\mu(s) = b_1\mu(s) \qquad (6)$$

since $\mu(0) = 0$. Also from (4) and (5)

$$W_\mu(s) = V_\mu(s) + (1 - b_1)\int_{\sigma=0}^{s} \mu'(\sigma)d\sigma$$

$$= V_\mu(s) + (1 - b_1)\mu(s) \qquad (7)$$

Thus the delayed effect of the velocity or the velocity lag function $W_{\mu}(s)$ can be generated on the differential analyser by programming equations (6) and (7) and taking $\mu(s)$ as the forcing function in differential equation (6).

The gust lag effect is slightly more complicated, as it is approximated by two exponential functions in $k_2(s)$. The gust lag is expressed by

$$u_{\vartheta}(s) = \int_{\sigma=0}^{s} \frac{k_2(s-\sigma)}{a} \frac{d\vartheta(\sigma)}{d\sigma} d\sigma$$

$$= \int_{\sigma=0}^{s} [1 - b_2 e^{-\lambda_2(s-\sigma)} - b_3 e^{-\lambda_3(s-\sigma)}] \frac{d\vartheta(\sigma)}{d\sigma} d\sigma \quad (8)$$

where $u_{\vartheta}(s)$ is the delayed disturbance effect.

This expression can be reduced to a set of simultaneous differential equations by the same method as that used for the velocity lag function. Defining

$$F_{\vartheta}(s) = \int_{\sigma=0}^{s} b_2[1 - e^{-\lambda_2(s-\sigma)}] \frac{d\vartheta(\sigma)}{d\sigma} d\sigma$$

and

$$G_{\vartheta}(s) = \int_{\sigma=0}^{s} b_3[1 - e^{-\lambda_3(s-\sigma)}] \frac{d\vartheta(\sigma)}{d\sigma} d\sigma$$

we get the following three equations with $\vartheta(s)$ as forcing function

$$F_{\vartheta}(s) + \frac{1}{\lambda_2} \frac{d}{ds} F_{\vartheta}(s) = b_2 \vartheta(s) \quad (9)$$

$$G_{\vartheta}(s) + \frac{1}{\lambda_3} \frac{d}{ds} G_{\vartheta}(s) = b_3 \vartheta(s) \quad (10)$$

$$u_{\vartheta}(s) = F_{\vartheta}(s) + G_{\vartheta}(s) \quad (11)$$

Thus $u_{\vartheta}(s)$ can be derived from these equations for any arbitrary function $\vartheta(s)$, and the equations are in a form suitable for solution on the differential analyser.

Differential analyser programme. The performance of the rigid aeroplane with lag is now described by the equation of motion

$$\frac{d}{ds}\mu(s) + CW_{\mu}(s) = Cu_{\vartheta}(s) \quad (12)$$

The delay in the velocity is generated by

$$\left.\begin{aligned} W_{\mu}(s) &= V_{\mu}(s) + (1 - b_1)\mu(s) \\ V_{\mu}(s) &+ \frac{1}{\lambda_1} \frac{d}{ds} V_{\mu}(s) = b_1 \mu(s) \end{aligned}\right\} \quad (13)$$

and the gust lag is introduced by equations (9), (10) and (11). These are the equations required for the differential analyser set-up.

FLEXIBLE AEROPLANE ENTERING A VERTICAL GUST WITH GUST LAG

Equation of motion. An extra degree of freedom is introduced into the problem by allowing for flexibility in the aircraft structure as shown in Fig. 4. The wings are assumed to be rigid in themselves, but to be flexible about the point where they are fixed to the body of the aeroplane. The restoring torque is $k\theta$, where θ is the angular displacement of the wings from the initial position before a disturbance arises. The equation of motion is then

$$\frac{W'b}{g4} \frac{d^2\theta}{ds^2} + \frac{(W+W')}{Wb} 4k\theta + \frac{\rho US}{2\theta_0} \int_{\sigma=0}^{s} k_1(s-\sigma) \times \frac{du(\sigma)}{d\sigma} d\sigma =$$

$$= \frac{\rho US}{2\theta_0} \int_{\sigma=0}^{s} k_2(s-\sigma) \frac{d}{d\sigma} v_g(\sigma) d\sigma$$

where W = half weight of fuselage
W' = weight of each half wing
b = wing span
θ_0 = maximum static deflexion under sharp-edged gust without lift lag.

This equation can be transformed into

$$\frac{d^2\Theta(s)}{ds^2} + \int_{\sigma=0}^{s} \frac{k_1(s-\sigma)}{a} \left[G_1 \frac{d^2}{d\sigma^2} \Theta(\sigma) + G_3 \Theta(\sigma) \right] d\sigma +$$

$$+ G_2 \Theta(s) = G_2 \int_{\sigma=0}^{s} \frac{k_2(s-\sigma)}{a} \frac{d}{d\sigma} \vartheta(\sigma) d\sigma \quad (14)$$

where Θ = wing deflexion ratio $= \theta/\theta_0$

$$= \frac{\text{wing deflexion in gust}}{\text{static deflexion under sharp-edged gust load}}$$

$G_1 = C(W + W')/W'$

$G_2 = \nu^2 = \left(\frac{\pi Nc}{U}\right)^2 = \left(\pi \times \frac{\text{Number of vibrations}}{\text{when aircraft travels one chord length } c}\right)^2$

$G_3 = C\nu^2$

N = fundamental natural frequency of wings.

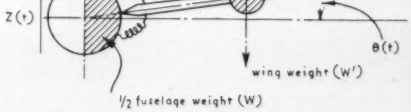

Fig. 4. Simple flexible aircraft

Equation (14) is much more involved than the relations for the previous cases. If a differential analyser is used for a detailed analysis the equation of motion is in its most suitable form as given by (14).

Differential analyser programme. For the differential analyser set-up, equation (14) is rewritten as follows:

$$\frac{d^2}{ds^2}\Theta(s) + W_q(s) + G_2\Theta(s) = G_2[F_0(s) + G_0(s)] \quad (15)$$

where

$$q(s) = G_1 \frac{d}{ds}\Theta(s) + G_2 \int_0^s \Theta(s) ds \quad (16)$$

and the functions W, F and G are the same as for the rigid aeroplane with gust lag, i.e. they are defined in equations (13) and (9), (10), (11).

It follows that the lag functions can be generated in exactly the same way as for the rigid aeroplane. The only difference arises with the velocity lag function $k_1(s)$, which now operates on the function $q(s)$ and not $\mu(s)$, i.e. $q(s)$ becomes the forcing function in (13).

RESULTS

As this paper is concerned mainly with the method of employing the differential analyser for the solution of the gust problem, it is proposed to indicate briefly the general nature of the solutions and their implications. In addition, the accuracy and speed of obtaining these solutions will be discussed. A complete presentation of the results of this work, which is of particular interest to aircraft designers, will be given later.

The rigid aircraft with lag. A range of solutions for a sudden and for several graded gusts with gradients rising linearly from zero to maximum in 4, 10, 20, 40 chord lengths is shown in Fig. 5. The independent variable is given in

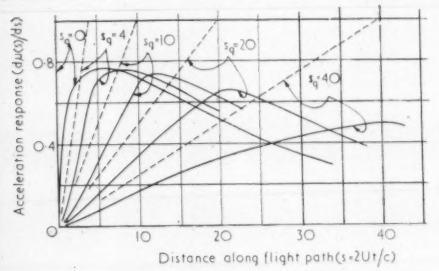

Fig. 5. Response of rigid aircraft ($C = 0{\cdot}04$) to sharp-edged and graded gust with lift lag

s_g, gust gradient in half chords.

chord lengths and the ordinates represent the vertical acceleration response. The peak value of the acceleration response falls as the gust severity diminishes. The acceleration response itself is a relative measure of the magnitude of stresses in the wing structure, and its maximum, being of particular interest, is defined as the alleviation factor, i.e. the reduction in the peak stress when compared with the maximum stress that would arise if the same gust was applied instantly

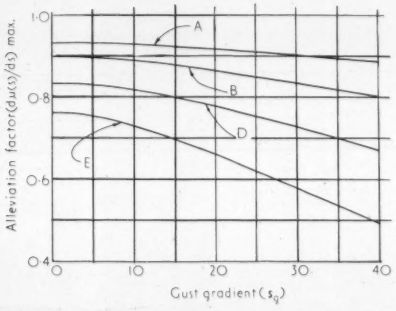

Fig. 6. Alleviation factor for rigid aircraft with lift lag against gust gradient s_g for a range of relative density parameters C

Curve *A*, $C = 0{\cdot}005$ (e.g. jet fighter at 36 000 ft); curve *B*, $C = 0{\cdot}01$ (e.g. Avro–Lincoln at 23 000 ft); curve *D*, $C = 0{\cdot}02$ (e.g. D.C.3 at 21 000 ft); curve *E*, $C = 0{\cdot}04$ (e.g. D.C.3 at 5000 ft).

without gust lag. The solutions shown in Fig. 5 are typical of civil airliners at low altitudes, since the aircraft relative density parameter C is large (in this case $C = 0{\cdot}04$).

From a series of solutions such as given in Fig. 5 a graph may be drawn up showing the alleviation factor plotted as a function of gust length for aircraft of various relative density parameters. Such a family of curves is given in Fig. 6 for a practical range of $C = 0{\cdot}005$, $0{\cdot}01$, $0{\cdot}02$, $0{\cdot}04$. The alleviation factor for rigid aircraft is therefore found to be less than unity in all cases and it diminishes with increased values of the relative density factor C.

The flexible aircraft without lag. The results for a flexible aircraft show that it would be dangerous to have relied upon data derived from an analysis of the rigid aircraft. The effect of wing flexibility has a number of important consequences. A typical set of response curves is shown in Fig. 7 for a

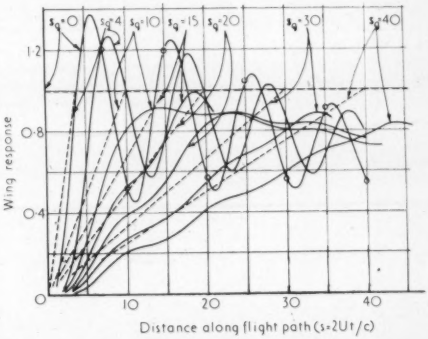

Fig. 7. Wing response Θ against time for flexible aircraft caused by linearly graded gusts

Wing response $= \theta/\theta_0$

$$= \frac{\text{dynamic deflexion}}{\text{deflexion under static lift; sharp gust without lag}}$$

$C = 0{\cdot}01$; $W'/(W + W') = 0{\cdot}1$; $\nu = 0{\cdot}2\,\pi$; $G_1 = 0{\cdot}1$; $G_2 = 0{\cdot}395$; $G_3 = 0{\cdot}00395$.

sharp-edged and six graded gusts. The abscissa is given in terms of chord lengths as for the rigid aircraft. The ordinate is now, however, a measure of the wing deflexion Θ due to the gust, where $\Theta = \theta/\theta_0$

and θ actual angular deflexion due to gust

θ_0 static angular deflexion due to the maximum lift caused by the same gust if applied instantly and if gust lag is neglected.

For each such family of solutions the various aircraft parameters are taken into account in the constants G_1, G_2 and G_3, which, as indicated previously, are non-dimensional functions of:

(i) the aircraft relative density parameter C
(ii) the wing weight ratio $W'/(W + W')$
(iii) the natural frequency of vibrations of the wings.

The deflexion, like the acceleration for the rigid aircraft, is here a measure of the stress in the wing structure and the maximum deflexion corresponds to the peak stress. The alleviation factor is defined as the ratio of the maximum

deflexion to the static deflexion θ_0 that would be produced by the maximum lift for a sharp-edged gust without lag, i.e. the alleviation factor can be read off directly from the curves since the dimensionless deflexion response Θ is given in terms of θ_0.

The introduction of an additional degree of freedom has made the response oscillatory as can be seen in Fig. 7 and two features arise:

(i) the maximum deflexion can go much beyond the static value θ_0
(ii) the maximum deflexion does not solely depend on the gust severity.

As follows immediately the peak stresses in the wings of an aircraft can increase considerably above the values indicated by the study of the rigid aircraft. Maximum deflexion does occur for the suddenly applied gust in this case, but as the gradient of the graded gust decreases, a "resonance" effect appears. In this particular family of solutions a gust which rises to a maximum in 10 chord lengths does in fact produce a less violent response in the aircraft than does one with a 15-chord rise time.

The general nature of this resonance effect is emphasized in Fig. 8 where the alleviation factor is plotted against the

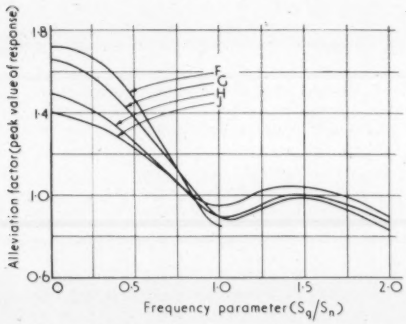

Fig. 8. Alleviation factor against frequency parameters s_g/s_N for several aircraft speeds when allowing for flexibility and gust lag

$$\frac{s_g}{s_N} = \frac{\text{gust gradient distance}}{\text{distance travelled during one wing vibration}}$$

$C = 0{\cdot}01$, $W'/(W+W') = 0{\cdot}8$; curve F, $\nu = 0{\cdot}05\,\pi$, $U = 8\,U_0$; curve G, $\nu = 0{\cdot}1\,\pi$, $U = 4U_0$; curve H, $\nu = 0{\cdot}2\,\pi$, $U = 2\,U_0$; curve J, $\nu = 0{\cdot}4\,\pi$, $U = U_0$.

frequency parameter s_g/s_N for four different aircraft speeds considering a particular type of aircraft as defined by

$$C = 0{\cdot}01$$
$$W/(W+W') = 0{\cdot}1$$

The frequency parameter is given as the ratio of the gust gradient distance s_g to the distance s_N the aircraft travels during one period of the natural wing oscillations. As can be seen, the alleviation factor increases considerably with speed U for the graded gusts if $s_g/s_N < 0{\cdot}6$. For higher speeds than those given, the alleviation factors for the graded gusts can increase even beyond that for the sharp-edged gust.

Considering the set of solutions as shown in Figs. 7 and 9 another interesting feature arises, namely the fact that an increase in the wing weight ratio $W/(W+W')$ reduces the damping of the oscillations. From the mathematical form of the equation it may appear that instability could arise for certain values of the parameters. The limiting stability condition can be derived by transforming the equation of motion from its integro-differential form (14) into a fourth order differential equation. The stability condition then follows as

$$G_1 G_2 - G_3 \geqslant 0$$

which in effect only means that $W \geqslant 0$ for stability. Hence instability does not arise for actual cases. However, it follows that a small relative weight of the fuselage in an aircraft means low damping for wing vibration.

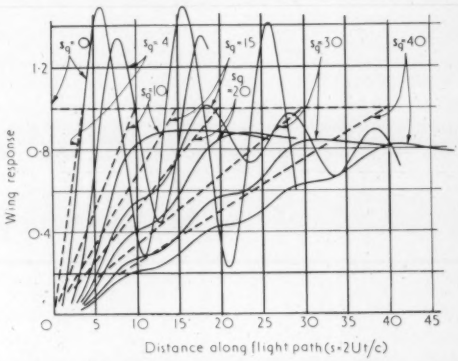

Fig. 9. Wing deflexion against time for flexible aircraft with relatively large wing weight ratio

$C = 0{\cdot}01$; $W'/(W+W') = 0{\cdot}8$; $\nu = 0{\cdot}2$; $G_1 = 0{\cdot}0125$; $G_2 = 0{\cdot}395$; $G_3 = 0{\cdot}00395$.

Speed and accuracy of solutions. The accuracy of a mechanical solution, either analogue or digital, of mathematical equation is in general a function of the time taken to obtain the solution. Mathematically, the longer the computing routine the more accurate the result. However, there are limits to the extent one can go in this direction in the interests of obtaining a solution at all. In addition the longer the solution takes the more likely is the chance of error, as the probability of a machine failure increases; in the analogue machine the accumulated error due to the inherent inaccuracy of the computing units (e.g. integrator slip) increases with time.

A compromise is therefore necessary, and in the case of an electro-mechanical differential analyser, which is by modern standards a slow machine, the scale factors are made as small as possible consistent with an overall accuracy of about 1%. This criteria was specially important in the work described here as some hundreds of solutions were required, and when the scale of the independent variable was kept at a safe minimum an average solution took 15–20 min to run, and the whole programme involved some three to four months of computing. This was extremely fast compared with a numerical solution carried out with the assistance of desk machines where a single solution took some three to four days to complete. A full investigation of the problem on this basis was, of course, impossible. With the above general

consideration in mind it was quite easy to achieve solutions in which the accuracy was better than 1% of full-scale values in the case of the flexible aircraft. The six integrators employed in the solution of the equations are each capable of an accuracy of 0·1% if they are scaled so that their full ranges are made use of. This had been determined by running the integrators for test problems of the same kind. The input functions, i.e. the graded gusts, are linear functions of s and therefore they have been generated simply by using a ratio unit connected to the bus bar representing s. Thus no error was introduced here.

The only other source of error in the computer set-up was due to the mechanical adding units which are liable to exhibit some slip when the output is the difference of two large quantities; however, this error could be controlled to be well below the accuracy of the integrators. With the scales chosen, the output is recorded on the output table was plotted with an accuracy of better than 0·2% of full-scale values. Thus as overall accuracy allowing for computing and recording errors of better than 1% could be confidently expected. This has been confirmed by the actual results. One typical solution which has been computed by using step-by-step methods is shown in Fig. 7. The points indicated by circles were obtained from the numerical solution.

ACKNOWLEDGEMENTS

The authors would like to thank Prof. D. M. Myers, under whose general direction this project has been carried out. They would also like to thank Mr. K. Sayers and Mr. J. Foster for their help when operating the differential analyser.

REFERENCES

(1) FISHER, H. R. *Aeronautical Research Council, Great Britain, Report and Memorandum*, p. 1463 (1932–33).

(2) BRYANT, L. W., and JONES, I. M. W. *Aeronautical Research Council, Great Britain, Report and Memorandum*, p. 1690 (1936).

(3) WILLIAMS, D., and HANSON, J. *Aeronautical Research Council, Great Britain, Report and Memorandum*, p. 1823 (1937).

(4) RHODE, R. V. *S.A.E. Journal*, p. 81 (1937).

(5) PIERCE, H. B. *National Advisory Committee for Aeronautics, United States, Tech. Note* No. 1320 (1947).

(6) HOOKE, F. H. *Aeronautical Research Consultative Committee, Australian Ministry of Supply, Rep. ACA*-54 (1954).

(7) MYERS, D. M. and BLUNDEN, R. W. *J. Instn Engrs Australia*, **24**, p. 10 (1952).

(8) PRITCHARD JONES, W. *Aeronautical Research Council, Great Britain, Report and Memorandum*, p. 2117 (1945).

NOTES AND NEWS

Correspondence

Comments on the A.S.T.M. Powder Data File

In February 1956 the writers published a list of errors in and comments on the X-ray Powder Data File.(1) This list was described briefly in the Institute's journals.(2) As a result of this publication, and of the appearance of a sixth set of data cards which was issued in 1956, a number of further errors have come to light and further comments have been sent to us. These have been collected in a booklet having the same title as that above, and copies have been sent to (i) all members of the X-ray Analysis Group of the Institute of Physics, (ii) all who have purchased copies of the Data File through the Institute, and (iii) all who have obtained copies of the first booklet from the writers. Others who would like to have copies of the booklets may obtain them on request from the Institute or from us.

The Committee of the X-ray Analysis Group of the Institute of Physics has authorized the publication of such lists of comments at approximately annual intervals. Users of the Data File are urged to send to the writers any material that they feel should be included in future "Comments."

Viriamu Jones Laboratory, University College, Cardiff, S. Wales.

J. W. HUGHES
ISABEL E. LEWIS
A. J. C. WILSON

REFERENCES

(1) Errors in the A.S.T.M. Index of X-ray Powder Diffraction Patterns. Cardiff: Viriamu Jones Laboratory. Pp. 39 (1956). [In June 1956 the Joint Committee on X-ray Diffraction Methods agreed that the name of the card file be "X-ray Powder Data File," and that the book index be called "Index to the X-ray Powder Data File." The title of the second booklet has, therefore, been altered correspondingly.]

(2) HUGHES, J. W., LEWIS, I. E., and WILSON, A. J. C. *Brit. J. Appl. Phys.*, **7**, p. 80 (1956). *J. Sci. Instrum.*, **33**, p. 86 (1956).

New books

Peaceful uses of atomic energy. Vol. 7. Nuclear chemistry and the effects of irradiation. (New York: United Nations; London: H.M. Stationery Office, 1956.) Pp. 691. Price 70*s*.

Although, as the title suggests, this volume will primarily interest chemists and metallurgists, nevertheless, rather more than one third of the eighty-six papers should be of interest to physicists. Thus the four papers on the fission process—which, after all, was discovered by radiochemical means—include an important theoretical paper on the distribution of nuclear charge in low energy fission, and an interesting review of spontaneous fission. The two sections dealing with the fission products include nine papers dealing with the discovery of new isotopes or isomers, or with measurements of half lives and characteristic radiations.

Among the many papers concerned with the heavy elements, there is an important and fascinating survey of the preparation and nuclear properties of the heaviest elements (plutonium to fermium) and a discussion of the electronic configuration of the actinide ions. Activation cross-sections for the important isotopes ^{233}Pa and ^{239}Np are reported in another paper in this section.

Those who are interested in the physics of the solid state will find much experimental information of interest and value in the nine papers of Session 11B, which dealt with the effects of radiation on uranium and its alloys, on graphite, and on structural materials. The seven theoretical papers in the final section include an extensive and authoritative paper on the theory of lattice displacements, and several other stimulating papers. Both sessions on radiation damage were distinguished by the lively discussions which are printed verbatim and clearly indicate that this is one of the important growing points in solid state physics.

The book is beautifully produced and extremely readable, and is a worthy record of a notable conference.

R. HURST

Peaceful uses of atomic energy. Vol. 9, Reactor technology and chemical processing. (New York: United Nations; London: H.M. Stationery Office, 1956.) Pp. 771. Price 70*s*.

In common with the other volumes of this series, this book is a collection of papers submitted to the Conference on the peaceful uses of atomic energy held in Geneva in 1955 which were assembled into groups for discussion at the various sessions. The reports of the discussions are limited and although there are some pertinent comments the greatest value by far lies in the papers themselves. Although the papers do not appear in this order, they may be conveniently grouped into those dealing with chemical processing, active waste disposal in its various forms, metallurgical problems including fabrication and corrosion, and technological problems of application of liquid metals as reactor coolants. The volume also contains two papers on the technological problems of homogeneous aqueous reactors. By far the largest proportion of the papers is of U.S.A. and U.K. origin.

In the area of chemical processing, a number of papers deal with the various methods of aqueous processing, and reference is also made to decontamination and operating experience with active plant. Another section deals with possible high temperature or pyrometallurgical processing. Papers at several sessions are devoted to waste handling, including extraction of fission products and disposal of active materials to ground or by sea, and also problems of filtration and air dispersion. In the metallurgical field there are extensive papers on the metallurgy of uranium and its alloys, and thorium, and others on plutonium intermetallic compounds and ceramic fuels. The effects of thermal cycling on uranium are reported but negligible mention is made of irradiation effects. Certain of the fabrication problems of fuel elements for air cooled and water cooled reactors are reported. The information on corrosion refers to water systems, and to liquid metals, which are discussed mainly in relation to the use of sodium and sodium potassium, where there are papers on general technological experience and on heat transfer problems, and one on the particular problems of the sodium-graphite reactor system. A Russian paper refers to experiences with lead and bismuth. The two papers dealing with the homogeneous aqueous reactor cover the chemistry and the problems of slurries of uranium and thorium oxides in water.

Many of the papers have been written as reviews or summaries and are well documented, and should be useful to both the reader who wishes to introduce himself to the subjects and the specialist, though for the latter there is much information which has been released subsequent to the Conference.

J. SMITH

Peaceful uses of atomic energy, Vol. 10. Radioactive isotopes and nuclear radiations in medicine. (New York: United Nations; London: H.M. Stationery Office, 1956.) Pp. ix + 544. Price 57*s*.

This is one of the sixteen volumes which have been required to publish the 1050 papers presented at the International Conference on the peaceful uses of atomic energy held at Geneva in August 1955. The lavish production of these volumes, which is scarcely matched by their scientific value, can perhaps be ascribed to the emotional content of the title and the prodigality of the United Nations.

The present volume deals with the use of atomic radiations in the diagnosis and treatment of disease and includes eighty-five papers together with the discussions which arose from them. The applications to therapy have on the whole been disappointing. Apart from the treatment of thyrotoxicosis with ^{131}I and polycythaemia vera with ^{32}P, the only worthwhile advances appear to have been in the construction of various radioactive sources and teletherapy units for the treatment of cancer, for which purpose they have, in some cases, advantages over the conventional radium and X-ray methods. The most important paper in this section is by J. S. Mitchell on "Some problems in radiotherapeutics," which emphasizes the difficulties in this field and the need for rigorous clinical evaluations. Many of the papers simply described the work going on in various countries, without any scientific data or clinical results, and this led to much fruitless repetition.

The diagnosis and study of disease with radioactive isotopes has proved more fruitful, but the results reported re-emphasize the general dictum that, in "tracer" work, it is very easy to perform the experiments, but much more difficult to interpret

the results. So far, the thyroid gland has received the most attention, and twenty-two papers are devoted to the use of ^{131}I in the study of thyroid function. It is of interest to note, in passing, that cancer of the larynx is the commonest type of malignant disease in East Pakistan.

Although the amount of hitherto unpublished work is relatively small, the volume provides a fair but mostly uncritical survey of current work in this field.

O. A. TROWELL

Peaceful uses of atomic energy. Vol. 11. Biological effects of radiation. (New York: United Nations; London: H.M. Stationery Office, 1956.) Pp. 402. Price 57*s*.

This volume is the outcome of inviting the maximum number of radiobiologists to present a paper at an international conference. Relatively little new information is recorded, partly because another international conference on radiobiology was taking place in Cambridge at the same time.

Sixty-three papers were presented and sixteen of these simply gave a brief résumé of the biological effects of radiation, on which topic there was a commendable degree of agreement. Four of the papers are reported twice. The subjects dealt with in more detail were carcinogenesis, radiation injury and hazards in man, metabolism of bone-seeking isotopes, protection and recovery from radiation, and genetic effects. On the last topic, the rather disquieting conclusions of T. C. Carter that "there is no agreement, even among the informed, about the exact nature and magnitude of the genetic danger from ionizing radiations," and that "we cannot today make any useful quantitative assessment of the genetic consequences of exposure of human populations to ionizing radiations at low dosage rates" are worth noting. In the long run perhaps the most important "peaceful use" of atomic energy may turn out to be the part which many biologists hope it will play in directing the attention of politicians and others to the subject of human genetics.

The Russian contribution is difficult to evaluate as Soviet radiobiology is dominated by the theme that many of the bodily manifestations of radiation damage are secondary consequences of a primary radiation injury to the brain, a view which is not held elsewhere. Many of the statements of A. V. Lebedinsky, for instance that 0·1r increases nerve reflex time by a factor of 2·5, that the nucleic acid content of lymph nodes is increased immediately and at one, two and six hours after irradiation, and that the leucopenia in dogs exposed to 100r is due to conditioned reflexes, are susceptible of experimental refutation, though they were apparently not challenged in the conference discussion.

The most important paper was that of Latarjet and Marcovich (Paris) in which, using a beautiful technique based on the "induction" of bacteriophage in a lysogenic strain of bacteria, they demonstrated a quantitatively measurable biological effect from a dose of 0·3r. At the other end of the scale it was reported that some insects will withstand 350 000r without apparent effect, and at least 5000r is needed to sterilize them. So perhaps insects will inherit the earth if the vertebrates fail to survive the atomic age. O. A. TROWELL

Peaceful uses of atomic energy. Vol. 12. Radioactive isotopes and ionizing radiations in agriculture, physiology and biochemistry. (New York: United Nations; London: H.M. Stationery Office, 1956.) Pp. ix + 553. Price 63*s*.

This volume comprises ninety-four papers, but many of them were not in fact read at the Conference. The record shows that in one session only nine out of twenty-six papers were read, and in another nine out of thirty-one; the remainder were presumably submitted in manuscript form for publication in this volume without criticism or comment. Nine of the papers are reported twice, presumably once as read at the conference and again as a more extensive script submitted later. The subject-matter falls under three headings.

(1) *Radiation-induced genetic changes in crop plants.* In many countries much effort is being made to produce mutations in plants by exposing them to relatively high doses of X- or γ-radiation. The great majority of the mutations produced are of course deleterious, if not lethal, but the hope is to produce occasional beneficial ones, for example, varieties of crop plants which are resistant to certain infectious diseases. So far very little of commercial value has been achieved and most of the authors were content to speculate on the possible benefits which they hope to realize.

(2) *Tracer studies in agriculture.* In this field the use of radioactive isotopes has led to considerable advances in the study of soil chemistry, plant nutrition, and the action of fungicides and insecticides. Two interesting new discoveries are that some plants can be nourished by absorption of nutrient solutions sprayed on to the foliage, and, that in certain forests, practically all the trees are united to their neighbours by natural root grafts, so that the whole forest is in fact a biological continuum through which fungus and other diseases can spread with great rapidity.

(3) *Tracer studies in physiology and biochemistry.* This is certainly the field in which the "peaceful uses of atomic energy" have, so far, been most profitably exploited. The use of radioactive isotopes has led to spectacular advances in almost all fields of biochemistry, and has given fundamentally new knowledge of the processes of intermediary cell metabolism, mineral metabolism, protein and nucleic acid synthesis, cell permeability, photosynthesis, etc., which could hardly have been obtained in any other way. In many cases, however, "tracer" work has raised more problems than it has solved. Particularly in the field of "metabolic turnover" the results are often very difficult to interpret with any certainty. Many of the earlier conclusions have had to be revised in the light of more critical biological judgment and considerable caution is necessary in accepting the conclusions of the many workers who have been attracted to this field by its current popularity and technical ease.

O. A. TROWELL

Peaceful uses of atomic energy. Vol. 15. Applications of radioactive isotopes and fission products in research and industry. (New York: United Nations; London: H.M. Stationery Office, 1956.) Pp. viii + 327. Price 54*s*.

The papers in this volume of the proceedings of a highly successful conference were the substance of three of the sessions. It cannot be claimed that they reveal any outstanding advances in industrial applications and research, but as radioisotope applications cover such a variety of subjects, the fact that we have here a collection, though by no means a comprehensive one, of authoritative papers in one book is of considerable worth. Nine of the papers are by Russian authors and provide a valuable introduction, in English, to their work.

The first session, Radioactive isotopes in research, is rather heavily weighed in favour of analytical chemistry, six of the sixteen papers being on this subject, with considerable overlapping particularly on radioactivation analysis. The first session starts well with a paper by Kondratyev giving an account of Russian work on tracer studies of chemical reactions, whilst Willard deals with the rather wider aspects of radio-isotope technique in chemical research but only in the bare outline. Other topics discussed are the use of radio-isotopes in catalysis, petroleum production research, adsorption and diffusion in alloys (all the three papers of this latter subject being by Russian authors).

The second session, Radioactive isotopes in control and technology shows clearly the similarity in development in Europe, Russia and America. Thickness gauges and allied instruments are naturally well to the fore (three papers), together with γ- and bremsstrahlung radiography (five papers) as having the longest history. Other papers of particular interest are Samarin's, on the study of the processes of the production of iron and steel, as the Russians have done much work here and a comprehensive review by Hull and Fries on techniques in petroleum refinery research and analysis. Other papers on wear, leakage and hydraulics, fluid dynamics and sand movement are also included.

The third session, Fission products and other applications is devoted almost entirely to radiation chemistry and the authors are almost exclusively American. The papers review, as might be expected, γ-ray induced chemical reactions, irradiation of polymers, and sterilization of food and its effects, but there is a very little previously unpublished work included; less popular topics include self-luminous compounds, nuclear batteries and the direct conversion of the energy of nuclear radiation to electrical power.

Each session is accompanied by a verbatim record of the proceedings but the discussion was, on the whole, disappointing. The translations are sometimes a little clumsy but the meaning is usually clear and in view of the speed with which these volumes have appeared, it is a forgivable blemish.

G. B. Cook

Nachrichtentechnische Fachberichte. Band 4. Elektronische rechenmaschinen und informationsverarbeitung. Edited by A. Walther. (Braunschweig: Friedr. Vieweg and Sohn, 1956.) Pp. viii + 229. Price *DM* 26.

This volume contains the proceedings of an international conference on electronic digital computing devices held in Darmstadt in October 1955. Scientists from 15 countries took part in the conference, which dealt with technical details of memory and switch elements, descriptions of several large machines, programming, developments in numerical mathematics and abstract switching theory. The text of the proceedings was prepared by transcription of a tape recording, subject to correction by the authors. This method makes possible an earlier publication, but has disadvantages. When an author presents a paper, he does not give all experimental and mathematical details, but is concerned rather with pointing out in the simplest language the principal features of his work. Some of the present volume therefore lacks the completeness which one expects of a well-written scientific paper. Nevertheless, the sixty-four papers collected here form an easily read, interesting and useful guide to the present status and probable future developments of a rapidly growing subject.

T. B. Rymer

Order–disorder phenomena. By E. W. Elcock. (London: Methuen and Co. Ltd., 1956.) Pp. x + 166. Price 11*s.* 6*d.*

"The essential process of ordering is one of those curious and immediately arresting phenomena that can hardly fail to arouse enthusiasm"—and the author's enthusiasm is communicated to the reader. This book is a useful addition, of the more recent, rather longer type, to the series of Methuen's monographs on physical subjects. The five chapters are a general introduction; the specification and determination of the state of order; approximate theoretical treatments; non-stoichiometric alloys; relation of ordering to ferromagnetism and antiferromagnetism. The treatment is confined to two-component systems and, in general, to alloys, though some inorganic compounds are included in the final chapter.

In a wide survey it is inevitable that the worker in each field will find minor blemishes in the exposition of his specialty, but I have not noted any serious defects in the X-ray sections. In a second edition more care should be devoted to proof-reading; "uberstrucktures" is neither English nor German, and Professor Lipson's initials are not A.H.

A. J. C. Wilson

Molybdenum. Metallurgy of the rarer metals. No. 5. By L. Northcott. (London: Butterworths Scientific Publications, 1956.) Pp. xii + 22. Price 40*s.*

This book, the fifth in this useful series, is timely in view of the possibilities that molybdenum may emerge as an engineering material in its own right, after many years as a "physicists" metal and an alloying constituent of steels. Before its outstanding strength at high temperatures can be utilized in gas turbines, however, formidable problems remain to be overcome, not least among them arising from the readiness with which the metal oxidizes when hot.

Surface treatments to minimize oxidation, as well as the physical metallurgy of the metal and its alloys, and methods for their preparation and fabrication in bulk and of adequate purity, have been, and remain, under intensive investigation. In these circumstances it must be a hard task for an author to prepare a balanced and well-digested account in which leading trends are clearly indicated. and this book betrays some evidence of the difficulties. It is none the less to be commended as an up-to-date collection of facts in an important area of modern metallurgical technology.

G. L. J. Bailey

Handbuch der Physik. Edited by S. Flügge. Volume XVII: **Dielectrica.** (Berlin: Springer-Verlag). Pp. vi + 406. Price *DM*94 .

The first article (150 pp.) by W. F. Brown, jr., gives an excellent survey of the dielectric properties of gases (at low and high densities), liquids, solutions and solids in steady as well as in alternating electric fields. Theory and measurements of dielectric losses and relations between molecular structure and dipole moments are discussed in detail. Clausius–Mosotti's equation comes under heavy fire from the author. The subtleties of modern dielectrics, i.e. piezo- and ferro-electricity and electro-striction, are treated in 130 pages by E. W. Forsbergh, jr. The dielectric constants of ferro-electrics (values up to 10^4) are presented together with the hysteresis loops and discontinuities closely analogous to ferromagnetics, the time lags, the Curie points and the results of X-ray and infra-red studies of the various crystals, particularly of barium titanate, and are followed by the

various theories of ferro-electricity. Piezo-electric phenomena and electro-striction in static and dynamic mechanical fields are included. The whole subject is of great complexity, but it becomes unnecessarily involved by the use of new technical terms that makes its reading rather difficult. Finally, there is an article by W. Franz (100 pp. in German) in which the electric breakdown in solids and liquids is reviewed critically and with clarity. As to solids, the usual distinction is made between thermal and electric breakdown; gas formation and other processes play a vital role in the breakdown of liquids. The theoretical section of solids in electric fields contains a treatment of the interaction between electrons and lattice, ionization by collision, external and internal field emission, energy distribution of electrons, rate of multiplication and other topics.

Common to the three authors of this volume is the perseverance with which they have assembled the vast aggregate of references—a *sine qua non* of a good "handbook." Print and illustrations: alpha double plus. A. VON ENGEL

Chemical Engineering Practice. Vol. 1, General; Vol. 2, Solid state. Edited by H. W. Cremer and T. Davies. (London: Butterworths Scientific Publications, 1956.) Vol. 1, pp. xiv + 494; Vol. 2, pp. vi + 632. Price 95*s*. per volume.

This work to be completed in twelve volumes (of which the first two volumes are reviewed) is intended to present all aspects of chemical engineering involved from the inception of a chemical engineering project to its completion. The objective is therefore an ambitious one, and possibly controversial in view of the difficulties in defining the limits of chemical engineering science. It is, however, gratifying to note that emphasis is placed on the fact that chemical engineering is concerned essentially with applied physics in addition to applied chemistry, for many chemical engineering operations are primarily concerned with the application of physical laws rather than with chemical reactions. The physicist who is concerned with chemical engineering problems should therefore welcome this approach which has been clearly emphasized in this work.

The work is intended for those who have already obtained a first degree in chemical engineering, and in practising the science wish to refer to the many fundamental and applied aspects of chemical engineering. Emphasis is placed on the theoretical background of the subject, and a clear distinction is made between chemical engineering and chemical technology. This is an important distinction and one which the practising chemical engineer must always bear in mind, since the theoretical approach to many chemical engineering problems does not always correlate with the practical data derived from chemical technology. The practising chemical engineer must therefore develop a sound sense of technical judgment founded on fundamental principles and allied with practical experience.

A work of this magnitude must necessarily cover a very wide field and in a short review it is only possible to outline the subjects which have been dealt with in these first two volumes.

The first volume opens with an introductory chapter on the origins of chemical engineering, followed by a chapter on the chemical engineer which adequately summarizes the diverse activities of the chemical engineer in modern chemical industry. There follows a chapter on economics of production as exemplified in process industries. The section on the investigation and development of an industrial process is covered in chapters on the preparation of material balances, and the preparation of energy balances. A further section on pilot plants and semi-commercial units includes chapters on general aspects, design, operation, reporting of results and a comprehensive bibliography. This first volume concludes with chapters on the preparation of flow diagrams for full scale production; and units, dimensions and calculations.

The second volume is of special interest to the physicist who is concerned with chemical engineering. The opening chapter on fundamental concepts of matter in the solid state is followed by a section on metals and metallic alloys, which includes chapters on the significance of mechanical properties and their measurement, alloy equilibrium diagrams, the range of steels, fatigue in metals and creep in metals. The volume proceeds to chapters on the mechanical and physical properties of plastics and glasses, corrosion of metals, porous masses, porous powder metallurgical products for filtration and related uses, and powder metallurgy. The volume concludes with a section on the important industrial uses of porous masses, which includes chapters on the purification of coal gas, flow in fuel beds, the use of porous masses in the treatment of water and sewage and transpiration cooling.

The chapters are illustrated by drawings, graphs, flowsheets, and, where appropriate, by numerical examples. Each chapter contains an adequate list of references to standard works and recent literature.

The impression is gained that the general and managing editor have succeeded admirably in collating the material which forms the tools of the practising chemical engineer. These first two volumes set a uniformly high standard and the work should comprise a valuable addition to chemical engineering libraries. H. THOMAS

Lectures on rock magnetism. By P. M. S. BLACKETT. (Jerusalem: The Weizmann Science Press of Israel, 1956.) Pp. 131. Price $5.00.

This account of the second Weizmann Memorial Lectures deals with the recent developments in this new branch of geophysics. In it Professor Blackett gives his views of the use of magnetic data to trace the history of the earth's magnetic field and to attempt to throw some light upon the theories of drift and polar movement. Particular attention is directed to the discussion of the evidence in support of these theories, and to some possible processes which might be responsible for the many reversely magnetized rock samples found in different parts of the world. At present, evidence cannot be regarded as providing any decisive solution, and it is clear that much new experimental work has to be carried out. In particular, there is little or no systematic magnetic data available on these natural materials. The book presents in easily readable form a lucid account of a fascinating and as yet unsolved problem.

W. SUCKSMITH

Notes and comments

Automatic measurement of quality in process plants

The Council of the Society of Instrument Technology Ltd., has approved a proposal to hold a Conference this year on the above subject. The Conference will be held at the University College of Swansea from the evening of Monday, 23rd, to midday on Thursday, 26th September, 1957.

The main object of the gathering is to provide an opportunity for the users and makers of automatic measuring equipment, and those concerned with research and developments in this field, to meet and discuss their work. It is hoped that the range of topics to be covered will include: *Chemical quality*: chromatography; mass-spectrography; pH-measurement; spectroscopy; titration. *Physical quality*: density; moisture content; refractive index; viscosity and "consistency."

Offers of further contributions on these and other similar topics will be welcomed by the Council. It is hoped that the papers will ultimately be published in book form, together with discussion submitted in writing after the Conference.

Because of limited accommodation, and to retain informality in the technical discussions, it will be necessary to restrict the total number attending.

All communications should be addressed in the first instance to: The Secretary, The Society of Instrument Technology Ltd., 20, Queen Anne Street, London, W.1.

Conversion factors for specific energy, energy and pressure

Mr. E. J. Le Fevre of the Mechanical Engineering Research Laboratory of the Department of Scientific and Industrial Research, has prepared a report giving the conversion factors resulting from recent international decisions regarding units and kindred matters that affect tables of thermodynamic properties of steam and other working media.

Interconversion tables for specific energy, energy and pressure are given. Copies of this six-page duplicated report are obtainable gratis from the Director, Mechanical Engineering Research Laboratory, East Kilbride, Glasgow.

Applications should quote HEAT NO. 111.

Zeitschrift für Instrumentenkunde

After a lapse of 13 years, caused by the war, the German *Zeitschrift für Instrumentenkunde* has made its reappearance. The new issue which opens the 65th volume appears almost exactly 75 years after its first publication in 1881. At that time the new journal was the first of its kind in the world to deal with the description of scientific instruments and it became the model for journals such as this one in other countries. Professors Glazebrook and J. J. Thomson cited the *Zeitschrift für Instrumentenkunde* as an example when in the 1920's they promoted the founding of our *Journal*.

The *Zeitschrift für Instrumentenkunde* was purposely designed to forge a link between the academic centres of scientific study and the fast growing industry in the new German Reich. In its volumes the growth of German technology and instrument making can be traced. The first article ever published in the journal describes a barometer and is signed by Mechaniker R. Fuess, who in the years to come gave his name to one of the most important German instrument firms. In spite of the old spelling with c's instead of Z's or k's, and with h's which have long since disappeared from behind t's, the foreign reader will still find the back numbers of the *Zeitschrift für Instrumentenkunde* pleasant reading. It is to be feared that he may not have such an easy passage with the neo-German of the most recent issue using words like *Feinwerk* which the reader may have difficulty in finding in a dictionary. We suggest that the Editors consider retaining the more conservative style of the old volumes. We welcome the reappearance of the Zeitschrift and wish the Editors (Prof. Dr. W. Keil of Stuttgart and Reg.-Rat Dr.-Ing. H. J. Schrader of Brunschweig) and the publishers (Friedr. Vieweg & Sohn of Braunschweig) all success in their venture.

World Directory of Crystallographers

The International Union of Crystallography is considering the possibility of preparing a world directory of crystallographers. This list would contain the names and addresses of all practising crystallographers, including advanced graduate students. It is planned to compile a preliminary list in time for the Fourth General Assembly to be held in Montreal, July 10–17, 1957. The Secretaries of the national committees (*Acta Cryst.*, **8**, 857, 1955) have been asked to prepare a list of crystallographers in their countries. Some scientists and technologists, however, who carry on crystallographic work (including X-ray, electron or neutron diffraction and microscopy or other techniques) are not members of scientific societies having a unique crystallographic interest, and might therefore be missed. Those who come into this category are asked to send their names and addresses, in printed letters, to Dr. Williams Parrish, Philips Laboratories, Irvington-on-Hudson, New York, U.S.A.

Journal of Scientific Instruments

Contents of the April issue

CONFERENCE REPORT

Summarized proceedings of a conference on contemporary optics, Sydney, 1956. By C. G. Bruce, R. G. Giovanelli and W. H. Steel.

ORIGINAL CONTRIBUTIONS

A high temperature microfurnace for the study of the devitrification of glass. By H. Bridge.

A photographic recording microphotometer. By J. Bor.

The floating-zone melting of refractory metals by electron bombardment. By A. Calverley, M. Davis and R. F. Lever.

Mercury-in-quartz thermometers for very high accuracy. By H. Moreau, J. A. Hall and Vera M. Leaver.

The measurement of the momenta of high energy charged particles in a diffusion cloud chamber. By B. B. Culwick.

Laboratory and workshop notes

An attachment to a Weissenberg camera for heating specimens between exposures. By L. S. Dent.

The application of a simple mercury discharge lamp to Schlieren photography. By D. H. Edwards and J. D. Owen.

NOTES AND NEWS

Correspondence

On processing titanium hydride replenishers. From D. Walsh and P. M. Shearman.

INSTRUMENTS, ELECTRONICS AND AUTOMATION EXHIBITION—A preview

Notes and comments

THIS JOURNAL is produced monthly by The Institute of Physics, in London. It deals with all branches of applied physics (including theory and technique).

All rights reserved. Responsibility for the statements contained herein attaches only to the writers.

EDITORIAL MATTER. Communications concerning editorial matter should be addressed to the Editor, The Institute of Physics, 47 Belgrave Square, London, S.W.1. (*Telephone:* Sloane 9806.) Prospective authors are invited to prepare their scripts in accordance with the *Notes on the preparation of contributions*. (Price 2*s*. 6*d*. including postage.)

REPRODUCTION. The Institute of Physics is a signatory to The Royal Society's Fair Copying Declaration. Details may be obtained upon application from The Royal Society, London, W.1.

ADVERTISEMENTS. Communications concerning advertisements should be addressed to the agents, Messrs. Walter Judd Ltd., 47 Gresham Street, London, E.C.2. (*Telephone:* Monarch 7644.)

CLAIMS FOR MISSING JOURNALS. Claims from regular subscribers to this *Journal* for missing numbers will only be considered if received within 60 days of the date of mailing plus normal outward time of transit and time for lodging the claim. Losses attributable to failure to notify a change of address or to similar omissions will not be considered.

SUBSCRIPTION RATES. A new volume commences each January. The charge is £5 per volume ($14.25 U.S.A.), including index (post paid), payable in advance. Single parts, so far as available, may be purchased at 10*s*. each ($1.50 U.S.A.), post paid, cash with order. Orders should be sent to The Institute of Physics, 47 Belgrave Square, London, S.W.1, or to any bookseller.

The effect of radiation damage on the electronic properties of solids*

By E. W. J. MITCHELL, M.Sc., Ph.D., A.Inst.P., Physics Research Laboratory, University of Reading

An outline is given of the way in which the concentration of defects introduced by irradiation may be estimated. The topics which are discussed are the effects of irradiation on the electron mobility in metals, the carrier concentration in germanium and the optical absorption in quartz and diamond. The emphasis in the discussion of results is on their contribution to the study of defects in solids.

1. INTRODUCTION

The discussion in this article is limited to the effects of atomic displacements produced by elastic collisions between the nuclei and the incident high energy radiation. Since most properties of materials are affected in some degree the discussion is further limited to electronic properties—the resistivity of metals and semi-conductors, and the optical properties of insulators.

There are two aspects of radiation damage work, one involving the study of the energy loss of fast particles and the other the study of defects in solids. The latter is well illustrated by the fact that the only experimental knowledge concerning the behaviour of interstitial atoms in simple metals is derived from radiation damage work. Similarly, fast particle irradiation is the only means available for introducing lattice defects into the simplest covalent solid, namely diamond.

2. THE ESTIMATION OF DEFECT CONCENTRATIONS[1]

In passing through matter charged particles lose energy by exciting electrons and also by Coulomb interaction (Rutherford scattering) with nuclei. For most velocities the rate of energy loss is very much greater for the first process than it is for the second. After nuclear encounters, the nuclei may have sufficient recoil energy to escape from their normal positions into interstitial positions. With heavy particle irradiation these primary knock-ons can produce further displacements. The minimum recoil energy required for an atom to be displaced (E_d) is discussed below.

Energy can be transferred to lattice vibrations by one of two processes during irradiation: the transfer of the excited electronic energy, or some part of it; and, the direct excitation of lattice vibrations which occurs with non-displacement collisions. Depending on the rate at which energy can be dissipated by the lattice these processes may lead to considerable excesses of vibrational energy in regions large compared with atomic dimensions. In the former case they are referred to as thermal spikes[2] and in the latter as displacement spikes[3] or *M*-regions[4] (Fig. 1).

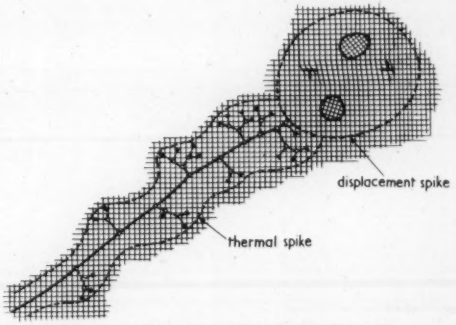

[*Reproduced from "Journal of Applied Physics"*]

Fig. 1. A two dimensional representation of radiation damage (after Brinkman)

× interstitial atoms
○ vacant lattice sites
——— path of primary knock-on
– – – path of subsequent knock-on
(intersections of background lines represent normal lattice sites)

Table 1. *Some maximum recoil energies and defect concentrations*

	E_{max} (eV)			Calculations for 12 MeV d^+		
	1 MeV e^-	2 MeV n^0	12 MeV d^+	β (eV cm)^2	N_d cm^{-3}	
C	360	$5{\cdot}7 \times 10^5$	6×10^6	$0{\cdot}29 \times 10^{-12}$	$2{\cdot}3 \times 10^{-4}$	$4{\cdot}1 \times 10^{19}$
Si	153	$2{\cdot}7 \times 10^5$	3×10^6	$0{\cdot}8 \times 10^{-12}$	$1{\cdot}4 \times 10^{-3}$	$7{\cdot}0 \times 10^{19}$
Cu	67·5	$1{\cdot}2 \times 10^5$	$1{\cdot}4 \times 10^6$	$1{\cdot}6 \times 10^{-12}$	$3{\cdot}3 \times 10^{-3}$	$2{\cdot}8 \times 10^{20}$
Ge	59·4	$1{\cdot}1 \times 10^5$	$1{\cdot}2 \times 10^6$	$1{\cdot}7 \times 10^{-12}$	$2{\cdot}8 \times 10^{-3}$	$1{\cdot}2 \times 10^{20}$
Au	21·8	$4{\cdot}5 \times 10^4$	$4{\cdot}8 \times 10^5$	$4{\cdot}0 \times 10^{-12}$	$5{\cdot}6 \times 10^{-3}$	$3{\cdot}3 \times 10^{20}$

The values of E_d used are: 65 eV — C, 30 eV — Si, 25 eV — Cu, 31 eV — Ge and 25 eV — Au.
The value of N_d for C refers to diamond.

The particles to be considered here are electrons, deuterons and neutrons. Atomic displacements can be induced by γ-irradiation[5] but these result primarily from collisions involving the Compton electrons which are produced

* Based on a lecture given to the Electronics Group of The Institute of Physics on 13 December, 1955.

uniformly throughout the solid. Protons[6] and α-particles[7] have been used in radiation damage studies but the calculation of defect concentrations is very similar to that for deuterons. Some examples of the recoil energies which can be obtained for different bombarding particles are shown in Table 1.

Procedure—General

The most reliable calculations are those in which empirical range-energy relations are used. This avoids the necessity of having to rely on a theory of the rate of energy loss of charged particles by electronic excitation. If the total rate of energy loss of the bombarding particle is $-\frac{\partial E}{\partial x} = f^n(E)$ the range is $R = \int_0^{E_i} \frac{dE}{f^n(E)}$. Two cases which will be of interest in this article are the range of electrons in carbon, as used by Clark and others[5]—$R = 0{\cdot}12\,E_i^{1{\cdot}38}$, $0{\cdot}15 < E_i < 0{\cdot}8$ MeV, Glendennin,[8] and of deuterons in germanium, as used by Fan and Lark-Horovitz[9]—$R = 6{\cdot}33 \times 10^{-4}.E_i^{1{\cdot}63}$, $2 < E_i < 10$ MeV, Heller and Tendam.[10] For a 1 MeV electron the range in diamond is 1·2 mm while for a 10 MeV deuteron in germanium the range is only 270 μ.

We have to find first the number and energy distribution of the primary knock-ons produced as a result of nuclear collisions. The probability of an incident particle (mass M_1) being scattered in a given direction is expressed in terms of the differential cross-section ($d\phi$) such that $N_i.d\phi(\theta).d\Omega =$ the number of particles scattered per second at an angle θ into a solid angle $d\Omega$, per scattering centre (mass M_2) (Fig. 2). N_i(cm^{-2} s^{-1}) is the incident flux.

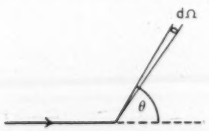

Fig. 2. The angle of scattering θ

The energy transferred to the primary knock-on is

$$E_p(\theta) = \frac{4M_1M_2}{(M_1 + M_2)^2}.E_i.\sin^2(\tfrac{1}{2}\theta) \qquad (1)$$

which for light bombarding particles gives

$$E_p(\theta) = 4\frac{M_1}{M_2}.E_i\sin^2(\tfrac{1}{2}\theta)$$

except that light particles are usually moving fast enough for the relativity correction to be appreciable, when

$$E_p(\theta) = \frac{4E_i}{M_2}.\frac{(\tfrac{1}{2}E_i + M_1c^2)}{c^2}.\sin^2(\tfrac{1}{2}\theta) \qquad (1a)$$

From these relations we can find the primary knock-on energy for each value of θ. Thus the number of primary knock-ons having energy in the range $E_p(\theta)$ to $E_p(\theta) + dE_p(\theta)$ is given by

$$N_p.dE_p(\theta) = N_i.d\phi[E_p(\theta)].2\pi\sin\theta.d\theta \qquad (2)$$

Electrons

In the case of most electron irradiations the primary knock-ons, because of the unfavourable mass ratio, do not have sufficient energy to produce further displacements. We are therefore not interested in the energy distribution of the primary knock-ons but only the total number produced with energy greater than the minimum displacement energy. A total cross-section $[\sigma(E_i)]$ may be defined such that the number of displacements per scattering centre (f) is

$$N_i.\sigma(E_i) = \int_{E_d}^{E_{MX}} N_p.dE_p(\theta)$$

where E_{MX} is given by equation (1a) above when θ is 180°.

The integration is performed for various values of E_i incident on atomic layers in the crystal at chosen depths x, the relation between these values being determined by $f^n(E)$ which can be obtained from the range-energy relation. A final integration over all values of E_i, that is over all x, gives the total number of displacements per scattering centre. The experiment of firing the bombarding particles into a thick specimen can be used for electron irradiations because "foreign" nuclei are not left in the crystal, and because the threshold energy E_t defined by

$$E_d = \frac{4E_t\,(\tfrac{1}{2}E_t + M_1c^2)}{M_2\,c^2} \qquad (3)$$

is within the energy limits for which the range-energy relation is known.

The procedure outlined above has been used by Clark and others[5] for calculating defect concentrations in diamond. They have used the relativistic expression for the differential cross-section per unit solid angle given by Mott and Massey[11]

$$d\phi = \frac{Z_2^2e^4}{4\mathbf{m}^2v^4.\sin^4(\tfrac{1}{2}\theta)}\left[1 - \frac{v^2}{c^2}\sin^2(\tfrac{1}{2}\theta)\right]\left(1 - \frac{v^2}{c^2}\right) \qquad (4)$$

where Z_2 is the atomic number of the scattering centre and v the incident electron velocity. For $E_i = 1$ MeV and $E_d = 60$ eV Clark and others find that there are 0·05 displacements produced per incident electron. Thus for a dose of 100 μA min (3×10^{16} incident particles per cm^2) they find $1{\cdot}6 \times 10^{15}$ displacements. The concentration in the x-direction is non-uniform, falling from high values to zero in about 1 mm, with a mean of about 2×10^{16} cm^{-3}.

Deuterons, etc.

The simplest set of conditions is when the specimen is sufficiently thin for the outgoing particles to have practically the same energy (say within 10%) as the incident particles. Then, since the cross-section does not vary violently with energy, we can treat the incident beam as monoenergetic throughout the crystal, with consequent simplification. A further advantage is that under these conditions there will not be a concentration gradient of defects in the crystal. Thus we can readily calculate the number of primaries. Because of the larger mass ratio the primary knock-ons in deuteron irradiations can produce further displacements and according to Kinchin and Pease[1] each primary produces $E_p/2E_d$ displacements in slowing down to rest.

The differential cross-section per unit solid angle for nuclear collisions is given by the Rutherford equation

$$d\phi = \frac{1}{E_i^2}.\left(\frac{Z_1Z_2e^2}{4}\right)^2\operatorname{cosec}^4(\tfrac{1}{2}\theta) \qquad (5)$$

whereupon, using equation (2), we find the energy distribution of the primaries as

$$N_p.dE_p = \beta.N_i.\frac{dE_p}{E_p^2E_i} \qquad (6)$$

where $$\beta = \pi\left(\frac{Z_1 Z_2 e^2}{M_1 + M_2}\right)^2 M_1 M_2$$

some values of which are shown in Table 1. Z_1 is the atomic number of the bombarding particle. The number of displacements per scattering centre (f) is

$$\int_{E_d}^{E_{MX}} N_p . dE_p + \int_{2E_d}^{E_{MX}} N_p \cdot \frac{E_p}{2E_d} \cdot dE_p = \frac{\beta N_i}{E_i E_d}\left(1 + \frac{1}{2}\ln\frac{E_{MX}}{2E_d}\right) \quad (7)$$

The work of Cooper and others[12] was carried out under these conditions. They irradiated thin copper wires with 12 MeV deuterons. Using equation (7) we find for 10^{17} d cm^{-2} and $E_d = 25$ eV $3{\cdot}3 \times 10^{-3}$ displacements per scattering centre, i.e. $2{\cdot}8 \times 10^{20}$ defect pairs cm^{-3}.

For thicker specimens, but sufficiently thin for the outgoing energy to be within the limits of the known range-energy relation, we have to carry out the above calculation for successive planes of atoms. The incident energy of the deuterons on each plane may be found from the range-energy curve. Thus for germanium bombarded by 9·6 MeV deuterons Fan and Lark-Horovitz[9] give the concentration of defects as $2{\cdot}1 \times 10^{-3}$ per scattering centre per 10^{17} cm^{-2} incident deuterons, or $9{\cdot}3 \times 10^{19}$ cm^{-3} (cf. Table 1 for monoenergetic deuterons).

Neutrons

We are concerned with displacements resulting from collisions between fast neutrons and the nuclei of the solid. In a pile, specimens are irradiated with both slow and fast neutrons. The presence of the slow neutrons means that in some cases transmutation can occur, e.g. germanium, James and Lark-Horovitz.[13] This has the effect of introducing a permanent chemical impurity. The concentrations, however, are low enough not to obscure seriously the displacement effects.

Two advantages of neutron irradiations are that the ranges of neutrons are very much greater than the thicknesses of specimens used and also that the cross-sections for nuclear encounters are known experimentally over a wide energy range. In many cases the cross-section (σ_a) is independent of energy over the requisite range and the scattering may be assumed under these conditions to be isotropic. Some values are given by Adair.[14]

Since all values of scattering angle are then equally likely, a given monoenergetic neutron irradiation $n(\epsilon).d\epsilon$ n cm^{-2} in the energy range ϵ to $\epsilon + d\epsilon$ will produce equal numbers of primary knock-ons of all energies up to $F_{MX}\epsilon$. The number of primaries in an energy range dE_p is independent of energy and is given by

$$N_p . dE_p = \frac{\sigma_a . n(\epsilon) d\epsilon}{F_{MX}\epsilon} \cdot dE_p \quad (8)$$

per scattering centre. Thus the calculation of the damage effects resulting from pile irradiation is intrinsically no more difficult than the calculation of the effects of deuteron irradiations.

At any point in a pile there will be thermal neutrons and neutrons which have not yet been completely moderated, having energies from the thermal value up to the fission energy. In the centre of a cell of the graphite lattice in the Harwell pile (BEPO) at about 50° C the neutron spectrum is given by

$$n(\epsilon)d\epsilon \simeq At.\left[(1/\epsilon_0^2)\epsilon . e^{-\epsilon/\epsilon_0} + (0{\cdot}05/\epsilon)\right]d\epsilon \quad (9)$$

where ϵ_0 is about 0·025 eV, $n(\epsilon)d\epsilon$ is the neutron dose cm^{-2} in the energy range ϵ to $\epsilon + d\epsilon$, A is a constant depending on the power level of the pile and is given approximately for each irradiation and t is the duration of the exposure. The second term is not applicable for energies up to 0·1 eV and the measured thermal dose is defined as

$$D = \int_0^{0{\cdot}1} n(\epsilon)d\epsilon = 0{\cdot}91At$$

For producing displacements we need ϵ greater than about 100 eV and above this the neutron spectrum is

$$n(\epsilon)d\epsilon \simeq 0{\cdot}055D\frac{d\epsilon}{\epsilon}$$

Assuming as before that a primary knock-on of energy E_p produces $E_p/2E_d$ displacements in slowing down to rest, the number of displacements per scattering centre is

$$\int_{E_d|F_{MX}}^{\epsilon_{MX}} \int_{E_d}^{F_{MX}\epsilon} N_p . dE_p + \int_{2E_d|F_{MX}}^{\epsilon_{MX}} \int_{2E_d}^{F_{MX}\epsilon} E_p/2E_d . N_p . dE_p \quad (10)$$

which, using equation (8), gives

$$\sigma_a \frac{0{\cdot}055D}{2E_d} \cdot \frac{E_{MX}}{2}$$

as long as $E_{MX} > E_d$. If the solid is diatomic there will be two such terms corresponding to the two types of primary knock-ons. For quartz Mitchell and Paige estimate a defect concentration under these conditions of 5×10^{18} cm^{-3} for $D = 10^{17}$ n cm^{-2}.

Loss of energy of moving atoms

We have assumed so far that the knock-ons only lose energy in nuclear encounters and that when the recoil energy exceeds $2E_d$ a further displacement is produced. It has also been assumed that the non-displacement collisions do not affect the calculation. However, as the moving atom slows down—although still having $E > 2E_d$—the number of non-displacement collisions will increase. If the rate of generation of vibrational energy in a small region by such collisions exceeds that at which the energy can be removed by thermal conduction the "local temperature" will rise. If this temperature rise is large enough it is supposed that no point defects will be produced or retained in the region.

There is as yet no direct evidence that such a process occurs. Indirectly, irradiation induced phase changes have been observed in some materials—notably quartz,[15] diamond[16] and zirconia.[17] It is likely that the new phases are the final products of the heated regions. The results for diamond and quartz are referred to below. The lack of precise knowledge about this process leads to the main uncertainty in the calculation of point defect concentrations induced by deuteron or neutron irradiation. Estimates have been made by Brinkman[3] and Mitchell and Paige.[4]

When the primary knock-ons are charged they will also lose energy by electronic excitation. This is most important when considering the energy loss of fission fragments[18] but is not significant for the knock-ons produced by pile irradiation of elements above carbon, or for 10 MeV deuteron irradiation of germanium or gold. The criterion which has been used is that the knock-ons are not on the average charged if their velocity is less than that of their least tightly bound electron.[19, 20]

The value of E_d

E_d is the minimum energy which an atom must be given to be knocked into an interstitial position. E_d represents the energy required to produce an interstitial when *all the surrounding atoms remain in their original positions*. This arises because the collision takes place quickly compared with the time of relaxation of the neighbouring atoms. The minimum displacement energy is therefore greater than the energy E_F required to produce an interstitial-vacancy pair by thermal activation, during which the surrounding atoms relax continuously to the changing equilibrium conditions. The difference between E_d and E_F is analogous to the difference between the optical and thermal activation energies of a localized electron in a solid. In this case according to the Frank–Condon principle the optical transition occurs before there is any relaxation in the positions of the surrounding atoms.

The Schottky defect (vacancy plus extra surface atom) rather than the Frenkel defect (interstitial—vacancy pair) is the defect produced most commonly by thermal activation and this is consistent with the few calculations of energy of formation which have been made. In copper, for example, Huntington[21] has estimated that between 5 and 10 eV is needed to produce an interstitial atom. Seitz[1] suggested that as a basis for initial calculations a value of $E_d \simeq 25$ eV should be considered. It is clear (Table 1) that for this sort of value electron irradiation provides a direct method of measuring E_d.

The results of Klontz and Lark-Horovitz[22] for germanium are shown in Fig. 3, from which a threshold electron energy of 0·65 MeV is deduced corresponding to $E_d = 31$ eV. A value of 25 eV has been found for copper by Eggen and Laubenstein.[23] In diamonds a visible absorption band is associated with displacements and the absorption is not directly affected by ionization processes. Dugdale[24] has used the depth of penetration of colour as a function of electron energy to determine E_d. He found from the extrapolation to zero effect a value $E_d = 65 \pm 5$ eV. Recently Loferski and Rappaport[25] have reported that what are considered to be atomic displacements, affecting the lifetime of carriers in a P/N junction in germanium, are produced at electron energies giving $E_d < 23$ eV.

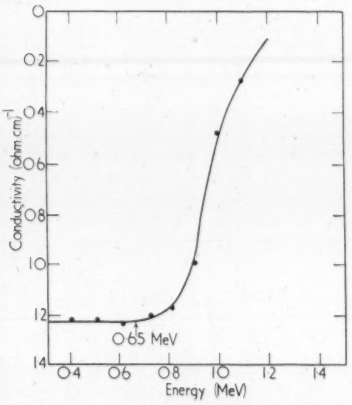

[*Reproduced from "Annual Review of Nuclear Science"*]

Fig. 3. The determination of the threshold energy for germanium. The conductivity after a constant dose is shown as a function of the energy of the bombarding electrons (after Klontz)

While these results show that the Seitz value is a useful approximation it is clear that a systematic study of displacement energies should be made. This work involves the full time use of an electron accelerator—a facility which is not yet available to solid state physicists in this country who are not engaged in technological work.

3. THE RESISTIVITY OF METALS

The resistivity of metals is altered by the additional electron scattering by defects induced during irradiation. At room temperature this may be negligible compared with the thermal scattering. Further, the defets may be annealed at room temperature. Measurements are therefore made at low temperature where the induced effects are large compared with the residual resistance, and where the probability of annealing is much less.

If aluminium is irradiated and measured at room temperature there is no detectable change in resistivity,[26] and only small changes with copper, silver and gold. When irradiated and measured at 10° K damage effects are readily determined. Fig. 4 shows the well-known results of Cooper and others.[12]

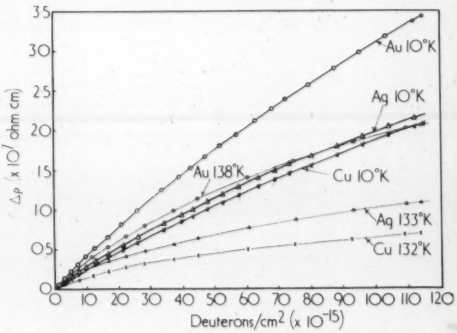

[*Reproduced by permission of The Physical Society*]

Fig. 4. The change of resistivity of copper, silver and gold as a function of deuteron dose (after Koehler and Seitz)

The two curves for each metal (10 and 130° K) show that at the higher temperature some annealing is taking place. At the lower temperature there is probably no annealing resulting from the ambient temperature, although the non-linearity of the change of the resistivity *versus* dose curve may arise from annealing in a thermal spike.

The initial slopes at 10° K give

	Cu	*Ag*	*Au*
$\Delta\rho$/dose ($\mu\Omega$ cm/10^{17}.d^+. cm^{-2})	0·23	0·26	0·38

According to Matthieson's rule the resistivities arising from different scattering processes may be added. Thus if Δ_ρ is

the change of the low temperature resistivity induced by irradiation

$$\Delta_\rho = \rho_{int} + \rho_{vac} + \rho_{agg}$$

where the component resistivities are due to electron scattering by interstitial atoms, vacancies and any aggregates which may be present.

Kinchin and Pease[1] have calculated the concentration of defects expected to be produced by the deuteron irradiation, and assuming that only single interstitials and vacancies are produced their results may be expressed in terms of resistivity per 1% vacancies and 1% interstitials as

	Cu	*Ag*	*Au*
$(\rho_{int} + \rho_{vac})$ $\mu\Omega$ cm	0·57	0·47	0·47

These values most likely represent lower limits because:

(i) Any annealing taking place at 10° K means that there were present fewer isolated point defects than has been determined by the damage calculation.

(ii) If *M*-regions are formed the concentration of isolated point defects is less than that given by the calculations. On the other hand there may be some extra scattering at the boundaries of the regions so that only part of the measured increase of resistivity has to be ascribed to the smaller concentration of point defects.

(iii) There will be some groups of defects present and there is the possibility that the scattering from a group is less than that produced by the same number of isolated defects.

Other estimates of resistivity due to defects

Various attempts have been made to calculate the extra resistivity due to 1% vacancies and to 1% interstitials; the values are shown in Table 2.

Table 2. *Theoretical values of resistivities due to 1% defects*

Dexter[27]	1952	Vacancies	Cu	Ag	Au	0·4 $\mu\Omega$ cm/1%
		Interstitials	Cu	Ag	Au	0·6
Jongenberger[28]	1953	Vacancies	Cu	Ag	Au	1·3 (1·8)*
	1955	Interstitials				4·5–5·5
Blatt[29]	1955	Interstitials				1·4 (0·7)†
Overhauser and Gorman[30]	1956	Vacancies	Cu			1·5
		Interstitials	Cu			10·5

* Numerical correction gives 1·8 according to Overhauser and Gorman.

† Applying his method to substitutional impurities of adjacent atomic number Blatt finds theoretical values too large by ×2. He suggests that this is a systematic error in the type of calculations so far made and that the calculated values for interstitials and vacancies should also be divided by 2.

The extra potential which a conduction electron sees is in part due to the defect and in part to the associated relaxation of the positions of surrounding atoms. Dexter concluded that the latter was not important for either vacancies or interstitials. Jongenberger obtained a contribution of 0·04 $\mu\Omega$ cm from the distortion surrounding a vacancy and 3·5 $\mu\Omega$ cm for the nearest neighbour displacements about interstitials. From their calculations on copper Overhauser and Gorman found for these two quantities 0·5 and 9·6 $\mu\Omega$ cm respectively.

The discrepancies between the values given in Table 2 arise mainly, therefore, from the differences found for the contribution to the resistivity from the local strain surrounding the defect. Although there are no direct experimental checks of the values in Table 2 an indirect comparison may be made using the results of quenching experiments.

This possibility is derived ultimately from the theoretical result[21] that for copper the energy of formation of an interstitial atom ($\simeq 5$ eV) is much higher than for a vacancy. It is assumed that the same is true for gold. At a high temperature, therefore, where there is a significant concentration of vacancies (N_v) in thermodynamic equilibrium the concentration of interstitials is negligible (N_I). As long as $N_v > 100\,N_I$ say, the resistivity increase obtained after quenching may be ascribed to vacancies.

By quenching from different temperatures the energy of formation of vacancies (E_v) may be found so that the fraction of vacancies can be determined using

$$N_v(T)/N_0 = e^{-E_v/kT} \qquad (11)$$

The activation energy (E_M) for the annealing of the frozen in vacancies (i.e. corresponding to their motion) may also be determined. Measurements have been made by Koehler,[31] Lazarev and Ovcharenko,[32] and by Bauerle and others.[33] The results are summarized in the table.

Table 3. *Results of quenching experiments*

		E_v	E_M	ρ_{vac} per 1%
Au	L and O	0·78	0·51	0·25 $\mu\Omega$ cm
Pt		1·16	1·06	3·2
Au	K		0·68 ± 0·03	
Au	B and others	1·02 ± 0·06	0·66 ± 0·06	0·36

The two main difficulties in the comparison with the theoretical values are:

(i) The experimental difficulty of quenching fast enough to ensure that all vacancies are frozen in. Bauerle and others[33] claim that 90% of the high temperature concentration is retained during their quenching treatment. However, it is difficult to be sure of the efficiency of the quenching and an independent check on the consistency of the activation energies may be made by comparing with self-diffusion data. If self-diffusion occurs by the generation and motion of vacancies as is believed to be the case in copper and gold[34] then the following relation should be true:

activation energy for self-diffusion, $E_{SD} = E_v + E_M$.

E_{SD} for gold has been measured by several workers.[35] The values 1·85 and 1·75 eV are taken from Zener's review. E_{SD} has since been measured by Kurtz and others[36] 1·96 eV, and most recently by Okkerse[37] 1·70 eV. In spite of the range of these experimental values there is better agreement with the results of Bauerle than with Lazarev and Ovcharenko.

(ii) The second difficulty arises because of the simplifying assumptions implicit in the thermodynamic equation (11). In deriving equation (11) it is assumed that the vibrations of atoms surrounding vacancies are the same as before the formation of the vacancies. If a vacancy has x nearest neighbours and if, in a direction joining an atom to the vacancy, the frequency is changed from ν to ν' there is an extra term—$\ln\left(\frac{\nu}{\nu'}\right)^x$—in the free

energy associated with N_v vacancies.[38] Consequently equation (11) should be replaced by

$$N_v(T)/N_0 = \left(\frac{\nu}{\nu'}\right)^x e^{-E_v/kT} \qquad (12)$$

Although $\frac{\nu}{\nu'}$ may not be large it is raised to a power which can be 12 (f.c.c. structure) so that the total effect may be appreciable. Since ν' will be expected to be less than ν, the estimate of the increased resistivity due to 1% vacancies based on the measured increase and equation (11) will be too large. The values given in Table 3 therefore represent the upper limits.

Considering both these points we conclude from the quenching experiments on gold that the resistivity due to 1% vacancies is not greater than 0·4 $\mu\Omega$ cm. This has to be compared with the lowest theoretical value of 0·4 and the highest of 1·8.

From the damage measurements a value of 0·5 $\mu\Omega$ cm per 1% Frenkel defect is obtained, that is vacancies (1%) and interstitials (1%), there being three sources of error which could lead to a higher value. Clearly further work is needed; the conclusion at present seems to be that the theoretical values of the resistivity per defect are too high.

For discussion of the annealing of the defects introduced by deuteron irradiation at 10° K the reader is referred to the papers of Koehler and Seitz,[39] Cottrell and Lomer,[40] and Seeger.[41]

4. SEMI-CONDUCTORS

Whereas the changes induced by irradiation in the conductivity of metals arise because of the increase of electron scattering, in semi-conductors both the concentration of charge carriers and the mobility are affected. This means that the conductivity of semi-conductors is very sensitive to radiation damage; a fact which led to the first experimental determination of the minimum displacement energy (Fig. 3). Beyond this, however, the interpretation of the radiation induced changes in terms of point defects is exceedingly complex. For details of the measurements in this field the reader is referred to the work of James and Lark-Horovitz,[13] Fan and Lark-Horovitz,[9] Cleland and others,[42] and Cleland and Crawford.[43]

In the case of metals the effect on the mobility is measured of all the types of defect introduced by the irradiation, that is the integrated effects of interstitial atoms, vacancies, small groups of either, and possibly *M*-regions. At the other extreme the optical absorption induced in insulators (large forbidden energy gap) provides a means of separating the effects of different types of defect. Some degree of separation of the effects of damage may be obtained from the electrical measurements on semi-conductors.

It is not sufficient simply to record the change in carrier concentration since this change is not uniquely determined by the irradiation dose. This was first shown by the work of Fan and Lark-Horovitz[9] with germanium. They compared the initial rates of removal of carriers per unit dose ($-dn/dD$, $-dp/dD$) for deuteron irradiated *n*- and *p*-type specimens of varying impurity concentrations.

These values were deduced from Hall effect measurements on specimens irradiated with 9·6 MeV deuterons at 200° K. They show clearly that $-dn/dD$ or $-dp/dD$ cannot be linked directly with calculated rates of defect production, even assuming some number of trapping levels per defect.

Table 4. *Rate of removal of carriers*

n-type		*p*-type	
N_D cm^{-3}	$-dn/dD$	N_A cm^{-3}	$-dp/dD$
$1{\cdot}04 \times 10^{15}$	25·8	$4{\cdot}8 \times 10^{15}$	20·8
$1{\cdot}58 \times 10^{16}$	228	$8{\cdot}5 \times 10^{15}$	17·3
$4{\cdot}80 \times 10^{17}$	1130	$1{\cdot}04 \times 10^{18}$	200

(N_D, initial donor concentration; N_A, initial acceptor concentration.)

The actual changes, in the measured quantities, produced by the irradiation of *n*-type specimens are shown in Fig. 5. The conductivity of both high and low resistivity material at

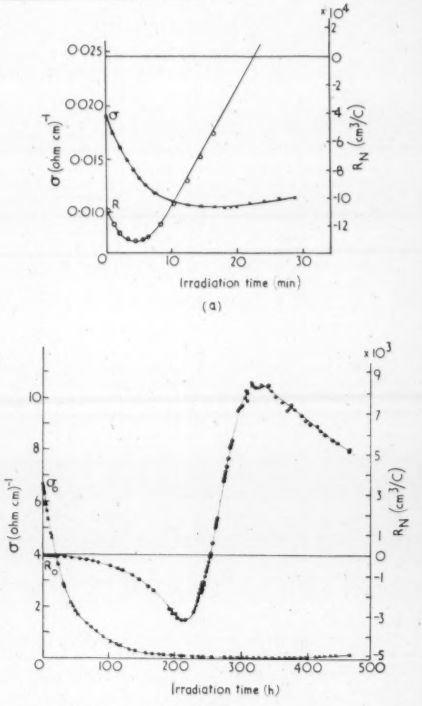

[*Reproduced by permission of The Physical Society*]

Fig. 5. The variation of conductivity (σ) and Hall constant (R_N) of germanium with time of irradiation (after Lark-Horovitz and Fan)

first decreases, reaches a minimum and slowly increases with time of irradiation. It was found that the dose (D_{min}) required to reach the minimum conductivity depended on the initial conductivity. Simultaneous measurements of the Hall effect showed that at about D_{min} the Hall coefficient changed sign, becoming positive (*p*-type).

In order to understand these effects we must consider the statistics governing the occupation of energy levels by electrons. Consider an *n*-type conductor. The concentration (vol^{-1}) at any energy level is determined by the position of the Fermi level (ϵ_F), or chemical potential of the electrons, and by the Fermi–Dirac distribution function (f). Thus at the bottom of the conduction band (Fig. 6)

$$f_C = 1/[1 + e^{+(\epsilon_C - \epsilon_F)/kT}]$$

and at an impurity level ϵ_I

$$f_I = 1/[1 + \tfrac{1}{2} e^{+(\epsilon_I - \epsilon_F)/kT}]$$

the factor $\frac{1}{2}$ arising, Wilson,[44] when it is assumed that the impurity can donate an electron of one spin.

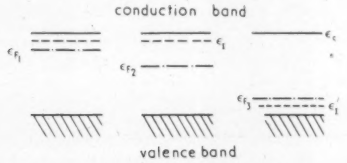

Fig. 6. Energy band diagram for *n*- and *p*-type semiconductors showing different positions of the Fermi level (ϵ_{F_1}, ϵ_{F_2} and ϵ_{F_3})

For an initial concentration $N_I = 10^{19}$ cm^{-3} at $\epsilon_I = 0{\cdot}03$ eV below the conduction band, the Fermi level (ϵ_{F_1}) is 0·04 eV below the band. N_I may be determined from the Hall and conductivity measurements and ϵ_{F_1} is essentially determined by the condition that the sum of f over the valence and conduction bands must give the total number of valance electrons plus N_I. There will be an almost 1 : 1 removal of electrons, from the conduction band, per acceptor level introduced by irradiation when the Fermi level is as high as ϵ_{F_1}.

For an *n*-type conductor of higher purity the Fermi level can be as ϵ_{F_2}. Clearly acceptor levels introduced between ϵ_I and ϵ_{F_2} have a much lower probability of being occupied by electrons than when the Fermi level was at ϵ_{F_1}. Thus the rate of removal of carriers will be less in the purer material, as observed.

In both cases a stage will be reached when the Fermi level is low enough for there to be an appreciable number of electrons missing from the valence band. Under these conditions the material becomes *p*-type.

When the starting material is *p*-type of high conductivity the effect of irradiation is shown in Fig. 7. The conductivity decreases and the hole concentration decreases at a diminishing rate tending to a similar concentration to that produced by prolonged irradiation of *n*-type specimens. The Fermi level (ϵ_{F_3}—Fig. 6) for high conductivity *p*-type material is close to ϵ_I' so that practically all donor centres produced by irradiation lose their electrons—that is, the concentration of holes in the valence band is reduced. Thus the maximum value of $-dp/dD$ is obtained using the most impure material.

For weakly *p*-type material it is found that the conductivity at first increases, indicating that in spite of the above process there must be sufficient acceptor levels produced in the lower half of the energy gap to accept electrons from the higher donors and still lead to a higher concentration of holes in the band.

Fan and Lark-Horovitz[9] have further shown how some information concerning the energy distribution of the induced traps may be obtained from the electrical measurements. This depends on the fact, which follows from the form of the Fermi–Dirac distribution function, that the maximum rate of carrier removal occurs when ϵ_F is close to the energy of a group of traps. One set of their results is shown in Fig. 8. *n*- and *p*-type samples were irradiated with 4·5 MeV electrons at 200° K and the rates of removal of carriers per unit dose was determined for the different positions of the Fermi level. This indicated that under these conditions the main groups of levels were about 0·2 eV below the conduction band and 0·2 eV above the valence band. Similar measurements on specimens irradiated with 9·6 MeV deuterons showed that the main concentrations of levels in this case were 0·1 eV above and below the band edges.

On the assumption that single vacancies and interstitials are produced during electron irradiation the 0·2 eV levels

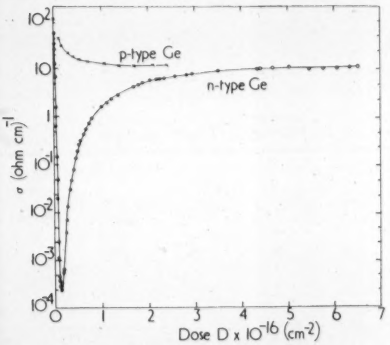

[*Reproduced by permission of The Physical Society*]

Fig. 7. Variation of the conductivity of *n*- and *p*-type germanium with deuteron irradiation (after Lark-Horovitz and Fan)

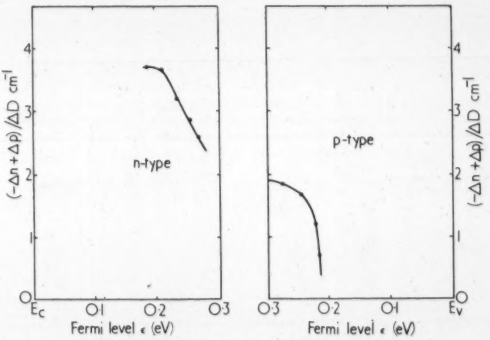

[*Reproduced by permission of The Physical Society*]

Fig. 8. Rate of carrier removal as a function of the position of the Fermi level for electron irradiated germanium (after Lark-Horovitz and Fan)

are believed to be associated with the simplest point defects. James and Lark-Horovitz[13] had previously suggested that each vacancy should contribute two acceptor levels, while the interstitial germanium atom should provide two donor levels. It will be of great interest to compare the effects of low temperature electron irradiations with the effects of quenching experiments from high temperatures. The comparison requires, however, that in the former case non-equilibrium electron distributions can be avoided, and in the latter that impurity effects can be eliminated.[45] Subsequent annealing experiments could then lead to information concerning aggregation which is necessary for the fuller interpretation of the trapping levels produced by higher energy irradiation.

5. THE OPTICAL PROPERTIES OF INSULATORS

The general procedure in this case is to measure the absorption spectra induced by irradiation and to try to identify the defect responsible for a given absorption band. In this way one endeavours to decide what kinds of defects are produced and the conditions under which they may be annealed. The following discussion of some of the work on diamond and quartz gives an indication of what is involved.

Diamond

The effects in diamond are illustrated in Figs. 9 to 11, which are taken from the work of Clark and others.[5, 46]

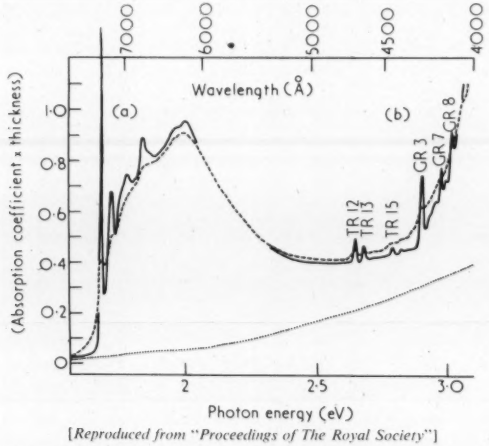

[*Reproduced from "Proceedings of The Royal Society"*]

Fig. 9. The absorption spectrum induced in a type 2*a* diamond by 1·0 MeV electron irradiation (. . . . . before irradiation); – – – – – after irradiation (measured at room temperature); ———— measured at liquid air temperature (after Clark, Ditchburn and Dyer)

In the present account we shall refer primarily to their work on type II*a* diamonds since these are optically simpler in the unirradiated state. The absorption induced by electron and γ-irradiations and the changes produced by subsequent heat treatment may be summarized as follows:

(i) The absorption systems (*a*) and (*b*) are induced by irradiation. Group (*a*) lines—main line 7400 Å—show a fine structure especially at low temperatures; group (*b*) lines are less dependent on temperature.

(ii) Heating at 450° C leads to a partial decrease of the strengths of the lines in both groups. This has only been observed in γ-irradiated specimens. For electron irradiations it is presumed to occur during the irradiation as a result of the heating of the specimen by the electron beam.

(iii) At 600° C group (*a*) and (*b*) lines decrease in strength and new lines (*c*) appear in the region of (*b*). The rate curves for the decrease of (*a*) and increase of (*c*) may be superposed and are of the bimolecular form.

(iv) Heating at higher temperatures leads to the disappearance of all lines including those produced during (iii). There remains a background absorption which is greater than that present initially. The induced background absorption has the same spectral form as that present before irradiation, i.e. only a single scaling factor is required for super-position.

After γ-irradiation the crystal will contain randomly distributed interstitial-vacancy pairs, the distance between the interstitial and the vacancy varying from a few angstroms, when the kinetic energy of the displaced atom is small, to a much larger value which depends on the dose. This represents practically the simplest case in radiation damage work. The effects of electron irradiation are slightly more complex because of the partial recovery and because they are not uniformly distributed through the crystal.

None of the bands decreases if the crystal is illuminated with light of energy up to that of the absorption edge. This absence of optical bleaching is strong evidence that the decreases of absorption observed during heat treatment are due to the migration of atoms or vacancies, and not of electrons which had become trapped at defects. There are

then two sources of optical absorption—the first involving the unpaired electrons of the four carbon atoms surrounding a vacancy, and secondly the four unpaired electrons of an interstitial carbon atom. Because the bonding of the carbon

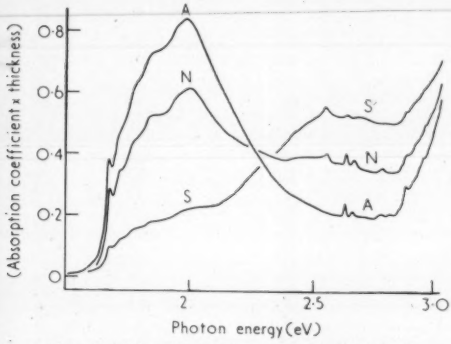

[*Reproduced from "Proceedings of The Royal Society"*]

Fig. 10. The absorption spectra of type 2*a* diamond. *A*, after a 1·0 MeV electron irradiation; *N*, after subsequent heating at 600° C for 4 h; *S*, for 100 h. (after Clark, Ditchburn and Dyer)

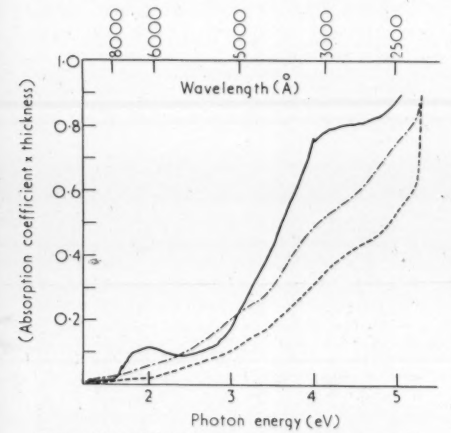

[*Reproduced from "Proceedings of The Royal Society"*]

Fig. 11. The absorption spectra induced in a type 2*a* diamond (– – – – – before irradiation; ———— after 0·6 MeV electron irradiation; —·—·—· after subsequent heating at 850° C for 21 h (after Clark, Ditchburn and Dyer)

atoms surrounding an interstitial is complete and because there is plenty of room for interstitial atoms, it is suggested that there is very little bonding of the electrons of the interstitial atom with the surrounding atoms. Thus thermal vibrations of the surrounding atoms will not be readily transmitted to the interstitial, suggesting that any absorption spectra associated with the electrons of the interstitial carbon atom will not be strongly temperature dependent. The electronic absorption due to the vacancy, however, is associated with electrons belonging to the surrounding carbon atoms which are almost normally bound to neighbouring atoms. The lattice vibrations will be readily transmitted to these electrons. By this reasoning Clark and others[46] have concluded that the group (*a*) lines are associated with the vacancy and group (*b*) with the interstitial.

There is some theoretical support for the conclusion following the molecular orbital calculation by Miss Kearsley[47] of the energy levels of the electrons surrounding a vacancy in diamond. Miss Kearley obtains a value of about 2·0 eV which is in reasonable agreement with the main line (1·67 eV) of the group (*a*) absorption system.

When the temperature is high enough the point defects will be mobile. In their second paper Clark and others[46] put forward the following interpretation of the changes in the absorption spectrum following heat treatment. The partial reduction in both systems is attributed to the recombination of close pairs of defects, probably by the diffusion of the vacancies. At the higher temperature the vacancies recombine with the more distant interstitials and combine with each other to form pairs of vacancies, giving the group (*c*) absorption lines. Both processes will give a bimolecular rate law. In the high temperature region the pairs migrate and aggregate, leading it is suggested to a breakdown of the structure and an associated continuous absorption tail. It is thought that the excess interstitials eventually migrate either to the surface or to internal surfaces.

With neutron irradiations (*a*), (*b*) and (*c*), groups are superposed on an increased background, which increases further, as in (iv), after heat treatment. The neutron irradiation induced background absorption probably results from the breakdown of the structure in the *M*-regions. Recent X-ray diffraction measurements by Levy and Kammerer[16] have shown that for high neutron doses (10^{20}–10^{21} n cm^{-2}) diamond becomes amorphous. It will be interesting to see whether recrystallization occurs after heat treatment. Clark and others have found that the induced background absorption cannot be decreased by heat treatment.

In type I diamonds, which show what is believed to be a false absorption edge at 3·74 eV due to impurity or some other kind of imperfection, the effects are more complicated. The vacancy band [group (*a*)] is formed after irradiation but other effects are masked by the natural absorption. There is a marked difference after heat treatment, however, for in type I diamonds a new absorption system appears with a main line at 5032 Å in absorption and emission, with associated structure on the high energy side in absorption and on the low energy side in emission. This is the well-known green luminescent centre which occurs naturally in some type I diamonds. The defect responsible is not yet known. Information concerning the symmetry of this centre has recently been obtained by Elliott and others[48] from measurements of the polarization of the luminescence when the centre is excited by plane polarized light. The results show that the centres have axes along ⟨111⟩ with little electronic relaxation between them. Although this is the most probable symmetry to find in diamond it is not the only one; for example, a pair of interstitials would give a ⟨110⟩ symmetry.

Quartz

After a sufficiently high neutron dose quartz, like diamond, becomes amorphous. The simplest explanation is that the

material in *M*-regions forms an amorphous phase after rapid "cooling." In the case of quartz one is fortunate in having a stable amorphous phase available, namely fused quartz, with which to compare the radiation induced effects. One of the most interesting optical effects is the position of the absorption limit in irradiated quartz.

In an ideal insulating crystal the optical absorption by electrons would be zero until the photon energy was large enough to excite electrons from the upper valence band to the conduction band. The absorption would then increase rapidly to values $\sim 10^5\ cm^{-1}$. It is difficult to measure absorption coefficients of $10^5\ cm^{-1}$ so that in general the detailed structure of this absorption edge for real crystals is not known, or can only be obtained from evaporated films. In crystalline quartz Mitchell and Paige[4] find the absorption edge to be at 8·5 eV (1460 Å) as in Fig. 12. At this energy the absorption coefficient was $500\ cm^{-1}$—the highest value which could be recorded using specimens 0·1 mm thick—and was increasing by $200\ cm^{-1}/0{\cdot}1$ eV.

In fused quartz, however, there is an absorption limit at 8·1 eV (Fig. 12) as measured by Mitchell and Paige using the same criterion as above. It is suggested that this is a strongly enhanced tail of the absorption edge. The presence of imperfections in the ideal crystal leads to a variation of interatomic distances in the neighbourhood of the imperfection. Thus the energy of some of the electronic transitions contributing to the absorption at the edge is altered. Fused quartz in this context can be regarded as grossly imperfect crystalline quartz; that is, the basic units (SiO_4) are the same but in fused quartz these units are not regularly arranged over distances greater than say 100 Å. Thus the X-ray diffraction pattern contains no sharp lines. The variation in the Si – O distance leads to an absorption edge broader than in crystalline quartz. In their experiments Mitchell and Paige observed the broadening only on the low energy side of the edge.

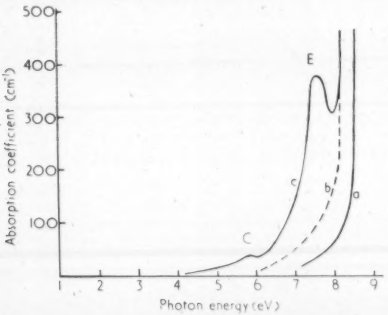

Fig. 12. The absorption spectra induced in quartz by pile irradiation: (*a*) crystalline quartz before irradiation; (*b*) fused quartz before irradiation; (*c*) crystalline quartz after irradiation

The same authors found after pile irradiation that whereas the absorption limit in fused quartz remained at 8·1 eV, the limit in crystalline quartz shifted from the edge to 8·1 eV. This shift is attributed to the formation of amorphous material in the crystal even at doses of 10^{18}–$10^{19}\ n^{\circ}\ cm^{-2}$.

If each *M*-region led, on the average, to a volume of amorphous phase v then the process would be expected to saturate according to

$$V_{am} = V_0(1 - e^{-\alpha v D})$$

where V_{am} is the volume of amorphous material, V_0 is the total volume of specimen and α the number of *M*-regions produced per dose *D*. The macroscopic density change as a function of dose which was observed by Wittels and Sherrill was not of this form. To account for the type of curve obtained experimentally (Fig. 13), and for the occurrence of amorphous regions at the much lower doses used by Mitchell and Paige, it has to be assumed that the average volume of an *M*-region is a function of dose. Possible mechanisms have been discussed by Primak and others[49] and by Mitchell and Paige. Both the density change and the enhanced absorption tail are removed by annealing at 950° C, although for the highest doses Wittels and Sherrill[15] found that the final state was polycrystalline.

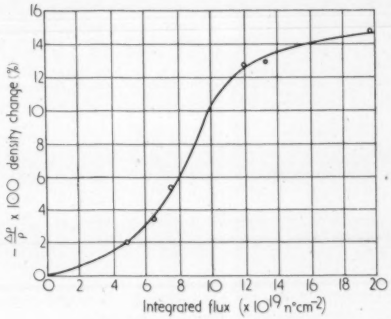

[*Reproduced from "Physical Review"*]

Fig. 13. Density change of quartz as a function of fast neutron bombardment (after Wittels and Sherrill)

Other optical effects are induced in quartz by irradiation damage, notably the C band at about 5·7 eV and the E-band at 7·6 eV. The nature of the defects responsible for these bands is not certain, but there is some evidence that they are associated with oxygen vacancies and interstitials respectively. The visible colouring—which occurs naturally in smoky quartz—has been shown to be an ionization effect associated with aluminium impurity.[50]

REFERENCES

(1) Seitz, F. *Disc. Faraday Soc.*, **5**, p. 271 (1949).
Bohr, N. *K. Danske Vidensk. Selsk. Mat-fys. Medd.*, **18**, p. 8 (1948).
Kinchin, G. H., and Pease, R. S. *Rep. Progr. Phys.*, **18**, p. 1 (1955).

(2) Seitz, F. *Phys. Today*, **5**, p. 6 (1952).

(3) Brinkman, J. A. *J. Appl. Phys.*, **25**, p. 961 (1954).

(4) Mitchell, E. W. J., and Paige, E. G. S. *Phil. Mag.* (1956).

(5) DUGDALE, R. A. Bristol Conference on "Defects in Crystalline Solids" (London: Physical Society, 1954).

CLARK, C. D., DITCHBURN, R. W., and DYER, H. B. *Proc. Roy. Soc. A*, **234**, p. 363 (1956).

CLELAND, J. W., CRAWFORD, J. H., and HOLMES, D. K. *Phys. Rev.*, **102**, p. 722 (1956).

(6) BRINKMAN, J. A., DIXON, C. E., and MEECHAN, C. J. *Acta. Met.*, **2**, p. 41 (1954).

SMOLUCHOWSKI, R. Bristol Conference on "Defects in Crystalline Solids" (London: Physical Society, 1954).

(7) LIND, S. C., and BARDWELL, D. C. *J. Franklin Inst.*, **196**, p. 521 (1923).

BRATTAIN, W. H., and PEARSON, G. L. *Phys. Rev.*, **80**, p. 846 (1950).

PEASE, R. S. *Acta. Cryst.*, **7**, p. 633 (1954).

(8) GLENDENNIN, L. E. *Nucleonics*, **2**, p. 12 (1948).

(9) FAN, H. Y., and LARK-HOROVITZ, K. Bristol Conference on "Defects in Crystalline Solids" (London: Physical Society, 1954).

(10) HELLER, Z., and TENDAM, D. *Phys. Rev.*, **84**, p. 905 (1951).

(11) MOTT, N. F., and MASSEY, H. S. W. *Theory of Atomic Collisions* (London: Oxford University Press, 1949).

(12) COOPER, H. G., KOEHLER, J. S., and MARX, J. W. *Phys. Rev.*, **94**, p. 496 (1954).

(13) JAMES, H. M., and LARK-HOROVITZ, K. *Semi-conducting Materials* (Ed. H. K. Henisch. London: Butterworths Scientific Publications, 1951).

(14) ADAIR, R. K. *Rev. Mod. Phys.*, **22**, p. 249 (1950).

(15) WITTELS, M., and SHERRILL, F. A. *Phys. Rev.*, **93**, p. 1117 (1954).

(16) LEVY, P. W., and KAMMERER, O. F. *Phys. Rev.*, **100**, p. 1787 (1955).

(17) WITTELS, M. C., and SHERRILL, F. A. *J. Appl. Phys.*, **27**, p. 643 (1956).

(18) BOHR, N., and LINDHARD, J. *K. Danske. Vidensk. Selsk. Mat-fys. Medd.*, **28**, p. 7 (1954).

(19) LAMB, W. E. *Phys. Rev.*, **58**, p. 696 (1940).

(20) STEPHENS, K. G., and WALKER, D. *Proc. Roy. Soc. A*, **229**, p. 376 (1955).

(21) HUNTINGTON, H. B. *Phys. Rev.*, **91**, p. 1092 (1953). (See also Ref. 34.)

(22) KLONTZ, E. E., and LARK-HOROVITZ, K. *Phys. Rev.*, **82**, p. 763 (1951) (Abs.) **86**, p. 643 (1952) (Abs.).

(23) EGGEN, D. T., and LAUBENSTEIN, M. J. *Phys. Rev.*, **91**, p. 238 (1953). (Abs.)

(24) DUGDALE, R. A. Private communication (1955).

(25) LOFERSKI, J. J., and RAPPAPORT, P. *Phys. Rev.*, **98**, p. 1861 (1955).

(26) KINCHIN, G. H., and PEASE, R. S. *Rep. Progr. Phys.*, **18**, p. 25 (1955).

(27) DEXTER, D. L. *Phys. Rev.*, **87**, p. 768 (1952).

(28) JONGENBERGER, P. *Appl. Sci. Res. B*, **4**, p. 237 (1953); *Nature* [*London*], **175**, p. 545 (1955).

(29) BLATT, F. J. *Phys. Rev.*, **99**, p. 1708 (1955).

(30) OVERHAUSER, A. W., and GORMAN, R. L. *Phys. Rev.*, **102**, p. 676 (1956).

(31) KAUFFMAN, J. W., and KOEHLER, J. S. *Phys. Rev.*, **97**, p. 555 (1955).

(32) LAZAREV, B. G., and OVCHARENKO, O. N. *Dokl. Akad. Nauk. S.S.S.R.*, **100**, p. 875 (1955).

(33) BAUERLE, J. E., KLABUNDE, C. E., and KOEHLER, J. S. *Phys. Rev.*, **102**, p. 1182 (1956).

(34) HUNTINGTON, H. B., and SEITZ, F. *Phys. Rev.*, **61**, p. 315 (1942).

(35) ZENER, C. *J. Appl. Phys.*, **22**, p. 372 (1951).

(36) KURTZ, A. D., AVERBACH, B. L., and COHEN, M. *Acta. Met.*, **3**, p. 442 (1955).

(37) OKKERSE, B. *Bull. Amer. Phys. Soc.*, **1**, p. 149 (1956).

(38) MOTT, N. F., and GURNEY, R. W. *Electronic Processes in Ionic Crystals* (London: Oxford University Press, 1948).

(39) KOEHLER, J. S., and SEITZ, F. Bristol Conference on "Defects in Crystalline Solids" (London: Physical Society, 1954).

(40) COTTRELL, A. H., and LOMER, W. M. *Phil. Mag.*, **46**, p. 711 (1955).

(41) SEEGER, A. *Z. Nat.*, **10**, p. 251 (1955).

(42) CLELAND, J. W., CRAWFORD, J. H., and PIGG, J. C. *Phys. Rev.*, **98**, p. 1742; **99**, p. 1170 (1955).

(43) CLELAND, J. W., and CRAWFORD, J. H. *Phys. Rev.*, **93**, p. 894; **95**, p. 1177 (1954).

(44) WILSON, A. H. *The Theory of Metals* (London: Cambridge University Press, 1953).

(45) LOGAN, R. A. *Phys. Rev.*, **101**, p. 1455 (1956).

(46) CLARK, C. D., DITCHBURN, R. W., and DYER, H. B. *Proc. Roy. Soc. A*, **237**, p. 75 (1956) and private communication.

(47) KEARSLEY, M. J. Private communication (1956).

(48) ELLIOTT, R. J., MATTHEWS, I. G., and MITCHELL, E. W. J. Paris Luminescence Conference, to be published.

(49) PRIMAK, W. *Phys. Rev.*, **98**, p. 1854 (1955).

(50) MITCHELL, E. W. J., and PAIGE, E. G. S. *Phil. Mag.*, **46**, p. 1353 (1955).

The light output of some phosphors excited with electrons of high current density

By P. A. EINSTEIN, M.Sc., A.M.I.E.E., Associated Electrical Industries Ltd., Aldermaston, Berks.

[*Paper received* 26 *November*, 1956]

The behaviour of phosphors at high current densities and at 50 kV has been examined using a pulse technique. For a number of phosphors, the onset of saturation occurs at a high value of current density (in the region of 10^{-1} A/cm^2).

Significant phosphor heating was avoided by use of single pulses of short duration, and did not become important up to current densities of 1 A/cm^2. The rise and decay time constants (though the processes are not exponential) in general increase with current density as has also been reported by other workers for lower current densities. Empirical laws relating time constants to current density have been established.

The behaviour of phosphors under intense excitation is of practical interest, particularly in connexion with projection cathode-ray tubes. The information usually required concerns the light yield from a given area, under equilibrium conditions, and its dependence on current density. The values of the rise and decay time constants also have practical significance.

SATURATION

Phosphors are known to saturate; the term is applied to the condition where the light yield at equilibrium output no longer shows a proportionate increase with change in exciting current density. In general, saturation commences at a current density in the region 10^{-4} to 10^{-2} A/cm^2 for most phosphors.[1–6] Unfortunately, the study of saturation at higher current densities and steady electron irradiation is complicated by the heating of the phosphor in the electron beam. For this reason, in the present work, the phosphors were excited by single pulses of short duration. In a later paper,[7] dealing with the thermal aspects of the problem, it will be shown that, for current densities up to the order of 1 A/cm^2 at 50 kV energy and short single pulses, the heating effect may be neglected.

APPARATUS

The apparatus is shown schematically in Fig. 1; 50 kV electrons were generated by the gun *C* and deflected electrostatically on to the phosphor at *K* by a rectangular voltage pulse applied across the deflector plates *G*. The central portion of the electron beam was selected by the movable aperture *E*, thus giving a substantially uniform current density distribution over the electron spot at *K*.

Current density control was effected by altering either filament temperature or condenser lens setting *D*; the projector lens *H* formed an image of aperture *E* of fixed magnification in the phosphor plane at *K*, and thus facilitated the determination of current density by measurement of the total current entering the Faraday cage at *L*. Current densities up to 3 A/cm^2 could be attained at *K* in a spot 80 μ in diameter. However, at this high value, the current density distribution was not entirely uniform as a rather higher percentage of the beam had to be allowed to pass through the aperture *E*.

The phosphor specimen at *K* consisted of a layer obtained by settling the powder from suspension in the customary manner, to a thickness of 0·1 mm. The settled area was made small (2 × 1 mm) so as to reduce any effects from a small amount of stray light resulting from electrons scattered from the tube walls, etc. The base plate *K* could be moved so as to expose a fresh phosphor surface to the beam after preliminary lining-up had been completed. The pulse generating circuits *N*, *O*, *P*, *Q*, were suitably interlocked in such a way that the cathode-ray tube *S* time base was fired at the requisite short time preceding the deflecting pulse. The light from the phosphor was observed by photomultiplier *I* (Mazda type 27M1), and displayed on the cathode-ray tube together with the deflecting pulse (inverted for convenience). The deflecting pulse could be fired either singly or in a sequence at the rate of 1·5 or 50 per second; the pulse length was variable from a minimum of 30 to 6000 μs.

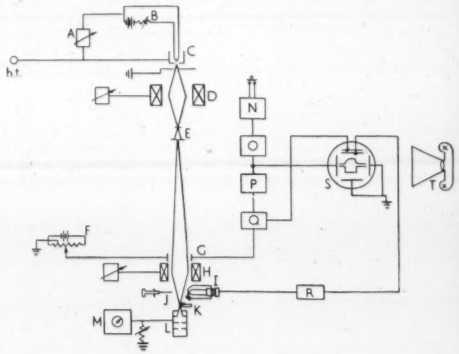

Fig. 1. Arrangement of apparatus for examining the behaviour of phosphors

A, gun bias control unit; *B*, filament control; *C*, gun; *D*, lens I with control unit; *E*, aperture; *F*, beam shift d.c. unit; *G*, deflector plates; *H*, lens II with control unit; *I*, photomultiplier with neutral density filters; *J*, monitor fluorescent screen; *K*, phosphor specimen; *L*, Faraday cage; *M*, beam current d.c. amplifier; *N*, low-frequency oscillator; *O*, trigger pulse generator; *P*, variable delay unit; *Q*, main pulse generator; *R*, photomultiplier power unit and amplifier; *S*, double-beam cathode-ray oscillograph; *T*, camera.

OPTICAL CALIBRATION

For the purpose of this calibration, a lamp-house unit was designed to simulate the phosphor (Fig. 2), and was placed in the position normally occupied by the phosphor.

An opal glass diffusing disk *O* of known area was illuminated by a pilot lamp *P* maintained at colour temperature of 2047° K.[8] (A more recent agreed value is 2042° K.) The light was interrupted by sector disk *S* driven by motor *M*, and the resulting pulse traces on the cathode-ray oscillograph

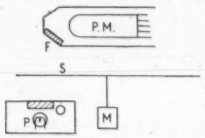

Fig. 2. Optical calibration unit

F, neutral density filter; *M*, motor; *O*, opal glass diffusing disk; *P*, pilot lamp; *P.M.*, photomultiplier tube; *S*, sector disk.

were photographed for various amplifier gain settings and neutral density filter values *F*. As the absolute luminance of the opal screen had previously been determined in a separate comparison against a standard lamp using a flicker photometer, a direct relation between cathode-ray tube trace height and "white" screen luminance in candelas per square centimetre (i.e. as appearing to the photomultiplier cell), was thus established. For assessing the performance of individual phosphors, corrections had subsequently to be applied to allow both for the spectral distribution of the phosphor and for the response characteristic of the photomultiplier cell. In view of the many factors and intermediate conversions, the light output scales should be taken only as approximate.

EXPERIMENTAL RESULTS

Four commonly used and commercially available phosphors were investigated. These were:

(*a*) ZnSCdS(Ag)	Derby	type 340	(green)
(*b*) ZnO	Derby	X-68	(blue-green)
(*c*) Willemite	British Thomson-Houston	34C-17-10A	(green)
(*d*) ZnS(Ag)	Levy and West	G-86	(blue)

The light output was observed for pulses of various lengths ranging from 30 to 6000 μs with current density as parameter ranging from 10^{-5} to 2·7 A/cm^2. The light output is defined as the intensity averaged over the time for which the phosphor is excited (i.e. the pulse length), and measured in candelas per square centimetre. It is determined by dividing the total area under the observed light pulse (including that under the decay region) by the pulse length. A typical pulse is shown in Fig. 3(*a*). In Fig. 3(*b*), the effect of phosphor heating becomes apparent. The light output falls away during the pulse as the temperature rises; the effect becomes more marked for longer pulse lengths, or for higher pulse repetition frequencies. The occurrence of this "droop" indicates the onset of significant phosphor heating.

To determine the current density *versus* average light intensity curves, the light pulses were photographed for a given current density setting, and the light yield determined by measuring the total area under the light pulse (on a convenient photographic enlargement). Fig. 4 shows the average light intensity over the pulse *versus* current density for the four phosphors examined. The ordinate scale units are "white" (*P.M.*) candelas per square centimetre, as seen by the photomultiplier, i.e. the scale gives the response to the phosphor of the photomultiplier calibrated against a white

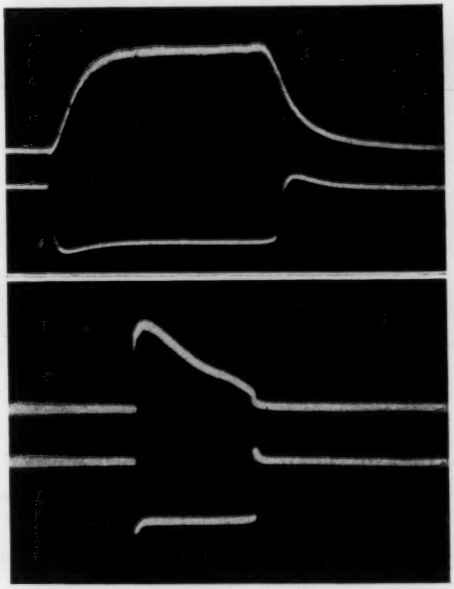

Fig. 3. Light yield *versus* time pulses

(*a*) Typical pulse 54 μs at 8 × 10^{-3} A/cm^2; (*b*) Pulse showing effect of phosphor heating, 200 μs at 2·7 A/cm^2.

Phosphor, Levy and West G-86 [ZnS(Ag)].
Beam velocity 50 kV.

source. Additional scales indicate the absolute luminous output in watts per square centimetre of the individual phosphors after applying an appropriate spectral correction. (This correction is only approximate.)

The point of immediate interest arising from Figs. 4(*a–d*) is the relatively high value of current density for which appreciable current saturation occurs. For the phosphors examined, this value lies in the region 10^{-1} A/cm^2, except in the case of Willemite, where it occurs around 10^{-3} A/cm^2. These values are much higher than those usually quoted from d.c. or scanned data (e.g. Bril and Kröger,[6] which show the onset of saturation in the region of 10^{-4} A/cm^2.) However, the present results were obtained at a beam energy of 50 kV, for which the electron penetration is relatively high.[9] The possibility of current saturation occurring later at higher voltages has been discussed by Dowling and Sewell[10] (compare their Fig. 7), and Strange and Henderson (Ref. 4, Part III).

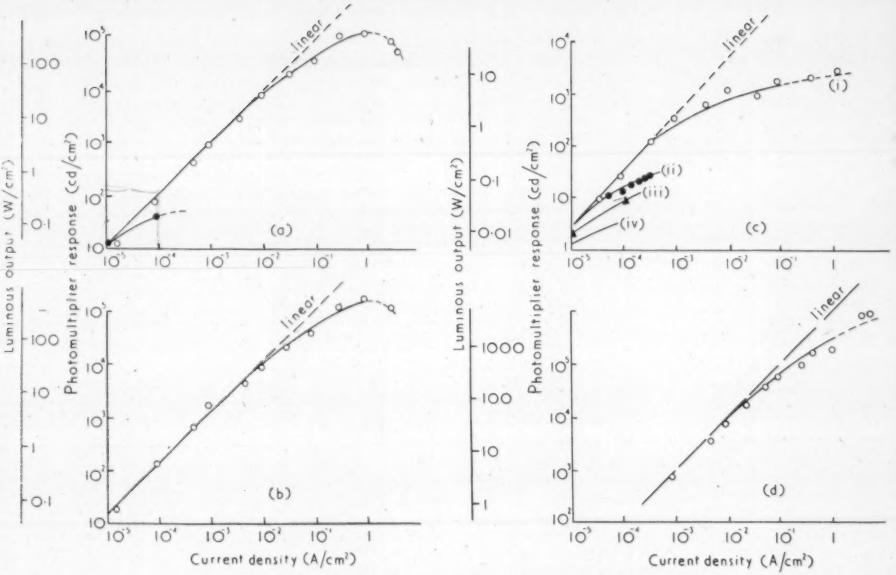

Fig. 4. Average luminous energy *versus* current density

(*a*) Derby 340, ZnS CdS(Ag), 50 kV, absolute efficiency (approximately) 10%.
○ = present experiment, 54 μs single pulses.
● = abstracted from Nottingham, 1939 (Ref. 3, Fig. 9, p. 81). ZnS Cds(Ag) (normalized).

(*b*) Derby X-68, ZnO, 50 kV, absolute efficiency (approximately) 14%.
○ = 54 μs single pulses.

(*c*) 34C–17–10A, Willemite, 50 kV, absolute efficiency (approximately) 3%.
Curve (i), present experiment, 6000 μs single pulses; curve (ii), Strange and Henderson (Ref. 4, Table 6), 5 kV; curve (iii), Nottingham, 1939 (Ref. 3, Fig. 4), 7 kV; curve (iv), Bril and Kröger,[6] 0·015% manganese.

(*d*) Levy and West G-86, ZnS(Ag), 50 kV, absolute efficiency (approximately) 10%.
○ = 30 μs single pulses.

DEPENDENCE OF TIME CONSTANTS ON CURRENT DENSITY

Very few phosphors show a purely exponential rise and decay with time under cathode-excitation. Even very simple theoretical models of cathodo-luminescence[4] lead to complicated expressions describing the growth and decay phenomena. Under such circumstances, the appending of "time constants" in the usual sense to describe the speeds of the process becomes arbitrary; however, such quantities are still of value from an engineering point of view, particularly for assessing the usefulness of a phosphor for a specific purpose. Consequently, rise and decay time constants are here defined as the reciprocals of the times (in seconds) to rise to two thirds or to fall to one third equilibrium value. The constants have been abstracted directly from photographs of cathode-ray oscillograph traces of light pulses, and are represented as functions of current density in Fig. 5. In every case, there exists a marked dependence of time constant, and, in particular, during the rise, on current density. This is not a direct result of possible phosphor heating, since a separate experiment in which the time constants were obtained as functions of temperature at a lower current density (Fig. 6) showed only slight increase with temperature up to 400° C.

The rise constant is more sensitive to changes in current density, and, in general, varies as (current density)$^{0.4}$. Willemite has a marked dependence of rise constant on current density (i), varying as $i^{1.75}$ between 10^{-3} and 1 A/cm^2. The decay of Willemite is unusual inasmuch as it first falls slightly with rising current density up to 10^{-2} A/cm^2 (Fig. 5), after which it increases gradually as $i^{0.3}$. The table sets out the rise and decay conditions for the four phosphors examined. The figures for ZnS(Ag) are in good agreement with those of Strange and Henderson (Ref. 4, p. 375) at lower current densities. (The comparison is made with a time constant value derived by combining the quoted values for the α- and β-processes.)

DISCUSSION

The point of main interest in this paper is the high value of current densities at which the phosphors examined appear to show appreciable saturation under pulse conditions. It is possible that the earlier onset of saturation reported by other workers may have been due to the use of lower voltages. The present work shows a linear relationship between current density and light-output up to 10^{-2} A/cm^2

for ZnO and ZnS–CdS, and 10^{-1} A/cm² for ZnS. Since it was estimated that heating did not become effective until 1 A/cm² for 50 μs single pulses, the above values represent

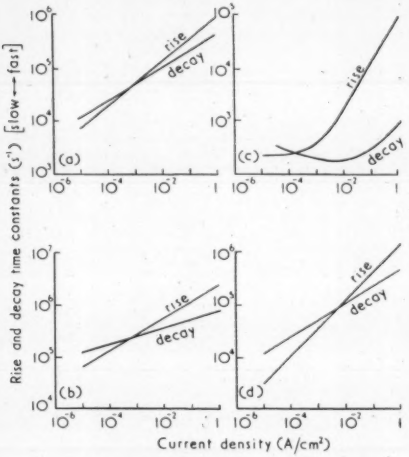

Fig. 5. Time constants *versus* current density
(*a*) Derby 340, ZnS CdS(Ag), 50 kV.
(*b*) Derby X-68, ZnO, 50 kV.
(*c*) 34C-17-10A, Willemite, 50 kV.
(*d*) Levy and West G-86, ZnS(Ag), 50 kV.

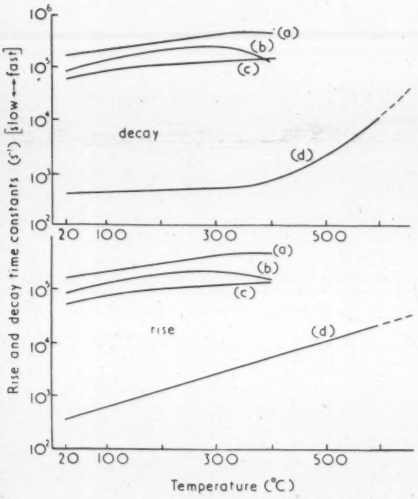

Fig. 6. Time constants *versus* temperature (50 kV, 10^{-3} A/cm²)

Curve (*a*) ZnO(X-68); curve (*b*) ZnS CdS(Ag) (340); curve (*c*) ZnS(Ag) (G-86); curve (*d*) Willemite.

Rise and decay constants as functions of current density

Phosphor		Rise constant Q (s^{-1})	Decay constant R (s^{-1})
ZnS (Ag)	G-86	$1{\cdot}7 \times 10^6\, i^{0.5}$	$5{\cdot}5 \times 10^5\, i^{0.3}$
ZnO	X-68	$2{\cdot}5 \times 10^6\, i^{0.3}$	$8{\cdot}5 \times 10^5\, i^{0.15}$
ZnS–CdS (Ag)	340	$7{\cdot}3 \times 10^5\, i^{0.4}$	$4{\cdot}65 \times 10^5\, i^{0.3}$
Willemite		$7 \times 10^4\, i^{1.75}$*	$8 \times 10^2\, i^{0.3}$

i = current density A/cm².
* After 10^{-3} A/cm².

the onset of true current saturation. In the case of Willemite, direct comparison with other published data is complicated by the fact that the properties of this phosphor are very sensitive to the activator concentration; this is borne out by the curves of Bril and Kröger[6] showing the effect on the saturation onset of a change in the manganese activator concentration. The diversity of the phosphor samples probably accounts for some of the disparity in the results of various authors shown in Fig. 4(*c*).

The processes underlying current saturation with electron excitation are complicated and particularly so in such systems as granular fluorescent screens where electron scattering and secondary electron generation (each dependent on penetration depth) occur. An attempt at explaining the phenomena is beyond the scope of this paper. It is doubtful whether much fundamental knowledge on cathodo-luminescence can be derived from granular screens; a better approach to this end would be the use of single crystals, such as were used by Ehrenberg and Franks.[9]

The fundamental processes underlying luminescence are discussed by Strange and Henderson[4] and Randall, Wilkins and Garlick,[11] among others. It may be deduced from these that, for the simplest case, i.e. a "random" or "monomolecular" process, the rise and decay phenomena are described by:

$$L = \frac{ABin}{Ai + B}\left\{1 - \exp\left[-(Ai + B)t\right]\right\} \quad \text{(rise)} \quad . \quad (1)$$

$$L = L_0 \exp(-Bt) \quad \text{(decay)} \quad . \quad (2)$$

where L is light yield, i is current density, t is time, and A, B and n are constants.

These equations describe exponential rise and decay curves, which were not observed. The observed current density dependence of the rise constant would, however, be explained (since the rise constant is given by $Ai + B$), but not the predicted independence of the decay constant B [equation (2)].

For a "bimolecular" process, the expressions describing rise and decay become much more complicated and include terms which show current density dependence of both rise and decay time constants. Both the non-exponential nature of the decay as well as the dependence of its time constant on current density might now be explained; however, this "bimolecular" process is not really admissible, since it does not satisfactorily cover current saturation. Possibly the one process changes over the other during the course of the pulse, but this is a matter for conjecture. Furthermore, in formulating these equations, only thin phosphor laminae were considered, and, to account for the electron penetration into the crystals, additional modifications would be required.

For these reasons, no model of the rise and decay processes is here put forward, except to state that the observed behaviour of the time constants with current density would not be unexpected.

A possible practical application of the increased speed of phosphors at high current density may arise in cases where

it is desirable to work with relatively short after-glow, such as flying-spot tubes, etc.

Future work of a more fundamental nature might be concerned with a study as described in the present paper, but using single crystals or thin transparent phosphor layers for which the thermal, electron penetration and light scattering conditions are simpler than for a granular screen, and where there is a better chance of establishing a correlation between theory and experiment. Further study of the saturation behaviour with voltage would be of interest as would also the use of even shorter pulses, since, for pulses short compared with the time constants of the phosphor, little saturation would be expected.

ACKNOWLEDGEMENTS

The author is indebted to Mr. M. E. Haine for encouragement during the work, to Messrs. D. Allenden and M. W. Jervis for the construction of the electronic equipment, to Mr. G. F. Fooks for carrying out some of the measurements, and to Dr. T. E. Allibone, Director of the Laboratory, for permission to publish this paper.

REFERENCES

(1) LEVY, L., and WEST, D. W. *J. Instn Elect. Engrs*, **79**, p. 11 (1936).
(2) MARTIN, S. T., and HEADRICK, L. B. *J. Appl. Phys.*, **10**, p. 116 (1939).
(3) NOTTINGHAM, W. B. *J. Appl. Phys.*, **10**, p. 73 (1939); **8**, p. 777 (1937).
(4) STRANGE, J. W., and HENDERSON, S. T. *Proc. Phys. Soc.* [*London*] *B*, **58**, p. 369 (1946).
(5) BRIL, A. *Physica*, **15**, p. 361 (1949).
(6) BRIL, A., and KRÖGER, F. A. *Philips Tech. Rev.*, **12**, 421, p. 120 (1950).
(7) ARCHARD, G. D., and EINSTEIN, P. A. *Brit. J. Appl. Phys.* (to be published).
(8) Brit. Stand. 233 (1953).
(9) EHRENBERG, W., and FRANKS, J. *Proc. Phys. Soc.* [*London*] *B*, **66**, p. 1057 (1953).
(10) DOWLING, P. H., and SEWELL, J. R. *J. Electrochem. Soc.*, **100**, p. 22 (1953).
(11) RANDALL, J. T., WILKINS, M. H. F., and GARLICK, G. F. J. *Proc. Roy. Soc. A*, **184**, p. 347 (1945).

Dynamic shear properties of some rubber-like materials

By W. P. FLETCHER, B.Sc., F.Inst.P., A.I.R.I., and A. N. GENT, B.Sc., Ph.D., A.Inst.P., A.I.R.I.,
The British Rubber Producers' Research Association, Welwyn Garden City, Herts.

[*Paper first received* 2 *August*, 1956 *and in final form* 14 *January*, 1957]

Measurements are described of the dynamic shear properties of a number of representative rubber-like materials, both vulcanized and unvulcanized, over a wide range of frequencies and temperatures. The major part of the transition from a rubber-like to a glass-like state has been investigated. Reduced values for the real component of the complex shear modulus and the ratio of the imaginary to the real part are presented, enabling the behaviour of the materials studied to be evaluated for other frequency and temperature conditions.

1. INTRODUCTION

In a previous publication[1] an apparatus was described for determining the dynamic shear properties of rubber-like materials over a wide range of frequencies and temperatures. Preliminary measurements were given for a Thiokol RD vulcanizate which undergoes a rubber-to-glass transition at temperatures near room temperature when deformations are imposed at frequencies in the range used: 0·01 to 30 rad/s. Measurements have now been made on a number of representative materials, both vulcanized and unvulcanized, over this frequency range and at appropriate temperatures. Most of the materials examined are in wide general use in circumstances where the dynamic mechanical behaviour is of importance.

The experimental results may be treated by the method of reduced variables developed by Ferry and others[2, 3] if the material satisfies certain theoretical conditions. The treatment yields a master curve relating a chosen dynamic property with reduced frequency; it is described briefly in Section 3 and is illustrated in Section 4 using the experimental measurements on a test-piece of unvulcanized natural rubber. In view of the limited frequency range of about three decades used in the present experiments in comparison with that required to encompass the rubber-to-glass transition—some ten decades—the present work does not constitute a rigorous examination of the applicability of the method of reduced variables. Indeed, the experimental difficulties involved in obtaining a complete confirmation are formidable. However, a considerable degree of success has been achieved in deriving master curves for all the materials examined from the experimental measurements, and previous workers[4–9] using a variety of polymeric materials have successfully reduced their experimental results in a similar manner.

The derived relationships enable the results to be presented very concisely. They may be used to predict the values of the dynamic properties over wide frequency and temperature ranges, although caution is advisable in deriving values at temperatures or frequencies far removed from those at which the measurements were made.

The method of reduced variables enables the frequency and temperature dependence of the dynamic properties to be studied independently. In Section 5 the temperature dependence is discussed for all the materials examined and compared with the generalized temperature dependence recently found to be widely applicable.[10, 11] The frequency dependence at suitable reference temperatures is described in the following sections.

2. EXPERIMENTAL

The materials used were:

A, unvulcanized natural rubber;
B, an unfilled natural rubber vulcanizate;
C, a vulcanizate of a typical tyre-tread compound, containing twenty-six volumes of carbon black per hundred volumes of natural rubber;

D, a natural rubber vulcanizate, containing twenty volumes of an ester plasticizer per hundred volumes of rubber;

E, a vulcanizate of a butadiene-styrene copolymer;

F, a vulcanizate of a similar copolymer, containing about forty volumes of an ether plasticizer per hundred volumes of rubber;

G, a vulcanizate of Thiokol RD; and

H, a standard sample of polyisobutylene.[12]

The mix formulations and vulcanization conditions which were employed in preparing the vulcanized test-pieces are given in the Appendix.

The test-pieces consisted of two moulded rubber cylinders bonded one to each end of a cylindrical steel block. The outer faces of the rubber cylinders were bonded to steel end plates which were clamped rigidly. The central block was locked into a carriage and subjected to a vertical force varying sinusoidally with time, causing the rubber cylinders to undergo a sinusoidal shear deformation.

The rubber cylinders were 1 in. in diameter and $\frac{1}{8}$ or $\frac{1}{4}$ in. in height. Adequate adhesion to the steel parts was obtained by means of bonding cements for the vulcanized rubber test-pieces, and by means of a resin bonding system for the unvulcanized natural rubber test-piece. The polyisobutylene samples were made to adhere by wiping the surfaces with benzene and pressing them into contact with the metal.

For measurements at low temperatures the test-piece and carriage were immersed in methyl alcohol which was circulated continuously, either through an external cooling coil surrounded by a mixture of methyl alcohol and solid carbon dioxide, or through a by-pass, the path being determined by a thermostatically-controlled solenoid-operated valve. For temperatures above room temperature the test-piece and carriage were immersed in a heated water bath.

During the course of a complete set of measurements, changes of up to 0·5° C in the temperature of the test-piece occurred. These changes affected the measured dynamic properties markedly in the neighbourhood of the transition to the glass-like state and in this region, therefore, three or four measurements were taken at each frequency and their mean values recorded.

The amplitude of vibration did not exceed 2% shear and no appreciable dependence of the measured properties on the amplitude of vibration could be detected for the majority of the materials examined. For the carbon-black filled natural rubber vulcanizate, where a considerable amplitude dependence has been described previously,[13] no indication was found of an increased effect at low temperatures. In view of the much greater dependence of the measured properties on the frequency of vibration and the temperature, and the difficulty of maintaining the vibration amplitude constant throughout the measurements, the effect of changes in the amplitude of vibration have been ignored for this material also. The significantly increased scatter in the experimental results for this material may be partly due to this cause.

A description of the apparatus and the methods of evaluating the dynamic properties has been given elsewhere.[1] The hysteresis loop given by a plot of instantaneous shear stress against instantaneous shear strain is recorded photographically; it is found to be substantially elliptical at the small strains used. From measurements of the ellipse dimensions, the values of the real and imaginary components, n and $\eta\omega$, of the complex shear modulus may be readily obtained. It has been found convenient to present the results in terms of the real component n and the ratio d of the imaginary to the real component (= tan δ, the tangent of the angle of mechanical loss).

3. METHOD OF REDUCED VARIABLES

Considerable advances have been made recently[2, 3, 14] in the methods of formulation of the temperature and frequency dependence of the stiffness of rubber-like materials. The material is assumed to comprise a variety of molecular mechanisms, whose contributions to the observed stress are assumed to relax separately and exponentially with time. If all the relaxation times depend similarly on temperature, an equivalence can be deduced between a change in the frequency of deformation and a change in temperature. Such a correspondence has been widely observed.[15, 16]

If the relaxation times are increased by a factor a_T when the temperature is changed from a standard temperature T_s to a temperature T, the real part n of the complex shear modulus at a frequency ω and temperature T is given by[2, 3, 14]

$$n(\omega, T) = \frac{T\rho}{T_s\rho_s} n(\omega a_T, T_s) \qquad (1)$$

where $n(\omega a_T, T_s)$ is the value at the standard temperature and a frequency ωa_T, ρ and ρ_s are the densities at T and T_s, the latter being absolute temperatures. $d(\omega, T)$ is given similarly by

$$d(\omega, T) = d(\omega a_T, T_s) \qquad (2)$$

Values of the factor a_T at various temperatures may be obtained from measurements of the steady flow viscosity for unvulcanized materials,[2, 3, 14] or from measurements of equivalent frequencies in vibration experiments. The values so obtained enable experimental results for n or d to be reduced to a standard temperature by means of equations (1) and (2). In this way the magnitude of either property over an extensive range of effective frequencies may be derived from measurements at a number of temperatures. Alternatively, when the behaviour at a reference temperature is known, the behaviour at other temperatures may be obtained from equations (1) and (2), using appropriate values for a_T.

The quantity a_T affords a convenient measure of the temperature dependence. It has recently been shown[10, 11] that the dependence of a_T upon T has the same general form for a wide range of materials; one, moreover, which is capable of physical interpretation in terms of the increase in the volume available for molecular motion. The relationship is[11]

$$\log_{10} a_T = -8{\cdot}86\,(T - T_s)/[101{\cdot}6 + (T - T_s)] \qquad (3)$$

where T_s is a reference temperature, chosen arbitrarily for one system, polyisobutylene, as −30° C. Values of T_s for other materials were then determined as those reference temperatures giving agreement of measured values of a_T over a range of temperatures with the values predicted by equation (3). Good agreement was obtained in this way[11] over temperature ranges of $T_s \pm 50°$ C. The values of T_s obtained were found to be about 50° C above the corresponding glass transition temperatures. It therefore appears that equation (3) provides an adequate representation of the variation of a_T over a temperature range extending upwards from the glass transition temperature for about 100° C.

Determinations of a_T from measurements of corresponding frequencies at different temperatures are described below for a number of rubber-like materials.

4. EXPERIMENTAL RESULTS: UNVULCANIZED NATURAL RUBBER

The measured values of the real part of the shear modulus for a sample of unvulcanized natural rubber have been plotted in Fig. 1 against the frequency of deformation at a number of temperatures. The corresponding measurements

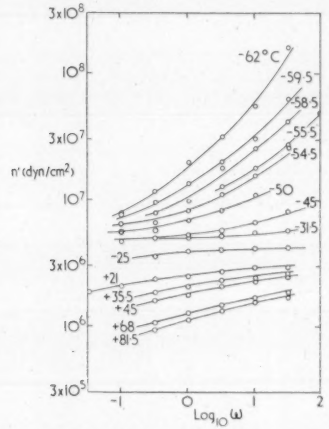

Fig. 1. Experimental relations between n' and $\log_{10}\omega$ at various temperatures for unvulcanized natural rubber *A*

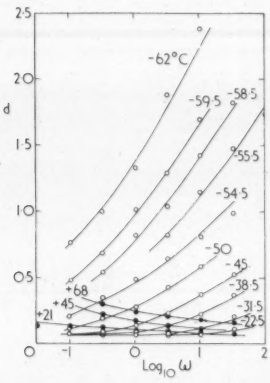

Fig. 2. Experimental relations between d and $\log_{10}\omega$ at various temperatures for unvulcanized natural rubber *A*

of the damping ratio d are given in Fig. 2. The modulus values have been multiplied by the correction factor $T_s\rho_s/T\rho$ necessary to eliminate kinetic theory changes with temperature and the corrected values are denoted by n'. The reference temperature chosen was $-25°$ C. If the correction had been omitted, however, the position of the experimental points would not have been greatly affected.

In accordance with the treatment described in Section 3, multiplication of the frequency scale by a suitably chosen factor should cause the experimental results obtained at one temperature to coincide with those obtained at another. Since logarithmic frequency scales have been used, the experimental curves of Figs. 1 and 2 should therefore superpose on lateral translation. The experimental results at the various temperatures have been subjected to suitable lateral shifts to bring them into superposition with the experimental results at $-25°$ C, to produce the composite curves shown in Fig. 3. It is clear that a considerable degree of superposition can be effected, within the experimental limitations discussed below.

The magnitudes of the lateral translations imposed are a measure of $\log_{10} a_T$. They were determined using the experimental results for d given in Fig. 2 and applied to the experimental results for n'. The successful superposition found in this case may therefore be considered additional support for the assumptions made in the theoretical treatment.

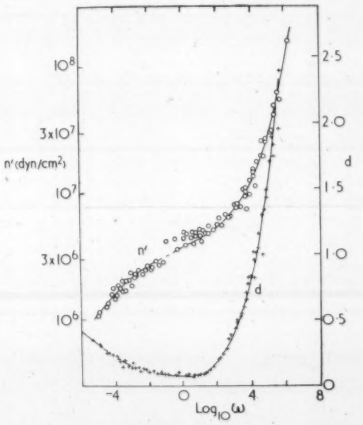

Fig. 3. Experimental relations between n' and $\log_{10}\omega$ and d and $\log_{10}\omega$, reduced to a standard temperature ($-25°$ C), for unvulcanized natural rubber *A*

The following experimental difficulties may be noted. Firstly, the experimental curves of Figs. 1 and 2 are relatively flat at temperatures between -20 and $+20°$ C, and the values of $\Delta(\log_{10} a_T)$ necessary to superimpose one curve with another in this region cannot be deduced accurately. The values for $\log_{10} a_T$ have therefore been obtained by interpolation from the results at low and high temperatures. The experimental results plotted at values of $\log_{10}\omega$ below -1 in Fig. 3 are subject to a possible error in $\log_{10}\omega$, due to imprecision in interpolating, of up to 0·5 units. The satisfactory agreement found to obtain between the values of a_T and the predictions of equation (3), discussed below, suggests that the error is small.

Secondly, marked increases in the measured values of n' were found at temperatures between -20 and $-40°$ C, and the results in this region did not superpose satisfactorily with those at other temperatures. This is evident in Fig. 3 where the points in question lie between values of $\log_{10}\omega$ of -1

and +2. The anomalous stiffening is ascribed to the occurrence of a small degree of crystallization during the conditioning period of about half an hour at each temperature.[17]

The composite curves of Fig. 3 represent the behaviour of unvulcanized natural rubber at a temperature of −25° C. They are in fairly good agreement with comparable published results.[9] The behaviour at other temperatures may be obtained by a shift of the origin of the frequency scale by an amount $\log_{10} a_T$, and an example of this procedure is given in Section 9.

5. TEMPERATURE DEPENDENCE FOR ALL THE MATERIALS EXAMINED

Values of a_T have been obtained for all the materials examined, by measurements of equivalent frequencies at different temperatures, as described in Section 4 for unvulcanized natural rubber. The values of $\log_{10} a_T$ are plotted against temperature in Fig. 4. The vertical positions of the curves in the figure have been adjusted by adding an appropriate constant amount to the values of $\log_{10} a_T$ for each material in order to achieve clarity of display and to bring the values of T_s, i.e. the temperatures at which $\log_{10} a_T$ is zero, into agreement with those defined below.

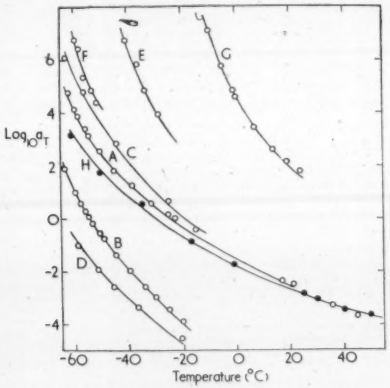

Fig. 4. Temperature reduction factors a_T necessary to reduce measurements at the indicated temperatures to standard temperatures. The standard temperatures used are given in Table 1. The experimental curves for materials *B* and *D* have been displaced vertically downwards by four units for clarity of display

The sensitivity to temperature is seen in Fig. 4 to decrease markedly as the temperature is increased. For the unvulcanized natural rubber *A*, for example, the change in temperature equivalent to a change in frequency by a factor of ten increases from approximately 5° at −60° C to 25° at +40° C.

In accordance with the observations of Williams and others[10, 11] on a variety of materials, the curves of $\log_{10} a_T$ against temperature for the different test-pieces were found to superpose when referred to suitably chosen reference temperatures T_s. The value of T_s for the polyisobutylene sample was chosen to be −30° C.[11] The values of T_s for the other materials were then determined as those giving superposition of the $\log_{10} a_T$ curves with the corresponding curve for polyisobutylene. The values obtained are listed in Table 1, together with two corresponding values obtained by Williams and others.[10, 11] They are seen to be about 50° C higher than the probable glass transition temperatures, in accordance with observations on other systems.[10, 11]

Table 1. *Reference temperatures* T_s

Material	T_s (°C)	T_s (°C) *determined by Williams and others* [10, 11]
Unvulcanized natural rubber *A*	−25	–
Unfilled natural rubber vulcanizate *B*	−21	—
Filled natural rubber vulcanizate *C*	−20	—
Plasticized natural rubber vulcanizate *D*	−33	—
Butadiene-styrene vulcanizate *E*	+ 3	− 5
Plasticized butadiene-styrene vulcanizate *F*	−16	—
Thiokol RD vulcanizate *G*	+35	—
Polyisobutylene *H*	−30	−30

In Fig. 5 the composite curve is given which is obtained from all the determinations of $\log_{10} a_T$ when referred to these values of T_s. It is seen that excellent superposition obtains. Moreover the relationship given in equation (3), represented by the full curve of Fig. 5, is seen to be in good agreement with the present experimental results.

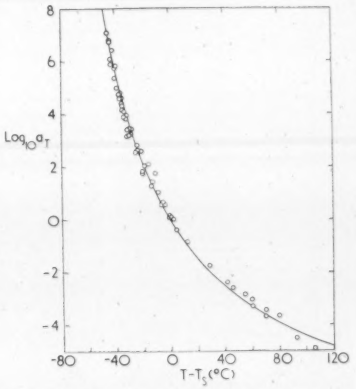

Fig. 5. Relation between the temperature reduction factor a_T and temperature for all the materials examined, referred to appropriate standard temperatures T_s. The values used for T_s are given in Table 1. The full curve is the relation given in equation (3)

The measurements of $\log_{10} a_T$ are seen in Fig. 5 to depart from the predictions of equation (3) at temperatures more than 50° C above T_s, as found previously.[10, 11] The departures are, however, relatively small.

6. EXPERIMENTAL RESULTS; NATURAL RUBBER VULCANIZATES

In Figs. 6 and 7 values of n' and d are given for an unfilled vulcanizate of natural rubber *B* and for one containing

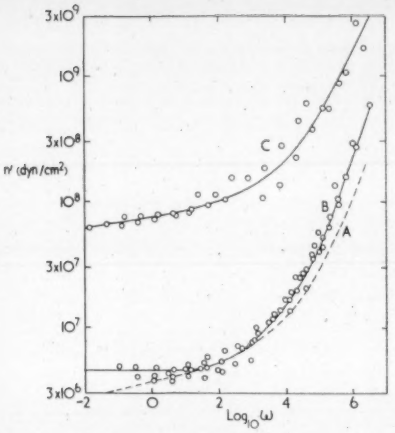

Fig. 6. Experimental relations between n' and $\log_{10}\omega$ reduced to the appropriate standard temperatures T_s, for a natural rubber vulcanizate B ($T_s = -21°$ C), and a carbon black filled natural rubber vulcanizate

C ($T_s = -20°$ C).

The broken curve relates to unvulcanized natural rubber

A ($T_s = -25°$ C)

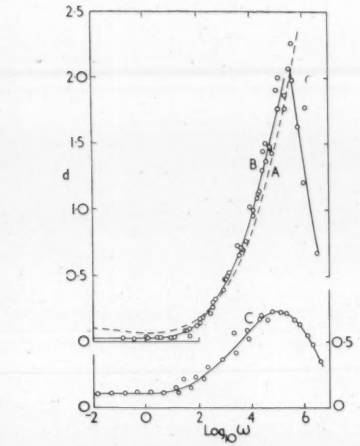

Fig. 7. Experimental relations between d and $\log_{10}\omega$, reduced to the appropriate standard temperatures T_s, for a natural rubber vulcanizate B ($T_s = -21°$ C), and a carbon black filled natural rubber vulcanizate

C ($T_s = -20°$ C).

The broken curve relates to unvulcanized natural rubber

A ($T_s = -25°$ C)

twenty-six volumes of carbon black per hundred volumes of rubber C. The experimental measurements of n for the latter have not been corrected for the kinetic theory dependence on temperature since no such dependence was observed even at low frequencies and high temperatures, and the values superposed more satisfactorily without correction. The superposition was much inferior for this material however. The results have been reduced to the respective standard temperatures T_s given in Table 1 in order that the temperature dependence of a_T given in equation (3) and Fig. 5 should be applicable, and in order to compare the materials under corresponding conditions. The broken curves of Figs. 6 and 7 are taken from the full curves of Fig. 3, and represent the behaviour of unvulcanized natural rubber A, at its standard temperature. The experimental results for a vulcanizate of natural rubber containing twenty volumes of dioctyl sebacate per hundred volumes of rubber D have been omitted from Figs. 6 and 7 since they were in close proximity to those obtained for the unplasticized vulcanizate B and of similar form. Attention has previously been drawn to the similar behaviour of plasticized and unplasticized rubbers;[18] it appears that the effect of plasticization is to a first approximation merely to reduce the value of T_s.

The value obtained for T_s for the vulcanized rubber B is seen in Table 1 to be some 4° C above that obtained for the unvulcanized rubber. This is in accord with measurements of the glass transition temperatures.[19] The value of T_s for the filled vulcanizate C is seen to be very similar to that for the unfilled vulcanizate, in agreement with earlier work.[18]

The curves of Figs. 6 and 7 appear to lie at somewhat lower frequencies for the vulcanized rubber B, and at still lower frequencies for the filled vulcanizate C, than for the unvulcanized rubber, but the differences are small and simultaneous changes in the shape of the curves make comparison difficult. Moreover, errors in determining T_s are reflected in corresponding errors in the position of the curves. Within the experimental errors, therefore, the transition appears to occur over similar frequency ranges for all the natural rubber materials.

The unvulcanized rubber A was found to undergo a second transition at low frequencies, shown more clearly in Fig. 3, associated presumably with the onset of molecular flow. The vulcanized rubber B, however, was found to have a substantially constant value for n' up to the rubber-to-glass transition region. The experimental points are not shown in Fig. 6 for values of $\log_{10}\omega$ below -1 to avoid an unduly contracted scale.

The filled material C, for which the low frequency values of n' are high, exhibits a more diffuse increase in n' with frequency.

The corresponding curves for d given in Fig. 7 show similar differences. The vulcanized rubber B exhibits, at low frequencies, values of d as low as 0·03, which is the lower limit of measurement using the present experimental method, whereas the unvulcanized rubber A exhibits a further rise in d as the frequency is reduced. The filled vulcanizate C has a greatly reduced maximum value for d, in accordance with the observations of Ecker[20] on similar systems. At low frequencies, the value of d is relatively high.[21, 22]

7. EXPERIMENTAL RESULTS: BUTADIENE-STYRENE MATERIALS

In Figs. 8 and 9 the values of n' and d are given for vulcanizates of a butadiene-styrene copolymer (Krylene) E and of a similar copolymer containing about forty volumes

of an ether plasticizer per hundred volumes of rubber *F*. The results have been reduced to the respective standard temperatures T_s given in Table 1. The broken curves of Figs. 8 and 9 are taken from Figs. 6 and 7 respectively, and

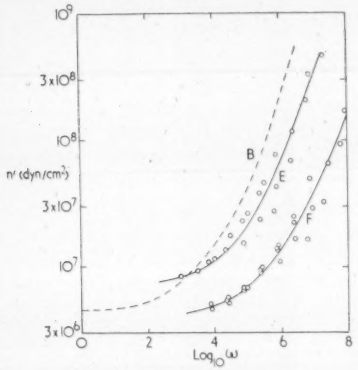

Fig. 8. Experimental relations between n' and $\log_{10}\omega$, reduced to the appropriate standard temperatures T_s, for a butadiene-styrene vulcanizate *E* ($T_s = +3°$ C) and a similar plasticized vulcanizate *F* ($T_s = -16°$ C). The broken curve relates to the natural rubber vulcanizate *B* ($T_s = -21°$ C)

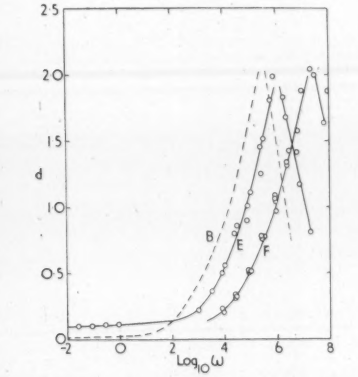

Fig. 9. Experimental relations between d and $\log_{10}\omega$, reduced to the appropriate standard temperatures T_s, for a butadiene-styrene vulcanizate *E* ($T_s = +3°$ C) and a similar plasticized vulcanizate *F* ($T_s = -16°$ C). The broken curve relates to the natural rubber vulcanizate *B* ($T_s = -21°$ C)

represent the behaviour of the unfilled natural rubber vulcanizate *B* at its standard temperature.

The value of T_s for material *E* is seen in Table 1 to be in fair agreement with a previous determination.[10, 11] For the plasticized material *F* it is greatly reduced. The experimental error in determining T_s was larger than for most of the other materials as the measurements were carried out over a considerably reduced temperature range. There is a corresponding uncertainty in positioning the curves of Figs. 8 and 9. It appears, however, that the principal effect of the presence of the plasticizer is to reduce the value of T_s, since only minor changes occur in the shape of the curves and the position is not greatly affected. Similar behaviour was described in Section 6 for plasticized natural rubber.

The experimental curves of Figs. 8 and 9 for the butadiene-styrene materials appear to be very similar in shape to the corresponding curves for the natural rubber vulcanizate *B*, and they lie in a similar frequency range. The low frequency values of d, however, are considerably larger than those for natural rubber, as has been frequently observed.[22, 23]

8. EXPERIMENTAL RESULTS: THIOKOL RD AND POLYISOBUTYLENE

In Figs. 10 and 11 the values of n' and d are given for a Thiokol RD vulcanizate *G* and for a standard sample of polyisobutylene H.[12] The results have been reduced to the respective standard temperatures given in Table 1. The broken curves of Figs. 10 and 11 represent the behaviour of unvulcanized natural rubber *A* at its standard temperature.

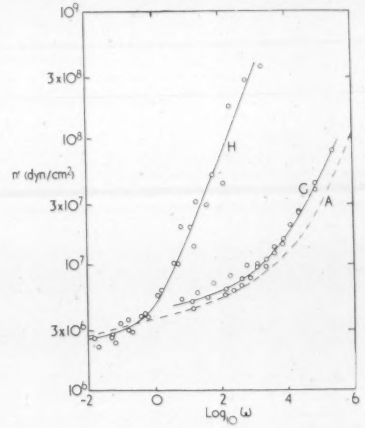

Fig. 10. Experimental relations between n' and $\log_{10}\omega$, reduced to the appropriate standard temperatures T_s, for a Thiokol RD vulcanizate *G* ($T_s = +35°$ C) and a standard sample of polyisobutylene *H* ($T_s = -30°$ C). The broken curve relates to unvulcanized natural rubber *A* ($T_s = -25°$ C)

The transition behaviour shown by the Thiokol RD vulcanizate *G* is closely similar to that shown by the unvulcanized natural rubber, and hence to vulcanized natural rubber, both in shape and position. The polyisobutylene sample, however, exhibits a more diffuse transition and it occurs at markedly lower frequencies. In the curves for d given in Fig. 11, for example, it is seen that the width of the transition peak is considerably greater than that observed for the other materials, while the maximum value of d occurs

at a frequency some three decades below that found for the natural rubber materials.

Although the position of the curves is subject to some uncertainty due to possible errors in determining T_s, an error of about 20° C would be necessary to cause the disparity in positions shown in Figs. 10 and 11. This is highly improbable. Moreover, the value for T_s used in the present work is identical with that obtained by Williams and others.[10, 11] It therefore appears that the transition in polyisobutylene occurs at lower frequencies than for the other materials studied, when referred to their respective standard temperatures.

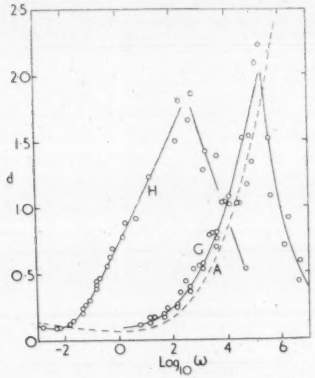

Fig. 11. Experimental relations between d and $\log_{10}\omega$, reduced to the appropriate standard temperatures T_s, for a Thiokol RD vulcanizate G ($T_s = +35°$ C) and a standard sample of polyisobutylene H ($T_s = -30°$ C). The broken curve relates to unvulcanized natural rubber A ($T_s = -25°$ C)

9. APPLICATION OF RESULTS TO OTHER TEMPERATURES

In order to obtain values of the dynamic shear properties at other temperatures T from the graphical presentations given in the preceding sections at standard temperatures T_s, two operations are necessary.

Firstly, the frequency scale requires multiplication by a factor a_T. With the logarithmic frequency scales used in the present graphical presentations this consists of transposing the scale by an amount $\log_{10} a_T$ to the right. (When $\log_{10} a_T$ is negative, the transposition is to the left.) The frequency scale is then appropriate to the temperature T. The required value of $\log_{10} a_T$ may be read from the full curve of Fig. 5 or calculated by means of equation (3), using the appropriate value of $T - T_s$.

Secondly, the values of n' read from the graph required multiplication by a factor $T\rho/T_s\rho_s$, generally close to unity, in order to compensate for kinetic theory changes with temperature. This factor may be approximated by T/T_s for most purposes.

As examples the values of n' and d are derived in Table 2 for two materials at a number of frequencies and temperatures by means of the graphical presentations given in previous sections for the variation with frequency of the dynamic properties at standard temperatures. The values of n' and d measured experimentally under these conditions are given for comparison; they are seen to be in fair agreement.

ACKNOWLEDGEMENTS

The authors thank Mr. J. F. Hawkes for the preparation of test specimens and assistance in carrying out the measurements. This work forms part of a programme of research undertaken by the Board of the British Rubber Producers' Research Association.

REFERENCES

(1) Fletcher, W. P., and Gent, A. N. *J. Sci. Instrum.*, **29**, p. 186 (1952).

(2) Ferry, J. D. *J. Amer. Chem. Soc.*, **72**, p. 3746 (1950).

(3) Ferry, J. D., Fitzgerald, E. R., Grandine, L. D., Jr, and Williams, M. L. *Industr. Engng Chem.*, **44**, p. 703 (1952).

(4) Grandine, L. D., Jr, and Ferry, J. D. *J. Appl. Phys.*, **24**, p. 650 (1953).

(5) Ferry, J. D., Grandine, L. D., Jr, and Fitzgerald, E. R. *J. Appl. Phys.*, **24**, p. 911 (1953).

(6) Williams, M. L., and Ferry, J. D. *J. Colloid Sci.*, **9**, p. 479 (1954).

(7) Williams, M. L., and Ferry, J. D. *J. Colloid Sci.*, **10**, p. 1 (1955).

(8) Williams, M. L., and Ferry, J. D. *J. Colloid Sci.*, **10**, p. 474 (1955).

Table 2. *Comparison of measured and interpolated values of n' and d*

	Unvulcanized natural rubber A			*Unfilled natural rubber vulcanizate B*		
Temperature (°C)	+45	−50	−50	−44·5	−44·5	−54·5
$T - T_s$ (°C)	+70	−25	−25	−23·5	−23·5	−33·5
$\log_{10} a_T$, *from equation* (3)	− 3·6	2·9	2·9	2·65	2·65	4·35
Frequency (*c/s*)	0·0505	0·016	1·6	0·016	1·6	0·016
ω (*rad/s*)	0·317	0·1	10	0·1	10	0·1
$\log_{10}\omega$	− 0·5	− 1	+ 1	− 1	+ 1	− 1
$\log_{10}\omega a_T$	− 4·1	1·9	3·9	1·65	3·65	3·35
n' (*c.g.s.* × 10^6) *from Figs.* 3 *or* 6	1·50	5·25	11·7	4·9	11·9	9·6
d, *from Figs.* 3 *or* 7	0·21	0·15	0·70	0·09	0·74	0·58
n' (*c.g.s.* × 10^6) *measured*	1·65	5·55	10·4	5·2	11·0	8·7
d, *measured*	0·23	0·11	0·57	0·09	0·70	0·50

(9) ZAPAS, L. J., SHUFLER, S. L., and DE WITT, T. W. *J. Polymer Sci.*, **18**, p. 245 (1955).

(10) WILLIAMS, M. L. *J. Phys. Chem.*, **59**, p. 95 (1955).

(11) WILLIAMS, M. L., LANDEL, R. F., and FERRY, J. D. *J. Amer. Chem. Soc.*, **77**, p. 3701 (1955).

(12) MARVIN, R. S. *Proc. 2nd Int. Congr. on Rheology*, p. 156 (Oxford, 1953) (London: Butterworths Scientific Publications, 1954).

(13) FLETCHER, W. P., and GENT, A. N. *Trans Instn Rubber Industr.*, **29**, p. 266 (1953).

(14) FERRY, J. D., and FITZGERALD, E. R. *Proc. 2nd Int. Congr. on Rheology*, p. 140 (Oxford, 1953) (London: Butterworths Scientific Publications, 1954).

(15) ALEKSANDROV, A. P., and LAZURKIN, YU. S. *J. Tech. Phys., USSR*, **9**, p. 1249 (1939); *Rubber Chem. Tech.*, **13**, p. 886 (1940).

(16) NOLLE, A. W. *J. Polymer Sci.*, **5**, p. 1 (1950).

(17) GENT, A. N. *Trans Instn Rubber Industr.*, **30**, p. 139 (1954).

(18) FLETCHER, W. P., GENT, A. N., and WOOD, R. I. *Proc. 3rd Rubber Techn. Conf.*, p. 382 (London, 1954) (Cambridge: W. Heffer and Sons, Ltd., 1954).

(19) BEKKEDAHL, N. *J. Res. Nat. Bur. Stand.*, **13**, p. 410 (1934); *Rubber Chem. Tech.*, **8**, p. 5 (1935).

(20) ECKER, R. *Kautschuk U. Gummi*, **9**, p. W.T.2 (1956).

(21) GEHMAN, S. D., WOODFORD, D. E., and STAMBAUGH, R. B. *Industr. Engng Chem.*, **33**, p. 1032 (1941).

(22) DILLON, J. H., PRETTYMAN, I. B., and HALL, G. L. *J. Appl. Phys.*, **15**, p. 309 (1944).

(23) FLETCHER, W. P., and SCHOFIELD, J. R. *J. Sci. Instrum.*, **21**, p. 193 (1944).

APPENDIX

The mix formulations and vulcanization conditions whereby the test-pieces of the vulcanized materials were prepared are given below. The amount of each ingredient is given in parts by weight.

	B	*C*	*D*	*E*	*F*	*G*
Natural rubber (smoked sheet)	100	100	100			
Butadiene-styrene 75/25 (Krylene)				100	100	
Thiokol RD						100
Stearic acid	2	2·5	2	1·5	0·72	1
Zinc oxide	5	5	5	3	3·6	5
CBS	0·8	0·5	0·8	0·9		0·75
DPG				0·1		
MBT					0·72	
TMT					0·036	
Sulphur	2·5	2·5	2·5	1·5	1·08	1·5
Phenyl-β-naphthylamine		1				
Pine tar		4·5				
Philblack O		50				
Tricresylphosphate						20
Di-octyl sebacate			20			
Ether plasticizer					*ca* 40	
Vulcanization time (min)	30	30	30	50	30	30
Vulcanization temperature (°C)	140	140	140	149	140	140

CBS = N-cyclohexyl benzthiazyl sulphenamide
DPG = Diphenyl guanidine
MBT = Mercaptobenzthiazole
TMT = Tetramethylthiuram disulphide

Secondary electron emission from barium dispenser cathodes*

By I. Brodie, M.Sc., A.Inst.P., and R. O. Jenkins, B.Sc., A.R.C.S., D.I.C., Ph.D., F.Inst.P., Research Laboratories, The General Electric Company Limited, Wembley, England

[*Paper first received* 25 *January, and in final form* 23 *February*, 1957]

Measurements of the total secondary electron emission coefficient under electron bombardment δ have been made at room temperature on "L" cathodes and porous tungsten cathodes impregnated with barium calcium aluminates. For "L" cathodes δ decreases with increasing porosity due to the increased surface roughness but δ is always above that for clean tungsten, due to the activation of the surface by adsorbed layers. For the impregnated cathode, δ increases with increasing porosity due to the larger contribution from the impregnant in the pore ends which has a larger value of δ than the surrounding activated tungsten. δ for the impregnated cathode is above that for the "L" cathode and comparable with that for bulk barium oxide. Decay of δ under electron bombardment is observed in the case of the impregnated cathode but the initial value can always be recovered by heating.

The various forms of barium dispenser cathodes were developed for use in thermionic devices where currents above $\frac{1}{2}$ A/cm^2 d.c. were required from the cathode with long life. One application is for use in a cavity magnetron. In this device the cathode may suffer intense bombardment by returning electrons so that in operation, particularly on long pulse or continuous operation the cathode temperature can rise sufficiently to make the ordinary oxide cathode unsuitable. Under these circumstances dispenser cathodes which operate at higher temperatures may prove more satisfactory. Electron bombardment of the cathode has another effect in that it produces secondary electrons which contribute to the working of the valve. The effective current density available from a cathode under magnetron conditions may thus be much larger than its primary thermionic emission. Alkaline earth oxides have a large secondary emission coefficient and from this point of view the oxide cathode has proved very satisfactory in magnetrons. It was therefore felt desirable to obtain data on the secondary emission coefficients of various dispenser cathodes in order to assess their relative suitability for use in magnetrons which rely on secondary emission to achieve the required cathode emission density.

THE CATHODES INVESTIGATED

The two types of barium dispenser cathode in general use were investigated, these being the "L" cathode[1] and that made from porous tungsten impregnated with barium calcium aluminates.[2,3] The construction of the cathodes tested is shown in Fig. 1. For the "L" cathodes the filling was pure barium oxide, obtained by decomposition of barium carbonate, and for the impregnated cathode the impregnant was a mixture of barium and calcium aluminate, corresponding to the molecular formula $\frac{1}{2}$ CaO . 3BaO . Al_2O_3. Each type of cathode was made with two grades of porous tungsten, having 45% and 25% porosity respectively.

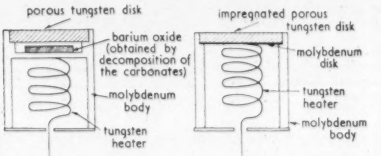

Fig. 1. Dispenser cathodes. (The cathode disks were 6·5 mm diameter and 1 mm thick)

(*a*) The "L" cathode.
(*b*) The impregnated cathode.

The appearances of the surface of "L" cathodes made from these two grades of porous tungsten differ markedly. The 45% material, after machining for the "L" cathode, has a dull granular surface, whereas machining after impregnating leaves it with a polished surface. The 25% tungsten can only be machined when impregnated with copper which is subsequently evaporated out from the pores,[4] leaving a smooth bright surface. Impregnating this material has no effect on the surface appearance, any excess impregnant being chipped away. No further surface treatment is given to the 25% material during assembly of either the "L" or impregnated type of cathode.

EXPERIMENTAL METHOD

The tube used for investigating the secondary emission properties of the cathodes is shown in Fig. 2. The electron gun system for the primary beam had a conventional oxide cathode with a modulator and two anodes A_1 and A_2 which gave electrostatic focusing. The electron beam from the gun passed through a 3 mm diameter hole in a disk of molybdenum, serving as the collector for secondary electrons, and then impinged normally on the surface of the cathode under investigation. This latter was placed 5 mm from the anode and took the form of a plane disk 6·5 mm in diameter. The purpose of the shutter, which could be interposed between the dispenser cathode and the molybdenum disk, was to prevent contaminants from each cathode affecting the other whilst they were being outgassed and activated. It

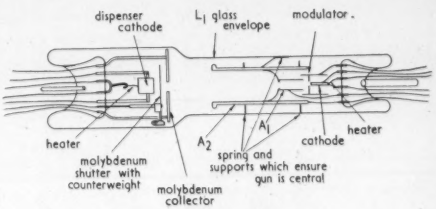

Fig. 2. The measurement tube

* G.E.C. Communication No. 720.

also prevented contamination of the molybdenum collector during processing of the dispenser cathode. The assembly was mounted in an L_1 glass tube and baked at 400° C for an hour on a mercury diffusion pump with liquid air trap. With the shutter closed the dispenser cathode was thoroughly outgassed, the oxide cathode processed in the normal way and finally a barium getter was deposited into the base of the valve furthest from the dispenser cathode. Before measurements were made the dispenser cathode was operated at about 1100° C for 5–8 h and its thermionic activity checked by taking pulse emission measurements. All secondary emission measurements were taken with the cathodes at room temperature; measurements at temperatures approaching that of the operating temperature of the cathodes are not possible with the present arrangement due to thermionic emission.

The current density in the primary beam was usually about 1 mA/cm^2 and could be varied by altering the potential of the modulator. The collecting field between the dispenser cathode and the molybdenum secondary collector was always greater than 1000 V/cm in order to ensure complete saturation of the secondary electron current. The energy of the primary electron beam was varied between 400 and 1500 V. The primary current was measured by increasing the potential of the dispenser cathode above that of the collector, thus preventing escape of secondaries. This value agreed well with the difference between the nett current to the dispenser cathode and the secondary current to the collector under the normal measuring conditions. This simple arrangement enabled the secondary electron emission coefficient δ to be found for the various types of dispenser cathode with an accuracy of about 5%.

THE EXPERIMENTAL RESULTS

"L" cathodes. The results for the "L" cathodes investigated are shown in Fig. 3. δ for cathodes made with 25% porous tungsten has a maximum value of 1·6 for 750 V electrons compared with a value of 1·45 for the 45% porous

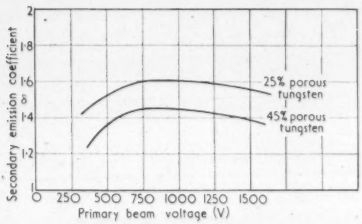

Fig. 3. Graph of secondary emission coefficient against voltage of primary beam for "L" cathodes. (No time decay effect observed with either cathode)

tungsten. It was observed that the "L" cathodes showed no significant decrease of δ with time under bombardment by 1500 V electrons, for periods up to 30 min. The values of δ also remained sensibly constant for variations in the primary beam current density between 1 and 20 mA/cm^2. Both types of cathodes showed slight fluorescence under bombardment by a beam of 2500 V electrons with a current density of 10 mA/cm^2, but this disappeared when the energy of the beam was brought below 1000 V. The colour of the luminescence was light blue.

Impregnated cathodes. The results for the impregnated cathodes are shown in Fig. 4. For the cathode with 45% porous tungsten the maximum value of δ decayed under electron bombardment from an initial value of 2·8 to a final value of 2·25 in about 15 min. Due to this decay the initial curve is likely to be slightly less accurate than the final curve

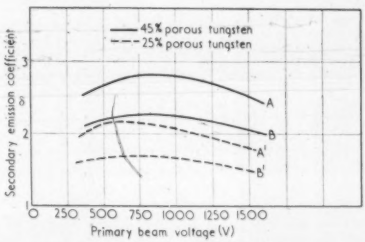

Fig. 4. Graph of secondary emission coefficient against voltage of pirmary beam for impregnated cathodes

A, *A'*, initial curves; *B*, *B'*, final curves.

although it is probably more significant. The final values of δ remained quite constant with time and primary current density and were reproduced quite well between different samples. The initial value of δ could always be recovered by heating the cathode to 1200° C for a few minutes.

The 25% porous tungsten impregnated cathodes showed similar trends. The maximum value of δ decreased fairly rapidly from 2·15 to a stable value of 1·70. In contrast with the "L" cathodes, both impregnated cathodes fluoresced strongly under bombardment by a beam of 2500 V electrons with a current density of 10 mA/cm^2 and some fluorescence was still visible with 400 V electrons. The luminescence from the 45% porous tungsten was appreciably stronger than that from the 25% porous cathode, the colour of the luminescence again being light blue.

DISCUSSION

For the "L" cathodes the secondary emission coefficients show an increase with decreasing porosity. This is in accordance with the well-known fact that the secondary emission coefficient of any surface decreases as the roughness of the surface increases.[5] The peak value of δ for a clean tungsten surface as given in the literature[5] lies between 1·3 and 1·45. Thus taking into account surface roughness the values for the "L" cathodes are significantly higher than that for clean tungsten. This is in agreement with Treloar's[6] results in which he found that the secondary emission coefficient for tungsten was increased by an adsorbed monolayer of barium on oxygen on tungsten. The type of surface examined by Treloar was very similar to that which is known to exist on the surface of an "L" cathode.[7]

For the impregnated cathodes the initial values of δ are much larger than for "L" cathodes; however, in this case the value of δ decreases with decreasing porosity. This is consistent with regarding the surface structure as patches of active material, with a high value of δ, in the pore ends surrounded by monolayer activated tungsten, and is in

accordance with the picture of the nature of the emitting surface of this type of cathode which has been put forward.[7] The material in the pore ends must contain one or more of the oxides of barium, calcium and aluminium and the secondary emission coefficient of this material can be estimated very approximately if it is assumed that the area of the pore ends is proportional to the porosity and that the value of δ for the surrounding activated tungsten is that of the smoother "L" cathode. Figures calculated on this basis are given in the table.

Values of δ for cathodes and impregnants

Type of impregnated cathode	*Porosity*	*Value of δ*	*Value of δ for impregnant*
Impregnant $\frac{1}{2}CaO \cdot 3BaO \cdot Al_2O_3$	45%	2·8 Initially	4·2
		2·25 Finally	3·0
Impregnant $\frac{1}{2}CaO \cdot 3BaO \cdot Al_2O_3$	25%	2·15 Initially	3·8
		1·70 Finally	2·0

It should be noted that both the magnitude and the decay of δ under electron bombardment support the view that the impregnant itself contributes strongly to the secondary emission, such decays being characteristic of alkaline earth oxides.[8,9] The marked increase in fluorescence over the "L" cathode shows the impregnant is in fact being bombarded. The values of δ calculated above for the impregnant are also consistent with what might be expected from a material containing the oxides of barium, calcium and aluminium.[5] The reason for the greater decay in the case of the 25% porous tungsten is not clear.

It is interesting to compare the results obtained here for impregnated cathodes with results taken under similar conditions for barium oxide which have been reported by Woods and Wright.[8,9] These workers found that for a sprayed oxide coating the secondary emission coefficient decayed from an initial value of 2 to below 1·5 fairly rapidly. For a thick evaporated film or a sprayed coating which had been pressed to give it a shiny surface, the initial value of δ was 2·8 which decayed to 2 in about 15 min. The initial values could always be recovered by heating the cathodes at 800° C for 5 min. The value of δ for the conventional barium strontium double oxide coating is somewhat higher, being about 4.[10] If the initial values measured in all cases are assumed to correspond to the values obtained at working temperature, it will be seen that both forms of "L" cathode are considerably inferior to the conventional oxide-coated cathode. On the other hand the impregnated cathode made with 45% porous tungsten is only slightly inferior to the conventional double oxide coated cathode and better than a sprayed barium oxide surface, while the 25% porous tungsten cathode is comparable with the sprayed barium oxide. The assumption that δ for a cathode at its operating temperature has the initial value seems justified by (i) the rapid recovery of the secondary emission when the cathode temperatures are raised, (ii) that for the oxide coating[8] and other materials[11] variations of δ with temperature appear to be relatively small, and (iii) that this is to be expected from considerations of electron energy.[11]

CONCLUSIONS

The measurements of secondary emission coefficients have shown that "L" cathodes have a lower value of δ than the oxide cathodes but higher than that for clean tungsten. The value for the cathode made with smooth high density porous tungsten is higher than that for the cathode of low density porous tungsten, which has a rougher surface. The barium calcium aluminate impregnated cathode has a higher secondary emission coefficient than "L" cathodes due to the impregnant in the pore ends having a higher secondary emission coefficient than the surrounding activated tungsten. Fairly rapid decay of δ for the impregnated cathode, similar to that of the oxide cathode, has been observed and is probably associated with decomposition of the surface of the impregnant under electron bombardment. Heating the cathodes gives complete recovery of the secondary emission coefficients, which are slightly inferior to those of the oxide cathodes. The experiments suggest that the impregnated cathode should have a high enough secondary coefficient to operate in many magnetrons, especially in view of the fact that cathodes with the double oxide interspersed in a coarse porous nickel surface are often used satisfactorily.

ACKNOWLEDGEMENT

In conclusion, the authors wish to thank the Admiralty for permission to publish this paper.

REFERENCES

(1) Lemmens, H. J., Jansen, M. J., and Loosjes, R. *Philips Tech. Rev.*, **11**, p. 341 (1950).

(2) Levi, R. *J. Appl. Phys.*, **26**, p. 639 (1955).

(3) Brodie, I., and Jenkins, R. O. *J. Appl. Phys.*, **27**, p. 417 (1956).

(4) Levi, R. *Philips Tech. Rev.*, **17**, p. 97 (1955).

(5) Bruining, H. *Physics and Applications of Secondary Emission* (London: Pergamon Press Ltd., 1954).

(6) Treloar, L. R. G. *Proc. Phys. Soc.* [*London*] *B*, **49**, p. 392 (1937).

(7) Brodie, I., and Jenkins, R. O. *Brit. J. Appl. Phys.*, **8**, p. 27 (1957).

(8) Woods, J., and Wright, D. A. *Brit. J. Appl. Phys.*, **3**, p. 323 (1952).

(9) Woods, J., and Wright, D. A. *Brit. J. Appl. Phys.*, **4**, p. 56 (1953).

(10) Woods, J., and Wright, D. A. Private communication.

(11) Bruining, H. *Die Sekundar-Electronen-Emission fester Korper* (Vienna: Verlag-Springer, 1942).

Vacuum-deposited films of nickel-chromium alloy*

By R. H. Alderson and F. Ashworth, B.Sc., Ph.D., A.Inst.P., Metropolitan-Vickers Electrical Co. Ltd., Trafford Park, Manchester, 17

[*Paper received* 15 *October*, 1956]

The preparation and properties of stable films of vacuum-deposited nickel–chromium alloy are described. Properties discussed include the film-alloy composition, the relationship between film thickness and resistance (Ω/square), the temperature coefficient of resistance, grain size in the film (electron micrographs), mechanical failure of stressed films, optical transmission as a function of film thickness, fundamental noise and electrical breakdown under low- and high-frequency conditions. Graphs summarize the data and micrographs illustrate grain growth, breakdown due to stresses in the film and electrical breakdown in microwave attenuators.

PREPARATION OF STABLE FILMS

All the work reported here relates to films of nickel–chromium alloys prepared in a conventional "evaporation plant" (Metropolitan-Vickers type 27 coating unit) but in all cases strict control of the evaporation source temperature, the degree of vacuum and substrate temperature have been maintained. The substrate was borosilicate- "heat-resistant" glass "of microslide quality" made by Chance Bros. Ltd.

Only film thicknesses up to a few hundred Ångström units were of interest in these studies and these could be readily made by the evaporation of a quantity of nickel–chromium alloy (80% nickel: 20% chromium) from a tungsten "boat" strip by resistance heating. Thicker films up to 0·1 mm have been prepared by evaporating nickel–chromium from a ceramic crucible heated by a radio-frequency induction coil, but these thicker films exhibit the bulk properties of the alloy and are of no special interest in this paper.

The most important parameters in the preparation of stable films of nickel–chromium alloys (and this applies to other evaporands likewise) are the source temperature, the degree of vacuum maintaining in the system and the temperature of the receiving surface during deposition from the vapour phase.

Earlier work by the authors has shown that stable films of nickel–chromium alloys can only be made if the substrate temperature is greater than 350° C and the vacuum in the system is better than 10^{-4} mm of mercury.

Fig. 1 illustrates how increasing the substrate temperature above 350° C speeds up the "forming" of the film after deposition. All films were deposited on glass substrates at 350° C and allowed to "stabilize" at 350° C for thirty minutes before they cooled down and were removed from the vacuum chamber.

Fig. 2 illustrates the resistance changes experienced by a freshly formed film of nickel–chromium alloy from the moment when deposition was completed. The film was allowed to "stabilize" at 350° C for thirty minutes, then allowed to cool to room temperature when its resistance value fell to 270 Ω/square. Resistance changes, when its temperature was again raised to 350° C and cooled to room temperature, were shown to be reversible, indicating that the film was fully stabilized.

Measurements of the resistance values of films during deposition must be made with care. Microslides (3 × 1 in.) of borosilicate glass having, for electrodes, previously deposited films of nickel–chromium alloy or of chromium metal covering areas of ½ × 1 in. at each end have been found to be the most reliable. Electrodes of this form and approximately 2000 Å thick are always used on "control" slides. Electrodes made by baking on films of "platinum" or "silver" paste are quite unreliable for this type of work and

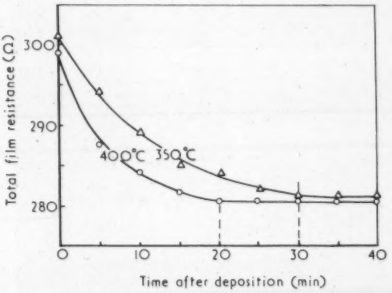

Fig. 1. Decay of resistance during baking of nickel–chromium films on glass

results quoted using such electrodes are suspect. Electrical contact is made by wrapping tinfoil around the electrode-ends of the slide and applying spring-loaded clips with wires attached. Using "control" slides of this type films may be formed with resistance values lying within ±0·1% of the desired values up to 300 Ω/square. This may be achieved

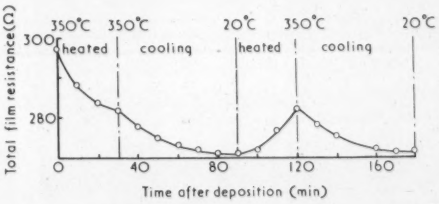

Fig. 2. Resistance changes from a freshly-formed layer of nickel–chromium film on glass

manually using a resistance bridge or by incorporating an automatic control such as that shown in Fig. 3, which switches off the evaporation source at a predetermined value of control slide resistance.

* The substance of this paper was presented at the Symposium on Thin Films arranged by the Electronics Group of The Institute of Physics and held in Reading, September, 1956.

PROPERTIES OF STABLE FILMS

Films prepared as described are particularly resistant to abrasion and corrosion. The films cannot be removed without scratching the glass base, and can be repeatedly polished to remove finger marks, grease and dirt. They can be removed from the base by immersing in hot concentrated sulphuric acid or warm concentrated hydrochloric acid.

necessary to maintain the source temperature at least at 1600° C.

Film resistance/film thickness. Nickel–chromium alloy in bulk has a high resistivity ($10^{-4}\,\Omega$ cm) compared with other conductors. It also has a low temperature coefficient of resistance (0·04% per °C). These properties are highly desirable in the production of high resistance elements,

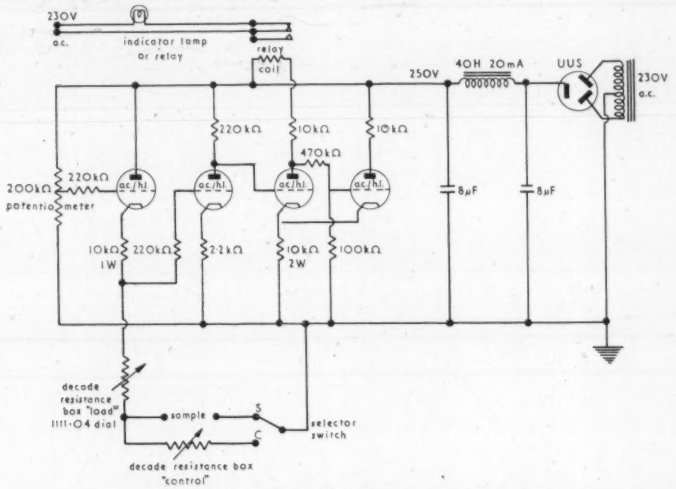

Fig. 3. Circuit for automatically controlling the evaporation source

The hardness of the films is attributed to a surface migration of the atoms after deposition and the formation of a stable structure during the processing at 350° C. The observed decrease of resistance value is compatible with a change in structure, or decay of lattice distortions.

Alloy composition/source temperature. Fig. 4 illustrates how the composition of the deposited film depends on the source temperature. In order to produce films with a composition approaching 80% nickel : 20% chromium it is

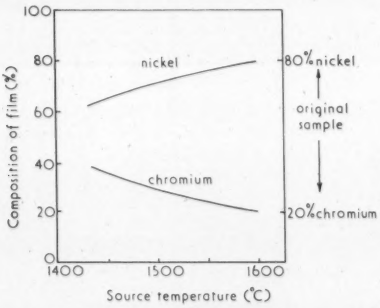

Fig. 4. Variation of composition with source temperature for nickel–chromium alloy films on glass

especially if these resistance elements are in the form of thin films.

The resistance along a conductor of length l and area of rectangular cross-section $(b) \times (t)$; (where t is the thickness) is given by:

$$R = \rho(l/bt) \text{ (where } \rho \text{ is the bulk resistivity).}$$

If the conductor is a film of unit length and unit breadth, and thickness t, then the resistance across a unit square will be given by:

$$R = \rho_t/t \text{ (where } \rho_t \text{ is the resistivity of the thin film).}$$

This gives a convenient measure for the resistance of a film in terms of "ohms per square." For conductors such as nickel–chromium, with a high value of ρ_t, it is possible to make much higher resistance elements for the same physical dimensions. Normally the limiting value of t, below which the films are neither continuous nor stable, makes the production of very high resistance elements difficult. It has been observed and confirmed by life tests that films of 300 Ω/square and less are always stable to within $\pm\frac{1}{2}$%. Such a film of 300 Ω/square has a thickness of approximately 50 Å. A film of 400 Ω/square deteriorates gradually in use. This corresponds to a thickness of 30–40 Å.

Fig. 5 illustrates the relationship between film thickness and resistance value (reduced to ohms per square) for film thicknesses up to 750 Å.

The bulk resistivity of 80 : 20 nickel–chromium alloy is of the order of $10^{-4}\,\Omega$ cm, while the value for films of the

order of 700 Å thick is approximately $1{\cdot}2 \times 10^{-4}\,\Omega$ cm increasing to approximately $1{\cdot}65 \times 10^{-4}\,\Omega$ cm for films as thin as 50 Å.

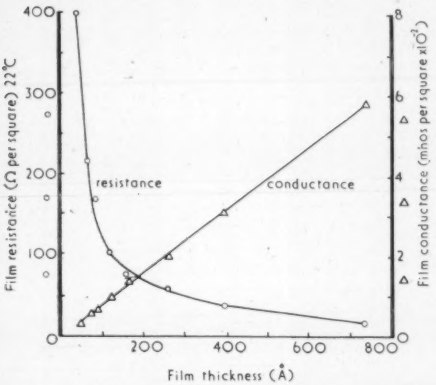

Fig. 5. Relationship between film thickness and resistance value for nickel–chromium alloy films on glass

Temperature/coefficient of resistance. The temperature coefficient of resistivity for nickel–chromium films varies between 0·01%* and 0·02% per °C depending on the composition (Fig. 4) and thickness. The value for bulk 80% nickel : 20% chromium alloy is 0·04% per °C.

Electron micrographs of grain growth. Electron micrographs, using replica techniques, indicate that "stabilized" nickel–chromium alloy films have a micro-structure, the "grain" size of which is related to the film thickness. Fig. 6 shows micrographs of films having thicknesses of the order of 50, 75 and 125 Å. The "grain" size lateral dimensions increase correspondingly, approximately 40, 100, 140 Å by estimation.

Mechanical breakdown of stressed films. Thin nickel–chromium films well bonded to borosilicate glass are not broken up by differential contraction on cooling from 350° C to room temperature even though the expansion coefficient between 20–350° C for 80% : 20% nickel–chromium alloy in bulk is $13{\cdot}0 \times 10^{-6}$ per °C and for borosilicate glass $3{\cdot}6 \times 10^{-6}$. But when films thicker than about 10 000 Å deposited on borosilicate glass are cooled from 350° C to room temperature the glass surface fails and flakes of nickel–chromium–glass fly off the surface—the bond between the nickel–chromium and the glass is stronger than the tensile strength of the borosilicate glass. Under similar circumstances thick nickel–chromium films freshly deposited on soda glass can withstand the stresses set up by differential contraction (expansion coefficient of soda glass is of the order of 12×10^{-6}).

When thick films of magnesium fluoride are deposited directly on the still hot, freshly deposited, thin nickel–chromium films the high stresses produced on cooling down cause them to break up. The series of electron micrographs shown in Fig. 7 illustrate this. Fig. 7(*a*) shows a good film consisting of nickel–chromium 75 Å thick (150 Ω/square) with coating of magnesium fluoride approximately 500 Å thick. Fig. 7(*b*) shows a similar film of nickel–chromium covered by a very much thicker film of magnesium fluoride, approximately 5000 Å. This film shows discontinuities and its resistance value was several megohms per square. There

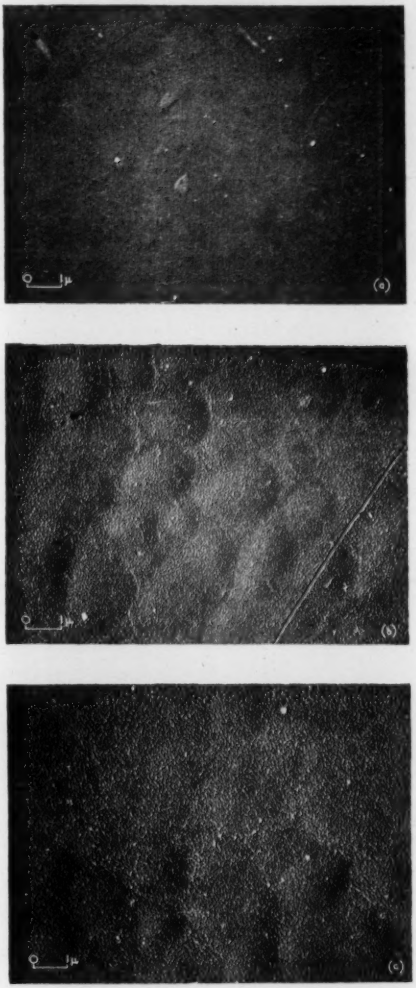

Fig. 6. Electron micrographs of grain size in nickel–chromium alloy films

Film thicknesses: (*a*) 50 Å; (*b*) 75 Å; (*c*) 125 Å.

* HOLLAND. *Vacuum Deposition of Thin Films.* (London: Chapman and Hall, Ltd., 1956), p. 251 quotes 0·006% per °C but does not define film composition.

is some electron diffraction evidence to suggest that these "faults" occur at intercrystalline boundaries.

Optical density. Optical density curves for a series of thicknesses of nickel–chromium films on borosilicate glass have been plotted (Fig. 8) and indicate the neutral absorption of these films up to 400 Å thickness. Thicker films show tendency for more absorption at the shorter wavelengths. This appears as a brownish tinting observed in transmission of white light through thick films.

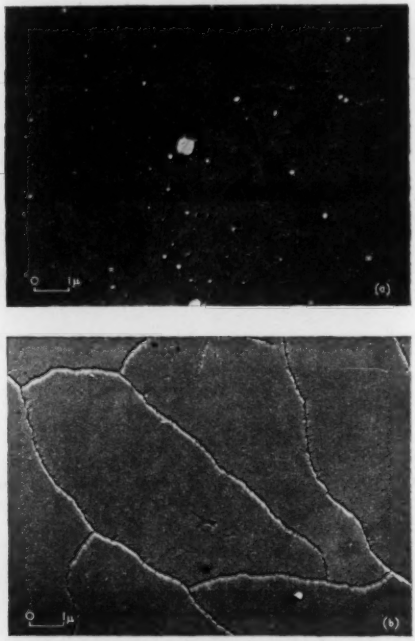

Fig. 7. Mechanical breakdown in stressed nickel-chromium alloy films, 75 Å thick

Magnesium fluoride films: (*a*) 500 Å; (*b*) 5000 Å thick.

Fundamental noise. Noise measurements have been made on several films of 300 Ω/square (total resistance values approximately 10 kΩ) (Fig. 9). Fundamental noise in these was rather more than in a nickel–chromium wire-wound resistor of similar order of resistance. At 0·75 mA current the increase in current noise was comparable in films and wire-wound resistor as shown by the broken curves in Fig. 9. For the films 0·75 mA corresponded to approximately 0·1 W dissipation per square inch of area.

Electrical breakdown, d.c. and l.f. Films of nickel–chromium alloy on glass substrates may be readily prepared having value from 300 Ω/square to less than 1 Ω/square and these can be used to make stable resistance elements. The range of resistance values is determined by the film "square-resistance" and the practical lengths and widths of film which are possible. A resistance of 100 000 Ω can be made with a

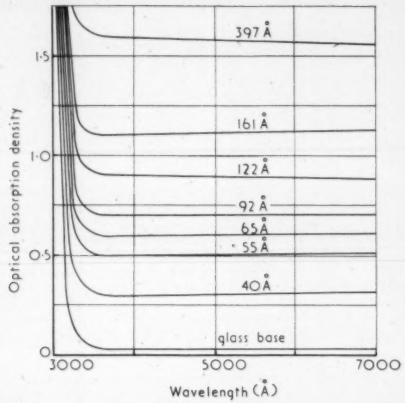

Fig. 8. Variation of optical absorption with thickness for nickel–chromium films

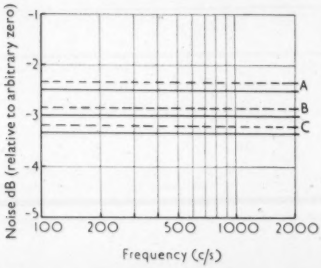

Fig. 9. Current noise in nickel–chromium films and wire-wound resistor

A: nickel-chromium film, 300 Ω/square. Total 11·2 kΩ.
B: nickel-chromium film, 300 Ω/square. Total 13·3 kΩ.
C: wire-wound resistor. Total 10 kΩ.

——— = noise at 0 mA.
– – – – = noise at 0·75 mA.

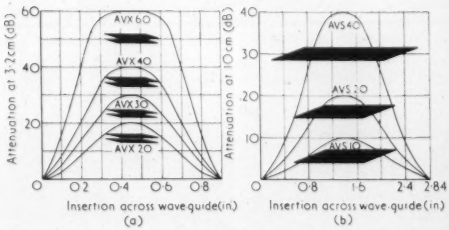

Fig. 10. Typical characteristic curves of wave-guide attenuator vanes

(*a*) AVX series for 3 cm wave-band. Wave-guide W.G. 16.
(*b*) AVS series for 10 cm wave-band. Wave-guide W.G. 10.

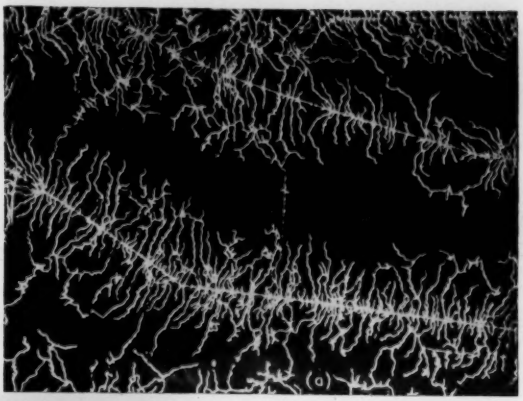

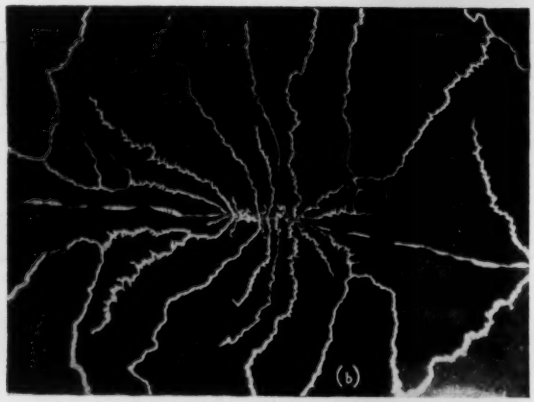

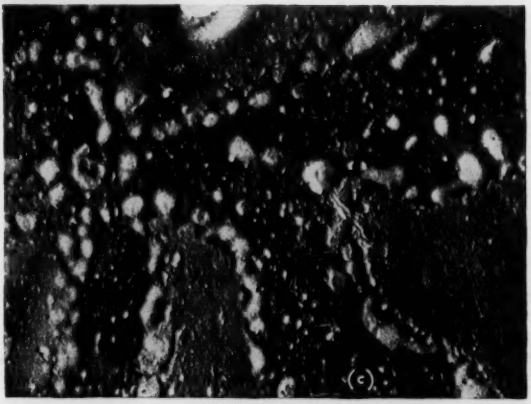

Fig. 11. Electrical breakdown in nickel–chromium alloy films used as microwave attenuator elements

(*a*) ×100, (*b*) ×750, (*c*) ×25 000.

film of 250 Ω/square and a length and width ratio of 400 : 1 which can either take the form of a zig-zag on a flat plate or a spiral round a tube. Resistance elements of this type are capable of dissipating more than 1 W/in.^{2} under d.c. or low-frequency conditions—in fact it is possible to boil water in a beaker, the outside surface of which has been coated with a resistive film of nickel–chromium connected directly to the mains! Films on glass may be operated continuously at 400° C without damage; at higher temperatures the glass breaks.

Electrical breakdown, h.f. In high-frequency applications films have been used extensively as microwave attenuator elements (Fig. 10). A typical attenuator, type WG. 10/10 (or AVS 10) for the 10 cm wave-band, consisting of a parallelogram of glass of overall length 9·5 in., and width 1·125 in. with a film resistance of 200 Ω/square, has a maximum attenuation of 10 dB when mounted centrally in the waveguide. Attenuators of this type are capable of dissipating a few watts of mean power, the limiting value being determined to some extent by the field distribution in which the attenuator is situated. At higher loadings the nickel–chromium films break down. A vane dissipating 1·5 W of mean power in a wave-guide transmitting 10 kW peak, of pulse length 3 μs and repetition frequency 50 pulses/second may fail depending on the field distribution, the initial breakdown pattern being composed principally of a few *longitudinal streaks* [such as those appearing in Fig. 11(*a*)]. At higher power levels, e.g. when dissipating 10·5 W mean power (70 kW peak, 3 μs pulse, 50 pulses/second) branching streaks develop and increase in number and severity as illustrated in Fig. 11(*a*). At 14 W (10 kW peak, 2 μs pulse, 700 pulses/second) similar breakdown patterns appear. Closer examination of these patterns [Fig. 11(*b*)] indicates that the low-power breakdown occurs along linear discontinuities in the glass surface, most probably scratch-lines introduced during polishing. The film first breaks down wherever it is locally thinnest and this can occur most obviously along scratches. The high-power breakdown originates at these scratches—where the highest voltage stress occurs, but follows trends similar to those observed in lightning streaks, in Lichtenberg figures or breakdown patterns in electrically stressed solids (e.g. irradiated Perspex). These *random* tracks are determined, in general, by the field pattern in the films and, in detail, by local variation in the film thickness and composition. The electron micrograph in Fig. 11(*c*) indicates that breakdown is a local overheating and melting of the film.

ACKNOWLEDGEMENTS

The authors wish to acknowledge with thanks, assistance given by the Director, British Scientific Industries Research Association, for making available a spectro-photometer for spectral transmission measurements, by the Director and Dr. A. C. Moore of the Telecommunications Research Establishment for facilities for noise measurements and by Metropolitan-Vickers Research Department staff, G. Saxon and G. W. Buckley, for evidence of electrical breakdown at radio-frequency, A. W. Agar and R. S. M. Revell for electron micrographs and G. Siddall for some of the preliminary measurements.

The authors wish to thank Dr. Willis Jackson, Director of Research and Education, and Mr. B. G. Churcher, Manager of the Research Department, Metropolitan-Vickers Electrical Co. Ltd., for permission to publish this paper.

The conductance of a column of vapour for gases at low pressures

By D. S. Stark, B.Sc., A.Inst.P., Services Electronics Research Laboratory, Baldock, Herts.

[*Paper first received* 29 *October*, 1956, *and in final form* 3 *January*, 1957]

Vacuum systems often contain stationary columns of vapour. A general expression is derived for the conductance of such a column for gases at low pressures.

A rough experiment using columns of mercury vapour yielded values for the conductance for air and hydrogen which were of the same order of magnitude as the values predicted from the expression given.

It is shown that the conductance of the vapour can be less than that of the pipe which contains it. This becomes increasingly probable as the pipe diameter and the vapour pressure are increased.

Vacuum pumping systems often contain stationary clouds of vapour. For example, pumping fluid vapour is likely to be found in condensation pumps, in the region immediately above and around the pumping jet.

Such a stationary cloud presumably causes an impedance to the flow of the gases being pumped. It is useful to estimate, even roughly, the magnitude of such an impedance and to find out how it depends on such factors as the pressure, temperature and molecular weight of both the vapour and the gas being pumped.

An attempt has been made to obtain an idea of the magnitude of the conductance of a specified column of vapour. Two methods were used: firstly the deduction of a general expression from the kinetic theory, and secondly an approximate experimental measurement.

Calculation from Kinetic Theory

Consider a tube of constant cross-sectional area A cm^2 (Fig. 1) which contains a vapour (molecular weight M_1) between perpendicular planes, A and B, impermeable to the vapour, distance L cm apart. Let there be uniformly n_1 vapour molecules per cubic centimetre, throughout this volume.

A vacuum pump is connected to the right of plane B, and a constant pressure, p_a microbars, of a given gas (molecular weight M) is maintained immediately to the left of plane A. The pressure immediately to the right of plane B is p_b. The planes A and B are supposed to have no impedance to the passage of the gas. When steady conditions have been established, therefore, gas will flow through the vapour at a constant rate from A to B. To avoid complication, it is

assumed that the tube itself has no impedance to the flow of gas, i.e. the reflexion of molecules at the walls is specular.

Let the molecular concentration of the gas be n molecules per cubic centimetre at any plane X, distance x cm from A, and suppose n is everywhere small compared with n_1.

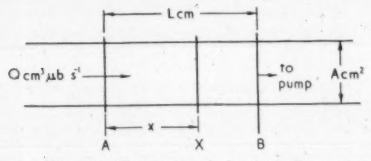

Fig. 1. Diagram illustrating derivation of equation (7)

The *net* number of molecules of gas crossing any plane X in unit time is independent of x, and is

$$N = -AD(dn/dx) \text{ (molecules per second)} \qquad (1)$$

where D is the coefficient of inter-diffusion for the given gas and vapour.

$$D = \frac{\sqrt{(V^2 + V_1^2)}}{3\pi(n + n_1)\delta^2} \quad \text{[See Refs. (1) and (2)]}$$

where V and V_1 are the arithmetic mean molecular velocities of the gas and vapour respectively, and δ is half the sum of the diameters of a molecule of vapour and a molecule of gas.

As n is small compared with n_1,

$$D = \frac{\sqrt{(V^2 + V_1^2)}}{3\pi n_1 \delta^2} \qquad (2)$$

which is independent of x.

Integrating equation (1) between $x = 0$ and $x = L$ gives

$$n_a - n_b = NL/AD \text{(molecules per cm}^3\text{)} \qquad (3)$$

where n_a and n_b are the values of n at A and B respectively.

Now $p_a = n_a kT$ and $p_b = n_b kT$ microbars, where $T°$ K is the temperature of gas and vapour and k is Boltzmann's constant.

$$p_a - p_b = kTNL/AD \qquad (4)$$

It is easily shown that the throughput Q of gas across any plane is given by

$$Q = NkT \text{ (cm}^3\ \mu\text{bs}^{-1}\text{)} \qquad (5)$$

The conductance of the vapour for the gas is defined by

$$U_v = Q/(p_a - p_b)$$

Substituting from equations (4) and (5),

$$U_v = DA/L \text{ (cm}^3\text{/s)} \qquad (6)$$

In equation (2)

$$v = \sqrt{(8RT/\pi M)} \quad \text{and} \quad n_1 = p_1/kT$$

hence $$U_v = \frac{k}{3\pi}\sqrt{\left(\frac{8R}{\pi}\right)}\sqrt{\left(\frac{1}{M} + \frac{1}{M_1}\right)}\frac{T^{\frac{3}{2}}}{\delta^2 p_1}\cdot\frac{A}{L} \text{ (cm}^3\text{/s)} \qquad (7)$$

If M is small compared with M_1 (as in the case of air or hydrogen relative to mercury), we have approximately

$$U_v = \frac{k}{3\pi}\sqrt{\left(\frac{8R}{\pi}\right)}\frac{T^{\frac{3}{2}}}{M^{\frac{1}{2}}\delta^2 p_1}\cdot\frac{A}{L} \text{ (cm}^3\text{/s)} \qquad (8)$$

For mercury vapour, expressing the pressure in millibars, equation (8) gives

$$(U_v)_{air} = 2{\cdot}06 \times 10^{-5}\cdot\frac{T^{\frac{3}{2}}}{p_1}\cdot\frac{A}{L} \text{ (l./s)} \qquad (9)$$

and $$(U_v)_{hydrogen} = 9{\cdot}75 \times 10^{-5}\cdot\frac{T^{\frac{3}{2}}}{p_1}\cdot\frac{A}{L} \text{ (l./s)} \qquad (10)$$

Equation (8) shows that the conductance is inversely proportional to the pressure of the vapour and also to the square root of the molecular weight of the gas. The explicit dependence on temperature is $T^{\frac{3}{2}}$, but in equilibrium the vapour pressure is itself a rapidly increasing function of temperature. Fig. 6, curve C, shows a plot of U_v against $1/p_1$, for air and mercury vapour, calculated from equation (9).

In Fig. 2 a comparison is made between the theoretical conductance of a long empty pipe, and the conductance of a column of vapour of the same diameter. Curves A and B are the calculated conductances for air in a column of mercury vapour at pressures of 10^{-2} mb (44° C) and 10^{-3} mb (15·5° C) as a function of diameter. Curve C gives the conductance of an empty pipe of circular section, at 20° C.

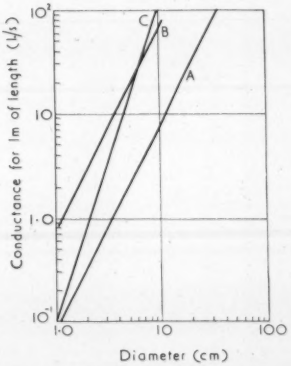

Fig. 2. Conductance plotted against diameter

Curve A, column of mercury vapour at 10^{-2} mb (44° C); curve B, column of mercury vapour at 10^{-3} mb (15½° C); curve C, long pipe, circular section (20° C).

It may be seen that for diameters exceeding a certain value the conductance of the vapour (which is proportional to the square of the diameter) becomes less than the conductance of the pipe containing it (which is proportional to the cube of the diameter). At this point the vapour becomes the more important factor in limiting the flow of gas through the pipe.

If D cm is the diameter for which the conductance of mercury vapour alone is equal to the conductance of pipe alone (for air), then $D = (6{\cdot}7 \times 10^{-3})/p_1$, where p_1 mb is the pressure of mercury vapour. This is deduced from equation (9), assuming that the temperature is constant at 20° C. It should be remembered that the pressure of air is assumed to be small compared with the pressure of vapour.

The pipe length is, of course, assumed to be great compared with (i) its diameter, and (ii) the mean free path of the gas molecules in the vapour, so that these make very many

collisions during their passage through the vapour. This should particularly be borne in mind for the lower pressures of vapour.

EXPERIMENTAL DETERMINATION

The experiment was not designed to provide an accurate verification of the theory given above, but simply to answer the following questions.

(*a*) Does a stationary barrage of vapour possess an appreciable impedance to the flow of gas?
(*b*) Is this impedance of the same order of magnitude as that calculated from equation (8) above, and does it vary as predicted by that equation?

The apparatus (Fig. 3) consisted of a long glass tube, surrounded by three separate jackets, through which water could be passed at various temperatures. A trapped 3½ in. mercury pump was attached at one end, and a measured

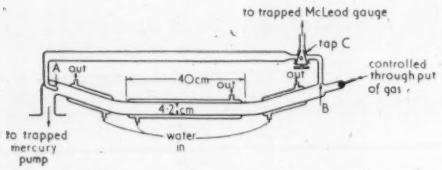

Fig. 3. Experimental arrangement for measurement of the conductance of a column of mercury vapour at various pressures

throughput of gas, Q l. mbs^{-1}, was introduced at the other. By means of the tap C, the trapped McLeod gauge could be connected to the vacuum at either A or B, reading the pressures p_a and p_b mb. The conductance of the tube between A and B was given by

$$U_t = Q/(p_b - p_a) \text{ (l./s)}$$

The value of U_t was measured for various throughputs, with the centre section first at 14° C, and then at 60° C. The end jackets were both kept at 14° C throughput. As expected, only a small variation with temperature was found.

Mercury was now poured into the tube—enough to occupy the length of the centre section. Thus the apparatus contained mercury vapour at a pressure roughly equal to the vapour pressure at the temperature of the apparatus. The pressures, p'_a and p'_b at A and B, were measured as before, for a series of known throughputs Q'.

The conductance of the tube plus vapour is given by

$$U = Q'/(p'_b - p'_a) \text{ (l./s)}$$

If we make the assumption that the impedance of the tube containing vapour is equal to the sum of the impedance of the tube alone and the impedance of the vapour alone, we obtain a relation between the reciprocals of the conductances.

$$1/U_v = (1/U) - (1/U_t)$$

The values of U_v derived in this way are apparent conductances of the vapour.

An allowance was made for the fact that the liquid mercury reduced the conductance of the tube by about 8%, simply owing to its obstructing part of the cross-sectional area. This was small compared with the expected reductions due to vapour impedance.

These measurements of U_v were made with the mercury maintained at each of six temperatures from 14 to 60° C, by controlling the temperature of the water circulating in the centre jacket. The two end jackets were kept cold (about 14° C), in order to reduce the amount of mercury vapour flowing up the cool tubes leading to the McLeod gauge, and thus to avoid any pumping action towards the gauge, which, if appreciable, would have been undesirable.

For each of six pressures of mercury vapour, therefore, the conductance of vapour alone U_v was estimated—in each case for a number of different values of throughput Q' both for air and for hydrogen. It was assumed that the pressure of vapour in the centre section of the tube was equal to the vapour pressure of mercury at the temperature of the apparatus. This was obviously only approximately so, as condensation in the cold ends would cause some reduction in pressure. However, the accuracy aimed at did not justify attempts at complicated corrections.

Fig. 4 is a plot of U_v against Q' (for air), for each of six pressures of vapour between $9{\cdot}2 \times 10^{-4}$ and $3{\cdot}2 \times 10^{-2}$ mb. For comparison, the conductance of the tube alone U_t is also plotted (as dotted line T).

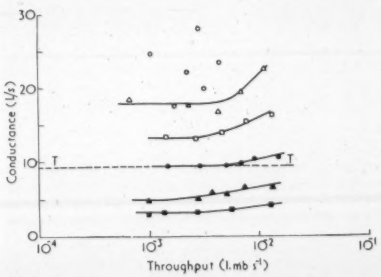

Fig. 4. Conductance of mercury vapour column (for air)

○ = 14½° C ($9{\cdot}2 \times 10^{-4}$ mb); △ = 22° C ($1{\cdot}75 \times 10^{-3}$ mb);
□ = 30° C ($3{\cdot}4 \times 10^{-3}$ mb); ● = 40° C ($7{\cdot}4 \times 10^{-3}$ mb);
▲ = 50° C ($1{\cdot}6 \times 10^{-2}$ mb); ■ = 60° C ($3{\cdot}2 \times 10^{-2}$ mb).

These values of U_v should only be taken as giving the order of magnitude of the conductance of the vapour. Their *relative* values, however, are more significant, though even here the accuracy is limited. This is because there was a tendency for the measured values to increase very slowly with time. For example, if the readings made first were repeated at the end of the experiments, they were found to have increased by up to 50%. This was thought to be due to the increasing film of condensed mercury droplets on the cold end walls of the tube. Mercury vapour condenses more efficiently on a mercury surface than it does on glass, so that as the area of condensed droplets increases, the mercury vapour in the centre section of the tube would condense more rapidly in the cooled ends. The pressure produced by equilibrium between the rate of evaporation of mercury from the warm surface, and the rate of condensation at the ends, would therefore be reduced, so increasing the conductance of the vapour. This seems a likely explanation, because after these deposits of mercury had been cleaned out, the readings returned to their early lower values.

Fig. 4 shows that for any pressure of vapour, U_v is fairly constant for the lower throughputs of air. It tends to increase at higher throughputs—possibly because the air then tends to "sweep" the vapour along with it.

Fig. 5 gives similar curves for hydrogen. The behaviour here is much the same, though the accuracy is less—owing

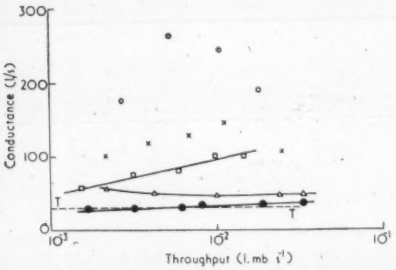

Fig. 5. Conductance of mercury vapour column (for hydrogen)

○ = 22° C ($1{\cdot}75 \times 10^{-3}$ mb); × = 30° C ($3{\cdot}4 \times 10^{-3}$ mb); □ = 40° C ($7{\cdot}4 \times 10^{-3}$ mb); △ = 50° C ($1{\cdot}6 \times 10^{-2}$ mb); • = 60° C ($3{\cdot}2 \times 10^{-2}$ mb).

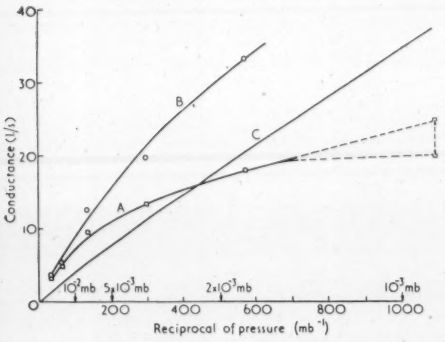

Fig. 6. Conductance of mercury vapour column (for air)

to the expected higher conductances for the light gas. In Fig. 6, curve *A*, the values of U_v for low throughputs of air are plotted against $1/p_1$ (where p_1 mb is the pressure of vapour). Curve *B* gives values of U_v, corrected by subtracting the estimated impedance of mercury vapour in the cold ends of the tube. For comparison, the conductance of vapour predicted from equation (8) is also plotted (curve *C*).

It can be seen that:

(*a*) the experimental values for U_v are of the same order of magnitude as the predicted values (usually within a factor of two);

(*b*) they lie on a smooth curve, and at higher pressures where the accuracy is best, there is a rough proportionality between U_v and $1/p_1$. At lower pressures the conductances are lower than the values predicted by extending the "proportional" part of the curve. This is no doubt because at these lower pressures the impedance of the vapour in the cold ends of the tube is a bigger fraction of that in the main tube. Curve *B* which gives values of U_v corrected for this effect is more nearly linear throughout.

For the reasons given above, it is not possible to obtain a direct comparison from Figs. 4 and 5, between the conductances of the vapour for air and hydrogen, as the two series of measurements were made at widely separate times. However, in order to obtain such a comparison, three measurements with air were immediately followed by three with hydrogen, the vapour temperature being kept constant at 50° C (pressure approximately $1{\cdot}6 \times 10^{-2}$ mb). The mean value for U_v for air was 5·9 l./s, and for hydrogen was 46·8 l./s. The ratio was therefore 7·9—compared with 4·73 predicted from equations (9) and (10).

The shape and size of the apparatus used was a compromise between the requirements explained below and those of manufacture. The diameter and length of the vapour column are *D* and *L*.

(*a*) The sensitivity of the method is increased if U_v/U_t is as small as possible. As $U_v \propto D^2$ and $U_t \propto D^3$, therefore $U_v/U_t \propto 1/D$, i.e. the accuracy is better for greater diameters.

(*b*) The sensitivity is improved if the pressure drop across the vapour is as large as possible compared with the pressure at *A*; therefore U_v should be small compared with the pumping speed at *A*. Therefore the diameter of the pump should be at least as great as *D*, and L/D should be as great as possible.

(*c*) The pressure of mercury vapour is determined by a balance between the rates of evaporation from the mercury surface and of condensation in the cold end tubes. To ensure that the pressure is not much less than the vapour pressure of mercury at the temperature of the apparatus, the surface area of mercury should be as great as possible compared with the cross-section of the tube.

CONCLUSION

The experimentally determined values of apparent conductance of a mercury vapour column to air and hydrogen were within a factor of two of the values deduced from equation (8), over a range of vapour pressures from 10^{-3} to 3×10^{-2} mb.

From this equation it follows that the conductance of the vapour can be much less than that of the pipe which contains it, and in such cases it is the more important factor in determining the overall conductance. This becomes increasingly probable as the pipe diameter and the vapour pressure are increased.

ACKNOWLEDGEMENTS

The author is indebted to the Admiralty for permission to publish this paper, and to Mr. J. Pollard for much helpful comment.

REFERENCES

(1) JEANS, J. *The Kinetic Theory of Gases*, 1st ed., p. 209 (Cambridge: The University Press, 1940).

(2) LOEB, L. B. *The Kinetic Theory of Gases*, 2nd ed., p. 267 (New York: The McGraw-Hill Book Co. Inc., 1934).

New books

Frequency modulation engineering. By C. E. TIBBS and G. G. JOHNSTONE. (London: Chapman and Hall, Ltd.). Pp. xii + 435. Price 45*s*.

The application of frequency modulation to radio transmission is literally as old as the use of continuous waves for telegraphic purposes. But in recent years the main interest in the technique of frequency modulation has been in its exploitation in the fields of broadcasting and communication at very high frequencies. When the first edition of this book was written by C. E. Tibbs in 1947, the subject of the relative merits of amplitude and frequency modulation was one of great controversy in technical circles. The intervening nine years have greatly clarified the position, and the fact that the British Broadcasting Corporation have already brought into operation the first group of a nation-wide network of broadcasting stations operating at carrier frequencies within the v.h.f. band of 87·5–100 Mc/s using the frequency modulation principle has greatly stimulated interest in the subject.

The publication of the book now under review is therefore very timely; it constitutes a major revision and expansion carried out by the second author, who is a member of the B.B.C. Engineering Training Department. After a chapter describing the principles of the frequency modulation of a carrier wave and the nature of the resulting sidebands, two chapters are devoted to the structure of electrical noise and its effect as a source of interference. Since the modern application of frequency modulation is to the transmission of carrier wave frequencies above 30 Mc/s, it is most useful to find that the authors have devoted two chapters to the propagation of v.h.f. waves and to the aerial systems with which they are used. These chapters are important in enabling the engineer to understand how distortion of the audio-frequency signals can arise due to wave reflection effects and —more important—to draw his attention to the care necessary in the design of receivers, with their limiters and discriminators, which form the subject of later chapters. A separate chapter on frequency modulation transmitters both explains the principles of these and gives engineering details of typical installations in use in this country and America. A brief outline of the special measuring techniques used in the practice of frequency modulation is noteworthy in that nearly all the illustrations, and all but one of the references at the end of the chapter, are taken from publications in the United States. This feature is probably not quite fair to the British radio industry to-day.

For those who are engaged in the study, development or exploitation of high fidelity broadcasting using the frequency modulation technique, this book can be recommended as an excellent guide to all the engineering aspects of the subject; and it will also be found most instructive to others who are interested in the corresponding techniques used for communications, radar and navigational aids at very high radio frequencies.

R. L. SMITH-ROSE

Solid state physics. Vol. 2. Advances in research and application. Edited by F. SEITZ and D. TURNBULL. (New York: Academic Press Inc., 1956.) Pp. xii + 468. Price $10.00.

Readers will be grateful to the authors of the five articles in this second volume of the series for preparing such thoroughly comprehensive reviews of their subjects. Each article could have made a useful monograph in itself, published separately. The first one, on "Nuclear magnetic resonance," by G. E. Pake, surveys the whole subject of nuclear spin effects in solid state physics at an advanced level. The basic quantum-mechanical theory of the interactions between the nuclear spins, the applied fields, and the lattice, and of the various broadening and line shift effects, is described, and an account is given of experimental methods and of the main results obtained so far. It is followed by an article by W. D. Knight on "Electron paramagnetism and nuclear magnetic resonance in metals." As would be expected from its author, this deals particularly and authoritatively with the shift in the nuclear resonance line produced by a paramagnetic electronic field near the nucleus; it will be especially valuable to those interested in using nuclear resonance to study the electronic structure of alloys. The third article, "Applications of neutron diffraction to solid state problems," by C. G. Shull and E. O. Wollan, describes the beautiful experimental work by neutron crystallographers on the location of hydrogen atoms in crystals, on ferroelectric structures, and on magnetic superstructures in compounds. Inelastic scattering and ferromagnetic scattering are briefly mentioned, and the general outlook in the article is similar to that in G. E. Bacon's recent book. Following this is an article entitled "The theory of specific heats and lattice vibrations," by Jules de Launay. This is the only "pre-nuclear" branch of solid state physics discussed in the present volume and, appropriately, the author develops his account from the historical standpoint, starting with the Dulong–Petit law and the theories of Einstein and Debye. The treatment is at a fairly elementary level and builds up gradually, through the theory of lattice vibrations and elastic waves, to the more recent treatments of two- and three-dimensional lattices. The final article, on "Displacement of atoms during irradiation," by Frederick Seitz and J .S. Koehler, deals comprehensively with the physical aspects of "knock-on" damage in crystals by heavy-particle irradiation. Similar in outlook to the recent article by Kinchin and Pease (*Rep. Progr. Phys.*, 1955), it explains in detail the basic theory of collision effects in solids and compares critically the estimated damage with that deduced from experiment. Much previously unpublished work is described and the authors have not hesitated to advance new opinions in some of the more controversial aspects of the subject; for example, in reference to the effect of displacement spikes, and in the interpretation of the annealing ranges in irradiated metals and alloys. The first part of the article will undoubtedly be valued as an exposition of the basic collision theory; the second as a starting point for planning new experiments.

These articles fully maintain the high standard set in the first volume. The experimental physicist will in general have to work hard to digest all that is in them, but will be amply rewarded by the things that he will so learn about the solid state.

A. H. COTTRELL

Irradiation colours and luminescence. By K. PRZIBRAM. (London: Pergamon Press Ltd., 1956.) Pp. xiv + 332. Price 63*s*.

The first edition of this book appeared in the German language and was published in Vienna in 1953. Since then the text has

been revised and the present edition has been translated into English by Dr. Caffyn of the University of Durham. The text deals with the phenomena of coloration by high energy radiation and the luminescence of crystals with special emphasis on natural minerals. In Part 1 a brief résumé of experimental techniques for coloration of crystals and for measurement of coloration and luminescence is given together with a chapter on coloration in synthetic alkali halides and chapters on the theoretical aspects of coloration and luminescence. The approach to experimental techniques is perhaps a little uncritical in places and the section on luminescence does not give an up-to-date perspective of such topics as phosphor constitution and mechanisms of energy storage. However, the first part may be of value to the mineralogist who does not have to be so concerned with fundamental processes or with the highly specialized techniques by which they are investigated. Part 2 of the text is concerned with natural minerals but detailed interest is centred on rock salt and on fluorite, both of which have received considerable attention in Professor Przibram's school in Vienna. The various chapters provide in the main a collection of descriptive observations on minerals, though in the chapter on rock salt there is an interesting discussion on the relation between the type of coloration and the growth characteristics of the crystals. In the case of fluorites the plethora of recorded observations is best indicated by the opening statement of the chapter concerned: "Probably no other mineral shows such an abundance of different hues and such brilliant luminescence phenomena as the fluorites." Current experiments in this country on synthetic fluorites with controlled impurity and defect contents may help to unravel the mass of data collected for crystals of natural origin.

The references in the text are copious and are well arranged in the indices, which include author and subject sections. I am sure that the mineralogists will be grateful for the encyclopaedic collection of data which the author has brought together in this book which gives so compactly the results of a lifetime of interest in this field. It will also form a useful, though expensive, reference source to those of us with a more fundamental interest in the phenomena it describes.

G. F. J. GARLICK

Spheroidal wave functions. By J. A. STRATTON, P. M. MORSE, L. J. CHU, J. D. C. LITTLE and F. J. CORBATO. (London: Chapman and Hall Ltd.; New York: John Wiley and Sons Inc., 1956.) Pp. xiii + 613. Price £5.

This book is really a second edition of an earlier book[1] with the tabular material greatly expanded.

If the scalar-wave equation is separated in spheroidal co-ordinates ξ, η, ϕ, the solution can be written in the form $je_{ml}(h, \xi)S_{ml}(h, \eta)\cos m\phi$, in the prolate case, and $je_{ml}(ih, -i\xi)S_{ml}(ih, \eta)\cos m\phi$, in the oblate case, where $w(z) \equiv je_{ml}(h, z)$ or $S_{ml}(h, z)$ satisfies the spheroidal wave equation

$$\frac{d}{dz}\left[(z^2-1)\frac{dw}{dz}\right] - \left(A - h^2z^2 + \frac{m^2}{z^2-1}\right)w = 0. \quad (1)$$

In this equation A, h and m (an integer) are parameters, the first of which is, in consequence of the boundary conditions, one of an infinite set of eigenvalues $A = A_{ml}(h)$ $(l = m, m+1, \ldots)$.

The solutions of equations (1) are thus functions of four variables, and their complete tabulation would occupy a prohibitive amount of space. One way of overcoming this difficulty would be to prepare comprehensive programmes for an automatic computer which would evaluate the solutions in any region of interest. Another way is to prepare a skeleton set of tables from which the required solutions can be calculated with a little effort. Nine-tenths of the present book is devoted to such tables.

The actual quantities tabulated are a_n and d_n, the coefficients in the expansions

$$je_{ml}(h, \xi) = \left(\frac{\xi^2-1}{\xi^2}\right)^{m/2} \sum_n a_n j_{n+m}(h\xi),$$

$$S_{ml}(h, \eta) = \sum_n d_n P^m_{m+n}(\eta),$$

in the prolate case, and in similar expansions in the oblate case. Here $j_n(z)$, $P^m_n(z)$ denote respectively the spherical Bessel function and the associated Legendre function. Also tabulated is a quantity t from which the separation constant A can be computed. The ranges covered are $m = 0(1)8$, $l = m(1)8$, $h = 0(0{\cdot}1)1(0{\cdot}2)8$. No special provision is made for interpolation in the h-direction. Entries in the table are all given to seven significant figures, and expressed in floating point form $0{\cdot}19061091 - 06 \equiv 0{\cdot}1906109 \times 10^{-6}$. The summation variable n extends until the last term is negligible; fourteen terms are necessary in the worst cases.

In the first sixty pages a comprehensive account is given of the principal mathematical properties of spheroidal wave functions, which includes various expansions, relations between solutions and the relation to Mathieu functions. It is mostly a straight reprint of a paper by Stratton and Chu,[2] and appeared also in the earlier book; a few known misprints, e.g. in equation (310), have not been corrected. In this connexion mention must be made of Chapter 16 of the recently published Bateman Memorial Volumes[3] which gives a detailed survey of the existing theory of spheroidal wave functions.

One of the difficulties in the theory is the variety of notations in current use. It is the hope of the present authors that the publication of their tables, which are easily the largest and most comprehensive in existence, will help to standardize the notation. This observation would have greater weight if the same notation had been used for the Introduction as for the tables.

Spheroidal wave functions will be of value to workers in many branches of physics, including acoustics, electromagnetic theory and quantum mechanics, in problems involving, for example, the radiation and scattering of waves by wires, strips and disks, and similarly in the study of diffraction through slits and circular apertures. The book is very clearly printed, and considering the amount of information it contains, the price is not unreasonable.

F. W. J. OLVER

REFERENCES

(1) STRATTON, J. A., MORSE, P. M., CHU, L. J., and HUTNER, R. A. *Elliptic cylinder and spheroidal wave functions.* (London: Chapman and Hall, Ltd., 1941.)

(2) STRATTON, J. A., and CHU, L. J. *J. Math. Phys.*, **20**, p. 259–309 (1941).

(3) ERDÉLYI, A., MAGNUS, W., OBERHETTINGER, F., and TRICOMI, F. G. *Higher transcendental functions.* Vol. 3. (London: McGraw-Hill Publishing Co. Ltd., 1955.)

Astronomical optics and related subjects. Edited by ZDENEK KOPAL. (Amsterdam: North-Holland Publishing Co.). Pp. xv + 428. Price 90*s*.

This book contains practically all of the contributions given at a Symposium on astronomical optics held at the University of Manchester during the period 19–22 April, 1955. The Symposium itself was organized by the Editor of the present volume, Professor Z. Kopal, together with Dr. W. L. Wilcock and Dr. E. Wolf. The topics included in the Symposium cover a very wide range—in many cases they appear to be much more "related" than "astronomical." This is so much the case that almost every worker in optics will find things of interest in this volume. The sessions of the Symposium were held under the following headings: Information theory and optics; Optical images and diffraction; Interferometry and coherence problems; Electronic devices in astronomical optics; Resolution problems and scintillation; Wide-angle systems and aspheric surfaces; Filter photography, and thin films. The contents of the papers given under the earlier headings underline the growing importance of Fourier methods in optics, both in relation to diffraction and coherence problems, and the utility of correlation functions. In the remaining sections the main emphasis is on the use of photoelectronic techniques, including photometry and television, and the use of filters, both of the absorption and interference types, in astronomical photography. It is regrettable that so little space is devoted to new telescope and camera systems for astronomy. Equally regrettable is the almost complete absence of mention of the optical techniques in radio-astronomy, for example telescopes, interferometers and the techniques used in meteor tracking. The inclusion of these topics would have resulted in a much longer Symposium and a correspondingly larger report, and this may have been the reason for excluding them.

Finally, one should not omit one's congratulations to the organizers of this Symposium for bringing together a collection of useful papers, and to the publishers for maintaining their usual good standards. It is a pity that this has had to be achieved at the expense of a price which will put this volume out of the reach of most individual workers in the field.

H. H. HOPKINS

Static and dynamic electron optics. By P. A. STURROCK. (London: Cambridge University Press, 1955.) Pp. x + 240. Price 30*s*.

Among the many treatises on electron optics this is a book apart. It bears on every page the imprint of the author's hand, who is a manipulative mathematician of rare fluency, with a strong penchant for elegance, order and conciseness. Without conciseness it would have been impossible to collect such a vast material between the covers of a small-octavo book of only 240 pages, but many a reader might wish that another 100 pages or so could have been added for explaining the results in terms more familiar to the average physicist.

Within the given limitations of space, the author has done extremely well in covering not only ordinary "static" electron optics, in a wider frame than usual, and from a higher point of view, but also "dynamic electron optics," that is to say the theory of particle accelerators. This last third of the book is probably its most important and original part, and fills a real gap in textbook literature.

The salient feature of this work is the systematic use of variational principles with Lagrangians (which the author regrettably calls "variational functions"), expanded in series of perturbation characteristics of progressive order. Almost every result is obtained by this powerful method, often by admirably short cuts, and many of these results are the author's own. The deductive process naturally starts from the top of the pyramid, and descends towards the basis. It brings with it, unavoidably, a didactical difficulty. A. and L. Föppl, who deduced the whole of elasticity theory in a similar way from Castiglione's Principle illustrated it by saying that one starts with a million-pound note, which has to be converted gradually into smaller change. The average reader will not understand much of it until the author has arrived at the small change to which he is used. Indeed, only few physicists, with a very mathematical turn of mind can be expected to learn any chapter of physics by a descent from the top of a pyramid. For the others it will be necessary to read Sturrock's chapters first forward, then backwards, and finally forward again. In the end most of them will learn that the repeated journey was not only necessary, but the best way to prepare them for original work.

Other features which make the reading rather difficult are the somewhat unorthodox notations, such as e.g. the "ray equation" (2.2.10), $d\boldsymbol{p}/ds = \delta n/\delta \boldsymbol{x}$. This is admirably concise, but the reader might be excused if he does not know what is meant by division by a vector. The unorthodox definitions are scattered over the pages and physical concepts are too often referred to by their symbol instead of by name. Clarendon does not always mean a vector in the book, $\boldsymbol{p}$ stands for the vector momentum as well as for the scalar value of the momentum on the axis. But in most cases the reader will have to admit that Dr. Sturrock's notations, as well as his units, are more logical and practical than those in common usage.

This book will be indispensable to all those who want to do original work in electron optics or on particle accelerators, and it must be seriously recommended to all mathematically minded physicists who have acquired an elementary knowledge of electron optics, and want an introduction to its higher flights.

D. GABOR

High speed aerodynamics and jet propulsion. Vol. 2. Combustion processes. (Princeton: Princeton University Press; London: Oxford University Press, 1956.) Pp. xv + 662. Price 84*s*.

The book consists of a series of reviews by leading American experts of the more fundamental knowledge of theory and experiment on various aspects of combustion connected with gas turbines, rockets and ram jets. The title combustion is taken in the widest sense to include nuclear reactors in the same sense that the maximum elements of a pile are called fuel elements. Thus the last chapter gives a very brief survey of the principles of nuclear heat liberation by the fission and fusion processes without, however, relating these in any way to the practical problem of using the heat.

The first three chapters deal with the thermodynamics of combustion—the theory and approximate calculation of reaction equilibria and flame temperatures, and the thermodynamic equations for fast flowing gases with heat release. Methods of calculation are given but no results or practical applications. Then follow two chapters on chemical kinetics giving a full account of the theory of activation energy, chain reactions and surface adsorptions with a sprinkling of examples of combustion reactions on the low temperature side (i.e. below 1000° C) where chemical kinetics are important and a section summarising the laboratory techniques available. The first of these chapters by H. S. Taylor can be recommended as a clear account suitable to teach the

physical chemistry to physicists. R. N. Pease deals particularly with the reactions of hydrogen, carbon monoxide, paraffins and boron hydrides with oxygen, and that of hydrogen with fluorine.

The third part of the book follows the logical sequence and deals with flame propagation in gases, the first chapter giving the differential equations for continuity and transport, the second being a condensed version of the chapter in Lewis's and von Elbes's book on the theory of combustion waves based on the concept of excess enthalpy although mentioning rival concepts, the laboratory experimental results being covered in a separate section. Combustion waves in turbulent gases are dealt with by Karlovitz in a chapter which is largely a series of summaries of different experimenters results but which cannot yet be digested into a coherent story, although they emphasize the generation of turbulence by the flame itself. Linear and turbulent diffusion flames are dealt with in the next chapter on the assumption that it is the physical mixing which governs the reaction rate.

Part four deals with liquid and solid fuels, Longwell dealing with atomization (without taking sufficient account of recent British work in this field) fuel spray mixing and evaporation and Spaldings's droplet combustion theory. Solid fuel is covered primarily from the point of view of the total combustion time of individual pulverized fuel particles. The two chapters on liquid and solid rocket propellants are of a directly practical character. Part five covers the theory of detonation processes.

Generally speaking the book emphasizes the large gap which exists between laboratory experiments and theory on the one hand and the practical problems of the combustion engineer on the other. There is no account of practical combustion aerodynamics nor an adequate theory of recirculation stabilized flames. M. W. THRING

Vacuum deposition of thin films. By L. Holland. (London: Chapman and Hall Ltd., 1956.) Pp. xix + 541. Price 70*s*.

Although the art of vacuum deposition is no longer in its infancy there was until recently no comprehensive textbook available to smooth the path of the newcomer to the subject, and to act as a source book to the initiated. Mr. Holland has performed a task of considerable proportions in synthesizing from the plethora of published papers and his own extensive experience an easily digestible and relatively compact book.

The author remarks in his preface that "It was obviously impossible to deal in detail with all the numerous applications of thin films, and the main subject matter has been planned to cover plant design, film production and the physical properties of thin films. . . ."

The construction and characteristics of demountable vacuum plants are set forth, including details of recent developments such as the booster diffusion and gas ballast rotary pumps. Descriptions are given of the associated apparatus evolved for numerous specialized applications such as the production of multilayer films, the metallizing of long rolls of "gassy" material, the deposition of electrodes on to crystal vibrators and shadow casting. The design of vapour sources and their emission characteristics is dealt with at length, as is the coating of plastics.

Evaporation techniques are described for the deposition of a comprehensive range of metals, both elements and alloys, and of dielectrics. The properties of the resultant films are considered, those of aluminium being treated in great detail. Of late years there has been a revival of interest in cathodic sputtering, and a full account is given of recent advances in technique and of new applications in this field. The final chapter is allotted to "The preparation and properties of a range of oxide films": the author does not confine himself here to films produced only by vacuum deposition.

The allocation of only one chapter to the growth, structure and physical properties of thin films is a fair reflexion of our very imperfect understanding of the fundamentals of the process.

The volume is well produced with a great many clear diagrams, useful tables and some interesting plates. In a compilation of this sort the index is of great importance and happily the indexing is of better than average quality. There is both a subject and an author index, the latter referring both to the pagination and to the adjoining list of 557 references. The arrangement of the chapters, however, is not satisfactory. For instance, the subject matter of Chapter 2, "The degassing of plastic materials *in vacuo*," should surely be adjacent to that of Chapter 12, "Evaporated coatings on plastic materials and lacquered components." This does not, of course, seriously detract from the value of the book, well-worn copies of which will be found in every deposition laboratory for years to come. J. E. KNOWLES

Steric effects in organic chemistry. Edited by Melvin S. NEWMAN. (New York: J. Wiley and Sons, Inc.) (London: Chapman and Hall Ltd.) Pp. vi + 710. Price 100*s*.

The earlier successful elucidation of polar effects (i.e. electron displacements in molecules which originate from the electronic structures of the groups present) on reaction rates and equilibria has, latterly, been followed by more detailed examination of, and possible over-emphasis on, steric factors (i.e. those dependent upon the spatial interaction between non-bonded atoms or groups). This comprehensive series of authoritative articles, concerned especially with aspects of the subject not previously covered in review articles, and well documented with more than 1600 up-to-date references (including 1955) to original publications, is therefore timely and valuable. The treatment is advanced and is directed mainly to the organic chemist familiar with modern electronic theories of structure and mechanism. The first ten chapters deal first with conformational analysis (i.e. the relative orientations of single bonds in open-chain and cyclic compounds), and then with steric effects in substitution, elimination and addition reactions, in rearrangements, equilibria and in molecular complexes and organometallic compounds. The remaining chapters, which are of more direct interest to the physicist, discuss steric effects on physical properties, calculation of the magnitude of steric effects and finally, in a most thought-provoking essay, the separation and quantitative evaluation of polar, steric and resonance effects in reactivity.

Concentration on steric effects occasionally causes insufficient cognisance to be taken of other relevant factors or of differentiation between various reaction mechanisms, each with its own specific steric requirements. It was surprising to find (p. 255) the conformations of *iso*bornyl and bornyl chlorides reversed, but the few errors detected do not detract appreciably from the valuable and stimulating character of the book. It well achieves its avowed aim which is "to enable the reader to interpret for himself reactions and phenomena involving a wide range of steric effects," and it can be highly recommended to all interested in structure and mechanism in organic chemistry. J. W. BAKER

Notes and comments

Elections to The Institute of Physics

The following elections have been made by the Board of The Institute of Physics:

Fellows: E. Atherton, A. Barker, E. George, R. L. Gordon, H. A. Hughes, S. E. Hunt, P. L. Kirby, C. Mack, R. Parker, H. V. Pilling, V. Robert, H. W. B. Skinner, E. G. Stanford, S. Thornton, B. M. Wheatley.

Associates: C. Ambasankaran, D. Aston, A. C. Baker, W. A. D. Baker, R. A. Bembridge, N. F. Blackburne, W. E. Boud, J. D. H. Bradley, M. Bridger, J. Bunton, G. H. Byford, J. A. Champion, J. Chayen, C. A. Cochrane, W. E. Craker, H. M. Dean, J. A. Dennis, R. Diamond, E. Dyson, R. Elam, J. Ellis, W. G. Ferrier, L. Finkelstein, D. F. Fyfe, B. E. Godfrey, B. J. Gumm, A. M. Hardie, J. Houghton, T. P. Hughes, T. F. B. Jaggar, J. K. Jones, P. G. Lea, Y. K. Lim, J. Luff, D. E. Macdonald, R. C. McVickers, I. G. Matthews, A. D. Maude, F. R. Morgan, J. A. Morgan, J. Nightingale, F. J. Pearson, J. Potts, J. A. Reynolds, J. Richards, A. Rimmer, S. F. Robinson, J. B. Rowcroft, C. Rubenstein, C. M. H. Smith, L. N. Snell, G. M. Somerville, D. G. Strahle, A. W. Stirling, J. G. Tapley, A. R. Thomas, P. M. Tipple, P. W. Turner, J. Varma, S. M. Y. Wafaquani, J. Wardley, H. Whitehouse, P. W. Wright, B. Yates, K. W. Young.

Seventy-four Graduates, sixty-six Students and five Subscribers were also elected.

Combustion and flame

We welcome a new scientific Journal which appears under the title *Combustion and Flame*. The Journal, which is to be published quarterly, is specially adapted for the publication of scientific papers in the field of combustion and flame and it will be issued on an international basis. The first issue contains 128 pages and the papers which appear are entitled: Stability limits of flames of ternary hydrocarbon mixtures; Ignition of dust layers on a hot surface; A photoelectric study of the light emission from carbon monoxide-oxygen thermal explosions; The slow oxidation of methane; Some properties of formaldehyde flames; Burning velocities of hydrogen cyanide in air and in oxygen; The explosibility characteristics of coal dust clouds using electric spark ignition; Self combustion of acetylene III; A cool flame phenomenon in the combustion of acetylene; Flame zone studies III.

The Journal, the first issue of which appeared in March, is edited by Dr. Bernard Lewis and Professor A. R. Ubbelohde. It is published for the Combustion Institute by Butterworth's Scientific Publications, 4–5 Bell Yard, Temple Bar, London, W.C.2. It is distributed in the U.S.A. by Interscience Publishers Inc., New York. The annual subscription is £5 5*s.* 0*d.*

British Standards Institution Yearbook, 1597

The Yearbook of the British Standards Institution has just been published. As usual, 400 pages of this 480 page publication are devoted to a complete numerical list of the British Standards and Codes of Practice current on the 1 January, 1957. These total approximately 3000.

Apart from its main purpose as a reference directory to all current British Standards, the Yearbook contains other information about B.S.I. and the services it offers, including notes on the British Standards mark of approval (the Kite) and the standards to which it is applied. Other information covers lists of addresses in the United Kingdom and overseas, where complete reference sets of all British Standards can be consulted, while the Yearbook also contains a comprehensive index in which all standards are listed according to subject.

Copies of *B.S.I.'s Yearbook*, which is an invaluable reference work to users of British Standards, have been sent free to all the Institution's subscribing membership, who may purchase additional copies at the published price of 15*s.* less members' discount. Non-members of the Institution may buy at the published price plus 1*s.* 6*d.* for postage and packing.

Erratum

On page 8 of the January issue of this *Journal*, the first line of the penultimate paragraph of the conference report entitled: Summarized proceedings of a conference on the electron microscopy of fibres, should read: Dr. P. Kassenbeck of l'Institut Textile de France . . .

Journal of Scientific Instruments

Contents of the May issue

ORIGINAL CONTRIBUTIONS

Papers

A high speed electronic analogue field mapper. By R. B. Burtt and J. Willis.
An improved automatic fraction collector. By G. F. H. Box and R. B. Bradbury.
An ultra-microtome. By A. L. Sims and T. S. Leeson.
A steady state method for the rapid measurement of the thermal conductivity of rocks. By A. Beck.
The a.c. properties of resistors and potential dividers at power and audio frequencies, and their measurement. By G. H. Rayner and L. H. Ford.
A photoelectric particle counter for use in the sieve range. By T. Beirne and J. M. Hutcheon.
A synthesizer for triangular wave functions. By Dan McLachlan.
Obliquity effects in interference microscopes. By C. F. Bruce and B. S. Thornton.
A fast kicksorter channel. By R. D. Amado and R. Wilson.

Laboratory and workshop notes

A precision electron-beam oscillograph with a spot diameter of a few microns. By M. von Ardenne.
A miniature dry-box for semi-conductor work. By P. R. Rowland and G. W. Whiting.
An automatic constant level device for liquid nitrogen. By D. E. Henshaw.
A simple instrument for the calibration of microscope fine-focus scales. By J. B. A. England.
A thermistor probe. By W. Belfield and R. W. Johnson.

NOTES AND NEWS

Correspondence

A proportional counter tube for X-ray diffraction analysis. From F. H Sumnet and D. P. D. Webb; A. R. B. Skertchly.
A Fourier analogue-computer of the Hägg–Laurent type. From V. Frank.
Comments on the A.S.T.M. Powder Data File. From J. W. Hughes, Isabel E. Lewis and A. J. C. Wilson.

New instruments, materials and tools
Manufacturers' publications
Notes and comments

THIS JOURNAL is produced monthly by The Institute of Physics, in London.

It deals with all branches of applied physics (including theory and technique). All rights reserved. Responsibility for the statements contained herein attaches only to the writers.

EDITORIAL MATTER. Communications concerning editorial matter should be addressed to the Editor, The Institute of Physics, 47 Belgrave Square, London, S.W.1. (*Telephone:* Sloane 9806.) Prospective authors are invited to prepare their scripts in accordance with the *Notes on the preparation of contributions.* (Price 2*s.* 6*d.* including postage.)

REPRODUCTION. The Institute of Physics is a signatory to The Royal Society's Fair Copying Declaration. Details may be obtained upon application from The Royal Society, London, W.1.

ADVERTISEMENTS. Communications concerning advertisements should be addressed to the agents, Messrs. Walter Judd Ltd., 47 Gresham Street, London, E.C.2. (*Telephone:* Monarch 7644.)

CLAIMS FOR MISSING JOURNALS. Claims from regular subscribers to this *Journal* for missing numbers will only be considered if received within 60 days of the date of mailing plus normal outward time of transit and time for lodging the claim. Losses attributable to failure to notify a change of address or to similar omissions will not be considered.

SUBSCRIPTION RATES. A new volume commences each January. The charge is £5 per volume ($14.25 U.S.A.), including index (post paid), payable in advance. Single parts, so far as available, may be purchased at 10*s.* each ($1.50 U.S.A.), post paid, cash with order. Orders should be sent to The Institute of Physics, 47 Belgrave Square, London, S.W.1, or to any bookseller.

SPECIAL ARTICLE

Physics below 1° K*

By E. Mendoza, M.A., Ph.D.,† H. H. Wills Physical Laboratory, University of Bristol

A temperature T can only be called "low" if kT is small compared with some energy level spacing characteristic of the system. On this criterion 1° K is often not a low temperature, and the region below 1° K is one in which many events occur. The adiabatic demagnetization of paramagnetic bodies is the commonest technique for attaining these low temperatures, though other methods also exist. The main limitation on experiments is the small amount of power which can be absorbed by the working substances. At temperatures down to 3×10^{-2}° K, a number of experiments have been performed, not only on the refrigerants but also on other substances. Results from several branches of physics, including solid state and nuclear physics, are briefly presented and discussed. Below 3×10^{-2}° K only the refrigerants have been investigated; the lowest temperature yet reached is about 2×10^{-5}° K.

It is nowadays comparatively easy to carry out experiments with liquid helium at temperatures down to 1° K. The marketing of a commercially manufactured helium liquefier in the U.S.A. and, in this country, the setting up of a service operated by the National Physical Laboratory whereby liquid helium can be bought, have reduced experiments at liquid helium temperatures almost to the level of routine operations. However, a practical limit is imposed on the lowest temperature attainable by pumping on the liquid helium; this is about 1° K.

The temperature region below 1° K therefore remains relatively inaccessible. Special means are needed to reach it, and a certain amount of skill—comparable with that needed a generation ago to produce liquid helium—is still necessary. It is the purpose of this article to review some of the techniques and results in this region, which is still largely unexplored.

It is perhaps necessary to begin by explaining that for many purposes 1° K is not a low temperature. A temperature of 1° K only looks very low, almost indistinguishable from absolute zero, if temperatures are plotted linearly; on a logarithmic scale—which is no more arbitrary than a linear one—or a $1/T$ scale—which is perhaps a better one—1° K is infinitely far from absolute zero.

But there is only one real justification for working below 1° K, and that is that phenomena are still to be found there.

In general, interesting events usually occur when the relative populations of energy levels alter rapidly with temperature; the entropy decreases rapidly with falling temperature and this can have a profound effect, not only on the equilibrium properties but also on the transport properties of the system. It is well known that if energy levels are spaced by a gap ϵ, their relative populations change rapidly at some temperature of the order of T_0 where $kT_0 = \epsilon$; further, a temperature can only be spoken of as "low" in connexion with this system if it is small compared with T_0. It is the common occurrence of level spacings of the order of 10^{-4} eV and less that gives the temperature region below 1° K its special importance.

It is equally well known that an energy level spacing can lead to absorption or emission of radiation of a certain frequency. Thus, spectroscopy in the centimetre or long infra-red regions is intimately bound up with some aspects of work below 1° K, as is the study of hyperfine structures of spectral lines where spacings of similar magnitudes are also involved.

It has happened that a good deal of the research which has so far been carried out below 1° K has concerned magnetic phenomena. This is partly because the interactions in many magnetic systems are of the right order of magnitude, but also to some extent it reflects the fact that the commonest method for reaching the low temperatures is itself a magnetic one, which makes further magnetic measurements easy to carry out. But the scope of experiments has broadened enormously in the past few years and though technical difficulties still prevent many desirable measurements from being made, problems of the most diverse kinds are now being tackled.

ADIABATIC DEMAGNETIZATION OF PARAMAGNETICS

Of the methods for lowering the temperature well below 1° K, the adiabatic demagnetization of paramagnetics, with a twenty-year history behind it, is by far the most highly developed. There are in addition two others—the adiabatic magnetization of a superconductor and the adiabatic dilution of a solution of ^{3}He in ^{4}He. But of these, the first is still being developed while the second has not yet been achieved; they will be briefly described in later sections. Here some of the more important general aspects of the demagnetization process will be described, and then some technical matters.

Most of the refrigerants for low-temperature work above 1° K are low boiling-point liquids; what makes them so useful is their property of maintaining a constant temperature even while heat is continually entering from the warmer surroundings. Some such quality is desirable in refrigerants for use below 1° K. Unfortunately none undergoes a phase change with a latent heat concentrated in a narrow range of temperature; but any refrigerant worthy of consideration must at least have a large specific heat to slow down the effect of stray heating and also to allow other bodies to be cooled by contact. This is true even if the temperature is maintained approximately constant by some cyclic process, and it is even more desirable if (as usually happens) the working substance, having once been cooled, is left to warm up slowly. In this section it will be shown that many paramagnetic salts possess this property and so make good refrigerants.

* Based on a lecture delivered to the London and Home Counties Branch of The Institute of Physics on 17 October, 1956.

† Now at The Physical Laboratories, University of Manchester.

Purely for the sake of illustration a familiar adiabatic process—the adiabatic expansion of a gas—will first be described. Thermodynamically it is analogous to the demagnetization process and the two have some important properties in common. Consider a gas at high pressure contained in a thermally insulated vessel; the pressure is released slowly. At high temperatures when the gas behaves perfectly, it obeys the law $T \propto p^{\gamma-1/\gamma}$, where γ is the ratio of specific heats; but for a large expansion the temperature may fall so far that this no longer applies. Then the process is best represented on an entropy-temperature diagram, Fig. 1(*a*), where the curves refer to one atmosphere pressure

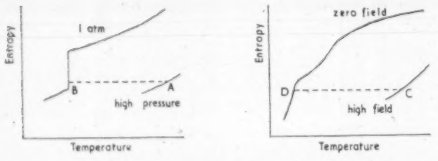

Fig. 1. Entropy-temperature curves

(*a*) For gas which becomes liquid at low temperatures. (*b*) For paramagnetic body.

and a high pressure. The entropy—the disorder—of an assembly of molecules increases with temperature and when the volume through which they can wander increases; thus the trend of the high temperature part of the one-atmosphere curve and the reduction of entropy by pressure are explained. At the boiling point there is a sudden reduction of entropy by an amount L/T (where L is the latent heat, T the boiling point) corresponding to the transition to a state of greater order. The adiabatic expansion to atmospheric pressure is represented by the horizontal line AB and the gas is seen to be partly liquefied. The most important aspect is that the final temperature reached from an expansion from any reasonably large pressure is determined not by the $p - T$ relation of the gas valid at high temperatures but by the boiling point of the gas; that is, by the interaction between the molecules.

The adiabatic demagnetization of a paramagnetic can be described in similar terms. Consider a body consisting of an assembly of ions whose magnetic moments originate in electron spins; it is thermally isolated from its surroundings and is in a strong magnetic field H. At high temperatures the interactions between ions are small and the magnetization is a function of (H/T) only. An entropy-temperature diagram in the field H and in zero field is useful for finding the temperature change on demagnetization. The curves in Fig. 1(*b*) can be understood by noting that the disorder of an assembly of magnetic ions increases with the temperature agitation and with the disorientation from parallel alinement of the magnetic moments of the individual ions; thus, at constant temperature, the entropy of the body is reduced by application of a field. The fall of entropy at low temperatures shown on the curve for zero field can be due to a variety of interactions, some of which will be described in a later section. At high temperatures, that is well above the region of the rapid fall of entropy, the temperature follows an adiabatic change of field according to $T \propto H$; but a demagnetization from a strong field to zero is represented by the horizontal line CD and once again the temperature finally reached is determined by the departure from perfect behaviour.

This magneto-caloric effect of course exists in, say, iron at room temperature. But the cooling effect is very small for a number of reasons. Firstly, any ordinary field is negligible by comparison with the Weiss internal field so that the amount of magnetic entropy which can be removed is very small; further, at room temperature the magnetic entropy is only a small part of the total, which is dominated by the temperature agitation; and lastly, it is essential that all irreversible effects—such as those due to hysteresis and eddy currents—should be absent. Thus magnetic cooling is only important for paramagnetics at low temperatures.

Perhaps, however, the most important feature of the process follows from the relation $C = T(\partial S/\partial T)$ between the specific heat C and entropy S; namely, that in just the temperature region reached by demagnetization from any reasonable field the specific heat is large. (At least, it is large by comparison with non-magnetic salts at comparable temperatures, though the absolute magnitude of the heat capacity per unit volume is very small by comparison with typical room temperature values.) The extraordinary degree of thermal isolation which can be achieved at low temperatures means that it is quite easy to make a specimen stay in the vicinity of its specific heat maximum for several hours after its initial cooling, unless, of course, energy is deliberately fed into it.

There are many substances which are suitable for use below 1° K. It is fairly obvious that they must be magnetically dilute—that is, that the magnetic ions must not be too close together—so as to reduce the temperature where departures from perfect behaviour become important. On the other hand, they must not be too dilute or else the heat capacity per unit volume will be too small. The commonest substances used till recent years have been salts where the magnetic ions are spaced apart by non-magnetic groups and a good deal of water of crystallization—such as the Tutton salt $Mn(NH_4)_2(SO_4)_2 \cdot 6H_2O$, the alum

$$Fe_2(NH_4)_2(SO_4)_4 \cdot 24H_2O$$

or the highly anisotropic rare earth salt

$$Ce_2Mg_3(NO_3)_{12} \cdot 24H_2O.^{(1)}$$

Nowadays substances containing no water are coming into favour, such as ferric acetyl acetonate[2] $(C_5H_7O_2)_3Fe$, ammonium hexafluoro chromite[3] $(NH_4)_3CrF_6$, synthetic ruby[4] which is Al_2O_3 containing some chromic ions and even builders' brick which contains some ferric ions as silicate. These and similar substances have their useful ranges in the region between 5×10^{-3} and 5×10^{-1}° K using fields of the order of 10 kG and starting temperatures near 1° K. It is a remarkable process which can allow a 200-fold reduction of absolute temperature to be achieved in one operation.

TECHNIQUES OF DEMAGNETIZATION

The sequence of operations which has to be carried out in practice is the following. A specimen of the working substance (usually in the form of a "pill" weighing a few grammes formed from compressed powder or cut from a single crystal), inside a calorimeter immersed in liquid helium is cooled to the starting temperature. Then the magnetic field is switched on slowly, the temperature rises and the heat of magnetization has to be removed, which

boils off some liquid helium; in these initial operations there is thermal contact between the specimen and the bath. When the specimen has cooled again to the starting temperature it is thermally isolated from the bath, the field is switched off and the salt demagnetized. The main experimental difficulty is to provide a thermal link between specimen and bath which can be made and broken at will. Mechanical methods, depending on surfaces which can be pressed together, have never been really successful and other means must be used.

Helium gas which can be introduced into the calorimeter at low pressure provides the simplest thermal link. But it is

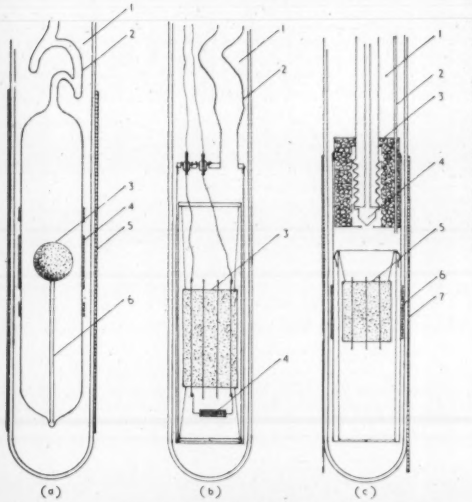

Fig. 2. Demagnetization calorimeters inside liquid helium flasks

(*a*) As used at Leiden and elsewhere for studies on the salts themselves. (1) liquid helium; (2) pumping tube; (3) sphere of salt; (4, 5) coil windings for susceptibility measurement; (6) glass stalk.

(*b*) As used at Bristol for work on metals. (1) liquid helium; (2) glass pumping tube with copper–glass seal to metal calorimeter; (3) pill suspended by threads; (4) radio resistor connected to fins in salt, with two more fins available for cooling other bodies.

(*c*) As used at Kharkov for work on superconductors. (1) liquid helium; (2) narrow tube for introducing exchange gas; (3) container of activated charcoal; (4) nozzle for opening charcoal "pump" to gas; (5) pill suspended by threads; (6, 7) coil windings for susceptibility measurement.

desirable to be able to pump it away again quickly, leaving a good vacuum. The high-speed pumping tube has to have kinks, radiation shields or shutters in it to stop radiation from room temperature shining directly on to the salt, Fig. 2(*a*, *b*). After demagnetization the salt has a strong "gettering" action; the vapour pressure even of the light isotope of helium, ^{3}He, is so low that *in equilibrium* there are very few gas molecules in the calorimeter; the continual desorption of helium from the calorimeter walls therefore causes a heat flow into the salt. To reduce this effect some workers recommend that just before demagnetization, when the salt has already been fairly well isolated, the bath temperature be raised for a short time to bake out the walls at about 2° K. With a well designed calorimeter and with the salt suspended on fine threads or mounted on a stalk of glass of low thermal conductivity, heat flows of the order of 1 erg/s are fairly easy to achieve. To warm a 5 g specimen of chrome alum, for example, from 0·06 to 0·08° K takes about 13 500 ergs, so that this heat leak is acceptable.

Samoilov[5] designed a most ingenious and efficient pumping system consisting of activated charcoal inside a chamber which could communicate with the calorimeter *via* a needle valve, Fig. 2(*c*). Thus the need for a wide pumping tube communicating with room temperature was avoided and the residual heat flow into the salt was very low indeed.

A very interesting and quite different kind of thermal link can be made from a wire which becomes superconducting. Several properties of superconductors will be discussed in a later section—here it is sufficient to mention that a metal in this state (exhibiting zero electrical resistance) can be transformed into the normal (resistive) state by applying a magnetic field of the order of a few hundred gauss; and that the thermal conductivity in the super-conducting state—showing no respect for the Wiedemann–Franz law—is much *lower* than when normal. The measurements for lead are shown in Fig. 3. To make an automatically acting heat switch it is

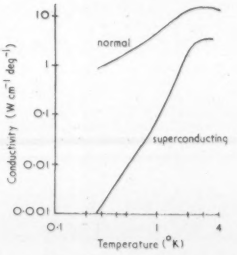

Fig. 3. Thermal conductivity of lead

only necessary to connect the salt to the calorimeter wall through a fine wire of lead; when the magnetizing field is on, the wire becomes normal and conducts the heat away; after demagnetization it becomes superconducting and is a fairly good thermal insulator. A wire 10 cm long and 0·1 mm diameter conducts only about 2 ergs/s into the cold salt, though the time needed for removing the heat of magnetization at 1° K is inconveniently long, about an hour. The superconducting heat switch is really seen to best advantage when it is used to make and break thermal contact between bodies which are both well below 1° K.

Though the magnets are often the biggest items of equipment, this article is not the place to deal with their design in detail. Large expensive electromagnets now have to compete with comparatively cheap iron-free solenoids energized by large generating sets (purchased from transport companies which now operate buses instead of trams). The only requirements are that the field of 10 to 50 kG should be ripple-free and fairly homogeneous over the volume of the salt, remembering that this is inside a calorimeter inside a liquid helium flask inside a liquid air flask.

HEAT CONTACT

In the early days of demagnetization there was much argument as to whether the salts were really cooled—that is, whether the temperature of the solid defined in terms of the relative populations of the vibrational energy levels could follow the magnetic temperature defined by the populations of the magnetic levels. In other words, it was recognized that the spins might attain thermal equilibrium among themselves but that the lattice might remain at a different temperature. It is now known that in most substances, the spin and lattice temperatures attain equilibrium quite quickly. This means that other bodies can be cooled by contact.

As refrigerants for cooling other bodies—thermometers or metal specimens, for instance—the salts suffer by comparison with liquid refrigerants. It is always difficult to make good thermal contact between solids and here this is aggravated by their poor thermal conductivity. Liquid helium at once suggests itself for making good thermal contact but its abnormal heat transport properties demand comparatively refined techniques if very rapid warming times are to be avoided; in practice it is only in experiments on the liquid helium itself that it is ever cooled below 1° K. The simplest technique that has been devised for establishing thermal contact to the salt is to form the pill round copper fins or wires which conduct the cold out. Mixing the powder with plastic may add strength and stop the pill from cracking. Large crystals grown round the wires provide better contact because their thermal conductivity is higher. It is possible to metallize a synthetic ruby and solder it to a stub to conduct the cold out, but this is not possible with salts which decompose on heating. Often the body to be cooled has a certain amount of power generated in it—for example, by the passage of the measuring current in a resistance determination—but if this is limited to a few hundred ergs per second at 0·5° K (or a few tenths of an erg per second at 0·05° K) the body settles down to a temperature quite close to that of the salt.

TEMPERATURE MEASUREMENT

Temperatures have to be measured below 0·5° K without recourse to gas thermometers or vapour pressure thermometers. Instead, radio resistors make very good thermometers at low temperatures. With most types the resistance increases monotonically with decreasing temperature, often with great rapidity—a behaviour attributed in part to their granular texture. Typical $\frac{1}{2}$ W resistors in the range between 10 and 100 Ω at room temperature are useful, the value at 1° K rising to between 100 and 10 000 Ω. If the end-caps are of good design, the reproducibility from run to run is adequate. The best are insensitive to magnetic fields and have small thermal time constants, while small measuring currents can give sufficient precision with negligible power generation. The only disadvantage stems from the habit of the manufacturers of changing the mixes so that published low temperature data suddenly become unreliable as a guide. In these as in other resistance measurements, the heat inflow through the leads can be made arbitrarily small by using thin long wires of constantan (of high thermal resistance) plated with a thin layer of tin (which becomes superconducting and gives rise to no generation of Joule heat).

It is, of course, necessary to calibrate the resistance as a function of the absolute temperature. There are a number of ways of doing this—all actually measure the Kelvin work temperature—and in the best thermodynamic tradition the refrigerant itself is the primary thermometric substance. The method described here uses operations which are almost equivalent to a Carnot cycle, possibly the only occasion in physics where this is ever done.

Imagine the thermometer of negligible heat capacity in good thermal contact with the salt, generating negligible power either through the measuring current or through eddy currents in changing magnetic fields. Assume that the energy levels of the salt are known to sufficient accuracy in the region above 1° K; if, for example, it is found to behave as a perfect paramagnetic above 1° K then the entropy S can be written down[6] as a function of

$$\alpha = \mu H/kT = 0{\cdot}67 \times 10^{-4} \times H/T$$

where μ is the Bohr magneton, k is Boltzmann's constant, H the magnetic field in gauss and T the temperature:

$$S/R = \alpha \coth \alpha - (2s+1)\,\alpha \coth (2s+1)\alpha + \ln \frac{\sinh (2s+1)\alpha}{\sinh \alpha}$$

(where $s = 3/2$ for chromic salts, 5/2 for ferric, as deduced from the susceptibility in low fields $4\mu^2 s(s+1)/3kT$ per ion). The formula for S takes account of paramagnetic saturation in high fields but not of interactions between ions; if necessary these can be allowed for to sufficient accuracy by introducing one parameter related to the Weiss constant if the susceptibility obeys a Curie–Weiss law. To find a point on the calibration curve of the thermometer two experiments are needed. In the first, Fig. 4, the final temperatures (recorded

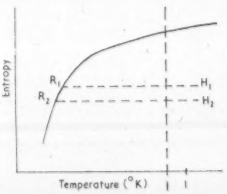

Fig. 4. Temperature measurement

At temperatures to the right of the vertical dotted line the behaviour of the salt is known.

as R_1 and R_2 ohms) corresponding to two demagnetizations from known initial conditions (H_1/T_1) and (H_2/T_2) are found; it is convenient if R_1 and R_2 closely straddle the calibration point required. Then ΔS, the entropy change between R_1 and R_2 is known. In the second experiment the salt is demagnetized to a lower temperature and then deliberately warmed up by introducing heat (perhaps by using the thermometer as a heater or by shining γ-rays from a suitable source) and the amount of heat ΔQ to warm the salt between R_1 and R_2 measured. Then $\Delta Q = T.\Delta S$ where T is an average temperature between R_1 and R_2. The complete calibration curve can be constructed from such data. In place of R, any other parameter can be used in a similar way.

Another commonly used secondary thermometer is the susceptibility of the salt itself, measured with a coil system or susceptibility balance. At high temperatures Curie's law or the Curie–Weiss law is obeyed and an extrapolation of the susceptibility some way below 1° K gives a good approximation to the absolute temperature. But at the lowest temperatures the corrections become very large and at some point the susceptibility even starts decreasing again with

decreasing temperature and hysteresis sets in. Here, other temperature-varying parameters—the remanence and the area of the hysteresis loop for a given field—have been used as secondary thermometers;[7] the hysteresis losses in an alternating field, deduced from the out-of-phase component of the susceptibility, have been used to supply the heat during the second part of the procedure for the absolute calibration. There is no need for leads or other connexions to the salt during any of these measurements. Many salts are quite unreproducible from run to run at low temperatures, however, particularly some of the alums which undergo partial or complete ferroelectric phase changes at about liquid air temperatures.[8] The advantage of the anhydrous salts mentioned earlier is that they are expected to be less variable in their behaviour.

Recently a novel method (useful down to about 0·05° K) has been devised[9] for finding the susceptibility-temperature relation for any new substance. It depends on the use of cerium magnesium nitrate, which has a number of special properties. It behaves like a perfect paramagnetic down to the region of 0·006° K and therefore has a very small specific heat down to, say, ten times that temperature; it is very reproducible in its behaviour; finally it is highly anisotropic. Below 1° K the susceptibility perpendicular to the hexagonal axis is about fifty times that parallel to it. This most useful property is applied in the following way: A single crystal sphere of the cerium salt is surrounded by a spherical shell made of the new substance (powdered and therefore isotropic). The whole is demagnetized and allowed to come to temperature equilibrium. A special coil system is arranged to measure the total magnetic moments parallel to the axis of the crystal and perpendicular to it, and it is easy to see that from these data the separate susceptibilities of the salts can be deduced. The cerium salt thus acts as the thermometer to calibrate the susceptibility of the other.

CASCADE DEMAGNETIZATION; TEMPERATURE STABILIZATION

Two extensions of the straightforward demagnetization process will be described next. Ultimately they are likely to prove to be very important technical developments, but they will not be described in any detail here because no new physical principles are involved.

The first is the use of a cascade arrangement to allow a demagnetization to be carried out from a temperature which is itself far below 1° K. It is the ratio (H/T) which determines the amount of entropy removed by a field so that a ten-fold decrease of starting temperature is worth a ten-fold increase of field, and a two-stage demagnetization can, in principle, produce a cooling which would otherwise require an impossibly large field.

In a preliminary experiment to study the process,[10] the apparatus had a large pill of ferric ammonium alum as the first stage and a smaller pill of diluted potassium chrome alum as the second; they were connected through a superconducting wire [Fig. 5(*a*)]. Both stages were magnetized at 1° K in 4·2 kG and then the magnet was moved slowly, so that the field was gradually removed from the first stage, thus cooling it, while allowing the second to follow slowly in temperature with minimum entropy production. By the time the first stage had been fully demagnetized the second was still in the full field while the wire, in the stray field of the magnet, was still normal; everything was at about 0·25° K. Then the magnet was switched off, thermal contact between the stages was broken, and the second stage reached 0·003° K. This temperature could only have been reached in a single stage using a far larger magnet. As described in a later section this method has been applied to reach spectacularly low temperatures.

The second important development particularly concerns the experimenter who wishes to make measurements on substances other than the salts themselves. The small heat capacity of the average pill means that a power generation of a few tens of ergs per second is the largest that can be tolerated for more than a few seconds. This has led to the development of the magnetic refrigerator.[11]

A block diagram of this elaborate arrangement is shown in Fig. 5(*b*). The thermal valves are superconducting wires

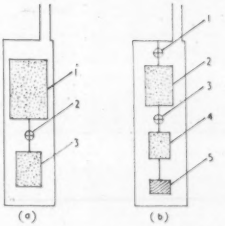

Fig. 5. Block diagrams

(*a*) Two-stage demagnetization. (1) first stage; (2) superconducting valve; (3) second stage.

(*b*) Magnetic refrigerator. (1, 3) superconducting valves; (2) working substance; (4) reservoir; (5) specimen to be cooled.

operated by small solenoids. The specimen to be cooled remains in thermal contact with a "reservoir" pill of salt (chosen for its high specific heat in the required temperature region), and feeds its power into it. The specimen and reservoir pill constitute the system to be refrigerated cyclicly. One full cycle of operations takes two minutes. For purposes of description consider the machine being used to maintain a temperature of 0·3° K. For rather more than half the cycle the specimen and reservoir pill are isolated by the lower valve so that in this time they warm up slightly above 0·3° K. At a certain phase C of the cycle the reservoir is connected through to the working substance which at that moment is also arranged to be at 0·3° K, and in a magnetic field of 2·5 kG. This field is slowly removed so that the reservoir falls to just 0·3° K; it is then isolated till the phase C of the cycle comes round again. In the meantime the working substance is taken round a cycle of magnetization and demagnetization using the thermal switch to the bath, so as to find itself in the correct condition at the phase C of the cycle. In this way a specimen generating 150 ergs/s can be kept indefinitely within better than 10% of 0·3° K. The machine has a lower limit of efficient operation at 0·2° K.

The details of the design—the correct dimensioning of the valves, the choice of working substances and the allowance for their non-ideal behaviour, and not least the commercial manufacture of the complete machine—constitute a fascinating piece of cryogenic engineering in this temperature range.

Another much simpler way of stabilizing the temperature of a salt in the presence of a power input has been proposed recently.[12] It is to demagnetize a single specimen, not to zero field but to some finite value thus reaching a certain

temperature which can be observed with a carbon resistance thermometer. Then as power is fed into the salt, trying to warm it up, the residual field is decreased. It is easy to design in principle a system whereby the resistance of the thermometer controls the magnet current and keeps the temperature constant. The limited amount of control available till the field becomes zero should be adequate for many experiments.

But even if large magnets are used with large pills of salt with careful attention to the problems of heat contact, the power that can be coped with remains pathetically small; 1000 ergs/s is still thought of as very large.

RESULTS BELOW 1° K

The second half of this article deals with a few results of experiments below 1° K, culled from different branches of physics, with some attempt to explain their significance. There are as yet no standard techniques or designs of apparatus applicable to all kinds of measurements. Every new experiment presents its own problems and a few of the more interesting ones are described here in brief detail.

RESULTS ON PARAMAGNETIC SALTS

The salts which were selected as working substances for the very first demagnetizations were those which obeyed Curie's law above 1° K. Their properties could be explained on a "paramagnetic gas" model in which all the details of the structure could be forgotten and only the widely spaced paramagnetic ions themselves needed to be considered. As indicated previously, the temperatures actually reached after demagnetization were determined by the fine structures of the lowest lying energy levels, so that the interpretation of the specific heat anomalies and the deviations from Curie's law were immediately interesting.

Nowadays, however, the energy level schemes are explored by microwave spectroscopy, which gives far more unambiguous information than the thermodynamic methods. In addition, these measurements need only be done above 1° K and are easier to do. The energy level schemes thus revealed can often be interpreted with the aid of the crystal structures. In the alums, for instance, each ion magnetic ion is surrounded by an octahedron of water molecules which exert strongly inhomogeneous electric fields and make it energetically favourable for the ion to be alined in certain directions with respect to the octahedron. This is one way of producing the fall of entropy in zero external field shown in Fig. 1(*b*). With many salts, however, it has happened in the past that the specific heat calculated from the level scheme has at first not agreed with the direct measurements below 1° K. Further searches at higher frequencies have then sometimes shown up hyperfine structures in the lowest lines which also contribute to the specific heat. This is one of the ways in which the thermodynamic measurements can usefully supplement the spectroscopy.

There remain some phenomena, however, which can only be studied below 1° K. In addition to the specific heat maximum produced by the effects of the environment of the magnetic ions, there is often a very sharp maximum at a lower temperature. Very weak hysteresis sets in at the same time, so that this must be a co-operative effect between ions. The area enclosed by the loop is usually only a few tenths of an erg compared with 10^2–10^6 erg for an average ferromagnetic at room temperature, while the remanence is only about 10^{-4} of the saturation magnetization. In the early days, this state was called metamagnetic, but now it is fairly certainly identified as antiferromagnetic. This statement depends partly on the observation that the differential susceptibility in zero field, after going through a maximum as the temperature is reduced, begins to decrease again. Thus $(\partial I/\partial T)_H$ is positive, where I is the intensity of magnetization. Therefore, by one of Maxwell's relations, $(\partial S/\partial H)_T$ is positive, the disorder increases when a magnetic field is applied. This is characteristic of an antiparallel array which must be upset by a magnetic field, and so the type of ordering is crudely identified as antiferromagnetic.

To single out one substance which has been much studied,[13, 14] chromium methylammonium alum has its transition temperature at 0·020° K. The crystals have cubic symmetry at room temperature but undergo a transition to tetragonal symmetry at about 160° K. In addition, a still lower symmetry makes its appearance below 0·020° K though it is not clear whether this is due to the effects of strain or not. The variation of differential susceptibility as the external magnetic field is varied is shown in Fig. 6.

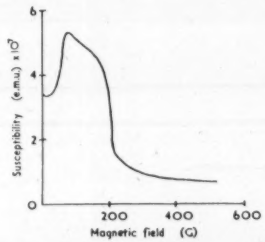

Fig. 6. Susceptibility of chrome methylammonium alum as function of magnetic field

Field applied parallel to cube axis, susceptibility measured in same direction, at constant entropy.

This complicated behaviour is attributed to the rotation of antiferromagnetic *domains*. The sharp upswing is thought to be due to the domains clicking over to positions nearly perpendicular to the field, then later they are gradually turned parallel to the field and the system becomes paramagnetic. In order to understand the details of the co-operative process it must be known how the Cr^{+++} ions actually interact with one another. It has been found that chromium potassium alum, which differs only in the non-magnetic ions lying between adjacent Cr^{+++} ions, has practically the same lattice spacing and yet the transition temperatures differ by a factor of two. This seems to show that direct dipole-dipole interactions between the Cr^{+++} ions cannot be the dominant forces because they would not vary so rapidly with distance apart. It has been suggested that a "super-exchange" takes place whereby the electron cloud of one Cr^{+++} ion overlaps a neighbouring anion which can exchange electrons with it. This in turn is overlapped by a second neighbouring Cr^{+++} ion and thus the two magnetic ions can effectively interact. Such super-exchange mechanisms have been identified in high temperature antiferromagnetics.

It is clear that there is a wealth of phenomena to be investigated here, though it can be anticipated that each salt will present its own surprise.

RESULTS WITH LIQUID ^{4}HE AND ^{3}HE

When liquefied, the isotope ^{4}He has quite normal properties down to a temperature of 2·168° K and it is called liquid He–I. At that temperature it transforms into another modification, liquid He–II, which has unexpected transport properties. The rare isotope ^{3}He, on the other hand, has no such abnormal properties.

Liquid He–II can be discussed and investigated at many levels. There are first a host of abnormal flow properties and their associated thermal effects, but these are of such bewildering variety and are so sensitive to minute disturbances that they tend to obscure rather than clarify the theoretical situation. They are, however, of great importance to the experimenter who wishes to cool a few cubic centimetres of liquid helium below 1° K, because a film of He–II can climb up any tube and by a refluxing action can cause a large inflow of heat into the cold body.

An early attempt to explain some of the facts of He-II was based on the idea that the assembly of (symmetrical) ^{4}He molecules should obey Bose–Einstein statistics and therefore undergo some sort of condensation at a low temperature, while ^{3}He obeying Fermi–Dirac statistics should not. But this simple approach cannot be developed quantitatively. The two-fluid model for He-II postulates the existence of a normal and a superfluid, or in other words it postulates a special energy spectrum and many experiments have aimed at determining this. One of the triumphs of the two-fluid model was the prediction of the existence of second sound, a mode of propagation of temperature waves almost without attenuation above 1° K. The study of this and of ordinary ultrasonic waves has yielded much knowledge of the energy spectrum.

In one set of measurements Chase and Herlin[15] used a device of Ashmead's for maintaining a mass of He-II cold for a long time and studying ultrasonic propagation. The conical plug and socket, Fig. 7, were made of thin stainless steel and were lapped to fit very closely together. The plug could be raised to let liquid helium into the chamber inside the powdered salt, and at the same time this provided thermal contact to the bath. Before demagnetization the plug was closed, and though the superfluid flow of He-II through the gap caused a heat leak that was still quite large, the 200 g mass of salt remained below 1° K for nearly an hour. The experimental chamber contained a quartz plate opposite a reflecting metal surface to generate ultrasonic pulses and study their propagation. In Osborne's experiments[16] a similar arrangement was used with a plane wire heater as generator of second sound and an Aquadag thermometer as detector.

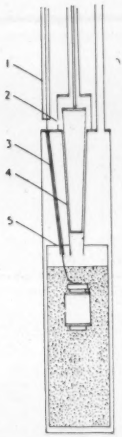

Fig. 7. Apparatus for measurements on liquid helium below 1° K

(1) coaxial cable; (2) hole for admitting liquid helium; (3) cable passing through tube filled with Vaseline; (4) stainless steel plug and socket, plug shown raised; (5) calorimeter containing salt and experimental chamber all filled with liquid helium. Coils for measuring temperature not shown.

From these and other experiments the energy spectrum of He-II is fairly well known. A physical interpretation, that some of the excitations are vortices and vortex rings in the superfluid, has recently been suggested. Experiments on the rate of loss of angular momentum of rotating masses of He-II are in accord with this idea, but so far nothing has been done below 1° K.

By contrast with ^{4}He, the behaviour of the rare isotope ^{3}He is relatively pedestrian. Nevertheless it is of interest below 1° K because its vapour pressure is very much higher—at 0·5° K it is about 0·15 mm as compared with $1{\cdot}7\ 10^{-5}$ mm for ^{4}He. Thus a bath of liquid ^{3}He could allow quite low temperatures to be reached simply by pumping. But the gas to make 1 mm^3 of liquid costs £40 to buy at present, so that this is not yet a very practicable method.

Another way of utilizing the considerable entropy of ^{3}He has been proposed[17] and is more acceptable because the process is a reversible one. A long tube packed tightly with fine powder with interstices of the order of 10^{-6} cm wide is freely permeable to He-II but almost impassable to ^{3}He. The flow rates differ by a factor 10^4 or 10^5. Such a "superleak" therefore acts as a semipermeable membrane and allows the osmotic pressure of ^{3}He dissolved in ^{4}He to be measured. Now osmotic pressures obey the appropriate gas laws for isothermal and—less familiarly—for adiabatic processes. In particular, if the solute can be expanded adiabatically and reversibly—a process represented in textbooks by the slow movement of an insulating piston confining the solute "gas" into a volume V—^{3}He should obey the law $TV^{2/3}$ = constant. The process can be carried out in practice by allowing superfluid ^{4}He to flow in through a superleak and dilute the solution, the surface of the liquid taking the place of the piston. The dilute solution can, of course, be reconcentrated later by reducing the effective pressure at the other end of the superleak below the osmotic pressure. The assumptions behind the above formula are that the osmotic pressure of the solute obeys the Fermi–Dirac gas law which happens to be identical with the classical one for a monotomic gas; that the entropy of the ^{4}He is negligible compared with that of the ^{3}He and that the superfluid arrives carrying zero entropy; and further, that the mass of ^{3}He in the vapour phase can be neglected. The formula must be modified because, among other things, solutions of ^{3}He in ^{4}He are known not to be perfect—there is an entropy of mixing—and indeed to exhibit a phase separation at low enough temperatures.[18] Nevertheless a 20 : 1 dilution should allow a temperature in the region of 0·2° K to be reached. This process should provide much data about ^{3}He — ^{4}He solutions, and might in the future compete with demagnetization for producing moderately low temperatures, especially for experiments where magnetic fields have to be completely absent.

RESULTS WITH SUPERCONDUCTORS

Several properties of superconductors have been mentioned already. Each metal has its own transition temperature; Fig. 8 shows the distribution of these plotted on a logarithmic scale of temperature. In the superconductive state the electronic motion is in some way more ordered than in the normal state above the transition temperature, and this

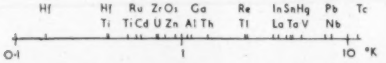

Fig. 8. Transition temperatures of superconducting elements

Logarithmic scale of temperature. For hafnium see Ref. (19); for titanium see Ref. (20).

produces a state of perfect diamagnetism ($B = 0$) as a result of which the electrical resistance is zero. However, as previously mentioned, the application of an external field of sufficient magnitude restores the resistance and other normal properties. The variation of critical field with temperature can be related to the latent heat of transition by an analogue of the Clausius–Clapeyron equation and the critical field curve is as important for a superconductor as the vapour pressure curve for a liquid. The one small practical difficulty in such measurements below 1° K is that when the magnetic field is applied the temperature of the salt is altered. An ingenious solution was that adopted by Cooke, Whitley and Wolf[21] using cerium ethyl sulphate as the refrigerant. This salt is highly anisotropic so that after demagnetization from a field applied in the direction of maximum susceptibility, a field applied perpendicularly hardly raises the temperature. Single crystals of the salt were stuck on to a foil of the metal and a simple measurement of the total magnetic moment sufficed to give the critical field data.

The absorption of latent heat when the metal becomes normal is the basis of another method of reaching temperatures below 1° K—namely the adiabatic *magnetization* of a superconductor.[22, 23] Only a very small amount of entropy is removed but this is to some extent compensated by the fact that quite large specimens can be used because only small magnetic fields are required. It is difficult to attain the theoretical efficiency because of the eddy currents induced when the specimen is partly normal.

One detailed picture of the origins of superconductivity[24] draws attention to the narrow wake of disturbance left behind by an electron travelling rapidly through the lattice. This can give rise to an interaction between two such electrons, but it is, of course, difficult to extend the discussion to 10^{23} interacting electrons. It was, however, guessed that a group of them would be separated from the rest at the Fermi level by a gap of order 10^{-4} eV. For some time, doubt was cast on the existence of such a gap because measurements at comparatively "high" temperatures near the transition temperature failed to disclose the expected exponential variation of specific heat with temperature. Instead, they showed a cubic dependence.

Goodman[25] measured the specific heat of aluminium in the superconducting state between 0·25° K and its transition temperature of 1·18° K and achieved sufficient accuracy to be able to decide between the two types of curve. The technical problem was to avoid the adsorption or desorption of helium gas from the specimen which would have produced spurious results. Liquid helium was condensed into the inner chamber attached to the salt, Fig. 9, to bring it to any desired initial temperature. The whole assembly was in a high vacuum. The aluminium specimen was connected to the salt through a superconducting heat switch. After

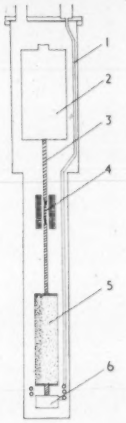

Fig. 9. Apparatus for measuring the specific heat of superconducting aluminium

(1) tube for introducing helium and pumping it away again; (2) aluminium specimen (heater and carbon thermometer inside—not shown); (3) copper heat link; (4) impure lead heat switch and niobium solenoid; (5) salt; (6) helium chamber. The coils for measuring the temperature of the salt are not shown.

demagnetization of the salt, the stray heat flow into the metal was only 2 erg/s and it was quite free from adsorbed helium. The results shown in Fig. 10 show that the exponential law is correct.

Within recent months, changes of infra-red absorption have been found[26] in superconductors above 1° K in the wavelength region between 0·5 and 5 mm; these confirm the

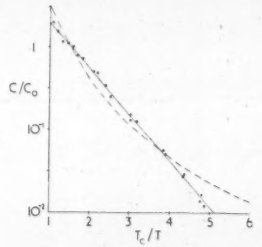

Fig. 10. Results obtained with apparatus shown in Fig. 9

Specific heat C of superconducting electrons plotted on logarithmic scale. (C_o is the electronic specific heat in the normal state at the transition temperature T_c.)

.. experimental points. ——— $6{\cdot}9 \exp(-1{\cdot}28Tc/T)$.
– – – – $3(T/Tc)^3$.

existence of the gap and may allow its fine structure to be determined.

RESULTS ON NORMAL METALS

Very little systematic work has been done on non-superconducting metals below 1° K. The electrical resistance and magneto-resistance of a few nominally pure metals have been measured, and these have shown that what was originally regarded as a rare anomaly is really quite common. This is that contrary to expectation the electrical resistance of several metals at low enough temperatures does not remain constant at a value determined by the amount of physical and chemical impurities present in the metal but increases by a few per cent as the temperature is decreased. It is now thought that one mechanism for producing this effect is some sort of ferromagnetic or antiferromagnetic interaction caused by the presence of paramagnetic impurity atoms—as, for example, with manganese in copper. These interactions can occur at surprisingly low concentrations. But it is easier to work with comparatively high concentrations of impurity (0·1–1%) which can be better controlled and which produce their effects above 1° K.

Specific heat measurements on pure metals could also be of some interest. Above 1° K the dominant contribution comes from the lattice vibrations but below 1° K from the conduction electrons. The surprising fact is that calculations which ignore most of the interactions between the conduction electrons seem to give the correct value of their specific heat. It would be expected, for example, that the interactions which in some metals give rise to superconductivity should also be present to some extent in all metals and that these should quite alter their specific heat. Measurements below 1° K could be revealing but only if they were sufficiently precise. Whereas techniques are adequate for distinguishing between a cubic or an exponential variation with temperature, they are not yet good enough for this purpose.

Rayne[27] carried out a few determinations by measuring the heat capacities of samples of salt plus metal, and then subtracting the contribution from the salt. But the scatter of the final data was great. One interesting fact emerged, however. A sodium sample showed a large specific heat anomaly at 0·8° K with some thermal hysteresis. Barrett's[28] X-ray studies on work-hardened sodium make it possible that this may have been caused by a partial transition from body-centred cubic to close-packed hexagonal structure. Other investigations have shown specific heat anomalies in other samples of sodium up to the region of 8° K and the effect is certainly sensitive to the presence of impurities. Though the observation of a transition at 0·8° K therefore has no fundamental physical significance, it does demonstrate that there is enough thermal agitation at this temperature to bring about a martensitic phase change in sodium.

RESULTS IN NUCLEAR PHYSICS

Usually one associates nuclear physics with great energies and it might seem curious that low temperatures should be able to contribute anything to the subject. The connexion is that many nuclei have magnetic moments; thus there exist many metals and compounds where the bound electrons contribute no temperature-dependent paramagnetism but where the nuclei give rise to a weak paramagnetism obeying Curie's law. The magnitude of the unit of nuclear magnetic moment is indeed very small—about 1/2000 of that of a spinning electron—because nucleon charges are of the same order as electron charges but their masses are 2000 times bigger. The same numerical factor governs the ratio of fine to hyperfine structures in spectral lines. It follows that any suitable metal placed in a magnetic field H at temperature T, where H/T is of order 10^6 G/deg, has many of its nuclei alined parallel to the field (just as an ordinary paramagnetic ion has a good deal of entropy removed if H/T is of order 10^3). Such a partly polarized system allows, in principle, many details of nuclear emission and capture processes to be detected by experiments on macroscopic blocks of material, whereas these details are obscured if the nuclei are oriented at random inside the block.

Since the highest steady field which can be conveniently produced is well below 10^5 G, the experiments must be done below 1° K. Dabbs, Roberts and Bernstein[29] produced partly polarized ^{115}In nuclei at 0·035° K in a field of 11 kG ($H/T = 3{\cdot}1 \times 10^5$ G/deg) using the arrangement of Fig. 11.

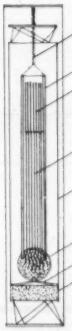

Fig. 11. Apparatus for polarization of ^{115}In nuclei

(1) tension springs; (2) plastic shield; (3) indium plates; (4) silver wires for heat links; (5) copper shield; (6) sphere of salt grown round flattened ends of wires; (7) rigid plastic mounting; (8) "guard" salt. The coils for measuring the temperatures are not shown.

The coolant was a crystal sphere of iron alum grown round silver wires which were soldered to the indium foils. The silver conductors and the indium were shielded inside a tube of plastic chosen for its low neutron absorption, and this assembly was rigidly mounted inside a metal cage cooled by a second block of salt. The whole was suspended by nylon threads. After demagnetization of the salts from 16 kG, the field round the indium was slowly raised to 11 kG. The small amount (2%) of polarization thus produced was used in the following way. A beam of thermal neutrons from a pile was monchromatized and polarized by reflexion from the 220 planes of a magnetized magnetite crystal and subsequently from the 110 planes of a copper crystal. The beam finally emerged with 87% of the neutrons having their spins parallel to a certain direction. They could also be turned antiparallel to this direction by passing them through an auxiliary inhomogeneous field, when they underwent a "Majorana flip." The beam then went through the cryostat on to the indium, and the capture cross-section was found to vary with the relative orientation of the spins of nuclei and neutrons. When they were parallel it was greater than when antiparallel,

showing that the spin of the compound nucleus was the sum (not the difference) of the two spins. In spite of the fact that the subsequent β-decay of the compound nucleus warmed the sample, it could be kept sufficiently cold for about ninety minutes.

This method is in principle applicable to any nucleus with non-zero magnetic moment, but to achieve polarizations of, say, 50% or more would require values of H/T which are near the limit of attainability at the present. For this reason it is called the "brute force" method and in fact other more subtle ways of orienting nuclei were successfully used before it.[30, 31] There are many variant methods and they will not be described here in detail. They depend on the use of crystals which are paramagnetic and also show a large hyperfine level splitting. In these the electrons inside each ion exert a magnetic field on the nucleus of the order of 10^5 or 10^6 G so that the nucleus shows a strong preference for certain directions inside the ion at temperatures of 0·1 or 0·01° K. All that is necessary then is to orient the ions themselves, which can be done in a low field of a few hundred gauss or even in a zero external field if the crystalline electric fields are strong enough. The anisotropy of neutron capture or γ-ray emission has been studied in several nuclei and some valuable data on spins and parities have been determined. The recent experiment on the non-conservation of parity[32] was of this kind.

In the experiment on ^{115}In described above, the object was to produce and study an ordered array of nuclei, a more or less parallel alinement. But an adiabatic demagnetization from such a condition should reach a very low temperature characteristic of the interaction *between* nuclei. If these forces were merely the direct interactions between dipoles, then nuclear ferromagnetism should be produced at a temperature of the order of 10^{-7}° K, but there are other types of coupling involving the participation of the conduction electrons which might raise this temperature by a factor 10 or 100. An experiment of this kind by Kurti and others[33] recently attained the world's record in low temperatures. They used a two-stage demagnetization (without attempting to break the thermal link between stages) with chrome potassium alum as the first stage and about 50 g of fine copper wires as the second. The second demagnetization was from 0·012° K and 28 kG. The susceptibility of the copper showed that a temperature of about 2×10^{-5}° K was held for a few seconds. This was only a preliminary experiment and it can be anticipated that the nature of the coupling between nuclei in a metal can usefully be studied in this way.

CONCLUSION

In a single experiment, a temperature near 2×10^{-5}° K has been reached and held for a few seconds. Between 10^{-3} and 3×10^{-2}° K a number of interesting experiments have been performed but only on the refrigerants—the paramagnetic salts—themselves. Above 0·03° K a large amount of work has been done not only on the salts but also on other substances.

The temperature region below 1° K is one where weak interaction forces can still give rise to interesting effects in a number of systems, even though the temperature is considered low by ordinary physical standards. There are severe practical limitations on the type of experiment which can be performed, but techniques are improving rapidly. It can be anticipated that many new results will emerge from research at these very low temperatures.

REFERENCES

(1) Cooke, A. H. *Progress in Low Temperature Physics*, **1**, p. 224 (Amsterdam: North Holland Publishing Company, 1955).
(2) Daunt, J. G., and Pillinger, W. L. *Annexe* 1955–3, *Suppl. Bull. Internat. Inst. Refrig.*, p. 158 (1955).
(3) Ambler, E., and Hudson, R. P. *Phys. Rev.*, **102**, p. 916 (1956).
(4) Heer, C. V., and Rauch, C. J. *Annexe* 1955–3, *Suppl. Bull. Internat. Inst. Refrig.*, p. 218 (1955).
(5) Samoilov, B. N. *Dokl. Akad. Nauk SSSR*, **86**, p. 281 (1952).
(6) Casimir, H. B. G. *Magnetism and Very Low Temperatures*, p. 28 (Cambridge: University Press, 1940).
(7) de Klerk, D., Steenland, M. J., and Gorter, C. J. *Physica*, **15**, p. 649 (1949).
(8) Pepinsky, R., Jona, F., and Shirane, G. *Phys. Rev.*, **102**, p. 1181 (1956).
(9) Cooke, A. H., Meyer, H., and Wolf, W. P. *Proc. Roy. Soc. A*, **233**, p. 536 (1956).
(10) Darby, J., Hatton, J., Rollin, B. V., Seymour, E. F. W., and Silsbee, H. B. *Proc. Phys. Soc. A*, **64**, p. 861 (1951).
(11) Heer, C. V., Barnes, C. B., and Daunt, J. G. *Rev. Sci. Instrum.*, **25**, p. 1088 (1954).
(12) Kurti, N. *Annexe* 1955–3, *Suppl. Bull. Internat. Inst. Refrig.*, p. 587 (1955).
(13) Gardner, W. E., and Kurti, N. *Proc. Roy. Soc. A*, **223**, p. 542 (1954).
(14) Beun, J. A., Steenland, M. J., de Klerk, D., and Gorter, C. J. *Physica*, **21**, p. 767 (1955).
(15) Chase, C. E., and Herlin, M. A. *Phys. Rev.*, **97**, p. 1447 (1955).
(16) Osborne, D. V. *Phil. Mag* (8) **1**, p. 301 (1956).
(17) London, H., reported by Brewer, D. F. *Nature* [*London*], **179**, p. 79 (1957).
(18) Walters, G. K., and Fairbank, W. M. *Phys. Rev.*, **103**, p. 262 (1956).
(19) Hein, R. A. *Phys. Rev.*, **102**, p. 1511 (1956).
(20) Steele, M. C., and Hein, R. A. *Phys. Rev.*, **92**, p. 243 (1953).
(21) Cooke, A. H., Whitley, S., and Wolf, W. P. *Proc. Phys. Soc. B*, **68**, p. 415 (1955).
(22) Dolecek, R. L. *Phys. Rev.*, **96**, p. 25 (1954).
(23) Mendelssohn, K., and Yaqub, M. *Annexe* 1955–3, *Suppl. Bull. Internat. Inst. Refrig.*, p. 583 (1955).
(24) Singwi. *Phys. Rev.*, **87**, p. 1044 (1952).
(25) Goodman, B. B. *Annexe* 1955–3, *Suppl. Bull. Internat. Inst. Refrig.*, p. 506 (1955).
(26) Biondi, M. A., Garfunkel, M. P., and McCoubrey, A. O. *Phys. Rev.*, **101**, p. 1427 (1956).
(27) Rayne, J. *Phys. Rev.*, **95**, p. 1428 (1954).
(28) Barrett, C. S. *Acta. Cryst.*, **9**, p. 671 (1956).
(29) Dabbs, J. W. T., Roberts, L. D., and Bernstein, S. *Phys. Rev.*, **98**, p. 1512 (1955).
(30) Daniels, J. M., Grace, M. A., and Robinson, F. N. H. *Nature* [*London*], **168**, p. 780 (1951).
(31) Bernstein, S., Roberts, L. D., Stanford, C. P., Dabbs, J. W. T., and Stephenson, T. E. *Phys. Rev.*, **94**, p. 1243 (1954).
(32) Wu, C. S., Ambler, E., Hayward, R. W., Hoppes, D. D., and Hudson, R. P. *Phys. Rev.*, **105**, p. 1413 (1957).
(33) Kurti, N., Robinson, F. N. H., Simon, F. E., and Spohr, D. A. *Nature* [*London*], **178**, p. 450 (1956).

The measurement of surface residual stress by X-rays

By G. A. HAWKES, B.Sc., The Fairey Aviation Co. Ltd., Hayes, Middlesex

[*Paper received* 28 *November*, 1956]

A multi-exposure, X-ray, back-reflexion technique, with graphical solution for the evaluation of the level of residual macro-stress in any particular surface direction in a polycrystalline material, is described. This technique has, in particular, been applied to the stress analysis of aluminium alloys and high tensile steel components and specimens.

1. INTRODUCTION

The basic principles of the X-ray methods of stress measurement have been previously published.[1-5]

Early techniques were based upon a two-exposure method, which assumed simple isotropic elastic behaviour in the material under question. The surface tangential stress acting in a given azimuth ϕ has been defined by the equation,[5]

$$\sigma_\phi = \frac{d_\psi - d_z}{d_z} \cdot \frac{E}{(1+\nu)\sin^2\psi} \qquad (1)$$

in which σ_ϕ is the stress component in surface direction ϕ, d_ψ is the interplanar spacing measured in a direction having azimuth ϕ and inclination ψ to the normal to the surface, and E and ν are respectively Young's modulus and Poisson's ratio of the material under examination.

2. EXTENSION TO GRAPHICAL SOLUTION

The main disadvantage of the two-exposure methods is that, eventually, complete reliance is placed upon two experimental points to determine the slope of a line.

However, equation (1) may be put in a convenient straight line form as will now be shown, and six back-reflexion photographs, taken at $\psi = 0$, 30 and 45°, will give five points through which to draw the straight line, each point being the mean of either two or four other points, obtained from film data. Furthermore, the form in which the experimental results appear provide an indication of the correctness of the fundamental assumptions made in developing the method.

$$\frac{d_\psi - d_z}{d_z} = \frac{\sin\theta_z - \sin\theta_\psi}{\sin\theta_\psi} \qquad (2)$$

where θ is the Bragg angle θ.

Hence equation (1) becomes

$$\frac{\sigma(1+\nu)\sin^2\psi}{E\sin\theta_z} = \frac{1}{\sin\theta_\psi} - \frac{1}{\sin\theta_z} \qquad (3)$$

Therefore $$\operatorname{cosec}\theta = \frac{\sigma(1+\nu)\sin^2\psi}{E\sin\theta_z} + \frac{1}{\sin\theta_z} \qquad (4)$$

If theoretical assumptions are correct, then $\operatorname{cosec}\theta$ is a linear function of $\sin^2\psi$ and from the resulting graph the value of $\sigma(1+\nu)/(E\sin\theta_z)$ may be determined and hence the stress σ.

In practice, it has been found convenient to take six back-reflexion photographs of the area of the specimen under examination. That is, two at normal beam incidence, two at 30° incidence (one on either side of the normal) and two at 45° incidence (also, one on either side of the normal); these angles of incidence are obtained by rotating the specimen, in the plane containing the primary beam and the direction of stress required, about an axis across the face of the area under examination. A rectangular film is used in the back-reflexion camera, the length of which is also in the above plane, and great care must be taken in the initial lining up to ensure the film holder and the X-ray beam are perpendicular. Vertical slit collimation is used with the slit at right angles to the length of the film, hence the length of the slit will not cause undue broadening of the diffraction pattern. A 0·030 in. slit is used for the normal and 30° incidence photographs, and a 0·020 in. slit for 45° incidence, to compensate for the spreading out of the irradiated area upon rotation. During exposure the specimen is oscillated over a small angular range (±1¼°) through its mean position in order to bring more crystal planes into a reflecting position. Specimen-to-film distance is determined indirectly by smearing the surface under examination with pure Vaseline, loaded with finely divided, strain free, silver powder of high purity.

From each back-reflexion photograph, two values of $\operatorname{cosec}\theta$ and the corresponding values of $\sin^2\psi$ are obtained, as explained below.

Referring to Fig. 1 the diffraction lines A and H are the $K\alpha_1$ lines of the appropriate high θ plane of the silver calibrat-

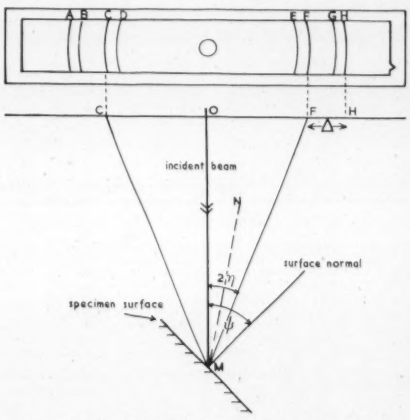

Fig. 1. Type of back-reflexion photograph obtained for stress measurements showing the geometry of the back-reflexion technique with the specimen surface in an inclined position

ing powder, B and G are the $K\alpha_2$ components; C and F are the $K\alpha_1$ lines of the appropriate plane in the material under examination, and D and E are the $K\alpha_2$ components. The position of the line peaks are noted, either visually by vernier scale or by a recording microphotometer.

As no particular attention is paid during initial lining up of the specimen to the specimen-to-film distance, it is necessary to standardize all films, the information on each being reduced in proportion, as determined by a convenient constant value of the diameter of the $K\alpha_1$ silver ring. The diameter referred to is AH and the numerical factor by which this diameter must be multiplied to reduce it to 7 cm is calculated. The distances AC and FH are then multiplied by this factor and the resulting two values recorded as Δ_1 and Δ_2. The relationship between Δ and cosec θ, and Δ and $\sin^2\psi$ is obtained from previously constructed graphs of Δ against these two functions, the necessary information for the construction of these graphs being obtained geometrically for the particular radiation employed (see Section 3).

The following is an illustrative example of a stress determination carried out on the surface of an aluminium alloy component using copper radiation. Measurements have been made in centimetres and reference should be made to Fig. 1 for line designations. In making the initial exposures and in subsequent measuring operations care is obviously taken to ensure that the film is not reversed in position, e.g. the fiducial mark on the camera, which is reproduced on the film, is always kept to the right.

First exposure: normal inclination.

Vernier readings: A, 14·935; C, 16·005; F, 24·955; H, 26·000.

Hence $AH = 11{\cdot}065$ and standardizing factor (S.F.) = 0·6327

$AC = 1{\cdot}070$ and (S.F.) $AC = \Delta_1 = 0{\cdot}6769$

$FH = 1{\cdot}045$ and (S.F.) $FH = \Delta_2 = 0{\cdot}6612$

Finally from the graphs (i) Δ against cosec θ, (ii) Δ against $\sin^2\psi$ (for $\psi = \eta$) we get

$\sin^2\psi = 0{\cdot}027$ when cosec $\theta = 1{\cdot}01397$

$\sin^2\psi = 0{\cdot}027$ when cosec $\theta = 1{\cdot}01411$

Second exposure: 30° inclination (rotated clockwise, looking down on the specimen, fiducial mark to the right).

Vernier readings: A, 16·920; C, 18·270; F, 26·875; H, 28·005.

Hence $AH = 11{\cdot}085$ and standardizing factor, (S.F.) = 0·6316

$AC = 1{\cdot}350$ and (S.F.) $AC = \Delta_1 = 0{\cdot}8526$

$FH = 1{\cdot}130$ and (S.F.) $FH = \Delta_2 = 0{\cdot}7137$

Finally from the graphs (i) Δ against cosec θ, (ii) Δ against $\sin^2\psi$ ($\psi = 30° + \eta$ for Δ_1 and $\psi = 30° - \eta$ for Δ_2) we get

$\sin^2\psi = 0{\cdot}395$ when cosec $\theta = 1{\cdot}01238$

$\sin^2\psi = 0{\cdot}124$ when cosec $\theta = 1{\cdot}01363$

In order to enable readers to check a complete example the vernier readings of the third, fourth, fifth and sixth exposures are given below.

Third exposure: 45° inclination (rotated clockwise, looking down on the specimen, fiducial mark to the right).

Vernier readings: A, 14·590; C, 16·155; F, 24·360; H, 25·680.

Fourth exposure: normal inclination.

Vernier readings: A, 17·765; C, 18·835; F, 27·830; H, 28·905.

Fifth exposure: 30° inclination (rotated anti-clockwise, looking down on the specimen, fiducial mark to the right).

Vernier readings: A, 17·285; C, 18·445; F, 27·020; H, 28·390.

Sixth exposure: 45° inclination (rotated anti-clockwise, looking down on the specimen, fiducial mark to the right).

Vernier readings: A, 16·920; C, 18·180; F, 26·430; H, 28·035.

Thus twelve points can be plotted on a graph of cosec θ against $\sin^2\psi$ as shown in Fig. 2. The mean point is taken

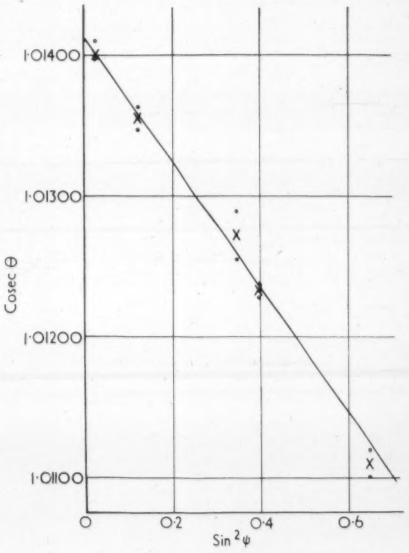

Fig. 2. Relation between cosec θ and $\sin^2\psi$

for positions of similar abscissae, leaving five points through which to draw the best straight line. The gradient of the line is determined and multiplied by the constant (for any one material), $(E \sin\theta_2)/(1+\nu)$, $(3{\cdot}42 \times 10^3$ t/in.^{2} for aluminium alloys).

The above result is therefore evaluated as $-15{\cdot}5$ t/in.^{2}, i.e. a compression of that order, which in this case would be quoted to $\pm 1{\cdot}5$ t/in.^{2} Limits of accuracy are discussed in Section 6.

3. THE GEOMETRY OF DIFFRACTION

Preparation of the graphs: Δ *against* cosec θ, Δ *against* $\sin^2\psi$. Referring to Fig. 1 MN is the normal to the reflecting planes contributing to line F. The diffracted beam for line F makes an angle $2\eta = 180° - 2\theta$ with the incident beam, where θ is the Bragg angle θ. If the inclination of the specimen normal

to the incident beam is ψ, then the inclination of the reflecting planes (for line *F*) is $\psi - \eta$ to the specimen surface and similarly $\psi + \eta$ for line *C*.

When the $K\alpha_1$ ring for silver *AH* has been reduced to 7 cm, we are able to determine the corrected specimen-to-film distance *D* from the lattice constant of silver and an application of Bragg's law for the particular radiation in use.

Thus, we calculate *D* or *OM*, *OH* is corrected to 3·5 cm and values may be assigned to *FH* (Δ). Hence, by giving Δ a range of values 0·5 to 1·5 cm for example, a series of values of 2η may be determined by applying the tangent ratio to triangle *FOM*, and since $2\eta = \pi - 2\theta$, cosec θ may be plotted against Δ.

Other curves may then be constructed for $\sin^2 \psi$ against Δ (i) when $\psi = \eta$, (ii) when $\psi = 30° + \eta$, (iii) when $\psi = 30° - \eta$, (iv) when $\psi = 45° + \eta$ and (v) when $\psi = 45° - \eta$.

4. APPLICATION TO HIGH TENSILE STEELS

The technique described has been applied very successfully to aluminium alloys using copper radiation with silver as the calibrating powder. In addition to these alloys, stress measurements have been carried out on beryllium copper strip using cobalt radiation and martensitic high tensile steels, using chromium radiation with silver powder again as the calibrating medium.

The problem with high tensile steels was twofold; firstly, a radiation had to be used which would produce a measurable line in the back-reflexion position, and secondly, verification was necessary to show whether or not the simple theory for isotropic behaviour could be applied to an anisotropic material.

Cobalt and iron radiation both furnish a ferrite or martensite line in the desirable 2θ range above 140° and are excellent selections when the steel hardness is sufficiently low so that sharp lines are obtained. In the tensile range we are considering, however, these high angle lines become diffuse and merge into the general film background. This situation is avoided by the use of the softer chromium radiation, with which the martensite (211) planes diffract at about 155°. The softness of the radiation possibly contributes further gain in line sharpness in the instance of a gradient of stress in depth, since it will diffract only from the extreme surface of the sample.

At the time of writing this paper, no satisfactory technique has been developed for measuring the residual stress level in the austenitic phase of high tensile steels as distinct from the martensitic ones.

The reliability of the results obtained for such stress measurements employing the simple isotropic theory was demonstrated by comparing theoretical stress figures with the corresponding X-ray stress figures. This procedure is briefly outlined below.

A specimen strip of 18 s.w.g. sheet (Firth–Vickers Stayblade, 17/7/1—chromium/nickel/aluminium, precipitation-hardening stainless steel) was fully heat-treated to 85 t/in.^{2} ultimate tensile strength, and an X-ray stress determination was carried out in the longitudinal direction of the specimen. The specimen was constrained to a circular arc and stress measurements were repeated on various tension and compression faces. At no time was the elastic limit of the specimen exceeded. After each measurement the radius of curvature of the strip was determined from clock gauge readings obtained by traversing the clock gauge along the strip. Hence, an initial surface stress value was obtained for the straight strip and also a series of values of X-ray surface stress and theoretical surface stress, the latter having been derived from elementary bending formulae. The results, given in Table 1, are in tons per square inch and the normal sign convention has been employed, i.e. positive for tension and negative for compression.

Table 1. *Comparison of the theoretical and X-ray stress measurements made on high tensile steel strip. Initial surface stress on straight strip* $-12·0$ *t/in.*^{2}

Theoretical surface stress with correction due to initial stress (t/in.^{2})	*X-ray stress* (t/in.^{2})
−21·7	−23·2
−36·4	−45·0
+20·3	+17·6
+33·0	+29·3
+38·6	+40·0

These results clearly indicate that the X-ray technique can be applied to the determination of engineering or macro-stresses in high tensile steels.

The profile of the (211) martensite line using chromium radiation is very broad, about 0·5 cm for steels heat-treated to the property level cited above, with a film-to-specimen distance of about 12 cm. Even so, it has been found that visual vernier scale measurements can be accurately repeated and recourse to some form of recording microphotometer is not essential. The reproducibility of result could possibly be accounted for also, by the fact that the final stress result is obtained from a measurement of line shift rather than actual line position.

Residual surface stresses have been measured in steels heat-treated up to the 120 t/in.^{2} ultimate tensile strength level, and the results of a few of such measurements are quoted in Table 2. The first two results are a hoop stress

Table 2. *Stress measurements made on various high tensile steel test-pieces*

Material and surface condition	*Ultimate tensile strength* (t/in.^{2})	*Direction and magnitude of X-ray stress* (t/in.^{2})
(1) R. ex 544 (modified En. 30B). Turned surface, hand polished stabilized 120° C for 24 h.	125	Hoop −28·5 Longitudinal −36·0
(2) R. ex 544 (modified En. 30B). Ground surface, stabilized 120° C for 24 h. Hand polished and finished on metallurgical polishing pad.	125	Longitudinal −19·0
(3) Same surface as for (2), plus anodic pickling in 75% sulphuric acid for 60 s at current density 100 A/ft^2.	125	Longitudinal −1·0
(4) En. 26. Ground surface, stress-relieved 175° C for 1 h. Hand polished.	88	Longitudinal −9·4
(5) Same surface as for (4), plus anodic pickling in 75% sulphuric acid for 60 s at current density 100 A/ft^2.	88	Longitudinal −3·4

***

and a longitudinal stress taken on a circular section fatigue test-piece, and later results illustrate the drop in the surface stress as a result of a particular type of surface preparation. These results were eventually considered, in conjunction with certain fatigue test data.

5. SURFACE PREPARATION

The surface preparation used in these laboratories for aluminium alloys is to dry polish down to 0000 grade emery paper concluding with a two minutes mixed acids etch. It has been shown that this treatment, or an electrolytic etch, or even no further preparation beyond the 0000 finish, has no significant effect on the X-ray stress measured.

The measurements conducted on high tensile steels have been carried out without surface preparation (further to that indicated in Section 4), for one or both of two reasons: firstly, it was desired that the surface condition should not be disturbed, and secondly, the value, as yet uncertain, of the stress imparted to the surface in consequence of surface preparation. Present investigations, though not complete, suggest that this imparted stress is considerably below previously published values.[6]

6. ACCURACY

A theoretical consideration of the limits of accuracy using the technique described above shows that even if vernier readings are in error by 0·01 cm, the error in the final stress figure is well within the usual scatter of points found on the cosec $\theta/\sin^2\psi$ graph. As a result, the narrowest limits quoted for measurements made on aluminium alloys are: $\pm 0{\cdot}3$ for approximately zero stresses, $\pm 1{\cdot}0$ at a 10 t/in.^{2} stress level, and $\pm 2{\cdot}0$ t/in.^{2} at a stress in the region of 20 t/in.^{2} These limits are approximately doubled for high tensile steel measurements.

ACKNOWLEDGEMENTS

The author wishes to acknowledge the work of Mr. G. Munday who was initially responsible for the development in this Laboratory of the technique as applied to aluminium alloys.

The author is also indebted to Mr. W. E. Cooper, Head of the Materials Laboratory, and the Directors of The Fairey Aviation Co. Ltd., for permission to publish this paper.

REFERENCES

(1) THOMAS, D. E. *J. Sci. Instrum.*, **18**, p. 135 (1941).
(2) FROMMER, L., and LLOYD, E. H. *J. Inst. Metals*, **70**, p. 91 (1944).
(3) THOMAS, D. E. *Amer. J. Phys.*, **19**, p. 190 (1948).
(4) GLOCKER, R. *Materialprüfung mit Röntgenstrahlen* (Berlin: Springer-Verlag, 1949).
(5) KLUG, H. P., and ALEXANDER, L. E. *X-ray Diffraction Procedures*, p. 539 (London: Chapman and Hall Ltd., 1954).
(6) BEU, K. E., and KOISTINEN, D. P. *Trans Amer. Soc. Metals*, **48**, p. 213 (1956).

The heating of fluorescent screens bombarded by electrons

By G. D. ARCHARD, A.Inst.P., and P. A. EINSTEIN, Associated Electrical Industries Ltd., Aldermaston, Berks.

[*Paper first received* 26 *November*, 1956, *and in final form* 9 *January*, 1957]

The temperature rises of fluorescent screens under various forms of electron bombardment (such as pulsed or scanned beams) are calculated in terms of screen dimensions and the thermal constants of the phosphor. Fair agreement is found between theory and experiment. Worked examples relating to practical cathode-ray tubes are given.

The light output of fluorescent screens is not only subject to current saturation[1-3] but depends on the temperature of the phosphor. Most phosphors cease to emit light at temperatures of the order of 250° C, but regain fluorescence on cooling. It is, therefore, of interest to determine the heating of fluorescent screens by electron beams, in particular when these are scanned or pulsed.

Müller[4] and Dumond, Watson and Hicks[5] calculated the temperature rise of rotating X-ray targets (corresponding to pulsed radiation). This work cannot be applied to the present case for two reasons: (*a*) electrons penetrate more deeply into phosphors than into customary X-ray targets and produce internal heating; (*b*) phosphors have much lower thermal conductivity than metals and the effects of successive pulses are materially superimposed.

The problem particularly envisaged in this paper is that of a scanned television tube. For the sake of simplicity, it is approached in several stages, in which the heating due to plane radiation (continuous or pulsed) and that due to a cylindrical beam are successively considered, and later combined. It is, of course, realized that the theory presented is only approximate, but it is offered in conjunction with experimental results as an indication of the true situation. It is hoped that further work on this problem may be forthcoming.

HEATING DUE TO PLANE RADIATION

If a phosphor layer of thickness a and thermal conductivity k is mounted on a material of thickness a' and thermal conductivity k', the far side of which is perfectly cooled, the temperature rise at the phosphor surface after infinite time will be:

$$\theta = Q\{(a/k) + [(a' - a)/k']\} \qquad (1)$$

(Anthony[6]), where Q is the rate per unit area at which heat is supplied to the surface.

If the heating is not continuous, but consists of pulses of length t_1 separated by intervals $t_2 - t_1$, the mean rate of supply will be $(t_1/t_2)Q$ and the mean temperature rise after infinite time will be correspondingly less than that given by equation (1). In general, the factor by which Q has to be

multiplied in order to give the mean rise will be less than (t_1/t_2), owing to the fact that the temperature rise is not a linear function of the time (Anthony[6]). A single cycle may be regarded as the combination of a pulse of positive heating of length t_2 superimposed on a similar pulse of negative heating of length $t_2 - t_1 (t_1 \ll t_2)$. Thus in effect this may be regarded as a pulse equal to $t_2 - (t_2 - t_1)$, i.e. t_1, as before. For $t_2 \gg t_1$, the mean temperature time curve obeys roughly a square root law, so that the factor in question is approximately:

$$[\sqrt{t_2} - \sqrt{(t_2 - t_1)}]/\sqrt{t_2} \simeq t_1/2t_2 (t_2 \gg t_1)$$

The mean temperature rise is thus:

$$\theta_{mean} = (t_1/2t_2) Q\{(a/k) + [(a' - a)/k']\} \qquad (2)$$

Superimposed on this temperature rise will be a ripple due to the individual pulses as shown schematically in Fig. 1.

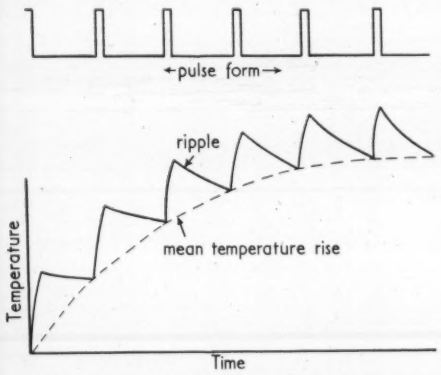

Fig. 1. Temperature variation due to repeated pulses (schematic)

This is estimated as follows. Electrons penetrate matter approximately in accordance with the Thomson–Whiddington law[7] and the heating due to them may be considered to take place in a thickness L of the phosphor, given by:

$$L \simeq h\Phi^2 \qquad (3)$$

where Φ is the accelerating voltage and h depends on the nature of the phosphor (for zinc sulphide at 50 kV, $L \simeq 14\ \mu$). In this, $h = A/\rho Z$, where A = atomic weight, Z = atomic number, ρ = density, a = quantity varying very slowly with atomic number, here about 5×10^{11}; for compounds an average A/Z is applied. It is realized that the Thomson Whiddington law is not followed exactly, but it appears to be a reasonable approximation for present purposes. Results thus obtained should, at any rate, be better than those which would follow from the assumption that all electrons stopped instantaneously at the surface of the phosphor and that their energy was converted into heat only there. Provided that L is small compared with the thickness of the phosphor, the temperature rise due to an individual pulse of length t_1 is given by Carslaw and Jaeger[8] as:

$$\theta_{pulse} = (\alpha Q t_1/kL)[1 - 4i^2\text{erfc}\,(L/2\sqrt{\alpha t_1})] \qquad (4)$$

where $\alpha = k/\rho c$ = diffusivity of phosphor (ρ = density, c = specific heat). In the case of the ripple the nature of the backing is immaterial, provided that the pulse is so short that no appreciable heat penetrates to the far side of the phosphor during the pulse. The function i^2erfc, tabulated by Carslaw and Jaeger, is given by:

$$i^2\text{erfc}\,x = \int_x^\infty \left(\frac{1}{\sqrt{\pi}} e^{-\xi^2} - \xi\,\text{erfc}\,\xi\right) d\xi$$

where

$$\text{erfc}\,x = \int_x^\infty \frac{2}{\sqrt{\pi}} e^{-\xi^2}\, d\xi$$

For zinc sulphide and $t_1 < 100\ \mu$s, the i^2erfc term is negligible.

When a steady state is reached (as on the right of Fig. 1), each pulse appears as a single saw-tooth, numerically given by equation (4), superimposed on a steady rise (dotted line), numerically given by equation (2). The effective temperature rise over a whole pulse, which will be correlated in the next section with the mean light output over a whole pulse, is thus of the order of $(\theta_{mean} + \frac{1}{2}\theta_{pulse})$, that is:

$$\theta_{plane} = (t_1/2t_2) Q\{(a/k) + [(a' - a)/k']\} + \\ + (\alpha Q t_1/2kL)[1 - 4i^2\text{erfc}\,(L/2\sqrt{\alpha t_1})] \qquad (5)$$

HEATING DUE TO CYLINDRICAL BEAM

If a uniform cylindrical beam of radius R falls on a phosphor of thermal conductivity k mounted on an infinitely thick base of thermal conductivity k', the ultimate temperature rise in the spot will be:

$$\theta = (QR/k) \int_0^\infty \frac{J_0(\lambda r) J_1(\lambda R)(k' sh\lambda a + k ch\lambda a)}{\lambda(k sh\lambda a + k' ch\lambda a)}\, d\lambda \qquad (6)$$

(this expression is based on the theory of Carslaw and Jaeger Ref. 8, p. 187) where J_0 and J_1 are Bessel functions of the first kind, of zero and unit order respectively, and r is the distance from the centre of the spot. This temperature distribution has been numerically computed for various values of R/a. The rise is greatest in the centre of the spot and falls to the order of half at the edges. For most of the practical cases considered it is found that the average rise over the whole spot (which is the rise observed) is approximately 2/3 of that at the centre. This factor was chosen because exact calculations based on equation (6) showed that the temperature distribution had roughly a bell-shaped form, still being finite at the geometrical edges of the spot. A study of several practical cases suggested that, whereas the ratio of average to peak value ranged from $\frac{1}{2}$ to 1 for extreme values of R/a, the best general compromise was 2/3.

Even at the centre of the spot, the temperature rise is not so high as it would have been if plane radiation had been used. Equation (6) shows that the ratio of temperature rise at the centre of the spot to temperature rise for plane radiation is:

$$\theta_{cyl}/\theta_{plane} = f(R/a) \qquad (7)$$

as plotted in Fig. 2. The curve is valid for all values of k' exceeding 0·002, and so holds for both glass and metal backed phosphors. Thus, the ratio of *average* temperature rise (cylindrical radiation) to temperature rise (plane radiation) is approximately (2/3) $f(R/a)$.

In order to find the heating due to an invividual pulse, equation (6) must be subjected to a Laplace transformation. This results in expressions so cumbersome as to be useless. A reasonable estimate may be obtained, however, by applying the factor $f(R/a)$ to the whole of equation (5), (the transient, or pulse, term as well as the term relating to steady heating) which gave the corresponding result for plane radiation. The total observed rise for repeated pulses of cylindrical radiation thus becomes:

$$\theta_{cyl} = (2/3) f(R/a)\left((t_1/2t_2)Q\left\{(a/k) + [(a' - a)/k']\right\} + \right.$$
$$\left. + (\alpha Q t_1/2kL)[1 - 4i^2\mathrm{erfc}\,(L/2\sqrt{\alpha t_1})]\right) \quad (8)$$

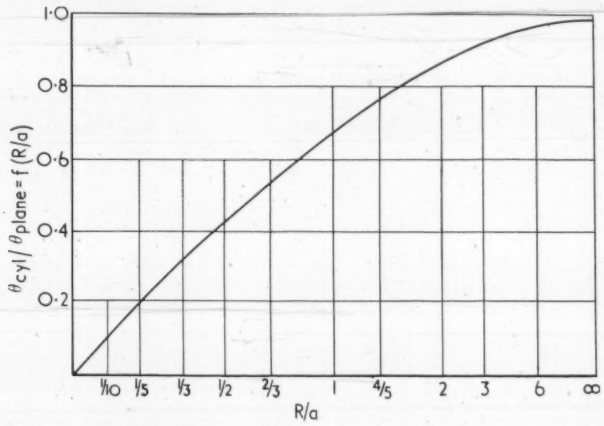

Fig. 2. Factor for converting effect of plane radiation into corresponding effect averaged over cylindrical beam $[f(R/a) = (2/\pi)\tan^{-1}(R/a)]$.
R, radius of beam; a, thickness of phosphor.

COMPARISON WITH EXPERIMENT

A cylindrical 50 kV electron beam of uniform current density was deflected on to a phosphor sample in pulses of various lengths from 10 μs upwards. The resulting light actuated a photomultiplier, the output of which was displayed on a cathode-ray tube. Fig. 3 is a typical photograph showing loss of output ("droop") as the phosphor became heated during the pulse. The effect increased with increase in current density, pulse length or pulse repetition frequency.

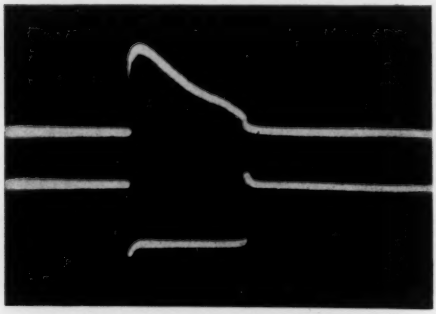

Fig. 3. Light output (*versus* time) pulse

Phosphor, Levy and West G 86 [ZnS(Ag)]; current density, 2·7 A/cm²; beam velocity, 50 kV; time, 200 μs; single pulse. [Lower trace: deflecting pulse (inverted).]

The ratio of observed light output averaged over a pulse to that which would have been expected in the absence of heating was determined—curves linking this ratio with temperature exist (Ref. 3, p. 409), but for the purpose of the present work, were derived independently (Fig. 4).

As an example, a cylindrical beam with $R = 0{\cdot}004$ cm was directed in pulses 100 μs long on to a phosphor sample 0·01 cm thick mounted on metal ($k' \gg k$). The repetition

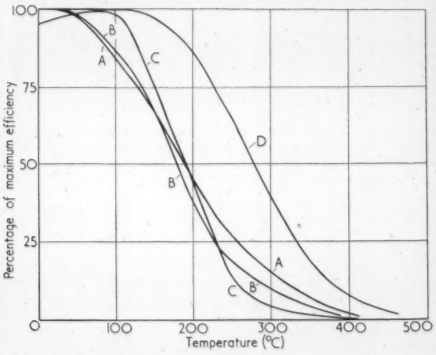

Fig. 4. Comparative efficiencies of phosphors with temperature change (50 kV, low current density)

Curve *A*, Derby, ZnO (X 68); curve *B*, Derby 340 [ZnSCdS(Ag)]; curve *C*, Levy and West, ZnS(Ag) (G 86); curve *D*, Willemite (British Thomson-Houston sample).

rate was 50 pulses per second, the current density 0·9 A/cm^2 and the accelerating voltage 50 kV. The thermal conductivity of the phosphor, determined by settling a sample from liquid suspension on to a copper block, placing another block on top, and carrying out heat flow measurements, was approximately 4×10^{-4} cal cm^{-1} °C^{-1} s^{-1}. The quantities to be inserted in equation (8) are thus: $Q = 0{\cdot}9 \times 50000/4{\cdot}2$ cal/cm^2, $t_1 = 10^{-4}$ s, $t_2 = 1/50$ s, $a = 0{\cdot}01$ cm; k' may be taken as ∞, L as 14×10^{-4} cm, α as 8×10^{-4}. R/a is 0·4, so, from Fig. 2, $f(R/a) = 0{\cdot}37$. These give:

$$\theta_{csl} = 350° \text{ C}.$$

The experimentally observed output was 4% which corresponded to a temperature rise of 280° C.

Comparison between theory and experiment is given for several other conditions in Fig. 5. In view of the approximations made, the agreement may be regarded as fair.

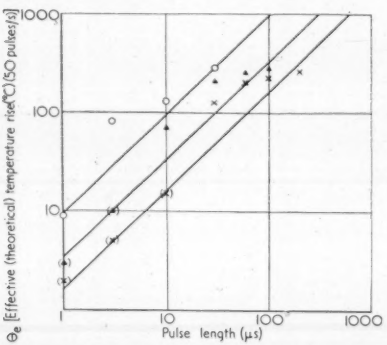

Fig. 5. Comparison of theoretical phosphor temperature with estimated temperatures (derived from efficiencies). [ZnS (Ag) G86]. Accelerating voltage, 50 kV

Estimated phosphor temperatures: ○ = 2·7 A/cm^2; ▲ = 0·9 A/cm^2; × = 0·45 A/cm^2; —— = theoretical.

HEATING DUE TO SCANNED BEAM

When a raster containing many lines is scanned by a beam of radius R at n frames per second, any elementary disk of radius R falls under the beam n times per second, but its temperature rise is greater than that calculated for a *pulsed* beam having n pulses per second, because the temperature of neighbouring disks is also raised.

If the raster is scanned so quickly that the phosphor at one corner of the frame has not cooled appreciably by the time the spot has reached the opposite corner, the temperature rise will correspond to plane continuous radiation. If the raster is scanned slowly, the temperature rise at one point will not be affected by that several spot radii away, and will nearly correspond to cylindrical pulsed radiation. In general, the temperature rise will lie between these in a manner dependent on the speed of scanning.

Equations (2) and (4) show that the mean temperature rise for pulsed radiation of a given pulse length depends on the repetition frequency, while the ripple does not. When the repetition frequency is high, the mean rise exceeds the ripple and when the repetition frequency is low the ripple exceeds the mean rise. It is, therefore, a reasonable compromise to calculate, for the case of a scanned beam, the mean rise on the assumption that the radiation is plane, and the ripple on the assumption that it is cylindrical. This means that the first term of equation (5) must be added to the second term of equation (8), giving:

$$\theta_{scan} = (t_1/2t_2)Q\left\{(a/k) + [(a' - a)/k']\right\} + \\ + (2/3)f(R/a)\,(\alpha Q t_1/2kL)[1 - 4i^2\text{erfc}\,(L/2\sqrt{\alpha t_1})] \quad (9)$$

(t_1 now signifies time to move across one spot width). This procedure may appear somewhat arbitrary, but it is the nearest approximation which can be applied under the circumstances. For values of (R/a) in the region of unity or higher, the error should not be great, and, in any case, it is likely to be less than that which would be introduced by merely regarding the radiation as plane.

The principle will be illustrated by considering an 18 in. television screen, which uses a raster of approximate dimensions 35 × 27 cm, with 400 lines at 50 frames per second. Suppose a layer of phosphor 0·0025 cm thick is mounted on glass 0·5 cm thick, and that the beam current is 200 μA at 20 kV. In order to cover the screen without gaps the spot diameter must be 0·06 cm. Thus, current density in spot equals 0·07 A/cm^2, and spot velocity equals 7×10^5 cm/s. Hence: $Q = 0{\cdot}07 \times 20000/4{\cdot}2$ cal/cm^2; $a = 2{\cdot}5 \times 10^{-3}$ cm, $a' = 0{\cdot}5$ cm, $\alpha = 8 \times 10^{-4}$, $k = 4 \times 10^{-4}$, $k' = 2 \times 10^{-3}$, $t_1 = 8{\cdot}5 \times 10^{-8}$ s, $t_2 = 1/50$ s, $L = 2{\cdot}2 \times 10^{-4}$ cm [corresponding to 20 kV; equation (3)]. Also $R/a = 12$, so that $f(R/a) \simeq 1$. This gives a temperature rise equal to 0·26° C. Since the time per spot width is small compared with the rise time of typical cathode-ray tube phosphors (5 μs) and the current density is 0·07 A/cm^2, there should be little saturation so that the phosphor will be working at maximum efficiency.

Suppose now that the same final picture brightness is required from a projection system, producing a final image of the same area (35 × 27 cm), using an $f/1$ lens to project the image. If the lens has a diameter and focal length 5 cm and field of view 55°, then for the best optical conditions the phosphor will have to have dimensions 6·1 × 4·7 cm, and to be situated 5·9 cm from the lens. The optical magnification will be 5·7. The lens receives 15% of the light emitted from the phosphor and transmits 90% of this. The phosphor must, therefore, have $5{\cdot}7^2/0{\cdot}15 \times 0{\cdot}9 = 250$ times the brightness required in the final image, so that the spot current density must be $0{\cdot}07 \times 250 = 18$ A/cm^2.

Suppose first that the phosphor is mounted on glass as before, the raster now having dimensions 6·1 × 4·7 cm. Equation (9) gives a temperature rise equal to 65° C. In this case, temperature is beginning to limit output.

Now suppose that the phosphor is mounted on metal. As the screen has, in this case, to be viewed from the electron side, the light yield will be twice the former, so that half the former loading is required, namely 9 A/cm^2. Equation (9) now gives a temperature rise equal to 11° C. If the phosphor is made four times as thick, the rise is still less than 13° C, so that the power in the beam could be raised appreciably before temperature limitation sets in.

CONCLUSIONS

Pulses of less than 1/2 J/cm^2 (e.g. 50 kV, 1 A/cm^2, 10 μs) impinging fifty times per second on a phosphor layer

1/10 mm thick, mounted on a 5 mm thick glass base cooled on the far side, do not cause temperature limitation of light output. Thus, for example, existing television tubes should not suffer from temperature limitation, except possibly in the case of the highest rated projection tubes. Even so, considerable reduction in the temperature rise of the phosphor can be brought about by mounting on a metal base.

ACKNOWLEDGEMENTS

The authors are indebted to Mr. M. E. Haine and the late Dr. G. Liebmann for helpful discussions, Mr. J. N. Esterson and Mr. G. F. Fooks for experimental assistance, and Dr. T. E. Allibone, Director of this Laboratory, for permission to publish this paper.

REFERENCES

(1) MARTIN, S. T., and HEADRICK, L. B. *J. Appl. Phys.*, **10**, p. 116 (1939).
(2) BRIL, A., and KRÖGER, F. A. *Philips Tech. Rev.*, **12**, p. 120 (1950).
(3) BRIL, A., and KLASENS, H. A. *Philips Res. Rep.*, **7**, p. 401 (1952).
(4) MULLER, A. *Proc. Roy. Soc. A*, **125**, p. 507 (1929).
(5) DUMOND, J. W. N., WATSON, B. B., and HICKS, B. *Rev. Sci. Instrum.*, **6**, p. 183 (1935).
(6) ANTHONY, M. L. *Amer. Soc. Mech. Engrs*, p. 236 (1951).
(7) WHIDDINGTON, R. *Proc. Roy. Soc. A*, **89**, p. 554 (1914).
(8) CARSLAW, H. S., and JAEGAR, J. C. *Conduction of Heat in Solids*, pp. 61, 187, 373 (London: Oxford University Press, 1947).

The penetration of irregularly-shaped particles through an airborne-dust elutriator

By J. G. DAWES, Ph.D., A.M.I.Min.E., F.Inst.P., G. K. GREENOUGH, B.Sc., and J. S. SEAGER, B.Sc.,
Safety in Mines Research Establishment, Ministry of Fuel and Power, Sheffield

[*Paper received* 9 *July*, 1956]

A connexion is established between the shape-factor distribution relating the projected-area diameters (D_M) and the Stokes' diameters (D_S) of particles in a dust cloud, and the penetration efficiency $E(D_M)$ of a standard elutriator for those particles determined by the microscope evaluation of thermal precipitator samples taken with and without the elutriator. From the measured characteristic $E(D_M)$ in a given dust cloud, it is possible to estimate the mean value of the shape factor D_S/D_M of the cloud, and its coefficient of variation.

1. INTRODUCTION

Walton[1] has given the theory of elutriators which can be used to obtain a size-selected fraction of airborne dust. They are used, in conjunction with a dust-collecting device, to obtain a representative sample of the portion of the dust which is likely to penetrate the respiratory system and reach the alveoli of the human lung.[2] In the theory the relevant parameter for describing the size of a dust particle is the Stokes' diameter (D_S). This is defined as the diameter of a sphere of the same material as the particle, which has the same terminal settling velocity as the particle when they are isolated in large bodies of still air. However, with the most common airborne-dust sampling instrument used for aetiological studies of pneumoconiosis in Great Britain, namely the thermal precipitator,[3] the size of the dust particles sampled is determined in terms of their projected area diameters (D_M). The projected area diameter of a particle is the diameter of the circle which has the same area as the particle when it is viewed under a microscope.

The projected area diameter D_M and the Stokes' diameter D_S of a particle may be related by a shape factor $\zeta = D_S/D_M$. The relation between the Stokes' diameters (D_S) of particles entering an elutriator and the proportion of particles of a given Stokes' diameter which penetrate the elutriator is called the Stokes'-diameter penetration characteristic $E(D_S)$. This is equal to the Stokes' diameter collection efficiency characteristic of a sampling instrument if the efficiency of the dust collection system of the instrument is 100% for all particles capable of penetrating the elutriator. There is a corresponding, but not identical, penetration characteristic based on D_M, i.e. $E(D_M)$, and it is necessary to distinguish between $E(D_S)$ and $E(D_M)$.

For spherical particles, since $D_M = D_S$, $E(D_M)$ is the same as $E(D_S)$, but such particles are of rare occurrence in the dust clouds encountered in industries such as coal mining.

When an airborne coal dust cloud is sampled by an instrument fitted with a standard elutriator,[2] which is designed so that only 50% of particles of unit density and diameter 5 μ, and none of size greater than $\sqrt{50}\,\mu$, would penetrate the elutriator if all particles were spherical, it is found that many particles of projected area diameter greater than $\sqrt{50}\,\mu$ are collected on the sample. Moreover, the penetration characteristic $E(D_M)$ is of a very different form from the characteristic $E(D_S)$ predicted by Walton's theoretical work which used the D_S convention for defining particle size. The reason for this is that in a dust cloud made up of irregularly-shaped particles, within a group of particles all having the same value of D_S, particles exist which cover a range of different microscope sizes D_M. Similarly for a group of particles of given size D_M, there is an associated distribution of Stokes' diameter sizes.

Data which demonstrate this have been given by Timbrell[4] who has proposed a bivariate frequency function for describing the frequency of occurrence, in a dust cloud, of particles with associated values of D_S and D_M. [The principal mathematical properties of a bivariate frequency function are described in a number of standard textbooks on statistics (e.g. Mood[5]).] It is convenient, when describing the properties of the bivariate distribution characterizing a given dust, to make use of appropriate shape-factor distributions. In the present context the relevant one is the frequency function of the shape factor $\zeta = D_S/D_M$ for particles in the size range D_M to $D_M + \delta D_M$. This function $p_M(\zeta)$ is, in general, different for different values of D_M, but will only

change slightly for a small change in D_M. For any value of D_M, the proportion of particles with shape factor between ζ and $\zeta + \delta\zeta$ is $p_M(\zeta)\delta\zeta$ and $\int_0^\infty p_M(\zeta)d\zeta = 1$. Since for constant D_M, $\delta(\zeta) = \delta D_S/D_M$, the proportion of particles of size D_M which have Stokes' diameter between D_S and $D_S + \delta D_S$ is

$$p_M(\zeta)\delta\zeta = (1/D_M)p_M(\zeta)\delta D_S \qquad (1)$$

One object of the present paper is to establish the relation between the penetration characteristics $E(D_S)$ and $E(D_M)$ as a function of $p_M(\zeta)$. Another is to indicate how information about the shape-factor distribution of a dust can be obtained from an experimental determination of the characteristic $E(D_M)$.

2. PERFORMANCE OF THE STANDARD ELUTRIATOR WITH SPHERICAL PARTICLES

A standard elutriator[2] designed for use with the thermal precipitator is shown in Fig. 1. The general equation given by Walton[1] for its performance is

$$E(D_S) = 1 - f/f_c \qquad (2)$$

where $E(D_S)$ is the penetration efficiency of the elutriator for particles of Stokes' diameter D_S and terminal settling velocity f; f_c is the terminal velocity of the largest size of particle which can just penetrate the elutriator. In the case of the standard elutriator, for which 50% of unit density spheres of 5 μ diameter penetrate the system, the penetration efficiency for spheres of density ρ is

$$E(D_S) = 1 - \rho D_S^2/50 \qquad (3)$$

and the largest sphere penetrating the elutriator and collected by the instrument sampling the cloud of spherical particles is of diameter $(50/\rho)^{\frac{1}{2}}$ microns.

The applicability of equation (3) was tested by two experiments (*A* and *B*) in which two thermal precipitators, one of them fitted with the standard elutriator (Fig. 1), were used to take samples simultaneously in a cloud of wax spheres.

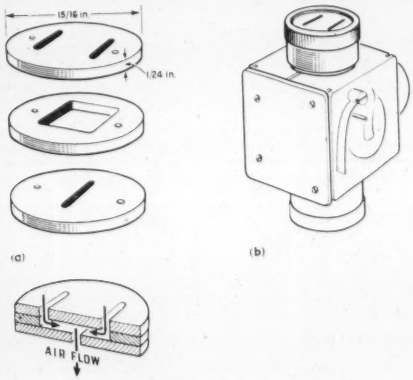

Fig. 1. Size selector for thermal precipitator
(*a*) Component parts. (*b*) Mounted on thermal precipitator head.

The penetration characteristic was determined by obtaining the elutriator efficiency for a number of different size ranges, using microscope evaluation. This was determined as the ratio of the number of particles collected in the given size range in the sample taken with the thermal precipitator fitted with the elutriator, to the number in the same size range in the sample taken with the ordinary thermal precipitator. It was assumed that the particles were true spheres and that D_M, the measured size parameter, was equal to D_S, the Stokes' diameter. On the basis of this assumption the experimentally determined penetration characteristic $E(D_M)$ was equivalent to the required characteristic $E(D_S)$. Fig. 2 compares the derived value of $E(D_S)$ and the corresponding theoretical characteristic.

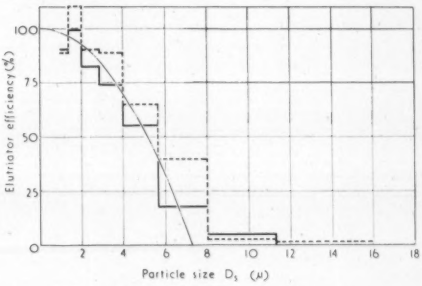

Fig. 2. Size selection characteristics of standard elutriator

· · ———— · · theoretical efficiency for spheres of density $\rho = 0{\cdot}94$ g/cm^3.

Experimental results for wax "spheres" of density $\rho = 0{\cdot}94$ g/cm^3:

———— experiment *A*.
– – – – – experiment *B*.

The agreement between theory and experiment is reasonable in view of the experimental errors involved. These include statistical counting errors, microscope sizing errors, the possibility of air inclusions in the wax spheres and of the lack of true sphericity in the wax particles in the test cloud. No satisfactory evidence of the existence of the two latter forms of error was, however, obtained by microscope examination of the samples.

3. PERFORMANCE OF THE STANDARD ELUTRIATOR WITH NON-SPHERICAL PARTICLES

Let the number-frequency size distribution of the dust cloud drawn into the elutriator be $f(D_M)$, where $\int_0^\infty f(D_M)dD_M = 1$, the size of the particles being measured by microscope examination of samples collected from the cloud. If the number of particles entering the elutriator is N, then the number of particles in the size range D_M to $D_M + \delta D_M$ is $Nf(D_M)\delta D_M$. The number of these contributing to the size range D_S to $D_S + \delta D_S$ is $Nf(D_M)\delta D_M(1/D_M)p_M(\zeta)\delta D_S$ from equation (1).

The proportion of particles in the size range D_S to $D_S + \delta D_S$ that penetrate the elutriator is $(1 - \rho D_S^2/50)$ [equation (3)]. Consequently the number of particles in the size range D_S to

$D_S + \delta D_S$ which are also in themicroscope size range D_M to $D_M + \delta D_M$ and which penetrate the elutriator is

$$Nf(D_M)\delta D_M(1/D_M)p_M(\zeta)(1 - \rho D_S^2/50)\delta D_S$$

for $0 \leqslant D_S \leqslant (50/\rho)^{\frac{1}{2}}$. For $D_S > (50/\rho)^{\frac{1}{2}}$ the number is zero.

The total number of particles in the size range D_M to $D_M + \delta D_M$ penetrating the elutriator is

$$Nf(D_M)\delta D_M \int_0^{(50/\rho)^{1/2}} \frac{1}{D_M} p(\zeta)\left(1 - \frac{\rho D_S^2}{50}\right) dD_S$$

Since the number of particles entering the elutriator in this size range is $Nf(D_M).\delta D_M$ the proportion of particles of size D_M which penetrate the elutriator (i.e. the efficiency of the elutriator for particles of microscope size D_M) is

$$E(D_M) = \int_0^{(50/\rho)^{1/2}} p_M(\zeta)\left(1 - \frac{\rho D_S^2}{50}\right)\frac{dD_S}{D_M}$$

$$= \int_0^{(50/\rho)^{1/2}} p_M(\zeta)\left(1 - \frac{\zeta^2 \rho D_M^2}{50}\right)\frac{dD_S}{D_M}$$

Then, effecting a change of variable and the corresponding limit

$$E(D_M) = \int_0^{(50/\rho)^{1/2}/D_M} p_M(\zeta)\left(1 - \rho\zeta^2 \frac{D_M^2}{50}\right) d(\zeta)$$

For convenience, write

$$D_M\left(\frac{\rho}{50}\right)^{1/2} = m$$

then

$$E(D_M) = \int_0^{1/m} p_M(\zeta)(1 - \zeta^2 m^2) d(\zeta) \qquad (4)$$

Thus, given the frequency function $p_M(\zeta)$ for different values of m, the collection efficiency of the standard elutriator for the corresponding value of the microscope diameter D_M can be computed.

In order to explore the validity of equation (4), a series of experiments were carried out in the dust tunnel[6] at this Establishment. The shape factor distribution $p_M(\zeta)$ for a number of values of D_M and the size-selection characteristic $E(D_M)$ of the standard elutriator were obtained for a dust cloud produced by dispersing coal dust which had been

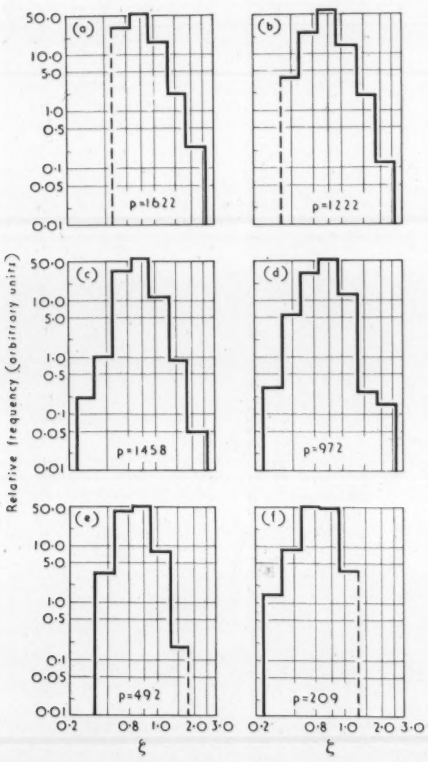

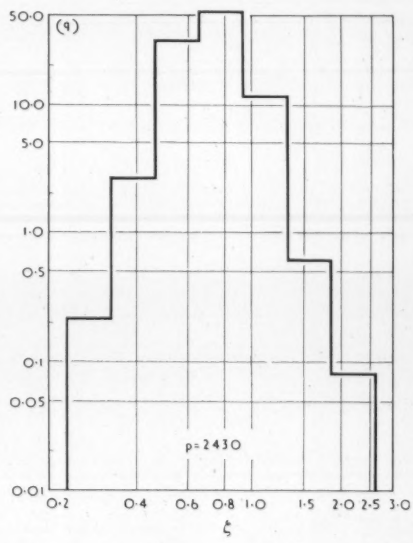

Fig. 3. Observed values of ζ for given ranges of D_M. Conifuge data on cloud of dispersed under-belt dust

(*a*) D_M range $\sqrt{2}$–2 μ. (*b*) D_M range 2–2$\sqrt{2}$ μ. (*c*) D_M range 2$\sqrt{2}$–4 μ. (*d*) D_M range 4–4$\sqrt{2}$ μ. (*e*) D_M range 4$\sqrt{2}$–8 μ. (*f*) D_M range 8–8$\sqrt{2}$ μ. (*g*) Assumed average distribution of ζ combined data from D_M ranges 2$\sqrt{2}$–4 and 4–4$\sqrt{2}$ μ.

collected from deposits formed under a conveyor belt in a coal mine. Inspection of the thermal precipitator samples produced no evidence that the airborne cloud contained aggregates, and it was assumed that the dust cloud-forming mechanism[7] had been successful in dispersing the bulk coal dust into a cloud of single particles.

The Conifuge,[8] a sampling device which grades the dust particles according to their Stokes' diameter, was used to determine the shape-factor distribution of the dust cloud. Comparison of the coal-dust particles with microscopic wax spheres (see Section 2) deposited on the same sample enabled the Stokes' diameters of the dust particles to be estimated. For a series of zones on the sampling slide, which corresponded to certain ranges of Stokes' size, the numbers of particles in different projected-area diameter size ranges were determined. The data from the several zones were entered into the rows of a two-way table, each cell of which then contained the number of particles for which D_S fell in a certain range and D_M fell in a certain range. From the columns of this table the distributions of D_S for the stated ranges of D_M shown in Figs. 3(*a*) to (*f*) were constructed. The shapes of the distributions, in so far as they are complete, are similar and it was assumed that for practical purposes the shape of $p_M(\zeta)$ was independent of D_M for the range of particle sizes considered. It will be noted that values of $\zeta > 1$ occur. This may be due to a number of factors. The effect could be produced by counting errors or by differences in density between particles in the cloud; or it may arise because some platelet or needle-shaped particles of coal are deposited on end on the slide. That this last phenomenon can occur has been demonstrated on similar samples which have been metal shadowed and then examined under the electron microscope.

The assumed average distribution for $p_M(\zeta)$, on the appropriate relative scale, is shown in Fig. 3(*g*). This assumption makes the computation of $E(D_M)$ from equation (4) an easy task. The computed function $E(D_M)$ is shown in Fig. 4,

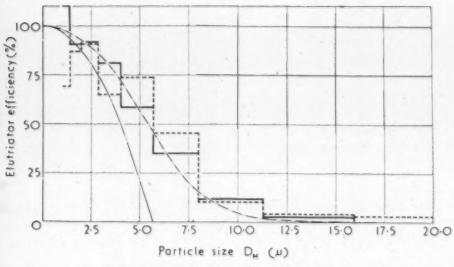

Fig. 4. Size selection characteristic for coal dust cloud

· — · — · computed characteristic assuming equation (4) and using data from Fig. 3(*g*).

· · — — — · · theoretical efficiency for spheres of density $\rho = 1{\cdot}57$ g/cm³.

Observed characteristics:

———— experiment C.

– – – – – – experiment *D*.

together with the results (*C* and *D*) of two experimental determinations of $E(D_M)$ for different size ranges, which were obtained from the thermal precipitator samples taken in the cloud in the dust tunnel, in the same way as in the previous experiment with wax spheres.

The agreement between the direct and indirect methods of deriving the size-selection characteristic is sufficiently good to justify both the use of equation (4) and the assumption that for practical purposes the distribution $p_M(\zeta)$ may be regarded as relatively independent of particle size.

In this way, a connexion between the Stokes' diameter penetration characteristic of an elutriator and its projected-area diameter penetration characteristic in a given dust cloud has been established.

4. DERIVATION OF PARAMETERS OF AVERAGE SHAPE-FACTOR DISTRIBUTION

Hitherto the experimental methods for obtaining information about the shape-factor distributions of a dust cloud have involved the use of fairly complex equipment; for example, the Conifuge,[8] which is not commercially available, is difficult to manufacture and demands the use of power supplies which are not always available in certain parts of many coal mines. The theory developed in Section 3 leads to the possibility that information about the shape-factor distribution of a dust cloud can be obtained by the use of simple equipment, namely two thermal precipitators, one fitted with a standard elutriator. Since in any case one thermal precipitator is required to obtain information on the concentration and size distribution of the dust cloud, the extra equipment necessary to provide data on the shape-factor distribution of the dust is the thermal precipitator fitted with the elutriator, and the sample evaluation techniques used are those adopted in usual thermal precipitator practice.

For practical purposes it appears that the distribution of the shape factor D_S/D_M is not greatly dependent on the value of D_M for which it is determined and, in principle at least, it is possible to obtain the average distribution of D_S/D_M of a dust cloud by the application of an inverse form of equation (4) to experimental results for $E(D_M)$.

It is impracticable, however, to determine $E(D_M)$ by microscope counting of thermal precipitator samples unless the extent of the ranges within which the particles are classified according to size progressively increases with particle size. This is so because of the difficulty of assigning different values of projected area diameter to irregularly-shaped particles of about the same size.

Even though the size ranges for the larger particles are greater than for the smaller ones, the numbers of larger particles present are much smaller in airborne dust clouds of the type usually encountered,[9] especially in the samples taken with the thermal precipitator fitted with the elutriator. Consequently, even though the microscopist evaluating the samples devotes particular attention to counting and sizing the larger particles, the experimental error of the ratio $E(D_M)$ for the larger sizes is of necessity higher than for the smaller particles.

Thus when attempting analysis of the $E(D_M)$ curve to obtain the shape-factor distribution, it is difficult to reconstruct a sufficiently accurate version of the smooth $E(D_M)$ curve from the average values for ranges of D_M which themselves are of variable accuracy, and which are all that experiments can yield.

Furthermore, whereas the efficiency characteristic $E(D_M)$ can be derived from the shape-factor distribution [using equation (4)] by integration, which reduces the effect of minor fluctuations due to experimental errors, the reverse

process of deducing the shape-factor distribution from the efficiency characteristic involves the use of derivatives which exaggerates the effects of experimental errors. Consequently, analysis directed at determining the form of the shape-factor distribution from the experimentally determined elutriator efficiency characteristic is not likely to be reliable. But, as will be shown, the efficiency characteristic is not sensitive to

series of characteristics shown in Fig. 5 were computed assuming the shape-factor distributions shown for all values of D_M and unit density particles. It will be noted that, even though there is a wide variation in the form of the shape-factor distributions assumed, there is not a large change in the general form of the size-selection characteristic.

However, if a relation is sought between the mean of the

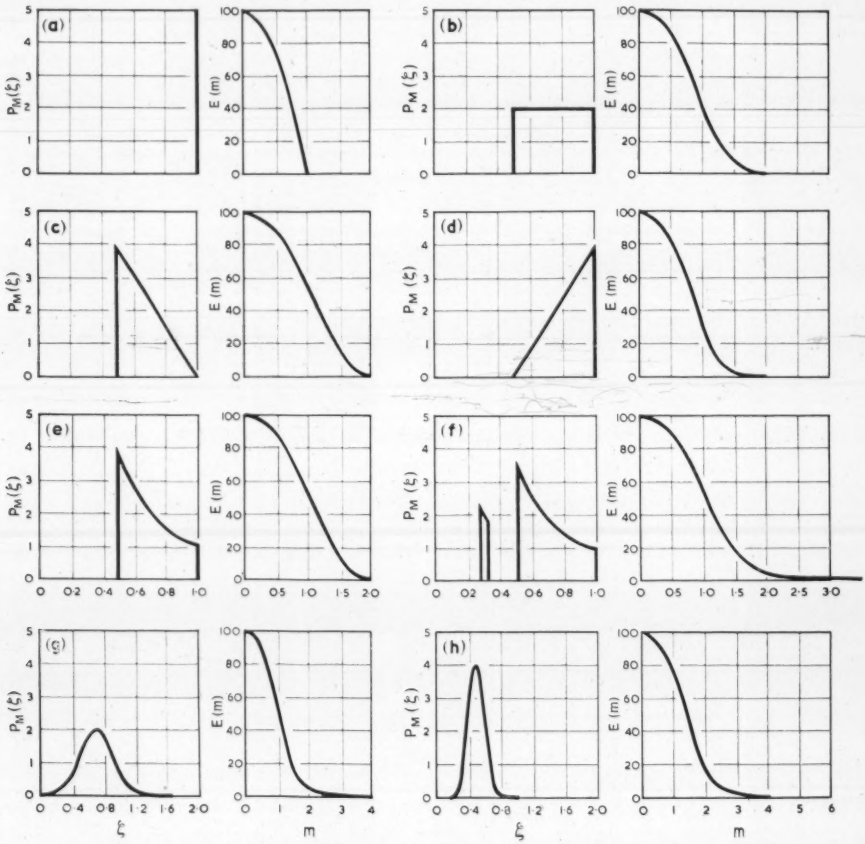

Fig. 5. Assumed ζ distributions and corresponding computed size-selection characteristics

variations in the details of the shape-factor distribution, which are reduced in effect by integration in the same way as experimental errors, and it is possible to establish relations between certain parameters of $E(D_M)$ and certain key parameters of $p_M(\zeta)$, which are almost independent of the form of the shape-factor distribution.

In order to explore the variation of the penetration characteristic of the standard elutriator as a function of the shape-factor distribution of the dust cloud sampled, the shape-factor distribution and the value of D_M for which the collecting efficiency is 50%, that shown in Fig. 6(*a*) is obtained. Similarly, the relation between the coefficient of variation of the shape-factor distribution and the ratio of the diameter for which the penetration efficiency is 10% to that for which it is 50% is shown in Fig. 6(*b*). The values of the parameters for the experimental data discussed in Section 3 are shown on Fig. 6.

If now the penetration characteristic of the standard

elutriator is determined by sampling in a given dust cloud with two thermal precipitators, one of which is fitted with the elutriator, and the samples are evaluated by microscope inspection, then if the projected area diameters for which the penetration efficiency is 10% and that for which it is 50% are determined, the mean of the average shape-factor distribution of the dust cloud sampled $[p_M(D_S/D_M)]$, and its coefficient of variation can be estimated by using the relations shown in Fig. 6.

The parameters obtained for the distribution $p_M(D_S/D_M)$

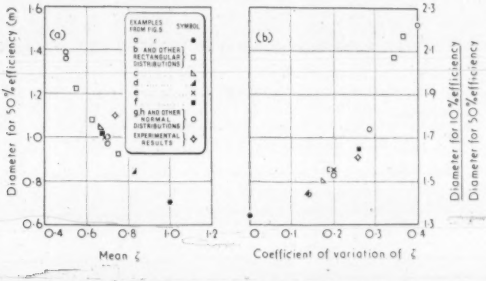

Fig. 6. Relations between parameters of the shape factor distribution and parameters of the size-selection characteristic

are useful for describing the dust cloud, and are of practical value as they can be an aid to distinguishing between different dust clouds of a given kind of material and to identifying the onset of aggregation in a dust cloud.

ACKNOWLEDGEMENTS

The authors wish to thank the Ministry of Fuel and Power for permission to publish this paper. They also wish to thank the Director and Mr. R. J. Hamilton of the National Coal Board Mining Research Establishment for the loan of the prototype Conifuge used in the experiments.

REFERENCES

(1) WALTON, W. H. *Brit. J. Appl. Phys., Supp.* 3, **5**, p. S 29 (1954).

(2) DAVIES, C. N. *Brit. J. Indust. Med.*, **9**, p. 120 (1952).

(3) GREEN, H. L., and WATSON, H. H. *Medical Research Council, Special Report* 199 (London: H.M. Stationery Office, 1935).

(4) TIMBRELL, V. *Brit. J. Appl. Phys. Supp.* 3, **5**, p. S 86 (1954).

(5) MOOD, A. M. *Introduction to the Theory of Statistics* (London: McGraw-Hill Publishing Co. Ltd., 1950).

(6) BURDEKIN, J. T., DAWES, J. G., and SLACK, A. *Safety Mines Res. Establ. Res. Rep.*, **141** (1957).

(7) HATTERSLEY, R., MAGUIRE, B. A., and TYE, D. *Safety Mines Res. Establ. Res. Rep.*, **103** (1954).

(8) SAWYER, K. F., and WALTON, W. H. *J. Sci. Instrum.*, **27**, p. 272 (1950).

(9) WYNN, A. H. A., and DAWES, J. G. *Safety Mines Res. Establ. Res. Rep.*, **28** (1950).

Electron microscope and diffraction studies of 7% chromium-molybdenum steels

By BETTY E. WILLIAMS, National Physical Laboratory, Teddington, Middlesex

[*Paper first received* 25 *May*, 1956, *and in final form* 7 *February*, 1957]

An investigation into the structural properties of some 7% chromium-molybdenum creep resisting steels has been carried out using electron microscopy and diffraction. The presence of fine precipitate of titanium carbide in good creep steels is observed.

The work described in this paper forms part of a larger investigation, the object of which was to improve the strength at high temperature of ferritic steels containing enough chromium to make them oxidation resistant at 600° C. When the work was started, it had been already shown that a steel containing 7% of chromium, 2% of molybdenum, 0·5% of titanium and 0·15% of carbon sometimes exhibited very good creep resistance when tested under standard conditions (tensile stress of 5 t/in.^{2} at 650° C) but that it did not always display these good qualities; the object of the investigation was to discover the cause of the difference between those samples which had good creep resistance, and those which had not.

Steels of this composition consist at the temperatures at which they are heat-treated (950–1250° C) of a mixture of α-iron, γ-iron and small hard crystals of titanium carbide. Both forms of iron contain some dissolved carbon and titanium. When the steels are cooled from the heat-treatment temperature the γ-iron is converted to α-iron, but forms a microscopically recognizable separate constituent. When the steels are subsequently heated to 600–750° C, both the α-iron present at the heat-treatment temperature, and that formed from γ-iron during subsequent cooling, precipitate their dissolved carbon in the form of finely dispersed carbide particles. These particles can rarely be seen with the optical microscope, and since they were thought to exert an important

influence on the creep resistance of the steels, they were studied in detail with the electron microscope, and by X-ray diffraction and electron diffraction.

Four techniques of examination were used:

(i) electron microscopy of replicas of the surfaces of polished and etched specimens;
(ii) chemical extraction of the carbides followed by X-ray diffraction;
(iii) electron microscopy and electron diffraction of chemically extracted residues;
(iv) electron microscopy and electron diffraction of extraction replicas.

DESCRIPTION OF TECHNIQUES

(i) *Preparation of replicas for electron microscopy.* A positive all-metal replica technique was used,[1,2] since Formvar replicas had proved uninformative and of too low resolution. To prepare an all-metal replica, it is necessary to coat the surface of polished and etched metal specimens with a very thin film, about 20 Å, of a hydrophilic material (in this case boron oxide[3]) to facilitate subsequent stripping. This coating is carried out in a vacuum immediately prior to the deposition of both the shadowing metal (gold/palladium 60/40) and the backing film of aluminium (calculated thickness 75 Å), Fig. 1. The metal replica will float off on to the surface of distilled water: this procedure was found to be unreliable and to produce replicas containing a large number of strain markings. More consistent stripping results are obtained by coating the metal replica, while still supported by the metal specimen, with a thin film of Formvar, from a $\frac{1}{2}$% solution in chloroform, and backing it with a thick film of nitrocellulose from a 2% solution in amyl acetate. When this film has dried, the edges are scored with a razor blade and the composite film, after being breathed on, lifted free. The nitrocellulose is washed off with amyl acetate and the Formvar with chloroform. If the film of Formvar is omitted disruption of the metal replica takes place because of swelling of the nitrocellulose during its removal.

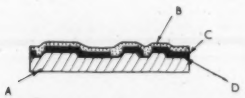

Fig. 1. Diagram of all-metal replica for electron microscopy

A, metal specimen; *B*, aluminium backing layer, approximately 75 Å thick; *C*, gold/palladium shadowing layer, approximately 10 Å thick; *D*, boron oxide stripping layer, approximately 20 Å thick.

(ii) *X-ray diffraction of chemically extracted residues.* A lump sample of steel weighing 1–2 g was suspended in a 10% solution of iodine in alcohol in a small stoppered bottle and left overnight without stirring. About 0·3 g of the sample dissolved, leaving a carbide residue of about 3 mg, partly on the bottom of the bottle and partly as a loose deposit on the surface of the sample. The sample was removed and placed in a beaker: the adhering residue was washed off using an alcohol wash bottle. To this was added the residue from the stoppered bottle. The combined residues were transferred to a centrifuge, where they were separated and washed with alcohol. After being dried they were weighed and examined using a Unicam camera and filtered cobalt radiation.

(iii) *Electron microscopy and electron diffraction of the residues.* The two techniques were used on the same specimen, the diffraction pattern usually being taken from the same field of view as the micrograph. Preparation of the specimen was carried out as follows: A support film of nitrocellulose was formed on a dish of distilled water by allowing a drop of 2% solution of nitrocellulose in amyl acetate to spread over the surface, the amyl acetate evaporating, leaving a continuous thin film. A drop of alcohol containing the residue was placed on the film and, in spreading out, carried fine particles to the outside of the drop. A specimen was selected from a region in which there was a concentration of particles.

(iv) *Electron microscopy and electron diffraction of extraction replicas.* This technique consists of removing fine precipitates from the surface, attached *in situ* to a Formvar replica.[4] Specimens were polished and etched as for a normal electron microscopic examination. A thin film of Formvar was obtained on the surface of the specimen by coating from a $\frac{1}{2}$% solution of Formvar in chloroform. Re-etching was then carried out through the Formvar film, using 4% nital. The specimen was washed in alcohol and the replica removed in the usual way (Fig. 2).

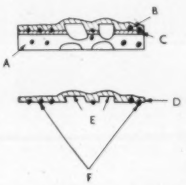

Fig. 2. Extraction replica technique

A, metal specimen containing large and small precipitate; *B*, Formvar; *C*, material removed by etching through Formvar; *D*, detached Formvar film; *E*, impressions of large particles; *F*, attached small particles.

The above four techniques help to give a more complete picture of the structure of the material than any one technique alone. Surface replicas of the solid sample are capable of showing precipitates down to about 200 Å in size, and although the size and location of the particles are demonstrated, no information as to their structure is obtainable. The structure of particles down to 1000 Å is obtained from chemically extracted residues by X-ray diffraction methods, using filtered cobalt Kα radiation (λKα = 1·790 Å). Below this size, only diffuse X-ray patterns are obtained owing to line broadening by finer particles, and their size and structure are determined by electron diffraction methods using 60 kV electrons (λ = 0·05 Å). From particles about 1000 Å in size, spotty electron diffraction rings are obtained and as the size of the particles decreases the rings become sharp and well-defined. Below 100 Å, in the instrument used, line-broadening measurements give an indication of the particle size only.

Examination of the residues does not show where the particles were in the α- or γ-regions of the original sample and to do this, the extraction replica was employed. Using this technique, particles below about 5000 Å are retained in their proper relative position in the film and larger particles can be detected by means of the impression left on the contact surface of the replica.

RESULTS

Three steels designated FC43, FC96 and FC105, all of the same nominal composition, were examined. They had been tested under 5 t/in.^{2} at 650° C, and a creep strain less than 0·15% at 200 hours and less than 0·3% at 1000 hours was regarded as satisfactory. Sample FC43 showed a satisfactory creep resistance when quenched from 1150° C and tempered at 750° C for a suitable time. This had to be less than two hours since, as shown in Table 1, when the tempering time was two hours or over the creep resistance deteriorated. A satisfactory standard of creep resistance could not be obtained with samples FC96 and FC105 when quenched from 1150° C and tempered, but was reached when these samples were quenched from 1250° C. The results of creep tests illustrating this behaviour are also given in Table 1.

Table 1. *Heat treatments and creep tests*

Steel No.	*Heat treatment*	*Creep strain %* 200 *h*	1000 *h*	2000 *h*
FC43	WQ 1150° C only	0·090	0·209	Test shut down
	WQ + ½ h 750° C	0·148	0·357	0·515
	WQ + 1 h 750° C	0·081	0·157	0·215
	WQ + 2 h 750° C	0·185	0·430	Test shut down
	WQ + 16 h 750° C	0·365	Test shut down	
FC96	WQ 1150° C + 1 h 750° C	0·25	Ruptured (912 h)	
	WQ 1250° C + 1 h 750° C	0·076	0·185	0·280
FC105	WQ 1150° C + 1 h 750° C	2·1	Ruptured (432 h)	
	WQ 1250° C + 1 h 750° C	0·08	0·175	0·250

WQ = water-quenched.

Table 2. *Electron microscopy and diffraction of extracted residues*

Sample	*Miscroscopy*	*Diffraction*
FC43. Water-quenched from 1150° C.	Large elongated particles, up to 10 μ in length.	Occasional single crystal pattern, probably TiC, through thin large particles.
FC43. Water-quenched + ½ h 750° C.	Large particles. Hint of very fine particles.	Hint of additional diffuse ring.
FC43. Water-quenched + 1 h 750° C.	Large particles and very fine particles [Fig. 4(*a*)].	TiC pattern showing line broadening corresponding to a particle size of ≃ 50 Å. A superimposed single crystal pattern due to a large particle [Fig. 4(*b*)].
FC43. Water-quenched + 2 h 750° C.	Large particles. Very fine particles sharper than those at 1 h 750° C.	TiC pattern showing little line broadening, i.e. particle size ≃ 100 Å. Some additional diffraction rings.
FC43. Water-quenched + 16 h 750° C.	Large particles. Fine particles more distinct [Fig. 5(*a*)].	TiC pattern with spotty rings, showing particle size of several hundred Ångstrom units. Additional diffraction rings, including those of 2 h 750° C, now sharp and consistent with face-centred cubic of a_0 = 3·6 Å. Possibly carbide of form $M_{23}C_6$ [Fig. 5(*b*)].
FC43. Water-quenched + 48 h 750° C.	Large particles. Aggregates of finer particles.	Very spotty TiC pattern. Faint pattern of $M_{23}C_6$ type.
FC96. Water-quenched from 1150° C + 1 h 750° C.	Fine precipitate only.	Pattern indicates range of particle sizes up to several thousand Ångstrom units. TiC + $M_{23}C_6$.
FC96. Water-quenched from 1250° C + 1 h 750° C.	Large particles plus much fine precipitate.	Spotty pattern superimposed on sharp rings indicating TiC particle sizes between 100–1000 Å.

M = (CrFeMo).

Microstructure and constitution of steel FC43. The structure of steel FC43 as water-quenched from 1150° C is shown by the optical micrograph in Fig. 3. It consists of a mixture of two types of area, respectively alpha and gamma at the quenching temperature, interspersed with coarse particles of titanium carbide. No change of structure visible under the optical microscope was produced by the tempering treatment at 750° C, and the X-ray examination of the extracted carbide residues revealed only titanium carbide. The changes produced by the tempering operation at 750° C were revealed, however, by examination of the carbide residues with the electron microscope, and these results are summarized in Table 2. In all conditions of heat-treatment, the coarse titanium carbide particles visible in the optical microscope were found, but in addition the samples tempered for short times showed in the electron microscope quantities of extremely fine particles, which became coarser as the tempering time increased (Figs. 4 and 5) and simultaneously the electron diffraction patterns showed diffuse halos of titanium carbide. These halos were at first broad, indicating a particle size of about 50 Å, but, with increase of tempering time, they became sharper, and ultimately spotty, suggesting that the particles grew as tempering continued; they finally became greater than 1000 Å. When the tempering time exceeded two hours, additional lines appeared in the electron diffraction pattern, attributable to the carbide $M_{23}C_6$ and when this constituent appeared, the creep resistance deteriorated. It is not possible to say that the quantity of $M_{23}C_6$ increased regularly in relation to the amount of titanium carbide, since the sample contained in the electron beam in any exposure is not necessarily representative of the residue as a whole, and irregular fluctuations of relative intensity of the beam occur. It is probable, nevertheless, that the tempering process consists of a precipitation and progressive coarsening of very fine titanium carbide particles, followed by the formation of $M_{23}C_6$, and that the highly creep resistant condition corresponds to the stage at which very fine titanium carbide is present.

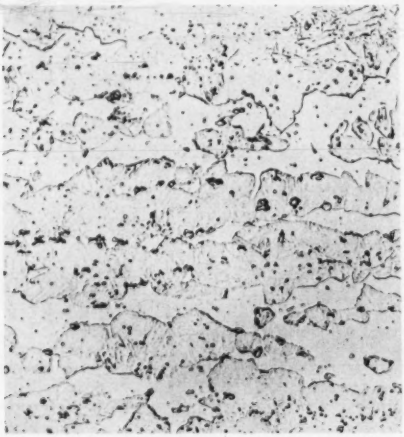

Fig. 3. Structure of steel FC43. Water-quenched from 1150° C for 15 min (×500)

It can be seen from Table 1 that the water-quenched and untempered sample has high creep resistance although no fine titanium carbide could be detected in its structure. The specimens were, however, heated to 650° C and held at this temperature for twenty-four hours before being loaded in the creep test, and it was confirmed that during this time titanium carbide was precipitated in particles of approximately 200 Å diameter.

An electron micrograph of sample FC43 in the condition in which it displays high creep resistance is shown in Fig. 6. The α- and γ-areas are readily distinguished, but at this stage no general precipitation can be detected with certainty. Precipitation, however, took place slowly during the creep test, and the structure after 8000 hours under 5 t/in.^{2} at 650° C is shown in Fig. 7. The α- and γ-areas have behaved differently. The α-areas are filled with a uniform precipitate which proved to be titanium carbide. Its microscopic

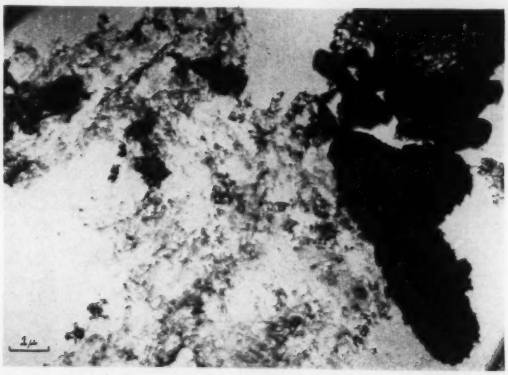

(*a*)

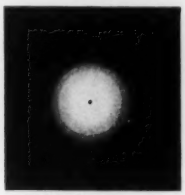

(*b*)

Fig. 4. (*a*) Electron micrograph, and (*b*) diffraction pattern of residue from steel FC43 (1 h at 750° C)

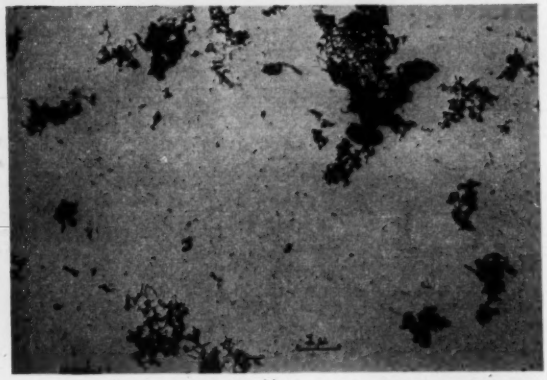

(*a*)

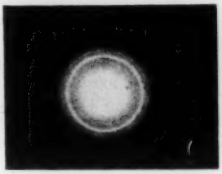

(*b*)

Fig. 5. (*a*) Electron micrograph, and (*b*) diffraction pattern of residue from steel FC43 (16 h at 750° C)

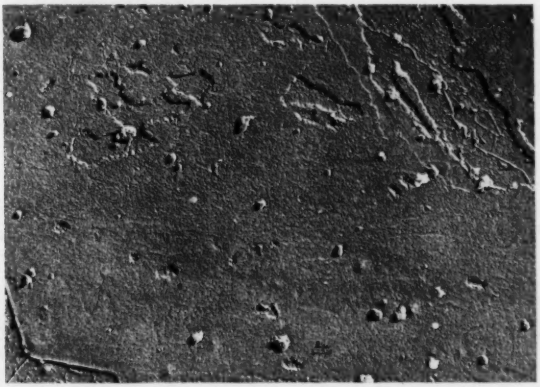

Fig. 6. Steel FC43 water-quenched from 1150° C and one hour at 750° C. An α + former γ structure

Fig. 7. Steel FC43 water-quenched from 1150° C, heated one hour at 750° C and creep-tested 8000 hours at 650° C and 5 t/in.^{2}, showing fine precipitate in α-grains

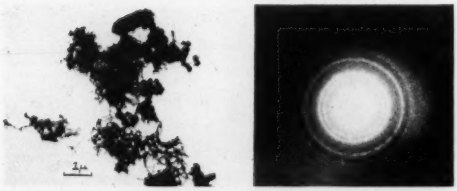

(*a*) (*b*)

Fig. 8. (*a*) Electron micrograph, and (*b*) diffraction pattern of residue from steel FC43, water-quenched from 1150° C, heated one hour at 750° C and creep-tested for 8000 hours at 650° C and 5 t/in.^{2}

appearance is illustrated in Fig. 8(*a*) and it produced the spotty electron diffraction pattern given in Fig. 8(*b*). The γ-areas contain a very coarse precipitate which proved on X-ray examination of residues to be not $M_{23}C_6$, as was produced by prolonged tempering at 750° C, but a mixture of $(MoFe)_2Ti$ with a trace of M_6C. The changes in this steel on prolonged heating are thus not the same at 650° C as at 750° C. The creep rate of the steel after 8000 hours at 650° C accompanied by the appearance of the $M_{23}C_6$ lines in the X-ray diffraction patterns of the carbide residues. A little fine titanium carbide was doubtfully detected in some of the electron diffraction patterns from the residues. These results are summarized in Table 2.

When quenched from 1250° C the proportion of γ-areas in the structure was less, and after tempering for one hour at 750° C a uniform fine precipitate was present, rather coarser

Fig. 9. Steel FC96, water-quenched from 1150° C

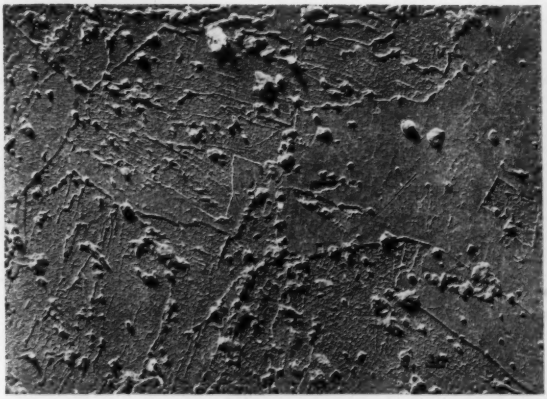

Fig. 10. Steel FC96, water-quenched from 1150° C and heated one hour at 750° C

was greater than at the beginning of the test, but still relatively low.

Microstructure and constitution of steels FC96 and FC105. The steels FC96 and FC105, which gave unsatisfactory creep resistance when quenched from 1150° C, but satisfactory creep resistance when quenched from 1250° C, contained a greater proportion of γ-areas when quenched from 1150° C than did steel FC43, as may be seen by comparing Fig. 9 with Fig. 6. The behaviour on tempering at 750° C differed markedly, for after only one hour large particles of precipitate greater than 1 μ diameter were found (Fig. 10) and were and more variable in the γ-areas than in the α-areas (Fig. 11). Fig. 12 is an extraction replica of one of these samples. Electron diffraction patterns from the particles suspended in the film showed them to be titanium carbide, both in the α- and in the γ-areas. A little $M_{23}C_6$ was observed in the X-ray diffraction patterns, but it was less than in the samples quenched from 1150° C, and it is clear that the effect of quenching from the higher temperature was to retard the formation of coarse $M_{23}C_6$ particles and favour the presence of finely distributed titanium carbide. The titanium carbide precipitate was coarser in these samples than in FC43 (the

prevailing size being about 1000 Å) and it would seem that high creep resistance can be associated with titanium carbide particles of any size between 50 Å and about 1000 Å.

Fig. 11. Steel FC96, water-quenched from 1250° C and heated one hour at 750° C

containing much titanium in solution in which titanium carbide, forming in preference to other carbides, grows slowly at 650° C. Water-quenching a γ-rich structure

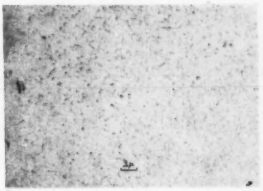

Fig. 12. Steel FC96, water-quenched from 1250° C and heated one hour to 750° C. Extraction replica

DISCUSSION OF RESULTS

The processes in these steels are complex and susceptible to alteration by slight changes of heat-treatment. A complete explanation of all the effects of structure upon creep resistance cannot yet be offered. It is clear, however, that, leaving the coarse and inert optically visible titanium carbide particles aside, the conditions which lead to low creep resistance are those which result in relatively coarse $M_{23}C_6$ particles of a size that can be detected by X-ray diffraction, and those which lead to high creep resistance are those which result in uniform fine dispersions of titanium carbide particles of a size which is not readily detected by X-rays, but are visible when electron diffraction is used. The ability of the titanium carbide dispersion to resist serious coarsening during long periods at the temperature of the creep test is no doubt an important feature.

Samples differing in creep resistance differ principally in the manner in which precipitates form during the tempering operation, and this in turn is influenced partly by the quenching temperature and partly by other factors which are not yet understood.

The areas, respectively alpha and gamma, at the quenching temperature behave differently on tempering, and it is unlikely that the behaviour will be fully elucidated by the examination of extraction residues in which the particles from the two types of area are mixed. The extraction replica, which enables the behaviour of each area to be studied separately, has many advantages.

The rate of growth of precipitate is less in α-areas than in γ-areas, the slow growing precipitate of titanium carbide forming mainly in the α-areas. For this reason a predominantly α-structure appears to be desirable. This phenomenon may be due to the greater solubility of titanium in the α-phase, and of carbon in the γ-phase. Water-quenching a predominantly α-structure produces a material produces material with relatively more carbon in solution, and this presumably favours the precipitation of the more rapidly growing $M_{23}C_6$.

There are certain points of difficulty. The steel FC43 deteriorated in creep resistance before the titanium carbide particles reached 1000 Å, whereas steels FC96 and FC105 maintained their creep resistance when the average particle size was 1000 Å. The quantity and distribution of the precipitates are probably concerned as well as their size. In steel FC43 a quantity of $M_{23}C_6$ was also present when the titanium carbide particles had grown to 1000 Å. This would probably have been formed at the expense of titanium carbide and in its neighbourhood the matrix, denuded of molybdenum and chromium by its presence, may well have been relatively weak.

ACKNOWLEDGEMENTS

The work described in this paper has been carried out as part of the General Research Programme of the National Physical Laboratory, and is published by permission of the Director of the Laboratory.

The author is indebted to Dr. E. A. Calnan for helpful advice and discussion. The materials, creep data and optical micrographs were provided by Mr. G. A. Mellor and Mr. S. M. Barker, while Mr. H. R. Sullivan prepared the residue samples and carried out the X-ray diffraction analyses.

REFERENCES

(1) SMITH, N. D. P. Private communication.
(2) CALBICK, C. J. *Bell Syst. Tech. J.*, **30**, p. 798 (1951).
(3) KAYE, W. *J. Appl. Phys.*, **20**, p. 1209 (1949).
(4) FISHER, R. M. *A.S.T.M. Special Technical Publication*, No. 155 (American Society for Testing Materials, 1954).

The movement of the second crossover potential of insulators

By A. B. McFarlane, M.Sc.(Eng.), A.C.G.I., A.M.I.E.E., Electronic Tubes Ltd., High Wycombe, Bucks.

[*Paper first received* 29 *May, and in final form* 31 *December*, 1956]

The secondary emission coefficient δ of metals and insulators has hitherto been considered to be a definite function of primary electron energy eV_s. The curve relating δ to V_s has two positions, one at low potentials in the range 10 to 100 V, and the other from 1000 V upwards, at which δ is equal to unity, with a maximum value between them. These two positions are known as the first and second crossover potentials respectively.

In a cathode-ray tube, the luminescent screen is an insulator, itself mounted on an insulating glass base. The curve relating δ to V_s then determines the highest potential to which the screen can be brought, this being at or near the second crossover. This effect is very pronounced and is well known in earlier cathode-ray tubes. It sets a quite definite limit to the luminance available and also to the high voltage which can usefully be applied to the tube.

It has now been found that by suitable treatment of the screen, for example by settling it in a strong silicate solution or by applying a layer of magnesium oxide smoke to the bombarded surface, the second crossover may be made to vary rapidly with the electric field applied. In this way the second crossover can be made to follow closely the applied anode voltage, thus allowing the application of almost unlimited values to the tube, with a consequent gain in luminance and performance.

LIST OF SYMBOLS

i_b, the bombarding beam current;
i_s, the secondary emission current from the screen;
i_c, the conductivity current through the screen;
δ, the maximum obtainable ratio i_s/i_b (i.e. secondary emission coefficient) for a particular bombarding energy eV_s;
δ_a, the apparent secondary emission coefficient ($\delta_a < \delta$) resulting from partial suppression of the secondary electron emission;
V_s, the bombarded screen potential (eV_s is the electron bombarding energy);
V_{sc}, the second crossover potential of the screen (i.e. the upper bombarding potential (V_s) at which δ is capable of being equal to unity);
V_a, the voltage applied to the anode of the cathode-ray tube (in the case of a typical cathode-ray tube the anode is also the collector electrode for the secondary emission);
R, the "lumped" resistance of the screen and glass together, assuming that the target may be adequately represented by a conducting layer connected to the collector electrode by a resistance.

1. INTRODUCTION

Curve A in Fig. 1 is typical of metal targets and shows the variation of the secondary emission coefficient δ as a function of the bombarding energy eV_s. Insulator targets are known to give much greater values of δ, but also the values are more difficult and uncertain to specify depending on their structure and the electrode arrangements. Nevertheless it is always supposed that a curve such as B of Fig. 1 could be taken to describe their properties.

A feature of both curves is that at some high potential, δ is equal to unity. This point is called the second crossover potential. The shape of the curves has a certain plausibility, the secondary emission increasing at first as the bombarding energy eV_s increases, and then decreasing when the incident electrons penetrate so deeply that the slower secondary electrons cannot escape.

Now the luminescent screen of a cathode-ray tube is essentially quite a good insulator, and it is deposited on a glass base which is itself highly insulating. The behaviour of insulated secondary emitters is known to be such that for bombarding potentials below the second crossover, a retarding field is set up automatically to limit the actual number of secondary electrons withdrawn, to be almost exactly equal to the incident current. The variation of δ_a in the neighbourhood is illustrated by a curve such as ABC in Fig. 2, and depends on several factors including the surface structure, the electrode configuration and the secondary electron emission energy. The load line R represents the resistance of the screen and glass.

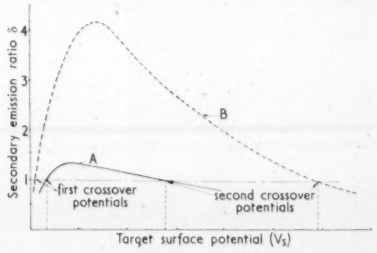

Fig. 1. The secondary emission ratio δ as a function of the bombarding energy

Curve A, measured curve for metal; curve B, assumed curve for insulators.

The intersection of these two curves for a particular value of applied voltage V_a determines the corresponding screen potential V_s. Clearly, for a particular value of beam current i_b the difference in these potentials depends on the magnitude of R and the shape of the δ_a curve. When $R = 0$ the load line lies parallel to the ordinate axis, and as $R \to \infty$ it rotates about O, and ultimately becomes parallel to the abscissa axis. In practice R is very high, usually in the region of $10^{12}\ \Omega$. V_a' and V_s' represent the conditions for a value of V_a below the second crossover potential. It is seen that even for high values of R, these two potentials are almost equal. As the applied voltage to the tube is increased the screen potential

increases in sympathy until it reaches the second crossover. Further increase in the applied voltage leads to a very little increase in the screen potential, as is shown again in Fig. 2. An increase in V_a from V_a'' to V_a''' merely causes a rise in V_s from V_s'' to V_s'''. This latter rise is very dependent on

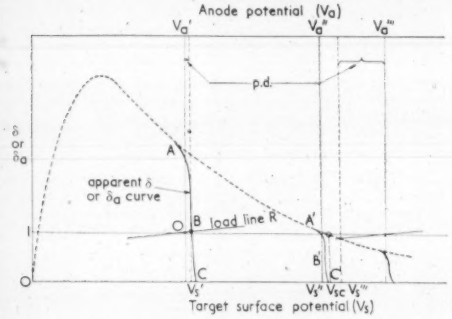

Fig. 2. The variation of V_s with V_a in a cathode-ray tube

p.d., potential differences between Aquadag collector and screen surface.

R and is small for high values of R. Increasing V_a further still, produces hardly any increase in V_s, which remains around the second crossover potential V_{sc}. Under these circumstances there is no point in applying an anode potential V_a much greater than V_{sc}, since no higher potential is available on the screen itself, and it is this latter potential which determines the light output.

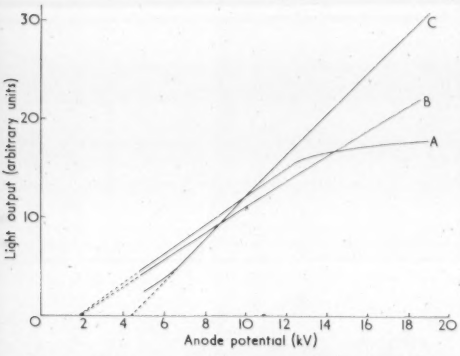

Fig. 3. Light output curves for screens deposited on glass (beam current 40 μA)

Curve *A*, standard screen; curve *B*, extra-silicated screen; curve *C*, magnesium oxide coated screen.

Preliminary experiments on aluminized tubes in which we can safely assume that the screen potential is always equal to the anode voltage, showed that the light output is almost linearly proportional to the screen potential over a range from 4 to 18 kV. Thus a light output-anode potential curve taken at constant beam current can be used as a rough indication of the way in which the screen potential varies with changes in anode voltage. Curve *A* of Fig. 3 shows such a relationship for earlier tubes having the standard screen (see Appendix). This indicates that the screen reaches a definite second crossover potential and will go no higher. As a result V_{sc} of Fig. 2 is often termed the "sticking potential."

2. DEVELOPMENT ON THE LUMINESCENT SCREENS OF CATHODE-RAY TUBES

The need for greater luminance in television and instrument tubes has led to developments in the properties of the screens, one consisting in the treatment of the screen to prevent "sticking" and another the application of very strong electric fields to the screen by means of a thin aluminium layer deposited over the surface. We shall be concerned here with the former method.

Two methods[1] of treating the screen reduced the tendency to "stick," one consisting of settling the screen in unusually strong silicate solution (extra-silicated screens—see Appendix) and the other the application of a thin layer of magnesium oxide smoke to the bombarded side of the standard screen.

Curves *B* and *C* of Fig. 3 show the degree of improvement attained. There is now no sign of a definite "sticking" potential. These curves are not isolated examples, and have been repeated quite closely many times. They are discussed in more detail in Section 4(*b*).

3. INTERPRETATION OF THE RESULTS

In view of the earlier experience of a definite second crossover, it could be argued that the improved screens have a second crossover well above 18 kV. Such an explanation is, however, not tenable if we are to attach any significance to the explanation given for the fall in δ at high bombarding potentials. The situation should become worse as the applied voltage is increased, and there is no obvious reason why the treatment of the screens should prevent electron penetration or permit more secondaries to escape. Silicaceous material and magnesium oxide smoke have very similar densities and are insulators, just like the screen itself.

We must conclude, therefore, that some other effect is brought into play and this could possibly be a variation in the potential of the second crossover with the applied electric field strength. The field strength is defined by the potential difference between corresponding V_a and V_s values as indicated in Fig. 2. There is reason to suppose[2] that δ itself can be strongly field dependent, and also that this effect could depend on features of the structure of the surface, which are so far ill defined.

An attempt was made, therefore, to test this hypothesis by measuring the actual current flowing through the screens of experimental tubes.

4. EXPERIMENTAL EVIDENCE TO SUPPORT INTERPRETATION

(*a*) *Experiments with screens on metal film* As has been stated already in Section 1, the light output measurement gives only an indication of the screen potential and the secondary emission curve. A measurement of electron currents is much more sensitive. To do this, however, we must be able to make good electrical contact with the screen,

and consequently the screens of Fig. 3 were deposited on a conducting base. We are, therefore, making an assumption that this does not appreciably affect the phenomenon which determines the screen potential. This is very reasonable since it has been found that the screens are sufficiently thick to prevent bombardment of the glass base affecting the "sticking" potential. It will be seen from the results of Section 4(*b*) that this assumption is valid.

The conducting base was made by evaporating a semi-transparent film of nickel on the inside surface of the glass bulb where the screen was to be settled. Provision was made for two external and diametrically opposite contacts to this film. This enabled the resistance of the film to be measured so that disconnexions would not vitiate the results. In contrast to the situation in ordinary tubes, the potential of this base could be adjusted at will. Thus with the circuit connected as in Fig. 4, curves corresponding to such portions as *ABC*,

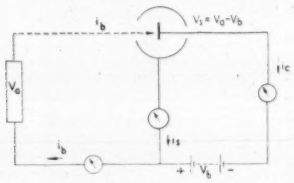

Fig. 4. Circuit for measuring δ

and *A'B'C'* of Fig. 2 were taken on each type of screen. The anode potential was adjusted to a particular value, and then with the target at +200 V with respect to the anode (i.e. collector electrode) to ensure that all the emitted secondary electrons returned to the target, the beam current was read on the i_c meter. The value of i_b was adjusted to 40 μA by altering the control grid bias on the electron gun. The potential of the nickel was then made negative to the anode by a certain amount, and the value of i_s was measured for this condition, whence δ_a ($=i_s/i_b$) was calculated. To check the condition for δ_a equal to unity, the current (i_c) flowing through the screen was also noted, since it reverses at this point. In addition, light output curves corresponding to those of Fig. 3 were also taken.

(*b*) *Results.* Fig. 5(*a*) shows the light output curves obtained on the three types of screen under consideration. Effectively there are two curves for each screen, one taken with the potential of the nickel base "floating," and the other with the nickel held at anode potential. These latter curves which represent the case when "sticking" is entirely eliminated have, in fact, been normalized at an anode potential of 10 kV taking that measured for the standard screen as reference. The result is the one curve *D* of Fig. 5(*a*). The selection of this potential is arbitrary, and a correction of −2·3 kV was applied to the values of V_a for the magnesium oxide coated screen to allow for "dead" voltage in penetrating the oxide layer. This normalization eliminates the effect of different amounts of light transmission through the various nickel films, and enables us to compare results more easily. Furthermore, curve *D* demonstrates that the light output is directly proportional to the screen potential, at least over the range from 5 to 16 kV.

Curves *A*, *B* and *C* are those taken with the nickel film "floating." The values actually measured have been multiplied by the respective factors used in the above normalization.

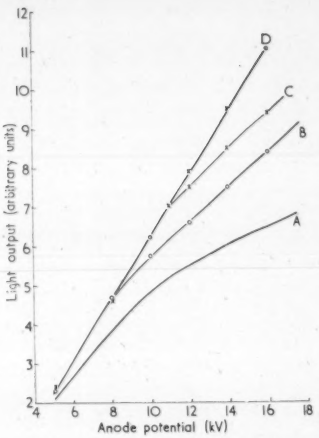

Fig. 5(*a*). Light output curves of luminescent screens deposited on a nickel base

Curve *A*, standard screen with nickel "floating"; curve *B*, extra-silicated screen with nickel "floating"; curve *C*, magnesium oxide coated screen with nickel "floating"; curve *D*, normalized curve for all screens when nickel is connected to anode potential.

○ = extra-silicated points. × = magnesium oxide points.

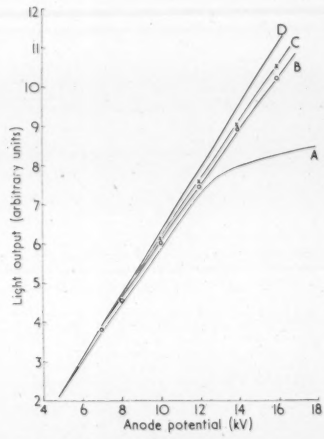

Fig. 5(*b*). Light output curves of luminescent screens deposited on glass but normalized with curve *D* of Fig. 5(*a*)

Curve *A*, standard screen; curve *B*, extra-silicated screen; curve *C*, magnesium oxide coated screen; curve *D*, as in Fig. 5(*a*).

Thus it is seen clearly that the standard screen is very bad for sticking, whilst the extra-silicated screen shows considerably less tendency to stick and the magnesium oxide coated screens even less still.

Now we are particularly interested in comparing the above curves *A*, *B* and *C* with those of Fig. 3, which are for similar screens deposited directly on the glass bulb. Curve *A*, Fig. 3, shows that the standard screen sticks very badly, whilst the other two screens behave reasonably well, the magnesium oxide coated one being the best of all. This latter result is seen more clearly if we compare curves *A*, *B* and *C* of Fig. 3 with curve *D* of Fig. 5(*a*). Fig. 5(*b*) shows the results when the curves have been normalized at 5 kV, this value being chosen as being below that at which "sticking" occurs for any of the screens, and at the same time being on the linear part of the light output curves. Again, the V_a values for the magnesium oxide coated screen were corrected as before for "dead" voltage.

Thus we see that the screens examined behave in very similar fashion when they are settled on a conducting base as when deposited directly on glass. The results are not identical, but then it is unlikely that a phenomenon such as secondary electron emission, which is so dependent on processing, should be exactly reproducible on a metal base as on glass.

Fig. 6 shows the δ_a measurements, and from these curves we derive Fig. 7, showing the variation of sticking potential with the potential difference between the nickel film and collector, for the three screens.

It is seen immediately that the standard screen has a relatively fixed second crossover, the variation for the voltage range from 150 to 800 V between film and collector being only 1·35 kV from 5·85 to 7·2 kV (i.e. a "slope" of 2·1). The extra-silicated screen varies much more rapidly covering 0·84 kV for 160 V. This gives a "slope" of 5·3. Finally, the screen coated with magnesium oxide smoke shows a still more rapid variation of second crossover, being 1·9 kV for 120 V difference in potential between film and collector. This gives a "slope" of 16.

All three curves of Fig. 7, extrapolated back to zero difference of potential, meet in the neighbourhood of 7 kV, which would indicate that the bombarding electrons penetrate to similar extents, and the second crossover at zero field is, as we should expect, not affected by the method of producing the screens. No significance is attached to the fact that the curves actually appear to cut the abscissa axis at potentials from 5·5 to 8 kV, as such a range is probably within the repeatability of making such tubes. Very marked changes in the rate of change of second crossover with the withdrawal field are obtained, however, by suitable processing. Measurements using an electrostatic voltmeter have shown that when the bombarded screen is "floating," it automatically adjusts its potential below that of the anode to make δ_a equal to unity (see Fig. 6).

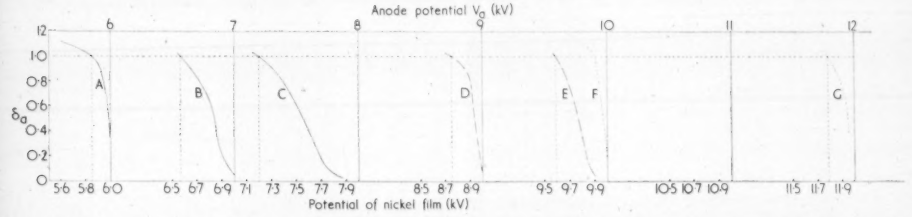

Fig. 6. The variation of δ_a with the potential of the conducting base at various anode potentials ($i_b = 40\ \mu$A)

Curves *A*, *B* and *C*, standard screen; curves *D* and *E*, extra-silicated screen; curves *F* and *G*, standard screen covered with magnesium oxide smoke.

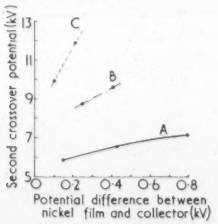

Fig. 7. The variation in the second crossover potential with accelerating field at the screen surface

Curve *A*, standard screen; curve *B*, extra-silicated screen; curve *C*, standard screen covered with magnesium oxide smoke.

5. CONCLUSIONS

Two sets of experiments, one on screens deposited on an insulating glass support and the other using similar screens on a thin metal film show similar behaviour in regard to light output as a function of electron accelerating potential. The measurements on the insulator can be interpreted by, and those on the metal film confirm the hypothesis that methods of producing the screens can be devised which cause the position of the second crossover to be very dependent on the electron withdrawing field. The validity of the idea of a second crossover is, therefore, in doubt, since it can be either a very indefinite and movable point, or relatively fixed. It may, however, be concluded that for small withdrawal fields all the screens tested have a second crossover of about 7 kV. The variation in crossover can easily be made so great that the high limit at which suitable luminescent screens may be operated is not indicated by tests up to 20 kV.

Since the preparation of this paper, Laponsky[3] and his associates have published results and conclusions that the second crossover of insulators can be considerably field

dependent. They attribute this fact to the roughness of the bombarded surface.

The exact explanation for the field dependence in the case of the extra-silicated and magnesium oxide coated screens has not been determined. Clearly the physical state of the bombarded surface is important. The results on the standard screen which itself has a "rough" surface show that the sticking potential is hardly field dependent. Thus "roughness" alone is not a sufficient definition of the surface of an insulator for the second crossover to be field dependent. The magnesium oxide particles were approximately 1 μ in size and gave the coated standard screen a very fluffy-matt surface. In the case of the extra-silicated screen it is conceivable that a surface of similar texture may be obtained from a silicate structure forming amongst the screen particles.

ACKNOWLEDGEMENT

The author wishes to thank the Management of Electronic Tubes Ltd. for permission to publish this paper. He would also like to thank Dr. C. S. Bull for his advice and many discussions.

REFERENCES

(1) McFarlane, A. B. *M.Sc.(Eng.) Thesis* (University of London, 1955).
(2) Bull, C. S., and Atherton, A. H. *J. Instn Elect. Engrs*, (III), **97**, p. 65 (1950).
(3) Laponsky, A. B., and others. *J. Electrochem. Soc.*, **103**, p. 498 (1956).
(4) McFarlane, A. B. Brit. Pat. No. 740, 454 (1953).

APPENDIX

The standard screen

A 12 in. bulb was filled with 3·5 l. of filtered tap water since the available supply was of suitable electrolytic properties for screening. Next 4·5 g of the luminescent powder were weighed out and thoroughly mixed with 45 cm^3 of 10% (by weight) potassium silicate solution. This mixture was diluted with a further 205 cm^3 of filtered tap water and vibrated for one to two minutes to break down any aggregates of powder. The solution was then poured into the bulb through a funnel. At the end of this was a rose which distributed the powder uniformly throughout the bulk of the water. The powder was allowed to settle for twenty-five minutes and then the settling liquid was carefully tipped out. Next the screen was dried slowly over a warm stream of air. The resulting screen was 6 mg/cm^2 thick.

The extra-silicated screen[4]

For this screen the above process was carried out, but the 45 cm^3 of 10% potassium silicate solution and 205 cm^3 of filtered tap water were replaced by 250 cm^3 of 10% potassium silicate solution (ratio SiO_2/K_2O in the silicate ranged from 1·8 to 2·2).

It must be pointed out that although the screen powder is settled in a solution of potassium silicate, the form in which the latter is present in the screen is not determined. Thus, we shall refer to any silicaceous material remaining in the screen from the potassium silicate solution as "silicate." Hence the term "extra-silicated."

New books

Raum-und bauakustik fur architekten. By WILLI FURRER. (Basel und Stuttgart: Birkhauser Verlag, 1956.) Pp. 200. Price *DM* 27.50.

Although the book on sound insulation and building acoustics is avowedly written for architects, in fact its use is as an up-to-date account of Continental practice in a form suitable for applied physicists and electrical engineers specializing in the field of building acoustics, and advising architects on detailed matters of design. The ordinary architect has enough to do without concerning himself with the specialist matters which make up the greater part of this book.

With this proviso, the book can be recommended to British practitioners as a useful summary of Continental experience and technique. A. T. PICKLES

Engineering dynamics. Vol. 2. By C. B. BIEZENO and R. GRAMMEL. (London and Glasgow: Blackie and Son Ltd., 1956.) Pp. x + 527. Price 90*s*.

In courses up to first degree standard in the various branches of engineering mechanics, problems discussed are simplified and idealized. The more difficult problems met with in practice have to be omitted or are not treated as fully as would be required in actual practice. For this reason, say the authors in their preface, most technical colleges have instituted special courses in higher mechanics. The authors, however, come from two of the well-known "technical high schools" of the Continent, Delft and Stuttgart, and one doubts whether many such courses are to be found in this country.

Engineering Dynamics is a textbook at the level of such post-graduate courses. The work is in four volumes of which Vol. 2 is under review. Vol. 1 is general, covering theory of elasticity together with analytical and experimental methods. Vol. 2 (elastic problems of single machine elements) deals with the parts from which machines are built as isolated elements, and leads from the abstract theory of Vol. 1 to Vol. 3 (steam turbines), and Vol. 4 (internal combustion engines) where the parts are considered in relation to the complete machine. Such appears to be the general plan of the whole work, from which it will be seen that it is primarily concerned with the dynamics of machines.

It should be remarked that the word dynamics in the title includes statics and Vol. 2 is mainly concerned with statical problems. Its four parts are I (beam and shaft), II (spring and ring), III (plate and shell), and IV (problems of elastic instability). The choice of problem is influenced by the special interests of the authors, and the work is not to be regarded as an encyclopedia. Each problem is solved by what the authors consider to be the best method, whether graphical, analytical or numerical, e.g. iterative and the work is carried through in detail to a complete numerical solution in many cases. In some cases more than one method is discussed. When iterative methods are used the convergence is established.

The range of problems may be sufficiently indicated by the headings of the subsections of Part I. The first section, the beam on rigid supports, commences with the derivation of Clapeyron's Theorem of three moments in a general form which does not assume *EI* constant along the beam. We then have in succession the beam on elastic supports, the beam on continuous elastic foundations, and finally the straight shaft which includes shafts with grooves and notches.

When the book was first published in German in 1939 the relaxation method was comparatively new, and the section on the circular shaft with a keyway, solved analytically, mentions in a footnote that relaxation offers an alternative solution of this and other problems, with a reference indicating that the method is described in Vol. 1.

The authors are scientists of international repute in this field and their book will well repay close study. It is not a book to read on the train, it demands concentration and assumes a very wide knowledge of mathematics. The English translation is from the second German edition by M. L. Meyer and is very well done. It only remains to add that the book is beautifully produced and is a pleasure to handle. A. W. GILLIES

Cambridge Aeronautical Series, Vol. 2. Wing theory. By A. ROBINSON and J. A. LAURMANN. (London: Cambridge University Press.) Pp. ix + 569. Price 75*s*.

Initiated by the work of Joukowski, Lanchester, Prandtl and others an enormous amount of research has been done during the last fifty years on the flow of air over wings. Those aspects of this subject, such as incompressible flow over wings of arbitrary shape and compressible flow over thin wings, in which the state of the flow can be described by a linear differential equation, have received especially close attention and at the present time few outstanding problems remain to be solved. The time is ripe therefore for a definitive work in these fields collecting, arranging and assessing the body of research which has been done. The present book, the senior author of which was formerly Deputy Head of the Department of Aerodynamics at Cranfield College of Aeronautics, partly supplies this need, for it gives an almost complete account of the more important aspects of the theory of such flows.

It is intended for research workers or students at the advanced level in universities and they are expected to have a sound knowledge of the theory of functions of a complex variable, but those parts of the general theory of hydrodynamics needed are discussed in Chapter I.

In Chapter II the incompressible flow round a two-dimensional aerofoil is discussed using complex variables throughout. To begin with results of a general nature are proved and then the principal properties of the Joukowski aerofoils are worked out. For more general aerofoils there are two principal problems—to find the pressure distribution round a given aerofoil and to find that aerofoil having a given pressure distribution. Both are treated in detail here using the methods of Theodorsen and Lighthill respectively. Finally the profile drag, which is zero in inviscid theory, is calculated by appealing to the properties of turbulent and laminar boundary layers.

The three dimensional aerofoil is discussed in Chapter III. The theory behind Prandtl's lifting line and Weissinger's extension of it to swept wings is given. The authors also consider the theory of the lifting surface in great detail, using sources, doublets, vortices and the acceleration potential.

The aerofoil in compressible flow is the subject of Chapter IV. If the flow is subsonic the theory of flow past a thin wing is the same as that of a compressible flow past a similar wing, modifications only entering when higher order approximations are taken into account. In supersonic flow, of course, the theory is entirely different from subsonic flow and, in fact, much simpler. The general theory is given using the concept of the finite part of an infinite integral. In the applications use is also made of source distributions, special co-ordinates and cone-fields, etc. A brief account of higher order theories and of transonic flow is also given. Long as this chapter is, such an important topic as wing-body interaction is not mentioned, and it is a pity that the authors could not find space for even a brief discussion.

Finally in Chapter V unsteady flow past aerofoils is considered, including problems of oscillating aerofoils and of accelerating aerofoils.

The book is well written, the ideas behind the theories and methods being clearly explained while their development is lucid and direct. Further the authors draw their references from papers published on both sides of the Atlantic and give a balanced picture of the present position in the field. Occasionally, however, the mathematics becomes recondite and perhaps only of academic significance; it could with advantage have been transferred to an appendix or omitted altogether. Subject only to this reservation the book is strongly recommended to all students of aeronautics as a standard textbook.

K. STEWARTSON

An introduction to electrostatic precipitation in theory and practice. By H. E. ROSE and A. J. WOOD. (London: Constable and Co. Ltd., 1956.) Pp. 166. Price 17*s.* 6*d.*

The Central Electricity Authority are spending about £2½ million per year on electrostatic precipitators for power stations, and with the increasing emphasis on clean air the number of dust-collecting plants installed in other industries is bound to increase. It is strange that a development of this magnitude should:

> "go down to the vile dust, from whence it sprung,
> Unwept, unhonour'd and unsung."

There is no well-known textbook on the subject, and the literature is widely scattered through a varied range of journals. The authors have therefore performed a very useful service in critically selecting and presenting this material, together with the results of their own researches, in this convenient monograph.

The book opens with an introductory chapter describing typical electrostatic precipitators. Subsequent chapters deal with electrical discharge theory; efficiency of dust collection; precipitation problems, such as re-entrainment and back ionization; precipitator design and construction; and power supply requirements.

The authors have presented a well-balanced account of present knowledge which can be thoroughly recommended. The picture is not a satisfactory one, however, and the following sentence (p. 74) is indicative of the state of the subject; "Examination of Fig. 4–1 and Fig. 4–8 shows that, if the scales of the figures are changed so that unity on Fig. 4–8 corresponds to 50% on Fig. 4–1, the agreement between the theoretical and practical curves is almost perfect." The situation is undoubtedly improving in recent years and it is hoped that this book will inspire physicists to study the subject and make it less of an art and more of a science.

J. S. FORREST

Lubrication of bearings. By F. T. BARWELL. (London: Butterworth's Scientific Publications, 1956.) Pp. xii + 292. Price 50*s.*

This book sets out to give a logical story of the fluid film lubrication of journal bearings, picking out (in a very personal selection) the significant features from the massive international literature. It is not a simple story; the newcomer will have to do some hard work, but it is probably as simple as it can be made in the present state of knowledge. By making fairly severe assumptions a straightforward procedure has been derived for design. The author deals with the assumptions very openly, and, by reference to the limitations of present knowledge, fulfils his second aim of showing research workers where further work is needed.

The book is filled out with a considerable amount of ancillary material. It is introduced by chapters on the nature of surfaces, on the basic principles of lubrication, on wear and on viscosity. These are excellent in intention, and useful reminders for those practising in this field, but they will not be easily understood by a newcomer to the subject. The later chapters deal with varying loads, vibrations in bearings, thrust and special bearings, bearing materials, test arrangements for bearings, and an interesting treatment of grease as a lubricant.

There are a few slips, and in some places the presentation needs simplifying. No doubt the author will see to these faults when he can take a more detached view for a second edition. It is already, however, a notable book, not least to be welcomed as a British book on a subject which has a notable British history.

D. CLAYTON

Notes on applied science No. 17. High voltage impulse testing. (London: H.M. Stationery Office, 1956.) Pp. 9. Price 1*s.* 6*d.*

Impulse tests have been and are being incorporated in national and international test specifications of high-voltage equipment subjected to lightning surges. In this note the relevant information is briefly summarized. It deals with the effects of lightning strokes on transmission systems, the production, standardization and measurement of impulse voltage and current waves, and the major considerations affecting the specifications of impulse tests on insulators, protective gaps, transformers, capacitors and surge diverters.

R. H. GOLDE

Principles and techniques of applied mathematics. By B. FRIEDMAN. (London: Chapman and Hall Ltd.; New York: John Wiley and Sons Inc., 1956.) Pp. ix + 315. Price 64*s.*

This book discusses linear spaces, spectral theory of operators, Green's functions, Eigenvalue problems of ordinary differential equations, and partial differential equations, in successive chapters. It is concerned with mathematics which may be applied, rather than with "applied mathematics." In fact, the only application, a discussion of the passage of a plane light wave through a pane of glass, is introduced only to formulate a suitable boundary condition at infinity.

It is addressed to physicists and engineers, though it demands quite extensive knowledge of mathematics, particularly linear algebra and complex integration. The emphasis is consequently on methods rather than abstract theory and the text is illustrated by many examples and problems. Many details and extensions of the text have been put into problems. In one or two cases the "hints" given in connexion with the problems are not very helpful.

The attempt to provide an introduction to Schwartz's distribution theory is not wholly successful and needs to be thought out more carefully. There are some inconsistencies and occasional looseness of expression. Nevertheless, the author is to be thanked for making the attempt. The discussion which will be stimulated will, no doubt, lead to a more satisfactory introductory treatment.

This book can be recommended to physicists with an interest in mathematics, who will find it a useful book to place alongside Courant and Hilbert. A. W. GILLIES

Grundzuge der tensorrechnung in analytischer darstellung: III Teil: anwendungen in physik und technik. By A. DUSCHEK and A. HOCHRAINER. (Vienna: Springer-Verlag, 1955.) Pp. vi + 250. Price DM 24.

This is the third volume of a series of books on tensor calculus the first two of which deal with tensor algebra and tensor analysis; it is devoted to the application of tensor calculus to problems of pure and applied physics. The main aim of the authors was to show that many of the laws of classical physics can be formulated more elegantly and their solutions often be simplified considerably by the consistent use of tensors. Of particular interest are the chapters on so-called "vector double fields," i.e. fields described by two field vectors A and B connected by an equation of the form $B = \lambda A$ where λ is a scalar function of space and where curl A and div B are given. The general theory of these fields is applied to electromagnetic and thermal fields. The final chapters of the book are devoted to the theory of relativity where tensor methods have been used right from the beginning. The usefulness of the book would have been greatly enhanced if the authors had not confined themselves to isotropic continua: the theory could have been presented without any appreciable increase in complication in a more general form so as to make it applicable to anisotropic media, thus covering the field of crystal physics which is the natural domain of tensor methods. R. FURTH

Progress in metal physics. Vol. 6. Edited by B. CHALMERS and R. KING. (London: Pergamon Press Ltd., 1956.) Pp. viii + 354. Price 70*s*.

Most workers in physical metallurgy and solid state physics are now familiar with the type of review likely to be found between the solid red covers of this admirable series. The current volume is no exception; its six survey articles are invaluable sources of information for all who are seriously concerned with the subjects discussed, but they are not recommended as light bedside reading for the tired technologist.

The book begins with a discussion by A. W. Lawson of the variation of the electrical resistivities of metals with hydrostatic pressure, a comparatively unknown field, dominated, of course, by Bridgman's work. H. K. Hardy takes seriously the editor's original promise that the historical background of a subject will be included on its first mention; his interesting article on filamentary growths of metals on both metals and non-metals begins with work in the early eighteenth century. In contrast to this, Dr. Hardy's former colleague, A. H. Sully, justifiably assumes that his readers already know something of the complexities of creep behaviour, and he concentrates on giving a patient and clear description of the sometimes conflicting results obtained recently in investigations of the structural changes during creep.

The remaining reviews are on the austenite: pearlite reaction ("what is known, and what is surmised"), by R. F. Mehl and W. C. Hagel, on the mechanism of evaporation, by O. Knacke and I. N. Stranski, and on mosaic structure, by P. B. Hirsch. For many metallurgists, the interest of the important transformation in steels will outweigh that of the rest of the book, and Professor Mehl's name is sufficient guarantee of its authority. Dr. Hirsch also writes on a subject to which he personally has contributed so much, and does so with marked success. This long article was closest to the personal interests of the present reviewer, and he can only express his thanks for being put right on so many points.

Until recently, "Metal Physics" was the scientific equivalent of one of Mr. Potter's "O.K. words," and it is apparently still so rated by the editors, who consider it worthy of capital initial letters, unlike physics and metallurgy. Lifemen in this field, however, now tend to refer to themselves as solid state physicists, and a series of review articles covering this wider subject is now being published in book form. Inevitably there will be some overlapping with the functions of the Progress in metal physics series, but if the present standards are maintained, the Progress series need not fear the competition. J. W. CHRISTIAN

Matrix calculus. By E. BODEWIG. (Amsterdam: North-Holland Publishing Co., 1956.) Pp. xi + 334. Price 53*s*.

With the development of high-speed electronic computers it has become practicable to carry out extended sequences of operations with matrices of moderately high order, and a book which develops those parts of matrix theory which are of practical interest is therefore particularly timely.

For a number of years the author has advocated the systematic use of a matrix notation which avoids reference to the individual elements of the matrix and instead treats the rows and columns as the important units. The first section of the book is devoted to an exposition of this idea and to the development of the fundamental properties of matrices. The treatment is given in elementary terms, and it is indeed at times almost naïve, but since the book is clearly intended for a wide range of readers, this is not altogether undesirable. The systematic use of a notation for the rows and columns certainly gives an overall simplification, but there are times when the author's enthusiasm runs away with him.

The remaining three sections describe methods for the numerical solution of the main problems of matrix algebra, the solution of linear equations, the inversion of matrices and the calculation of latent roots and vectors. Each section is divided into two parts, one on direct and one on iterative methods. Most of the methods of practical importance are mentioned, perhaps the most notable omission being Lanczos' method for the calculation of latent roots.

When one turns to the author's assessments of the methods discussed the situation is unsatisfactory. It is difficult to believe that Dr. Bodewig has extensive experience of computation with matrices of even moderately high order or of the use of electronic computers, and it is sound advice on these topics that is badly needed. Two examples will suffice to illustrate these shortcomings. The use of Jacobi's method of orthogonal transformations to reduce a symmetric matrix to diagonal form is recommended only when the matrix is of "almost diagonal form." It would seem that the author is unaware that the method has been programmed for a number of electronic computers and is generally used for symmetric matrices of quite general type. These programmes have been designed to find all the latent roots by continuing the iteration until the off-diagonal elements are zero to working accuracy and, provided all the roots are wanted, it has proved quite a

good method. As a second example the author recommends that in the Givens' method the latent vectors be found by solving the linear system $(\lambda I - S)y = 0$, where S is the co-diagonal form, starting with the first equation of this system. Very little experience is required to show that this is unsatisfactory. There are numerous examples of this apparent lack of experience.

As a survey of methods for dealing with matrix problems the book has much to recommend it, but the practical advice should be treated with caution. J. H. WILKINSON

Selected combustion problems, Vol. 2. (London: Butterworths Scientific Publications; New York: Interscience Publishers Inc., 1956.) Pp. viii + 495. Price 90*s*.

The second combustion colloquium of the Advisory Group for Aeronautical Research and Development (AGARD) was held at Liège in December 1955. Eighteen papers were presented by American, British, French and Italian authors, divided into groups covering (*a*) aircraft engines and fuels, (*b*) ignition and flammability, (*c*) transport properties, (*d*) high-altitude combustion problems, and (*e*) similarity, scaling and fundamental parometers in combustion. The proceedings of the colloquium which have now been published in book form contain all the papers together with reports of the discussions to which they gave rise.

The papers are somewhat uneven in quality. Most of them are intentionally more reviews than original contributions to scientific knowledge, but they are evidence of the great efforts that are currently being made by combustion engineers to understand and absorb what is relevant of physics and chemistry and relate it to their design and development problems. Clearly these efforts have a reciprocal effect on the scientific field also, as new concepts are invented, scientists' hypotheses applied and tested, and new experiments are made. A student of combustion who had been in outer space since 1945 (one is tempted to say that some give this impression) would hardly recognize the subject on his return.

Only a few of the papers can be mentioned in a short review. One on the fundamental principles of flammability and ignitions, by Lewis and von Elbe, provoked considerable discussion, chiefly focused on the authors' "excess enthalpy hypothesis." Although this theory was put forward several years ago it is curious to note that, whereas it makes no headway, in that it does not make clear what was previously in darkness, its advocates are still as faithful as ever. Although the matter was left undecided at Liège, the discussion may have some effect by demonstrating the strength of the opposition.

The section on transport properties is distinguished by an encyclopaedic review by Hilsenrath of the National Bureau of Standards. This provides, in forty-five closely printed pages, a catalogue of compilations and reviews of thermodynamic and transport properties, an indexed bibliography of recent research in this field, details of the tabulations of the N.B.S. and American Petroleum Institute, and a report on the activities of the main groups in the United States. The book is worth buying for this paper alone.

The sections on high-altitude combustion and scaling inevitably overlap. Current understanding of these matters has greatly increased, with the recognition of the role of the volumetric chemical reaction rate and its dependence on pressure. The change which this recognition has brought about is notable in the papers by Way, and Bragg and Holliday. These papers, respectively from the American and British aircraft industries, are good examples of the reciprocal influence of science and engineering mentioned earlier.

The use of models, it can now be said, is a practical and useful procedure in aircraft combustion development. The same is not yet true of rockets as the papers by Ross and Croco testify. This is because of the greater tendency of rocket flames to exhibit vibratory phenomena, to which, alas, gas turbine chambers are also becoming increasingly prone. However, so many problems have been solved which appeared intractable a few years ago, that even rocket combustion may become amenable to analysis. If this does occur, AGARD will be able to claim a share of the credit.

D. B. SPALDING

Neiderfrequenz- und Mittelfrequenz-Messtechnik für das Nachrichtengebiet. By A. WIRK and H. G. THILO. (Stuttgart: S. Hirzel Verlag, 1956.) Pp. vii + 234. Price *DM*28.

The authors of this book are at the Siemens and Halske A.G. and it could be summarized briefly as providing the background which would be useful to a telecommunication engineer concerned with measurements, and more particularly to one using the equipment of this firm.

The book deals with the following subjects: methods of measurement and screening, current sources for measurement purposes, current and voltage measurement, methods of detection and indication, frequency measurement, distortion measurement, noise and its measurements, measurement of complex impedances and four-terminal networks, and the determination of the overall performance of a telecommunication circuit. The book is by no means exhaustive in its treatment, which is mainly descriptive and with a minimum of mathematics. Each section concludes with examples of instruments, giving a basic circuit diagram, a general specification and an illustration of the external appearance of each instrument. G. H. RAYNER

Frequency modulation. By L. B. ARGUIMBAU and R. D. STUART. (London: Methuen and Co. Ltd., 1956.) Pp. vii + 96. Price 8*s*. 6*d*.

This is a handy-sized monograph for those who wish to know something about frequency modulation as a system. It aims to state the advantages and limitations and the fundamental reasons why these arise. Transmitting and receiving circuits are discussed only in their broad outlines to bring out the general principles. A. J. MADDOCK

Records and research in engineering and industrial science. By J. EDWIN HOLMSTROM. 3rd Ed. (London: Chapman and Hall Ltd., 1956.) Pp. xii + 491. Price 60*s*.

For those frustrated readers who find it increasingly difficult to keep abreast of advancing knowledge even in their own limited field, here is real encouragement. Could anything be more stimulating than the author's claim, made in the first edition of this book sixteen years ago and still not withdrawn, that "the whole of knowledge is available for everyone to use." Certainly knowledge is available as are the valuable minerals in all the seven seas, but both kinds of treasure are hard to come by. In *Records and research* the author sets out to provide facilities to ease the path of the seeker after knowledge in the fields of engineering and industrial science, and it must be said at once that he has achieved a great measure of success. Both for interest and usefulness the book

deserves real credit, but the serious student approaching its pages may wish that the two functions had not been quite so interwoven; a book of reference yes, most valuable, a disquisition on the nature and methods of science, excellent and decidedly interesting. But a reference book stands at one's elbow ready for the urgent question: the answers must be found quickly; while rambles through such pleasant fields as the communication of ideas, manipulation of information, note-taking and writing to fix thinking are a more leisured occupation. These are subjects for the library shelf and the armchair, not for the office desk.

I should like to see the material of chapters 1, 2, 3, 7 and 9 co-ordinated and brought together with its own attractive board under some such title as "Science into technology." What a stimulating volume for the 6th-form boy or the undergraduate! Encouraging him to stray into byways of science and to meet surprisingly, and not at all out of place, people like Albert Schweitzer and Sir Walter Scott. Chapter 7 is a mine of great value to the student willing to dig, while chapter 9 on Records would form an excellent round-off for my student's guide. It would be taken from the shelf and provide inspiration long after college days were over.

Having thus decanted the "armchair" delights I would then put the contents of the remaining four chapters, 4, 5, 6 and 8, unashamedly in a serious book of reference, organization national and international, and reference locating records: its leaves would be quickly thumbed.

But it isn't two books but just one, and as such very well worth while.

P. DUNSHEATH

Physics of non-destructive testing. Supplement No. 6 to the *British Journal of Applied Physics*. (London: The Institute of Physics, 1957.) Pp. iii + 72. Price 25*s*.

Supplement No. 6 to this *Journal* contains a selection of papers presented during the past few months at meetings of the Non-destructive Testing Group of The Institute of Physics. They include most of those read at a conference held in Bristol in July 1956 and it is intended, through this Supplement, to enable engineers, metallurgists and indeed all those concerned with non-destructive testing, to appreciate the importance of the new methods which are resulting from applications of physics to this field and to give them an opportunity of considering how far further suggestions for utilizing the physical behaviour of substances under various conditions can be used and developed as methods for non-destructive testing.

The following titles give some idea of the range of subjects that are covered in the papers: Some aspects of the mechanical testing of non-metallic solids; Symposium on optical and surface methods of non-destructive testing; The potentialities of X-ray diffraction studies in non-destructive testing; Symposium on principles of penetrant methods; Magnetic properties and the structure of metals; Principles and applications of nuclear magnetic resonance; Optical fluorescence in non-destructive testing; The effects of penetrating radiations on materials; Physical methods in medical diagnosis; The detection of fatigue in metals; Structural changes and energy dissipation during fatigue in copper; Measurement of elastic constants by the ultrasonic pulse method; The testing of fibres and their molecular structure.

The Supplement contains both a name and a subject index and nearly one hundred illustrations.

[NOTE: Supplements are no longer sent automatically to subscribers to this *Journal*.]

Laboratory and workshop notes 1953–1955. Compiled and edited by Ruth Lang. (London: Edward Arnold (Publishers) Ltd.) Pp. xii + 246. Price 30*s*. net.

The warm reception given to the first three volumes of these Notes, originally published in the *Journal of Scientific Instruments*, prompted the Board of the Institute of Physics to invite Dr. Ruth Lang to prepare this fourth volume which, in his preface, Sir John Cockcroft cordially recommends to laboratory workers. This series of volumes has become known in some quarters as "a catalogue of ingenuity," and this can equally be said of the new collection. It is divided into the following sections: Graphs, records and charts; Mechanical design and devices; Laboratory and workshop methods and tools; Optical and thermal devices and techniques and infra-red spectroscopy; Devices for liquids and gases; Vacuum and high pressure devices and techniques; Electrical devices and techniques.

A further handbook of industrial radiology. Edited by W. J. Wiltshire. (London: Edward Arnold (Publishers) Ltd.) Pp. viii + 338. Price 30*s*.

The *Handbook of industrial radiology*—now in its second edition—was based on a series of lectures given by the Non-Destructive Testing Group of the Institute of Physics. Those lectures were mainly confined to essentials and the handbook was, and still is, of the greatest value to all concerned with the application of radiology to industrial purposes.

Today, the basic principles of radiological inspection remain unchanged; the methods and techniques discussed in the handbook are still essential. At the same time, the ceaseless flow of scientific progress has brought much that is new. The development of accelerators has made possible the production of radiation of high energy and in great intensity; the advent of a supply of radio isotopes, with their convenience and adaptability, has facilitated many applications of radiological methods; electronic progress has made automatic inspection more practicable in suitable cases. These and other such advantages have greatly extended the radiologist's potential field of activity.

It was clear that some collected account of these new developments should be made available to workers in radiological inspection, and to provide such an account is the main purpose of the present volume. The ground covered in the handbook is not repeated, but some of the subjects crowded out of that book (fluoroscopy, stereoscopy and so on) have been included and somewhat fuller treatment has been given to some matters, such as the various radiation scattering processes and the factors affecting radiographic qualities. The present book may be regarded as the complement of the handbook and is in no sense intended to supersede it. As before, each chapter has been written by a specialist in the subject dealt with. The titles of the chapters are: High voltage X-ray generators; Natural and artificial sources for gamma-radiography; Scattered radiation; Radiographic quality and sensitivity; Films and their processing; The reproduction of radiographs; Fluoroscopy; Electrical methods for detection and measurement; Weld radiography; Castings and their radiography; Microradiography; Flash radiography; Stereo methods; Industrial Xeroradiography; An introduction to applied X-ray diffraction methods.

Once again through the generosity of the editors and the authors the royalties from the sales of the above two books will be passed to the Institute of Physics' Benevolent Fund. Not only for this reason but for their own advantage we cordially invite readers to order their copies forthwith.

Notes and comments

British Conference on automation and computation

At the invitation of The Institution of Civil Engineers, The Institution of Mechanical Engineers and The Institution of Electrical Engineers, exploratory Conferences were held on 6th March and 16th April, 1957, as a result of which the representatives of some twenty organizations, with interests in the fields of automation and computation, approved proposals for closer collaboration, and agreed to recommend them to their Councils for adoption. The proposals, if accepted by the bodies concerned, will result in the setting up of a British Conference on automation and computation which will be organized in three groups of Societies, having the following fields of interest:

Group A. The engineering applications of automation techniques; *Group B.* The development and applications of computers, automatic controls and programming techniques; *Group C.* The sociological and economic aspects of automation and computation procedures.

The following bodies would be invited to act as the conveners and sponsors of the three groups:

Group A.

Convener: Institution of Mechanical Engineers; *Additional Sponsors:* Institution of Civil Engineers, Institution of Chemical Engineers, Institution of Electrical Engineers, Institution of Production Engineers.

Group B.

Convener: Institution of Electrical Engineers; *Additional Sponsors:* Institute of Cost and Works Accountants, Institute of Physics, Office Management Association, Society of Instrument Technology.

Group C.

Convener: British Institute of Management; *Additional Sponsors:* Industrial Welfare Society, Institute of Cost and Works Accountants, Institute of Personnel Management, Institution of Production Engineers.

An essential feature of the proposals is that liaison between the groups should be established on a permanent basis from the outset, and it is foreseen that the central unit of the Conference which will be established for this purpose will undertake such other duties as may be deputed to it by the groups; for example, the preparation of periodical digests of published papers falling within the general fields of automation and computation.

All societies and institutions interested in the subject will be most welcome to support the activities of the Conference by applying for membership of the appropriate group or groups. Further information may be obtained from the Secretary, The Institution of Electrical Engineers, Savoy Place, London, W.C.2.

The Board of the Institute of Physics has accepted the proposals and appointed Dr. A. D. Booth and Dr. H. R. Lang as its representatives to Group B; they were its representatives at the exploratory Conferences.

Radiofrequency Spectroscopy Symposium

The Committee which was appointed at the symposium held under the auspices of the Liverpool and North Wales Branch of The Institute of Physics in Bangor last September, announces that it is arranging for the next symposium to be held in the University of Southampton from 19–21 September. The meeting will be mainly concerned with investigations by electron resonance techniques. Further details are available from Dr. D. J. E. Ingram, The University, Southampton, or the Deputy Secretary, The Institute of Physics, 47 Belgrave Square, London, S.W.1.

Journal of Scientific Instruments

Contents of the June issue

SPECIAL ARTICLE

Instrument transducers. By J. Thomson.

ORIGINAL CONTRIBUTIONS

A water-cooled mercury arc lamp for the excitation of Raman spectra. By L. A. Woodward and D. N. Waters.

An apparatus giving thermogravimetric and differential thermal curves simultaneously from one sample. By D. A. Powell.

Single crystal oscillation photographs about three crystallographic axes from a single setting on a Weissenberg camera. By J. Shankar and P. G. Khubchandani.

An automatically recording vacuum balance. By M. I. Pope.

Optical and instrumental limitations to the accuracy of "oximetry". By R. H. Kay and R. V. Coxon.

A solid state paramagnetic resonance spectrometer. By P. M. Llewellyn.

An evaporated gold bolometer. By E. Archard.

The design of calorimeters for the determination of ion beam intensities. By E. R. Harrison.

Laboratory and workshop notes

A vapour trap for vacuum systems. By G. K. T. Conn and H. N. Daglish.

An autographic testing machine. By A. A. Barker.

High-temperature plasticity measurements in controllable atmospheres. By J. D. Mackenzie.

A demountable seal for high vacuum work. By V. A. Heathcote and W. E. Read.

Lattice parameter determination from broad diffraction lines. By F. R. Brotzen and E. L. Harmon.

A new demountable ultra-high vacuum joint. By J. Drowart, P. Goldfinger and R. van Steenwinkel.

An instrument for use in ultra-microtomy. By A. L. Sims and T. S. Leeson

NOTES AND NEWS

Correspondence

A simple arrangement for obtaining optical transforms of crystal structures.

New books

New instruments

Notes and comments

THIS JOURNAL is produced monthly by The Institute of Physics, in London.

It deals with all branches of applied physics (including theory and technique). All rights reserved. Responsibility for the statements contained herein attaches only to the writers.

EDITORIAL MATTER. Communications concerning editorial matter should be addressed to the Editor, The Institute of Physics, 47 Belgrave Square, London, S.W.1. (*Telephone:* Sloane 9806.) Prospective authors are invited to prepare their scripts in accordance with the *Notes on the preparation of contributions*. (Price 2*s.* 6*d.* including postage.)

REPRODUCTION. The Institute of Physics is a signatory to The Royal Society's Fair Copying Declaration. Details may be obtained upon application from The Royal Society, London, W.1.

ADVERTISEMENTS. Communications concerning advertisements should be addressed to the agents, Messrs. Walter Judd Ltd., 47 Gresham Street, London, E.C.2. (*Telephone:* Monarch 7644.)

CLAIMS FOR MISSING JOURNALS. Claims from regular subscribers to this *Journal* for missing numbers will only be considered if received within 60 days of the date of mailing plus normal outward time of transit and time for lodging the claim. Losses attributable to failure to notify a change of address or to similar omissions will not be considered.

SUBSCRIPTION RATES. A new volume commences each January. The charge is £5 per volume ($14.25 U.S.A.), including index (post paid), payable in advance. Single parts, so far as available, may be purchased at 10*s.* each ($1.50 U.S.A.), post paid, cash with order. Orders should be sent to The Institute of Physics, 47 Belgrave Square, London, S.W.1, or to any bookseller.

Summarized proceedings of a conference on electron microscopy—Reading, July 1956

The annual conference of the Electron Microscopy Group was held in the Departments of Chemistry and Physics of the University of Reading on July 24–26, 1956. Papers covering the theory, construction, and application of the instrument were read, and in addition five papers on the applications of electron diffraction were presented.

ELECTRON OPTICS

The conference opened with a paper by MR. A. W. AGAR and MR. M. E. HAINE (Associated Electrical Industries Ltd., Aldermaston, Berks) on a magnetic-electrostatic gun alinement section for an electron microscope, which could be used for either transmission or "reflexion" working. This section, although only about 2 in. long, allows for tilt and position alinement in two perpendicular co-ordinates, and a beam tilt up to 18° in one co-ordinate for reflexion working. The tilts are all arranged so as to produce no movement of the illuminating spot in the image plane. This performance is achieved by the use of two electro-magnets for deflexion in one co-ordinate, the magnet pole-pieces being insulated from the core and used as electrostatic deflector plates for deflexion in the perpendicular co-ordinate. Mumetal is used throughout for the magnet cores and polepieces.

Mr. Haine then read another paper on contrast with elastic and inelastic scattering processes. He calculated the contrast due to elastic and inelastic scattering of electrons in the electron microscope on a wave-optical basis. Various approximations were made, especially in the case of inelastic scattering where additional scattering data is required for a rigorous analysis. He showed that the major contribution to contrast arises from the elastic wave which is scattered from the gap left in the illuminating wavefront by the inelastically scattered electrons. The next most important effect is by phase contrast with elastic scattering. If phase or amplitude contrast is very small, the inelastically scattered electrons have little effect except for extended objects.

MR. T. MULVEY (Associated Electrical Industries Ltd., Aldermaston, Berks) described an improved electron-optical system for an X-ray microanalyser. In X-ray microanalysis as introduced by Castaign and Guinier in 1949,[1] one of the chief difficulties encountered is that the electron current obtained in the fine electron "probe" has been small (10^{-8} A). Calculation shows that with good lens design, a current of about 10^{-6} A should be possible in a probe of one micron diameter. A lens system has been designed to do this, giving the possibility of extending the micro-analysis to light elements, such as carbon. A way of using a standard optical microscope to view the selected area has also been incorporated in the design.

Mr. Haine and Mr. Agar then read a further paper on the design of a double condenser lens and its alinement criteria. They analysed the tolerances for the alinement of the source and for the condenser lens pole bores in the magnetic electron microscope illuminating system. It was shown that, for a single stage condenser lens, the source alinement tolerance is about 1 mm. In the case of a double condenser lens, a much smaller tolerance is allowable if it has to be ensured that the illumination is not lost at critical focus when the magnification of the condenser system is changed. The design of a suitable double magnetic condenser lens was discussed, taking into account the conditions of optimum operation, reasonable size, and reasonable symmetry tolerances for negligible astigmatism.

INSTRUMENTATION

Investigations of electron emission systems containing hairpin filaments were described by MR. K. DOLDER (Atomic Energy Research Establishment, Harwell). It is commonly observed that two or more electron sources can co-exist in such systems and experiments were described which indicated that one source was the filament tip and the other a small emitting space charge which, for low values of grid bias, could split into a number of discrete components. This splitting was attributed to electron space charge oscillations. Measurements with a system containing two hairpin filaments enabled the frequency f of these oscillations to be estimated from the average distance between adjacent electron sources. The results were compared with the Tonks and Langmuir formula:[3] $f = 8980\sqrt{n}$ c/s, where n is the number of electrons/cm^3 of the space charge. Agreement was found if it was assumed that electrons entered the oscillating charge with only thermal energies. Measurements of anomalous angular distributions of emission from hairpin systems were described and they were shown to be the result of space charges situated close to the filament. The conditions under which a virtual (space charge) cathode formed in hairpin systems was discussed and its properties were outlined. Optimum operating conditions for hairpin systems were suggested.

In a brief note MR. AGAR discussed the minimum brightness of the image for high resolution working. He used a ×10 light microscope for viewing the fluorescent screen and deduced that for any fringe width at the object, optimum visibility is obtained when the electron optical magnification is such as to give a 70 μ fringe on the fluorescent screen. Thus for a 10 Å fringe at the object, the electron optical magnification should be 70000 diameters, and the screen brightness not less than $\bar{2}\cdot5$ log. foot lamberts, with the illuminating system operating under conditions required for high resolution.

MR. R. MILLER and DR. J. W. SHARPE (Royal Technical College, Glasgow) outlined a method of measuring the amount of rotation produced by the lenses of a three-stage electron microscope.[4] A shadowcast replica of a diffraction grating was inserted in the microscope in such a way that the lines were parallel to the axis of tilt of the stereo device. Micrographs were taken at various magnifications and combinations of lens polarities, and an estimate of the rotation produced by each lens was obtained. The authors found the calibration to be of use in stereoscopic work as it has enabled the amount of back rotation of the plates to be calculated

A set of lens currents was standardized to give a total rotation of 45° and thus (on the Metropolitan-Vickers type E.M.3 machine) give the axis of tilt parallel to one side of the photographic plate.

A simple photomultiplier photometer suitable for electron microscopy was described by DR. R. BARER and DR. R. G. UNDERWOOD (Department of Human Anatomy, University of Oxford). They found a need for a portable, robust and highly sensitive photometer for use as an exposure meter in both light optical and electron microscopy (especially by the reflexion method). An obvious solution was to use a photomultiplier tube, but the stabilized power supply usually considered necessary was both bulky and expensive. The performance of type 931A photomultipliers (by Radio Corporation of America) was tested on unstabilized mains supplies and it was found that for many purposes the stability was quite adequate. Additional stabilization was rarely required when the instrument was used as an exposure meter for photography, and even when used with a recording microdensitometer the stability was good over periods of a few minutes. Excellent long-term stability could be provided by a simple constant voltage transformer. The instrument finally developed consisted of a photomultiplier with unstabilized 800 V d.c. supply, feeding into a balanced valve voltmeter circuit, using a single double-triode valve. Sensitivity could be varied in steps of three over a range of 243 times. The output varied linearly with light level to within 2%. An important feature was the provision of a device whereby the sensitivity was always adjusted to the same value whenever the reading was taken irrespective of the actual value of the mains voltage. This was achieved by balancing the voltage applied to one dynode against that of a small battery. The instrument is thus in a sense manually stabilized and will give accurate results provided no gross mains fluctuations occur during the short time necessary to take a reading.

DR. K. ITO (Japan Electron Optics Laboratories, Tokyo) read a paper describing some changes in specimens which take place when the specimen is heated and cooled in the microscope. The apparatus used was described in some detail.

MR. HAINE and MR. R. PAGE described a new 100 kV three-stage electron microscope (type E.M.6 by Metropolitan-Vickers Electrical Co. Ltd.) which gave facilities for transmission, reflexion working and electron diffraction. The instrument is capable of a regular instrumental resolving power of at least as good as 15 Å. It was fitted with specimen and camera airlocks and a multi-plate camera. The instrument was designed essentially for very high performance, and made full use of the many features developed in the Associated Electrical Industries' and Metrovick Laboratories. The microscope was mounted on a desk stand of the same type as this company's type E.M.3 microscope, but it had a larger viewing window.

SPECIMEN TECHNIQUES

DR. G. M. JEFFREY and DR. J. SIKORSKI (Textile Physics Laboratory, University of Leeds) described the development of an ultrasonic apparatus for specimen preparation in the study of the fine structure of keratin. They used a low frequency ultrasonic system in preference to a high frequency apparatus as the more favourable for the dispersion of fibres into their fundamental morphological units, i.e. microfibrils. The preliminary experiments were made using a Mullard ultrasonic generator, type E 7590 B with a standard magnetostrictive transducer, immersed in a large volume of water in order to provide adequate cooling. The sample, contained in a cellophane bag, was suspended in front of one of the transducer faces at a distance of about 1 to 2 cm. The acoustic output of the transducer (9·5 W/cm^2 at 25 kc/s) was found adequate to disperse collagen into fine undamaged fibrils which showed the usual bands in the electron micrographs. It was realized, however, that a higher acoustic output may be required to disperse the highly cross-linked keratin. Furthermore it was thought advisable to reduce the danger of heat denaturation of keratin by removing the sample away from the source of eddy-current heating, i.e. the transducer. These requirements were satisfied by using an acoustic transformer described by Neppiras[5] in connexion with a high frequency reciprocating drill. The transformer is essentially an acoustic loudspeaker working backwards, to provide a step-up ratio of acoustic energy from the transducer. From the fundamental acoustic equations it is possible to obtain an explicit solution assuming the boundary of the horn as exponential in shape.[6] For the resonant transformer the particle velocities, and therefore the amplitudes, are increased at the small end, as compared with the large end, in the inverse ratio of areas—or diameters, for circular cross-section. The nodal plane, where particle velocities are zero, determines the position at which any clamping could be applied. The resonant length of the transformer, made from brass, was chosen as a half-wavelength and the step-up ratio as 2, thus giving an acoustic output 19 W/cm^2, if the transducer coupling was perfect; allowing for 20% at this interface, the acoustic energy transmitted into the suspension should be about 15 W/cm^2. The input end of the transformer was screwed into a brass element attached to the transducer by means of the bolts, holding the laminations together (Fig. 1).

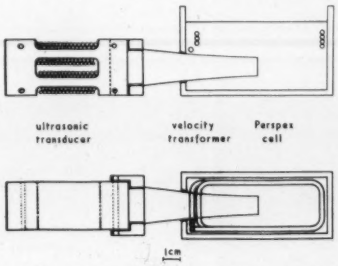

Fig. 1. An ultrasonic apparatus used for the dispersion of fibrous proteins

A more efficient coupling could be obtained by silver-soldering the transformer to the transducer, but the present arrangement is efficient enough to provide vigorous cavitation. The transformer was inserted into a hole drilled in a side wall of an open Perspex cell, of a diameter equal to the nodal diameter. The waterproof compound (Bostik 771) forms a seal between the transformer and cell wall; thus a flexible support is provided, allowing for a finite thickness of the wall. The transducer and the whole assembly were cooled by immersion in transformer oil, which was continuously circulated from the containing vessel through a coil submerged in cold running water and finally returned directly on to the transducer/transformer interface. An additional cooling of the suspension was effected by circulating cold water through a coiled glass

tube which fitted into the cell; thus the overall temperature of the suspension could be maintained below 30° C indefinitely. Attempts at ultrasonic dispersion of untreated keratin fibres were not successful. Therefore, the ultrasonic dispersion was tried either on cortical cells separated from untreated fibres, by well-known methods of enzymic digestion, and subsequently chemically treated, or cortical cells obtained from already chemically pre-treated fibres. In either case even prolonged ultrasonic irradiation of water suspensions failed to reveal any change in keratin material. However, some swelling agents, known also for their ability to attack hydrogen bonds, produced the desired effect. Saturated urea or lithium bromide were found convenient (Fig. 2).

Fig. 2. Lincoln wool (cortical cell) treated in peracetic acid and exposed to ultrasonic vibrations in lithium bromide solution (×6800)

Dr. K. Little (Medical Research Council, Harwell, Berks) discussed some practical points in the preparation of connective and hard tissue sections. Work on these was still in the stage when it is necessary to use fairly low magnifications for comparison with orthodox histology, and the main immediate objective was to observe the interrelation of components. For this Dr. Little found it best to use large sections ($\frac{1}{2}$ mm across and upwards) while thick sections (0·1–0·5 μ) viewed stereoscopically were much easier to prepare than serial sections, and had the advantage of introducing less distortion on cutting. In dental enamel, with apatite crystallites of 2000 Å in length and over, thick sections were found essential. It was found that for embedding, a monomer must be used which could be polymerized without any great volume change (butylisobutyl methacrylate mixture), otherwise the specimen was distorted on its removal. Polymerization with ultra-violet light gave more control over the consistency, while a poor solvent such as amyl acetate was best for removing the embedding medium. Except in sections sufficiently thin for the embedding medium to be needed to hold things together, removing it was found to reduce artefacts and mistakes in interpretation, since its density is similar to that of some tissue components. Removal also increased the resolution. Except in the case of mature enamel, sections could be cut with a glass knife. It was found to be advisable not to shadow specimens intended for stereoscopic viewing.

(*a*)

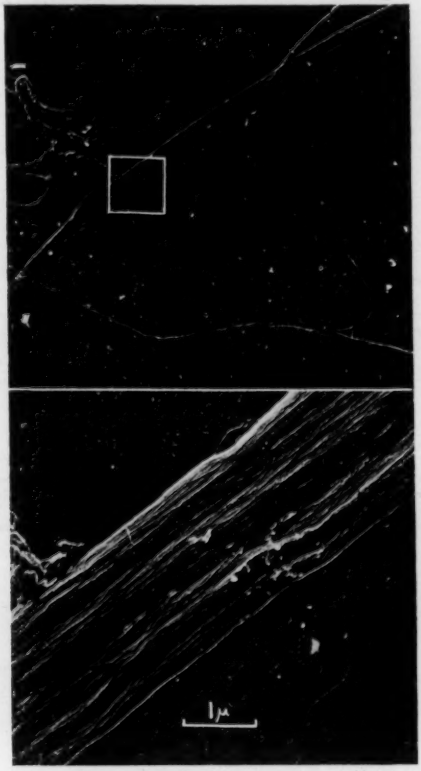

(*b*)

Fig. 3. Micrograph of a spruce tracheid mechanically beaten, carbon replica shadowcast with gold palladium

(*a*) × 6000
(*b*) × 15000

Mr. D. H. Page (British Paper and Board Industry Research Association, Kenley, Surrey) described a three-stage method for the carbon replication of extensive areas of fibres, the two intermediate casts being made in polymerized methyl methacrylate and polyvinyl alcohol. As a partial embedding technique is avoided, the surface presented for replication is extremely rough and the final carbon replica is very fragile. However, a handling technique that ensures that the replica can be mounted on its grid intact over large areas, is incorporated. The method is capable of resolving cellulosic

microfibrils (100–200 Å thick) and the initial methacrylate cast is retained intact and can be used for further replications (Fig. 3). In addition to its application to the study of fibres the method has been extended to the field of rough surfaces in general, particularly wood and paper surfaces. Mr. Page showed stereomicrographs at low magnification revealing information on both the gross and detailed structure of the specimens, and indicated the roughness of surfaces that can be replicated by this method.

MR. R. G. BAKER and DR. J. NUTTING (Department of Metallurgy, University of Cambridge) discussed direct carbon replicas in the study of fracture surfaces. They pointed out that the development of the direct carbon replica technique has greatly facilitated the study of fracture surfaces. Not only can high magnifications be used, but the greater depth of focus available in the electron microscope has meant that replicas of even very rough surfaces can be examined satisfactorily. The method has been used to examine fractures of many different types. Fractures in martensitic, temper brittle and tough steels from both izod and tensile tests can be easily replicated. Replicas have also been made of fatigue fractures in both steel and brass specimens. By taking extraction replicas, information can be derived about the role of other phases, e.g. carbides in the fracture path, and information can be derived on both the mode of initiation and of propagation of fracture.

MR. D. E. BRADLEY (Associated Electrical Industries Ltd., Aldermaston, Berks) described the direct stripping of carbon films from etched metal surfaces. In the early work on carbon replicas, unsuccessful attempts had been made to strip carbon films directly from steel surfaces by floating them on to a water surface. It was felt that it might be possible to wet-strip carbon films from non-ferrous metals in spite of the lack of success with steels. The technique employed consisted of coating the etched specimen with about 100 Å of carbon and floating this onto water, with or without a backing of Bedacryl (polyacrylic ester by Imperial Chemical Industries Ltd., used as 7% solution in benzene). This method had previously been employed by Diehle, Mader and Seeger on electropolished copper, aluminium and nickel. It was found that it was possible to strip carbon directly from many metals, including silicon, germanium, titanium, brass, uranium, aluminium and others. The most suitable specimen so far had been found to be brass, and slides were shown of the sort of structure from which carbon replicas could be stripped. The depth of etch in one case was very deep and many pyramid-like protrusions resembling possible sub-grain structure were found. However, there was no indication of re-entrant structure which might key the carbon film to the surface. It was pointed out that this method was so simple as to be worth trying on any specimen on the chance that it might succeed. If it did so, the resulting replica would be reliable, free from artefacts, and at the same time the structure surface of the metal specimen would be preserved. If it did not succeed, the use of etchants for loosening the film would have to be employed as suggested by Nutting, but, in this case, the structure would be destroyed in the process.

MR. H. L. NIXON and MR. H. L. FISHER (Rothamsted Experimental Station, Harpenden, Herts) read a paper describing modifications to the original spray droplet technique of Backus and Williams,[7] as a result of which practical difficulties in the application of the method are overcome. Droplets are caught in a cascade impactor,[8] which makes it possible to select the size range desired. The use of much smaller droplets than those used in the original method makes it necessary to use a smaller standard particle, and they have used the Dow latex LS 040A, their estimate for the diameter of which is 850·33 Å, in good agreement with the 880 Å given by the manufacturers. This latex has not yet been measured by methods other than electron microscopy, but since the same considerations apply, a critical review of the data for the original Dow latex 580G is useful in assessing the validity of measurements on LS 040A made with the electron microscope. From such a review they conclude that there are good reasons for suspecting a possible fixed error of up to 18–20% in all counts made by methods of this kind, owing to errors in the determination of the mass of a single standard particle. Until the reasons for different values of particle diameter for the same latex obtained by different methods of measurement are better understood it seems reasonable to accept the value given by electron microscopy, which lies between that obtained by sedimentation and the interparticle distance as measured by X-ray diffraction. Making this assumption, the mean mass of a single Dow LS 040A particle is $3{\cdot}75 \times 10^{-16}$ g. The modified method gives results in very close agreement with the known amounts of tobacco mosaic virus present in dilutions from a concentrated purified preparation, and with the results of serological precipitin tests on such dilutions.

MR. R. W. HORNE and MISS E. M. GREEN (Cavendish Laboratory, University of Cambridge) gave an account of studies of tobacco mosaic virus and turnip yellow mosaic virus using the carbon replica technique. X-ray diffraction experiments have suggested that the protein content of tobacco mosaic virus rods are arranged in the form of a helix with a pitch of 23 Å and a repeat distance of 69 Å.

Fig. 4. Tobacco mosaic virus (×140 000)

Electron microscope studies of tobacco mosaic virus at high instrumental magnification using carbon replicas have revealed periodicities along the axis of the rod with a mean distance of 46 Å. Many of the rods observed appear to have an angular cross-section (Fig. 4). Carefully prepared suspensions of tobacco mosaic virus were dried down on clean

glass surfaces. Carbon was evaporated directly on to the rods at an angle of 30° to the normal approximately 50 Å thick. The carbon was then stripped off and placed in 2 N KOH at 60° for 20 min to remove any remaining virus rods pulled away after stripping. After a suitable washing period the replicas were mounted on copper grids and examined in the Siemens–Elmiskop microscope at instrumental magnification of ×40 000 and ×80 000. Although the total object thickness of the specimen is reduced by using carbon replica techniques and several interesting features observed, further work will be necessary to investigate the possible artefacts caused by the piling up of carbon on the specimen surface. Turnip yellow mosaic virus was examined using this technique and revealed a definite angular shape to the individual particles with some indication of surface structure.

MR. A. W. AGAR described a method for the measurement of thickness of thin carbon films.[9] This device consisted of a light condenser (a ×10 reducing lens) and a similar lens to make the beam of light parallel again having passed through focus, together with a photomultiplier, the output from which was measured by a sensitive microammeter. The slide on which the carbon film was deposited was placed at the focus of the light beam. The optical density of carbon films, found by this method, was compared with the thickness of the films as determined by interferometers. The graph of optical density against film thickness was, with the exception of a small inverted "foot," a straight line. This method could be used to determine the thickness of a carbon film while evaporation was proceeding.

MR. M. S. C. BIRBECK and DR. E. H. MERCER (Chester Beatty Research Institute) described the use of amoebae as test objects for fixation and embedding. Amoebae are single-celled organisms of a convenient size for comparative study in the light and in the electron microscope. The organism may be watched during fixation, dehydration and embedding and gross alterations in structure noted. Dark ground illumination was found to be particularly satisfactory since both the external cell membrane and numerous intracellular particulates are well displayed. Immediately following the addition of the standard osmium fixative all movement ceases. After prolonged fixation (more than 2 h) Brownian movement appears pointing to a destruction of the intracellular gel. A similar change occurs after some hours in 70% ethanol, and the external membrane also becomes more refractile. Both prolonged fixation or dehydration lead to a poorly preserved structure judged electron microscopically. However, even when fixation and dehydration appear to be successfully effected further faults appear during polymerization in methacrylates. These seem to be due to an uneven and too rapid polymerization within the cell, which may cause a gross cracking or swelling of limited regions.

CHEMICAL APPLICATIONS

An electron-optical study of the oxidation of thin lead films was described by MR. D. KIRKWOOD and DR. J. NUTTING (Department of Metallurgy, University of Cambridge). Single crystal films of lead sulphide were produced by vacuum evaporation of the sulphide on to a freshly cleaved surface of rocksalt [(100) face of lead sulphide parallel to (100) cleavage face of rocksalt]. The oxidation of this film at 300° C was studied by stripping the film and examining it with the electron microscope and by transmission electron diffraction. The reactions varied with film thickness. Thin films (approx. 150 Å) produced hexagonal plates which grew very slowly. Thicker films (approx. 400 Å) showed greatly increased nucleation, with particles clustering in bands along certain crystallographic directions; a background structure was observed consisting of needles orientated at 45° to the plates. These needles were interpreted from the electron diffraction examination to be recrystallized lead sulphide. The plane spacing of the reaction product agreed most closely with those calculated by Wilman for lanarkite ($PbOPbSO_4$).

MR. R. H. OTTEWILL (Department of Colloid Science, University of Cambridge) and MR. R. W. HORNE (Cavendish Laboratory, University of Cambridge) gave an account of an electron microscope examination of freshly prepared silver iodide sols. Freshly prepared silver iodide sols have been examined in a high resolution electron microscope (a Siemens–Elmiskop type UM 100) which has a potential resolving power of 6–10 Å. Numerous small particles of the order of 10–25 Å have been resolved (Fig. 5). Only particles which

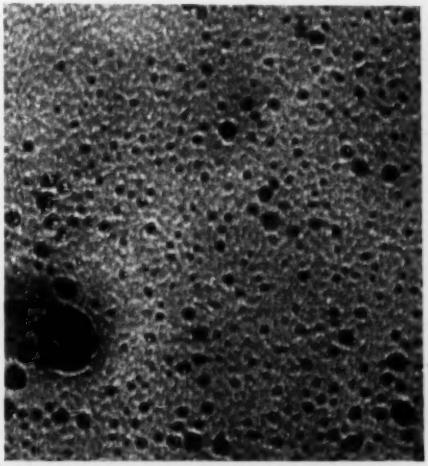

Fig. 5. Silver iodide sol (×300 000)

were clearly resolved from the background structure and which could be reproduced on duplicate plates were measured, although there was evidence that smaller particles varying from 6–10 Å were present. The sols were always freshly prepared in order that ageing phenomena, which included possible changes in the form and size of the particles due to recrystallization or slow flocculation, should not become important. The presence of very small particles in the sol demonstrates that colloidal particles may exist almost down to the range of atomic dimensions, and suggests that such preparations may be useful as a standard of resolution in the 10 Å region.

MR. J. A. GARD (Department of Chemistry, University of Aberdeen) described some electron microscope studies on calcium silicates. The minerals okenite,[10] foshagite and tricalcium silicate hydrate are too finely divided for single-crystal X-ray work, and the symmetry is too low for determination of the unit cells from powder or fibre diffraction patterns. Correlation of the latter with electron-diffraction

patterns recorded in the electron microscope from single crystals enabled the unit cells to be derived. It was shown also that orientation during dehydration to wollastonite was preserved completely in the case of foshagite, but only partially in the case of okenite. Electron diffraction of small single crystals can also give information about reflexions which are too weak to record on X-ray powder patterns. The (00l)-spacings of tobermorite from Loch Eynort are stable, while those of other tobermorite minerals shrink during dehydration. Electron diffraction showed that the superlattice reflexions are much more complex in the Loch Eynort mineral, and that the principal cleavage is (100), while that of the other minerals is (001).[11] A fundamental difference in structure was thus revealed between minerals which gave identical X-ray patterns.

Dr. D. Scott and Mrs. H. M. Scott (Mechanical Engineering Research Laboratory, East Kilbride) described an electron microscope study of the structural changes of greases in rolling bearings. As the fine fibres in greases are of dimensions beyond the resolving power of the best light microscopes, the electron microscope was used to study the primary fibre changes which take place in a grease subjected to mechanical working. Methods of specimen preparation were discussed and the method used was described. The oil phase was removed by vacuum vaporization to leave the fibres unchanged in size, shape and arrangement for viewing in the electron microscope. The electron micrographs showed differential breakdown of the fibres by different degrees of mechanical working (Fig. 6). The grease actually

Fig. 6. Fibre structure of an unused lime base grease. The oil phase was removed by vacuum vaporization (×20 000)

worked between the rolling and sliding surfaces suffers a rapid degradation of the fibre structure and shows that the severity of operating conditions in these parts of a bearing are greater than those imposed by a conventional grease worker or tester.

Mr. G. A. Bassett (Tube Investments Research Laboratory, Saffron Walden, Essex) described an attempt to study the crystallinity of polyethylene by electron microscopy. Solvent cast films of polyethylene have been examined in the electron microscope. A well defined spherulitic structure has been observed and the system of radiating fibrils of which each spherulite is made up (Fig. 7). The helically wound

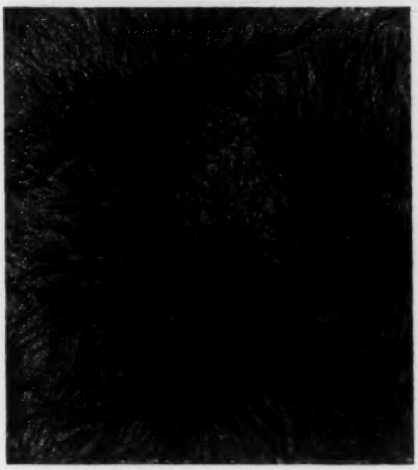

Fig. 7. Transmission electron micrograph of solvent cast film of polyethylene showing spherulite structure (×64 000)

ribbon structure of the type proposed by Keller has not been observed although the dimensions of the proposed helices are well within the resolutions of the microscope used (a Siemens–Elmiskop type I). Along some of the spherulite fibrils a periodic structure with a repeat distance of about 100 Å has been observed. This is about the same magnitude as some repeat distances observed by low-angle X-ray scattering by various workers. The contrast in the micrographs of polyethylene film appears largely to arise from changes in the thickness of the film; this has been demonstrated by the similarity between a carbon replica of the film surface and direct transmission micrographs of the polymer film. At magnifications of over ×500 000, no structure whatever is detectable in accurately focused micrographs of the polyethylene film. When the microscope image is slightly out of focus the phase contrast introduced produces a detailed small scale structure. This may be some manifestation of the intertwining of the polymer chains but at the present time the theory of image formation under these conditions does not permit of any detailed interpretation along these lines. Dark field electron microscopy appears in principle to offer a method to distinguish between the crystalline and amorphous regions of the polyethylene film. In practice it appears that the polymer is very rapidly rendered amorphous by the cross-linking action of the electron beam of the microscope. This precludes the taking of micrographs while preserving the crystalline nature of the polymer film examined. Some exploratory experiments have been made using electron

stains as a means to delineate between the crystalline and amorphous regions of the polymer. Treatment of polyethylene films with uranium nitrate solution has shown up a marked periodic structure along the spherulite fibrils. The morphology of thin films of some other polymers have also been studied, notably nylon and polymethylene.

BIOLOGICAL APPLICATIONS

The experimental "ageing" of connective tissue in rabbits' ears was described by MISS P. TYMMS (Department of Experimental Pathology and Cancer Research, School of Medicine, University of Leeds). During work by Dr. B. Jolles, of Radiotherapy Department, General Hospital, Northampton, it became necessary to carry out an electron microscope examination of the collagen fibres in the subcutaneous connective tissue of rabbits' ears. The ears had been subjected to mechanical stresses and strains. Variation in treatment was effected by varying the duration of the whole period of treatment, or by varying continuity of treatment. In two cases, treatment was carried out after the death of the animal. In general, the effect of stretching the ears was to remove the amorphous ground substance (AGS) which was present as a coating material in fibrils from untreated ears (Fig. 8). If, after a period of treatment, the ear was "rested" (i.e. left untreated) for two or three weeks, there was a re-accumulation of AGS on the fibrils. The ears treated after the death of the animal also showed a removal of AGS, so that, to some extent, the removal may be due to mechanical factors. Previous work[12] has shown that with increasing age there is a decrease in amount of AGS coating the fibrils, and it is thought that a similar effect has been produced here by mechanically "ageing" the ears. This effect, however, cannot be regarded as being exactly comparable with senescence, since the re-accumulation of AGS on resting the ears shows it to be a reversible process.

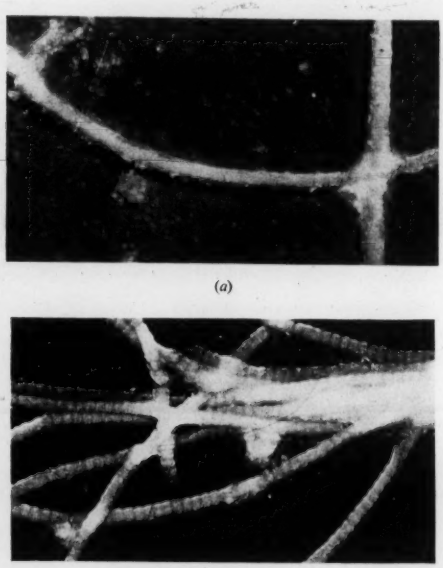

(*a*)

(*b*)

Fig. 8. Collagen fibrils from rabbit's ear (×26 400)
(*a*) untreated.
(*b*) stretched.

The value of carbon replicas in the electron microscopy of *Synura* and *Mallomonas* was discussed by MR. D. E. BRADLEY (Associated Electrical Industries Ltd., Aldermaston, Berks) and DR. K. HARRIS (University of Reading). *Synura* and *Mallomonas* are small unicellular organisms classed in the order Chrysophyceae which belongs to the Algae. They are found in many ponds and ditches from February to April. Both organisms are covered with minute silica scales, the structure of which varies according to the species and is

Fig. 9. Shadowcast carbon replica of scales of *Mallomonas Leboimii* (×3500)

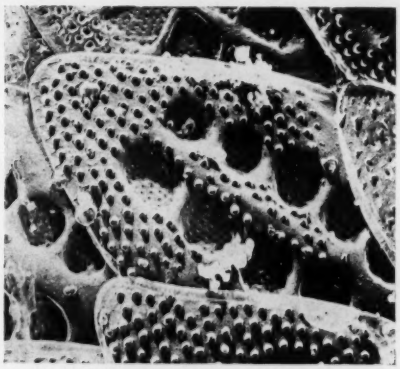

Fig. 10. Shadowcast carbon replica of scales of *M. Lychenensis* (×12 000)

hence of great value in the identification and classification of species. The optical microscope reveals the gross features of these scales, but the electron microscope alone can show up the very fine detail and elaborate sculpturing. Some species of *Mallomonas* were first described and electron micrographs shown of actual scales and carbon replicas of scales (Fig. 9). It was found that, in this case, carbon replicas were more satisfactory because of the relative thickness of the scales themselves. In addition, replicas differentiated between the inner and outer surfaces of the scales, and also permitted the study of complete organisms. Micrographs were also shown of several complete organisms. In the case of *Synura*, it was found that both replicas and a direct examination is necessary in order to obtain a complete picture of the morphology of the scales, which are rather thinner and more delicate than those of *Mallomonas* (Fig. 10). Comparison between direct electron micrographs and replicas indicated that many features were internal. In addition, the delicate scales of *Chrysosphaerella*, an organism belonging to a genus closely related to *Synura*, were shown and replicas were used to clarify the structural details. It would appear that a whole new field has been opened up for the electron microscope in the study of what can be broadly described as "pond life."

Dr. G. Eaves and Miss P. Tymms (Department of Experimental Pathology and Cancer Research, School of Medicine, University of Leeds) then gave a note on the structure of the collagen fibril. Sections of collagen fibrils in the subcutaneous connective tissue of mouse skin were examined. In these sections the typical periodic structure was clearly visible, and the density of the sectioned fibrils appeared to be much greater than that of the methacrylate embedding material (Fig. 11). It was thought that the appearance of fibrils in both transverse and longitudinal sections provided additional evidence for the solidity in structure of the fibrils (as opposed to the hollow structure ascribed to them by some workers).

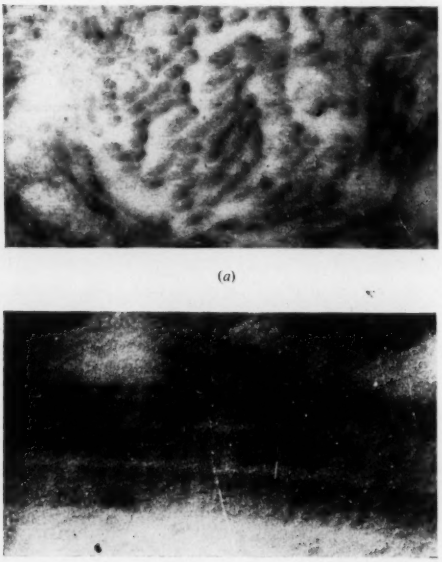

(*a*)

(*b*)

Fig. 11. Mouse skin collagen

(*a*) Transverse section (× 57 200).
(*b*) Longitudinal section (× 143 000).

CONFERENCE REPORT

Dr. J. W. Menter (Tube Investments Research Laboratory, Saffron Walden, Essex) gave an account of those parts of the Madrid Conference of the International Union of Crystallography which were of interest to the Group.

METALLURGICAL APPLICATIONS

An electron microscope study of the effect of lubricant on the initiation of wear was described by Dr. D. Scott and Mrs. H. M. Scott (Mechanical Engineering Research Laboratory, East Kilbride). As the initiation of damage in wear experiments can be expected to occur over a submicroscopic area the electron microscope was used to study the initiation of wear under various conditions. Micrographs of replicas revealed that small-scale features of interest in the study of wear can yield experimental evidence for postulated theories of the mechanism of wear and lubrication. Metal surfaces from wear experiments with a special crossed-cylinder machine were examined and revealed differential surface changes due to lubricant effect (Fig. 12).

An X-ray and electron optical investigation of tempered alloy steels were described by Dr. J. F. Radavich (Purdue University, Indiana) and Mr. R. G. Baker (Department of Metallurgy, University of Cambridge). An investigation of the tempering of alloy steels is being carried out using electron microscopy, electron diffraction, X-ray diffraction and X-ray fluorescent analysis to study the precipitated phases. An attempt is being made to correlate the microstructural changes observed with the changes in hardness and, where possible, with other mechanical properties. Direct carbon extraction replicas are used in each of the methods. They are mounted on copper grids for examination in the electron microscope and electron diffraction camera, on glass fibres for X-ray diffraction examination and on mylar films for X-ray fluorescent analysis. The preliminary results have been encouraging although more work is clearly necessary on the development of the techniques before their full potentialities are realized. It is possible, however, to identify and follow changes in the composition of alloy carbides produced over the whole range of tempering temperatures. The methods used are considerably quicker and are capable of much greater accuracy than the more conventional techniques, which involve electrolytic extraction of the carbides followed by X-ray examination and conventional chemical analysis.

Mr. E. Smith and Mr. J. A. Coiley (Department of Metallurgy, University of Cambridge) discussed some observations on the etching of ferrous materials. During an electron microscope investigation of the structure of etched specimens of ingot irons, plain carbon and certain alloy steels, using the direct carbon replica technique, a structure was observed within the ferrite grains and in some ferrite grain boundaries. This structure consisted of spot-like markings with a diameter and spacing of about 300 Å and a density of $1{\cdot}5 \cdot 10^{10}/\text{cm}^2$. The authors presented evidence to show that these markings were due to an inherent structure of the ferrite and not due to a fine precipitate or oxide formation on the surface. They suggested that the markings were due to carbon

rich regions within the grains and at the grain boundaries, and compared these regions with the carbon atmospheres around dislocations, of the type postulated by Leak and Thomas. The authors showed that if the markings did in fact represent some types of dislocations within the ferrite, then certain anomalies concerning the structures of the materials examined arose; these anomalies were briefly discussed.

Fig. 12. Reversed print of a shadowed Formvar replica showing wear damage on the surface of a hard steel cylinder (×16 000)

MR. W. I. MITCHELL and DR. J. NUTTING (Department of Metallurgy, University of Cambridge) described an electron metallographic of creep in aluminium–4% copper alloys. In an investigation of abnormal precipitation of θ' phase in Al–4% Cu alloy the effect of creep upon this precipitation was observed. Using oxide replicas stripped by electropolishing, comparison was obtained between slip observed in optical micrographs and sub-surface precipitation under the same spot on the specimen. Correlation was found between deformation and precipitation and at low temperatures precipitation occurred along slipped planes. Stripping by electropolishing does not, in contrast to $HgCl_2$, destroy the specimen. Thus the possibility of stripping serial replicas from different layers of the same spot arises. An attempt was made, using this technique, to investigate the nature of the abnormal precipitation in normally aged specimens. Due to the difficulty of the technique the results were indefinite but suggest two types of the effect associated with either unstable dislocation walls or stabilized single dislocations.

ELECTRON DIFFRACTION

DR. J. A. CHAPMAN (Physics and Chemistry of Surfaces Laboratory, University of Cambridge) gave an account of an electron diffraction study of retracted monolayers. Transmission electron diffraction patterns have been obtained from monolayers of long-chain polar compounds deposited by retraction on to thin evaporated metal films. The pattern from a fatty acid monolayer on evaporated silver or platinum consists of two diffuse rings (together with a third ring arising from contaminating bulk crystallites). The presence of two rings indicates some short-order regularity in the arrangement of the molecules and it is shown that the rings can be explained if it is assumed that the polar end-groups of the fatty acid molecules are arranged in much the same way as they are in the β-form of the bulk crystal. The chains in the monolayer, however, instead of being inclined to the basal plane as they are in the bulk crystal, are perpendicular to the substrate. The cross-sectional area per molecule is about 21 Å^2. The loose packing of the hydrocarbon chains in monolayers explains why no crystalline structure is revealed in reflection electron diffraction patterns.

An electron diffraction study of crystal imperfections was described by DR. T. B. RYMER (University of Reading). It is possible with suitable precautions to measure with an accuracy of 0·01% both the radii of electron diffraction rings and also the voltage applied to the diffraction camera.[13] With some specimens, such as vacuum evaporated sodium chloride, caesium iodide, etc., the lattice constants measured in this way agree with those determined by X-rays. In other cases, lattice constants derived from measurements of the different rings of a diffraction pattern differ among themselves and from the X-ray results. This indicates a distortion of the crystal structure. Three types of distortion have been identified:

(i) A homogeneous stress acting throughout the whole specimen.[14]
(ii) Stress set up in face-centred cubic crystals by sessile dislocations.[15]
(iii) Stacking faults in face-centred cubic crystals.[16]

Each type of distortion causes a characteristic variation in the apparent lattice constants derived from measurements of the different diffraction rings of a pattern, and it is therefore possible to determine the type of distortion in any particular case.

The radii of Laue zones in electron-diffraction patterns were discussed by MR. J. A. GARD. A procedure[17] was described in which a series of electron-diffraction patterns is recorded from a crystal tilted through known angles. One of the patterns is used as the datum for location of the centres of Laue zones on the other patterns. The tilt mechanism of the type E.M.3 instrument (by Metropolitan-Vickers Electrical Co. Ltd.) may be calibrated optically, but a small correction is necessary for the parallax between the specimen and the tilt axis.[18] A graph showed corrections necessary when large angles of tilt are used. When the "camera constant" is determined using a standard substance deposited along with the specimen on the grid, it was shown that the effective camera length need not be known accurately, and that a change in the specimen height from normal does not appreciably affect the accuracy.

DR. M. J. WHELAN, MR. R. W. HORNE and DR. P. B. HIRSCH (Cavendish Laboratory, University of Cambridge) gave an account of some electron optical transmission studies of metals. It occurred to them that much information might be obtained on the distribution of dislocations in metals by examining thin foils directly in the electron microscope. They described some experiments which they had performed on aluminium foils prepared by beating and etching. In the beaten foil, subgrains about 1 μ in size were observed, and the angular misorientation across the sub-boundaries was of the order of 1 or 2° (Fig. 13). In some boundaries the individual dislocations were clearly visible (Fig. 14), and the dislocation density estimated from such photographs was of the order of 10^{10}/cm^2. The dislocations and hence the sub-

grain boundaries always appeared darker than the surrounding regions, and this was interpreted in terms of more electrons scattered into Bragg reflexions from strained regions than from unstrained regions of the crystal lattice. Some dark field experiments supporting this view were described. Hexagonal networks and cross-grids of dislocation lines have been observed in agreement with dislocation theory.

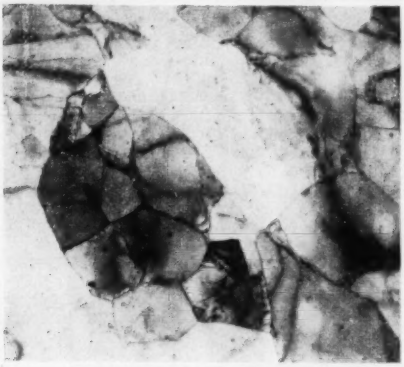

Fig. 13. Substructure in A beaten at room temperature. The average subgrain size in 1 μ, the average angular misorientation about $1\frac{1}{2}^{\circ}$. The dislocation density is about 10^{10} per cm^2

Fig. 14. A sub-boundary consisting of uniformly spaced dislocations. The average spacing of the dislocation is about 175 Å

Measurements of angular misorientations on several subgrain boundaries has enabled dislocation theory to be checked quantitatively. The reasonable agreement between theory and experiment indicated that the dislocations observed have unit Burgers vectors. Dislocations have been observed to move when working at large beam currents. Two types of movement are commonly observed. The first is a slow and jerky movement visible to the eye, which possibly corresponds to creep. The second is a fast movement, and is made visible by the trail left behind by the moving dislocation and the subsequent diffusion of these defects away from the slip plane. Cross slip by the Mott–Frank mechanism is observed frequently (Fig. 15). Finally a ciné film of the movement of dislocations was shown.

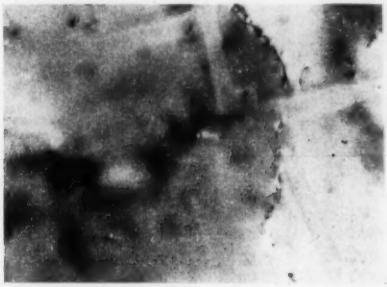

Fig. 15. Cross-slip by the screw dislocation mechanism. This plate was taken immediately after a dislocation had passed, and shows the band of contrast left behind. The bands are parallel to traces of (111) slip planes, and the contrast is thought to be due to point defects generated by the moving dislocation. At the point where the direction of the band changes through a right-angle the dislocation transfers from one slip plane to another

PHYSICAL APPLICATIONS

The final paper of the conference was a most stimulating description by Dr. J. W. Menter (Tube Investments Research Laboratory, Saffron Walden, Essex) of his work on the direct observation of crystal lattices and their imperfections by electron microscopy.[19] During the course of some work on imperfections in glass Dr. Menter observed a crack which was, at one point, of the order of 10 Å wide, i.e. in the region of the resolution limit of the electron microscope. It occurred to him that it might be possible to visualize, in the same way, rows of atoms, and imperfections in these rows, in a crystal. The publications of previous workers on the limit of resolution had stated that an instrumental resolution of 3 Å or better would be necessary to visualize the heavier atoms, but if the atoms were regularly arranged in a crystal, then the reflexions from the planes would reinforce one another and the rows of atoms be visualized in spite of having only 8 Å or so instrumental resolution. A suitable crystal was sought and the phthalocyanines, and in particular platinum phthalocyanine, was thought to be a possibility. It grows in long flat ribbon-like crystals, the surface of the ribbon being (001) and the ribbon axis [010]. The angle $(001)\hat{}(20\bar{1})$ is 88° so that a crystal of this habit lying on a horizontal supporting film has the $(20\bar{1})$ planes almost vertical, the spacing of these planes being 11·94 Å. These planes in fact proved to be resolvable and the spacing found agreed with that found by X-ray diffraction. Imperfections in the lattices were demonstrated in the micrographs (Figs. 16, 17, 18).

Dr. Menter then discussed the mechanism of the formation of this high resolution image in terms of the Abbé Theory of image formation for light microscopy. The image of the planes is formed as a result of interference between the zero

order and first order spectrum from the (20$\bar{1}$) planes which act as a diffraction grating. The ultra high resolution arises from the fact that the diffracted beam from a small crystal traverses a very narrow zone of the objective lens so that the imperfections in a wide range of materials in relation to properties such as strength, plastic flow, and fracture.

Although pointing out that the resolution of two lattice planes is not a direct measure of the resolving power of the

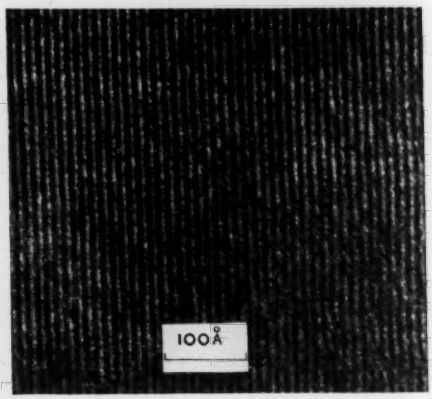

Fig. 16. Part of platinum phthalocyanine crystal showing (20$\bar{1}$) planes resolved, spacing 12 Å. Magnification (×1 500 000)

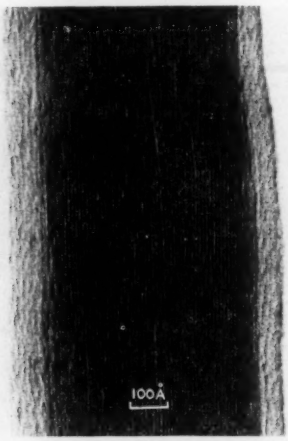

Fig. 17. Copper phthalocyanine crystal showing a number of dislocations. Magnification (×700 000)

effect of spherical aberration is not severe. Experiment has justified in general terms the validity of this approach. Dr. Menter suggested that the method might be extended to the study of crystals of even smaller lattice dimensions than the phthalocyanines, making possible the direct study of the

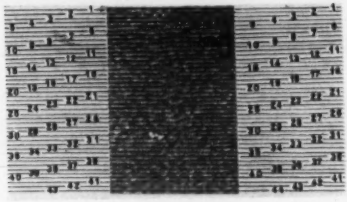

Fig. 18. Edge dislocation in platinum phthalocyanine crystal. Magnification (×750 000)

instrument, Dr. Menter suggested that we now have a comparative measure of the resolving power of one electron microscope relative to another.

C. E. CHALLICE

REFERENCES

(1) CASTAING, R., and GUINIER, A. *Proceedings of Conference on Electron Microscopy, Delft* (1949).

(2) DOLDER, K. T., and KLEMPERER, O. *J. Electronics*, **1**, p. 601 (1956).

(3) TONKS, L., and LANGMUIR, I. *Phys. Rev.*, **33**, p. 195 (1929).

(4) MILLER, R., and SHARPE, J. W. *J. Appl. Phys.*, **27**, p. 860 (1956).

(5) NEPPIRAS, E. A. *J. Sci. Instrum.*, **30**, p. 72 (1953).

(6) CRANDALL. *Theory of vibrating systems and sound* (London: Macmillan and Co. Ltd., 1927).

(7) BACKUS, R. C., and WILLIAMS, R. C. *J. Amer. Chem. Soc.*, **71**, p. 4052 (1949).

(8) MAY, K. R. *J. Sci. Instrum.*, **22**, p. 187 (1945).

(9) AGAR, A. W. *Brit. J. Appl. Phys.*, **8**, p. 35 (1957).

(10) GARD, J. A., and TAYLOR, H. F. W. *Min. Mag.*, **31**, p. 5 (1956).

(11) GARD, J. A., and TAYLOR, H. F. W. *Min. Mag.*, **31**, p. 361 (1957).

(12) EAVES, G. *Ph.D. Thesis* (University of Leeds, 1953).

(13) RYMER, T. B., and WRIGHT, K. H. R. *Proc. Roy. Soc. A*, **215**, p. 550 (1952).

(14) HALLIDAY, J. S., RYMER, T. B., and WRIGHT, K. H. R. *Proc. Roy. Soc. A*, **225**, p. 584 (1954).

(15) RYMER, T. B. *Proc. Roy. Soc. A*, **235**, p. 274 (1956).

(16) RYMER, T. B., FAYERS, F. J., and HEWITT, S. J. *Proc. Phys. Soc. [London] B*, **69** (1956).

(17) GARD, J. A. *Brit. J. Appl. Phys.*, **7**, p. 361 (1956).

(18) GARD, J. A. *J. Sci. Instrum.*, **33**, p. 307 (1956).

(19) MENTER, J. W. *Proc. Roy. Soc. A*, **236**, p. 119 (1956).

Some considerations of the magnetostrictive composite oscillator method for the measurement of elastic moduli

By N. B. TERRY, B.Sc., Ph.D., A.Inst.P., Mining Research Establishment, National Coal Board, Isleworth, Middlesex

[*Paper first received* 6 *November*, 1956, *and in final form* 18 *April*, 1957]

The development of the composite oscillator method, using nickel transducers, to enable measurement of the rigidity moduli as well as the Young's moduli of small cylindrical specimens is described. The magnitude of the cementing errors for the different modes of excitation is examined both theoretically and experimentally. An analysis is given which shows the advantages, for the technique described, of resonating at the fundamental mode for specimens of relatively low characteristic acoustic impedance. A further consideration of errors due to cross-sectional mismatch between transducer and specimen is made and finally some measurements on coal specimens are given.

1. INTRODUCTION

For the past thirty years the composite oscillator method of measuring elastic moduli, using piezoelectric excitation, has found extensive use particularly in America, where in fact it was first developed in 1925 by Quimby.[1] The specimen, in the form of a thin cylinder, is cemented to a quartz cylinder of equal cross-section. The quartz cylinder forms one arm of a convenient bridge and, depending on its cut and on the distribution of electrodes, may be set into longitudinal vibration (Balamuth[2]) or torsional vibration (Rose[3]) by application of an alternating voltage. The mechanical resonance frequencies of the composite cylinder may be detected by measuring the variation of the electrical impedance of the composite rod (Cooke[4]) or the variation of the current amplitude flowing through the cylinder (Zacharias[5]) and may easily be shown[1] to be given by:

$$c_1\rho_1 \tan (2\pi f l_1/c_1) + c_2\rho_2 \tan (2\pi f l_2/c_2) = 0 \qquad (1)$$

Here ρ_i is the density of a cylinder ($i = 1$ and 2 for transducer and specimen respectively), l_i is the length of a cylinder rod, f is a longitudinal or torsional resonance frequency of the composite cylinder and c_i is the velocity of the longitudinal or torsional elastic waves along the length of a cylinder. Since we have

$$c_i = 2l_i f_i \qquad (2)$$

where f_i is the natural frequency of a cylinder vibrating alone in its fundamental longitudinal or torsional mode, and since the cross-sectional areas are equal, equation (1) may be re-written in the more convenient form:

$$M_1 f_1 \tan (\pi f/f_1) + M_2 f_2 \tan (\pi f/f_2) = 0 \qquad (3)$$

where M_i is the mass of a cylinder. For a thin cylinder set into longitudinal oscillation, Young's modulus E_i along the length is given by:

$$E_i = c_i^2\rho \qquad (4)$$

and for a cylinder of circular cross-section set into torsional vibration, the rigidity modulus G_i is given by

$$G_i = c_i^2\rho i \qquad (5)$$

where the axis of the cylinder is the axis of torsion. Thus if frequencies f and f_1 and the masses M_1 and M_2 are measured, f_2 can be calculated from equation (3) and the relevant modulus for the specimen from equations (2) and (4) or (2) and (5).

In general the composite oscillator method has previously found application to the precise measurement of the elasticities of crystalline and polycrystalline materials and absolute accuracies of the order 0·1% are possible. Changes in elastic moduli, caused by varying a physical parameter such as temperature, may be measured to within 0·01%. The piezoelectric method is not the most suitable for measurements on organic specimens, such as resins, wood, coal, etc., since these substances show large variations in their elasticities and many measurements on different specimens are required for representative evaluation. Clearly the fragility and expense of the quartz resonators has restricted the more general application of the method. However, Terry and Woods[6] have shown that measurements of Young's moduli may be made by using nickel rod transducers excited magnetostrictively. By selecting nickel wire transducers of diameters ranging down to half a millimetre, they were able to carry out measurements of Young's moduli on crystalline specimens of very small lateral dimensions and of lengths ranging down to about $\frac{1}{2}$ cm. Since the nickel rods are robust and easily prepared, and the associated circuits are very simple, the magnetostrictively excited composite oscillator is admirably suited for use with organic materials, particularly when only small specimens are available. This paper has the objective of describing the development of the magnetostrictive method to enable the rigidity moduli as well as the Young's moduli of specimens to be measured and to examine theoretically and experimentally the conditions for the optimum employment of the method.

2. EXCITATION

It will be shown later (see section 5) that for accurate measurements the transducer has to be selected so as to have a natural frequency approximately equal to or higher than that of the specimen. Thus for very short specimens, correspondingly short nickel rods have to be used and it is found that the fundamental resonant vibrations are rather feeble. Terry and Woods[7] have described a simple modification to the Pierce magnetostrictive oscillator which has a high sensitivity and enables the resonances to be detected. However, for specimens having a natural frequency less than about 40 kc/s the simple arrangement shown in Fig. 1 may be used. Coil A, of inductance about 10 mH is fed from a signal generator with an alternating current of from 10 mA to about 50 mA, whilst the pick-up coil B, which is of some-

what higher inductance, is connected to the amplifier of an oscilloscope. Coils *A* and *B* are each enclosed in earthed copper screens to reduce the inductive linkage between them. The nickel rod is placed inside the two coils and the signal generator is tuned to the mechanical resonance frequencies which are indicated as maximum voltage outputs from the pick-up coil *B*.

In order to obtain longitudinal vibrations, the nickel rod is prepolarized longitudinally by placing in a solenoid having a field of about 200 oersteds. It is found that the nickel rods retain their remanent polarization for long periods so that changes in their resonance frequencies due to variations of magnetic state are negligible. As a precaution, however, a rod can easily be polarized just before use.

3. TORSIONAL VIBRATIONS

It was found that sufficiently powerful torsional vibrations could be obtained by utilization of the Wiedemann effect—if a rod of magnetostrictive material is placed with its axis orientated in the direction of a longitudinal magnetic field, and an electric current is passed along the rod, the combination of the circular magnetic field due to the current and the longitudinal magnetic field produces a state of torsion in the rod, the axis of the latter being the axis of torsion.

It is convenient if the nickel rods can be operated on remanent circular polarization. In order to produce this a large current of several hundred amps is momentarily passed through each rod. If the rod is now subjected to an alternating longitudinal field, by placing say, in coil A of Fig. 1,

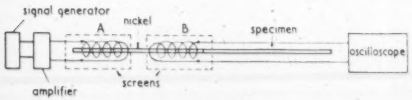

Fig. 1. Arrangement for exciting and detecting magnetostrictive oscillations

energized as described, strong torsional oscillations are produced. Table 1 gives the measured frequencies of torsional resonance for a set of nickel rods of diameters $\frac{3}{8}$ in.; these had all been cut from the same hard nickel rod.

Table 1. *Torsional vibrations of nickel rods of diameter $\frac{3}{8}$ in.*

Length of rod l_1 *(cm)*	*Natural resonance frequency* f_1 *(kc/s)*	*Velocity of torsional waves* $c_1 = 2l_1f_1$ *(cm/s)*
4·479	33·64	$3{\cdot}014 \times 10^5$
5·982	25·17	3·011
7·553	19·95	3·018
9·005	16·74	3·014
10·09	14·95	3·016
11·90	12·67	3·011
15·44	9·753	3·012
17·90	8·412	3·011

As a check on the accuracy of the composite oscillator method when using magnetostriction for the excitation of torsional modes, measurements were made on a single brass specimen of diameter $\frac{3}{8}$ in. cemented to a number of nickel rods of equal diameters but different natural frequencies, and also on a number of different steel rods, cut from a steel rod of diameter $\frac{3}{8}$ in.; each steel specimen was matched in frequency to the selected transducer. The results of measurements of the fundamental (or 1st harmonic) mode and the 2nd harmonic mode are given in Table 2.

All the results given in Table 2 above contain an error due to the presence of the cement at the interface, but it is shown in section 4 that the error for the 2nd harmonic mode is negligible. The measured density of the steel used was $7{\cdot}80$ g/cm^3. From equation (5) and the mean result of Table 2 the rigidity modulus is found to be $8{\cdot}21 \times 10^{11}$ dyne/cm^2; the result quoted by Kaye and Laby[8] is $8{\cdot}12 \times 10^{11}$ dyne/cm^2. It may be seen, therefore, that the results completely verify the internal consistency of the method and give a reasonable external check on its accuracy; better agreement could not be expected since the mechanical properties of steel vary with treatment and composition.

4. CONSIDERATION OF ERRORS DUE TO THE CEMENT

Balamuth[2] pointed out the advantages to be obtained by adjusting the length of the specimen until its natural frequency is approximately equal to that of the transducer and of exciting the composite rod at its second harmonic mode; this practice has been followed by all subsequent workers. In this way the cemented interface appears at a stress node with the result that the resonance frequency is less dependent on the elasticity of the cement film [equation (1) has been derived by neglecting the cement film].

It will be shown later, considering errors due to the mounting of the composite rod (see section 5), that for specimens of low elastic moduli, cemented to nickel rods, more accurate measurements can be made in practice by measuring the fundamental resonance frequencies rather than the frequencies of the higher harmonic modes, so that it is necessary to consider the magnitude of the error due to the cement when the interface corresponds to a stress antinode. Terry and Woods,[6] by regarding the cement as a third cylinder in a tripartite oscillator, have shown that the fractional error R_1 in the calculated value of the elastic wave velocity c_2 due to neglecting the cement is given by

$$R_1 = \frac{-M_3}{M_2}\left[\cos^2\theta_2 + \left(\frac{\rho_2 c_2}{\rho_3 c_3}\right)^2 \sin^2\theta_2\right]\left[\frac{2\theta_2}{2\theta_2 - \sin 2\theta_2}\right] \quad (6)$$

where $\theta_i = \pi f/f_i$ and the subscript 3 refers to the cement.

For operation at the 2nd harmonic mode, with $f \simeq f_1 \simeq f_2$ as proposed by Balamuth, $\theta_2 \simeq \pi$ and from equation (6),

$$R_1 \simeq -\frac{M_3}{M_2} \quad (7)$$

By careful cementing with the aid of a jig, the ratio M_3/M_2, which depends on the degree of planeness of the end surfaces, can be kept to negligible proportions. If, however, the composite rod is vibrated in its fundamental mode, and the specimen and transducer have been selected to have approximately equal natural frequencies so that $f_1 \simeq f_2 \simeq 2f$, we have $\theta_2 \simeq \frac{1}{2}\pi$ and from equation (6),

$$R_1 \simeq -\frac{M_3}{M_2}\left(\frac{\rho_2 c_2}{\rho_3 c_3}\right)^2 \quad (8)$$

From equation (4) or (5), equation (8) may alternatively be written

$$R_1 \simeq -\frac{l_3 K_2}{l_2 K_3} \quad (9)$$

where K is the appropriate elastic modulus.

Table 2. *Torsional elastic wave velocities in brass and steel cylinders*

Length of specimen (*cm*)	*Mass of specimen* (*g*)	*Natural frequency of transducer* (*kc/s*)	*Fundamental mode*		*Second harmonic mode*		*Percentage error in* (1) *due to cement* $\frac{100[(1)-(2)]}{(2)}$	*Theoretical percentage error in* (1) *due to cement*
			Frequency of composite rod (*kc/s*)	(1) *Calculated torsional wave velocity* (*cm/s*)	*Frequency of composite rod* (*kc/s*)	(2) *Calculated torsional wave velocity* (*cm/s*)		
				STEEL				
12·68	69·48	12·67	6·318	$3{\cdot}196 \times 10^5$	12·73	$3{\cdot}247 \times 10^5$	−1·6	−2·3
10·39	56·91	14·95	7·550	3·167	15·27	3·248	−2·5	−2·7
9·599	52·58	16·74	8·317	3·175	16·81	3·243	−2·1	−2·9
8·108	44·45	19·95	9·848	3·157	19·97	3·243	−2·6	−3·5
6·406	35·10	25·17	12·40	3·135	25·23	3·240	−3·2	−4·4
			Mean	3·166	*Mean*	3·244		
				BRASS				
7·029	42·29	12·67	6·620	$1{\cdot}915 \times 10^5$	13·11	1·951	—	—
		14·95	7·074	1·923	14·49	1·940	−1·0	−1·0
		16·74	7·353	1·923	15·46	1·940	—	—
		19·95	7·788	1·925	16·86	1·934	—	—
			Mean	1·922	*Mean*	1·941		

It is clear from equation (9), therefore, that for a composite rod vibrated in its fundamental mode, the fractional error in c_2 due to the cement depends on the relative elasticities of specimen and cement. The cements used are usually thermoplastic resins and if the specimen is of an organic nature it is not difficult to select a cement such that $K_2/K_3 \simeq 1$. If this is done the cementing errors are negligible in spite of the fact that the interface occurs at a stress antinode. For example, for measurements of the elastic moduli of coal specimens, Santolite M.H.P. (parasulfonamide) has been used as a cement. By moulding rods of Santolite of $\frac{3}{8}$ in. diameter and sticking these to nickel rods of similar diameter the torsional wave velocity has been determined as $9{\cdot}5 \times 10^4$ cm/s and the density is 1·35 g/cm^3. These values are very close to those obtained for the specimens of coal measured (see Table 3).

For specimens of higher elastic moduli, for example, steel and brass specimens, equation (8) shows that a measurable error results when vibrating the composite rod in its fundamental mode if a resin cement of low elastic modulus, such as Santolite, is used, while for the second harmonic mode the error is negligible. A comparison of the torsional wave velocities calculated from measurements of the resonance frequencies corresponding to the two modes (see Table 2) gives the experimental errors due to the cement. These may be compared with the theoretical cementing errors calculated from expression (8) and also given in Table 2. (The average amount of Santolite cement used was 4 mg for the steel specimens and 2 mg for the brass specimen.) It can be seen that the observed errors show reasonable agreement with the predicted values; closer agreement for the steel specimens might have been obtained had these had more perfectly plane ends instead of slightly rounded ones.

5. OPTIMUM MODE OF OSCILLATION

Because of eddy current losses, the efficiency of the nickel transducers is considerably impaired at frequencies above about 100 kc/s. If small specimens are used, therefore, it is not practical to vibrate the composite rod at its higher harmonics and in general only the fundamental or second harmonic mode is used. A comparison of the accuracy of measurement obtained for these modes will now be given.

If R_2 is defined as

$$\frac{\text{fractional error in the calculated value of the elastic wave velocity } c_2}{\text{fractional error in the measured value of the resonance frequency } f}$$

i.e. $R_2 = \dfrac{f}{c_2}\left(\dfrac{\partial c_2}{\partial f}\right)_{c_1}$, from equation (3) we have

$$R_2 = \frac{\theta_2 + \theta_1\left(\dfrac{\rho_2 c_2}{\rho_1 c_1}\sin^2\theta_2 + \dfrac{\rho_1 c_1}{\rho_2 c_2}\cos^2\theta_2\right)}{\theta_2 - \sin\theta_2\cos\theta_2} \qquad (10)$$

where, as before, $\theta_i = \pi f/f_i$.

An examination of equations (6) and (10) shows that both functions R_1 and R_2 rise to large values as θ_2 becomes less than about $\pi/2$. For accurate work this restricts f/f_2 to a value above about 0·5 and therefore limits the smallest size of specimen that can accurately be measured with a given transducer. Moreover, it is found that for most organic materials, if the specimen size relative to the transducer is such that f/f_2 is greater than 0·5, the additional attenuation of the longer specimen makes detection of the fundamental mode difficult. From these considerations it is convenient to select the specimen to have an approximately equal natural frequency to that of the transducer.

If this is the case, from equation (3) it can be seen that for the fundamental mode, $\theta_1 \simeq \theta_2 \simeq \frac{1}{2}\pi$ and from equation (10),

$$R_2 \simeq 1 + (\rho_2 c_2/\rho_1 c_1) \qquad (11)$$

For the 2nd harmonic mode, however, $\theta_1 \simeq \theta_2 \simeq \pi$ and from equation (10),

$$R_2 \simeq 1 + (\rho_1 c_1/\rho_2 c_2) \qquad (12)$$

For a legitimate comparison of the fundamental and 2nd harmonic modes we may only consider those types of errors in the resonance frequencies which are approximately equal in magnitude for the two modes. Clearly errors due to

instability in the oscillator used for measuring the frequency fall into this category. More serious are the changes in the resonance frequencies due to the mounting of the composite rod; these are found experimentally to be much the same for both modes. For very accurate work mounting errors may be minimized by supporting the composite rod vertically by thin wires attached to a displacement node. In practice, however, where many measurements are required it is of great practical advantage to be able to simply rest the nickel rod horizontally in the coil formers with the specimen held free of the latter. Experiment shows that in this way the error introduced in the measured resonance frequency will be no more than about 0·1% provided the amplitude of vibration is not too small; for the arrangement of Fig. 1 the current in the exciting coil should be greater than 10 mA.

Equations (11) and (12) show that the magnitude of the error in the value of the calculated velocity c_2, resulting from an incorrect estimation of the resonance frequency, depends on the ratio of the characteristic acoustic impedances ($\rho_i c_i$) of specimen and transducer. For example, if these are equal the percentage error in c_2 will be double that in f for both modes. Under no circumstances can the fractional error in c_2 be less than that in f, but if the characteristic impedance of the specimen is much greater than that of the transducer, equation (12) shows that R_2 is nearly unity and that the most accurate measurements are possible at the second harmonic mode with the advantage of a powerful resonant vibration and negligible cementing errors. If on the other hand, the specimen has a lower characteristic impedance than the transducer (and this is the case for most organic specimens used with a nickel transducer), equation (11) shows that the most accurate work is possible at the fundamental mode. For example, considering a coal specimen cemented to a nickel transducer of equal cross-section, since for the nickel $\rho_1 c_1 \simeq 45 \times 10^5$ c.g.s. units and for coal $\rho_2 c_2 \simeq 2 \times 10^5$ c.g.s. units, it can be seen from equation (12) that an error of 0·1% in the estimation of the 2nd harmonic resonance frequency will give rise to an error of over 2% in the calculated value of c_2, whereas a similar error in the determination of the fundamental resonance frequency will, from equation (11), give rise to an error in c_2 of little more than 0·1%. Fortunately, as has been shown in section 4, by a correct choice of cement the errors due to the cement can be kept negligible even for the fundamental mode.

If long specimens can be prepared, an alternative arrangement is to resonate the composite rod at frequencies corresponding to the vibration of the transducer as a half wave, the specimen length being selected so that the specimen vibrates not as a half wave, but as a number of half waves, say n. In this case we have $\theta_1 \simeq \pi$ as before, but $\theta_2 \simeq n\pi$ so that from equation (10), $R_2 \simeq 1 + (\rho_1 c_1/\rho_2 c_2)1/n$. Thus even if $(\rho_1 c_1/\rho_2 c_2)$ is large, R_2 can be kept low by selecting a large enough value of n; the practical limit to n is determined by the attenuation in the specimen. If this procedure is followed the cement is situated at a stress node so that cementing errors can be kept low without careful selection of the cement.

6. MISMATCHING OF THE CROSS-SECTIONS

Equation (1) is derived on the assumption that the waves are plane. If, however, the transducer and specimen have different cross-sections, the pressure cannot be uniform over the cross-sections at the interface so that in fact the waves cannot be plane and equation (1) cannot be justified theoretically. Equation (3), therefore, may be regarded as an empirical equation suggested by equation (1) and may be written in the form

$$\rho_1 c_1 A_1 \tan\theta_1 + \rho_2 c_2 A_2 \tan\theta_2 = 0 \qquad (13)$$

where A_i is the cross-sectional area.

Where a large number of measurements are required, it is of considerable practical advantage if these can be made without the necessity to match the cross-sections accurately. The effect of mismatching the cross-sections was therefore investigated in the following manner.

A Permendur rod of length 18·83 cm and of initial diameter 1·46 cm was turned to a number of shapes similar to that shown in Fig. 2 by reducing the diameter of portion *BC*

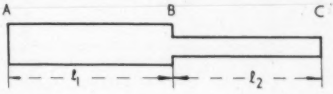

Fig. 2. Shape of Permendur rod used for investigations into the effect of cross-sectional area mismatch. *AB* is regarded as the transducer and *BC* as the specimen

(Permendur was used rather than nickel since it is easier to machine). At each stage the 1st and 2nd harmonic resonance frequencies of the rod, vibrated both torsionally and longitudinally, were recorded. Portion *AB* of the rod was regarded as a transducer of length l_1 and its resonance frequency calculated from $f_1 = c_1/2l_1$, where c_1 is the elastic wave velocity measured before machining the rod. The wave velocities c_2 in the portion *BC*, which was regarded as the specimen, were

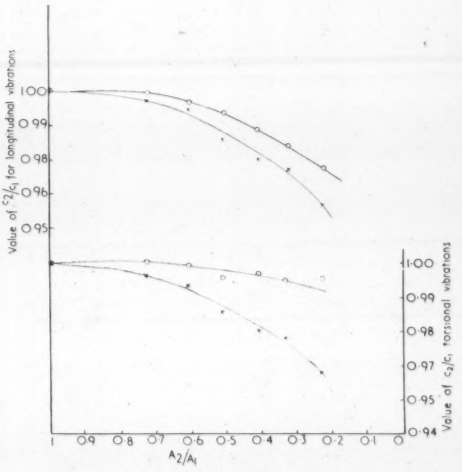

Fig. 3. Variation of calculated wave velocity with change of cross-section in the specimen portion *BC* of the Permendur rod shown in Fig. 2

X, fundamental mode; *O*, second harmonic mode; A_1, cross-sectional area of portion *AB* of Permendur rod (see Fig. 2); A_2, cross-sectional area of portion *BC*; c_1, true wave velocity in the Permendur rod; c_2, calculated wave velocity using equation (13).

calculated from equations (2) and (13). The rod was cut so that the two sections were equal in length to within 0·1% of the total length; the results obtained are given in the graph of Fig. 3.

From the results of experiments consisting of cementing crystalline and aluminium specimens to nickel rods of various diameters and vibrating these longitudinally in the fundamental mode, Terry and Woods[6] concluded that values for c_2 could be calculated from equation (13) with an accuracy of at least 1% within the range examined, i.e.

$$1 \leqslant A_1/A_2 \leqslant 3$$

It can be seen from Fig. 3 that the experiments on Permendur described above indicate a less generous tolerance, but it should be remembered that they refer to the case where the transducer and specimen have equal characteristic acoustic impedances and are both of circular cross-section. Evidently the error introduced by cross-sectional mismatch depends on the relative characteristic acoustic impedances of specimen and transducer as well as their relative natural frequencies. To derive a general law would obviously involve prohibitive labour and it is better to examine the tolerance for the particular material to be measured. For example, a coal specimen of square cross-section was cemented to a number of nickel rods of various diameters and vibrated longitudinally in the fundamental mode. The values of the calculated wave velocities were found to be independent of the cross-sectional area of the transducer within the range examined, i.e.

$$1 \leqslant A_1/A_2 \leqslant 4{\cdot}5$$

It should be noted that in the experiments described it has been assumed that the elastic wave velocity is independent of the diameter of the rod. There is, however, dispersion for the longitudinal waves due to lateral dilatation and this has been investigated by Bancroft.[9] His results show that for a Permendur rod of the dimensions described the longitudinal wave velocity increases by only 0·02% as the diameter is halved. Thus the effect can be neglected for these experiments.

7. SOME RESULTS OF MEASUREMENTS

Some results on specimens of Barnsley Hards coal are included to illustrate the versatility of the method. Coal, because of its cracked and inhomogeneous nature is probably one of the most difficult materials to examine for elastic behaviour, and in fact, if the elastic moduli are measured statically by compressing cubes or bending strips, coefficients of variation of up to 25% are quite often obtained. Nevertheless, it can be seen from Table 3 below that fairly reproducible results are obtained by using the composite oscillator method; this is probably due to the fact that the small specimens used can be selected so as to be free of gross flaws. The longitudinal measurements were carried out on specimens of approximately $\frac{1}{4}$ in. square cross-section cemented to nickel rods of circular cross-section and $\frac{1}{8}$ in. diameter. The torsional measurements were made on cylinders of $\frac{3}{8}$ in. diameter cemented to nickel rods of equal cross-section; all specimens were cut parallel to the bedding plane and had been desiccator dried for several weeks prior to measurement. The density of the samples were measured by R. L. Bond[10] as 1·364 g/cm^3 using the helium displacement method.

8. CONCLUSION

It has been shown that the composite oscillator method, using nickel transducers, can be used to measure the Young's moduli and rigidity moduli of materials. Provided the cement is carefully selected, theory shows that the error due to the cement can be kept low for all modes of oscillation. The advantages of measuring the resonance frequency of the fundamental mode for specimens of low characteristic acoustic impedance has been illustrated. It can be seen that the permitted tolerance of the mismatch of the cross-sections of transducer and specimen depends on the relative characteristic acoustic impedances as well as the natural frequencies of specimens and transducer and an independent investigation with the type of material on which measurements are required is recommended.

ACKNOWLEDGEMENTS

The author wishes to express his thanks to Mr. I. Evans for helpful discussion and to his other colleagues at the Mining Research Establishment for their assistance.

This paper describes work carried out as part of the Research Programme of the Mining Research Establishment and is

Table 3. *Measurements on Barnsley Hards coal specimens*

Natural resonance frequency of transducer (kc/s)	*Length of specimen* (cm)	*Type of vibration*	*Fundamental resonance frequency of composite rod* (kc/s)	*Velocity of elastic waves in the specimen* (cm/s)	*Young's modulus* (dyne/cm^2)	*Rigidity modulus* (dyne/cm^2)	*Standard error of the mean* (dyne/cm^2)
13·24	5·026	longitudinal	8·358	$1{\cdot}71 \times 10^5$	$3{\cdot}99 \times 10^{10}$		
19·58	2·539		15·80	1·73	4·08		
26·92	3·739		11·30	1·67	3·80		
26·92	2·539		16·62	1·72	4·03		
26·92	2·541		16·54	1·71	3·99		
			Mean	1·71	3·98		$0{\cdot}04 \times 10^{10}$
12·67	4·088	torsional	5·949	$0{\cdot}98 \times 10^5$		$1{\cdot}31 \times 10^{10}$	
14·95	3·850		6·156	0·94		1·21	
14·95	4·249		6·094	1·03		1·45	
14·95	3·683		6·979	1·03		1·45	
16·74	3·199		7·758	0·99		1·34	
16·74	3·391		7·425	1·00		1·36	
16·74	3·790		6·820	1·02		1·42	
			Mean	1·00		1·36	$0{\cdot}04 \times 10^{10}$

published by permission of Dr. W. Idris Jones, Director General of Research in the Scientific Department of the National Coal Board. The views expressed are those of the author and not necessarily those of the Board.

REFERENCES

(1) QUIMBY, S. L. *Phys. Rev.*, **25**, p. 558 (1925).
(2) BALAMUTH, L. *Phys. Rev.*, **45**, p. 715 (1934).
(3) ROSE, F. C. *Phys. Rev.*, **49**, p. 50 (1936).
(4) COOKE, W. T. *Phys. Rev.*, **50**, p. 1158 (1936).
(5) ZACKARIAS, J. *Phys. Rev.*, **44**, p. 116 (1933).
(6) TERRY, N. B., and WOODS, H. J. *Brit. J. Appl. Phys.*, **6**, p. 322 (1955).
(7) TERRY, N. B., and WOODS, H. J. *Proc. Leeds Phil. Soc.*, **6**, p. 251 (1954).
(8) KAYE, G. W. C., and LABY, T. H. 10th Ed., p. 38 (London: Longmans Green Ltd., 1948).
(9) BANCROFT, D. *Phys. Rev.*, **59**, p. 588 (1941).
(10) BOND, R. L. Private communication (1956).

The frequency dependence of noise temperature ratio in microwave mixer crystals

By M. E. SPRINKS, B.Sc., Ph.D., A.Inst.P., G. T. G. ROBINSON, A.M.Brit.I.R.E., Grad.I.E.E., and B. G. BOSCH, Dipl.Ing., Electronics Department, University of Southampton

[*Paper first received* 14 *January, and in final form* 18 *February*, 1957]

The contribution of flicker noise to the overall noise temperature ratio of microwave crystals has been widely noted and the previous estimates have shown that this contribution extends at least to frequencies of the order of 45 Mc/s. The normal range of intermediate frequencies employed in radar receivers is 10 to 60 Mc/s.

The paper attempts to assess the rate of variation of noise temperature ratio and to indicate how the values would affect the overall receiver noise factor of a given system having an intermediate frequency lying within this range.

In assessing the performance of a microwave crystal diode as a frequency convertor it is common practice to employ a system which, in effect, measures the overall noise factor of a specimen receiver. Consequently the parameters of the crystal are measured in conjunction with certain properties of the measuring equipment. The quantity measured is the noise factor N where:

$$N = L(N_{IF} + t - 1) \qquad (1)$$

L being the conversion loss of the crystal, N_{IF} the noise factor of the intermediate frequency amplifier, and t the noise-temperature ratio of the crystal, all quantities being quoted as linear ratios.

The noise factor of the intermediate frequency amplifier is assumed to be constant during the operation of the equipment and the term in the equation which accounts for local oscillator noise has been omitted on the assumption that a noise filter cavity is employed. Although this system is completely satisfactory in the production testing of crystals designed for use in one type of equipment, it is open to criticism if the crystal is more generally applied to systems with widely differing intermediate frequencies. The basic reason for this is the marked variation of the noise temperature ratio of the crystal with frequency. An examination of this variation is necessary before a translation may be made from the measured figure of merit of the crystal to the value to be expected in any particular application.

MEASURING EQUIPMENT

In essence the equipment required for such a series of measurements is a standard form of noise measuring receiver and depends for its operation upon the comparison of two noise levels at the input. Such receivers have been described in standard textbooks[1] and have also been developed by research establishments to carry out specific measurements such as the noise temperature ratio measuring set described by Hodgson.[2] The present system may be represented in block diagram form as in Fig. 1. A klystron of type CV323 supplies local oscillator power, *via* a noise filter cavity and a 10 dB directional coupler, to the crystal which is mounted in a broad-band wave-guide mixer unit. A fluorescent tube

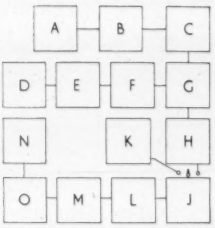

Fig. 1. Block diagram of complete apparatus

A, klystron type CV323; *B*, level setting attenuator; *C*, noise filter cavity; *D*, matched load; *E*, fluorescent noise source; *F*, sub-standard attenuator; *G*, 10 dB coupler; *H*, broad-band mixer unit; *J*, input circuit; *K*, noise diode; *L*, amplifier in range 10 to 60 Mc/s; *M*, mixer stage; *N*, detector and indicator; *O*, intermediate frequency amplifier, 5 Mc/s.

microwave noise source, which gives an output power nominally 15·5 dB above kTB, is incorporated in the system in order that an assessment may be made of overall noise factor when required. (The quantity kTB is the maximum thermal noise power available, in a bandwidth B, from a source maintained at a standard temperature T, assumed to be 290° abs, and k is Boltzmann's constant.) The actual noise power incident upon the crystal may be adjusted by means of a glass vane attenuator and, since the crystal mount

***

is a broad-band device, a correction must be made for the image frequency noise power absorbed. During the measurement of the noise temperature ratio of a crystal the fluorescent tube is inoperative and this branch of the microwave circuit is effectively terminated by the matched load. Any noise then generated by the crystal in excess of kTB is generated at the intermediate frequency as a result of the local oscillator drive, and constitutes the quantity to be considered in the definition of noise temperature ratio. This noise level is a function of the local oscillator drive power and a single value has been chosen for the silicon specimens which gives 1 mA rectified crystal current. This corresponds to a typical scheme of operation for the particular crystal types tested.

The noise generated by the crystal may be considered to have two components. There is a basic frequency independent component which, in the case of the new crystals tested, would probably be very little in excess of kTB and could be found by extrapolation of the total noise *versus* frequency curve. A second, frequency dependent, contribution is present which is of such an order of magnitude that it may completely dominate the basic noise even at frequencies of the order of several tens of megacycles per second. Since the variation of this second component with frequency is almost inverse the term flicker noise has been applied to it. In the equipment the total noise is measured by comparison to a noise diode at the input of the amplifier, and when the noise outputs of the crystal and diode are equal an expression may be applied

$$t = l + 20\,IR \qquad (2)$$

where t is the noise temperature ratio of the crystal, i.e. the number of times by which its noise output exceeds kTB, I is the diode current to give equality of noise output, and R is the diode load.

The range of frequency considered to be significant in the problem has been arbitrarily chosen as 10 to 60 Mc/s and, in order to cover the range, the main "intermediate frequency" amplifier has the form of a superheterodyne receiver. A single stage of amplification is used at the crystal "intermediate frequency" and is followed by a second frequency conversion stage and a high-gain amplifier of centre frequency 5 Mc/s.

An indication of noise output is made by a diode detector and modified valve voltmeter unit. The overall gain is of the order of 120 dB, although since comparison of the noise levels is carried out at the input of the system no precise information is required of the bandwidth or of the detector law. Coverage of the complete frequency range is achieved by variable capacity tuning in conjunction with a series of plug-in coils. The input circuit to the main amplifier incorporates the impedance transformation network, which is arranged to give operation of the system for minimum noise factor, and the selector switch between the diode and crystal noise sources with their associated current monitoring points.

The measurements depend for their accuracy upon the noise diode circuit design and the valve used is an Osram type A2087 with its filament fed from a transformer which provides an infinite range of variation of secondary voltage from zero to seven volts. Accurate alinement of the individual tuned circuits in the amplifier is accomplished by adjustable inductance cores, thus eliminating any tracking errors, and a similar method is used to tune out any stray capacitances which may affect adversely the true noise output of the crystal and comparison diode circuits. It is possible, by means of the indicator unit control, to back off the noise originating in the receiver itself and so use the maximum sensitivity of the instrument in the required comparison measurements.

EXPERIMENTAL RESULTS

Four types of crystal were measured, each specimen having been maintained as far as possible in the condition that it left the manufacturer. Consequently the quoted values of noise temperature ratio relate to cyrstals which have not deteriorated by use in a normal radar receiver and have not been intentionally damaged in any way to simulate burn-out or partial burn-out. Coaxial silicon crystals of types CV2154, SIM2 and CS3B were chosen for the tests and a comparison was made with the germanium type IN263 crystal recently introduced by the Philco Co.[3] Flicker noise was seen to contribute significantly to the noise temperature ratio in the frequency range of 10 to 60 Mc/s in such a manner that the coefficient a in the equation

$$N' = k(1/F^a) \qquad (3)$$

assumes values slightly in excess of unity. In this equation, N' is the flicker noise contribution at some frequency F and k is constant. A specimen curve is shown in Fig. 2.

The measurements of two silicon samples are quoted corresponding to the best crystal of a batch of twenty-four

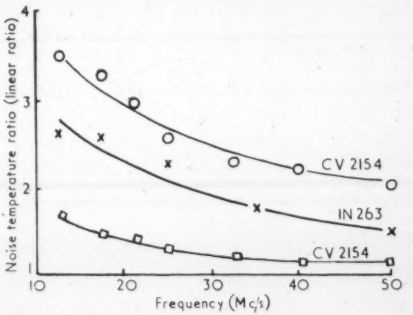

Fig. 2. The variation of noise temperature ratio with frequency

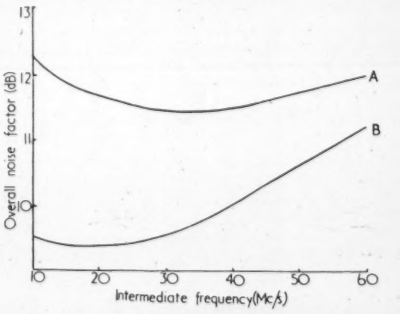

Fig. 3. Overall noise factor of a specimen receiver
A, typical silicon crystal; *B*, best silicon crystal.

and to a crystal which is representative of the most frequently occurring value of noise temperature ratio.

The experimental results quoted could contribute to a detailed analysis of microwave receiver performance as indicated by Strum[4] but a limited analysis may be made in the light of equation (1) if some particular valve type is chosen for the initial intermediate frequency stage. Detailed information of the variation of noise factor with frequency has been given by Moxon[5] and an example might be taken of the pentode type EF54. This valve, although not currently used, will illustrate the general variation of total noise factor with frequency. If a conversion loss of 6 dB is taken for the crystal, two curves may be plotted of total noise factor using the results of Fig. 2. The best crystal of the batch of twenty-four gives a broad minimum of noise factor at 20 Mc/s and illustrates the dominance of the intermediate frequency amplifier term at the higher frequencies. The crystal more representative of the batch shows a somewhat sharper minimum at 30 Mc/s and indicates that the noise factor at 10 Mc/s, where crystal noise predominates, is of the same order as that at 60 Mc/s, where intermediate frequency amplifier noise governs the overall figure. These specimen curves are given in Fig. 3.

CONCLUSION

The effect of the variation of overall noise factor with frequency due to crystal noise temperature ratio has been illustrated. More importantly, the results seem to illustrate the need to include the frequency dependence of noise temperature ratio as part of the testing and specification of performance of crystals, since in many cases the choice of intermediate frequency may rest entirely with the individual user. From a knowledge of the typical noise temperature ratio values for any crystal type it then becomes possible to design for optimum noise factor if a detailed analysis of intermediate frequency amplifier performance is made. Alternatively, the information may be used to supplement that already available of the noise generated by crystals under radio-frequency and direct current drive conditions.[6]

ACKNOWLEDGEMENTS

The authors wish to convey their appreciation of the help given by the Admiralty, under whose contract the work was carried out, and particularly by Mr. Bristow of the Admiralty Signal and Radar Establishment. Thanks are also due to Prof. Zepler for providing facilities in the Electronics Department and for his constant interest in the progress of the work.

REFERENCES

(1) TORREY, H. C., and WHITMER, C. A. *Crystal Rectifiers*, Vol. 15, p. 283 *et seq.* (Massachusetts Institute of Technology, 1948).
(2) HODGSON, C. T. Telecommunications Research Establishment *Memorandum* 553 (Ministry of Supply, 1953).
(3) CAVALIERI, A. L., Jr. *Philco Bull.*, **6**, (3), p. 17 (1956).
(4) STRUM, P. D. *Proc. Inst. Radio Engrs*, **41**, p. 875 (1953).
(5) MOXON, L. A. *Recent Advances in Receiver Design*, p. 32 (London: Cambridge University Press, 1953).
(6) NICOLL, G. R. *J. Instn Elect. Engrs*, **101**, (111), p. 317 (1954).

The impedance of the oxide-coated cathode at ultra-high frequencies

By L. J. HERBST, B.Sc., Ph.D., A.Inst.P.,* College of Technology, Birmingham

[*Paper first received* 8 *January, and in final form* 13 *February*, 1957]

The impedance of the oxide-coated cathode has been measured on a number of disk seal triodes at frequencies ranging from 500 to 2365 Mc/s. Mean values of the parallel elements R and C_2 which constitute the coating impedance were 15 Ω ($\sigma = 0{\cdot}29\ \Omega^{-1}\,m^{-1}$) and 6·5 pF ($\epsilon = 3{\cdot}2$) respectively. The value of R decreased with increasing temperature. The temperature dependence of R was found from conductance measurements over a range of 150° K.

LIST OF SYMBOLS

R = r.f. resistance of cathode coating to currents flowing through it in a direction perpendicular to the coating surface (Ω)
σ = r.f. specific conductivity of cathode coating under conditions of current flow as for $R(\Omega^{-1}\,m^{-1})$
C_1 = capacitance between grid wires and coating surface (F)
C_2 = capacitance of cathode coating (F)
ϵ = dielectric constant of C_2
G = equivalent parallel conductance formed by C_1 in series with the parallel combination of R and C_2 (Ω^{-1})
P = filament power in absence of cathode current (W)
$P - \delta P$ = filament power required to keep the temperature of coating at the same value as P when the cathode passes direct or r.f. currents (W)
f = frequency (c/s) ($\omega = 2\pi f$)
$\hat{v}$ = peak r.f. voltage between grid and cathode (V)
V = rectified d.c. voltage indicated by voltmeter connected across the external grid and cathode terminals (V)
T = cathode temperature (° K)

INTRODUCTION

A new method of measuring the resistance of the oxide-coated cathode at ultra-high frequencies has been described in a previous paper,[1] a knowledge of which is assumed. Recalling the method briefly, a radio-frequency voltage from a separate oscillator was applied between the grid and the cathode of the disk seal triode under test. The valve was connected up as a rectifier and the r.f. voltage was deduced from the d.c. voltage reading of a high resistance voltmeter connected across the grid-cathode path. The experimental procedure was to change the heater power when applying r.f. power so as to maintain constant temperature of the

* Now at British Telecommunications Research Ltd., Taplow, Bucks.

cathode coating which was observed with the aid of a photocell. Experimental evidence obtained during d.c. tests indicated that nearly all heater power was transferred to the coating and that a change in heater power resulted in an equal change of power in the coating. Hence G, the equivalent loss conductance between grid and cathode, is given by

$$G = 2\delta P/\hat{v}^2 \tag{1}$$

Furthermore, it was assumed that $\hat{v} = V$, leading to

$$G = 2\delta P/V^2 \tag{2}$$

whilst, according to Fig. 1, G is related to C_1, C_2 and R by

$$G = \omega^2 C_1^2 R/[1 + \omega^2(C_1 + C_2)^2 R^2] \tag{3}$$

Ref. (1) was an account of a preliminary investigation followed by some further work, described here and based on

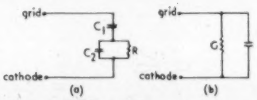

Fig. 1. (*a*) Circuit between grid and cathode. (*b*) Equivalent admittance between grid and cathode

a series of measurements made on a number of valves with widely differing grid-cathode clearances. These measurements lead to an evaluation of the coating impedance components R and C_2. The effect of electron inertia has been taken into account when deducing the r.f. voltage from the d.c. voltmeter readings.

THE RELATIONSHIP BETWEEN $\hat{v}$ AND V

General considerations. For voltages exceeding a few volts, the d.c. voltage developed across the load resistance of a thermionic valve rectifier is very nearly equal to the peak value of the r.f. voltage, i.e. $\hat{v} = V$ (see Fig. 2) provided that:

(*a*) the load resistance is high compared with the valve resistance during the short fraction of the cycle when conduction current flows through the valve;

(*b*) the time-constant of the capacitance-resistance combination across which V is developed is very large compared with the period of one cycle;

(*c*) transit time effects may be ignored.

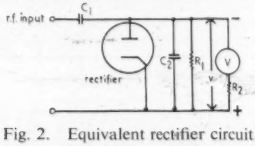

Fig. 2. Equivalent rectifier circuit

C_1 = coupling capacitor formed by r.f. probe and coaxial line structure.
C_2 = insulating mica capacitor (310 pF).
R_1 = leakage resistance of C_2 (200 MΩ).
V = d.c. valve voltmeter (input resistance R_2 = 24 MΩ).

Conditions (*a*) and (*b*) are easily satisfied, and the effect of transit time is discussed in the next paragraph.

The effect of electron inertia. When the effect of transit time during rectifier operation becomes appreciable, the reservoir capacitor C_2 in Fig. 2 will charge to a potential below $\hat{v}$, because of electrons which have left the cathode when the field was positive and fail to reach the anode owing to the reversal of field whilst they are still in transit. Megaw[2] has made an extensive investigation of the problem but ignored the effect of initial electron velocity which was not important in his case. Here allowance has been made for the initial electron velocity by assuming that all electrons leave the cathode with the same velocity equal to the mean value. Consider the case shown in Fig. 3 where C_2 of Fig. 2 has charged to a value $-V$ volts between anode and cathode of a planar diode.

Clearly
$$V = \hat{v}\sin\alpha \tag{4}$$

and the problem resolves itself to finding $\sin\alpha$ for a given value of V, the interelectrode clearance, and frequency such that the electron with the maximum range, i.e. the electron leaving the cathode at the instant A (Fig. 3) will just fail to

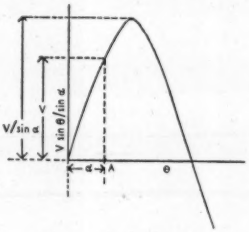

Fig. 3. Rectifier action

reach the anode. Ignoring space-charge, the equation of motion for an electron leaving the cathode at that instant is

$$\ddot{x} = \frac{e}{m}\cdot\frac{\hat{v}}{a}[\sin(\omega t + \alpha) - \sin\alpha] \tag{5}$$

where t is the time ($t = 0$ for $\theta = \alpha$), a the grid-cathode spacing (m), x the distance traversed by the electron in the direction of the anode, and e and m have their usual meanings.

Solving equation (5) and allowing for a uniform initial electron velocity of $1{\cdot}96 \times 10^5$ m/s, a value obtained by assuming a Fermi distribution of electrons at 1260° K,[3] the equations leading to a solution of $\sin\alpha$ are

$$\cos(\omega t_0 + \alpha) = \frac{7{\cdot}00aF}{V}\sin\alpha + \cos\alpha - \omega t_0 \sin\alpha \tag{6}$$

$$\frac{V}{224a^2F^2}\cdot\frac{G(\omega t_{0,\alpha})}{\sin\alpha} + \frac{3{\cdot}12 \times 10^{-2}}{aF}(\omega t_0) = 1 \tag{7}$$

$$G(\omega t_{0,\alpha}) = \omega t_0\cos\alpha + \sin\alpha - \sin(\omega t_0 + \alpha) - \frac{(\omega t_0)^2}{2}\sin\alpha \tag{8}$$

F being the frequency (Mc/s) and t_0 the time of flight during which the electron moves towards the anode. $\sin\alpha$ was found by solving equations (6) and (7), ωt_0 being found graphically in terms of $\sin\alpha$ from equation (6).

INTERPRETATION OF RESULTS

General considerations. G is given in terms of V, P and $\sin\alpha$ by equations (1) and (4), leading to

$$G = 2\delta P\sin^2\alpha/V^2 \tag{9}$$

Table 1. *Summary of results*

Valve No.	Grid-cathode clearance (mm)	C_1 (pF)	Frequencies at which measurements were made (Mc/s)	C_2 (pF)	R (Ω)	σ ($\Omega^{-1}m^{-1}$)	ϵ	T_1(°K)	T_2(°K)	GT_1/GT_2	RT_1/RT_2	$\left\{\phi = \frac{1.99\log_{10}(RT_1/RT_2)}{10^4[(1/T_1)-(1/T_2)]}\right\}$
1	0·14	0·86	500, 730, 1190, 1555, 1810, 2365	9·(5)	1 (2)	0·36	4·7	1140	1286	1·62	2·01	0·64
2	0·16	0·76	500, 1615	4·(5)	1 (9)	0·23	2·2	1239	1388	1·31	1·54	0·43
3	0·14	0·86	500, 1615	6·(0)	2 (1)	0·21	3·0	1241	1390	1·38	1·78	0·57
4	0·14	0·86	500, 730, 1190, 2335	6·(5)	1 (9)	0·23	3·2	1233	1399	1·48	1·91	0·87
5	0·13	0·93	500, 1615	5·(5)	1 (6)	0·27	2·7	1250	1398	1·28	1·60	0·48
6	0·14	0·86	500, 1615	4·(0)	1 (2)	0·36	2·0	1234	1391	1·69	2·60	0·66
7	0·10	1·22	611, 1935	1·(2)	1 (1)	0·40	5·9	1260	Not measured			
8	0·16	0·76	500, 730, 1190, 2335	7·(0)	1 (2)	0·36	3·4	1225	1315	1·29	1·52	0·63
9	0·20	0·61	500, 1615	7·(0)	1 (0)	0·44	3·4	1258	1401	1·37	1·56	0·47
10	0·20	0·61	500, 690, 1025, 1565, 2040	5·(0)	1 (7)	0·26	2·5	1267	1402	1·28	1·48	0·44
11	0·21	0·58	500, 730, 1190, 1560, 2040	4·(5)	3 (0)	0·15	2·2	1171	1321	1·25	1·49	0·36
12	0·41	0·30	500, 1615	4·(0)	1 (3)	0·33	2·0	1251	1396	0·97	1·02	0·04
13	0·44	0·28	500, 730, 1035, 1630, 2040	4·(5)	4 (4)	0·10	2·2	1282	1435	1·15	1·31	0·28

First the r.f. relationship of the current/voltage characteristic (i/v) for G had to be found in order to establish whether G could in fact be represented by equation (3) and, if so, to determine R and C_2. A knowledge of the temperature variation of G was also needed for calculating G under oscillatory conditions, during which the cathode temperature might differ appreciably from the value corresponding to P owing to coating heating by circulating currents and electron back-bombardment.

The investigations, listed in Table 1, extended from frequencies where transit time corrections were small ($\sin\alpha$ being in excess of 0·90) to the highest frequencies at which sufficient r.f. power could be developed across the coating to give a reasonably accurate measurement of δP. The accuracy of the expression $\delta P/V^2$ allowing for errors of measurement was $\pm 15\%$. A selected list of conductance measurements is shown in Tables 2. G_a and G in Tables 2 denote conductances calculated by ignoring transit time corrections ($\sin\alpha = 1$) and by allowing for them respectively; $\sin\alpha'$ shown in these tables is obtained by ignoring initial electron velocity.

An important result emerging from the tests at 500 and 730 Mc/s was this: G was found to be independent of δP for all valves within the accuracy of measurements. At these frequencies the effect of transit time corrections on the relative values of G over the range δP is negligible for standard and medium clearance, and only slight for large clearance valves. Conductance determinations were made for six standard clearance valves at 500 Mc/s with δP up to 1·2 W and the constancy of G over the full range of δP was in all cases well up to the standard for valves Nos. 3 and 11, at 500 and 730 Mc/s as shown in Tables 2. It was concluded that the ultra-high frequency i/v characteristic of G is linear and that, since G is regarded as a passive network, the ultra-high frequency i/v characteristic of R is linear also.

The transit time corrections could be expected to be valid if G_a was no longer independent of δP when the difference in $\sin\alpha$ over the range of measurement at a fixed value of P became appreciable, and if the application of the corrections resulted in G being independent of δP. Such behaviour has, in fact, been generally observed. At the highest frequencies the two conductance measurements corresponding to $\sin\alpha$ values of 0·55 and 0·62 in Table 2 cover an insufficient range

Tables 2. *Selected results of impedance measurements*

All measurements were made at T_1 of Table 1.
G is not shown at the lower frequencies where $\sin\alpha > 0{\cdot}90$.

500 *Mc/s*
Valve No. 3

	δP	G_a	$\sin\alpha$
58·5	0·229	$1{\cdot}34 \times 10^{-4}$	0·94
78·5	0·450	$1{\cdot}46 \times 10^{-4}$	0·94
103·5	0·756	$1{\cdot}41 \times 10^{-4}$	0·95
123·5	1·040	$1{\cdot}37 \times 10^{-4}$	0·96

730 *Mc/s*
Valve No. 11

	δP	G_a	$\sin\alpha$
48·4	0·151	$1{\cdot}21 \times 10^{-4}$	0·88
63·4	0·248	$1{\cdot}24 \times 10^{-4}$	
73·4	0·356	$1{\cdot}32 \times 10^{-4}$	
88·4	0·486	$1{\cdot}25 \times 10^{-4}$	
103·4	0·686	$1{\cdot}28 \times 10^{-4}$	
118·4	0·883	$1{\cdot}28 \times 10^{-4}$	0·92

1190 *Mc/s*
Valve No. 8

	δP	G_a	$\sin\alpha$
23·3	0·121	$4{\cdot}48 \times 10^{-4}$	0·82
33·3	0·229	$4{\cdot}04 \times 10^{-4}$	
41·3	0·378	$4{\cdot}44 \times 10^{-4}$	0·86

1560 *Mc/s*
Valve No. 11

	δP	G_a	G	$\sin\alpha'$	$\sin\alpha$
18·6	0·170	$9{\cdot}80 \times 10^{-4}$	$4{\cdot}02 \times 10^{-4}$	0·61	0·64
23·6	0·220	$7{\cdot}92 \times 10^{-4}$	$3{\cdot}56 \times 10^{-4}$	0·64	0·67
28·6	0·348	$8{\cdot}50 \times 10^{-4}$	$4{\cdot}04 \times 10^{-4}$	0·66	0·69
33·6	0·478	$8{\cdot}48 \times 10^{-4}$	$4{\cdot}40 \times 10^{-4}$	0·69	0·72
38·6	0·575	$7{\cdot}72 \times 10^{-4}$	$4{\cdot}12 \times 10^{-4}$	0·71	0·73

2335 *Mc/s*
Valve No. 1

	δP	G_a	G	$\sin\alpha'$	$\sin\alpha$
9·3	0·078	$1{\cdot}80 \times 10^{-3}$	$5{\cdot}50 \times 10^{-4}$	0·47	0·55
15·6	0·212	$1{\cdot}74 \times 10^{-3}$	$6{\cdot}72 \times 10^{-4}$	0·58	0·62

to give significant differences in $\sin\alpha$. Nevertheless there is considerable support for the validity of the transit time corrections. All G evaluations were henceforth made by allowing for transit time corrections in the manner indicated.

The evaluation of coating impedance. Assuming G to be given by equation (3), R and C_2 may be calculated from a knowledge of C_1 and measurements of G_1 and G_2 at frequencies f_1 and f_2 according to the equations

$$R = \frac{\omega_2^2 - \omega_1^2}{\omega_1^2\omega_2^2} \cdot \frac{G_1G_2}{G_2 - G_1} \cdot \frac{1}{C_1^2} \tag{10}$$

$$C_2 = \frac{1}{R}\left\{\left[1 - \frac{G_2}{G_1}\left(\frac{\omega_1}{\omega_2}\right)^2\right] \Big/ \left[\omega_2^2\frac{G_2}{G_1}\left(\frac{\omega_1}{\omega_2}\right)^2 - \omega_1^2\right]\right\}^{\frac{1}{2}} - C_1 \tag{11}$$

whilst the validity of equation (3) may be verified by plotting $y = 2F^2/G$ against $x = F^2$ (F being the frequency in Mc/s). Such a plot should result in a straight line expressed by

$$y = y_0 + mx \tag{12}$$

$$y_0 = 10^{-12}/2\pi^2C_1^2R \tag{12a}$$

$$m = 2[(C_1 + C_2)/C_1]^2R \tag{12b}$$

Extensive conductance measurements were made on six valves (see Table 1) and the plots of y *versus* x are reproduced for those valves in Figs. 4(*a–f*). The graphs of Fig. 4 provide a general confirmation of G being representable by equation (3); R and C_2 were evaluated from y_0 and m after what appeared to be the best straight line had been drawn through the points on the graph. To allow for the estimated error of $\pm 15\%$ in $\delta P/V^2$, a straight line $(y_1 - y_2)$ was drawn in place of y for each value of x where y_1 and y_2 differed by 15% from $2F^2/G$. (C_1 was determined from a knowledge of the cathode coating area and the grid-cathode clearance; the latter was measured optically and was also deduced from Langmuir plots of the static characteristics.)

The graphs are also a test of the validity of the transit time corrections. In view of all the uncertainties involved, the departures from linearity, brought out clearly by the generous

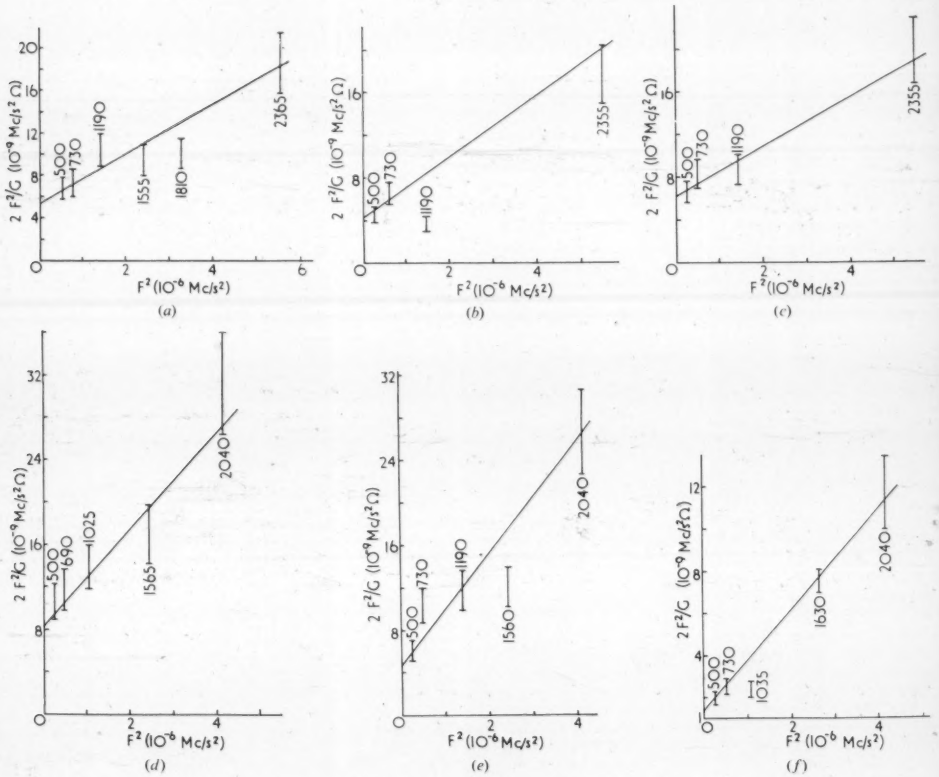

Fig. 4. Plot of $2F^2/G$ *versus* F^2

Figures against each line denote frequency (Mc/s).

(*a*) Valve No. 1. (*b*) Valve No. 4. (*c*) Valve No. 8. (*d*) Valve No. 10. (*e*) Valve No. 11. (*f*) Valve No. 13.

scale chosen for y, are not alarming. The departures themselves do not follow a regular pattern which might suggest a frequency dependence of R or C_2. Whilst no obvious explanation is advanced to account for some of the discrepancies, emphasis must be placed on the satisfactory nature of the graphs for the medium- and large-clearance valves Nos. 10 and 13.

So far there has been no experimental evidence in support of the allowance for initial electron velocity made when deriving $\sin\alpha$. It is only at frequencies of 2000 Mc/s or above that the difference between $\sin\alpha$ and $\sin\alpha'$ (zero initial electron velocity) is of some consequence. Values of G, ignoring and allowing for initial electron velocity, will be in the ratio $(\sin\alpha'/\sin\alpha)^2$ and, taking a typical case of a standard clearance valve at 2335 Mc/s, this ratio will be 1·3. Generally, since $\sin\alpha > \sin\alpha'$, y corresponding to the highest value of F^2 in Fig. 4 will be displaced upwards by about one-fifth of the magnitude shown therein if initial electron velocity is ignored; corresponding displacements at the lower frequencies will be negligible. The linearity of the plots would thus be seriously disturbed by ignoring initial electron velocity. Hence, in an indirect way, experimental evidence is provided that the allowance for initial velocities is at least of the right order of magnitude.

Values of R and C_2 were found for the six valves plotted in Figs. 4(*a–f*) from equations (12*a*) and (12*b*). (In all evaluations of G an allowance of 5% was made for the heat loss in the transfer of energy from heater to coating, this allowance being based on experimental evidence obtained from the d.c. tests.)

Values of R and C_2 for valves Nos. 2, 3, 5, 6, 9 and 12 were found from conductance measurements at 500 and 1615 Mc/s with the aid of equations (10) and (11).

The temperature dependence of G. Conductance measurements were made at 500 Mc/s at a temperature of about 150° K in excess of the normal operating temperature by applying a filament power of about 4 W. At 500 Mc/s electron inertia corrections were small and G_{T1}/G_{T2}, the ratio of conductances at temperatures T_1 and T_2, was found by taking the mean of four measurements each at T_1 and T_2. For two valves temperature comparisons of G were also made at higher frequencies. (Conductance measurements were kept to a minimum because of the obvious risk involved when operating at such high heater power.) The ratio G_{T1}/G_{T2} was now found by taking the mean of several G_{aT1}/G_{aT2} ratios for equal values of V, this procedure eliminating the need to apply transit time corrections. From equation (3)

$$\frac{R_{T_1}}{R_{T_2}} = \frac{G_{T_1}}{G_{T_2}}\left(\frac{C_{1T_2}}{C_{1T_1}}\right)^2\left[\frac{1+\omega^2(C_{1T_1}+C_2)^2R_{T_1}^2}{1+\omega^2(C_{1T_2}+C_2)^2R_{T_2}^2}\right] \qquad (13)$$

the suffices T_1 and T_2 referring to the values of various quantities at T_1 and T_2. The ratio R_{T1}/R_{T2} was readily found from equation (13), accurate to 1%, by a method of successive approximation. Allowance was made for the variation of C_1 with temperature due to the expansion of the cathode sleeve support leads in the direction of the grid frame.

Fig. 5 shows the calculated G_{T1}/G_{T2} curves plotted against frequency for three valves and based on the determinations of G_{T1}/G_{T2} at 500 Mc/s. Measured values for valves Nos. 1 and 13 at frequencies other than 500 Mc/s are also shown. For valve No. 1, where measured conductance comparisons were most accurate on account of the comparatively large variation of R with temperature, the agreement between calculated and measured G_{T1}/G_{T2} ratios at the four frequencies is very good indeed. For valve No. 13, on the other hand, the inaccuracies inherent in the present technique are more pronounced and the agreement between calculated and experimental values is not so good.

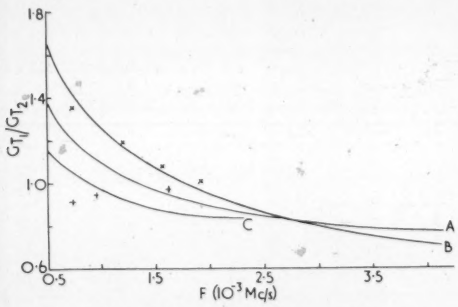

Fig. 5. Variation of G with temperature

Curve *A*, valve No. 3; curve *B*, valve No. 1; curve *C*, valve No. 13.

× = measured ratio, valve No. 1.

+ = measured ratio, valve No. 13.

CONCLUSIONS

Taking the mean of the results for all valves in Table 1, with the exception of Nos. 11 and 13 which had little or no emission when the tests were made, $R = 15\,\Omega$ and $C_2 = 6{\cdot}5$ pF corresponding to $\sigma = 0{\cdot}3\,\Omega^{-1}\,m^{-1}$ and $\epsilon = 3{\cdot}2$. An assessment of the accuracy of R and C_2 is rather difficult owing to the uncertainties involved in the transit-time corrections made to the voltage readings; R and C_2 can only be expressed to one significant figure, hence the bracketing of the second digit in Table 1. No previous measurements of coating impedance at ultra-high frequencies have come to the author's notice, but Rodenhuis[4] has assumed values of $\sigma = 0{\cdot}3\,\Omega^{-1}\,m^{-1}$ and $\epsilon = 4$ when calculating losses in the cathode coating at ultra-high frequencies. The low values of σ for valves Nos. 11 and 13 may be due to deterioration of the vacuum; in any case very low d.c. conductivity invariably accompanies failure in emission.

The r.f. i/v characteristic of R was found to be linear up to the highest value of δP in the conductance measurements. The upper limit of δP at 500 Mc/s was usually about 1 W and the peak r.f. voltage across the coating would then be 5·5 V for R equal to 15 Ω. The d.c. i/v characteristic of the oxide coating is expected to be linear for a fully activated coating according to Wright.[5] Few measurements have been reported at temperatures in excess of 1000° K, but Loosjes and Vink[6] have obtained some values of σ at 50 c/s for temperatures up to 1250° K and have found the i/v characteristic of the oxide coating at that temperature to be linear. Their measurements extended up to similar voltages across the coating as the present author's.

ACKNOWLEDGEMENTS

The work described herein was part of a research programme which was carried out under the direction of Professor M. R. Gavin and which led to the author being awarded the Ph.D. degree by the University of London.

Thanks are due to Dr. J. E. Houldin for helpful discussions,

to the workshop staff, Mr. L. Brierley and the late Mr. A. Derby for construction of the equipment, and to the Research Laboratories of the General Electric Co. Ltd., for provision of the disk seal triodes.

REFERENCES

(1) HERBST, L. J., and HOULDIN, J. E. *Brit. J. Appl. Phys.*, **6**, p. 236 (1955).
(2) MEGAW, E. C. S. *Wireless Engr*, **13**, p. 65 (1936).
(3) HERMANN, G., and WAGENER, S. *The Oxide Coated Cathode*, Vol. 2, p. 24 (London: Chapman and Hall, 1951).
(4) RODENHUIS, K. *Philips Res. Rep.*, **5**, p. 46 (1950).
(5) WRIGHT, D. A. *Semiconductors*, p. 115 (London: Methuen and Co. Ltd., 1950).
(6) LOOSJES, R., and VINK, H. J. *Philips Res. Rep.*, **4**, p. 449 (1949).

A

Fluoroscopy with an enlarged image

By R. HALMSHAW, B.Sc., A.R.C.S., A.Inst.P., and C. HUNT, Armament Research and Development Establishment, Ministry of Supply, London

[*Paper received* 2 *January*, 1957]

Comparisons of attainable sensitivity have been made between two types of fluoroscopic set, one having an ultra-fine focus tube used with projective magnification and the other a conventional high current tube used with the specimen close to the screen. A marked gain in sensitivity was obtained with the former, values better than 1½% being obtained over a range of thickness of aluminium, and better than 3% on steel, using wire penetrameters.

Sensitivities have been calculated, in terms of the performance of the eye at different brightnesses and possible methods of improving sensitivity are considered.

Fluoroscopy has two major potential advantages over radiography on film: these are, firstly that the cost of inspection can be very considerably reduced because the image is viewed on a fluorescent screen instead of being recorded on a film, and secondly that the specimen can be moved whilst being viewed, causing a change in the image which frequently facilitates interpretation.

The major limitations of fluoroscopy are also well known: these are that the attainable sensitivity of flaw detection is much poorer than with film radiography, and that the penetrable thickness of material with any specific X-ray energy is much smaller. It is, however, a very attractive method of inspection in cases where a permanent record is not required.

Two quite separate lines of approach have been suggested for the improvement of fluoroscopy. In one it is argued that because the image on the screen is necessarily blurred, owing to screen unsharpness, the additional geometric unsharpness caused by using an X-ray tube with a large focus will not be important. The aim is therefore to use high-current tubes, with necessarily large focal spots, so as to obtain screen images as bright as possible and so minimize the loss in visual acuity which occurs at lower brightnesses.

The second line of approach suggests that because fluorescent screens produce a grainy image, the image of the specimen detail should be magnified on to the screen by using a very fine focus tube and placing the specimen some distance from the screen (projective magnification technique). To obtain the necessary small focus, the rating of the X-ray tube must be reduced and this consequent low tube current results in a lower screen brightness. It is suggested that the loss in visual acuity of the eye due to the lower brightness may be more than offset by the enlarged size of the image detail on the screen. So far as is known, no results of a direct comparison of the two methods have been published.

O'Connor and Polansky[1, 2, 3] reported a detailed examination of the factors influencing fluoroscopic sensitivity and by using a tube having a 1 mm focus, so that some projective magnification could be employed, obtained sensitivities of 1½–2% in aluminium and magnesium with the American Society of Mechanical Engineers type penetrameter. By using a rotating anode tube with intermittent operation they were able to employ tube currents of 20–70 mA and so utilize a very high screen brightness.

APPARATUS

Two X-ray sets were available for this work.

Set A: an ultra-fine focus tube with a constant potential generator having a maximum rating of 140 kV, 1 mA, and a focal spot which, in projection, was elliptical and 0·2 × 0·3 mm in size.

Set B: a medium focus tube with a Villard-type generator, having a maximum rating of 148 kV, 20 mA and a projected focal spot, rectangular in shape and 4 × 5 mm in size.

The measured outputs of the two tubes used are given in Table 1.

Table 1. *X-ray output at* 120 *kV (nominal), measured at* 20 *in. distance*

	Output (r mA^{-1} *min*$^{-1}$*)*		*Output at rated current (r/min)*	
	Unfiltered	*Filtered through ½ in. Al*	*Unfiltered*	*Filtered through ½ in. Al*
Fine focus tube	9·9	1·8	9·9	1·8
Medium focus tube	1·26	0·4	25·2	8·0

FACTORS AFFECTING TECHNIQUE

The factors which have some influence on the ability to detect flaws in a specimen by fluoroscopy are very numerous, although some are obviously of secondary importance only. Some are limited by the equipment and some are interdependent: the following require further consideration.

Dark adaptation. In practically all fluoroscopic work the screen brightness is such that for the eye to perform efficiently, dark adaptation of the observer is essential. Chamberlain[4]

has discussed the effectiveness of dark adaptation and has shown that, whereas dark adaptation of the eye as a whole continues to show a rapid improvement for at least thirty minutes, it does, in fact, continue slowly for many hours (Fig. 1). It was therefore made standard practice to have at least twenty minutes in complete darkness before commencing viewing. The fluoroscopy room was, of course, blacked out, with controlled red light for adjusting specimens and making notes. In addition, work was always planned so that the examinations at the lowest brightnesses were made towards the end of a session when dark adaptation was more complete.

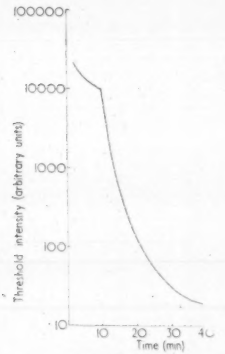

[*Reproduced from "Radiology"*]

Fig. 1. The progress of dark adaptation

Protection: method of viewing the screen. The radiation which penetrates the specimen is only partially absorbed in the fluorescent screen and the unabsorbed portion must be prevented from reaching the observer. There are two well recognized methods: one is to use a mirror system to view the screen indirectly and the second is to interpose sufficient lead glass between the screen and the eye to reduce the intensity of the transmitted radiation to a safe value. As it was not proposed to use X-ray energies above 150 kVp it was decided to use direct viewing with an appropriate thickness of lead glass. The thickness of glass required was approximately $\frac{3}{4}$ in. and was placed immediately in front of the screen. This glass must produce some back-scattered radiation which would have an effect on the screen analagous to scattered radiation from the specimen, and reduce image contrast; this effect does not seem to have been discussed in the literature although it would be comparatively easy to have the screen spaced a considerable distance from the protective glass if this would lead to any significant improvement.

Observers. The great majority of the observations have been made by the two authors. Preliminary tests showed that they agreed closely in their ability to discern detail, and of three other observers who were used for short spells of viewing, one agreed closely with the two principals, one could see less and one claimed to see slightly more.

Over a period of six months the two principal observers improved in ability to locate and recognize detail, so much so that many of the earlier observations on sensitivity had to be repeated, a systematic improvement being found.

Fluorescent screens. All fluorescent screens produce an image with a grainy appearance, although the precise cause of this graininess is not well understood. In general, the smaller the graininess of the screen the lower is the light output for a given intensity of X-rays. In choosing a screen, therefore, a compromise has to be made between graininess and brightness. Graininess is not an easy property to measure, and one accepted method of comparing screens is to measure the unsharpness produced in the image of a sharp metal edge, laid on the screen.[5]

A second important property of screens is their light output per unit of X-ray energy at different kilovoltages. O'Connor[1] investigated twenty different screens available in the U.S.A. and advantage has been taken of his results to limit this investigation to a few screens. He showed that all screens of the yellow-green fluorescent type have the same characteristics of output with variation in X-ray energy, up to 400 kVp; all show a peak response at approximately 120 kVp. The screens chosen for examination and the results obtained are shown in Table 2.

Table 2. *Characteristics of fluoroscopic screens*

	Unsharpness (mm)	*Relative brightness (arbitrary units)*
(1) Radelin FG	1·07	1·7
(2) Radelin F	0·80	1·3
(3) CAWO	0·80	1·5
(4) "Seifert"	0·52	1·0
(5) Sirius H.S.	1·33	2·0

From these results, the two screens having the smallest values of unsharpness, Nos. 3 and 4, were chosen for use.

The area of screen illuminated was governed more by practical considerations than by theory. The area had to be large enough to allow a reasonable portion of a specimen to be seen at a time and, bearing in mind that projective magnification may be used, a screen area of 10 × 10 in. seemed a reasonable size. It is true that the visibility of an illuminated area is dependent on the size and brightness of the surrounding area, but a study of the literature[6, 7] did not suggest that this was likely to be other than a very secondary effect, so far as fluoroscopy was concerned.

For the measurement of screen brightness no photometer was available capable of measurement down to the lowest brightnesses being used and direct measurements were possible only above 0·01 ft-lambert, for which an S.E.I. photometer was used. A photometer unit consisting of a gas-type photocell and a logarithmic amplifier, designed primarily as a densitometer, was calibrated from brightness measurements with the S.E.I. photometer, and by this means measurements were made, down to 0·001 ft-lambert.

Projective magnification. By placing the specimen between the X-ray tube and the screen, at a distance from the screen, the image of the specimen is projected larger than natural size. By this means, fine detail in the specimen can be made more easily discernible: there are two physical principles involved; the image size of specimen detail is made proportionally larger than the screen graininess and so is less influenced by the spatial fluctuations in light intensity due to graininess. Secondly, at low brightnesses, the visual acuity of the eye is low and it is possible to perceive large images when small detail may be lost.

Projective magnification has another advantage: when the specimen is moved away from the screen the proportion of scattered radiation from the specimen which reaches any point on the screen is reduced and so the ratio I_S/I_D becomes smaller and, as will be shown later, the sensitivity becomes better.

Projective magnification is practicable only with a very fine focus X-ray tube: if a normal focus tube is used the image of the specimen very rapidly becomes blurred as the specimen is separated from the screen, and the discernibility of detail is poor. The magnitude of projective magnification which is useful is therefore related to the size of the focal spot of the X-ray tube, and this relation has been discussed in a number of papers.[1, 8, 9]

The values of optimum projective magnification determined directly from equations for the summation of screen and geometric unsharpness are independent of the size of the detail being examined, but at these magnifications the actual unsharpness on the screen is very large (0·8–1·5 mm), and it is suggested that there are other effects which might influence the value of projective magnification at which the best sensitivity is attained. These are the reduction in contrast due to unsharpness,[5] the discernibility of blurred detail as compared with sharp images[10] and the ability of the eye to see detail as the brightness is reduced. These factors appear too complex to be amenable to calculation and the optimum values of projective magnification were determined by direct observation.

In general, in fluoroscopy with a fine-focus tube, the tube should be as near the screen as practicable, so as to obtain a higher brightness, and the factors which limit tube-screen distance are the need to obtain a reasonably large area of screen and the ability to obtain the necessary projective magnification. This last factor is the real limitation, as the construction of most X-ray tube-heads prevents specimens being brought closer than a certain distance to the target. In practice, for thin plates, where a projective magnification of about ×6 was found to be required to obtain the best sensitivity, a tube-screen distance of less than 20 in. could not be used.

SENSITIVITY

The type of penetrameter on which most comparison data is available is the wire-type, which has been shown by a number of experimenters to be sensitive to changes in both contrast and definition. Accordingly, this type of penetrameter was used for most of the experiments and in all cases the penetrameter was on the surface of the specimen nearest the tube and away from the screen.

All penetrameter measurements are liable to a subjective error in that as penetrameters have regular spacings, the position of successive wires or steps is known and the presence of detail may be imagined rather than seen. To investigate this, when the sensitivities attainable with different techniques and specimen thicknesses had been determined by the usual method of counting the number of wires visible down a series of wires of decreasing diameter, a number of checks were made. On a particular thickness the wire corresponding to the limit of visibility was placed on the plate in any clock-face position and the viewer invited to locate it. One viewer averaged six correct places out of seven attempts and the other five out of seven over a number of different specimen thicknesses, which confirmed that the chosen wire was being seen, not imagined, and on the other hand that a sufficiently critical standard of discernibility was being set.

EXPERIMENTAL RESULTS

Comparison of sensitivities obtained with no image magnification. The experimental results, given as averages of several readings by two observers, are shown in Tables 3 and 4.

Table 3. *Sensitivity: comparison between different sets with specimen close to screen. Aluminium plates: wire penetrameter: 20 in. tube-screen distance*

thickness x (in.)	*Fine focus set (A) Sensitivity %*			*Medium focus set (B) Sensitivity %*	
	Kilovoltage	*Seifert screen*	*CAWO screen*	*Kilovoltage*	*CAWO screen*
¼	75	5·9	9·5	68	7·4
½	85	4·7	5·5	74	4·8
¾	95	3·6	4·2	80	3·8
1	107	3·1	3·4	86	3·1
1¼	120	2·5	2·5	91	—
1½	135	2·1	2·1	98	2·1
1¾	140	—	1·8	104	—
2	140	2·7	1·9	110	2·3
2½	140	3·5	2·4	126	2·4
3	140	3·9	—	140	3·0
3½	140	4·5	—	140	3·6
4	140	—	—	140	3·9

Table 4. *Sensitivity: comparison between different sets with specimen close to screen. Steel plates: wire penetrameters: 20 in. tube-screen distance*

thickness x (in.)	*Fine focus set (A)*		*Medium focus set (B)*	
	Kilovoltage	*Sensitivity (%)*	*Kilovoltage*	*Sensitivity (%)*
0·1	130	9·8	110	7·8
0·2	140	7·8	130	6·5
0·3	140	7·4	140	6·0
0·4	140	7·4	148	5·9
0·5	140	7·4	148	5·9
0·6	140	7·8	148	5·9
0·7	140	7·8	148	6·2
0·8	140	7·9	148	6·9
0·9	140	7·9	148	7·2
1·0	140	8·0	148	7·9

The following conclusions can be drawn:

(*a*) Used without projective magnification, the sensitivity obtainable with either set is approximately the same for thicknesses up to 2 in. aluminium, but beyond this point, the high-current tube gives better results, as might be expected.

(*b*) Using two different screens with the ultra-fine focus set, the results show that with thin specimens the screen having the smaller unsharpness gives better results, but for thicknesses greater than 2 in. aluminium, the brighter screen is better, in spite of its larger unsharpness.

The effect of projective magnification. Determination of the values of projective magnification giving the best sensitivity. A wire penetrameter was used to represent specimen detail and, attached to plates of different thicknesses, was moved away from the screen towards the X-ray tube. A rapid increase in observable detail was apparent, but the position of the specimen for maximum detail was found not to be critical and there was therefore a considerable spread in the experimental results.

A large number of readings were taken, with different observers, and two conclusions were immediately apparent:

(*a*) the amount of projective magnification which gives the best sensitivity is dependent on the diameter of the wire which is just discernible, so that the optimum value varies with specimen thickness;

(*b*) the values determined by experiment are, in general, considerably greater than those predicted from theoretical considerations. Fig. 2 shows curves of optimum values of projective magnification for the Seifert screen for different specimen thicknesses of steel and aluminium. These are based on averages of a large number of experimental observations which showed a considerable variation between different observers.

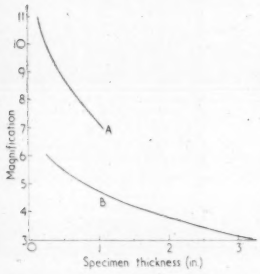

Fig. 2. Experimentally-determined curves of optimum values of projective magnification (focus 0·3 mm)

Curve *A*, aluminium specimens; curve *B*, steel specimens.

Using these values of projective magnification, the best attainable sensitivities were determined, and the results are shown in Tables 5 and 6.

Table 5. *Sensitivity: the effect of projective magnification. Fine focus set: aluminium specimens. Wire penetrameter: 20 in. tube-screen distance*

thickness x (in.)	*Kilovoltage*	*×2 Projective magnification*	*Optimum magnification*	
		S %	*S* %	*M*
$\frac{1}{4}$	75	4·7	3·1	×6
$\frac{1}{2}$	85	3·2	2·4	×5·5
$\frac{3}{4}$	95	—	—	—
1	107	2·4	1·6	×4·8
$1\frac{1}{2}$	135	2·0	1·35	×4·3
2	140	1·8	1·4	×3·9
$2\frac{1}{2}$	140	2·0	1·4	×3·5
3	140	2·1	1·6	×3·1
$3\frac{1}{2}$	140	—	1·8	×3·0
4	140	—	2·1	×2·9

Table 6. *Sensitivity: the effect of projective magnification. Fine focus set: wire penetrameter: Seifert screen: 20 in. tube-screen distance. Steel specimens*

thickness x (in.)	*Kilovoltage*	*Sensitivity %*		
		×3 Projective magnification	*×6.6 Projective magnification**
0·1	130	5·9	5·0
0·2	140	4·9	3·8
0·3	140	3·9	3·3
0·4	140	3·4	3·0
0·5	140	3·2	2·9
0·6	140	3·3	2·8
0·7	140	3·4	3·1
0·8	140	3·5	3·2
0·9	140	3·5	3·2
1·0	140	4·0	3·3
1·1	140	4·6	3·6

* Maximum magnification attainable at 20 in. tube-screen distance, but not optimum values.

The following conclusions can be drawn:

(*a*) a small amount of projective magnification (×2) results in a considerable gain in sensitivity, particularly with large thicknesses of aluminium. For example, on a 3-in. specimen the sensitivity improves from 4 to 2¼%. The same effect is seen on steel;

(*b*) with steel specimens, the difference between the attainable sensitivity with the fine focus set used with projective magnification, and the medium focus set, is more marked than on aluminium, although the values of projective magnification required to give the best results on wire penetrameters are somewhat large. A moderate amount of magnification (×3) will, however, give considerably better sensitivities than can be obtained using the medium focus set;

(*c*) with large steel thicknesses, from ¾ to 1 in., the difference in sensitivity between the two sets, when no projective magnification is used, becomes smaller, but the attainable sensitivity is much worse than can be obtained with the fine focus set, using projective techniques; e.g. with 0·9 in. steel the sensitivity is 8% compared with 3½%.

Other experimental results not detailed here showed that:

(*d*) when different screens are used with projective magnification the difference in attainable sensitivity is negligible except with very thin specimens;

(*e*) results at 20 and 40 in. tube-screen distance, using projective magnification and kilovoltages chosen to give the best results at each distance, are very nearly the same. There is a slight gain in sensitivity at 20 in. compared with 40 in., and a further slight gain at 12 in. tube-screen distance.

The detectability of artificial cracks formed by having a gap of known width between two flat metal faces was also examined experimentally. The "cracks," in aluminium, were adjusted between widths of 0·001 and 0·015 in. and were of four different depths, ⅛, ¼, ⅜ and ½ in.; they were placed on the tube side of a block of aluminium, the plane of the crack being parallel to the X-ray beam; projective magnification as given in Fig. 2 was used.

The results obtained are summarized in Fig. 3. These curves show the maximum thickness through which an artificial crack of a given width and depth can be detected.

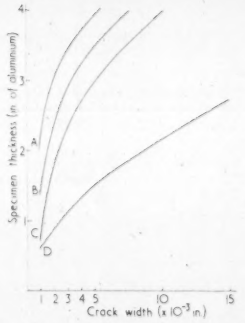

Fig. 3. The detectability of artificial cracks in aluminium using the fine focus set and projective magnification.

Curve *A*, crack ½ in. deep; curve *B*, crack ⅜ in. deep; curve *C* crack ¼ in. deep; curve *D*, crack ⅛ in. deep.

COMPARISON OF THEORETICAL AND OBSERVED SENSITIVITIES

It is possible that the limits of sensitivity may be set by either radiographic factors, such as scattered radiation, screen unsharpness, etc., or by the limitations of the eye, and an equation showing the relative effects of these factors which could be compared with experimental results would be of considerable use in indicating in what direction improvements may be sought after. It does not appear to be possible to calculate sensitivity from fundamental data and make allowance for the lack of definition of the image, but considerable information can be obtained from a knowledge of the performance of the eye on sharp images at the brightness levels used in fluoroscopy, which, when compared with the experimentally obtained sensitivities, should show the relative importance of the factors controlling the definition of the image.

Most of the published measurements on the eye's ability to discern detail have used visual acuity as a measure of the eye's performance, and as can be seen from the definition of visual acuity, it is not easy to relate this to the ability to see single details, such as lines or spots, when these may be of different contrasts; visual acuity, in fact, does not take account of contrast at all, but assumes it to be 100%. A certain amount of data was found on the visibility of detail at different known contrasts, but this was somewhat inadequate and independent measurements were made.

Two test charts were prepared: the first had six rows of circular spots, from 5 to $\frac{1}{4}$ mm diameter, of different contrasts from 100 to 9·5%, as suggested by Morgan and Sturm,[11] and the second was of single lines, 1 cm long, of widths from 4 to $\frac{1}{4}$ mm, and contrasts from 97 to 5%. The contrast of the pattern is as defined by Rose.[12]

$$\text{contrast} = \frac{\text{difference in transmission between image and background}}{\text{transmission of background}}$$

These contrast charts were placed on the front of the protective lead glass about 1 in. in front of the fluorescent screen and the visibility of the spots or lines determined at different brightnesses, which were obtained by placing different thicknesses of metal in the X-ray beam. Thorough dark adaptation was used (thirty minutes) and a viewing distance of 10 in.; several sets of observations were made by two observers and the results are shown in Figs. 4 and 5.

The results obtained by Morgan and Sturm,[11] at three brightnesses, are also shown, for comparison, on Fig. 5. The brightnesses which they employed were estimated from their values of the number of light photons $mm^{-2}\,s^{-1}$ emitted by the screen, using a conversion factor of 1 ft-lambert = 1×10^{11} photons $mm^{-2}\,s^{-1}$. It will be seen that except at the lowest brightness, their results agree closely, but the relation which they suggest from fluctuation theory between the diameter of the smallest visible spot d, contrast C and brightness B, namely d^2 proportional to $1/BC^2$, is not valid for the whole range of B and C shown on Fig. 5, and does not apply to the discernibility of single lines as shown in Fig. 4.

From the point of view of determining limiting visibilities, it can be shown that the contrast of the just-visible fluoroscopic image, over the range of specimen thickness examined, is between 2 and 10%, and over this limited contrast range, it can be shown that the equation

$$d = 1/100BC^{3/2} \qquad (1)$$

is a reasonable fit to the discernibility curves for single lines, with

$$d = 1/20B^{2/3}C^{3/2} \qquad (2)$$

becoming a better fit at contrasts around 10%. In a similar way

$$d = 0{\cdot}13/CB^{1/2} \qquad (3)$$

can be shown to be a reasonable fit to the discernibility curves for circular spots at contrasts near to 10%.

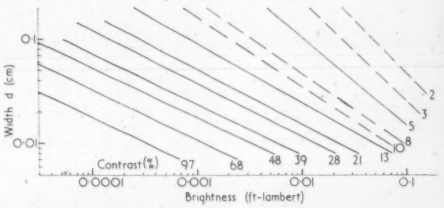

Fig. 4. The discernibility of 1 cm long lines of varying widths d and contrasts, at different brightnesses
Dotted curves indicate estimated values.

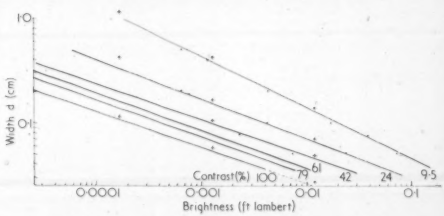

Fig. 5. The discernibility of circular spots of varying diameters d and contrasts, at different brightnesses
+ = Morgan and Sturm values.[11]

These empirical equations for the discernibility of sharply defined images can be combined with the radiographic factors to produce equations of radiographic sensitivity applicable to fluoroscopy.

By definition, contrast $C = (\Delta B/B) \times 100$ (in %) where B is the screen brightness, which is proportional to the X-ray intensity incident on the screen, and ΔB is the brightness difference due to an image-detail on the screen. Then taking the intensity of the X-ray beam reaching the screen, as consisting of two components, I_D the direct, image-forming radiation and I_S, the scattered radiation, it can be shown that

$$C = (\Delta B/B) \times 100 = \mu \Delta x 100/[1 + (I_S/I_D)] \qquad (4)$$

where μ is the coefficient of linear absorption.

This can be substituted in equation (1), taking $d = \Delta x$ for a circular-section wire, so that an equation for sensitivity can be derived.

If the image on the screen is $M\times$ natural size, owing to projective magnification, then

$$\text{sensitivity}\,(\%) = \left(\frac{\Delta x}{x}\right) 100 = \frac{1}{x}\left[\frac{1 + (I_S/I_D)}{\mu}\right]^{0{\cdot}6}\left(\frac{1}{BM}\right)^{0{\cdot}4} \qquad (5)$$

Similarly, for cylindrical cavities of depth equal to diameter:

$$\text{sensitivity} = \frac{3 \cdot 65}{x}\left[\frac{1 + (I_S/I_D)}{\mu M B^{\frac{1}{2}}}\right]^{\frac{1}{2}} \qquad (6)$$

To compare these equations with direct measurements of sensitivity, values of $[1 + (I_S/I_D)]$, μ and B are required. These have been determined for aluminium plates, using the appropriate X-ray kilovoltages, both with the specimen plates close to the screen and at the position for projective magnification, and are shown in Table 7.

Table 7. *Measurements of scattered radiation, absorption coefficient and screen brightness for different thicknesses of aluminium plate*

	$[1 + (I_S/I_D)]$			*Screen brightness (ft-lamberts)*	
Aluminium thickness (in.)	*Specimen against screen*	*With projective magnification*	μ (cm^{-1})	*Specimens against screen*	*With projective magnification*
$\frac{1}{2}$	1·64	1·16	1·23	0·078	0·017
$\frac{3}{4}$	1·83	1·19	1·10	0·053	0·014
1	2·01	1·23	0·94	0·036	0·012
$1\frac{1}{2}$	2·5	1·37	0·70	0·022	0·0095
2	3·0	1·49	0·70	0·012	0·0047
$2\frac{1}{2}$	3·7	1·65	0·70	0·0072	0·0023
3	4·4	1·81	0·70	0·0046	0·0011
$3\frac{1}{2}$	5·1	2·0	0·70	0·003	(0·00053)
4	—	2·2	0·70	—	(0·00024)

The brightness values shown in brackets are extrapolated.

Using this data the values of sensitivity calculated from the equations derived from the visibility of sharp images can be compared with experimentally observed values of fluoroscopic sensitivity.

Table 8. *Comparison of calculated and observed sensitivities on aluminium plates*

	Wire penetrameter sensitivities					*Sensitivity Cylindrical holes depth = diameter*	
	Optimum projective magnification			*No projective magnification*		*Optimum projective magnification*	
Aluminium thickness (in.)	*Calculated Based on equation (5)*	*Based on equation (2)*	*Observed*	*Calculated*	*Observed*	*Calculated*	*Observed*
$\frac{1}{2}$	2·0		2·35	2·6	4·7	3·8	4·3
$\frac{3}{4}$	1·6		1·9	2·4	3·6	2·8	—
1	1·5		1·6	2·3	3·1	2·3	2·6
$1\frac{1}{2}$	1·4		1·3	2·2	2·1	2·1	2·1
2	1·5		1·4	2·7	2·7	2·0	2·1
$2\frac{1}{2}$	1·8	1·55	1·4	3·1	3·5	2·15	2·1
3		1·77	1·6	3·4	3·9	2·3	2·4
$3\frac{1}{2}$		2·0	1·8	3·8	4·5	2·65	2·8
4		2·3	2·1	—	—	3·0	3·1

These results lead to a number of conclusions.

(*a*) The equations for sensitivity are based on the experimentally-determined discernibility of sharp images of lines, whereas the fluoroscopic image is seen on a "grainy" screen. The good agreement between the observed and calculated values, when projective magnification is used, suggests that under these conditions the unsharpness of the screen is relatively unimportant.

(*b*) The greatest discrepancy between observed and calculated values is for small thicknesses, when the specimen is close to the screen, and it is precisely under these conditions, when the observed image is smallest, that screen unsharpness is likely to have the most influence. With specimens up to $1\frac{1}{2}$ in. thick, when no projective magnification is used, the diameter of the thinnest visible wire is less than the screen unsharpness, so that in this range the image contrast is affected by unsharpness.

(*c*) From equations (5) and (6) an improvement in sensitivity can be brought about by a decrease in $[1 + (I_S/I_D)]$, or an increase in μ, M or B. The first is obviously not practical, as with projective magnification, I_S/I_D is already almost as small as possible. Increase of μ is also unlikely to have a large effect, as to hold B constant while obtaining an increase in μ (decrease in kilovoltage) would require very large increases in X-ray output. Increase of M has great disadvantages in that a smaller area of specimen is examined at any one time, so that increase in B seems to be the only practical method of improving sensitivity.

Equation (5) shows that a tenfold increase in B would reduce the numerical value of sensitivity by a factor of 0·4, and a hundredfold increase in B by a factor of 0·16; that is, a sensitivity of 4% would improve to 1·6 and 0·64% respectively, although it should be pointed out that there is some possibility that the latter value would not be attained owing to other limiting factors.

This increase in B could possibly be obtained in two different ways. The first is by refinements in X-ray tube design, allowing the tube to be operated at a higher current, without an increase in focal spot size. Some experiments were made to verify the improvements which could be obtained in this direction by over-running a fine focus tube for short periods at twice the output of set A, and the sensitivities obtained were shown to be in close agreement with the values predictable from equation (5) for a doubling of B.

At the time that this work was being completed, descriptions of a rotating-anode tube with forced oil-cooling on the tube envelope, built for the U.S. Naval Ordnance Laboratory were published.[13] This tube has a rating of 5000 W at 140 kVp from a 0·5 mm focus, compared with O'Connor's original tube having a rating of 900 W and a 1 mm target, and considerable gains in fluoroscopic sensitivity are claimed.[14]

A second possible method of increasing the screen brightness is to increase the X-ray kilovoltage. The brightness increase will be accompanied by a decrease in μ, but the overall effect can be shown to be a gain in sensitivity. Taking a specific example, if the kilovoltage is increased from 140 to 200 kV, then for a specimen of 3 in. aluminium, calculation suggests that for the same milliamperage, the sensitivity should be improved by a factor of 0·7: that is, a wire penetrameter sensitivity of 1·15% should be possible, compared with 1·6%.

CONCLUSIONS

(*a*) It has been shown that fluoroscopy, utilizing a fine focus tube, with which a projected image technique can be used, enables better wire penetrameter sensitivity to be attained than with a higher output medium focus tube, with which the specimen has to be close to the screen. Comparable figures are:

	Wire penetrameter sensitivity (%)				
	½ in. Al	*2 in. Al*	*4 in. Al*	*½ in. Fe*	*1 in. Fe*
Ultra-fine focus tube (1 mA)	2·35	1·35	2·1	2·9	3·3
Medium focus tube (20 mA)	4·9	2·05	4·1	5·8	7·8

(*b*) The sensitivities attainable on wire penetrameters, the minimum detectable sizes of artificial cracks and cylindrical cavities, suggest that fluoroscopy with a magnified image gives adequate sensitivity for many types of inspection work in the thickness-range $\frac{1}{4}$–4 in. aluminium, 0–1 in. steel, using 140 kVp X-rays. Comparable figures are:

	Wire penetrameter sensitivity (%)			
	1 *in. Al*	2 *in. Al*	$\frac{1}{2}$ *in. Fe*	1 *in. Fe*
Fluoroscopy	1·6	1·35	2·9	3·3
Radiography on film (140 kV maximum)	0·6	0·6	0·9	1·0
	fine-grain film			tungstate screens

(*c*) The need for thorough dark adaptation of the eye has been shown. A dark adaptation time of five minutes, which gives partial cone-adaptation only, has been shown to be inadequate and a minimum adaptation time of twenty minutes is suggested.

(*d*) Measurements made on different fluoroscopic screens have shown that, whereas with specimens against the screen, screen unsharpness is an important factor in the visibility of detail, with projected image techniques it is of secondary importance only.

(*e*) The magnitude of projective magnification to be used with any particular specimen thickness has been shown not to be solely dependent on screen unsharpness and focus size, but to vary with specimen thickness. Curves of optimum projective magnification against thickness are given.

A small amount of projective magnification ($\times 2$) has been shown to give a marked improvement in sensitivity, but the optimum values for a 0·3 mm focus size have been shown to vary between three and six for different thicknesses of aluminium.

(*f*) Data obtained on the ability of the eye to discern sharp detail of different contrasts at different brightnesses has led to formulae for sensitivity, in terms of measurable quantities, which agree well with observed sensitivities. These formulae emphasize that in order to improve sensitivity the overriding requirement is an increase in screen brightness, and the amount of improvement to be expected can be estimated.

FUTURE DEVELOPMENTS IN FLUOROSCOPY

The formulae derived for sensitivity suggest that, in order to improve the attainable sensitivity, the major requirement is an increase in brightness and while this could be attained in part by an increase in kilovoltage, the primary need is for an increase in tube current. The amounts of projective magnification found to be advantageous with the 0·3 mm focus tube ranged between $\times 3$ and $\times 6$, and already limit the area of specimen under examination at one time, so that although an increase in M improves sensitivity, such an increase would cause severe practical limitations. It is suggested, therefore, that decreases in focal spot size, below 0·3 mm, would have little practical advantage and that the optimum size of focus is between 0·3 and 0·5 mm. The need, therefore, is for an X-ray tube operating up to 200 kVp, with a focus of this size, and with as large an output as possible. There seems to be no *a priori* reason why a rotating anode tube could not be designed with the anode at earth potential, in which case it ought to be possible to arrange water cooling of the anode directly, thus permitting a large increase in focal spot loading.

The efficiency of conversion of X-ray energy to light by the fluorescent screen is very low and there also seems to be some prospect of improvement from new developments in this field. Electroluminescent materials have been developed and have been shown[15–17] to give image intensification—the so-called "solid-state image intensifier." There appears to be three possible mechanisms[18]: (*a*) an electroluminescent cell, in series electrically with a dielectric which becomes conductive during exposure to X-rays; (*b*) a light-amplifying phosphor layer, in series optically with an ordinary fluoroscopic screen; (*c*) a photoelectroluminescent screen, sensitive to X-rays. Development does not appear to have proceeded far enough for intensification factors to be measured, but figures of $\times 30$ have been mentioned.[19]

The electronic image intensifier might perhaps also be considered as a form of more efficient fluoroscopy screen, in that by its use large gains in brightness are obtained. A new factor, however, limits its performance: the magnitude of the quantum fluctuations at the stage in the intensification process where the number of quanta is smallest, usually the absorption of X-rays by the primary screen, is magnified in the subsequent stages of intensification and so limits the information conveyed by the large number of quanta emitted by the final screen; with low X-ray intensities, these fluctuations are, in fact, visible.

ACKNOWLEDGEMENT

Crown copyright is reserved. This paper is reproduced by permission of the Controller of H.M. Stationery Office.

REFERENCES

(1) O'Connor, D. T., and Polansky, D. *Navord Report* 2168 (Maryland: U.S. Naval Ordnance Laboratory, 1951).
(2) O'Connor, D. T., and Polansky, D. *Non-destr. Test.*, **10**, pp. 10–21 (1951).
(3) O'Connor, D. T. *Non-destr. Test.*, **11**, pp. 11–21 (1952).
(4) Chamberlain, W. E. *Radiology*, **38**, pp. 383–425 (1942).
(5) Halmshaw, R. *J. Photo. Sci.*, **3**, pp. 161–168 (1955).
(6) Steinhardt, J. *J. Gen. Physiol.*, **20**, pp. 185–209 (1936).
(7) Hecht, S., and Shlaer, S. *J. Opt. Soc. Amer.*, **37**, pp. 531–545 (1947).
(8) Nemet, A., and Cox, W. F. *Brit. J. Radiol.*, **29**, pp. 335–7 (1956).
(9) Burger, G., Combee, B., and Tuuk, J. *Philips Tech. Rev.*, **8**, p. 321 (November 1946).
(10) Kruithof, A. *Philips Tech. Rev.*, **11** (11), p. 333 (May 1950).
(11) Morgan, R. H., and Sturm, R. E. *Amer. J. Roentgenol.*, **62**, pp. 617–34 (1949).
(12) Rose, A. *J. Soc. Motion Picture Televis. Engrs*, **47**, pp. 273–294 (1946).
(13) O'Connor, D. T., and Criscuolo, E. *Non-destr. Test.*, **13**, pp. 18–26 (1955).
(14) Criscuolo, E., and Polansky, D. *Non-destr. Test.*, **14**, pp. 30–32 (1956).
(15) Cusano, D. A. *Elect. Engng*, **74**, p. 170 (1955).
(16) Orthuber, R. K. *J. Opt. Soc. Amer.*, **44**, pp. 297–9 (1954).
(17) Kazan, B., and Nicoll, F. *Proc. Inst. Radio Engrs*, **43**, pp. 1888–97 (1955).
(18) Williams, F. E. *Amer. J. Roentgenol.*, **75**, pp. 77–82 (1956).
(19) Diemer, G., and Klasens, H. A. *Philips Res. Rep.*, **10**, pp. 401–424 (1955).

The ultrasonic degradation of polystyrene at a frequency of 1 Mc/s

By N. H. LANGTON, M.Sc., Ph.D., A.M.Brit.R.E., A.Inst.P., and P. VAUGHAN, A.P.I., The National College of Rubber Technology, Northern Polytechnic, London, N.7

[*Paper received* 25 *January*, 1957]

Experimental results obtained by irradiating fractionated polystyrene in benzene with ultrasonics of 1 Mc/s frequency are given. Degradation is observed to take place, and the consequent variation of degree of polymerization P with length of time of irradiation is shown. The results are compared with those obtained by other workers who used lower frequencies, and discussed with reference to the degradation equation of Schmid. An alternative equation which fits the experimental results better is examined.

Over the past few years a number of papers have been published describing the degradation of high polymers when irradiated with ultrasonics of various frequencies. By degradation is meant the breaking of the long chain molecules of the high polymer into units of shorter length. This occurrence can be detected by measuring the intrinsic viscosities of the irradiated solutions, when it will be found that there is a decrease in intrinsic viscosity from that of the unirradiated solution. The intrinsic viscosity at any time is connected with the degree of polymerization P, where $P = M_p/M_m$ and M_p and M_m are the molecular weights of the polymer and monomer respectively, by the equation $[\eta] = \alpha P$, where α is a constant.

The degradation of polystyrene in solution has previously been investigated mainly by Schmid,[1] Schmid and Rommel,[2] Melville and Murray,[3] Jellinek and White,[4] and Brett and Jellinek.[5] These workers used, respectively, ultrasonic frequencies of 284 kc/s,[1, 2] 213 kc/s[3] and 500 kc/s.[4, 5] An equation describing the degradation was first proposed by Schmid,[6] who worked upon the assumption that the degradation was caused by frictional forces due to the relative motion of solute and solvent. Although this description of the mechanism of the phenomena is now regarded as incorrect, Schmid's equation is still valid and has been used as the basis of a wider theory developed by Jellinek and White.[4] The work of Melville and Murray,[3] and in particular that of Brett and Jellinek,[5] indicate that the degradation is probably caused by the presence of cavitation in the irradiated solution. In this paper the authors describe experiments on the degradation of polystyrene dissolved in benzene, using an ultrasonic frequency of 1 Mc/s, and the results are discussed in the light of Schmid's equation and compared with those for lower frequencies obtained by the workers referred to above.

EXPERIMENTAL

The apparatus used and its arrangement is shown diagrammatically in Fig. 1. The 1 Mc/s quartz crystal transducer T was immersed in a glass tank holding about ten gallons of water, and was fed from a standard Mullard high-frequency generator type E. 7562 which was capable of producing a maximum power output of 300 W ultrasonic power in water. The working face of the quartz crystal had a diameter of 6·3 cm, and the ultrasonic beam, which was practically parallel, was projected on to an inclined watchglass reflector R the centre of which was about 15 cm from the face of the transducer. The ultrasonic beam was thereby reflected to a focus at the water surface, where it normally caused the usual fountain and exhibited the effects of cavitation. This arrangement of transducer and reflector was kept unaltered during the entire run of experiments. A thick Duralumin plate D with a circular hole of 1 cm radius was held horizontally just in the water surface, the latter always being kept at the same level with respect to the centre of the transducer face. The hole was of a size to just take the end of the irradiation tube I, as shown in Fig. 1, so that the tube could always be placed in the same position with respect to the reflector at the beginning of each experiment. By working the transducer at the same voltage each time, these precautions ensured that the ultrasonic power entering the irradiation tube was as nearly as possible the same for each experimental run. This power was measured calorimetrically as described below.

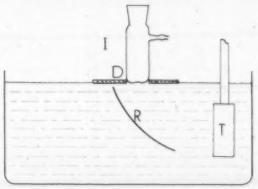

Fig. 1. Experimental arrangement of apparatus for the ultrasonic degradation of polystyrene (cooling finger not shown)

The absorption of the ultrasonic energy by the solution and the glass walls of the tube tended to cause a considerable rise of temperature. It is necessary to prevent this, as it has been shown by Schmid that the degradation effect is less at elevated temperatures. The temperature was controlled by inserting a cold finger into the irradiation tube. Brett and Jellinek[5] show that the position of a cooling coil in the irradiation tube must be accurately reproducible, as a small change in its position can have a large effect upon the degradation rate. This positioning was made repeatable by constructing the irradiation tube from a standard Quickfit open tube with a socket number B. 19, and using the cooling finger FC14/00 which is made to fit the B. 19 socket. The end of the open tube was closed and made slightly concave inwards to take the ultrasonic fountain, the inner surface of the curved bottom being about ½ cm from the lower end of the cooling finger. The tube was also fitted with a side-tube, to which was usually attached a U-tube containing a few drops of mercury. This acted as a crude indicator of any pressure build-up which would be caused by inefficient cooling, and also ensured that the system remained closed during each experiment so that there would be no loss of solvent vapour. A thermocouple could be introduced through this side tube, and this was done to enable the efficiency of the cooling system to be tested. It was found that when no

water was flowing, the temperature of 12 cm³ of the solution rose from 22·5° C to a steady value of 52·0° C after eight minutes' irradiation, whilst with the cooling water flowing, the temperature rise was from 22·0 to 25·7° C. This small increase of temperature would have no appreciable effect upon the ultrasonic degradation. The experiments were always carried out with 12 cm³ of solution, which filled the irradiation tube to a depth of 4·5 cm, and during the experiments, an ultrasonic disturbance could be seen at the surface of the solution and the characteristic cavitation noise heard.

The polystyrene solution was prepared by dissolving 50 g in 1 l. of ethyl methyl ketone, allowing it to stand for several days, and then adding methanol to precipitate the polymer. The highest molecular weight fraction precipitates first, and a first fraction of 17·008 g was obtained this way. This was separated from the remaining solution by decantation and dried in an oven at about 50° C. By adding more methanol, a second fraction of lower molecular weight was obtained, the yield being 25·25 g. This was also collected and dried. These polystyrene fractions were then dissolved in pure benzene and made up to known concentrations. The first fraction was used up in preliminary work, and it was the second fraction which was used in the experiments described here. Of this fraction, 18·500 g were dissolved in 1 l. of benzene to make the stock solution, and the 12 cm³ used in each irradiation experiment were obtained from this.

RESULTS

The ultrasonic degradation in the irradiated solution was detected and measured in the usual manner by observing the changes in intrinsic viscosity. Solution viscosities were measured with an Ostwald type U-tube viscometer, immersed in a thermostatically controlled water bath, the temperature of which was kept at 28 ± 0·05° C. Most of the measurements were taken with a No. 1 viscometer, B.S. 188/4233/55, which had a "pure benzene" time of 153·49 s at this temperature, although occasionally a modified No. 1 viscometer, B.S. 188/79248, having a "pure benzene" time of 233·37 s was used as a check. In all cases, 12 cm³ of solution of concentration $c = 1{\cdot}805$ g/100 cm³ were irradiated, and immediately afterwards 10 cm³ of this solution were diluted to 20 cm³ with pure benzene to make a solution of concentration $c/2$. This solution was then used for the viscosity measurements, the viscometer being allowed to stand in the water bath for at least twenty minutes before commencing the timing. At least four readings of the time of flow were observed. This procedure was then repeated with the solution diluted to $c/4$, $c/8$, $c/16$ and $c/32$ concentrations, although the last dilution generally gave results which were unreliable. Each irradiation time was repeated several times, and the results averaged. The graphs of these results expressed in the form η_{sp}/c plotted against c are shown in Fig. 2. A series of straight lines of approximately the same slope were obtained, and these lines are extrapolated to zero concentration to obtain values of the intrinsic viscosity $[\eta]$, where $[\eta] = (\eta_{sp}/c)_{c=0}$. From the values of η so obtained, it is possible to calculate the degree of polymerization P from the equation $\eta = 8{\cdot}0 \times 10^{-4} P$, the value of the constant in this equation being taken from Brett and Jellinek.[5] The values of η and P for each irradiation time are given in the table. These results are plotted in Fig. 3, which shows how

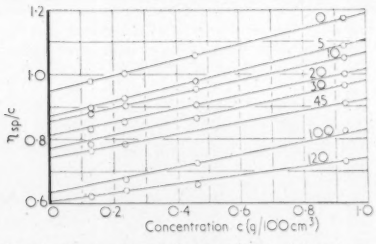

Fig. 2. Graph of intrinsic viscosity (η_{sp}/c) against concentration C for various irradiation times t. The values of t are given on the curves in minutes

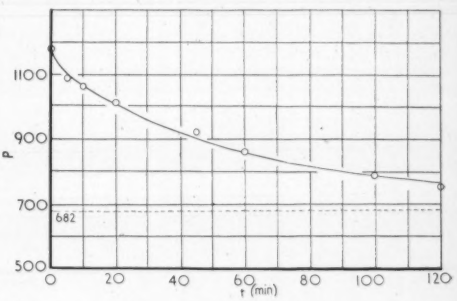

Fig. 3. The decrease of the degree of polymerization P with increasing time of irradiation t

the value of P decreases as the solution is irradiated for longer periods of time.

Values of $[\eta]$ *and* P *for various irradiation times* t

t(min)	$[\eta]$	P
0	0·946	1183
5	0·868	1085
10	0·850	1062
20	0·809	1011
30	0·767	960
45	0·738	920
60	0·688	860
100	0·630	788
120	0·602	753

This degradation table is typical of ultrasonic degradation, and is similar to that obtained by other workers who have used lower ultrasonic frequencies. The initial portion of the resulting curve shows that the degradation rate is relatively large for the first five minutes or so, after which it gradually decreases and the curve becomes flatter and tends to a limiting value P_∞.

DISCUSSION OF RESULTS

The ultrasonic degradation equation proposed by Schmid is

$$dX/dt = + K_1(P_t - P_\infty) \qquad (1)$$

where X is the number of broken bonds per litre of solution after t seconds of irradiation, P_t the degree of polymerization which is reached at the end of the irradiation period, P_∞ the

final limiting degree of polymerization and K_1 a constant. Since the number of chain breakages X is inversely proportional to P_t, putting $X = A/P_t$, where A is a constant, gives

$$dP_t/dt = -KP_t^2(P_t - P_\infty) \qquad (2)$$

where $K = K_1/A$ and is a rate constant. Hence,

$$\int[dP_t/P_t^2(P_t - P_\infty)] = -Kt + \text{constant}$$

This equation gives

$$-[P_\infty/P_t] - \ln[1 - (P_\infty/P_t)] = Kt + \text{constant} \qquad (3)$$

The values of P in this equation refer to number averages, whilst the experimental results are weight averages. In spite of this, however, both Schmid[1] and Brett and Jellinek[5] obtain straight lines from their experiments when the left-hand side of equation (3) is plotted against the irradiation time t.

We see that the left-hand side of the above equation cannot be evaluated unless the numerical value of the constant P_∞ can be found. The finding of this value from the experimental results may have caused some error in previous work, because P_∞ was apparently obtained either by extrapolation or inspection, and it is doubtful if an accurate value can be obtained in these ways, especially when the degradation curve values are not found for long irradiation periods. Brett and Jellinek, for example, give a value $P_\infty = 663$, which is that found for $t = 120$ min and is greater than the experimental value for $t = 240$ min. For this reason it was thought that the introduction of a method for calculating P_∞ from the experimental curve would be advantageous. The method used here is that due to Guggenheim.[7] This method involves the calculation of the term $\ln(P_t - P_{t+T})$ where T is an arbitrary time interval which should be greater than the half-life period of the degradation for accuracy. The value $T = 50$ min was always taken. Values of $\ln(P_t - P_{t+T})$ are plotted against t and the slope of the straight line obtained measured. The lines thus obtained are shown in Fig. 4, calculated from the results of Melville and Murray,[3] Brett and Jellinek[5] and the present writers. Two sets of results of Melville and Murray are shown, both for degradation in air (run 2) and in a vacuum (run 1), the other results are for degradation in air at atmospheric pressure. It is seen that in all cases the experimental points give very good straight lines, except for t less than about ten minutes. The limiting value P_∞ is obtained from the equation

$$(P_t - P_\infty)/(P_0 - P_\infty) = \exp(-kt) \qquad (4)$$

where k is the slope of the straight line. The values of P_∞ thus found were, Brett and Jellinek, $P_\infty = 613$, Melville and Murray, $P_\infty = 1176$ for a vacuum and 1119 for air, Langton and Vaughan, $P_\infty = 682$. Since the experiments of Schmid and Rommel showed that P_∞ was the same regardless of the value of the initial degree of polymerization P_0, the value of P_∞ can be taken as a criterion against which the effects of input power and frequency upon the amount of degradation can be deduced. Unfortunately there are not enough data at present available to make any deductions of this nature, although it does appear that the frequency has little effect upon the rate of degradation, or upon the value of P_∞.

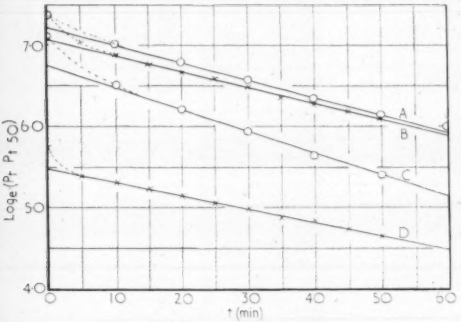

Fig. 4. Graph of $\log_e(P_t - P_{t+50})$ against irradiation time t

Curve *A*, Melville and Murray, run 1 (vacuum); curve *B*, Melville and Murray, run 2 (air), 213 kc/s; curve *C*, Jellinek, 500 kc/s; curve *D*, Langton and Vaughan, 1 Mc/s.

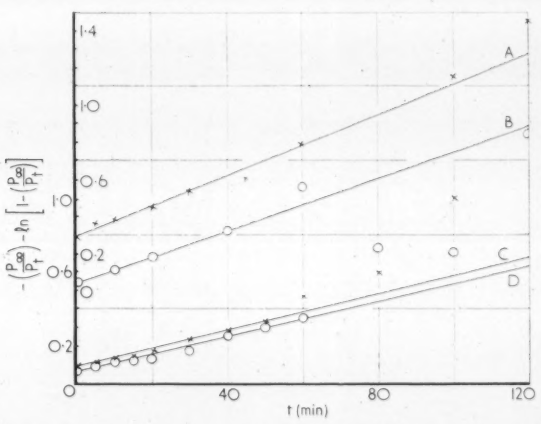

Fig. 5. Graph of $-(P_\infty/P_t) - \ln[1 - (P_\infty/P_t)]$ against irradiation time t. (Vertical scale repeated for clarity, inner scale refers to curves *A* and *B*)

Curve *A*, Langton and Vaughan; curve *B*, Jellinek; curve *C*, Melville and Murray, run 1; curve *D*, Melville and Murray, run 2.

Using the values of P_∞ calculated by this method, equation (3) was plotted for the four sets of experimental results, as shown in Fig. 5. The linearity of the points is not good, being best in the cases of the results of Brett and Jellinek and the writers. The extent of agreement in the first case, with the new value of P_∞ is not as good as that shown in the original paper. The results of Melville and Murray give poor agreement. On the whole, the agreement is better for irradiation periods less than about sixty minutes.

It is easy to show that Guggenheim's method as used above for finding P_∞ is equivalent to assuming a degradation equation of the form

$$dP_t/dt = -k(P_t - P_\infty) \tag{5}$$

Comparison of Figs. 4 and 5 show that equation (5) describes the experimental results better than equation (3). A third possible equation is

$$dX_t/dt = +k(X_\infty - X_t) \tag{6}$$

This equation can be integrated in terms of P, but when plotted it leads to a curve in all cases and hence is unsuitable and the graphs are not shown.

Attempts to measure the ultrasonic power entering the irradiated solution were made by several methods. The temperature rise of the solution without cooling was observed, as also was the temperature rise in a rubber bung with an embedded thermocouple. By plotting the cooling curves after the ultrasonics had been switched off an estimate of the heat losses could be obtained in the usual way. There was little agreement between the results for the various methods. The most consistent results were obtained using 10 cm^3 of distilled water irradiated in the tube used for the main experiments, measuring the temperature rise with a thermocouple and correcting for the thermal capacity of the glass tube. The average of the results gives an ultrasonic power absorption of about 7 W, but this figure is not reliable.

Some measurements were also taken of the degradation with smaller power inputs, obtained by using the quartz crystal transducer at lower voltages. For an irradiation time of thirty minutes, $P_{30} = 944$ for 4000 V, 1119 for 3000 V, and for 2000 V the value of 1200 which was found is the same, within the limits of experimental error, as that of the unirradiated solution. Thus the effect of the ultrasonics decreases as the input power to the solution decreases, as has been noticed before. It is thought that degradation ceases when the input power is too small to produce cavitation, but it is not easy to detect when this occurs by observing the solution, though, as far as could be seen, there was no cavitation in the solution when the crystal voltage was 2000 V.

CONCLUSIONS

The degradation curve obtained from the experimental values of P_t, which have an estimated accuracy of about $\pm 4\%$, show that the degradation at 1 Mc/s is similar to that previously observed at 213 and 500 kc/s by other workers. The results do not agree very well with Schmid's equation, the agreement being better for short irradiation times than for times longer than about sixty minutes. The same is true for the results of Brett and Jellinek and for those of Melville and Murray, which were re-examined using values of the limiting degree of polymerization P_∞ calculated by Guggenheim's method. The use of this method showed that the equation

$$dP_t/dt = -k(P_t - P_\infty) \tag{7}$$

agreed with experiment better than the equation of Schmid, which has always been used previously, except for irradiation periods below about ten minutes.

ACKNOWLEDGEMENT

The authors are grateful to Dr. J. Glazer, Senior Lecturer at the National College of Rubber Technology, for drawing their attention to Guggenheim's method.

REFERENCES

(1) SCHMID, G. *Phys. Z.*, **41**, p. 326 (1946).
(2) SCHMID, G., and ROMMEL, O. *Z. Electrochem*, **45**, p. 659 (1939).
(3) MELVILLE, H. W., and MURRAY, A. J. R. *Trans. Faraday Soc.*, **46**, p. 996 (1950).
(4) JELLINEK, H. H. G., and WHITE, G. *J. Polymer Sci.*, **6**, pp. 745, 759 (1952); **7**, pp. 21, 33 (1951).
(5) BRETT, H. W. W., and JELLINEK, H. H. G. *J. Polymer Sci.*, **13**, p. 441 (1954).
(6) SCHMID, G. *Z. Phys. Chem.*, **186**, p. 113 (1940).
(7) GUGGENHEIM, M. *Phil. Mag.*, **7**, p. 538 (1926).

Size of the focal spot in a betatron

By D. Greene, M.Sc., Ph.D., A.Inst.P., Betatron Research Group, Christie Hospital and Holt Radium Institute, Withington, Manchester

[*Paper received* 18 *February*, 1957]

The X-ray source in a 20 MeV betatron has been examined and has been found to be about 1 cm wide. It is suggested that there are two X-ray sources, the small platinum target and the "donut" wall, to which electrons may be scattered from the target.

The resolving power of a finite sized ionization chamber is discussed in an Appendix.

Introduction

In a betatron used to produce X-rays at an internal target it is usually assumed that the X-ray source is very small because: (1) the X-ray target itself is usually small. In the Metropolitan-Vickers' betatron[1] on which the present results were obtained, the area presented by the platinum target to the incident electrons is about 1 mm square; (2) the guiding field of the betatron is designed to focus the electrons both in the plane of the orbit and in planes normal to it; (3) the electrons strike the target by spiralling out from the stable orbit. The pitch of this spiral is small, so the electrons strike only the tip of the target in a number of successive cycles round the spiral.

In a betatron used for X-ray therapy it is necessary to limit the beam to a well-defined cross-section, and desirable that the cut-off at the edge should be sharp. On the assumption that the focal spot is small, it would seem possible to achieve the latter condition.

Measurements

Fig. 1 shows the intensity distribution across a beam which is limited by a collimator with walls tapering to converge on the target. The intensity measurements were made using a

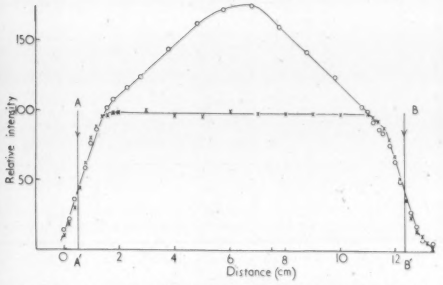

Fig. 1. Intensity distribution across the betatron X-ray beam at 80 cm from target

Baldwin Ionex ionization chamber, 6 mm in diameter and 2 cm long, at a depth of 4 cm below the surface of a water phantom, so that electronic equilibrium had been established. The circles correspond to readings taken with the collimator in position, and the crosses show the results obtained when a laminated copper "beam flattening" filter is fitted to the target end of the collimator. The symmetry of the beam edges and the fact that the filter does flatten the beam show that the collimator is correctly alined.

It can be seen that the beam edge is not sharp, but falls off fairly uniformly over a distance of about 1·5 cm. The lines AA' and BB' show where the intensity would be expected to fall off sharply if there were a point source of radiation, and it can be seen that the intensity starts to decrease well inside these lines.

The lack of sharpness at the beam edge could be explained, (i) as a result of the poor resolving power of the finite sized ionization chamber used; (ii) as due to secondary radiation scattered inside the beam; (iii) as a penumbra produced by a large focal spot.

(i) *Resolving power.* The resolving power of a finite sized ionization chamber is discussed in the Appendix, and it is there shown that if the observed beam edge extends over a distance greater than the chamber width, it can be assumed that the results give a correct measure of the shape of the beam edge. The results in Fig. 1 show the beam edge extending over more than twice the chamber diameter.

(ii) *Scatter.* It is generally agreed[2, 3] that for 20MV X-rays the depth dose curves do not vary appreciably with field size, and therefore that the contribution from scattered radiation is very small. In Fig. 1 the intensity at AA' and BB' is down to 45% of that inside the flattened beam. If it is assumed that the focal spot is very small, the contribution of the primary at or just outside these points is zero, so the 45% would be entirely due to scatter. This is not consistent with the depth dose results.

(iii) *Focal spot.* The size of the focal spot was examined using the apparatus shown in Fig. 2. A slit 15 cm long and 0·2 mm wide was formed by a pair of 15 × 7 × 5 cm lead blocks C with their 7 × 5 cm faces separated by paper spacers D. The faces forming the slit were machined flat. The ionization chamber E was fixed to the back of this slit which was set up parallel to the central axis of the betatron

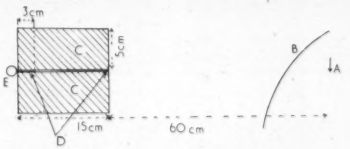

Fig. 2. Slit arrangement used to look at X-ray source

A, betatron target; *B*, "donut" wall; *C*, lead blocks; *D*, paper spacers; *E*, ionization chamber.

beam, with the slit front 60 cm from the target. A series of readings was taken with the ionization chamber as the system was traversed across the beam, and a typical result is shown in Fig. 3(*a*). Here the circles correspond to direct measurements and it can be seen that they give a peak superimposed on a continuous background which extends for some distance on each side of the results shown. This background can be

accounted for mainly by direct penetration of the lead, as is shown by the solid circles of Fig. 3(*a*), which correspond to readings taken with the slit closed. The difference between the two curves is plotted in Fig. 3(*b*), which shows the way in which the intensity through the slit varies with slit position.

In so far as the slit limits the radiation received at the ionization chamber to a narrow parallel beam, Fig. 3(*b*) gives the intensity distribution across the X-ray source. The beam received at the ionization chamber is in fact not parallel,

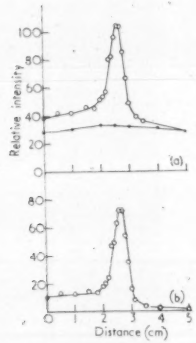

Fig. 3. Curves showing variation of intensity through slit against slit position

but diverges to a width of 1·8 mm at the plane through the target. The experimental curve will therefore show a peak 1·8 mm wider at the base than the real one. This error is small compared to the width of the peak of Fig. 3(*b*), so the intensity distribution across the source will not be far from that shown.

These results were obtained when the slits were traversed in the plane of the betatron orbit. Similar results were obtained when the slits were traversed in the plane normal to the orbit.

Absorption experiments have been carried out with the slits pointing at different parts of the source, and these show that the radiations from the peak, and from the sides of the peak, are of similar quality. These absorption experiments are not very critical, because absorption coefficients are not very energy-dependent in this range.

It has been found by direct measurement that the slit system is pointing to within 1 mm of the target when giving the maximum reading.

DISCUSSION

The slit experiments show that the X-ray source in the betatron used for these measurements is about 1 cm diameter. The penumbra to be expected from a source with the intensity distribution shown in Fig. 3(*b*) has been calculated, and the result given agrees reasonably well with Fig. 1.

Published isodose curves for other betatrons[2, 3] show the same features at the beam edge as Fig. 1, so it seems that the efforts reported here are not unique to the betatron on which the present measurements were made.

In view of the discussion in the Introduction, these are surprising results. It is suggested that there are, in fact, two sources of radiation in a betatron: the target and the "donut" wall. Electrons scattered through small angles at the target, and so losing little energy, may reach that part of the "donut" wall adjacent to the collimator, where additional radiation is produced in the glass. There is as yet no experimental evidence to confirm this hypothesis.

APPENDIX

Resolving power of a finite sized ionization chamber

It is frequently necessary to make ionization chamber measurements where the intensity is varying rapidly over the region occupied by the chamber. This situation arises, for example, at the edge of an X-ray beam.

The effect of the finite size of the chamber on the measured distribution can be considered by taking a series of assumed distributions and calculating the results that would be expected for a chamber of known dimensions. If the intensity distribution is given by $I = f(x)$, and the outline of a right section of the chamber by $y = A(x)$, the response of the ionization chamber when centred at the position x is proportional to $\int_{x-a}^{x+a} f(x)A(x)dx$. It is assumed (1) that the chamber is of uniform cross-section, (2) that the intensity distribution is uniform along the length of the chamber, and (3) that the length of the chamber in the x-direction is $2a$.

This integral has been computed graphically in a number of cases, and two sets of results are shown in Fig. 4. The solid lines represent the assumed intensity distributions, and

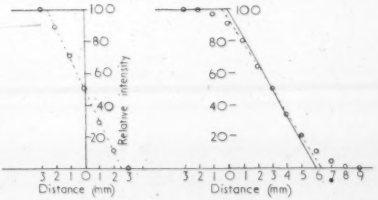

Fig. 4. Assumed and calculated intensity distributions. Solid lines show assumed intensity distribution. Points show the calculated results for a 6 mm diameter ionization chamber

the points are the computed readings for a 6 mm diameter chamber centred at the corresponding point on the x-axis. It can be seen that where the intensity drops precipitously to zero, the ionization chamber extends the calculated points over a distance equal to its own diameter. Where the intensity decreases uniformly to zero over 6 mm, the dotted straight line through the points diverges by less than half a millimetre from the solid line. The maximum deviation of the calculated points from the solid line occurs where the line breaks discontinuously. One would not expect such sharp discontinuities to occur in practice, so that this effect would be minimized.

If the intensity distribution across a beam edge is to be measured, the minimum width of the edge is the penumbra width, which is usually known. From the results given here, the maximum chamber width that is permissible to give accurate results is equal to this penumbra width. Conversely, if the measured beam edge extends over a distance greater

than the chamber width, it can be assumed that the chamber will correctly measure the shape of the beam edge.

REFERENCES

(1) MAJOR, D., PERRY, F. R., and PHILLIPS, K. *Proc. Instn Elect. Engrs* (A), **102**, p. 845 (1955).

(2) JOHNS, H. E., DARBY, E. K., HASLAM, R. N. H., KATZ, L., and HARRINGTON, E. L. *Amer. J. Roentgenol.*, **62**, p. 257 (1949).

(3) LAUGHLIN, J. S., BEATTIE, J. W., LINDSAY, J. E., and HARVEY, R. A. *Amer. J. Roentgenol.*, **65**, p. 787 (1951).

The preparation of electron microscope replicas from rough porous surfaces

By D. M. HALL, M.Sc., Dominion Physical Laboratory, Lower Hutt, New Zealand

[*Paper first received* 27 *December*, 1956, *and in final form* 19 *February*, 1957]

A two-step collodion-carbon replica process is described for obtaining replicas from rough porous surfaces such as fractured teeth. Specimens are soaked in water and allowed to dry slowly so that a water block immediately below the surface prevents the collodion penetrating too deeply into the pores and ensures that the replicas can be stripped. The use of an amyl acetate/water interface to float the carbon replica while the primary collodion replica is being dissolved results in less damage to the carbon film than other methods used.

During recent electron microscope studies of human teeth[1] it became essential to observe the fine structure of enamel and dentine with replicas which had to be removed from rough porous surfaces of fractured teeth.

Previous studies of dentine and enamel have been confined to the study of (*a*) replicas from polished and etched surfaces, (*b*) thin sections of demineralized teeth, and (*c*) replicas from fracture surfaces. The latter replicas were released, however, by digesting the underlying teeth, and the small supplies of good teeth to this Laboratory precluded such a method.

In the course of subsequent work it was found that collodion replicas could be stripped from a rough surface of a tooth provided the tooth immediately below the surface was in a moist state. The use of a thick collodion primary replica shadowed with uranium, and a secondary carbon replica preserved both the fine and the coarse detail.

PREPARATION OF REPLICAS

Most of the teeth used for the studies were premolars fixed in ethyl alcohol for a period of two days, but a number of teeth which had been fixed in 1% osmic-acid-veronal buffer were also used. A tooth chosen for preparation was allowed to soak in distilled water for several hours. On removal from the water a cool air blast was used briefly to remove the water from the surface of the tooth and the tooth was then held tightly in the jaws of a clean metal bench vice. The edge of a chisel was placed obliquely in the antero-posterior depression of a premolar and struck a sharp blow. The two surfaces of this fracture were immediately flooded with a solution of 1% collodion in amyl acetate and allowed to dry. This film was backed with a drop of thick gelatin solution and dried with an air current at room temperature. The collodion gelatin film was stripped with tweezers, cut with scissors to a suitable size for grids, placed on a glass slide with the collodion side up and, after shadowing with uranium oxide, a carbon film of approximately 100 Å thickness was deposited in the manner described by Bradley.[2] Some pieces of the composite film were placed gelatin side down on the surface of a beaker of warm water and, when the gelatin had dissolved completely, approximately 10 ml. of amyl acetate was added to the surface of the water with a pipette, taking care not to sink the carbon replicas below the surface of the water. The carbon replicas floating on the surface of the water were then covered to a depth of approximately 2 mm by amyl acetate. Since only 0·18 g of amyl acetate go into solution with 100 ml. of water at 20° C, the replicas are not disturbed due to mixing of the two liquids.

When the collodion was dissolved, the replicas were carefully scooped up in a glass bucket made from the bottom of a test tube, and placed in another beaker of water. This second step was necessary as it had been found impossible to remove the replicas on metal grids when they were held in the water-amyl acetate interface. A drop of Aerosol wetting agent solution was added to the water in the beaker to lower the surface tension and stop the replica from shattering when being removed. A grid held by a pair of tweezers was placed face down on a replica and moved slowly down through the water until in a vertical position, when it was slowly withdrawn.

The grid and replica were allowed to dry while still held by the tweezers, since any assistance in drying the grid, such as placing the grid on absorbent paper, tended to break up the thin carbon film. When the film was dry the grid was immersed in a container of amyl acetate for an hour to remove any traces of collodion. Upon removal the replica was ready for use in the electron microscope. A micrograph of a replica of a fracture surface of human dentine is shown in Fig. 1.

In the examination of general porous materials the process described above can be used if the material is saturated with water before it is fractured.

If an examination of a non-fractured surface is required, e.g. a surface prepared by polishing and etching, then the specimen is saturated with water and removed to a pad of damp cotton wool with the required surface uppermost. This surface is viewed through binocular microscope ($\times 20$ is useful) until the free water boundary has retracted to the

surface of the block (say ten minutes' time). The boundary is then allowed to retract a further small distance (say for two minutes) before the collodion is flooded on to the surface as in the process first described.

A micrograph of a replica from a fractured surface of a mullite crucible is shown in Fig. 2. The rough nature of the surface is evident but fine details of the mullite crystals can also be observed when a magnification of 15 000 or more is used.

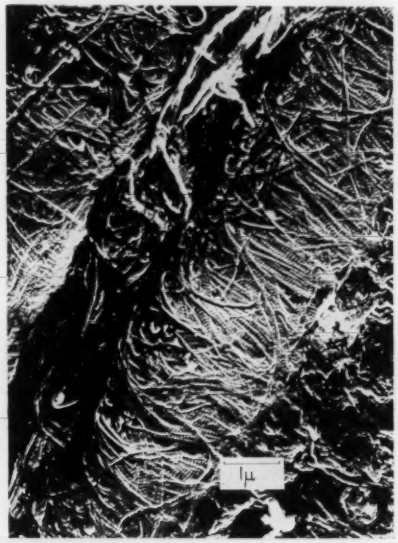

Fig. 1. Carbon replica of fractured dentine etched in HCl and tri-calcium phosphate at pH3 for two minutes. Shadowed at tan $^{-1}\frac{1}{2}$ with uranium oxide

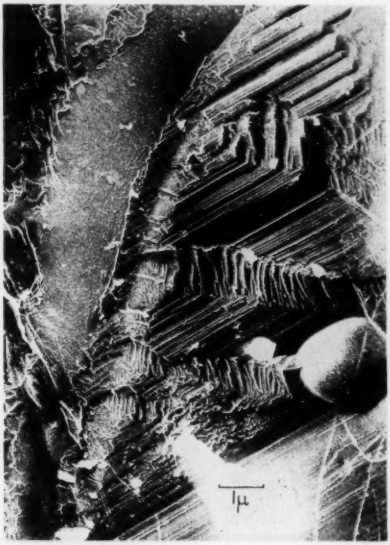

Fig. 2. Carbon replica of fracture surface of porous mullite crucible. Shadowed at tan $^{-1}\frac{1}{2}$ with uranium oxide

DISCUSSION

It was found that the important steps in the process were as follows.

(*a*) To keep the specimen moist until it is to be replicated. If a porous specimen becomes dry before the collodion is applied to the surface, the collodion is absorbed well into the pores and the film becomes firmly keyed to the surface and cannot be removed. Conversely, when the collodion is applied to the specimen before the water has been absorbed from the surface, such areas show lack of detail when replicated. This condition is avoided by observing the moisture disappear from the surface when viewed by a stereoscopic microscope.

(*b*) The gelatin used to back the collodion film must be dried at air temperature since dry heated air causes the gelatin to become fragile and also makes the removal of the collodion more difficult.

(*c*) The use of an interface of water and amyl acetate keeps the replicas flat while the collodion is dissolving and reduces the tendency of the replica to break into fragments.

The 1% collodion in amyl acetate which is used for the negative replica is applied in sufficient quantity to ensure that the collodion film, when dry, is many times thicker than the depth of relief.

The author has made several hundred successful replicas of teeth and has used the method occasionally for other rough porous surfaces.

REFERENCES

(1) Shroff, F. R., Williamson, K. I., Bertaud, W. S., and Hall, D. M. *Oral Surgery, Oral Medicine and Oral Pathology*, **9**, p. 432 (1956).

(2) Bradley, D. E. *Brit. J. Appl. Phys.*, **5**, p. 65 (1954).

The time-dependence of the recording properties of G5 nuclear emulsion

By W. C. Barron, B.Sc.,* The Physical Laboratories, University of Manchester, and
A. W. Wolfendale, B.Sc., Ph.D., A.Inst.P., Department of Physics, The Durham Colleges in the University of Durham

[*Paper received* 14 *March*, 1957]

The fading of fast proton and μ-meson tracks in G5 nuclear emulsion has been studied as a function of time and conditions of storage. The storage time for a 50% reduction in the blob density of the tracks is estimated to be 1040 $\pm$ 200 days for storage at 5° C and 520 $\pm$ 50 days at 25° C. No difference in fading has been found between the emulsions stored in air and those stored in commercial argon. The mechanism responsible for the fading appears to be the thermal ejection of electrons from the latent image.

The sensitivity of the emulsion after storage has also been studied. A reduction in blob density of the tracks of fast particles of less than 5% after a storage time of 450 days has been found.

1. Introduction

When nuclear emulsions are exposed for considerable periods of time the fading of tracks formed by particles passing through the emulsion during the early part of the exposure is likely. An upper limit to the duration of the exposure is therefore imposed above which confusion in the analysis of events and, in some cases, a loss of events, becomes important.

Various workers have studied the fading properties of the earlier types of nuclear emulsion, (e.g. Ilford C2), in detail, but information on the modern electron-sensitive emulsions such as Ilford *G*5 is scarce. This experiment was carried out partly in order to "monitor" the exposure of a large stack of stripped emulsions underground and partly to study fading for its own sake. The large stack of emulsion was exposed under what were thought to be the best conditions and a quantity of trial emulsion strips, which has been exposed to μ-mesons and a beam of protons soon after manufacture, were stored under these and other conditions. Periodic developments (using a standard technique designed to give reproducible results) of these trial strips served as a check on the fading of the emulsion and gave information on the increase of fading with time.

In order to study the mechanism of fading the trial strips were stored under two conditions of surrounding gas, atmospheric air and commercial argon, and at two temperatures, 5° C and 25° C. The variation with time of the blob densities of both proton and fast μ-meson tracks were studied so that any dependence of fading on particle mass as distinct from velocity could be determined.

A check on the variation with time of the sensitivity of the emulsion for recording proton tracks was afforded by exposing stored trial strips to the proton beam again, and comparing the blob densities of the "old" and "new" protons in the same strips.

2. Experimental Procedure

2.1. *The treatment of the emulsion prior to exposure*

140 cc of 400 μ, *G*5 nuclear emulsion were poured at the Holborn underground laboratory. Strips were cut having dimensions 10 $\times$ 5 cm and 5 $\times$ 5 cm. The strips were left for 3 days in air at 25° C and relative humidity 51% for the water content to reach equilibrium.

The larger strips were placed, in stacks of 5, in metal containers and the containers filled with commercial argon at near atmospheric pressure. The volume of argon was about 70 c.c. The remainder of the strips were placed, again in stacks of 5, in cardboard containers and the boxes sealed by immersion in paraffin wax. The smaller strips were thus surrounded by atmospheric air, the volume being about 10 c.c. The strips in each stack were tightly clamped between Perspex sheets so that only the edges of the strips were in contact with the surrounding gas.

2.2. *Exposure of the emulsion to the standard particles*

A beam of particles of the same inherent ionization was required so that, with a standard development technique, the developed strips would give constant grain densities for the standard particle tracks in strips having the same history. Protons and fast μ-mesons were used as standard particles. The protons were derived from the Birmingham synchrotron. These particles had kinetic energy 950 $\pm$ 50 MeV giving an ionization near plateau level on the low energy side of the minimum. The strips were inclined to the beam with the protons traversing the emulsions at a mean angle of 26° to the plane of the emulsion. The flux of protons over the central regions of the emulsions was $(8 \pm 2) \times 10^4$ particles/cm^2.

The μ-meson tracks were obtained by exposing the strips vertically to the cosmic ray flux at sea level for 9 days. Scattering measurements on straight μ-meson tracks were made at a later date and particles with momentum $\geq$ 2 GeV/c selected, i.e. μ-mesons at plateau ionization. Thus the emulsion strips contained protons and μ-mesons of nearly the same ionization, the differences in ionization being small compared with those due to fading and the statistical uncertainty of the ionization measurements.

2.3. *Storage of the emulsions underground*

The strips were stored horizontally in the Holborn underground laboratory, some in a refrigerator and some at room temperature. In order to reduce the background of slow electrons some strips were surrounded by 5 cm of lead. The storage area had been surveyed previously with a portable Geiger counter unit to ensure that the radioactive background was not excessive.

2.4. *The development technique*

The emulsion strips were developed in the laboratory at

* Now at A.E.R.E., Harwell, Berks.

Manchester after being carried horizontally from the underground laboratory. The emulsions were first mounted on prepared glass sheets and then developed using the "Temperature-Development" method of Dilworth and her co-workers.[1, 2] In this method the final grain density depends mainly on the temperature and duration of the hot stage. The temperature chosen for the hot stage was 18·6° C with a time duration of 90 min. In order that the blob density of any development with a different hot-stage temperature could be normalized, the variation of blob density with hot-stage temperature was determined in the region of 18·6° C. This variation was found to be 10% per °C. Of the developments, only one fell outside the range 18·4 to 18·6° C.

2.5. *The standard emulsions*

After exposure to protons and μ-mesons one set of emulsions was developed and the remainder returned to Holborn. This set constituted the standard with which the strips developed later were compared.

The lengths and angular distributions of the tracks were measured. Tracks were accepted as due to protons from the synchrotron if their lengths and angles were within two standard deviations of the mean values. It was estimated that the resultant contamination by "spurious" particles was negligible.

For tracks at near plateau ionization either grain or blob counting methods can be used to give the track density. Since the blob counting method is less subjective it was adopted in this analysis.

The mean blob density of the standard proton tracks was $20{\cdot}0 \pm 0{\cdot}1$ blobs per 100 μ track length in the central regions of the emulsions. The variation in blob density over the area, and through the depth of the emulsion was small. This variation is considered in detail in section 3.2 where it is compared with the variation of the faded emulsions.

The blob density of the tracks of μ-mesons with momentum >2 GeV/c was similarly measured and gave $19{\cdot}7 \pm 0{\cdot}2$ blobs per 100 μ track length.

The remaining emulsion strips, stored under different conditions, were brought to the laboratory above ground at periodic intervals and the emulsions were developed under similar conditions. The blob densities of the tracks of the protons and μ-mesons in the central regions of the emulsion strips were then measured.

3. THE EXPERIMENTAL RESULTS ON FADING

3.1. *The increase of fading with time*

The blob densities for protons and μ-mesons are plotted against the time between exposure and development in Figs. 1 and 2. Fig. 1 gives the variation for emulsions stored in air at the two temperatures: the corresponding variations for storage in argon are given in Fig. 2. The errors shown on the points are the standard deviations of the mean value found by averaging over the 5 strips in each container. Small corrections to the points have been made for the variation in hot-stage temperature; only one correction is important—that at 470 days for storage in air where the temperature was 1·0° C above the usual value and the blob densities have been reduced by 10%.

It is apparent from the figures that there is no significant difference in fading between the proton and fast μ-meson tracks. This result is as expected and need not be considered further.

In order to determine a characteristic "lifetime" of the emulsions for fading, e.g. the storage time required to give a 50% reduction in blob density, extrapolation of the experimental results to longer times is required. A numerical relation between the blob density and time is therefore necessary.

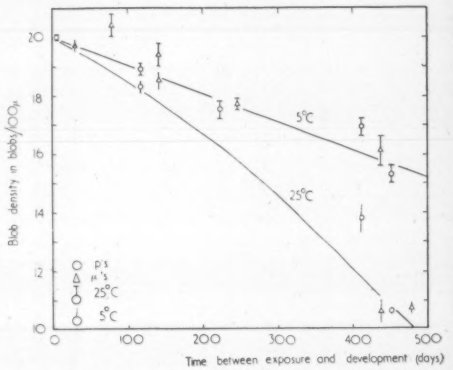

Fig. 1. The fading of emulsion strips stored in air

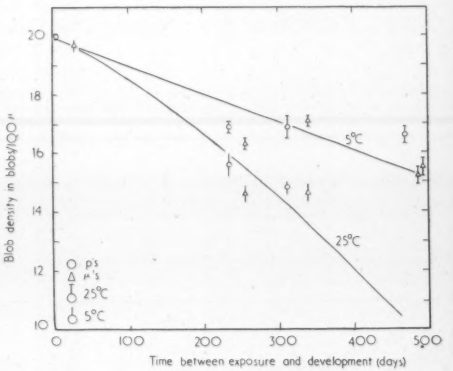

Fig. 2. The fading of emulsion strips stored in argon

If n_0 and n_t are respectively the blob densities of the standard tracks and tracks developed after storage for t days, then a relation of the form

$$n_t = n_0(1 - \alpha t^{\beta})$$

gives a rough fit to the experimental results. α and β are constants for a particular set of storage conditions.

Since there is no significant difference between the fading of μ-meson and proton tracks the two sets of points have been considered together. Similarly since no difference is observed between emulsions exposed in argon and air at the same temperature, the constants have been evaluated for the points grouped together at each temperature.

The storage times for a 50% reduction in blob density found in this way are

520 ± 50 days at 25° C and
1040 ± 200 days at 5° C.

The curves drawn using the empirical relation are also given in Figs. 1 and 2. It will be noticed that in a number of cases the difference between a point and the curve is several times the standard deviation of the point. The most likely reason for this is the lack of complete reproducibility of the development. The r.m.s. deviation from the curve is about 4%: this value is rather small considering the generally accepted difficulty in obtaining reproducible grain and blob densities.

3.2. *The variation of fading over the emulsion strips*

An important feature of the fading is its variation over the surface and through the depth of the emulsion. A study of these variations should give information on the mechanism of fading.

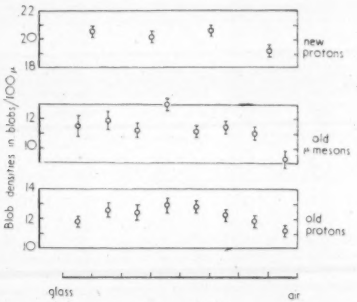

Fig. 3. The variation of blob density through the depth of the emulsion

Fig. 3 shows the variation through the depth of one of the most faded strips. This strip carries proton tracks of "age" 3 days as well as protons of "age" 452 days and μ-mesons of "age" 477 days. (A further consideration of strips of this type is given in section 4.) There is no significant difference between the unfaded and faded tracks as far as variation through the depth is concerned. The small variation shown is consistent with that expected from the development procedure.

The variation of blob density over the surface of the emulsion was also studied. No significant difference was found between the various regions.

4. THE EXPERIMENTAL RESULTS ON EMULSION SENSITIVITY

A number of containers were returned to the synchrotron after a period of storage underground and a further beam of protons passed through the emulsions. The second beam was inclined at a different angle of incidence in order to facilitate identification. The mean blob densities of the "new" protons were determined and these are given in Fig. 4. It is apparent that the variation of sensitivity is small, certainly less than 5% over a period of 500 days, and it is not inconsistent with zero. In view of the variation in blob density of about 4% resulting from the lack of complete reproducibility of development (see section 3.1) a more detailed analysis of the sensitivity variations is not profitable.

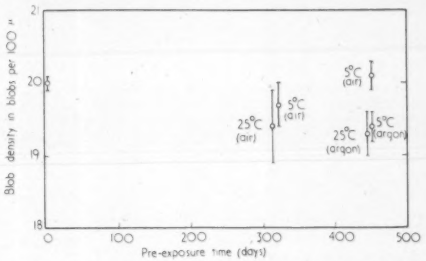

Fig. 4. The variation of emulsion sensitivity with time

5. DISCUSSION OF THE RESULTS

5.1. *The origin of the fading*

Comparison with the results of other workers is difficult since most of the earlier work was carried out on emulsions of lower stability—e.g. Ilford *C*2. The results of these experiments can be summarized as follows.

The fading of the latent image specks is due to two main causes

(*a*) chemical—a reaction between the silver of the specks and substances present in the emulsion, causing oxidation of the silver and consequent loss of silver ions from the latent image, and

(*b*) physical—a loss of electrons from the latent image to the conductance band by thermal excitation.

Many workers have shown that oxygen is an efficient agent in producing fading in the manner of (*a*) and Albouy and Faraggi[3, 4] have suggested that the reaction is

$$2\,Ag + O + H_2O \rightarrow 2\,Ag^+ + 2\,OH^-$$

The observed increase in fading with water content of the emulsion is also consistent with this reaction. These workers also found a variation in fading over the depth of the emulsion due, presumably, to the time taken for the diffusion of oxygen through the emulsion.

Mather[5] has stored non-electron-sensitive *NTB* and *C*2 emulsions under low pressures of air, in the region 0·1–10 mm of mercury, and has shown that the rate of fading is reduced by a factor of about 10 compared with emulsion stored at atmospheric pressure. Mather finds that the rate of fading in "vacuum" at 22° C for tracks due to slow protons, in *NTB* and *C*2 emulsion, is 0·08% per day.

The residual fading in Mather's experiments has been considered by Beiser[6] who considers that some, or all, may be due to loss by thermal excitation.

Leide[7] has recently studied the fading of slow proton tracks in *G*5 emulsion. The study was made over a much shorter time (2 months) than in this experiment, but the range of temperature was greater and the effect of varying the humidity was also investigated. The results are in general agreement. It is found that fading is constant in the interior

of the emulsion and increases rapidly with the temperature of storage.

Considering these results and those of the present investigation it seems likely that the main mechanism of fading in *G5* emulsion, stored under the conditions described in section 2, is that of thermal ejection. The following aspects of the results give rise to this conclusion.

(1) There is no significant difference between the fading of emulsions stored in air and the inert gas, argon.

(2) There is no significant variation in blob density over the area of the faded emulsions whereas diffusion of gas (through the edges of the emulsion) would cause a variation if mechanism (*a*) were important.

(3) The reduction in fading at the lower storage temperature is in qualitative agreement with a thermal mechanism.

(4) The rate of fading observed at 25° C, over the first 80 days, is $(0{\cdot}059 \pm 0{\cdot}015)\%$ per day. This value is rather smaller than that found by Mather, 0·08% per day, for the vacuum-stored emulsions at 22° C, and attributed to the thermal mechanism. A difference in this direction is expected since the *G5* emulsion has larger grains than *C2* and *NTB* emulsions and Albouy and Faraggi[8] have pointed out that the stability should increase with grain size.

6. CONCLUSIONS

From observations on emulsions stored underground for periods of time up to about 500 days it is concluded that the blob density of tracks at minimum ionization falls by 50% in 1040 ± 200 days at 5° C and 520 ± 50 days at 25° C.

The reduction in emulsion sensitivity over this period is less than 5% and therefore negligible in comparison with the effect of fading.

It is concluded that the fading of *G5* nuclear emulsion at temperatures in the region 5–25° C is probably due to the thermal ejection of electrons from the latent image.

ACKNOWLEDGEMENTS

The authors wish to thank Professor G. D. Rochester for his interest in the work and for many helpful discussions, and Professor S. Devons for his support during the latter stages of the work. We are greatly indebted to Professor P. B. Moon and the staff of the Birmingham synchrotron for making possible the machine exposures. We are indebted to Dr. A. M. Short, Mr. J. V. Major, Mr. A. J. Apostolakis and Mr. J. O. Clarke for helpful assistance throughout the period of the experiments.

REFERENCES

(1) DILWORTH, C. C., OCCHIALINI, G. P. S., and PAYNE, R. M. *Nature* [*London*], **162,** p. 102 (1948).

(2) DILWORTH, C. C., OCCHIALINI, G. P. S., and VERMAESEN, L. *Bulletin du Centre de physique Nucleaire de L'Universite Libre de Bruxelles.* No. 13*a* (Feb. 1950).

(3) ALBOUY, G., and FARAGGI, H. *J. Phys. Radium,* **10,** p. 105 (1949).

(4) ALBOUY, G., and FARAGGI, H. *C.R. Acad. Sci.* [*Paris*], **228,** p. 68 (1949).

(5) MATHER, K. B. *Phys. Rev.*, **76,** p. 486 (1949).

(6) BEISER, A. *Phys. Rev.*, **80,** p. 112 (1950); **81,** p. 153 (1951).

(7) LEIDE, G. *Ark. Fys. Bd.* **11,** p. 329 (1956).

(8) ALBOUY, G., and FARAGGI, H. *Fundamental Mechanisms of Photographic Sensitivity.* Ed. J. W. Mitchell, p. 290 (London: Butterworths Scientific Publications, 1951).

Correspondence

The electrical conductivity and permittivity of mixtures

In two articles published in this *Journal*, Pearce[1,2] presents interesting experimental data on the electric conductivity and permittivity of mixtures and discusses the validity of a number of theoretical formulae. In addition he proposes an "empirical" formula based on the results of his own and other experiments.

A theoretical discussion of the same problem was published by the writer[3,4] a few years ago. Some of the results of this work are briefly mentioned below in connexion with Pearce's conclusions. For a full discussion the reader is referred to the original papers.

From general principles it can be easily shown (see Burger[5] or de Vries[3,4]) that the permittivity of the mixture can be written as:

$$\epsilon_m = \frac{(1-p_1)\epsilon_2 + p_1 k_1 \epsilon_1}{1 - p_1 + p_1 k_1} \qquad (1)$$

where the notation of Pearce has been adopted (that is, ϵ_m equals permittivity of the mixture, ϵ_1 and ϵ_2 refer to the discontinuous and continuous phases respectively, and p_1 equals the fraction of the total volume occupied by the discontinuous phase). Here

$$k_1 = E_1/E_2 \qquad (2)$$

is the ratio of the average electrical field vectors in the discontinuous and continuous phases. Equation (1) is equivalent to Pearce's "empirical" expression; the empirical constant $v = 1 - k_1$ and its physical meaning follows from equation (2). It will be clear that k_1 depends on ϵ_2/ϵ_1, p_1 and the geometry of the system, i.e. the shape, size and orientation of the particles that form the discontinuous phase and their distribution in space.

Since a general analytical solution of the problem meets with great mathematical difficulties, even for particles of regular shape (e.g. ellipsoids) and with a simple distribution (e.g. random or in a regular lattice), simplifying assumptions have been introduced to calculate k_1. The writer has given a unified treatment of the formulae proposed by Maxwell, Burger, Eucken, Ollendorf, Bruggeman (extended to particles of ellipsoidal shape), Böttcher and Polder and van Santen and has shown how they differ in the assumptions underlying the calculation of k_1 or the similar quantity $K_1 = E_1/E = k_1/(1 - p_1 + p_1 k_1)$, where E is the overall average of the electrical field factor. In most of these theories a random distribution and orientation of the particles is explicitly or implicitly assumed and this case will be discussed in what follows.

The assumptions of Maxwell and Burger lead to a value of k_1 that is independent of p_1, and therefore to the same result as Pearce proposed in his empirical formula. The only difference lies in the fact that a certain value of k_1 depending on ϵ_1/ϵ_2 and the shape of the particles follows from the theory, whereas in the empirical formula v is chosen so as to obtain a best fit to the experimental data. The theory shows that k_1 depends strongly on ϵ_1/ϵ_2 as is also illustrated by Fig. 4 of Pearce.[2]

The writer has also shown that Bruggeman's theory contains an illogical element and that a correct analysis based on his assumptions leads to a formula with k_1 independent of x_1 and equal to the value in the theories of Maxwell and Burger.

Although all the proposed theoretical formulae are approximate, and, therefore, not of general validity, the question of their applicability is of great practical importance. Much confusion has arisen from the fact that they often have been tested against data on mixtures with particles of an unknown shape, which in some cases is accounted for by a suitable choice of an empirical form factor (see de Vries[3]). A comparison of the theoretical values with experimental data on mixtures with spherical particles has shown that in most cases the experimental values lie between the predictions of the formulae of Maxwell and Bruggeman. If ϵ_1/ϵ_2 differs from unity by less than a factor 10^2 the former gives the better results, whereas the latter is better for values of ϵ_1/ϵ_2 of order 10^3. The applicability of Böttcher's formula is restricted to cases where ϵ_1/ϵ_2 is close to unity or where p_1 is small. In these cases the differences between the various formulae are small anyhow.

C.S.I.R.O. Division of Plant Industry,
Deniliquin,
New South Wales,
Australia.

D. A. DE VRIES

[11 October, 1956]

I was not previously aware of the papers by de Vries and I thank him for drawing my attention to them. Ref. (3) is in Dutch, but I understand that all essential points are covered in Ref. (4) and in what follows I shall deal only with the latter.

The empirical factor v introduced in Ref. (2) is clearly envisaged as independent of p_1. De Vries does not think of k_1 in these terms since he explicitly refers to its dependence on p_1. Once the assumption is made that E_1/E_2 is independent of p_1, formula (1) can be readily derived from first principles. It therefore appears to me that de Vries' suggestion that it is equivalent to my "empirical" expression is somewhat misleading.

There may be advantages in regarding the relationship between the Maxwell and the empirical expression from the standpoint adopted by de Vries in his note but at the moment they escape me. The practical forms and effects of the two expressions are very different.

In his final paragraph de Vries quotes more or less from Ref. (4) the comparison between the predictions of the formulae of Maxwell and Bruggeman. In this reference the supporting experimental data is in three parts. The first relates to three sets of tests comprising about twenty results of electrical conductivity measurements on dispersions of droplets of one liquid in another with a higher conductivity. There is a good indication that for one set the experimental error is of the same order as the difference between predictions of the two formulae. Although inconclusive the results are on the whole better represented by the curves derived from the Bruggeman formula than by those deriving from Maxwell's expression. This is not altogether surprising since for the latter it was postulated that the spheres should be "at such distances from each other that their effect in disturbing the

course of the current may be taken as independent of each other,"[6] whilst for the majority of the results quoted the dispersed phase is from 10% to over 90% of the total volume.

In the same way the values of thermal conductivity of packed columns of equal spheres, which constitute the second part of the experimental evidence offered by de Vries, are for conditions outside the scope of the expressions being compared and are therefore irrelevant as a test of the validity of either.

The third piece of experimental evidence offered consists of three values of diffusion rate of columns of glass spheres which is equivalent to the electrical condition where $_2\epsilon_1 = 0$. From a small amount of experimental work of my own and an examination of other workers' results I am already inclined to think that Bruggeman's equation for spheres fails as $_2\epsilon_1 \to 0$ and I have in hand further work aimed at investigating the matter more fully.

If the method described in Ref. (5) is employed to compare Maxwell's equation with Bruggeman's it will be clear (see

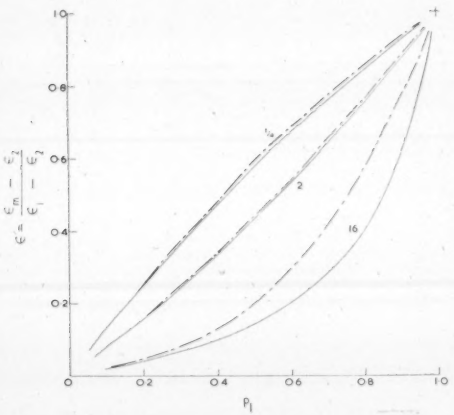

Curves of ϵ' against p_1 for three values of $2\epsilon_1$. The full curves were calculated from Maxwell's formula and those shown chain dotted from Bruggeman's expression for spheres. The numbers against the curves are the values of $_2\epsilon_1$ to which they relate

figure) that for values of $_2\epsilon_1$ not far removed from unity say $\frac{1}{4} < {}_2\epsilon_1 < 4$ differences are for practical purposes negligible. Important differences only appear outside this range and as is shown in Ref. (1) Bruggeman's expression is a good representation of experimental results when $_2\epsilon_1 \to \infty$. In my view the evidence offered by de Vries affords inadequate support for the conclusions he has drawn regarding the validities of the two formulae.

It is claimed that Bruggeman's theory contains an "illogical element," but logic is sometimes a matter of opinion and in this case its quality seems to be entirely dependent on whether a criterion proposed by de Vries is to be regarded as valid.

Mining Research Establishment, Isleworth, Middlesex.

C. A. R. PEARCE

[4 December, 1956]

REFERENCES

(1) PEARCE, C. A. R. *Brit. J. Appl. Phys.*, **6**, p. 113 (1955).
(2) PEARCE, C. A. R. *Brit. J. Appl. Phys.*, **6**, p. 358 (1955).
(3) DE VRIES, D. A. *Mededelingen Landbouwhogeschool Wageningen*, **52**, p. 1 (1952); also Thesis, University of Leiden, 1952.
(4) DE VRIES, D. A. *Annexe* 1952-1 *au Bulletin de l'Institut International du Froid*, p. 115 (1952).
(5) BURGER, H. C. *Phys. Z.*, **20**, p. 73 (1915).
(6) MAXWELL. *Treatise on Electricity and Magnetism*, 3rd ed. Vol. 1, p. 440 (London: Oxford University Press, 1892).

The depth of surface damage produced by lapping germanium monocrystals

Work on the preparation of germanium transistors by the alloy process has shown their performance to be dependent on the methods used for lapping and etching the wafers. Lapping produces, at the surface, a dense pattern of conchoidal fractures the dimensions of which are dependent on the size of the abrasive particles. Underlying the surface is a disturbed layer which has a very high dislocation density. The depth of damage has been estimated, from the variation of the effective diffusion distance L of minority carriers, as the disturbed layer is progressively removed by etching (with CP_4* at 20° C). L reaches an asymptotic value L_b when the whole of the layer is removed; L_b is dependent on the bulk lifetime of the germanium and the recombination velocity s of the surface. Using a modification of the Morton–Haynes travelling light spot method, the initial distance between the potential probe and the light spot is chosen to be large compared with L_b, and L is taken for our present purpose as the increase in the spot-to-probe distance required to reduce the floating potential of the probe by a factor of e.

The wafers were cut in the (111) plane from a monocrystal and lapped between mild steel plates (in a machine to be described elsewhere) using a suspension of emery abrasive in paraffin, to produce surfaces flat and parallel within $\pm 1\ \mu$

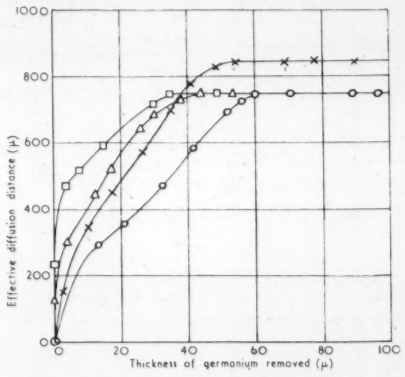

Fig. 1. Relationship between effective diffusion distance and thickness of germanium removed for abrasives with the following average particle diameters: □, ½ μ; Δ, 5 μ; ×, 15 μ; ○, 25 μ

over the whole wafer area. Material was removed during lapping at the average rate of 25 μ per hour at each surface. Fig. 1 shows the relationships between the distance L and thickness of germanium removed for abrasives having average particle diameters of $\frac{1}{2}$, 5, 15 and 25 μ. The average

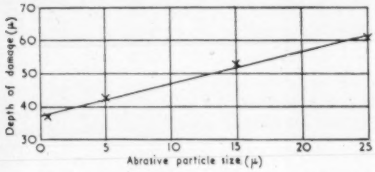

Fig. 2. Relationship between depth of damage and particle size

particle diameter was determined by microscopical examination. The thickness of the wafer was measured at each stage by a dial gauge having a ball point radius of 1·5 mm. Fig. 2 shows the relationship between depth of damage (estimated from Fig. 1) and particle size. It would appear that the total depth of damage is made up of an approximately constant portion of 35–40 μ (possibly corresponding to the layer of high dislocation density) and a portion (possibly corresponding to the conchoidal surface fractures) about equal in thickness to the abrasive particle diameter.

The depth of damage produced by 15 μ abrasive has also been estimated from a study of the etching rate of germanium, the etchant being CP_4 at 20° C. The rate is fast initially but stabilizes after about 50 μ of material has been removed. A microscopic examination of the surface at several stages of etching showed that the etch pattern observed at early stages disappears when the thicknesses of germanium given in Fig. 2 are removed, leaving the surface flat, apart from etch pits due to dislocations in the bulk material.

The above results suggest a much larger depth of damage than that inferred by T. M. Buck and F. S. McKim* from measurements of the photomagnetoelectric effect.

Acknowledgement is made to the Engineer-in-Chief of the General Post Office for permission to make use of the information contained in this paper.

Post Office Research Station,
Dollis Hill,
London, N.W.2.

D. Baker
H. Yemm

* Buck, T. M., and McKim, F. S. *J. Electrochem. Soc.*, **103**, p. 593 (1956).

New books

Mass spectrometer researches. By G. P. BARNARD. (London: H.M. Stationery Office, 1956.) Pp. iii + 62. Price 3*s*. 6*d*.

This booklet deals with hitherto unpublished aspects of work begun at the National Physical Laboratory in 1945 which, it was then hoped, would lead to the construction of a mass spectrometer capable of determining absolute values of isotope ratios. After describing an experimental sector mass spectrometer, built with greater mechanical precision than ever previously attempted, the author discusses the conventional type of electron bombardment ion source and describes some new source designs using trochoidal electron beams. Particular emphasis is given to factors controlling sensitivity resolving power and mass discrimination. Whilst the main objectives of the work were not realized this booklet gives an interesting account of the difficulties of making absolute measurements with an instrument where half understood secondary phenomena play such an important part.

J. BLEARS

The encyclopedia of chemistry. Editor in Chief: G. L. CLARKE. (New York: Reinhold Publishing Corp.; London: Chapman and Hall Ltd., 1957.) Pp. xiv + 1037. Price 156*s*.

It should be said at once that this is an interesting compilation. Destructive criticism of a dictionary or encyclopaedia is very easy as any specialist must feel dissatisfied with the articles in his field, and it is more reasonable to consider the purpose of the work and how far it is fulfilled. Unfortunately the Preface is no guide, and in speaking of "the multitude of chemists, physicists, engineers, biologists, research workers, teachers and students who comprise the scientific population of the world" as "those whom the book is intended to serve" it appears to make claims which are unduly wide. An encyclopaedia can be either a first guide to a new topic or a more or less popular account designed to answer the more obvious questions of the non-specialist reader.

In the complete absence of references and of indications for further reading beyond what is given in general terms in the article on "chemical literature," the first-named object can hardly be the aim; and if the second is intended, it would be observed that some of the articles are so condensed as to be difficult to follow. An example is "thermodynamics" which may be an excellent summary, but would convey little to the ordinary reader even if the cognate topics indicated (entropy, thermochemistry, stoichiometry, temperature scales) were also read. Another matter is that articles often leave the reader in the air; thus, under entropy, Boltzmann's constant is mentioned, in the index the other mention of this constant is apparently a misprint. In the biography of Boltzmann the constant is not mentioned, but his law is; however, the law does not appear in the index. Having said so much that is unfavourable, something must be added on its merits. It is well printed and well written and is very solid. It is not broken up with tables or formulae, or with the usual not very illuminating illustrations. The articles in their various degrees of compression are complete and seem very accurate. Biographies are included and are good, and here, as indeed throughout the work, the choice ranges over the world and is without any special bias to the American worker or the American publication. Pitfalls looked for had been avoided, thus in the biographies nearly all the birthplaces are given except Faraday's (so avoiding the question of the claim of Clapham [Yorks]). Information on U.S. research institutions is extensive, but other countries do not seem to be included. The Royal Institution is not in, but is mentioned under Faraday, Davy and Bragg. Crystallography, and indeed all associated sciences, are compressed to an extent that renders them hardly worth inclusion; there is no mention of the Barker Index. There are few misprints, the only one noticed that may not be obvious was "pliocarpine (Pliocarpus jaborandi)" on p. 41; it is not in the index under either spelling.

The book does, however, encourage browsing. It seems probable that if placed in a library various classes of readers would come to value it. Some of the articles have a novel approach which can be quite illuminating.

J. G. COCKBURN

Physical properties of solid materials. By C. ZWIKKER. (London: Pergamon Press Ltd., 1954.) Pp. viii + 300. Price 60*s*.

To provide a summary of the physics of solids in less than three hundred pages is an ambitious project; in doing this it is not clear what class of reader the author has in mind. The book covers a much wider field than that which is now called "solid state physics," namely the study of semi-conductors, electrons in metals and dislocations, including as it does sections on high polymers, properties of powders, friction and corrosion and classical elasticity. An experienced research worker looking through such a book will probably find something new to him, such as the use of radium to prevent the fouling of optical glass by fungi or the heat conductivity of moist brick. And perhaps a post-graduate student will find it profitable, as showing that there is more to solid state physics than the behaviour of germanium. But much of it seems to the present reviewer to be too scrappy to be of much use either to the beginner or to the expert. Three-and-a-half pages on rectifiers contain three quite sophisticated diagrams of energy levels at a Schottky barrier and one wonders if this section is any use. There is a proof of the Fermi–Dirac statistics; is this the place that anyone would look for it? And lack of space leads to some odd statements. For instance, "the electrical conductivity of metals and semiconductors is determined by the number of electrons in the conduction band and the number of holes in the full band and by the mean free paths of these electrons and holes, covered before they are trapped or stopped"—reminiscent rather of an examination candidate in a hurry than of a textbook. But none the less the book is stimulating as showing how many fields of knowledge could be brought within the orbit of the physics of solids.

N. F. MOTT

Peaceful uses of atomic energy. Vol. 14. General aspects of the use of radioactive isotopes: Dosimetry. (New York: United Nations; London: H.M. Stationery Office, 1956.) Pp. viii + 305. Price 45*s*.

The fourteenth volume of the Proceedings of the 1955 Geneva Conference commences with 13 papers summarizing the use of radioisotopes in the technology and industry of various countries at this time. Then follow 7 papers describing in some detail the production of various radioisotopes such as I. 131, C. 14, P. 32, S. 35, fission product Xe. 135 and other

fission product gamma sources, beta ray sources, La. 140, etc. Five papers then describe various aspects of handling and transport including a paper on radiation analytical facilities.

The second half of the volume, containing 27 papers, is concerned with dosimetry ranging from problems of kilocurie cobalt sources and radiation from reactors to very low level counting. Papers in this section include the design and development of a variety of counters employing physical methods, some on chemical and calorimetric techniques, applications of scintillation counting in medicine, special problems such as that of measurement of moisture content in soils by a neutron device. Special applications include the development of high resolution radiation detectors using both auto-radiographic techniques and a beta ray microscope while another paper describes the development of a series of precision radioactive airborne particle detectors.

R. F. JACKSON

Light-scattering in physical chemistry. By K. A. STACEY. (London: Butterworth's Scientific Publications, 1956.) Pp. viii + 230. Price 40*s*.

Measurement of light scattered by a cloud of particles suspended in a liquid enables, surprisingly, more to be deduced about their individual nature when they are invisible molecules than when their sizes are large enough to be accessible to ordinary microscopic examination. This is because small size and small difference in refractive index greatly simplify the theory of scattering. This book explains the ideas which have been obtained or confirmed about the molecules of high polymers, proteins and polyelectrolytes by measuring the intensity of light scattered at an angle to the incident beam, the transmission of light and the depolarization of the scattered light. Each of these groups of macromolecular substances has a separate chapter, with a hundred odd references at the end.

There are also chapters on the theory and the practice of light scattering. The latter shows the essential part played by the photomultiplier and deals with practical points in cell design, elimination of extraneous particles from the solution, the use of standard solid spheres of silica or high polymers and the measurement of refractive index. The chapter on the theory of light scattering is not up to the standard of the others. Symbols are used ambiguously, printing is inaccurate, and there is a lack of logical development in the arguments which suggests they are transcriptions of lecture notes rather than the independent analysis which the subject demands. The statements in the first chapter regarding the average molecular weights obtained by different methods require justification.

C. N. DAVIES

Changes of state. By H. N. V. TEMPERLEY. (London: Cleaver-Hume Press Ltd., 1956.) Pp. xi + 324. Price 50*s*.

The physics student is usually astonished when he learns about the unsatisfactory state of the theory of phase transitions and when he realizes that such apparently fundamental phenomena as freezing and melting at a definite temperature are still imperfectly understood. Considering the large volume of work being carried out at present on the properties of the solid state, it is rarely borne in mind that the study of transitions of higher order is hardly twenty-five years old. In these conditions, Dr. Temperley's book on changes of state provides an extremely useful survey of the whole field.

After a short historical introduction, the author sets out a classification of changes of state which is followed by a discussion of the more general theoretical aspects presented by the problem. The residual five-sixths of the book are devoted to a treatment of specific changes which are each discussed separately. The first of these is the transition between vapour and liquid and here the theoretical treatment is, of course, largely determined by the type of liquid model employed. The melting point is treated next and this is followed by a chapter headed "solutions" in which transitions in systems of more than one component are investigated, including order–disorder transitions in alloys. The last four chapters are devoted in turn to ferromagnetism (and anti-ferromagnetism), ferroelectricity, superconductivity and the lambda transition in liquid helium. It is here, in these more specific cases—where generalization has to give way to detailed information—that the reader will find the author's survey particularly helpful.

The author has defined his purpose in the preface when he says that it is his aim to help research workers to "find their way around" a fascinating but complicated field. This he has certainly achieved to a large degree and not in the least by his extensive reference to original publications and to books and summaries.

K. MENDELSSOHN

Defects in crystalline solids. Report of the Conference held in Bristol, July 1954. (London: The Physical Society, 1955.) Pp. 460. Price to non-members, 40*s*.

The study of defects in crystalline solids, in particular point defects and dislocations, has advanced rapidly in recent years, more particularly perhaps at first, through the investigation of their effects on mechanical and electrical properties. The significance of such defects in relation to other physical properties has, however, been increasingly studied and many new and powerful experimental methods for the investigation of the properties and behaviour of lattice defects have emerged. The conference here reported was primarily concerned with the role of defects in properties other than mechanical and electrical and with the advances in experimental methods. The report is necessarily a somewhat miscellaneous collection of papers and it is impossible in a brief review to do more than indicate broadly the main themes considered.

Among the experimental methods, emphasis naturally falls on magnetic resonance measurements to which some quarter of the forty-seven papers are devoted. Some of the latest results in the study of defects produced by irradiation are discussed and papers dealing with miscellaneous methods of investigation of defects through their role in precipitation processes, diffusion, etch pit formation and chemical reactivity are included. Some effects of defects on optical properties and on thermal conductivity in certain cases are reported. Structural features—types of dislocation source, dislocation networks, jogs, stacking faults and sub-structures—form the subject of a number of papers and work is reported on the role of defects in crystal growth.

The report naturally is not a comprehensive survey but it constitutes a valuable collection of representative papers.

R. KING

Notes and comments

Elections to The Institute of Physics

The following elections have been made by the Board of The Institute of Physics:

Fellows: A. W. Agar, G. W. Bloomfield, A. C. Copisarow, J. M. Cowley, R. G. W. Croney, J. C. Duckworth, R. D. B. Fraser, A. K. Head, L. E. Lawley, A. W. Pybus, R. M. Sillitto, R. Street, G. A. P. Wyllie.

Associates: J. Allen, D. E. T. Ashby, N. Brearley, L. J. Copley, I. R. Cowan, D. G. Davis, D. N. Davies, W. H. Davies, T. W. G. Dawson, G. A. Doran, A. V. S. de Reuck, D. I. Gaffee, L. F. Hawkes, D. E. Henshaw, V. M. Hickson, R. Hinkley, A. E. Jenkinson, N. Joel, N. K. Jones, A. Keller, L. Krause, J. Law, P. L. M. le Roux, B. Love, W. Mason, L. A. Massam, A. Moore, E. L. Murray, R. E. Newnham, A. F. Nicholson, P. N. Nikiforuk, F. B. Powell, D. D. Randall, E. B. Rodmell, R. L. Rutter, J. V. Sanders, J. Shaw, T. Shingler, E. E. Smith, A. K. Som, G. N. Thomas, L. Thomas, R. H. Whittle, L. H. Wells, A. Williamson, B. Zacharov.

Thirty-nine Graduates, forty-one Students and four Subscribers were also elected.

Conference on magnetism and magnetic materials

A conference on magnetism and magnetic materials will be held in Washington, D.C., on 18, 19 and 20 November, 1957, by the American Institute of Electrical Engineers in co-operation with the American Physical Society, the American Institute of Mining and Metallurgical Engineers, The Institute of Radio Engineers, and the U.S. Office of Naval Research. Authors should submit titles of proposed papers by 1 July and abstracts by 15 August. For further details write: L. R. Maxwell, U.S. Naval Ordnance Laboratory, White Oak, Silver Spring, Maryland, U.S.A.

Report of the International Commission on radiological units and measurements

The 1956 recommendations of the International Commission on radiological units and measurements have been published as the National Bureau of Standards Handbook 62. This report, which is divided into four chapters and contains 48 pages, covers the recommendations of the Commission as agreed upon at its meetings in Geneva in April 1956, and replaces its earlier report issued in 1953. The new report includes an extensive amount of basic information and data necessary to make radiation dose measurements in energy units (rads), and to convert data expressed in roentgens to the equivalent in energy units.

Chapter 1 contains a comprehensive discussion of radiological quantities, units, and symbols. In Chapter 2 guidance is provided for the clinical application of absorbed dose measurements. Chapter 3 presents a detailed treatment of the physical aspects of absorbed dose determination. Reports of the subcommittees are given in the final chapter. Chapter 4 also includes lists of the primary standards, X-ray standards, and radioactivity standards available in various countries and laboratories, as well as an extensive bibliography covering much of the subject-matter contained in the report.

Copies of this publication may be obtained from the Superintendent of Documents, U.S. Government Printing Office, Washington 25, D.C., price 40 cents.

Journal of Scientific Instruments

Contents of the July issue

SPECIAL ARTICLE

The Physical Society's Exhibition—London, 1957. By E. J. Harris.

ORIGINAL CONTRIBUTIONS

Papers

A low-frequency selective amplifier. By C. K. Battye.

Design and performance of a high-efficiency laboratory electro-magnet. By L. O. Bowen.

Magnet current stabilizer for an electron spin resonance spectrometer. By R. J. Abraham, D. W. Ovenall and D. H. Whiffen.

A method of stabilizing the specimen temperature for single crystal X-ray crystallography. By D. E. Henshaw.

The use of ferroelectric ceramics for vibration analysis. By R. C. Kell, G. A. Luck and L. A. Thomas.

The operation of a miniature camera by remote control. By D. E. Blackwell and D. W. Dewhirst.

A frequency modulated microwave spectrometer for electron resonance measurements. By A. C. Rose-Innes.

A compressometer for obtaining stress-strain curves of rock specimens up to fracture. By E. R. Leeman and C. Grobbelaar.

An automatic null method recording manometer. By H. R. B. Hack.

A thermostat using a resistance thermometer and a galvanometer–photocell amplifier. By P. M. Hu and R. W. Parsons.

Laboratory and workshop notes

An electromechanical timer. By W. Nisbet.

A controllable source of low-pressure hydrogen. By A. E. Barrington and F. T. Turner.

The location of events in nuclear emulsions. By J. H. Fremlin and Mrs. J. Mathieson.

A new capillary viscometer. By N. N. Greenwood and K. Wade.

An apparatus for growing single crystals of gallium arsenide. By J. L. Richards.

NOTES AND NEWS

Correspondence

A new type of ionization-pump. From G. Comsa and G. Musa.

Measurement of low deuterium concentration in water by means of float method. From B. Brigoli, E. Cerrai and M. Silvestri.

New instruments, materials and tools

New books

Notes and comments

THIS JOURNAL is produced monthly by The Institute of Physics, in London. It deals with all branches of applied physics (including theory and technique).

All rights reserved. Responsibility for the statements contained herein attaches only to the writers.

EDITORIAL MATTER. Communications concerning editorial matter should be addressed to the Editor, The Institute of Physics, 47 Belgrave Square, London, S.W.1. (*Telephone:* Sloane 9806.) Prospective authors are invited to prepare their scripts in accordance with the *Notes on the preparation of contributions*. (Price 2*s.* 6*d.* including postage.)

REPRODUCTION. The Institute of Physics is a signatory to The Royal Society's Fair Copying Declaration. Details may be obtained upon application from The Royal Society, London, W.1.

ADVERTISEMENTS. Communications concerning advertisements should be addressed to the agents, Messrs. Walter Judd Ltd., 47 Gresham Street, London, E.C.2. (*Telephone:* Monarch 7644.)

CLAIMS FOR MISSING JOURNALS. Claims from regular subscribers to this *Journal* for missing numbers will only be considered if received within 60 days of the date of mailing plus normal outward time of transit and time for lodging the claim. Losses attributable to failure to notify a change of address or to similar omissions will not be considered.

SUBSCRIPTION RATES. A new volume commences each January. The charge is £5 per volume ($14.25 U.S.A.), including index (post paid), payable in advance. Single parts, so far as available, may be purchased at 10*s.* each ($1.50 U.S.A.), post paid, cash with order. Orders should be sent to The Institute of Physics, 47 Belgrave Square, London, S.W.1, or to any bookseller.

Summarized proceedings of a conference on stress analysis—Cranfield, September 1956

The Tenth Annual Conference of the Stress Analysis Group of The Institute of Physics was held at the College of Aeronautics on 19, 20 and 21 September, 1956, in conjunction with the Royal Aeronautical Society. Papers were read which could be divided into four main subjects: kinetic heating, extensometry and instrumentation, jet efflux and crack propagation, and the proceedings are summarized in this report. A review of recent improvements in methods of experimental stress analysis in the U.S.A. and Canada was given by Mr. A. F. C. Brown.(1)

KINETIC HEATING

MR. K. L. C. LEGG and MR. G. STEVENS (Short Bros. and Harland Ltd., Belfast) read a paper on "Temperature distribution in aircraft structures and the influence of mechanical and physical material properties." Thermal effects in aircraft may arise from kinetic heating, engine installations and auxiliary systems. The first source is potentially of greater importance, although problems in connection with the second source can be severe, especially with vertical take-off aircraft of the "Flying bedstead" type.

The difficulty encountered in a formal analysis of heat conduction problems when practical boundary conditions are to be satisfied frequently suggests a finite difference approach. This may take the form of direct numerical integration or the use of digital or analogue computors or network analysers in which electrical circuits are arranged to be analogous to the thermal system. Several examples illustrating the use of these finite difference methods were given, such as the growth of temperature in a thick plate, the transient distribution of temperature in a rib carrying a hot duct; the chordwise distribution of temperature and transient loss in torsional stiffness in a thin wing due to kinetic heating, and the distribution of temperature and spanwise thermal stress due to kinetic heating in a bay of an integrally stiffened panel as shown in Fig. 1.

The importance of experimental methods was emphasized, and a brief description and illustration of a model fuel tank for simulated kinetic heating tests were given. An urgent plea was made for correlated data on thermal contact resistance of typical aircraft joints.

Data was given on some physical and mechanical properties of materials likely to be used for airframes where thermal effects are expected. These include thermal expansion,

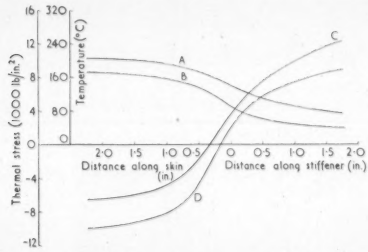

Fig. 1. Distribution of temperature and spanwise thermal stress in a 0·11 in. thick titanium skin with a central integral stiffener 0·2 in. wide, 2·0 in. deep. Pitch of stiffeners 6·5 in.

Curve *A*, temperature, $t = 135$ s; curve *B*, temperature, $t = 80$ s; curve *C*, maximum tensile thermal stress in stiffener, $t = 135$ s; curve *D*, maximum compressive stress in skin, $t = 80$ s.

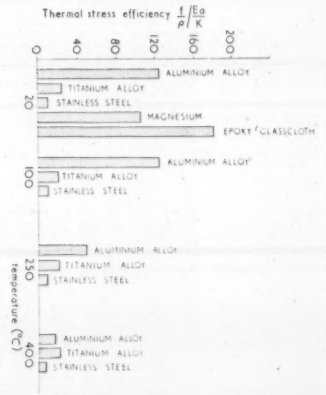

Fig. 2. Comparison of materials at different temperatures

conductivity, diffusivity, creep, fatigue, specific strength and stiffness. A parameter which the authors have chosen to call the "thermal stress efficiency" is shown in Fig. 2. This parameter

$$\frac{f}{\rho}\Big/\frac{E \cdot a}{K}$$

may be deduced from the boundary equation for a thermally thick solid subject to external heat transfer, namely,

$$-K\frac{\partial T}{\partial x} = h(T_A - T_S)$$

where f = ultimate tensile strength, ρ = density, E = Young's modulus, a = coefficient of expansion, K = thermal conductivity, h = heat transfer coefficient, T_A = atmospheric temperature, and T_S = solid temperature.

The thermal stress efficiency may be regarded as an indication of the ratio of the specific strength to the maximum thermal stress for any heating condition. From this the authors pointed out the versatility of aluminium alloys although they are penalized by loss of strength when subjected to elevated temperatures. Plastic materials promise to be useful at elevated temperatures but insufficient data are available.

MR. W. H. HORTON (Royal Aircraft Establishment, Farnborough) read a paper on "Experimental methods in kinetic heating tests." At any point on the surface of a body travelling at supersonic speed heat is provided according to the basic equation:

$$\partial Q/\partial t = q = hA(T_a - T_s)$$

where Q = quantity of heat, t = time, A = area heated, h = heat transfer coefficient, T_a = adiabatic wall temperature, and T_s = surface temperature.

The variation of h and T_a with time can be determined for any flight but T_s is a complex function of aerodynamics, heat flow and structural characteristics, which is not readily predictable. To carry out static and dynamic ground tests it is necessary to produce the thermal environment corresponding to the basic equation.

From the correct initial conditions of boundary temperature, the predetermined values of A, h and T_a and progressively measured values of T_s, an analogue computor determines the instantaneous values of $hA(T_a - T_s)$. This is compared with the value of q obtained by measurement of the radiant heat entering and leaving the surface. The difference between the calculated and the required q is fed into a servo-system which adjusts the power supply to the heat source so that the error is very small.

For Mach numbers up to five at ground level an infra-red heat source is used. This consists of $\frac{3}{8}$ in. diameter quartz tubes, 13 in. long, which have an output of 1 kW and a response time of $\frac{1}{4}$ s at 220 V and an output of 3 kW at 440 V. The best material for the reflectors is Alzac super purity aluminium (by Alluminate Co.) electro-polished and anodized. Surface coatings and temperature measurement were described. A novel thermocouple consisted of a $\frac{1}{8}$ m diameter nickel tube which contained two 0·0025 in. diameter chrome-aluminium thermocouple wires, insulated by magnesium oxide.

The intensity of radiation was measured with a specially designed wide range, rapid response, robust pyrometer. It consisted of a very thin, flat, circular disk of constanton placed in contact with an infinite thermal mass (a cooling fluid) at its edges. The temperature rise at the centre of the disk is proportional to the radiation which falls on it and is measured by the potential between a copper lead at the centre and a copper ring at the edge of the disk. The instrument has a response time of 0·02 s and can measure up to 100 kW/ft.^{2}

Recent developments in voltage regulation were discussed, a working test system was described and the possibilities and techniques of computors were outlined.

MR. J. A. G. HOLMES (Bristol Aircraft Ltd.) read a paper on the "Analysis of strain gauge results under transient temperature conditions." Because the strain gauge signal is affected by the gauge temperature, "temperature compensation" is usually obtained with a dummy gauge kept at the same temperature as the test station. This is impossible when the transient effects of kinetic heating are to be studied. Mounting a compensating gauge on the tested structure permits the measurement of uniaxial stresses only. When biaxial transient thermal stresses are to be measured, the dummy gauge is kept at a constant temperature and the gauge output due to the temperature change is determined in a calibration test.

Fig. 3 shows the temperature output of four gauges tested six times, expressed as percentage true strain reading. The curves show the envelope of all readings. The maximum scatter is equivalent to ± 2500 lb/in.^{2} in steel at 200° C. With this method accurate temperature measurement at the gauge station is important because an error of 1° C may represent up to 500 lb/in.^{2} in steel.

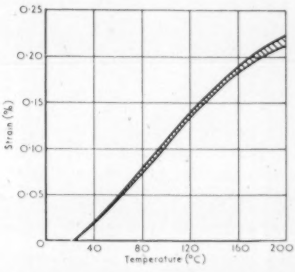

Fig. 3. Temperature variation of output of wire wound strain gauges on mild steel

If the total stress is to be divided into the parts due to loading and due to heating, separate tests must be carried out omitting one of the causes. The properties of the materials under transient temperature conditions must be obtained in order to convert measured strain to stress.

EXTENSOMETRY AND INSTRUMENTATION

MR. R. J. WILKINS (University College, London) read a paper on "Extensometry with particular reference to mechanical methods." These extensometers are dealt with in many publications and copies were available at the lecture of the two publications *Some strain gauges used in Building research*[2] and *Development of the measurement of strains in structures*.[3] The author was, therefore, able to devote more of his time to the history of extensometry and the discovery of Hooke's law which was illustrated by extracts from *The diary of Robert Hooke* (1672–1680).[4] The various slides shown were considered by the audience to have some general entertainment value.

The paper by DR. J. H. LAMBLE, MR. A. G. YOUNG and MR. E. S. DAHMOUCH (Faculty of Technology, University of Manchester), "Strain measurement by mechanical extensometers," described the Solex type extensometers. Gauge lengths from 60 to 2 mm had been tried. At the maximum magnification of 2×10^5, the range of the instrument is 4×10^{-5} in. For measurement of the lateral contraction of tensile specimens a Solex head was combined with a ball-ended micrometer anvil which facilitated adjustment and resetting of the "snap gauge." The extensometers are difficult to attach to some specimens but a thin coat of varnish helps to prevent slipping. A differential method of pneumatic amplification has been suggested by M. de Leiris[5] but not been tried by the authors.

The Johansson Mikrokator is a fragile extensometer of the

twisted strip type. The rotation of the pointer at the centre of the twisted strip is proportional to the change of tension of the strip which is caused by the movement of the knife edges in contact with the specimen. The contact pressure must be sufficient to prevent slipping and must be even on both knife edges. The sensitivity is 1×10^{-5} for a range of 0·0005 in. or 5×10^{-4} for a range of 0·002 in.

A satisfactory extensometer and strain gauge calibrator used by the authors was that designed by Prof. Wright Baker.[6] In this a rod is constrained to move axially in a slotted tube by diaphragms fastened to the ends of the rod and tube. An eighty threads per inch screw moves the rod relative to the tube. This movement is measured by the extensometer under calibration (attached to the tube and the rod) and by the gauging head of the high precision Talymin gauge (by Taylor, Taylor and Hobson Ltd.).

A paper by MR. J. PARKER and DR. S. S. GILL (Faculty of Technology, University of Manchester), "Some strain measuring techniques for experiments in plasticity," described the methods employed to obtain accurate, sensitive measurements of shear, longitudinal and hoop strain of a tubular specimen under combined torsion and internal pressure.

The shear strain was measured by viewing, through a telescope, lines reflected on to a curved scale 40 in. radius by two mirrors fixed on the specimen, 3 in. apart. The 40 in. scale measures more than 4% strain.

To measure the longitudinal strain, two circumferential grooves 0·0005 in. wide, 3 in. apart were turned in the specimen and viewed through two microscopes with micrometer eye-pieces. To avoid lateral movement, the microscope fine focusing slides were replaced by spring steel ligament hinges. This arrangement was calibrated with an etched glass reference scale and could measure 0·6% strain without resetting of the microscopes.

The hoop strain was measured by two pairs of Solex pneumatic gauging heads of the direct contact type, arranged to contact the specimen at 90° intervals. A dual reading Solex air controller gave direct readings of diameter changes. The gauge heads were calibrated with slip gauges. The range of this arrangement was 1% strain of a 1½ in. diameter tube but it could be readily reset because the heads were screwed into their mount. All strain measurements are sensitive to 1×10^{-5} in. and give consistent results.

MR. F. J. TRANTER (Aeronautical Inspection Directorate Laboratories, Harefield) read a paper, "The calibration of a highly sensitive extensometer." To meet the demand for an instrument of accuracy $\pm 1 \times 10^{-5}$ in. over the full range required for proof stress determination, a Lamb's extensometer of 2 in. gauge length was tested. Calibration with slip gauges and a twisted strip indicator mounted in a rigid frame showed that the extensometer, as purchased, gave low, inconsistent readings. New, accurately cylindrical rollers were made, the bearing surfaces were ground and lapped flat and the mirrors were adjusted to be parallel with the rollers. This resulted in consistent but incorrect readings.

The length and radius of curvature of the scale were found to be in error but correction for these increased the error of the instrument. Careful examination of the instrument showed that the spring which maintains the two flat plates in contact with the rollers also prevented the relative movement of the plates. The insertion of a ball-thrust bearing below the spring enabled the plates to move freely under their own weight. This modification allowed the Lamb extensometer to function correctly.

The modified instrument is accurate to $\pm 1 \times 10^{5}$ in. and has a sensitivity of 10^{-6} in. When used as a projection instrument the lamp must be removed far from the specimen to prevent local heating. A Lamb extensometer with a straight scale is considered to be less accurate than a dial gauge extensometer.

MR. V. M. HICKSON (Royal Aircraft Establishment, Farnborough) read a paper on "Strain distribution in notched and cracked sheets," describing a new method of measuring static elastic and plastic strains which is being developed. It is based on the general principle of taking displacement measurements of surface grids. The technique comprises:

(*a*) the polishing of the surface of the specimen and the production of a rectangular or equiangular system of guide lines and scratches in areas of interest. This marking process is performed with templates, scribers and rouge paper drawn across the measuring stations;

(*d*) the taking of replicas at successive loads. The principle used is to heat a small aluminium alloy platen (½ in. square) and to coat its surface with a hot melt composition (wax) of bitumen, carnauba and beeswax. It is then applied by means of a spring-loaded device to the measuring station, allowed to cool until thermal stress has dissipated, and is removed by impact on the short stem which is machined integral with the platen. A good replica of the scratches is thereby formed on the thin wax film. The replica scratch spacings are dimensionally accurate to a high degree;

(*c*) the comparison of two replicas from the same station, e.g. zero load and maximum load, in a special jig. The replicas are mounted on a block which runs on an accurate V-slide. A microscope fitted with a measuring eye-piece is focused on each replica in turn, and, after adjustment to pseudo-coincidence is made, relative displacements of corresponding scratches are measured. Using the present equipment, measurements of relative displacement to one micron can be made, representing an elastic stress of 1000 lb/in.^{2} on 0·4 in. gauge length or, for example, a measurement of plastic strain to 1% on 0·004 in. gauge length.

The replicas are designed to be self-compensating for ambient temperature, on the principle that a thin film of wax of low modulus must closely follow the thermal expansions and contractions of the aluminium base material of the platen, and this material has a coefficient of expansion very near to that of the specimen. Thus, within limits, the ambient temperature during replication will not affect the relative measurements of the two platens, provided that they are compared at the same temperature. It is important that the wax has suitable properties for the highest accuracy. These include having adhesion to the specimen within certain limits, and a long softening range rather than a sharp melting point.

The particular advantage of this system over conventional methods of measuring static strain is the extreme flexibility which permits the observer to measure surface strains over a very wide range, in any desired direction and over any gauge length shorter than the maximum dimension of the platen, smaller gauge lengths, of course, resulting in lower accuracy. The replicas appear to be reasonably permanent, permitting observations at long intervals of time. This "recording" facility has been demonstrated in an experiment to show the use of the technique in measuring manufacturing stress, it being considered practicable to take replicas before, during and after assembly of an aircraft structure, and also during its working life, subsequent comparison of replicas giving the required strains.

The development work is still in progress, attention being directed to designing measuring equipment which is more accurate and convenient to use, and to producing a replica material with a lower softening range.

MR. R. D. TRUMPER and MR. A. FAGG (Fairey Aviation Co., Hayes) presented a paper on "Temperature compensation of strain gauges." Variation of temperature causes a change of sensitivity and a false signal due to the change of resistance on heating. There is no change in sensitivity up to 100° C for Araldite, 125° C for Bakelite cement J11185, 200° C for Bakelite cement G11091 and it may be possible to use Silicone 810 cement with glass fibre base up to 500° C. The resistance of Nichrome strain gauges increases with temperature while that of Advance gauges decreases, but the false signal depends on the differential expansion of gauge wire and specimen as well as on the change of resistance of the wire. A change of state at 180° C of Bakelite cement cured at 130° C precludes its use above that temperature.

For slow changes of stress dummy gauges attached to light alloy structures caused errors of ± 300 lb/in.^{2} For transient temperatures up to 250° C the adhesion and volumetric stability of Bakelite were improved for use with self-compensating gauges. Linear resistance change - temperature graphs showed that satisfactory adhesion up to 240° C is obtained with Bakelite cement G11091 cured for two hours at

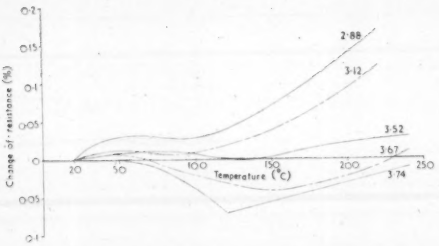

Fig. 4. Temperature sensitivity of self-compensated gauges on steel

Figures on curves refer to the resistance ratio of Advance/Nichrome gauges.

280° C. This increased curing makes the cement brittle and may cause gauge failure at 0·5% strain instead of the usual 2%. Self-compensation was obtained by winding appropriate quantities of Nichrome and Advance wires side by side on the same former. Fig. 4 shows that complete compensation is impossible because of the non-linear expansion and resistance - temperature characteristics of wires and specimens.

The gauge must be matched to the specimen material. The difference of $3{\cdot}3 \times 10^{-6}$ in the coefficients of expansion of spring steel and mild steel could cause an error of 5 t/in.^{2} at 150° C in spring steel if a gauge suitable for mild steel were used. A direct comparison with conventionally compensated Nichrome gauges for slow heating is given in Fig. 5. The self-compensated gauge, although not the best possible combination, is seen to be superior to the others. Under rapid heating, gauges on the outside of the structure will be hotter, those on the inside cooler than the structure. A test on a thin steel sheet under rapid radiant heating (20 to 190° C in 6 min) showed errors in the self-compensated gauge up to 26 t/in.^{2}, those in the differential gauge being much greater. It is suggested that gauges will have to be on the inner surface of the skin, be compensated as with the conventional type and in contact with a stabilizing thermal mass; the heat drop across the gauge would have to be allowed for.

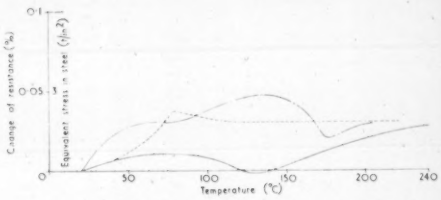

Fig. 5. Temperature drift of three compensated systems

T-connexion
differential connexion
self-compensated.

In the discussion MR. G. P. TONKIN (Bristol Aircraft Ltd.) said that he found that, for static work in wind tunnels above 200° C, all organic cements were unsuitable. Their plasticity was too great, although they became satisfactory again when the temperature was reduced. He found that ceramic cements were necessary.[7] Fig. 6 is a comparison of gauge-bar combination sensitivities for two organic and one inorganic (ceramic) cement, showing almost linear; presumably modulus caused increase for the latter and non-linear decrease for the former, due to slip. Further graphs showed a linear increase of sensitivity with temperature up to 230° C for Vida (by Jones and Stroud Ltd.) and 0·001 in.

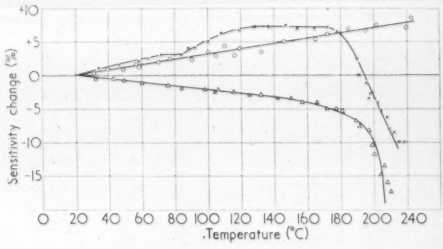

Fig. 6. Comparison of different gauges on uniformly loaded square mild steel bar

○ = Bristol Aircraft plated gauge pair
× = Baldwin AB7 bonded with Araldite 1
△ = Tillquist gauge pair.

Advance/Fortafix gauges. Results from vibration, extensometer, and static bending test to determine Young's modulus at different temperatures proved at least that there was no slip.

MR. J. ARROWSMITH (A. V. Roe and Co. Ltd., Manchester) read a paper on "Digital recording of test data." In aircraft engineering progress is often limited by the speed at which recordings of test measurements can be analysed. Recordings made during a test have to be calibrated, corrected for instrument errors and probably reduced to coefficient form.

Physical quantities are usually represented by analogy, such as a voltage level or the position of a needle on a dial. This method has culminated in the use of mirror galvanometer photographic trace recorders and auto-observers. These instruments are reliable but only suitable for up to about a score of simultaneous recordings.

In supersonic flight up to 200 quantities may have to be recorded continuously for sometimes up to one hour and subsequently arithmetical work may have to be performed on them. Recordings made by analogy involve:

(1) signal from transducer fed to airborne recorder;
(2) developing of film;
(3) measuring and tabulating of successive ordinates;
(4) arithmetic operations involved in correcting and calibrating;

a systematic conversion from analogy to digital form. Two operations could be eliminated if the pulses were recorded in digital notation on a medium suitable for input into a digital computer. Accuracy could be improved, arithmetic operations and the printing of numbers in decimal notation could be done automatically.

High-speed analogue to digital converters are necessary for recording in digital form. These devices sample varying voltages by finite steps and transform the instantaneous values into pulse notation. To be effective, the digitizer should be capable of dealing with approximately 1000 quantities per second, and to have a resolution better than 1%. This rate of operation would allow fifty transducers to be recorded twenty times per second or any combination which gives a product of 1000, and if binary code was used for the digitized outputs, they would require to be expressed in seven digits, giving a resolution of 1 in 127.

A flight recording system utilizing this technique is illustrated in Fig. 7. The signals from the transducers are sampled

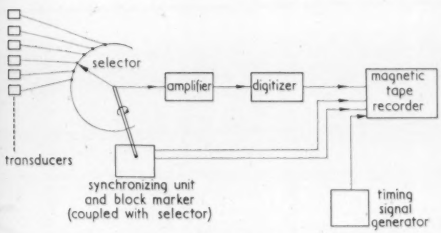

Fig. 7. Diagram of flight recording system

consecutively and passed through an amplifier to raise the potentials to a level of 10–30 V and applied to the digitizer. The principle of operation of the digitizer is that the ratio of the input voltage to a reference voltage is expressed in digital notation. For instance, if the reference was chosen as 30 V and this represents seven binary digits, that is 127 units, then any input voltage X would be expressed as 127 X/30 binary units. This system requires that the reference voltage is always greater than the input voltage. Magnitudes of the recordings must therefore be estimated. Too high a margin of safety causes a loss in accuracy of resolution. If the resolution is expressed in eight binary digits (1 in 255) or more the construction of the digitizer becomes more difficult.

The outputs of the digitizer are fed into a magnetic tape recorder. The digits may be recorded as square pulses in parallel blocks of seven across the tape, plus a synchronizing pulse track, a timing track and a block marker. Magnetic tape recorders are now commercially available and a typical recorder carries reels of tape 2400 ft in length on a 10½ in. diameter spool. It is possible to run the tape for this type of recording as slowly as 2 in./s. This is adequate for most purposes, but the tape spool can also be reloaded in flight.

One disadvantage of magnetic tape recording (in analogue or digital form) is that the recordings cannot be quickly observed, and insignificant information may therefore be processed. One method to overcome this difficulty is to pass the recording tape through a digital to analogue converter, producing a graphical output of the varying quantities plotted against time. The time periods over which the significant recordings occur can then be noted. When the magnetic tape containing the original digitized information is fed into the computer, the latter can be programmed to ignore information which is not contained within the required time periods. To do this, the timing track on the tape can give the time in either binary or binary coded decimal every second or so. A time unit would be required in the airborne system to generate a pulse code output for each successive time interval. The time would appear on the analogue record in the particular code used as a series of dots.

The computer must have a magnetic tape input unit, its computing speed should be fast and the equipment for output of data should operate at the computing speed. The following assessment has been made based on the performances of a typical modern single-address type of computer. Suppose that the operations to be performed on any one quantity are: (*a*) read in number; (*b*) multiply by a calibration factor; (*c*) add a correction term; (*d*) output the result.

Operations (*a*), (*b*) and (*c*) require four instructions: (1) read to store; (2) set multiplier; (3) multiply; (4) add.

This should take about 5 ms, and converting from binary to decimal form would take about 40 ms. Thus twenty-two numbers are processed per second. The printing equipment should be capable of dealing with, say thirty numbers per second, each of three decimal digits. A parallel printer is required because a standard serial operation teleprinter could only deal with four numbers per second at the most.

In this system of recording all manual operations such as trace reading, slide rule or desk calculator operations and tabulating are eliminated. Data is handled in digital form throughout all processing operations, and, in consequence, the original accuracy as recorded on the magnetic tape is maintained.

Digital information in addition to being recorded in the aeroplane, could also be telemetered to a ground station. The advantage is that pulse code modulation of a standard frequency modulated transmitter could be used instead of conventional analogue telemetery. The system could be so arranged that the presence of a pulse shifts the transmitter to one side of centre frequency, and the absence of a pulse shifts the transmitter to the opposite side of centre frequency. Once the data is in digital form it will maintain its accuracy throughout transmission. Slight losses in definition do not affect the magnitude of the quantity represented. The Morse code is a good example of this.

In the discussion MR. A. F. APPLETON (Bristol Aircraft Ltd.) raised the problem of the high "signal-to-noise" ratio which occurred in rotating switches when low voltages were transmitted.

MR. W. J. WALKER (Sir W. G. Armstrong Whitworth Aircraft Ltd., Baginton, nr. Coventry) read a paper "A novel design for a self-balancing and recording bridge," which described a system of bridge balancing which utilizes a binary combination of parallel resistors as the variable arm of the bridge. This can be recorded directly without any additional translating equipment. The principles of a closed loop servo-system are employed, but the servomechanism consists of a group of relays, which give a step-by-step mode of operation, free from hunting. The relay system also allows a very rapid method of balancing to be adopted, where any one of 2^n discrete values can be found in n steps. No approximation is involved in the balancing method and the range of accuracy is, therefore, extended beyond that possible with unpoled apex slide wire or parallel potentiometer methods of adjusting the variable.

The basic principles can be adapted to a number of problems, particularly in the analogue-to-digital conversion of current values. An example of digital conversion was given where the strain readings on a perforated tape are translated from binary to decimal values using analogue methods. A simple extension of the principles gives a rapid and economic means of initial zero balancing of strain gauges, where the individual apex potentiometers at each station can be replaced by a single group of ten fixed resistors.

The experience gained during two years use under difficult conditions has influenced the design of a second recorder. The speed of operation is expected to increase from one gauge reading per second to three with the same accuracy. The range of the bridge is $\pm 1{\cdot}6\%$, giving 1024 discrete levels in steps of $0{\cdot}003\%$. A general design method for any required range was given.

JET EFFLUX

A symposium was held which occuped most of the second day of the Conference. Papers were read by MR. M. O. W. WOLFE (Royal Aircraft Establishment, Farnborough), DR. R. FRANKLIN (University of Southampton), MR. D. J. MEAD (University of Southampton), MR. D. LAMBE (Vickers Aircraft Ltd., Weybridge), DR. B. L. CLARKSON (De Haviland Aircraft Co. Ltd., Hatfield) and MR. K. W. HETZEL (Vickers Armstrong (Aircraft) Ltd., Winchester). This symposium has been published in the *Journal of the Royal Aeronautical Society*.[8]

CRACK PROPAGATION

DR. A. A. WELLS (British Welding Research Association, Abingdon) read a paper entitled "Crack propagation." He described how cracking can be conveniently classified into the three stages of crack nucleation, stable growth and unstable growth, and stated that, for certain types of structure, prevention of unstable growth rather than prevention of crack nucleation could be adopted for design. This therefore focused attention on the criteria for instability in crack growth.

Two criteria of instability have been applied to the crack (length l) in a flat sheet under uniaxial tension σ. The first criterion gives the mean stress on the net area equal to the yield stress of the material. The second gives energy release from strain energy greater than or equal to surface energy, and hence the product $\sigma^2 l$ a constant value (this is the Griffiths criterion). The former criterion corresponds to a fully plastic, and the latter to a fully brittle material. In real materials the behaviour would be expected to be mixed; in high strength aluminium alloys, for example, local yield is observable at the crack roots. The effect of local yielding was shown to correspond theoretically to an imaginary increment in effective crack length so that $\sigma^2(l + \delta)$ should be a constant, where δ is a constant for a material depending on elastic modulus, surface energy and yield stress.

It was concluded that more rigorous solutions for the onset of unstable cracking are now required from plasticians, and that approaches of this type show promise of allowing structures to be economically designed which will tolerate, without sudden and complete failure, the existence of cracks until they are large enough to be found by inspection.

MR. C. R. FLETCHER (Bristol Aircraft Ltd.) read a paper entitled "The onset of fast crack propagation in aluminium alloy sheet materials," which was based on test work connected with evaluation of "fail safe" characteristics for aircraft structures. The need for "fail safe" design was considered only as an extension to the airframe structure of the philosophy already established for duplication of engines, controls, etc.

Results were described for many tension tests on flat sheet specimens initially slit centrally. An initial period of slow crack propagation was always found, clearly separated from the final period of rapid propagation; no changes were detectable on the fracture faces which were as in Fig. 8.

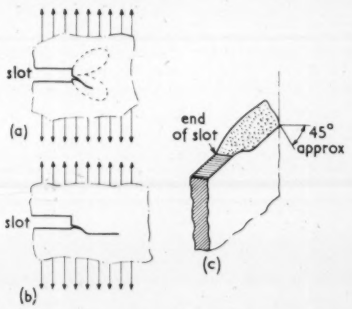

Fig. 8. (*a*) Initial period. Dotted lines show areas of surface distortion indicating high local strain. (*b*) Crack straightened out when fracture surfaces lie in the shear plane. (*c*) Sketch showing how fracture surface twists into the shear plane

The variation of σ with l was not found to give $\sigma^2 l$ a constant; the relation (at onset of slow and of fast cracking) for a typical test series is given in Fig. 9. Tests on D.T.D. 687, D.T.D. 710 and A.S.T.M. 2024-T3 showed similar results.

Results were not affected by fatigue instead of static loading, nor by sideways impacting to produce the crack if the plate was supported laterally. A crack from an unreinforced cut-out failed at the same stress as a slit of the same length as the cut-out plus crack length; the large area removed by the cut-out did not affect the failing stress. However, specimen size, shape and thickness all affected the $\sigma : l$ relationship considerably.

Designs of crack "stoppers" had also been examined on these specimens (on an equal weight basis). Cracking was unaffected until the crack end approached the "stoppers"

fairly closely. The relative efficiency of various types of "stopper" is shown in Fig. 10.

It was concluded that, although this empirical approach was providing much useful information, many problems still needed examination. In particular, the results cannot be directly applied to cylindrical pressure vessels because of effects of curvature on local stress distributions at the crack ends; the effects of cracks spreading from, instead of into, crack "stoppers" also needed consideration.

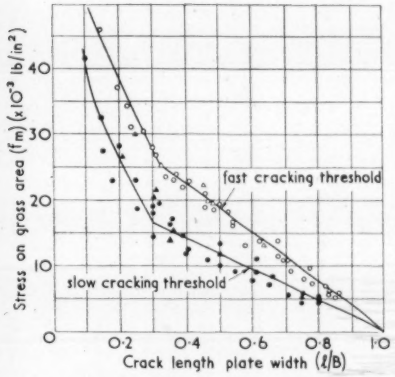

Fig. 9. Crack propagation in 20 in. long, 10 in. wide, 0·04 in. thick tensile specimens of D.T.D. 746

● and ○ = loading parallel to grain.
▲ and △ = loading normal to grain.

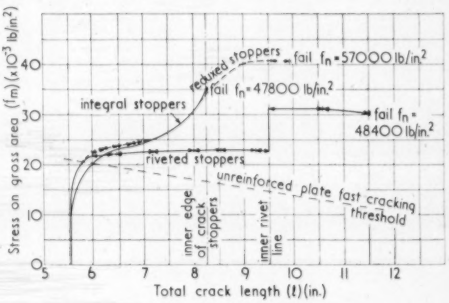

Fig. 10. Tests on 0·028 in. thick specimens of D.T.D. 746/D.T.D. 646 with crack stoppers. Ultimate strength of material is 62 000 lb/in.^{2}

⟷ indicates major jumps in crack propagation.

In the discussion, MR. J. R. DIXON (Bristol Aircraft Ltd., at University College, London) described a photoelastic investigation of tensile specimens containing a narrow slit with a small hole drilled at each end.

Stress distributions obtained showed the usual "butterfly wings," but at the sheet edge the direct stress was sometimes below 1·0 σ due to interaction between the slit and the free edge. Stress concentrations at the ends of the "cracks" were found to vary with "crack" length and with loading technique, as shown in Fig. 11. Results agreed well with the theoretical solution for an ellipse of major axis equal to "crack" length and having the same curvature at the "crack" end. Addition of longitudinal "crack stoppers" only modified stress distributions when the "crack" end was close to the "stopper," and of transverse "crack stoppers" only when they were very close to the "crack."

The effectiveness of drilling holes at the ends of cracks has been checked by COL. H. T. JESSOP (University College, London), and large stress concentrations were found which were reduced by increasing the hole size. Col. Jessop also remarked that stress distribution work had so far concentrated on the line of cracking, but that the typical "butterfly wing" effect represented plastic zones away from this line, and suggested that this could result in a shielding effect at the line. He considered that a surface coating photoelastic technique would be needed to investigate plastic effects in metallic specimens.

Then followed a paper called "The propagation of fatigue damage measured by periodic polishing" by MR. B. K. FOSTER and MR. T. F. ROYLANCE (University of Nottingham). In this a method of investigating the propagation of fatigue damage in a rotating bending specimen and its application to cumulative damage tests was described.

A specimen is run at a certain stress level for n_0 cycles. Material to a depth r_0 is removed from the surface of the specimen by polishing or grinding and polishing and it is then re-run for a further n_0 cycles, the load being adjusted so that the same stress amplitude is maintained. This procedure is repeated, always removing the same amount r_0 from the surface after running for n_0 cycles, until the total number of cycles $\Sigma n_0 = 2N$, where N is the life expected of a specimen run in the conventional manner without stopping periodically and polishing material away. From this point, the specimen is allowed to run on without stopping until failure. If this additional number of cycles is N, within the limits of the scatter band, it is assumed that the polishing operations have always completely removed all damaged material. If, on the other hand, the specimen fails before the additional number of cycles N or before reaching $\Sigma n_0 = 2N$ during the periodic polishing part of the test, then it is assumed that all the damaged material was not removed and that the fatigue process could continue unhindered. By making tests with various values of r_0 and n_0 the relationship

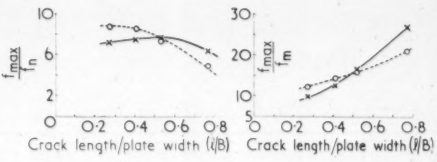

Fig. 11. Stress concentrations at the ends of 0·027 in. radius "cracks" in 8 in. long plates 4 in. wide

○ = load applied through clamped end plates.
× = load applied through four-point loading "tree."
f_m, mean stress on gross section.
f_n, mean stress on net section at "crack."

between the depth r, to which damage has propagated, and the number of cycles n, at a given stress, can be derived. Tests at various stresses enable a family of curves to be obtained showing the propagation of the damage front towards the centre of the specimen.

Such a family of curves for mild steel specimens, minimum diameter 0·3 in. and endurance limit ±18 t/in.^{2} is shown in Fig. 12. The curves for 20, 21 and 22 t/in.^{2} are experimental; the remainder are conjectural apart from the points on the fracture line. Straight lines have been drawn on the graph which is plotted in logarithmic co-ordinates, as a reasonable representation of the results so far obtained. Curves plotted from the results of tests on different materials and with different specimen shapes would not necessarily be linear.

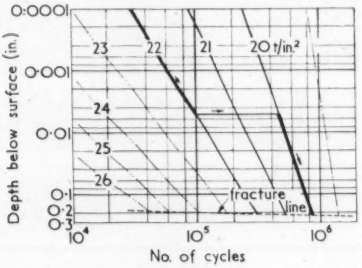

Fig. 12. Damage propagation curves for mild steel specimens

Chain dotted lines are conjectural.

In a cumulative damage test in which a specimen is loaded at one stress for a time and then loaded to failure at a second stress, the damage would propagate as indicated by the appropriate curve for the first stress as far as the number of cycles at which the stress is changed. It would then propagate according to the curve for the second stress, starting at the depth reached at the first stress but at an equivalent number of cycles. An example is shown in Fig. 12 by the heavy lines on the 22 and 20 t/in.^{2} curves.

Prediction of the cumulative damage ratio $\Sigma\frac{n}{N}$ for this case (10^5 cycles at 22 t/in.^{2}, remainder at 20 t/in.^{2}) using the damage curves, gives a value of $\Sigma\frac{n}{N}$ of 0·77, whereas the linear damage rule usually attributed to Miner[9] puts $\Sigma\frac{n}{N} = 1$.

Experiments under cumulative damage conditions have been made and the results were found to be in good agreement with predictions using the damage curves.

Thompson[10] has reported that the life of a specimen run under push-pull conditions could be extended apparently indefinitely by electrolytic polishing at intervals. Thus, although the work reported above concerns one particular specimen and one method of loading, it would seem that the principle could be applied to other types of specimen and other loading conditions.

ACKNOWLEDGEMENTS

Thanks are due to the authors, to Mr. I. L. G. Baillie, Miss M. E. Michael and Mr. J. C. Simmons for their assistance in the preparation of this report.

H. FESSLER

REFERENCES

(1) BROWN, A. F. C. *D.S.I.R., Overseas Technical Reports No.* 1 (London: H.M. Stationery Office, 1956.)

(2) *Some strain gauges used in building research.* Note No. A 33 (revised) (Watford, Herts.: Building Research Station, 1955).

(3) WILKINS, R. J. *Civil Engineering*, **51**, p. 537 (1956).

(4) *The diary of Robert Hooke* (1672–1680) (London: Taylor and Francis Ltd., 1935).

(5) DE LEIRIS, M. *Proc. 5th and 7th International Congress of Applied Mechanics*, 1938 and 1948.

(6) WRIGHT BAKER, H. *Bulletin of Mechanical Engineering Education*, 1952 (Manchester: College of Technology).

(7) TONKIN, G. P. *Bristol Aircraft Wind Tunnel Report* 266 (December 1955).

(8) *J. Roy. Aero. Soc.*, **61**, p. 103 (1957).

(9) MINER, M. A. *J. Appl. Mech.*, **12** (3), A, 159–164 (1945).

(10) THOMPSON, N. *Nature* [*London*], **175**, p. 980 (1955).

On the elementary theory of thermoelectric phenomena

By R. STRATTON, B.Sc., Ph.D., A.Inst.P., Metropolitan-Vickers Electrical Co. Ltd., Trafford Park, Manchester 17

The theory of thermoelectric phenomena is deduced from the general theory of conduction in a metal or semi-conductor. The calculation, which is well known, is discussed in great detail to bring out the significance of the various thermoelectric parameters. All the relations between the thermoelectric parameters are deduced from physical properties rather than by simply carrying out mathematical transformations. The sources of the heat and electromotive force developed are clearly indicated.

1. INTRODUCTION

The physical processes underlying thermoelectric phenomena are not always easily understandable when considered in terms of standard thermodynamic treatments. In an attempt to clarify these processes it was found better to start from the general theory of thermal and electrical conduction in metals and semi-conductors. Such an approach has, for example, been used by Seitz[1] and the following treatment amplifies this method and endeavours to bring out as clearly as possible the basic physical ideas.

For the sake of simplicity the discussion is restricted to conductors containing one type of charge carrier only moving in a single band of conducting levels. (Detailed results for the thermoelectric power of semi-conductors with both electrons and holes and with various scattering mechanisms have recently been reviewed by Johnson.[2])

Section 2 contains a discussion of the basic equations, from the general theory of conduction of an electron gas, which relate the electrical current and heat flow with the electrostatic field and temperature gradient. These are then used (Section 3) to calculate the variation of the Fermi level for (1) a single conductor, (2) a junction between two conductors, and (3) a thermocouple circuit. The thermoelectric e.m.f. (Seebeck e.m.f.) developed and the contact potential difference between two conductors for a non-uniform temperature distribution are also derived.

The reversible heat developed in the circuit is simply the Seebeck e.m.f. multiplied by the current and a detailed calculation is carried out in Section 4 which localizes the sources of this heat.

In Section 5 an analysis is also given for the energy flux which can be used to define the Peltier coefficient.

In the Appendix a recent paper by Laurela[3] is discussed. It is shown that the value of the thermoelectric power for a p–n junction is based on an erroneous definition. The correct value is given.

2. BASIC EQUATIONS

From the general theory of conduction of an electron gas, obeying Fermi–Dirac statistics, free, except for collisions with an associated mean free path l, it can be shown (cf. Seitz,[1] p. 178) that the electrical current density (I_x); thermal current density (C_x), i.e. the transport of kinetic energy and electrostatic field (E_x) are connected by the equations. (The equations are developed for electronic conductors with carriers of charge $-e$. To apply the results to p-type semi-conductors the sign in front of e must everywhere be reversed while Fermi energies are measured from the top of the valence band.)

$$E_x = +\frac{I_x}{\sigma} - \frac{1}{e}\frac{d\zeta}{dx} + \theta\frac{dT}{dx} \tag{1}$$

$$C_x = -\kappa\frac{dT}{dx} + I_x\left(T\theta - \frac{\zeta}{e}\right) \tag{2}$$

where

$$\sigma = -\frac{e^2}{3}K_1\sqrt{\frac{2}{m}} \tag{3}$$

$$\kappa = -\frac{1}{3}\left(\frac{K_3K_1 - K_2^2}{K_1T}\right)\sqrt{\frac{2}{m}} \tag{4}$$

$$\theta = \frac{1}{eT}\left(\zeta - \frac{K_2}{K_1}\right) \tag{5}$$

ζ is the Fermi energy measured from the conduction band edge, T is the temperature and

$$K_i = \frac{4\pi(2m^*)^{3/2}}{h^3}\int_0^\infty \varepsilon^i l\frac{\partial f_0}{\partial\varepsilon}d\varepsilon \tag{6}$$

(m^* is the effective mass, ε is the kinetic energy of the electrons and f_0 is the Fermi function).

The various integrals K_i can only be evaluated if the detailed scattering mechanism is specified so that the mean free path l is expressible as a function of ε. (As an example it will sometimes be assumed that scattering is caused by the thermal lattice vibrations when l may be shown to be a constant independent of ε for the case of semi-conductors.)

If the Fermi energy and temperature are constant, equation (1) reduces to $E_x = I_x/\sigma$, so that σ is the electrical conductivity; if only the temperature is constant the equation reduces to

$$E_x = \frac{I_x}{\sigma} - \frac{1}{e}\frac{d\zeta}{dx} \tag{1a}$$

The second term on the right-hand side gives rise to a diffusion current since the varying Fermi energy will be associated with a carrier density gradient. [However, this is only of importance (in the case of constant temperature) for potential barriers on semi-conductor contacts where there are rapid variations in carrier density.]

If the electrical current vanishes then equation (2) reduces to $C_x = -\kappa(dT/dx)$ so that κ is the thermal conductivity while equation (1) reduces to

$$E_x = -\frac{1}{e}\frac{d\zeta}{dx} + \theta\frac{dT}{dx} \tag{1b}$$

with θ as the absolute thermoelectric power.

The rate at which heat accumulates in a unit volume of the material is

$$\frac{dH}{dt} = I_x E_x - \frac{dC_x}{dx} \tag{7}$$

The first term in this equation is the electrical work done and corresponds to the change in potential energy of the carriers, while the second is the divergence of the heat current and is the rate at which heat (i.e. kinetic energy of the carrier) flows into the volume.

Substituting into equation (7) from equations (1) and (2)

$$\frac{dH}{dt} = \frac{I_x^2}{\sigma} - I_x\left(\frac{1}{e}\frac{d\zeta}{dx} - \theta\frac{dT}{dx}\right) + \\ + \frac{d}{dx}\left(\kappa\frac{dT}{dx}\right) - I_x\left[\frac{d}{dx}(T\theta) - \frac{1}{e}\frac{d\zeta}{dx}\right] \tag{8}$$

The first term in the first line is the Joule heat while the first term in the second line arises from the ordinary flow of heat. Both these terms are independent of the relative directions of the current and thermal gradient and are thus irreversible. The remaining terms, on the other hand, depend upon both the directions of the current and the thermal gradient. They are thus reversible and give rise to the thermoelectric effects.

The reversible terms in equation (8) may be simplified to

$$\frac{dH}{dt} = -I_x\frac{d\theta}{dx}\cdot T \tag{9}$$

However, we will sometimes use the separation of this quantity into potential (first line) and kinetic energy (second line) contributions as shown in equation (8).

Finally, the total energy transported or energy flux C_T will also be discussed. This is given by

$$C_T = C_x + I_x V(x) \tag{10}$$

where $V(x)$ is the electrostatic potential ($E = -dV/dx$). C_T satisfies the conservation equation

$$-dC_T/dx = dH/dt \tag{11}$$

which can be derived from equation (7).

The reversible part of C_T may be written, using equation (2), as

$$C_T = I_x[\theta T - (\zeta/e) + V(x)] \tag{12}$$

involving an arbitrary constant depending on the zero of potential energy adopted.

Substituting for θ from equation (5) gives

$$C_T = -(I_x/e)[(K_2/K_1) - eV(x)] \tag{12a}$$

From this it can be seen that the average kinetic energy transported per electron is (K_2/K_1) since $-I_x/e$ is the total number of electrons flowing in the x direction per unit area and unit time. The value of this energy depends on the mean free path but in general it will be of the same order of magnitude as the average kinetic energy of the electron gas in thermal equilibrium as may be seen from equation (6).

3. VARIATION OF THE FERMI LEVEL (SEEBECK E.M.F.)

(Relation between absolute thermoelectric power and Fermi level)

3.1 *Single conductor.* Equation (1*b*) for the electric field with zero electrical current will now be considered in more detail. Integrating between two points X_a and X_b of the conductor gives

$$-eV_{ab} = +\int_a^b eE_x dx = +(\zeta_a - \zeta_b) + e\int_a^b \theta dT \tag{13}$$

This equation is illustrated in Fig. 1 for the case of a metal (positive Fermi energy). It brings out the important point that the change in the Fermi level is

$$f(T_a, T_b) = e\int_a^b \theta dT \tag{14}$$

and it is this quantity which produces the thermal e.m.f. The Fermi level may be defined as the energy at which the

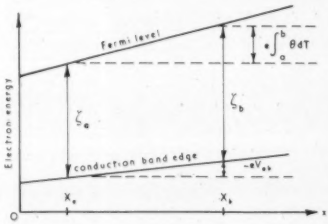

Fig. 1. Energy diagram for a metal with a temperature gradient

Fermi function or occupation probability is one half. It is measured from an energy zero which is arbitrary but constant throughout the system. (If the temperature is constant, then $-eV_{ab} = \zeta_a - \zeta_b$ and the Fermi level is constant while the Fermi energy will vary if the electrostatic potential does, e.g. at the surface of a semi-conductor.)

Equation (14) can also be written as

$$\frac{1}{e}\frac{df(T_0, T)}{dT} = \theta \tag{14a}$$

where T_0 is some fixed temperature *so that the absolute thermoelectric power is equal to the rate of change of Fermi level with temperature* divided by e. (N.B. This is not the same thing as the rate of change of Fermi energy since the origin of this quantity also changes with T.)

3.2 *Contact potential difference—Seebeck e.m.f.* Consider the contact between two dissimilar conductors at a uniform temperature T. Since the Fermi level in the two metals is the same in thermal equilibrium there is a contact potential difference (C.P.D.) (cf. Fig. 2).

$$V_{ab} = \text{C.P.D.} = \frac{1}{e}(\chi_a - \chi_b) \tag{15}$$

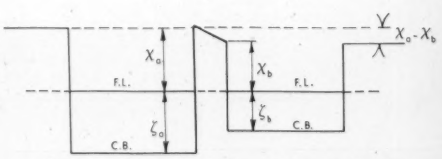

Fig. 2. The contact between two dissimilar metals (F.L., Fermi level; C.B., conduction band)

where χ_a and χ_b are the work functions of the conductors. This C.P.D. is the change in *potential* energy when an electron is taken from just outside conductor a to just outside conductor b.

We now assume that the temperature across the contact is non-uniform and consider the potential difference between points X_a and X_b in the two conductors respectively (Fig. 3). Taking the contact region as infinitesimally thin, the Fermi level will be constant across it while the potential energy

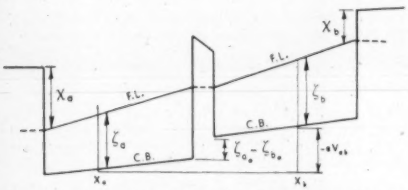

Fig. 3. The contact between two dissimilar metals with a temperature gradient

changes by $(\zeta_{a0} - \zeta_{b0})$ just as in the case of uniform temperature treated above. (The Fermi levels are evaluated near the contact region for both conductors.)

Using equation (1*b*) for zero current gives

$$-eV_{ab} = (\zeta_a - \zeta_b) + e\int_{T_a}^{T_0} \theta_a dT + e\int_{T_0}^{T_b} \theta_b dT \qquad (16)$$

(N.B. At constant temperature this reduces to

$$-eV_{ab} = \zeta_{a0} - \zeta_{b0}$$

i.e. the change in Fermi energy across the junction.)

Equation (16) can be simplified for the particular case

where $T_b = T_a = T - eV_{ab} = \zeta_a - \zeta_b - eF_{ab}[T, T_0]$ (17)

where $$F_{ab}[T, T_0] = \int_T^{T_0} (\theta_b - \theta_a) dT \qquad (17a)$$

and is the Seebeck e.m.f. This quantity will be discussed later in connexion with a closed loop, but for the moment it should be noticed that it has been defined so as to equal minus the rise in the Fermi level divided by e. (The difference $\theta_b - \theta_a$ is known as the thermoelectric power of the junction.)

If the two points are taken to be just outside the conductors then $(+V_{ab})$ is the contact potential difference. The Fermi energies are now $-\chi_a$ and $-\chi_b$ respectively since they are always measured from the bottom of the conduction band which is the electrostatic potential of space outside the metals. Thus

$$\text{C.P.D.} = \frac{1}{e}(\chi_a - \chi_b) - \int_{T_a}^{T_0} \theta_a dT - \int_{T_0}^{T_b} \theta_b dT \qquad (18)$$

or if $$T_a = T_b = T$$

$$\text{C.P.D.} = \frac{1}{e}(\chi_a - \chi_b) + F_{ab}(T, T_0) \qquad (18a)$$

Thus when a temperature gradient is established between two dissimilar conductors the C.P.D. is altered because the work functions depend on the temperature (especially for semi-conductors) and there is an additional term equal to the Seebeck e.m.f.

3.3 *The thermocouple loop.* Consider now a loop of two dissimilar conductors a and b with a break XY in conductor b. The temperature is taken as non-uniform and in particular the two junctions are at temperatures T and T_0 respectively. The loop is illustrated in Fig. 4(*a*) while Fig. 4(*b*) is the corresponding energy diagram. From the previous analysis

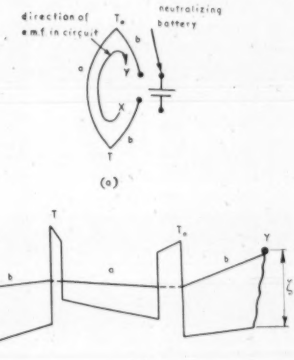

Fig. 4. (*a*) Open thermocouple. (*b*) Energy level diagram for open thermocouple

it is clear that the Fermi level rise in going from X to Y is [using equation (16)]

$$f_{XY} = -e\int_{T_X}^{T} \theta_b dT + e\int_{T}^{T_0} \theta_a dT - e\int_{T_0}^{T_Y} \theta_b dT$$

so that if $T_X = T_Y = T$

$$f_{XY} = -eF_{ab}(T, T_0)$$

i.e. *independent* of the position of the break XY.

If a battery with an e.m.f. equal to $F_{ab}(T, T_0)$ is now connected between X and Y so that its e.m.f. acts from X to Y it will exactly compensate for the rise in Fermi level and produce a steady system with no current flowing as was originally assumed for the calculation of the Seeback e.m.f. Thus the broken circuit can itself be considered as a battery with an e.m.f. of $F_{ab}(T, T_0)$ acting from Y to X. This may be considered to be the definition of the Seebeck e.m.f.

If the circuit is closed, the Fermi levels at X and Y must be brought together. This can only be done if a current is allowed to flow which exactly counterbalances the rise in Fermi level. Thus integrating equation (1) right round the circuit gives

$$\oint E_x dx + I_x \oint \frac{dx}{\sigma} - F_{ab}(T, T_0) = 0$$

The line integral over E_x vanishes since it measures the change in potential energy in going once round the circuit which is zero because the Fermi level is continuous as has been stated. [This should not be confused with the usual calculation of the Seebeck e.m.f. from the line integral over E_x (cf. Seitz,[1] p. 180) which really refers to an open circuit

with zero current as outlined in the first part of this section.] Thus

$$I_x R = F_{ab}(T, T_0) \tag{19}$$

where R is the total resistance of the loop

$$R = \oint \frac{dx}{\sigma} \tag{20}$$

The sign convention is such that I_x flows from the junction of temperature T to that at T_0 through conductor a (Fig. 5).

Fig. 5. Closed thermocouple

Suppose, for example, that T is the cold and T_0 the hot junction. $(T_0 > T)$ then $F_{ab}(T, T_0)$ is positive if $\theta_b > \theta_a$. Thus the current flows from the material with the greater thermoelectric power to that with the lower across the cold junction. Here it is important to take the algebraic value of θ since it is negative for metals and n-type semi-conductors and positive for p-type semi-conductors.

Consider a metal n-type semi-conductor contact (N.S.C.). In general $|\theta(M)| < |\theta\,(\text{N.S.C.})|$so that $\theta(M) > \theta\,(\text{N.S.C.})$. Thus current flows from the metal to the n-type semi-conductor across the cold junction. The opposite case arises for a metal-p-type semi-conductor contact (Fig. 6).

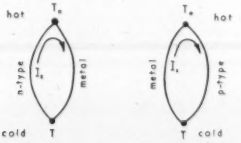

Fig. 6. Contact between a metal and a semi-conductor

From the Seebeck e.m.f. both the total heat produced and the energy flux could be directly evaluated. A better insight into the underlying physical principles can, however, be obtained by analysing these quantities from their fundamental definitions [equations (9) and (12)] and then pointing out the relation to the Seebeck e.m.f. This is done in the next sections.

4. HEATING

When a current I_x passes round a closed thermocouple circuit the heat developed may be calculated by summing the expression dH/dt around the circuit. Thus restricting the discussion to the reversible portion of dH/dt, the total heat developed is [equation (9)]

$$\frac{dH_T}{dt} = \oint \frac{dH}{dt} \cdot dx \doteq -\, I_x \oint \frac{d\theta}{dx} \cdot T \cdot dx \tag{21}$$

This integral will now be separated into four parts. Let X_{a0} and X_{b0} be two points of the conductors a and b respectively sufficiently close to the hot (T_0) junction for the temperature at the points to be still T_0. Similarly, choose points X_a and X_b near the cold (T) junction. Then

$$\frac{dH_T}{dT} = -\, I_x \left(\int_{X_a}^{X_{a0}} \frac{d\theta}{dx} \cdot T \cdot dx + \int_{X_{a0}}^{X_{b0}} \frac{d\theta}{dx} T dx + \right.$$
$$\left. + \int_{X_{b0}}^{X_b} \frac{d\theta}{dx} \cdot T \cdot dx + \int_{X_b}^{X_a} \frac{d\theta}{dx} T dx \right) \tag{21a}$$

The two integrals across the junction will be considered first. They may be simplified to

$$-\, I_x T_0 \int_{X_{a0}}^{X_{b0}} \frac{d\theta}{dx} dx = -\, I_x T_0 (\theta_{b0} - \theta_{a0}) \equiv -\, I_x \pi_{ab}(T_0)$$

$$-\, I_x T \int_{X_b}^{X_a} \frac{d\theta}{dx} dx = -\, I_x T (\theta_a - \theta_b) \equiv -\, I_x \pi_{ba}(T)$$

Here we have introduced the Peltier coefficient $\pi(T)$ which is defined as

$$\pi_{ab}(T_0) \equiv -\frac{1}{I_x} \int_{X_{a0}}^{X_{b0}} \frac{dH}{dt} \cdot dx = T_0(\theta_{b0} - \theta_{a0}) \tag{22}$$

and has the dimensions of a voltage.

From equation (22) it can be seen that heat is evolved at the cold junction and absorbed at the hot junction. For if $\theta_b > \theta_a$, $F_{ab}(T, T_0)$ is positive and, therefore, I_x will be positive and $\pi_{ab}(T_0)$ is positive while $\pi_{ba}(T)$ is negative. Thus dH/dt is positive at the cold junction and negative at the hot junction. If $\theta_b < \theta_a$, the signs of $F_{ab}(T, T_0)$, I_x, $\pi_{ab}(T_0)$, $\pi_{ba}(T)$ are all reversed and the same conclusion holds.

Referring to equation (8) it will be seen that the Peltier coefficient can be written as

$$\pi_{ab}(T) = \frac{1}{e}[\zeta_b - \zeta_a] - \frac{1}{e}[(\zeta_b - \zeta_a) - eT(\theta_b - \theta_a)]$$

where the first term in square brackets comes from the potential energy $(I_x E_x)$ and the second from the kinetic energy $(\partial C_x/\partial x)$ contributions to (dH/dT). Using the definition of θ, equation (5), this reduces to

$$\pi_{ab}(T) = \frac{1}{e}(\zeta_b - \zeta_a) - \frac{1}{e}\left[\left(\frac{K_2}{K_1}\right)_b - \left(\frac{K_2}{K_1}\right)_a \right] \tag{23}$$

This result may be easily interpreted. The quantity $(\zeta_a - \zeta_b)$ is the increase in potential energy when an electron crosses the junction from a to b (cf. Figs. 2 and 3). Also it has already been pointed out [cf. remarks following equation (12a)] that (K_2/K_1) is the average kinetic energy transported per electron.

Consider, for example, the contact between two covalent non-degenerate n-type semi-conductors and assume lattice scattering then

$$K_2/K_1 = 2\,kT\,(\text{covalent}) \tag{24}$$

and the kinetic energy term disappears. (It will always be at most of the order (kT) for any other type of scattering provided the semi-conductor is non-degenerate.) Hence the only contribution to $\pi_{ab}(T)$ is from the potential energy term. Fig. 7 shows such a junction with $\theta_b > \theta_a$. If electrons cross

from a to b (I_x from b to a) they have to get rid of some excess energy since their kinetic energies are of similar value in the two crystals. Thus heat is evolved in agreement with the previous discussion for the case $\theta_b > \theta_a$. When electrons cross from b to a they must be supplied with energy so that heat will be absorbed.

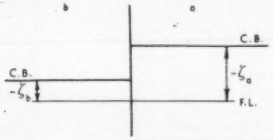

Fig. 7. Contact between two n-type semi-conductors

In the case of metal contacts (cf. Fig. 8) the kinetic energies are of the order of the Fermi energies. Thus the change in potential energy is almost exactly compensated by the kinetic energy change leading to a small (second order) value for π. In fact (cf. Seitz,[1] p. 179)

$$\frac{K_2}{K_1} - \zeta = k^2T^2\frac{\pi^2}{3}\left[\frac{1}{\zeta_0} + \frac{l'(\zeta_0)}{l(\zeta_0)}\right] \tag{25}$$

(where ζ_0 is the value of ζ at $T = 0$)
so that

$$\theta = -\frac{k^2T}{e}\left[\frac{1}{\zeta_0} + \frac{l'(\zeta_0)}{l(\zeta_0)}\right] \tag{26}$$

and

$$\pi_{ab}(T) = -\frac{k^2T^2}{e}\left\{\left[\frac{1}{\zeta_0} + \frac{l'(\zeta_0)}{l(\zeta_0)}\right]_b - \left[\frac{1}{\zeta_0} + \frac{l'(\zeta_0)}{l(\zeta_0)}\right]_a\right\} \tag{27}$$

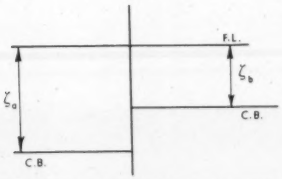

Fig. 8. Contact between two metals

Returning now to equation (21) there still remain the two integrals over the bulk of the materials. They may be written as

$$\frac{dH_B}{dt} = -I_x\left(\int_T^{T_0} Td\theta_a + \int_{T_0}^{T} Td\theta_b\right) \tag{28}$$

in order to change to an integration over T instead of θ we introduce the Thomson coefficient by

$$\tau = T(d\theta/dT) \tag{29}$$

or alternatively

$$dH/dt = -\tau I_x(dT/dx) \tag{29a}$$

the latter being the more usual definition.

Substituting into equation (28)

$$\frac{dH_B}{dt} = -I_x\left[\int_T^{T_0}(\tau_a - \tau_b)dT\right] \tag{30}$$

To assist in the interpretation of τ the results are again separated into potential and kinetic energy contribution using equation (8). Thus

$$\int_a^b \tau\frac{dT}{dx}dx = -\left[(\zeta_a - \zeta_b) + \int_a^b \theta dT\right] - \left[\left(\frac{K_2}{K_1}\right)_b - \left(\frac{K_2}{K_1}\right)_a\right]$$

The first term again corresponds to the increase in potential energy (cf. Fig. 1) and equation (13), while the second gives the change in average kinetic energy transported.

The total rate at which heat is developed is given by [equations (18), (19) and (27)].

$$\frac{dH_T}{dt} = -I_x\left[\pi_{ab}(T_0) - \pi_{ab}(T) + \int_T^{T_0}(\tau_a - \tau_b)dT\right] \tag{31}$$

Now clearly we would also have calculated dH_T/dt by using the Seebeck e.m.f., i.e.

$$(dH_T/dt) = -I_xF_{ab}(T, T_0) \tag{32}$$

so that

$$F_{ab}(T, T_0) = \pi_{ab}(T_0) - \pi_{ab}(T) - \int_T^{T_0}(\tau_b - \tau_a)dT \tag{33}$$

Equation (33) can be obtained directly from the relation between $F_{ab}(T, T_0)$ and θ [equation (17)] by integrating by parts and using equations (22) and (29) which give the relation between $\pi_{ab}(T)$ and $\tau_a(T)$ with θ respectively. The previous evaluation of dH_T/dt has, however, localized the regions where the various heat exchanges take place. From equation (31) it can be seen that $F_{ab}(T, T_0)$ could be replaced by a source of e.m.f. equal to π at each of the junctions and a distribution of sources along the conductors of e.m.f. equal to $\tau dT/dx$. This replacement is often used in the elementary theory of thermoelectricity which starts with this distribution of sources of e.m.f. and uses thermodynamic arguments to relate them. It should be pointed out that this distribution of sources of e.m.f. is purely conventional, the real distribution being given by $\theta dT/dx$ [cf. equation (14a)] continuous throughout the loop. There is no discontinuity of Fermi level or source of e.m.f. at the junctions.

5. ENERGY FLUX

The total energy transported per unit area is given by [equation (12)]

$$C_T = I_x[\pi - (\zeta/e) + V(x)]$$

where we have defined the absolute Peltier coefficient (π) as

$$\pi = T\theta \tag{34}$$

From Fig. 1 it will be seen that if potential energy is measured with respect to the *Fermi level as zero* then an energy flux can be defined which is given by

$$C_T' = I_x\pi \tag{35}$$

This is, however, *not* the total energy flux C_T since the Fermi level is a function of position. Thus measuring energy from an arbitrary but constant energy zero (to be denoted by a suffix a) we have, using equation (13),

$$C_T = I_x\left[\pi - \frac{\zeta}{e} - \frac{1}{e}(\zeta_a - \zeta) - \int_{T_a}^{T}\theta dT\right]$$

$$= I_x\left(\pi - \int_{T_a}^{T}\theta\, dT - \frac{\zeta_a}{e}\right) \tag{36}$$

***

Now C_T is connected with the rate of evolution of heat at a point by the conservation equation (11).

Substituting for C_T gives

$$\frac{dH}{dt} = -\frac{dC_T}{dT}\frac{dT}{dx} = -I_x\frac{dT}{dx}\left(\frac{d\pi}{dT} - \frac{\pi}{T}\right)$$
$$= -I_x\frac{dT}{dx}\cdot T\frac{d}{dT}\left(\frac{\pi}{T}\right) \quad (37)$$

Thus from the definition of the Thomson coefficient it follows that

$$\tau = Td(\pi/T)/dT \quad (38)$$

which can be directly proved by using equations (29) and (34).

It should be observed that applying the conservation equation at a contact leads to the obvious result

$$\pi_{ab}(T) = \pi_b(T) - \pi_a(T)$$

This applies even if C_T' is used instead of C_T since the Fermi level is constant across the contact. It should, however, be emphasized that C_T' is *not* a total energy flux since energy is referred to a varying energy zero which is constant only across the contact.

6. CONCLUSIONS: RELATIONS BETWEEN THE THERMOELECTRIC PARAMETERS

For convenience the various relations between the thermoelectric parameters will be re-stated. The fundamental relations are

$$F_{ab}(T, T_0) = \int_T^{T_0}(\theta_b - \theta_a)dT \quad (17)$$

$$\pi_{ab}(T) = \pi_b(T) - \pi_a(T) = T(\theta_b - \theta_a) \quad (22)$$

$$\tau(T) = Td\theta/dT \quad (23)$$

The thermoelectric parameters are further related by

$$F_{ab}(T, T_0) = \pi_{ab}(T_0) - \pi_{ab}(T) - \int_T^{T_0}(\tau_b - \tau_a)dT \quad (33)$$

$$\frac{d}{dT}\left(\frac{\pi}{T}\right) = \frac{\tau(T)}{T} \quad (37)$$

$$F_{ab}(T, T_0) = \int_T^{T_0}\frac{\pi_{ab}}{T}dT \quad (39)$$

[the latter result being obtained from equations (17) and (22)].

Since the whole report consists of a discussion of an accepted theory only a few conclusions, concerning points which are perhaps not well understood, will be listed here.

(1) The thermoelectric power can be defined as the rate of change of Fermi level with T (measured with respect to some arbitrary and constant zero). It is not equal to the rate of change of Fermi energy which is usually measured from the (variable) conduction band edge.

(2) While π measures the rate at which heat is evolved at a junction it does not represent a localized e.m.f. at the junction, the Seebeck e.m.f. being continuously distributed along the thermocouple.

(3) π is equal to the energy flux per unit current when the energy is measured with respect to the Fermi level. Since the latter varies with position in the thermocouple, π is, in fact, not equal to the total energy flux per unit current which takes account of the variation of the Fermi level [cf. equation (12)].

(4) The reason why semi-conductors have much larger π than metals is because the potential and kinetic energy contributions almost cancel one another in the case of metals while the latter contribution is very small for semi-conductors.

(5) When the temperature is uniform the contact potential difference between two conductors is the difference between their work functions. However, when the junction is at a different temperature from the open ends the C.P.D. is larger by the Seebeck e.m.f. This effect should be experimentally observable.

ACKNOWLEDGEMENTS

The author has greatly benefited from many stimulating discussions with Mr. G. R. Antell. He wishes to thank Mr. R. P. Chasmar for valuable advice, Dr. R. W. Sillars for detailed criticisms, Dr. Willis Jackson, Director of Research and Education, and Mr. B. G. Churcher, Manager of the Research Department, Metropolitan-Vickers Electrical Co. Ltd., for permission to publish this paper.

REFERENCES

(1) SEITZ, F. *Modern Theory of Solids* (London: McGraw-Hill Book Co. Ltd., 1940).

(2) JOHNSON, V. A. *Progress in Semi-Conductors* (London: Heywood and Co. Ltd., 1956).

(3) LAURELA, E. *Ann. Acad. Sci. Fennicae*, No. 178 (1955).

APPENDIX

In a recent paper, Laurela[3] derives the thermoelectric power for a p–n junction and gives a result inconsistent with the value to be expected from Section 2. The latter is

$$\theta_{np} \equiv \theta_p - \theta_n = \frac{1}{eT}\left\{-\left[\zeta_p - \left(\frac{K_2}{K_1}\right)_p\right] - \left[\zeta_n - \left(\frac{K_2}{K_1}\right)_n\right]\right\} \quad (40)$$

ζ_n being measured from the conduction band edge E_c and ζ_p from the top of the valence band (cf. Fig. 9). This gives a Peltier coefficient

$$\pi_{np} = \frac{1}{e}\left\{-(\zeta_p + \zeta_n) + \left[\left(\frac{K_2}{K_1}\right)_n + \left(\frac{K_2}{K_1}\right)_p\right]\right\} \quad (41)$$

Since ζ_n and ζ_p are negative π_{np} is positive so that heat will be evolved when conventional current flows from p to n.

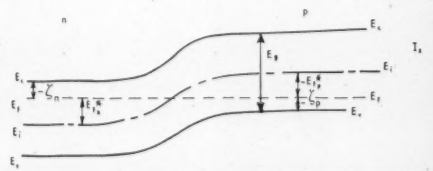

Fig. 9. p–n junction

Thus when an electron from the n side reaches the junction it combines with a hole from the p side and it gives up potential energy $(\zeta_p - \zeta_n)$. There will also be a contribution from the kinetic energy terms representing the total kinetic energy destroyed.

Laurela uses a different notation. Fermi energies (E_F^*) are measured from the intrinsic energy level (assuming for simplicity equal hole and electron masses)

$$E_i = \tfrac{1}{2}(E_c + E_v) \tag{42}$$

Thus
$$E_F^* = E_F - \tfrac{1}{2}(E_c + E_v) \tag{43}$$

Applying this to the n and p regions

$$E_{Fn}^* = E_{Fn} - E_{in} \tag{44}$$

$$E_{Fp}^* = E_{Fp} - E_{ip} \tag{45}$$

But $E_{Fn} = E_{Fp}$ in equilibrium so that

$$E_{in} - E_{ip} = -(E_{Fn}^* - E_{Fp}^*) \tag{46}$$

Now $V = -E_i/e$ measures the change of potential energy across the junction. Laurela defines θ_{np} as

$$\theta_{np} = \frac{d}{dT}(V_p - V_n) \tag{47}$$

or
$$\theta_{np} = -\frac{1}{e}\frac{d}{dT}(E_{ip} - E_{in}) = +\frac{1}{e}\frac{d}{dT}(E_{Fp}^* - E_{Fn}^*) \tag{48}$$

i.e. the change of Fermi energy and not Fermi level as it should be. Equation (47) is in fact incorrect.

Using equation (48) Laurela finds that

$$\theta_{np} = +\frac{E_g - (E_{Fn}^* - E_{Fp}^*)}{eT} + \frac{3k}{e}$$

or using our definitions of the Fermi energy

$$\theta_{np} = -\frac{(\zeta_p + \zeta_n)}{eT} + \frac{3k}{e} \tag{49}$$

as opposed to our results, equation (40), which depends on the mean-free-path as it should.

ORIGINAL CONTRIBUTIONS

The oxidation of evaporated barium films (getters)

By R. N. Bloomer, B.Sc., A.Inst.P., Research Laboratory, Associated Electrical Industries Ltd., Aldermaston, Berks

[*Paper received* 20 *February*, 1957]

Mott's theory of the oxidation of metals is summarized and expressed in terms comparable with the throughput, capacity, and speed of pumping, which are measured in the present work on barium getters.

It has been found that there is a critical temperature, about 40° C for barium, below which a thin protective film of oxide is formed. Above 40° C, barium films oxidize right through, and so in this case, the capacity of getters for oxygen depends upon the amount of metal used. The feature of the mechanism which limits the speed of pumping of oxygen has been found, and hence the speed has been increased in various ways.

The theory of Mott concerns only the growth of an oxide film that is already at least a monolayer thick. In the present study it has been found that the first monolayer spreads from nucleation centres in the barium surface.

1. INTRODUCTION

Previous work by Wagener[1, 2] and Bloomer[3, 4] has shown that evaporated films of barium (getters) take up molecular oxygen: it is unnecessary for the gas to be either ionized, excited, or nascent. The experiments have been continued, in an attempt to discover some of the details of the way in which oxygen reacts with barium to increase the thickness of an oxide layer growing upon the metal. These experiments are now described, and an explanation of them given. For this, two theoretical ideas are used: firstly, the ionic theory of the oxidation of metals developed by Mott,[5, 6, 7] later with, and by, Cabrera and his co-workers[8, 9, 10, 11, 12]; secondly, the assumption that the condensation of the first monolayer of oxygen can only start at and continue about nuclei in the surface of the metal film.

2. THEORETICAL

2.1. *An outline of Mott's theory of the oxidation of metals*

In the theory of Mott[7] it is first supposed that one or two monolayers of oxygen atoms have been adsorbed upon the surface of the metal, to give the beginning of an oxide layer. The theory concerns only the further thickening of this layer.

It is assumed that there are empty electron levels in the oxygen adsorbed on the interface between the oxide layer and the surrounding oxygen gas. Electrons will pass through the oxide layer, from the metal, to fill these empty levels. When the oxide layer is very thin, say only a few tens of Angstrom units, the electrons pass through by the quantum-mechanical tunnel effect: when the layer is thicker the electrons can still pass if they are first raised to the conduction band of the oxide, for example, by photo-electric or thermionic emission from the metal. The energy barrier that has to be overcome in such emissions—between the conduction bands of the metal and its oxide—is less than the work function of the clean metal in vacuum. The removal of electrons from the metal to the adsorbed oxygen causes a potential drop across the oxide, in conventional sign from metal to oxygen. The electric field which is thus set up across the oxide is strong enough in the case of thin layers to promote the diffusion of positive metal ions. Such diffusion is through interstitial positions within the oxide lattice. In these movements of electrons and metal ions, the electrons will arrive first, because of their greater speed for a given energy. The

density of these dissociated metal atoms in interstitial sites is assumed to be small enough for the space charge effects of the electrons and the ions to be negligible.

The variation with temperature of the diffusion of the metal ions through the oxide lattice sets the character of the laws of oxidation. This variation with temperature can be expressed in the usual way by an exponential term. Thus, at sufficiently high temperatures, the metal ions will dissolve and migrate in the oxide. A strong field, like that across an oxide layer less than about 50 Å thick, is unnecessary for this motion. In these circumstances, the oxide film can continue growing indefinitely. By contrast, at relatively low temperatures, the oxide layer can only grow because metal ions move across it by virtue of the strong field, and without much help from thermal energies. Therefore the oxide layer will grow at a rate which decreases rapidly as the film thickens and the field weakens. By taking some very slow growth rate as defining the end of oxidation, Mott has deduced the value of a critical temperature. Below this temperature the oxide layer can grow to some small thickness, about 50 Å, only: above this temperature the layer can grow indefinitely.

The critical temperature T_c can be expressed by the formula

$$T_c = W/32k \qquad (1)$$

if oxidation is defined as ceasing when the rate of growth of the oxide layer falls to 10^{-10} cm/s.

W = the energy barrier to the movement of a metal ion from the metal into any interstitial position in the oxide lattice, and

k = Boltzmann's constant

This is the value at which measurements have been stopped in the present work. The derivation of equation (1) is relegated to Appendix 1.

Two other quantities treated in Mott's theory can be measured indirectly in experiments like the present ones with barium getters. Firstly, the limiting thickness X_L, at which oxidation stops when the temperature is $T < T_c$, is

$$X_L = C/(1 - T/T_c) \qquad (2)$$

[see Appendix 1, equation (4)] in which C = (the potential difference between the surface of the Fermi distribution in the metal and the empty electron levels in the oxygen adsorbed on the outer surface of the oxide)/(the average field strength at the interface between the metal and the oxide).

Thus, C can be expressed in terms of the appropriate potential energy gaps, V and $W_i + U$, and the half-width a of the potential energy barrier for metal ions between the metal and the oxide layer. These quantities are conventionally represented in Figs. 1(*b*) and (*c*), which are taken from Mott's papers.

We have

$$C = Va/(W_i + U) \qquad (3)$$

if the electronic and ionic charges are the same. [If they are unequal, a correction factor e_i/e, the ionic charge/the electronic charge, is necessary on the r.h.s. of (3).]

Secondly, the ionic current through the oxide film varies with temperature and oxide film thickness, X, in differing manners below and above the critical temperature, T_c, defined by (1). For $T < T_c$ and thin oxide layers across which the fields are strong,

$$\text{ionic current} \propto \exp -(W_i + U)/kT \,.\, \exp aV/XkT \qquad (4)$$

in which the constant of proportionality is $naqf$, where

n = the number of metal ions, in unit area of the metal surface, which are able to move into the oxide; for example, those at the edge of an atomic layer or some similar irregularity. [See *P*, Fig. 1(*a*).]
q = the charge on a metal ion, and
f = the frequency of atomic vibration in the metal and oxide.

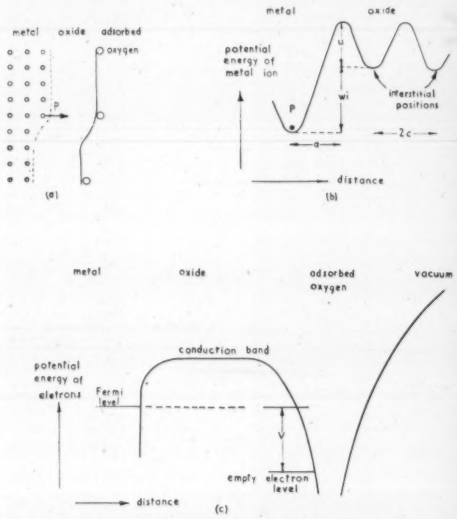

Fig. 1. The oxidation of metals after Mott

(*a*) The oxide layer grows by the transfer of metal ions like *P*.
(*b*) Energy barriers to metal ion movement.
(*c*) Energy barrier to electron movement.

For $T > T_c$ and thicker oxide layers, in which the fields are too weak to influence the diffusion of the metal ions,

$$\text{ionic current} = \text{const.}\ V/XkT \,.\, \exp -(W_i + U)/kT \qquad (5)$$

in which the constant is Nc^2qf, where

N = the number of metallic ions per unit volume of oxide which are occupying interstitial positions, and
c = half the distance between interstitial positions.

2.2. *Some deductions from Mott's theory relevant to the present studies*

In the present work three quantities are deduced from measurements of the pressure drop in a constrictive pipe of known conductance, through which oxygen reaches the getter by free molecular flow. These quantities are (*a*) the amount of gas, i.e. the number of molecules, taken up by the getter deposit in unit time (throughput), (*b*) the volume of gas taken up in unit time at any particular pressure (speed of pumping), and (*c*) the total amount of gas taken up during the active life of the getter (capacity). For each of these, there is an equivalent quantity deducible from Mott's theory. Such correlates are now examined as useful tests of the theory.

The capacity of a getter for oxygen is proportional to the thickness of a homogeneous oxide layer grown upon it.

Consequently, in equation (2) the limiting thickness X_L may be replaced by the quantity of gas, Q, which is taken up by the getter at a temperature $T < T_c$. In the present work, Q is measured in the gas phase. Strictly, the constant in (2) must be changed by a factor which is proportional to the spatial density of oxygen in barium oxide. However, if the capacity is Q_1 at T_1, and Q_2 at $T_2 < T_1$, $Q_1 \propto (1 - T_1/T_c)^{-1}$ and so on.

Hence, $$T_c = (Q_1T_1 - Q_2T_2)/(Q_1 - Q_2) \qquad (6)$$

Thus, the critical temperature can be found from the r.h.s. quantities measured in the present work. The Mott theory predicts that the capacity will increase with temperature below T_c. The capacity will be independent of the thickness of the getter deposit, provided the thickness is greater than the limiting value appropriate to the temperature of the experiment. But, above the critical temperature, the capacity will be limited only by the thickness of barium deposited when the getter is fired. These contrasting features can be tested after the critical temperature has been found.

The throughput of oxygen gas to the getter is proportional to the metal ion current in the oxide layer growing upon the barium. For the present work to be a valid check of the theory, it is necessary for the throughput that is measured in the experiments to be limited by the properties of the getter film, not by the constrictive pipe. Thus, a valid comparison can be made from measurements of throughput towards the end of the active life of the getter, when the throughput is falling with time. Now, it is predicted from the Mott theory that, for a given thickness of oxide layer, the throughput to the getter will increase exponentially with temperature [see equation (5)], for temperatures greater than T_c [see equation (1)]. At temperatures less than T_c, the throughput at any particular thickness will not vary as rapidly with temperature [see equation (4), in which the two exponential terms have opposite signs of variation with temperature].

Consider now the measured speed of pumping of a getter film. This will, if anything, be less than the theoretical speed deduced from the kinetic theory of gases, because only a fraction (called the condensation coefficient) of the oxygen molecules incident upon the growing oxide layer will combine with barium ions which have reached this surface after diffusing through the oxide. The condensation coefficient might, of course, be limited by the rate of adsorption of oxygen on to the oxide surface, a matter not treated in Mott's theory. But, if so, the condensation coefficient (proportional to the measured speed of pumping of a constant area of getter) would decrease exponentially with increase of temperature, since desorption is an activated phenomenon. On the other hand, if the condensation coefficient is limited by the number of metallic ions in unit area of the free surface of the oxide at any time, variation of this coefficient with temperature is predicted by the theory. Above the critical temperature, the number of metallic ions in unit area [proportional to N in equation (5)] will increase with temperature, because of the increased solubility of these ions in the oxide lattice (quite apart from their greater mobility). Below the critical temperature, the speed of pumping will depend upon n [equation (4)], which is the number of sites in unit area of the metal from which ions can become free to go into the oxide interstitially. Now n, unlike N, is probably independent of temperature. Thus, the distinction between the variations of speed with temperature predicted by the two mechanisms (limitation either by the superficial density of interstitial ions or by oxygen adsorption) is less below than above the critical temperature. However, below the critical temperature, if the condensation coefficient is limited by the interstitial ion density, the speed of pumping will increase with the number of surface defects or discontinuities [as at P in Fig. 1(*a*)] in unit area of the metal surface. Therefore, below the critical temperature, it should be possible to test whether or not the metallic ion density is limiting the speed of pumping, by depositing getters upon sundry substrates. Above the critical temperature, the test can be made by finding how speed varies with temperature.

2.3. *The part played by nucleation centres in the adsorption of the first monolayer of oxygen*

Experiments by Arizumi and Kotani,[15] and Bloomer reported in his paper,[4] have shown that the adsorption of the first monolayer or so of oxygen upon barium is conditional. Some barium films are initially inert towards oxygen, although these, after an induction period, suddenly start to take up oxygen. Moreover, for all barium films, the speed of pumping increases in the first few minutes of the active life, see Bloomer.[4] Thus, there is evidence that oxidation can only start at certain nuclei in the barium surface.

Consider a simple picture of the process of nucleation, like that suggested by Evans[13] for the sideways growth of corrosion films on metals. Suppose that there are a fixed number of nuclei from which the oxygen monolayer grows outward. At any instant the layer will have grown to an equal extent from each centre, by the adsorption of oxygen at the outer edge. The speed of pumping of oxygen by this process will be proportional to the area on to which adsorption takes place. This area is that of the annulus, one adatom wide, at the circumference of the circularly growing layer. Thus the speed of pumping is $S \propto 2\pi rd$

where r = the radius of the circular layer, and
d = the diameter of the oxygen adatom.

The actual number of oxygen molecules which become adsorbed in unit time on unit area is constant at any given pressure, and so the area of the layer will increase linearly with time.

Therefore, $r \propto t^{\frac{1}{2}}$ where
r is the radius at any time t from the start of growth.

Hence $S \propto t^{\frac{1}{2}}$

or $$S = K_1t^{\frac{1}{2}} \qquad (7)$$

The constant K_1 is a measure of the number of nuclei in unit area of the metal film. The relation (7) can be expected to hold only until the edges of growing layers become contiguous. This will happen when nearly a monolayer of gas has been adsorbed. As this condition is approached, the speed of pumping will be found to fall below the curve given by equation (7).

By contrast, the oxide layer might build up into hemispherical caps, say, about the nuclei, rather than spread outwards in a monolayer. In such a case, the four simple relations terminating in (7) in the preceding paragraph must be modified as follows:

$S \propto 2\pi r^2$, (r is here the radius of the hemispherical cap)
$r \propto t^{1/3}$
$s \propto t^{2/3}$ (s is the surface area of the hemispherical cap)
and $S = K_2t^{2/3}$ (8)

Law (8) would hold until neighbouring caps touched, but before it failed the amount of oxygen taken up would be

equivalent to that in several monolayers upon the apparent surface of the getter mirror. The actual number of monolayers will be $n^{-\frac{1}{2}}$, where n is the number of nuclei in unit area of the getter surface. Now K_2, like K_1 in (7), also varies with n. Hence, if the growth of the oxide about the nuclei is three dimensional, the number of monolayers taken up in the period when law (8) holds will be dependent upon the slope of the plot of S against $t^{2/3}$ for this period. (The number of monolayers will be proportional to $K_2^{-1/2}$.) This relation contrasts with the independence of the slope (K_1) and the limiting thickness of a single monolayer in the case of two dimensional growth about nuclei. Therefore, from experimental plots of S against $f(t)$, and the area beneath them, it can be decided if the growth about nuclei is two- or three-dimensional.

3. EXPERIMENTAL APPARATUS AND METHODS

The basis of the method is the proportionality of the throughput and the pressure drop for a pipe through which gas streams at pressures so low that the molecules flow freely (without mutual collisions), demonstrated experimentally by Knudsen[14] and utilized by Wagener[1] for studies of barium getters. A bulb containing the getter is connected with a gas supply by a pipe of conductance K (l./s). When the getter is active, the pressure near it, p_g (microns of mercury), will be less than the pressure, p_m, at the other end of the pipe. Then the throughput $\dot{Q}$ (l.μ/s) and the speed of pumping S (l./s) of the getter are

$$\dot{Q} = K(p_m - p_g) \tag{9}$$

$$S = K(p_m/p_g - 1) \tag{10}$$

The capacity of the getter, Q(l.μ), can be obtained from the area under a $K(p_m - p_g)$ against time curve.

The particular form of apparatus used in the present work had been described previously by Bloomer.[4] One change has been made in the method of controlling the oxygen pressure in the apparatus when the getter film is being kept at any temperature below 0° C. At these temperatures, any water vapour in the oxygen supplied from an unbaked glass storage system might condense, so spoiling pressure measurements taken with a pair of ionization gauges, of which only one is attached to that part of the apparatus remaining at room temperature. It has been found convenient to control the oxygen pressure in the apparatus by heating ground crystals of potassium permanganate in an appendix to the main manifold. This manifold is connected to the bulb containing the getter by the pipe of conductance K. The appendix is baked initially in each experiment along with the rest of the high vacuum system. Grinding the crystals reduces the probability of their thermal fracture, which is otherwise a cause of intolerable pressure fluctuations. This method, and the other way of controlling the pressure of oxygen in the manifold (namely, using a baked needle valve to connect the vacuum system with unbaked storage bulbs containing oxygen at near-atmospheric pressure), have both been used, for experiments with barium films kept above 0° C. The results then obtained have been equally satisfactory.

4. RESULTS AND DISCUSSION

4.1 *Capacity at different temperatures—the critical temperature*

A typical plot of throughput against time [i.e. $K(p_m - p_g)$ versus t, see equation (9)], obtained in an experiment with a getter film at room temperature, is shown in Fig. 2. The total capacity of the getter is obtained from the area under this curve by arbitrarily taking the end of the active life to be when the throughput begins to fall rapidly (time = 80 min in Fig. 2). The total capacity/apparent surface area of the

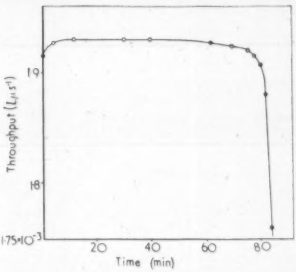

Fig. 2. A typical curve of throughput plotted against time

Film area = 11 cm²; film temperature = 20° C; capacity = 9·04 l.μ ≡ 28 monolayers.

getter is equivalent to the thickness of oxide layer formed. It is instructive to convert this apparent thickness to the equivalent number of monolayers of close-packed oxygen atoms.

The capacity of unit area of films kept at and below room temperature have been obtained in this way, see Table 1. From the variation of capacity per unit area with temperature, the critical temperature T_c can be found using equation (6).

Table 1. *The variation of capacity per unit area (expressed in monolayers) with temperature, and the critical temperature deduced therefrom*

Temp. °K T_1	No. of monolayers Q_1	T_2	Q_2	Critical temp. °K $T_c = \frac{Q_1T_1 - Q_2T_2}{Q_1 - Q_2}$
283	25·9	274	19·5	310
293	25·2	278	12·4	308
283	22·2	263	11·9	306

A plot of oxide film thickness (number of monolayers) at different temperatures, but with the same thickness of barium in each experimental run, has a break at about the critical temperature, as shown in Fig. 3.

This result agrees with the prediction of Mott's theory.

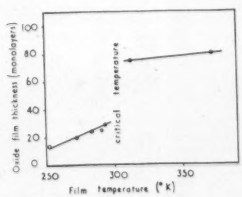

Fig. 3. The influence of temperature upon oxide layer thickness

There is a critical temperature. Since the critical temperature is definite, see Fig. 3, the effective value of W [the work function for the transit of ions from metal to oxide, see equation (1)], must be definite also. By analogy with the electronic work function of metals against vacuum, W might have been expected to vary over the metal-oxide interface, in patches, see Becker[16] and Herring and Nichols.[17] If there is a variation, however, it is the patches with the lowest values of W which will contribute most to the oxidation.

There is an important difference between the thermionic work function and the energy W, and hence the analogy fails. The thermionic (electronic) work function depends largely upon the electron affinity of the emitting atoms, although there is some small variation of work function from one crystalline face to another. Contrariwise, the energy difference W will depend greatly upon the spacing between metal and oxygen ions in the oxide; for, unlike an electron in the case of thermionic emission, a metal ion during oxidation is moved in the beginning from the metal to a definite position, not to infinity. Hence, the low value of critical temperature (that is of W) for barium is not a necessary consequence of the low work function of barium atoms. This conclusion is upheld by a comparison of critical temperatures for oxidation with thermionic work functions for other metals, as shown in Table 2.

Table 2. *The thermionic work function ϕ and the critical temperature T_c, for various metals*

Metal	ϕ *(eV)*	*Reference*	T_c	*Reference*
Aluminium	4·2	Wright[18]	600° K	Cabrera and Hamon[11]
Copper	4·6	Wright[18]	293° K	Rhodin[20]
Zinc	4·3	Wright[18]	498° K	Vernon and co-workers[21]

4.2. *Variation of capacity/unit area with thickness of barium film*

Fig. 4 is a plot of the oxide film thickness against thickness of barium in the getter deposit (i.e. time of firing the getter). It shows that the thickness of oxide layer built up when a barium film is kept just above the critical temperature is proportional to the time during which the barium was evaporated at a steady rate at the start of the experiment. At the end of these runs, the initially opaque barium film had become translucent. Below the critical temperature the oxide layer thickness is independent of the barium film thickness. At the end of each of these experiments, the getter film was still opaque and mirror-like. It was checked that these experiments were well founded, for the values of oxide layer thickness obtained were independent of the area of the evaporated barium film when, in otherwise identical runs, this was varied between 5 and 50 cm^2.

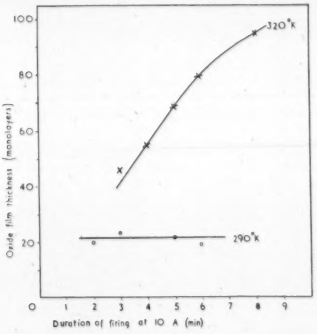

Fig. 4. The variation of oxide thickness with barium thickness below and above the critical temperature

This result shows that the oxide layer on barium is protective only below the critical temperature, in accordance with Mott's theory.

4.3. *Variation of throughput with temperature*

Throughputs measured towards the end of the active life of getter films are shown in Fig. 5, plotted against time. The curves of results obtained at different temperatures have been displaced along the time axis in order to separate them clearly. The curves are horizontal when the throughput is limited by the constrictive pipe, but fall with time when the throughput is limited by the getter. It is seen that the slopes of the curves vary with temperatures higher than the critical temperature: at lower temperatures the slope is the same for all curves.

For temperatures above T_c, the experimental plots of Fig. 5 cannot be interpreted directly by equation (5) (see section 2.1), since the oxide film thickness X is not the same for the falling regions of all the curves. The film thickness in these regions is greater the higher the temperature of the experiment. Nevertheless, the slope in these regions decreases with increase of temperature, because of the dominance of the single exponential term of equation (5). Now, for temperatures below T_c, the values of thickness are about the same for the falling regions of all the experimental curves of Fig. 5. From equation (4), (see section 2.1), it is deduced directly that the slope in the falling region should be largely independent of temperature (see section 2.2). Thus, the observed influence of temperature upon the slopes of the falling portions of the curves in Fig. 5 is, in all cases, as predicted by Mott's theory.

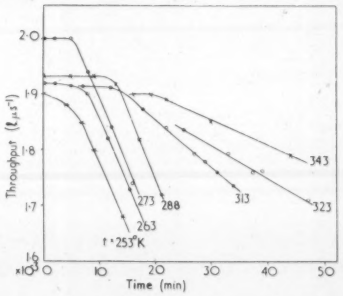

Fig. 5. The influence of temperature upon the rate of decay of the throughput

4.4. *Variation of speed with temperature*

The speed of pumping of oxygen by unit area of the apparent surface area of a barium getter mirror has been measured in a range of temperature above and below the

critical temperature. The values obtained are plotted in Fig. 6: the curve has a definite break at about the critical temperature. For comparison, one tenth of the theoretical speed of pumping of unit area of a surface, deduced from the kinetic theory of gases, is shown for the range of temperature covered by the measurements.

The speed of pumping of oxygen by barium is only a small fraction—about 1/25—of the speed for unit area predicted by the kinetic theory of gases. Furthermore, the speed of pumping is only independent of temperatures below the critical value T_c: above the critical temperature, the speed

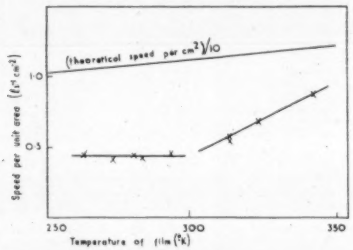

Fig. 6. The influence of temperature upon the speed of pumping

increases. Hence, by the argument given in section 2.2 (fourth paragraph) it is deduced that the speed is limited by the superficial density of interstitial barium ions in the surface of the growing oxide.

4.5. *Barium deposited on sundry substrates*

The experiments whose results are given in this section were made with the object of trying to change the speed of the getter for oxygen, by altering the number of defects in the barium and its growing oxide layer. These tests were suggested by the Mott theory [see equation (4), in which occurs the factor n, the number of metal ions per unit area which are at some atomic irregularity in the metal surface, for example, at places like P in Fig. 1(*a*)].

The results given so far in this paper have been obtained with barium deposited on glass that was allowed to reach a temperature set by the stopping of radiation from the red-hot getter wire during the deposition of the barium. This temperature was about 70° C. Now, during the deposition of some films, the glass was deliberately heated to a higher temperature, about 200° C, in order to cause crystalline changes. For these films, the values of speed per unit area, measured at 20° C, was $0{\cdot}30\ \mathrm{l.s^{-1}\,cm^{-2}}$. For normal films deposited at about 70° C, the speed per unit area was $0{\cdot}44\ \mathrm{l.s^{-1}\,cm^{-2}}$. The lower speed of films deposited on the hotter glass suggests that the barium atoms are then mobile enough for crystalline changes to occur, so removing some of the irregularities in places such as P, Fig. 1(*a*).

In the first attempts to increase the speed, barium was deposited upon previously oxidized barium layers. These layers were prepared by raising a barium getter film above the critical temperature of about 40° C, and then introducing oxygen at a pressure of several centimetres of mercury. The layer of completely oxidized barium became misty white, but translucent. A barium film for an experiment was then deposited upon this layer, under high vacuum conditions. These films were arranged to be several times thicker than the protective layer of oxide (about 25 monolayers) which forms at room temperature, see section 4.1. The speed of pumping per unit area, at 20° C, was found to be $0{\cdot}44\ \mathrm{l.s^{-1}\,cm^{-2}}$ (the same as in the case of the normal barium films on glass). Thus, these attempts failed to increase the density of irregularities.

It is well known that barium oxide made by reducing the carbonate, as in the conventional oxide-coated thermionic cathode, has a particularly defective lattice, see Wright.[19] Accordingly, barium films were deposited upon barium oxide/strontium oxide layers, prepared in the experimental tubes by the breakdown of the carbonates. The speeds of barium films of increasing thickness were measured at 20° C, and are shown in Table 3.

Table 3. *The speed of barium films, at 20° C, deposited upon BaO/SrO*

Time of deposition at a uniform rate (min)	*Speed of pumping per unit area ($\mathrm{l.s^{-1}\,cm^{-2}}$)*
2	2·6
3	1·7
5	1·6

Thus, these attempts to increase the density of irregularities like P, Fig. 1(*a*), and hence of interstitial barium ions in the oxide, were successful.

The experiments above, in which the speeds per unit area were changed, must not be interpreted by means of the Mott theory alone, without some further evidence that the surface roughness of the barium films is about the same for all the substrates (glass, oxidized barium, or BaO/SrO). If the true area of a film is greater than the apparent area, the speed (per unit apparent area) and the capacity (expressed as the number of monolayers of oxygen upon the apparent area) will be increased, both by the same factor. Accordingly, capacities as well as speeds have been measured. The results are summarized in Table 4.

Table 4. *Capacity and speed, measured at 20° C, for unit apparent area of barium deposited upon sundry substrates*

Substrate	*Speed per unit area ($\mathrm{l.s^{-1}\,cm^{-2}}$)*	*Capacity: number of monolayers of oxygen upon unit apparent area*
Glass	0·44	25
Oxidized barium	0·44	45
BaO/SrO 2 min (see Table 3)	2·6	40
3 min	1·7	50

It is seen that the changes in speed and capacity are largely independent of each other. Hence the changes cannot be explained by variation of surface roughness alone: the changes can be explained by means of Mott's theory.

In the case of getter films deposited upon oxidized barium, the capacity is increased, but the speed is unchanged compared with films upon glass. This increase of capacity is interpreted as a reduction of the critical temperature, that is of W, see equation (1). Alternatively, or additionally, the explanation could be that the value of the distance a, see Fig. 1(*b*), is increased. For films deposited upon the mixed oxides prepared from the carbonates, the increase of speed, yet with an unchanged capacity, is interpreted as evidence that the superficial density n of sites like P, see Fig. 1(*a*),

controls the condensation coefficient of oxygen upon a growing barium oxide layer.

4.6. *The speed of pumping of oxygen by continuously deposited barium*

The taking up of oxygen by a barium surface on to which the metal, as well as the gas, is impinging, has been studied. Fig. 7 shows plots of the speed increasing during such runs. In these experiments, the apparent area of the getter film did not change. The rate of arrival of barium atoms at the surface was estimated approximately from the time taken to form a just opaque layer, before the start of the speed measurements. The rate was of the order of 10^{13} cm^{-2} s^{-1} (greater for curve 1 than curve 2 of Fig. 7). The rate of sorption of oxygen molecules was about 5×10^{12} cm^{-2} s^{-1} in both cases,

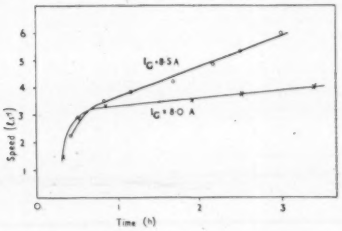

Fig. 7. Increase of speed during continuous firing of getter (heating current = I_G)

There are two ready explanations of the steady increase of speed when barium was evaporated on to a growing oxide film. Firstly, that the area of the getter film increases as more barium is evaporated; secondly, that irregularities made in the growing film persist, the rate of their introduction depending on the rate of arrival of barium. The first is believed not to have happened in these experiments, for, once a getter wire has been fully opened by a first firing

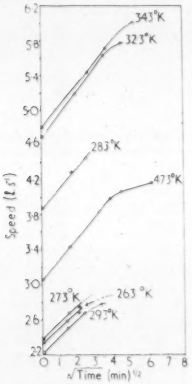

Fig. 8. The increase of speed in the early stages of oxidation of barium at different temperatures

(this had been done here), the area of the deposited getter mirror does not increase as more barium is evaporated.

4.7. *Variation of speed with time during the initial growth of activity*

The speed of pumping increases with time at the start of an experimental run, as has been reported earlier, see Wagener[22] (1951) and Bloomer.[4] The values of speed measured from the start of typical runs are shown plotted against $t^{\frac{1}{2}}$ in Fig. 8, for a range of different temperatures. The amount of oxygen taken up whilst $S \propto t^{\frac{1}{2}}$ has been calculated for the runs plotted in Fig. 8, and in each case has been converted to the equivalent number of monolayers upon unit area of the apparent surface. These amounts, and the slopes of the plots of S against $t^{\frac{1}{2}}$ are shown in Table 5.

Table 5. *The increase of speed at the start of runs*

Temperature °K	*Slope of S v.s $t^{1/2}$ plots* $C = dS/dt^{1/2}$ $l.s^{-1}\ min^{-1/2}$	*Number of monolayers taken up whilst* $S \propto t^{1/2}$
263	0·19	0·9
273	0·20	0·9
283	0·25	1·4
293	0·20	1·3
323	0·28	2·4
343	0·27	4·2

The details of the calculation of the number of monolayers are given in Appendix 2. A plot of the number of monolayers against T is shown in Fig. 9. Again, there is a break in the curve at about the critical temperature.

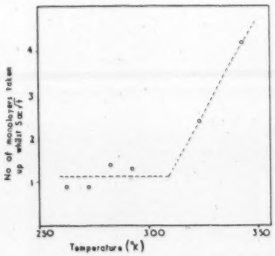

Fig. 9. The variation with temperature of the amount of oxygen taken up whilst speed is proportional to (time)$^{\frac{1}{2}}$

The law of increase of speed during the formation of the first monolayer of oxide shows that the oxide layer grows about nuclei in the surface. In the absence of such nuclei, barium films are inert towards oxygen, see Bloomer.[4] When the barium film is above the critical temperature, the amount of oxygen taken up whilst the speed is increasing proportional to time$^{\frac{1}{2}}$ is greater than a monolayer and increases with temperature. This is evidence that the barium ions diffuse through the oxide rafts whilst these grow outwards (in other words, the edges of a growing oxide raft dissolve in the metal).

CONCLUSIONS

The variation with temperature of the amount of molecular oxygen which is taken up by barium films is explained by Mott's theory of oxidation. At temperatures below about

40° C, the oxide film on barium is protective, and grows to a thickness of about 50 Å only. At higher temperatures, barium films are oxidized right through.

The speed of pumping of oxygen by unit area of a barium film is limited by the superficial density of interstitial barium ions in the free oxide surface.

In the beginning, the oxidation spreads from nucleation centres in the metal surface, and continues until a complete monolayer has been built up. Thereafter, the growth of the oxide layer is as predicted by Mott's theory.

ACKNOWLEDGEMENTS

It is a pleasure to thank Mr. B. M. Cox who has done most of the experimental work, Mr. M. E. Haine for advice and encouragement, and Dr. T. E. Allibone for permission to publish this paper.

APPENDIX 1

The critical temperature

For thin oxide films at a low temperature T, Mott[7] has deduced that the rate of growth dX/dt at any thickness X is

$$dX/dt = nfv \exp(-W/kT) \exp(aV/kTX) \quad (1)$$

In equation (1),

$W = W_i + U$, the potential energy differences W_i, U and V, and the distance a being defined in Fig. 1(*b* and *c*) of the present paper.

n = the number of metal atoms per unit area at positions like P in Fig. 1(*a*).

f = the frequency of atomic vibrations, which is assumed to be the same for metal ions at places like P and at interstitial positions in the oxide.

v = the volume of oxide per metal ion,

k = Boltzmann's constant, and

e = the charge on a metal ion during motion into and through the oxide layer.

The number of metal atoms in unit area of the metal surface is $a^{-2}\,\mathrm{cm}^{-2}$, and $a \sim 10^{-7}$ cm. Mott assumes that only about 1/100 of these will be at places like P. The present measurements of pumping speed per unit area suggest that the fraction is 1/25–1/10 in the case of barium. Accordingly, put $n \sim 0{\cdot}1a^{-2} = 10^{13}\,\mathrm{cm}^{-2}$. Now, $f = 10^{12}\,\mathrm{s}^{-1}$. Also, $v \simeq a^3 = 10^{-21}\,\mathrm{cm}^3$, since $c \simeq a$, see Fig. 1(*b*). We define the end of oxidation as occurring when dX/dt has fallen to $10^{-10}\,\mathrm{cm\,s}^{-1}$, the value at which measurements have been stopped in the present work. At this stage, the oxide layer will have grown to a thickness X_L.

By substitution of numerical values in (1), we have

$$10^{-10} = 10^{12}10^{13}10^{-21} \exp(-W/kT) \exp(aV/kTX_L)$$

Whence $-141n10 = aV/kTX_L - W/kT$,

and $$X_L = aV/(W - 32kT) \quad (2)$$

Therefore, $X_L \to \infty$, i.e. the metal oxidizes right through, when the temperature is greater than a critical value T_c, given by $T_c = W/32k$.

Equation (2) can be written

$$X_L = (aV/W)(1 - T/T_c)^{-1} \quad (3)$$

$$= C(1 - T/T_c)^{-1} \quad (4)$$

writing $C = aV/W$. Equation (4) is the form given in the text of the paper as equation (2).

APPENDIX 2

Calculation of the number of monolayers taken up whilst $S \propto t^{\frac{1}{2}}$

If p_m and p_g are the pressures at the manifold and getter tube ends of a constrictive pipe of conductance K, the speed of pumping of the getter is

$$S = K(p_m/p_g - 1) \quad (1)$$

[equation (10) in section 3]. For values of $p_m/p_g > 20$, as in all the examples given in Table 5, the relation (1) may be written

$$S = Kp_m/p_g \quad (2)$$

without appreciable loss of accuracy. But at the start of the active life of a getter $S \propto t^{\frac{1}{2}}$.

Thus $$S = Ct^{\frac{1}{2}} \quad (3)$$

Hence during this period,

$$p_g = Kp_m/Ct^{\frac{1}{2}} \quad (4)$$

from (2) and (3).

Now throughput [see equation (9) in section 3] is

$$\dot{Q} = K(p_m - p_g)$$
$$= K(p_m - Kp_m/Ct^{\frac{1}{2}}) \text{ using (4)} \quad (5)$$

Let t_l be the time for which $S \propto t^{\frac{1}{2}}$.

Then the quantity of gas taken up during this time is

$$Q_{t_l} = \int_0^{t_l} Kp_m(1 - K/Ct^{\frac{1}{2}})dt$$
$$= Kp_m(t_l - 2Kt_l^{\frac{1}{2}}/C) \quad (6)$$

Now during the majority of the active life of the getter, the throughput is restricted by the conductance K, and is

$$\dot{Q} = Kp_m \quad (7)$$

at any instant, since p_g is negligible, and the total capacity is $Qt_L = Kp_mt_L$, where t_L is the duration of the active life of the getter. The period t_l, during which $S \propto t^{\frac{1}{2}}$ is equivalent to a period $t_{l'}$ during the part of the oxidation when (7) applies. From (6) and (7), it is seen that $t_{l'}$ and t_l are related, for

$$Q_{t_l} = Kp_mt_{l'}$$
$$= Kp_m(t_l - 2Kt_l^{\frac{1}{2}}/C),$$

whence $$t_{l'} = t_l - 2Kt_l^{\frac{1}{2}}/C \quad (8)$$

Now, if the number of monolayers taken up during the lifetime t_L of the getter is N_m, the number taken up during the $S \propto t^{\frac{1}{2}}$ regime at the start is

$$n = N_mt_{l'}/t_L \quad (9)$$

Formula (9) has been used for computing the values of n given in Table 5. The variation of K with temperature has been ignored, in view of the approximation accepted by assuming the equivalence of (1) and (2), and also of (5) and (7).

REFERENCES

(1) WAGENER, S. *Brit. J. Appl. Phys.*, **1**, p. 225 (1950).
(2) WAGENER, S. *Nature [London]*, **173**, p. 684 (1954).
(3) BLOOMER, R. N. *Nature [London]*, **178**, p. 1000 (1956).
(4) BLOOMER, R. N. *Brit. J. Appl. Phys.*, **8**, p. 40 (1957).
(5) MOTT, N. F. *Trans Faraday Soc.*, **35**, p. 1175 (1939).

(6) MOTT, N. F. *Trans Faraday Soc.*, **39**, p. 472 (1940).
(7) MOTT, N. F. *Trans Faraday Soc.*, **43**, p. 429 (1947).
(8) CABRERA, N. *C.R. Acad. Sci.* [*Paris*], **220**, p. 111 (1945).
(9) CABRERA, N. *Phil. Mag.*, **40**, p. 175 (1949).
(10) CABRERA, N., and MOTT, N. F. *Rep. Progr. Phys.*, **12**, p. 163 (1948).
(11) CABRERA, N., and HAMON, J. *C.R. Acad. Sci.* [*Paris*], **224**, p. 1713 (1947).
(12) CABRERA, N., TERRIEN, J., and HAMON, J. *Comptes Rendus*, **224**, p. 1558 (1947).
(13) EVANS, U. R. *Trans Faraday Soc.*, **41**, p. 365 (1945).
(14) KNUDSEN, M. *Ann. Phys.* [*Leipzig*], **28**, p. 999 (1909).
(15) ARIZUMI, T., and KOTANI, S. *J. Phys. Soc.* [*Japan*], **7**, p. 300 (1952).
(16) BECKER, J. A. *Rev. Mod. Phys.*, **7**, p. 95 (1935).
(17) HERRING, C., and NICHOLS, M. H. *Rev. Mod. Phys.*, **21**, p. 185 (1949).
(18) WRIGHT, D. A. *J. Instn Elect. Engrs*, **100**, Part III, p. 125 (1953).
(19) WRIGHT, D. A. *J. Electronics*, **1**, p. 521 (1956).
(20) RHODIN, T. N. *J. Amer. Chem. Soc.*, **72**, p. 5102 (1950).
(21) VERNON, W. H. J., AKEROYD, E. I., and STROUD, E. G. *J. Inst. Metals*, **65**, p. 301 (1939).
(22) WAGENER, S. *Brit. J. Appl. Phys.*, **2**, p. 132 (1951).

Measurements of the impedance parameters of junction transistors

By E. E. WARD, Electrical Engineering Department, University of Birmingham

[*Paper received* 19 *February*, 1957]

The paper describes with practical details equipment for making null measurements of the earthed-base impedance parameters and of α^1. Measurements on collector open-circuit are included and typical results at frequencies up to 30 kc/s are given.

There are now several sets of parameters in use for predicting the behaviour of transistor circuits, and the present paper describes equipment for measuring the impedance parameters given in the accepted notation by

$$v_1 = i_1 Z_{11} + i_2 Z_{12}$$
$$v_2 = i_1 Z_{21} + i_2 Z_{22}$$

and also for measuring α^1 which is defined as $\alpha^1 = \alpha/(1 - \alpha)$, where $\alpha = Z_{21}/Z_{22}$. To increase the frequency range over which accurate measurements can be made the switching of circuits has been avoided wherever possible and three separate instruments have been built as shown below. In practical technique the most useful and frequent single measurement is of α^1; other measurements are made if needed. Evidently the four impedance parameters and α^1 contain redundant information and afford a check by their agreement.

MEASUREMENT OF α

Since the value of α is close to unity it is best calculated from measurements of $\alpha^1 = \alpha/(1 - \alpha)$ and these have been made by the circuit of Fig. 1, wherein the base current is E/R, the collector current is $-\alpha^1 E/R$, $i_1 = e/R_1$ and $i_2 = -\mathrm{j}EwC$. The condition for a null gives

$$\alpha^1 = \frac{R}{R_1}\left(\frac{e}{E}\right) - \mathrm{j}RwC$$

The resistors R and R_1 are fixed, making $R = 100\ R_1$; thus when the ratio $e/E = 1$ the real part of α^1 is 100. Measurements have been made over the range 1 to 100 kc/s; the transformers are wound on *T* and *U* stampings of high permeability alloy; the assembled cores measure $2 \times 1\frac{3}{16}$ in. and are stacked $\frac{5}{16}$ in. deep; the centre-tapped input winding is wound with twisted twin wire. For frequencies above 5 kc/s an elementary heterodyne detector is used consisting of an anode-bend demodulator and heterodyne oscillator followed by audio amplification.

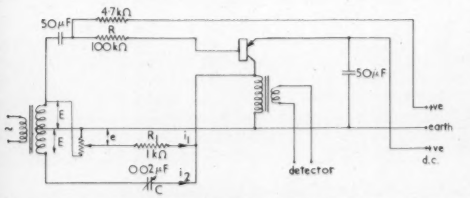

Fig. 1. Measurement of α^1

MEASUREMENT OF Z_{21} AND Z_{11}

In the circuit of Fig. 2 the switches are thrown to position *A*. If Z_x greatly exceeds Z_{11} the emitter current is e/Z_x and the collector e.m.f. is eZ_{21}/Z_x. When the detector current vanishes

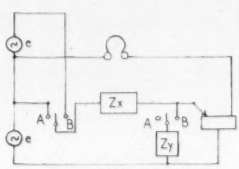

Fig. 2. Measurement of Z_{11} and Z_{21}

this e.m.f. is equal to e and hence $Z_x = Z_{21}$; no current flows in the collector circuit at balance.

The switches are now thrown to positions *B*; the impedance Z_x passes a current $2e/Z_x$ and the emitter current is reduced to its former value by adjusting Z_y for a null. Then at balance $Z_y = Z_{11}$. The alternating collector current at balance is zero.[5]

Fig. 3 shows the practical circuit; it will be seen that the impedance Z_x, which in Fig. 2 is equal to the collector impedance and of the order of several megohms, is replaced by a resistor of 100 kΩ fed from a potential $0{\cdot}1e$ taken from a tapping on the transformer. This is the largest value of standard resistor needed in any of the measurements. Its ratio of length to diameter is great in order to reduce errors

at high frequencies. Great care has been taken in screening the detector transformer; its windings are on brass formers, radially slit to avoid a closed circuit, the earthing connexion being exactly opposite to the slit so that the core is not excited by capacity currents. Stray capacitances are balanced out by the zero adjustment shown. The input transformer has 185

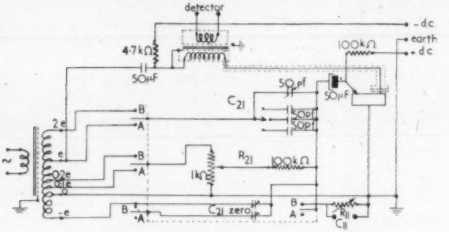

Fig. 3. Circuit of instrument based on Fig. 2

primary turns and is fed from a 600 Ω source; there are 80 secondary turns between the 2*e* connexion and earth; the detector transformer has 550 primary turns and a secondary winding of 55 turns for feeding a 75 Ω cable. The cores are the same as described above.

MEASUREMENT OF Z_{22} AND Z_{12}

In the circuit of Fig. 4 the impedance Z_y is set to zero and at balance $Z_x = Z_{22}$; the emitter circuit is open for alternating currents but a d.c. path is provided.

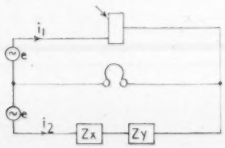

Fig. 4. Measurement of Z_{22}

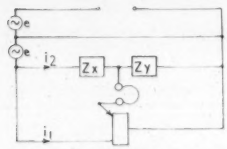

Fig. 5. Measurement of Z_{12}

Z_{12} is measured by the arrangement of Fig. 5, which is a modification of Fig. 4; switches are arranged so that the two may be interchanged instantaneously; in the circuit of Fig. 4, Z_x only is adjusted for balance which occurs when $Z_{22} = Z_x + Z_y$ and $i_1 = i_2$. In Fig. 5, Z_y is varied for balance, which occurs when $i_1 Z_{12} = i_2 Z_y$. Since i_2 is unchanged and i_1 is merely reversed in sign by the interchange of the circuits, they remain equal and $Z_y = Z_{12}$. No current flows in the emitter at balance. This method of measurement can only be used if Z_{22} greatly exceeds Z_{12} as it does in a junction transistor since otherwise the balance conditions of the two circuits seriously interact. With present transistors the effect is small and exact balance of both circuits is normally reached at the second attempt.

The practical circuit is shown in Fig. 6; the principal components have already been described; good screening of

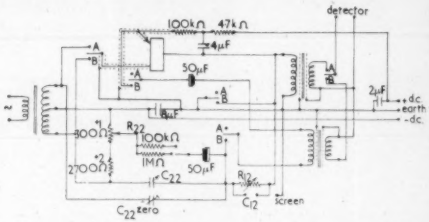

Fig. 6. Circuit of instrument based on Figs. 4 and 5

the emitter and collector leads is needed since stray capacitance currents flowing in the open emitter circuit will cause serious errors at high frequencies.

ACCURACY OF MEASUREMENT

The components of the three instruments were calibrated at 1000 c/s using laboratory standards and showed no variations exceeding 1% over a long period. It is likely that an overall accuracy of a few parts per cent was achieved at this frequency.

Tests have been made to find out how much of this accuracy was lost at higher frequencies; the greatest error was found in the resistive parallel component of Z_{12} which was measured 3·2% low at 250 kc/s, but the components of Z_{21} could not be investigated above 25 kc/s. Supplementary tests were made to reveal interaction due to internal inductance; the measurement of R_{12}, for example, was not noticeably changed at 250 kc/s, when an additional capacitor was added equal to the probable value of C_{12}.

The accuracy of reading is given by the width of the silence zone over which no signal can be heard through the noise of

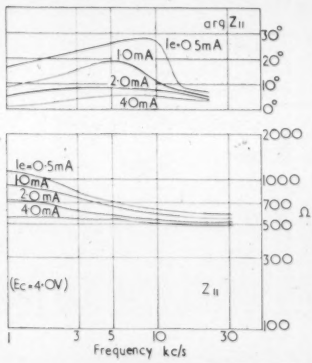

Fig. 7. Measured modulus and argument of Z_{11}

the transistor. At 1000 c/s this was ±3% for the two components of α^1 and ±1·4% for all other components.

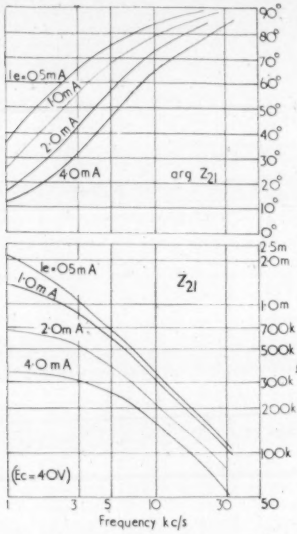

Fig. 8. Measured modulus and argument of Z_{21}

The collector circuit impedance of the circuit of Fig. 2 at balance may be derived from the minimum detectable error signal. For normal noise conditions in the transistor this minimum was about 500 μV in the collector circuit over the range from 1 to 250 kc/s. Since the signal voltage at the collector winding was usually 200 mV, and the collector current was about $0{\cdot}5/Z_{22}$ mA, the effective collector load impedance was therefore close to 400 Z_{22}.

MEASUREMENTS MADE

For a small British transistor of current manufacture (1954), the measured modulus and argument of Z_{11} are shown in Fig. 7; the collector potential was −4·0 V; the curves of Z_{12} were similar. Z_{21} is likewise shown in Fig. 8, and Z_{22} is similar to it.

ACKNOWLEDGEMENTS

The author is glad to acknowledge his debt to the Electrical Engineering Department, The University of Birmingham, to Professor A. Tustin, sometime Head of the Department, and to Mr. J. Gregory, who built and operated the equipment.

REFERENCES

(1) Blumlein, A. D. British Patent No. 581164.
(2) Bousquet, A. G. *General Radio Experimenter*, **27**, No. 10 (1953).
(3) Clark and Vanderlyn. *J. Instn Elect. Engrs*, **96**, Part III, p. 189 (1949).
(4) Tuttle, W. N. *Proc. Inst. Radio Engrs*, **21**, p. 844 (1933).
(5) Ward, E. E. British Provisional Patent 30955/54.

The emission from oxide cathodes in low pressure discharges

By M. A. Cayless, B.Sc., A.R.C.S., A.Inst.P., The British Thomson-Houston Co. Ltd., Rugby

[*Paper received* 25 *January*, 1957]

It is shown that measurements made in vacuum on oxide-coated discharge cathodes are unreliable as a measure of the properties of the cathode in the gas atmosphere of the discharge. Several known methods of measuring the zero-field emission of cathodes in gas atmospheres are found to give rise to difficulties when applied to oxide cathodes in several millimetres pressure of rare gas. A method is described in which these difficulties are avoided and it is applied to a study of cathodes of the fluorescent lamp type. It is found that the zero-field emission of these cathodes at operating temperatures is considerably higher than the thermionic emission measured in vacuum, but still much smaller than the discharge current which they normally pass. It is shown that the various secondary and field emission processes must play a prominent part in the normal operation of these cathodes which, in fact, need not necessarily be particularly good thermionic emitters.

INTRODUCTION

This paper describes work which forms part of an investigation into the way in which oxide cathodes operate in low pressure discharges, particularly those of the fluorescent lamp type. These are usually through mercury rare-gas mixtures at several millimetres pressure and the cathodes often consist of coiled-coil tungsten helices coated with mixtures of the alkaline-earth oxides. Usually a hot-spot forms on the cathode and the discharge is often self-sustaining without any form of auxiliary cathode heating. Other types of cathode can be used, however, e.g. pellets or rods of various sintered materials, and the methods of investigation to be described are not restricted to the more usual type and have proved valuable in assessing the value of experimental kinds.

PRELIMINARY EXPERIMENTS

In a series of preliminary experiments a considerable number of measurements were made of the thermionic emission obtained in vacuum from standard fluorescent lamp cathodes. These were made in the usual way by means of Schottky and Richardson plots obtained from carefully prepared test diodes. The cathodes used were, for the most part, coiled-coil filaments of 0·003 in. diameter tungsten coated with a mixture of barium, strontium and calcium

carbonates in the proportions by weight of 5 : 3 : 2. These were broken down into oxides and activated by heating to temperatures in the range, 1450 to 1600° K, which is frequently used in lamp manufacture.

The emissions obtained in this way were surprisingly poor, and not much variation was found when different processing schedules were used.[1] The following general features were observed:

(*a*) saturated emissions of 1–10 mA at 1000° K for cathodes which normally pass discharge currents of 200–300 mA;
(*b*) work functions, obtained from Richardson plots, of about 1·5 V;
(*c*) considerable slumping of emission when current was drawn at temperatures between 1000 and 1250° K;
(*d*) temporary re-activation when heated above 1250° K, though this could not be repeated indefinitely;
(*e*) somewhat improved re-activation (about twice as much) if current was drawn during (*d*).

Further observations suggested that the inability to obtain fully activated cathodes was because the high temperature (1500–1700° K) necessary to obtain free barium by the tungsten reaction[1, 2]

$$6\,BaO + W \leftrightharpoons Ba_3WO_6 + 3\,Ba$$

resulted in its immediate evaporation.

To reduce this evaporation some cathodes were activated by heating to very high temperatures in a pressure of 3 mm of argon. On re-evacuating, higher emissions at 1000° K were obtained, for example, 16 and 50 mA after activation for 15 s at 1700 and 1900° K respectively. However, continued running at 1000° K resulted in a marked falling-off of the emission with time. At lower temperatures the increased emission was retained for much longer periods. By striking an arc during the activation period the emission could be raised to 100 mA at 1000° K, but again this was only temporary.

These results make it clear that measurements of the emission of these cathodes made in vacuum are an unreliable indication of their behaviour in the discharge. It seems quite possible that the state of the cathode when immersed in the discharge is quite different from that in vacuum. For this reason some measure of the emission capabilities of cathodes under discharge conditions is required.

METHODS OF MEASURING EMISSION IN A GAS

The ordinary diode method cannot be used in the presence of a gas since a discharge occurs at high anode potentials and the current is space-charge limited with all practicable electrode arrangements at low anode potentials. The electronic mean-free-path is less than 0·1 mm in 3 mm pressure of argon and thus it is quite impracticable to keep the anode-cathode spacing below this value.

Several authors have described methods of measuring the emission when there is zero field at the cathode surface by evaporating electrons from the cathode into the plasma of an auxiliary discharge, a procedure which is in some respects equivalent to mounting an anode within the mean-free-path. For example, Found[3] describes two methods which he applied successfully, but both these failed when applied to the cathodes under investigation since the discharge invariably tended to switch from the auxiliary cathode to that under test before the critical point was reached. Furthermore, the auxiliary discharge was clearly distorted by the current taken by the cathode, and Found's analysis is therefore of doubtful validity. A variation of one of these methods due to Koller[4] failed for similar reasons.

Other authors[5, 6] have used an alternative approach in which an anode is mounted a few millimetres away from the cathode and a short discharge (no positive column) passed. The cathode is heated and the current/voltage characteristics of the discharge are measured for various cathode temperatures. At discharge currents less than the thermionic emission of the cathode a retarding field forms at the cathode surface, and at higher currents an accelerating field. The point at which the field is zero at the cathode surface is identified by the behaviour of the characteristic, and the discharge current at this point is the "zero-field emission" of the cathode.

The details of the identification of this "zero-field point" vary, depending on the type of cathode, temperature range, gas pressure, etc., but generally the situation is as shown schematically in Fig. 1. The various parts of the characteristic are accompanied by certain visual appearances and these different modes are shown on the figure. They are described in detail by Malter, Johnson and Webster.[7] Between *A* and *B* the visible glow is confined to a thin layer at the anode surface; between *B* and *C* the glow moves out into the inter-electrode space as a detached "ball of fire" and the voltage falls to a low value; at *C* the glow envelops the cathode, but there is usually a visible dark space between *C* and *D* (compare [8]); at *D* the current passes the zero-field value and an accelerating field develops at the cathode, marked by an increase in the voltage *DE*; at *E* a hot-spot forms on the cathode and the voltage again falls, this mode of discharge usually being referred to as an arc. Sometimes discontinuities are observed at the transition points, but if a sufficiently large ballast resistance is employed the whole characteristic can be observed for a considerable range of cathode temperatures.

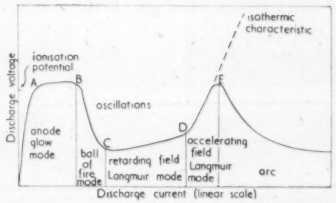

Fig. 1. Schematic characteristic of hot cathode discharge

The method usually employed is to identify the point *D* at which the voltage begins to increase. This point will move (schematically) along the characteristic *BCD* and its extension as the cathode temperature is increased (see[6] for example). Johnson and Webster[9] employ a slightly different method, identifying a point at which the emission is half that at *D*.

The zero-field emission is higher than the temperature limited (zero-field) thermionic emission because other factors also contribute to the discharge current. Possible components are:

(*a*) zero-field thermionic emission;
(*b*) positive ion current;
(*c*) secondary emission by positive ions;
(*d*) secondary emission by metastable atoms;
(*e*) photoelectric emission;
(*f*) emission of negative ions.

However, the positive ion current (*b*) is a small fraction of the electron current at the zero-field point because of the space-charge relation in the cathode sheath.[10] Hence the component (*c*) is also likely to be small. The magnitudes of (*d*), (*e*) and (*f*) are unknown but unlikely to be very large. When the field becomes accelerating, as the current increases, the positive ion current increases rapidly[3, 10] and hence (*c*) also. (*d*) and (*e*) may also become more prominent because of increased excitation in the neighbouring part of the discharge. There is, in addition:

(*g*) field enhanced thermionic emission caused by the Schottky and, with oxide cathodes, other effects.[11]

The zero-field emission is, nevertheless, a valuable guide to the behaviour of a cathode in a discharge, in some respects as useful as the thermionic emission, to the value of which it sets an upper bound.

MEASUREMENTS WITH OXIDE-COATED CATHODES

With oxide-coated cathodes in pressures of the order of a few millimetres of rare gas the identification of the zero-field point on the characteristic is more difficult. Druyvesteyn and Warmoltz[5] obtained useful results, but at lower pressures. At the higher pressures the point *D* becomes difficult to identify and does not appear to coincide with the visual changes described above. Pengelly and Wright[6] state that oxide cathodes were unstable in their "first mode," which is near the zero-field point. Oscillations in the region *BD*, of sometimes as much as 15 V, make the characteristic more indeterminate. They also mask the half-way point used by Johnson and Webster[9] who used non-oscillatory discharges in helium.

A detailed study was therefore made of short discharges in 3 mm argon with oxide-coated tungsten coiled-coil cathodes of the type described in the first section. The anode was usually a 13 mm square of tantalum mounted 10 mm from the cathode. Experiments with movable anodes showed this to be a suitable distance, the voltage increasing regularly and linearly as the distance was increased from 1 mm to a point between 10 and 20 mm, when a Faraday dark space formed and large irregular variations occurred. The discharges were run from a 250 V supply and a large resistive ballast.

It was found that the characteristics of these cathodes differ from Fig. 1, taking the form shown in Fig. 2 when the cathode is heated to a moderate temperature. The characteristic shown is one in which the various transition points are particularly clear.

Starting at low currents, the anode glow and ball of fire modes occur as previously described. There is, however, no sharp transition point between the latter and the retarding field Langmuir mode, but the ball gradually moves towards the cathode and envelops it as the discharge current is increased until it completely surrounds it, there being a visible dark space of one or two millimetres width. Near the point *D* the glow suddenly shrinks on to the cathode surface, the dark space disappearing and the glow having a characteristic appearance of "pinching" the cathode. Frequently the glow changes colour at the same time. The unsymmetrical oscillations occurring between *B* and *D* are shown by the broken lines, obtained with a d.c. oscilloscope. The minimum *C* has no particular significance, the characteristic in this region being only the mean voltage registered by the moving coil meter. The oscillations grow smaller and more sinusoidal on approaching *D* and disappear on reaching it.

Between *D* and *E* the glow shows an increasing tendency to concentrate at a particular region of the cathode until at *E* hot-spots form and the voltage drops as the discharge becomes an arc. The dependence of this transition on the heating of the cathode by the discharge is shown by the dotted line, which was obtained by passing current pulses, of 10^{-4} s duration, from a thyratron switching circuit, which were

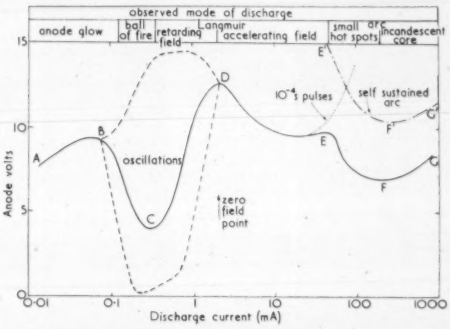

Fig. 2. Typical observed characteristic with oxide cathode. Triple oxide on tungsten coiled-coil cathode at 900° C in 3·1 mm argon. Voltage across cathode 7·8, anode cathode separation 0·8 cm. (The anode volts appear low in this case because of the high cross-cathode voltage)

——— characteristic obtained with moving coil meters.
– – – – amplitude of oscillations observed with d.c. oscilloscope.
..... characteristic of 10^{-4} s pulses.
—·—·— characteristic of self-sustained arc.

insufficient to heat the cathode. Furthermore, the discharge is self-sustaining in the region *EFG*, the characteristic being *E'F'G'* when no heating current is supplied to the cathode. In this case, if the discharge current is decreased below that at *E'* the voltage increases rapidly and the discharge becomes a glow discharge.

With this particular kind of cathode two distinguishable types of arc operation occur. Between *E* and *F* heating is mainly by bombardment and tiny hot spots form on the oxide surface, frequently pulsating regularly or "dancing" from one place to another. At currents above *F* the whole core of the cathode becomes incandescent as the ohmic heating by passage of the arc current becomes the dominating factor. Self-sustained lamp cathodes usually operate near the point *F'*.

The point near *D* at which the glow shrinks on to the cathode is taken as the zero-field point separating the two types of Langmuir mode. Fig. 3 shows how this point moves as the cathode temperature is changed. The disappearance of oscillations near this point [compare refs. (7) and (12)] and the fact that the zero-field emission measured in this way varies exponentially with inverse temperature (see next section) support this interpretation. Further theoretical reasons are given in a later section.

The decrease in voltage between *D* and *E* is most interesting. This is in direct contrast to the increase shown by other types of cathode (Fig. 1). That it is associated with secondary processes (listed above) is demonstrated by comparing Fig. 3

with Fig. 4, which show curves obtained with cathodes made with identical tungsten coils coated with triple alkaline-earth oxides and lanthanum hexaboride respectively, the latter having properties which lie between those of the oxides and pure metals.[12] In Fig. 4 the dip is not nearly so pronounced

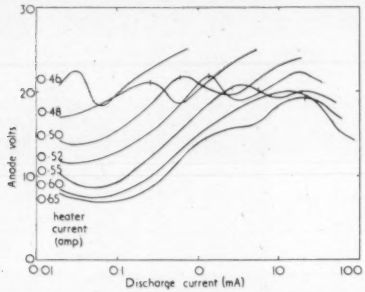

Fig. 3. Characteristics of oxide cathode 39A

The intersections on Figs. 3 to 6 show the visually observed zero-field points.

and is soon followed by the rapid increase in voltage found with pure metals. Tungsten, for example, shows no sign of a dip at this point, the voltage increasing at once, as in Fig. 1. Poorly emitting and poisoned oxide cathodes have characteristics similar to those in Fig. 4.

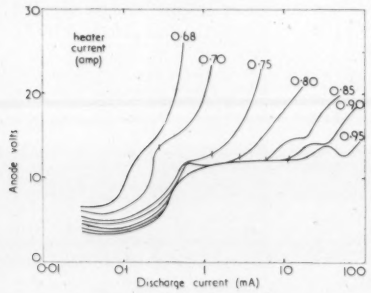

Fig. 4. Characteristics of boride cathode 40A

Among the many kinds of cathode examined in this way, only those in which the voltage remains low even when the cathode temperature is such that D is well separated from E (by a decade or more of current) have been found suitable for use as self-sustained lamp cathodes. This is interpreted as meaning that the secondary properties must play a prominent part in the functioning of these cathodes. Much further work on these properties is required for a fuller understanding of the part they play.

As Fig. 3 demonstrates, the zero-field point does not always occur exactly at the point D of Fig. 2, and in practice it is found possible to locate the point more accurately by passing a fixed discharge current (more accurately, by using a constant ballast resistance) and varying the filament temperature by means of the auxiliary heating current. The resulting characteristics are shown in Figs. 5 and 6 which correspond to Figs. 3 and 4 respectively. The points at which the glow shrinks on to the cathode are shown by short intersections and the discharge currents shown are those measured at these points. They appear near the minimum at low discharge currents, but move towards the maximum at higher currents. In the former case the voltage increases rapidly after the minimum is passed and the discharge soon becomes

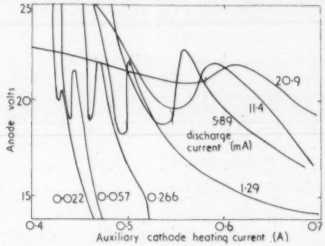

Fig. 5. Constant current characteristics of oxide cathode 39A

The discharge currents shown on Figs. 5 and 6 are those measured at the zero-field point.

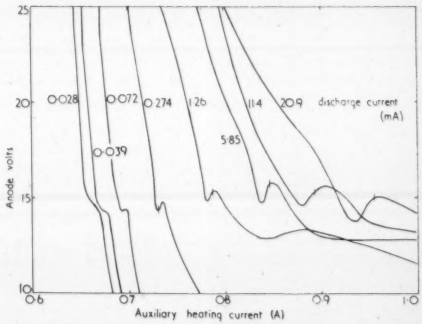

Fig. 6. Constant current characteristics of boride cathode 40A

a glow discharge, but if the current is high enough the voltage will remain low, forming a self-sustaining arc. The explanation of the maximum and minimum awaits a more detailed theory of the discharge, but the movement of the zero-field point towards the maximum is probably caused by the increasing part played by the secondary processes as the current is increased. In making measurements it is convenient to observe the visual change to identify the zero-point at the higher currents, and to use the minimum at low currents when the glow is not easily seen: measurements show that this is usually justified.

COMPARISON WITH VACUUM EMISSION

In a large number of experiments the zero-field emission has been measured as described in the last section and compared with the vacuum emission measured immediately before or afterwards. Cathode temperatures were measured with an optical pyrometer in preliminary experiments for different

values of the heating current, both with and without gas. No corrections were made for emissivity. Fig. 7 shows a typical comparison in the form of Richardson lines for the fluorescent lamp cathode used to obtain Figs. 3 and 5. To avoid difficulties presented by the voltage drop along the cathode, which is quite high with this type, only a section of the whole cathode was used, the large secondary coiling being pulled straight.

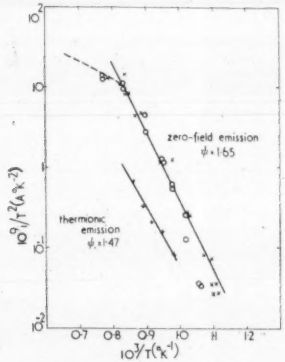

Fig. 7. Richardson lines for oxide cathode 39A

× Points from constant temperature characteristics.
○ Points from constant current characteristics.
+ Points from vacuum measurements.

The values of ψ shown in Figs. 7 and 8 are the apparent work functions of the lines shown. The units of the ordinates are equal to the emission current in milliamperes when $T = 1\,000°$ K.

The zero-field emission is seen to be about an order of magnitude higher than the vacuum emission. The apparent work functions are comparable, though it is doubtful whether much meaning can be attached to them. Not all cathodes showed such a good comparison over the entire range, but usually agreement was good in the centre two decades, and most irregularities could be accounted for by difficulties in locating the points at the ends. In addition there was always a systematic discrepancy at high currents which is indicated by the broken curve in Fig. 7, and which is due to the point D approaching point E (Fig. 2). This is discussed in the next section.

The difference between the vacuum and zero-field emissions is attributed largely to the comparatively large secondary effects occurring with oxide cathodes. Fig. 8 shows comparable Richardson lines obtained from the lanthanum boride cathode used for Figs. 4 and 6. Here the difference is much smaller, compatible with smaller secondary effects, and the work functions are in close agreement with each other and the published value.[13]

Repeated determinations of the Richardson lines made alternately in vacuum and in gas with the same cathode, showed variations which could be ascribed to changes in the cathode structure, for example, by barium evaporation in vacuum. These variations were smaller in the case of the more stable boride cathodes. Similar experiments carried out with pure tungsten cathodes have revealed small systematic variations, probably attributable to changes in the surface of the tungsten under bombardment.

Although the zero-field emission of the oxide cathodes is some ten times greater than the thermionic emission measured in vacuum, it is still considerably less than the discharge current at which they normally operate, when heated to a comparable temperature. This again emphasizes the importance of the secondary processes in the running of the discharge. It is not, in fact, essential that a cathode should have a particularly good thermionic emission to ensure good performance.

Cathodes which were made to provide good thermionic emission in vacuum (well activated O-nickel based cathodes) were found to give comparably high zero-field emission in the discharge, but were rather erratic and quickly deactivated if operated for long with accelerating fields and under the consequent bombardment. If the coating was not completely destroyed reactivation would occur on changing back to a retarding field.

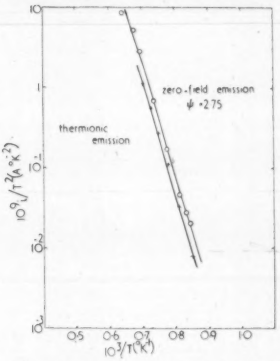

Fig. 8. Richardson lines for boride cathode 40A

○ Points from constant current characteristics.
+ Points from vacuum measurements.

BEHAVIOUR OF THE CATHODE SHEATH

In order to understand the visible changes which occur in the transition from retarding to accelerating fields it is necessary to consider the situation in the space charge sheath in front of the cathode.

There are two cases, in which the sheath thickness is (*a*) much less than, and (*b*) much greater than the mean-free-paths λ_e, λ_p of the electrons and ions in the gas. It is sufficient to consider here the case of a plane cathode, emitting an electron current density j_e, and to which flows a positive ion current density j_p. In what follows m_e, m_p, μ_e, and μ_p are the molar masses and the mobilities of the electrons and ions respectively, V is the potential drop across the sheath and its thickness. All the relations are given in practical units.

In case (*a*) we have the Langmuir relation

$$d_s^2 = 5{\cdot}462 \times 10^{-8} V^{3/2} j_p^{-1} m_p^{\frac{1}{2}} L \quad \text{cm}^2 \qquad (1)$$

where L is a factor which varies between 1, when $j_e = 0$ (single sheath) and 1·8605 for $j_e m_p^{\frac{1}{2}} = j_p m_e^{\frac{1}{2}}$, when the field is zero at the cathode (double sheath).[10]

In case (*b*) an easy integration of Poisson's equation, assuming negligible field at the plasma edge gives

$$d_m^3 = 0{\cdot}995 \times 10^{-13} \frac{\mu_e \mu_p}{\mu_e j_p - \mu_p j_e} V^2 \quad \text{cm}^3 \qquad (2)$$

[This equation is incorrectly quoted by Druyvesteyn and Penning as their equation (88), p. 128 of ref. (14).] Thus in this case d varies between a finite value d_{mp} when $j_e = 0$ to an indefinitely large value as $\mu_p j_e$ approaches $\mu_e j_p$, and the field tends to zero at the cathode.

In the case of argon at 3 mm pressure and $V = 10$ V, values of the quantities (estimated from kinetic theory and experimental data) are $\lambda_p = 1{\cdot}7 \times 10^{-3}$ cm, $\lambda_e = 10^{-2}$ cm, $\mu_p = 10^3$ and $\mu_e = 2 \times 10^5$ cm^2 s^{-1} V^{-1}. Values of d given by equations (1) and (2) using these values are shown in Fig. 9 as functions of j_p. (A more realistic approach to the motion of positive ions[15] leads to much more complicated equations, which yield the same main conclusions, however.)

Most of the measurements are performed in the region where assumption (*b*) is valid. The wide dark space when the cathode field is zero or retarding corresponds to the condition $\mu_e j_p = \mu_p j_e$ [compare ref. (8)], its size being limited to the few millimetres observed by considerations other than those dealt with here. As soon as the discharge current exceeds the zero-field value the positive ion current increases, (2) becomes finite and the sheath shrinks to a small fraction of a millimetre. For example, under the conditions of the above example, if the zero-field emission is 20 mA, an increase in discharge current to 21 mA will result, according to (2), in the dark space shrinking to about 0·02 cm if field emission and the increased influence of secondaries is ignored.

At high zero-field emissions it is possible for the discharge to function under conditions (*a*) (see Fig. 9). This tendency

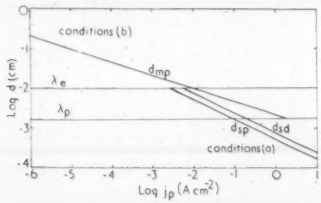

Fig. 9. Thickness of cathode sheaths and mean-free-paths in 3 mm argon

λ_e, λ_p: Electronic and ionic mean-free-paths;
d_{sp}: Thickness of ionic single sheath, $d > \lambda$;
d_{sd}: Thickness of double sheath, $d > \lambda$;
d_{mp}: Thickness of ionic single sheath, $d < \lambda$;
The thickness of the double sheath when $d < \lambda$ is indefinitely large.

is accelerated by the formation of hot-spots, which provide the required current density, and occurs when the point *D* of Fig. 2 approaches the point *E*. This results in the anomaly mentioned earlier and indicated on Fig. 7, and in these circumstances this method of measuring the zero-field emission is inapplicable.

The discharge in the region *DE* is thus shown to be in the Langmuir mode with an accelerating field and a space-charge sheath wider than the mean-free-paths. The change to the arc is characterized by the space-charge sheath becoming smaller than the mean-free-paths as a result of hot-spot formation. Conversely the hot-spots are maintained by the increased energy of bombardment resulting from the ions being unimpeded by collisions in the sheath. Thus there is a complementary relationship between sheath width and hot-spot formation, which has wide implications. This will be discussed in another paper.

DISCHARGES IN MERCURY AND RARE-GAS MIXTURES

Although the experimental results quoted in this paper have been obtained with discharges in pure argon, the addition of mercury, or the use of another rare gas, makes little difference and the method is equally applicable. Results obtained when mercury was present are qualitatively the same as those discussed above, only the potentials and light output being changed.

CONCLUSIONS

A method has been evolved for measuring the zero-field emission of discharge cathodes which is particularly suitable for oxide-coated types in a few millimetres of rare gas, avoiding the difficulties which occur in this case when basically similar methods are used.

It is shown that the zero-field emission of oxide cathodes of the fluorescent lamp type, although higher than the thermionic emission by a factor of up to ten, is still considerably smaller than the discharge current at which they normally operate at comparable temperatures. Both these differences are largely due to the various processes of field and secondary emission, which are shown to be particularly prominent in the case of oxide cathodes. The elucidation of the parts played by these processes presents a wide field for further research.

The visual change which takes place in the neighbourhood of the cathode when the field changes from retarding to accelerating is satisfactorily explained in terms of the simple theory of space-charge sheaths.

ACKNOWLEDGEMENTS

The author is indebted to his colleagues at the Research Laboratory of the British Thomson-Houston Co. Ltd. for many helpful discussions and, in particular, to Miss A. D. Forster-Brown who has carried out many of the experiments.

REFERENCES

(1) Cayless, M. A., and Watts, B. N. *Brit. J. Appl. Phys.*, **7**, p. 351 (1956).
(2) Hughes, R. C., Coppola, P. P., and Evans, H. T. *J. Appl. Phys.*, **23**, p. 635 (1952).
(3) Found, C. G. *Phys. Rev.*, **45**, p. 519 (1934).
(4) Koller, L. R. *Physics*, **7**, p. 225 (1936).
(5) Druyvesteyn, M. J., and Warmoltz, N. *Physica*, **4**, p. 41 (1937).
(6) Pengelly, A. E., and Wright, D. A. *Brit. J. Appl. Phys.*, **5**, p. 391 (1954).
(7) Malter, L., Johnson, E. O., and Webster, W. M. *R.C.A. Rev.*, **12**, p. 415 (1951).
(8) Druyvesteyn, M. J., and Warmoltz, N. *Physica*, **4**, p. 51 (1937).
(9) Johnson, E. O., and Webster, W. M. *R.C.A. Rev.*, **16**, p. 82 (1955).
(10) Langmuir, I. *Phys. Rev.*, **33**, p. 954 (1929).
(11) Wright, D. A., and Woods, J. *Proc. Phys. Soc. B*, **65**, p. 134 (1952).
(12) Eckart, C., and Compton, K. T. *Phys. Rev.*, **24**, p. 97 (1924).
(13) Lafferty, J. M. *J. Appl. Phys.*, **22**, p. 299 (1951).
(14) Druyvesteyn, M. J., and Penning, F. M. *Rev. Mod. Phys.*, **12**, p. 140 (1940).
(15) Sena, L. *J. Phys. USSR*, **10**, p. 179 (1946).

The spectral reflectivity of back-surface and front-surface aluminized mirrors

By G. G. TWIDLE, M.Sc., A.R.C.S., Light Division, National Physical Laboratory, Teddington, Middlesex

[*Paper received* 22 *February*, 1957]

Results are given of a determination of spectral reflectivity of back- and front-aluminized quartz mirrors in the wavelength-range 0·25–1·35 μ. A résumé is given, including reference to other recent work on front-surface mirrors, showing what are thought to be the highest values of reflectivity obtainable over the range 0·1–12 μ. The technical precautions necessary for the attainment of these optimum values are discussed in practical terms.

1. INTRODUCTION

The general technique for producing evaporated aluminium mirrors for optical instruments is now well known. Several original papers are available giving measured values of the front surface reflectivity and also, in some cases, the optical constants of the aluminium films. There is, however, little information on the reflectivity of back-surface mirrors and the factors which may influence it. With but few exceptions the published values of front-surface reflectivity have been expressed in the form of small-scale graphs which cannot be read very accurately and, further, there has been no serious attempt to systematize all the available information and to present it in a self-consistent form, showing the best values of reflectivity over the widest possible spectral range.

The measurements of back reflection described in the present paper were required for assessing the maximum optical transmission likely to be obtainable for a quartz double-monochromator having six back-reflecting mirror surfaces, fairly accurate values of reflectivity therefore being necessary. It was thought useful to extend the work to include also a measurement of front-surface reflectivity over the wavelength range envisaged, namely 0·25 to 1·3 μ, and to attempt to collate the results with the other published figures.

2. PREPARATION OF MIRRORS

Several experimental mirrors were prepared using, as a base, fused quartz plates about 2 mm thick. They had been supplied by the manufacturer with the standard plate-glass finish. Some of the plates were cleaned in Teepol solution followed by distilled water, and others in concentrated nitric acid, concentrated potassium hydroxide solution and dilute nitric acid in succession, interspersed by rinses in distilled water. While in the solutions the plates were rubbed with clean cotton wool, and were finally dried with cotton wool and well-washed cotton material. They were further subjected to the normal high-voltage discharge while in the evaporation chamber at backing-pump pressure.

Aluminium of 99·99% purity was evaporated from a spiral of 0·7 mm diameter tungsten wire. The spiral was previously cleaned in the usual way and loaded under vacuum with as much aluminium as it would take. This quantity was considerably in excess of that required for the mirror deposition. The quartz plates were set to face the source squarely at distances of either 8 or 13 cm so that two corresponding thicknesses of deposit were obtained from a single evaporation. The thicknesses of aluminium deposited, found from the weight and the bulk value of the density, were approximately 0·07, 0·15 and 0·38 μ. The evaporation time for the last two thicknesses was about 30 s and for the first, on a separate run, 15 s with the plate at the 13 cm distance. At a thickness of 0·07 μ the aluminium was just transparent to the light from the source at the end of the evaporation period, while the thicker films were opaque. No shutter was used except for one of the mirrors of intermediate thickness, where an electro-magnetically operated shutter protected the quartz plate from the initial stream of vapour.

The finished mirrors were not protected from the air although they were kept in a desiccator while awaiting measurement.

3. MEASUREMENT OF REFLECTIVITY

The spectral reflectivity of each mirror was measured using the apparatus shown in Fig. 1. Radiation from the exit slit *S* of a double monochromator was brought to a focus on one element of a Hilger–Schwarz linear compensated thermopile,

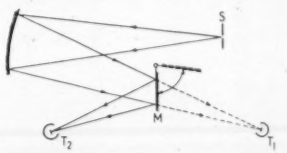

Fig. 1. Apparatus for measuring spectral reflectivity of each mirror

S, Exit slit of monochromator; M, mirror under investigation; T_1 and T_2, Hilger–Schwarz linear compensated vacuum thermopiles.

T_1. The mirror under investigation, *M*, could be swung into the beam so that after reflection the image of the slit *S* was formed on one element of a similar thermopile T_2. The angle of incidence at the mirror was about 20° for which the reflectivity for unpolarized light is not significantly different from that for normal incidence.

The ratio of the sensitivities of the thermopiles at each wavelength was found both by direct comparison and also from two sets of observations on the same mirror, for one of which the thermopiles were interchanged.

A mercury lamp was used to provide spectral-line radiation over the spectral range 0·2484 to 1·357 μ, with a tungsten strip-filament lamp to fill in from 0·60 to 0·95 μ.

When the beam of radiation is reflected from the back of the mirror, multiple images are formed due to inter-reflections within the quartz plate. However, their relative displacement caused by the oblique incidence enabled the image produced by a single reflection at the quartz–aluminium interface to be selected by the narrow thermopile target, thus making correction for the effects of front surface reflection and absorption in the quartz simpler and more certain. Allowance for these was made by the use of refractive index data and independently

measured transmission values for the unaluminized plates, so that the final results, in the case of back reflection, represent simply the reflectivity of the quartz–aluminium interface.

4. RESULTS

A total of seven mirrors was measured for back reflection. The results for two were rejected on grounds of internal inconsistency. Results for the remaining five exhibited an extreme spread of not more than 1% at any one wavelength in the spectral range 0·37 to 1·35 μ. Towards the farther ultraviolet differences steadily increased to a range of about 8% at 0·25 μ. The scatter of observations here appeared largely random. There were some systematic differences between different specimens, but these could not be correlated with any known features. In particular, there was no correlation with the method of cleaning the quartz or with the thickness of the aluminium. The mean results for these five mirrors are therefore taken, and are shown by the encircled points in Fig. 2. The representative curve drawn through them disregards the high values near 0·25 μ, for which the available radiation intensity was much lower than elsewhere, and the experimental error correspondingly higher. However,

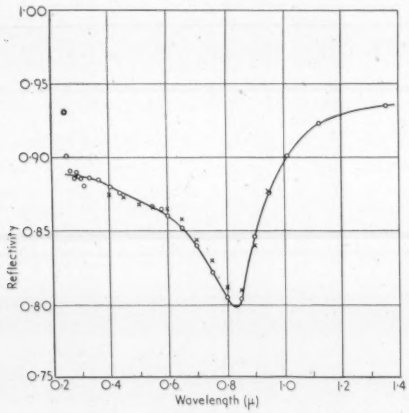

Fig. 2. Back-surface reflectivity. This curve shows the reflectivity of the aluminium–quartz interface

○ indicates the mean values of results for five mirrors.
× indicates values calculated from the optical constants given by Schultz[1] and Schultz and Tangherlini.[2]

the possibility that these high values have a real significance must not be overlooked. The five mirrors measured included the one screened by a shutter at the start of the coating process. The curve for this mirror did not differ appreciably from the mean curve shown in Fig. 2.

The same seven mirrors were measured for front reflection, and no result was rejected. Again, the extreme values of reflectivity at any one wavelength in the range 0·37 to 1·35 μ differed by only a small amount, never more than 1·5%. Differences again increased steadily from 0·37 to 0·25 μ, but in contrast with the back-surface reflectivity, the values of front-surface reflectivity in this spectral region showed a predominantly systematic dependence upon the thickness of the aluminium film. The greater the thickness the lower was the ultraviolet reflectivity. The method used to clean the quartz base was without influence on the results.

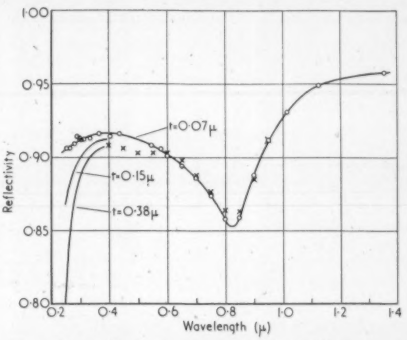

Fig. 3. Front-surface reflectivity. This curve shows the reflectivity of an aluminium film 0·07 μ thick

○ indicates the measured values.
× indicates values calculated from the optical constants given by Schultz[1] and Schultz and Tangherlini.[2]
t = thickness.

The highest reflectivity was shown by the just transparent 0·07 μ thick film and these maximum values are shown in Fig. 3. The decreasing values in the ultraviolet associated with the two greater thicknesses are also shown, each based on the average of three mirrors.

The final adopted values of both front and back spectral reflectivity are given in full in the table.

Spectral reflectivity of evaporated aluminium on fused quartz

Wavelength (μ)	Reflectivity: Back surface (Mean of five mirrors)	Reflectivity: Front surface (For a 0·07 μ thick film)
0·2482	(0·937)	—
0·2537	0·901	0·906
0·2653	0·891	0·906
0·2804	0·886	0·909
0·2894	0·890	0·914
0·2968	0·887	0·913
0·3022	0·886	0·912
0·3132	0·881	0·912
0·3342	0·886	0·913
0·3650	0·885	0·916
0·4047	0·880	0·914
0·4358	0·876	0·916
0·5461	0·867	0·908
0·5780	0·865	0·906
0·6000	0·860	0·901
0·6500	0·852	0·894
0·7000	0·840	0·886
0·7500	0·822	0·874
0·8000	0·805	0·858
0·8500	0·804	0·859
0·9000	0·846	0·888
0·9500	0·876	0·912
1·0140	0·901	0·931
1·1287	0·923	0·949
1·3570	0·935	0·958

5. DISCUSSION AND CONCLUSIONS

The author has discovered no published data on the back-reflecting properties of aluminium films on quartz with which to compare the present values. The consistency of these latter in the visible and infra-red suggest that they are reliable optimum values. The largely random nature of the spread of results in the ultra-violet makes it unsafe to deduce that higher values than those shown by the mean curve of Fig. 2 are really attainable. However, with the exception of doubtful values at about 0·25 μ, it is considered that the mean curve shown can be taken as representative to within $\pm 2\%$ or less, in the ultra-violet range, and $\pm 0{\cdot}5\%$ elsewhere.

The explanation of the spread in the ultra-violet is not certain, but may well be connected with optical scattering associated with slightly different states of polish of the quartz plates which, as has been mentioned, were only of plate-glass quality. It is notable that effects due to possible contamination of the initial deposit, for example by the formation of oxide, were absent and also that it proved immaterial which of two orthodox methods was used to clean the quartz base.

Values for the visible and near infra-red have been calculated from the optical constants as found by Schultz[1] and Schultz and Tangherlini[2] and are shown by crosses in Fig. 2. The agreement is satisfactory.

The full curve shown in Fig. 3 is probably the maximum attainable front-surface reflectivity to within the limits stated. Hass[3] has given rather small-scale graphs showing slightly higher values in certain regions of the spectrum for a mirror made by a higher rate of evaporation than that used here, but the differences are small. Hass also clearly shows the deleterious effect of too slow a rate of evaporation, an effect that has been known qualitatively for some time and was avoided as far as possible in the present work.

The decrease in ultra-violet reflectivity with increasing thickness is almost certainly due to increasing granulation and consequent increase in scatter, although Hass, Hunter and Tousey[4] have published results, during the course of the present work, showing that this effect is greatly reduced by still faster coating, giving opaque films in as short a time as 2 s. Under these conditions they claim no adverse effects up to an aluminium thickness of 0·6 μ, even in the vacuum ultra-violet. It is unlikely, however, that the reflectivity is measurably influenced by scattering at any wavelength longer than about 0·2 μ, under our conditions of evaporation, provided the aluminium thickness is limited to the range 0·07 to 0·1 μ. Confirmation over part of the range is again given by the optical constants found by Schultz[1] and Schultz and Tangherlini,[2] which give the values shown by crosses in Fig. 3.

The graph shown in Fig. 4 is compiled from the present results together with far ultra-violet values given by Banning,*[5] Purcell[6] and Hass, Hunter and Tousey[4] and infra-red values given by Beattie†[7] and shows the general concordance of the more recently obtained values of front surface reflectivity over the wavelength range 0·1 to 12 μ.

The technical conclusions are that for *back-surface mirrors* orthodox cleaning of the base is sufficient, while the best optical polish is obviously desirable. The rate of evaporation should be such as to give a just opaque film in less than 20 s, at a pressure of less than 10^{-4} mm of mercury. Thickness of the film, above opacity, is without effect, while shuttering at the beginning of deposition was not found to be necessary under these conditions. For *front-surface mirrors* the same conditions are satisfactory provided that the film thickness is limited to 0·07 to 0·1 μ for highest reflectivity in the nearer ultra-violet. Considerably faster rates of evaporation are necessary to get good results in this region with thicker films, and particularly to get optimum performance in the vacuum ultra-violet. The long-term adhesion of the aluminium to the base may well be affected by the method used to clean the base, but this aspect of the general problem did not arise in the work reported here and was not investigated. It is merely noted that no obvious deterioration, from blistering for example, has taken place in the nine months since the mirrors were prepared.

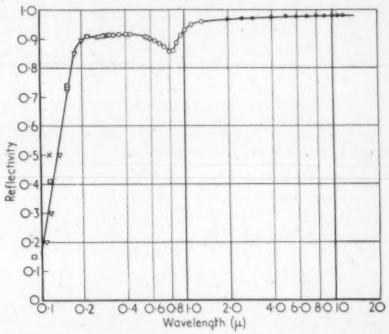

Fig. 4. Reflectivity of an opaque or nearly opaque evaporated aluminium film over the spectral range 0·1–12 μ, compiled from the following sources:

○ Present results.
● Beattie.[7]
□ Hass, Hunter and Tousey.[4]
▽ Banning.[5]
× Purcell.[6]

ACKNOWLEDGEMENT

The work described above has been carried out as part of the research programme of the National Physical Laboratory and this paper is published by permission of the Director of the Laboratory.

Note added in proof. Further results given by Hass, Hunter and Tousey [*J. Opt. Soc. Amer.*, **46**, p. 1009 (1956)] for the reflectivity of front-surface aluminium mirrors in the vacuum ultra-violet are in accord with the curve given in Fig. 4.

REFERENCES

(1) SCHULTZ, L. G. *J. Opt. Soc. Amer.*, **44**, p. 357 (1954).
(2) SCHULTZ, L. G., and TANGHERLINI, F. R. *J. Opt. Soc. Amer.*, **44**, p. 362 (1954).
(3) HASS, G. *J. Opt. Soc. Amer.*, **45**, p. 945 (1955).
(4) HASS, G., HUNTER, W. R., and TOUSEY, R. *J. Opt. Soc. Amer.*, **46**, p. 369 A (1956).
(5) BANNING, M. *J. Opt. Soc. Amer.*, **32**, p. 98 (1942).
(6) PURCELL, J. D. *J. Opt. Soc. Amer.*, **43**, p. 1166 (1953).
(7) BEATTIE, J. R. *Phil. Mag.*, **46**, p. 235 (1955).

* Read from results given graphically.
† This author also gives the corresponding optical constants.

Determination of the impurity concentrations in a semiconductor from Hall coefficient measurements

By P. A. Lee, B.Sc., Ph.D., A.Inst.P., The British Thomson-Houston Co. Ltd., Rugby

[*Paper received* 26 *February*, 1957]

The equation is derived for the carrier concentration as a function of temperature and the concentrations of the acceptors and donors in a semiconductor. As a result, it is shown how these impurity concentrations may be found experimentally from a determination of the Hall coefficient as a function of the temperature. These methods are applied to the case of *p*-type silicon which is dealt with in some detail.

Much interest has been shown in recent years in developing methods for analysing the impurity concentration in semiconductors and in particular in germanium and silicon, e.g. radiochemical[1] and mass spectrometer techniques.[2] These semiconductors may now be produced with impurities which are well beyond the limit of detection of most of these methods and it is necessary to resort to the measurement of the Hall coefficient as a means of analysis. Several authors have given the results of their analysis of the impurity concentrations in semiconductors from the measurement of the Hall coefficient as a function of the temperature.[3,4] This technique has been used in this Laboratory for some time for studying semiconductors and it is shown here how this analysis may be most conveniently carried out.

In an extrinsic semiconductor the carrier concentration is a function of both the temperature and also the impurity concentration which may consist of both donors and acceptors. This function is derived here for a *p*-type semiconductor where the acceptor concentration is in excess of the donor concentration, but the calculations apply equally to an *n*-type semiconductor with an obvious interchange of parameters.

Semiconductor with both donors and acceptors

We will assume the conventional case where the donor impurity level is near to the conduction band and the acceptor impurity level close to the valency band. We assume furthermore that the donors are fully ionized and thus the concentration of holes p is given by the mass action relation:

$$pN_A^-/N_A^\times = K_A \tag{1}$$

where N_A^- is the number of ionized acceptors per cubic centimetre, $N_A^\times$ the number of neutral acceptors per cubic centimetre, and K_A the equilibrium constant.

From statistics we know that

$$K_A = (2\pi m^* kT/h^2)^{3/2} \exp(-E_A/kT) \tag{2}$$

where m^* is the effective mass of a hole, and E_A the ionization energy of acceptors.

If N_A is the total number of acceptors per cubic centimetre, then

$$N_A = N_A^- + N_A^\times \tag{3}$$

and if N_D is the total number of donors per cubic centimetre, then for neutrality:

$$p = N_A^- - N_D \tag{4}$$

From equations (1), (3) and (4) it follows that:

$$p = \left(\frac{K_A + N_D}{2}\right)\left\{\left[1 + \frac{4K_A(N_A - N_D)}{(K_A + N_D)^2}\right]^{\frac{1}{2}} - 1\right\} \tag{5}$$

This is the equation that we require and holds from very low temperatures up to temperatures where the intrinsic properties of the semiconductor start to predominate over the extrinsic properties. For convenience we may consider two distinct regions.

(i) At high temperatures where all the impurities are ionized we have:

$$K_A \gg N_A \quad \text{and} \quad K_A \gg N_D$$

and therefore it follows that:

$$\frac{4K_A(N_A - N_D)}{(K_A + N_D)^2} \to \frac{4(N_A - N_D)}{K_A} \ll 1$$

By expanding $\left[1 + \frac{4(N_A - N_D)}{K_A}\right]^{\frac{1}{2}}$ into a binomial series we get:

$$p = N_A - N_D \tag{6}$$

In this region the carrier concentration p is independent of the temperature.

(ii) At very low temperatures we have:

$$K_A \ll N_A \quad \text{and} \quad K_A \ll N_D$$

and therefore it follows from equation (5) that:

$$p = [K_A(N_A - N_D)/N_D] \tag{7}$$

Thus at these temperatures p is proportional to

$$\exp(-E_A/kT)$$

from equations (2) and (7), the constant of proportionality depending only on the ratio of the impurities N_A/N_D.

There is an intermediate region towards which the curve will tend only if $N_A \gg N_D$ (or more exactly if $N_A - N_D \gg K_A$ and $K_A \gg N_D$).

In this case $\frac{4K_A(N_A - N_D)}{(K_A + N_D)^2} \gg 1$ and thus:

$$p = [K_A(N_A - N_D)]^{\frac{1}{2}} \tag{8}$$

In this region p is proportional to $\exp(-E_A/2kT)$.

Graphs of equation (5) are shown in Fig. 1 where the hole concentration p is plotted on a log scale along the ordinate and the inverse of the temperature $1/T$ along the abscissa. Three cases are shown.

(i) Fig. 1(*a*) shows the case of $N_A - N_D > N_D$ and refers to a strongly *p*-type sample.

(ii) Fig. 1(*b*) shows the case of $N_A - N_D < N_D$ where the impurities are nearly balanced with the acceptors in excess.

(iii) Fig. 1(*c*) shows the exceptional but unlikely case of $N_A - N_D = N_D$ or $N_A = 2N_D$ exactly.

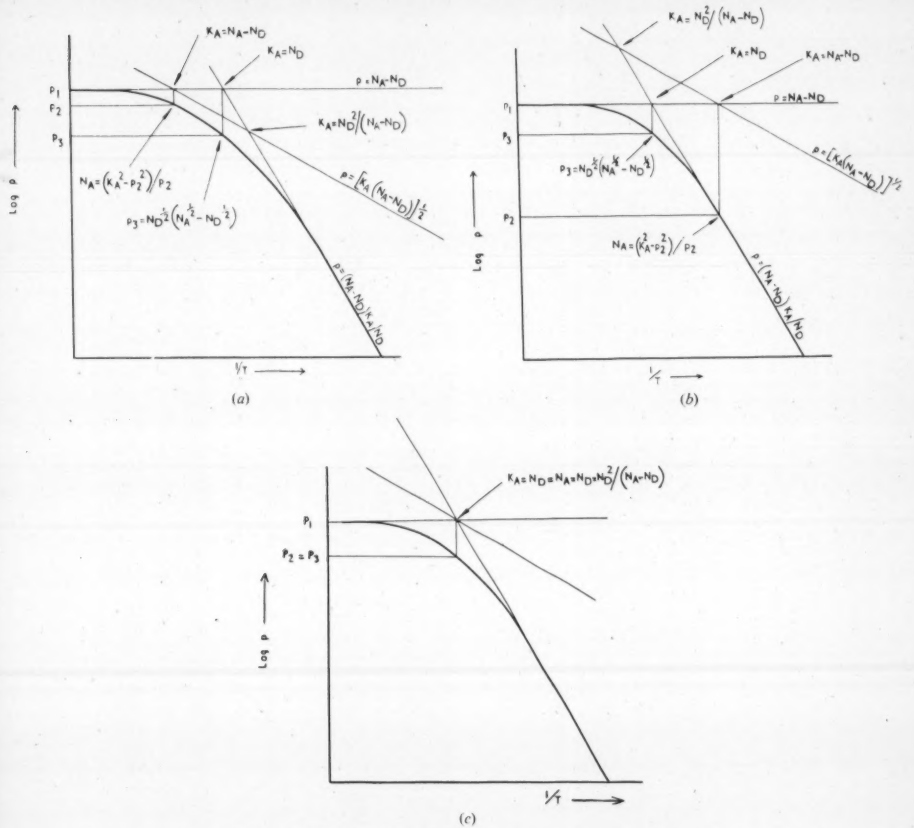

Fig. 1. Graph of carrier concentration *versus* reciprocal temperature
(*a*) $N_A - N_D > N_D$. (*b*) $N_A - N_D < N_D$. (*c*) $N_A - N_D = N_D$.

These criteria form a useful definition when referring to so-called "balanced or unbalanced" semiconductors.

Also shown in Fig. 1 are the straight lines given by equations (6), (7) and (8). Various intercepts which are of interest have been calculated and are as indicated in Fig. 1. It is to be noted that the position of the horizontal line given by equation (6) depends only on $N_A - N_D$ while the intercept of this line with that given by equation (7) depends only on N_D. That is, for a fixed N_A, the intercept will move to lower or higher temperatures according as N_D is decreased or increased, since $N_D = K_A$ at this point.

SEMICONDUCTOR WITH ACCEPTORS ONLY

If we put $N_D = 0$ in equation (5) we obtain:

$$p = \frac{K_A}{2}\left[\left(1 + \frac{4N_A}{K_A}\right)^{\frac{1}{2}} - 1\right] \tag{9}$$

As before we can divide the temperature dependance of p into two distinct regions:

(i) At high temperatures $K_A \ll N_A$ and thus

$$\left.\begin{aligned}\left(1 + \frac{4N_A}{K_A}\right)^{\frac{1}{2}} &\to 1 + \frac{2N_A}{K_A}\\ \text{and} \qquad p &= N_A\end{aligned}\right\} \tag{10}$$

(ii) At low temperatures $K_A \ll N_A$ and thus

$$\left.\begin{aligned}4N_A/K_A &\gg 1\\ \text{and} \qquad p &= (K_A N_A)^{\frac{1}{2}}\end{aligned}\right\} \tag{11}$$

In this range p is proportional to $\exp(-E_A/2kT)$ and the curve does not change its gradient to $\exp(-E_A/kT)$ as is the case if donors are present.

DETERMINATION OF N_A AND N_D FROM THE HALL COEFFICIENT

The Hall coefficient R for a rectangular filament is given by

$$R = \frac{V_H t}{Hi} \times 10^8 \text{ cm}^3 \text{ coulomb}^{-1} \quad (12)$$

where V_H is the Hall voltage in volts, t the thickness of specimen in centimetres, H the magnetic field in gauss, and i the current through specimen in amperes.

In the extrinsic range the carrier concentration p is given by the relation:

$$p = 3\pi/8Re \quad (13)$$

where e is the electronic charge equal to $1{\cdot}6 \times 10^{-19}$ coulombs.

Thus we may obtain an experimental curve of p as a function of the temperature by measuring the Hall coefficient R over a range of temperatures.

To determine the impurity concentration N_A and N_D we must compare equation (5) with this experimental curve. Basically this implies a determination of K_A as a function of temperature, which in turn implies finding the ionization energy of the acceptors E_A and the effective mass of holes m^*. The value of E_A may be found from the curve at low temperatures [equation (7)]. The effective mass may be assumed from other data, e.g. cyclotron resonance[5] or if not otherwise known may be used as an adjustable parameter to obtain a better fit between the experimental and theoretical curves.

An alternative and perhaps simpler method is as follows. At the temperature at which the two tangents to the curve intercept it is seen from Fig. 1 that the value of p is given by:

$$p_3 = N_D^{\frac{1}{2}}(N_A^{\frac{1}{2}} - N_D^{\frac{1}{2}}) \quad (14)$$

If p_1 is the saturation value of p given by equation (6) then it follows that:

$$N_A = [(p_1 - p_3)^2]/(p_1 - 2p_3) \quad (15)$$

$$N_D = p_3^2/(p_1 - 2p_3) \quad (16)$$

It is interesting to note that since:

$$p_1/p_3 = (N_A/N_D)^{\frac{1}{2}} + 1 \quad (17)$$

and $N_A > N_D$ for a p-type semiconductor then

$$p_1 > 2p_3 \quad (18)$$

A certain amount of care is necessary when applying the above procedure for two reasons. Firstly it is to be noted from equations (2) and (7) that it is $\log_e (p/T^{3/2})$ which is proportional to $1/T$ and not $\log_e p$. This means that in some instances the value of p_3 may be too high and it is necessary to correct for this. This is found to be particularly important for balanced samples where it is sometimes found that equation (18) does not hold, but applying the above correction usually overcomes this difficulty. Secondly, if acceptors are present only, then the point p_3 will not exist and p_2 may be used in error. In practice, there are some donors, and measurements at sufficiently low temperatures will reveal any mistake that might otherwise be made.

Should facilities not be available for lowering the temperature to the extent that we are able to draw the tangent given by equation (7) a rough estimate of the impurities may be made using the following procedure. In many cases we know the identity of the majority impurity and merely wish to know its magnitude. In this case we may be able to plot a graph of K_A as a function of temperature.

First of all we obtain $N_A - N_D$ from the value at which p saturates (p_1). We now calculate the temperature at which K_A equals this value and from the curve find the value of $p(p_2)$ at this temperature. From Fig. 1 it follows that:

$$N_A = (K_A^2 - p_2^2)/p_2 \quad (19)$$

In practice this method does not yield very accurate results, and is only mentioned for completeness.

Using this method we can also calculate the limits of determination of impurities in a semiconductor as shown in the next section.

p-TYPE SILICON

It is well known that even after extensive purification of silicon the predominant impurity remaining is boron, which makes the silicon p-type in character. The above analysis was developed to investigate these samples where the majority impurity N_A may be as low as 10^{13} atoms per cubic centimetre. Fig. 2 shows a graph of K_A [equation (2)] plotted on a log scale *versus* the reciprocal of the temperature for the case of boron as an acceptor where it is assumed that $E_A = 0{\cdot}045$ eV[6] and $m^* = 0{\cdot}4\ m$[7] where m is the free electron mass.

As indicated above we can find the limits of detection for various temperature ranges as follows for boron as the major impurity from Fig. 2.

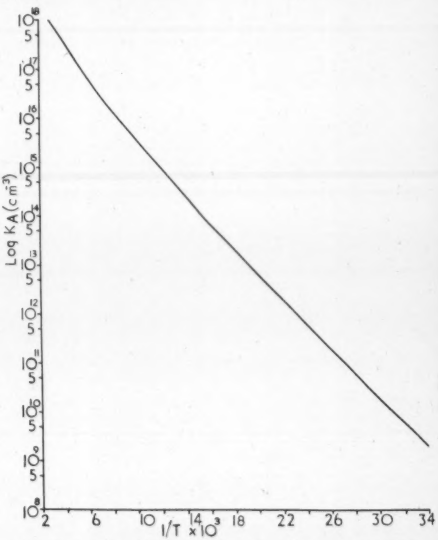

Fig. 2. Graph of the equilibrium constant K_A for $E_A = 0{\cdot}045$ eV and $m^* = 0{\cdot}4$ m

(i) For measurements down to 90° K (boiling point of oxygen), we may find N_A and N_D providing $(N_A - N_D) > 2 \times 10^{15}$ cm^{-3} (value of K_A at 90° K).

(ii) For measurements down to 55° K (triple point of oxygen) we may find N_A and N_D providing $(N_A - N_D) > 2 \times 10^{13}$ cm^{-3} (value of K_A at 55° K).

(iii) For concentrations less than this it is necessary to make measurements down to 20° K (boiling point of hydrogen).

Similar estimates may be made for other impurities in silicon and also other semiconductors.

Fairly extensive measurements of the Hall coefficient have been made on silicon down to 90° K and these have recently been extended to 20° K using liquid hydrogen. The results of these measurements on various samples will be published at a later date.

ACKNOWLEDGEMENTS

The author wishes to thank his colleagues Dr. F. W. G. Rose and Mr. F. Paton of the BTH Research Laboratory for many interesting discussions whilst preparing this manuscript.

REFERENCES

(1) JAMES, J. A., and RICHARDS, D. H. *Nature* [*London*], **176**, p. 1026 (1955).

(2) HANNAY, N. B., and AHEARN, A. J. *Analyt. Chem.*, **26**, p. 1056 (1954).

(3) DEBYE, P. P., and CONWELL, E. M. *Phys. Rev.*, **93**, p. 693 (1954).

(4) MORIN, F. J., and MAITA, J. P. *Phys. Rev.*, **96**, p. 28 (1954).

(5) DRESSELHAUS, G., KIP, A. F., and KITTEL, C. *Phys. Rev.*, **98**, p. 368 (1955).

(6) BURSTEIN, E., PICUS, G., HENVIS, B., and WALLIS, R. *J. Phys. Chem. Solids*, **1**, p. 65 (1956).

(7) DEXTER, R. N., and LAX, B. *Phys. Rev.*, **96**, p. 223 (1954).

NOTES AND NEWS

Correspondence

Action and viscous flow

T. V. Starkey has recently published four papers[1-4] which propound and apply a theory of viscous flow based on the concept of "action." In the first of these[1] he uses the fact that "viscosity" has the same dimensions as "action per unit volume" as a basis for a deduction that solute particles will behave as "macromolecular vortices." From this he deduces three equations for the viscosity of solutions of particles of different shapes, and shows that they are equivalent to the equations of Einstein, Staudinger and Hever, and Huggins. By applying the theory of least action he deduces that particles of a solution (or presumably of a suspension) flowing along a tube, will move towards the tube axis, forming a "Kármán vortex street." From this he deduces a viscosity-concentration relation for high concentrations. He concludes by considering the qualitative result of particle shape upon the viscosity and the change of viscosity with rate of shear, which this theory predicts. The second and third papers[2, 3] consist principally of experimental demonstrations of the fact that suspended particles tend to move to regions of least shear, a phenomenon which he claims can be deduced from the principle of least action, and which he attributes to the Magnus effect.[2] In the most recent paper[4] the theory of least action is shown to lead to the correct velocity profile, both in a circular tube and in a rotating co-axial cylinder viscometer. It is also pointed out that a suspension in viscous flow possesses several features in common with a fluid in turbulent flow.

Certain points in the theory as presented by Dr. Starkey appear to require clarification. Firstly, it does not necessarily follow, from the fact that two quantities have the same dimensional form, that they are physically identifiable. Energy and turning moment both have the dimensions $M L^2 T^{-2}$. It would then not seem to follow from the dimensional similarity of "action per unit volume" and "viscosity" that the two are related, and more justification than has been given by Dr. Starkey is required before the two can be equated with confidence. Secondly, it is questionable whether the principle of least action may be applied without modification to a system in which energy is being converted into heat. A paragraph by Jeans[5] is quoted as justification for such procedure, but an examination of this paragraph shows that the principle of least action must be modified before it is applicable to such a system. Jeans shows that this may be done by the addition of a series of "generalized forces." These are found by subtracting from the externally applied forces those forces caused by the non-reversible processes. Thus the effect of the latter must be known before it is allowable to minimize the action. This is clearly illustrated in the example which Jeans gives (p. 496, Ref. 5). It follows that this reference cannot be used to justify the application of the principle of least action in the way in which it has been done by Dr. Starkey.

The same objection can be levelled against the argument used in the fourth paper[4] which is used to show that the velocity profile of a fluid flowing at low Reynolds' numbers will be that which would dissipate the least energy. In the evaluation of the term δW, which is the work required to displace the system from one configuration to some slightly different configuration, all forces must be included. The force exerted by the fluid because it resists deformation as well as the external force which causes the fluid to move must be considered; and as these are equal and opposite δW must always be zero. Thus the strict application of the principle to conditions where both kinetic and potential energies are absent can produce no prediction.

A further point which would appear to require clarification is the effect of Reynolds' number on the formation of a "Kármán vortex street" along the axis of a tube. The original derivation of the idea that such a configuration would be set up appears to apply to very low Reynolds' numbers, as only viscous forces need be considered. This is also implied when the concept is used to obtain a viscosity-

concentration relation.[1] However, the phenomenon is later[2] attributed to the Magnus effect which would not operate at low Reynolds' numbers as it depends upon the fluid density and not upon the fluid viscosity. Further evidence that the movement of particles towards the axis of a tube depends upon momentum forces rather than viscous forces can be found in Dr. Starkey's own observations. These showed that the movement of colloidal carbon particles across the direction of flow became less as the velocity of flow was reduced.[2] Also a cine film of stable suspensions of spheres flowing through a tube[7] shows no sign of a "Kármán vortex street" formation. The viscosity-concentration relation which is deduced on the assumption that this phenomenon occurs should be generally applicable, but it only agrees at low concentrations with the equation given by Oliver and Ward.[6] Oliver and Ward's equation agrees well with the results of a large number of workers who used well dispersed suspensions.

An alternative approach to the problem is made below which produces similar predictions to those of Dr. Starkey, and which illustrate the limitations of the original theory. Maxwell[8] has produced a theory of fugitive elasticity, and this may be slightly modified to produce the desired result. Consider an elastic solid which is deformed with a modulus of rigidity of n. Suppose that after a time interval L the internal shear stress in the material is relaxed, so that it can undergo a further deformation. If this process is repeated a large number of times and if n is large and L is small, the resultant movement of the material is the same as that of a fluid of viscosity $n\,L$. During any one elastic deformation the process is reversible, and the principle of least action may be applied with safety. Action is the time integral of the difference between the kinetic and potential energy of the system. If the Reynolds' number is small the kinetic energy may be neglected in comparison with the potential energy. Under these conditions the principle of least action leads to the well-known condition that, for equilibrium, the potential energy is a minimum. That is, the velocity profile will be such that the energy stored in the fluid just before each relaxation is a minimum, and will be such that the rate of dissipation of energy is a minimum. An identical conclusion will follow if the fluid is non-Newtonian. This result is the same as Dr. Starkey's.[4]

The limitations of the theory may now be illustrated by considering, as an example, a hard non-settling sphere in a fluid with a parabolic velocity profile flowing at very low Reynolds' number. The exact solution of such a problem is known[9] so that it is possible to check the predictions of the theory.

Casual inspection might suggest that the principle of least action would predict that the sphere would move across the direction of flow to the region of least shear, as when it is in this position the rate of dissipation of energy is least, and thus the potential energy of the system just before relaxation will be a minimum. This, however, is not the result of the exact analysis, which shows that no such transverse motion will take place. If only a single deformation is considered it is at once obvious that any movement of the sphere normal to the direction of flow will require energy. The fact that the sphere is then in a region of lower shear will reduce the energy stored in the system, but this reduction will always be less than the increase caused by the movement itself. While less energy would be needed for the succeeding deformation, the reduction of stored energy only follows the non-reversible relaxation process. It is thus seen that the failure of the sphere to move across the direction of flow is a direct result of the irreversible nature of the viscous deformation. It might be noted that this result applies only to low Reynolds' numbers, so that it is not relevant to the observation of Dr. Starkey, that colloidal carbon particles when suspended in water appeared to move towards the axis of the tube through which they were flowing.[2]

It is concluded that a more detailed analysis is required before Dr. Starkey's theory of the equivalence of viscosity and action per unit volume can be considered as rigorously proved. It has been suggested that Maxwell's theory of fugutive elasticity might be helpful in this respect.

The author would like to express his appreciation to Dr. R. L. Whitmore and Dr. A. Middleton for criticism of the manuscript.

Nottingham and District Technical College,
Nottingham.

A. D. MAUDE

[20 February, 1957]

REFERENCES

(1) STARKEY, T. V. *Brit. J. Appl. Phys.*, **6**, p. 34 (1955).
(2) STARKEY, T. V. *Brit. J. Appl. Phys.*, **7**, p. 52 (1956).
(3) STARKEY, T. V. *Nature* [*London*], **178**, p. 207 (1956).
(4) STARKEY, T. V. *Brit. J. Appl. Phys.*, **7**, p. 448 (1956).
(5) JEANS, J. H. *The Mathematical Theory of Electricity and Magnetism*, 5th ed., p. 492. (London: Cambridge University Press, 1948).
(6) OLIVER, D. R., and WARD, S. G. *Nature* [*London*], **171**, p. 396 (1953).
(7) HIGGINBOTHAM, G. H. *Ph.D. Thesis* (Birmingham, 1951).
(8) MAXWELL, C. *Phil. Trans.*, **156** (1866), quoted in NEWMAN, F. H., and SEARLE, V. H. L., *The General Properties of Matter*, 4th ed., p. 215 (London: Edward Arnold and Co., 1948).
(9) FAXEN, H. *Arkiv. Mat. Astro. Fysik.*, **20**, p. 5 (1927), quoted in HASIMOTO, H., *J. Phys. Soc. Japan*, **11**, p. 793 (1956).

The alleged difficulties referred to by Dr. Maude appear to me to be wholly subjective. In regard to the first of these, it is agreed that dimensional identity does not imply physical identity. It is pointed out, however, that in paper (4) the equation:

$$A = (8lV/\pi R^4)\eta$$

(in which A is the action per unit volume involved in transferring a volume V of a liquid of viscosity η through a tube of length l and radius R) was derived without reference to dimensions; it could not have been obtained by their use.

Secondly, the operation of "generalized forces" was considered. In the problem under examination no changes occur either in the kinetic or the potential energy of the system and the work done on the system by external forces is wholly dissipated as heat. A quantitative equivalence between heat dissipation and work done, therefore, exists, and it is this equivalence which forms the basis of the argument in question. Dr. Maude's statement that "the Magnus effect would not operate at low Reynolds' numbers" appears to be wrong. The alternative approach suggested seems consequently quite unnecessary.

The Technical College of Monmouthshire,
Crumlin, Mon.

T. V. STARKEY

[6 March, 1957]

New books

Recent advances in science: Physics and applied mathematics. Edited by MORRIS H. SHAMOS and GEORGE M. MURPHY. (London: Interscience Publishers Ltd., 1956.) Pp. xi + 384. Price $7.50.

In the spring of 1954 a symposium on recent advances in science was organized by New York University. Distinguished specialists gave a series of lectures to non-specialists on various branches of physics and applied mathematics. This book is a somewhat belated publication of twelve essays based on these lectures. The first is on Methods of Applied Mathematics by Richard Courant and it is followed by The Future of Operations Research by P. M. Morse. There are then eight essays on various fundamental aspects and applications of atomic, nuclear and solid state physics; the authors are H. A. Bethe, R. M. Bozorth, L. J. Haworth, N. F. Ramsey, I. I. Rabi, W. Shockley, C. H. Townes, and V. F. Weisskopf. There follows a contribution from F. A. Brickwedde on Low Temperature Physics (Cryogenics) and the book is concluded with a general article by E. U. Condon on Physics and the Engineer.

The choice of subjects is somewhat arbitrary and there has been little attempt to correlate the various essays. However, this book, written at a fairly elementary level by some of the most distinguished American scientists of to-day, is of considerable importance. It may be recommended wholeheartedly to anyone with a scientific background and an interest in modern developments in pure and applied physics.

M. R. GAVIN

1956 heat transfer and fluid mechanics institute. Preprint of papers. (Stanford: University Press; London: Oxford University Press, 1956.) Pp. 278. Price 45*s*.

The preface states that this "is the ninth of the series initiated in 1948 for the purpose of making available to engineers of the Western region a program of high scientific caliber representing fundamental research in heat transfer and fluid mechanics."

A field as large as this has in the past led to a wide diversity of papers and this year's issue is no exception. Many of the papers are to be published in the journals of professional societies and in view of their heterogeneity one would imagine that this will meet the needs of many workers. Nevertheless the issue forms an interesting collection ranging from problems of boiling and evaporation through problems of conduction and forced convection and viscous flows (incompressible and compressible) to the thermodynamics of irreversible processes. The papers your reviewer found most interesting—no doubt a purely personal matter—were those dealing with thermodynamical as distinct from "thermostatical" problems (No. 15 below) and the flow past a flat plate (No. 11) certainly if this latter is the forerunner of further work. However, it is impossible in the space available to discuss the papers individually and the most one can do is to display the following list of contents and let every man make his own choice:

(1) Ebullition from solid surfaces in the absence of a pre-existing gaseous phase. By S. G. Bankoff.

(2) Effect of an ultrasonic field on boiling heat transfer-exploratory investigation. By S. E. Isakoff.

(3) Solving the melting problem using the electric analogy to heat conduction. By D. R. Otis.

(4) Effect of axial fluid conduction on heat transfer in the entrance regions of parallel plates and tubes. By P. J. Schneider.

(5) Heat transfer in a pipe with turbulent flow and arbitrary wall-temperature distribution. By C. A. Sleicher, Jr., and M. Tribus.

(6) Heat transfer of a laminar pipe flow with coolant injection. By S. W. Yuan and A. B. Finkelstein.

(7) Heat transfer by forced convection from a horizontal flat plate into a turbulent boundary layer. By A. C. Spengos and J. E. Cermak.

(8) On the changing size spectrum of particle clouds undergoing evaporation, combustion, or acceleration. By A. H. Shapiro and A. J. Erickson.

(9) Experimental study of the velocity and temperature distribution in a high velocity vortex type flow. By J. P. Harnett and E. R. G. Eckert.

(10) Natural convection heat transfer from a horizontal cylinder rotating in air. By D. Dropkin and A. Carmi.

(11) An analog solution of the Navier–Stokes equation for the case of flow past a flat plate at low Reynolds numbers. By E. Janssen.

(12) On the supersonic flow of a viscous fluid over a compression corner. By R. L. Chuan.

(13) Heat transfer to a yawed infinite cylinder in compressible flow. By E. Reshotko.

(14) The unsteady laminar boundary layer on a flat plate. By Sin-I Cheng and D. Elliott.

(15) Thermodynamics of the first order. By Y. S. Touloukian and R. S. Lykoudis.

(16) Non-linear problems in thermodynamics of irreversible processes. By I. Prigogine.

(17) Thermoelasticity and irreversible thermodynamics. By M. A. Biot.

[The last named is not in the pre-print volume but is available as a separate Cornell Aernautical Laboratory Report.]

L. HOWARTH

Thermodynamic tables and other data. Edited by R. R. HAYWOOD. (London: Cambridge University Press, 1956.) Pp. 24. Price 2*s*. 6*d*.

A set of short tables of the thermodynamic properties of the more common gases. It collects together in a conveniently accessible form values for the specific volume, enthalpy and entropy of ammonia, carbon dioxide, Freon-12 and methyl chloride at saturation and at two values of superheat. In addition it includes four tables giving the internal energy, enthalpy, entropy and density of superheated steam from 1 to 5000 PSIA and from 150 to 1600° F. Tables are also included for the saturation properties of steam and the properties of compressed water. The most commonly required constants of the various gases are given as a preamble.

S. ANGUS

Notes and comments

The Education of Physicists in Universities and Colleges of Technology

In November 1956 a conference was held on "Degree and diploma courses in applied physics." The conference was organized jointly by the Institute of Physics and The London and Home Counties Regional Advisory Council for Higher Technological Education and was held at the Institution of Electrical Engineers, London. The aim of the conference was to provide an opportunity for the discussion of the question of courses in applied physics and the need to develop them in a manner differing from that of a university honours degree course while, at the same time, demanding similar intellectual ability. It is hoped thereby to produce men and women with a knowledge of fundamental physical principles and an aptitude for the application of physical knowledge, in order to meet the needs of industry for both research and development.

The conference high-lighted many of the problems and differences of opinion which must arise where such schemes are discussed and it was felt that, because of the interest which this subject has stimulated, the proceedings of the conference, in a slightly edited form, should be made generally available. This has now been done and the proceedings, reprinted from the *Bulletin* of The Institute of Physics and under the above title, can be obtained from The Institute of Physics, 47 Belgrave Square, London, S.W.1. Price 6*s*.

British Computer Society

Some months ago a working party examined a proposal to form a national society to meet the need for a forum for the exchange of information between the people concerned with computers and automatic data-handling techniques in their scientific, engineering, business and other aspects, and agreement has now been reached to form a new body to be called the British Computer Society. The London Computer Group which was formed in 1956 and which has so far catered primarily for business interests has agreed to take part in the formation of the new Society and to add its resources to it; all existing members of the Group will automatically become members of the new Society, the objects of which are: (*a*) To provide an organisation for those interested in and to further the development and use of computational machinery and the techniques allied thereto; (*b*) To facilitate the exchange of information and views and to foster well-informed public opinion on this subject; (*c*) To hold conferences and meetings for the reading of papers and delivery of lectures; (*d*) To publish a Journal, and other information for the benefit of its members.

It is intended to incorporate the Society as a company limited by guarantee. A provisional Council has been formed with the following membership: A. D. Booth; E. E. Boyles; A. J. Bray; E. C. Clear Hill; A. S. Douglas; R. G. Dowse; F. S. Ellis; H. W. G. Gearing; A. Geary; C. G. Holland Martin; D. W. Hooper; E. N. Mutch; R. E. Stevens; F. Yates.

The Society intends to form regional and specialist groups, and at the outset will set up a Business group and an Engineering and Scientific group.

All those interested in obtaining further information should apply to the Honorary Secretary, The British Computer Society, 29 Bury Street, London, S.W.1.

Journal of Ultrastructure Research

A new scientific journal has been announced entitled: *Journal of Ultrastructure Research* which is to be edited by Dr. Fritiof S. Sjöstrand and Dr. Arne Engström, both associated with the Karolinska Institutet, Stockholm.

The purpose of the *Journal* will be to assemble, in one medium, papers dealing with the ultrastructure of the elementary structural as well as functional components of cells and tissues. The first volume, priced at $15.00, will consist of four issues. Manuscripts by Ebba Andersson, A. J. Dalton, R. Ekholm, E. Faure-Fremiet. D. Ferreira, A. Frey-Wyssling, B. Vincent Hall, E. L. Kuff, M. G. Menfee, and Ch. Rouiller have been accepted for publication in the initial issues.

Further information can be obtained from the editorial offices of the *Journal*, Department of Anatomy, Karolinska Institutet, Stockholm 60, Sweden. Subscription orders should be sent to the publishers, Academic Press Inc., 111 Fifth Avenue, New York 3, New York, U.S.A.

Journal of Scientific Instruments

Contents of the August issue

SPECIAL ARTICLE

Ultra-high vacua. By J. Yarwood.

ORIGINAL CONTRIBUTIONS

Papers

The recording of electron diffraction patterns from single crystals using the Metropolitan-Vickers type E.M.3 electron microscope. By R. E. Burge, H. R. Munden and C. D. Curling.

A half-silvered mirror tangentimeter. By H. J. G. Hayman, F. Deutsch and H. Tabor.

A sensitive electronic strain gauge. By H. L. Allsopp and D. F. Gibbs.

The optimum design of quarter-squares multipliers with segmented characteristics. By M. E. Fisher.

Two portable thermistor radiometers. By W. H. Ward.

A bolometer detector for the measurement of shock velocity in low density gases. By J. G. Cloustón, L. J. Drummond and W. F. Hunter.

A projection spectrum comparator. By C. F. Smith.

A precision bath thermostat. By W. Wilson and N. W. B. Stone.

An exposure calculator for isotope radiography. By T. A. Cosh.

Laboratory and workshop notes

A method for the measurement of solid film thicknesses in the 5 to 30 micron range. By Garry Thomson.

A revolution counter for high-speed shafts. By J. A. Sanderson.

NOTES AND NEWS

Correspondence

A simple arrangement for obtaining optical transforms of crystal structures. From H. Lipson.

Avoiding the need for dividing units in setting electronic differential analysers. From M. E. Fisher.

New books

Notes and comments

THIS JOURNAL is produced monthly by The Institute of Physics, in London. It deals with all branches of applied physics (including theory and technique).

All rights reserved. Responsibility for the statements contained herein attaches only to the writers.

EDITORIAL MATTER. Communications concerning editorial matter should be addressed to the Editor, The Institute of Physics, 47 Belgrave Square, London, S.W.1. (*Telephone:* Sloane 9806.) Prospective authors are invited to prepare their scripts in accordance with the *Notes on the preparation of contributions*. (Price 2*s*. 6*d*. including postage.)

REPRODUCTION. The Institute of Physics is a signatory to The Royal Society's Fair Copying Declaration. Details may be obtained upon application from The Royal Society, London, W.1.

ADVERTISEMENTS. Communications concerning advertisements should be addressed to the agents, Messrs. Walter Judd Ltd., 47 Gresham Street, London, E.C.2. (*Telephone:* Monarch 7644.)

CLAIMS FOR MISSING JOURNALS. Claims from regular subscribers to this *Journal* for missing numbers will only be considered if received within 60 days of the date of mailing plus normal outward time of transit and time for lodging the claim. Losses attributable to failure to notify a change of address or to similar omissions will not be considered.

SUBSCRIPTION RATES. A new volume commences each January. The charge is £5 per volume ($14.25 U.S.A.), including index (post paid), payable in advance. Single parts, so far as available, may be purchased at 10*s*. each ($1.50 U.S.A.), post paid, cash with order. Orders should be sent to The Institute of Physics, 47 Belgrave Square, London, S.W.1, or to any bookseller.

Electron micrographs from thick oxide layers on aluminium*

By C. J. L. Booker, B.Sc., A.R.I.C., J. L. Wood, M.A., Ph.D., Department of Chemistry, Sir John Cass College, London, and A. Walsh, B.Sc., Department of Applied Physics, Northampton College of Advanced Technology, London

[*Paper first received* 17 *January, and in final form* 28 *May*, 1957]

Electron micrographs have been obtained of the pore structure in the thick oxide layer formed by anodizing aluminium in sulphuric acid. The pores are shown to be minute tubes of approximately 200 Å diameter running perpendicularly through the oxide and ending almost in contact with the underlying metal. The pore base thickness has been estimated, and the effect of a change in anodizing conditions on the pore base pattern is shown.

1. Introduction

The work described in this paper forms part of a wider investigation into the capacitance-resistance hygrometer which has been described previously.[1, 2] In this instrument

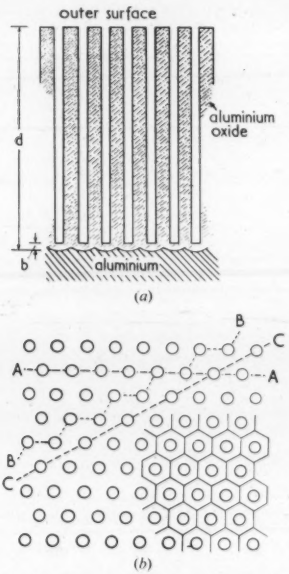

Fig. 1. (*a*) Model section of pore structure. (*b*) Model plan of pore structure illustrating:
(i) hexagonal distribution; (ii) origin of pore base pattern; (iii) three possible cleavage lines obtainable in a cross-section *AA*, *BB*, *CC*.

the relative humidity is indicated by the electrical characteristics of a porous aluminium oxide layer formed by anodizing an aluminium surface in sulphuric acid. Porous oxide layers can also be formed in other acid electrolytes, but their electrical characteristics prove less suitable as hygrometer elements. A theoretical consideration of the electrical properties requires a knowledge of the pore dimensions as indicated diagrammatically in Fig. 1; this information was obtained from the electron microscope.

Previous workers have used only layers sufficiently thin to act as transmission specimens in the electron microscope.[3–6] The hygrometer elements make use of much thicker layers (e.g. 30 μ) and these could only be examined by replica methods.[7] Replicas may be taken from (i) the cross-section through the oxide layer normal to the plane of the metal surface, (ii) the outer surface of the oxide layer, and (iii) the metal surface at the metal-oxide interface. Keller, Hunter and Robinson[8] have applied method (iii) in their investigations of oxide layers formed by anodizing in sulphuric, oxalic, chromic and phosphoric acids. These workers proposed an idealized model of the pore structure based on a hexagonal-type packing of the pores, in which the pore diameter depended on the electrolyte used, and the pore spacing increased linearly with the anodizing voltage. However, the layer thicknesses used were not reported but were probably much thinner than those used in the present work.

The only previous report of method (ii) is by Vermilyea[9] on anodized tantalum surfaces using nitrocellulose replicas. Edwards and Keller[6] have obtained polystyrene-silica replicas[10] of an oxide cross-section. However, the resolution obtained did not show much detail of the pore structure. With the same technique the porous structure of a rupture surface of a thick oxide layer was demonstrated by Huber.[11] In the present work method (i) has provided most information and this has been supplemented by methods (ii) and (iii).

2. Experimental Methods

2.1 *Preparation of the oxide layers.* Specimens of 99·99% purity aluminium strip (10 cm lengths, 5 mm wide and 0·85 mm thick) were electropolished for 5 min at 20 V in a perchloric acid and ethyl alcohol bath (1 : 5 by volume) by anodic treatment with a current density of 100 mA cm^{-2}; using carbon cathodes fitted in Soxhlet thimbles. The bath was maintained at room temperature.

For anodizing, the area of the electropolished surface required was "stopped off" with polystyrene. A cathode of lead or aluminium foil was used with 17·5% v/v sulphuric acid contained in a glass cell maintained at 19 ± 1° C. The following three sets of conditions were used:

(i) 50 mA cm^{-2} for 1 h; voltage rose from 17 to 27 V.
(ii) 100 mA cm^{-2} for 30 min; voltage rose from 20 to 32 V.
(iii) 50 mA cm^{-2} for 1 h, and then 200 mA cm^{-2} for 1 min.

* Material taken from a thesis to be presented by C. J. L. B. in support of candidature for the Ph.D. degree of the University of London.

2.2 *Preparation of replicas*

2.2.1 *Cross-sections.* The anodized specimen was mounted in Araldite D cold setting resin, left to set overnight, and then hardened at 80° C for one hour. A cross-section normal to the plane of the oxide layer was ground down on an emery wheel and then on abrasive papers moistened with white spirit. Final polishing on a wheel fitted with a Selvyt cloth using magnesium oxide slurry gave a surface finish suitable for the preparation of replicas.

The two-stage Formvar-carbon technique was used, described by Bradley,[12] and modified slightly, as follows. The Formvar replica was backed up with a 1% solution of Celloidin (nitrocellulose) in ethyl acetate and stripped from the surface with Sellotape. A carbon film was deposited on the replica surface and then shadowed *in situ* with gold-palladium alloy, the direction of shadowing being along the metal-oxide boundary at an angle approximately cot^{-1}3 to the surface. The composite replica was freed from the Sellotape and mounted on copper supporting grids. By consecutive treatment with ethyl acetate and chloroform the plastic cast was dissolved away, leaving the shadowed carbon replica on the grids ready for examination in the electron microscope.

2.2.2 *Outer surface.* The same technique was used for the preparation of replicas, except that a thicker nitrocellulose layer was necessary to back up the Formvar, the stronger "Scotch" acetate tape was required, and the outline of required area of the replica was scored with a razor blade before stripping.

2.2.3 *Metal-oxide interface.* The oxide layers were dissolved by repeated immersions for periods of 5 min in a boiling aqueous solution of 2% chromic oxide and 3·5% phosphoric acid[13] until the specimen reached constant weight. The underlying metal thus exposed was then re-anodized in 12% disodium hydrogen phosphate containing 0·4% sulphuric acid[14] to obtain a uniform thin anodic film replicating the metal surface without introducing fresh structure. This replica was then removed for examination in the usual way.

3. RESULTS AND STRUCTURAL INFORMATION

3.1 *Cross-sections.* In the replicas of the mounted sections the metal-oxide and Araldite-oxide boundaries could be easily distinguished. The general appearance of the oxide layer itself was of a smoothly polished surface occasionally interrupted by irregularities where the oxide had broken away in minute "chips," leaving areas as shown in Fig. 2. This interpretation was confirmed by examining stereo-pairs of micrographs of the "craters" remaining behind.

Detail of the porous structure was revealed in the following three ways:

(i) The craters left behind in the surface provide a most valuable way of examining the pore arrangement, particularly as they are most frequently found near the metal-oxide boundary. In some the cleavage has taken place along the pore axis, displaying very plainly the parallel alignment of the pore channels. Fig. 2 illustrates this. A feature of some craters close to the metal-oxide interface is a close-packed hexagonal pattern (see Fig. 3).

(ii) Although the greater part of the cross-sectional surface of the oxide appeared smooth, it was possible to resolve a fine structure, shown in Figs. 4 and 5. A large variety of these "raindrop" type patterns was observed, and since their origin was in the pore structure it was possible to evaluate the pore diameter and spacing from an analysis of the patterns.

(iii) In parts of replicas near the outer surface a distinct coarsening of the pore structure was observed, as shown in Fig. 6. This may be attributed to the greater opportunity here for chemical attack by the electrolyte during anodizing.

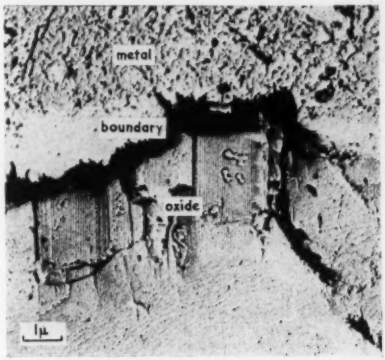

Fig. 2. Cross-section through oxide near boundary with metal, showing "craters" containing pore structure. 8000 × (EM3)

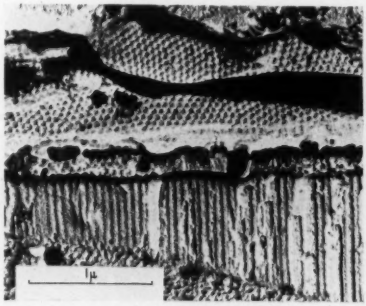

Fig. 3. Hexagonal pattern in a "crater" at the metal-oxide boundary. 25000 × (Siemens)

3.1.1 *Measurements from "craters."* It is not possible to estimate the diameter of the pores but only the lateral spacing between the parallel channels in the fracture surface exposed in the crater. From samples produced with the same anodizing conditions, the lateral spacings may vary over a considerable range. Some variation in the replica scale depending on the inclination of the fracture plane to the direction of viewing is to be expected; this may be up to 10%. However, three different types of fracture cleavage may occur, represented in Fig. 1(*b*), by *AA*, *BB* and *CC*. Measurements from a number of micrographs gave values of the pore spacing s which varied between the following limits: 50 mA cm^{-2} for 1 h, s = 450 to 600 Å, 100 mA cm^{-2} for 30 min, s = 450 to 550 Å.

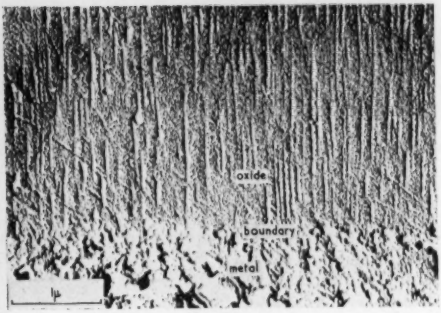

Fig. 4

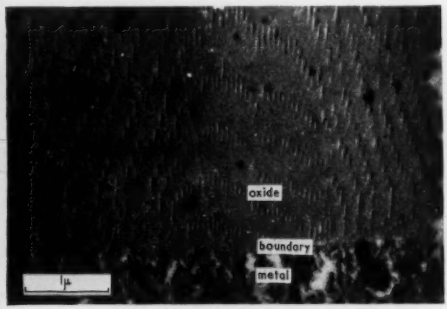

Fig. 5

Figs. 4 and 5. Smooth oxide cross-sections showing "raindrop" patterns; i.e. elongated pore sections in the surface. 17000 × (EM3)

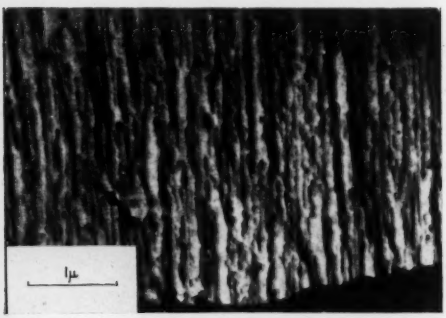

Fig. 6. Oxide cross-section near the outer surface, showing a coarsening of the pore structure. 18000 × (EM3)

Assuming hexagonal packing, the number of pores per square centimetre may be readily obtained from the spacing by means of the relationship $n = \frac{2}{s^2\sqrt{3}}$.

The appearance of Fig. 3 suggests that here the metal has been pulled away from the oxide surface and the pattern visible in the upper half of the figure is that of the metal originally in contact with the oxide layer. The pattern then indicates that the pore channels are hexagonally packed and measurements from this give a pore spacing of 550 Å for specimens anodized at 50 mA cm^{-2} for 1 h.

3.1.2 *Measurements from the "raindrop" pattern.* In a crater the pores are exposed along their length. Where the polished surface cuts the pores obliquely, however, the resulting cavity is filled with the replicating plastic, and appears in the carbon replica as a "raindrop." The raindrops vary both in length and spatial distribution in the surface, giving rise to a great variety of patterns as in Figs. 4 and 5, which are typical of a large number of micrographs. By means of an optical projection analogue it was possible to demonstrate that all these patterns could arise from a regular hexagonally packed arrangement of pores in which the structure had been cut by the plane of polishing, inclined at an oblique angle to the pore axis. As the dihedral inclination of the plane was varied, so the type of pattern changed.

It would not be justifiable to estimate the diameter of the pores from the raindrop trace given by a single pore, which has rather ill-defined boundaries. However, by assuming that the patterns result from a hexagonal arrangement, a number of ways of estimating the pore diameter has been developed, all of which essentially average the trace impressions. For example, providing that the spacing s is known, the number of traces in an area of the surface indicates the angle at which the pores intersect the surface plane in that area. The mean trace length then indicates the pore diameter.

Another method, illustrated diagrammatically in Fig. 7, can be used in certain parts of the surface where the type of

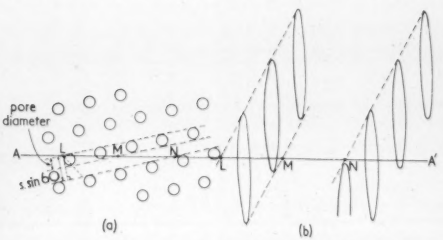

Fig. 7. Diagram illustrating the calculation of pore diameter from the "raindrop" type pattern. AA' is axis of intersection cutting pore channels

(*a*) Plane normal to pore axis.
(*b*) Surface of micrograph.

pattern indicated in Fig. 5 occurs. The line AA' in the surface cuts the pores as shown, so that $\frac{LM}{LN} = \frac{\text{pore diameter}}{s \sin 60}$

The ratio of the distances LM to LN may be estimated from the micrograph with more certainty than the dimensions of an individual trace. With a specimen anodized at 100 mA cm^{-2} for 30 min a series of micrographs extending across the thickness of the oxide layer (127 μ) showed well developed

patterns throughout, and the measurements obtained gave values for the pore spacing between the limits $s = 490$ to 530 Å, and for the pore diameter $D = 150$ to 200 Å.

3.1.3 *Pore base thickness, b* [see Fig. 1(*a*)]. Examination of the "raindrop" type pattern in the vicinity of the oxide-metal interface showed that in samples anodized under both conditions the pore traces continued to within 500 Å of the metal surface. It is not possible to determine exactly the minimum distance between the pore base and the metal, and in certain regions no gap is discernible.

3.2 *The oxide outer surface.* In some cases the Formvar replica penetrated a considerable way into the pores, and could be stripped from the surface without breaking the projections, which then became covered with the evaporated carbon film. It was perhaps surprising to find that the outer surface was sufficiently regular to allow these replicas to be obtained, so that electropolishing of the aluminium specimens and careful control in subsequent anodizing must be of importance. The uniformity of some specimens 30 μ thick was observed by interference colours.

The tubular projections in the carbon replicas are often tangled together giving a grass-like appearance shown in Fig. 8, which made an estimate of the number per unit area

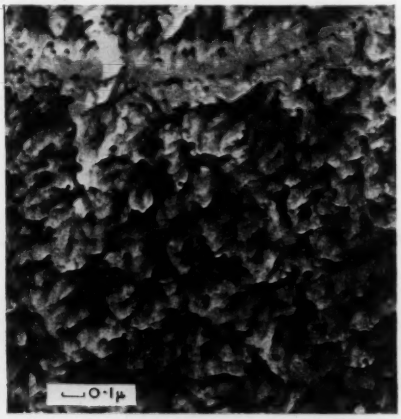

Fig. 8. Impressions of pores in the replica at the oxide outer surface. 40000 × (Siemens)

imprecise. The pore diameter was estimated from observations of individual projections, whose appearance suggested only a slight widening of the pores near the outer surface. In many cases the Formvar did not appear to penetrate deeply into the pores, and outer surface replicas of another type resulted, as in Fig. 9. These provided less information about the pores.

3.2.1 *Measurements from the outer surface.* The number of pores per square centimetre at the outer surface may be obtained directly from a count of the impressions in a replica of this surface, and this gave 13×10^9 cm^{-2} for a specimen anodized at 100 mA cm^{-2}. In some replicas the projections formed by the impressions of the Formvar into individual pores can be observed, and the pore diameter in these ranges from 250 to 300 Å (samples anodized at 100 mA cm^{-2}).

3.3 *The metal surface.* This was examined in a manner comparable with that used by Keller and his co-workers.[8] A similar honeycomb-type of structure was observed, and its dimensions were consistent with their interpretation; that each "cell" in the structure is associated with the base of a single pore. Brown[15] has reported that an electropolished aluminium surface, examined by reanodizing to form a

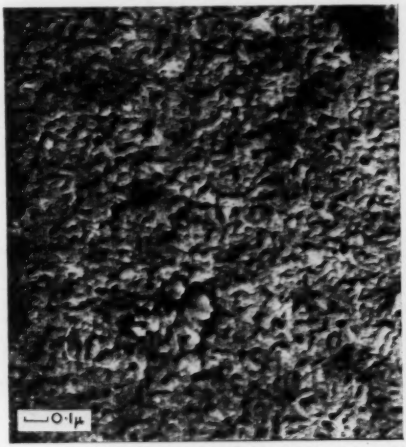

Fig. 9. Another type of oxide outer surface replica. 40000 × (EM3)

replica in a similar way, has a structure of comparable appearance and dimensions. Since electropolishing results from simultaneous anodizing and dissolution in an acid electrolyte this so-called "self-structure" may well arise in the same way as the metal surface structure observed in the present investigation where the anodizing and dissolution processes are consecutive. Recently published work by Welsh[16] on electropolished aluminium surfaces strongly supports this idea (see below).

3.3.1 *Measurements from the metal surface.* By counting the number of cells per unit area in the pore base pattern, the spacing s may be evaluated. For samples anodized at 50 mA cm^{-2}, $s = 600$ Å, while for those anodized at 100 mA cm^{-2}, $s = 590$ Å. The difference is not significant due to the wider variation about these mean values.

3.3.2 *Variation in anodizing conditions.* The dependence of the pore structure on the anodizing conditions is of considerable interest, especially with regard to the electrical properties of the layer. These conditions may be varied either from sample to sample, or during the course of a single experiment; in the present work only the current density was varied in order to display any consequent structural changes. Unfortunately, no satisfactory replicas were obtained from the surfaces prepared in this way.

An alternative was to examine the surface of the metal after removal of the oxide layer in search of a change in the pore base structure. Fig. 10 shows the pore base pattern resulting from normal anodizing conditions (50 mA cm^{-2} for 1 h) while Fig. 11 was obtained with changed anodizing

conditions (50 mA cm^{-2} for 1 h and then 200 mA cm^{-2} for 1 min). A comparison of these two micrographs demonstrates that a change in anodizing conditions introduces a pronounced irregularity into the pore base pattern.

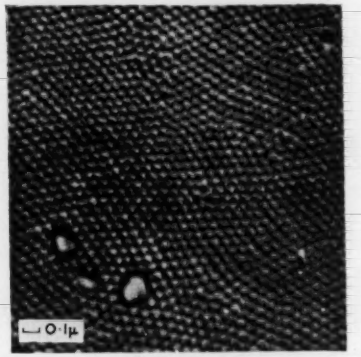

Fig. 10. Pore base replica of an oxide surface formed under constant anodizing conditions. 25 000 × (EM3)

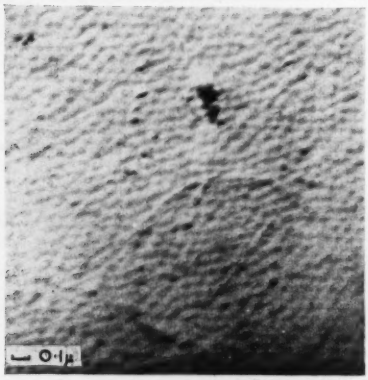

Fig. 11. Pore base replica of an oxide layer formed with a change in anodizing conditions in the last minute. 25 000 × (EM3)

4. DISCUSSION

4.1 *The effect of electropolishing.* It seems unlikely that the arrangement and dimensions of the pore structure are determined by the preliminary electropolishing. The results of Keller and co-workers[8] give a pore spacing which is determined by the anodizing voltage; the values obtained in the present work compare favourably with those of Keller, whereas the size of the surface furrowing expected with the conditions of electropolishing used would be about 700 Å according to Welsh.[16] Furthermore, a change in the current density during anodizing alters the pore base pattern.

4.2 *The hexagonal packing.* The most striking evidence for the hexagonal packing of the pores comes from the pore base patterns (Figs. 3 and 10). The oblique projections of a hexagonal packing only differ from those of a square one in the ratio of spacing s to pores per unit area n; this is about 15% greater for the hexagonal packing. Our measurements agree best with the hexagonal-packing ratio, although the limits of error do not rule out the alternative. The packing, shown both by pore bases and cross-sections, is not entirely regular, and small variations in the spacing and orientation of the pattern occur. Regularity of the packing usually extends over areas of about 1 μ^2.

4.3 *The pore base pattern.* The experiments leading to Figs. 10 and 11 demonstrate the effects of the anodizing conditions on the pore base. Although no information is provided about the effect of anodizing changes on the pore channels themselves, it does indicate that although the pore pattern is set down in the first moments of anodic oxidation the structure of the pore base itself is dependent on the conditions at the last moment of anodizing. This also confirms the opinion that the anodic oxidation proceeds at the base of the pores as indicated by the dyeing experiments of Rummel.[17]

4.4 *Pore volume.* Taking the pore diameter as 190 Å, the spacing as 500 Å with a hexagonal arrangement and constant pore cross-section, the pore volume is 13%, which agrees reasonably well with the values given in the literature.[4,8,18–20]

4.5 *Adsorption.* The structural dimensions obtained by electron microscopy indicate a surface area of 0·11 m^2 cm^{-2} of superficial oxide surface. A value of 0·20 m^2 cm^{-2} is obtained by a surface area determination by nitrogen adsorption at 90° K on 100 rods anodized at 33 mA cm^{-2} in 17·5% v/v sulphuric acid for 30 min. The surface was outgassed at 120° C for 15 h before adsorption. This suggests that irregularities in the oxide surface occur which are beyond the resolving power of the electron microscope.

5. CONCLUSIONS

The methods described here show how investigations with the electron microscope may be extended to the study of the thick porous oxide layer formed by anodizing aluminium. In particular, the parallel arrangement and hexagonal packing of the pore channels, together with their alignment normal to the metal surface has been shown. The pore structure appears to extend throughout the entire thickness of the oxide to the pore base layer, whose thickness may be estimated; and the pore diameter and spacing do not show much variation through the oxide layer. Although somewhat coarser in structure, the outer surface appears comparatively regular. Finally, an examination of some pore base replicas confirms the current opinion that pore growth proceeds from the pore base layer.

6. ACKNOWLEDGEMENTS

This work forms part of a research programme of the Food Investigation Organization of the D.S.I.R., to which one of us (C. J. L. B.) is indebted for a grant. The authors thank Dr. V. E. Cosslett for the use of the Siemens electron microscope at the Cavendish Laboratory, Cambridge, and Dr. J. S. S. Reay of Imperial College, London, for carrying out the surface area determination. Samples of super-purity aluminium were kindly supplied by the British Aluminium Company.

7. REFERENCES

(1) CUTTING, C. L., JASON, A. C., and WOOD, J. L. *J. Sci. Instrum.*, **32**, p. 425 (1955).

(2) JASON, A. C., and WOOD, J. L. *Proc. Phys. Soc. [London] B*, **68**, p. 1105 (1955).

(3) MAHL, H. *Korrosion u. Metallsch.*, **17**, p. 1 (1941).

(4) FISCHER, H., and KURZ, F. *Korrosion u. Metallsch.*, **18**, p. 42 (1942).

(5) WILSDORF, H. *Z. angew. Physik*, **2**, p. 17 (1950).

(6) EDWARDS, J. D., and KELLER, F. *Trans Am. Inst. Mining Met. Engrs, Inst. Metals Div. Tech. Pub., No.* 1710 (1944).

(7) BOOKER, C. J. L., WOOD, J. L., and WALSH, A. *Nature [London]*, **176**, p. 222 (1955).

(8) KELLER, F., HUNTER, M. S., and ROBINSON, D. L. *J. Electrochem. Soc.*, **100**, p. 411 (1953).

(9) VERMILYEA, D. A. *J. Appl. Phys.*, **26**, p. 489 (1955).

(10) HEIDENREICH, R. D., and PECK, V. G. *J. Appl. Phys.*, **14**, p. 23 (1943).

(11) HUBER, K. *J. Colloid Sci.*, **3**, p. 197 (1948).

(12) BRADLEY, D. E. *Brit. J. Appl. Phys.*, **5**, p. 65 (1954); *J. Inst. Metals*, **83**, p. 35 (1954).

(13) EDWARDS, J. D. *Proc. Amer. Soc. Test. Mat.*, **40**, p. 959 (1940).

(14) KELLER, F., and GEISLER, A. H. *Trans Am. Inst. Mining Met. Engrs*, **156**, p. 82 (1944); *J. Appl. Phys.*, **15**, p. 696 (1940).

(15) BROWN, A. F. Symposium on the Metallurgical Applications of the Electron Microscope, Nov. 16 (1949), *Inst. Metals Mon. Rept. Ser.*, **8**, p. 103 (1950).

(16) WELSH, N. C. *J. Inst. Metals*, **85**, p. 129 (1956).

(17) RUMMEL, TH. *Z. Phys.*, **99**, p. 518 (1936).

(18) COSGROVE, L. E. *J. phys. Chem.*, **60**, p. 385 (1956).

(19) BURWELL, R. L., SMUDSKI, P. A., and MAY, T. P. *J. Am. Chem. Soc.*, **69**, p. 1525 (1947).

(20) BAUMANN, W. *Z. Phys.*, **111**, p. 708 (1939).

Barium getters and carbon monoxide

By R. N. BLOOMER, B.Sc., A.Inst.P., Research Laboratory, Associated Electrical Industries Ltd., Aldermaston, Berks.

[*Paper first received* 24 *April, and in final form* 21 *May*, 1957]

The absorption of carbon monoxide by evaporated barium films has been studied in a pressure range 10^{-6}–10^{-7} mm of mercury. The mechanism is shown to be similar to that for oxygen (Bloomer[1,2]), and is explained with the aid of Mott's[3] theory. Carbon monoxide is dissociated at the surface of the barium film, and an oxide layer containing free carbon is formed. Below 80° C, the layer of reaction products is protective once it has grown to a thickness of about 50 Å. Above, 80° C, the whole of the barium is used up in the reaction.

The condensation coefficient at room temperature is 0·012. Thus, about 1 in 80 of the carbon monoxide molecules striking the getter surface in any period is taken up by a barium film at room temperature (1 in 40 at 170° C). The condensation coefficient is limited to these low values by the superficial density of interstitial barium ions in the free surface of the oxide layer. A nearby ionizing discharge has very little influence upon the fraction of incident molecules which is condensed upon and taken up by a barium film.

1. INTRODUCTION

It is well known that carbon monoxide is a common residual gas in radio valves and the like. Heated metals evolve this gas because carbon and oxygen impurities diffuse separately to the surface, there combine, and are given off as carbon monoxide (Smithells and Ransley[4]).

The absorption of carbon monoxide by barium getters has been studied recently by Arizumi and Kotani,[5] Wagener,[6] and by Morrison and Zetterstrom.[7] In the experiments of Arizumi and Kotani, the conditions of deposition of the barium films changed in successive runs, and were found to control the characteristics of the absorption. Hence, it is difficult to deduce the mechanism of the absorption from this study. Wagener found that the quantity of carbon monoxide taken up by barium at room temperature was small, suggesting that a layer of impervious material is formed by the reaction. It was found that a barium film which had been poisoned by carbon monoxide did not take up oxygen when this gas was introduced afterwards. At higher temperatures (110° C, 160° C), the capacity for carbon monoxide did increase, although at 60° C it was about the same as at room temperature. No explanation for this was given. Morrison and Zetterstrom presented data of engineering value, but did not investigate the details of the mechanism of absorption. It is significant that these workers found that the capacity at 150° C was greater than at 25° C.

The present author[1,2] has studied the absorption of oxygen by barium, and confirmed Mott's[3] theory of the oxidation of metals. The present work was undertaken to see how far the characteristics of the pumping of carbon monoxide by barium can be explained with the aid of Mott's theory. In this theory, it is assumed that oxide layers grow by the diffusion of metal ions, from the parent metal to the gas layer adsorbed on the free surface of the oxide. This motion of ions is through interstitial positions in the lattice of the oxide, and is controlled by the electric field due to contact potential difference in the case of thin oxide layers (50 Å, or thereabouts). In thicker oxide layers, the metal ions can only move by virtue of their thermal energy, and so the oxide layer can only grow to more than 50 Å thick when the temperature is high enough. An outline of Mott's theory was given in the paper on the oxidation of barium.

2. APPARATUS AND EXPERIMENTAL METHOD

The experimental method is based on Knudsen's Law of flow of gases at low pressures. The pressure drop, $p_m - p_g \sim 10^{-5}$ mm of mercury, across a constriction of known

conductance, $K = 0{\cdot}1$ l.s^{-1}, is measured continuously with ionization gauges, one placed in a manifold into which the gas being studied is introduced, and the other placed beyond the construction and near the getter. Now the throughput of gas to the getter at any instant is $Q = K(p_m - p_g)$; and so the total quantity of gas taken up by the getter in a period t_1 can be found, from the area under a Q versus t curve, between the limits $t = 0$ and $t = t_1$. At any time, the speed of pumping of the gas by the getter is $S = K(p_m/p_g - 1)$.

The particular form of apparatus used in the present experiments has been described before, Bloomer.[8] For the present work, carbon monoxide was prepared by the reaction of sulphuric acid and potassium ferrocyanide. The carbon monoxide was dried, by storing it in a gas handling system containing a trap cooled by liquid nitrogen. Barium films were obtained from commercial getters of three different makes. The experimental procedure was the same as in the work with oxygen.

3. RESULTS

The speed of pumping of carbon monoxide by barium was found to vary with time, as shown in the typical experimental curves of Fig. 1. Curves of similar form, with an initial

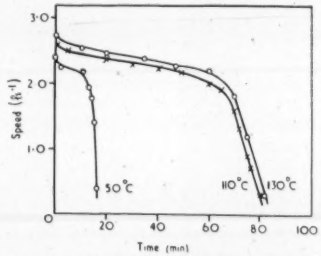

Fig. 1. The variation with time and temperature of the speed of pumping of carbon monoxide by barium $p_m = 4 \times 10^{-5}$ mm of mercury.

rapid fall, followed by a slower steady fall, and a final rapid fall to near zero speed, were obtained when the area of the getter film was changed by two or three times, and the pressure in the manifold was altered by an order or so. Fig. 2 is a plot of the values of speed per unit area of the getter film, measured at different temperatures a few minutes after the start of each run, that is after the initial rapid, but small, drop in speed. The ratio of the speed of pumping of unit area of film to the theoretical speed of pumping through a unit area hole in a thin diaphragm is called the condensation coefficient, and is a measure of the fraction of the molecules which are absorbed upon striking the getter. Corresponding values of condensation coefficient and temperature have been found to be:

20° C, 0·012; 70° C, 0·013; 120° C, 0·022; 170° C, 0·025.

For carbon monoxide at room temperature, the theoretical speed of pumping is 11·9 l.s^{-1} cm^{-2}. (The theoretical speed at room temperature was used when calculating condensation coefficients, because in the experiments, the temperature of only the getter film, and not the walls of all the apparatus, was varied.)

The speed of pumping increased slightly with the amount of ionizing electron current in a diode near the getter. It was found that the influence of electron current was unchanged when the distance between the getter and the nearby ionization gauge was altered in successive runs. It was checked that the ratio of ion current to electron current in

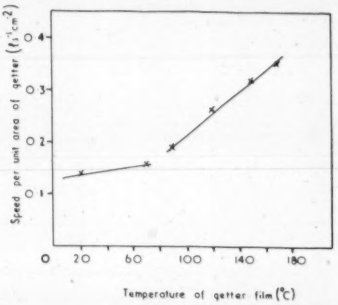

Fig. 2. The variation with temperature of the speed of pumping of unit (apparent) area of getter film

the ionization gauge was independent of changes of electron current in the range from a few microamperes to a few milliamperes. Therefore, the electron current in the ionization gauge itself was varied, to investigate the influence of an ionizing electron discharge (180 V) upon the speed of pumping of the getter. Two typical curves of the variation of speed with electron current are shown in Fig. 3. The rate of rise

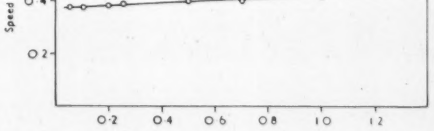

Fig. 3. The variation of the speed of pumping with electron current

of speed with electron current increased steadily with temperature. Mean values were found to be as follows:

20° C, 0·074 l.s^{-1} cm^{-2} mA^{-1}; 70° C, 0·094; 110° C, 0·10; 150° C, 0·11(4).

The capacity of barium getters for carbon monoxide was found to increase with temperature, as reported by Wagener[6] and Morrison and Zetterstrom,[7] but it has been found that the increase is not at a steady rate. Below 80° C, the amount of carbon monoxide taken up is independent of the thickness of the barium deposit, but increases slightly with temperature. Above 80° C, the capacity increases in proportion with the thickness, and is independent of temperature. This behaviour is illustrated in Figs. 4 and 5. In Fig. 4, the amount of carbon monoxide taken up, expressed as the number of close-packed monolayers of gas molecules calculated from the apparent surface area of the getter film, is plotted against the time of

firing of the getter at the start of each experiment. The duration of the firing time at a constant heating current was found to control the thickness of the barium deposit. Fig. 5 is a plot of the number of close-packed monolayers of carbon monoxide taken up by unit area at different temperatures. For this series of experiments, the thickness of the barium

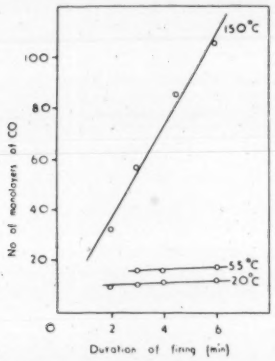

Fig. 4. The variation of capacity of getter with thickness of deposit, at different temperatures

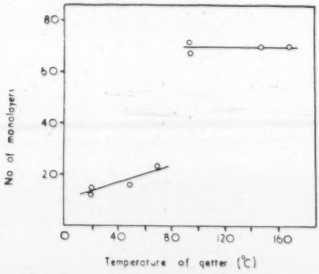

Fig. 5. The influence of temperature upon the capacity, for carbon monoxide, of equal thickness barium films

deposit was kept constant (the getter was fired for four minutes at the same constant heating current as was used in the experiments reported in Fig. 4). When they were kept below 80° C, getter films which had ceased taking up carbon monoxide looked unchanged and mirror-like. When kept above 80° C, getters which had ceased to take up carbon monoxide had become translucent, and were stained brown.

4. COMMENTARY

The present work shows that the capacity of barium films for taking up carbon monoxide does not increase with the thickness of the original film, when the temperature is below about 80° C. Thus, a protective layer of reaction product is formed. In contrast, at temperatures higher than the critical value of 80° C, the whole of the barium film is used up in the reaction with carbon monoxide. This behaviour is reminiscent of the oxidation of barium, for which the critical temperature is about 35° C, Bloomer.[1,2] It is probable that carbon monoxide breaks up into carbon and oxygen at the barium surface, since getter films which had reacted completely and gone translucent were stained brown. The oxygen (atomic), which is formed at the barium surface, would react with the metal. Thus, the similarity between the absorption of oxygen and carbon monoxide is to be expected.

A critical temperature above which an oxide layer ceases to be protective is predicted in Mott's[3] theory of the oxidation of metals. It is shown that the critical temperature (on the absolute scale) is proportional to the height of the energy barrier to the movement of metal ions from the underlying metal into interstitial positions in the lattice of the growing oxide. Thus, for the carbon monoxide reaction, a higher energy barrier than for oxygen is implied, and is probably caused by the presence of the free carbon in the oxide. It is clear that this temperature is not characteristic of the energy of dissociation of the gas, for this is smaller for carbon monoxide (1·15 eV) than for the formation of nascent oxygen (3·35 eV). Arizumi and Kotani[5] found that a getter which had ceased to pump carbon monoxide at lower temperatures started to absorb the gas when heated. This is evidence that the getter was raised above the critical temperature.

The form of the speed versus time curves, like those of Fig. 1, has a ready explanation. The small but rapid fall in speed in the first few minutes of a run is caused by the absorption of gas upon the fresh getter surface. When the getter film is kept below the critical temperature of 80° C, the amount of gas taken up during this rapid fall in speed is just enough to form a close-packed monolayer upon the apparent surface area of the getter, as is shown in Fig. 6.

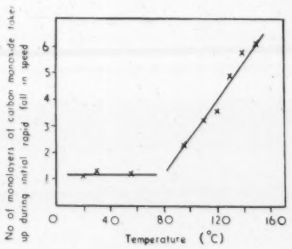

Fig. 6. The variation with temperature of the amount of gas taken up initially

Above the critical temperature, the amount taken up is greater and increases with temperature. The slower, steady falling off in speed, which takes place throughout the active life of a getter film, is evidence that the diffusion of barium ions through the layer of reaction product (oxide) is impeded, probably because the layer contains free carbon. The linear fall of speed with time follows naturally from the linear increase with time of the thickness of the layer containing free carbon. An alternative explanation could be that the fall of speed is caused by a concentration gradient of interstitial barium in the growing oxide layer, but against this is the fact that there is no falling off in speed in the case of oxygen.

The rapid fall in speed at the end of life is approached more slowly above than below the critical temperature.

Above the critical temperature, the getter film is used up at the edges sooner than in the middle parts where it is thicker, and so at the end of life there is some reduction in the area of the still active part of the film. This causes the onset of the rapidly falling part of the speed versus time curve to be less abrupt above the critical temperature.

The condensation coefficient of carbon monoxide upon barium appears to be limited by the superficial density of barium ions at the free surface of the getter film, for the speed varies with temperature at different rates below and above the critical temperature, as does the rate of diffusion of ions by way of interstitial positions, according to the theory of Mott. Clearly, the rate of arrival and condensation of carbon monoxide molecules is not limiting the speed, which has been found to be independent of pressure and less than the theoretical value. By contrast, the throughput of gas to the getter does, of course, depend upon the pressure. It is only in the rapidly falling part of the speed versus time curve, near the end of the active life of the getter, that the throughput is limited by the capabilities of the getter, and not by the conductance of the constriction and the manifold pressure. Since the rate of change of speed with ionizing electron current does not alter abruptly at the critical temperature, although the speed (condensation coefficient) does, it is concluded that activated or ionized molecules are not taken up by the getter directly. This is consistent with the earlier evidence that the absorption is preceded by dissociation of the carbon monoxide.

5. CONCLUSIONS

(1) The product of the reaction between barium and carbon monoxide forms a protective layer at temperatures less than 80° C. At higher temperatures, the whole of a barium film is used up in the reaction.

(2) The reaction product is probably barium oxide, containing free carbon.

(3) About 1 in 80 of the incident molecules of carbon monoxide, striking the barium surface in a given period, is taken up at room temperature, and about 1 in 40 at 170° C. These fractions are set by the superficial density of interstitial barium ions in the free surface of the oxide layer.

(4) An ionizing electron current has only a very slight influence upon the speed of pumping of carbon monoxide.

(5) The absorption of carbon monoxide is preceded by the adsorption of a monolayer or so of the gas. No nucleation centres are necessary for this adsorption to occur, since barium getters always take up this gas without an induction period, and the speed of pumping falls, rather than rises, in the first few minutes after the gas is introduced.

ACKNOWLEDGEMENTS

It is a pleasure to thank Mr. B. M. Cox for much help with the experiments, Mr. M. E. Haine for advice and encouragement, and Dr. T. E. Allibone, Director of the Research Laboratory, Associated Electrical Industries, Ltd., for permission to publish this paper.

REFERENCES

(1) BLOOMER, R. N. *Nature* [*London*], **179**, p. 493 (1957).

(2) BLOOMER, R. N. *Brit. J. Appl. Phys.*, in press (1957).

(3) MOTT, N. F. *Trans Faraday Soc.*, **43**, p. 429 (1947).

(4) SMITHELLS, C. J., and RANSLEY, C. E. *Proc. Roy. Soc. A*, **155**, p. 195 (1936).

(5) ARIZUMI, T., and KOTANI, S. *J. Phys. Soc. Japan*, **7**, p. 415 (1952).

(6) WAGENER, S. *Vacuum*, **3**, p. 11 (1953).

(7) MORRISON, J., and ZETTERSTROM, R. B. *J. Appl. Phys.*, **26**, p. 437 (1955).

(8) BLOOMER, R. N. *Brit. J. Appl. Phys.*, **8**, p. 40 (1957).

A system for recording transmission errors in universal joints

By A. J. BARTLEY, B.Sc., A.M.I.Mech.E., and R. W. GREGORY, M.A., Ph.D.,* Department of Mechanical Engineering, University of Durham

[*Paper first received* 27 *February, and in final form* 29 *March*, 1957]

This paper describes the development of a new system for recording the "performance characteristics" of universal joints. The system is described in detail and some test results obtained with a single Hooke's joint are included. The system could also be used for recording the twist in a shaft subject to torque and would be most suitable for use on shafts where the twist is to be measured over two reference points which are so remote from each other that more conventional systems could not be used.

1. INTRODUCTION

Ideally, the velocity ratio of a universal joint connecting two co-planar shafts should be unity in all circumstances; in particular, it should be independent of speed, torque and transmission angle. Certain joints, notably Hooke's couplings, are inherently imperfect in the sense that the theoretical velocity ratio is not constant except at zero transmission angle, while others, even when kinematically perfect, are subject to errors arising from elastic distortion and the need for adequate working clearances between mating parts.

A study of errors in universal joints is desirable not only for its general kinematic interest but also because such joints are often incorporated in the transmission systems of precision machine tools. Since errors of only a few minutes of arc may be important in such cases an attempt has been made to devise measuring apparatus which will enable universal joints to be tested to this degree of precision under machine shop conditions and which will, at the same time, accommodate transmission angles up to a maximum of 40°. The

* Now at University of Cambridge.

latter requirement rules out the possibility of making a mechanical connexion between measuring devices on the input and output shafts; in fact, such a connexion could only take the form of another, equally imperfect, universal joint or its equivalent.

An apparatus which appeared to be satisfactory for this purpose was developed in 1948 by Dr. M. Grützmacher as part of the rehabilitation programme sponsored in Germany by the Department of Scientific and Industrial Research. This system was originally developed for measuring the dynamic deflexion of gear teeth but was subsequently further developed by the Mechanical Engineering Research Laboratory (M.E.R.L.) for use on other problems in the field of dynamic metrology including its application to universal joints. The equipment developed at M.E.R.L.[1] was loaned to the authors under a D.S.I.R. research contract but was found to have certain drawbacks and the alternative measuring system, described in the following pages, was therefore developed.

The possible use of the optical properties of polaroid as a basis for measuring small angular displacements was also investigated[2] and rejected in favour of the method here described. This method, although similar to that developed by M.E.R.L. in so far as both make use of time-modulated signals generated in pick-ups associated with the input and output shafts, differs from the original both in respect to the means by which the signals are generated and, more fundamentally, in the circuit employed for demodulation.

2. THE MEASURING SYSTEM

2.1 *Principle of operation.* Fundamentally, the measuring system operates by comparing two non-sinusoidal, alternating signals generated in pick-ups associated with the input and output shafts. These signals are similar in that the pick-ups are identical but the signal from the output shaft is time-modulated, i.e. displaced in time, with respect to the input shaft signal due to transmission errors in the universal joint. Information as to the nature and magnitude of the transmission errors can be obtained by comparing the signals in a suitable electronic circuit.

This principle is not new but usually sinusoidal signals are employed and comparison effected in a phase discriminator whose output is proportional to the sine of the phase difference between the signals. In the simpler types of circuit, the desired output is contaminated by a large unwanted carrier ripple which must be eliminated by a low-pass filter and, in the process, the useful output may be seriously distorted unless the ratio of carrier to desired signal frequency is large. Such distortion can be avoided, however, by using an alternative method of detection (see section 2.2) which gives negligible carrier ripple and so needs no filtration.

The pick-ups can be designed so that, in the absence of transmission errors, the frequency of either generated signal is any integral number, N, times the angular velocity of the shafts. It can be shown that sensitivity is directly proportional to the frequency ratio N, whereas the range of error which can be accommodated without overloading is inversely proportional to N. All experiments described in this paper have been carried out with $N = 72$, which figure is considered to be a reasonable compromise between the conflicting requirements of sensitivity and range.

The pick-ups operate photoelectrically and may be designed to generate a variety of non-sinusoidal wave forms. This flexibility can be used to advantage in eliminating the non-linearity which, as previously mentioned, is an inherent defect of systems operating with sinusoidal carrier signals.

2.2 *Description of electronic circuit.* Fig. 1 is a block diagram showing the elements of the measuring circuit and the waveforms of the signals at various points in the circuit. Detailed diagrams of the circuit are given in Figs. 2(*a*) and 2(*b*).

Pick-ups 1 and 2 are associated, as shown in the top left-hand corner of Fig. 1, with two disks mounted respectively on the input and output shafts of the joint being tested. As

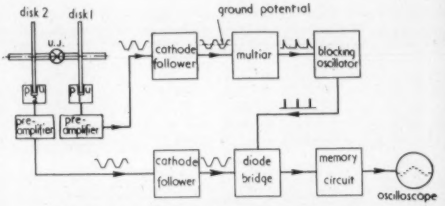

Fig. 1. Block diagram of equipment

the disks rotate, voltages are generated in the pick-ups in a way which is described in detail in section 2.3 but which is irrelevant at the moment. Both signals are approximately 35 V peak-to-peak after pre-amplification and have waveforms similar to a rack profile. The pre-amplifiers are a.c. coupled and the output signals are therefore balanced with respect to earth. Signal 1 is injected through a cathode follower into a multiar[3] which generates a positive trigger pulse each time signal 1 goes negative through earth potential. The triggers operate a monostable blocking oscillator, which generates large pulses a few microseconds in duration, and these pass to an electronic switch consisting of four diodes in a bridge circuit. The switch closes for the duration of each pulse and connects signal 2, *via* a cathode follower, to a " memory " capacitor M. The capacity of this capacitor is sufficiently small with respect to the output impedance of the cathode follower to ensure that it is charged practically to the full potential of signal 2 by the time the switch reopens.

Between pulses, the bridge is non-conducting and the resistance across the "memory" capacitor is a parallel combination of its own leakage resistance, the back resistance of the diodes and the input resistance of the cathode follower output stage. These resistances are all very large and the potential on the capacitor therefore remains virtually unchanged between pulses. At the same time the potential on capacitor C decreases exponentially as charge leaks away through the parallel resistance R. The time constant CR must be small enough for the diodes to pass a heavy current during each pulse and yet be sufficiently large to prevent conduction between pulses. Since the time interval between pulses depends on shaft speed it is necessary to increase R (or C) as speed is reduced but the value of the time constant is not critical and three switched values of R suffice, in practice, to cover the complete working range from 200–1200 rev/min.

If a perfect universal joint is tested, the signals from the pick-ups have a fixed phase relationship. The potential of signal 2 is therefore the same at every inspection; that is, each time the electronic switch conducts the "memory" capacitor is charged to the same potential and the output from the measuring system remains constant. On the other

hand, when transmission errors cause relative time modulation of the signals from the pick-ups, the potential of signal 2 varies from one inspection to the next and the output is an escalator wave made up of 72 steps per shaft revolution. (The pick-ups are so phased that signal 2 is always inspected on a falling flank. Straightness of this flank is necessary and sufficient to ensure linearity of the measuring system.)

as for the signal from pick-up 1 when the frequency ratio is 72 and the universal joint is rotating at 800 rev/min) and signal 2 had the same peak-to-peak amplitude but the frequency and waveform could be varied.

Figs. 3 and 4 relate to two tests which were made with the frequency of signal 2 adjusted to 16 c/s. In the first test the signal was sinusoidal and in the second test a squared-off

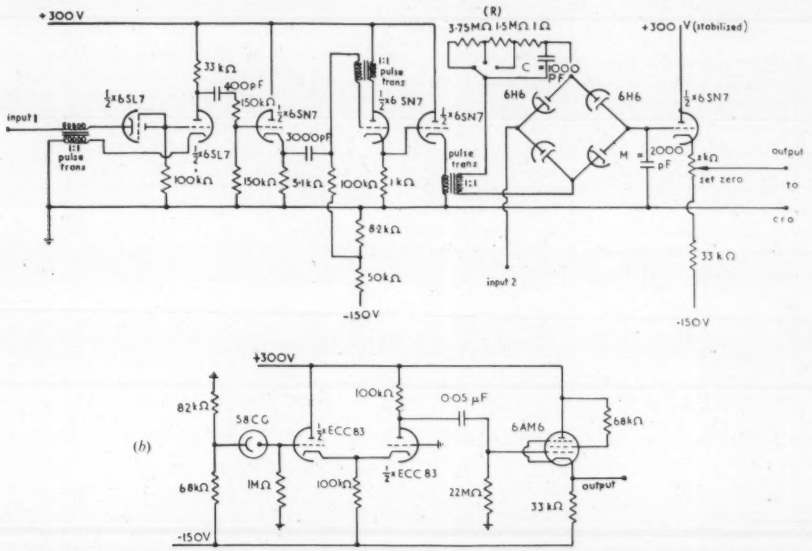

Fig. 2. (*a*) Diagram of time-demodulator circuit. (*b*) Diagram of pre-amplifier circuit

On account of the small size of the steps in the escalator wave, carrier ripple is negligible in the output. The escalator therefore approximates to a smooth curve through the inspected points but it is important to appreciate that this envelope is *not* a continuous record of transmission error. The error is only observed at 72 points per revolution and in conceiving these points to be joined by a smooth curve it is tacitly assumed that the function is well behaved. In so far as it is commonplace to draw a smooth curve through a finite number of experimentally observed points, this is not a serious limitation of the method but it is as well to realize that a transient error whose life cycle is less than the time interval between pulses may not be recorded.

2.3 *Acceptance tests on the measuring system.* In order to estimate the probable performance of the measuring system as a whole, the component parts were first tested separately. The more important of such preliminary tests were made on the demodulating system and were designed to assess the fidelity with which a known input signal could be reproduced. For this purpose signals 1 and 2, which are generated in the two pick-ups in the complete test rig, were injected from laboratory oscillators. Several series of tests were made. In one such test, signal 1 was sinusoidal with amplitude 35 V peak-to-peak and frequency 960 c/s (the amplitude and frequency but not the waveform are the same

sinusoid, obtained by passing a sine-wave through a limiting circuit, was used. The figures are photographic records taken from an oscilloscope and show the injected signal 2 (continuous trace) and the stepped output waveform from

Fig. 3. Sinusoidal test signal with its associated escalator type trace superimposed

the detecting system. The input signal is seen to be faithfully reproduced even when there are sudden discontinuities in the waveform.

Similar satisfactory results were obtained in further series

of tests in which the frequency of signal 1 was adjusted to selected values in the range corresponding to shaft speeds between 200 and 1200 rev/min. The frequency, amplitude and waveform of signal 2 was altered from time to time during these tests.

It may be objected that the mean frequencies of the two input signals from the pick-ups are necessarily the same and

Fig. 4. Squared-off sinusoidal test signal with its associated escalator type trace superimposed

that the preliminary tests should have been made using one fixed frequency oscillator and one frequency modulated oscillator. This would certainly have been the most realistic arrangement but unfortunately such test gear was not available. However, to guard against the possibility that the excellent reproduction evident in Figs. 3 and 4 might be due to the relatively low frequency of signal 2, another series of tests were made with the oscillator frequencies set at 720 and 704 c/s approximately. No deterioration in performance was observed and the detecting system was therefore considered to be entirely satisfactory.

2.4 *Description of experimental rig.* Having "proved" the demodulating unit, an apparatus was built to extend the tests to include the photoelectric pick-ups. This apparatus is shown in Fig. 5. A Hooke's joint is mounted between two

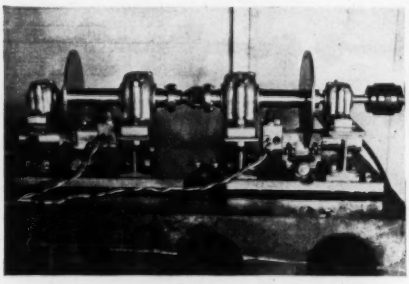

Fig. 5. Photograph of experimental apparatus

shafts each of which is supported by two journal bearings. The input shaft assembly is shown on the right-hand side of the picture and is rigidly clamped, *via* its baseplate, to a cast iron foundation block. The output shaft assembly is free to rotate about the axis of the joint and can be clamped to the foundation block so as to give any desired transmission angle up to 15°. In all other respects the two assemblies are identical but of opposite hand.

Signals 1 and 2 are derived from the disks and pick-ups associated with the input and output shafts respectively. Each disk has seventy-two $\frac{3}{16}$ in. diameter holes equally spaced on a pitch circle of such diameter (8·596 in.) that the holes and the spaces between holes subtend equal angles of $2\frac{1}{2}°$ at the centre of the disk.

A cross-sectional elevation through one pick-up is shown in Fig. 6. In its essentials it consists of a light source, a rectangular aperture and a photocell. The disk is arranged to rotate between the light source and the aperture so that the light beam illuminating the photocell is periodically interrupted. The dimensions of the aperture and its position relative to the hole is such that the inspected flank of the rack-shaped waveform corresponds to an angular movement of 5/3 degrees; the maximum transmission error which can be recorded, therefore, is $\pm 5/6$ degrees. The light filament is

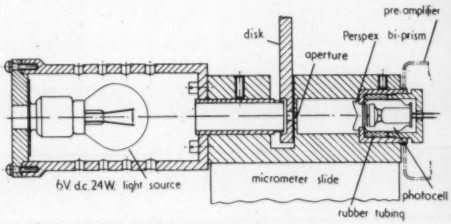

Fig. 6. Sectional elevation through pick-up (one-third normal size)

arranged perpendicular to the longitudinal axis of the aperture in order to render the illumination of the photocell as even as possible. In addition, a Perspex bi-prism is placed in front of the photocell to split the light beam into two parts before it reaches the cathode. The object of this is to ensure that the central area of the cathode, which contains a $\frac{1}{8}$ in. diameter hole for the passage of the anode lead, is not illuminated as otherwise it would result in curvature of the flanks of the waveform and hence lead to non-linear operation.

Each photocell and its preamplifier is wired on a small chassis which can be inserted in the main body of the pick-up and the complete assembly is mounted on a horizontal micrometer slide secured to the baseplate as shown in Fig. 5. The purpose of the slides is to facilitate correct positioning of the pick-ups with respect to the disks.

As can be seen from the circuit diagram, Fig. 2(*b*), each preamplifier consists of a double triode amplifying stage coupled to a cathode follower by a high-pass network having a time constant of 0·11 sec. The minimum speed at which tests are to be made on universal joints is 200 r.p.m. This figure corresponds (for disks with 72 holes) to a carrier signal with a period of 1/240 sec which is sufficiently short compared with the time constant of the coupling network to obviate distortion in the pre-amplifier and hence to ensure that the sensitivity of the measuring system is independent of speed.

2.5 *Calibration procedure and disk correction.* To calibrate the apparatus it is necessary, in theory, to rotate one disk through a known angle with respect to the other and observe the effect on the output trace. As this would have to be done when the system is rotating it is clearly a more practical proposition to leave the relative angular positions of the disks unaltered and move one of the pick-ups by means of its micrometer slide. The micrometer slide moves the

pick-up in a straight line and not along the pitch circle of the holes as is theoretically necessary but the required range of angular movement is so small that no significant error results from this approximation. The linear movement of the pick-up can be controlled to an accuracy better than 0·001 in. which, when referred to the disk, corresponds to an angular movement of less than one minute of arc.

Fig. 7 shows a typical set of calibration results which were obtained at the speed used in the subsequent practical tests, namely 400 rev/min, but any other speed would have been

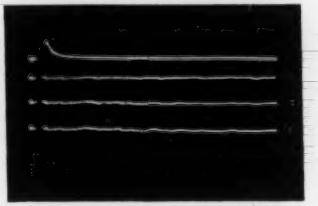

Fig. 7. Calibration results (speed 400 rev/min)

equally satisfactory. In order to exclude transmission errors from the results, the universal joint was replaced during calibration with a rigid straight shaft. The pick-ups were positioned so that their output signals were exactly in-phase and the resulting trace was then displayed on a cathode-ray oscilloscope to give line (*a*) in Fig. 7. One of the pick-ups was then displaced through a known distance (in this case 0·02 in. which is equivalent to 16′ of arc) with the result that the potential of the output signal increased and the trace displaced upwards to position (*b*) in Fig. 7. Similarly, by moving the pick-up in the opposite direction the trace was displaced vertically downwards to position (*c*). Knowing the distance moved by the pick-up it was possible, by measuring the corresponding trace displacement on the oscilloscope, to estimate the sensitivity of measurement per unit angular displacement. In Fig. 7, for example, the sensitivity is about 0·4 mm per minute of arc.

In principle, considerable improvement in sensitivity can be obtained by increasing the gain of the oscilloscope amplifier but high sensitivities can only be usefully employed when the errors to be measured are small and under these conditions the residual errors in the trace, due to disk imperfections assume greater relative importance. The overall residual error in the present disks is about ¼′ of arc and if the displacement of the trace due to this error is limited to 1 mm the maximum sensitivity is limited to 4/3 mm per minute of arc. The nature of the error distribution is evident from Fig. 7.

When the disks were tried out originally, the residual error was greater than ¼′ of arc but it was found possible to reduce gross errors by coating the leading edges of the affected holes with thin layers of paint.[4] Holes in both disks were treated in this way according to whether the affected step traces were "high" or "low." Some of this labour could undoubtedly have been avoided if the machining of the disks had been subject to a more rigid dimensional specification. In the present disks, the overall amplitude of the errors is approximately 0·001 in. and an improvement of at least 40% could therefore be achieved by specifying bilateral tolerances of ±0·0001 in., on the central bore of the disks, on hole size and on hole position. These tolerances should not be excessively difficult to hold because they are relative rather than absolute tolerances (that is to say they represent the permissible variation in one disk with respect to the other) and any errors which are present in both disks have no effect on the results. Thus by machining the disks together as a pair, the aforementioned tolerances become easier to maintain.

Although the system is sensitive to the types of errors discussed above it is not very sensitive to errors in radial positioning of the holes. Indeed, it can be shown that such an error can be as great as 0·01 in. without causing any serious effect.

3. TEST RESULTS

Practical tests were conducted on a single Hooke's joint as the behaviour of such a joint can be predicted theoretically. Since this joint is not a "constant velocity" joint, transmission errors are large and a low sensitivity of measurement had to be used in order to keep the output trace on screen. Figs. 8

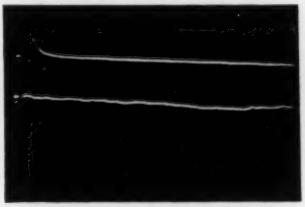

Fig. 8. Test results for a single Hooke's joint. Transmission angle 0°. Speed 400 rev/min. No load

and 9 illustrate the behaviour of the joint at transmission angles of 0° and 10° respectively.

Although the results were nominally obtained under conditions of "no-load" it was found necessary to apply a small resisting torque to the output shaft in order to take up backlash which was causing erratic fluctuations of the peaks of the trace.

In Fig. 9 an attempt has been made to fit the theoretical curve to the actual curve for comparative purposes. The

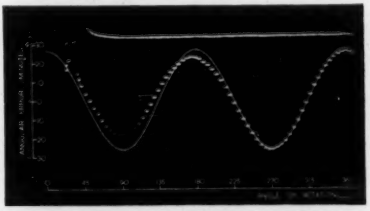

Fig. 9. Test results for a single Hooke's joint. Transmission angle 10°. Speed 400 rev/min. No load

deviations which are apparent between the two curves were present in all the test results to a greater or lesser degree depending upon the angle of transmission of the joint. It is

not proposed to explain this inconsistency as the data available at present is insufficient.

The top trace in Figs. 7, 8 and 9 is a record of a pulse used to trigger the time base of the oscilloscope in order to facilitate photography. The pulse has no significance in regard to the operation of the measuring system.

4. CONCLUSIONS

The merits of the system can be listed as follows:

(*a*) The measuring elements associated with the input and output shafts are mechanically independent and can therefore be mounted in any convenient positions.
(*b*) The equipment, as at present constructed, is capable of recording angular displacements of a few minutes of arc with little interference from mechanical or electrical "noise." It is anticipated that further development will lead to appreciable improvement in this respect.
(*c*) Sensitivity is independent of speed.
(*d*) Cyclic changes in input speed have no effect on the measurements.
(*e*) The system is linear in operation.
(*f*) Calibration can be done without interrupting a test.
(*g*) Subject to the minor limitations mentioned in Section 2.2 sudden changes in the relative angular displacement of the measuring elements are recorded faithfully.

A disadvantage of the method is that the greatest angular error which can be recorded is limited to 5/6°, with the existing 72-hole disks. As mentioned in Section 2.4, this restriction follows from the fact that the effective range of measurement is limited to the angle corresponding to the inspected flank of the carrier signal. In order to increase the range it would be necessary to use disks with fewer holes of larger diameter and to increase the length of the apertures. This entails operating with fewer inspections per revolution and, in consequence, errors in excess of 5/6° cannot be recorded with the same fidelity as smaller ones.

The mechanical independence of the measuring elements suggests a number of alternative applications of the system. For example, the equipment could be used to measure torque in a rotating shaft or, by mounting the elements at the extremities of a crankshaft, to record torsional oscillations. Indeed, the method is suitable for any application in which it is desired to compare angular rotations at two remote stations.

ACKNOWLEDGEMENTS

The work described has been carried out as part of the research programme of the Mechanical Engineering Research Board of the Dept. of Scientific and Industrial Research. The paper is published by permission of the Director of Mechanical Engineering Research.

Thanks are due to Professor A. F. Burstall of King's College, University of Durham, in whose Department the work was carried out and to Messrs. Vickers Armstrongs Ltd. of Newcastle upon Tyne for the loan of variable speed units for the drive to the test rig.

REFERENCES

(1) TIMMS, STEVENSON and CHALMERS. *The Dynamic Measurement of Small Angular Displacements*, Mechanical Engineering Research Laboratory Report No. Mech./Met. 55.
(2) BARTLEY, A. J. *J. Sci. Instrum.*, **33**, p. 20 (1956).
(3) CHANCE, B., Ed. *Waveforms*, Radiation Laboratory Series No. 19 (New York: McGraw-Hill Book Co. Inc., 1949).
(4) DEAN, S. K., and KILBURN, M. A. *Engineer*, **200**, p. 686 (1955).

The effect of oxygen and sulphur on the thermionic emission from matrix cathodes

By J. F. RICHARDSON, B.A., Grad.Inst.P., Physics Department, University College of North Staffordshire

[*Paper received* 5 *March*, 1957]

The poisoning of the emission from matrix cathodes by oxygen and sulphur is reversible. Recovery of the emission is more rapid from oxygen poisoning. The shape of the recovery curves indicates that the poisoning agent is present on the surface and has also diffused into the cathode pores.

Recently,[1] a report has been made of the effect of oxygen and sulphur on thermionic emission from oxide-coated cathodes and on their electrical conductivity. A similar study has now been made on the effect of these elements on the matrix cathode (M-cathode). This cathode has been described by several authors.[2–4] For the present work a mixture of 69·9% of 4–5 μ grain-diameter nickel powder (containing as major impurities 0·1% carbon, 0·001% sulphur and 0·02% iron) with 30% barium carbonate and 0·1% reducing agent (see below) was ball-milled in amyl acetate, dried and pressed, by a blow in a fly press, into the form of a disk which closed one end of a 5 mm diameter O-nickel tube.

The cathode was then mounted as part of a planar diode, the anode consisting of an A-nickel disk 1 cm diameter and 4 mm thick. The electrode separation was 1 mm. To break down the carbonate the cathode was gradually heated to 950° C, the pressure being maintained below 10^{-4} mm of mercury. The cathode was sintered at 1100° C for thirty minutes, and activated at this temperature by applying 100 V to the anode. During the next twenty-four hours the cathode was aged, the temperature being reduced gradually to 850° C over the first two hours. The tube was then gettered and sealed-off.

Three reducing agents were used at various times, zirconium, zirconium hydride and silicon. No difference in the performance of the resultant cathodes could be detected. Richardson plots gave straight lines over the temperature range 600–900° C and their slopes indicate work functions of 1·7 to 1·8 eV. The interpretation of such slopes as leading directly to work-functions is open to doubt, and this point is being investigated further in these laboratories. All temperatures were measured by means of a tungsten–nickel thermocouple.

Poisoning was achieved by including in the valve an alumina-coated tungsten filament on which was painted a suspension of barium peroxide in amyl acetate and 5% collodion as binder, to provide oxygen, or a filament coated with a similar suspension of molybdenum disulphide[1] for the sulphur. Oxygen or sulphur was released by passing a current through the filament. The valves containing the sulphur filament could be baked only up to 250° C for outgassing, since at higher temperatures sulphur was liberated. To study cathode recovery the emission was poisoned to 10% of its value at a fixed temperature and anode voltage, and the reactivation then continously recorded.

RESULTS

Oxygen poisoning. Typical recovery curves are shown in Fig. 1. Recovery of cathode emission at 800° C or higher was relatively rapid taking about ten minutes at 800° C. At lower temperatures the recovery was not as rapid as at the higher temperatures (e.g. after two minutes the recovery was 99% at 950° C, 79% at 700° C and 73% at 650° C). Variations in anode voltage had little effect between 0 and 12 V positive. This voltage was not exceeded since the first

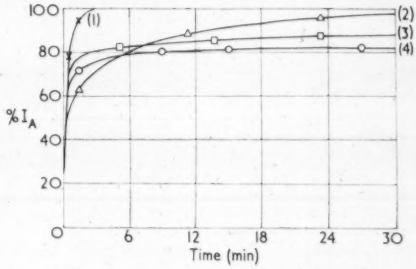

Fig. 1. Oxygen poisoning of *M*-cathode

Curve (1). $V_A = 8$ V, $T = 950$° C. Poisoned gradually to 10% I_A over 1 min.
Curve (2). $V_A = 8$ V, $T = 775$° C. Poisoned rapidly to 10% and maintained at that value for 1 min.
Curve (3). $V_A = 8$ V, $T = 700$° C. Poisoned gradually to 10% I_A over 1 min.
Curve (4). $V_A = 8$ V, $T = 650$° C. Poisoned gradually to 10% I_A over 1 min.

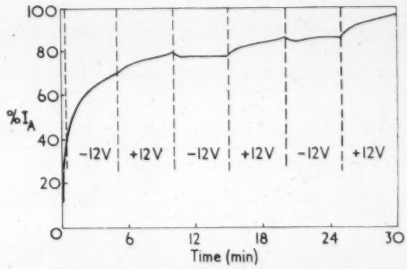

Fig. 2. Oxygen poisoning of *M*-cathode
Voltage reversed at 5 min intervals.

ionization potential of oxygen is 13·6 V. However, if the voltage was reversed at regular time intervals, a plot similar to that in Fig. 2 was obtained. The emission during the periods when the voltage was negative was measured by reversing the voltage for sufficient time to take a reading.

The curve indicated that the cathode was repoisoned during the negative voltage periods.

If the cathode was poisoned rapidly to 10% of its emission [Fig. 1, curves (1), (3) and (4)] the initial recovery was very rapid, but if it was poisoned to the same extent over a longer period [Fig. 1, curve (2)] the initial recovery was much slower. After approximately fifteen minutes the recovery in each case was the same.

Sulphur poisoning. With sulphur, typical curves for which are shown in Fig. 3, the recovery was very similar to that from oxygen poisoning, but slower. The first ionization potential of sulphur is 10·3 V so voltages below this value only were used. The reduction of emission to 10% of the initial value by sulphur poisoning took longer than for poisoning by oxygen at the same cathode temperature and

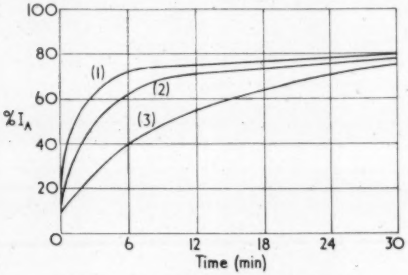

Fig. 3. Sulphur poisoning of *M*-cathode

Curve (1). $V_A = 8$ V, $T = 800°$ C. Poisoned gradually to 10% I_A over 1 min.
Curve (2). $V_A = 8$ V, $T = 750°$ C. Poisoned gradually to 10% I_A over 1 min.
Curve (3). $V_A = 8$ V, $T = 700°$ C. Poisoned rapidly to 10% I_A and maintained at that value for 1 min.

under approximately comparable conditions. The initial rate of recovery was appreciably less rapid than from oxygen poisoning, though, as for oxygen, the rate of recovery did depend on the rate of poisoning. After some minutes the emission from the cathode recovering from sulphur poisoning was about 20% below that from a comparable cathode at the same temperature recovering from oxygen poisoning. No repoisoning of the cathode by sulphur was detected on reversing the voltage across the diode.

CONCLUSIONS

The poisoning of electron emission from *M*-cathodes by both oxygen and sulphur is reversible, although the recovery from sulphur poisoning is slower than from oxygen poisoning. Sulphur is a less effective poisoning agent than oxygen but no quantitative work has been carried out on this aspect as yet.

The recovery curves indicate that the poisoning is due to two processes. One is the sorbtion of poisoning material on the cathode surface and the second is by diffusion of material into the cathode. As reactivation occurs the surface material is lost quite readily, giving the rapid initial increase in emission, whereas the material in the cathode diffuses out comparatively slowly, giving the gradual return to complete activation. More material will diffuse into a cathode the longer the poisoning period and so it will reactivate more slowly, as the results show. These results appear compatible with the fact that the sulphur atom or ion is larger than the oxygen atom or ion and hence would be more difficult to diffuse into or out of the matrix. The recovery rate may also be influenced by the gas pressure in the region near the cathode surface.

The repoisoning of the cathode by oxygen when the voltage across the valve is reversed could be due to either the oxygen leaving the cathode as negative ions, or some material leaving the anode and moving to the cathode. It has been found[5] that with oxide-coated cathodes the oxygen which leaves the cathode after poisoning is in the form of O_{16}^- ions. It is hoped soon to use a mass spectrometer to study the recovery process to determine if this observed effect is due to ionized oxygen. From energy considerations sulphur should be able to ionize to about the same extent as oxygen. That such an effect has not been observed with sulphur may be due to the insensitiveness of the method employed in these preliminary experiments.

ACKNOWLEDGEMENTS

The author wishes to express his thanks to Prof. F. A. Vick, who supervised the work, for the laboratory facilities provided, and also to Metropolitan-Vickers Electrical Co. Ltd. for permission to publish and without whose support this work would not have been possible.

REFERENCES

(1) Higginson, G. S. *Brit. J. Appl. Phys.*, **8**, p. 148 (1957).

(2) MacNair, D., Lynch, R. T., and Hannay, N. B. *J. Appl. Phys.*, **24**, p. 1335 (1953).

(3) Dodds, J. M. *Nature [London]*, **174**, p. 1176 (1954).

(4) Beck, A. H., Brisbane, A. D., Cutting, A. B., and King, G. *Vide*, **9**, p. 302 (1954).

(5) Shepherd, A. A. *Brit. J. Appl. Phys.*, **4**, p. 70 (1953).

The ageing of gas-filled standard lamps on a.c. and d.c.

By W. Barnett, R. G. Berry, B.Sc., Grad.I.E.E., and J. S. Preston, M.A., M.I.E.E., F.Inst.P., F.I.E.S.,
Light Division, National Physical Laboratory, Teddington, Middlesex

[*Paper received* 14 *March*, 1957]

A comparison is made of the rates of fall of light output and current, at constant voltage, and colour temperature 2700° K approx., of 100–110 V 100 W gas-filled photometric standard lamps, on a.c. and d.c. supplies. The rates are appreciably greater on d.c. than on a.c., and this is shown to be due to specific effects of d.c.-operation on filament resistance, and filament emissivity. These effects are shown to be fully reversible, after many hours of burning, by reversal of the d.c. polarity, and not inconsistent with migration of tungsten along the surface of the filament. A practical conclusion is that the usefully smaller rate of depreciation characteristic of a.c.-operation may be fully retained on d.c. by reversal of polarity at regular convenient intervals. An a.c. supply, with its easy voltage regulation, is then legitimate for burning the lamps for the lengthy periods of the normal preliminary ageing tests.

A

1. INTRODUCTION

The light-output of a tunsten filament lamp, at constant voltage, behaves somewhat irregularly within the first 10 or 20 h of burning. Thereafter, however, it falls fairly steadily throughout life. An obvious reason is gradual evaporation of the filament. This gets thinner, its resistance increases, and so both the current and the power consumed gradually fall, while concomitant blackening of the bulb may also add to the reduction in light-output. A less obvious, and perhaps less important, reason might be roughening of the surface of the filament, owing to progressive structural changes. Its radiating properties would then tend more and more toward those of a true grey body. The selective emission of *visible* radiation—a well-known property of a rolled or drawn tungsten surface in its initial condition—would thus be somewhat reduced and, of the total power consumed, a rather larger fraction would be radiated in the *invisible* infra-red.

For lamps to be used as secondary standards of light, the light-output must not fall by more than 2–3% per 100 h of use, at a reasonable operating temperature or voltage. A greater ageing rate may indicate a technically faulty lamp. It also makes re-calibration necessary too often for convenience or economy. The rate is found by burning the lamps for 100 h or so, and comparing them every 25 h or so with similar but already seasoned lamps, unburned except for the quite short time taken by the observations. For such photometric measurements, including the subsequent calibration and use of the lamps, a d.c. supply is used, to enable the lamp-voltage to be set, without difficulty, as accurately as possible. Naturally then, it is necessary also to burn the lamps on d.c., not a.c., during the ageing runs, if the purpose is to obtain a direct measure of the ageing rate which is consistent with the way the lamps are subsequently to be used as standards.

Burning, or ageing, on a.c. would in fact yield too optimistic a figure for lamp performance, from this viewpoint. Comparison of N.P.L. results with those of other laboratories has, on occasion, revealed differences which can be resolved only by assuming the ageing rate on a.c. to be about one-half that on d.c., at the same r.m.s. voltage. Lieb[1] found a higher rate with d.c. than with a.c. He also found that, in gas-filled lamps, the filament resistance increased more rapidly on d.c. than on a.c., though in vacuum lamps the increase was, contrariwise, the more rapid on a.c. Filaments operated on d.c. also showed the greater degree of surface-disorder. Johnson[2] and de Vos[3] found that the surface structure produced by d.c. operation was a regular pattern of ridges, though this pattern appeared also with a.c. operation, in regions of large temperature gradient near the ends of the filament, so that it was probably associated in some way with migration of tungsten along the surface.

The present paper describes systematic experiments to find what effect the nature and polarity of the electric supply have upon both the light-output and filament resistance. It confirms the older findings. Principally, however, it presents new results, which are of fundamental interest and show how the smaller a.c. rate of ageing can be preserved while lamps are being measured, or used as standards, on d.c. This in turn makes a.c., with its greater convenience, quite appropriate for burning the lamps during the preparatory ageing process, so that two considerable practical advantages are won by a single means. The work is restricted to gas-filled lamps, but a second study, of vacuum lamps, is planned.

The lamps used were of the special 100–110 V, 100 W type, made by the General Electric Co. Ltd., of England, for use as secondary standards of luminous flux, and described by Leeds and Winch[4] and Winch.[5] The single-coil filament—a complete octagonal wreath—is fed by symmetrically placed leading-in wires supplying the two halves in parallel. The filament is welded to these and to the six other supporting wires. All the lamps were set at a colour temperature near 2700° K, with voltages near 100 V. These voltages were never varied, except for one burning period only, in the first experiment. The exception is without significance here, however.

2. INITIAL OBSERVATIONS

Eleven such lamps were being aged at N.P.L. for internal use. They were burned on a d.c. supply as usual and measured, at 30 h and intervals thereafter, in a 1 m spherical integrator with a high-precision photoelectric photometer. The full lines in Fig. 1 show the changes in light-output against duration of burning. At 93 h an inquiry was thought desirable into the inconsistent shapes of the graphs so far. At *A* and *B* the lamps had been removed from the ageing racks, measured, and replaced in the symmetrical bayonet sockets of the racks *regardless of polarity*. Thus, there was a chance of reversal, for any lamp, at *A* and at *B*. It was seen that for period *BC* some lamps continued to fall, but others quite unexpectedly rose in output. Was this due, then, to reversals of polarity of the latter at *B*? If so, why did *all* the lamps fall in the period *AB*, after a chance that some could have been reversed at *A*? Only speculative answers were possible to the second question—an over-methodical operator at *A*, or some over-shoot of initial vagaries in the

lamps. The first question was nevertheless persistent. Therefore, the lamps were given a short run *CD*, in the hope of obliterating past history, the polarity now being noted. Then followed a run *DE* on the same polarity, and a run *EF* with polarity reversed on *all* the lamps. The whole graphs, and particularly the change of gradients at *E*, then showed that reversal of polarity indeed had an effect, tending to oppose the previous trend, and in seven cases even changing the sign of a previously established rate of fall. Moreover, while such an effect could obviously not persist indefinitely after a single reversal, its "time-constant" was certainly of the order of hours, as witness the incomplete effect of the short "stabilizing" run *CD*.

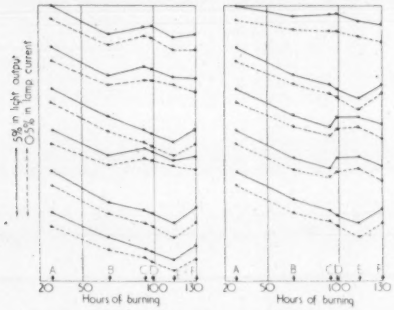

Fig. 1. Changes in light output and lamp current during the ageing of eleven gas-filled lamps at constant voltage. The vertical scales are relative and are, respectively, as indicated on the left-hand side of the diagram. The electric supply was d.c,but subject to chance-reversal after each occasion of measurement except *D* where it was unchanged, and *E* where it was deliberately reversed on all the lamps

The broken lines in Fig. 1 show measured lamp-currents, on a relative scale ten times more open than the scale of light-output. An immediate further conclusion is that there are concurrent and consistent changes in filament resistance, with the light-output changing roughly as the tenth power of amperes or watts consumed. Quite notable is the fact that the filament resistance can *fall* for some time after a reversal of the polarity of the supply.

3. THE MAIN EXPERIMENT

Twelve fresh lamps, not previously burned by the makers, were then obtained and used in a systematic experiment. Four were placed on an a.c. supply, four on d.c. of fixed polarity, and four on d.c. whose polarity was reversed every two hours. Because the last group had to be switched off to change the polarity each time, the first two groups were switched off and on likewise, to preserve similarity in this respect. The results are shown in Fig. 2 (a.c., and alternated d.c. groups) and the left half of Fig. 3 (constant d.c. group). Over the last 100 h the mean rates of fall in light-output were the same, namely, 0·9% per 100 h, for both the groups of Fig. 2. The rates of fall in current (and power) were also the same, namely, 0·18% per 100 h (one lamp in the alternated d.c. group changed anomalously at about 90 h). In contrast, the rates for the constant d.c. group were 3·8% per 100 h in light-output, and 0·38% per 100 h in current.

A marked difference between the a.c. and normal d.c. ageing rates was thus confirmed. Also, as anticipated by

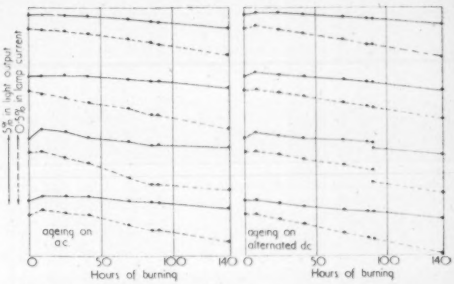

Fig. 2. Graphs similar to Fig. 1, for the ageing of four gas-filled lamps on a.c. 50 c/s, and another four on d.c. with deliberate reversal of polarity every two hours, all at constant voltage

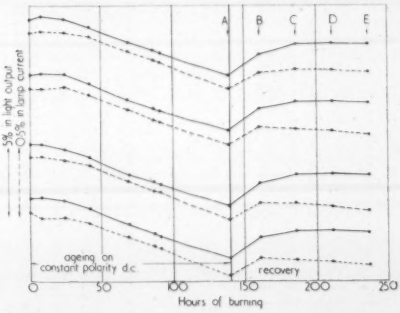

Fig. 3. Graphs similar to Fig. 1, for the ageing of four gas-filled lamps on d.c. of constant polarity (left half of diagram), and showing the recovery of the same lamps produced by reversing the d.c. polarity at *A*, and then changing over from d.c. to a.c. from *B* onward (right half of diagram), all at constant voltage

reason of the long time-constant mentioned above, reversal of supply-polarity every 2 h was shown to be sufficient, in regard to ageing rate, to make a d.c. supply equivalent to a 50 c/s a.c. supply, and so to secure the lower rate of depreciation characteristic of operation on a.c.

4. A COROLLARY

The utilitarian question then arose whether the four lamps in the constant d.c. group could be "conditioned" in some way so as probably to behave, afterwards, as though they had had the same history as their eight fellows. A running-schedule based on intelligent guesswork produced the results shown in the right half of Fig. 3. At *A*, the d.c. was reversed,

provoking a sharp rise in output (average rate 7½% per 100 h). At *B* it was thought wise not to continue with d.c., because detailed and more frequent observations on one of the lamps showed that its ageing curve had reached the "turnover" point. So an a.c. supply was used from that point onward until the output had passed a maximum and was falling at about 0·35% per 100 h. This whole treatment took about 100 h more of burning. At the end of it, at 235 h, the mean light output was about 2·0% less than it had been at 25 h. In the same period the output of the a.c. group would have fallen about 1·9%, had they been run on to 235 h—assuming a steady rate of fall throughout. Thus, the whole of the excess fall in light output caused by running the four lamps on d.c. for the first 140 h had, we may presume, been recouped by the conditioning treatment. The lamp-currents, i.e. the filament resistances, are seen to have recovered similarly. At this juncture the potential value of the lamps, as future standards, forbade further experiment, in the reasonable anticipation that any other adverse effects of the earlier d.c. ageing had likewise been obliterated.

5. CONCLUSIONS

The main practical conclusion is that regular reversal of the d.c. supply, during the use of gas-filled standard lamps, can usefully diminish the rate of depreciation of their light output. Reversal on each occasion of use—lasting perhaps five minutes—is convenient, and more than sufficient to secure the minimum rate. In this case the rate will be the same as for an a.c. supply of the same voltage (r.m.s.), which type of supply can then legitimately be used for the preliminary ageing tests, with the attendant advantage of easy voltage regulation. Probably this conclusion holds good, qualitatively, for all gas-filled lamps. Quantitatively, other factors may no doubt have an influence. For instance, at low operating temperatures the ageing rate may in any case be too small to be of much consequence. At the higher temperatures, and with the relatively smaller bulbs of general lighting service and projector lamps, more rapid blackening of the bulb may dilute the effect.

The question of whether the effects observed persist throughout the whole life of a lamp, and whether indeed they influence the time at which ultimate failure occurs, is left open. Vacuum lamps, it is to be noted, are not here dealt with at all.

It is of interest to see what evidence may be derived, from the results themselves, about the probable causes of the difference in ageing rates, among the mechanisms suggested at the outset of this paper. We shall require to use the further experimental observations that for a lamp of the type here used, at the colour temperature 2700° K, a deliberate change in voltage V of 1% is accompanied by a change of 0·51% in current i and 3·9% in luminous output L. From this we derive

$$\frac{d(\log L)}{d(\log W)} = \frac{3{\cdot}9}{1{\cdot}51} = 2{\cdot}58$$

where W = power consumed.

It is reasonable to suppose that the fall in light output for a.c. ageing is due chiefly or even solely to two causes. The first is the uniform thinning of the filament due to slow evaporation, and the second is blackening of the bulb by the evaporated material. The former entails a steady fall in the power consumed at constant voltage, at a rate which we have seen to be 0·18% per 100 h. The contribution of this cause to the fall in light output is not simple to calculate exactly. The relevant differential can, however, readily be shown to lie somewhere between unity and the value of 2·58 given above. We may take a figure of 2 and so write, approximately—

total a.c. ageing rate of 0·9% in light output
= 0·36% (due to fall in power) + 0·54% (due to blackening).

This merely serves to give a very rough indication of the relative effects of the two causes mentioned. Only the total is of any consequence in the arguments which follow below.

Now it also seems reasonable to suppose that, for d.c. operation, the general thinning of the filament and the bulb-blackening proceed at the same rate as for a.c.—or at least at no greater rate, otherwise the complete recovery of light output under the conditioning treatment of section 4 would not have been found possible. Further, there is evidence that some additional mechanism of a different kind must be operating during d.c. ageing; for on d.c. the light output falls ten times as fast as the power, whereas on a.c. it falls only five times as fast. Schwarz,[6] as well as de Vos,[3] refers to the possibility of migration of tungsten along the filament, and cites an experiment in confirmation. He found that the ultimate failure of filaments running on d.c. occurred most often at a point very near to the junction of the filament with the positive leading-in wire. Moreover he observed that this point was within the region so strongly cooled by the lead-in that it emitted practically no light. The suggestion is that in any section of a filament, tungsten migrates along the section leaving a constriction near the cool filament-support at the positive end of the section, and a "bulge" near the support at the negative end, while the filament cross-section is elsewhere unaffected. In such a case, with the constriction and bulge in regions not hot enough to emit appreciable light, the resulting increase in filament resistance will be equivalent, in effect, to the insertion of an equivalent extra resistance in the external circuit of a normal lamp. The change in light output is then calculable from the change in current, from the data given earlier, according to the differential—

$$\frac{d(\log L)}{d(\log i)} = \frac{3{\cdot}9}{0{\cdot}51} = 7{\cdot}65$$

The rate of fall of current on d.c. is, as we have seen, 0·38% per 100 h. We now assume this to be composed of 0·18% due to thinning of the filament as on a.c., and 0·20% due to effects of migration as just pictured. The contribution of the latter to the fall in light output will then be $0{\cdot}2 \times 7{\cdot}65 = 1{\cdot}53\%$. We can then write—

total d.c. ageing rate of 3·8% in light output
= 0·9% (due to same causes as on a.c.)
+ 1·53% (due to effects of migration on resistance)
+ 1·37% unaccountable.

The component of 1·37% per 100 h seems large enough to be certainly significant, and to be due to some cause not so far considered. It is suggested that it arises from transfer of some of the available radiated power from the visible to the infra-red. The amount involved in the transfer is quite small, and can readily be associated with a possible progressive change in the spectral emissive properties of the filament arising from a change in surface-structure—changes which presumably take place much more slowly, if at all, with a.c. or alternated d.c. operation. For consistency with the results

of section 4, we must, of course, assume that both the migration of tungsten and the changes in emissivity and surface structure are capable of reversal.

In brief, then, the present analysis strongly suggests that the reasons for the more rapid ageing on d.c. than on a.c. are (*a*) migration of tungsten toward the negative end of each filament section, causing a "necking" at the positive end, and a consequent accelerated rise in filament resistance, and (*b*) a more rapid change in the spectral emissivity of the filament, due probably to changing surface structure and resulting in a significant rate of increase in the ratio of infra-red to visible in the radiation emitted by the filament.

Finally, it can be inferred from the recorded observations that a substantially better maintenance of light output would generally result from operating lamps at constant current instead of constant voltage. On the other hand, this procedure might lead to earlier failure because it involves a steady increase in filament temperature throughout life. As a matter of fact, constant voltage operation has most often been customary, for reasons of convenience. Discussion of the various factors which might influence a choice between the two conditions of operation in any given case is, however, outside the scope of this paper.

ACKNOWLEDGEMENT

The work described above has been carried out as part of the research programme of the National Physical Laboratory, and this paper is published by permission of the Director of the Laboratory.

REFERENCES

(1) LIEB, J. W. *Trans Illum. Engng Soc. N.Y.*, **18**, p. 5 (1923).
(2) JOHNSON, R. P. *Phys. Rev.*, **54**, p. 459 (1938).
(3) DE VOS, J. C. *Thesis Amsterdam (V.U.)*, p. 61 (1953).
(4) LEEDS, R. E., and WINCH, G. T. *G.E.C. J.*, **22**, p. 232 (1955).
(5) WINCH, G. T. *Trans Illum. Engng Soc.*, **21**, p. 92 (1956).
(6) SCHWARZ, K. E. *Elektrolytische Wanderung in flüssigen und festen Metallen* (Leipzig: J. A. Barth, 1940).

The use of low-inertia integrating motors

By R. F. FARR, M.A., F.Inst.P., Department of Clinical Physics, Christie Hospital and Holt Radium Institute, Manchester 20

[*Paper received* 20 *March*, 1957]

The relative advantages and the performance of these small permanent-magnet motors which have, over a certain range, a speed proportional to the applied voltage, are discussed. The current-voltage characteristics, which allow the motor to be described by a simple equivalent circuit, are used to derive the speed-voltage characteristic when it is driven by a voltage source of appreciable internal resistance. Choice of the type of motor is discussed in relation to the integration of relatively large and of small voltages.

Small, permanent-magnet motors have been designed (by Electromethods Ltd.) which have, over a certain range, a speed S accurately proportional to the applied voltage E. Such motors may be used to drive light mechanisms. They may also be used to integrate E with respect to time, for which purpose it is convenient to use the built-in revolution counter available with the motors. It is this latter application and the characteristics of the motors when driving this specific load that will first be considered.

Fig. 1 shows the speed-voltage characteristic, and Fig. 2 the current-voltage characteristic, of a certain 24 V motor, when new, operated from a voltage source E of very low resistance and driving the standard revolution counter. The instantaneous value of I, the current drawn by the motor, fluctuates a few per cent, due to variation of friction as the motor and counter revolve. These fluctuations become more pronounced as the speed is reduced. From the mean curve (Fig. 2) and the known armature resistance r' ($= 700\ \Omega$) the back e.m.f. E' has been calculated. The relative speed S so derived

$$S \propto E' = E - Ir'$$

is drawn as the solid curve in Fig. 1, in which experimental points are also plotted.

At the nominal voltage E_n the motor runs at a full speed S_n closely equal to 2000 rev/min. It deviates from the ideal linear characteristic

$$S/S_n = E/E_n \qquad (1)$$

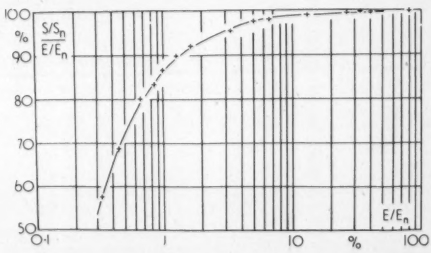

Fig. 1. Speed-voltage characteristic of a typical motor driving a counter from a voltage source of low internal resistance. Speed S expressed as a fraction of the full-speed S_n. Applied voltage E expressed as a fraction of the nominal voltage E_n. ($E_n = 24$ V)

by about 1% at $E = 0{\cdot}1\ E_n$ and by about 10% at $E = 0{\cdot}015\ E_n$. The motors may therefore be used[1] for accurate integration over a range of voltage from $0{\cdot}1\ E_n$ to $1{\cdot}0\ E_n$. Their operation (*a*) over this 10 : 1 range of voltage and (*b*) at lower voltages, will be considered in turn. These ranges also correspond to the two sections of the current-voltage characteristic: *EF*, along which *I* varies almost linearly with *E*, and *BE*, along which it is nearly constant.

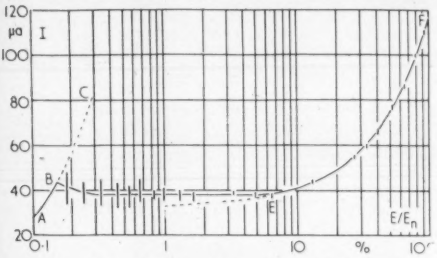

Fig. 2. Current-voltage characteristic of a typical motor driving a counter from a voltage source of low internal resistance. *I* is current in microamperes. Applied voltage *E* expressed as a fraction of the nominal voltage E_n. ($E_n = 24$ V)

OPERATION OF MOTOR WITH COUNTER OVER UPPER RANGE OF SPEED AND VOLTAGE

Over the range $1{\cdot}0\ E_n$ to $0{\cdot}1\ E_n$, the mean value of *I* fits to within 1% the linear relation

$$I = I_0 + E'/R_0 \qquad (2)$$

Curves *a–g* (Fig. 3) refer to a number of 24 V motors. The parameters I_0 and R_0 vary somewhat from motor to motor but representative values are

$$I_0 = 40\ \mu\text{A} \quad R_0 = 0{\cdot}25\ \text{M}\Omega$$

Apart from the small armature loss I^2r', the power consumed by the motor is therefore

$$E'I = E'I_0 + (E')^2/R_0 \qquad (3)$$

The first term represents losses proportional to the speed and the second those proportional to the square of the speed. The latter account for 70% of the power at full-speed and may principally be attributed to eddy-currents. In this motor, losses have been reduced by arranging the coil to rotate in the air-gap between the permanent magnet and a stationary core and by the use of a gold commutator and brushes and of jewelled bearings.

Considering motors wound for different nominal voltages but of otherwise identical construction and driving the same load at the same speed, equation (3) shows that

$$I_0 \propto E_n^{-1} \qquad R_0 \propto E_n^2 \qquad (4)$$

Thus, if E_nI is plotted against E/E_n, identical curves should be obtained for the different types of motor. This is roughly true (Fig. 3) curves *a–g* referring to the 24 V motors and curves *h*, *j*, *k* referring to single 12, 6 and 1·5 V motors respectively. As regards the slope (E_n^2/R_0) the motors appear to fall into two groups. As regards the intercept on the vertical axis (E_nI_0) the values lie within ±25% of a mean. For the purpose of the following discussion, equations (4) can be taken to hold.

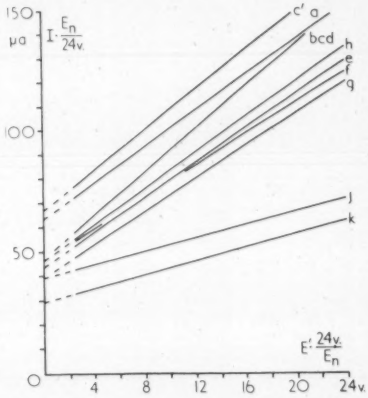

Fig. 3. Part of the current-voltage characteristics of a number of motors. *I* is current in microamperes. Back e.m.f. *E′* expressed as a fraction of the nominal voltage E_n

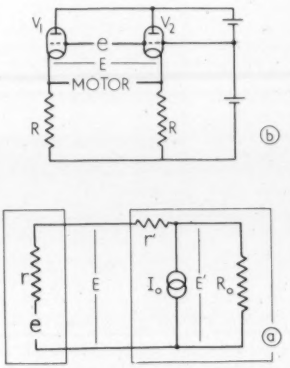

Fig. 4(*a*). Voltage source of e.m.f. *e* and internal resistance *r* drives a motor of armature resistance *r′*, represented by an equivalent circuit consisting of a resistance R_0 in parallel with a constant-current source I_0. The voltage applied to the motor is *E* and the back e.m.f. is *E′*

(*b*) A motor is driven by a voltage *E* derived from a voltage signal *e* through a simple balanced amplifier, used as an impedance-changer

Over the range of voltage specified, equation (2) shows that the motor may be represented in the equivalent circuit (Fig. 4*a*) as a constant-current device I_0, shunted by a

resistance R_0. When the motor is driven by a source of e.m.f. e and internal resistance r

$$S \propto E' = (e - I_0 r')R_0/(R_0 + r + r') \qquad (5)$$

If E' and therefore S are to vary linearly with e it is necessary either (*a*) whenever the signal voltage e' ($\neq 0$) is applied, to provide in series with it a fixed voltage $I_0(r + r')$, which may be possible in some applications, or (*b*) of more general application, to use a source of low internal resistance.

The allowable upper limit of r depends upon (*a*) the degree of linearity and the range of speed or voltage required, and (*b*) as determining I_0, the type of motor used and the load it drives. In considering the non-linearity introduced by r, the armature resistance will be neglected. It will be supposed that this additional deviation from linearity shall not exceed 2% over a range of voltage from $0{\cdot}1\ E_n$ to $1{\cdot}0\ E_n$. Then

$$(0{\cdot}1\ e - I_0 r)/(e - I_0 r) \geqslant 0{\cdot}098$$

and since $e \simeq E_n$

$$r \leqslant 0{\cdot}002\ E_n/I_0$$

For a typical 24 V motor driving the revolution counter, r has therefore an upper limit of 1200 Ω, and for the other motors it can be written

$$1200\ (E_n/24)\ \Omega$$

The motor may be driven directly from a source of sufficiently low impedance, such as a photovoltaic cell or a thermocouple, but where e is derived from a source with a high impedance, such as an ionization chamber, an impedance-changing circuit must be interposed between the source and the motor.[2] The choice of motor voltage E_n, in relation to the design of the d.c. amplifier, will be considered in two cases (*a*) when a sufficient signal voltage is available and the simplest circuit is to be used, and (*b*) when the signal voltage is small.

Choice of motor. (*a*) *Simple impedance-changer.* A simple cathode-follower may be used but it is advantageous to use a balanced circuit (Fig. 4*b*). For then, when integrating at the lower end (2·4 V) of the linear range of a 24 V motor, a 20% change of the common filament voltage will not affect the output by more than 1%, allowing the use of unstabilized filament supply. Then E is very closely equal to

$$(e - 2I_0/g_m) \cdot g_m X/(1 + g_m X) \qquad (6)$$

where g_m is the mutual conductance of each triode and

$$X = RR_0/(2R + R_0)$$

Thus $r = 2/g_m$, and, for a typical 24 V motor, g_m has a lower limit of 1·6 mA/V.

In general, it is necessary to operate a valve at a high value of the quiescent anode current i_a in order to obtain a high value for g_m. On the other hand, it may be desirable to operate it at a low value of i_a, (*a*) to minimize the grid current, in some applications, and (*b*) to avoid overload of the motor. The former may limit the use of this simple circuit. The latter will be considered further.

At full speed, the anode current of V_1 (positive-going grid) is

$$E_n/2X + 2(I_0 + i_a)$$

Now suppose that V_2 is cut-off and that the anode current of V_1 does not rise much above this value, being limited by grid-current. Then the maximum output voltage is

$$E_{max} \simeq E_n/2 + (i_a - I_0)X$$

If E_{max} is not to exceed, say, $1{\cdot}5\ E_n$ then

$$i_a \leqslant E_n/X + I_0$$

If R_0 is simply the parallel impedance of the motor, the maximum allowable quiescent current is so low as to result in an insufficiently high mutual conductance. R_0 may therefore be reduced by shunting the motor with a suitable resistance, which may conveniently take the form of a voltmeter indicating the instantaneous value of E. R_0 should not be reduced so far as to make $g_m X$ so small that the voltage gain (equation 6) is affected by changes in g_m. Thus, neglecting I_0

$$i_a \leqslant g_m(E_n/g_m X)$$

From this point of view, a high value of g_m/i_a is required, which involves operating the valve with low rather than high values of i_a and g_m. For the 24 V motor, if $g_m X$ is to be about 20, g_m/i_a should be about 1·2 per volt.

Under the conditions discussed here, viz.,

$$g_m \geqslant 1{\cdot}6(24/E_n) \quad \text{(mA/V)}$$
$$g_m/i_a \geqslant 1{\cdot}2(24/E_n) \text{ (per volt)}$$

only the 24 V motor can be driven satisfactorily by the simple circuit of Fig. 4(*b*) and a relatively large signal voltage is therefore required.

Choice of motor. (*b*) *Integration of small voltages.* The case will next be considered where the motor is required to run at full speed at a voltage e less than the lowest nominal voltage (1·5 V) of the available motors. It will be assumed that a cathode follower output stage is used, preceded by an amplifier of voltage gain A, and that overall negative-feedback reduces the overall voltage gain to G. This has the effect of reducing, by a factor A/G, both the output impedance and the effect upon G of changes in A. It must now be considered whether it is better to use a motor of low E_n, requiring a lower overall amplification but a higher degree of negative feedback to ensure a sufficiently low output impedance; or to use a motor of high E_n, requiring a larger overall amplification but less negative feedback.

(i) The necessary gain G varies as E_n^{-1}. Equation (4) shows that, to obtain the necessary output impedance, A/G must vary as E_n^{-2}. The necessary gain before feedback A, therefore, varies as E_n^{-1}, and economy in voltage amplification is ensured by the use of a motor with a large E_n. (ii) However, this may lead to a value of A/G which, while large enough to fulfil condition (5), renders G susceptible to changes in A. A/G may be regarded as having an irreducible minimum value. Then, for A/G = constant, A varies as E_n. Under these conditions, economy in voltage amplification is secured by the use of a low-voltage motor.

It is clear that, for the integration of small voltages, having regard to both low output impedance and linearity and stability of gain of the d.c. amplifier, there is an optimum voltage of motor to be used. Its value depends upon the output impedance of the last stage and on the minimum value chosen for A/G. These considerations lead to a choice between the two motors of lowest nominal voltage.

BEHAVIOUR OF MOTOR WITH COUNTER OVER LOWER RANGE OF SPEED AND VOLTAGE

The motor will rotate and drive the revolution counter when $E = 0{\cdot}002\ E_n$, with a power input of only 2 μW, of which about half represents armature loss. It therefore

presents an attractive method of integrating low voltages when the power available is small, but it is important to realize the inherent non-linearity that will then arise. Fig. 1 shows that the deviation from the ideal characteristic (equation 1) increases from 13% at $E = 0{\cdot}01\ E_n$ to over 50% at $E = 0{\cdot}002\ E_n$. For example, when integrating in the range 0·005 to 0·003 E_n, the ratio of the extreme speeds is 0·7 of the ratio of the corresponding voltages.

In the range 0·07 E_n to 0·003 E_n, the mean current remains sensibly constant at about $1{\cdot}2\ I_0$, so that $R_0 = \infty$. The behaviour of the motor when driven by a voltage source of e.m.f. e and internal resistance r is therefore obtained by modifying equation (5) to

$$S \propto E' = e - 1{\cdot}2\ I_0(r + r')$$

Below about 0·003 E_n, the fluctuations of current are pronounced. The mean current rises until at B the motor stalls and the curve meets AC, which represents the armature resistance r'.

OTHER LOADS

The foregoing results refer to new motors driving the standard revolution counter. Any increase of the torque will produce a proportionate increase in I_0, and the range over which a linear speed-voltage characteristic is obtained will be reduced. The stalling speed will rise as point B moves up AC (Fig. 2).

Ageing and prolonged use of the motor will, for two reasons, result in an increase of non-linearity. I_0 will rise due to (*a*) mechanical wear of the bearings and counter train, and (*b*) demagnetization of the field magnet, causing the motor to run at a higher speed at a given voltage, with a consequent increase in the first term of equation (3). Such changes are observed in a motor, the characteristics of which, when new (curve *c*), and after about 1 million revs, in 2 years' intermittent use (curve *c'*), are shown in Fig. 3.

CONCLUSIONS

These motors have a linear speed-voltage characteristic over a wide range, provided that the torque and the internal resistance of the voltage source are both small. With these limitations, they have a wide field of possible uses: (*a*) for driving very light mechanisms at a controlled speed and (*b*) with the revolution counter, for integrating with respect to time slowly varying d.c. voltages. The advantages of these motors in these applications, over (i) velodyne motors and (ii) Miller integrators, have been discussed elsewhere.[1,2] In the second application, they have the merit that the signal can be amplified and indicated, and also integrated, using one amplifier. Furthermore, the motor, being reversible, will integrate a d.c. voltage that is both positive- and negative-going and it more easily permits the use, with its attendant advantages, of a balanced amplifier, than does the Miller circuit. For example, in the integration of a voltage over a long period of time, steady zero-drift may be compensated by reversing, at regular intervals, the connections at both the output and input terminals of the amplifier.[3]

A particularly straightforward application of the motor is seen[2] in the integration of a voltage in the range 2–24 V from a high impedance source, through a simple impedance-changing circuit (Fig. 4*b*).

REFERENCES

(1) WHEATLEY, B. M. *Brit. J. Radiol.*, **26**, p. 382 (1953).
(2) FARR, R. F. *Brit. J. Radiol.*, **30**, p. 213 (1957).
(3) BRADDICK, H. J. J. Private communication.

An iterative analogue computer for use with resistance network analogues.

By I. C. HUTCHEON, M.A., A.M.I.Mech.E., A.M.I.E.E., Research and Development Department, George Kent Ltd., Luton, Beds.

[*Paper first received* 20 *March, and in final form* 2 *April*, 1957]

When field problems involving sources or sinks are solved using resistance network analogues, currents must be applied to the nodes of the network such that each current is a desired function of the associated node potential.

This requires repeated re-adjustment of every current until each is correct. A method is described whereby the adjustments are made automatically by a scanning switch, a function generator, an a.c. amplifier, and a set of triode valves each connected to a network node and having a memory capacitor connected to its grid. The solution is thus achieved rapidly, and changing problems can be solved continuously.

Suitably modified, the apparatus may find uses such as solving other differential equations or providing a set of non-linear resistors for fluid flow analogues.

Partial differential equations of the type

$$\frac{\partial^2\phi}{\partial x^2} + \frac{\partial^2\phi}{\partial y^2} = f(\phi) \qquad (1)$$

describe the distribution of a variable ϕ in a two-dimensional field from which a quantity $f(\phi)$ is withdrawn per unit area. In principle they can be solved when the boundary conditions are given, but in practice an algebraic solution is often difficult or impossible.

As Liebmann[1,2] has shown, they can be solved with quite high accuracy by the use of a network of resistors to simulate the medium in which the field exists. Potentials corresponding to the boundary values of ϕ are applied to the boundaries of the network, and currents corresponding to $f(\phi)$ are withdrawn from the nodes. The resulting distribution of potential over the network gives the distribution of ϕ over the field. The network may be one-, two- or three-dimensional, but most problems can be reduced to one or two dimensions and consideration will be limited to these cases.

Adjustment of any one current modifies the potentials at all the nodes, and hence the (interim) desired values of all the other currents. It is therefore necessary to repeat all the adjustments several times until the desired relation between current and potential holds at every node.

This procedure has been made easier in the case where $f(\phi) = -K^2\phi$ by a method[3] in which the errors in adjustment are displayed on an oscilloscope by means of a scanning switch. It is then possible to see which are the worst errors and to reduce them first and by the (interim) optimum amount.

In another method, described by Karplus,[4] the current adjustments are made automatically by conventional analogue computer units connected to the nodes of the network and maintaining continuously the desired relationship between the currents and the potentials. Each computer unit generates the desired function independently, and there are as many units as there are nodes: the method therefore becomes somewhat expensive if extended to two-dimensional networks.

Automatic methods of solution are valuable, however, since they may considerably extend the scope of resistance network analogues by permitting the continuous solution of changing problems, or the determination of critical values (eigenvalues) of parameters which give particularly significant solutions.

The method to be described provides for the currents to be adjusted automatically one after another by means of a single function generator, a scanning switch and an a.c. amplifier. These work in conjunction with a set of triode valves, each connected to a node of the network and controlling the current applied to it. Each triode possesses a "memory" capacitor connected to its grid whose potential is adjusted once every cycle in relation to the node potential and remains steady in between adjustments. Any desired relationship can be obtained between current and node potential by adjusting the function generator, and this item may economically be made accurate since only one is used. The only moving part is the switch, and if this is rotated at suitable speed, the solution can be reached in a few seconds or less. The amplifier is simple, and the triode characteristics are unimportant. The method has been used experimentally with one-dimensional networks and should extend readily to two dimensions.

PRINCIPLE OF THE ANALOGUE

Consider for simplicity the one-dimensional case. Equation (1) may be written in finite difference form:

$$\frac{d^2\phi}{dx^2} = \frac{\phi_{n+1} - \phi_n}{h^2} - \frac{\phi_n - \phi_{n-1}}{h^2} = f(\phi_n) \qquad (2)$$

where h is the interval in x (the mesh interval) between adjacent nodes. In this case the analogue is a line of equal

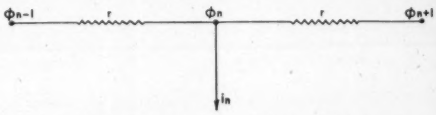

Fig. 1. Typical node of a one-dimensional network

resistors r, represented by a typical node in Fig. 1. If current i_n is withdrawn from a node at potential ϕ_n, then

$$\frac{\phi_{n+1} - \phi_n}{r} - \frac{\phi_n - \phi_{n-1}}{r} = i_n \qquad (3)$$

which is exactly analogous to equation (2) if

$$i_n = \frac{h^2}{r} f(\phi_n) \qquad (4)$$

Equation (2) can therefore be solved by the circuit of Fig. 2 if the grid potential of each triode is adjusted so that the potential V_n across its cathode resistor R is

$$V_n = Ri_n = h^2 \frac{R}{r} f(\phi_n) \quad (n = 1, 2 \ldots 5) \tag{5}$$

ϕ_0 and ϕ_6 are applied boundary potentials, V_b is a common h.t. supply, and the solution is given by the values of ϕ_{1_5} along the network. h in this case is 1/6th the range of x considered, but closer spacing would be used in most practical problems. Boundary currents may be specified instead of potentials.

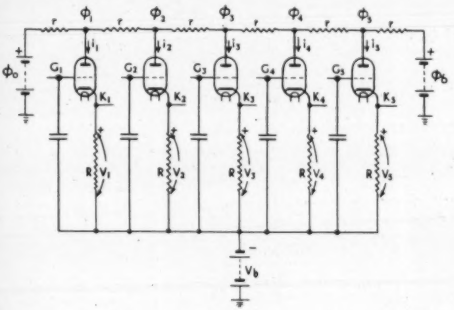

Fig. 2. Network with triodes to control (positive) currents

The circuit of Fig. 2 deals only with cases where i and hence $f(\phi)$ are always positive. If they are always negative the same circuit suffices with the polarities of all ϕ reversed and

$$V_n = -h^2 \frac{R}{r} f(\phi_n) \tag{6}$$

If $f(\phi)$ changes sign, so must i and reversible current-controlling elements are required as typified in Fig. 3.

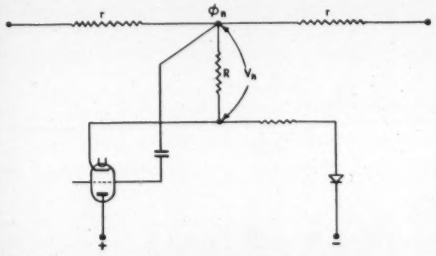

Fig. 3. Reversible control element

METHOD OF AUTOMATIC CURRENT ADJUSTMENT

Fig. 4 shows a system which automatically adjusts and re-adjusts the grid potentials of the triodes until the current through each is correct. It applies to the circuit of Fig. 2 where $f(\phi)$ is always positive, a modified arrangement being required for adjusting reversible elements such as shown in Fig. 3.

The section S_ϕ of a ganged three-pole switch presents the node potentials in turn to a function generator F as the switch is continuously rotated. The outputs $F(\phi)$ are applied to one input terminal of an amplifier A whose other input

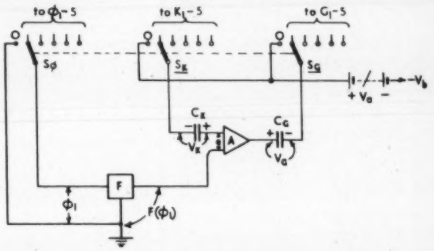

Fig. 4. Scanning and current-adjusting circuit

receives the cathode potentials in turn *via* switch section S_K. Any differences, e, are amplified and applied *via* S_G to the appropriate grids so as to modify the cathode currents and reduce all e's towards zero.

Each triode possesses a memory capacitor which holds the grid potential steady between adjustments. Every adjustment modifies the potentials over the whole network, and the final equilibrium is thus approached in stages over several cycles.

The amplifier is conveniently a.c.-coupled through input and output capacitors C_K and C_G respectively, which are large enough to maintain essentially steady potentials during equilibrium operation. Once every cycle, or more often if desired, a zeroing operation is performed which sets the potentials on these capacitors and allows them to be considered as batteries for purposes of analysis. In Fig. 3, zeroing occurs as the switch wipers reach position O, and gives

$$V_K = V_G = F_0 + V_b - V_a \tag{7}$$

where F_0 is the output of the function generator when its input is shorted (Fig. 5) and V_a is a potential which can be adjusted manually to alter the zero of the function.

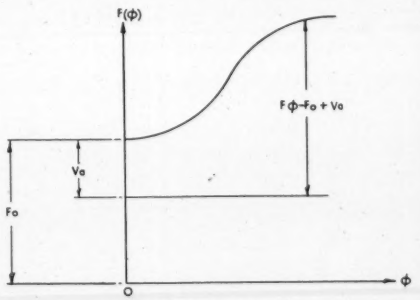

Fig. 5. Typical function

When equilibrium has been established, all the triodes carry currents $i_n = V_n/R$ such that

$$F(\phi_n) - V_n + V_b - V_K = e \qquad (8)$$

for every triode element, and, if the amplifier gain is high, the errors e approximate to zero. Equations (7) and (8) give the equilibrium cathode potentials

$$V_n = F(\phi_n) - F_0 + V_a \text{ approx.} \qquad (9)$$

Thus the common h.t. potential V_b which appears in every inspection of cathode potential, is opposed by an exactly equal potential on C_K and does not affect the operation. Similarly, steady potentials in the function generator output and the amplifier input or output have no effect. This use of a.c. coupling allows a very simple amplifier to be used, eliminates amplifier drift effects and permits a.c. amplification of the function within the function generator. The input of the function generator must, of course, be directly coupled.

SOME PRACTICAL DETAILS

The foregoing remarks assume that each memory capacitor exactly retains its potential between adjustments. In fact, however, grid current in the triodes and capacitor leakage cause slow drifts which must be corrected by continuing to revolve the switches after balance has been reached.

Most valves are found to have grid current well below 0·1 μA, and 1 μF memory capacitors give a drift rate less than 0·1 V/s which is low enough for most purposes if the cycle time is less than about one second. Selection of valves or faster cycling would reduce the drift rate or alternatively permit a considerable reduction in the value of these capacitors. The effects of leakage resistance become negligible if the potential drift over a cycle from this cause is below say 0·1% of the actual potential. This requirement is met if the self time constant of each capacitor exceeds say 1000 times the cycle duration, and good quality paper capacitors used at room temperature are quite adequate for durations up to a few seconds.

The above slow drifts are corrected by small signals applied automatically during every adjustment. Errors are avoided if C_K and C_G are large enough to pass the necessary currents while still maintaining substantially constant potentials. Thus C_K may have a time constant with the amplifier input impedance which is of the same order as the time between zeroing operations, while C_G may have the same value as the memory capacitors. If a rapid approach to balance is required, C_G should be larger, e.g. about equal to the total of memory capacitors between zeroing positions. The charge passed through C_G while several valves are adjusted has to be made up during zeroing and, if this is infrequent, the amplifier should have a proportionately low output impedance. Zeroing may be carried out any number of times in a cycle, greater frequency permitting smaller coupling capacitors but requiring more switch positions. Both coupling capacitors must have high leakage resistance since each sustains the h.t. potential, and C_K at least should be a polystyrene or equivalent type.

Undesired transient signals can be prevented from reaching the amplifier or the memory capacitors by performing the switching in the following sequence:

S_ϕ makes
S_K makes
S_G makes
S_G breaks
S_K breaks
S_ϕ breaks

Any type of function generator could be used which has sufficient accuracy and a response which ensures that the function voltage is fully generated during the time between S_ϕ making and S_K making. There are several types which fulfil this not very onerous requirement, and the biased-diode generator which approximates the function by a number of straight-line segments appears very suitable. The diode network may be followed by an a.c.-coupled amplifier if it is necessary to amplify the function voltage, and in any case should have a low output impedance so as to be unaffected by stray currents running to earth from the main amplifier. Its input impedance must be high enough to leave the network potentials substantially unaffected.

The high impedance input connexion to the main amplifier needs to be well screened to avoid pick-up during switching. This can be achieved by building C_K into the amplifier and using a co-axial lead to the switch that has its sheath connected to the low impedance input. The latter may be connected to the amplifier chassis, this being allowed to float. Similar remarks apply to the high impedance input of the function generator but in this case the chassis is earthed.

EXPERIMENTAL MODEL—RESULTS

A model has been made designated "NOLA" (Non-Linear Analyser) which has eight triode elements, each of which is a 12AX7, 12AT7 or 12BH7 double triode. Cathode resistors are inter-changeable and of the order 10 kΩ; the memory capacitors are each 1 μF, but smaller values would probably suffice.

Switching is effected by three 44-position switch sections, ganged together and turned by hand. A fourth section is included for other purposes, and the correct switching sequence is obtained by using studs joined together in twos, threes and fours while omitting the remaining studs in every five.

The amplifier has a single stage giving a gain which is variable up to about 50, and a cathode follower output. A five-section biased diode square root function generator has been used for some tests, and this also has a cathode follower output. Other tests have been made with no function generator, i.e. a function of $\times 1$.

Solutions are generally reached, to the extent that no further change can be observed, within about 10 turns of the switch. They are held by continuing to revolve the switch and drift slowly if it is not turned.

As a test problem, equation (2) was solved for the case

$$F(\phi) = (2\phi)^{1/2} \quad \text{i.e. } f(\phi) = \frac{1}{h^2}\frac{r}{R}(2\phi)^{1/2} \qquad (10)$$

where $r = 5$ kΩ, $R = 10$ kΩ, $h = X/9$, X = the range of x considered.

If we assume that $\phi = d\phi/dx = 0$ when $x = 0$, the algebraic solution is

$$\phi = 22{\cdot}78\,(x/X)^4 \qquad (11)$$

which is compared with the analogue solution in the following table.

Comparison of analogue solution with equation (11)

x/X	ϕ by equation (11)	ϕ by analogue
4/9	0·889	0·89 (set manually)
5/9	2·170	2·17
6/9	4·500	4·49
7/9	8·337	8·2
8/9	14·22	14·2
9/9	22·78	22·6
10/9	34·72	34·6
11/9	50·83	50·7
12/9	72·00	71·9
13/9	99·17	99·2 (set manually)

All resistors were to $\pm 0{\cdot}1\%$ tolerance, but the voltage measurements were made on an ordinary high-resistance voltmeter. Fig. 6 shows some further analogue solutions where the boundary values of ϕ have been chosen arbitrarily and $\phi \neq 0$ when $d\phi/dx = 0$. This case has so far resisted exact analysis, but an approximate solution, obtained for x as a power series in ϕ shows the upper curve to be accurate to about 1% at its worst point.

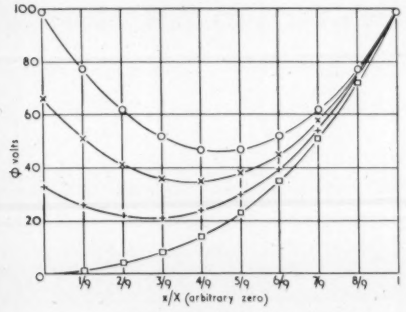

Fig. 6. Analogue solutions of equation (10)

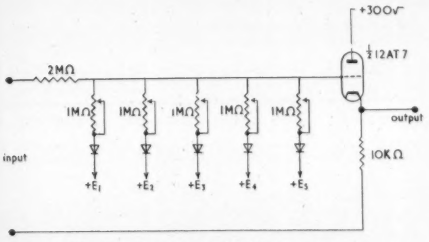

Fig. 7. Square-root function generator

Fig. 7 shows the circuit of the function generator which comprised five biased diodes and a cathode follower output. The break points were set by adjusting E_{1-5}, and the slopes of the intermediate segments by adjusting the 1 MΩ potentiometers. Voltages were measured on the same voltmeter, outputs being taken from a datum given by shorting the input. Values of inputs and outputs at the break points were:

Input (volts)	0	3	8	18	32	50	72
Output above datum (volts)	0	2·45	4	6	8	10	12

POTENTIALITIES OF THE METHOD

The currents withdrawn from the network can be made to depend on the local values of x and y by pre-adjusting the cathode resistors, enabling equations of the form

$$\frac{\partial^2\phi}{\partial x^2} + \frac{\partial^2\phi}{\partial y^2} = f(x\,y)\,.\,f(\phi) \qquad (12)$$

to be solved. Circuit modifications should enable the potential differences between nodes to be used to control the currents, permitting $\partial\phi/\partial x$ and $\partial\phi/\partial y$ to be introduced on the right-hand side of the above equation.

The addition of another switch section enables the triode elements to be separated. If the current through each is made a function of the potential across it, the elements become a set of non-linear resistors which may be interconnected to solve, for example, flow problems in networks of pipes.

Similarly it is possible to set up currents which are related to potentials existing within a rotating machine by means of a commutator instead of many slip rings.

The accuracy with which Poisson type equations are solved should approach that achieved by Liebmann if a suitably accurate function generator is used. Extension to two dimensions requires the development of a three-pole switch having 100 or more ways, the correct switching sequence being given inherently by the design of the contacts.

ACKNOWLEDGEMENTS

The author is indebted to Dr. D. B. Spalding of the Imperial College of Science and Technology for stimulating an interest in this field and for much valuable advice.

He also thanks Mr. E. D. Low for deriving a general solution to the test problem by approximate methods.

REFERENCES

(1) Liebmann, G. *Brit. J. Appl. Phys.*, **4**, p. 193 (1953).

(2) Liebmann, G. *Brit. J. Appl. Phys.*, **1**, p. 92 (1950).

(3) Liebmann, G., and Bailey, R. *Brit. J. Appl. Phys.*, **5**, p. 32 (1954).

(4) Karplus, W. J. *Brit. J. Appl. Phys.*, **6**, p. 356 (1955).

(5) Provisional Patent Specification No. 348 (Jan., 1957).

The optical density and thickness of evaporated carbon films

By Anna Cosslett, D.Phil., and V. E. Cosslett, Ph.D., F.Inst.P., Cavendish Laboratory, Cambridge

[*Paper first received* 14 *March, and in final form* 21 *May*, 1957]

Measurements of the variation in optical density with thickness of evaporated carbon films (50–1500 Å thick) give a value of the absorption coefficient considerably lower than that recently found by Agar.[1] Our mean value is close to that for natural graphite and electron diffraction patterns suggest that the films consist of randomly orientated graphite lamellae of varying width embedded in a variable amount of amorphous carbon. The optical density of films of the same nominal thickness may vary as much as 25%, probably due to variations in the degree of orientation of the lamellae and in their lateral extension. The much greater difference (60%) between our films and those of Agar is ascribable to more radical differences in the method of evaporating and collecting the carbon. This dependence of optical properties on method of preparation means that there can be no universally valid calibration curve for finding film thickness from optical density. The method proposed by Agar is reliable only if the details of preparation are standardized and a calibration curve is produced for each set of conditions.

INTRODUCTION

The use of evaporated carbon films has become so general in electron microscopy,[2] for support films as well as replicas, that considerable importance attaches to knowledge of their thickness. When they are also used as standard specimens in electron scattering and interferometry investigations this knowledge must be as exact as possible. Agar[1] has recently described a rapid method of finding the thickness by measuring the optical density. For calibration purposes the thickness was determined by the Tolansky multiple beam interferometer, or, for the thinnest films, by a two-beam shearing system (in reflection) due to Dyson, and the optical density by a densitometer employing a photomultiplier. For some time we have been using a transmission interference microscope (Smith)[3] for measuring the thickness of ultra-microtome sections on the one hand, and on the other hand of layers of carbonaceous material deposited on a specimen exposed to an electron beam ("contamination"). In order to check the calibration of the interference microscope we have made extensive measurements on evaporated carbon films over a wide range of thickness, and find that our results differ greatly from those of Agar. The purpose of this communication is to point out that the optical density-thickness curve which he obtained cannot be accepted as a generally valid calibration for carbon film thickness, as he suggested. Deductions from it, based on a simple measurement of optical density, may yield a film thickness that is in error by as much as 100%. Our investigation has shown that there is a significant difference introduced by the method of measuring thickness, but a much greater variation with conditions of evaporation. Determination of the refractive index and absorption index of the films suggests that they are essentially graphite. Electron diffraction patterns partially support this view, but point to the structure being one of random orientation of very small platelets instead of parallel arrangement as in graphite. It has been possible to detect some significant changes in the diffraction pattern which may account for the variation in optical properties with conditions of evaporation.

Investigation of the causes of this discrepancy, which is most probably connected with the well-known variation in the properties of graphites from different sources, is still in progress. However, we think an immediate statement of the complexity of the situation is necessary to prevent erroneous use of Agar's calibration curve. Copies of it were distributed at the meeting of the Electron Microscopy Group at Reading in July 1956, and may be applied to films prepared in quite different conditions from those which he had used. Two cases have already come to our notice where our own measurements of thickness would give a more reasonable interpretation of results. In the meanwhile Calbick[4] has published a value for the optical absorption coefficient of carbon films which differs still further from our values; at the same time he draws attention to the great variation in properties with method of evaporation and collection of the films.

EXPERIMENTAL METHOD

Carbon films were prepared, as described by Bradley,[2] by evaporation from an incipient arc between spectroscopically pure carbon rods in vacuo and were collected on cleaned glass microscope slides placed at different distances from the source. Part of the film was floated off in water, leaving the other part with as clean an edge as possible (not necessarily straight). The optical density was measured in a Walker densitometer with a standard glass wedge. If I_0 is the light intensity recorded through a clear region of the slide and I that through the slide plus carbon film, then the optical density is taken as

$$D = \log_{10}(I_0/I)$$

Properly speaking, the experimental values of D should be corrected for loss of light by reflection, but the correction is small compared with the other errors, especially for very thin films. It has not been applied to the experimental results by either ourselves or Mr. Agar.

The optical absorption coefficient is defined by

$$I = I_0 \cdot e^{-\alpha t}$$

where t is the thickness of the film in centimetres. Hence the value of α is obtained from the slope of the density-thickness curve: $\alpha = 2{\cdot}3\, dD/dt$. Graphite films may be treated in terms of the optical theory of dispersion in metals and an extinction coefficient k defined such that

$$k = \alpha\lambda/4\pi$$

where λ is the wavelength of the incident light; k is important in considering the reflectance of the films and in finding the real part of the refractive index n from the complex value $\boldsymbol{n}$.

The thickness and refractive index of a film were found with the Baker doubly-refracting interference microscope employing a shearing type objective (Smith).[3] Monochromatic light ($\lambda = 5461$ Å) suffers a phase change θ (in radians) in passage through the film, which is found by

matching the transmitted to the reference image seen in a half-shade eyepiece (Smith),[5] with the aid of a calibrated analyser. The film thickness is given by

$$t = \lambda \,.\, \theta / 2\pi(n - \mu)$$

where μ is the refractive index of the surrounding medium. To find t it is necessary to employ a double immersion method, measuring the phase change with the film alternately in air and in a liquid of known refractive index such as water or glycerine. The results give n as well as t and the real part of the refractive index n can then be found from

$$n = n - ik$$

with the value of k obtained from the absorption measurements.

Most of the measurements were made with a $\times 40$ objective and with a $\times 10$ eyepiece in the auxiliary microscope of the half-shade eyepiece. Measurements were made at several points along the edge of a film and between 10 and 20 readings were made at each point. The standard error of the mean was between 0·10 and 0·15 degree. For very thin films ($\sim$ 100 Å), with readings of a few degrees only, the error in the refractive index is 5% and in the film thickness 12–15%. With a film of thickness 150 Å this corresponds to an error of $\pm$20 Å. For thick films the percentage error in refractive index is only 1% and in thickness 2%, but the standard error in the mean of a set of readings is increased owing to the lower sensitivity of matching in the half-shade eyepiece, due to greater absorption of light. The error in optical density measurement is about 2%, being greater for thick films and smaller for thin films.

In order to eliminate the possibility of any systematic error in the method of measuring thickness, a number of films were checked by the Tolansky multiple beam method. The results agreed to better than 10%, even with films of 150 Å thickness.

To check the reliability of the double immersion procedure for determining the refractive index of a moderately absorbing material, such as carbon is, the refractive index of mineral graphite was measured. Very thin flakes of graphite were obtained by rubbing a piece of it over a microscope slide. Using water as immersion medium, with air as comparison, the refractive index was calculated from the expressions given above. Films of thickness ranging from 250 to 1000 Å were measured. The average value of n was 2·04. No values for the refractive index of graphite could be found in the literature, but from the measurements of Huntjens and van Krevelen[6] of its reflectance in air and in cedar oil a calculated value of 2·02 is obtained. The agreement is well within the estimated error.

RESULTS

The general nature of the results is shown by plotting optical density D against thickness t (see figure, curve C). The experimental values are plotted, without correction for reflectance. The best straight line through the experimental points falls short of the origin and the few points for films thinner than 100 Å indicate that the curve has indeed a concave curvature (upwards) in this region. The value of the absorption index, taken from the straight portion of the curve, is $1{\cdot}35 \times 10^5$ and the extinction coefficient $k = 0{\cdot}55$. From the data of Huntjens and van Krevelen we calculate a value for k of 0·56 for graphite. It is seen that the scatter of experimental points is considerable for the thinner films, but does not exceed the range of $\pm$15% quoted above.

The curve obtained by Agar is shown also in the figure (curve A). Its slope corresponds to a value for α of $2{\cdot}15 \times 10^5$ and for k of 0·90, more than half as large again as our values. Agar's published curve shows no experimental points, but he states that the thickness measurements were accurate to $\pm$10%, "with only two or three exceptions," the error being greatest with the very thin films. His curve, besides being steeper than our own, is concave *downwards* near the origin, implying that thin films have a higher absorption coefficient than thick ones. Calbick has published only an abstract of his work,[4] with no curve, but gives a value for α of 4×10^5 which would correspond to $k = 1{\cdot}7$. Not only is this value much higher still than that of Agar, it is above that for steel and not far short of that for nickel.

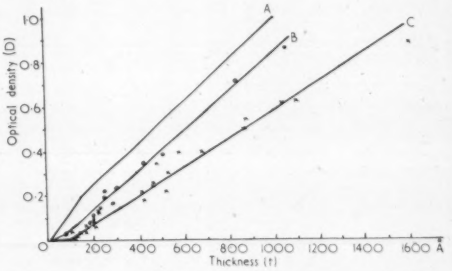

Variation of optical density D with thickness t of carbon film, for Agar's films as measured by him A; for his films as measured by us B; and for our films measured by us C

In order to test the consistency of our respective methods of measuring optical density and film thickness, Mr. Agar kindly made available to us a representative selection of the films he had prepared and measured. Our results from these are plotted in the figure (curve B). For a given film our measurement of optical density agrees very closely with that of Agar, but we find the thickness to be consistently greater than he does by an amount of the order of 150 Å. Our points therefore fall on a straight line parallel to Agar's own curve, to an accuracy of rather better than $\pm$10%, giving the same value for absorption coefficient as he obtained. The best line through the experimental points now falls short of the origin, however, indicating a concave curvature upwards or perhaps a sigmoid curvature in this region. It is significant that Agar's films have a uniformly high refractive index of 2·3.

It was noticeable that films of approximately the same thickness, prepared in our own evaporator, varied markedly in reflectance and optical density. As expected, films of unusually high D were found to have high values of n, owing to the effect of the higher value of k; the real part of the refractive index, n, usually lay between 1·9 and 2·1. In one extreme instance there was a variation in n from 1·85 to 2·35 and in D from 0·016 to 0·14 over the surface of a given film, the corresponding variation in thickness being within the relatively narrow range 160 to 220 Å. The change in D over the surface was visible to the naked eye. This observation is in itself sufficient warning that the optical density is not a reliable guide to film thickness, except within very crude limits.

In order to investigate whether these differences in optical

properties might be correlated with structural changes in the deposited films, electron diffraction patterns were obtained from films of differing thickness and refractive index. The patterns show only a few very broad rings but there are significant differences between those given by films of high and low refractive index. The two most prominent rings correspond to the 10 and 11 reflections from two-dimensional sheets of graphite, and these are present for both types of film. The normally strong 002 reflection could barely be detected from films of low refractive index, indicating absence of the characteristic interplanar spacing of graphite, whereas it was readily visible in the patterns from films of high refractive index. Detailed investigation of these variations has been begun, but the preliminary conclusion appears justified that evaporated carbon films consist of more or less randomly orientated carbon hexagons embedded in a variable amount of amorphous material, as found by Hirsch[7] in certain types of coal. The radii of the main rings correspond to a two-dimensional graphitic structure with $a = 2{\cdot}4$ Å, compared with the value of 2·46 Å for pure graphite. The latteral extent of these flakes is found from the ring width to be 6 to 8 Å in the films of low refractive index, corresponding to only two or three linked carbon rings (Diamond).[8] A detailed account of these structural investigations will be published later.

DISCUSSION

It is evident from the results presented in the figure that there are two main contributory factors to the discrepancy between our measurements and those of Agar. The fact that our measurements of his films give a line parallel to but displaced from his curve indicates an important influence, of some 150 Å magnitude, of the technique used to measure film thickness or of the time interval between the measurements ("ageing"). That the curve for our own films lies still farther away from curve *B*, and at a very different slope, indicates that the method of preparing the films also has a great effect on their optical properties. In numerical terms, a film of optical density 0·5 would be read from Agar's curve *A* as having a thickness of 450 Å, from our measurement of his films *B* as 600 Å, and if prepared in our evaporator as 850 Å.

The discrepancy between the two methods of measurement, which is equivalent to $\lambda/36$, is most probably due to lack of correction for change in phase at the film boundaries. We have checked the double beam interferometer results against the Tolansky method for a number of films and found good agreement. Agar, on the other hand, used a reflection instead of a transmission double-beam method for most of his thickness determinations, especially for the thinner films where any consistent error would be most serious. Thus there is a significant difference in the optical interaction of the imaging beam with the carbon film in the two methods of measurement. Alternatively it may be that ageing effects occur in carbon films as in many metal films, although a uniform absolute change throughout such a wide range of thickness would hardly be expected.

The difference in slope of curve *C* as compared with curves *A* and *B* must be due to some radical difference of the films prepared by us from those prepared by Agar, which we have not yet been able to identify. It is most probably concerned with a difference in the size and packing of the elementary graphite platelets and perhaps with the ratio of amorphous to graphite carbon in the deposit. Variations of this sort may be due to the use of a different grade of carbon, but is more probably connected with the details of evaporation or collection. The temperature and speed of evaporation could radically affect the fineness of the graphite particles produced. Calbick[4] reports the collection of particles as large as several microns in some conditions. Alternatively the sensitivity of the optical properties of thin films to the state of the substrate on which they are formed is well known (cf. Heavens).[9] For instance, the sense of curvature of the optical density curve near the origin has been reported as both concave and convex upwards by different investigators of the same metal, in the same way as curves *A* and *C* in the figure differ. Differences in the method of cleaning the slides, or even in the type of glass, might well change the structure of the film; this could account for the fact, mentioned above, that Agar's films have a uniformly high refractive index as well as high absorption coefficient.

For the present purpose of deducing film thickness from optical density measurements the conclusion must be that the method only has validity for a particular set of experimental conditions. It appears to be reliable, to $\pm 10\%$ or better, for thicknesses down to 100 Å so long as the conditions of evaporation and collection are kept constant. It follows that anyone wishing to employ the method must make his own calibration against the readings of an optical interferometer or other independent means of finding film thickness.

The validity of the difference between our measurements and those of Agar on the same films still remains to be decided. At the moment there are some grounds for assuming that our readings are the more reliable. Both curves *A* and *C* have been used by Möllenstedt and Keller[10] in interpreting the results they obtain for the phase shift in an electron interferometer when a carbon film is placed in one beam but not in the other. The value for the inner potential of carbon obtained from our curve (15 V) is in better accord with accepted values than that given by Agar's curve (24 V). Similarly we are informed by Agar (private communication) that our results give better agreement with theory than do his in the interpretation of electron scattering data obtained from carbon films by Haine and Agar.[11] Whilst these observations cannot be accepted as definitive, owing to the insecure state of the theoretical treatment of both problems, it justifies a certain degree of confidence in our methods. We are continuing measurements by different methods of films prepared in a variety of conditions, in the hope of finally resolving these discrepancies.

REFERENCES

(1) AGAR, A. W. *Brit. J. Appl. Phys.*, **8**, p. 35 (1957).
(2) BRADLEY, D. E. *Brit. J. Appl. Phys.*, **5**, p. 65 (1954).
(3) SMITH, F. H. Brit. Patent Specification 639014, 1950; *Research*, **8**, p. 385 (1955).
(4) CALBICK, C. J. *J. Appl. Phys.*, **27**, p. 1389 (1956) (Abstract only).
(5) SMITH, F. H. *Nature* [*London*], **173**, p. 362 (1954).
(6) HUNTJENS, F. J., and VAN KREVELEN, D. W. *Fuel*, **33**, p. 88 (1954).
(7) HIRSCH, P. B. *Proc. Roy. Soc. A*, **226**, p. 143 (1954).
(8) DIAMOND, R. To be published.
(9) HEAVENS, O. S. *Optical Properties of Thin Films*, Chap. 6 (London: Butterworths Scientific Publications, 1955).
(10) MÖLLENSTEDT, G., and KELLER, M. *Z. Phys.*, **148**, p. 34 (1957).
(11) HAINE, M. E., and AGAR, A. W. *Proc. Intern. Conf. Electron Microscopy, Stockholm* (1956), p. 64. (Stockholm: Almquist and Wiksell, 1957).

On the mechanism of the production of dark-current pulses in photomultipliers

By Zs. NÁRAY and P. VARGA, Central Research Institute of Physics, Budapest, Hungary

[*Paper received* 26 *March*, 1957]

It was found that the dark-current pulses of photomultipliers are chiefly produced by the particles emerging from the glass envelope, i.e. if the envelope is at a more negative potential than the cathode, electrons are emitted by the envelope, and if the envelope is at a more positive potential than the cathode the electrons—produce scintillations in the glass envelope and a photon feedback takes place. By this mechanism the fact that the shield has a greater effect on the dark-current pulses of higher amplitudes can be satisfactorily explained.

Morton and Mitchell[1] as well as Rodda and Heath[2] have shown that the dark-current pulse rate in multipliers, where the photocathode is located inside the bulb (for example, types 931-A, Mazda 27M1, etc.), depends on the potential between the photocathode and the shield, that is the conducting layer deposited on the outer surface of the envelope of the multiplier. Experience shows that if the potential of the shield approximates to that of the photocathode the dark-current pulse rate decreases as a function of the shield potential. If, however, the shield potential is negative (in the so-called negative region of the shield characteristic) or positive with respect to the cathode potential (in the so-called positive region of the shield characteristic) the dark-current pulse rate may increase slowly or rapidly depending on the sign of the shield potential. Investigating the nature of the shield effect one of the authors[3] has found that the shield potential mainly affects the rate of dark-current pulses of large amplitudes. It should be noticed that the shield potential only slightly affects the photocurrent. The optimal signal-to-noise ratio was obtained at a shield potential approximating to the cathode potential.

The dark-current pulse rate of photomultipliers can be reduced by orders of magnitude by the suitable choice of the shield potential. From this fact one may infer that the main contribution to the dark current is not made by the thermionic emission of the photocathode.[4] Thus it seemed important to investigate by what mechanism the shield effect is produced. The authors began by considering the role the gas contained in the multiplier plays in producing the shield effect. To this end the temperature dependence of the shield effect was investigated.

TEMPERATURE DEPENDENCE OF THE SHIELD EFFECT

Morton's suggestion that the shield effect "is probably due to the effect of the potential of the inner surface of the glass near the photocathode on ions in the tube" seems to be plausible. Thus the shield effect ought to be strongly temperature dependent, since, as is well known, the number of gas molecules inside the tube decreases rapidly when the gas is cooled. To check this suggestion the authors have investigated whether the shield effect decreases with decreasing temperature.

It has been found that if the potential U_c of the cathode of the multiplier is negative with respect to the earth potential, the shape of the dark-current pulse rate *versus* shield-potential curves remains essentially unchanged at temperatures ranging from -78 to $+20^\circ$ C (see Fig. 1). On the other hand, at a constant shield potential, the dark-current pulse rate varies as a function of temperature according to Engström's measurements.[5]

According to the authors' measurements the temperature dependence of the dark-current pulse rate of the multiplier can be written in the form

$$N_d = F_1(U_s) \cdot F_2(T)$$

Here U_s and T denote shield potential and temperature, respectively. This empirical relation seems to prove the independence of the shield effect on the temperature and this in turn contradicts the assumption that the gas molecules produce the current.

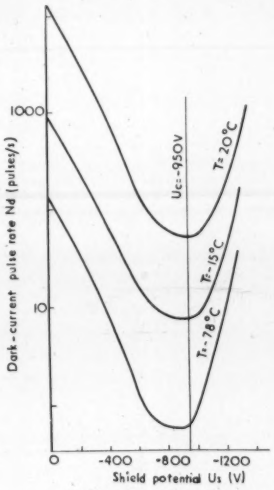

Fig. 1. The shield characteristic at various temperatures

This result concerning the temperature dependence of the dark-current pulse rate is consistent with the hypothesis of Rodda,[6] who assumes that at a negative shield potential thermal electrons are emitted from the bulb and reach the cathode. This assumption is confirmed by the amplitude dependence of the shield effect too, as for the electrons emerging from the shield the photocathode can also be regarded as a surface of secondary emission, and thus the amplitudes of the pulses produced by these electrons exceed the average amplitude. Rodda interprets the increase of the dark-current pulse rate at a positive shield potential by "the

electrons which leave the cathode and strike the glass envelope after several stages of multiplication giving rise to scintillations." By means of an optical feedback these scintillations give rise to photoelectric emission from the photocathode, and thus further dark-current pulses are produced. Possibly one pulse may be due to several primary electrons.

As the next step the authors investigated the negative and positive region of the shield characteristic separately and obtained the following results.

NEGATIVE SHIELD POTENTIAL

Under normal operating conditions the thermionic emission of the inner surface of the glass envelope cannot be directly observed, the current being too small. Thus the investigations aimed at proving that photoelectrons are emitted from the inner surface of the glass envelope. If there is photoemission, the existence of thermionic emission can also be assumed, thus accounting for the negative region of the shield characteristic.

To observe the photo-effect the measurement had to be arranged in such a way (Fig. 2) that only the inner surface of the shield was illuminated, the shield current to be measured being thus produced only by the electrons emitted by the inner surface of the envelope, and incidental positive ions from the electrodes being excluded. If photo-emission from the inner surface of the envelope really takes place, shield current must be observed only in the case of a *negative* shield potential.

Measurements were carried out with an oblique beam of light on the glass bulb, the angle of incidence being chosen sufficiently large for the light to be totally reflected from the inner surface of the glass envelope. In this case, as is well known, the amplitude of the light vector exponentially decreases in the area behind the reflecting surface (in this case the inner wall of the glass envelope). The light may produce photoelectrons in the thin layer which is unavoidably deposited on the inner surface of the envelope during the manufacture of the tube. As the measurement requires a strong illumination of the inner surface of the envelope the multiplier is immersed in a fluid (benzene) with approximately the same refraction index as that of the glass envelope, thus avoiding reflexion losses on the outer surface. Owing to the unfavourable geometry of the arrangement the electrodes could not be protected from the incidence of a large amount of scattered light. Thus current was produced in the case of both the negative and positive shield potentials.

To avoid these difficulties the following method can be applied: at first the shield is connected at positive voltage and the multiplier illuminated by an obliquely incident light beam (see Fig. 2). It is evident that in this case the shield current is produced by the photoelectrons emerging from the electrodes under the influence of the scattered light. (The scattered light incident on the electrodes is also visible to the naked eye.) An illumination corresponding to this scattered light is then produced by a light beam incident on the electrodes which is perpendicular to the envelope. The intensity of the perpendicular beam is varied until the shield current becomes identical for the right and the oblique angle of incidence. Then the shield is connected to negative voltage without changing the position of the two light sources. The results of this experiment are summarized in the table for two typical multipliers *A* and *B*.

As the table shows, the quotient of the shield current produced by the oblique and perpendicular light beam is much greater at a negative than at a positive shield potential. Considering that in the case of an oblique angle of incidence the illumination of the inner surface of the glass envelope exceeds the illumination caused by the perpendicular beam, the results of these experiments confirm the assumption that

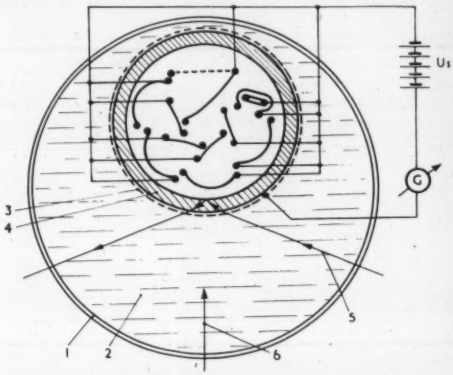

Fig. 2. The shield current in the case of total reflexion
(1) glass vessel; (2) benzene; (3) aquadag layer (which is removed from the part illuminated); (4) multiplier envelope; (5) light beam incident obliquely; (6) light beam incident perpendicularly.

from the inner surface of the envelope photoelectrons can be ejected; thus the negative region of the shield characteristic can be accounted for by the thermal electrons emitted under operating conditions from this surface.

Results of measurement taken for proving the photoeffect on the inner surface of the envelope

Multiplier	*A*		*B*	
Shield potential (V)	−1000	1000	−1000	1000
Current at oblique incidence, I_o (μA)	0·057	0·097	0·055	0·14
Current at perpendicular incidence, I_p (μA)	0·0067	0·097	0·002	0·14
I_o/I_p	8·5	1	27	1

POSITIVE SHIELD POTENTIAL

The scintillations accounting for the positive region of the shield potential can be observed in the following manner: As Fig. 3 shows, multiplier II is placed near multiplier I. The variation of the counting rate of multiplier II is investigated as a function of the shield potential of multiplier I which operates in a conventional circuit. With a cathode potential of −1000 V with respect to earth potential, and by varying the shield potential from −1000 to 0 V in multiplier I, the counting rate of multiplier II increases. This increase, though small, can be proved directly and quickly by extending the shield potential range up to +300 V as then the increase in the counting rate of multiplier II is a great deal higher, about eight to ten times as much as in the former case. In the course of further investigations the authors found that

the scintillation effect depends only on the potential between the shield and the cathode, since the same result is obtained if the other electrodes are also connected to the cathode of multiplier I.

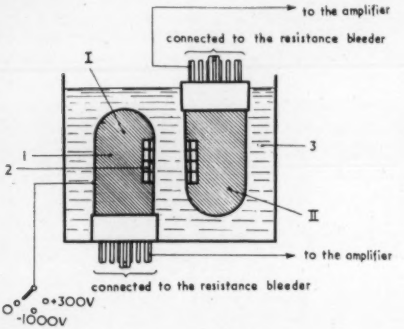

Fig. 3. Measuring arrangement for detection of scintillation

I and II, photomultipliers; (1) aquadag layer; (2) the aquadag net deposited on the glass surface opposite the cathode; (3) benzene.

In checking measurements the authors have found that if the shield and all the electrodes of multiplier I are joined, the variation of their common voltage does not affect the counting rate of multiplier II.

It can thus be concluded that the coupling of the two multipliers can only be brought about by the photons produced by the scintillations on the envelope of multiplier I. The scintillations are due to the electrons emerging from the electrodes (mainly from the photocathode).

Summarizing the results of the investigations of the shield effect, one can conclude that the predominant component of the dark current in photomultipliers is produced by different mechanisms in the positive and negative region of the shield characteristic as follows.

At a negative shield potential the thermal electrons ejected from the inner surface of the envelope give rise to secondary electrons in the cathode, which are multiplied in the well-known manner. As the electrons emitted from the inner surface of the envelope must pass through one more multiplier stage than the thermal electrons emitted from the photocathode, the amplitudes of the former exceed those of the latter and the amplitude dependence of the shield effect can be accounted for.

At a positive shield potential the electrons emerging from the inner electrodes produce scintillations on the glass envelope. The photons thus produced give rise to electrons on the cathode, which increase the dark-current pulse rate. Since this mechanism may give rise to several photons and consequently, several photoelectrons on the cathode, the amplitudes of the corresponding dark-current pulses may exceed those of the pulses produced by the electrons flying from the cathode directly to the first dynode.

ACKNOWLEDGEMENTS

Our thanks are due to Prof L. Jánossy for helpful advice and to Mrs. V. Bárdos for carrying out the experimental work.

REFERENCES

(1) MORTON, G. A., and MITCHELL, J. A. *R.C.A. Rev.*, **9**, p. 632 (1948).

(2) RODDA, S., and HEATH, F. G. Brit. Patent Specification 645763.

(3) NÁRAY, Zs. *Acta Phys. Hungar.*, **5**, p. 159 (1955).

(4) NÁRAY, Zs. *J. Sci. Instrum.*, **33**, p. 476 (1956).

(5) ENGSTRÖM, R. W. *J. Opt. Soc. Amer.*, **37**, p. 420 (1947).

(6) RODDA, S. *Photoelectric multipliers* (London: Macdonald, 1953).

Correspondence

The diffusion of barium in discharge tubes

Among the complications occurring in experiments on the sputtering of cathode materials in discharge tubes are the processes involved in the transport of the sputtered material from the cathode to the wall, or collecting surface, where it is deposited. This problem has been treated[1] on the basis of the diffusion of sputtered atoms through the gas.

On this theory, if the gas is at a pressure of a few millimetres of mercury, the sputtered material would form a quite diffuse area on a wall more than a few millimetres from the cathode. This is, in fact, often observed. Sometimes, however, highly localized spots with quite sharp boundaries are observed on the walls of discharge tubes containing self-heated cathodes as shown in the figure. The formation of these cannot be accounted for on the basis of the diffusion of atoms.

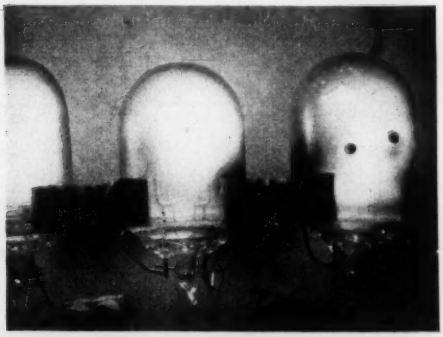

Barium-containing spots sputtered from the cathode of discharges in 3 mm pressure of argon and mercury vapour. Diffuse areas of sputtered nickel are visible at the sides. The bulbs are 35 mm in diameter

Analysis of the spots shows that they always contain a low work function cathode material, usually barium. This suggests that the material is transported as ions, the diffusion of which will be modified by the work function of the wall. Materials of high work function form more diffuse areas, such as those seen at the sides in the figure (nickel). (These distinct types, in a less marked form, are well known as blemishes on fluorescent lamps.)

Consider the ion and electron current densities j_p, j_e to two regions of the wall, of effective work functions ϕ_1 and ϕ_2 ($\phi_1 > \phi_2$). Suppose the plasma densities near the wall to be n_1 and n_2 and let V be the potential of the plasma above the wall and T_e the electron temperature. Then the ratio of the wall currents will be

$$\frac{j_{p2}}{j_{p1}} = \frac{j_{e2}}{j_{e1}} = \frac{n_2 \exp\left[-e(V+\phi_2)/kT_e\right]}{n_1 \exp\left[-e(V+\phi_1)/kT_e\right]}$$

$$= (n_2/n_1)\exp\left[(\phi_1 - \phi_2)/kT_e\right]$$

n_2 and n_1 will differ slightly because of the different current densities in the plasma,[2] but the dominant factor is the exponential factor which shows that the area of low work function will receive a substantially larger ion current than the other. Thus a point which gains an initial excess of (say) barium, and hence a low work function, will develop rapidly at the expense of its surroundings.

Research Laboratories,
British Thomson-Houston Co. Ltd.,
Rugby.

M. A. CAYLESS,
A. D. FORSTER-BROWN

[7 June, 1957]

REFERENCES

(1) ECKER, G., and EMELÉUS, K. G. *Proc. Phys. Soc. [London]*, *B*, **67**, p. 546 (1954).
(2) CAYLESS, M. A. To be published.

The deterioration of nitro-cellulose films used for electron microscopy

It is well known that sheets of nitro-cellulose discolour and become brittle when exposed to the sun and that it is essential to keep the solution used for electron microscope substrates in a dark bottle to retard deterioration. However, no similar remarks have been seen concerning the prepared collodion covered grids used as the usual substrates for electron microscopy. Most microscopists prepare a small stock of grids in advance and often hold the prepared specimens for a time before examination in the microscope is completed.

We have noticed that these thin films deteriorate in strong light in a remarkably short time. A few hours near a window is sufficient to result in noticeable splitting in the electron beam. Sunshine is more rapid and even the light from the hot tungsten filament in the shadowing equipment is now suspect. Since it is impossible to obtain high resolution micrographs with substrates which move and tear we now take the precaution of preparing fresh grids each day and keeping specimens and unused grids out of the light in a drawer until required. We try to keep the time of evaporation of shadowing material to a few seconds. These two precautions have reduced trouble with splitting of the collodion films in the beam.

Because little information is available on the deterioration of thin collodion films, it would be interesting to know whether other microscopists use these precautions.

Dominion Physical Laboratory,
Lower Hutt,
New Zealand.

D. M. HALL

[9 April, 1957]

The mechanism of particle acceleration in high current spark discharges

In recent years, attention has been drawn to the high current spark discharges in light gases as one approach to thermonuclear power. This note is concerned with a possible explanation of particle acceleration in a contracted spark channel with which Kurchatov and others[1] have experimented in deuterium or some other light gas at low pressure. In order to analyse the mechanism involved, the application

of the theory of microwave cavity resonator was examined. Here it is convenient to derive the electromagnetic fields from the usual scalar and vector potentials, ϕ and **A**. In a highly ionized gas, such as that in a spark channel, however, we may assume that the net space-charge density is everywhere zero at all times and then the scalar potential will vanish. Thus we may try to find a solution of the following equation

$$(1/C^2)\ddot{A} - \nabla^2 A = 4\pi i \tag{1}$$

subject to boundary conditions where A is normal to electrode surfaces or zero and parallel to dielectric wall of discharge tube or zero.

Now it is clear that the problem is very similar to that of a microwave cavity resonator excited by a given current. Therefore the vector potential and the current in the spark gap are expanded in terms of characteristic wave functions A_a, having an orthogonality property and normalized in the volume of the discharge tube[2] giving

$$A = \Sigma_a J_a(t) A_a(x, y, z), \quad i = \Sigma_a I_a(t) A_a(x, y, z) \tag{2}$$

Here $I_a(t)$ is called the exciting current of ath mode and given by

$$I_a(t) = \frac{1}{V}\int\int\int i \,.\, A_a^* dV \tag{3}$$

and $J_a(t)$ is called a resonator co-ordinate to give the amplitude of excitation of its particular mode. Substituting equation (2) in equation (1) and taking account of the energy losses in the gap, we obtain for the time dependence of each resonator co-ordinate:

$$\ddot{J}_a + (w_a/Q_a)\dot{J}_a + (Ck_a)^2 J_a(t) = 4\pi C^2 I_a(t) \tag{4}$$

Since the phenomena of spark discharge are not so rapid as those of a microwave with resonant frequency w_a of gap as a cavity (some hundred Mc/s) equation (4) may be written approximately:

$$J_a(t) = (4\pi/k_a^2) I_a(t) \tag{5}$$

As is readily understood from equation (3), we may further consider only particular modes which have a similar spatial distribution to that of discharging current and therefore will be excited by it most effectively. In fact, electromagnetic field in the gap at the contraction of discharging path is just like that of E_0-mode in cylindrical cavity and the current in contracted channel seems to be most effective to excite this mode (see figure). Thus we may conclude that in the gap space of a high current spark discharge, an electromagnetic field like that of E_0-mode in a cylindrical cavity with dielectric wall is excited by the discharging current at the contraction. Therefore as soon as the discharging path is contracted by the so-called pinch effect to be a channel of plasma, the excitation current of E_0-mode becomes great and the intense fields of the mode will build up. And it is remarkable that the field distribution suggests the kink of discharging current and the abrupt drop of voltage across the gap as are observed by Kurchatov and others at the contraction of the discharging path.

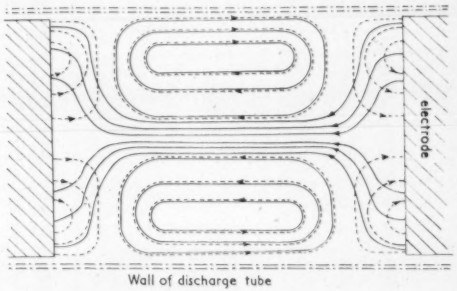

Current distribution (solid line) and E_0-mode potential (dashed line) at the contraction of spark channel

Thus for the gap of length L with electrodes of radius R, the longitudinal electric field along the tube axis is roughly estimated by equation (5):

$$E_z(O) \simeq \frac{4\pi \times 10^{-9} \dot{I} \cos\left(\frac{2\pi}{L} z\right)}{\left(\frac{2\pi}{L}\right)^2 + \left(\frac{3{\cdot}83}{R}\right)^2} \text{ (in V/cm)} \tag{6}$$

Here $\dot{I}$ is the time derivative of current density in the contracted spark channel expressed in A/cm^2 sec.

In Kurchatov's experiments, the current density of the channel is reported to be about 5×10^3 A/cm^2 and it is formed in a fraction of a microsecond. For these values equation (6) gives an effective potential difference of about 4×10^5 V in the middle of the gap of 1 m (tube radius 20 cm), which is sufficient to accelerate charged particles to generate hard X-rays or to induce $(d - d)$ reaction in deuterium gas to some extent.

Engineering Faculty,
Tohoku University,
Sendai,
Japan.

SHIGEO NAGAO
[18 February, 1957]

REFERENCES

(1) *Nucleonics*, **14**, p. 36 (1956).
(2) CONDON, E. U. *Rev. Mod. Phys.*, **14**, p. 341 (1942).

New books

Advances in electronics and electron physics. Vol. 8. Edited by L. MARTON. (New York: Academic Press Inc.; London: Academic Books Ltd., 1956.) Pp. xi + 562. Price 104*s*.

The series of reviews, *Advances in Electronics and Electron Physics* has now reached its eighth year of existence and is well recognized as a most useful contribution in bringing together, each year, collected information on selected subjects. In the short space here it is only possible to give an indication of the field covered by the authors of each of the nine reviews.

In "Some new applications and techniques of molecular beams," J. G. King and J. R. Zacharias set out to show how a molecular beam can be employed as a device to observe some other phenomenon and not merely to study the molecules themselves. The large range of concentration over which such a device can be used and the relatively high signal-to-noise ratio make the technique a powerful one. L. Kerwin's "Mass spectroscopy" obviously has some relationship to the previous paper and continues from a previous one in this series published in 1948. What a pity this author employs the words "spectroscope" and "spectroscopy" throughout: the instrument is a meter, not a scope. Another review allied to a previous one in the series in 1951 is "Field emission," by W. P. Dyke and W. W. Dolan: particular note is taken of the latest techniques employing very high current-densities and the theory is examined in the light of these.

Two articles have a bearing on techniques used in nuclear physics: "Amplitude and time measurement in nuclear physics," by E. Baldinger and W. Franzen, and "Pulse amplitude analysis," by J. L. W. Churchill and S. C. Curran, the titles of both of these giving every indication of their contents.

C. Süsskind in "Electron guns and focusing for high-density electron beams" describes the principal methods being employed in electron gun design to obtain beams of a sufficient number of electrons whilst holding together the resulting beam against space-charge and other forces leading to divergence. To provide bright visual displays on a cathode-ray tube screen persisting for an extended period of time corresponding to information which has been "written" in a fraction of a second, various designs of storage tube are being employed: these are described in "Viewing storage tubes," by M. Knoll and B. Kazan.

An important paper is presented by G. H. Metson with the title "On the electrical life of an oxide-cathode receiving tube." The work here described is concerned with specially made valves with projected lives of twenty years or so and the great influence of core material and vacuum conditions are demonstrated. Several papers have appeared in this series from time to time on magnetrons and the present volume contains a further one on "Magnetron mode transitions," by E. C. Okress.

A. J. MADDOCK

Chemical processing and equipment. Prepared by the U.S. Atomic Energy Commission. (New York: McGraw Hill Book Company Inc.; London: McGraw Hill Publishing Co., Ltd., 1956.) Pp. 316. Price 45*s*.

The description of the Idaho plant which recovers highly enriched uranium from uranium–aluminium fuel elements by a solvent extraction process is comprehensive, although it would have been more satisfactory if a greater proportion of the contents of the book had been allocated to this subject. The facilities, process and equipment are outlined, the only notable omissions being those of throughput and solvent extraction column diameters. The plant was designed for direct rather than remote maintenance and there is a useful account of the decontamination methods used to reduce the radiation levels before personnel can approach the equipment. The authors indicate that the very much larger equipment required to recover plutonium from irradiated natural uranium would be difficult to decontaminate and maintain directly, because of its size, and suggest that remote maintenance or removal may be desirable for such an equipment. It is not made obvious that economic considerations would support this approach. It is unfortunate that details of the plant adopted are emphasized and the considerations leading to the choice have not been fully discussed.

The remainder of the book is a useful catalogue of equipment which has been developed or adapted by many of the U.S. atomic energy establishments for handling laboratory quantities of highly radioactive materials. Useful reference data, listing the numbers of detailed drawings which are available on request and relevant articles in the open literature are included with the description of each item of equipment. There is no doubt that a high degree of ingenuity and engineering skill has been applied to the handling of high levels of radioactivity on the laboratory and plant scale.

Although not a textbook it should be invaluable to the specialist and even more so to workers concerned with reactor experimentation requiring a knowledge of dealing with radioactive substances in the course of research and development programmes.

L. G. RALFE

Die masssysteme in physik und technik. By G. OBERDORFER. (Vienna: Springer-Verlag, 1956.) Pp. vi + 140. Price 27*s*.

In this little book Dr. Oberdorfer attempts a critical investigation of the basis on which the systems of measuring of the physical quantities are based. He begins by discussing the nature of units and the form of correlating equations and then deals with the question of dimensions, basic and derived quantities. Then follows an account of the systems used in mechanics, electricity and magnetism and in heat. At the end of the book the author gives a most useful list of the more important physical quantities, their dimension and the units employed. For the non-German reader the heavy and somewhat verbose style is likely to create difficulties.

K. MENDELSSOHN

Elsevier's dictionary of cinema sound and music. By W. K. CLASON. (Amsterdam: Elsevier Publishing Co.; (London: Cleaver-Hume Press.) Pp. 948. Price £6.

This is one of a series of technical multilingual dictionaries in course of publication by the Elsevier Publishing Co. It is edited by the head of the translation department of Philips' Electrical Works, Eindhoven, and is in English (and American), French, Spanish, Italian, Dutch and German. In parallel columns covering two facing pages are first the serial numbers of the technical terms (3213 in all), next the terms in English or American arranged alphabetically, then the subjects (acoustics, cinema or music), followed by definitions of the terms in English. Then comes a column for the equivalents in each of the other five languages, with genders and synonyms. This is a most convenient arrangement. Since certain modifications in orthography were introduced recently in Holland, both new and old spellings are given in the Dutch language

column, where appropriate. In the second column, various synonyms are given, including slang expressions and each one in turn is given a place and number in the alphabetical list. For example, 546—cimbol, cimbalom, cimbelom, dulcimer: 547—cimbalom, cimbal, cimbelom, dulcimer: 548—cimbelom, cimbal, cimbalom, dulcimer: 949—dulcimer, cimbal, cimbalom, cimbelom. In each case the information given in the other columns is repeated. This seems to me to be needless duplication: space—and cost—would have been saved by a system of cross-references. The definitions in column four are very uneven in standard. Some are excellent, though a proportion of them could be understood only by those technically trained in the subject. Some are inadequate, e.g. *acoustic bass:* an organ stop on the pedal organ; *e-string:* the string with the highest note on any string instrument; *drumming:* sound made by drums; and from its definition—"section of the science of acoustics"—I still do not know what *acouophony* means. A few are wrong, e.g. *concave lens:* a lens thicker at the centre than at the edges; *mains noise:* noise generated within the mains; *mute:* means to alter the pitch of musical instruments. These will no doubt be corrected in later editions. It would need someone with a more liberal education than mine to check some of the terms used in cinema studios, e.g. *ashcan, dinky inky* (syn. inky dinky). Eric Partridge and other students of languages have a field for research here. Where appropriate, the usual mathematical symbol is appended to the definition of a quantity, and it would have added to the value of the dictionary if the corresponding symbols could have been added to the columns for other languages.

The whole book is excellently—indeed lavishly—produced. The printing is bold and clear on good paper and the binding pleasing and serviceable. There are very few misprints. A short bibliography of dictionaries and textbooks is appended. As far as I can tell the equivalents in the various languages seem to be accurate and reasonably comprehensive. There is no doubt that this dictionary will be a real aid to translators having to cope with technical terms in the fields covered.

F. A. VICK

Kernmomente. By H. KOPFERMANN. (Frankfurt: Akademische Verlagsgesellschaft, 1956.) Pp. xvi + 463. Price DM. 54.

The study of nuclear moments has provided some of the most valuable clues for our understanding of nuclear structure; in addition it has revealed a surprising variety of interactions between nuclear moments and their surroundings which are finding increased uses in the study of molecules and solid bodies. To write an account of all this wide-flung activity was a task which only such an established master of the subject as Professor Kopfermann could hope to tackle with success. Actually the book under review is the second edition of a monograph written about 15 years earlier; but the material has grown enormously during that time and consequently the book had to be completely rewritten.

Although the author originally made his name as an expert in the use of optical methods, his account of hyperfine structure and techniques for measuring it occupies only a small section of the book. Extensive chapters deal with the variety of techniques which have grown up in the last twenty years around Rabi's discovery of the resonance method, using molecular beams. The extension of this principle to condensed phases, the nuclear paramagnetic resonance methods of Bloch and Purcell, is treated in equal detail, including such refinements as Hahn's spin echo and the Overhauser effect. There is an extensive chapter on the study of nuclear moments by the absorption of microwaves and finally a description of the present state of the shell model and of its success in accounting for the observed nuclear moments.

Experimental methods are only briefly described, without any "tap grease." On the other hand the theoretical foundation and the formulae needed for the quantitative discussion of the phenomena are given throughout but without excessive mathematical complications. The style is lucid but very condensed; concentration is required in reading those long German sentences packed with information. In view of this it will be good news to many that an English translation is to be published later this year by the Academic Press (New York and London).

O. R. FRISCH

Laboratory Administration. By E. S. HISCOCKS. (London: MacMillan and Co. Ltd., 1956.) Pp. xvi + 392. Price 36*s*.

Books on laboratory or research administration are comparatively rare, and it is only in recent years that the subject has been thought worthy of consideration out of the context of the research which it serves. The probable reason is that the administration of scientific work is to some extent an art as well as a routine, and only with the recent growth of laboratories of increasingly standardized shape, size and organization has it been possible to discern which portions of the administrative framework can be clearly standardized. Mr. Hiscocks is therefore something of a pioneer and it is good to report that his book is well produced, and reasonably cheap, and that most of it is extremely readable. It is, to some extent, a compilation rather than an informative monograph and inevitably, therefore, one encounters sections that are obvious to the point of dullness; but even these sections have their own value if read by the administered as well as the administrators, for they should help the former to an appreciation, not always present, that the latter are rather more than a necessary evil.

The book is subject to the following criticisms in the opinion of the reviewer:

(1) Its value is limited by being presented (for perfectly good reasons, as the author explains) very much from a Civil Service viewpoint; almost all examples of methods, techniques, and problems are from the Scientific Civil Service. It is true that the Scientific Civil Service is the biggest employer of scientists in this country at present, but its methods of scientific administration still carry as strong an imprint of Civil Service organization as of scientific thought and method; more examples from the Universities and Research Associations and from industry would have presented a more comprehensive picture.

(2) Many of the tables and statistics which make the book unnecessarily lengthy are very much out of date and virtually valueless.

(3) The key to successful laboratory administration lies in Sir Edward Appleton's statement that "administration in a laboratory should be an enabling process"; this is quoted by Mr. Hiscocks on p. 3 of his book, but there is more than a suspicion that at times he succumbs to the temptation to codify and rationalize the work he knows so well, while losing sight of its purpose.

None of these criticisms detracts seriously from the undoubted value of the book, and Mr. Hiscocks is to be congratulated for setting a challenge which will almost certainly stimulate others to write inferior books on this subject. Though, happily, it is not true to say that this book should be at every scientific administrator's bedside, it should certainly be available in an adjacent library.

G. W. LOBB

Metallurgical analysis by means of the Spekker photoelectric absorptiometer. By F. W. Haywood and A. A. R. Wood. 2nd Ed. (London: Hilger and Watts Ltd., 1957.) Pp. viii + 292. Price 40*s*.

The first edition of this book was published in 1944, only three years after the pioneer exploitation of the Spekker instrument by Vaughan and his collaborators. Part I was concerned with the general principles of "colorimetric" analysis, and with the construction and manipulation of the instrument. There was also a chapter dealing with "Possible future developments." In Part II, methods for the analysis of a number of standard engineering alloys were described, "only those which have been proved trustworthy in industry" being included. It was stressed that the collection was not complete, and that with such a new development references to the literature were few.

In the thirteen years that have elapsed, the Spekker instrument and the techniques associated with it have not only become firmly established, but, to some limited extent, have in turn given way to the somewhat more refined spectrophotometric techniques made possible by the Uvi-Spek, Unicam Sp. 600, and similar instruments. The further refinements made possible by recording instruments, firmly established abroad, are now just round the corner. These developments do not detract from the popularity and value of the Spekker instrument, which has itself run to a second edition, the H. 760.

In the present volume, methods are again given for the analysis of the alloys of aluminium, copper, iron and magnesium, and there is a new section on zinc alloys. Under aluminium, methods have been added for the determination of antimony, lead and magnesium, while bismuth and lead have been added to the section on copper alloys. The section on magnesium alloys covers the same ground as before, but that on Ferrous Alloys (now headed: Steels) has doubled in content, and it now gives methods for aluminium, boron, carbon, lead, niobium, nitrogen, phosphorus and tungsten, none of which was present in 1944. There is also a new section dealing with zinc alloys. The methods described call for little comment: the arrangement is good, setting out as it does full details of reagents, procedure, blank preparation, light source, filters, cells, water setting, temperature, calibration, accuracy, time required and references.

Looking back, it is perhaps interesting to note that few of the speculations made in 1944 under "Possible future developments" have come to fruition, except that for the full development of absorptiometry a monochromator will be essential. The second edition of this volume can be fully recommended to all concerned with metallurgical analysis.

R. C. Chirnside

Peaceful uses of atomic energy. Vol. 8. Production technology of the materials used for nuclear energy. (New York: United Nations; London: H.M. Stationery Office, 1956.) Pp. 627. Price 70*s*.

Vol. 8 of the Proceedings of the Geneva Conference deals with the production technology of special materials used in nuclear reactors. It covers seven sessions of the Conference and can be conveniently divided into three sections: "Fissile and fertile materials," "Moderators" and "Canning materials." Each session contains a verbatim report of the discussion that took place immediately following the presentation of the papers.

The first section is devoted to the treatment of uranium and thorium ores, metal production and analytical procedures. The use of "ion exchange" techniques in ore preparation and in analysis is noteworthy. The section on moderators covers heavy water, graphite, berylliium and beryllia, whilst zirconium is the only canning material—other than beryllium—that is considered as a "special" material. The session dealing with heavy water, graphite and zirconium are characterised by three excellent comprehensive papers from the United States. Benedict surveys processes for D_2O production whilst Currie's paper on graphite will long remain an important reference. On zirconium, Shelton's 40 000 word epic gives some idea of the problems faced in the production and fabrication of such a metal. The separation of hafium from zirconium is considered in some detail and analytical methods are well covered.

The great value of this volume is in bringing together so much information on hitherto unpublished—and often classified—topics. It is important to appreciate that it is not a book in the conventional sense, but a collection of papers—and discussions—written by authors who have worked independently on very similar subjects. The similarity of approach is remarkable. There is no doubt that this volume provides a valuable source of information both to the specialist and to the reader with more general interests.

Roy Huddle

Proceedings of the CERN Symposium. Vol. 1. High energy accelerators. Scientific editor: E. Regenstreif (Geneva: CERN European Organization for Nuclear Research, 1956). Pp. xiii + 567. Price 40 *Sw. f.*

Vol. 1 of the Proceedings of the CERN Symposium, on High Energy Accelerators, gives the full text of the 80 or so papers submitted and the ensuing discussions in the first week of the Symposium held in Geneva last year. In addition to papers from CERN member countries, notable contributions came from the U.S.A. and U.S.S.R. This was the first time that a conference on this scale had been devoted to high energy accelerators and certainly the Proceedings are the first volume to bring together under one cover such a wealth of information on this subject. The introduction to the volume by J. B. Adams is an excellent summary of the meeting.

A number of the papers, from groups with machines in operation, give information on the operation and use of large accelerators and show that not the least of the problems is the organization necessary to achieve the maximum amount of useful physics research with such accelerators. The machines concerned are the proton synchrotrons at Berkeley (6 GeV), Brookhaven (3 GeV), and Birmingham (1 GeV), and the synchrocyclotron at Moscow (600–700 MeV).

The detailed design problems of new accelerators under construction or being planned occupy a major part of the contributions and cover such topics as injection, extraction, magnet tolerances and r.f. generation—particularly in connexion with strong focusing machines: also included are details of practical tests on model machines. The new machines include the proton synchrotrons for 2·5 GeV at Saclay, 3 GeV at Princeton, 7 GeV at Moscow, 10 GeV at Moscow, 11 GeV at Canberra, 12·5 GeV at Argonne, 25 GeV at CERN, 33 GeV at Brookhaven, and 50 GeV at Moscow. Some papers deal with electron synchrotrons, in particular the 6 GeV Cambridge (U.S.A.) and 1 GeV Frascati machines. The design study by the Stanford group of very large linear electron accelerators is interesting, especially as one 2 miles long for 20 to 70 GeV is seriously considered. The theoretical aspects of orbit stability, including the problems of the transition energy, resonant particle oscillation, and radiation in circular electron machines, are presented in a number of papers.

Another large group of papers deals with new ideas for accelerators for higher energies or higher intensities in an attempt to avoid the rapidly increasing size and cost incurred by merely scaling up present designs of accelerator. The design of fixed field alternating gradient accelerators with radial sector or spiral ridge magnets to give high currents is discussed as a practical possibility for the near future. One interesting idea for obtaining higher interaction energies is to arrange for two streams of particles to collide, sufficiently high intensities being achieved by storing particles in magnetic rings which can be part of the accelerators or separate units. Proposals from the U.S.S.R. include one in which protons would be accelerated in a contracted toroidal electron-proton plasma in which the magnetic field would be such as to maintain 100 GeV protons on a radius of only 3 metres.

This book is excellently produced and should certainly be in the possession of any individual or institution wishing to have the latest information on the high energy accelerator field. The only disappointing feature is that the list of machine parameters which was issued to participants at the meeting should have been omitted from the Proceedings.

P. D. WHITAKER

Proceedings of the CERN Symposium 1956. Vol. 2. Pion physics. Scientific editors: A. CITRON, G. VON DARDEL, B. D'ESPAGNAT, Y. GOLDSCHMIDT-CLERMONT and C. PEYROU. (Geneva: CERN European Organization for Nuclear Research, 1956.) Pp. xii + 443. Price 40 *Sw.f.*

The Editors are to be congratulated on the production of a first class report less than six months after the symposium. The second volume contains about eighty papers submitted during the second week of the conference, brief reports of the discussions are also included. Many of the papers are of great value since they contain hitherto unpublished material which will not appear elsewhere. With one exception, all the papers are in English.

The first part of the volume contains twenty-three papers on techniques used in high energy nuclear physics. Bubble chambers, cloud chambers, Čerenkov and fast counting techniques are described in detail and very useful bibliographies are included. This part of the report should be of value to readers interested in technical developments in modern nuclear physics.

The technique section is followed by papers on antiproton physics, nucleon–nucleon scattering, theoretical aspects of pion physics, pion–nucleon scattering, photoproduction of pions, pion production by nucleons and mesonic atoms. Each section includes an introductory or review paper which provides the background for the remaining papers. The section on pion physics will be of the greatest value to workers in the field because of the large number of detailed Russian papers, many of which are now available in English for the first time.

The production is excellent and the book is well illustrated.

C. C. BUTLER

Photoconductivity conference. Edited by R. G. BRECKENRIDGE, B. R. RUSSELL, and the late E. E. HAHN. (New York: John Wiley and Sons Inc.; London: Chapman and Hall Ltd., 1956.) Pp. xiii + 653. Price £5 8*s*.

Photoconductivity has been a subject of interest and importance for a considerable time, but increasingly so in the last ten years. It is important in its own right as the basis of methods for detecting radiation and for providing radiation-controlled indicating and switching devices. It is potentially valuable in connexion with solar batteries and with some types of solid state light amplifier and wavelength converter. It is also of indirect value as a tool for studying several aspects of solid state physics. The processes are however highly complex, and in general, difficult to interpret. Considerable progress has been made with understanding the behaviour of germanium, but less with other materials. Research on these is continuing very actively. The relative contributions of the surface and the bulk of the solid are sometimes difficult to separate, but when this can be done, the subject may make an important contribution to surface physics as well as to knowledge of the bulk properties.

The interest and progress in the subject are illustrated by the size and range of this volume, reporting a conference on photoconductivity held in November 1954. Thirty papers are included, dealing with the basic theory and fundamental physical processes, and with the properties of the materials in use as photoconductors. The first papers are general, applying to the basic processes in any material. The later papers deal specifically with germanium, silicon, zinc oxide, indium antimonide, tellurium, and the lead sulphide group of compounds. The papers are all authoritative and well presented and are followed in many cases by a short account of the discussion which ensued. The authors include many names well known in solid state physics, and all are experts on the subjects they are discussing. One can say with confidence that familiarity with the contents of these papers is essential to all workers in this and related subjects. It is to be noted, however, that Rose's paper has appeared identically in the Solid State Issue of *Proc. Inst. Radio Engrs.* for December 1955, while several of the other papers are only slightly different from publications that have been presented elsewhere.

D. A. WRIGHT

Relaxation methods in theoretical physics. Vol. 2. By R. V. SOUTHWELL. (Oxford: Clarendon Press, 1956.) Pp. vi + 274. Price 55*s*.

It is difficult to review a work by an author whose name is almost synonymous with the subject on which he writes. This third volume on relaxation method (the first was applied to engineering science), is a collection of problems with "relaxation" solutions which have been published in various journals over the past ten years by the author, or by his associates, often in joint papers. References are given to the originals and generous acknowledgement is given to his "erstwhile team of co-workers."

The problems in this volume all lead to equations of considerable difficulty from the iterative viewpoint, the straight biharmonic equation being probably the simplest. To those who have toyed with anything more complicated than, say, the harmonic problem, such comments as "sound intuition brings a reward . . ." (p. 250), and "though satisfactory in the hands of experienced computers . . ." (postscript to the first chapter), will evoke a heartfelt assent. It is very fitting that this volume is dedicated to Miss Vaisey for on the sole evidence of work completed, she must combine sound intuition and experience to a remarkable degree.

One serious reservation should perhaps be made on all this work. Statements such as "If Z_2 is deemed a sufficiently close approximation . . ." (p. 260) are of very little help in the vexed problem of convergence. It is salutary to find that in Fig. 130, the revised solution which "as reworked . . . includes one more significant figure" alters the solution at one point by 500 in 1200. The original solution was therefore not correct even to the second figure, although one assumes that the residuals were reduced to the order of tens. It is clear from this that the order of the residuals is an inadequate guide to the order of the error in the required quantities.

This reviewer feels that the question "How do we know how accurate we are?" demands more attention than it gets. The summary rejection of the modification due to Fox (paragraph 235) is to be regretted. This method could give valuable information on mesh size which is one important feature governing accuracy.

In several chapters the problem to be considered is not clearly stated, and the natural division of material is not made. For example, in the mixed plastic-elastic problem the conditions on the interface are vital to the existence or uniqueness of the solution. In one sentence, continuity of displacement, stress, and strain is assumed. This assumes continuity of the tangential stress σ_t, for no very good reason, and is in effect assuming arbitrarily that $\Delta\lambda$ shall be zero. It is implied that the assumption is necessary, is it enough to produce a unique solution?

But this is a minor point of presentation, and all students of relaxation methods will be grateful for this comprehensive monument to the energy and ingenuity of a devoted band of men and women. C. SNELL

Rheology: theory and applications. Vol. 1. Edited by FREDERICK R. EIRICH. (New York: Academic Press Inc.; London: Academic Books Ltd., 1956.) Pp. xiv + 761. Price 143*s*.

The preparation of three large volumes dealing with rheology represents perhaps the most ambitious attempt yet made to provide something like a comprehensive survey of this somewhat ill-defined subject. In any such work the question of the choice of subject-matter is bound to be difficult, and this is particularly true in the subject of rheology, in which so many distinctive methods of approach are to be found. The editor of these volumes has achieved a reasonable balance between the more general and mathematical type of treatment and the more specific study of particular materials, and each chapter is sufficiently detailed to give a really useful understanding of the state of development of the subject. The appearance in one volume of discussions on both metals and non-metals (mainly polymers and polymer solutions) shows a welcome tendency for these two broad schools to begin to use a common language.

It is not possible to comment in detail on the individual contributions to Volume 1. The subject of the deformation of metals and crystals includes contributions by W. Prager, by D. C. Drucker, by J. Fleeman and G. J. Deenes, and by J. M. Burgers and W. G. Burgers. Various aspects of viscosity in pure liquids and in polymer solutions are discussed by A. Bondi, by T. G. Fox, S. Gratch, and S. Loshaek, by J. Riseman and J. G. Kirkwood and by H. L. Frisch and R. Simha, and streaming birefringence and stress birefringence in polymers are dealt with by A. Peterlin. More general contributions include the phenomenological theory of large elastic deformations, by R. S. Rivlin, viscoelastic behaviour, by T. Alfrey, phenomenological macrorheology, by M. Reiner, and non-Newtonian flow, by J. G. Oldroyd. More specialized subjects include rheological properties under high pressure, by R. B. Dow, and ultrasonic investigations in liquids, by R. B. Lindsay.

Though there is inevitably a certain amount of overlapping, and some subjects which particular readers might have wished to see included are missing, the general standard of this work is very high, and it can be confidently recommended. The production and indexing are excellent, and if the price will unfortunately restrict its acquisition by individual readers, one can only hope that it will be the more readily available in every library. L. R. G. TRELOAR

Synthetic polypeptides. Preparation, structure, and properties. By C. H. BAMFORD, A. ELLIOTT and W. E. HANBY. (New York: Academic Press Inc.; London: Academic Books Ltd., 1956.) Pp. xiii + 445. Price 80*s*.

To quote from the Preface: "It will be unnecessary to tell potential readers that the peculiar interest attached to synthetic polypeptides lies in their relation to the proteins." Thus they are everybody's business, and not least the physicist's; though to be sure, as high polymers, they are very good examples, too, of how little real separation there is these days between physics and chemistry and biology (and technology) in this sort of field. The authors have ranged widely over it, and tell us this comparatively new story in a way only they could have done so well, so important a proportion of the basic investigations on which it rests having been carried out by them personally and their collaborotars in the Courtaulds Research Laboratory at Maidenhead. The physics is predominantly X-ray diffraction analysis and infra-red spectroscopy, and the underlying principles and their special application to the problem of synthetic polypeptides and related structures are expounded in a particularly thorough and helpful manner. Indeed, we owe a great deal to the authors for this most excellent, comprehensive and timely book, which has the property of making itself indispensable from the moment one sets eyes on it. W. T. ASTBURY

Journal of Scientific Instruments

Contents of the September issue

SPECIAL ARTICLE

Some new electrical and magnetic ceramics. By G. Campbell.

ORIGINAL CONTRIBUTIONS

Papers

An optical probe for accurately measuring displacements of a reflecting surface. By K. W. T. Elliott and D. C. Wilson.

The design of an apparatus for biological experiments at high hydrostatic pressure. By A. C. Downing and D. R. Wilkie.

Counter diffractometer—the effect of vertical divergence on the displacement and breadth of powder diffraction lines. By E. R. Pike.

A new self-recording rheogoniometer. By A. F. H. Ward and P. Lord.

Cooled photoconductive detectors using indium antimonide. By D. W. Goodwin.

Laboratory and Workshop Notes

A valve for the grease-free manipulation of mercury. By G. A. Bottomley.

Elimination of pen to paper friction in Murday system recording milliameters. By J. S. Heeks and D. W. Ovenall.

A quenching probe unit for Geiger–Müller tubes. By F. W. Lovick.

A graphical method for the correction of counting rates for dead time. By Y. W. Chan.

NOTES AND NEWS

New instruments, materials and tools — New books

Manufacturers' publications — Notes and comments

THIS JOURNAL is produced monthly by The Institute of Physics, in London. It deals with all branches of applied physics (including theory and technique).
All rights reserved. Responsibility for the statements contained herein attaches only to the writers.
EDITORIAL MATTER. Communications concerning editorial matter should be addressed to the Editor, The Institute of Physics, 47 Belgrave Square, London, S.W.1. (*Telephone:* Belgravia 6111.) Prospective authors are invited to prepare their scripts in accordance with the *Notes on the preparation of contributions*. (Price 2*s*. 6*d*. including postage.)

REPRODUCTION. The Institute of Physics is a signatory to The Royal Society's Fair Copying Declaration. Details may be obtained upon application from The Royal Society, London, W.1.

ADVERTISEMENTS. Communications concerning advertisements should be addressed to the agents, Messrs. Walter Judd Ltd., 47 Gresham Street, London, E.C.2. (*Telephone:* Monarch 7644.)

CLAIMS FOR MISSING JOURNALS. Claims from regular subscribers to this *Journal* for missing numbers will only be considered if received within 60 days of the date of mailing plus normal outward time of transit and time for lodging the claim. Losses attributable to failure to notify a change of address or to similar omissions will not be considered.

SUBSCRIPTION RATES. A new volume commences each January. The charge is £5 per volume ($14.25 U.S.A.), including index (post paid), payable in advance. Single parts, so far as available, may be purchased at 10*s*. each ($1.50 U.S.A.), post paid, cash with order. Orders should be sent to The Institute of Physics, 47 Belgrave Square, London, S.W.1, or to any bookseller.

Contact stresses in toroids under radial loads

By H. Fessler, M.Sc., Ph.D., and E. Ollerton, B.Sc.(Eng.), Departments of Civil and Mechanical Engineering, University of Nottingham

[*Paper received* 25 *April*, 1957]

The investigation was restricted to the measurement and calculation of shear stresses only, since these are considered the most important. The stresses were determined using the frozen stress photoelastic technique. A large range of toroids, with positive, zero and negative surface curvatures was tested. The shapes and sizes of the contact areas were in close agreement with Hertzian theory, and the values and positions of the maximum shear stresses agreed with calculated values based on the analysis by Thomas and Hoersch.

It was found that for many practical cases of rolling contact the maximum range of the orthogonal shear stress exceeds the maximum shear stress. This is because the orthogonal shear stress is reversed as one body rolls over the other. A method of calculating the greatest range of orthogonal shear stress has been developed from Hertz's theory. The measured stress ranges and their positions agreed with the calculated values.

Contact stresses in toroids are of general interest because forces are frequently transmitted between surfaces having two principal curvatures. Ball bearings, wheels on rails, and gear teeth are examples of this.

The general solution of contact stresses in semi-infinite elastic bodies was derived by Hertz[1] in 1881. The geometric shapes of the bodies determine the proportions of the contact area, which is elliptical. Hertz obtained the stresses in terms of certain Newtonian potential functions. In 1913 Fuchs calculated the stresses by arithmetic integration and in 1917 Belajef obtained a general solution for the stresses in the bodies by the use of elliptical coordinates. Morton and Close[2] calculated the stresses in a sphere under normal load. In 1932, Thomas and Hoersch[3] converted Hertz's general solution into an expression containing standard elliptic integrals, for the stresses along the axis of symmetry only. They determined yielding in steel bodies by Fry's method of strain etching. This method was also used by Föppl[4] in 1936 to illustrate his evaluation of the stresses in spheres and cylinders in contact. In 1953 Radzimovsky[5] studied parallel cylinders in rolling contact and determined theoretically the stresses in the plane of rolling. He also put forward a strength theory based on the Huber–Mises criterion of failure under combined stresses.

The purpose of the present investigation was:

(*a*) to verify the Thomas and Hoersch solution for the value and position of the maximum shear stresses;
(*b*) to investigate to what extent the theory applies to finite bodies;
(*c*) to arrive at a general method of estimating the contact stresses near discontinuities in curvature of the bodies;
(*d*) to determine the magnitude and position of the maximum range of shear stress which would occur if the bodies were in rolling contact.

Shear stresses only were studied because they (not the direct stresses) are considered to be the criterion of fatigue failure.

Calculation of Maximum Shear Stress

Thomas and Hoersch's solution, as applied to toroids with two coincident planes of symmetry, may be summarized as follows. To calculate the stresses in any particular case, the following must be known. The radial load P and for bodies 1 and 2; Young's moduli E_1 and E_2; Poisson's ratios ν_1 and ν_2; and the principal radii of curvature R_{i1}, R_{j1}, and R_{i2}, R_{j2}, where i and j are the coincident planes of symmetry of both toroids.

Thomas and Hoersch define

$$B = \tfrac{1}{2}\left(\frac{1}{R_{i1}} + \frac{1}{R_{i2}}\right) \text{ and } A = \tfrac{1}{2}\left(\frac{1}{R_{j1}} + \frac{1}{R_{j2}}\right) \tag{1}$$

chosen so that $B > A$ and show that

$$\frac{B}{A} = \frac{k^{-2} \cdot E(k') - K(k')}{K(k') - E(k')} \tag{2}$$

where $k = b/a$ is the ratio of semi-minor to semi-major axis of ellipse of contact

and
$$k' = \sqrt{(1 - k^2)} \tag{3}$$

$$E(k') = \int_0^\infty (k^2 + \omega^2)^{\frac{1}{2}}(1 + \omega^2)^{-1} d\omega \tag{4}$$

$$K(k') = \int_0^\infty (1 + \omega^2)^{-1}(k^2 + \omega^2)^{-\frac{1}{2}} d\omega \tag{5}$$

This can be evaluated with tables and B/A plotted against k. A graph of k for different values of B/A was published by Thomas and Hoersch.[3] It is also proved that

$$a^3 = 3\Lambda P \,.\, E(k')/2\pi k^2 \tag{6}$$

where
$$\Lambda = \frac{1}{A + B}\left(\frac{1 - \nu_1^2}{E_1} + \frac{1 - \nu_2^2}{E_2}\right) \tag{7}$$

i.e. a constant depending on the shapes and properties of the bodies in contact.

Thus the semi-major axis a and the shape k of the ellipse of contact can be predicted. They also show that the direct stresses along a radial line through the centre of contact are given by:

$$\left.\begin{aligned} X_x &= \frac{a}{\Lambda} M(\Omega_x + \nu\Omega'_x) \\ Y_y &= \frac{a}{\Lambda} M(\Omega_y + \nu\Omega'_y) \\ Z_z &= \frac{a}{\Lambda} \cdot \frac{M}{2}\left(\tau - \frac{1}{\tau}\right) \end{aligned}\right\} \tag{8}$$

where the z axis coincides with the line of loading and the x and y axes lie in the planes of symmetry of both toroids and x coincides with the major axis of the ellipse.

$$M = 2k^2/(1 - k^2)E(k') \tag{9}$$

$$\Omega_x = -\tfrac{1}{2} + \tau/2 + \frac{z}{a}[F(\phi, k') - E(\phi, k')] \tag{10}$$

$$\Omega_x = 1 - \tau/k^2 - \frac{z}{a}[F(\phi, k') - k^{-2} \cdot E(\phi, k')] \tag{11}$$

$$\Omega_y = \tfrac{1}{2} - \tau/k^2 + 1/2\tau - \frac{z}{a}[F(\phi, k') - k^{-2} \cdot E(\phi, k')] \tag{12}$$

$$\Omega_y' = \tau - 1 + \frac{z}{a}[F(\phi, k') - E(\phi, k')] \tag{13}$$

$$\tau = \left(k^2 + \frac{z^2}{a^2}\right)^{\frac{1}{2}}\left(1 + \frac{z^2}{a^2}\right)^{-\frac{1}{2}} \tag{14}$$

$F(\phi, k') = K(k')$ between the limits z/a and ∞ (15)

$E(\phi, k') = E(k')$ between the limits z/a and ∞ (16)

At a chosen value of k, the shear stresses $\frac{1}{2}(X_x - Z_z)$ and $\frac{1}{2}(Y_y - Z_z)$ can therefore be evaluated for different distances z from the contact surface, plotted against z and the maximum value and its position determined. This procedure was repeated with different values of k to give theoretical curves of maximum shear stress and its depth, plotted against the contact axis ratio. These curves, shown in Figs. 5 and 6, apply to both bodies, since the theory does not distinguish between them.

CALCULATION OF MAXIMUM RANGE OF SHEAR STRESS

Radzimovsky[5] and Smith and Liu[6] pointed out that when two toroids are in rolling contact, the greatest variation of shear stress may not occur on the axis of symmetry but at some other point in the principal plane of motion.

Consider a point at a given depth below the surface as the load passes over it. The difference of the principal stresses increases from zero to a maximum when the load is directly over the point and decreases after that. The greatest value of maximum shear stress therefore occurs on the axis of symmetry. This value can be calculated by the method of Thomas and Hoersch.

Alternatively one may consider the orthogonal shear stress Z_x or Z_y (see Fig. 1). At a point in the plane of rolling this

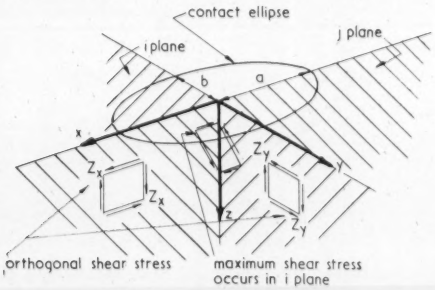

Fig. 1. Definition of stresses

increases from zero to a maximum value as the load approaches the point, but decreases to zero when the load is directly above the point (because this shear stress is zero on an axis of symmetry). As the load moves on, the orthogonal shear stress at the point increases to a second maximum value, but the direction of the shear stresses is opposite to that of the first maximum. This may be illustrated by considerations of symmetry or of equilibrium. The sum of these two maximum values is referred to as the range of shear stress.

This range of shear stress may be greater than the largest value of the maximum shear stress, and when this occurs is considered to be the factor controlling fatigue failure of the bodies. To calculate the range of shear stress one must be able to calculate the orthogonal shear stress at any point in the principal planes. The equations were derived as follows.

In his account of Hertz's theory, Love[7] derives the displacements of an element in the body. From these

$$\mathrm{u} = \frac{-z}{4\pi\mu}\cdot\frac{\partial\phi}{\partial x} - \frac{1}{4\pi(\lambda+\mu)}\frac{\partial\psi}{\partial x} \tag{17}$$

$$\mathrm{w} = \frac{-z}{4\pi\mu}\frac{\partial\phi}{\partial z} + \frac{(\lambda+2\mu)}{4\pi\mu(\lambda+\mu)}\frac{\partial\psi}{\partial z} \tag{18}$$

where μ and λ are the Lamé parameters,

$$\phi = \iint \frac{P'}{r}dx'dy' \text{ and } \psi = \iint P' \log(z + r)dx'dy' \tag{19}$$

Because $r = \sqrt{(x^2 + y^2 + z^2)}$

$$\partial\psi/\partial z = \phi, \text{ and } \partial^2\psi/\partial x\partial z = \partial\phi/dx$$

Using the above

$$Z_x = X_z = \mu\left(\frac{\partial\omega}{\partial x} + \frac{\partial u}{\partial z}\right) \text{ reduces to } -\frac{z}{2\pi}\frac{\partial^2\phi}{\partial x\partial z} \tag{20}$$

Love also shows that

$$\phi = \frac{3P}{4}\int_\gamma^\infty \left(1 - \frac{x^2}{a^2+\psi} - \frac{y^2}{b^2+\psi} - \frac{z^2}{\psi}\right) [(a^2+\psi)(b^2+\psi)\psi]^{-\frac{1}{2}}d\psi \tag{21}$$

where γ is the positive root of the equation

$$1 - \frac{x^2}{a^2+\gamma} - \frac{y^2}{b^2+\gamma} - \frac{z^2}{\gamma} = 0 \tag{22}$$

From this the shear stress at any point,

$$Z_x = -\frac{3Pxz^2}{2\pi}\cdot\frac{[(a^2+\gamma)\gamma]^{-\frac{1}{2}}(b^2+\gamma)^{-\frac{1}{2}}}{\left[\left(\frac{x}{a^2+\gamma}\right)^2 + \left(\frac{y}{b^2+\gamma}\right)^2 + \left(\frac{z}{\gamma}\right)^2\right]} \tag{23}$$

On the plane of symmetry, $y = 0$ it may be written as

$$Z_x = -\frac{3P}{2\pi a^2}\cdot Q = -\frac{ak^2}{\Lambda E(k')}\cdot Q \tag{24}$$

where

$$Q = \frac{\frac{x}{a}\left(\frac{z}{a}\right)^2\left[\left(1+\frac{\gamma}{a^2}\right)\frac{\gamma}{a^2}\right]^{-\frac{1}{2}}\cdot\left(k^2+\frac{\gamma}{a^2}\right)^{-\frac{1}{2}}}{\left(\frac{ax}{a^2+\gamma}\right)^2 + \left(\frac{az}{\gamma}\right)^2} \tag{25}$$

in the same way it can be shown that the shear stress on the plane $x = 0$

$$Z_y = -\frac{3P}{2\pi b^2} \cdot R = -\frac{b}{\Lambda} \cdot \frac{1}{kE(k')} \cdot R \qquad (26)$$

$$\text{where } R = \frac{\frac{y}{b}\left(\frac{z}{b}\right)^2\left[\left(1+\frac{\gamma}{b^2}\right)\frac{\gamma}{b^2}\right]^{-\frac{1}{2}}\left(\frac{1}{k^2}+\frac{\gamma}{b^2}\right)^{-\frac{1}{2}}}{\left(\frac{by}{b^2+\gamma}\right)^2+\left(\frac{bz}{\gamma}\right)^2} \qquad (27)$$

The maximum values of Z_x and Z_y occur in the planes $y = 0$ and $x = 0$ respectively. The orthogonal shear stresses at any point $(x, 0, z.)$ or $(0, y, z.)$ in these planes may therefore be calculated if the load P and the curvatures and elastic constants of the bodies are known. Because it is not practicable to differentiate the expressions for the stresses with respect to their position, they were evaluated in the regions where the experimental maxima occurred. These calculated values of greatest range of shear stress and its position are plotted against the shape of the ellipse of contact in Figs. 7 and 8.

SHAPES OF MODELS

Either principal curvature of either toroid may be positive (convex), zero (plane) or negative (concave). Bodies with two positive principal curvatures were called barrels; those with one positive and one negative curvature, saddles. Each model is defined by a point in Fig. 2. Every test is indicated by a straight line connecting the shapes which were loaded

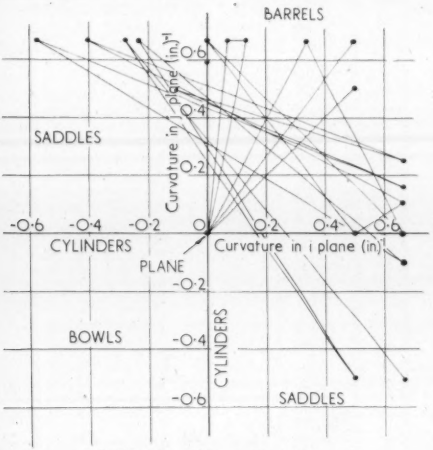

Fig. 2. Shapes of models

against each other. It may be seen that the tests consisted of: barrels loaded against barrels, cylinders, planes, and saddles; sphere against plane; cylinders against cylinders; and saddles against saddles. Bowls, that is bodies with two negative curvatures, were excluded.

Within the practical limits of the material (Araldite casting resin B) and apparatus, the shapes were chosen to give the greatest possible variation in the shape of the contact ellipse—from a circle between crossed cylinders and a sphere on a plane, to a rectangle between parallel cylinders (shown by the isolated dot on the j axis).

The required shapes were turned as smooth as possible on a lathe with a radius attachment. A $\frac{3}{4}$ in. diameter hole was bored through the centre of these solids of revolution to locate the principal planes of the model. Each solid of revolution was cut on a diametral plane to produce two identical, independent models.

EXPERIMENTAL TECHNIQUES

The models were located on $\frac{3}{4}$ in. diameter steel bars fastened to rigid steel platens in the apparatus shown in Fig. 3. The upper platen was free to slide vertically on guides, and loads could be applied on the line of intersection of the coincident principal planes of the models.

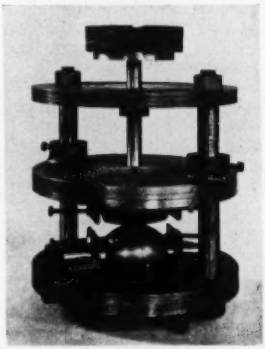

Fig. 3. Photograph of apparatus showing models located on bars

It was found that the compressive stresses induced during a "stress freezing" cycle altered the appearance of the contact surface by deforming the microscopic surface irregularities. This permitted the direct measurement of the ellipse of contact. Fig. 4 shows two different models, illuminated to show the contact areas. Lines were scribed with a toolmaker's height gauge at the extremities of the contact area and the axes of the ellipse of contact were thus measured to within $\pm 0{\cdot}001$ in.

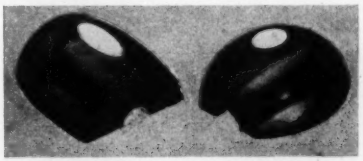

Fig. 4. Contact areas on two toroids

Slices containing the principal planes were cut from each model using a diamond-impregnated mild steel slitting wheel. The yz slice, containing the minor axis of the ellipse of contact, was cut first and removed before the remainder of the other slice was cut out. The usual slice thickness was 0·05 in.

The fringe pattern in the slices showed large stress gradients at the edges of the contact areas which agreed closely with the position of the scribed lines. Thus the axis of symmetry of the *yz* slice was determined and found to contain the zero isoclinic line. The maximum fringe order was determined by Tardy compensation and its distance from the contact surface was measured with a travelling microscope.

For the determination of the greatest orthogonal shear stress, the circular polariscope was set to particular isoclinic angles and the positions and values of the maximum fringe orders on these isoclinics were measured. The greatest orthogonal shear stress for each isoclinic angle was calculated and plotted against the isoclinic angle to determine the maximum value in the plane. The co-ordinates of this maximum value were obtained in the same way.

Because the distance of the greatest orthogonal shear stress from the centre line was 0·7 to 0·95 of the semi-axis of the ellipse of contact (see Fig. 8) it was possible to determine this stress also for the *xz* slices, the central portion of which was lost in cutting the *yz* slices.

Thus the investigation was extended to the plane of the major axis of the ellipse of contact. The corresponding values of maximum shear stress were obtained from *xz* strips cut from the centre of the *yz* slice.

The Young's modulus and material fringe value of each pair of models (that is each solid of revolution) were determined from a rectangular tensile specimen cut from one of the models after testing. The accuracy of strain measurement was greatly improved by scribing three lines near each end of the specimen; thus up to nine different gauge length and elongation measurements could be made on one specimen after one test. The slope of a plot of elongation against gauge length gave a reliable value of strain.

CONTACT AREA

Experimental convenience limited the size of the models to radii of curvature as small as $1\frac{1}{2}$ in., but it was also desirable to employ large loads which produce large contact areas. (The stresses and their distances from the surface increase with increasing load and can therefore be measured more accurately.)

Because Hertz's theory assumes semi-infinite bodies, it was necessary to determine the greatest ratio of semi-major axis of ellipse of contact a to smallest radius of curvature R to which the theory could be applied. Contact areas were compared because, unlike stress determinations, these measurements are a non-destructive test. To save time, four pairs of models were loaded at room temperature and the contact area was determined by the transfer of Prussian blue from one model to the other. The large loads required (up to four tons) were applied in a compression testing machine.

Equation (6) predicts that a^3 should be proportional to the load P. Measured values of a and b were plotted against $P^{\frac{1}{3}}$ so that equal errors of measurement of the axes of the contact ellipse should produce equal scatter on the graph irrespective of the values of a and b.

Tests were carried out with a/R varying from 0·05 to 0·3, the greatest value permitted by the strength of the model material. No evidence of the expected size effect was found as the experimental values for all but the small values of a agreed with the theoretical values within the limits of experimental accuracy. The small values of a were greater than predicted. This was attributed to imperfect transfer of the marking medium.

In order to decide whether the load should be transmitted to the models through the diametral plane or through a round bar in the locating groove, some of the above tests were carried out with "plane–plane," "bar-bar," and "bar-plane" supports. No significant difference was found and therefore subsequent tests were all carried out with "bar-bar" supports because this was more convenient.

For the "frozen stress" tests, where the stresses were determined, the measured values of the axes of contact were also compared with the theoretical values. The theoretical values of a were calculated from equation (6) in terms of the applied load P, the radii of curvature and the measured Young's moduli of the bodies. Poisson's ratio was taken as 0·5.

The differences between measured and theoretical values are therefore dependent on the accuracy of measurement of a and b, inaccuracies in the radii of curvature and Young's moduli and friction in the guides of the loading rig (which can reduce P). The last was deemed the greatest source of error. The results of twenty-one tests (forty-two models) are summarized in Table 1.

Table 1. *Comparison of contact areas*

Experimental/theoretical	*Mean value*	*Standard deviation*
semi-axes of ellipse a and b	0·959	0·042
ratio $k = b/a$	1·024	0·052

These results merely establish the accuracy of the experimental techniques used here. The theoretical contact surface of toroids under radial load was established by Hertz[1] with glass bodies coated with lamp black.

STRESSES

Equations (8), (24) and (26) show that all the stresses are proportional to a/Λ. It is also evident from equation (6) that a/Λ has the dimensions of stress. The results are therefore presented non-dimensionally as stress $\times\Lambda/$(a characteristic length). The length chosen was the semi-axis of the contact ellipse in the plane in which the stresses are determined, i.e. in the direction of rolling. It should be noted from equation (8) that the theoretical curve for the maximum shear stress $\frac{1}{2}(Z_z - X_x)$ or $\frac{1}{2}(Z_z - Y_y)$, depends on ν. The curve presented is for $\nu = 0{\cdot}5$.

Consideration of equations (24) and (26) shows that the orthogonal shear stresses $\times\Lambda/$(a length) are not only non-dimensional but also independent of the load and properties

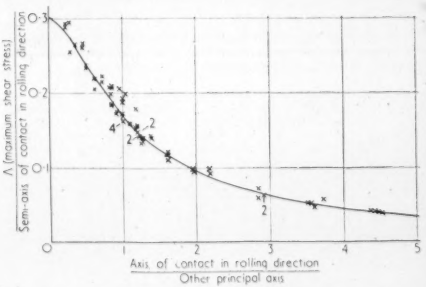

Fig. 5. Maximum shear stresses

Figures near points indicate the number of co-incident observations.

of the materials in contact. These results are therefore quite general and depend only on the shape of the bodies, and the positions considered, when presented in the above manner.

Fig. 5 shows the maximum shear stress for all models tested, plotted against the measured value of the ratio of the axes of the contact ellipse. The full line represents the stress calculated according to the method of Thomas and Hoersch. Four points are obtained from each test, two from each of the bodies in contact.

The ratio of the depth of the maximum shear stress below the contact surface to the semi-axis of the contact ellipse in the same plane is plotted in Fig. 6. The full line shows the

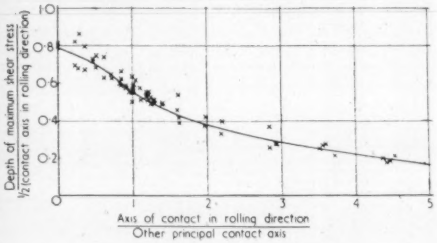
Depth of maximum shear stress
½(contact axis in rolling direction)
Axis of contact in rolling direction
Other principal contact axis

Fig. 6. Depth of maximum shear stresses

theoretical values. The marked difference between pairs of points was attributed to the large ratios of contact ellipse axis to torus radius which occurred in these tests. It should be noted that the mean values of pairs of points lie very much closer to the theoretical line. Relative horizontal displacement of points in a pair are due to (small) differences in the measured axes of the contact ellipses of the two mating bodies.

Figs. 5 and 6 provide the first real verification of Thomas and Hoersch's calculations known to the authors. Measurement of zones of yielding by strain etching is considered a poor method of verifying an elastic stress distribution. The tests reported here cover the range of contact ellipse ratios from zero for parallel cylinders (or a cylinder on a plane) to very long narrow contact areas (ratio of axes $4\frac{1}{2}$). A wide range of shapes of bodies was used.

The range of shear stress calculated in the new derivation from Hertz's theory is based on the orthogonal shear stress in the principal planes. It is possible that the greatest range of reversing shear occurs in the principal planes in directions inclined at some angle θ to the axes. This possibility was investigated experimentally.

The procedure previously outlined to determine the greatest orthogonal stress was repeated for different values of θ. This was a very tedious procedure because the shear stress in the θ direction is not symmetrical about the Z axis. For any constant depth, the maximum range of shear stress may occur at any depth below the surface between the depths of the greatest values on the left and right of the axis of loading. After it had been established that the greatest range at inclination $\theta = 30°$ occurred at the depth of the greatest shear stress, this was assumed to apply for other values of θ because it also applies for $\theta = 0$ (due to symmetry).

It was found that no range of shear stress greater than the range of orthogonal shear stress existed in the barrel $R_i = 1{\cdot}50''$, $R_j = 7{\cdot}58''$ when loaded through the barrel $R_i = 1{\cdot}499''$, $R_j = 15{\cdot}06''$. This result was assumed to apply for all shapes.

The experimental values of maximum range of shear stress are plotted in Fig. 7 and compared with the line calculated from the new theory with the same abscissa as Fig. 5. The new theoretical calculations were considered to be experimentally verified.

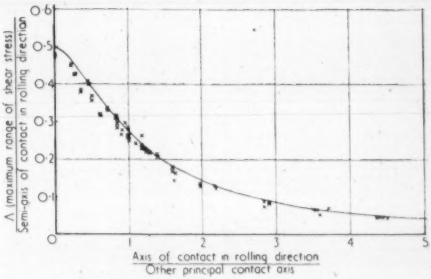
Δ (maximum range of shear stress)
Semi-axis of contact in rolling direction
Axis of contact in rolling direction
Other principal contact axis

Fig. 7. Maximum range of stress

Fig. 8 shows the position of the maximum range of shear stress. The large scatter of the experimental points from the theoretical curves is due to small changes of stress over a large area near the maximum value and to the large curvature of the contact areas. The distance from the centre line is of no practical interest unless the rate of stress reversal for a given rolling speed of the loaded torus becomes important.

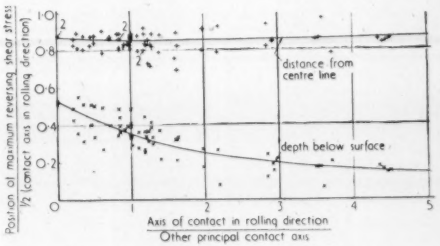
Position of maximum reversing shear stress
½(contact axis in rolling direction)
distance from centre line
depth below surface
Axis of contact in rolling direction
Other principal contact axis

Fig. 8. Position of maximum range of stress
Figures near points indicate the number of co-incident observations.

Radzimovsky[5] used Belajef's method to calculate the value and position of the range of shear stress for parallel cylinders. His results are compared with those from the new theory and photoelastic test in Table 2.

Table 2. *Comparison of results*

	$\frac{\text{Maximum half range}}{\text{Maximum pressure}}$	$\frac{z}{b}$	$\frac{y}{b}$
Radzimovsky	0·256	0·5	±0·85
New theory	0·250	0·53	±0·87
Experimental	0·237	0·517	±0·868

The relative magnitude of the maximum shear stress and the range of shear stress depends on the shape of the ellipse

of contact. The ratio of the stresses, calculated and measured, is plotted in Fig. 9. The full theoretical line is for $\nu = \frac{1}{2}$ (since the maximum shear stress curve depends on ν), and the broken line for $\nu = \frac{1}{4}$. The photoelastic material used has a value of $\nu = \frac{1}{3}$. Fig. 9 can be used to determine whether the stresses on the 45° planes (maximum shear stress planes) or the 90° planes (orthogonal shear stress planes) will give the greatest range of shear stress, as one body rolls over the other.

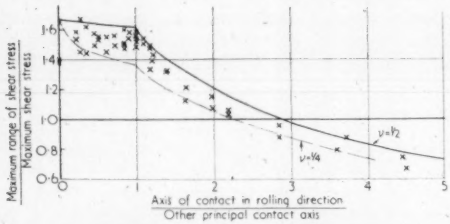

Fig. 9. Ratio of shear stresses

The maximum shear stresses occur in planes containing the minor axis of the ellipse and the direction of the normal load. If the contact axis ratio is greater than unity, the vertical plane of rolling contains the major axis of the ellipse of contact. The plane containing the maximum shear stress is therefore perpendicular to the rolling direction, and it has been shown experimentally by the authors that in this case there is no reversal of shear stress on the planes of maximum shear, as one body rolls over the other. This means that when the contact ratio exceeds 2·25, the actual value of the maximum shear stress is equal to the greatest range of shear stress inside the bodies when $\nu = \frac{1}{4}$.

When the contact axis ratio is less than unity the vertical plane of rolling coincides with the plane containing the maximum shear stress. In these circumstances there is a small reversal of shear stress on the 45° planes at the depth of the maximum shear stress as rolling proceeds. The value of the negative peak shear stress has been evaluated experimentally for different shapes of contact, and found to be approximately 10–15% of the maximum shear stress for any particular shape. Since the orthogonal shear stress is more than 30% greater than the maximum shear stress in this region, the former will still give the greatest range of shear stress in rolling contact.

CONVERSION OF STRESSES

The results of the previous Sections show that the important shear stresses can be calculated for any true toroid subjected to radial loads. However, the theories cannot be applied to regions where one or more of the principal curvatures of the bodies is discontinuous. In such cases the stresses must be determined experimentally. The only practicable known method of doing this is the frozen stress photoelastic technique (employed in this investigation), in which the stresses in models are measured. These stresses must be converted to the corresponding values in the prototype, which may be a different size and will almost certainly have different values of Young's modulus and Poisson's ratio (these are 2000 to 3000 lb/in.^{2} and 0·5 respectively for "frozen stress" materials). To effect this conversion it is assumed that the stresses obey the same rules as they would if adjoining parts of the bodies, where the curvatures are continuous, were in contact.

In a paper on contact stresses between railway wheels and rails Frocht[8] proposed a simple conversion formula for the maximum shear stress. From equation (8) the maximum shear stress $\frac{1}{2}(Z_z - Y_y)$ may be seen to have a factor a/Λ, which depends on the materials, size and load. Frocht's formula converts a/Λ to the appropriate value but neglects the effect of variation of Poisson's ratio on the term $\nu\Omega'_{,}$. This effect may cause considerable errors, and it is considered by the authors that no reliable simple formula for the conversion of the maximum shear stress can be devised.

The range of shear stress is determined by equations (24) or (26). From equations (25) and (27) it may be seen that the factors Q and R are pure functions of the geometry only of the bodies. For the range of shear stress σ of geometrically similar model m and prototype p it is therefore accurate to write

$$\frac{\sigma_p}{\sigma_m} = \frac{a_p}{\Lambda_p} \cdot \frac{\Lambda_m}{a_m} \tag{28}$$

From equations (6) and (7) it follows that, if the bodies in contact have the same E and ν

$$\frac{\sigma_p}{\sigma_m} = \left(\frac{P_p}{P_m}\right)^{\frac{1}{3}} \left(\frac{\Lambda_m}{\Lambda_p}\right)^{\frac{1}{3}} = \left(\frac{P_p}{P_m}\right)^{\frac{1}{3}} \left(\frac{L_m}{L_p}\right)^{\frac{1}{3}} \left(\frac{1-\nu_m^2}{1-\nu_p^2}\right)^{\frac{1}{3}} \left(\frac{E_p}{E_m}\right)^{\frac{1}{3}} \tag{29}$$

where L is a characteristic length. The stress in any material is therefore readily calculated if the corresponding stress in the model is known.

The position of any particular stress (e.g. the depth z below the surface) is directly related to a, the semi-major axis of the ellipse of contact. Therefore

$$\frac{z_p}{z_m} = \frac{a_p}{a_m} = \left(\frac{P_p \Lambda_p}{P_m \Lambda_m}\right)^{\frac{1}{3}} = \left(\frac{P_p}{P_m} \cdot \frac{E_m}{E_p} \cdot \frac{L_p}{L_m} \cdot \frac{1-\nu_p^2}{1-\nu_m^2} \cdot\right)^{\frac{1}{3}} \tag{30}$$

The conversion is only approximate in regions of discontinuous curvature because the true expressions for the stresses there are unknown.

CONCLUSIONS

A method of calculating the orthogonal shear stresses in toroids under radial loads has been developed, and it has been shown experimentally that the range of orthogonal shear stresses is often the greatest range of shear stress when the toroids are in rolling contact.

The greatest value of this range of shear stress and the maximum shear stress have been determined experimentally for a large range of toroid shapes. These results verify the new theory for the range of shear stress and the Thomas and Hoersch theory for the maximum shear stress with regard to both magnitude and position of the stresses.

For many practical cases of rolling contact the range of orthogonal shear stress is the greater and it is therefore the appropriate criterion for fatigue failure. In regions of discontinuous curvature of the bodies in contact the range of shear stress may be determined approximately from the results of a photoelastic test by a simple conversion formula.

The shape and size of the contact areas of the models were in close agreement with those predicted by Hertzian theory.

The results are presented in non-dimensional form so that the stresses in any actual case may be readily computed when

the shape of the area of contact is known. This shape may be calculated from the curvatures of the toroids or read off a graph published by Thomas and Hoersch.[3]

Although Hertz's theory assumes semi-infinite bodies, the experiments showed that it may be used to predict the important shear stresses for finite bodies. For ratios of semi-major axis of the ellipse of contact to smallest radius of curvature of either toroid up to 0·5, the differences between theoretical and experimental values were small.

ACKNOWLEDGEMENTS

This work is sponsored by the British Transport Commission to whom thanks are due for permission to publish this paper. The authors also wish to thank Dr. N. T. Bloomer for his assistance with the mathematical analysis.

REFERENCES

(1) HERTZ, H. *J. Math.* (*Crelle's J.*), **92**, p. 156 (1881).
(2) MORTON, W. B., and CLOSE, L. J. *Phil. Mag.* (6), **43**, p. 320 (1922).
(3) THOMAS, H. R., and HOERSCH, V. A. *Bull. Engng Exp. Station* No. 212 (University of Illinois, 1930).
(4) FÖPPL, L. *Forschung auf dem Gebiete des Ingenieurwesens Ausgabe A*, **7**, p. 209 (1936).
(5) RADZIMOVSKY, E. I. *Bull. Engng Exp. Station*. No. 408 (University of Illinois, 1953).
(6) SMITH, J. O., and CHANG KENG LIU. *J. Appl. Mech.*, **20**, p. 157 (1953).
(7) LOVE, A. E. *Theory of Elasticity*, 4th ed., p. 192 (London: Cambridge University Press, 1927).
(8) FROCHT, M. M. *Report of Committee* 4 *Rail. Amer. Rly. Eng. Assoc. Bulletin* V55, No. 514, p. 773 (1954).

The application of a transient method to the measurement of the thermal conductivity of rocks and building materials

By G. GAFNER, M.Sc., National Physical Research Laboratory, Pretoria, South Africa

[*Paper received* 14 *March*, 1957]

A transient method of measuring the thermal conductivity of insulators has been modified to allow measurements to be made on rocks and building materials in the approximate thermal conductivity range 0·008 to 0·07 J/cm °C s, with an accuracy of 7% or better. A detailed description is given of the apparatus, experimental procedure and corrections to be applied to the results obtained.

Most steady-state methods for the determination of the thermal conductivity of rocks and other materials in the same conductivity range (0·008 to 0·07 J/cm °C s) suffer from the inherent disadvantage of being slow. The divided bar type of apparatus, commonly in use, requires three days per test in which three accurately ground samples are used. A further objection to this type of method is that a representative result is not obtained when the three samples do not have identical conductivity, as is often the case in practice. As a large amount of work has been done in recent years on the development of transient methods for measurements on insulating materials, it was decided to carry out an investigation to assess the applicability of these methods to measurements on medium conductors. On reviewing the current literature on this subject it appeared that three established methods might be modified to allow measurements to be made on materials of somewhat higher conductivity than they had originally been designed for. The following is a brief description of these methods.

Clarke and Kingston[1] suggested a method in which a constant known quantity of heat is supplied to one face of a slab of test material. An analysis of the temperature change with time of the other face leads to the thermal constants of the test material. No further experimental work was done with this method as no way of avoiding the use of a double sample, one on either side of the heater, could be found.

Beatty, Armstrong and Schoenborn[2] developed an elegant method using a constant temperature boundary condition, applied as follows. One face of the test slab, initially at constant temperature, is suddenly brought into contact with an isothermal heat source at higher temperature. The temperature-time change of a heat sink of known thermal capacity in contact with the opposite side of the test slab is recorded. The thermal constants of the test slab can be deduced from this record. An extended series of tests with this method gave results with a spread of 20%, and as an improved technique using a block of pure melting ice to establish the constant temperature boundary condition did not lead to a very marked improvement in the reproducibility of the results obtained, the method was abandoned. It is interesting to note that this method gives the thermal diffusivity and specific heat of the sample from a test taking two minutes or less when small rock samples are used.

A further method, developed by Clarke for measurements on insulating materials, utilizes a heat source at adjustable temperature and a heat sink of known thermal capacity on opposite faces of the slab of test material. The temperatures of the heat source and sink rise in unison when a constant temperature difference is maintained between them. The thermal conductivity of the sample can be evaluated from the rate of rise of temperature of the heat sink once the initial transient has passed. This method is adapted to measurements on medium conductors in this paper.

THEORY

The problem is that of a semi-infinite slab (*b*) (see Fig. 1) in thermal contact with a heat source (*a*) at the $x = 0$ face, and a heat sink of known thermal capacity at the $x = d$ face. The slab and heat sink are initially at the arbitrary zero of temperature. At time $t = 0$ the temperature of the heat source is raised to V_a and adjusted thereafter to maintain a constant temperature difference $V = V_a - V_c$ across the test

slab. The solution to this problem is obtained by solving, with the Laplace method

$$\frac{\partial v}{\partial t} = \frac{k}{\rho c}\frac{\partial^2 v}{\partial x^2}$$

under the initial and boundary conditions

$$\left.\begin{aligned} v &= 0, \text{ at } t = 0 \text{ for all } x \\ v &= V_a, \text{ at } x = 0 \\ v &= V_c, \text{ at } x = d \end{aligned}\right\} \text{ for all } t$$

where $$V_a - V_c = V$$

and $$mc'\frac{\partial v}{\partial t} = -k\frac{\partial v}{\partial x}, \text{ at } x = d$$

where v is the temperature at a plane x at time t in the sample of thickness d, having specific heat c, thermal conductivity k and density ρ. The mass of the heat sink per unit area of sample is m and its specific heat is c'.

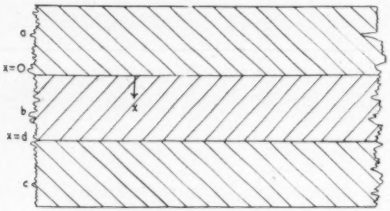

Fig. 1. Schematic representation of the test sample, heat source and heat sink

The solution of these equations for V_c is given by Clarke, from a personal communication by D. G. Lampard, as

$$V_c = V\left\{\frac{kt}{d[(\rho cd/2) + mc']} - \frac{1}{6}\frac{\rho cd/4 + mc'}{(\rho cd/4) + mc' + (mc')^2/\rho cd} - 2\sum_{s=1}^{\infty}\frac{\exp(-\alpha_s^2 kt/\rho cd^2)}{[1 + (\rho cd/mc') + mc'\alpha_s^2/\rho cd]\cos\alpha_s - [1 + (\rho cd/mc')]}\right\}$$

where $\pm\alpha_s$ are the roots of

$$\cos\beta - \frac{mc'}{\rho cd}\beta\sin\beta - 1 = 0$$

The value of $\frac{d}{dt}(V_c)$ when t is large enough to neglect all exponential terms is

$$\frac{d}{dt}(V_c) = \frac{kV}{d[(\rho cd/2) + mc']} \qquad (1)$$

This is recognized as the steady-state equation for linear heat flow with a correction term for heat stored in the test slab. It is surprising that this correction term is only one-half of the actual heat capacity per unit area of the sample surface. The accuracy of equation (1) can be verified by simple considerations of the heat flow through the slab when its temperature level rises linearly with time, as follows:

Consider the sample to consist of n equal elements (see Fig. 2). The thermal capacity of the slab is realized by having a thermal capacity of $\frac{\rho cd}{n-1}$ on each of the isothermals $V_1, V_2 \ldots V_{n-1}$. The rest of the system, having no heat capacity, will be purely conductional even though the whole temperature level of the system rises continuously.

For the first element

$$Q_{0,1} = \frac{k(V_0 - V_1)}{d/n}$$

where $Q_{0,1}$ is the heat flow per unit area from the isothermal V_0 to the V_1 isothermal.

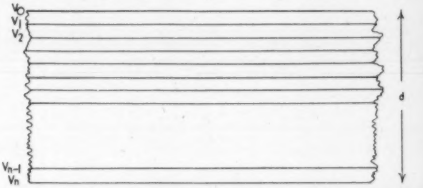

Fig. 2. Test sample divided into $(n-1)$ segments, each bounded by two isothermals

For the second element

$$Q_{1,2} = \frac{k(V_1 - V_2)}{d/n} = \frac{k(V_0 - V_1)}{d/n} - \frac{\rho cd}{(n-1)}\frac{dV}{dt}$$

For the nth element

$$Q_{n-1,n} = \frac{k(V_{n-1} - V_n)}{d/n} = \frac{k(V_{n-2} - V_{n-1})}{d/n} - \frac{\rho cd}{(n-1)}\frac{dV}{dt} \cdots =$$

$$\cdots = \frac{k(V_0 - V_1)}{d/n} - (n-1)\frac{\rho cd}{(n-1)}\frac{dV}{dt}$$

Summing these equalities we find

$$nQ_{n-1,n} = \frac{k(V_0 - V_1 + V_1 - \ldots + V_{n-1} - V_n)}{d/n} - \sum_{s=1}^{n-1} s\frac{\rho cd}{(n-1)}\frac{dV}{dt}$$

Thus $$nQ_{n-1,n} = \frac{k(V_0 - V_n)}{d/n} - \sum_{s=1}^{n-1} s\frac{\rho cd}{(n-1)}\frac{dV}{dt}$$

Now $$\sum_{s=1}^{n-1} s = \frac{n(n-1)}{2}$$

Thus $$Q_{n-1,n} = \frac{kV}{d} - \frac{\rho cd}{2}\frac{dV}{dt}$$

$Q_{n-1,n}$ is the heat flow per unit area per unit time into the heat sink and thus equals $mc'\frac{dV}{dt}$, thus $\frac{dV}{dt} = \frac{kV}{d[(\rho cd/2) + mc']}$

This solution is exact as n does not appear in it.

DESCRIPTION OF THE APPARATUS

The heat sink of the apparatus (see Fig. 3) consists of a copper block of which the specific heat had been accurately measured using an adiabatic calorimeter. The block is approximately $3\frac{1}{2}$ in. in diameter and 1 in. thick and has one accurately lapped flat surface. This surface is fitted with three small steel pegs spaced equally around the perimeter which prevent the sample from sliding off the block on

insertion into the apparatus. A baked pyrophyllite guard cylinder with an inside diameter of 5 in. and depth of 1½ in. with an inlaid heating wire prevents lateral and downward heat loss from the block. The temperature of the guard cylinder is measured by five series-thermocouples glued on to the inner surfaces, spaced so as to give a good representation of the average temperature. The copper block is fitted with two thermocouples set into radial holes. The thermocouple in the hole just below the lapped face of the block is connected differentially with another similar thermocouple set into a radial hole in the base of the heat source. The temperature of the copper block is measured with the second thermocouple set into a hole in the middle thereof. The block is supported on the base of the guard cylinder by three small Perspex pillars and insulated from it by low conductivity mineral wool.

The heat source of the instrument consists of a 5½ in. outside diameter brass container with an accurately lapped copper base. Water is placed in this container during the test and is temperature controlled by means of a heater set into a spiral copper tube in the water. An electrically driven impeller ensures good heat exchange between the heater and water. Pressure on the sample is obtained by means of a spring loading system acting as shown in Fig. 3. Mineral wool insulation is packed around the sample to minimize side losses to the air during the test.

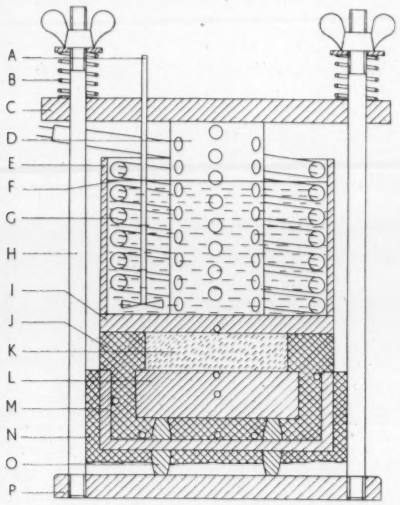

Fig. 3. Cross-section of the apparatus

○, thermocouple junctions; *A*, stirrer; *B*, loading spring; *C*, loading bar; *D*, loading cylinder; *E*, brass container; *F*, water level; *G*, heater in copper tubing; *H*, loading frame; *I*, copper base of container; *J*, mineral wool insulation; *K*, test sample; *L*, copper heat sink; *M*, pyrophyllite guard cylinder; *N*, felt insulation; *O*, Perspex supports; *P*, base plate.

A smaller apparatus was built for measurements on rocks, and is essentially the same as the larger save that the size was scaled down to suit the 1⅛ in. diameter rock samples.

EXPERIMENTAL PROCEDURE

The test sample, in the form of a disk of diameter 7 cm and thickness between 0·5 and 3 cm, is lapped plane and parallel to better than 0·02 mm. The faces are then coated with a thin layer of silicone grease and the sample inserted in the apparatus. A pressure of 30 lb/in² is applied by means of the loading system. The water container is filled with water which is approximately 10° C hotter than the sample and copper block. This temperature difference is maintained throughout the test by manual adjustment of the voltage across the heater in the water with the help of a variable transformer. The e.m.f.'s of the thermocouples in the block and guard cylinder are measured every two minutes by means of a vernier potentiometer and maintained equal to each other by varying the current through the guard heater. The temperature difference is chosen so as to give a temperature rise of the copper block of approximately 20 μV (0·5° C) per two minutes. Temperature measurements are continued for a period of 20 min after the passage of the initial transient, that is once the rise of temperature of the copper block has become linear with time.

METHOD OF CALCULATION

Three corrections have to be applied to the observed rate of rise of temperature of the copper block before this can be substituted into equation (1) to give the measured thermal conductivity of the test sample. These corrections allow for:

(1) *Non-linearity of the thermal e.m.f.-temperature curve.* The microvolt was used as a unit of temperature in order to save having to convert each reading into the corresponding temperature. This procedure is only justified if the thermal e.m.f. changes linearly with temperature. This is not the case for the copper-constantan thermocouples used, the thermoelectric power changing by 0·7 μV every ten degrees between 20 and 70° C. This is compensated for by adding 0·22% to the observed rate of rise of temperature of the copper block for each 100 μV of temperature difference between the block and heat source.

(2) *Heat flow from the heat source into the block through the insulation around the sample.* The magnitude of this effect was determined by carrying out tests on three 7 cm diameter disks of wood fibreboard of known thermal constants, with temperature differences of 200, 400 and 800 μV. The heat flow through the disk was calculated from equation (1) in each case and subtracted from the experimentally observed heat flow into the copper block. This gave the extraneous heat flow which was found to be directly proportional to the temperature differential for a given thickness and linearly related to the reciprocal of the sample thickness for a given temperature difference. The exact relationship was established with the help of the nine experimental points and Fig. 4 shows the resulting family of curves, each corresponding to a specific sample thickness, relating the temperature difference across the sample to the extraneous heat gain of the copper block. The insulation around the sample was packed in the same way in each test. The same procedure was followed, using 3·5 cm disks, to obtain the correction applicable to the smaller apparatus. The correction is applied by subtracting the quantity deduced from the graph from the observed rate of heat flow into the copper block in each test. Heat flow rates were conveniently expressed as the rise in temperature of the copper block, measured in microvolts, per two minutes.

(3) *Heat exchange between guard cylinder and copper block.* Tests were made with large fixed temperature differences

between the guard cylinder and the block. The correction to be applied followed from a comparison of these results with those obtained when the test was made with temperature equality between the block and guard. The correction was found to be such that when the guard was hotter by 2·5° C the rate of rise of temperature of the block increased by 1 μV per 2 min (40 μV = 1° C). As the temperature difference is easily maintained to 0·1° C in practice, the correction is very small. Flow in the small apparatus was such that the correction was twice as large as in the large apparatus.

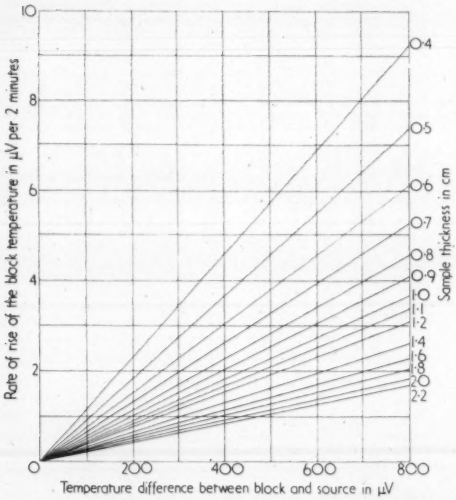

Fig. 4. Graph for the evaluation of the correction for heat flow from the source to the block through the insulation

FILM RESISTANCE EVALUATION

Large apparatus. The most homogeneous material in the thermal conductivity range under consideration is fused quartz. Three samples of diameter 7 cm and thicknesses 0·7, 1·5 and 2·4 cm were obtained and each tested five times with a new film each time. Table 1 gives the results of these tests. The "thermal conductivity" value as tabulated is not corrected for the contribution of the film.

The true thermal resistance of the sample must equal the observed thermal resistance less the film resistance, i.e.

$$\frac{d}{k_m} - r_f = \frac{d}{k_t} \qquad (2)$$

where d = sample thickness
k_m = uncorrected thermal conductivity
k_t = true thermal conductivity
and r_f = film resistance.

Using the results of Table 1 in equation (2), eliminating k_t which is assumed to be constant, the value

$$r_f = 6{\cdot}1 \pm 1{\cdot}3 \text{ cm}^2 \text{ °C s/J}$$

is obtained. This value is undesirably large but is inevitable as a film had to be used which did not appreciably penetrate porous samples.

Table 1. *Results used for the determination of the large apparatus film resistance*

Sample number	*Thickness (cm)*	*Uncorrected thermal conductivity at 30° C in J/cm °C s*	*Standard deviation from the mean*
1	2·406	0·0133	0·0002
2	1·518	0·0131	0·0002
3	0·732	0·0123	0·0003

Small apparatus. Three samples of fused quartz and two of crystalline quartz were available for the determination of the film resistance in this apparatus. Each of these was tested five times with a new film each time and Table 2 gives the results obtained.

Table 2. *Results used for the determination of the small apparatus film resistance*

Material	*Sample number*	*Thickness (cm)*	*Uncorrected conductivity at 30° C in J/cm °C s*	*Standard deviation from the mean*
Fused quartz	4	1·206	0·0128	0·0001
	5	0·567	0·0123	0·0001
	6	0·305	0·0118	0·0001
Crystalline quartz	7	0·952	0·0561	0·0005
	8	0·635	0·0515	0·0005

The value for the thermal resistance of the film is obtained from Table 2 and equation (2) as before. The result obtained is

$$r_f = 2{\cdot}8 \pm 0{\cdot}7 \text{ cm}^2 \text{ °C s/J}$$

The difference between the two values obtained is unhappily large and can only be attributed to the fact that good thermal contact is more readily obtained on a small surface than on a larger one. The difference is, however, larger than anticipated. The deviation from the mean gives the uncertainty which must apply to any measurement made in either of these two apparatuses.

COMPARISON OF RESULTS WITH THOSE OBTAINED BY OTHER METHODS

Large apparatus. Tests were carried out on three samples of fused quartz and three types of brick and the results compared with those obtained by other workers. Table 3 gives these results.

Table 3. *Comparison of results from the large apparatus with those obtained by other methods*

Material	*Thickness (cm)*	*k at 30° C by this method*	*Standard deviation*	*k at 30° C by steady-state methods*	*% difference between results*
Fused quartz	2·406	0·0138	0·0002	0·0136	1
	1·518	0·0139	0·0002	0·0136	2
	0·732	0·0138	0·0003	0·0136	1
Brick 1	1·923	0·0094	0·0001	0·0094	0
Brick 2	2·444	0·0079	0·0001	0·0082	−4
Brick 3	2·554	0·0088	0·0002	0·0088	0

The results given in Table 3 for fused quartz are those obtained by Mr. E. H. Ratcliffe at the National Physical Laboratory, Teddington, for smaller disks during a comprehensive survey of the thermal conductivity of quartz, using an absolute steady-state method.[4] Those given for bricks were obtained by Mr. F. J. Lotz of the South African National Building Research Institute in a large steady-state apparatus. Both sets of results are considered to be most reliable. Because of the known inhomogeneity of brick, samples were chosen so as to have the same density as the bulk sample which was tested in the steady-state apparatus. The agreement shown between results obtained by the two methods is most satisfactory.

Small apparatus. Tests were made on three samples of fused quartz and two of crystalline quartz (three being available, the thinnest, however, having too low a thermal resistance to give a reliable result). Table 4 gives the results of these tests together with those obtained on the identical samples by Ratcliffe.

Table 4. *Comparison of results from the small apparatus with those obtained by other methods*

Material	*Thickness (cm)*	*$\bar{k}$ at 30° C by this method*	*Standard deviation*	*$\bar{k}$ at 30° C by steady-state method*	*% difference between results*
Fused quartz	1·206	0·0131	0·0001	0·0136	−4
	0·567	0·0131	0·0001	0·0136	−4
	0·305	0·0133	0·0001	0·0136	−2
Crystalline quartz	0·952	0·0678	0·0005	0·0632	7
	0·635	0·0670	0·0005	0·0632	6

The heat flow was perpendicular to the optic axis of the crystalline quartz. The fact that the fused quartz results are almost as much below as the crystalline quartz results are above those of Ratcliffe is most mystifying and no reason could be found for this discrepancy. Ratcliffe's fused quartz results were satisfactorily corroborated by the larger apparatus and it is highly unlikely that his values are in error by anything like as much as 7%. One is thus forced to conclude that the results obtained from the small apparatus cannot be relied upon to better than 7%. Many tests were carried out on a representative selection of rock samples but no results are given as no accurately established values are available for comparison.

CONCLUSION

The method has been established to be reliable to better than 5% when 7 cm diameter samples are used. This, coupled with its simplicity and speed, suggests that its adoption as a rapid laboratory method would not be amiss. The only obvious limitation is the smallness of the sample used, which cannot be increased very much without introducing further inaccuracies due to the fact that the magnitude of the correction for the heat capacity of the sample increases with sample thickness. Having to establish the specific heat of the sample accurately would increase the time taken for each test to such an extent that the attractiveness of the method would be lost. It follows from this that the usefulness of the method increases with the homogeneity of the test sample. A sample thickness of 1 cm is recommended for materials with conductivity of 0·01 and 3 cm for materials with conductivity approximately 0·07 J/cm °C s.

The method has also been successfully applied to measurements on the effect of moisture content on conductivity. Owing to the small temperature differences which can be used and the short duration of the test moisture migration effects are kept to a minimum. The method is most suited to measurements at room temperature but this range can be extended by enclosing the whole apparatus in a hot- or cold-box at the appropriate temperature.

ACKNOWLEDGEMENTS

This paper is published with the permission of the South African Council for Scientific and Industrial Research. The author also wishes to express his gratitude for the assistance and constructive criticism received from Dr. S. C. Mossop and Mr. A. E. Carte of this laboratory. Acknowledgement is also made to the Director of the National Physical Laboratory, Teddington, for permission to use hitherto unpublished data on the thermal conductivity of fused and crystalline quartz.

REFERENCES

(1) CLARKE, L. N., and KINGSTON, R. S. T. *Aust. J. Appl. Sci.*, **1**, p. 172 (1950).
(2) BEATTY, K. O., JR., ARMSTRONG, A. A., JR., and SCHOENBORN, E. M. *Indust. Engng Chem.*, **42**, p. 1527 (1950).
(3) CLARKE, L. N. *Aust. J. Appl. Sci.*, **5**, p. 178 (1954).
(4) Private communication from the National Physical Laboratory, Teddington.

The measurement of Meyer hardness and Young's modulus on the Rockwell test machine

By D. K. MACKENZIE, B.Sc., and T. P. NEWCOMB, M.Sc., Ferodo Ltd., Chapel-en-le-Frith, Stockport, Cheshire

[*Paper received* 16 *April, and in final form* 13 *June*, 1957]

A method is described in which the Rockwell hardness machine is used to determine the Meyer hardness and Young's modulus of a material. Meyer hardness values so derived for a number of materials are compared with those obtained from hardness measurements made on a Vickers hardness machine, and values of Young's modulus compared with figures quoted in standard tables.

In the Rockwell hardness test a ball is pressed into the specimen under a minor load (usually 10 kg), and the penetration indicator is set on the datum line. This minor load serves to diminish the effects of surface imperfections. A further load, the major load, is then applied and removed, and the resulting depth of penetration h_2 determined with the minor load still applied. The Rockwell number H_R, is then defined as $H_R = \text{constant} - h_2$. If a comparison is required between the hardness as measured by the Rockwell test and the Meyer hardness (p_m = total load/projected area of indentation) the depth of penetration and radius of curvature of the indentation r must be converted to the projected area of contact ($\frac{1}{4}\pi d^2$) by the approximate relationship $\frac{1}{4}\pi d^2 = 2\pi r h_2$. The Meyer hardness can then be calculated from p_m = major load/$2\pi r h_2$. Neglecting the elastic recovery which occurs on removal of the major load, r may be taken as the ball radius r_1. If elastic recovery is appreciable a considerable error may be introduced into the calculations on which the hardness values are based.(1)

The error due to elastic recovery may be eliminated by measuring the penetration with the major load applied, and calculating the projected area of indentation from this penetration, provided it is assumed that there is little change in the diameter of the impression during the release of the major load. However, errors then are present due to elastic deformation of the machine and of the specimen as a whole. In the following work, methods are described of eliminating these errors, and of determining the elastic recovery of the material from which Young's modulus may be calculated by means of Hertz's equation.

EXPERIMENTAL DETAILS

Using the standard Rockwell hardness testing machine, the depths of penetration of a spherical indenter into flat specimens of different nominal hardness were measured with the major load applied and with the major load removed. In addition, the specimen was compressed between flat anvils under the same load and the deflexion determined. By this means a measure of the errors due to machine distortion and the bulk deformation of the specimen was obtained. If these errors are subtracted from the corresponding ball penetration reading, the actual depth of the impression h_1 before elastic recovery occurs is determined, h_1 being the sum of the elastic and plastic deformations. The penetration h_2 recorded with the major load removed gives a measure of the residual plastic deformation.

Measurements of h_1 and h_2 were made using balls of $\frac{1}{4}$ and $\frac{1}{2}$ in. diameter and major loads L from 20 to 100 kg, five independent readings being taken at each load and averaged. The measurements were consistent to an accuracy of $\pm 2\%$.

Typical results are shown in Fig. 1 for aluminium and Perspex. These results show that the depth of penetration is linear with load, all lines passing through the origin.

From this information the Rockwell number, the Meyer hardness and Young's modulus may be calculated. Measurements of the Meyer hardness were also obtained by alternative methods for comparison with the Rockwell results;

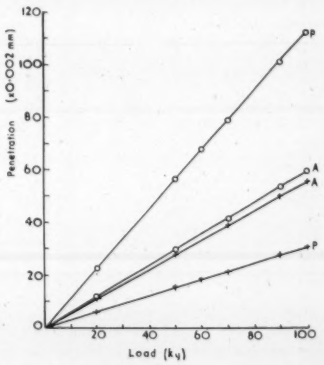

Fig. 1. Typical penetration *versus* major load measurements. ($\frac{1}{4}$ in. diameter ball.)

Curves *A*, aluminium; curves *P*, perspex.
○ = h_1 (load-on) results.
+ = h_2 (load-off) results.

thus for polymers, p_m values were determined by actual measurements of the projected area of indentation, whereas for metals, Vickers hardness measurements were used to provide a standard of comparison.

DISCUSSION OF RESULTS

(*a*) *Comparison of hardness determinations.* By definition, the Meyer hardness is given by $p_m = 4L/\pi d^2$ (see Fig. 2). Since the diameter d of the impression remains substantially constant after removal of the major load,

$$d^2 = 8r_1h_1 = 8r_2h_2 \qquad (1)$$

where r_1 is the ball radius, and r_2 is the radius of curvature of the indentation after release of elastic stresses. The Meyer hardness can thus be calculated from $p_m = L/2\pi r_1 h_1$. Meyer

hardness figures derived from this expression are shown in Table 1 for polymers together with values of p_m based on measurements of the impression diameter d. The Rockwell hardness numbers H_R are also included in the table. From these results, illustrated graphically in Fig. 3, it can be seen that the conventional numbers are in poor agreement with values of Meyer hardness.

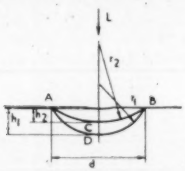

Fig. 2. Ball indentation

ADB, indentation under load; *ACB*, remaining plastic indentation after removal of major load.

Table 1. *Comparison of hardness measurements for plastic materials*

Material	p_m(kg/mm²) from diameter (Rockwell)	p_m(kg/mm²) from depth (Rockwell)	Rockwell number L scale $\frac{1}{4}$ in. ball 60 kg
Perspex	25	23	112
Bakelite	30	32	117
Celluloid	9	11	78
Polymer "A"	40	40	104
Polymer "B"	10	11	56
Polymer "C"	19	17	78

In the case of metals the Meyer hardness increases steadily as the load increases, owing to work hardening of the material during the indentation process. However, values may be obtained from the Rockwell test which will compare with Vickers hardness measurements (V.D.H. $= 0{\cdot}9272\, p_m$) by using a $\frac{1}{16}$ in diameter ball under a sufficiently high load (110 kg) to cause the material to be fully worked. Results obtained by the two methods are shown in columns one and two of Table 2.

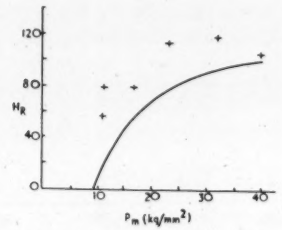

Fig. 3. Variation of H_R with p_m (depth).

Full line indicates theoretical relationship if no elastic recovery occurred.

Table 2. *Comparison of hardness and Young's modulus measurements for metals*

Metal	p_m(kg/mm²) from Vickers	p_m(kg/mm²) calculated from Rockwell	Measured moduli from Rockwell E(kg/mm² × 10³)	Hoyt's values E(kg/mm² × 10³)
Zinc	47	47	8·1	8·1
Brass sheet	121	114	10·9	10·6
Copper sheet (hard)	93	97	12·5	11·9
Copper sheet (soft)	45	48	10·5	10·6
Steel	186	182	22·6	20·8
Gauge plate	222	212	21·7	20·8
Aluminium	42	40	7·5	7·4

(*b*) *Evaluation of Young's modulus.* Assuming that d remains constant during the release of elastic stresses, Hertz's equation for the elastic recovery of spherical surfaces takes the form

$$d = 2{\cdot}22\left[\frac{L}{2}\,\frac{r_1 r_2}{r_2 - r_1}\left(\frac{1}{E_1} + \frac{1}{E_2}\right)\right]^{\frac{1}{3}} \qquad (2)$$

where E_1 and E_2 are the Young's moduli for the indenter and specimen materials respectively and L is the applied load.(1)

The Young's modulus of the material can therefore be determined from equations (1) and (2) assuming that $E_1 = 20{\cdot}4 \times 10^3$ kg/mm² and that h_1 and h_2 are the readings corresponding to a major load L.

The values obtained for metals are shown in column 3 of Table 2 together with figures taken from standard tables(2) (column 4).

ACKNOWLEDGEMENTS

The authors wish to thank Dr. R. T. Spurr and Mr. A. Jenkins of the Technical Division of Ferodo Ltd. for assistance and criticism, and the directors of Ferodo Ltd. for permission to publish this paper.

REFERENCES

(1) TABOR, D. *The Hardness of Metals* (Oxford: Clarendon Press, 1951).

(2) HOYT, S. L. *Metals and Alloys Data Book* (New York: Reinhold Publishing Corporation, 1943).

High-temperature tensometry and its application to amorphous polyethylene terephthalate

By E. L. Foster, D.Phil., and H. Heap, Imperial Chemical Industries Ltd., Harrogate, Yorks.

[*Paper received* 25 *April*, 1957]

Amorphous polyethylene terephthalate will crystallize at elevated temperatures either by the action of the temperature alone or as a result of a stretching process. An apparatus has been constructed by means of which the stress-strain curves of amorphous polyethylene terephthalate in the rubber-like state may be investigated under conditions where the material is heated for a period of not more than one second before the application of the strain. In this way spontaneous crystallization is minimized and the crystallization due to stretching may be studied. The effects of both temperature and straining rate on the shape of the stress-strain curve have been investigated and the results indicate that the crystallization is stress-controlled. The application of the results to the fibre spinning and drawing processes is discussed.

In the field of synthetic fibre-forming polymers, materials may frequently be encountered which undergo a transition from a glass-like state to a rubber-like state in a narrow temperature range. Furthermore, once in the rubber-like state, it is often possible to induce partial crystallization either by the action of a stretching process or by the influence of temperature alone. Of these two cases, crystallization by the action of a stretching process is undoubtedly the more important from a practical point of view, since it leads to oriented crystalline material with greatly enhanced strength.

Polyethylene terephthalate, the polyester from which Terylene fibres are made, is a material of this type. If this material in the amorphous state is heated to temperatures above the glass-rubber transition, crystallization will occur at a rate dependent, among other things, on the temperature,[1–3] this crystallization having a spherulitic character.[4–6] If, however, a filament of amorphous polyethylene terephthalate is heated for only a very short time, crystallization does not take place to any significant extent under the action of the heat alone. This is shown by the fact that spun filaments, which have passed quickly through the range from the melt temperature to room temperature, in a time of the order of one-tenth of a second, are found to be in the amorphous state. If, on the other hand, a filament passes rapidly through such a hot region while undergoing a stretching process, in which the tension is high, it is observed that the crystallization may be greatly accelerated due, it is believed, to a partial alinement of the molecular segments in the course of the stretching.

The spinning and drawing of synthetic fibres such as these both involve some degree of hot stretching, and if a good understanding is to be obtained of the molecular mechanisms which occur during these processes, a knowledge of the stress-strain relationships of the amorphous material is an important contribution. Attempts to measure the stress-strain characteristics of fibres at elevated temperatures are not uncommon, but the methods used have normally been confined to carrying out the test in a tube either with a current of hot air passing through it or with a heater wound around it. In such cases, the heating of the filament is relatively slow and its rate depends to a great extent on how rapidly the tube itself may be heated. In the present experiments, however, it is desirable that the stress-strain relationships should be determined under conditions such that the filament is at the high temperature for as short a time as possible, so as to minimize the amount of crystallization which takes place merely as a result of thermal activation.

Probably the most satisfactory way to bring about a rapid temperature rise of the type required is the sudden immersion of the filament under test in a hot liquid medium immediately prior to the test, and the performance of the stress-strain test under immersed conditions. This is the basis on which the present technique of measurement has been built.

EXPERIMENTAL

An Instron tensile testing machine with a wide range of stretching rates up to a maximum of 50 cm/min was available for the measurement of the stress-strain curves, and the major experimental problem was the design of a suitable modification which would enable the filament to be immersed in a hot liquid immediately prior to the test. This modification, shown schematically in Fig. 1, consisted of a metal

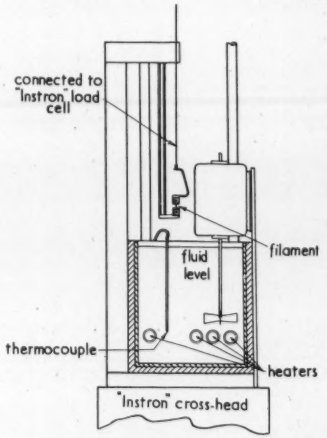

Fig. 1. Schematic diagram of high-temperature attachment

tank covered with a layer of Sindanyo board for heat insulation and mounted on a steel framework which could be bolted rigidly to the cross-head of the Instron machine. Four cartridge heaters mounted through the side of the tank heated the liquid which it contained and efficient stirring was effected by means of a small motor-driven paddle. The temperature of the liquid was controlled jointly by a Variac transformer governing the current passing to the main heaters,

together with a Sunvic thermostat controlling a subsidiary heater. A chromel-alumel thermocouple was used to measure the liquid temperature in conjunction with a Cambridge meter with auto-compensated junction reading to $\frac{1}{2}$° C.

The single filament under test was mounted between two clamps, the upper one freely suspended from the load-cell of the Instron machine and the lower one attached firmly to the steel framework supporting the tank and therefore moving down with the cross-head. The steel framework was so constructed that the tank could be raised rapidly with the aid of counterbalancing springs so as to immerse the filament in the liquid contained in the tank.

In the testing of single filaments, where the cross-section is uniform, the use of mechanical grips is unsatisfactory owing to either breakage or slippage in the grips. The technique found to be most satisfactory was to mount the filament across two opposite sides of a thin piece of card in the shape of a hollow rectangle using a heat resistant cement. These two sides of the card were then mounted in mechanical grips and the remaining two sides cut away just before testing. This method also considerably reduced the possibility of damage to the filament before test. Cold-setting Araldite cement was tested under dead weight loading conditions with loads of the magnitudes experienced in these tests, and allowed no slipping up to 160° C. This was therefore chosen for cementing the filaments to the cards.

The usual procedure employed was to set the bath temperature, mount the filament in the grips and then switch off the stirrer to prevent this causing fluctuations in the measured load. The tank was then raised quickly and the stretching of the sample commenced almost immediately. This is quite permissible since calculation shows that even with filaments as thick as those used here, the heating process is virtually complete in less than one second.

Silicone oil is a suitable liquid to use in the tank since the evidence is that it does not attack polyethylene terephthalate. A useful guide in this respect is the fact that immersion in silicone oil does not lower the glass-rubber transition temperature at all, and certainly no difference can be detected between properties measured in air and in silicone oil at room temperature.

In preliminary tests it was established that there was no significant variation of temperature along the path of extension of the filament in the oil. When the stirrer was switched off, several minutes elapsed before any drift from the stabilized temperature could be detected.

In order to obtain measurable loads when stretching at the higher temperatures, the measurements were carried out on relatively thick filaments, about $13–14 \times 10^{-3}$ cm in diameter. These filaments had zero orientation as measured by birefringence and anisotropy of fluorescence, and X-ray photographs revealed no crystallization. Stress-strain curves were measured over the temperature range 90–120° C, and the rate of straining was varied by varying both the initial filament length and the machine speed. Initial filament lengths and diameters were measured by means of a cathetometer and a microscope respectively. The initial filament lengths were in the range 2–10 mm.

No reliable conclusions may be drawn from the initial slopes of the stress-strain curves since the response of the recording pen was not sufficiently rapid to record this region truly.

DISCUSSION OF RESULTS

Fig. 2 is an example of some of the stress-strain curves observed at 100° C and it is seen immediately from this that the shape of the stress-strain curve is markedly dependent on the rate of straining. At the lowest rates of straining, the behaviour of the material tends towards that of a simple viscoelastic material and a filament will extend to very great extensions at low stress. At the highest rates of straining, on the other hand, the stress-strain curve is a sigmoid,

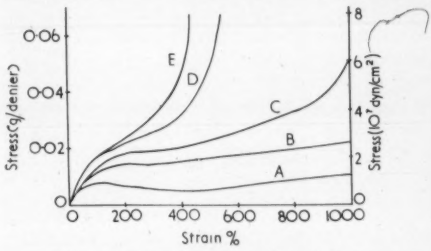

Fig. 2. Stress-strain curves at 100° C

Rates of straining per minute: curve *A*, 59%; curve *B*, 222%; curve *C*, 286%; curve *D*, 400%; curve *E*, 462%.

characteristic of a material which undergoes some process of reinforcement and once this reinforcement has occurred, the filament breaks at high stress with very little further extension. At intermediate rates of straining there is a gradual transition from one form of stress-strain curve to the other. X-ray photographs of filaments after equal extensions at high and low rates of straining at the same temperature show that the reinforcement is indeed a rapid partial crystallization. Furthermore, this crystallization must be brought about solely by the higher rate of straining since this is the only factor which is changed.

Fig. 3, showing the pattern of stress-strain curves at 120° C, gives some indication of the role of the temperature. The

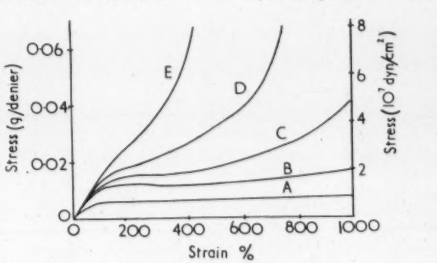

Fig. 3. Stress-strain curves at 120° C

Rates of straining per minute: curve *A*, 2630%; curve *B*, 7150%; curve *C*, 11 900%; curve *D*, 14 300%; curve *E*, 18 500%.

basic feature of a transition from one type of stress-strain curve to another with increasing rate of strain, which was observed in Fig. 2, occurs again here, but the range of rates of straining over which this transition takes place is now more than an order of magnitude higher than at 100° C.

Although the pattern of stress-strain curves is undoubtedly made more complicated by the fact that even at the lowest rates of straining some reinforcement does occur, presumably due to crystallization as a result of temperature only, the

gradual transition from one type of stress-strain curve to the other over a wide range of straining rates with no well-defined "transition point" seems to be an inherent property of the material. This fact makes it difficult to effect a true comparison between the curves at different temperatures. In this case, a comparison has been made, however, using an arbitrary curve which was chosen to be near the high straining rate end of the transition, since interest is centred mainly on the case when most of the crystallization is due to the stretching process. The curve chosen, called for convenience the "characteristic" curve, is one which reinforces sufficiently rapidly to attain a stress of 7×10^7 dyn/cm^2 at 500% extension. By interpolation it is then possible to estimate the "characteristic" rate of straining which is necessary to give rise to this "characteristic" curve at each temperature at which sets of curves have been obtained. It is also considered that the point of inflexion on this curve is of some importance, since it indicates the region in which the rate of reinforcement becomes significant. The stress at the point of inflexion on the "characteristic" curve may be termed the "characteristic" stress and has also been derived by interpolation.

Fig. 4 shows that the "characteristic" stress is virtually independent of temperature over the whole temperature

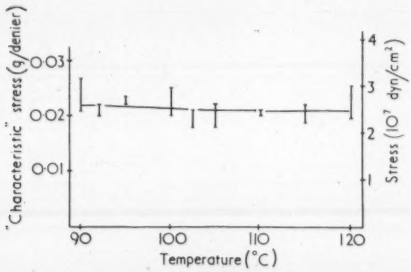

Fig. 4. Variation of "characteristic" stress with temperature

range covered. This is roughly the behaviour which would be expected if the reinforcement is sharply dependent on the degree of molecular alinement, since this is stress-dependent in a rubber-like material. If, then, the simplifying assumption is made that the material behaves as a simple viscoelastic substance until the reinforcement sets in, the rapid change of the "characteristic" rate of straining with temperature becomes readily understandable. This "characteristic" rate of straining is, to a rough approximation, the rate of straining necessary to generate an approximately constant stress at various temperatures, and may thus be expected to be approximately inversely proportional to the viscosity of the material.

This interpretation is supported by the fact that the logarithm of the "characteristic" rate of straining is linear with the inverse of the absolute temperature, as shown in Fig. 5. From this linear relationship it is possible to derive a value for the activation energy to be associated with the viscous flow process. This activation energy is of rather doubtful value, however, since it is not improbable that its true magnitude will depend on the degree of alinement of the molecules during the flow process. In view of this, the derived value of 55 kcal/mol. must be considered to be in relatively good agreement with the value of 40 kcal/mol. which has been derived from melt viscosity measurements.[7]

These results do serve to illustrate the essential difference between the spinning and drawing processes. In spinning from the melt, where the material is extruded from an orifice and is wound up at high speed, most of the extension takes place at the high temperature end of the thread-line, so that,

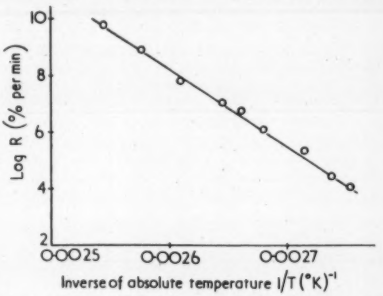

Fig. 5. Variation of "characteristic" strain rate R with temperature

owing to the very low viscosity of the material at this high temperature, very little stress is set up and the resultant filament has very little orientation and no reinforcement takes place. In the drawing process, on the other hand, where the material is stretched on passing through a heated zone, the maximum temperature attained by the filament is limited to a value just above the glass-rubber transition temperature, so that the rate of straining resulting from the applied stretch ratio gives rise to sufficient stress to cause reinforcement and a well-oriented crystalline filament results. These results also show that this rapid type of crystallization which is brought about by a stretching process is more correctly termed "stress-induced crystallization" than "strain-induced crystallization."

This type of stretching behaviour contrasts with that of materials like 6·6 Nylon which are initially crystalline and in which the degree of orientation in the stretched filaments is related more to the strain.[8]

ACKNOWLEDGEMENTS

The authors wish to thank Mr. D. Webster for assistance in the experimental work.

REFERENCES

(1) KELLER, A., LESTER, G. R., and MORGAN, L. B. *Phil. Trans. A*, **247**, p. 1 (1954).
(2) MORGAN, L. B. *Phil. Trans. A*, **247**, p. 13 (1954).
(3) HARTLEY, F. D., LORD, F. W., and MORGAN, L. B. *Phil. Trans. A*, **247**, p. 23 (1954).
(4) KELLER, A. *J. Polymer. Sci.*, **17**, p. 291 (1955).
(5) KELLER, A. *J. Polymer. Sci.*, **17**, p. 351 (1955).
(6) KELLER, A., and WARING, J. R. S. *J. Polymer. Sci.*, **17**, p. 447 (1955).
(7) MARSHALL, I., and TODD, A. *Trans. Faraday Soc.*, **49**, p. 67 (1953).
(8) CULPIN, M. F., and KEMP, K. W. *Proc. Phys. Soc. [London]*, *B***69**, p. 1301 (1956).

A method of measuring the thermal constants of granular materials

By T. S. E. Thomas, B.Sc., Ph.D., Vickers Group Research Establishment, Weybridge

[*Paper first received* 12 *January*, 1956, *and in final form* 30 *May*, 1957]

Thermal constants of granular materials are determined by measuring the temperature changes at the centre and surface of a metal cylinder containing the material. Heat is supplied to the cylinder wall at a constant rate by a resistance winding, and surface heat loss is eliminated by an outer screening tube kept at the same temperature by manual or automatic control.

The usual methods for measuring thermal conductivity involve a long delay before the temperature distributions reach steady state values, and for industrial testing quicker methods have been devised. In the Vernotte method[1] the conductivity is found from measurement of the temperature changes when a constant heat flux is transmitted through a slab of the material. In the probe method,[2, 3] a probe is inserted into a large mass of material, and measurement of its temperature rise when electrically heated enables the conductivity of the surrounding material to be found.

The method described here uses only a small quantity of material and, in addition to the conductivity, the specific heat is found from the same test. The method has so far only been used for granular materials, but it is possible that with some modifications it would be suitable for easily machinable solids such as plastics. The material is placed in a thin-walled metal cylinder on which is a resistance winding R_1 (Fig. 1). The wall is heated at a constant rate by the winding current and temperature measurements are made by two thermocouples; one at the centre of the cylinder and the other attached to the cylinder wall.

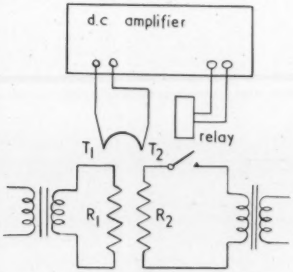

Fig. 1. Temperature control circuit

The mathematical theory, which takes into account the heat capacity of the wall, shows that when the surface heat flux is uniform the temperature difference between the centre and the surface finally becomes constant and the rate of rise is everywhere the same.

Heat from the cylinder winding is dissipated both by conduction into the interior and by conduction, convection and radiation to its external surroundings. This external heat loss is eliminated by surrounding the cylinder with a coaxial cylinder of greater diameter and length. This also has a resistance winding R_2, and its temperature can be adjusted to be the same as that of the inner cylinder.

APPARATUS

The dimensions are not critical. The length of the cylinder should be at least four times its diameter in order to eliminate end effects. The temperature difference between the centre and the surface varies as the square of the diameter, but the duration of the initial transient also increases with the diameter. A convenient design is as follows. The inner cylinder (2) in Fig. 2 is an aluminium tube 2½ in. diameter and 10½ in. long; the wall thickness being 0·033 in. The base (5) is a thin plywood disk and there is also a wooden crossbar (4)

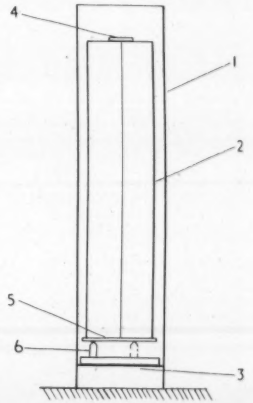

Fig. 2. Diagram of conductivity apparatus

at the top end to support the central thermocouple. The screening cylinder (1) is an aluminium tube 3 in. diameter and 13½ in. long. About 1 in. from the bottom there is a metal disk (3) supported by brackets. This carries a wooden disk in which three short ebonite rods (6) are inserted. The base of the inner cylinder rests on the pointed ends of these rods which act as thermal insulators. Constantan resistance wire (26 s.w.g.) is used for the windings of both tubes, and the wire ends are attached to small ebonite collars fixed to the cylinders by small bolts. The pitch of the winding is four turns per inch.

On account of the thermal resistance of the wire insulation the wire temperature will be above that of the cylinder. In the experiments recorded in Fig. 3 the heating current was 0·476 A and (assuming that $k = 0{\cdot}005$ c.g.s. units) the excess temperature is calculated to be about 0·5° C. It is not possible to calculate the heat flow to the outer cylinder from the wire. An upper limit may be found by assuming the whole inner cylinder to be at this temperature. The charts given in books on heat transfer[4] show that in this case thermal conduction is the dominating transfer mechanism. For 0·5° C excess temperature the heat flow by conduction per inch tube length is found to be 0·011 W. The total heat

input per inch length is 0·91 W and so the ratio (loss)/(input) is 1/83. Since the wire only covers one-tenth of the cylinder surface the actual loss will be much less than 0·011 W and consequently it can be neglected.

The temperature difference between the two cylinders is measured by a differential thermocouple T_1T_2 (Fig. 1). The Nichrome/constantan junctions of 36 s.w.g. wire are soldered to the heads of short 8 B.A. brass bolts and these are screwed into the cylinder walls, thus ensuring good thermal contacts. The central thermocouple has a spot-welded joint with no extra metal.

The temperature of the screening cylinder can be maintained at the same temperature as the inner cylinder by a second observer adjusting the power supply with a galvanometer connected to the differential thermocouple. A more convenient, and perhaps more accurate, method is to use the thermal e.m.f. to operate a relay with the aid of a sensitive amplifier (Fig. 1). The Tinsley direct current amplifier [5] is suitable for this purpose, and it was found that 2 μV, corresponding to a temperature difference of 1/20° C, was sufficient to operate an ordinary telephone relay.

THEORY

The differential equation for symmetrical radial heat flow is

$$\frac{\partial^2 v}{\partial r^2} + \frac{1}{r}\frac{\partial v}{\partial r} = \frac{1}{K}\frac{\partial v}{\partial t} \tag{1}$$

where v is the temperature, k is the thermal conductivity, c is the specific heat, ρ is the density, $K = k/c\rho$ is the thermal diffusivity, a is the cylinder radius and t the time.

The boundary condition when $r = a$ is

$$F = k\frac{\partial v}{\partial r} + w\frac{\partial v}{\partial t} \tag{2}$$

where F is the heat flux per unit area (from the winding) and w is the heat capacity per unit area of the cylinder wall. As the wall is thin and a good conductor the temperature difference between its faces is negligible. The solution of the differential equation can be found by the Laplace transform method (see Appendix). It consists of two terms; a linear variation of temperature with time and a transient term which is negligible when t is large. This is verified by the experimental curves in Fig. 3. The linear term is

$$v = \frac{F}{w + ka/2K}\left[t + r^2/4K - \frac{a^2}{8K}\left(\frac{4Kw + ka}{2Kw + ka}\right)\right] \tag{3}$$

Considering the surface temperature v_s and the centre temperature v_c ($r = a$ and $r = 0$) the following equations are obtained:

$$v_s - v_c = \tfrac{1}{2}Fa^2/(2Kw + ka) \tag{4}$$

$$\partial v/\partial t = 2KF/(2Kw + ka) \tag{5}$$

It is easily deduced that the thermal diffusivity K and the thermal conductivity k are given by

$$K = \tfrac{1}{4}a^2(\partial v/\partial t)/(v_s - v_c) \tag{6}$$

$$k = \tfrac{1}{4}[F - w(\partial v/\partial t)]a/(v_s - v_c) \tag{7}$$

In practice the wall heat capacity is found from a test made with the cylinder empty. The packing density ρ is found by dividing the mass of the cylinder contents measured after the experiment by the cylinder volume. The specific heat is then given by $c = k/K\rho$.

RESULTS

Experiments have been made with glass sand (which is almost pure silica), coke dust, pumice, cement and Nonpareil insulating powder. The temperature-time curves obtained with sand and coke dust gave two parallel lines, as predicted by the theory, and the curves are reproduced in Fig. 3. The heat input was the same in the two tests. The curves obtained with the other materials did not give parallel lines, there

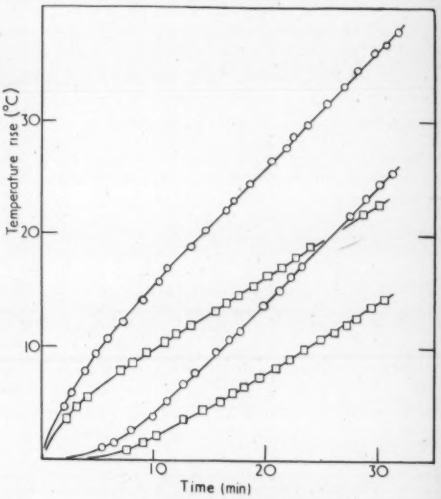

Fig. 3. Temperature/time curves
○ = coke dust. □ = sand.

being a difference of about 5% between the rate of rise at the surface and centre. This shows that the error due to axial heat flow along the central thermocouple wire is significant when the conductivity is below a certain limit. The results of the tests are given in the table in c.g.s. units.

Experimental results

Material	ρ	K	k	c
Glass sand	1·54	$2{\cdot}9 \times 10^{-3}$	$7{\cdot}5 \times 10^{-4}$	0·17
Coke dust	0·73	2·9	4·2	0·20
Cement*	1·06	1·3	2·4	0·17
Pumice*	0·84	1·7	2·4	0·17
Nonpareil powder*	0·32	2·4	1·7	0·22

* These results are approximate.

It can be concluded from the above results that this method will give an accurate estimate of the thermal constants when the thermal conductivity is above 4×10^{-4} cal s^{-1} cm^{-1} °C^{-1} and possibly this limit can be reduced by using thinner and more fragile thermocouple wires.

ACKNOWLEDGEMENTS

The first experiments with this apparatus were made at the Dominion Physical Laboratory, Lower Hutt, New

Zealand, and I am indebted to Prof. A. J. C. Wilson of University College, Cardiff, and Dr. W. H. George of Chelsea Polytechnic for facilities for further work in their laboratories.

REFERENCES

(1) CLARKE and KINGSTON. *Austral. J. Appl. Sci.*, **2**, p. 235 (1951).
(2) HOOPER and LEPPER. *J. Amer. Soc. Heat. Vent. Engrs*, **22**, p. 129 (1950).
(3) BLACKWELL. *J. Appl. Phys.*, **25**, p. 157 (1954).
(4) FISHENDEN and SAUNDERS. *Introduction to Heat Transfer* (London: Oxford University Press, 1950).
(5) GALL. *J. Instn. Elect. Engrs*, **89**, (II), p. 434 (1942).

APPENDIX

Solution of the differential equation

The Laplace transform of the equation is:

$$\frac{d^2\bar{v}}{dr^2} + \frac{1}{r}\frac{d\bar{v}}{dr} - q^2\bar{v} = 0 \tag{8}$$

where $q^2 = p/K$

$$\left(\text{Laplace transform } \bar{v} = \int_0^\infty f(t)e^{-pt}dt\right)$$

The general solution involves modified Bessel functions of the first order $I_0(qr)$ and $K_0(qr)$. Since K_0 is infinite when $r = 0$, terms containing it will not occur so $\bar{v} = AI_0(qr)$ is a solution.

The transform of the boundary condition from equation (2) is

$$k(\partial\bar{v}/\partial r) = F/p - wp\bar{v}\ (r = a) \tag{9}$$

and on substituting for $\bar{v}$,

$$A = F/p[kqI_1(qa) + wpI_0(qa)] \tag{10}$$

v is found from $\bar{v}$ by using the inversion integral

$$v = \frac{F}{2\pi i}\int_{\gamma-i\infty}^{\gamma+i\infty} \frac{I_0(qr)e^{zt}dz}{z[kqI_1(qa) + wzI_0(qa)]} \tag{11}$$

where $q^2 = z/K$

This has a double pole at $z = 0$ and single poles at the roots of $kqI_1(qa) + wzI_0(qa) = 0$.

Since I_0 and I_1 are positive functions, it follows that all the roots are negative and consequently the terms in v corresponding to these roots will each contain a negative exponential which tends to zero as t increases.

On expanding the various functions in power series and taking the limit $z \to 0$ it will be found that the residue (coefficient of $1/z$) is

$$\frac{F}{2\pi i}\left[t + r^2/4K - \frac{a^2}{8K}\left(\frac{4Kw + ka}{2Kw + ka}\right)\right] \Big/ (w + ka/2K) \tag{12}$$

and by the Cauchy residue theorem it follows that this (multiplied by $2\pi i$) is the term in v corresponding to $z = 0$

Measurement of the diffusion rate of hydrogen in nickel

By A. G. EDWARDS, M.Sc., Ph.D., Associated Electrical Industries Ltd., Aldermaston, Berks*

[*Paper received* 30 *April*, 1957]

The diffusion rate of hydrogen within nickel has been measured by making observations on the rate of escape of the gas from a hydrogen-soaked nickel wire heated *in vacuo*. The value obtained agrees, within experimental error, with data on solubility and permeation rate through foils interpreted on the assumption that energy barriers to gas penetration through surfaces are small.

1. INTRODUCTION

The passage of a gas molecule through a metal membrane into a vacuum vessel involves the following three processes, the first and last of which can be further subdivided if required.

(1) Penetration through the gas metal interface on the entrance side.

(2) Diffusion through the bulk metal.

(3) Penetration through the metal vacuum interface at the exit side.

In principle, any one of these processes may be effective in limiting the overall rate of transfer of gas molecules through the foil. In practice, it is not agreed in what systems, if any, surface barriers to interface penetration exist. Fast,[1] for example, considers that they are to be found in the system hydrogen–iron, but this is not supported by the work of Stross and Tompkins.[2]

Experimental work which has a bearing on this problem has largely been confined to determinations of permeation rates of gases through metals, and measurements of solubility of gases in metals. The permeation rate is the rate of penetration of the gas through the foil, normally from a vessel containing the gas at a pressure p into a vacuum. Its variation with temperature is of the form

$$P = P_0 e^{-b_p/T} \tag{1}$$

where P_0 is in 1 μ gas per cm^2 metal per cm thickness per s for a pressure of 1 atm; b_p is in ° K; T is the absolute temperature.

If the permeation rate is assumed to be inversely proportional to thickness, as is usually done, this implies that surface barriers are small. The diffusion of a gas within a metal is not affected by interface effects. The diffusion rate is the rate of transfer of the gas through unit area of the metal for unit concentration gradient. Its relation to temperature is of the form

$$D = D_0 e^{-b_D/T} \tag{2}$$

where D_0 is in cm^2 s^{-1}, and b_D in ° K.

The solubility of a gas in a metal varies with temperature in the manner

$$S = S_0 e^{-b_s/T} \tag{3}$$

where S_0 is in 1 μ gas per cc metal, and b_s is in ° K.

If we now consider a foil of unit thickness at temperature T separating gas at pressure p from vacuum, and we further suppose there are no surface barriers, we have

$$\left.\begin{aligned} & P = DS \\ \text{i.e.} \quad & P_0 e^{-b_p/T} = D_0 S_0 e^{-b_D/T - b_s/T} \\ \text{whence} \quad & P_0 = D_0 S_0 \text{ and } b_s + b_D = b_p \end{aligned}\right\} \tag{4}$$

The nomenclature followed here is similar to that of Smithells and Ransley,[3] i.e. the temperature coefficients are not quoted as atomic or molecular heats. This is done to avoid the confusion which surrounds the use of these terms in the literature.

2. THEORY

The following theory of the outgassing of a long cylinder into a vacuum is based on the assumptions that (1) the gas is initially uniformly distributed throughout the body, (2) there are no surface barriers to its escape from the body into a vacuum, and (3) diffusion is covered by Fick's law, the diffusion coefficient being independent of concentration.

We then have the following relationship presented by Euringer[4] and by Barrer.[5]

$$dQ/dt = \frac{2C_0 D}{a} \sum_{\nu=1}^{\infty} \exp \frac{-D\xi_\nu^2 t}{a^2} \tag{5}$$

where dQ/dt = rate of escape of gas per centimetre length per second (1 μ/s);

C_0 = gas concentration in the wire at $t = 0$ (1 μ/cc);

D = diffusion rate in square centimetres per second;

a = radius of the wire in centimetres;

ξ_ν = the νth root of the equations $J_0(\xi_\nu a) = 0$.

The first three roots are

$$\xi_1 = \frac{2{\cdot}405}{a} \quad \xi_2 = \frac{5{\cdot}52}{a} \quad \xi_3 = \frac{8{\cdot}654}{a}$$

Now suppose that evolution takes place from a wire of length L into a vessel pumped at a speed S_0 l./s, we will then have the pressure given by

$$p = \frac{LA\pi C_0 D}{S_0} \Sigma \exp \frac{-D\xi_\nu^2 t}{a^2} \tag{6}$$

Now compare this with

$$y = \Sigma \exp s\xi_\nu^2 \tag{7}$$

These two curves become identical if

$$s = Dt/a^2$$

$$y = \frac{pS_0}{4\pi C_0 DL}$$

Thus, if an experimental plot is made of log p against log t, and another of log y against log s (by calculation), the two curves obtained will be superposable, and by comparing the corresponding values of s and t and of y and p, values of D, the diffusion rate, and C_0, the initial concentration can be obtained.

If s is small, equation (7) reduces to the form

$$y = \frac{1}{2\sqrt{(\pi s)}} \tag{8}$$

* Now at Siemens Edison Swan Research Laboratory.

This approximate form can sometimes be used to overcome the difficulty associated with any preliminary outgassing which takes place at room temperature. We see from equation (6) that the outgassing characteristics would not be affected in shape by changes of temperature if pressure were plotted against the parameter Dt. Therefore, in plotting pressure against time for outgassing at a fixed temperature, allowance can be made for earlier outgassing at different temperatures by selecting a time origin a short period before the specimen actually reaches its final outgassing temperature. The period can be found as an intercept by plotting $(\text{pressure})^{-2}$ against time for the early part of the outgassing run where equation (8) holds true.

3. EXPERIMENTAL ARRANGEMENTS

The general method adopted is to soak a heated cylindrical specimen of nickel thoroughly in hydrogen and allow it to cool while still surrounded by the gas. The gas is then pumped away, and the background pressure reduced by mild flaming of the glass envelope and continued pumping. Finally, the specimen is heated to a fixed temperature and the pressure in the system plotted as a function of time.

It is desirable that the temperature of the specimen should follow a step function, that is, it should be possible to increase it from room temperature to its outgassing value very quickly. This makes some form of direct electrical heating essential, since the dropping of a cold body into a hot evacuated enclosure, where heat can only be received by radiation, leads to an asymptotic approach of body temperature to enclosure temperature, the time constant of which may be quite long. With direct electrical heating, on the other hand, it is easy to arrange an initial high rate of dissipation, followed by an immediate reduction of power to a "maintenance" level when the specimen has reached the prescribed temperature.

It is also important that all the specimen should be at the same temperature. A cool portion will initially affect the shape of the outgassing curve very little, but at a later stage, when the majority of the specimen is nearly gas free, its slowly varying outgassing rate will contribute an ever-increasing relative amount to the pressure in the system.

The specimen arrangement adopted in the present case is shown schematically in Fig. 1. A 30 cm length of 1 mm diameter nickel wire (extra high purity commercial grade) is used in the form of a wide-spaced hairpin, with large radius of curvature at the bend. The ends are welded to the centre of smaller molybdenum hairpins, the ends of which are brought out by way of tungsten leads, through the hard glass envelope of the tube. Three platinum/platinum rhodium thermocouples are attached to the specimen as shown, the wire diameter being kept down to 0·001 in. to reduce heat loss by conduction.

The specimen tube is connected to an ion gauge, and a cold finger with high conductance tubing, but between the cold finger and the mercury vapour traps of the pumping system, a constriction with a pumping speed of 50 cc/s is included, which determines the speed of pumping from the specimen tube largely independent of fluctuations in diffusion pump performance.

The electrical connexions are also shown in Fig. 1. Each molybdenum hairpin is fed by the centre tapped secondary of a high current low voltage transformer driven from a Variac. The centre taps are connected across the secondary of a third Variac driven transformer, and the current delivered by this is monitored. With this arrangement, TC_1 can be brought to any desired reading by varying V_1, TC_2 by varying V_2 and TC_3 by varying V_3, the controls being largely independent of each other. If the three thermocouples read the same, the temperature is assumed to be uniform throughout the specimen.

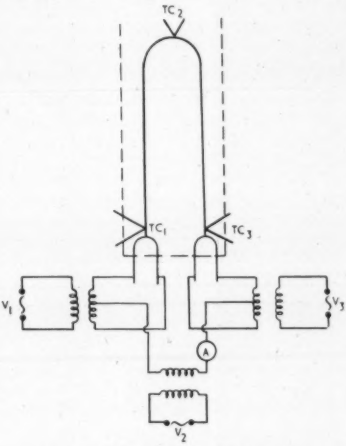

Fig. 1. Arrangement of specimen

The all-glass apparatus is vacuum baked overnight, and after applying liquid air to the cold traps, the nickel specimen is outgassed for some while at red heat. The whole system is then filled with hydrogen, which has been dried by passing over copper turnings refrigerated in liquid air into a storage flask containing a tray of phosphorus pentoxide. When required for use, the hydrogen is again passed over refrigerated copper into the system. The specimen is heated to 870° C approximately, with the hydrogen at about 32 cm of mercury pressure for a period of five minutes, after which the heating current is turned off, and a similar period allowed for cooling before the hydrogen is pumped away.

Throughout this process the ion gauge is maintained hot by means of a thermal tape. The background pressure in the system can be further diminished by flaming the specimen tube lightly. Finally, liquid nitrogen is poured into the cold finger, thus giving it a high pumping speed for water vapour, the specimen tube reflamed, and the heating tape turned off. Flashing of the molybdenum hairpins ensures that they are hydrogen free before the beginning of the experiment. The background pressure can be reduced in this way to 10^{-7} mm of mercury or less.

To start an outgassing run, a current is passed through the specimen 10 to 20 times as great as that finally required under equilibrium conditions. When TC_2 shows the required temperature, the current is reduced to the maintenance value previously determined, and TC_1 and TC_3 adjusted to read the same value. Uniform temperature conditions can be set up in less than a minute.

Thereafter, conditions are maintained by manual Variac

adjustments, and pressure recorded as a function of time throughout the duration of the run.

4. RESULTS

The effective duration of the outgassing runs varied from a few minutes to a few hours, according to the temperature. In Fig. 2 are shown on the same plot the theoretical curve of y as a function of s, taken from Euringer,[4] and the points for the three outgassing runs at different temperatures. The theoretical curve is then drawn to give the best fit to the experimental points.

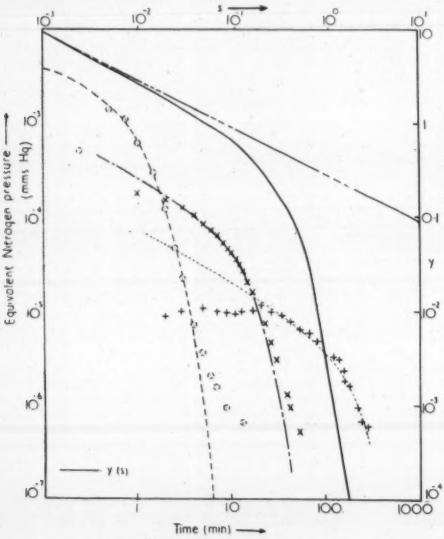

Fig. 2. Outgassing curves for wires

—○———○— 496° C.
×—·—×— 291° C.
+·····+ 162° C.
——— $y(S)$.

The fit is not perfect for the following reasons: (*a*) for small values of time the specimen has not yet reached equilibrium temperature, (*b*) the effect of initial outgassing at room temperature is most significant at small values of time (adequate correction for this in the manner indicated cannot always be made), and (*c*) at low pressures (large values of time) the effect of background pressure becomes significant. The warming action of the wire on the surrounding envelope gives an effective background much higher than the "cold" value at the beginning of the run.

These effects seem adequate to explain the departure of experimental points from the theoretical curve except in the case of the lowest temperature runs. The initial constancy of outgassing rates in this case is difficult to explain.

From each curve a value for diffusion rate and initial concentration is obtained, and these are recorded in Table 1.

Table 1. *Experimental results for diffusion rate and initial concentration*

Outgassing temp., °C	*Diffusion rate cm² sec⁻¹*	*Initial concentration 1 μ/g*	*Stoving pressure, cm of mercury*	*Stoving temp., °C*	*Stoving time min*
162·5	9×10^{-8}	5·3	33	~870	6
186	$1{\cdot}23 \times 10^{-7}$	—	33	~870	6
205	$3{\cdot}0 \times 10^{-7}$	6·6	32	~870	5
237	$4{\cdot}6 \times 10^{-7}$	6·4	32	~870	5
291	$1{\cdot}04 \times 10^{-6}$	6·05	32	~870	5
332·5	$1{\cdot}9 \times 10^{-6}$	5·4	33	~870	11½
355	$3{\cdot}1 \times 10^{-6}$	8·1	32½	~870	5
426	$7{\cdot}3 \times 10^{-6}$	11·2	32	~870	5
496	$1{\cdot}34 \times 10^{-5}$	10·2	31	~870	5

Since $D = D_0 e^{-b_D/T}$

$$\log_{10} D = \log_{10} D_0 - \frac{b_D}{2{\cdot}302T}$$

and we should obtain a straight line for the plot of $\log_{10} D$ against $1/t$.

The present results are presented in this way in Fig. 3, together with those of Euringer.[4] The best straight line corresponds to

$$b_D = 5100°\,\mathrm{K}, \quad D_0 = 1{\cdot}07 \times 10^{-2}\,\mathrm{cm^2\,s^{-1}}$$

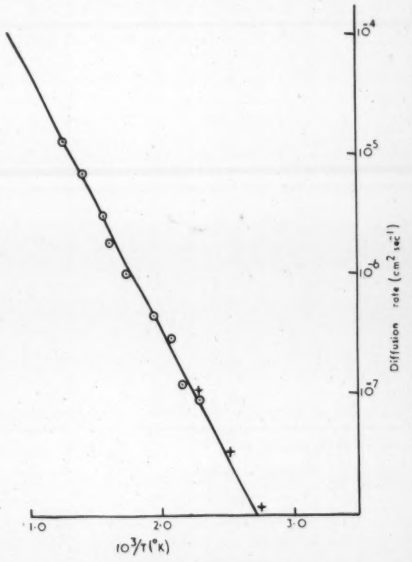

Fig. 3. Variation of diffusion rate with temperature

++ Euringer's results [Ref. (4)].
○○○○ Experimental points.
——— $D = De^{-(b_0/T)}$; $b_D = 5100°$K;
$D_0 = 1{\cdot}07 \times 10^{-2}\,\mathrm{cm^2\,s^{-1}}$.

The values for initial concentration show a scatter of about 2 : 1, and are considerably lower than those reported

for the solubility of hydrogen in nickel at the nominal stoving temperature. The scatter is, in part, attributable to the rather imprecise temperature control during the heating of the wire.

Table 2. *Summary of published data: hydrogen nickel system*

Permeation rate

$$P = P_0 e^{-b_p/T}$$

P_0 1 μl/sec/cm²/cm thickness at 1 atm	b_p (°K)	Reference
	7300–6550 (below Curie point) 6560–6020 (above Curie point)	Post, C., and Ham, W., *J. chem. Phys.*, **6**, p. 599 (1938).
$9{\cdot}9 \times 10^{-1}$	7710	Lombard, V., *C.R. Acad. Sci. [Paris]*, **177**, p. 116 (1923).
$6{\cdot}5 \times 10^{-1}$	6930	Deming, H., and Hendricks, B., *J. Amer. Chem. Soc.*, **45**, p. 2857 (1923).
11×10^{-1}	6900	Borelius, G., and Lindblom, S., *Ann. Phys. [Leipzig]*, **82**, p. 201 (1927).
$8{\cdot}0 \times 10^{-1}$	6700	Ham, W., *J. chem. Phys.*, **1**, p. 476 (1933).
11×10^{-1}	6130	Smithells, C. J., and Ransley, C. E., *Proc. Roy. Soc. A*, **150**, p. 172 (1935).
	6700	Post, C., and Ham, W., *J. chem. Phys.*, **5**, p. 915 (1937).

Solubility

$$S = S_0 e^{-b_s/T}$$

S_0 1 μl/cm³ for 1 atm.	b_s (°K)	Reference
1360	1325	Smittenberg, J., *Receuil Trav. chim. Pays. Bas.*, **53**, p. 1065 (1934).
1500	1475	Armbruster, M. H., *J. Amer. Chem. Soc.*, **65**, p. 1050 (1943).
	1525	Sieverts, A., *Z. phys. Chem.*, **60**, p. 129 (1907).
(300–500° C)	1075	Luckemeyer, Hasse, L., and Schenck, H., *Arch. Eisenhüttenw.*, **6**, p. 209 (1932).
(500–900° C)	2250	

5. COMPARISON WITH PUBLISHED DATA

The present data on diffusion rate are in reasonable agreement with those of Euringer, as is apparent from Fig. 3. No other published work is directly comparable, but we may compare the present results with combinations of earlier data on permeation and solubility, a selection of which (quoted in Barrer[5] and Dushman[6]) is given in Table 2. The permeation rate measurements show a number of values near $b_p = 6800°$ K, and the solubility measurements near $b_s = 1400$. The difference between these two, 5400, is reasonably near the present experimental value for the temperature coefficient of diffusion which is 5100. In view of the disagreement in the exponential coefficients, any close agreement in the multiplying factors is not to be expected.

6. CONCLUSION

The observed outgassing of hydrogen soaked nickel can be explained in terms of Fick type diffusion without significant surface barrier effects. The diffusion rate is given by

$$D = D_0 \exp - b/T$$

where $D_0 = 1{\cdot}1 \times 10^{-2}$ cm² s^{-1}, $b = 5100°$ K.

7. ACKNOWLEDGEMENTS

The author would like to acknowledge the help he has received from Mr. J. Smalley with the experimental work, and to thank Dr. T. E. Allibone, the Director of the Laboratory, for permission to publish this paper.

8. REFERENCES

(1) FAST, J. D. *Phillips tech. Rev.*, **7**, p. 74 (1942).

(2) STROSS, T. M., and TOMPKINS, F. C. *J. Chem. Soc.*, **49**, p. 230 (1956).

(3) SMITHELLS, C. J., and RANSLEY, C. E. *Proc. Roy. Soc. A*, **150**, p. 172 (1935).

(4) EURINGER, G. *Z. Phys.*, **96**, p. 37 (1935).

(5) BARRER, R. M. *Diffusion in and through solids* (London: Cambridge University Press, 1941).

(6) DUSHMAN, S. *Scientific foundations of vacuum technique* (London: Chapman and Hall, 1949).

On the screen brightness required for high resolution operation of the electron microscope

By A. W. AGAR, B.Sc., F.Inst. P., A.M.I.E.E., Aeon Laboratories, Beech Hill, Englefield Green, Egham, Surrey

[*Paper first received* 30 *August*, 1956, *and in final form* 28 *May*, 1957]

To determine the relationship between the screen brightness and the regularly obtainable resolution, the screen brightness, measured by a S.E.I. photometer was plotted against the minimum width of Fresnel fringe which was clearly visible all round a circular hole in a carbon film. It was found that there is an optimum fringe width at which the brightness is used most economically. It is also shown that unless the brightness exceeds a certain value (for a given resolution) it is not possible to be certain that this resolution can be attained.

When operating an electron microscope at high resolution, it is advantageous to examine the Fresnel diffraction fringes formed round the edges of holes in a film in an out-of-focus image. This enables the astigmatism of the objective lens to be corrected, and also provides a sensitive test for other factors limiting the resolution of the instrument (Haine and Mulvey).* Any factor which would limit the resolution of the microscope will visibly affect the Fresnel fringes when they are of a width comparable with the resolution required. For routine high resolution working, it is found very desirable to be able to check by visual inspection of the screen that all factors limiting the resolution are below the tolerance limits. The visibility of fringes of an appropriate width is therefore an important factor in high resolution work, and its relation to the brightness of the image on the fluorescent screen was therefore investigated.

A thin carbon film with a large number of holes in it was used as the object, and the instrumental magnification used was relatively low (20 000 ×) so as to allow a wide range of brightness. A 10 × telescope was used for viewing the screen. After a short period of dark adaption, the brightness of the image on the screen was set at some suitable value and measured by a S.E.I. photometer. The astigmatism was corrected as accurately as possible in direction and magnitude by adjustment of the corrector controls. The focus of the objective was then varied until the over-focused fringe was just visible as a distinct line all round the inside edge of the hole, and the resulting image was photographed.

A further exposure, very close to focus, was also made, to give a measure of the correction actually attained.

The experiment was repeated at a number of different intensities (over a range of 100 : 1), the astigmatism corrector being put out of adjustment between each attempt. Three different operators recorded their results in this way.

The fringe widths on the photographic plates were measured with an accurate eyepiece scale on a low-power microscope, and the mean minimum visible fringe width was plotted against the brightness (on a logarithmic scale), as shown in Fig. 1. This shows very clearly the steep increase in brightness required to view very narrow fringes, which is due to the limited resolution of the phosphor and the eye.

It is interesting to note that no fringes narrower than 25 μ were detected, and there is some suggestion of a "cut-off" width at about 35 μ. This agrees very well with the recognized figure of about 70 μ for the resolution of the phosphor used, as it might be expected that some intensity dip might be perceptible down to about half this limit.

A fringe of width w at the object examined at an instrumental magnification M_1 gives a fringe of width $M_1 w$ on the screen, and requires some brightness B_1 for visibility. If the magnification be changed to $M_2 (M_2 > M_1)$, the fringe width on the screen becomes $M_2 w$ and requires some lower brightness B_2 for visibility (B_1 and B_2 are determined from Fig. 1). However, this increased magnification results in a loss of screen brightness by a factor M_1^2/M_2^2, and it is not immediately obvious if the net result is an increase or decrease of brightness required.

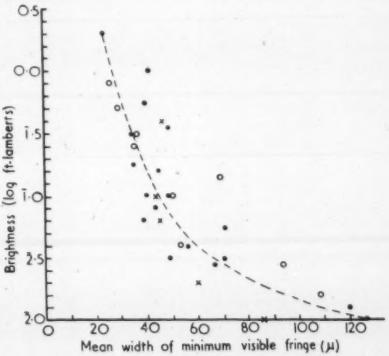

Fig. 1. Variation of minimum visible fringe width with brightness

• • • observer "A"
× × × observer "B"
○ ○ ○ observer "C"

The relative brightness required to see the image of the fringe on the screen for given illumination conditions and fixed fringe width at the object, but at differing magnification, may be defined as

$$(B_n/B_1)(M_1^2/M_n^2)$$

M_1, and hence B_1, may be chosen arbitrarily. The relative brightness required for the visibility of fringes of varying width on the screen is shown in Fig. 2. It should be noticed that the ordinate is still plotted on a logarithmic scale.

The curve of Fig. 2 reaches a minimum when the fringe width on the screen is 70 μ, though it is fairly flat between 50 and 100 μ fringe width. Thus, for any desired fringe width at the object, the instrumental magnification should be adjusted to enlarge this to 70 μ on the screen to ensure maximum visibility. It may be significant that this figure

* HAINE, M. E., and MULVEY, T. *J. Sci. Instrum.*, **31**, p. 326 (1954).

corresponds to the resolution of the phosphor used, but no experiments with different screens were made.

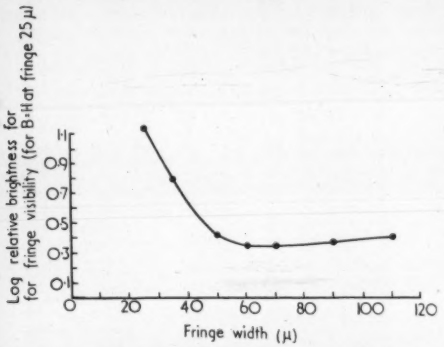

Fig. 2. Relative brightness required for viewing fringes (values of ordinates for $B = 1 \cdot 1$ at fringe 25 μ)

If it is possible to see a minimum fringe of 10 Å (referred to the object), then the attainable resolution will be better than 10 Å. Depending on the experience of the operator and other conditions (such as dark adaption), the resolution attainable, after visual correction of astigmatism, could be of the order of 5 Å. However, it should be remembered that Fig. 1 effectively gives threshold values of brightness at which a fringe of a certain width can be seen, and it is very desirable that one should operate above this level if strain is to be avoided and consistent results are to be obtained. (The scatter in the points gives some idea of the desirable safety factor). It seems reasonable then to adopt the convention of insisting on visibility of a fringe of minimum width equal to the required resolution. Thus if 10 Å resolution is required, the optimum instrumental magnification is 70000, and the screen brightness must be greater than $\bar{2} \cdot 5$ log foot Lamberts under the conditions of illumination suitable for high resolution operation.

ACKNOWLEDGEMENTS

The author is indebted to Mr. M. E. Haine for suggesting the investigation, and wishes to thank Dr. T. E. Allibone for permission to publish this note.

Non-linear forced vibration of a stretched string

By E. W. Lee, B.Sc., Ph.D., Department of Physics, The University, Nottingham

[*Paper first received* 8 *April, and in final form* 2 *May*, 1957]

A stretched string clamped at both ends and driven transversely at the centre is found to undergo non-linear oscillations. Discontinuities in the amplitude of the vibration are observed as the driving frequency is changed (jump phenomena) and the frequency at which these jumps occur depends markedly on whether the frequency is being increased or decreased (hysteresis). The behaviour is in qualitative agreement with simple theory.

1. INTRODUCTION

There is at present considerable interest in the behaviour of vibrating systems having non-linear restoring force. Their general properties are fairly well known. In the case of free vibration the natural frequency is a function of the amplitude and in the more complicated case of forced vibration discontinuities in the amplitude occur as the frequency of the driving force is changed. These discontinuities are usually referred to as "jump phenomena" (Stoker[1]). Hysteresis is also observed in that the frequency at which these jumps occur depends on whether the driving frequency is being increased or decreased.

Nevertheless, naturally occurring practical examples of vibrating systems in which non-linearity is really important are difficult to find. One such example is the vibration galvanometer studied by Appleton.[2] There, however, the hysteresis in the resonance curve amounted to only $0 \cdot 2$ c/s at 70 c/s so that it would be rather difficult to observe with ordinary laboratory equipment. Vibrators which have been specially designed to have a markedly non-linear restoring force have been described by Ludeke.[3]

In this paper a very simple arrangement is described which is inherently non-linear, and in which the non-linearity is considerable. Jump phenomena and hysteresis are readily observed and the apparatus is therefore very suitable for student demonstration.

2. EXPERIMENTAL ARRANGEMENT

The apparatus makes use of the fact that a wire vibrating transversely between two fixed points undergoes oscillations which are not simple harmonic except for infinitesimal amplitudes by virtue of the fact that the tension in the wire, and hence the restoring force on an element of it, increases with the displacement of that element from its equilibrium position. Such a wire can be set into forced vibration by a strong magnetic field at right angles to the wire at the mid-point and passing alternating current down the wire. An almost identical arrangement has been described by Muniz.[4] The wire is thus set into vibration at the frequency of the electric current. This is obtained from an r.c. oscillator (it is essential that the oscillator frequency be stable) through a step-down transformer. The magnetic field is supplied by a magnetron magnet and the amplitude of the vibration of the wire is measured by placing a paper scale immediately behind it. It is essential that the wire be clamped at both ends. If the ends of the vibrating wire are merely bridges the wire slips over them as it vibrates (particularly at large amplitudes) and

the non-linearity is much reduced. For this reason Constantan wire was used on account of its hardness. Copper wire, although otherwise satisfactory, tends to break at the points where it is clamped.

3. THEORY

The exact theory of the stretched string vibrating at large amplitudes has been given by Carrier[5] who considered free vibrations only. The case of forced vibrations is much more complicated. In the present example it is quite easy to set up the equations of motion rigorously but it is impossible to solve explicitly the equations obtained. The treatment given below makes no claim to be exact and the results obtained cannot be considered to be any more than a guide to the sort of behaviour one might expect such a system to exhibit.

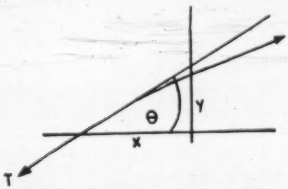

Fig. 1. Segment of vibrating string

Consider free vibrations first, the equation of motion of an element of the string (see Fig. 1) is

$$\frac{\partial}{\partial x}(T\sin\theta) = \rho A\frac{\partial^2 y}{\partial t^2} \tag{1}$$

where T is the tension in the string of cross sectional area A and linear density ρ. If T_0 is the tension in the undisturbed string the strain in the string when displaced is $\frac{1}{2}(\partial y/\partial x)^2$ and hence the tension becomes

$$T = T_0 + \tfrac{1}{2}AE(\partial y/\partial x)^2$$

where E is Young's Modulus of the string material. Equation (1) then becomes

$$\frac{\partial}{\partial x}[T_0 + \tfrac{1}{2}AE(\partial y/\partial x)^2]\sin\theta = \rho A\frac{\partial^2 y}{\partial t^2}$$

After carrying out the differentiation, neglecting powers of $\partial y/\partial x$ greater than the second and expressing $\sin\theta$ in terms of $\partial y/\partial x$, one obtains for free vibrations,

$$T_0\frac{\partial^2 y}{\partial x^2} + \frac{3}{2}AE(\partial y/\partial x)^2\frac{\partial^2 y}{\partial x^2} = \rho A\frac{\partial^2 y}{\partial t^2} \tag{2}$$

in which T_0 has been neglected in comparison with AE, which is easily seen to be justified. Equation (2) is a first order approximation to the equation of motion of the string. However, in the present experiment we are only interested in the displacement of a fixed point on the string and we therefore ignore the wave aspect of equation (2) and merely try to obtain from it the equation of motion of a fixed point. To do this it is expedient to assume that a solution of equation (2) exists of the form $y = \sin\dfrac{n\pi x}{l}\,f(t)$. Substitution in equation (2) gives

$$\frac{n^2\pi^2}{l^2}\sin\frac{n\pi x}{l}f''(t) + \frac{T_0}{\rho}f(t) + \frac{3}{2}\frac{AE}{\rho}\frac{n^2\pi^2}{l^2}\cos^2\frac{n\pi x}{l}[f(t)]^3 = 0 \tag{3}$$

where $f''(t)$ represents $\partial^2 f/\partial t^2$ and l is the total length of the string. Very little can be done with this equation as it stands because of the third term, but by considering only the fundamental mode and replacing $\cos^2 n\pi x/l$ by its average value, namely $\frac{1}{2}$, for $n = 1$, equation (3) can be reduced to a more manageable form. Furthermore, at the centre $x = l/2$ and $\sin n\pi x/l = 1$. Equation (3) then becomes

$$y'' + \frac{\pi^2}{l^2}\frac{T_0}{\rho}y + \frac{3}{4}\frac{\pi^4}{l^4}\frac{AE}{\rho}y^3 = 0$$

In the presence of an externally applied acceleration, this must be added to the right-hand side. In our case this is $Hi\delta/m'$ where H is the strength of the magnetic field which acts over a length δ of the wire at the centre and $i = i_0\cos\omega t$ is the current in e.m.u. in the wire. m' is the effective oscillating mass of the wire which is taken to be its actual mass ρl. The complete equation of motion of a point at the centre of the wire is thus

$$y'' + \frac{\pi^2}{l^2}\frac{T_0}{\rho}y + \frac{3}{4}\frac{\pi^4}{l^4}\frac{AE}{\rho}y^3 = \frac{Hi_0\delta}{\rho l}\cos\omega t \tag{4}$$

The usual way of dealing with an equation of this form is to assume a solution of the form $y = a\sin\omega t$ and substitute. Such a solution turns out to be admissible provided that

$$\omega^2 = \omega_0^2 + \frac{3}{4}\beta a^2 - \frac{G}{a} \tag{5}$$

with $\omega_0^2 = \dfrac{\pi^2}{l^2}\dfrac{T_0}{\rho}$, $\beta = \dfrac{3}{4}\dfrac{\pi^4}{l^4}\dfrac{AE}{\rho}$ and $G = \dfrac{Hi_0\delta}{\rho l}$. This cubic equation for the amplitude is then solved as a function of the impressed frequency by standard graphical methods (see, for example, Joos,[6] Stoker[1]). Since all the constants in equation (5) are known (T_0 was calculated from the resonant frequency of the wire for very small amplitudes) the amplitude of the motion can be calculated. The result is shown in Fig. 2.

4. EXPERIMENTAL RESULTS AND DISCUSSION

The wire used in the experiment certainly showed the behaviour which was expected and Fig. 2 shows that the observed behaviour is at least in qualitative agreement with that obtained from equation (5). Jump phenomena are clearly exhibited and there is considerable hysteresis. That these two effects are brought out so clearly is due to the very light damping of the wire. No attempt was made to take account of damping effects since these seriously complicate the analysis, but a measure of the damping was obtained experimentally from the observation that the amplitude of the free vibration decayed to half its original value in 4 s.

Quantitatively there is little agreement between theory and experiment especially at low frequencies where the observed amplitude is always greater than the theoretical. Further unexplained behaviour was observed in the variation of the lower jump frequency with driving current. More detailed analysis (Stoker[1]) of the stability of a system of this kind shows that the lower jump frequency should occur at a frequency ω given by

$$\omega^2 = \omega_0^2 + \frac{9}{4}\beta a^2$$

where a is the smaller of the two amplitudes at this frequency.

The calculated and experimental results are shown in Fig. 3 from which it appears that for driving currents greater than 0·1 A r.m.s. the wire ceases to behave as a hard spring,

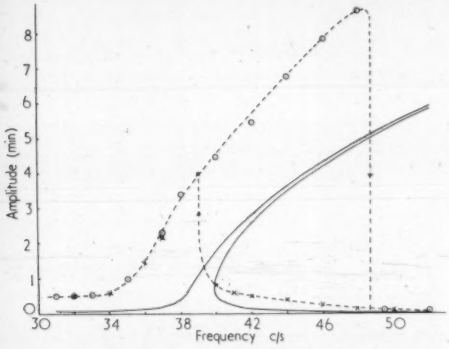

Fig. 2. Amplitude-frequency characteristics of string in its fundamental mode

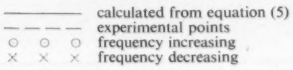

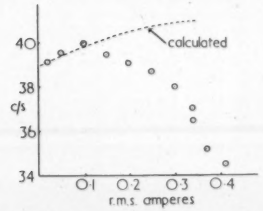

Fig. 3. Variation of lower jump frequency with driving current in the wire

i.e. $\beta > 0$, and thereafter behaves as a soft spring with $\beta < 0$. The amplitude-frequency behaviour is always that of a hard spring with the resonance curve bent towards the high frequency side. In view of the obvious limitations of the theoretical analysis it is futile to consider possible reasons for these discrepancies.

Unlike many non-linear systems this example could not be made to exhibit sub-harmonic response. The reason is simply that the string possesses an infinite number of possible modes of vibration with frequencies ω_0, $3\omega_0$, $5\omega_0$, etc. Consequently if a driving force whose frequency is close to one of these frequencies is applied to the string it vibrates with the frequency of the driving force, which it can do quite easily since it is in no way restricted to vibrate at frequencies close to its fundamental frequency but may vibrate at any frequency close to one of its own natural frequencies. When the string is made to vibrate in this way it shows exactly the same non-linear behaviour as for the fundamental mode.

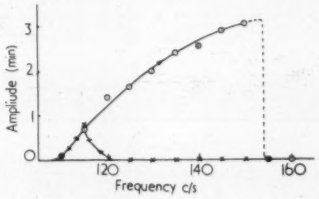

Fig. 4. Observed amplitude-frequency characteristic of string vibrating in its third harmonic

Fig. 4 shows the amplitude-frequency characteristic of the string vibrating at its third harmonic.

REFERENCES

(1) STOKER, J. J. *Nonlinear Vibrations* (New York: Interscience Publishers Inc., 1950).

(2) APPLETON, E. V. *Phil. Mag.*, **47**, p. 609 (1924).

(3) LUDEKE, C. A. *Amer. J. Phys.*, **16**, p. 430 (1948).

(4) MUNIZ, E. O. *Amer. J. Phys.*, **21**, p. 232 (1953).

(5) CARRIER, G. F. *Quart. Appl. Math.*, **3**, p. 157 (1945).

(6) JOOS, H. *Theoretical Physics*, p. 93 (London: Blackie and Sons, Ltd., 1947).

High vacuum shaft seals, flanged joints and the gassing and the permeability of rubber-like materials

By R. H. V. M. Dawton, Atomic Energy Research Establishment, Harwell, Berks.

[*Paper first received* 15 *November*, 1956, *and in final form* 26 *February*, 1957]

Various designs of high vacuum shaft seals are given and their performance measured by the pressure rate of rise in a closed system. Experiments show that there is little to choose between them from their vacuum performance, although the washer in which a tension spring is embedded is at times to be preferred. A large portion of the leak is condensable indicating something more complicated than the direct passage of air through the seal. Experiments give measurements of the gassing from rubber-like materials including neoprene and butyl rubber when totally enclosed in a vacuum system, and also measurements of their permeability to gases. All the synthetic materials tested gassed considerably more than did rubber. In the permeability experiments it was found that the time required for gases to pass through diaphragms varies from several minutes to an hour, depending on the gas. The permeability, unlike the gassing effect, is considerably less with the synthetic rubbers tested than with rubber. Data are given of the testing of flanged gasket joints and their effect on a vacuum system during the first twenty hours of pumping when the joint gassing is liable to be confused with a leak. Data are also given on the flange clamping pressure necessary for a tight joint.

The object of this paper is to record the results of some high vacuum measurements, e.g. gassing rates and permeability rates, on shaft seals and flanged joints, and also to measure the effect of rubber-like materials when used on continuously pumped high vacuum equipment.

1. High Vacuum Shaft Seals

Shaft seals on large vacuum equipment have been used for some time[1] but the lack of data on their leak rate makes it impossible to predict the effect of using such seals on small vacuum systems. The data obtained in this paper was obtained as follows. The seal was attached to a known volume (about 500 cm^3) and pumped down to 10^{-5} mm of mercury (see Fig. 1). The pumps were then isolated from

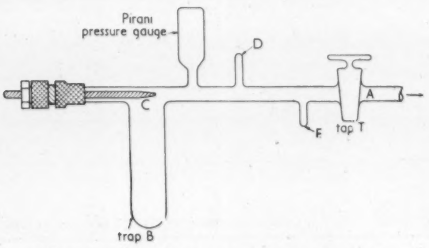

Fig. 1. Apparatus used for testing shaft seals

A, to liquid air trap, mercury pump and rotary pump; trap *B*, an appendage which can be immersed in liquid air; *C*, seal under test; *D*, when used McLeod gauge and its liquid air trap sealed on here (calibration only); *E*, fine control leak valve sealed on here (calibration of gauge only).

the system and the pressure rise observed on a mirror galvanometer attached to a Pirani gauge. Pressure changes down to $\frac{1}{2} \times 10^{-4}$ mm of mercury could be measured. The precautions taken to ensure reliable results are given in Section 4.

Initial experiments showed that if the sealing of the shaft is by a tube-like rubber sheath (Fig. 2), the resulting joint is relatively unsatisfactory when compared with the sealing obtained by a flat rubber washer such as is used in the Wilson seal design. For this reason, the main experiments were limited to the flat washer type of seal. As is well known, the shaft causes the washer to curve outwards at the centre, and it is usually stated that the atmospheric pressure forces the washer against the shaft to help form the seal. In actual fact it is not the atmospheric pressure which is predominant in forming the seal but rather the snap of the washer material. This can be demonstrated if the washer is mounted inside

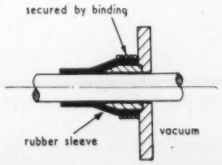

Fig. 2. Vacuum shaft joint using a rubber sleeve (this design is unsatisfactory compared with those in Fig. 3)

out, so that it curves the other way, when the seal still performs its duty. Further, when the seals are used hot, at say 100° C, far better performance is obtained if the washer is given additional elastic properties by having within it a spring to keep it to the shaft [see Fig. 3(*d*)].

Leakage rates. The term leakage rate is used despite the fact that most of the leakage was found to be condensable and is therefore not a simple leakage of air. The composition of the condensable vapour is not known but it could be moisture which the shaft and lubricant have acquired on exposure to air. At room temperature the various types of seals tested (Fig. 3) are all so similar that there is no need to discriminate between them. The results given below are for seals using a $\frac{3}{8}$ in. shaft diameter. Lubrication is required, and in general a thin high vacuum oil, such as Apiezon B oil, is better than a high vacuum grease. For a static shaft the leakage is about $1{\cdot}2 \times 10^{-3}$ l. μ/s after eight hours' pumping. For a slowly rotating shaft (1 rev/s without end play) the leakage is increased some three times. For reciprocating motions the leakage is proportional to the distance the shaft moves and independent of the time or

speed, if the speed is below 4 cm/s, and under these conditions the leakage is 0·01 l. μ/cm of to and fro motion. At higher speeds the leak per unit motion of the shaft increases. An important result is that the leak on the in motion of the shaft is some six times that of the out motion of the shaft. This should be remembered when designing apparatus. It also suggests that the main cause of the leakage is the lubricant's clinging to the shaft and so entering the main vacuum system. This suggestion is supported by the facts

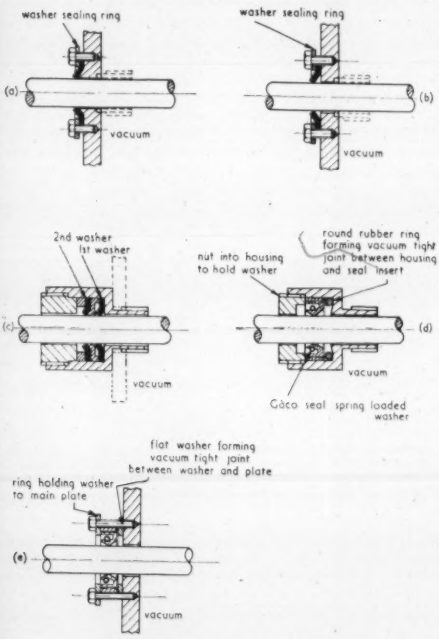

Fig. 3. Different types of shaft seals

(*b*) is a simplified form of (*a*). (*e*) is an alternative and more simple mounting than that of (*d*).

that a thick lubricant results in a greater leakage, and also that if the atmosphere around the seal is removed (by building round it a vacuum chamber and evacuating) very little change in the reciprocating leakage is observed until some minutes have elasped to allow the lubricant to de-gas. Further, on removing the vacuum and replacing the atmosphere, the original leakage does not occur until some minutes have elapsed. Seals in which the shaft has a conical motion (again about 1 rev/s, the speed of hand operation) give a leakage rate of the same order as for rotating shafts.

All the leakages quoted above are when no liquid air refrigerant is used on the test system. If liquid air refrigerant is used, the apparent leak rates are reduced to about one-tenth of the values given. Some 90% of the leak is therefore condensable and it appears to originate from the lubricant. (For this reason seals were tried without lubricant but were not a success. With rubber washers it was impracticable to move the shaft; with neoprene some movement was possible, but owing to the distortion of the washer which these movements involved, large leakages were frequent.) A more simple design of seal such as that shown in Fig. 5 has a leak rate about one-tenth of that for the seals of Fig. 3 if not too heavily greased. With care, limited rotational and rectilinear motions are possible.

Tolerances on dimensions of seals and failure of seals. Washers cut from sheet material are satisfactory, provided that the hole into which the shaft moves appears to the unaided eye to be smooth, round, and squarely cut at the edges. The washer should have a smooth surface and should not be too soft. A shore hardness of 50 to 55 appeared suitable for washers from sheet material, and a shore hardness of 85 appeared suitable for the M.I. Gaco type of seal. Shafts from glass, steel and brass were tried and all gave similar results. It is most important that the shaft surface be smooth, e.g. a stainless steel shaft which has been polished by buffing will, if roughened by fresh FF emery paper, have an increased leak rate. This increase is particularly marked for reciprocating motion, when the increase is fourfold. For reciprocating motion, circumferential markings give a higher leakage than do longitudinal markings (see Table 1). The

Table 1. *Effect of shaft roughness on leak rates of shaft seals*

Type of shaft (all silver steel)	*Static leak rate (10^{-3} l.μ/s)*		*Stroke leak (l.μ/cm of stroke)*	
	Liquid air	*No liquid air*	*Liquid air*	*No liquid air*
Smooth shaft (buffed)	0·060	0·51	0·0012	0·011
Circumferentially marked shaft	0·062	0·55	0·0061	0·052
Longitudinally marked shaft	0·082	0·46	0·0039	0·048
Standard stainless steel shaft	0·061	0·55	0·0039	0·034

The circumferential and the longitudinal marking was by fresh FF emery paper. Apiezon B oil was used as a lubricant. The seal type is shown in Fig. 3(*d*).

diameter of the shaft is not critical, but, for example, in the case of a $\frac{3}{8}$ in. diameter shaft it should be to within $\pm\frac{1}{32}$ in. of its correct size.

In all, about 30 seals were tested. Each was given several thousand reciprocating strokes of 5 cm length, and a similar number of rotations. Some seals were kept assembled for two months. No failure of any kind occurred or was suspected at room temperature.

Tests at 120° *C.* Tests made at 120° C indicated that, except for the spring-loaded seals, failure began after some two days' heating. Neoprene lubricated with silicone high vacuum oil appeared to last rather longer than did other combinations. The spring-loaded type of washers, of which four were tested, gave a definitely better performance. Two were tested for 100 h, and two for 200 h, each at 120° C, and in no case did a failure occur. Rather more frequent lubrication is, however, needed at this temperature, and during periods of a few hours when the shaft is stationary the washer tends to stick to the shaft. It is best freed by a rotation of the shaft. The static leakage rate for the spring-loaded washer, during the first few hours of heating is increased some twenty times and falls to five times after 48 h of heating.

The reciprocating leak is not much affected, being increased by a factor of about two.

Construction of seals and effect of side thrust. The design of seals should be considered from the point of view both of simplicity of construction and of the ability of the seal to fulfil its purpose. Seals without the 30° lip behind the washer are simplest to manufacture and work well, but the hole behind the washer must not be too large as otherwise on inserting the shaft the washer will bulge inwards and not outwards as is preferable. If, however, the shaft is to be used at an

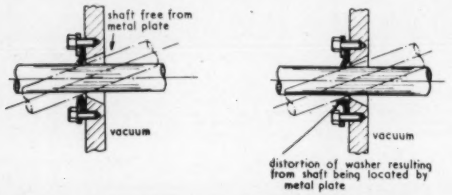

Fig. 4. Diagrams showing the reduction in distortion if the washer itself can locate the shaft and take the side thrust

angle to the seal and the washer itself is insufficient to deal with the side thrust, then the metal support, with a 30° lip, should be as close to the washer as possible to prevent washer distortion. In cases where the side thrust on the washer is small enough for the washer to do the locating, it is best not to use the lip, since washer distortion is then reduced (see Fig. 4). The simplest and most satisfactory seal seems to be the Gaco M.I. type mounted as in Fig. 3(*e*); but if mounted in a housing [Fig. 3(*d*)], it should not be a tight fit, as otherwise it becomes difficult to remove for replacement. The tightening screw should not be jammed too tight, and if the seal is used at say 100° C this screw is frequently found loose when the seal is cooled. This loosening is the result of

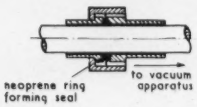

Fig. 5. A seal with a low gassing rate and suitable for occasional movements

expansion of the seal material, and if remembered and taken up no trouble occurs, but where repeated heating and cooling are to take place, it is better to insert a thrust spring between the seal insert and the tightening screw. Shafts should always have their ends tapered for about the first $\frac{3}{8}$ in. to allow them to be re-inserted in the seal without damage to the washers.

Some seals are fitted with two washers, the space between which can be evacuated. The space is generally called the pump-out space and it is useful at times to test the seal for leakage. Evacuation of this space is not always a temporary cure for a leaky first washer, as the pumping speed at the pump-out is low and air tends to leak in *via* the threads of the clamping screw and past the edge of the second washer. It is often overlooked that a leak in a simple seal [e.g. Fig. 3(*a*)] can often be made tight by a fillet of Apiezon Q between the shaft and the washer.

2. GASSING RATES AND PERMEABILITY OF RUBBER, NEOPRENE AND BUTYL RUBBER

A vacuum system may be impaired in two ways by the use of rubber, namely by gassing from the material due to vaporization and possible gas pockets; and by permeability, that is the passage of the atmosphere through the pores of the material into the vacuum system. The gassing effect (for continuously pumped systems) is found in general not to be serious, except perhaps for the first hours of pumping, but the permeability leak can be very much greater and often prohibits the use of rubber diaphragms and bellows on high vacuum systems. A good deal of work has already been done on the permeability of rubber and rubber-like materials[2, 3] at pressures of about 1 mm of mercury. The permeability varies considerably for different substances—neoprene, for instance, has a permeability of about one-tenth that of rubber. Also the passage of gas through the material involves a considerable time-lag, which for a $\frac{1}{16}$ in. thick diaphragm may be from a few minutes to about an hour before any effect is manifested on the gauges. Some further experiments on the permeability were made by the author and they showed that, using vacua of better than 5×10^{-5} mm of mercury, this time-lag was still clearly marked. The permeability values were also in good agreement with those given in ref. (2). Attempts to reduce the permeability leak by covering the surface with, for example, a "high vacuum paint" proved unsuccessful.

Gassing rates (tests on four rubbers). Some 100 cm^2 of material were cut to random shapes from $\frac{1}{16}$ in. thick sheet and were placed in a 150 cm^3 flask on a vacuum system, and the gassing recorded as time proceeded. At first the gassing fell rapidly but later the rate decreased. For example, a square centimetre of $\frac{3}{16}$ in. thick rubber at the end of the second hour, seventh hour and seventieth of pumping gave off gas at the rate of 1×10^{-3}, $0{\cdot}5 \times 10^{-3}$ and $0{\cdot}01 \times 10^{-3}$ l. μ/s respectively. The materials tested were natural rubber type J.1260 from Premier Waterproof and Rubber Co. Ltd.; cured rubber, loaded with 25% by weight of carbon black, from Greengate and Irwell Rubber Co. Ltd.; neoprene GN from Spencer Moulton and Co.; and butyl of code number BU. 12000, from Firestone Tyre and Rubber Co. All these materials gave a higher gassing rate than did rubber, and particularly so the neoprene which was up by a factor of 10. If a liquid air refrigerant trap is used in the system, some 95% to 99% of the gases are removed from the system. It is evident from this that, with liquid air refrigerant efficiently employed, the pressure increase from rubber used totally within a vacuum system is often much less than usually believed. Figs. 6 and 7 give detailed information of the gassing of two of the four materials tested, and includes also information on the pump-down time of a previously evacuated sample after exposure to dry air. These results, except for the top chain line of the graphs, were taken by isolating the vacuum system from the pumps and noting the time required for the pressure to rise by 10^{-4} mm of mercury. (During the first part of the curve, when the gassing was relatively large, the pressure rise used was more than 10^{-4} mm of mercury, but this is not of importance.) The time for this rise, together with the volume of the system, enables the gassing rate to be determined. Since, however, other experiments showed that the gassing rate tends to increase as the pressure falls, it is of importance to measure

the gassing at pressures usually met with in vacuum systems, say around 10^{-5} mm of mercury. Thus during the latter part of the gassing curves for rubber, the base pressure was considerably less than 10^{-4} mm of mercury, and the gassing rate at the base pressures was measured by taking the product of the base pressure and the speed of pumping. These results are shown by the chain curves at the top of Figs. 6 and 7, and besides giving the gassing rate at lower pressures (marked along the curve) they provide a useful check on the results given by the first method.

This second method was not applied to the system when liquid air refrigerant was used. Only the isolation method was used but pressure rises of a lower value (around 2×10^{-5} mm of mercury) could be measured when liquid air was employed, firstly because the rate of pressure rise

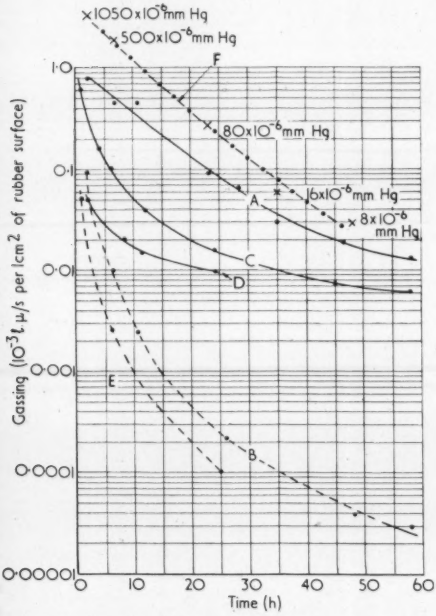

Fig. 6. Gassing rate for natural white rubber type J.1260

A, total gassing (initial curve); *B*, non-condensable gassing (initial curve); *C*, repeat of *A* after 24 h exposure to air; *D*, repeat of *C* after $\frac{1}{2}$ h exposure to air; *E*, repeat of *B* after $\frac{1}{2}$ h exposure to air (the repeat of *B* after 24 h exposure coincided closely with *B*); *F*, total gassing (second method) same experiment as curve *A*—figures give pressure at which gassing was measured.

was slower and secondly because tap gassing difficulties encountered when no liquid air is used (see Section 4) were absent.

Permeability experiments. Membranes of two thicknesses, $\frac{1}{16}$ in. and $\frac{1}{8}$ in., were used, and were mounted to form a wall of the vacuum enclosure. The experiments showed that the gas flow through the membrane was approximately inversely as the thickness, for the two thicknesses used. The outside of this diaphragm could be in contact with an atmosphere of gas, e.g. oxygen, nitrogen, by filling an auxiliary

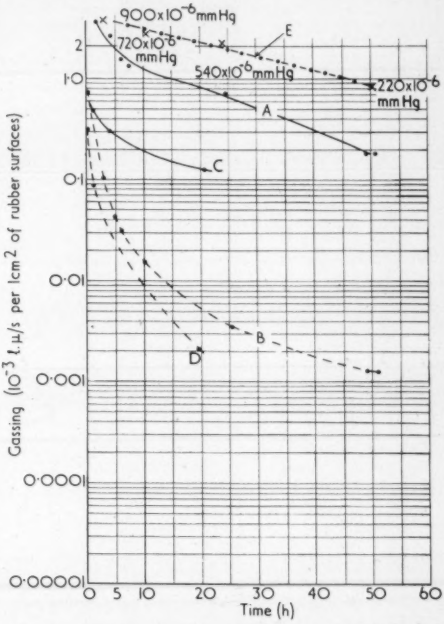

Fig. 7. Gassing rate for rubber loaded with 25% by weight carbon black. Neoprene is very similar. Butyl is also similar although its total gassing is rather less

A, total gassing (initial curve); *B*, non-condensable gassing (initial curve); *C*, repeat of *A* after $\frac{1}{2}$ h exposure to air; *D*, repeat of *B* after $\frac{1}{2}$ h exposure to air; *E*, total gassing (second method) same experiment as curve *A*—figures give pressure at which gassing was measured.

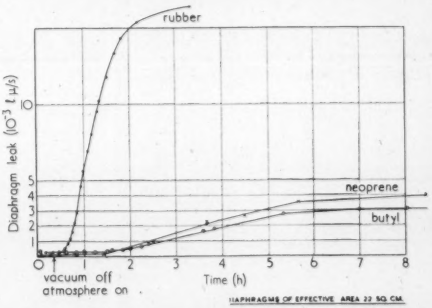

Fig. 8. Passage of air through $\frac{1}{16}$ in. thick diaphragms of effective area 22 cm²

gas chamber on the atmospheric side of the diaphragm. Liquids, e.g. high vacuum oils, could also be substituted for the gases, or, in other circumstances, the auxiliary chamber could be evacuated. The membrane was $3\frac{1}{4}$ in. diameter and supported by a perforated plate containing $\frac{3}{16}$ in. holes and having a hole area of 22 cm^2. The results are shown in Figs. 8, 9 and 10.

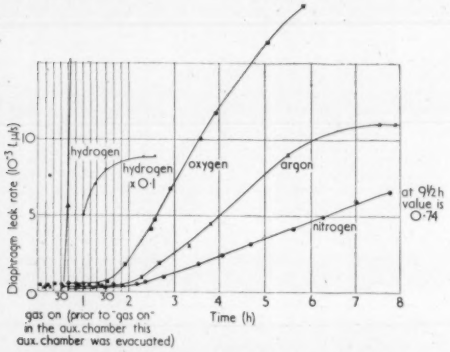

Fig. 9. Passage of gases through $\frac{1}{8}$ in. thick rubber diaphragm (J.1260) of effective area 22 cm^2. (Air calibration of Pirani used throughout)

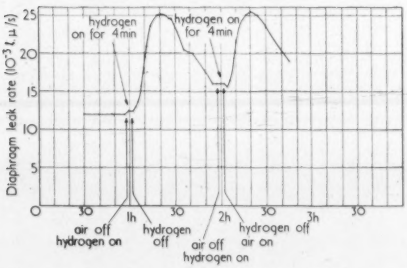

Fig. 10. Experiment on $\frac{1}{8}$ in. thick rubber (J.1260) (similar to Fig. 9 except that the hydrogen replaced the atmosphere for four minutes only)

Note: The rising curve if hydrogen is left on reaches a value of 82 l. μ/s.

3. HIGH VACUUM FLANGED JOINTS

In testing these joints the same method, i.e. the pressure rise in a closed vessel using a Pirani gauge, was used. The object was to determine the effect of joints on a small vacuum system, especially during the first few hours of pumping when their gassing may be confused with an air leak in the apparatus. Tests were also made on a silastic gasket in the hope that it might provide a suitable joint for working at temperatures of some 200° C to 300° C. At 300° C it appeared that a life of some 50 h could be expected; failures were the result of small holes appearing in the material causing it to become porous. This porosity may develop from faulty manufacture. The gassing at 300° C was considerable.

Room temperature experiments (*Figs.* 11 *to* 15). For experiments on rubber gaskets and neoprene gaskets, two types of flanges were used: flat smooth flanges and flanges

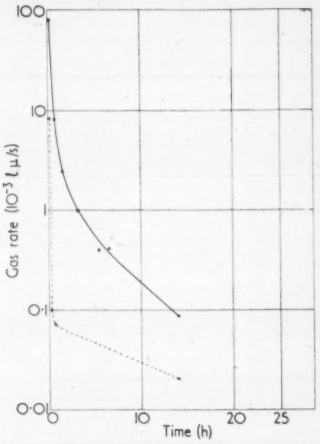

Fig. 11. Blank test of flange apparatus. The flange is removed and the glass system sealed off

Full curve, total gassing; broken curve, non-condensable.

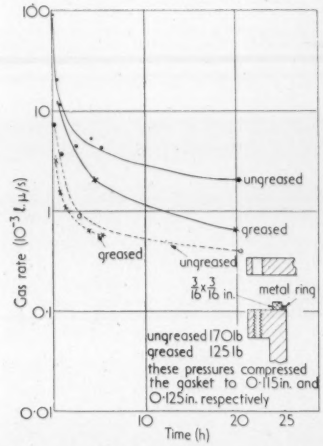

Fig. 12. Gassing rate for rectangular white rubber ring (see insert). Gasket diameter $1\frac{1}{2}$ in.

Full curves, total gassing; broken curves, non-condensable.

which fully trap the gasket by the tongue and groove method. The finished surfaces of the flanges were obtained by machining smooth and rubbing down with F grade emery paper on a surface plate. A similar surface was given to the tongue

and groove joint by finishing with F emery paper while the flange was in the machining lathe.

The gaskets used were all 1½ in. in diameter and of various

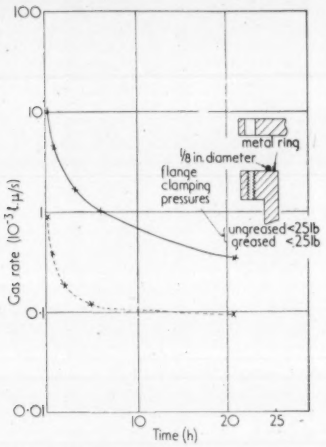

Fig. 13. Gassing rate for ⅛ in. round white rubber (see insert). Gasket diameter 1½ in.

Full curve, total gassing; broken curve, non-condensable.

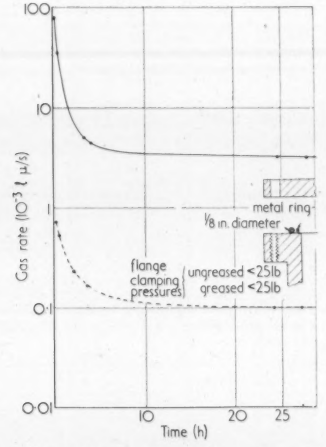

Fig. 14. Gassing rate for ⅛ in. diameter neoprene (see insert). Gasket diameter 1½ in.

Full curve, total gassing; broken curve, non-condensable.

rectangular and round sections. The materials had a shore hardness of between 40 and 50. Gaskets of a broad section, say $\frac{3}{16}$ in. thick and ½ in. wide, were not so satisfactory as gaskets less wide, say of section $\frac{3}{16} \times \frac{3}{16}$ in., owing to the greater clamping force which the former required for a tight joint. (By "tight" is meant the state when further flange pressure causes no observable change in the leak rate.) With gaskets of circular section the clamping pressure, as might be expected, was considerably less, being some 25 lb wt instead of the 200 lb wt required for the $\frac{3}{16} \times \frac{3}{16}$ in. square section. The circular gaskets were very satisfactory as vacuum seals, but if they were jammed tight they tended, after several days, to split round their periphery and so lose their effectiveness. To a very minor extent this was occasionally noticed on rectangular gaskets between flat flanges. The circular sectioned gaskets were, however, very useful for flanged glass apparatus where low clamping forces were

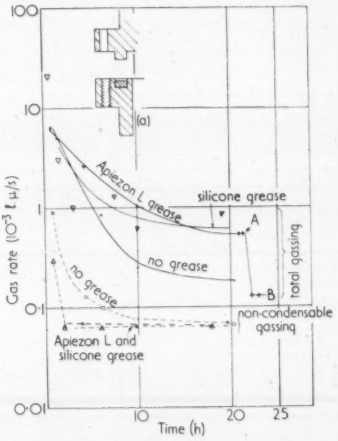

Fig. 15. Gassing rate for recessed flange white rubber (see insert). Mean gasket diameter 1½ in.

●, total gassing (no grease); +, total gassing (grease); ▽, total gassing (silicone); ○, non-condensables (no grease); ×, non-condensables (grease); △, non-condensables (silicone).

Note: At *A* the seal was heated to 70° C for 2 min and allowed to cool. After 15 min the gassing value was steady at *B*.

preferred. With all gaskets, provided the flange unevenness is not too great, the thinner the gaskets, or in the case of the gaskets of circular section, the smaller the section diameter, the less is the rate of gassing due to vapours from the rubber itself. The gassing from neoprene gaskets is several times that from rubber.

The effect of gasket grease. The effect of greasing the gasket is to reduce leakages resulting from insufficient flange clamping pressure: it seems to have no obvious effect on the leak or gassing rate of the so-called tight joint. Further, grease reduces by only a small amount the clamping pressures required for a joint clamped to the extent that it is called vacuum tight. The lubrication properties of grease (Apiezon L was used) caused frequent trouble when flat flanges were used. Thus all gaskets having ⅛ in. round or $\frac{3}{16}$ in. square sections invariably buckled inwards under the vacuum when greased and used on flat flanges. A small metal ring of sectional diameter about two-thirds that of the gasket placed within the gasket prevents this and yet does not complicate

the joint. There is also a tendency for these greased gaskets to increase in diameter owing to pressure between the flanges. This can be prevented by a metal ring placed round the outside of the gasket. In general, however, troubles from this expansion of the gasket indicate excessive clamping pressure. It is sometimes worth remembering that Apiezon B oil on gaskets has a similar effect to Apiezon L grease and is not nearly so slippery. Figs. 12 to 15 give drawings of the flanges and gaskets tested; the pressure figures indicate clamping pressures beyond which an increase gives no further reduction of the leak rate.

By reducing the pumping speed between the gasket and the vacuum system it was hoped that the resulting increase of gas pressure at the gasket might bring about a lower gassing rate from the gasket. To test the effect of the increases of gas pressure on gasket materials experiments were tried in which 100 cm^2 of the material (in the form of $\frac{1}{16}$ in. sheet) were placed in a 150 cm^3 flask which could be evacuated either through a $\frac{1}{4}$ l./s pumping line or through a $0{\cdot}13 \times 10^{-3}$ l./s pumping line. The results showed that except during the early stages of the outgassing from neoprene (a substance of relatively high gassing rate), the rate of gassing was much the same whichever of the two pumping speeds was used, and that unless pressures of some tens of microns were developed by the restrictive pumping, no advantage could be obtained. Further, the restrictive pumping would prolong the time required for the main out-gassing of the gasket. It can therefore be inferred that this is not a satisfactory method by which gasket performance can be improved.

High temperature experiments at 200° C to 300° C. The only possibility at present of a rubber substance for a gasket at 250° C is a silastic material. Its chief drawback is the tendency to flow under stress and, because of this, the tests were made using the gasket fully trapped in a groove. It was soon found that the gasket expanded considerably on heating, the amount for a rise from 20° C to 300° C requiring a motion of about 0·01 in. in the flange spacing for a gasket 0·0625 in. thick. If this motion was not allowed for, the joint invariably became slack when cooled to room temperature. The expansion was allowed for by loading the clamping bolts with Terry springs of outside diameter 0·3 in. made from steel wire 0·06 in. in diameter. Each produced a pressure of 28 lb wt when cold, so that with the atmosphere and six springs a total clamping pressure of 195 lb wt was obtained. When the seal was hot, care was taken that the heat did not reduce too much of the tension. The gasket was cut from $\frac{1}{16}$ in. sheet silastic material by scissors and fitted to the female groove. Before assembling it was smeared with a thin layer of silicone high vacuum grease.

The added complication of the expansion with temperature made it seem advisable to subject the joint to a few temperature cycles during test to be sure that the joint remained sealed. In all, three gaskets were tried, the first with the flange not spring loaded. If the repeated tightening necessary with each cooling be disregarded the results for the first gasket agree tolerably well with those for the other two, whose flanges were spring loaded.

The experiment was divided up into eight periods which were alternatively a period of 2 h at room temperature and a period ranging from 10 to 25 h hot. The hot gassing rate was 0·21. μ/s falling to 0·06 l. μ/s towards the end of the experiment. Some 90% of this gas was condensable by liquid air. At 300° C failure was at the end of 70 h and rapidly developed so that at 74 h the vacuum system would not pump below 10^{-2} mm of mercury. An examination of the gasket showed this failure was caused by about half of the total material used in the gasket becoming filled with tiny holes giving the appearance of a fine sorbo rubber. The second gasket with spring-loaded flanges was subjected to a temperature of 200° C. At this temperature no failure occurred and the experiment was terminated after a total of 100 h of heating.

4. NOTES ON THE EXPERIMENTAL APPARATUS AND PROCEDURE

It would be inappropriate to conclude this paper without mention of the precautions taken to ensure reliable data. An example of a possible source of error is the 0·8 mm bore glass tap greased with Apiezon L, which is employed for isolating the system from the pumps when measuring the rate of rise of pressure. Blank experiments showed the gas from these taps is small compared with the substance under test, provided the following points are remembered: (1) when on an evacuated system the tap should be turned a few times a day; (2) where the system is let up to atmosphere for about an hour the tap, when again under vacuum if warmed and turned a few times to recondition it, will give a low gassing rate 2 to 3 h after pumping commences; (3) a freshly greased tap has to be pumped some 50 h to obtain a low gassing rate and here as always warming by hot air and turning the tap helps greatly in removing gas. The experiments indicated that at pressures below $\frac{1}{2} \times 10^{-4}$ mm of mercury the gassing from taps appeared to increase rapidly. The reason for using a tap and not a mercury cut-off is that the latter requires liquid air refrigerant and this is inadmissible if the total gassing from materials is to be measured.

The apparatus used for the measurements is given in Fig. 1 where it is shown fitted with a seal under test at C. To determine a leak rate tap *T* is closed and the necessary motions of the seal made, when from the rise of pressure and the volume of the apparatus the leakage can be determined. For convenience, liquid air refrigerant is applied by immersion of the appendage. There is an advantage of using this type of trap in that the speed of pumping through the system is not reduced, but care must be taken to make the appendage wide enough. The condensable vapours are usually present in ten to fifty times the amount of the non-condensable gases, and hence the speed of the appendage trap at its junction with the main pipe line should be at least this number of times faster than that of the main pump at this same point. The permeability of materials to gases was measured by using the air calibration of a Pirani gauge and hence, e.g. the response to hydrogen was favoured. In the other experiments, some of the lower base pressures were measured by an ionization gauge, although in general a Pirani gauge and mirror galvanometer were used.

The apparatus of Fig. 16 was designed to measure simultaneously the condensable and the non-condensable gases. In the first section of the apparatus the total gassing was measured by the usual methods, and in the second section, denoted by volume 2, the non-condensable gassing was measured. Since the gas flow through pump 1 was independent of the pressure in volume 2, it was evident that volume 2 behaved as though vessel *A* were connected directly to it. Tests were made on this system using a Metropolitan-Vickers O2 diffusion pump for pump 1 (an oil pump was necessary because liquid air refrigerant, if used on volume 1, tended to complicate the measurement of the condensable vapours from the substances under test) and a glass mercury diffusion pump for pump 2, which was backed by a suitable rotary

pump. In using the apparatus there was a danger that some of the vapour passing through pump 1 might be decomposed by collisions with hot oil molecules and produce non-condensable gases which would be recorded by volume 2 (e.g. if methane were formed it would so behave since its vapour pressure at liquid air temperature is 90 mm of mercury). Hence tests were performed by measuring the non-condensable

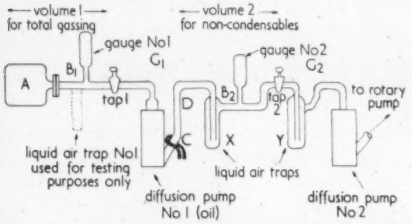

Fig. 16. Apparatus for measuring simultaneously condensable and non-condensable vapours from a sample of material

C, additional water cooling; *D*, wide bore pipe.

gassing rate in volume 2 and then checking it in volume 1 by applying liquid air refrigerant to the trap (shown dotted in Fig. 16) attached to volume 1 especially for this purpose. The results gave agreement to about 10%.

The following details are important for good performance of an apparatus of this type:

(i) The liquid air trap *X* must be fast, giving a speed, for vapours, at least 100 times that of pump 2 at B_2. For this reason a conventional trap should be used and not an appendage type, unless two of the latter are used in series.

(ii) The closer trap *X* is to pump 1, the lower the pressure will be in pump 1 and the less its oil will gas into volume 2 on a sudden reduction of pressure in the pump (e.g. if tap 1 be closed to record a zero on gauge 2).

(iii) Liquid air trap *Y* should be used even if pump 2 is an oil pump since pressures at G_2 are often very low.

(iv) The effects of gassing from pump 1 must be considered, as the non-condensable constituent is recorded by G_2. The result of tests made on this point can be summarized as follows. On closing tap 1 the gas flowing through the system from vessel *A* is stopped, and the immediate non-condensable gassing from pump 2 is then 5% to 10% of the non-condensable gas flowing from volume 1 to volume 2 prior to closing trap 1. If this tap is kept closed, so that there is no load on the pump, then after an hour the gassing from the isolated pump is relatively low. Pumps which have been left at atmospheric pressure require some 24 h of use before low gassing rates are obtained. The magnitude of this effect on the apparatus can be reduced by using as small a pump as convenient and also by under-running the heater, a legitimate action since the backing pressure is low.

REFERENCES

(1) WILSON, R. R. *Rev. Sci. Instrum.*, **12**, p. 91 (1941).
(2) VAN AMOONGEN, G. J. *J. Appl. Phys.*, **17**, p. 972 (1946).
(3) RIDDLE, G. L. *Chem. Industr.*, p. 36 (1947).

Correspondence

The γ-ray scintillation spectrometer

An earlier paper[1] describes the use of a two-crystal scintillation spectrometer in the analysis of the γ-ray spectrum of a mixture of fission products. Since the work was completed certain refinements have been made to the original design of the spectrometer; these are described briefly below.

The two-crystal spectrometer operates by the subtraction of the Compton spectrum in an anthracene crystal from the combined photoelectric and Compton spectra in a sodium iodide crystal. In this way each energy from a mixture of γ-ray emitters is characterized by a photoelectric peak alone, in the region below 2 MeV. Although the Compton continua in the two crystals could be matched at the higher energies in this region, there was a slight degree of mis-match at the lower energies. This is due to re-capture of scattered quanta, increasing with decreasing energy, in the sodium iodide crystal. In this crystal the total absorption peak is thus increased at the expense of a reduction in the height of the Compton continuum. It has been found that the effect of this secondary process may be compensated by placing an absorber before the anthracene crystal. For sodium iodide and anthracene crystals of length 1 in. and diameter 1·5 in., a lead absorber of thickness 0·15 in. introduces the necessary selective attentuation of radiation incident upon the anthracene crystal without interfering with the photoelectric (or total absorption) spectrum in the sodium iodide crystal.

As previously reported,[1] both crystals exhibit a negative temperature coefficient of pulse amplitude. For the combination of crystal and photomultiplier tube (E.M.I. type 6097) typical values of the coefficient are 0·1% per °C and 0·5–1·0% per °C for sodium iodide and anthracene crystals respectively. These values conform with those reported by Ball and others[2] in a recent paper. Since the effect of temperature is appreciably greater for anthracene than for sodium iodide it has been found desirable to protect the two crystals from marked changes in laboratory temperature. This has been achieved quite simply by enclosing both the counters and the counter mounting in a Perspex box (dimensions approximately 1 × 1 × 2 ft high) fitted with a hinged door for access to the sample platform. The interior of the box is maintained (to within 0·3° C) at a few degrees above normal room temperature by two 40 W electric lamps controlled by a stem type of thermostat. Mixing of the air within the box is by convection promoted by slots and holes at the top and bottom.

The two-crystal spectrometer operates with a single-channel pulse amplitude analyser and recording ratemeter. The channel of the analyser, previously kept at a constant width, is now made proportional to pulse amplitude (i.e. to energy). This is achieved by setting the pulse analyser to a constant bias voltage and by varying the attentuation of the pulse amplifier according to the rotation of the recorder chart. In a simple practical arrangement a wire-wound variable resistor R, coupled to the recorder chart, is connected between the head amplifier and main amplifier (A.E.R.E. type 1049B). Linearity of energy scale is preserved over the range $R \gg r$ where r is the input impedance of the main amplifier. This arrangement may be used without modification to existing amplifiers; an alternative version might introduce the variation of attenuation, or gain, at a higher level of pulse amplitude, i.e. within the main amplifier. The use of a constant relative channel width is attractive because of the following advantages: (i) the magnification of low γ-ray energies, due to the increase of crystal efficiency with decreasing energy, is less exaggerated; (ii) the low energy peaks are no longer distorted by channel widths comparable to the peak width; and (iii) all pulses are accepted by the analyser at a constant height. Spectrometer recordings illustrating this method of varying channel width have been reported elsewhere.[3] A spectrometer using a constant relative channel width has been recently described by Astrom.[4] In this method the bias voltage is varied by potentiometer in the conventional manner. The potentiometer also varies the lower level of the channel by a fixed proportion of the bias voltage.

Atomic Energy Research Establishment, Harwell, Berks.

D. H. Peirson
P. Iredale

[26 June, 1957]

REFERENCES

(1) Peirson, D. H. *Brit. J. Appl. Phys.*, **6**, p. 444 (1955).

(2) Ball, W. P., Booth, R., and MacGregor, M. *Nuclear Instruments*, **1**, p. 71 (1957).

(3) Peirson, D. H. *Atomics*, **7**, p. 316 (1956); Iredale, P. *A.E.R.E. Memorandum No. EL/M96* (London: H.M.S.O., 1957).

(4) Astrom, B. *Nuclear Instruments*, **1**, p. 143 (1957).

Scaling laws for space charge dynamics

In a note published on p. 44 of the January issue of this *Journal*, Haine derives some scaling relations for electron optical systems in which the current is space-charge limited. The scaling relations for a space-charge limited current within electrode systems of arbitrary shape were first stated by Langmuir and Compton.[1] Since then these relations have been restated in more detail by Hamaker,[2] Meltzer,[3] and Reifenschweiler[4] for the general case where the current is either completely or partially limited.

Briefly, the scaling laws are as follows. We assume that a steady state electron flow has at any point a single-valued velocity, that the speed is non-relativistic, and that the self-magnetic field can be neglected. If now all dimensions are scaled by a factor α, the electrode potentials by a factor β, and e/m (charge to mass ratio of the particles) by a factor γ, the particle trajectories will remain unaltered in shape, provided that both the current density and the velocity at the electrodes are scaled by the factors $\alpha^{-2}\beta^{3/2}\gamma^{1/2}$ and $\beta^{1/2}\gamma^{1/2}$ respectively. These scaling relations are identical with those applying in the absence of space charge, with the addition that the current density must vary as $\alpha^{-2}\beta^{3/2}\gamma^{1/2}$. Furthermore, these relations apply independently of whether the current is completely or partially space-charge limited.

In one form or another these scaling relations are well known[5,6] and are of particular importance in the study of ion sources and ion beams.[4,7] For example, as an initial aid in the design of a 500 keV d.c. accelerator having an equivalent proton beam current of 25 mA,[8] an electron

model was constructed in which the dimensions were scaled 1/5 and the potentials 1/100, and the electron beam current was approximately 1 mA.

Atomic Energy Research Establishment, Harwell, Berks. E. R. HARRISON

[8 February, 1957]

REFERENCES

(1) LANGMUIR, I., and COMPTON, K. T. *Rev. Mod. Phys.*, **3**, p. 273 (1931).
(2) HAMAKER, H. C. *Physica*, **9**, p. 135 (1942).
(3) MELTZER, B. *Proc. Phys. Soc.* [*London*] *B*, **42**, p. 813 (1949).
(4) REIFENSCHWEILER, O. *Ann. Phys.* [*Leipzig*], **14**, p. 33 (1954).
(5) SPANGENBERG, K. R. *Vacuum Tubes*, p. 181, 1st Ed. (New York: McGraw-Hill Book Co. Inc., 1948).
(6) IVEY, F. H. *Adv. Electronics Electron Phys.*, **6**, p. 137 (1954).
(7) THONEMANN, P. C. *Progr. Nuclear Phys.*, **3**, p. 219 (1956).
(8) HOBBIS, L. C. W., HARRISON, E. R., and WHITBY, H. C. To be published.

New books

Thermodynamic functions of gases. Vols. 1 and 2. Edited by F. DIN. (London: Butterworth's Scientific Publications, 1956.) Vol. 1. Pp. viii + 175. Vol. 2. Pp. vi + 201. Price 63*s*. each.

To the technologist and process designer in the field of industrial gases the thermodynamic diagram has the importance of a chart to the navigator, and it should be adequately reliable for all practical purposes. Once an accurate thermodynamic diagram has been constructed for a particular gas it should be valid for all time and of value to all users. The construction of a diagram with claims to accuracy is therefore both a heavy responsibility and a public service. It was to provide this service that the Department of Scientific and Industrial Research decided to sponsor a Committee to organize the preparation of reliable thermodynamic diagrams for all important industrial gases. The two volumes now published, nearly ten years after the birth of the Committee, report the painstaking work of members of four research organizations, two academic and two industrial, who between them have prepared thermodynamic diagrams for eight gases. Vol. 1 describes the work on ammonia, carbon dioxide and carbon monoxide, while Vol. 2 deals with air, argon, acetylene, ethylene and propane. Large-scale diagrams on a temperature-entropy basis are published separately at a modest price. A foreword to Vol. 1 is contributed by Prof. D. M. Newitt, Chairman of the Thermodynamics Committee, and the work of General Editor has been performed by Dr. F. Din of The British Oxygen Company who has written an instructive introductory chapter and has also been responsible for three of the surveys. The remaining surveys have been prepared by members of the research organizations of Imperial College, Leeds University and Imperial Chemical Industries Ltd.

The authors would be the last to claim that their work is final or complete. The first necessity for the preparation of a reliable thermodynamic diagram is the availability of accurate and comprehensive experimental data but the surveys have disclosed large gaps in the necessary information which experimental physicists should be encouraged to close. Accurate experimental determination of gas properties is a difficult matter but the authors appear to have been troubled by surprisingly few serious discrepancies. Careful discrimination has been necessary, however, in selecting experimental data, deriving other properties by means of thermodynamic relations, filling gaps and smoothing the surfaces so as to present a thermodynamically consistent whole. The survey reports which describe the preparation of the diagrams invest them with an authority not possessed by earlier charts. In each case the authors have attempted to estimate the margins of uncertainty attaching to their work, and it is to be hoped that the diagrams will not be indiscriminately used without reference to the text.

The work is described in the preface as preliminary. Prof. Newitt hopes that it will stimulate further research and promises that it will be carefully reviewed and amended where necessary to provide the basis for a final authoritative compilation of thermodynamic data which will meet with international acceptance. There can be no finality about a work of this sort but one hopes that it will be regularly reviewed and extended so as to become a standard work of reference. It is obviously easy to find grounds for criticism of the first edition, but critical comments should be regarded as suggestions for future improvement rather than as a reflexion on the present work. The choice of units has been left to the individual authors with the result that the same property for different substances is variously expressed in joules/mole °K, calories/mole °C and Kcals/kg °K. It is particularly confusing to the user of the tables to find pressures in bars in one case and atmospheres in others. When temperatures are spaced at 10° intervals cross-reference becomes difficult when °K and °C are used in different cases. The reference points are likewise inconsistent. Although it may not be possible for lack of data to fix the zero of entropy and enthalpy at 0° K in every case it is regrettable to find, in the case of ethylene, a choice of reference point which gives rise to negative values of entropy and enthalpy.

Few errors have been noted, but it may be pointed out that, in Table 5, Vol. 2, p. 29, the upper limit of ΔS should be at $P = 200$, instead of $P = 100$. On p. 9 of the same volume there is a spelling mistake which it might be 'discreet' to ignore. Apart from these no more serious errors have been noticed than a few misplaced commas and the work has clearly been edited with care. A. M. CLARK

Statistical mechanics. By T. L. HILL. (London: McGraw-Hill Publishing Co, Ltd., 1956.) Pp. xiii + 432. Price 67*s*. 6*d*.

A considerable number of books on statistical mechanics have appeared in recent years to which the present one makes a very welcome addition because its main part is devoted to a detailed and systematical treatment of the theory of dense fluids and the transition phenomena.

The first chapters give an introduction into the equilibrium theory of classical and quantum statistical mechanics and thermodynamics which uses elegant advanced mathematical methods, but is likely to discourage readers who have not already acquired a fairly good knowledge of the subject. This introduction is followed by a comprehensive presentation of fluctuation theory whose main object seems to be to show that fluctuations of thermodynamic parameters are "insignificant in magnitude and, consequently, of little interest or importance in thermodynamics and statistical mechanics". This sounds rather odd, considering the immense practical

part fluctuations play nowadays in the limitation of the accuracy of measurement of such parameters. The rest of the book deals most expertly with imperfect gas and condensation theory, distribution functions, co-operative phenomena, and the free volume and hole theories of liquids and solids.

The main emphasis throughout the book is laid on recent progress in these fields, which makes the book particularly useful for research workers in statistical physics and physical chemistry. It is regrettable, however, that practically no mention is made of the tremendously important and fundamental contributions to the development of statistical mechanics and fluctuation theory by Einstein, Ehrenfest, Smoluchowski and others whose names are not even to be found in the index. In the reviewer's opinion the author would do well to add a chapter on non-equilibrium statistical mechanics in a future edition, at the expense of details in the main part of the book which are not strictly essential for the argument.

R. FURTH

Table of the Fresnel integral to six decimal places. Compiled by T. PEARCEY. (London: Cambridge University Press, 1956.) Pp. 63. Price 12*s*. 6*d*.

The Fresnel integral occurs in wave problems in theoretical physics, notably in diffraction. The two components $C(u) = \int_0^u \cos\frac{\pi t^2}{2}\,dt$ and $S(u) = \int_0^u \sin\frac{\pi t^2}{2}\,dt$ when compounded and projected on to the plane $t = 0$ give the Cornu spiral which has long been used as a graphical means of calculation in diffraction problems.

The present table uses x as argument, where $u = \sqrt{\frac{2x}{\pi}}$, giving six decimals for x from 1·0(0·01)50·00 and seven for x from 0(0·01)1·00. C and S are side by side in the same table. Second differences are recommended, and given, for interpolation; the necessary table of proportional parts appears at the end of the book. Previous tables do not cover such a range of x.

The whole is well produced (in Australia by the Commonwealth Scientific and Industrial Research Organization) with a comfortable format and in accordance with modern standards of table making.

E. D. VAN REST

Physical techniques in biological research. Vol. 2. Physical Chemical Techniques. Edited by G. OSTER and A. W. POLLISTER. (New York: Academic Press Inc.; London: Academic Books Ltd., 1956.) Pp. xv + 502. Price 92*s*.

This is the second of a series of three volumes describing techniques derived from physics and physical chemistry which may be applied to problems arising in researches on biological systems. Each description follows along the same general lines. The theoretical basis of the method is outlined in a simple manner, followed by practical details of instruments and technique, together with examples illustrating the application to problems of biological interest.

Broadly, the central problems of interest in the biological field concern the nature of the molecules and the structure of the macromolecules comprising biological tissues, their localization within the tissue, and ultimately their interaction, partly as organized aggregates, during physiological processes (e.g. cell division and tissue formation). Vol. 2 deals mainly with techniques for studying the first group of problems. Thus Chapter 5 (N. Applezweig and T. F. Cleary) introduces the powerful technique of chromatography which may be used for the separation and quantitative assay of chemical components derived from the highly complex mixture in tissues. These authors succinctly comment that with the exception of the microscope it is hard to conceive of a more useful tool to the biologist than chromatography. A section is devoted to the application in steroid research. The techniques of electrophoresis, according to which molecules may be separated into classes depending on their total surface charge by suitable application of electric fields are clearly described by K. Stern (Chapter 6). An authoritative account of sedimentation, diffusion and viscosity in solutions of macromolecules is given in Chapter 3 by A. Ogston, an exception to the otherwise all-American authorship of this volume. The principles of the methods and the type of information obtainable, namely particle mass, shape and volume, are made clear. There is a brief introduction to the study of biological macromolecules by X-ray diffraction methods (G. Oster, Chapter 9). Recent results, obtained by this technique, for the structure of desoxyribosenucleic acid has proved to be a great stimulus to all workers interested in the functioning of the gene. Magnetic methods for elucidating certain aspects of molecular structure, and applied so far mainly to simple molecules, are described by Scott Blois (Chapter 8).

Recent electron microscope studies of cells have revealed a very extensive complex system of surfaces (membranes) inside the cytoplasm of cells. There is therefore interest in chemical reactions occurring at ordered arrays of molecules, and A. Rothen (Chapter 4) surveys the production and measurement of thickness of surface films, and their chemical reactivity.

There can hardly be any branch of experimental biology in which tracer techniques have not or could not be used with profit. J. Sacks (Chapter 1) outlines radioactive decay processes and the manipulation and measurement of both stable and radioactive isotopes. The production and dosimetry of ionizating radiations are described by J. S. Kirby-Smith (Chapter 2), brief reference only being made to the mode of action of radiation on chemical and biological systems. Finally, there is a detailed account of the fundamental physical chemistry of the electrical potential differences which occur in systems containing solutions of electrolytes, and also methods for potential measurements (K. S. Spiegler and M. R. J. Wyllie, Chapter 7).

These volumes, addressed mainly to biologists, are well produced and provide a comprehensive account of techniques. They will be valuable as a compact source of reference.

H. G. DAVIES

Momentum transfer in fluids. By W. H. CORCORAN, J. B. OPFELL and B. H. SAGE. (New York: Academic Press Inc.; London, Academic Books Ltd., 1956.) Pp. xi + 394. Price 72*s*.

This presentation of fluid mechanics in a single volume is both readable and thorough. The topics selected for study have been chosen for their special interest to chemical engineers: in furtherance of this plan a fair number of problems of practical importance have been worked out in numerical detail. A study of the general theory coupled with its application to workaday problems provides a sound basis for an engineering text-book. Turbulence and boundary layer theory receive full treatment and there are also adequate discussions of the Navier Stokes equations and of Bernouilli's Theorem. The body of the text avoids tensor notation but the theory of tensors is worked out in an appendix from very first principles. The final subject discussed is the relation between Correlation and Spectral Theories of isotropic

turbulence, which brings the development of the theory well up to date.

The book is attractively produced and well written: for a book of reference the price may not be altogether forbidding.

I. I. BERENBLUT

Solid state physics. Advances in research and applications. Vol. 3. Edited by F. SEITZ and D. TURNBULL. (New York: Academic Press Inc.; London: Academic Books Ltd., 1956.) Pp. xiv + 588. Price 96*s*.

The six articles in this third volume maintain the tradition of the series in that each is a self-contained work of reference on its branch of the subject. The electronic theory of solids plays a smaller part than in previous volumes, and only one of the present articles, that on Group III–Group V compounds, by H. Welker and H. Weiss, deals with it explicitly. The small effective masses and high mobilities of electrons in these compounds, which include indium-antimonide, are of considerable theoretical and practical interest. The place of electron theory is taken by statistical thermodynamics in three of the other articles. Thus L. Guttman writes on order-disorder phenomena in metals from the standpoint of pair-density functions and makes interesting comments on the nature of thermodynamic singularities at order-disorder transitions. In his account of phase changes, D. Turnbull deals mainly with the Volmer–Becker type of nucleation theory, applied to liquids and solids, and his article will be appreciated by chemists and metallurgists as well as solid-state physicists. A chemical and thermodynamical outlook also prevails in the article on relations between the concentrations of imperfections in crystalline solids, by F. A. Kröger and H. J. Vink, which deals exhaustively with the rules governing the types and numbers of electronic and point defects in crystals. Of the two remaining articles, the first—the continuum theory of lattice defects, by J. D. Eshelby—will be admired by theoreticians for its formal elegance, while the second—ferromagnetic domain theory, by C. Kittel and J. K. Galt—will be enjoyed by experimentalists as a most pleasant account of this rich field.

A. H. COTTRELL

Chemical engineering practice. Vol. 3. Solid systems. Edited by H. W. CREMER and T. DAVIES. (London: Butterworth's Scientific Publications; New York: Academic Press Inc., 1957.) Pp. vi + 534 + xvii. Price 95*s*.

This is the third of twelve volumes on chemical engineering practice of which the first two volumes have been reviewed previously. The volume deals with solid systems and is therefore primarily concerned with applications of physics to the problems and techniques of chemical engineering.

The opening section on size reduction includes chapters on principles of crushing and grinding, methods of sizing analysis, crushing and grinding equipment, the mechanics of pulverizers and special applications of grinding machines. There follows a section on screening, grading and classifying which includes chapters on tabling and jigging, flotation, sedimentation, wet classification, dense medium coal washing and air flow selection. A section on the mixing of solids is followed by a section on storage and handling of storage of solids; which includes a chapter on sampling, measuring and gauging of solids. The volume concludes with a section on cleaning gaseous media with chapters on cyclones and electro-precipitation.

The general and managing editor have maintained a sound balance in the presentation of the theoretical background and the technological applications. In this field of chemical engineering empirical data is important and the tabulations of the performance characteristics of equipment is both instructive and useful, while the detailed presentation of selected applications keeps the subject-matter in its right perspective. Equipment and techniques which have only been developed within recent years are described and the work is abreast with modern trends in technological development.

The volume contains an adequate list of references and bibliography, while diagrams and flowsheets are well set out. The overall impression is that the standard set in the first two volumes has been maintained, and that the editors have satisfactorily co-ordinated the presentation of the work.

H. THOMAS

Proceedings of the International Conference on Electron Transport in Metals and Solids. Held at the National Research Laboratories, Ottawa, September 10–14, 1956. *Canadian Journal of Physics*. Vol. 34, December 1956, No. 12A (issued as a supplementary number).

It is a pleasure to review the proceedings of a conference which was clearly well organized and of value to all who attended. Papers were presented dealing with research and problems at the frontiers of present knowledge, and time was evidently available for adequate discussion. The problems dealt with include the general one of interaction of electrons and lattice vibrations, conduction in solid solutions, resistance due to imperfections, and some aspects of magneto-resistance and nuclear magnetic resonance. These subjects were concerned especially with metals, as were the papers on electron interaction and on means of studying the Fermi surface. Heat conductivity was dealt with both in metals and in semi-conductors, and other aspects of semi-conductors discussed were impurity band conductivity and the nature of the bonds. Although all the subjects discussed are important, possibly the most interesting problems raised were the resistance minimum at low temperature with some metals, the mechanism of electron scattering by dislocations, plasma oscillations in semi-conductors, and heat transfer in semi-conductors.

The organizers and editors are to be congratulated on the rapid publication of this most stimulating book.

D. A. WRIGHT

Structure Reports for 1940–1941. Vol. 8. General Editor: A. J. C. WILSON. Section Editors: N. C. BAENZIGER, J. M. BIJVOET and J. MONTEATH ROBERTSON. (Utrecht: N. V. A. Oosthoek's Uitgevers Mij, 1956.) Pp. viii + 384. Price £7 11*s*.

It is hardly necessary to say that the publication of this volume will be greeted with pleasure by crystallographers and others concerned with structural data. The gap between the old *Strukturbericht* (Vol. 7 for 1939) and the new *Structure Reports* is now closed, and we may therefore anticipate a gradual reduction in the time-lag before each new year's work is reported.

No special features are to be expected in the lay-out of a volume which falls between the last of the old *Strukturbericht* series and a volume (9) of *Structure Reports* already published. The attempts in the early volumes of *Strukturbericht* to establish a systematic classification for inorganic and organic compounds according to structure-type are no longer maintained. The Editors state that no systematic search for pre-1940 omissions has been made; there are, however, a number of references to structures published in the period 1940–1941 but already described in Volumes 9–13 of *Structure Reports*.

W. H. TAYLOR

Notes and comments

Elections to The Institute of Physics

The following elections have been made by the Board of The Institute of Physics:

Fellows: F. Berz, E. L. Deacon, J. L. Farrands, F. Fowweather, R. G. Gosling, F. W. Hayward, W. E. Lamb, E. Stanley, H. Tipton, S. A. Young.

Associates: F. G. Blackler, D. G. Blears, A. C. Causon, J. C. Frame, A. Gerrard, T. P. Gray, A. Bose, S. M. Hamberger, B. V. Hamon, C. J. Hunt, T. W. Johnson, B. W. Leake, J. G. W. Lee, I. W. McLean, I. H. Mahadeva, H. F. W. Mander, E. H. B. Martin, A. W. Matz, E. H. Medlin, J. S. Morgan, J. D. Stuart, M. E. J. West, J. E. Wright, F. R. Young.

Fourteen Graduates and eighteen Students were also elected.

Conference on peaceful uses of atomic energy

The British Government have accepted an invitation from the Secretary-General of the United Nations to participate in a second International Conference on the peaceful uses of atomic energy, to be held in Geneva in 1958 from 1 September to 13 September inclusive. The last Conference, in 1955, occurred at a time when a great deal of work previously classified by the U.K., America and Canada was released for publication, and the same will be true of the next one since further important fields of work have recently been declassified.

A provisional topical agenda has been agreed by the seven-nation Advisory Committee, of which Sir John Cockcroft is the United Kingdom member, providing for 12 plenary sessions embodying papers of a general survey type, and four parallel series of technical sessions (68 3-hour sessions in all).

The technical sessions cover the following subjects:

Series 1: Chemistry and the chemical processing of irradiated fuel; reactor technology; radiation damage in reactor materials; handling of highly irradiated materials; treatment of radioactive wastes.

Series 2: Nuclear physics, including the physics of fission and fusion reactors; reactor theory; fuel cycles and the economics of nuclear power; research test and prototype power reactors; reactor experiments.

Series 3: Production and uses of isotopes and ionizing radiations in research, medicine, agriculture and industry; dosimetry; biological effects of radiation; radiological protection; reactor safety and location; meteorological and oceanographical aspects of the large-scale use of atomic energy.

Series 4: Raw material supplies; winning and refining of uranium and thorium; methods of separation of isotopes; metallurgy and fabrication of fuel elements; processing of other nuclear materials.

The conference will be conducted under the same rules of procedure as in 1955, which are published as Annex II in Volume 16 of the "Proceedings of the International Conference on the peaceful uses of atomic energy". Officials of the Conference, namely, the President, Vice-Presidents, Secretary-General, Deputy Secretary-General, Chairmen and Vice-Chairmen of the technical sessions will be announced later.

Arrangements for United Kingdom participation are being organized through an Executive Committee (Chairman, Sir John Cockcroft; Secretary, Mr. B. W. Mott), and a Papers' Committee (Chairman, Dr. B. F. J. Schonland; Secretary, Dr. T. A. Hall), on which are representatives of the United Kingdom Atomic Energy Authority, the Central Electricity Authority, Industry, Universities and other bodies. Titles and 500-word abstracts of papers must be in the hands of the Secretary-General of the United Nations by 1 March, 1958, and final texts by 1 June, 1958. At present the Papers Committee is engaged on the compilation of a provisional list of titles, with the object of ascertaining the approximate total number likely to be submitted by the United Kingdom and the distribution between the various sessions. It is hoped that this information will be available by 1 September, 1957. Organizations represented on the Papers Committee will be approached by their representatives for contributions, but others are invited to communicate directly with the Papers Secretary, at the Atomic Energy Research Establishment, Harwell, Berkshire, if they have titles to submit or if they seek further information. Enquiries concerning matters other than the submission of papers should be addressed to the Secretary of the Executive Committee, at the same address.

Journal of Scientific Instruments

Contents of the October issue

SPECIAL ARTICLE

Physics and the new electronics. By R. A. Smith.

ORIGINAL CONTRIBUTIONS

Papers

Energy stabilization of an electrostatic accelerator. By B. Millar, R. Bailey and J. L. W. Churchill.

The Leon tube: An instrument for measuring flow speeds in water. By J. F. Kemp.

The adjustment of optical systems. By W. S. Blaschke.

New infra-red detectors using indium antimonide. By D. G. Avery, D. W. Goodwin and Miss A. E. Rennie.

The plotting of strain-hysteresis loops. By W. H. Cogill.

Spherical aberration in the Fizeau interferometer. By W. G. A. Taylor.

A simple pulse spectrograph. By N. R. Hansen.

A precision capsule-type pressure gauge for the range 0–20 mm of mercury. By R. W. Crompton and M. T. Elford.

An electrical resistance analogue with a graded mesh. By P. J. Palmer and S. C. Redshaw.

A mercury-in-glass gas burette. By H. A. Wyllie.

A sensitive aerodynamic drag balance as an indicator of low air speeds. By J. F. Kemp.

Second-harmonic acceleration in the cyclotron. By K. E. A. Effat and J. H. Fremlin.

Laboratory and workshop notes

A polythene tubing control valve for liquids. By A. J. H. Sale.

Measurement of thickness distribution of thin films by α-particle absorption. By W. H. T. Davieson.

Static calibration of X-cut quartz plates used in dynamic pressure measurement. By D. H. Edwards and J. C. Breeze.

A method of storing electron microscope specimens. By T. B. Vaughan.

NOTES AND NEWS

Manufacturers' publications

Notes and comments

THIS JOURNAL is produced monthly by The Institute of Physics, in London. It deals with all branches of applied physics (including theory and technique).

All rights reserved. Responsibility for the statements contained herein attaches only to the writers.

EDITORIAL MATTER. Communications concerning editorial matter should be addressed to the Editor, The Institute of Physics, 47 Belgrave Square, London, S.W.1. (*Telephone:* Belgravia 6111.) Prospective authors are invited to prepare their scripts in accordance with the *Notes on the preparation of contributions*. (Price 2*s*. 6*d*. including postage.)

REPRODUCTION. The Institute of Physics is a signatory to The Royal Society's Fair Copying Declaration. Details may be obtained upon application from The Royal Society, London, W.1.

ADVERTISEMENTS. Communications concerning advertisements should be addressed to the agents, Messrs. Walter Judd Ltd., 47 Gresham Street, London, E.C.2. (*Telephone:* Monarch 7644.)

CLAIMS FOR MISSING JOURNALS. Claims from regular subscribers to this *Journal* for missing numbers will only be considered if received within 60 days of the date of mailing plus normal outward time of transit and time for lodging the claim. Losses attributable to failure to notify a change of address or to similar omissions will not be considered.

SUBSCRIPTION RATES. A new volume commences each January. The charge is £5 per volume ($14.25 U.S.A.), including index (post paid), payable in advance. Single parts, so far as available, may be purchased at 10*s*. each ($1.50 U.S.A.), post paid, cash with order. Orders should be sent to The Institute of Physics, 47 Belgrave Square, London, S.W.1, or to any bookseller.

Summarized proceedings of a conference on X-ray analysis—Cardiff, April, 1957

The Spring Conference of the X-ray Analysis Group of The Institute of Physics was held in the Physics Department of University College, Cardiff, on 5 and 6 April, 1957. The topics under discussion were the structures of minerals and inorganic compounds.

FIRST SESSION: THE STRUCTURES OF INORGANIC COMPOUNDS

The first session was held under the Chairmanship of Prof. E. G. Cox (School of Chemistry, Leeds); five papers were presented of which the first three were reviews and the last two descriptions of recent structural analyses.

Dr. P. G. Owston (Akers Research Laboratories, The Frythe, Welwyn) in presenting a review of the structure of transition metal complexes remarked that the recent development of industrial uses of atomic energy has reminded chemists of the existence of about one hundred elements other than carbon, some of which had been sadly neglected in the past. Much information of a general stereochemical character may be gained from a study of the colour and the magnetic properties of transition metal co-ordination compounds,[1] and the use of X-ray diffraction has frequently confirmed and extended these results. The stereochemistry of many complexes with co-ordination numbers from two to eight can be satisfactorily interpreted in terms of hybrid orbitals involving *s*, *p* and *d* orbitals. However, there is still a number of compounds containing more than one metal atom in which the nature of the linkage between the metal atoms is still obscure. In $K_4Ru_2Cl_{10}O \cdot H_2O$ the two halves of the anion are apparently linked by a linear Ru–O–Ru bridge.[2] In cupric and chromous acetates, crystallographic and magnetic studies indicate direct interaction between the metal atoms.[3] Interaction between metal atoms linked by carbonyl groups has also been observed.[4]

More recently, a series of novel compounds known as π-complexes, involving unsaturated organic molecules and ions, have been prepared and studied, and progress made in the interpretation of this new type of bonding.[5] Ferrocene, $Fe(C_5H_5)_2$, is probably the most familiar example[6] and its structure has been accurately determined by means of X-ray diffraction.[7] However, this is one of the few transition metal complexes for which bond lengths are well-established. The difficulty lies mainly in the location of light atoms such as carbon and nitrogen in the presence of heavy atoms such as those of the first transition series. The difficulty is emphasized by recent work on complex thiocyanates. In several recent structure analyses[8] the conclusions about the shape of the thiocyanate group are conflicting, and progress in the understanding of metal complexes will be hampered until crystallographers find a satisfactory method of locating light atoms in the presence of heavy ones.

Dr. J. D. Dunitz (Royal Institution, London) discussed the stereochemistry of metal complexes in rather more detail. The broad generalizations of the theory of hybridized bond orbitals are insufficient to explain some of the finer structural details. In particular, the available experimental evidence shows that, in cupric complexes, the regular octahedral configuration is distorted so as to produce four short bonds and two long ones. There are several examples of this peculiar behaviour of copper, but the most striking is seen in CuF_2.[9] The difluorides of all the metals of the first transition series have the rutile structure with regular octahedral co-ordination about the metal atom, except for CuF_2, which has a markedly deformed structure, with four shorter bonds at 1·93 Å and two longer ones at 2·27 Å; ZnF_2 again has a regular co-ordination. An explanation of the structure of cupric complexes can be obtained from crystal-field (or ligand-field) theory.[10]

The five 3*d* orbitals are degenerate if the force field is spherically symmetrical, as in an isolated ion or atom. In a crystal, however, the force field is in general no longer spherically symmetrical and the five-fold degeneracy is removed. The orbitals split into two groups, one doubly degenerate and the other triply degenerate, and simple electrostatic considerations show that the doubly degenerate orbitals have a higher energy than the triply degenerate. This statement is equivalent to one made by Jahn and Teller some twenty years ago.[11] The cupric ion has nine 3*d* electrons, and these may be fed into the five available orbitals. The triply degenerate orbitals will be completely filled, but there will be one "hole" left on the doubly degenerate orbitals. The hole could be associated with either one of two orbitals, whose directional properties are such that four slightly long and two normal bonds could result, or alternatively four normal and two considerably longer. The latter is confirmed experimentally, and it is presumed that the hole is in the $d(x^2 - y^2)$ orbital, and the extra electron in $d(z^2)$.

This elegant explanation of the abnormality of cupric complexes can be extended, and Cr^{2+} and Mn^{3+} complexes, with one electron in each of the triply degenerate orbitals and one in only one of the doubly degenerate orbitals, should also be distorted from a regular octahedron. This again is confirmed experimentally.[12]

In tetrahedral complexes similar ideas can be applied but the order of stability of the orbitals is reversed. It can be shown that regular tetrahedral complexes should not occur if there are three, four, eight or nine 3*d* electrons. No examples are known for d^3 and d^4. For d^8 and d^9 the distortion should be in opposite senses and this is again confirmed by a flattening of the tetrahedron in Cs_2CuCl_4[13] and $CuCr_2O_4$[14] and an elongation in $NiCr_2O_4$.[15]

In the discussion that followed, the questions indicated the great interest that the speakers had aroused; the frequency with which the speakers found it necessary to reply that no satisfactory theoretical explanation had yet been given or that the experimental evidence was inconclusive showed how much there is still to do in this field.

Dr. S. C. Abrahams (Chemistry Department, Glasgow) then reviewed recent structural studies of compounds of

sulphur, selenium and tellurium. The elements of Group VIB of the Periodic Table form a typical sub-group in which the basicity of the element increases with the atomic number, and a consideration of the bonds formed by these elements might show some interesting gradations. Furthermore, about two hundred papers have been published in the last ten years on this topic, so that a wealth of data is available. The subject has been discussed more fully than is possible here[16] and references to individual structure analyses are given there.

In order to classify all the structural determinations, it is convenient to consider the central building component AB_n, where A is sulphur, selenium or tellurium; B is the same or some other atom or atoms; and $n = 1, 2, 3, 4$ or 6. From the range of lengths found for the S–S bond ($A = B = S$ and $n = 1$) the value 2·08 Å may be selected for the single bond length and 1·89 Å for the double bond length. Longer bonds are occasionally found, as in S_2F_{10} and $S_2O_4^{2-}$. The lengths of Se–Se single and double bonds may be established as 2·35 and 2·19 Å respectively, but insufficient data are available to characterize Te–Te bonds in the same way.

In the cyclic molecule S_8 all the bonds are of equal length and apparently have some double bond character. In open chains of sulphur atoms there appears to be an alternation of long and short bonds with the outermost bonds short. In these chains the dihedral angle between the plane of any three linked atoms and that formed by an added atom is found to vary over a range of more than 40°. On the other hand the valency angle of the central sulphur atom in S⟨S⟩S is always close to 106°. Similarly for selenium the angle varies little from 104°, and the only known case for tellurium is in the hexagonal form of the element where the angle is also 104°.

Having established these general points for the case where $A = B$ and $n = 2$, Dr. Abrahams then moved on to a consideration of molecules in which $A \neq B$, and was able to draw some very interesting conclusions. Thus X–S–O angles are remarkably constant, at about 106°, whereas X–S–X and X–S–Y angles vary between 66° and 120°. Similar, but less extensive, results are found in selenium and tellurium compounds.

If $n = 3$, as in $(CH_3)_2SO$ or F_2SeO, the molecules form a shallow pyramid with one of the tetrahedral positions presumably occupied by the lone pair of electrons on the central atom. The ions SO_3^{2-} and SeO_3^{2-} are also pyramidal, but the neutral molecule SO_3 is planar.

When $n = 4$, as in $SeCl_4$, there seems to be no doubt that the molecules are not regular tetrahedra, but are trigonal bi-pyramids with one of the equatorial atoms removed. When $n = 6$, as in SF_6 or $TeBr_6^{2-}$ regular octahedral structures are invariably found, despite the additional pair of electrons in $TeBr_6^{2-}$.

A comprehensive review of this sort points up those portions of the field that are anomalous, and which require further theoretical or experimental work before a satisfactory solution can be found. For this reason the structure of $S(CH_3)_3^+$ is now being investigated, since OH_3^+ is believed to be pyramidal, whereas $O(HgCl)_3^+$ is planar.

Dr. MARY R. TRUTER (School of Chemistry, Leeds) next spoke about an interesting and ambitious programme on which she and her students are engaged. The programme calls for the accurate determination of the bond lengths of a simple crystalline organic compound both in its free state and when it is co-ordinated to a metal atom. Two pairs of related molecules were discussed: thiourea and *bis*thiourea zinc dichloride, $Zn[SC(NH_2)_2]_2Cl_2$, on the one hand, and thioacetamide and *tetrakis*thioacetamide cuprous chloride, $Cu[(CH_3)CS(NH_2)]_4Cl$, on the other. Of these four molecules, thiourea and the cuprous salt of thioacetamide had been studied by X-ray diffraction previously, but the work was carried out some twenty years ago and it was necessary to refine the earlier structures. The structures of all four molecules have now been determined by three-dimensional analysis, but the refinement is not yet complete. In particular it has been found necessary to correct the bond lengths for the effects of anisotropic thermal motion[17] and this stage of refinement is now in progress for the two lighter molecules. Three of the molecules are found to possess some crystallographic symmetry, but the fourth, thioacetamide, goes to the opposite extreme, and there are two molecules in the asymmetric unit of the space group $P2_1/a$.

In a sense the results are very satisfactory yet disappointing. Table 1 gives the provisional bond lengths. The bonds from zinc to chlorine or sulphur and from copper to sulphur agree well with the sum of the tetrahedral single bond radii, and the bonds are clearly single bonds. Corresponding bond lengths in thiourea and thioacetamide agree extremely well. On the other hand, these lengths also agree, within the experimental error, with the corresponding lengths after co-ordination has taken place. Thus there is as yet no conclusive evidence from this work that co-ordination affects bond lengths. The main difficulty lies in the rather large standard deviations of the bond lengths in the metallic complexes. Thus the standard deviation of the C–S length in the zinc complex is 0·023 Å, so that the S–C length of 1·767 Å is barely significantly different from the length of 1·707 Å in thiourea itself. Further refinement will undoubtedly lower the standard deviations, and it may then be possible to recognize some significant differences.

Table 1. *Comparison of bond lengths in thiourea and thioacetamide before and after co-ordination*

(All distances in Å)

Bond	$SC(NH_2)_2$	$(CH_3)CS(NH_2)$	$Zn[SC(NH_2)_2]_2Cl_2$	$Cu[(CH_3)CS(NH_2)]_4$	*Sum of tetrahedral radii*
Zn–Cl	—	—	2·312	—	2·30
Zn–S	—	—	2·343	—	2·35
Cu–S	—	—	—	2·345	2·34
S–C	1·707	1·694	1·767	1·683	—
C–N	1·311	1·316	1·30	1·302	—
			1·26		
C–C	—	1·483	—	1·460	—

Dr. P. T. DAVIES (Thornton Research Centre, Chester) presented the last paper of the first session. He dealt with the crystallography of $2PbO \cdot PbBr_2$, a compound known to exist in deposits in gasoline engines. Crystals were prepared by fusion of the stoichiometric amounts of lead oxide and lead bromide in an alumina crucible. A needle of about 0·15 mm maximum cross-section was selected and reflexions obtained to the limit of copper radiation about the needle axis, [*c*]. The crystals were orthorhombic and consideration of the absent reflexions led to the choice of the centrosymmetric space group Pbnm with four units of $2PbO \cdot PbBr_2$ in the unit cell. The cell dimensions are

$$a = 9{\cdot}87, \quad b = 12{\cdot}25, \quad c = 5{\cdot}88 \text{ Å}$$

The structure was solved in [*hk*O] projection, but the analysis was made difficult by the presence of the heavy atoms which led to rather large absorption errors. The lead atoms were located from a Patterson synthesis by use of the Buerger minimum function and the phases of the *hk*O reflexions calculated. Sixty of the ninety-two observed reflexions were then included in a Fourier synthesis. From the Fourier map it proved possible to locate the probable positions of the bromine atoms. Structure factors based on the lead and bromine positions gave an R factor of 30%. The diffraction pattern for the crystal rotated round [*c*] showed a close correspondence between alternate layer lines, indicating that the lead and bromine atoms lie in sheets separated by *c*/2. A choice was made between the permissible values of $z = \frac{1}{4}$ or $\frac{3}{4}$ by trial and error calculation of the *hkl* reflexions.

It has not proved possible to locate the oxygen atoms since the absorption errors are too large. Measurements are being repeated with silver radiation and a crystal of accurately known size in order to minimize and correct for these errors.

In the discussion Miss M. M. AITKEN (University Museum, Oxford) described a recent structure analysis of mercury dithizonate. In this compound the S–Hg–S angle is 155° and the Hg–S distance 2·42 Å, corresponding to a single covalent bond. Two nitrogen atoms lie about 2·4 Å from the mercury atom, a distance which is much longer than the normal single bond distance. The situation seems to be intermediate between linear two-covalent mercury and tetrahedral four-covalent mercury. Dr. G. W. R. BARTINDALE (Manchester College of Science and Technology) asked Dr. Truter for the exact angles round the metal atoms in her complexes, and he was informed that the Cl–Zn–Cl angle was smaller than the S–Zn–S angle, and that the tetrahedron round the copper atom was elongated down the four-fold inversion axis.

SECOND AND THIRD SESSIONS: THE STRUCTURES OF MINERALS

The major part of the second session, under the chairmanship of Dr. C. W. BUNN (Imperial Chemical Industries Ltd., Welwyn Garden City), was devoted to the discussion of recent work on the plagioclase felspars. Before moving on to this topic, the conference heard two unrelated contributions.

In the first paper, Dr. ARNE MAGNÉLI (University of Stockholm) described recent developments in the work by his research group on the titanium oxides. Employing photographic focusing techniques, they had been able to show that the true phase diagram of the Ti–O system is even more complex than has been proposed.[18] In particular, Dr. Magnéli described three composition regions. Firstly, for samples low in oxygen, it has been shown that the α-Ti lattice can accommodate oxygen up to $TiO_{0{\cdot}50}$;[19] with annealing temperatures of 400–800° C, however, two weak lines, (001) and (003), are observed for $TiO_{0{\cdot}35}$ and more oxygen-rich samples; these lines are incompatible with a random distribution of oxygen atoms in the close-packed hexagonal structure. They may be explained if it is assumed that the oxygen atoms are arranged preferentially in every second layer of octahedral interstices extending normally to the hexagonal axis of the titanium host lattice. Variations in cell dimensions at about $TiO_{0{\cdot}35}$ accompany the first appearance of the extra lines.

In the $TiO_{1{\cdot}00}$ range, the results of previous work[20] on the structural characteristics of titanium oxide with the defective sodium chloride structure have been confirmed for preparations obtained in the arc furnace. For samples annealed at 800° C, a new phase of this composition has been found.[21, 22] It has low symmetry and is thought to be a deformed sodium chloride with ordered atomic vacancies; the present results indicate that it may be compared with niobium oxide.[23]

Finally, within the composition range $TiO_{1{\cdot}75}$—$TiO_{1{\cdot}90}$, seven distinct phases have been identified,[24] with compositions described by the general formula Ti_nO_{2n-1} ($n = 4$ to 10). The powder patterns suggest that these oxides constitute a "homologous series" formed by regularly distributed atomic dislocations appearing in a basic structure of the rutile type; comparison may be made with the series $(Mo,W)_nO_{3n-1}$ based on the ReO_3-type structure,[25, 26] and also an analogous oxide series V_nO_{2n-1}($n = 4$ to 8) has been found.[27] For greater oxygen contents, it is not at present possible to decide if there are further distinct members of this homologous series, or if there is a transition at some composition into a phase of extended homogeneity range.

During the discussion, Dr. Magnéli explained the accuracy with which the value of *n* in the homologous series appeared to be integral; he did not yet know if the structures could simplify at higher temperatures. In reply to Prof. J. D. BERNAL (Birkbeck College, University of London), Dr. Magnéli said that the compounds of the homologous series were strongly coloured (bluish-black) and semi-conducting.

In the next paper, Dr. M. G. BOWN (University of Cambridge) described new single-crystal work which he and Dr. Gay were carrying out on the pyroxene group of minerals. This group, with general structural formula $XY(SiO_3)_2$, can be sub-divided into monoclinic and orthorhombic members. In the type structure of the monoclinic members, diopside $CaMg(SiO_3)_2$, chains of linked SiO_4 tetrahedra run along the short *c*-axis of the C-face centred cell.[28] The orthorhombic form occurs when the cations X and Y are relatively small and very similar in size (e.g. $FeMg(SiO_3)_2$); the structure is basically the same as that of the monoclinic pyroxene except for a decrease in the co-ordination of the X ion.

The most important rock-forming pyroxenes occur in the system $CaSiO_3$–$MgSiO_3$–$FeSiO_3$ (with less than 50% $CaSiO_3$); orthorhombic pyroxenes only appear as the low temperature forms of minerals with less than 5% $CaSiO_3$, whilst monoclinic pyroxenes exist over the whole field. Broadly speaking, there are two varieties, augites with greater than 20% $CaSiO_3$, and pigeonites with less; this is not an arbitrary distinction, for there is a miscibility gap across the middle of the trapezoidal composition diagram. It is thus possible that a molten magma cooling slowly will precipitate separate and separable crystals of pigeonite and augite. On further cooling, the pigeonite crystals precipitate augite lamellae, whilst the associated augite crystals precipitate pigeonite lamellae. Depending on the rate of cooling, the pigeonite may partially

or completely invert to hypersthene, the orthorhombic modification stable at low temperatures.

Examination of two-phase crystals has confirmed that the (001) plane is common to the co-existing augite and pigeonite. It is not clear why the exsolution of the lamellae should occur on (001); the difference (of the order of 2½°) in β-angle of the two phases means that the Si–O chains must bend by this amount in crossing from host to the lamellae. Further, examination of pigeonite in a two-phase crystal and in a homogeneous volcanic specimen has confirmed that the space group is $P2_1/c$[29] (not C2/c as for diopside). The extra pigeonite reflexions can be slightly diffuse with respect to the main reflexions common to both monoclinic structures. Another effect which varies from specimen to specimen is the strength of a streak sometimes to be seen joining corresponding augite and pigeonite spots. It has not so far been possible to correlate these effects with composition, cooling rate or each other.

Investigation of pyroxenes with other cations has shown that only when the two ions are of the same size and relatively small are the orthorhombic and pigeonite structures found (Fig. 1). Finally, Dr. Bown illustrated by several examples

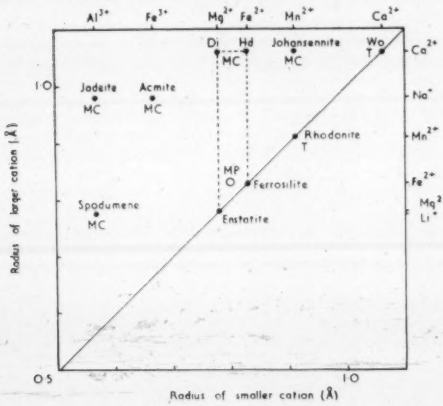

Fig. 1. Fields of occurrence of the various pyroxene structures as a function of the ionic radii of the cations

O, orthorhombic; *MC*, monoclinic *C* lattice; *MP*, monoclinic *P* lattice; *T*, triclinic.

the power of single-crystal methods in interpreting complex inter-related growths of these minerals.

Dr. K. W. ANDREWS (United Steel Co. Ltd., Rotherham) expressed the hope that powder work might also be carried out on these minerals which can occur as the components of slags. Replying to a question from Dr. Andrews, Dr. Bown said that there was no additional information from this investigation so far on the pure end members $MgSiO_3$ and $FeSiO_3$ or their relationships to the structures he had described.

There followed three papers on the plagioclase felspars, in the first of which Dr. P. GAY (University of Cambridge) reviewed recent X-ray work. Although the plagioclases are all based structurally upon a linked framework of Si–O tetrahedra, there are complex sub-solidus relationships. The various phases can be recognized by their single-crystal diffraction patterns, but the details of the structural arrangements responsible for these patterns are largely unknown.

In classifying the various diffraction patterns, it is convenient to divide all the possible reflexions into four groups; (*a*) those with h and k even, l even, (*b*) with h and k odd, l odd, (*c*) h and k even, l odd, (*d*) h and k odd, l even, the indexing being in terms of the triclinic cell of anorthite ($CaSi_2Al_2O_8$) with *c*-axis of the order of 14 Å. The type (*a*) reflexions common to all plagioclases are in the main strong; the occurrence of the weaker subsidiary reflexions (*b*), (*c*), (*d*) distinguish the various diffraction patterns. Pure anorthite shows all four reflexion classes, whilst the other end member, albite ($NaSi_3AlO_8$), shows only type (*a*); albite, therefore, has a similar triclinic cell to anorthite but with *c*-axis of the order of 7 Å. For the low temperature plagioclases, six different structural regions have been observed over the whole of the series.[30] The most interesting diffraction patterns are those observed from the intermediate structural region, which show, in addition to the type (*a*) reflexions, pairs of spots of differing intensity in non-Bragg positions replacing type (*b*) spots; further, the separation of these split (*b*) reflexions is variable and apparently a continuous linear function of the composition.[30] At higher temperatures, over the composition range from pure albite to about 90–95% anorthite, all structures can be converted into a 7 Å *c*-axis albite-like structure. Pure anorthite, however, undergoes a reversible change to a transitional structure at 1100° C, which persists (for quenched specimens) up to the solidus.[31]

From indirect evidence, it seems likely that, except at the anorthite end of the series, the principal structure rearrangement in the low → high transformation is the disordering of the Si–Al arrangement. For calcic specimens, retaining the 14 Å *c*-axis at high temperatures, it is thought that the Si–Al arrangement is always ordered and that changes in the cations are responsible for the high-low inversion.[32] No satisfactory explanation has so far been developed for the non-Bragg reflexions of the intermediate plagioclases.

In the subsequent paper Dr. H. D. MEGAW (University of Cambridge) described a model by which some features of the diffraction patterns of the plagioclases might be explained. The model assumes the existence of stacking faults such that part of the structure on one side of the fault plane is displaced relative to that on the other side by a constant "slip" vector; the faults arise by a growth or annealing process. These fault planes occur with a probability which is constant for a given material but depends on the composition. A unit cell of the structure suitable for mathematical treatment is defined by the three possible fault planes ($1\bar{1}2$), (013), (001); the volume of this cell is twice the volume of the normal cell.

The mathematical treatment develops in three dimensions, Wilson's method for layer structures.[33] When the general results of the theory are applied to the plagioclase felspar model, it is predicted that some reflexions remain as sharp Bragg maxima, others become broadly diffuse, whilst displaced reflexions are to be associated with half integral values of l, i.e. with reflexions which do not exist for the ordinary anorthite cell. Thus the non-Bragg pairs of reflexions of the intermediate plagioclases are not to be regarded as being related to the type (*b*) reflexions of the anorthite structures. The model also predicts other displaced reflexions which may account for the "satellite" reflexions which have also been described.[34]

For the intermediate plagioclase patterns, the values of the predicted and observed displacements can only be compared

if the variation of the probability of faulting with composition is known. At present it is possible only to use the observational data to see if reasonable values of the probability are obtained. In this way, it seems likely that whilst one probability is related to the square of the albite content, the other two are sensibly constant. The physical significance of the constant probabilities of faulting at all compositions is not understood. It is tempting to associate the onset of these faults at compositions of the order of 75% anorthite with the stoichiometric ratio; this may give physical meaning to the doubled cell of the mathematical treatment, which sets in only at this point. Such speculation, concluded Dr. Megaw, could only be placed on a firmer basis when the structures of the anorthites were known.

Finally in this group of papers, Mr. C. J. E. KEMPSTER (University of Cambridge) described work carried out in collaboration with Mr. S. CHANDRASEKHAR, and Dr. E. W. RADOSLOVICH on the structures of the anorthites. For both body-centred and primitive anorthite, the type (*a*) reflexions predominate, and their intensities are remarkably similar; in primitive anorthite the type (*c*) reflexions are rather more intense than the type (*b*) reflexions common to both this and the body-centred structure.

For primitive anorthite, the initial syntheses were carried out using only the type (*a*) reflexions; this imposed a higher symmetry on the syntheses. Each peak therefore represents four atoms in different parts of the unit cell, and is elliptical or "split." The calcium peak, which is more split than the rest, was then used as a heavy atom to determine the signs of the strong type (*c*) reflexions. The inclusion of these terms in the synthesis led to a trial structure with C-face centred symmetry which was refined in projection. Again the calcium peak was more elliptical than the rest, and a similar procedure was used to introduce terms due to the types (*b*) and (*d*) reflexions into the synthesis. At the present time, the reliability index is about 18% for all reflexions, and a three-dimensional difference synthesis is being carried out; it is not yet possible for a distinction between Si–O and Al–O bonds to be made. The work on body-centred anorthite has proceeded along similar lines and is at a comparable stage of development.

During the investigation of the structures of other plagioclases it has been found that, although the symmetry only allows one calcium atom per half cell, the calcium peak is always very elliptical, and similar to the split calcium peak in the initial syntheses for the anorthites. An anisotropic temperature factor twenty times as large in one direction as in the other would be needed to account for the observed eccentricities and this seems unlikely. To overcome this difficulty, a splitting into two "half-atoms" may be postulated; it seems plausible that there are two possible sites about $\frac{1}{2}$ Å apart separated by a low potential energy barrier. Instead of an ordered array of calcium atoms, there may be a random distribution between the two sites giving an imperfect structure. It has also been reported that the sodium atom in the high- and low-albite structures is similarly elongated.[35] It seems probable that there must be some form of imperfection in the arrangement of the cations over the whole series.

Opening the discussion of the felspar papers, Mr. J. R. S. WARING (University of Cambridge) drew attention to a possible connexion between the changes in physical optics and the mean position of the cation with variation in composition of the plagioclase. With increasing calcium content, the average co-ordinate of the cation moves from one side, through and then well beyond the position of the true mirror plane of monoclinic felspars; this follows qualitatively the changes shown in the extinction angles on (001) and (010).

Dr. R. F. YOUELL (University of Leeds) expressed the hope that this latest work upon the classification of the felspars would in time lead to a clearer understanding of the formation of their alteration products.

Replying to other questions on the application of the work on the plagioclases, Dr. Gay explained how, by means of its diffraction pattern, the material could be allocated to a particular structural category so providing a crude form of geological thermometer. With additional evidence from the associated minerals, this could be used in restricted cases to help to trace the sequence of crystallization of the plagioclase-bearing rocks; a study of this kind had been carried out upon the well-known Skaergaard intrusion. Prof. BERNAL drew attention to the work of Dornberger-Schiff[36] on the classification of disordered structures. Dr. Megaw said that she felt the present stacking fault theory for plagioclases could not be compared with classification so far proposed; in reply to Dr. W. A. WOOSTER (University of Cambridge), she said that a careful examination of the reciprocal lattice distribution of the displaced maxima predicted by the theory had not so far been carried out.

The evening discourse was given by Dr. D. C. MARTIN (Assistant Secretary to the Royal Society). He spoke about the International Geophysical Year (I.G.Y.), and his talk was profusely illustrated by slides and colour films. The audience was able to gain a good impression of the tremendous scope of the I.G.Y. programme and of the truly international efforts that are being made to ensure success.

On Saturday morning, the Group met again under the chairmanship of Prof. Cox to hear further discussion of mineralogical problems. The first paper by Dr. H. F. W. TAYLOR (University of Aberdeen) described the transformations of tobermorite ($Ca_5Si_6O_{22}H_{10}$) under various conditions. Most of the work had been carried out on material from Ballycraigy, N. Ireland, with an 11·3 Å basal spacing. For temperatures between 300 and 700° C, only the "9·35 Å hydrate" phase is found. The unit cell of this phase is probably closely similar to that of the unaltered material except for the c dimension; the pseudo-cell ($a = 5{\cdot}58$, $b = 3{\cdot}66$, $c = 18{\cdot}7$ Å) is A-centred not body-centred as in the unaltered material. In the apparently irreversible transformation, the results suggest that Si–O–Si links between metasilicate chains in adjacent layers[37] are formed to an increasing extent with rise in temperature. The variable water content[38] and disorder of the structure may be related to the placing of these interlayer bonds.

At about 800° C, a single crystal of the 9·35 Å hydrate alters to one of β–$CaSiO_3$, twinned in two orientations by reflexion across the (100) plane of tobermorite (tobermorite crystals of other origin behave differently on heating, and do not form the 9·35 Å hydrate). The orientation relationships of this change suggest considerable movements of the silicon atoms but little or no movement of the calcium ions. The change in the lime–silica ratio of the product can be explained if silica is expelled and a defect $CaSiO_3$ structure is formed. Tobermorite can also be hydrothermally converted into xonotlite ($Ca_6Si_6O_{17}(OH)_2$) most conveniently by treatment with supercritical water at 330° C; there is no intermediate formation of the 9·35 Å hydrate. The change is an oriented one in which the single crystal of tobermorite is converted into a crystal of xonotlite twinned in two orientations; the

probable mechanism of this change requires movement of the calcium ions.

In conclusion, Dr. Taylor expressed the hope that by work of this kind a position might be attained where the relationships of structures to their chemistry would be as well defined for the silicates as they are in the field of organic chemistry.

Dr. H. P. STADLER (King's College, Newcastle-upon-Tyne) expressed doubt that in these transformations the silicon atoms were more likely to migrate than the calcium ions. Dr. Taylor, whilst agreeing that the evidence was not conclusive, said that the strongest support for his views came from the transition of xonotlite to β-wollastonite, where a comparison of the structures showed that positions of both calcium and oxygen atoms were effectively unchanged. Dr. R. F. Youell endorsed the plea for closer co-operation between silicate chemists and crystallographers; he drew attention to a programme of work on the reactivity of silicates by single-crystal methods. In addition to a study of the chlorite–olivine transformation, more recently it has been found that the hydrous iron silicate, cronstedtite, undergoes transformations involving oxidation, dehydration and recrystallization whilst still diffracting coherently; work was also in progress on amesite and other silicates.

There followed two closely related papers, in the first of which Dr. E. J. W. WHITTAKER (Ferodo Ltd., Stockport) described the structure of para-chrysotile. The principal commercial asbestos is chrysotile [$Mg_3Si_2O_5(OH)_4$], a form of serpentine, which is recognized to occur in three modifications. In all cases, the fundamental structural unit is a layer consisting of a two-dimensional silicate net which replaces two-thirds of the hydroxyl groups on one side only of a layer of the brucite structure. The dissimilar faces of this composite sheet tend to make it curl with the brucite net on the outside of the arc; the various forms of the serpentine minerals arise from the various ways in which this tendency to curl is reconciled with the crystallographic requirements for stacking the layers. In chrysotile, the layers are curved cylindrically, and achieve partial order by stacking in the form of concentric cylinders. There is more than one possible way of stacking together the layers, and this leads to the production of macroscopic specimens containing several different stacking patterns.

It has been known for some years that some chrysotile specimens give weak diffuse reflexions on extra layer lines with a fibre axis identity period of 9·24 Å, in addition to the strong reflexions on layer lines with a 5·33 Å spacing.[39] Equi-inclination rotation photographs of the sixth extra layer reveal a series of sharp reflexions (which can be indexed as *h*60 reflexions) from a helical cylindrical lattice. Contrary to previous views,[40] it can be shown that the extra layer lines are produced by a variety of chrysotile with the usual cylindrical morphology, but with an unusual orientation of the axes of the layers; this new variety has been called para-chrysotile. By analogy with the structure of ortho- and clino-chrysotile it can be shown that the layers in para-chrysotile are subject to random translations of $nb/6$ parallel to the fibre axis; thus sharp reflexions are not observed on layer lines with $k \neq 6$. It can also be deduced that only one of three conceivable ways of stacking the layers is in accordance with the observations, and that this stacking arrangement suggests that the layers are subject to a distortion similar to that found for the other varieties of chrysotile. The symmetry of the serpentine layer precludes the possibility of a further polymorph related to para-chrysotile in the same way as clino- and ortho-chrysotile are related.[41]

Dr. J. ZUSSMAN (University of Manchester) described electron-diffraction studies of serpentine minerals carried out by himself and Prof. G. W. BRINDLEY (Pennsylvania State University) with technical assistance from Mr. J. COMER. From previous X-ray work, the cell dimensions of the main types of serpentine are known (Table 2). Specimens representative of each variety were studied by electron microscopy and selected area electron-diffraction techniques; in this contribution, the observations are concerned mainly with antigorite.

Table 2. *Cell dimensions of serpentine minerals (in Å)*

	a	*b*	*c*	β	*Reference No.*
Chrysotile	5·32	9·2	14·6	93·2° or 90°	(41, 45)
Lizardite	5·31	9·2	7·31	90°	(46)
Antigorite	43·5	9·2	7·28	91·4°	(47)

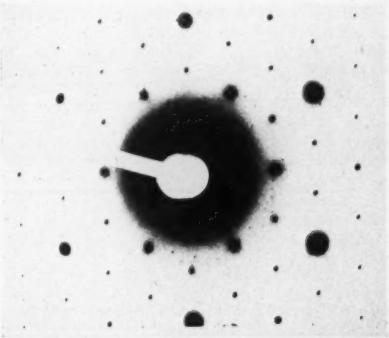

(*a*)

[Reproduced from *American Mineralogist*.]

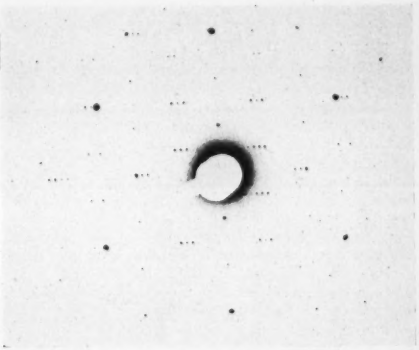

(*b*)

[Reproduced from *American Mineralogist*.]

Fig. 2. (*a*) Electron diffraction pattern from platy lizardite crystal, Kennack Cove, Lizard, Cornwall. (*b*) Electron diffraction pattern from platy antigorite crystal, Antigorio

For lizardite electron-diffraction single crystal patterns [Fig. 2(*a*)] show a hexagonal array of spots corresponding to a centred rectangular net of sides $a = 5{\cdot}2$ Å, $b = 9{\cdot}1$ Å, which compare closely with the cell dimensions from X-ray work. The patterns from platy antigorite crystals, on the other hand, show layer lines with $b = 9{\cdot}3$ Å, but with clusters of spots replacing the single spots of lizardite on these layer lines [Fig. 2(*b*)]. The cell dimension derived from these spot clusters is $38{\cdot}3$ Å. It was further found that not only different specimens but different crystals of the same specimen yield different values of a. When the various values of a are recorded, they are found to cluster into groups such that, with one exception, no member of the particular group has a dimension which differs by more than 2% from the mean; the differences in the mean values (of the order of 2·5–3 Å) are far greater than the experimental limits of error. The large a dimension of antigorites has been attributed to the super-periodicity of an undulating sheet structure.[42] It can then be suggested that the value of a is related to the number of small cells in each undulation, and that there may be a correlation between the spacing of the antigorite groups and half the period of the small cell ($\frac{1}{2} \times 5{\cdot}3 = 2{\cdot}65$ Å).

One particular antigorite (YuYen stone) showed very closely spaced spots for which $a \sim 90$–110 Å for some crystals. In addition electron micrographs of some of these crystals show interference fringes which are thought to be similar to those found for platinum phthalocyanine;[43] the spacing and orientation of these fringes correspond with the data from electron-diffraction patterns from the same crystals. Finally, Dr. Zussman mentioned the examination of a synthetic (Mg, Ge) serpentine, and a natural material from Unst. In both cases, the a cell dimension is of the order of 5·3–5·4 Å and not a multiple repeat as suggested by previous X-ray powder work.[44] The new evidence points quite clearly against these materials having the antigorite structure, and gives some weak confirmation that they both have a six-layered ($c \simeq 44$ Å) unit cell.

During the discussion, Dr. Zussman described further X-ray work which he and Prof. Brindley had carried out to study the thermal transformation of serpentine to forsterite. The results indicate that the transformation of chrysotiles proceeds with the intermediate formation of a chlorite-type structure, whilst antigorites form a mixed layer aggregate with changing proportions of the two constituents.[48]

After a short break, the meeting continued with a description of the crystal structure of botallackite by Mr. P. G. Embrey [British Museum (Natural History)]. Botallackite [$Cu_4(OH)_6Cl_2$], first described by Church,[49] was for many years discredited; an optical, chemical and X-ray examination of material collected at the same time as the original specimen re-established the mineral as a distinct species.[50] In 1952, Mr. A. W. G. Kingsbury found, at a new locality, Cligga Head, Cornwall, a small cavity containing single crystals of the mineral of size suitable for X-ray work. The space group was established as $P2_1/m$ with $a = 5{\cdot}632$, $b = 6{\cdot}124$, $c = 5{\cdot}715$ (all $\pm 0{\cdot}003$) Å, $\beta = 92{\cdot}75 \pm 0{\cdot}1°$; measurements of specific gravity, and the structure analysis, indicate the formula given above rather than $Cu_4(OH)_6Cl_2 \cdot 3H_2O$ as previously supposed.

The structure determination proved remarkably straightforward as the Patterson projections are closely similar to the electron density maps because of the pseudo-hexagonal symmetry. Good agreement between the F_o's and F_c's was obtained after correction for absorption (due to the platy habit of the crystal) had been made. The structure is composed of sheets of copper atoms, linked by OH and Cl in distorted octahedral co-ordination, lying parallel to (001). The mineral is isomorphous with $Cu_4(OH)_6Br_2$,[51] and is identical with the IIα modification of basic cupric chloride prepared by Feitknecht and Maget.[52] Synthetic work[53] has shown that botallackite is unstable and changes, through an intermediate phase, to the hexagonal paratacamite [$8Cu_2(OH)_3Cl$]. Although it has been established that natural botallackite changes readily to paratacamite, no traces of the intermediate phase have yet been found in nature. The structure of paratacamite has only been compared with that of $Co_2(OH)_3Cl$,[54] which in turn has not been fully determined; like botallackite it appears to have a layer structure. The best known of the polymorphs of $Cu_2(OH)_3Cl_2$, the orthorhombic variety, atacamite, has had its atomic parameters accurately determined;[55] the Cu–OH and Cu–Cl distances compare closely with those determined for botallackite.

In the next contribution, by Mr. H. P. Rooksby and Mr. M. H. Francombe (G.E.C. Research Laboratories, Wembley), two examples of structure transitions were discussed. In the first, relating changes in magnetic state with atomic arrangement, structural deformations in spinel-type compounds were described. Magnetite itself shows a small lattice distortion below $-160°$ C associated with a magnetic anomaly; it has recently been shown that nickel chromite is tetragonally deformed at room temperature, the tetragonal→cubic transition taking place at about 35° C.[56] More striking effects are shown by the system of solid solutions $FeFe_{2-x}Cr_xO_4$ at low temperatures; although no structural distortions are observed at ordinary temperatures, the variation of lattice parameter with composition seems to indicate four stages in the change from the "inverse" atomic arrangement of magnetite ($x = 0$) to the completely "normal" arrangement in ferrous chromite ($x = 2$).[57] At liquid air temperatures, when $x = 0{\cdot}8$ a new distortion is found which is tetragonal with c/a just greater than unity. Up to $x = 1{\cdot}3$ this tetragonal deformation gets larger; however, at this point, deformations occur along two of the original four-fold directions so that the symmetry becomes orthorhombic. With increasing x, a progressive change of the orthorhombic deformation occurs until at $FeCr_2O_4$ it has merged into a tetragonal deformation with axial ratio much less than unity. Experiments at selected compositions have shown that the change to the orthorhombic structure at $-180°$ C takes place in two distinct stages.[58] The origin of the structural changes is, at present, largely conjecture, but there does seem to be some correlation between the type of distortion and the distribution of magnetic atoms on the tetrahedral and octahedral sites.

For the second example Mr. Rooksby discussed the ferroelectric silver niobate and tantalate. At normal temperatures, the structure of silver niobate can be compared with sodium niobate[59] though the substitution of silver for the smaller sodium ion reduces the magnitude of the lattice distortion. With increasing temperature, the silver niobate goes through a sequence of anisotropic changes of structure-cell dimensions similar to those observed in sodium niobate; only above 560° C does the structure simplify to an ideal cubic perovskite type.[60] In the tantalate as well, a tetragonal deformation is found, but this exists over a smaller temperature interval than for the niobate. It appears that the upper transition temperature at which these structures become completely isotropic is determined primarily by packing considerations, whilst the lower transition temperature is in all probability linked with ferroelectric or anti-ferroelectric strain phenomena.

Replying to the discussion, Mr. Francombe said that no

structural details of the tantalate were yet available. He drew attention to the system (Na, Cd)NbO_3 where the introduction of cadmium atoms produces another type of superlattice with the cadmium atoms apparently occupying the A sites of the perovskite structure.

The last paper of the meeting was read by Dr. J. W. JEFFERY (Birkbeck College, University of London); practically all of the experimental results and interpretation described were the work of the late Dr. H. S. SIMONS.

The material, "fly ash" or pulverized fuel (p.f.) ash, is the product of modern generating stations burning finely ground coal. Under the microscope the ash is seen to consist mainly of spheres of 20 to 100 μ diameter, classifiable into several types.

The first X-ray photographs using a 9 cm Debye–Scherrer camera showed that the main constituents were α-quartz (SiO_2) and mullite ($3Al_2O_3 . 2SiO_2$), but it was not until the Nonius focusing camera was used that it became possible to identify the eight or more minor components. This camera can separate two lines at about $\theta = 20°$ whose distance apart is equal to the α_1, α_2 separation of a Debye–Scherrer camera of the same dispersion. The final identification was always made by comparison with standard photographs, but extensive use was also made of the A.S.T.M. indexes. About a hundred different samples were investigated. The range of mineralogical composition is: quartz: 3–25%; mullite: 0–40%; magnetite + haematite: 0–25%; other minerals: 0–15%; glass: 20–85%.

Several problems arose in connexion with the iron content. Changes on roasting were due to the oxidation of magnetite (Fe_3O_4) to haematite (α–Fe_2O_3); maghemite (γ–Fe_2O_3) did not occur. The different states of combination of iron, indicated by chemical studies made at the Central Electricity Research Laboratories, were found to consist of (*a*) a minute amount of iron sulphate; (*b*) dicalcium ferrite ($2CaO . Fe_2O_3$); (*c*) magnetite and haematite inseparably mixed, and (*d*) glass.

Calcium was present as anhydrite ($CaSO_4$), lime (CaO) and gypsum ($CaSO_4 . 2H_2O$). In wet dumps, ettringite ($3CaO . Al_2O_3 . 3CaSO_4 . 32H_2O$) is formed and is probably responsible for some of the consolidation.

P. GAY
P. J. WHEATLEY

REFERENCES

(1) NYHOLM, R. S. *Quart. Rev.*, **7**, p. 377 (1951).

(2) MATHIESON, A. MCL., MELLOR, D. P., and STEPHENSON, N. C. *Acta Cryst.*, **5**, p. 185 (1952).

(3) VAN NIEKIRK, J. N., and SCHOENING, F. R. L. *Acta Cryst.*, **6**, p. 227 (1953).

VAN NIEKIRK, J. N., and DE WET, J. F. *Acta Cryst.*, **6**, p. 501 (1953).

(4) CAVALCA, L., and BASSI, I. W. *Ricerca Sci.*, **23**, p. 1377 (1953).

HALLAM, B. F., MILLS, O. S., and PAUSON, P. L. *J. Inorg. Nuc. Chem.*, **1**, p. 313 (1955).

(5) RUNDLE, R. E., and GORING, J. H. *J. Amer. Chem. Soc.*, **72**, p. 5537 (1950).

WEISS, E., and FISCHER, E. O. *Z. Anorg. Allgem. Chem.*, **286**, p. 142 (1956).

HOLDEN, J. R., and BAENZIGER, N. C. *J. Amer. Chem. Soc.*, **77**, p. 4987 (1955).

DEMPSEY, J. N., and BAENZIGER, N. C. *J. Amer. Chem. Soc.*, **77**, p. 4984 (1955).

WUNDERLICH, J. A., and MELLOR, D. P. *Acta Cryst.*, **7**, p. 130 (1954).

WUNDERLICH, J. A., and MELLOR, D. P. *Acta Cryst.*, **8**, p. 57 (1955).

WEISS, O., and FISCHER, E. O. *Z. Anorg. Allgem. Chem.*, **278**, p. 219 (1951).

WEISS, O., and FISCHER, E. O. *Z. Anorg. Allgem. Chem.*, **284**, p. 69 (1956).

DUNITZ, J. D., ORGEL, L. E., and RICH, A. *Acta Cryst.*, **9**, p. 373 (1956).

(6) PAUSON, P. L. *Quart. Rev.*, **9**, p. 391 (1955).

(7) DUNITZ., J. D., ORGEL, L. E., and RICH, A. *Acta Cryst.*, **9**, p. 373 (1956).

(8) ZDANOV, G. S., and ZVONKOVA, Z. B. *Uspekhi Khimii*, **22**, p. 3 (1953).

SAITO, Y., TAKEUCHI, Y., and PEPINSKY, R. *Z. Krist.*, **106**, p. 476 (1955).

LINDQVIST, I. *Acta Cryst.*, **9**, p. 29 (1956).

LINDQVIST, I., and STRANDBERG, B. *Acta Cryst.*, **10**, p. 173 (1957).

(9) STOUT, J. W., and REED, S. A. *J. Amer. Chem. Soc.*, **76**, p. 5279 (1954).

BILLY, C., and HAENDLER, H. M. *J. Amer. Chem. Soc.* To be published.

(10) ORGEL, L. E., and DUNITZ, J. D. *Nature* [*London*], **179**, p. 462 (1957).

(11) JAHN, H. A., and TELLER, E. *Proc. Roy. Soc., A*, **161**, p. 220 (1937).

(12) BUERGER, M. J. *Z. Krist.*, **95**, p. 163 (1936).

MASON, B. *Amer. Miner*, **32**, p. 426 (1947).

HEPWORTH, M. A., JACK, K. H., and NYHOLM, R. S. *Nature* [*London*], **179**, p. 211 (1957).

(13) HELMHOLZ, L., and KRUH, R. F. *J. Amer. Chem. Soc.*, **74**, p. 1176 (1952).

(14) MIYAHARA, S., and OHNISHI, H. *J. Phys. Soc., Japan*, **12**, p. 1296 (1956).

(15) LOTGERING, F. K. *Philips Res. Rep.*, **11**, p. 190 (1956).

(16) ABRAHAMS, S. C. *Quart. Rev.*, **10**, p. 407 (1956).

(17) CRUICKSHANK, D. W. J. *Acta Cryst.*, **9**, p. 757 (1956).

(18) DE VRIES, R. C., and ROY, R. *Amer. Ceram. Soc. Bull.*, **33**, p. 370 (1954).

(19) EHRLICH, P. *Z. Anorg. Chem.*, **247**, p. 53 (1941).

(20) EHRLICH, P. *Z. Elektrochem.*, **45**, p. 362 (1939).

(21) KUYLENSTIERNA, U., and MAGNÉLI, A. *Acta Chem. Scand.*, **10**, p. 1195 (1956).

(22) WANG, C. C., and GRANT, N. J. *J. Metals*, **8**, p. 184 (1956).

(23) BRAUER, G. *Z. Anorg. Chem.*, **248**, p. 1 (1941).

(24) ANDERSSON, S., and MAGNÉLI, A. *Naturwissenschaften*, **43**, p. 495 (1956).

(25) MAGNÉLI, A. *Acta Cryst.*, **6**, p. 495 (1953).

(26) MAGNÉLI, A., BLOMBERG-HANSSON, B., KIHLBORG, L., and SUNDQVIST, G. *Acta Chem. Scand.*, **9**, p. 1382 (1955).

(27) ANDERSSON, G. *Acta Chem. Scand.*, **8**, p. 1599 (1954).

(28) WARREN, B., and BRAGG, W. L. *Z. Krist.*, **69**, p. 168 (1929).

(29) MORIMOTO, N. *Proc. Japan Acad.*, **32**, p. 750 (1956).

(30) GAY, P. *Miner. Mag.*, **31**, p. 21 (1956).

(31) GAY, P. *Miner. Mag.*, **30**, p. 428 (1954).

(32) GAY, P., and TAYLOR, W. H. *Acta Cryst.*, **6**, p. 647 (1953).

LAVES, F., and GOLDSMITH, J. R. *Acta Cryst.*, **7**, p. 131 (1954).

(33) WILSON, A. J. C. *X-ray Optics*, p. 49 (London: Methuen, 1949).

(34) COLE, W. F., SÖRUM, H., and TAYLOR, W. H. *Acta Cryst.*, **4**, p. 20 (1951); see also Ref. (30).

(35) FERGUSON, R. B., TRAILL, R. J., and TAYLOR, W. H. *Acta Cryst.* To be published.

(36) DORNBERGER-SCHIFF, K. *Acta Cryst.*, **9**, p. 593 (1956).

(37) MEGAW, H. D., and KELSEY, C. H. *Nature* [*London*], **177**, p. 390 (1956).

(38) MCCONNELL, J. D. C. *Miner. Mag.*, **30**, p. 293 (1954).

(39) ARUJA, E. *Diss. Ph.D.* (University of Cambridge, 1943).

(40) HARGREAVES, A., and TAYLOR, W. H. *Miner. Mag.*, **27**, p. 204 (1946).

(41) WHITTAKER, E. J. W. *Acta Cryst.*, **6**, p. 747 (1953).

(42) KUNZE, G. *Z. Krist.*, **108**, p. 82 (1956).

ZUSSMAN, J. *Miner. Mag.*, **30**, p. 498 (1954).

(43) MENTER, J. W. *Proc. Roy. Soc., A*, **236**, p. 119 (1956).

(44) BRINDLEY, G. W., and VON KNORRING, O. *Amer. Miner.*, **39**, p. 794 (1954).

(45) WHITTAKER, E. J. W. *Acta Cryst.*, **4**, p. 187 (1951).

(46) WHITTAKER, E. J. W., and ZUSSMAN, J. *Miner. Mag.*, **31**, p. 107 (1956).

(47) ARUJA, E. *Miner. Mag.*, **27**, p. 65 (1945).

(48) BRINDLEY, G. W., and ZUSSMAN, J. *J. Amer. Miner.*, **42**, p. 461 (1957).

(49) CHURCH, A. H. *J. Chem. Soc.*, **3**, p. 212 (1865).

(50) FRONDEL, C. *Miner. Mag.*, **29**, p. 34 (1950).

(51) AEBI, F. *Helv. Chim. Acta*, **31**, (1), p. 369 (1948).

(52) FEITKNECHT, W., and MAGET, K. *Helv. Chim. Acta*, **32**, (2), p. 1639 (1949).

(53) AEBI, F. *Acta Cryst.*, **3**, p. 370 (1950); see also Ref. (52).

(54) DE WOLFF, P. M. *Acta Cryst.*, **6**, p. 359 (1953).

(55) WELLS, A. F. *Acta Cryst.*, **2**, p. 175 (1949).

(56) DELORME, C. R. *C.R. Acad. Sci.* [*Paris*], **241**, p. 1588 (1955).

(57) YEARIAN, H. J., KORTRIGHT, J. M., and LANGENHEIM, R. H. *J. Chem. Phys.*, **22**, p. 1196 (1954).

(58) FRANCOMBE, M. H., and ROOKSBY, H. P. *Nature* [*London*], **178**, p. 586 (1956).

FRANCOMBE, M. H. *J. Phys. Chem. Solids.* To be published.

(59) FRANCOMBE, M. H. *Acta Cryst.*, **9**, p. 256 (1956).

(60) FRANCOMBE, M. H., and LEWIS, B. *Acta Cryst.* To be published.

Summarized proceedings of a meeting on low temperature distillation—London, March, 1957

An all-day discussion meeting on low temperature distillation was held by the Low Temperature Group of the Physical Society at The Institute of Physics, London, on Friday, 22 March, 1957. Summaries of the papers that were read and discussed are given in this report.

EXPERIMENTAL RESULTS FOR THE DISTILLATION OF LIQUID AIR IN A SMALL PACKED COLUMN

The first paper, by Dr. G. G. HASELDEN and Mr. R. A. NOTTLE (Imperial College of Science and Technology, London), was read by Dr. Haselden, who said that the air liquefaction and rectification plant at Imperial College had been designed on ambitious lines so that comprehensive research could be done on a pilot plant scale. It had taken some years to build the plant and to get it working satisfactorily, and only recently had results been obtained from it.

Three thousand cubic feet of air per hour is compressed to 200 atm, water removal is by freon precooling and, after passage through the heat exchanger, 15% liquefaction of the air is obtained at the expansion valve. Carbon dioxide removal is by filters in the liquid. The distillation cycle adopted is such that the column will operate over a wide range of flow-rates, reflux ratios and product ratios, and can be fed with either liquid or vapour. Only a part of the total air supply is fed to the column, the remainder being used to provide re-boil heat and refrigeration in the condenser. The control of this small, complex plant has been found to be a major problem, and can only be achieved by direct and precise control of column feed-rate and pressure.

The column is 3 in. in diameter and is packed with $\frac{1}{4}$ in. hundred-mesh brass McMahon saddles. Copper-constantan thermocouples are arranged at 6 in. intervals up the column, and coincident with most of the thermocouples are sampling points for liquid and vapour. The vapour sampling tubes withdraw the sample from across the entire width of the column and are shrouded to prevent the ingress of liquid. Liquid samples are collected in troughs and run into float chambers. When the chamber is full the float rises and lets out a liquid sample. Samples are taken as a continuous purge, and a full set can be withdrawn in a minute. Unfortunately, it has been found that the liquid samples are unreliable because of the relatively large amount of purge liquid which has to be withdrawn. Liquid sampling has therefore been abandoned.

Results. The temperature distribution in the column was taken as the criterion of stability, and a run was judged to be reliable when this remained constant for half an hour. Fig. 1 shows the argon and oxygen compositions of vapour samples at various heights in the column for four runs, from which it appears that the analyses are self-consistent. However, when the measured temperatures are compared with those calculated from the known liquid-vapour equilibrium data, the measured temperatures appear much higher, although the terminal conditions agree. The measured argon distribution also differs slightly from that calculated. The heights of theoretical plates (HETP) calculated separately for the three components agree in the middle of the column but differ at the ends. They also display a definite variation with the concentration of the components and hence are not constant at all levels in the column. They average about 5 in. The effects noticed are too great to be explained by experimental error and point to the need for more detailed investigation of the distillation of multicomponent mixtures.

In the discussion which followed, Dr. P. M. SCHUFTAN (British Oxygen Engineering Ltd., London), said that in industrial practice HETP's of 3 in. could be obtained and he wondered whether carbon dioxide blockages in the packing were giving unequal distribution. Dr. Haselden replied that American claims of HETP's of 2–3 in. had been made for total reflux experiments, but that at minimum reflux greater values had been reported. He did not think that the column had ever run for sufficient periods for significant amounts of carbon dioxide to have accumulated in the column.

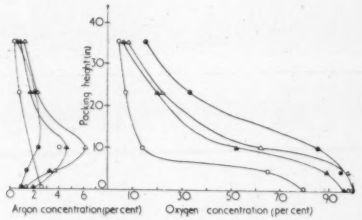

Fig. 1. Measured argon and oxygen concentrations *versus* packed height

● = run 1; ▲ = run 2; △ = run 3; ○ = run 4.

Dr. F. DIN (British Oxygen Research and Development Ltd., London) asked how the argon analyses were carried out and whether 100% equilibrium between liquid and vapour compositions was assumed when calculating the theoretical temperature distribution. The reply was that argon was analysed by a catharometer and perfect equilibrium was assumed in the theoretical calculations.

Mr. A. G. MACKIE (British Oxygen Engineering Ltd., London) asked whether a larger diameter column had been tried and the answer was in the negative. Dr. J. B. GARDNER (British Oxygen Research and Development Ltd., London) agreed that the difficulties in obtaining consistent results with a small unit were great. He wondered whether the equilibrium data of Weishaupt [see Ref. (11)], which were often used in column calculations, were suspect. Dr. Haselden agreed that Weishaupt's data were not all that could be desired, but any inaccuracies in them could not possibly account for the effects noted.

IRREVERSIBILITY IN AIR SEPARATION COLUMNS

The next paper, by Dr. J. B. GARDNER and Mr. K. C. SMITH (British Oxygen Research and Development Ltd., London), was read by Mr. Smith.

When air is separated a minimum quantity of work—the isothermal reversible work of separation—must be performed. This work is given by the equation

$$W_{rev} = \Delta H - T_0 \Delta S_{rev}$$

where T_0 is the ambient temperature and ΔH and ΔS_{rev} are the differences in enthalpy and entropy between air and the products of separation; ΔH is nearly zero and ΔS_{rev} is a function of the purity of the products. For the separation of air into oxygen and nitrogen plus argon at 20° C, the value of W_{rev} in practical units is 0·42 kWh per 1000 ft^3 of air separated or 1·98 kWh per 1000 ft^3 of oxygen product.

In any practical process there will be a number of thermodynamically irreversible features, such as pressure drops, temperature differences and heat inleaks. These will appear as irreversible entropy increases and will require the performance of additional work equal to $T_0\Delta S_{irrev}$. Some irreversible features are inherent in the process used, no matter how good the operation. Others are "design" factors due to practical limitations in the equipment.

Any adiabatic rectification column is intrinsically irreversible, since perfect phase equilibrium cannot be achieved at all points in the column. If a hypothetical column with an infinite number of plates operating at minimum reflux is considered, its operation requires the pumping of 3760 cal (per mole oxygen produced) from the condenser temperature 77·4° K, to that of the boiler 90·2° K. The work required equals 2·82 kWh per 1000 ft^3 oxygen which, compared with the isothermal reversible work of separation, represents an efficiency of 70%. If 20% above minimum reflux is provided and temperature differences of 2° are allowed in the condenser and reboiler, the efficiency drops to 44%. The McCabe–Thiele diagram[1] shows that a fully reversible column requires the operating and equilibrium lines to coincide over the whole range. This implies a continuously variable reflux ratio which could theoretically be achieved by adding appropriate quantities of heat at all levels in the column below the feed instead of solely at the boiler, and abstracting them above the feed at all levels instead of solely at the condenser.

Work penalties due to irreversibility in an air separation column

Irreversibility arising from:	*Work equivalent (kWh/1000 ft³ oxygen)* *Ideal case (A)*	*Practical case (B)*	*Penalty (B–A)*
Adiabatic rectification	2·30	2·30	
Reflux above minimum	0·57	0·57	
Expansion valves	0·22	0·38	0·16
Undercooler	0·02	0·09	0·07
ΔT's in condenser-reboiler		0·48	0·48
ΔP's across trays		0·54	0·54
Heat inleak		0·54	0·54
Total:	3·11	4·90	1·79

The table shows the penalties for irreversibility in a typical air separation double column. Even in an ideal column the provision of extra reflux contributes to the irreversible entropy increase, as do the expansion of the liquid streams in Joule–Thomson throttling valves and the operation of the undercooler. In an actual column the penalties in addition to those incurred in the ideal column are attributable to design factors, but the largest single factor causing irreversibility is that due to adiabatic rectification itself, which is approximately the same in an ideal column and in an actual column.

The totals show that in an actual column the irreversible losses are equivalent to 4·90 kWh per 1000 ft^3 oxygen, of which 3·11 kWh are intrinsic and 1·79 kWh due to design factors. These figures assume that the compression is performed reversibly. Actually, the penalties are almost twice these due to compressor and driving motor inefficiencies.

The practical result of these irreversible effects is an increase in the required air delivery pressure to the lower column. Thus each degree Kelvin across the reboiler-condenser is responsible for 0·35 atm increase in the admission pressure. Heat inleak is in a different category and requires an addition to the refrigeration load. It is theoretically possible to improve efficiency by providing intermediate columns and condensers, but it is doubtful whether the extra complications are justified. On the design side, improvement in efficiency usually involves an increase in the capital cost. Any real improvement in intrinsic efficiency, if at all possible, probably lies in the development of a radically different process.

Dr. T. J. WEBSTER (British Oxygen Research and Development Ltd., London), asked whether superheating in the oxygen boiler diminished the efficiency. Mr. Smith replied that it probably did, because of the increased ΔT's. Mr. P. SAHGAL (Imperial College, London), asked the size of the plant for which the heat inleak figure given by Mr. Smith applied. Mr. Smith said the figure was for a fairly large plant, say 400 m^3 oxygen per hour.

RECTIFICATION CALCULATIONS IN AIR SEPARATION COLUMNS

The paper, by Mr. B. CURRY and Miss V. M. SMITH (British Oxygen Engineering Ltd., London), was presented by Mr. Curry.

Rectification calculations have to be carried out for three principal reasons: to design new plants, to compare different processes and to evaluate the performance of producing plants. In all these cases high accuracy is not called for since design margins are always allowed. What is important is that the same routine should always be followed so that the results for different plants are strictly comparable. It is also important to choose methods of wide applicability, and speed is often of vital importance.

Of the well-known standard methods, the McCabe–Thiele method[1] is limited to two components and assumes constant molal overflow. Ponchon[2] and Savarit's[3] graphical method takes account of the variation in overflow and can be extended to three component mixtures. Sorel's[4] plate-to-plate method requires solutions by trial and error. It is accurate and comprehensive, but very tedious unless electronic computation can be called to aid. Sorel and Lewis's[4, 5] method is a simplification at the sacrifice of accuracy. Smoker's[6] method is a rapid analytical method for two components, but of doubtful validity, whilst Underwood's[7] method is an extension of Smoker's method to multi-component systems.

The selection of a suitable method for air rectification calculations is dictated by the following three considerations: air is a three-component mixture, the effect of the 1% argon, which is a "sandwich" component, being considerable; the variation in overflow cannot be ignored; and the relative volatility of the components is not constant over the range. The authors' method is a modified form of Sorel's method in which the overflow rate is assumed to be a linear function of the oxygen concentration. At first sight this might seem rather a crude assumption, but the method becomes increasingly accurate as the number of outlets and feed points, which give terminal conditions, increases.

The first step in the method is to produce the overall heat balance and then to establish the equation of the form:

$$L = A - Bx$$

for the relation between overflow rate L, and oxygen concentration x. Due allowance must be made for heat inleak into the section under consideration. Using the appropriate equilibrium data, one then works from the top tray downwards, determining the quantities and concentrations on each tray. It is preferable to take the equilibrium data from tables rather than graphs as this reduces chance errors and eyestrain. The results are usually presented in the form of a graph showing argon concentration *versus* oxygen concentration in the liquid on each tray.

The justification of the authors' method lies in the fact that their predictions are usually fulfilled in practice. Apparently low tray efficiencies are due to over cautious safety margins included by designers. Other standard methods indicate that some separations are impossible that have in fact been achieved. Mr. Curry gave some specific examples in air separation where the authors' calculation methods have been thoroughly proved.

In the discussion Dr. R. W. SARGENT (L'Air Liquide, Paris), agreed that the assumption of a linear relationship between the overflow rate and the composition gave very good results in practice, even with mixtures of five and six components. However, he thought that the nitrogen composition as the other variable gave better results than the oxygen composition.

A DISTILLATION PACKING DESIGNED FOR USE IN PARTIAL CONDENSERS AND EVAPORATORS

Dr. HASELDEN, in a paper by himself and Mr. A. WAHHAB (Imperial College of Science and Technology, London), said that Mr. Smith had pointed out in his paper that adiabatic distillation was a major source of irreversible entropy increase in air separation. If the distillation could be coupled with the heat exchange, which is also a fundamental part of the process, then an increase in the overall efficiency should result. In an attempt to achieve this end, they had taken an extended plate heat exchanger of the type manufactured by the Marston Excelsior Co. and adapted it for simultaneous distillation by incorporating the novel "overflow" packing shown in Fig. 2. The packing comprises a corrugated sheet brazed between flat metal plates $\frac{7}{16}$ in. apart. Rectangular holes $\frac{1}{4} \times \frac{3}{16}$ in. are cut in the corrugations to permit the upward flow of vapour and the downward flow of liquid. Liquid flows down the side walls and collects in the troughs where the corrugated sheet is brazed to the walls. This liquid overflows through the rectangular holes down the under surface of the corrugation and thence through the holes in the next lower corrugation back to the wall. The vapour takes a zigzag path as it rises through the holes in the corrugations. This packing is known to have good heat transfer characteristics, but in the present paper Dr. Haselden proposed to talk only about its properties as a distillation packing.

So far work has been carried out with the usual test mixtures at normal temperatures on an experimental column made up of a single sandwich 4 in. wide. It has been found that the efficiency is sensitive to vertical alinement, and for the best results the column must remain within 1° of the vertical in the plane of the sandwich. Experimental values of the height of each theoretical unit (HTU) as low as 1 in. have been measured but they are found to lie normally in the range 2–3 in. The packing is found to function well over a wide range of vapour flows. In general it is found that HTU values increase substantially at minimum reflux conditions, but absence of similar experimental tests with normal packings under these conditions makes comparison with other packings difficult.

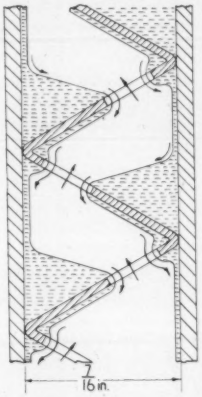

Fig. 2. Overflow packing for use in partial condensers and evaporators

In the discussion Dr. J. B. GARDNER wondered whether the effect of inclination out of the vertical would not be more critical in larger sizes. Dr. Haselden said that for large sizes a method had been developed in which the packing could be divided into a number of liquid-tight sections. Mr. SHAW (Atomic Energy Research Establishment, Harwell), asked whether it was proposed to make the whole column from this packing or just the condenser. Dr. Haselden replied that in general the new packing was not likely to replace the whole conventional column but, in air separation, the section below the feed. Dr. T. J. WEBSTER thought cleaning would present a problem and Dr. Haselden agreed that the new packing would in general only be suitable for use with clean liquids, as for instance in the rectification of air or light hydrocarbons. Dr. Gardner said that even air columns needed cleaning up occasionally, but agreed that washing with solvents would be possible with the new packing.

NEW DATA FOR THE PHASE EQUILIBRIA OF THE NITROGEN–OXYGEN SYSTEM AT 1·3 ATM

The paper was presented by Mr. A. H. COCKETT (British Oxygen Research and Development Ltd., London).

Data previously available on the nitrogen–oxygen system was based on the work of Inglis[8] and Dodge and Dunbar,[9] who incorporated Inglis' results into their own work. There is reason to believe that these results are of doubtful accuracy and a new investigation at a constant pressure of 1·32 atm, the upper column pressure in an air separation plant, has been carried out.

The arrangement of the apparatus is shown in Fig. 3; *A* is the equilibrium vessel in the cryostat. Vapour was circulated through the liquid in the equilibrium vessel by means of the double action electromagnetically operated pump *B*. The

analytical section, which could be isolated from or included in the circulation system, contained the quartz fibre gas density balance *C*, pressure adjusting bulbs *D*, the wide bore mercury manometer *E*, on which all relevant pressures were read, and subsidiary manometers. Liquid samples were drawn off from the equilibrium vessel and evaporated into the flask *F*, after which they were passed into the gas density balance of analysis.

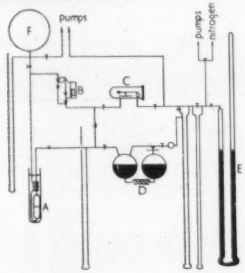

Fig. 3. Liquid-vapour equilibrium apparatus

It was found that six hours' circulation of vapour through the liquid was needed for the attainment of equilibrium, although usually it was more convenient to circulate overnight, i.e. about sixteen hours. The essential measurements required were the temperature and pressure in the equilibrium vessel and the pressure at which the density of the vapour was equal to that of pure nitrogen.

The results of this work when plotted on a temperature-composition diagram show that there is an appreciable deviation from Raoult's law and that the present results differ from those of Dodge and Dunbar,[9] particularly for mixtures containing less than 50% of nitrogen in the liquid. This difference is more pronounced in a graph showing the relative volatility, α, as a function of nitrogen concentration.

It has been shown by Herington[10] that if one plots

$$\log \gamma_1/\gamma_2 = (\log \alpha - \log p_1/p_2)$$

where γ_1, γ_2 represent activity coefficients, nitrogen and oxygen, α, the relative volatility and p_1, p_2 the vapour pressures of pure nitrogen and oxygen, against nitrogen concentration in the liquid, the areas above and below the axis should be equal for thermodynamic consistency. Judged by this test, the present results are satisfactory.

In the discussion Dr. R. W. SARGENT asked how the present results compared with those of Weishaupt[11] and Sagenkahn and Fink.[12] Mr. Cockett replied that it was only possible to compare the present results with those of Sagenkahn and Fink at one temperature and here the agreement was good. The agreement with Weishaupt's data was still being looked into but it appeared to be good.

THE VAPOUR PRESSURE OF THE ISOTOPIC SPECIES OF CARBON MONOXIDE

Mr. T. F. JOHNS (Atomic Energy Research Establishment, Harwell) in the next paper said that at Harwell low temperature distillation of carbon monoxide is used as a means of enriching the ^{13}C isotope of carbon and the ^{18}O isotope of oxygen. They have a column containing between 600 and 700 theoretical plates. One might expect that the order of volatility of the isotopic species of carbon monoxide would be $^{12}C^{16}O$ most volatile, followed by $^{13}C^{16}O$, and finally $^{12}C^{18}O$, least volatile. In point of fact, as between the two latter, $^{12}C^{18}O$ is the more volatile.

The method of measuring the vapour pressures was to measure the difference between that of the isotope mixtures and pure $^{12}C^{16}O$, the vapour pressure of the latter being assumed known. The samples of pure $^{12}C^{16}O$ and the isotope mixture were condensed into two cylindrical cavities drilled into a copper block connected to the limbs of a differential aneroid manometer. A third larger cavity was also drilled into the block and into this cavity liquid oxygen could be condensed. The copper block with the tubes of poor conducting metal leading away from it was suspended in a vacuum chamber surrounded by liquid nitrogen. The temperature of the block could be brought below that of the surrounding liquid nitrogen jacket by pumping away the liquid oxygen, after which the temperature remained almost steady for long periods, rising very slowly. The aneroid manometer had an "optical-lever" method of magnifying its deflexion. A pressure difference of 1 mm gave a movement of 20 mm on the light beam.

Typical results are shown in Fig. 4, in which the ratio of the difference between the vapour pressures of mixtures of $^{13}C^{16}O$

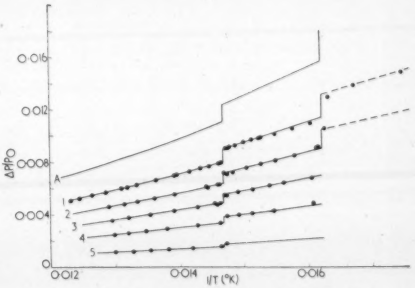

Fig. 4. Vapour pressure data for $^{13}C^{16}O$

Curve *A*, 100% $^{13}C^{16}O$; curve (1) 72·79% $^{13}C^{16}O$; curve (2), 57·76%; curve (3), 44·75%; curve (4), 30·57%; curve (5), 13·98%.

and $^{12}C^{16}O$ to that of pure $^{12}C^{16}O$ is indicated as a function of the reciprocal of the temperature. These results show that the ideal solution law is followed, so that it is possible to extrapolate the results to give the ratio for pure $^{13}C^{16}O$. The breaks in the curves represent the triple points and the transitions between the α and β solids. On the scale of the graph they appear as vertical jumps but, since the triple points and transition points of the isotopes are not identical, they are in fact steeply rising curves.

Mr. Johns then dealt with the possible reasons why the $^{12}C^{18}O$ isotope is more volatile than $^{13}C^{16}O$. In brief, the $^{12}C^{18}O$ molecule is the more asymmetric of the two and as a result it has a slightly larger molecular volume. This has the effect of giving an increased vapour pressure.

Similar results have been obtained with methane and oxygen. The most difficult part of the work was the initial purification of the gases and demonstrating that they were pure. This was achieved by distilling the liquefied gases in a small fractionating column having the equivalent of fifty

to sixty theoretical plates, until the overhead fraction had a constant vapour pressure. The vapour pressure at the triple point was shown to be independent of the proportion of the material frozen.

In the discussion Dr. K. A. G. MENDELSSOHN (Clarendon Laboratory, Oxford), asked why oxygen was used for the undercooling in preference to nitrogen. Mr. Johns replied that nitrogen freezes when it is pumped, and that in practice lower temperatures can be reached with oxygen. Also a greater weight of oxygen can be condensed into the cavity. Dr. T. J. WEBSTER asked whether it was certain that the two isotope cavities in the copper block were always at the same temperature. Mr. Johns said that experiments with identical substances in the cavities showed no vapour pressure difference after thermal equilibrium had been obtained in about fifteen minutes. Dr. F. DIN asked for more details of the small rectifying column for the initial purification. Mr. Johns said that the column consisted of a five-start brass screw thread of $\frac{3}{8}$ in. diameter, inside a concentric tube. It worked very well, the secret of success being the very small heat input of 0·1 W.

DISTILLATION OF BORON TRIFLUORIDE FOR THE PRODUCTION OF ^{10}B

The paper was presented by Dr. P. T. NETTLEY on behalf of himself and Dr. H. KRONBERGER (United Kingdom Atomic Energy Authority, Risley and Capenhurst).

Kilogramme quantities of highly enriched ^{10}B are required by the U.K.A.E.A. in a number of reactor and nuclear physics experiments. Fractional distillation of boron trifluoride at −95° C is used to produce the isotope. It is interesting to note that the heavier isotopic species $^{11}BF_3$ is the more volatile.

Information from Russian workers showed that the ratio of the vapour pressures p_{heavy}/p_{light} is equal to 1·009 ± 0·003 at −103° C. To obtain the basic design data (separation factor and HETP) for a plant more precisely, a short glass column, 4 ft high and 2·2 in. diameter, has been operated between −95 and −115° C. This column was packed with $\frac{1}{16}$ in. gauze Dixon rings and was thermally insulated by a silvered vacuum jacket. Evaporation was obtained by immersing a heated coil in the liquid boron trifluoride; the condenser was cooled with liquid nitrogen.

The condenser system for controlling the column temperature with different evaporation rates was ingenious and is depicted in Fig. 5. A large vessel *A* is kept filled with liquid nitrogen at −196° C. Compartment *B* immediately below *A* contains boron trifluoride boiling at the triple point pressure and temperature, 69 mm of mercury and −127° C. Boron trifluoride vapour condenses as a solid on the surface cooled by liquid nitrogen until the thickness of solid has sufficient thermal resistance. Boron trifluoride then condenses as a liquid at the triple point, −127° C, on this surface and refluxes. Heat to evaporate the liquid boron trifluoride in compartment *B* is supplied either by an electrical heater immersed in this liquid or by vapour in the column below condensing at the top of compartment *C*. The relative amounts of liquid and solid boron trifluoride in compartment *B* are dependent on the heat input to this compartment, the thickness of the solid layer being determined by the thermal conductivity of the solid. If the heat input is increased the thermal resistance of the solid layer is too large, therefore part of the solid melts and falls back into the liquid until the solid layer has the correct thermal resistance and equilibrium is re-established. Changes of heat input therefore have very little effect on the temperature of liquid boron trifluoride boiling in compartment *B*. This temperature is always close to the triple point temperature. The temperature of the boron trifluoride in the column itself can be varied by admitting gaseous nitrogen to compartment *C*. The boron trifluoride vapour in the column then has to diffuse through a blanket of gaseous nitrogen before it condenses. This raises the column temperature above the triple point temperature by an amount determined by the column evaporation rate and the quantity of gaseous nitrogen present.

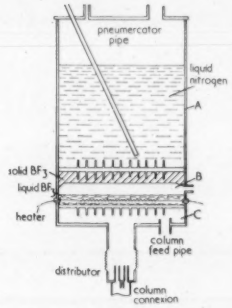

Fig. 5. Overhead condenser

Concentration measurements along the column at total reflux enabled $(q - 1)/h$ to be determined, where q is the ratio of the vapour pressures, p_{heavy}/p_{light}, and h is the HETP. Values of q and h were determined individually by continuously withdrawing material at a determined rate from the bottom of the column and feeding it back into the top. This gave a ^{10}B transport down the column which modified the concentration gradient obtained on total reflux. Data from these experiments gave a value of $q = 1{\cdot}0065 \pm 0{\cdot}003$ at −100° C; h varied from 2 to 5 cm as the mean vapour velocity in the column varied from 20 to 50 cm/s.

These data have been used to construct and operate a plant to produce boron containing 95% ^{10}B. The plant consists of two columns, each having packed lengths of 57·5 ft, in series. The first column produces material containing 50% ^{10}B at the boiler. This is fed into a point near the top of the second column, which is smaller in diameter than the first column, where it is enriched to 95% ^{10}B in the boiler. The small column strips down to 30% material at the condenser and this is fed back into the large column at the appropriate point. Waste material containing 9% ^{10}B is withdrawn from the condenser of the large column. The plant has an equilibrium time of twenty-three days and has been producing boron containing 95% ^{10}B with an output in excess of the design production rate which was 15 kg/year.

Dr. Nettley exhibited slides showing the experimental and production columns.

In the discussion, Dr. J. B. GARDNER asked whether, in view of the long equilibrium time, any special precautions had been taken to ensure that the columns did not have to shut down and also what steps had been taken to ensure that the column was adiabatic. Dr. Gardner also asked whether it had been found necessary to pre-flood the packing.

Dr. Nettley replied that in order to minimize the possibility

of shut down, commercial boron trifluoride is purified by distillation at −80° C prior to being fed into the plant. Commercial boron trifluoride contains oxides of sulphur and hydrates of boron trifluoride, all of which are solid at column temperatures and could cause blockages in pipes. Liquid nitrogen is stored in large storage tanks under pressure. This pressure is used to force the liquid nitrogen to the condensers at the top of the column. Liquid nitrogen feed lines have been duplicated to make failure of the coolant supply unlikely. The columns are thermally insulated by aluminium vacuum jackets. Failure of the vacuum would result in high inleak of heat which would cause the columns to flood. To avoid this happening both columns have a double vacuum jacket and the inner and outer jackets have separate pumping systems. Vacuum failure in one jacket does not cause the columns to flood. The heat inleak into each column is between 50 and 100 W compared with heat inputs of 1150 and 550 W to the boilers of the large and small columns respectively. Because the product is withdrawn from the boilers, higher inleak of heat could be tolerated.

Dr. H. LONDON (Atomic Energy Research Establishment, Harwell), pointed out that non-adiabatic conditions in columns packed with Dixon gauze rings do not appear to decrease the performance of the packing. Dr. Nettley said that the columns had been pre-flooded. No data had been obtained for the separation performance of the packing when distilling boron trifluoride without pre-flooding. It had been noted that pre-flooding doubled the pressure drop in the column. It is considered that this is due to the packing having a higher liquid hold-up in the pre-flooded condition and that pre-flooding is necessary.

THE DISTILLATION OF HYDROGEN FOR THE PRODUCTION OF DEUTERIUM

This paper was presented by Mr. W. H. DENTON (Atomic Energy Research Establishment, Harwell). The A.E.R.E. has been interested in hydrogen distillation for some years and is now developing the process on a production scale. There are now plenty of fundamental data on the liquid-vapour equilibria of the hydrogen–hydrogen deuteride and hydrogen deuteride–deuterium systems which have been accumulated in the Universities and on which design calculations can be made. At Cambridge there is an experimental column with single bubble cap plates of 50% efficiency. This column works well but it is expected that hydraulic problems will arise on a larger scale associated with the extremely low density of liquid hydrogen. To produce one ton of heavy water per year 1000 m^3 of hydrogen gas must be liquefied and distilled per hour. Ninety plates in a 10 ft diameter column will be needed.

Much attention has been given to the separation of deuterium from ammonia synthesis gas. In this process the nitrogen is completely condensed by heat exchange, leaving a pure hydrogen feedstock to the column. Refrigeration is provided by turbines expanding pure gas from the column. The biggest problem in this process is the effective re-evaporation of the nitrogen which is returned to the ammonia synthesis plant. Reversing exchangers are effective for the preliminary condensation of the nitrogen down to a temperature of 40° K, but they become impossible for removing the last traces of nitrogen below this temperature.

Because of the difficulties inherent in the separation of deuterium from ammonia synthesis gas, consideration has also been given to processes which involve liquefaction and distillation of hydrogen only. In these processes the hydrogen is re-cycled between the deuterium separation unit and a unit in which exchange takes place between the hydrogen and a deuterium-containing compound, such as water or hydrogen sulphide.

Dr. J. B. GARDNER, in the discussion, asked whether the ortho-para conversion presented any problems and whether any difficulties were anticipated with the turbine bearings at low temperature. Mr. Denton said that the hydrogen did not remain in the plant as liquid long enough for the ortho-para conversion to be important. Nevertheless, it was necessary to ensure that this conversion was not catalysed by an incorrect choice of materials of construction. The turbine bearings were at room temperature. Dr. R. W. SARGENT said that part of the trouble with the separation of the solid nitrogen was that it would not stick to the surfaces of the heat exchangers. He thought that consideration should be given to adsorbing it at the triple point.*

F. DIN

REFERENCES

(1) MCCABE, W. L., and THIELE, E. W. *Industr. Engng Chem.*, **17**, p. 605 (1925).

(2) PONCHON, M. *Tech. Mod.*, **13**, pp. 20, 55 (1921).

(3) SAVARIT, R. *Arts et Métiers*, pp. 65, 142, 178, 241, 266, 307 (1922).

(4) SOREL, E. *Comptes Rendus*, **58**, pp. 1128, 1204, 1317 (1889); **68**, p. 1213 (1894).

(5) LEWIS, W. K. *Industr. Engng Chem.*, **14**, p. 492 (1922).

(6) SMOKER, E. H. *Trans. Amer. Inst. Chem. Eng.*, **34**, p. 65 (1938).

(7) UNDERWOOD, A. J. V. *Trans. Inst. Chem. Eng. Lond.*, **10**, p. 131 (1932).

(8) INGLIS, J. K. H. *Phil. Mag.*, (6), **11**, p. 640 (1906).

(9) DODGE, B. F., and DUNBAR, A. K. *J. Amer. Chem. Soc.*, **49**, p. 591 (1927).

(10) HERINGTON, E. F. G. *J. Inst. Petrol*, **37**, p. 332 (1951).

(11) WEISHAUPT, J. *Angew. Chemie*, **B20**, p. 321 (1948).

(12) SAGENKAHN, M. L., and FINK, H. L. *O.S.R.D., Report No.* 4493 (1944).

* Similar papers to the last three were read at the International Symposium on Isotope Separation in Amsterdam during April. Full accounts will be published by the North Holland Publishing Co.

Viscous flow between rotating cylinders and a sheet moving between them

By M. R. Hopkins, M.Sc., Ph.D., F.Inst.P., Department of Physics, University College of Swansea

[*Paper received* 17 *April*, 1957]

The motion of a sheet, emerging from a liquid and passing between a pair of cylindrical rollers, is considered. An expression for the thickness of the liquid layer finally left on the sheet is derived in terms of the viscosity of the liquid, the size of the rollers, the speed at which the sheet moves through them and the force with which they are pressed together.

The coating of a sheet with a thin layer of liquid by passing the sheet through a bath of the liquid and then removing the excess by means of pairs of cylindrical rollers is a process of considerable industrial importance. There are often several pairs of rollers. They serve to pull the sheet through the bath, but their main function is to control the thickness of the layer of liquid finally left on the sheet. The system is

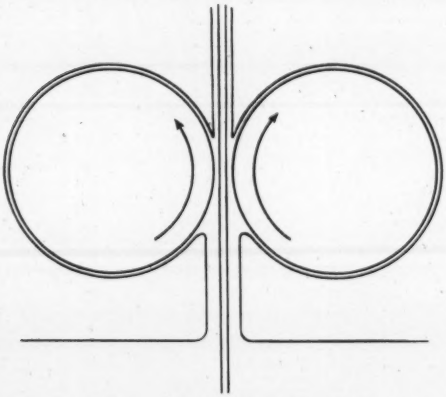

Fig. 1. Schematic diagram of system

illustrated in Fig. 1. The removal of liquid takes place in two ways:

(i) All the liquid approaching the line of closest approach (the "nip") of the rollers from underneath does not go through. Some of it flows back.

(ii) As the sheet emerges above the nip, the liquid is shared between the sheet and the rollers. That which adheres to the rollers is removed by brushes bearing on the under-side of the roller surfaces. This liquid drops back into the bath.

The first of these effects would be expected to predominate in the bottom pair of rollers, i.e. those nearest to the bath, and the second in the case of subsequent pairs. In fact, since the action of the upper pairs of rollers is merely that of sharing the liquid between themselves and the sheet, they need not be considered further. It is the action of the bottom pair that will be considered in detail. An example of the kind of system described is that which is used to coat steel sheet with molten tin in the manufacture of tinplate. This is by no means the only example; the use of rollers in controlling the thickness of a liquid coating applied to a sheet is a process which is common to a number of industries.

The diagram of Fig. 1 is schematic only, the scale being very much distorted. In the example cited, the rollers are about four inches in diameter, the thickness of the sheet just over a hundredth of an inch and the thickness of the tin on the sheet above the rollers of the order of a ten-thousandth of an inch. The rollers are forced together by spring pressure.

The physical problem is that of determining the relation between the controllable parameters (pressure between the rollers, speed, etc.) and the properties of the material.

VISCOUS FLOW BETWEEN ROLLER AND SHEET

Owing to the symmetry of the system, it is sufficient to consider the flow of a viscous fluid between one roller and one side of the sheet (Fig. 2).

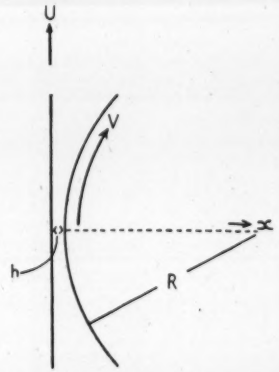

Fig. 2. Diagram showing flow of viscous fluid between one roller and one side of sheet

The problem of the distribution of pressure between two cylinders rotating and almost touching while completely immersed in a fluid has been discussed in the literature.[1–4] The method used by Gatcombe is applicable to the present problem. The usual assumptions of the hydrodynamical theory of lubrication are made (the fluid is Newtonian; the

flow is laminar; inertial effects in the fluid are neglected; the fluid pressure is constant in the x direction of Fig. 2).

If we let $v = v(x, y)$ be the velocity of the fluid,
$p = p(y)$ the pressure in the fluid in excess of atmospheric pressure,
R the radius of the roller,
h the distance of closest approach of the roller and the sheet,
η the viscosity,
U the velocity of the sheet,
and V the tangential velocity of the roller at its surface,

the differential equation to be satisfied is approximately

$$\frac{\partial^2 v}{\partial x^2} = \frac{1}{\eta}\frac{dp}{dy} \tag{1}$$

which may be integrated, with the boundary conditions

$$\left.\begin{aligned} v &= U \text{ at } x = 0 \\ v &= V \text{ at } x = h + y^2/2R \\ &= h\sec^2\theta, \text{ where} \\ \theta &= \tan^{-1} y/(2Rh)^{\frac{1}{2}} \end{aligned}\right\} \tag{2}$$

The solution in the region where the liquid fills the gap is

$$v = \frac{1}{2\eta(2Rh)^{\frac{1}{2}}}(x^2\cos^2\theta - xh)\frac{dp}{d\theta} + \frac{x}{h}(V - U)\cos^2\theta + U \tag{3}$$

If $\bar{v}$ is the mean velocity of the fluid at the distance of closest approach of the roller and sheet, we have at every θ

$$\int_0^{h\sec^2\theta} v\,dx = \bar{v}h = \text{constant} \tag{4}$$

Inserting (3) we find that in the region where the liquid fills the gap

$$\frac{dp}{d\theta} = \frac{12\eta(2Rh)^{\frac{1}{2}}}{h^2}(W\cos^2\theta - \bar{v}\cos^4\theta) \tag{5}$$

where $W = \frac{1}{2}(U + V)$

Assuming that the liquid fills the gap down to $-y_0 \gg (2Rh)^{\frac{1}{2}}$ and that p is zero there we have, practically $p = 0$ at $\theta = -\pi/2$ and hence

$$p = \frac{12\eta(2Rh)^{\frac{1}{2}}}{h^2}\left[\frac{W}{4}(\pi + 2\theta + \sin 2\theta) - \right.$$
$$\left. - \frac{\bar{v}}{32}(6\pi + 12\theta + 8\sin 2\theta + \sin 4\theta)\right] \tag{6}$$

Equation (5) is equation (15) of Gatcombe's paper[2] and equation (6) is substantially equation (3) of the paper by Banks and Mill.[4]

In contrast to the problem of completely submerged rotating cylinders we cannot now proceed to put $p = 0$ when $\theta = +\pi/2$. Let α be the value of θ corresponding to the value of y at which the liquid above the nip of the rollers divides between the roller and the sheet. Then, since p becomes zero when θ becomes α, we have from equation (6)

$$\frac{\bar{v}}{W} = \frac{8(\pi + 2\alpha + \sin 2\alpha)}{6\pi + 12\alpha + 8\sin 2\alpha + \sin 4\alpha} \tag{7}$$

We must now determine α. Let D be the point where the liquid divides between the roller and the sheet (Fig. 3). (If the surface tension of the liquid is small there will be a sharp curve at D.) The velocity v at D must be zero—a finite velocity there would mean a discontinuity in the vector velocity of a particle, requiring infinite accelerations of an impossible nature. At this stage let us make the simplifying assumption, which is justified in the practical case, that the sheet is pulled upwards by an external mechanism at a velocity U which is equal to V. Then D, the point where the liquid divides, is halfway between the roller and the sheet.

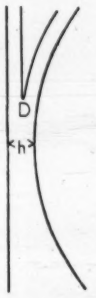

Fig. 3. Point of division of liquid between roller and sheet

α may then be determined from the condition that v is zero at D.

At D, $x = \frac{1}{2}h\sec^2\alpha$. Substituting this in the right-hand side of equation (3), making the left-hand side zero, and using equation (5) gives us

$$\bar{v}/V = \tfrac{1}{2}\sec^2\alpha \tag{8}$$

Combining equations (7) and (8), we have

$$\tfrac{1}{2}\sec^2\alpha = \frac{8(\pi + 2\alpha + \sin 2\alpha)}{6\pi + 12\alpha + 8\sin 2\alpha + \sin 4\alpha}$$

which may be written

$$3(\pi + 2\alpha) + 2\sin 2\alpha + 6(\pi + 2\alpha)\cos 2\alpha + $$
$$+ 5\sin 2\alpha\cos 2\alpha = 0 \tag{9}$$

The solution of this equation is

$$\alpha = 1{\cdot}0402 \tag{10}$$

which makes the relation between $\bar{v}$ and V

$$\bar{v}/V = 1{\cdot}3015 \tag{11}$$

We are now in a position to write down the pressure p in terms of known quantities, i.e.

$$p = \frac{12\eta(2Rh)^{\frac{1}{2}}V}{h^2}\left[\frac{1}{4}(\pi + 2\theta + \sin 2\theta) - \right.$$
$$\left. - \frac{1{\cdot}3015}{32}(6\pi + 12\theta + 8\sin 2\theta + \sin 4\theta)\right] \tag{12}$$

and to evaluate

$$F = \int p\,dy = (2Rh)^{\frac{1}{2}}\int_{-\pi/2}^{\alpha} p\sec^2\theta\,d\theta$$

where F is the total force (per unit width of sheet) between the roller and the sheet.

The result is $$F = 2{\cdot}5680\,\eta RV/h \qquad (13)$$

The thickness c of the fluid film on the sheet is given by

$$c = \frac{\bar{v}}{V}\frac{h}{2}$$

which, with the previous equation, gives

$$c = 1{\cdot}671\,\eta RV/F \qquad (14)$$

where the quantities are in c.g.s. units. This is the relation which is required. It is at least qualitatively in agreement with the experimental data, for it predicts that the coating thickness should increase with the speed and the size of the rollers and decrease with roller pressure and the temperature of the liquid (i.e. decrease with decreasing viscosity). The numerical factor might be altered by writing down the exact form of the differential equation instead of the approximate form in equation (1) and solving it numerically. The approximate solution in equation (14) is, however, of interest in that it shows how the physical quantities involved are related.

This work was done while the author was Head of the Physics Section of the Swansea Laboratories of the British Iron and Steel Research Association and formed part of the research programme of the Coatings Committee of the Association.

REFERENCES

(1) MARTIN, H. M. *Engineering*, **102**, p. 119 (1916).
(2) GATCOMBE, E. K. *Trans. Amer. Soc. Mech. Engrs*, **67**, p. 177 (1945).
(3) HERSEY, M. O., and LOWDENSLAGER, D. B. *Trans. Amer. Soc. Mech. Engrs*, **72**, p. 1035 (1950).
(4) BANKS, W. H., and MILL, C. C. *Proc. Roy. Soc. A*, **223**, p. 414 (1954).

Arc motion with magnetized electrodes

By A. E. GUILE, B.Sc.(Eng.), Ph.D., A.M.I.E.E., T. J. LEWIS, B.Sc.(Eng.), M.Sc., Ph.D., A.M.I.E.E., and S. F. MEHTA, B.E., Department of Electrical Engineering, Queen Mary College, London.

[*Paper first received* 14 *March, and in final form* 16 *July*, 1957]

The velocities of d.c. arcs moving in air at atmospheric pressure between horizontal and parallel cylindrical electrodes have been measured. The arcs moved freely in straight regular tracks in an axial direction under the action of magnetic fields set up by the current flow in the electrodes. Ferrous and non-ferrous electrodes were used and it was found that the axial velocity increased with the current in all cases, but was very much greater in magnitude for the steel electrodes. The hypothesis that the magnetic properties of the steels were responsible for the higher velocities was tested by magnetizing these materials in the axial direction along the electrodes. The cathode and anode spots then described helical paths with the anode moving in an opposite sense to the cathode, the circumferential component of the velocity being provided by the axial flux. It was deduced that magnetic fields within the electrode surfaces determined the motion.

It is suggested that transverse galvanomagnetic and thermomagnetic forces modify the electron emission and are responsible for the cathode motion. It appears that these forces also influence the motion of the anode spot.

INTRODUCTION

The motion of an arc in a magnetic field is governed by complex thermal and electrical forces acting on the arc column and on the active cathode and anode roots. The direction of the motion can in most cases be obtained by application of the usual rules of electromagnetic theory, treating the arc merely as a current-carrying conductor, but the magnitude of the motion cannot be determined so easily.[1] Furthermore, this treatment is not satisfactory as can be seen from the well-known phenomenon of the retrograde motion of the arc on mercury and solid metal electrodes under suitable conditions of magnetic field, current and vapour pressure.[2, 3]

Theories of this retrograde motion have been proposed by von Engel and Robson[4] and by St. John and Winans[2] among others, and involve processes, not in the column, but in the cathode-fall region. Electron and positive-ion motions in this high-field region determine the sites of new cathode spots for which electron emission is favourable. In this way, the arc progression is determined by microscopic conditions at the cathode.

The important role of the cathode processes in determining arc motion is further illustrated by experiments to be described below. These experiments provide evidence that magnetic fields within the cathode surface and to some extent in the anode surface play a very significant role and it may be that, in many cases, these alone determine the arc motion.

EXPERIMENTAL PROCEDURE

A drum camera operating at 960 frames/s was used to photograph arcs in free air between two horizontal and parallel cylindrical electrodes of approximately 1 cm diameter situated one above the other with the anode uppermost. The spacing was 3·2 cm and current was fed into and out of the electrode system at one end. The electrodes were smooth but not highly polished.

After initiation by an exploded wire at the current-feed end of the electrodes, the arc travelled along them either under the action of the magnetic field due to current in the electrodes, or else under the combined action of this field and an axial field set up in the electrodes by external means. The two

types of magnetic field operating on the arc are shown in Figs. 1 and 2. If an electrode is ferromagnetic then the magnetic flux density within it is increased and there is a discontinuity in the flux density at the surface as shown in Figs. 1 and 2. Interaction between arc current I and circumferential flux density B_c causes the arc to move in an axial direction with a velocity v_a (Fig. 1). Similar considerations for the anode will produce the same direction of motion.

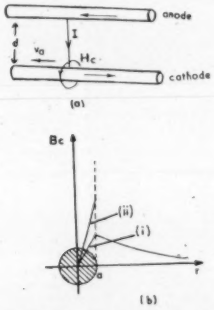

Fig. 1. (*a*) Axial motion due to circumferential flux.
(*b*) Circumferential flux density for:
(i) non-magnetic cathode.
(ii) magnetic cathode.

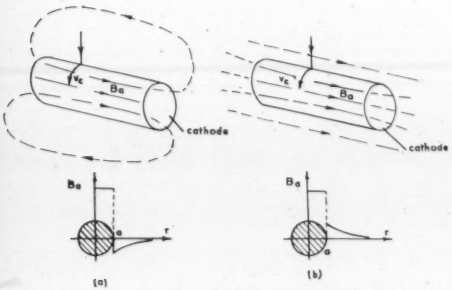

Fig. 2. Circumferential motion due to axial flux
(*a*) Permanently magnetized cathode.
(*b*) Electromagnetized cathode.

For ferromagnetic electrodes, it is also possible to produce appreciable axial flux density B_a either by means of an external electromagnet or else by magnetizing them permanently. An important distinction of later significance should be noted. Whereas the field directions will be the same inside and outside the electrodes when magnetized electrically, they will be opposite when the electrodes are permanently magnetized as shown in Fig. 2. Interaction between I and B_a will produce a circumferential force and a circumferential velocity v_c, and if B_c and B_a are present simultaneously then a helical motion of the arc might be expected.

RESULTS

Axial cathode velocities. Tests were made with copper, aluminium, brass, mild steel and magnetic stainless steel electrodes without axial magnetic field to determine the relationship between axial velocity v_a and current I. The results are summarized in Fig. 3.

The surface smoothness was similar at least for the drawn rods of brass, copper, aluminium and mild steel and although effects due to differences in emission properties are to be expected, nevertheless, it is significant that the velocities for the steels are distinctly higher than those of the other metals. The mild steel and the stainless steel have similar permeabilities so that differences in velocity may be due to surface conditions.

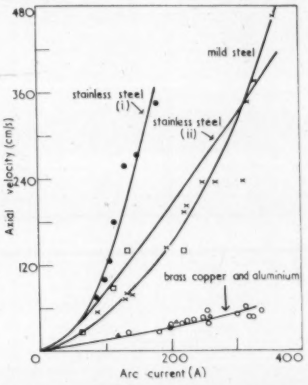

Fig. 3. Axial velocities of cathode and anode spots.
●● —— Stainless steel curve (i), axial cathode velocity measured with axial flux zero.
—— Stainless steel curve (ii), axial cathode velocity measured with axial flux present.
× × —— Mild steel—axial cathode velocity.
□ □ Mild steel—axial anode velocity.
○ ○ —— Brass, copper and aluminium—axial cathode velocity (points are those for brass).
△ △ Brass, axial anode velocity.

In the case of mild steel, for currents above those shown in Fig. 3 the nature of the cathode tracks changed. At lower currents the track was regular and continuous and melting had occurred as the arc moved forward. As the current was increased, the track became discontinuous with sections in which there was no cathode spot. This random jump occurs when the column driven forward by the magnetic field touches the electrode and two unstable arcs in parallel exist momentarily. This mode of discontinuous movement is similar to that outlined by Dunkerley and Schaefer.[5] This broken track was replaced at currents of about 500 A by a third type of continuous high velocity track. For this track there was surface discoloration and slight pitting, but no evidence of extensive melting. At still higher currents the cathode movement became random.[1] These various tracks are interesting and indicate that the arc motion is intimately connected with cathode phenomena,[6] but a full discussion is outside the scope of the present treatment. We shall confine our attention to the lower current range in which the motion is regular and melting has occurred.

Circumferential cathode velocities. The hypothesis that the magnetic properties of steel account for its cathode velocity being higher than that of non-magnetic materials, was investigated by introducing an axial magnetic field (Fig. 2). The cathode spot then described a helical path with the circumferential velocity v_c in the sense given by the normal laws for a magnetic field in the direction of that inside the cathode. This result is surprising and shows that the forces responsible for the circumferential motion lie within the cathode spot itself. This was verified by the fact that the helix direction was the same whether the cathode was an electromagnet or a permanent magnet, although the external fields away from the cathode surface were in opposite directions.

Reversal of the axial magnetism caused reversal of the sense of the helix, and in some tests the helix path completed three turns around the cathode. The track showed that the arc column had followed the path without short-circuiting back on to the cathode at a nearer spot.

For stainless steel cathodes magnetized electrically, the velocity v_c has been related to I and to the axial flux density B_a, and the results are summarized in Figs. 4 and 5. These

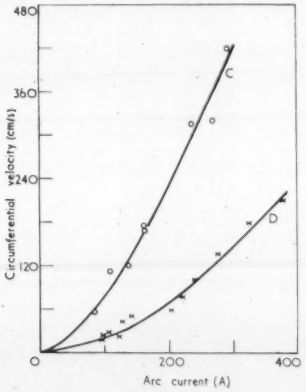

Fig. 4. Circumferential velocities of the cathode spot for a stainless steel cathode magnetized in the axial direction

C, $B_a = 1{\cdot}07$ Wb/m^2; D, $B_a = 0{\cdot}35$ Wb/m^2.

figures together with Fig. 3 offer strong evidence for the mechanism of arc motion being centred in the cathode spot itself and not in the arc column. This is borne out by the fact that the anode spot and column movements have little effect on regular cathode movement and only cause random jumps.[1] Some points on curve (i) in Fig. 3 for magnetic stainless steel cathodes refer to tests in which the anode was of the same material, and to others in which an aluminium anode was used. Although the anode spot remained stationary on the aluminium the cathode velocities were unaffected.

The relationship between v_a and v_c. In order to check whether the regular axial velocity v_a arises from magnetic fields *within* the cathode in the same way as the circumferential velocity v_c, the following procedure was adopted. For a given magnetic cathode carrying a current I, the circumferential magnetizing force at the surface H_c, was calculated from the equation

$$H_c = I/(2\pi a) + I/2\pi(d - a) \qquad (1)$$

where a is the electrode radius and d is the electrode spacing. B_c was then obtained from the magnetization curve and using this value of flux density in the axial direction, i.e. writing $B_a = B_c$, the corresponding value of v_c was then obtained from Figs. 4 and 5 for the same current I. This

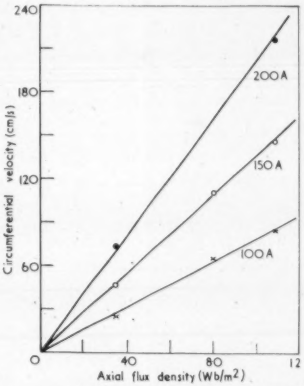

Fig. 5. Linear relationship between axial flux density B_a and the circumferential velocity v_c for stainless steel cathode spots

value of v_c is then compared in Fig. 6 with v_a for the same current I from curve (ii) of Fig. 3.*

Exact agreement is not to be expected for several reasons. (i) It is not certain that the axial force producing v_a can be computed from the product IB_c using equation (1) since the current distribution will be complex both at the point of emission and in the underlying metal, e.g. when there are multiple emission spots.[7] The force on individual spots will be different from that computed above and the circumferential field acting on spots remote from the current-feed end will be less than that given by application of equation (1). Since it is likely that the arc root progresses as a whole by forward movement of these outer spots, then the velocity v_a may well be lower. The axial field, however, has the same value at all cathode spots so that v_c is not reduced in this way. (ii) As discussed in the footnote both v_a and v_c [curve (ii), Fig. 3] are lower than if measured separately. They will not be reduced proportionally due to the magnetic saturation.

In view of these points and possible variations in surface conditions the agreement is surprisingly good, and it is

* The velocity of the cathode spot along the helix path is determined by a magnetic flux density which is the resultant of B_a and B_c. Due to magnetic saturation, there will be no constant proportionality between the velocities v_a and v_c and the corresponding flux densities B_c and B_a. Since v_a is measured as the axial component of the helix motion, the value will be less than that which would be obtained in the absence of B_a. This lower value is shown as curve (ii) in Fig. 3, whereas v_a, when B_a is zero, is shown as curve (i). The circumferential velocity v_c is also calculated from the helix motion and will also therefore be less than that if B_c were zero in the tests.

reasonable to conclude that both axial and circumferential cathode movements are governed by forces within the cathode spot itself, due to local surface magnetic fields which are in the same direction as the field in the bulk metal.

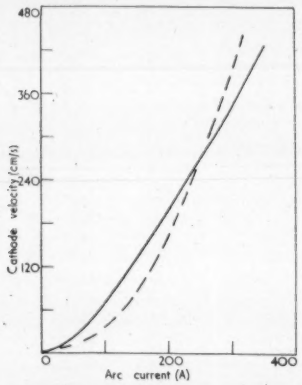

Fig. 6. Comparison between axial and circumferential velocities on a stainless steel cathode

——— Experimental values for v_a from curve (ii) of Fig. 3.
— — — Circumferential velocity computed as indicated in the section on the relationship between v_a and v_c.

Anode motion. Anode tracks are usually less regular than those on the cathode, but in spite of this some regular tracks up to 7 cm in length have been found. For given conditions of current I and magnetic field B_a, the axial velocities attained are approximately the same for both electrodes as shown in Fig. 3. With an axially magnetized anode, helical motion occurs, which, for a given current I and magnetic flux density B_a is in the reverse sense to that on the cathode. That this movement also is due to a surface field is shown by the sense of the helix being the same for permanent magnet and electromagnet anodes. This result is surprising and shows that electromagnetic forces within the anode spot are important.

Apart from the generally accepted picture that the hot anode spot is created by bombarding electrons accelerated through the anode fall, there is little further description of the anode mechanism and certainly little evidence on anode motion. The fact established here that the motion is influenced by magnetic fields in the surface is important therefore in any theory of the anode spot to be developed.

ELECTRODE PROCESSES

The actual mechanism of electron emission from the cathode spot into an arc at atmospheric pressure has never been fully described. Cold field emission,[8] thermionic emission, thermal ionization above the cathode spot,[9] and pure electron emission from high density vapour in the spot[10] have been cited as the appropriate mechanisms in various cases. In the present experiments, melting has occurred as the spot moved forward so that it may be that emission has proceeded from the cold type beginning at suitable microscopic sites, towards the thermionic type of emission at the higher temperatures. Ahead of the moving cathode spot there must always be sites on which emission is growing with time and which transiently take over the full current of the arc as it moves, only to wane and drop out again as the arc moves on. The mechanism of this transference cannot be discussed in detail here, but we need to know how the presence of a magnetic field within the surface can influence the direction of motion by causing emission sites to one side of the existing cathode spot to be preferred and the arc to be transferred in that direction. On a microscopic scale the surface irregularities would determine the local magnetic fields. In particular, although with a permanent magnet electrode the field in the air away from the metal will be in a reverse direction to the internal field, there will be local fields in air between asperities on the surface which could be in the same direction. It is possible that these local fields act on the cathode fall of the arc since at atmospheric pressure the fall extends over distances of less than 10^{-5} cm. Thus it might be argued that the action occurs in the cathode fall and not in the cathode spot. It is not easy in the present instance to distinguish clearly between phenomena in the cathode spot, i.e. in the metal and in the cathode fall, and it is better to consider the whole as a transition region from the solid metal through a liquid phase to a vapour in which large temperature and density gradients exist. The surface magnetic fields then produce forces throughout the region and as a result must in some way encourage emission on one side of the cathode spot.

At any established spot within the cathode area there is a large electron current density J_x normal to the electrode surface and also a large temperature gradient dT/dx where x is the direction of the surface normal. In all the experiments, the magnetic flux (B_a or B_c) is perpendicular to this normal direction, so that transverse galvanomagnetic and thermomagnetic forces can arise.[11] These forces have been mentioned by Smith[10] and by Ware[12] in connexion with the retrograde mercury arc.

The transverse effects defined in terms of certain coefficients are given below. In each case the coefficient is considered to be positive.

The Hall and Ettingshausen effects. Due to a current density J_x and a magnetic flux density B_z a transverse electric field E_y and a transverse temperature gradient dT/dy occur with

$$E_y = RJ_xB_z \quad \text{and} \tag{2}$$

$$dT/dy = -PJ_xB_z \tag{3}$$

where R and P are the Hall and Ettingshausen coefficients respectively.

The Ettingshausen–Nernst and Righi–Leduc effects. If the current density J_x is replaced by a temperature gradient dT/dx then the transverse effects are

$$E_y = -QdT/dx\ B_z \quad \text{and} \tag{4}$$

$$dT/dy = S\,dT/dx\ B_z \tag{5}$$

where Q and S are the Ettingshausen–Nernst and Righi–Leduc coefficients. The definitions above are based on the assumption of a uniform electron density. If a density gradient exists then it produces galvanomagnetic effects similar to those of equations (2) and (3).[12]

In normal situations these forces are small but they may be appreciable in the cathode spot where current densities of 10^6 A/cm^2[7] and temperature gradients of perhaps 10^8 °K/cm[13] as well as large electron density gradients may

exist. Bearing in mind that large flux densities occur for the steel electrodes and also that the various coefficients above are as much as ten times greater than those for non-ferrous materials,[14] it is plausible to attribute the higher velocities on steel to these effects. It appears that for circumferential motion of the cathode spot with the stated conditions of P, Q, R and S positive, the four effects could produce an electric gradient such as to cause electrons to move to the side of the cathode spot in the direction of the observed motion, and also a temperature gradient such that the same side to which the electrons tend to move would become hotter than the other. This situation might easily cause a preferred direction of motion since it will encourage field-aided thermionic emission from suitable nearby sites in that direction, and these may then evolve into new cathode spots. Ware,[12] in discussing the transverse effects for a low-pressure arc plasma has concluded that the thermomagnetic effects will rarely be important in laboratory discharges. This conclusion may not be valid for the situation described here because values of electron density, density gradient and thermal gradient in the micro-regions of the cathode spot of an arc at atmospheric pressure, may well be far in excess of those values for parts of the discharge away from the electrodes.

It is hazardous at this stage to suggest reasons for the contrary helix motion of the anode spot. Whereas on the cathode under the above conditions the galvanomagnetic and thermomagnetic forces are in the same sense, the galvanomagnetic forces are reversed with respect to the thermomagnetic ones on the anode. This may account for the less definite and opposite motion of the anode spot.

CONCLUSIONS

In the present experiments magnetic fields within the cathode and anode spots largely determine the arc direction and velocity. The magnetic fields acting on the positive column appear to be of secondary importance in determining regular motion, at least in the case of magnetic electrodes. These results are novel, and it is suggested that the transverse galvanomagnetic and thermomagnetic effects may be responsible. It may be that arc motion and the erratic and continual motion of arc spots in general may be as much determined by conditions within and at the edges of spots as with conditions in the high-field regions above the spots. It might be argued that the transverse effects would seem to be too small to govern the behaviour, but it should be remembered that comparatively small effects might upset the delicate and transient balance of forces within the spots. In this connexion it should be noted that glow-arc transitions can be induced by quite minor changes of the cathode surface[15, 16] and that the process of glow-arc transition is probably occurring continually as the arc moves. Work is continuing to establish further details of the electrode processes causing arc movement.

ACKNOWLEDGEMENTS

Thanks are due to Professors W. J. John and M. W. Humphrey Davies for encouragement and to Mr. P. Batty and Mr. G. A. White for assistance with the experimental work, and the British Electrical and Allied Industries Research Association for use of the camera. This work arose out of an investigation on arcing devices being undertaken for that Association in the Department.

One of the authors (T.J.L.) gratefully acknowledges the award of a Turner and Newall Fellowship by the University of London.

REFERENCES

(1) GUILE, A. E., and MEHTA, S. F. *Proc. Instn Elec. Engrs A.* (In the press.)

(2) ST. JOHN, R. M., and WINANS, J. G. *Phys. Rev.*, **98**, p. 1664 (1955).

(3) GALLAGHER, C. J., and COBINE, J. D. *Phys. Rev.*, **71**, p. 481 (1947).

(4) VON ENGEL, A., and ROBSON, A. E. *Phys. Rev.*, **93**, p. 1121 (1954).

(5) DUNKERLEY, H. S., and SCHAEFER, D. L. *Jour. Appl. Phys.*, **26**, p. 1384 (1955).

(6) COBINE, J. D., and GALLAGHER, C. J. *Phys. Rev.*, **74**, p. 1524 (1948).

(7) FROOME, K. D. *Proc. Phys. Soc.* [*London*], **60**, p. 424 (1948); *B*, **62**, p. 805 (1949).

(8) LANGMUIR, I. *Gen. Elec. Rev.*, **26**, p. 731 (1923).

(9) SLEPIAN, J. *Phys. Rev.*, **27**, p. 407 (1926).

(10) SMITH, C. G. *Phys. Rev.*, **62**, p. 48 (1942).

(11) BRIDGMAN, P. W. *The Thermodynamics of Electrical Phenomena in Metals* (New York: Macmillan and Co., 1934).

(12) WARE, A. A. *Proc. Phys. Soc.* [*London*] *A*, **67**, p. 869 (1954).

(13) COBINE, J. D. *Gaseous Conductors* (New York: McGraw-Hill Book Co. Inc., 1941).

(14) *International Critical Tables*, **6**, p. 414, 1st Ed. (New York: McGraw-Hill Book Co. Inc., 1929).

(15) EDELS, H. *Nature* [*London*], **172**, p. 362 (1953).

(16) PRICE, W. L., GAMBLING, W. A., and EDELS, H. *Nature* [*London*], **176**, p. 28 (1955).

A simple calibration technique for improving the accuracy of a Smith resistance thermometry bridge

By G. C. Lowenthal, B.A., B.Sc., A.Inst.P., Defence Standards Laboratories, Department of Supply, Melbourne, Australia

[*Paper received* 23 *November*, 1956]

The Smith resistance thermometry bridge (type 3) used at Defence Standards Laboratories is subject to irregular drifts which cause errors exceeding $\pm 0{\cdot}002^\circ$ C between 0 and 100° C and $\pm 0{\cdot}01^\circ$ C at 630° C. These errors cannot be dealt with successfully by potentiometric calibrations. An analysis shows, however, that provided certain conditions are satisfied, an external decade of stable 10 Ω resistors can be used to reduce the errors to $\pm 0{\cdot}0005$ and $\pm 0{\cdot}001^\circ$ C respectively, since the calibration is sufficiently simple and quick to be repeated as often as required.

A platinum resistance thermometer having the resistance R_T at a temperature T and the resistances R_0 and R_{100} at the freezing and boiling points of water respectively, defines a so-called platinum temperature T_{Pt} in accordance with the relation

$$T_{Pt} = \frac{100(R_T - R_0)}{R_{100} - R_0} \qquad (1)$$

T_{Pt} is corrected to International Temperature T by means of the Callendar equation

$$T = T_{Pt} + \delta\left(\frac{T}{100}\right)\left(\frac{T-100}{100}\right) \qquad (2)$$

the value of the constant δ being determined by a thermometer calibration at the boiling point of sulphur.

Obviously, only T_{Pt} as defined by (1) is affected directly by errors in resistance measurements and because of the form of (1) the effect of such errors will vanish, provided they are (*a*) the same for every resistance reading, or (*b*) proportional to every resistance reading. In addition they must be reproducible during a thermometer calibration and subsequent series of temperature measurements. The resistance bridge must, therefore, be free from drifts or fluctuations during a time interval sufficiently long to cover these measurements, or means must be avilable to measure these fluctuations so that they can be allowed for in any subsequent calculations of temperature.

Errors arising from the Smith bridge balance equation

The circuit diagram of the type 3 Smith bridge[1] is given in Fig. 1(*a*) and reference to this figure will explain the symbols used in the analysis below. Its balance equation is

$$P = \frac{R}{S}(Q + L_3) + \frac{bL_2}{a+b+L_1+L_2}\left(\frac{Q+L_3}{S} - \frac{a+L_1}{b}\right) \qquad (3)$$

which, subject to the conditions,

(i) $L_1 = L_2 = L_3$,

(ii) $L_1 + L_2 \ll a + b$,

(iii) $\dfrac{a}{b} = \dfrac{Q+R}{S-R}$,

reduces to

$$P = \frac{R}{S}Q \qquad (4)$$

Lead resistances are, in general, less than 1 Ω and can be made equal within 0·1% using the bridge itself for this comparison. This is adequate to satisfy condition (i). Maximum allowable lead resistances to satisfy condition (ii) were discussed by Gautier.[2] To check on condition (iii), the bridge is connected as shown in Fig. 1(*b*) and if it balances for all values of Q and a, (iii) is obviously satisfied. In practice, there will be a small out-of-balance current due to the fact that bridge resistors will invariably differ slightly from their nominal values. Hall[3] gave some numerical

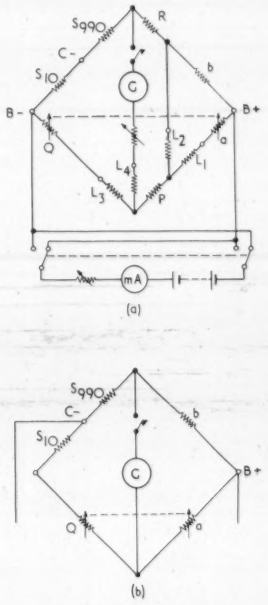

Fig. 1. The Smith bridge circuit

(*a*) Connexions for resistance measurements; and (*b*) connexions for the *a*/*b* ratio test. $S = b = 1000\ \Omega$, $R = 10\ \Omega$, $a = (Q + 10)/0{\cdot}99\ \Omega$, L_1, L_2, L_3, L_4 = thermometer leads.

data of the effect of such errors on calculated temperatures. For the present purpose, a more general treatment will be adopted. Equation (3) can be written in the form

$$P = \frac{R}{S}Q + \frac{R}{S}E \qquad (3a)$$

and if $L_1 = L_2 = L_3 = L$ (say), then

$$E = L + \frac{SbL}{R(a+b+2L)}\left(\frac{Q+L}{S} - \frac{a+L}{b}\right) \qquad (5)$$

If (iii) were attained, the magnitude of E would depend only on that of L and normally would be less than 150 $\mu\Omega$: an error which is sufficiently small to be neglected. In fact (iii) will not in general be attained as that E will depend on the values of its components Q, a, b, S and R. The variation ΔE can be determined by partial differentiation of E with respect to these components:

$$\Delta E = \frac{L}{RA^2}\Big\{bA\,.\,\Delta Q - [b(Q+L) + S(b+L)]\Delta a + \\ + [(a+2L)(Q+L) + S(a+L)]\Delta b - A(a+L)\Delta S - \\ - [b(Q+L) - S(a+L)]\frac{A}{R}\Delta R\Big\} \qquad (6)$$

where $A = a + b + 2L$ and ΔQ, Δa, etc., are independently determined corrections. For a reasonably well adjusted bridge, ΔE will be so small relative to Q (see Table 1 below),

Table 1. *Subsidiary ratio corrections*

Q arm setting, Ω	ΔQ, Ω	Δa, Ω	$\frac{\Delta E}{L}$
500	0·040	0·025	0·001
10 × 100	0·070	0·045	0·001
1 × 1000	0·512	0·153	0·018
2000	0·862	0·210	0·022
2500	0·900	0·220	0·019
3000	1·195	0·200	0·025
3500	1·220	0·210	0·022
4000	1·475	0·150	0·026
5000	1·830	0·190	0·027
6000	2·180	0·230	0·028
6700	2·210	0·270	0·025
7000	2·580	0·255	0·029
8000	2·915	0·240	0·030

that its determination to the nearest 5% will, in general, be quite sufficient. Since L is very small relative to the other resistors it can be neglected in comparison with a, b and Q in (6). Nominal values can be used for b (1000 Ω), S (1000 Ω) and R (10 Ω), and the term involving ΔR can be omitted since it is negligible compared to the other terms. Hence (6) becomes

$$\Delta E \simeq \frac{100L}{a+1000}\left(\Delta Q - \frac{Q+1000}{a+1000}\Delta a\right) + \\ + \frac{aL}{10(a+1000)}\left(\frac{Q+1000}{a+1000}\Delta b - \Delta S\right)$$

which can, in turn, be reduced to

$$\Delta E \simeq \frac{100L}{Q+1000}(\Delta Q - \Delta a) + \frac{QL}{10(Q+1000)}(\Delta b - \Delta S) \qquad (7)$$

at least for temperature measurements above 0° C where a will differ from Q by less than 2%.

In the D.S.L. bridge $\Delta b - \Delta S$ has been approximately 0·1 Ω for the last eight years, which means that for Q values corresponding to the temperature range 0° C to 500° C and for a lead resistance of 0·5 Ω, the contribution of the final term of (7) to ΔE varies from about 0·003 to 0·005 Ω. Since the resulting errors in temperature measurements are negligible, (7) can be finally simplified to

$$\Delta E \simeq \frac{100L}{Q+1000}(\Delta Q - \Delta a) \qquad (8)$$

ΔQ and ΔE will be the only remaining sources of error which might affect calculated temperatures significantly. Hence, instead of (3) reducing to (4), it reduces to

$$P = \frac{R}{S}(Q + \Delta Q + \Delta E) \qquad (9)$$

where ΔE is defined by (8).

Values of $\Delta E/L$ for the D.S.L. bridge are shown in Table 1. They have changed very little during the last four years, as might be expected, for the Q and a coils have similar drift rates. Values of Δa are determined from the out-of-balance current measured during the a/b ratio tests.[4] The measurement of ΔQ has yet to be discussed. Even if lead resistances reach 1 Ω, the errors in temperature measurements caused by the values of $\Delta E/L$ given in Table 1 are less than 0·001° C at any point within the platinum thermometer range, and less than 0·0005° C within the fundamental interval.

FURTHER SOURCES OF ERRORS IN RESISTANCE MEASUREMENTS

There are other sources of errors in resistance measurements, such as inadequate temperature control of the bridge coils and inadequate insulation resistance. They can be checked relatively easily and will not be discussed here.

Errors due to changes in the resistance of the contacts of the decade switches can become significant notwithstanding the 1/100 ratio arms. To avoid these errors, the switches must be kept scrupulously clean from sludge which is continuously formed around them by oil spray from the constant temperature bath mixing with small metal particles resulting from the movement of the brushes. If this sludge is allowed to accumulate on and between the contact surfaces, it can cause irregular variations exceeding 0·01 Ω in the sum of the contact resistances and can also lower the insulation resistance between the Q and a arms. For this reason, the switch contacts on the D.S.L. bridge are cleaned with toluol at monthly intervals. If the switches are clean, several rapid sweeps over all ten contacts will leave the bridge reading unaffected.

Short term fluctuations and drifts in the resistances of the bridge coils constitute the most serious obstacle to the realization of precision measurements. They are most noticeable in the 1000 Ω resistors but are also apparent in the 100 Ω coils. (It would be necessary to take special steps to detect fluctuations in coils lower than 100 Ω since they no longer exercise any significant effect on total bridge resistance.) Consequently, it is often impossible to make accurately reproducible readings even from day to day and, in the absence of means for either preventing or monitoring these resistance fluctuations, temperature measurements cannot generally be made to much better than ±0·002° C even within the fundamental interval.

THE USE OF A DECADE OF STABLE 10 Ω RESISTORS FOR SMITH BRIDGE CALIBRATION

The problem of bridge resistance fluctuations could be solved by redesigning the bridge[5] or by replacing the relevant bridge coils.[6] Either method, however, would be very

costly and could hardly be applied to an existing bridge. Instead, the D.S.L. bridge is simply and quickly calibrated when required, sometimes before every reading, by using it to measure a decade of stable 10 Ω manganin resistors.[7] Although such a procedure permits a check only on the 1000 Ω coils and the sum of the 100 Ω coils, these relatively few measurements will result in a satisfactory calibration, provided the following conditions are satisfied.

(1) It must be possible to establish a sufficiently accurate relation between the correction for each 100 Ω dial setting and that for the entire 100 Ω decade.

(2) Significant errors in the lower four of the six Q arm decades must be proportional to corresponding resistance readings or equal for all such readings.

(3) Significant errors due to the a/b subsidiary ratio must satisfy the same requirements.

Condition (3) has been fully dealt with above. To establish (1) and (2), it is necessary to fully calibrate the bridge preferably more than once during the first few years of its lifetime. Some results obtained during two full calibrations of the D.S.L. bridge are shown in Table 2(*a*). They are given for the three higher decades only. The resistors of the three lower decades, namely the 0·01 Ω, the 0·1 Ω and the 1 Ω decades, have at no stage deviated significantly from their respective nominal values. Concerning the higher decades, Table 2(*a*) shows that the small errors in the 10 Ω coils remained adequately stable and it should be safe to assume that this behaviour is still continuing. The resistances of the 100 Ω coils measured in 1951 were very nearly proportional to those measured in 1947. Table 2(*b*), which gives examples of results obtained with the new calibration method, indicates that this proportionality has been preserved. Since the total correction for this decade can be readily determined by a measurement against one of the 10 Ω calibrating resistors, corrections for each coil can be deduced from the results of earlier calibrations, or, more simply, by assuming that every coil of the decade has the same correction, namely one-tenth of the measured decade correction. Table 2(*a*) shows that correct values would still be obtained for some of the dial settings, and that the error for any other setting would not exceed 0·0005° C.

Since the R/S ratio will never be exactly 1/100 and since the a/b subsidiary ratio also has a slight effect on results, corrections obtained by this method differ from those which would be obtained by a direct potentiometric calibration of the Q arm. However, any changes in the R/S ratio affect all bridge readings by exactly equal proportions, while, at least in the case of the D.S.L. bridge, the ΔE term of (9) and other error terms that have been mentioned are either small enough to be virtually proportional to these readings or are virtually constant. Hence, provided thermometers are used for which L is less than 0·5 Ω and provided reasonable care is taken when this new calibration method is used, the sum of the various errors originating in the bridge will not cause errors in temperature measurement exceeding those given in the summary, which are, in the large majority of cases, small enough to be neglected in comparison with other errors to which temperature measurements are subject.[8]

Table 2. *D.S.L. Smith bridge: Q arm calibrations*

(*a*) *Potentiometric method*

Relative accuracy ±1 p.p.m. or ±0·001 Ω

Dial marking	*Sections*	*Resistance at 30° C (in absolute ohms* 1947	1951
X by 1000	1	1 000·627	1 000·540
	2	2 001·09	2 000·90
	3	3 001·52	3 001·23
	4	4 001·94	4 001·52
	5	5 002·43	5 001·90
	6	6 002·91	6 002·28
	7	7 003·34	7 002·66
	8	8 003·91	8 003·04
	9	9 004·31	9 003·41
	10	10 004·78	10 003·78
X by 100	1	100·008	100·007
	2	200·027	200·021
	3	300·037	300·028
	4	400·060	400·043
	5	500·081	500·061
	6	600·104	600·079
	7	700·124	700·092
	8	800·135	800·099
	9	900·150	900·109
	10	1 000·162	1 000·118
X by 10	1	10·001	10·001
	2	20·002	20·002
	3	30·003	30·003
	4	40·004	40·004
	5	50·005	50·005
	6	60·005	60·006
	7	70·006	70·007
	8	80·008	80·008
	9	90·009	90·009
	10	100·010	100·010

(*b*) *New method*

Relative accuracy ±1 p.p.m.

Dial marking	*Sections*	*Resistance at 30° C* *January* 1955	*April* 1955	*July* 1955
X by 1000	1	1 000·504	1 000·516	1 000·524
	2	2 000·843	2 000·869	2 000·885
	3	3 001·174	3 001·202	3 001·224
	4	4 001·443	4 001·486	4 001·517
	5	5 001·786	5 001·841	5 001·882
	6	6 002·124	6 002·190	6 002·242
	7	7 002·52	7 002·60	7 002·65
	8	8 002·84	8 002·93	8 002·99
	9	9 003·14	9 003·24	9 003·31
	10	10 003·44	10 003·55	10 003·64
X by 100	10	1 000·064	1 000·077	1 000·084

ACKNOWLEDGEMENTS

Acknowledgement is made to the Chief Scientist, Department of Supply, Australia, for permission to publish this

paper. The author also wishes to thank Mr. R. G. Ackland for many helpful suggestions during its preparation.

REFERENCES

(1) Smith, F. E. *Phil. Mag.*, **24**, p. 561 (1912).
(2) Gautier, M. *J. Sci. Instrum.*, **30**, p. 381 (1953).
(3) Hall, J. A. *Phil. Trans. A*, **229**, p. 1 (1929–30).
(4) Goodwin, W. N. *Weston Engineering Notes*, **2**, No. 5 (1947).
(5) Barber, C. R., Gridley, A., and Hall, J. A. *J. Sci. Instrum.*, **32**, p. 213 (1955).
(6) Barber, C. R., Gridley, A., and Hall, J. A. *J. Sci. Instrum.*, **29**, p. 65 (1952).
(7) Lowenthal, G. C., and Ackland, R. G. *J. Sci. Instrum.* To be published.
(8) National Physical Laboratory. Notes on Applied Science, No. 12, "Calibration of Temperature Measuring Instruments," p. 4 (London: H.M.S.O., 1955).

The damping effect of surrounding gases on a cylinder in longitudinal oscillation

By M. T. Browne, B.Sc., A.R.C.S., and J. R. Pattison, B.Sc., Ph.D., A.Inst.P.,* Department of Physics, Imperial College of Science and Technology, London

[*Paper received* 17 *May*, 1957]

The external damping influences on a longitudinally vibrating cylindrical bar are examined quantitatively. Experiments undertaken to confirm the theoretical estimations indicate a possible precision method for the determination of gas viscosities.

In a number of methods used for investigating internal damping in solids, the specimen is in the form of a cylindrical bar supported at a node of vibration so that it is able to vibrate under free-free conditions. Under such conditions, external sources of damping are present in addition to that under study. These are (*a*) viscous damping along the cylindrical surface; (*b*) acoustic radiation from the vibrating surfaces; and (*c*) damping loss in the specimen support. A theoretical evaluation of these damping sources may be made without difficulty.

Theoretical Treatment of External Damping

Consider a cylindrical bar of length $2l$ and diameter $2r$ with plane ends, supported at its centre. If the bar is set into free-free longitudinal oscillations about a central node, and the peak velocity along the axis of a thin disk section distant x from the node is u, then

$$u = U \sin(\pi x/2l) \tag{1}$$

If v denotes the peak radial velocity of the circumference of the disk element, then

$$v = V \cos(\pi x/2l)$$

But if μ is Poisson's ratio for the bar material, V, the peak radial velocity at the node of longitudinal vibrations, is related to U, the peak axial velocity at the free ends of the bar, by

$$V = (\mu r/l)U$$

Hence
$$v = (\mu r/l)U \cos(\pi x/2l) \tag{2}$$

A simple unit of damping is the damping capacity $\Delta W/W$ used by Föppl,[1] where ΔW is the energy absorbed in each cycle of vibration and W is the total energy of vibration. The logarithmic decrement δ is more commonly used and has the following relation to the damping capacity

$$\Delta W/W = 1 - e^{-2\delta}$$

so that
$$\delta \simeq \Delta W/2W \text{ for small } \delta.$$

For the bar under consideration, if ρ_M is the density of the material

$$W = \tfrac{1}{2}\rho_M \int_{-l}^{l} \pi r^2 u^2 dx$$

using equation (1)

$$W = \tfrac{1}{2}\pi r^2 l \rho_M U^2 \tag{3}$$

For the viscous damping along the cylindrical sides of the bar, the equation obtained by Stokes[2] may be used. The tangential force F on a unit plane area, moving at a velocity $u \cos 2\pi ft$, which varies sinusoidally with time t at a frequency f, owing to a medium of density ρ and viscosity η is given by,

$$F = u \cos 2\pi ft \,.\, \sqrt{(\pi f \rho \eta)}$$

If we consider the surface area of a thin disk element of the bar Δx thick, the work done by the force F in time Δt is

$$F \,.\, 2\pi r \,.\, u \cos 2\pi ft \,.\, \Delta t \,.\, \Delta x$$

Hence ΔW_V, the energy dissipated by the bar in overcoming viscous forces in each cycle of oscillation, can be obtained by summation over one cycle and over the length of the bar using equation (1) to substitute for u.

$$\Delta W_V = (\pi r l U^2/f)\sqrt{(\pi f \rho \eta)}$$

From equation (3), δ_V the decrement corresponding to viscous damping is

$$\delta_V = \Delta W_V/2W = (1/fr\rho_M)\sqrt{(\pi f \rho \eta)} \tag{4}$$

The calculation of the damping effects due to the acoustic radiation from a vibrating bar is simplified by considering

* Now at British Iron and Steel Research Association, London.

the end faces of the bar and the cylindrical surface as two separate sources of radiation, and this condition may be reproduced by suitable baffles surrounding the ends of the bar.

The real component R of the radiation impedance of a rigid circular piston of radius r, vibrating in a plane infinite baffle, has been obtained by Morse[3] in the form

$$R = \pi r^2 \rho c \left[1 - \frac{J_1(2kr)}{kr}\right] \tag{5}$$

where c is the velocity of sound in the medium of density ρ, $k = 2\pi f/c$, and J_1 is the Bessel function of the first kind of order one.

Therefore, considering the circular ends of a vibrating cylindrical specimen as piston radiators, the energy dissipated in one cycle of vibration by these pistons is

$$\Delta W_{R_1} = RU^2/f$$

Hence, using equations (3) and (5), the decrement due to radiation from the ends of the bar is given by

$$\delta_{R_1} = \frac{\Delta W_{R_1}}{2W} = \frac{\rho \,.\, c}{lf\rho_M}\left[1 - \frac{J_1(2kr)}{kr}\right] \tag{6}$$

The acoustic energy radiated by the cylindrical surface of a vibrating bar may be calculated approximately by treating it as short cylinders expanding and contracting normally and using the equation obtained by Morse[4] for the energy radiated per unit length. The cylinder sections vibrate in phase so that the total radiated energy from the cylindrical sides of the bar in each cycle is given by

$$\Delta W_{R_2} = \pi^3 \rho r^2 \int_{-l}^{l} v^2 dx$$

$$= \pi^3 \rho r^4 \mu^2 U^2 / l \quad \text{by equation (2)}$$

Hence, the decrement due to radiation of energy from the cylindrical sides of the bar is given by

$$\delta_{R_2} = \pi^2 r^2 u^2 \rho / l^2 \rho_M \tag{7}$$

The remaining source of external damping is provided by the support for the vibrating bar. Various designs may be employed but a common one consists of a single wire attached at the node of longitudinal free-free vibration. Since the wire is fixed at a node, the only velocity amplitude acting on it is V, the peak radial velocity at the surface of the bar. The wire is considered to be small enough in cross-section to neglect variations in radial velocity across it and to ignore longitudinal velocities.

If it is assumed that all the energy taken from the specimen by the support is dissipated in the wire alone, and not reflected by the fixture from which the wire is hung, then the elastic energy ΔW_S absorbed in one cycle of vibration is given by

$$\Delta W_S = (V^2 \rho_S c_S / f) S$$

where ρ_S is the density of the suspension wire material, c_S is the velocity of sound in the wire, and S is the cross-sectional area of the wire. Hence, putting $V = (\mu r/l)U$, the decrement δ_S corresponding to the damping introduced by the specimen support wire is given by

$$\delta_S = (\mu^2 \rho_S c_S / \pi l^3 f \rho_M) S \tag{8}$$

The simplest way of reducing this decrement to as small a value as possible is to reduce the cross-sectional areas of the suspending wire. This may be done in such a way that a more positive support is obtained by using three rigid needles with the points contacting the rod surface symmetrically in the plane of the node of longitudinal vibrations, instead of a single wire.

When the damping in a bar vibrating under free-free conditions is measured by an instrument which does not introduce further damping effects, the measured decrement δ_M is the sum of the decrements corresponding to internal damping in the bar δ_I and the external damping.

$$\delta_M = \delta_I + (\delta_V + \delta_{R_1} + \delta_{R_2} + \delta_S) \tag{9}$$

The magnitude of the external damping represented by the last four terms on the right-hand side of equation (9) is a function of certain characteristics of the specimen bar and surrounding medium shown in equations (4), (6), (7) and (8). For a given size and material of the specimen and for a given medium, the external damping is a function of the density of the medium.

The viscous damping δ_V is a function of $\sqrt{\rho}$, where ρ is the density of the medium, since the viscosity of the medium is unchanged by alteration of the pressure. Since the velocity of sound in the medium is also unchanged by change in pressure, provided that the mean free path of the molecules does not become comparable in magnitude to the wavelength of the sound wave, the piston radiation damping δ_{R_1} is directly proportional to density. Hence equation (9) may be written

$$\delta_M = \delta_I + \delta_S + A\sqrt{(\rho)} + B\rho \tag{10}$$

where, from equation (4)

$$A = (1/fr\rho_M)\sqrt{\pi f \eta} \tag{11}$$

and, from equations (6) and (7)

$$B = \frac{c}{lf\rho_M}\left[1 - \frac{J_1(2kr)}{kr}\right] + \frac{\pi^2 v^2 \mu^2}{l^2 \rho_M} \tag{12}$$

For specimens of a reasonable size, say 9 in. long and $\frac{1}{4}$ in. diameter, the values for decrements given in Table 1 are obtained from equations (4), (6), (7) and (8) for free-free oscillation in air at 0° C and 760 mm of mercury pressure.

Table 1. *Typical values of damping*

Material	*Frequency (c/s)*	$\delta_I \times 10^5$	$\delta_V \times 10^5$	$\delta_{R_1} \times 10^5$	$\delta_{R_2} \times 10^5$	$\delta_S \times 10^5$	$(\delta_E/\delta_M) \times 100\%$
Nickel	10420	73	0·30	0·72	0·011	0·50	2·1
Aluminium	11170	5	0·95	2·52	0·042	1·86	51·8

The fundamental frequency f of free-free vibrations is given by the equation obtained by Lord Rayleigh[5]

$$f = \frac{1}{2l}\sqrt{\left[E \Big/ \rho_M\left(1 + \frac{\pi^2 \mu^2 r^2}{4l^2}\right)\right]}$$

where E is Young's modulus for the bar material.

Considerable divergence exists between published values for internal damping due in many cases to the vibrational stresses applied being sufficient in magnitude to cause irreversible internal changes. The value tabulated for the internal

damping of nickel obtained by Ide[6] for annealed nickel at zero magnetic field and small vibrational stress is the smallest value known to the authors for this metal. The internal damping value for aluminium was obtained by Hanstock and Murray[7] using small vibrational stresses. The decrement due to suspension damping in Table 1 is for three taut steel wires of 0·5 mm diameter fixed symmetrically in the plane of the node of vibration.

Table 1 shows that the maximum influence of external damping is exerted by the piston radiation and that support damping is the next in order of importance. The effect of external damping on an aluminium specimen is greater than that on a nickel specimen of the same size, owing to the relatively smaller total energy of vibration W at the same peak axial velocity of the free ends of the bars, as well as the lower internal friction.

The support damping may be easily reduced to a negligible value by replacing the 0·5 mm diameter wires by steel needles, each having an effective contact area with the specimen of less than 0·05 mm diameter. Thus the support damping decrement is reduced by a factor of more than 1/100 since it is proportional to contact area. Both radiation damping decrements are linear functions of the density of the surrounding atmosphere and thus may be reduced by a factor of 1/100 by vibrating the specimen in an enclosure at 7·6 mm of mercury. This would also reduce the viscous decrement by a factor of 1/10. The improved suspension and reduced pressure enclosure reduce the ratio of external to total measured damping δ_E/δ_M to 0·06% for nickel and to 2·7% for aluminium specimens.

Where values of the internal damping of a material are required, it is necessary to reduce the influence of the external sources of damping as much as possible, but if it is intended to measure external damping as a check on the equations given in this paper for the logarithmic decrements of external damping, then the opposite process is necessary.

THE MEASUREMENT OF EXTERNAL DAMPING

In order to measure the external damping on a vibrating bar due to the surrounding gaseous medium, it is necessary to reduce the internal damping and the external damping introduced by the specimen suspension as much as possible. Further, since the damping due to surrounding gas will be relatively small compared to the total damping effect from other sources, it is necessary to employ a very accurate measuring technique.

Thus needle supports were used and Monel metal was chosen for the rod material since this metal was found by Ide[6] to have an internal friction decrement of 3×10^{-4} ratio in zero magnetic field, which was small compared with his results for other magnetic materials.

A further increase in the surface damping relative to internal damping can be obtained by using a tube with plugged ends instead of a solid rod. This has the effect of reducing W the total energy of vibration of the specimen and hence all the decrements for external damping (including suspension) are increased. There is a limit to the enhancement of the surface damping effects by reducing the value of W. The air enclosed in the tube will exert a damping effect on the vibrations, which is considerably smaller than that of the same volume of metal. However, W is evaluated from the vibrational energy contained in the solid tube so that the tube walls must not be so thin that the energy in the enclosed air is comparable in magnitude to that in the tube alone.

A magnetic material was chosen for the specimen rod because of the ease with which vibrations can be produced by magnetostrictive effects using a coaxial drive coil. The apparatus used for measuring decrements has been described elsewhere.[8] It consists of an electronic arrangement giving a measurement of N the number of cycles of oscillation of a decaying signal occurring during the fall from a particular amplitude value to one of half value. The decrement is then given by

$$\delta = \log_e 2/N$$

An improved model of the apparatus described[8] gave a constant range of three cycles in any set of consecutive readings, whatever the value of N, with a standard deviation of 0·87. Hence, for the experiments to be described in which $\bar{N} > 1500$ cycles, the expected error in $\bar{N}$ evaluated from ten consecutive readings was less than $\pm \frac{100 \cdot 0{\cdot}87}{1500 \cdot \sqrt{10}}\%$, that is, less than $\pm 0{\cdot}018\%$.

A Monel metal tube 9 in. long and $\frac{1}{4}$ in. overall diameter was used in the experiments. The tube wall thickness was 0·0055 in. and the ends of the tube were sealed by Perspex disks 0·05 in. thick. The tube was supported at its centre by three needles symmetrically fixed and mounted in a glass enclosure as illustrated in Fig. 1.

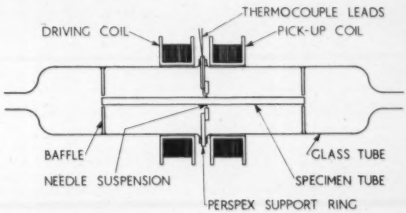

Fig. 1. Specimen mounting

The tube ends were located in the central holes of two brass disks of $\frac{1}{8}$ in. thickness fixed to the glass enclosure. These disks acted as baffles to separate the piston radiation region from the cylindrical radiation region. A small copper constantan thermocouple junction was fixed to the tube surface near to the node of fundamental longitudinal vibration, the leads being carried out through holes in the Perspex support which were subsequently sealed. A further thermocouple attached to the glass enclosure measured the ambient temperature at which the experiments were performed.

The specimen support ring was symmetrically perforated so that the two flanged tubes forming a vacuum-tight enclosure could be evacuated by a pump connected to one of the inlet ports at either end. The enclosure was pumped out and filled from a pressure cylinder with the gas under investigation. Liquid oxygen traps were used to ensure dry gases and the pressures inside the enclosure were measured by a mercury manometer and a McLeod low-pressure gauge.

The enclosure walls were lined with glass wool to reduce acoustic coupling between the vibrating specimen and the enclosure. The driving coil was connected to a decade oscillator, the output of which was adjustable in 1 c/s steps to tune with the tube specimen. The electronic measuring instrument connected to the pick-up coil, described elsewhere,[8] was brought into action by a switch in the driver coil circuit cutting off the oscillator output. The decaying

signal output from the pick-up coil initiated a count of the number of cycles for a half amplitude decay which always started from the same signal amplitude. Thus, provided that the magnetostrictive eddy-current effects producing the signals always occur under the same conditions, measurements will always be taken for the same amplitude range of mechanical vibration of the given specimen. In this way, the effects of amplitude-dependent damping are minimized.

The specimen tube was placed between the poles of an electromagnet which provided a polarizing magnetic field corresponding to maximum magnetic damping in the specimen. The maximum damping, rather than the minimum, was used in order to work on a position of stability in the damping/magnetic induction curve for the specimen material.

The specimen temperatures were disturbed by reductions of pressure in the enclosure and a minimum period of three minutes was necessary to allow a steady temperature to be regained. The magnetic properties of Monel metal are strongly influenced by temperature changes at ordinary room temperature and it was further necessary to carry out experiments when the ambient temperature was not changing during the time of a test run.

For an open tube of external diameter $2r$, length $2l$, wall thickness t, vibrating with a peak longitudinal velocity U

$$W = \tfrac{1}{2}\pi(2r - t)tl\rho_M \cdot U^2$$

If this tube is plugged at each end by thin plane plugs of mass M each, the resulting addition to W is MU^2. To avoid errors in the evaluation of $2W/U^2$ due to the difficulty in measuring t accurately, $2W/U^2$ may be obtained by subtracting one half of the mass of the tube, measured before plugging, from the total mass of the tube and plugs after fixing.

For the tube used in the experiments described $2W/U^2 = 1{\cdot}348$ g, $f = 9777$ c/s, $l = 11{\cdot}41$ cm, $r = 0{\cdot}1587$ cm, and $\mu = 0{\cdot}326$.

Hence, in equation (10)

$$\delta_M = \delta_I + \delta_S + A\sqrt{(\rho)} + B\rho$$

$$A = 0{\cdot}075\,81\sqrt{(\eta)} \text{ c.g.s.}$$

$$B = \left\{6{\cdot}007\left[1 - \frac{J_1(2kr)}{kr}\right]c + 135{\cdot}8\right\} \times 10^{-6} \text{ c.g.s.}$$

If ρ_0 is the density of the gas surrounding the specimen at room temperature and pressure p_0, then at any subsequent pressure p

$$\delta_M = \delta_I + \delta_S + A\sqrt{(\rho_0/p_0)}\sqrt{(p)} + B(\rho_0/p_0)p$$

A simpler relation between δ_M and p may be obtained in two ways.

Firstly, if δ'_M is the measured decrement at a given pressure p_1 then for any other pressure p

$$\delta_M - \delta'_M = A\sqrt{\left(\frac{\rho_0}{p_0}\right)}[\sqrt{p} - \sqrt{p_1}] + B\frac{\rho_0}{p_0}[p - p_1]$$

or

$$\frac{\delta_M - \delta'_M}{\sqrt{p} - \sqrt{p_1}} = A\sqrt{\left(\frac{\rho_0}{p_0}\right)} + B\frac{\rho_0}{p_0}[\sqrt{p} + \sqrt{p_1}] \qquad (13)$$

Equation (13) gives a linear relationship between a function of δ_M and p and a function of p.

A second relationship may be obtained by making the given pressure p_1 low enough to cause slip[9–12] between the specimen and the gas and so remove the viscous damping effects, but not low enough to interfere with the radiation damping by making the mean free path of the gas molecules comparable in magnitude with the wavelength of the sound wave. In this case

$$\delta_M - \delta'_M = A\sqrt{\left(\frac{\rho_0}{p_0}\right)}\sqrt{p} + B[p - p_1]\frac{\rho_0}{p_0}$$

or

$$\frac{\delta_M - \delta'_M}{\sqrt{p}} = A\sqrt{\left(\frac{\rho_0}{p_0}\right)} + B\frac{\rho_0}{p_0}\sqrt{p}\left[1 - \frac{p_1}{p}\right]$$

and since $p_1 \ll p$

therefore

$$\frac{\delta_M - \delta'_M}{\sqrt{p}} = A\sqrt{\left(\frac{\rho_0}{p_0}\right)} + B\frac{\rho_0}{p_0}\sqrt{p} \qquad (14)$$

The linear relationships (13) and (14) relate to different functions of δ_M and p and different functions of p, but the slope and constant term are identical in equation. Therefore both equations may be plotted with the same axes to give one curve.

$$f(\delta_M, p) = A\sqrt{\left(\frac{\rho_0}{p_0}\right)} + B\frac{\rho_0}{p_0}\phi(p) \qquad (15)$$

EXPERIMENTAL RESULTS

Six different pressures were used for the four gases studied and at each pressure ten half-decay readings were taken. The mean values of $\bar{N}$ and δ_M are given in Table 2.

Taking p_1 as 134 mm of mercury in equation (11) and p_1 as 1 mm of mercury in equation (12) nine values of the functions (δ_M, p) and $\phi(p)$ were obtained in equation (15) for each gas. These data are plotted in Fig. 2 and the regression lines evaluated, giving equal weight to each value, yield the following constants (Table 3).

The theoretical values of B obtained by the substitution of known data in equation (12) are consistently high compared

Table 2. *Damping measurements in various gases*

	Mean half-decay N cycles				*Measured damping* $\delta_M \times 10^7$			
Pressure $p(mmH_g)$	*Nitrogen at* 17·9° C	*Oxygen at* 17·5° C	*Air at* 16·6° C	*Carbon dioxide at* 18·1° C	*Nitrogen at* 17·9° C	*Oxygen at* 17·5° C	*Air at* 16·6° C	*Carbon dioxide at* 18·1° C
1	1702·1	1684·7	1687·3	1759·2	4072·3	4114·4	4108·0	3940·1
134	1641·6	1616·9	1625·5	1684·3	4222·4	4286·9	4264·1	4115·4
230	1622·6	1595·8	1606·3	1660·8	4271·9	4343·6	4315·2	4173·6
348	1603·9	1575·4	1587·6	1637·7	4321·7	4399·8	4366·0	4232·5
504	1583·8	1553·3	1567·3	1612·7	4376·5	4462·4	4422·6	4298·1
760	1556·1	1523·7	1540·0	1578·6	4454·4	4549·1	4501·0	4390·9

The theoretical values of B obtained by the substitution of known data in equation (12) are consistently high compared

to the experimental determinations given in Table 3 and also appear to vary in an unsystematic fashion.

Substituting for A and inserting the values for ρ_0 given by Kaye and Laby[13] at a pressure p_0 of 760 mm of mercury,

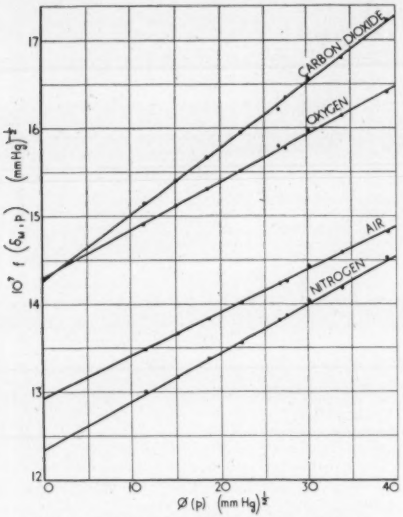

Fig. 2. Relation between damping and pressure

Table 3. *Values of damping constants*

Gas	Experimental determinations		Theoretical value
	$A\sqrt{(\rho_0/p_0)} \times 10^7$ $(mmHg)^{-\frac{1}{2}}$	$B(\rho_0/p_0) \times 10^8$ $(mmHg)^{-1}$	$B(\rho_0/p_0) \times 10^8$ $(mmHg)^{-1}$
Nitrogen	12·32	0·554	1·25
Oxygen	14·28	0·549	1·55
Air	12·92	0·490	1·34
Carbon dioxide	14·26	0·755	3·57

values for absolute viscosity η are derived. These data are given in Table 4 together with comparative values obtained by interpolation from the smoothed figures published by Johnston and McCloskey,[14] using the oscillating disk method.

Table 4. *The absolute viscosity of various gases*

	Absolute viscosity η (p) $\times 10^7$			
	Nitrogen at 18° C	Oxygen at 18° C	Air at 17° C	Carbon dioxide at 18° C
Present work	1712	2008	1813	1450
Johnston and McCloskey	1746	2021	1804	1452

CONCLUSIONS

The viscosity values obtained are in good agreement with published values and it is concluded that with certain experimental refinements, such as using a vibrator material which is less influenced by temperature change and placing the gas-filled enclosure in a temperature-controlled bath, a precision method for the measurement of gas viscosities could be developed, using the principles described.

A theoretical treatment of the radiation damping would need to be far more complex than that attempted here. For the simple apparatus described the assumptions, of infinite baffles with pistons radiating into free space uncoupled to other parts of the vibrating specimen or the rest of the apparatus, are obviously inapplicable. However, the plotted curves demonstrate that the radiation damping is proportional to gas density and does not interfere with viscous damping. It is possible that the radiation damping effect exerted by various structures could be investigated using apparatus based on that described.

ACKNOWLEDGEMENTS

The authors wish to thank Prof. P. M. S. Blackett for the facilities provided and Dr. R. W. B. Stephens for his interest and criticism. The Central Research Fund of the University of London provided part of the apparatus and the financial support of the Department of Scientific and Industrial Research is gratefully acknowledged.

REFERENCES

(1) Föppl, O. *J. Iron Steel Inst.*, **134**, p. 393 (1936); **135**, p. 451 (1937).

(2) Stokes, G. G. *Trans. Cambridge Phil. Soc.*, **9**, (II), p. 8 (1851).

(3) Morse, P. M. *Vibration and Sound*, p. 333 (New York: McGraw-Hill Book Co., Inc., 1948).

(4) Morse, P. M. *Vibration and Sound*, p. 299 (New York: McGraw-Hill Book Co. Inc., 1948).

(5) Strutt, J. W. *The Theory of Sound*, Vol. 1, p. 252 (London: Macmillan, 1944).

(6) Ide, J. M. *Proc. Inst. Radio Engrs*, **19**, p. 1216 (1931).

(7) Hanstock, R. F., and Murray, A. *J. Inst. Metals*, **72**, p. 97 (1946).

(8) Pattison, J. R. *Rev. Sci. Instrum.*, **25**, p. 490 (1954).

(9) Maxwell, J. C. *Phil. Mag.*, **19**, p. 31 (1860).

(10) Maxwell, J. C. *Phil. Trans. Roy. Soc.*, **156**, p. 249 (1866).

(11) Meyer, O. E. *Pogg. Ann.*, **125**, p. 177 (1865).

(12) Stacy, L. J. *Phys. Rev.*, **21**, p. 239 (1923).

(13) Kaye, G. W., and Laby, T. H. *Tables of Physical and Chemical Constants*, p. 37 (London: Longmans Green, 1948).

(14) Johnston, H. L., and McCloskey, K. E. *J. Phys. Chem.*, **44**, p. 1038 (1940).

On the ultimate concentration distribution in zone-melting

By I. Braun, B.Sc., D.Sc.,* H. H. Wills Physical Laboratory, University of Bristol

[*Paper received* 15 *March*, 1957]

This paper treats the question of the ultimate concentration distribution, that is the distribution which is unaffected by further passes. An exact solution is given of this ultimate distribution for any value of the distribution coefficient k, taking into account the end-effect due to the normal freezing in the last zone. Graphs of the ultimate distribution are given for different values of k and the zone-length. To know how many passes are needed to reach the ultimate distribution, these graphs have been compared with the graphs of the successive concentration profiles. After a certain number of passes the concentration profiles oscillate around the ultimate distribution. These oscillations become smaller and smaller with increasing number of passes. There exists therefore an optimum number of passes with the lowest concentration profile.

A complete solution of the equations governing zone-melting, taking into account the effect of "normal freezing" in the last zone, has been given previously.[1] To calculate the ultimate or limiting distribution with consideration of the end-effect, Pfann's[2] assumptions concerning the distribution coefficient k are used throughout. Also for simplicity we assume that the initial concentration distribution is equal to unity $[C_0(x) = 1]$.

The following notation is used:

x = distance along the bar measured from the starting end.
p = integration variable, equivalent to x.
N = total length of the bar. N is assumed to be an integral number of zone-lengths l, and for simplicity we take $l = 1$.

Each zone is designated by the co-ordinate of its starting point (see Fig. 1). Thus the zones are numbered from (0) to $(N-1)$.

$C_n^{(N-m)}(x)$ = concentration distribution of the nth pass in the $(N-m)$th zone or region.
$C^{(N-m)}(x)$ = ultimate distribution in the $(N-m)$th region.

According to the rigorous theory of zone-melting[3] the concentration of solute after n passes must satisfy the equation:

$$C_n(x) = k \cdot \left[\int_0^{x+1} C_{n-1}(p) \cdot dp - \int_0^x C_n(p) \cdot dp \right] \qquad (1)$$

for $0 \leqslant x \leqslant N-1$. In the last region $C_n(x)$ must satisfy the equation:

$$C_n(x) = \frac{k}{N-x} \cdot \left[\int_0^N C_{n-1}(p) \cdot dp - \int_0^x C_n(p) \cdot dp \right] \qquad (2)$$

for $N-1 \leqslant x \leqslant N$. The ultimate distribution is obtained if

$$C_{n-1}(x) = C_n(x) = \ldots \equiv C(x) \qquad (3)$$

and in this case equations (1) and (2) are reduced to:

$$C(x) = k \cdot \int_x^{x+1} C(p) \cdot dp \qquad \text{for } 0 \leqslant x \leqslant N-1 \qquad (4)$$

and $$C(x) = \frac{k}{N-x} \cdot \int_0^N C(p) \cdot dp \text{ for } N-1 \leqslant x \leqslant N \qquad (5)$$

Since the total amount of impurities is always conserved $C(x)$ must satisfy the boundary condition:

$$N \cdot C_0 = N = \int_0^N C(p) \cdot dp \quad \text{with } (C_0 = 1) \qquad (6)$$

Pfann,[2] who treated the case of a semi-infinite bar, gave as solution of equation (4):

$$C(x) = A \cdot e^{Bx} \quad \text{where } k = B/(e^B - 1) \qquad (7)$$

A, the integration constant, was determined by equation (6). It can easily be shown that if $C(x)$ is supposed to be an analytic function for every value of x, the solution of equation (4) is unique and of the form (7). One may prove this by developing $C(x)$ in a Maclaurin series, which is only permissible if $C(x)$ is an analytic function. But equation (7) does not satisfy simultaneously equation (5). The question therefore arises: does there exist a function $C(x)$ satisfying simultaneously the equations (4) and (5) and the boundary condition (6)? If there does not exist such a function $C(x)$, then an ultimate distribution can never be reached, i.e. every zone pass will change the concentration profile.

It will now be shown that a function $C(x)$ can be constructed satisfying equations (4), (5) and the boundary condition (6), i.e. there exists an ultimate distribution.

THEORY

For the finite concentration profiles[1] we have already obtained the result that $C_n(x)$ is a continuous, but only *partially* analytic function, where the end- or starting-points of the zones are singularities. It is therefore reasonable to expect that the ultimate distribution $C(x) = \lim_{n \to \infty} C_n(x)$ conserves this character. We therefore postulate that $C(x)$ is a *continuous* but *non-analytic* function, having singularities at the end- or starting-points of the zones. Let us write $C(x)$ in the form:

$$C(x) = C^{(N-1)}(x) + C^{(N-2)}(x) + \ldots + C^{(0)}(x) = \sum_{i=0}^{N-1} C^{(N-1-i)}(x) \qquad (8)$$

with the convention that the upper index indicates the region in which the function is valid (see Fig. 1). Thus $C^{(N-m)}(x) \neq 0$ for $N-m \leqslant x \leqslant N-m+1$, but $C^{(N-m)}(x) = 0$ for any

* Now at Hebrew Institute of Technology, Department of Physics, Haifa, Israel.

other value of x. With this convention the boundary condition (6) becomes:

$$N = \int_{N-1}^{N} C^{(N-1)}(p)\,.\,dp + \int_{N-2}^{N-1} C^{(N-2)}(p)\,.\,dp + \ldots + \int_{0}^{1} C^{(0)}(p)\,.\,dp \quad (9)$$

and since we assume $C(x)$ to be continuous we have for the singularities at the end-points of the zones the conditions:

$$\left.\begin{aligned} C^{(N-1)}(N-1) &= C^{(N-2)}(N-1) \equiv C(N-1) \\ C^{(N-2)}(N-2) &= C^{(N-3)}(N-2) \equiv C(N-2) \\ &\ldots\ldots\ldots\ldots \\ C^{(1)}(1) &= C^{(0)}(1) \equiv C(1) \end{aligned}\right\} \quad (10)$$

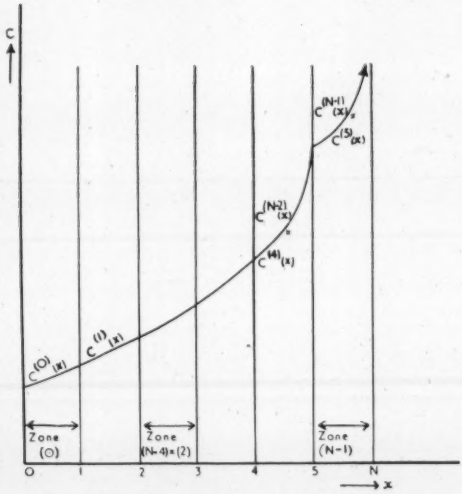

Fig. 1. Schematic representation of ultimate distribution. ($N = 6$)

$$C^{(N-1)}(x) = C^{(5)}(x)$$

Let us now calculate the different $C^{(N-1-i)}(x)$-functions of equation (8) starting with the function valid in the last zone $(N-1)$, where we have:

$$C(x) = C^{(N-1)}(x) \qquad \text{for } N-1 \leqslant x \leqslant N.$$

$C(x)$ must satisfy equation (5) in this region, and by assuming that $C^{(N-1)}(x)$ is analytic in this region, the unique solution of equation (5) is of the form of the normal freezing curve:

$$C^{(N-1)}(x) = C(N-1)\,.\,(N-x)^{k-1} \quad \text{for } N-1 \leqslant x \leqslant N \quad (11)$$

For $0 \leqslant x \leqslant N-1$, $C(x)$ must satisfy equation (4) and we have therefore, in particular in the $(N-2)$th region with equations (4) and (8):

$$C(x) = C^{(N-2)}(x) = k\,.\int_{x}^{x+1} C(p)\,.\,dp = = k\,.\left[\int_{x}^{N-1-\varepsilon} C^{(N-2)}(p)\,.\,dp + \int_{N-1+\varepsilon}^{x+1} C^{(N-1)}(p)dp\right] \quad (12)$$

since $x = N-1$ is a singularity, ϵ being an infinitesimal number. Taking the derivative of equations (12):

$$\frac{dC^{(N-2)}}{dx} = k\,.\,[C^{(N-2)}(N-1-\varepsilon) - C^{(N-2)}(x) + C^{(N-1)}(x+1) - C^{(N-1)}(N-1+\epsilon)] \quad (13)$$

and since $C(x)$ is assumed to be a continuous function we get for $\varepsilon \to 0$ from equation (13):

$$\frac{dC^{(N-2)}}{dx} = k\,.\,[C^{(N-1)}(x+1) - C^{(N-2)}(x)] \quad (14)$$

Introducing equation (11) into equation (14) yields an ordinary differential equation:

$$\frac{dC^{(N-2)}}{dx} = k\,.[C(N-1)\,.(N-x-1)^{k-1} - C^{(N-2)}(x)] \quad (15)$$

Integration of equation (15) gives:

$$C^{(N-2)}(x) = C(N-1)\,.\,e^{k(N-x-1)} - -C(N-1)\,.k\,.F_1\,(N-x-1) \quad (16)$$

$$\text{with} \quad F_1(u) = u^k \sum_{r=0}^{\infty} \frac{(u\,.\,k)^r}{k\,.\,(k+1)\,.\,(k+2)\ldots(k+r)} \quad (17)$$

where $u = N-x-1$. This function $F_1(u)$ also appears in the computation of the successive concentration profiles in the $(N-2)$th region.[1]

The same procedure can be applied to calculate $C(x)$ in the $(N-3)$th region. With equation (4) we have, for $N-3 \leqslant x \leqslant N-2$:

$$C(x) = C^{(N-3)}(x) = k\,.\left[\int_{x}^{N-2-\varepsilon} C^{(N-3)}(p)\,.\,dp + \int_{N-2+\varepsilon}^{x+1} C^{(N-2)}(p)\,.\,dp\right] \quad (18)$$

Differentiating and using the assumption of continuity of $C(x)$, we have for $x = N-2$:

$$C^{(N-3)}(N-2) = C^{(N-2)}(N-2) \equiv C(N-2)$$

Equation (18) yields for $\epsilon \to 0$:

$$\frac{dC^{(N-3)}}{dx} = k\,.\,[C^{(N-2)}(x+1) - C^{(N-1)}(x)] \quad (19)$$

Introducing equation (16) into equation (19) and integrating:

$$C^{(N-3)}(x) = [C(N-2) - k\,.\,C(N-1)\,.(N-x-2)]\,e^{k(N-x-2)} + k\,.\,C(N-1)\,.\,F_2(N-x-2) \quad (20)$$

with

$$F_2(u) = u^k \sum_{r=1}^{\infty} \frac{r\,.\,(k\,.\,u)^r}{k\,.\,(k+1)\ldots(k+r)} \qquad u = N-x-2 \quad (20a)$$

As before in the case of $F_1(u)$ the function $F_2(u)$ is needed for the calculation of $C_n^{(N-3)}(x)$.[1]

Continuing this process for lower and lower regions we obtain, by induction for any region, i.e. for $N-m-1 \leqslant x \leqslant N-m$:

$$C^{(N-m-1)}(x) = \left[C(N-m) - k\,.\,C(N-m+1)\,.(N-x-m) + \frac{k^2}{2}\,.\,C(N-m+2)\,.\,(N-x-m)^2 + \ldots + (-1)^{m-1}\,.\,\frac{k^{m-1}}{(m-1)!}\,.\,C(N-1)\,.\,(N-x-m)^{m-1}\right] e^{k(N-x-m)} + (-1)^m\,.\,k\,.\,C(N-1)\,.\,F_m(N-x-m) \quad (21)$$

or in summation form:

$$C^{(N-m-1)}(x) = e^{k(N-x-m)} \left[\sum_{i=0}^{m-1} (-1)^i \cdot \frac{k^i}{i!} \cdot C(N-m+i) \cdot (N-x-m)^i \right] + + (-1)^m k \cdot C(N-1) \cdot F_m(N-x-m) \qquad N-m-1 \leqslant x \leqslant N-m \quad (21a)$$

with

$$F_m(u) = u^k \cdot \sum_{r=0}^{\infty} \frac{\binom{m+r-1}{r} \cdot (k \cdot u)^{m+r-1}}{k \cdot (k+1) \ldots (k+m+r-1)} \qquad u = N-x-m \quad (22)$$

where, as in the binomial coefficient,

$$\binom{m+r-1}{r} = \frac{(m+r-1)!}{(m-1)!r!}$$

The values of the different constants $C(N-m-i)$ can be calculated as functions of $C(N-1)$ as follows:

From equation (16) we obtain for $x = N-2$ the starting points of the $(N-2)$th region:

$$\left. \begin{aligned} C^{(N-2)}(N-2) &= C(N-2) \equiv C(n-1) \cdot \psi_2 \\ \text{with} \qquad \psi_2 &= e^k - F_1(1) \end{aligned} \right\} \quad (23)$$

We designate by $F_1(1)$ the value of $F_1(u)$ for $u = 1$. For $x = N-3$, the starting point of the $(N-3)$th region, we get from equation (20):

$$C^{(N-3)}(N-3) \equiv C(N-3) = = e^k \cdot [C(N-2) - k \cdot C(N-1)] + k \cdot C(N-1) \cdot F_2(1)$$

and introducing into the last relation the value of $C(N-2)$ from equation (23):

$$\left. \begin{aligned} C(N-3) &= C(N-1) \cdot \psi_3 \qquad \text{with} \\ \psi_3 &= e^{2k} - k \cdot e^k + k \cdot [-F_1(1) \cdot e^k + F_2(1)] \end{aligned} \right\} \quad (24)$$

Continuing this procedure we get by induction in general for any starting point $x = N-m$:

$$C(N-m) = \psi_m \cdot C(N-1) \quad (25)$$

with

$$\psi_m = \sum_{j=0}^{m-2} (-1)^j \cdot (m-1-j)^j \cdot \frac{k^j}{j!} \cdot e^{(m-1-j)k} - - k \cdot \left[\sum_{j=0}^{m-2} (-1)^{m-j} \cdot e^{jk} \cdot \sum_{i=0}^{m-2-j} \frac{(j.k)^i}{i!} \cdot F_{m-1-j-i}(1) \right] \qquad m > 1 \quad (26)$$

These ψn-functions are written explicitly below for successive values of m:

$$\psi_2 = e^k - k \cdot F_1(1)$$

$$\psi_3 = e^{2k} - k \cdot e^k - k \cdot [F_1(1) \cdot e^k - F_2(1)]$$

$$\psi_4 = e^{3k} - 2 \cdot k \cdot e^{2k} + \frac{k^2}{2!} \cdot e^k - - k \cdot [F_1(1) \cdot e^{2k} - |F_2(1) + k \cdot F_1(1)| \cdot e^k + F_3(1)]$$

$$\psi_5 = e^{4k} - 3 \cdot k \cdot e^{3k} + (2)^2 \cdot \frac{k^2}{2!} \cdot e^{2k} - (1)^3 \cdot \frac{k^3}{3!} \cdot e^k - - k \cdot \left[F_1(1) e^{3k} - |F_2(1) + 2 \cdot k \cdot F_1(1)| \cdot e^{2k} + + \left| F_3(1) + k \cdot F_2(1) + \frac{k^2}{2!} \cdot F_1(1) \right| \cdot e^k - F_4(1) \right]$$

$$\psi_6 = e^{5k} - (4) \cdot k \cdot e^{4k} + (3)^2 \cdot \frac{k^2}{2!} \cdot e^{3k} - (2)^3 \cdot \frac{k^3}{3!} \cdot e^{2k} + + (1)^4 \cdot \frac{k^4}{4!} \cdot e^k - k \cdot \left[F_1(1) \cdot e^{4k} - |F_2(1) + 3 \cdot k \cdot F_1(1)| \cdot e^{3k} + + \left| F_3(1) + 2 \cdot k \cdot F_2(1) + (2)^2 \cdot \frac{k^2}{2!} \cdot F_1(1) \right| e^k - - \left| F_4(1) + k \cdot F_3(1) + \frac{k^2}{2!} \cdot F_2(1) + \frac{k^3}{3!} \cdot F_1(1) \right| \cdot e^k - F_5(1) \right]$$

Introducing the values of the different constants from equation (25) into equation (21), we obtain the ultimate concentration distribution in any region $(N-m\,1)$:

$$C^{(N-m-1)}(x) = C(N-1) \cdot \left\{ e^{k(N-x-m)} \cdot \left[\sum_{i=0}^{m-1} (-1)^i \cdot \frac{k^i}{i!} \cdot \psi_{m+i} \cdot (N-x-m)^i \right] + + (-1)^m \cdot k \cdot C(N-1) \cdot F_m(N-x-m) \right\} \quad (27)$$

with $m > 1$, where the respective ψ-functions are given by equation (26). To simplify the application of these formulae, the concentration profiles are written explicitly below:

$$\left. \begin{aligned} C^{(N-1)}(x) &= C(N-1) \cdot (N-x)^{k-1} && N-1 \leqslant x \leqslant N \\ C^{(N-2)}(x) &= C(N-1) \cdot [e^{k(N-x-1)} - k \cdot F_1(N-x-1)] && N-2 \leqslant x \leqslant N-1 \\ C^{(N-3)}(x) &= C(N-1) \cdot \left\{ [\psi_2 - k \cdot (N-x-2)] \cdot e^{k(N-x-2)} + k \cdot F_2 \cdot (N-x-2) \right\} && N-3 \leqslant x \leqslant N-2 \\ C^{(N-4)}(x) &= C(n-1) \cdot \left\{ \left[\psi_3 - k \cdot \psi_2 \cdot (N-x-3) + \frac{k^2}{2!} \cdot (N-x-3)^2 \right] \cdot e^{k(N-x-3)} - k \cdot F_3(N-x-3) \right\} && N-4 \leqslant x \leqslant N-3 \\ C^{(N-5)}(x) &= C(N-1) \cdot \left\{ \left[\psi_4 - k \cdot \psi_3 \cdot (N-x-4) + \frac{k^2}{2!} \cdot \psi_2 \cdot (N-x-4)^2 - - \frac{k^3}{3!} \cdot (N-x-4)^3 \right] \cdot e^{k(N-x-4)} + k \cdot F_4(N-x-4) \right\} && N-5 \leqslant x \leqslant N-4 \end{aligned} \right\} \quad (28)$$

The coefficient $C(N-1)$ can be determined by the boundary condition that the total amount of impurities remains constant. Introducing therefore into equation (9) the respective functions of equation (28), we get the value of $C(N-1)$:

$$C(N-1) = N \Big/ \left\{ \frac{1}{k} + k \left[\sum_{i=1}^{N-1} (-1)^i \cdot \int_0^1 F_i(p) \cdot dp + + \sum_{i=2}^{N-2} \frac{k^i}{i!} \cdot \int_0^1 p^i \cdot e^{kp} \cdot dp \cdot \sum_{j=1}^{N-1-i} \psi j \right] \right\} \quad (29)$$

by introducing $\psi_1 \equiv 1$, and where

$$\int_0^1 p^n \,.\, e^{kp} \,.\, dp = \frac{e^k}{k} \cdot \left[\frac{1-n}{k} + \frac{n(n-1)}{k^2} - \frac{n(n-1)(n-2)}{k^3} + \cdots \right.$$
$$\left. \cdots + (-1)^{n-1} \frac{n!}{k^{n-1}} + (-1)^n \frac{n!}{k^n} - (-1)^n \frac{n!}{k^n} \right]$$

Equation (29) yields after integration explicitly for increasing values of N for:

$N = 3$

$$C(2) = 3 \Big/ \left\{ \frac{1}{k} [1 + (1 + \psi_2)(e^k - 1) - |e^k(k-1) + 1|] - k \,.\, (f_1 - f_2) \right\}$$

$N = 4$

$$C(3) = 4 \Big/ \left\{ \frac{1}{k} [1 + (1 + \psi_2 + \psi_3)(e^k - 1) - (1 + \psi_2)|e^k(k-1) + 1| + \frac{1}{2}|e^k(k^2 - 2k + 2) - 2|] - k \,.\, (f_1 - f_2 + f_3) \right\}$$

$N = 5$

$$C(4) = 5 \Big/ \left\{ \frac{1}{k} \left[1 + (1 + \psi_2 + \psi_3 + \psi_4)(e^k - 1) - (1 + \psi_2 + \psi_3)|e^k(k-1) + 1| + (1 + \psi_2) \cdot \frac{1}{2} \cdot |e^k(k^2 - 2k + 2) - 2| - \frac{1}{6}|e^k(k^3 - 3k^2 + 6k - 6) + 6| \right] - k(f_1 - f_2 + f_3 - f_4) \right\}$$

and so on for higher values of N with

$$f_i = \int_0^1 F_i(p) \,.\, dp$$

Finally we can write the ultimate concentration distribution in accordance with equation (8), by using equation (28) in the form:

$$C(x) = C(N-1) \,.\, \left\{ (N-x)^{k-1} + \sum_{j=1}^{N-1} \left[e^{k(N-x-j)} \cdot \sum_{i=0}^{j-1} (-1)^i \cdot \frac{k^i}{i!} \cdot \psi_{j+i} \,.\, (N-x-j)^i + (-1)^j \,.\, k \,.\, F_j(N-x-j) \right] \right\} \quad (30)$$

with the convention that only those terms in equation (30) are different from 0, whose argument $u = N - x - j$ ($j = 0, 1, 2, \ldots, N-1$) has a value between 0 and 1 ($0 \leqslant u \leqslant 1$). The ψ-functions are given by equation (26) and the value of $C(N-1)$ by equation (29). The ultimate distribution given by equation (30) satisfies equations (4), (5) and the exact boundary condition (6). The theory is correct for any value of k.

NUMERICAL CALCULATION

Two problems were treated numerically:

(i) the form of the ultimate concentration distribution for different values of k and the zone-length; and

(ii) the number of successive passes needed to reach the ultimate distribution for given values of N and k:

(i) In Fig. 2 the ultimate distributions for different values of k with the same zone-length l ($l = 1$, $N = 3$) have been compared. For values of k close to unity ($0{\cdot}65 \leqslant k < 1$), there is a middle part with nearly constant concentration. In

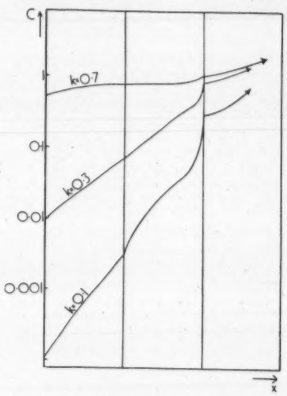

Fig. 2. Ultimate concentration profiles with same $N = 3$ and different k

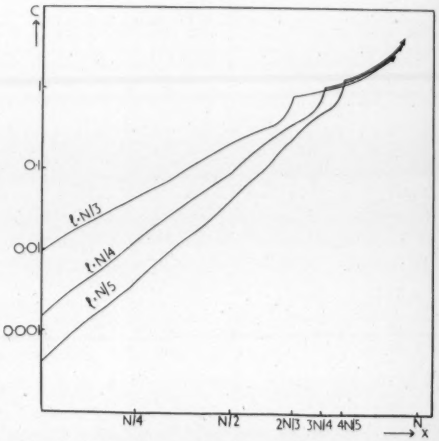

Fig. 3. Ultimate concentration profiles with same $k = 0{\cdot}3$ and different zone-lengths l

Fig. 3 ultimate concentration profiles with the same value of k are compared with profiles of different zone-lengths l. As found by Burris, Stockman and Dillon[3] a shorter zone-length produces a steeper ultimate distribution.

(ii) For a certain k and N different concentration profiles $C_n(x)$ with increasing n have been compared with the ultimate distribution $C(x)$. In Fig. 4, the case of $N = 3$ and $k = 0{\cdot}3$

has been treated. We see that the successive distributions $C_n(x)$ do not approach the ultimate distribution step by step, but oscillate around $C(x)$.

Thus in the case of $k = 0{\cdot}3$, $N = 3$ it is more advantageous to use eight passes than eleven passes, since $C_8(x)$ is situated lower than $C_{11}(x)$. $C_7(x)$ is the first concentration profile just crossing $C(x)$. If n increases more and more the oscillations around $C(x)$ decrease. In this case ($k = 0{\cdot}3$, $N = 3$) the optimum number of passes is $n = 8$. A rough estimate (not reproduced here) showed that for any N and $k = 0{\cdot}3$ the successive concentration profiles cross the ultimate concentration distribution for about $n = 2N + 1$ and the optimum number of passes is reached for about $n = 2N + 2$.

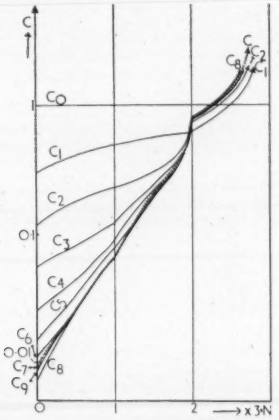

Fig. 4. Position of ultimate distribution C in relation to successive concentration profiles

$C_n(k = 0{\cdot}3, N = 3)$. $C_{11} \sim C_{10} \sim C_7$

———— = successive concentration profiles.

++++++ = ultimate distribution.

In Fig. 5 again successive concentration profiles are plotted together with the ultimate distribution in the case of $k = 0{\cdot}1$, $N = 3$. The first concentration profile crossing $C(x)$ is $C_6(x)$; $C_7(x)$ is the profile with the lowest concentration and therefore, in this case, $n = 7$ is the optimum number of passes. For longer bars ($k = 0{\cdot}1$, $N > 3$) an estimate showed that the successive concentration profiles cross the ultimate distribution for about $n = 2N$ and the optimum number of passes is reached for $n = 2N + 1$. We can therefore conclude that for $0{\cdot}1 \leqslant k \leqslant 0{\cdot}3$ we do not obtain lower concentration profiles if we increase n beyond $2N + 2$. In practice the oscillations around $C(x)$ can probably be neglected, since the assumptions of a constant zone-length and of uniform composition of the melt are difficult to realize.

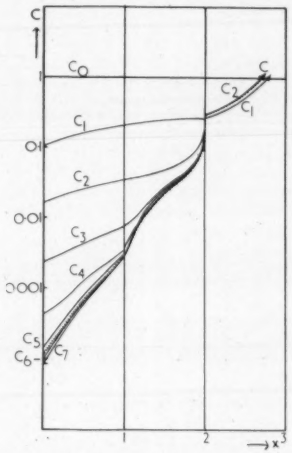

Fig. 5. Position of ultimate concentration profile in relation to successive concentration profiles ($k = 0{\cdot}1$, $N = 3$)

———— = successive concentration profiles.

++++++ = ultimate distribution.

ACKNOWLEDGEMENT

The author is greatly indebted to Prof. F. C. Frank for having initiated this problem and for invaluable discussions and to the Technoin Society of Great Britain for a maintenance grant.

REFERENCES

(1) BRAUN, I., and MARSHALL, S. *Brit. J. Appl. Phys.*, **8**, p. 157 (1957).

(2) PFANN, W. G. *J. Metals, N.Y.*, **4**, p. 747 (1952).

(3) BURRIS, L., STOCKMAN, C. H., and DILLON, I. G. *J. Metals, N.Y.*, 7, p. 1017 (1955).

New books

Pressure measurement in vacuum systems. By J. H. Leck. (London: The Institute of Physics, 1957.) Pp. 144. Price 30*s*.

Mr. Leck's book will prove a valuable addition to those already published in the "Physics in Industry" series. It meets the need for a comprehensive treatment of the subject of pressure measurement in vacuum systems and provides a complete guide to the choice of suitable pressure gauges and the correct interpretations of their readings.

Five types of pressure gauge are considered and the material is presented in six independent chapters the titles of which are: Mechanical manometers; Thermal conductivity gauges; Ionization gauges; The Knudsen radiometer gauge; Surface reaction techniques; Gauge calibration. Practical considerations are covered by the inclusion of numerous examples of design taken from literature; gauges of primarily historic interest such as the viscosity manometer have not been considered.

The book contains nearly one hundred illustrations together with a subject and name index. A comprehensive list of references is also included. R. G. A.

The physics of flow through porous media. By A. E. Scheidegger. (Toronto: University Press; London: Oxford University Press, 1957.) Pp. xii + 236. Price 110*s*.

The extensive literature on flow through porous media, stemming mainly from research workers in many industries, is inadequately cross-referenced and uneven in quality. Although many "correlations" amongst relevant factors have been proposed, their limitations are not easy to discern, mainly on account of the obscuration of underlying physical principles. Scheidegger's book is therefore important.

The eight parts of the book cover the general principles of porous media and fluids, followed by a discussion of hydrostatic problems, including adsorption and capillary pressure. Dynamical problems are discussed on two levels, firstly in so far as they may be regarded as deriving from Darcy's Law and, secondly, taking account of the more refined aspects of permeability such as those advanced by Kozeny and other workers. In the last part these considerations are applied to multiple phase flow. The treatment is concise and clear. At no point does the discussion evade difficulties.

The book will be useful not only to academic research workers but also to those workers in industry who encounter problems of flow through porous media. The latter will find here, probably for the first time, a worthy introduction to the subject. The former will appreciate that the references (of which there are more than 1000) include papers published in 1956. All workers in this field should have this book by them. R. L. Brown

Physical properties of crystals. By J. F. Nye. (London: Oxford University Press, 1957.) Pp. xv + 322. Price 50*s*.

Crystal physics is a vast field and it would hardly be possible to give an adequate representation of all its aspects in a single textbook. The author of the present book has therefore restricted it to the theoretical treatment of the macroscopic properties of crystals which can be mathematically represented by Cartesian tensors and matrices and which are supposed to be continuous functions of space.

The general mathematical principles, needed for this treatment, are presented in part I. Part II deals with equilibrium properties and contains a particularly interesting chapter on the thermodynamics of these properties. Part III deals with non-equilibrium properties and is mainly based on the Onsager reciprocal relations which play a fundamental part in the thermodynamics of irreversible processes. Part IV finally is devoted to crystal optics.

The book is very clearly written and the arguments at the same time mathematically precise and on the whole easy to follow. The reader will find the summaries at the end of each chapter and the numerous exercises very useful. Of particular value are the many excellent tables and diagrams of the symmetry properties of the various physical quantities to be found in the text and in the appendices at the end of the book. Methods of measurement are indicated and some numerical values given; the orders of magnitude of the various effects are also discussed.

The book fills a gap in the existing literature on crystal physics and can be warmly recommended to all students and research workers in this field. Its usefulness could, however, be still increased by adding brief qualitative explanations of the various effects on the basis of the atomic structure of crystalline bodies and some references to practical applications. A chapter on ferromagnetism ought to be included and the section on ferroelectrics extended in view of the enormous practical importance of these substances. Finally a section on the transformation properties of non-Cartesian tensors would be appreciated by the mathematically minded reader. Room for these additions could be found by cutting out some non-essential details. R. Fürth

The mechanism of phase transformations in metals. Institute of Metals Report Series No. 18. (London: The Institute of Metals, 1957.) Pp. 346. Price 50*s*.

This book contains the papers contributed to a symposium organized by the Institute of Metals, and held at the Royal Institution, London, on 9 November, 1955, together with some of the contributions to the discussions. The subject matter of papers includes nucleation and growth processes, precipitation phenomena, superlattice formation, martensitic transformation, allotropic changes in cobalt, and the $\beta \rightarrow \alpha$ transformation in uranium alloys. The book is well printed, and the diagrams and plates are clear and good, and much of the discussion is extremely interesting. The book can be wholeheartedly recommended. W. Hume-Rothery

Moderne messmethoden der physik. Volume 2. By Franz X. Eder. (Berlin: Veb Deutscher Verlag der Wissenschaften.) Pp. xvi + 648. Price DM 38.

The second volume of this book deals exhaustively with the measurement of thermal data. In the first section the author gives an outline of the basis of temperature measurement and then discusses various types of thermometer. Special problems of thermometry such as the measurement of very low temperatures, the calibration of thermometers and their use under various conditions are described in separate

chapters. The determination of thermal expansion and calorimetry form the subjects of the second and third sections. Here, as in the rest of the book, short mention is made of recent results which have been obtained with the methods described. The next section deals with phase changes of pure substances and gives examples of the determination of the transition temperatures and of the latent heats involved. The last chapter of this section gives an account of the Joule–Thomson effect. The transfer of heat by conduction, convection and radiation is discussed in section five together with a very detailed description of the different methods of measurement. This section also contains a description of heat exchangers and regenerators. A long section of over 120 pages is devoted to the production of low temperatures, ranging from simple cooling mixtures to the adiabatic demagnetization methods. In the two final sections measurements on systems of several components and the production of high temperatures are discussed.

The book, in contradistinction to many of the recent German publications, is written in a refreshingly clear and simple style. In spite of the very great number of methods and devices which are described, the essential features are well brought out in each case. The text is supported by a good bibliography, containing over 1000 references to original papers. The author has gone to great trouble in including the most recent developments and has produced a very useful and eminently readable book.

K. MENDELSSOHN

Progress in low temperature physics. Vol. 2. Edited by C. J. GORTER. (Amsterdam: North-Holland Publishing Co., 1957.) Pp. xi + 480. Price 84*s*.

The second volume of *Progress in low temperature physics* provides, like its predecessor, a well chosen and useful series of articles on topical subjects in the field. Six of these are devoted to the properties of helium itself which, following six similar articles in the first volume, give an indication of the far-reaching interest shown in this substance. P. Winkel and D. H. N. Wansink deal with the transport phenomena in the bulk liquid while K. R. Atkins gives a survey of the phenomena observed in helium films. While the investigation of the transport properties of the liquid now presents a tolerably clear picture, we still lack a clear understanding of the essential mechanism of superflow. Progress in the elucidation of the excitation spectrum is shown in H. C. Kramers' article on the properties of liquid helium below 1° K. Such properties as have been measured so far clearly indicate the transition at about 0·6° K of the pure phonon excitations to excitations of a different type which may possibly be connected with vortex motion. The problem of these excitations is discussed from the theoretical point of view in J. de Boer's beautifully clear article on the influence of quantum and exchange effects on the thermodynamical properties of liquid helium. A survey of the thermodynamical properties of solid helium, both from the experimental and theoretical points of view, is given by C. Domb and J. S. Dugdale. Much of it emphasizes the pioneer work, twenty years ago, by the late Sir Francis Simon on the melting curve. Finally there is a summary by H. van Dijk and M. Durieux on the temperature scale in the liquid helium region. While it is true that this scale is to some extent based on measurements of paramagnetic susceptibilities, there is little doubt that the remaining difficulties are mainly due to insufficient knowledge of the properties of helium.

In the realm of magnetism the editor, C. J. Gorter, has contributed an article on paramagnetic relaxation which is followed by an article on nuclear orientation by J. M. Steenland and H. A. Tolhoek. The latter provides a useful survey of a borderline field in which low temperature methods have been most useful in obtaining information on nuclear processes. A lucid exposition of a difficult subject is given by D. Shoenberg in his article on the de Haas–van Alphen effect in which the theory is compared with the great number of recently obtained experimental results. B. T. Matthias' short article on superconductivity deals with the empirical relation, established by the author between the occurrence of superconductivity in elements and compounds and the number of valency electrons. Another article on metal physics, by E. H. Sondheimer, treats theoretically the electron transport phenomena. A comprehensive review of the properties of semiconductors at low temperatures is given by V. A. Johnson and K. Lark-Horovitz which also contains an excellent bibliography. F. H. Spedding and his co-workers have summarized the low temperature properties of the rare earth metals, to the investigation of which this group has made such outstanding contributions. Finally, D. Bijl has contributed a critical survey of the representation of specific heat and thermal expansion data which contains the proposal of a new method of representation.

The book is excellently produced and extremely well edited. It will be of great value to those working in the low temperature field and useful for others who wish to keep abreast with recent developments. It is unfortunate that the price will put it out of reach of most research students.

K. MENDELSSOHN

Technical aspects of sound. Vol. II. Edited by E. G. RICHARDSON. (Amsterdam: Elsevier Publishing Co.; London: Cleaver–Hume Press Ltd., 1957.) Pp. xii + 412. Price 70*s*.

In the preface to Vol. I the editor, Prof. E. G. Richardson, states that his object has been to cover the technical aspects of acoustics often omitted from more general works on the subject. He has chosen experts, each in his special field, to write the several parts into which the subject matter has been divided, in a manner best suited to the research worker, industrialist or advanced student. The first volume dealt with the sonic range and in the main with airborne sound. The second volume, the subject of the present review, is concerned with the ultrasonic range and underwater acoustics. It is divided into three main sections: I, Ultrasonic transducers and applications (by B. E. Noltingk and N. B. Terry); II, Underwater acoustics (by E. Meyer, K. Tamm and H. Oberst); and III, Aircraft noise with a chapter on Underwater propulsion noise (by A. A. Regier, H. H. Hubbard, L. W. Lassiter and E. G. Richardson).

The four chapters of Division II describe mainly the work of Prof. Erwin Meyer and his collaborators Drs. K. Tamm and H. Oberst in Germany, on absorbers for water-borne sound known as "Fafnir" and "Alberich." The former is a type of aperiodic sound absorber consisting of an arrangement of rubber spikes or wedges containing air cavities. This type of absorber is now commonly used as a sound absorbent lining for acoustic water-filled tanks. "Alberich" was used by Germany during the war as a sound absorbent coating for submarines to make them less easily detected by Asdics. This absorber is of the "resonant" type—a relatively thin layer of rubber containing air cavities of appropriate size being attached to the steel hull of the submarine.

Division I which deals in two chapters with ultrasonic

transducers and ultrasonic applications is full of interesting information. The authors of this section, however, seem to be under the impression (paragraph 2, p. 32) that ultrasonic applications, due to improvements in ultrasonic h.f. transducers, have only taken place in post-war years (which war is not stated!). Since the early days of the 1920's " . . . few really practical applications of ultrasonic techniques could be made. The next widely used instrument was the ultrasonic flaw detector developed between 1939 and 1945." This astonishing statement is contradicted on p. 94. Fig. 52 and Fig. 54, p. 100, show "a standard type of laminated nickel transducer" and pp. 123–4 refer to "the most important ultrasonic application," the magnetostriction echo sounder, credit for which is left to the descriptive literature of Messrs. Kelvin and Hughes and "Atlas Werke." These developments were, in fact, due to the work of your reviewer and his collaborators in 1929 and published in British Patent No. 375375, 1931, and in the *Journal of the Institution of Electrical Engineers*.*

The material of the book has much to commend it, written, as it is, by authors of international repute, but this cannot be said with the same conviction of the choice of subjects and the general arrangement. There is a feeling of "randomness" and lack of coherence running through the book in spite of its otherwise good qualities. For example, Chapter 11 (Division III) on "Sounds of propulsion in water" looks as if it had strayed from Division II where it might more appropriately have been incorporated. Perhaps this lack of coherence is, however, inevitable in a book of this nature.

The volume has been well printed, illustrated and bound, and is likely to prove a valuable source of reference to research workers and those occupied in the applications of acoustics in industry. The editor expresses the hope in the preface of Vol. II that as new aspects of the subject appear or when old aspects change, further volumes will be issued.

A. B. WOOD

* WOOD, A. B., SMITH, F. D., and MCGEACHY, J. A. *J. Instn Elect. Engrs*, **76**, p. 550 (1935).

The Barker index of crystals, a method for the identification of crystalline substances. Vol. II. Crystals of the monoclinic system. Editors: M. W. PORTER and R. C. SPILLER. **Part 1. Introduction and tables.** Pp. v + 383, 43 text-figs. **Part 2. Crystal descriptions M. 1 to M. 1800.** Pp. viii + 380 (unnumbered). **Part 3. Crystal descriptions M. 1801 to M. 3572.** Pp. viii + 344 (unnumbered). (Cambridge: W. Heffer and Sons Ltd., 1956.) Price (bound), Vol. II (the three parts), £10.

The Barker index is a method for the identification of non-cubic crystalline substances by means of the measurement of the angles between the normals to faces. This does require, of course, that the specimen should develop a sufficient number of reasonably good faces to permit of the necessary measurements. In the case of minerals, this mostly limits the use of the method to crystals which have grown in veins and cavities where conditions permitted the development of good faces. But in the case of laboratory products, both organic and inorganic, a much larger proportion of the materials can be crystallized with faces. Hence it is desirable that in each laboratory where such crystals are produced there should be at least one research worker capable of utilizing the morphological properties of these crystals for identification and of recording the angles of any new substances produced.

The Barker index is being produced by an international committee with English, Dutch and American members. The first volume appeared in 1951 and this consisted of an explanatory first part, including a number of useful tables, and the crystal descriptions for the uniaxial systems and for the orthorhombic system; there were 2991 substances including organic and inorganic compounds, minerals, metals, and intermetallic compounds.

Part 1 of the present volume contains brief directions for the use of the Barker index, and this, along with corrigenda and addenda for Volume I, is supplied also in two loose copies for sticking into bound volumes. Then there is a 45-page introduction to the application of the Barker method to monoclinic crystals. The tables consist of the following: multiple-tangents, classification angles, refractive indices, densities, melting points, list of compounds in the sequence of Parts 2 and 3, alphabetical list of English chemical and mineralogical names, alphabetical list of Groth's German names.

Parts 2 and 3 contain the crystal descriptions of 3572 monoclinic substances, each taking on the average between one-third and one-half of a page. The printing and the photo-reproduction of the tabular matter has been done by Messrs. Percy Lund Humphries, and the whole production is excellent. The third and final volume is yet to come, and this will contain about a thousand triclinic substances.

N. F. M. HENRY

Progress in nuclear physics. Volume 5. Edited by Prof. O. R. FRISCH. (London: Pergamon Press Ltd., 1957.) Pp. vii + 325. Price 80*s*.

Each year Professor Frisch succeeds in bringing forward a number of excellent review articles on topics in Nuclear Physics. These are intended for specialist workers in the subject, and there is no attempt to make the articles popular. They range from articles on instrumentation, for example, "New electronic techniques for the nuclear physicist" by K. Kandiah and G. B. B. Chaplin, a large part of which is devoted to the coming use of transistors, to up-to-date review articles, such as that on "The neutrino" by B. W. Ridley. The latter writer is fortunate in having the recent discovery by Reines and Cowan of direct effects produced by the neutrino flux of a nuclear reactor to describe. The article is an extremely comprehensive account of what may be called the "pre-non-conservation-of-parity" period of beta-spectra. But it is well known that the experiments of S. C. Wu and others since the end of 1956 have shown that parity is not conserved in these weak interactions, and have opened up a fundamentally new vista on such processes. Some of Ridley's conclusions may therefore require reconsideration.

There is an interesting article by F. D. Brooks on the mechanism of light emission in organic scintillators. These are part of the stock-in-trade of nuclear physicists, but very few trouble to understand how they work. Another useful technical article is that of C. Dodd in "The bubble chamber" which is the analogue in high energy machine physics of the Wilson Cloud Chamber and which is becoming of increasing importance in the study of individual particle collisions or decays.

There are, of course, several other articles to which it has not been possible in a short review to make any reference. The book as a whole can be highly recommended to all those interested in nuclear physics research work.

H. W. B. SKINNER

Fibres, plastics, and rubbers. By W. J. ROFF. (London: Butterworth's Scientific Publications, 1957.) Pp. xvi + 400. Price 63*s*.

This volume, which is intermediate between a collection of tables and a text-book, should go a long way towards satisfying the need for a reasonably comprehensive yet compact reference book on the structure and physical and chemical properties of a wide range of high polymer materials. For convenience of reference a double classification is adopted, the first being in terms of materials (cellulose, rubber, etc.) and the second in terms of properties (tensile properties, water absorption, electrical properties, etc.). Each section includes a descriptive introduction or summary of background knowledge which is sufficient to provide an intelligent guide to the significance of the more detailed numerical information.

In a few places the presentation seems somewhat uncritical, and the terminology is occasionally misleading. A few examples may be quoted. Under "Friction," no indication is given of the inadequacy of the classical concept of a "coefficient of friction" in the case of fibres. The heading (p. 337) "Wet strength expressed as percentage of tensile strength" reads oddly. On page 92, "natural rubber" is used as a synonym for raw or unvulcanized rubber, and "vulcanized rubber" is contrasted with "natural rubber." (It is more usual to speak of raw or vulcanized natural rubber.) On p. 96 a figure is given for the "latent heat of melting" of natural rubber; without qualification this is highly misleading.

Apart from such small defects, however, the book is highly commendable. The indexing and references are adequate and the general layout is very pleasing.

L. R. G. TRELOAR

Neutron transport theory. By B. DAVISON with the collaboration of J. B. SYKES. (London: Oxford University Press, 1957.) Pp. xx + 450. Price 75*s*.

This book by Dr. Davison, formerly of the Atomic Energy Research Establishment, Harwell, is the first comprehensive account of neutron transport theory to be published. It will be warmly welcomed by workers in the fields of atomic energy and nuclear physics, and by others interested in general transport theory. It contains a wealth of material, presented lucidly and with mathematical rigour. The comparatively simple theories often used in nuclear reactor design are obtained as approximations to the general theory.

The book begins with a review of the various neutron interactions with atomic nuclei, followed by the derivation of the basic Boltzmann transport equation. The solution of this equation is investigated first under the assumption that the nuclear cross-sections are energy-independent, *i.e.* one-velocity group theory. Some standard problems which possess exact analytical solutions are worked out, and the author then discusses in detail the numerous approximate methods which have been developed. They include diffusion theory, the Serber–Wilson, variational and perturbation methods, and the spherical harmonics method, the latter being compared with Chandrasekhar's method of discrete ordinates. The application of the Monte Carlo method is also discussed, and the numerical method of B. G. Carlson is described in an Appendix. The next part of the book deals with the more difficult problem of determining critical size and neutron distribution when the energy-dependence of the nuclear cross-sections is taken into account. Multi-group theory and other approximate methods are fully discussed. The book concludes with a general treatment of slowing-down problems, including the determination of the neutron density at large distances from the source.

The non-specialist reader of the book may wish that it had been possible to include some worked examples, to illustrate the analysis and to compare the results yielded by the various approximate methods, but perhaps the numerical computation involved would have been excessive. The general impression remains of an excellent and timely book that will prove to be a notable contribution to the literature of mathematical physics.

J. CODD

Atomkraft. Der bau von atomkraftwerken und seine probleme. By FRIEDRICH MÜNZINGER. (Berlin: Springer Verlag, 1957.) Pp. xi + 224. Price DM 29.40.

This book is a second edition, rewritten and greatly enlarged, of a work first issued in July 1955. It is a useful collection of information about the various power reactor designs now under consideration in the U.K., U.S.A. and Canada, and their likely role in the economy over the next few decades.

The first section of the work deals, in four chapters, with the fundamental scientific and technological principles involved in reactor design. The second section, which forms almost two-thirds of the work, consists of a description of twenty-four different reactor systems which are now under consideration together with details, as far as they are known, of design and comparative costs. The last, and shortest, section deals with the economic aspects of a nuclear power programme.

The book should be of great value to German engineers and economists, for whom it was written, and of general interest to the non-specialist. The book, however, is deserving of better production and layout, and should contain fewer printing errors.

K. J. BOBIN

Hygrometry. By H. SPENCER-GREGORY and E. ROURKE. (London: Crosby Lockwood and Son, Ltd.) Pp. xv + 254. Price 36*s*.

It is greatly to be regretted that Dr. H. Spencer-Gregory has died since the book was published, and after reading this largely personal record of the work he and Rourke did together it is obvious that we may have to wait a long time for a successor who will match Dr. Gregory's enthusiasm and skill. This book is very welcome, in spite of a lack of balance, a shortage of references, and some defects in writing.

The subject is covered twice. A long introductory chapter with a practical bias is complete in itself; and then nine other chapters go into great detail on the theoretical aspects of the standard methods of measuring humidity, the diffusion hygrometer, and the special problems of hygrometry in gases at high pressure. Though the theory can be challenged in places, nearly all of it is worth thinking about, and most physicists working on water vapour will find something helpful in it.

H. L. PENMAN

Notes and comments

Teaching aids

A teaching aids sub-committee has recently been formed by the Science Masters' Association to collect information concerning teaching aids and prepare lists of these for circulation to its members. It would be appreciated if representatives of industrial organisations would supply the Committee with details of any booklets, wall-charts, models, showcases and filmstrips they may have which would be of use to schools. The details should include the name of the teaching aid, type and cost and be sent to the Secretary, 24 Coniston Road, Bromley, Kent.

Paul Instrument Fund grants

The Paul Instrument Fund Committee, composed of representatives of the Royal Society, the Physical Society, the Institute of Physics and the Institution of Electrical Engineers, was set up in 1945 "to receive applications from British subjects who are research workers in Great Britain for grants for the design, construction and maintenance of novel, unusual or much improved types of physical instruments and apparatus for investigations in pure or applied physical science."

A grant has been made from this fund to Dr. E. T. Hall, senior research officer at the Research Laboratory for Archaeology and the History of Art, Oxford, for the construction of an apparatus with which magnetic measurements may be made of archaeological material and for the development of an instrument for applying the method of neutron activation analysis to archaeological problems. A grant has also been made to Dr. C. M. Smyth and Mr. F. Y. Poynton (Northampton Polytechnic, London), for continuation of the construction of an ultrasonic microscope for which a grant was made in December 1954.

Formation of data-processing section

The Society of Instrument Technology is setting up a special section to cater for the current interest in data-processing systems. This section began to hold meetings in London this Autumn and the following four papers were scheduled for the first session: 10 October—A system for handling wind-tunnel data, by J. F. M. Scholes; 14 November—A digital plotting table, by J. Morrison; 28 January—Digital codes and coding, by M. P. Atkinson; 29 April—A joint meeting on scanning and logging, with papers by D. H. Whiting and J. Dunkley and J. Churchill.

Initial emphasis will be on systems for handling experimental data, and for industrial monitoring and control. The section will be concerned with system design as well as with the detailed design of equipment; it will also deal with the use and organization of systems and with design-study work.

Membership of the section is open to all members of the Society, who may also join the other special group, the Control Section. Members receive the quarterly "Transactions" of the Society, in which the data-processing papers will be published. Further information may be obtained from the Secretary, Society of Instrument Technology, 20 Queen Anne Street, London, W.1. Anyone interested in contributing to the activities of the section should write to the Section Secretary, W. T. Bane, 137 Kenilworth Court, London, S.W.15.

The Combustion Engineering Association

Economies in fuel, if real gain is to be achieved, must be practised on a nation-wide scale. The Combustion Engineering Association seeks to secure this by bringing together all interested parties to ventilate their problems and difficulties and benefit from the views and experiences of others. Membership of the Association is open to all industrial fuel users; consulting engineers; manufacturers of combustion and ancillary equipment; heating and ventilating engineers, and distributors of solid and liquid fuels. A Conference was held by the Association on 5 and 6 November at Harrogate at which was examined in detail the Third Progress Survey of the National Industrial Fuel Efficiency Service. Details may be obtained from the Association, 6 Duke Street, St. James's, London, S.W.1.

Journal of Scientific Instruments

Contents of the November issue

CONFERENCE REPORT

Instruments for use in occupational hygiene. By C. N. Davies.

ORIGINAL CONTRIBUTIONS

Papers

A high-precision photoelectric polarimeter. By E. J. Gillham.
Some improvements in the operation of the optical diffractometer. By C. A. Taylor and B. J. Thompson.
A low frequency random signal generator. By J. C. West and G. T. Roberts.
The time behaviour of logarithmic amplifier input circuits. By T. P. Flanagan.
Some further results on the rubber membrane theory and Laplace's equation. By W. Fulop.
Fizeau-type interference between beams of light reflected from three surfaces. By A. H. Cook.

Laboratory and workshop notes

A simple glass sliding joint for vacuum work. By G. W. Gore.
A fast cycle furnace. By D. B. Irving.
A rotating torque switch operable by light yarns. By R. L. Pocock.
Adjustable apertures for electron diffraction cameras. By J. C. Mills.
A reservoir for paper chromatography for use inside a rectangular glass container. By A. L. Sims.
A "subtractor" for radio-frequency bridges. By E. A. Faulkner.
Notes on the continuous recording of radiation using the Moll thermopile. By F. A. Burden and A. Hoffman.
A single-flash rotary disk optical shutter. By R. L. Gregory.
Use of coarse gratings to find the refractive index of materials. By G. M. Sreekantath and C. A. Verghese.

NOTES AND NEWS

New instruments, materials and tools.
New books.

THIS JOURNAL is produced monthly by The Institute of Physics, in London. It deals with all branches of applied physics (including theory and technique).

All rights reserved. Responsibility for the statements contained herein attaches only to the writers.

EDITORIAL MATTER. Communications concerning editorial matter should be addressed to the Editor, The Institute of Physics, 47 Belgrave Square, London, S.W.1. (*Telephone:* Belgravia 6111.) Prospective authors are invited to prepare their scripts in accordance with the *Notes on the preparation of contributions*. (Price 2*s*. 6*d*. including postage.)

REPRODUCTION. The Institute of Physics is a signatory to The Royal Society's Fair Copying Declaration. Details may be obtained upon application from The Royal Society, London, W.1.

ADVERTISEMENTS. Communications concerning advertisements should be addressed to the agents, Messrs. Walter Judd Ltd., 47 Gresham Street, London, E.C.2. (*Telephone:* Monarch 7644.)

CLAIMS FOR MISSING JOURNALS. Claims from regular subscribers to this *Journal* for missing numbers will only be considered if received within 60 days of the date of mailing plus normal outward time of transit and time for lodging the claim. Losses attributable to failure to notify a change of address or to similar omissions will not be considered.

SUBSCRIPTION RATES. A new volume commences each January. The charge is £5 per volume ($14.25 U.S.A.), including index (post paid), payable in advance. Single parts, so far as available, may be purchased at 10*s* each ($1.50 U.S.A.), post paid, cash with order. Orders should be sent to The Institute of Physics, 47 Belgrave Square, London, S.W.1, or to any bookseller.

Summarized proceedings of the eleventh annual conference of the Stress Analysis Group—Leicester, April 1957

The Stress Analysis Group of the Institute of Physics held a two-day conference at Leicester in April 1957, at which fifteen papers were discussed. These covered the established methods of stress analysis and some newer developments as well. Among them were three papers on fundamentals and the examination of stresses and strains on a microscopic scale. Two of these were on metals whilst the third was on rubber. An innovation was the holding of informal discussion groups on selected topics and these were agreed to have been successful.

The eleventh annual conference of the Stress Analysis Group was held at the University College of Leicester on 9 to 11 April, 1957. The conference this year only covered a period of two whole days, instead of the usual three, because it was only six months since the last conference, which was a joint conference with the Royal Aeronautical Society. Fifteen papers on a variety of subjects connected with stress analysis were read and discussed. Messrs. E. K. FRANKL, B. SUGARMAN and I. L. G. BAILLIE were the chairmen at the technical sessions.

Visits were made during the conference to the lens and optical measuring instrument factory of Taylor, Taylor and Hobson Ltd., and to the machine tool works of Jones and Shipman Ltd. An innovation was the holding of informal discussion group meetings on photoelasticity, strain gauging, other surface strain measurements and the scope of experimental stress analysis methods. The groups met during the second evening of the conference and were well attended.

FUNDAMENTALS OF STRESS ANALYSIS

The conference started with a session on fundamentals. Dr. L. R. G. TRELOAR (British Rayon Research Association, Manchester) gave an interesting discourse on the elasticity and structure of rubber-like materials, which he illustrated with simple but effective demonstrations. The elasticity of such materials is fundamentally different in origin from that of crystalline solids or glasses. Being associated with the random thermal fluctuations of the form of the long-chain molecules of which they are composed, it is in some way analogous to the elasticity of a gas. Dr. Treloar showed an illustration of the fact that the tension in a piece of stretched rubber increases as the temperature is raised. This consisted of a bicycle wheel in which the spokes were made of stretched rubber. When the wheel was heated locally with an electric fire, it was distorted by the contraction of the heated spokes and the unbalance caused it to rotate. The mathematical development of the statistical theory of elasticity has provided a quantitative basis for the interpretation of the principal physical properties of rubbers, including the form of the stress-strain relations under any type of deformation. This theory predicts a non-linear relationship in tension but a linear relationship in shear and this is borne out in practice. The stress-optical coefficients of rubbers can be calculated in a similar way with this theory. Rubbers are susceptible to changes of state and in particular to crystallization which may occur spontaneously on extension. The crystallization is never complete but has a marked effect on the elastic properties, particularly at low temperatures.

Dr. P. B. HIRSCH (Cavendish Laboratory, University of Cambridge) gave an account of a technique which has recently been devised at the Cavendish Laboratory for making dislocations visible in metal films. The films are etched or electro-polished down to a thickness of 1000 Å, when they become transparent in the electron-microscope. Thermal stresses are set up by the heating of the foil in the electron beam and dislocations can be observed to move under the action of these stresses. The dislocations are revealed by the altered scattering power in the strained field around them. An example is shown in Fig. 1 (see p. 483) for the case of aluminium where a dislocation is shown to have left a trail behind it in moving across a grain. In this particular case cross-slip has occurred from one slip plane to another within the grain. Cross-slip does not occur in stainless steel, but under certain conditions the dislocations split into partial dislocations with stacking faults between them. This is illustrated at A and B in Fig. 2 (p. 483) in which C is a twin boundary. This difference in behaviour between dislocations in aluminium and stainless steel is due to the difference in stacking fault energy in the two metals which is high in aluminium and low in stainless steel. The difference in mechanical properties is partly due to the same cause.

The paper by Mr. P. J. E. FORSYTH (Metallurgy Department, Royal Aircraft Establishment, Farnborough) was an interesting sequel to that of Dr. Hirsch, for in it he considered the effect on the strength of metals of the microstructure rather than the inter-atomic forces. These features are such as can be revealed with the optical microscope and the slides with which the talk was illustrated gave evidence of very fine metallurgical technique. Mr. Forsyth discussed first the effects of grain size. The grain boundaries in pure metals and single-phase alloys form obstacles to the movement of dislocations so that the finer the grain size is, the stronger is the metal. There is in fact a rough correlation between the yield point and grain size of the form $\text{Y.P.} \propto 1/l$, where l is the grain diameter. Under certain conditions, such as ageing, which results in the formation of precipitates along the boundaries, inter-crystalline weakness develops and failure under load occurs before the full strength of the grain can be attained. In alloys a further obstacle to the movement of dislocations may be offered by particles of a second phase and, if the distance between the particles is less than the mean diameter of a grain, hardening will result. In two-phase structures where one phase is markedly softer than the other all the deformation may occur in the softer phase, the hard phase remaining undeformed. This is well illustrated in Fig. 3 (p. 483) which shows the deformation in the alpha phase of an alpha-beta brass. In fatigue deformation under

uni-directional stress, slip bands are generally localized in a few grains and they are also more intense, apparently representing very considerable local dislocation movements. Fig. 4 (p. 483) shows groups of slip bands or striations in pure aluminium and it is in these bands that fatigue cracks begin. Cold working, by rolling for example, hardens the material by locking dislocations and distorting the crystal lattice. The introduction of these effective barriers to dislocation movement increases the stress which is needed to force the dislocations through the lattice and promotes an increase in fatigue properties. Aluminium alloys which age-harden have been shown to exhibit slip band extrusion, believed to be associated with the formation of soft zones along the slip bands. An example is shown in Fig. 5 (p. 484) of extrusion under fatigue loading from slip bands in an aluminium 4% copper alloy.

PHOTOELASTICITY

A second group of papers was mainly on photoelasticity. Miss M. CLUTTERBUCK (General Electric Co. Ltd., Applied Electronics Laboratory, Stanmore) spoke on her examination of the effect of Poisson's ratio on stress distribution and was reassuring to users of analogue techniques such as photoelasticity. It is in the stress freezing method that the greatest disparity in Poisson's ratio occurs between that of the model and prototype. Theoretical investigations on the Poisson's ratio effect are scanty, exceptions being in the work of Michell,[1] Filon[2] and later of Bickley[3] and Stevenson.[4] These all apply to two dimensions, the only three-dimensional work being that of Neuber for the hyperbolic notch. Miss Clutterbuck's contribution is to make photoelastic comparisons on the same material, cold and also after stress freezing, the Poisson's ratios being 0·36 and 0·48 for the two states. This is for the two-dimensional case of a loaded hole in a large plate and the results were compared for Poisson's ratio effect. Any differences were found to be within the limits of experimental error. The same conclusions applied to cases of multiple loaded holes and also on a round-ended lug. For a three-dimensional example, a cylinder with a hyperbolic notch was compressed cold and hot. Examination in this case was by the scattered light method with which the accuracy claimed was only within 7%. Here again any differences due to Poisson's ratio were within the range of experimental errors. An additional observation from this work is that unless the strains are the same in the model and prototype in the vicinity of loading points, much greater errors in these regions can be introduced from this cause than from differences in Poisson's ratio.

A paper by Dr. H. FESSLER and Mr. E. OLLERTON (Department of Civil and Mechanical Engineering, University of Nottingham) was on the contact stresses in toroids under radial loads. The work arose as an extension of a photoelastic investigation into the stresses occurring due to the contact between railway wheels and rails. The classical theory of Hertz, as evaluated by Thomas and Hoersch,[5] gives the three orthogonal stresses on the axis of loading. Tests made with photoelastic models of finite size, using the stress freezing method, gave good approximations to the theoretical stresses. The shapes of the ellipses of contact were also in accordance with those predicted by the theory. When the toroids are in rolling contact tangential stresses occur and the maximum range of shear stress does not occur on the loading axis. The investigation was mainly concerned with the determination of this stress and its position for a wide range of shapes of toroids.

Mr. L. D. MCCONNELL (Rolls Royce Ltd., Derby) discussed the design of lugs loaded by pins, as influenced by photoelastic work. The most important variable is the ratio of the pin diameter to the width of the lug. For a neat fit pin in a thin lug the lowest value of the peak stress occurs when this ratio is about 0·4. This figure is modified by the shape of the head of the lug, the amount of material beyond the pin and whether the head is rounded or square. A fully rounded head gives about 20% more stress than a square head whilst a banjo shape may cause an increase of as much as 50%. Another important factor is the bending of the pin. This causes an uneven distribution of stress in the lug and may raise the optimum value of the ratio of pin diameter to lug width to as much as 0·6. The clearance of the pin in the hole is also significant. Between a clearance of 0·002 in./in. and an interference fit of 0·003 in./in. there is not much difference in maximum stress. There is as yet little information on the improvement which may be gained by using higher degrees of interference. Clearances between 0·002 and 0·01 in./in. result in an increase in stress and this is particularly marked in the case of large diameter pins. When a pin joint has to rotate under load the conditions are altered and it is better to allow some clearance so that the pin can roll on the surface of the hole without sliding.

The paper by Messrs. A. S. MCLAREN and I. MACINNES (Department of Natural Philosophy, Royal College of Science and Technology, Glasgow) was on the influence of bending of the adhering sheets on the stress distribution in an adhesive lap joint. Earlier work by Mylonas[6] demonstrated photoelastically that the stress distribution in the joint was far from uniform and that high stress peaks could occur at the free surfaces of the glue. In the authors' investigation the effect of the deformation of the adhering sheets was allowed for. A study was also made of the relief of stress which occurred when the edges of the sheets were intentionally bent in the same sense as occurs under the action of tension on the joint. In the ensuing discussion mention was made of a way of reducing the modulus of Araldite at room temperature by adding a rubbery substance to the mixture before curing.

The contribution of Messrs. M. L. MEYER and A. N. OAK (Postgraduate Department of Applied Mechanics, University of Sheffield) was about an investigation which had been made after the failure of a crankshaft in service. The chief interest is in a comparison of three methods of measuring the fillet stresses under simulated gas pressure loads. The first method which was intended to give a qualitative result quickly, was a two-dimensional photoelastic test on a plane model representing a section of the crankshaft at its plane of symmetry. The second method was a three-dimensional photoelastic investigation which involved the casting of a full-sized Araldite model and applying the stress-freezing process. Slices were cut out on the axis of symmetry so as to give a direct comparison with the results from the plane model. For a direct measurement of the fillet strains under load, the crankshaft was clamped firmly in its crankcase and load was applied with a screw and measured by a load cell fitted with strain gauges. Strains on the fillets jointing the crankpins to the webs and on the webs themselves were measured with a Solex pneumatic extensometer on a gauge-length of 2 mm. The results of the three-dimensional photoelastic tests were in fair agreement with those derived from the extensometer measurements, the differences which occurred being attributed to the very small radii of some of the fillets. The two-dimensional photoelastic results were less reliable but gave a useful indication of the relative magnitudes of the stresses.

ELECTRICAL RESISTANCE STRAIN GAUGES

Only one paper at the conference was on electrical resistance strain gauges. This was by Mr. P. R. LANE (British Welding Research Association, Abington Hall, Cambridge) on the use of strain gauges inside vessels subjected to high pressures. For the measurement of strains in branch connexions inside these vessels, wire-wound gauges having a resistance of 120 to 200 Ω were used. Most of the tests were made at a pressure of 1000 lb/in.^{2} but a few were made at pressures up to 10 000 lb/in.^{2} The large size of the vessels (up to 3 ft 6 in. diameter by 11 ft long) made the use of water more convenient as a pressure medium and this necessitated the waterproofing of the gauges. This was effectively accomplished by the use of a bitumen compound which merely required to be melted and poured on. The leads had to be tested for pinholes and were brought out through a steel cone into which they were sealed with a low melting alloy. Over the whole range of pressure it was found that there was no change in the gauge factor, whether the compensating gauges were used inside or outside the pressure vessel. Special tests were devised to investigate this matter further and it was concluded that there must be a direct effect of pressure on the strain gauge wire which was equal and opposite to that of the hydrostatic pressure on the block to which the compensating gauge was fixed. This conclusion might not apply to gauges made from a different wire.

OTHER METHODS OF STRESS ANALYSIS

There were several papers on other methods of experimental stress analysis. Dr. H. HUGHES and Dr. K. W. ANDREWS (United Steel Companies Ltd.) described the use of a transportable X-ray unit for stress determinations. The equipment had been specially designed with all the necessary movements to make it convenient for use on a large component. Dr. Andrews drew attention to the possibilities and limitations of X-rays for stress analysis, emphasizing the fact that measurements could only be made at or very near to a surface. The quantity measured is the elastic strain of the lattice in a metallic crystal, but care is necessary in the interpretation of the results when the material has been strained plastically. The use of X-rays for the measurement of the stresses on the surface of a tube bent into a U-shape was quoted. The extent to which the stresses could be removed by heat treatment was one of the objects of this investigation. The stresses in various parts of railway wheels were measured after different heat treatments and compressive stresses up to 18 tons/in.^{2}, were recorded for the rim.

Dr. P. J. PALMER (Department of Civil Engineering, University of Birmingham) described an application of the *moiré* method to the bending of plates at right angles to their surface. The experimental technique is particularly suited to this class of problem, which is not readily soluble by photoelastic means. The principle is illustrated in Fig. 6. An illuminated screen is ruled with lines at about eleven per inch so that the black and white lines are of equal width. The pattern of lines is reflected at the polished surface of the model and recorded with a camera at the middle of the screen. Thus the point *L* on the model reflects the screen to the camera at the points *M* and *N* before and after loading. Two exposures are taken on the same photographic plate, one with and one without load on the model, and the interference pattern gives the slope of the model directly. The moments and stresses can be derived by plotting the gradients and differentiating them. An example of the use of the method is reproduced in Fig. 7 (p. 484). This shows a plate clamped at its edges with a rectangular hole, under uniform loading. The model was made from black Perspex. The order of accuracy for bending moments is 10% and for deflexions 5%. One comment of the author which is worth

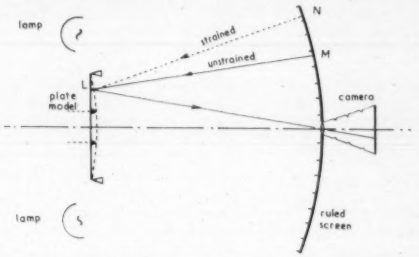

Fig. 6. Principle of *moiré* apparatus for bent plates

recording is that better pictures are obtained with the model bent so as to have a convex curvature towards the screen. This is because there are more lines per inch when the model is loaded in this manner, although the number of fringes is the same for a given curvature irrespective of sign.

Mr. J. A. N. LEE and Dr. R. C. COATES (Department of Civil and Mechanical Engineering, University of Nottingham) discussed the problem of the small deflexions of a point-loaded rectangular plate with two stiffened edges. This problem bears on the case of the pre-stressed concrete bridge which under certain conditions may be reduced to that of a thin plate. Stiffening the edges of the deck gives a useful relief of stress, but it is difficult to allow for any increase in torsional rigidity by other than experimental means. The results of an analytical method have been compared with those of a relaxation determination, neglecting the torsional rigidity in both cases. The particular interest in this investigation is in the use of a plaster of Paris model to see whether this neglect is justifiable. The plaster could be formed into substantial stiffening ribs which were integral with the deck. Nevertheless, the experimental results gave good confirmation of the simplified theory. The authors found it necessary to remove the air bubbles from the plaster cream before it was formed in the mould. This could not be done by the use of vibration but the application of a vacuum was effective.

ELASTIC STRESSES IN DESIGN

Among papers of a more general nature was one by Mr. C. SNELL (Department of Mechanical Engineering, University College, London) entitled "Some factors concerning the use of elastic stresses in design." Mr. Snell's avowed object was to stimulate thought and discussion on the advantages to be gained by a more serious consideration of the elastic stresses as a guide to safe design. He began by saying that it was remarkable that elastic theory was used as much as it is, since the three basic assumptions on which it is founded are not fulfilled. The assumptions are that a material obeys Hooke's law, that it is isotropic and that it is homogeneous. Departures from Hooke's law are not generally important because it is re-established after yielding has occurred and large changes in the geometry of components do not generally

occur. Lack of isotropy is always present, more in non-ferrous than ferrous materials, but it too is unlikely to be important. Mr. Snell quoted a ratio of 30 times for the moduli of spruce along and across the grain and said that this difference could only double the maximum stress for a hole in a plate under simple tension for this material. He considered that the finite grain size of metals was the feature of greatest importance in the application of elastic theory. The fact that engineering materials consist of a matrix of randomly-oriented grains makes the concept of stress at a point meaningless. Mr. Snell strongly deprecated the use of fatigue specimens with stress concentrations having a radius as small as 0·01 in., for this reason. Turning to repeated loading tests, Mr. Snell discussed the relationship between the theoretical stress concentration factor, K_t, and the strength reduction factor in fatigue, K_f. His conclusion is that, provided the stress range does not exceed twice the dynamic limit of proportionality of stress with strain, the two factors will often be equal. For carbon steels and austenitic steels, but not high tensile steels, K_f will be lower than K_t by virtue of the remarkable property of these materials to withstand repeated yielding without failure. The paper provoked a discussion on the recent tendency to insist on full-scale tests to destruction, such as those on the Comet aircraft. Views seemed to be about equally divided on the need or otherwise for these tests and it did not seem likely that agreement would have been reached even if much more time had been available.

VIBRATION TESTING

A paper of interest to those who are interested in the vibration testing of finished components came from Messrs. W. Brundrett and D. G. Seymour (Component Development Department, Bristol Aero-Engines Ltd.). The usual moving-coil type of vibration exciter is unsatisfactory for heavy duty, particularly at high frequencies. It was decided therefore to construct a robust type of exciter with a very high field strength and with a moving coil consisting of a single short-circuited turn. This coil, which was made from chrome copper strip 0·5 × 0·2 in., formed the secondary winding of two primary coils wound on C cores which linked with the coil. This exciter is now regularly used for tests on compressor and turbine blades vibrating at their fundamental frequencies, which range up to about 2500 c/s. The blade is clamped at its root in a freely suspended massive block and the exciting force is applied by a resonant system comprising a driving rod attached to the block with the moving coil at the remote end. The moving-coil system is not considered as likely to be useful for frequencies about 3000 c/s, but for higher frequencies a piezo-electric exciter has been devised. This employs two barium titanate ceramic disks firmly clamped between copper electrodes. The natural frequency of this unit, which is $5\frac{1}{2}$ in. long × $3\frac{1}{8}$ in. diameter, is of the order of 20 kc/s. It is threaded at both ends, at one end for attachment to the work-piece and at the other for the attachment of weights so that it can be tuned to lower frequencies.

The last paper of the Conference was by Dr. O. Kantorowicz (Pametrada Research Station, Wallsend) on wave speed curves relating to rotating machinery. In it he outlined a method used by the Pametrada Research Station for the examination of transverse vibrations in turbine disks. If a transverse wave motion is set up which rotates backwards with a speed equal to the forward speed of the rotor it will appear as a stationary pattern to an observer at rest. Such vibrations can be set up by a spatial inequality in steam distribution and have been shown to be responsible for catastrophic failures of impulse turbine disks in the past. More recently, fatigue failures of blades, shrouds and binding wires began to occur and it was realized that standing waves might be the cause, when they moved in a field containing resonators tuned to the same frequency. The method of analysing the performance which was mentioned previously is to plot the wave speed for each resonance as a function of frequency.(7) Resonators which may produce anomalous dispersion are often to be found in the blading and these show up in the curves. Dr. Kantorowicz illustrated his talk with a number of examples relating to steam turbines and also to large marine gearing.

ACKNOWLEDGEMENT

The author wishes to thank the Director of the National Physical Laboratory for granting facilities for the preparation of this article.

A. F. C. Brown

REFERENCES

(1) Michell, J. H. *Proc. Lond. Math. Soc.*, **31**, p. 100 (1900).

(2) Filon, N. G. *Brit. Assoc. Rep.*, p. 305 (1921).

(3) Bickley, W. G. *Phil. Trans A*, **127**, p. 383 (1928).

(4) Stevenson, A. C. *Phil. Mag.*, **34**, p. 766 (1943).

(5) Thomas, H. R., and Hoersch, V. A. Bull Engng Experimental Station No. 212 (University of Illinois, 1930).

(6) De Bruyne and Houwink. *Adhesion and adhesives* (New York: Elsevier Publishing Corp., 1951).

(7) Kantorowicz, O. *Proceedings of the Conference on Steam Turbine Research* (London: Institute of Mechanical Engineers, 1952).

The effects of dust and force upon certain very light electrical contacts

By A. J. Maddock, D.Sc., F.Inst.P., M.I.E.E., C. C. Fielding, B.Sc.,* J. H. Batchelor, B.Sc.,† and A. H. Jiggins, B.Sc., A.Inst.P.,‡ British Scientific Instrument Research Association, Chislehurst, Kent

[*Paper first received* 17 *June, and in final form* 14 *August*, 1957]

A study has been made of electrical contacts of platinum–gold–silver and of gold when operated at contact loadings of the order of milligrams. The general random nature of failures to make contact is demonstrated and two major causes are considered as contributing to these, dust and surface films. This paper is concerned firstly with the effects of dust and a relation between dust concentration and number of failures has been established: it appears that dust is more likely to be troublesome at very low contact loadings. The second part deals with the effects of contact force, for the practical case of relatively uncleaned contacts, from 0–4000 μg. The work here described extends to lower contact loadings than has hitherto been reported: resistance values rise very rapidly at loads below 1 mg.

1. INTRODUCTION

Several years ago, an investigation was carried out to study the behaviour—or perhaps it should be called the misbehaviour—of certain very light electrical contacts. The particular contacts existed in a low-current moving-coil relay and consisted of point-to-plane type, the point being the fixed contact and the plane (in the form of a blade) the moving contact. The nominal radius of the points was within the range 0·001 to 0·005 in. and the loading at make amounted to approximately 0·1 to 2 mg, depending on the type of relay. Movement of the blade on switching on the operating current to the relay was very slow due to the heavy electromagnetic damping and the relays were used, and tested, under very quiet conditions so that, as far as practicable, the effects of vibration were minimized: this of course was a factor against helping the relay to make but was determined by the special conditions of use. For the most part both blade and points were made of platinum–gold–silver alloy (PGS alloy).

It had been reported that on taking a given set of 100 relays and testing them a certain percentage would fail to make contact and that, after storing for some time and again testing and repeating the procedure, the same percentage of failures occurred though in different relays of the set. Such a result is consistent with random behaviour of contact and is very much in line with the work of Williamson, Greenwood and Harris[1] in their study of the influence of dust particles.

Since the effects of vibration had been almost completely eliminated (except for a few gross changes brought about by very heavy vibration and which were eliminated from the results) the major causes of failures-to-make were considered as being most likely due to dust particles on the contacts and to surface films—e.g. chemical films or adsorbed films. In an attempt to separate out the effects of these two major causes (and it is not suggested that they are the only ones) experiments were carried out first on the effects of dust upon these contacts and these are reported in Section 3, whilst later experiments were concerned with the effects of force upon the resistance of the contact and thus had a bearing on the effects of surface films: the data obtained in this respect are given in Section 4.

2. EXPERIMENTAL PROCEDURE

In view of the random nature of the behaviour of these contacts it was thought that experiments concerned with the effects of dust should be planned so that a large number of contacts could be studied more or less simultaneously and on a statistical basis. This was particularly necessary since it was desired to vary the concentration of dust in the atmosphere around the contacts and the group behaviour seemed more likely to give results which could be better correlated. A special apparatus was constructed having 100 sets of contacts, which could be selected one at a time, and which occupied a reasonably small volume in which one might expect the conditions at all the points to be sensibly similar, at least on an average basis.

A description of the apparatus is given in Appendix I and, although known and referred to as the 100-contact apparatus, in fact only some 80 contacts could be alined to behave regularly and respond at loadings comparable to those in the individual relays. However, this was a sufficiently large number and the results were expressed in terms of the percentage failures for a given atmospheric condition: the results are quoted in terms of total failures, that is the sum of all contacts which failed to make at all and those which gave partial contact, usually of very high resistance. The voltage in the contact circuit was 3 V and the current at make was set by external resistance to be 200 mA.§ The contact loading adopted for most of the work with this apparatus was 1·8 mg.

The complete contact apparatus was housed in a drybox, with rubber inset gloves for manipulation, but with the torsion control device and the controls from the turret rods brought outside. In this way, once the apparatus had been set up for a run, control of the contacts could be effected from outside and, as the interior of the box comprised a volume completely sealed off from the outside air, the conditions inside with regard to dust concentration could be controlled. A second drybox, attached to the side of the first, and with a door between them, could be used as a lock between the main box and the room: this allowed apparatus to be inserted without

* Now at Ministry of Supply.
† Now at Muirhead Ltd.
‡ Now at Woolwich Polytechnic.

§ The current was read on a milliammeter. Failure to make was indicated by zero current whilst a partial failure would be indicated by a much lower current (or a flickering current) than the normal full current of 200 mA.

unduly affecting conditions in the main box and enabled initial assembly and cleaning to be carried out more easily.

When the contacts were to be cleaned this was done by brushing the surfaces, using camel-hair brushes, firstly with carbon tetrachloride and secondly with acetone. Reduction of the dust concentration was achieved by allowing the dust to settle and be caught on the surfaces which were treated with a special sticky varnish: some notes on the attaining of low dust concentrations are given in Appendix II. A 4 in. diameter hole in the top of the box, normally closed, could be opened to admit dust from the room to enter the box to raise the concentration from a lower value. The dust concentration was determined by means of an Owen's jet dust counter and the particles obtained in this were counted under the microscope using dark-ground illumination. The dust concerned was the normal found in an experimental laboratory (linoleum-covered floors) and the concentration is expressed in particles per cm^3, particles of all sizes being counted down to the lowest visible by this method of observation, estimated as about $\frac{1}{2}\mu$.

In the case of the effects of contact force the behaviour of individual relays was studied with only mild initial cleaning of the contacts. By this means it was hoped to determine what might be the effects under conditions of actual use: for these latter tests gold contacts were used.

3. RESULTS OBTAINED AT DIFFERENT LEVELS OF DUST CONCENTRATION

3.1. *Behaviour at normal dust concentrations.* In the course of some preliminary testing it was observed that for all cases where the contacts were assembled and cleaned in the normal room atmosphere the number of failures for each actuation of all the contacts was roughly the same, the overall average of six actuations being 19·1%: this state of affairs seemed to apply for a run when all the contacts had been freshly cleaned or whether one or two actuations were carried out after only the one cleaning. By noting carefully which contacts of the set failed and by obtaining the running totals for these several actuations the build up of total failures was as given in row (*d*) of Table 1.

practice since any test means an actuation must take place with its attendant number of failures. This relationship is that normal to the number of survivors after a given time when the failures are random in nature and of a fixed loss per unit action.

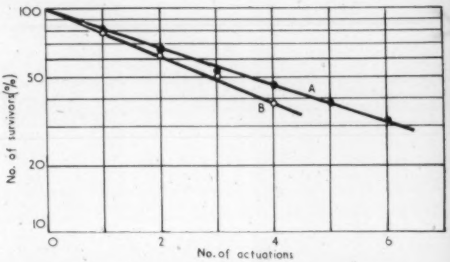

Fig. 1. Survivors and number of actuations

Another set of experiments, but carried out at a different dust concentration, gave very similar results for four actuations and these are plotted as curve *B* in Fig. 1. It will be noted from Fig. 1 that after seven or eight actuations only about 20% of the contacts will not have failed to make.

The failures reported in this sub-section will be due to all factors, dust, surface films and any other causes.

3.2. *Failures as a function of dust concentration.* A number of tests were made in the drybox commencing with the contacts cleaned and tested first at room concentration of dust (usually around 1100–1200 particles per cm^3) and then secondly after the dust had been allowed to settle for several days and the concentration had fallen to a low value (around 100 particles per cm^3). The general outcome of all these tests was that the percentage failures increased slightly (to about 23% from an initial figure of around 21%) as the dust concentration decreased.

Table 1. *Behaviour of contacts for repeated actuations generally at normal ambient dust concentration*

(*a*) Experiment number	4	6	8	9	10	11
(*b*) Number of actuations from start	1	2	3	4	5	6
(*c*) Number of contacts in use	80	85	79	78	75	75
(*d*) Number of failures per actuation in %	19	16·5	21·5	18	19·5	20
(*e*) Total number of failures from start	15	28	38	43	49	53
(*f*) Running average of number of contacts involved per actuation	80	82·5	81	80·5	79·2	78·7
(*g*) Total failures in % [100 (*e*)/(*f*)]	19	34	47	54	62	68
(*h*) Total survivors in % [100 − (*g*)]	81	66	53	46	38	32

The results of row (*h*) are plotted on a semi-logarithmic scale in Fig. 1, curve *A*, which indicates an exponential relationship of the form:

$$y = 100 \exp(-0{\cdot}194x)$$

y being the number of survivors after the number of actuations *x*. From this the average failure rate is 19·4% of contacts for each actuation. A continuous line has been plotted joining the points though, in fact, it is a discontinuous function since we can only go in unit steps of *x*. The line projects back well to 100% for zero actuations, indicating all good contacts, a state of affairs which cannot be tested in

It is, of course, the volume concentration that is measured by the dust counter in all cases, whereas it will be the surface concentration of the dust on the contacts which is of consequence in affecting the failure rate. The inference from these experiments is that the dust present on the contacts immediately after cleaning—and determined, therefore, in these cases by the volume concentration in the room—generally adheres to the contacts and may be further added to in some measure by more dust being collected as the latter settles down in the box: a small increase, therefore, rather than a decrease in the number of failures is observed.

To obtain values for the number of failures at low dust

concentration, it is now obvious that observations must be commenced at low values, the contacts being cleaned and assembled in the box at the lowest dust level at which it is desired to test. Additionally, a study can then be made of the effect on the contacts as the dust concentration is allowed to increase after the initial test and without any intermediate cleaning. A large number of runs was made to establish the relationship between dust concentration and percentage failures. The results of these are given by the set of points around curve *A* in Fig. 2, the line through these points

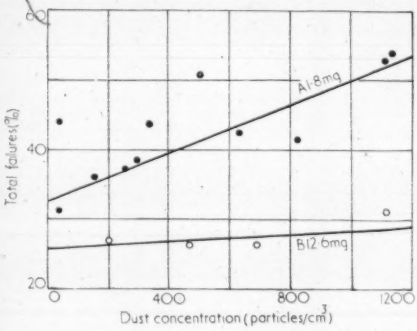

Fig. 2. Failures at different dust concentrations

representing the general trend of the relationship. From the correlation coefficient derived from the experimental data it was established that there was only a 2% probability that the points are so distributed by chance. The general trend, therefore, seems to be a linear one at least from 1200 particles per cm^3 downwards. It shows that the failures increase steadily as the dust concentration increases, but that even if there were not dust particles present a considerable number of failures would still occur, the intercept on the failure axis showing this value to be about 32% for this particular apparatus. This intercept is due to at least a second factor which is most likely to be a surface film on the contacts.

Great accuracy cannot be achieved in an experiment of this kind for several reasons: (*a*) although strict precautions were taken the apparatus was still subject to some disturbance from vibration, (*b*) it was sometimes difficult to judge the alinement of a contact, (*c*) each run took a day to complete during which time conditions could vary somewhat. Nonetheless, it is felt that the relationship given represents the general trend especially as quite a large number of other groups of runs, not shown on the diagram, had exhibited the same trend.

Four runs taken at a higher contact force (increased by a factor of seven) resulted in the points and curve *B* of Fig. 2. The percentage failures are now much less dependent on dust concentration, though a linear relationship is still indicated, and the second factor is the predominating one though reduced somewhat by the increased force.

These sets of experiments show that when proceeding from a high to low value of dust concentration little change takes place in the failure rate, whereas proceeding from low to high values of dust level the failure rate increases linearly. Practically, this means that it will be the highest level of dust concentration to which the contacts are ever exposed that will determine the failure rate.

3.3. *Effects of contact force.* To determine the effect of different contact force seven runs at a concentration of 670 particles per cm^3 and four at 800 were made and showed the expected decrease of failures with increase of loading. The results of both these sets are given in Fig. 3 with the most probable line (curve *A*) running through them (these two values of dust concentration are sufficiently close for one line to be drawn through all the points). This decrease is similar to the findings of other workers at much larger contact forces. On the assumption that a similar relationship is followed at all dust levels two other lines (*B* and *C*) at different dust concentrations have been plotted on the same diagram, the values for two points to determine each of these having been taken off curves *A* and *B* of Fig. 2.

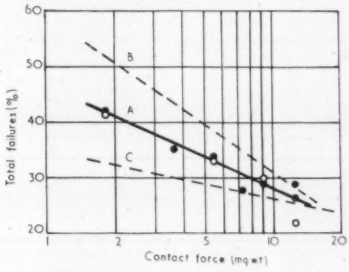

Fig. 3. Failures at different loadings

A, 670–800 particles/cm^3; *B*, 1100 particles/cm^3; *C*, 0 particles/cm^3.

Two points of interest appear from this: (*a*) there probably exists, even at zero dust concentration, a similar relationship between contact force and percentage failures: this means that surface films are also affected by contact force, (*b*) the several curves at different dust levels intercept the zero dust curve at about 15 mg weight: this implies that, for this particular apparatus, the effect of dust is sensibly negligible above this loading and all failures are due to other factors such as surface films.

4. FURTHER STUDY OF THE EFFECT OF CONTACT FORCE

In this fuller study of the effects of contact force it was desired to link up with the results of Holm at loadings of a few milligrams and to extend the investigation down into the microgram region as near to zero force as possible. The contact resistance was measured in moving-coil relays (as outlined in Section 1) fitted with fine gold contacts. One relay covered the range 0–600 μg and another 500 to 4000 μg, the control force being generated by means of current through the deflecting coil: zero force was considered to be acting when the contact point and its optical reflexion in the blade first met. Definite, though high resistance contacts were obtained under these circumstances and it is estimated that the loading was probably less than 5 to 10 μg. The contacts were washed initially in carbon tetrachloride and acetone and were protected from a vertical fall of dust but were not totally enclosed.

Previous work had shown that the contact resistance depended markedly also on other factors such as time of current flow, value of the contact current and the voltage in

the circuit. By adopting currents less than 2 mA and a potential of 2 V the effects of these were negligible in comparison with the effect of force on the contacts: such low values result, however, in high resistances being obtained.

4.1. *Results obtained over the force range.* In Fig. 4 are shown all the readings taken on one particular pair of contacts, the result of twenty-one runs from low to high contact force over the range 0–600 μg. To summarize the result the median points were taken at each vertical line, i.e. the eleventh point of each set, this being taken as an estimate of the most probable resistance at any given contact force and the circles indicate these points: the line XX' is the best straight line through these points. It was considered preferable to express the results in this manner rather than by arithmetical means

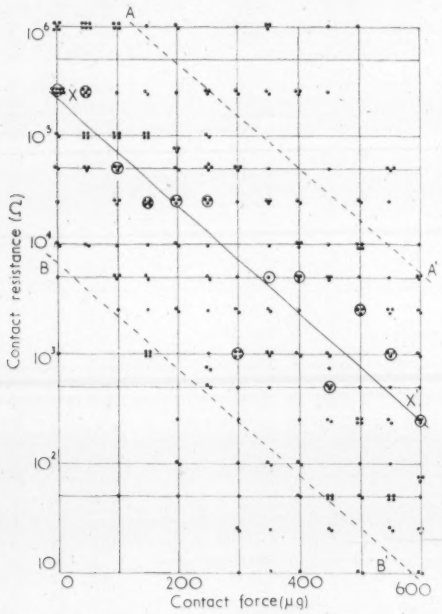

Fig. 4. Variation of contact resistance with contact force (0–600 μg). Twenty-one separate runs with gold contacts

when the values cover such a wide range. Lines AA' and BB' have been drawn parallel to XX' such that about 80% of the points are enclosed by them on each side of the median line. The general upward trend of the results is apparent, indicating a rapid increase of contact resistance as contact loading is decreased. A similar set of results was obtained in twenty-four runs taken on another pair of contacts in the higher force range 500–4000 μg: however, a much smaller rate of change with loading was obtained but with evidence of a sharper upward tendency at the 500 μg level.

Fig. 5 is an attempt to summarize the data obtained still further to show the variation of resistance from "zero" force upwards and to compare it with results quoted elsewhere. Curve *A* is drawn to link up all the median points obtained in the two sets of experiments, i.e. the circles of Fig. 4 and similar points for the higher force range mentioned above. This curve, *A*, is the most probable one taking into account all the median points for the two force ranges taken together (shown as circles and crosses respectively). Curve *B* of Fig. 5

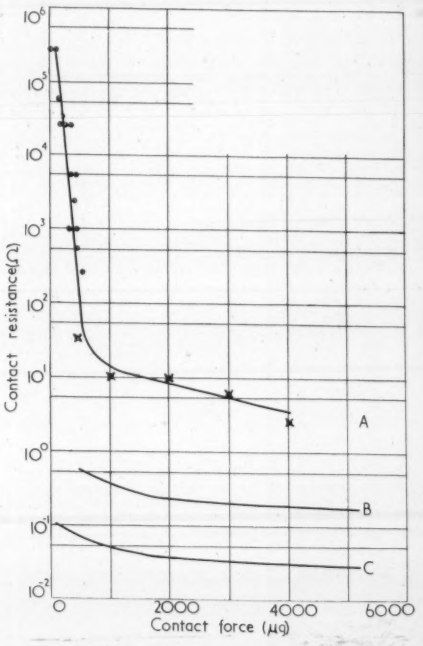

Fig. 5. Resultant curves for variation of contact resistance with contact force (0–5000 μg) for gold contacts

A, most probable values from present experimental results; *B*, Holm's results for contacts covered with a mono-molecular oxygen layer; *C*, theoretical curve for perfectly clean contacts.

is plotted from results quoted by Holm[2] for gold contacts with a mono-molecular oxygen film on the surface. Since the contact current and circuit voltage are not quoted for his results it is difficult to compare them closely with curve *A*. However, since we carried out no rigorous cleaning of the contacts it can be assumed that, besides the mono-molecular oxygen layer, the contacts had a certain amount of dust and grease and possibly thicker adsorbed films on their surfaces. A much higher resistance than that obtained by Holm is therefore to be expected: in general the shapes of the curves are similar, but we have been able to extend the picture to lower levels of contact force and show the very rapid rise of resistance at these low levels. Curve *C* is a theoretical curve of the resistance of perfectly clean gold contacts; it is, therefore, the lowest possible value that could ever be achieved. It is obtained by first calculating the actual contact area from

a knowledge of the load and elastic constants of the contact material, and then calculating the resistance caused by constricting the lines of current flow in this area as is treated by Holm.[3] On this basis the true pressure at the minute contact areas is sensibly constant no matter what the force is: the material yields until the load is just supported over an area proportional to the force.

The difference between this constriction resistance and the total contact resistance obtained in practice is called the film resistance. It is expressed as σ/S, where σ is the resistance of 1 cm^2 of the film and S is the contact area calculated from the radius of contact obtained in the calculation for the constriction resistance. The values of σ obtained in this way for our general curve A and the curve B of Fig. 5 are given in the table below:

Table 2. *Specific resistance of films at different loadings*

Contact force (μg)	*Film resistance* (Ω) *Curve A*	*Curve B*	σ_A ($10^{-9}\ \Omega$ cm^2)	σ_B
1000	15	0·28	26·4	0·5
2000	8·5	0·19	23·8	0·52
3000	5·3	0·16	19·6	0·59
4000	3·5	0·15	15·6	0·67

It is seen that σ_B does not vary much over the force range though with a small upward trend towards the higher force level. Holm also quotes some other results[4] for gold contacts at loads from 1–400 g and obtains a similar slight increase and states that the value of σ for gold, copper and tin is of the order of 5–12 $\times$ $10^{-9}\ \Omega$ cm^2, fairly independent of temperature, load and metal: this is an order higher than for his curve B, but the same slow rise is evident. In contrast to the figures for curve B, our contacts show a higher specific resistance for the films and, more particularly, vary with load quite markedly in the opposite sense. We attribute this to a gradual penetration of the composite film on our uncleaned contacts with increasing force: the very rapid change in contact resistance in the very low force region of curve A indicates possibly that considerable penetration of a relatively thick or high resistance film is occurring here. In partial support of this we would add that contact resistances of the order of 1 Ω are obtainable at a contact force of 100 μg after careful cleaning, fitting in well with curve B and emphasizing the wide variations that may be obtained.

5. CONCLUSIONS

A quantitative relation between dust concentration and contact failures has been shown to exist, the magnitude of which depends upon the force between the contacts. At the low levels of force here studied dust plays a large part in such failures. It has been shown that the dust is apparently retained on the contacts and the failure rate is determined by the highest concentration of dust to which the contacts have been exposed, subsequent lowering of the concentration does not reduce the failures unless the contacts can be cleaned and sealed in an enclosure at the lower concentration.

The results here quoted on the effects of contact force serve as a guide to indicate the general trend of contact resistance at very low force levels and show that the contact resistance may attain very high values at loadings below 1 mg unless the surface films can be permanently removed. They also indicate that the rate of change of resistance at these very low levels is much greater than is obtained over the more normal loading from milligrams to grams.

6. ACKNOWLEDGEMENTS

Thanks are due to the Admiralty, on whose behalf much of this work was carried out, and the Council of B.S.I.R.A. for permission to publish this paper. It is a pleasure to record the valuable work done during part of the investigation by J. H. Hamblyn.

REFERENCES

(1) WILLIAMSON, J. B. P., GREENWOOD, J. A., and HARRIS, J. *Proc. Roy. Soc. A*, **237**, p. 560 (1956).
(2) HOLM, R. *Electric Contacts*, p. 88 (Stockholm: H. Gebers, 1946).
(3) HOLM, R. *Electric Contacts*, pp. 21 and 73 (Stockholm: H. Gebers, 1946).
(4) HOLM, R. *Electric Contacts*, p. 111 (Stockholm: H. Gebers, 1946).

APPENDIX 1

Brief description of multi-contact apparatus (*Fig.* 6). The moving member A carries, on each side, 25 of the blade

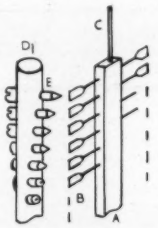

Fig. 6. General arrangement of contacts

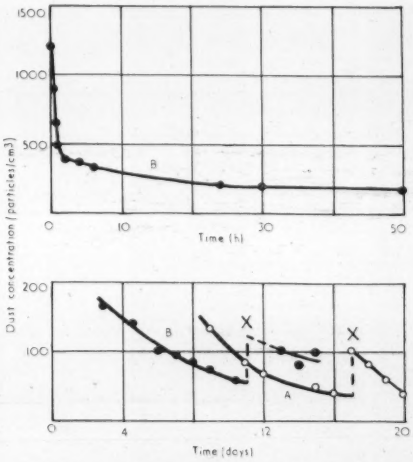

Fig. 7. Dust concentration with time in drybox
A, without; B, with sticky varnish; X, box shaken.

contacts *B* spaced 3/16 in. apart; it is supported at the top by light torsion strip *C* and is connected at the bottom by a similar strip to a rotatable head by means of which member *A* can be rotated to bring the blades into contact with the points.

Four rotatable turret rods *D* (only one of these, D_1, is shown) are situated at the corners of a rectangle and each carries 25 contact points *E* arranged around their length in helical form with 3/16 in. vertical spacing and 14° angular spacing. Thus by rotating the turret rods through 14° at a time each contact point may be brought into position to make contact with one of the blades, and as front and back surfaces of the latter are used 100 contact pairs in all are available. The angular spacing of the contact points provides a blank position where no point will touch a blade so that a rod can be completely out of action, whilst the one diagonally opposite is being used to make contact to the blades. Damping vanes are provided on each side of member *A* dipping into beakers filled with oil.

APPENDIX II

Dust concentration in sealed boxes. Preliminary tests with a closed biscuit tin showed that, if left undisturbed, the volume concentration fell from an initial value of 1200 particles/cm^3 to 100 in 1½ days and continued thereafter at a slow rate to 50 particles/cm^3 at 2½ days, continuing thence to 25 after 6 days. On shaking the box violently the count rose to 750 and, on subsequent standing, repeated the decline curve in similar manner to the first.

Tests on one of the dryboxes then gave the results of Fig. 7, curve *A*. As the volume is so much greater the rate of decrease is less than above: here a value of 170 particles/cm^3 was reached in 8 days and 40 in 17 days from an initial value of 1200. A second test was then made with a special sticky varnish applied to the three sides and bottom of the box with the results shown in curve *B*. (The lower graph shows the low level conditions in greater detail.) Again starting at 1200 particles/cm^3 the value falls rapidly to 300 in 8 hours, 200 in 1 day and then a slow and fairly steady drop to 100 at the end of 6 days. If the box is subsequently disturbed to some extent the dust count does not rise very high due to the effect of the sticky varnish. The rate of fall of dust concentration is more rapid when the surfaces are coated with sticky varnish. The drybox thus enables a controlled atmosphere, as regards dust concentration, to be obtained down to 100 particles/cm^3 in quite a short time and to 50 particles if ten days are allowed to elapse. Lower values can be obtained by providing a greater area of sticky varnish and by circulating the air inside the box by means of a small fan, so that there is more chance of the whole volume contacting a sticky surface.

The breakdown of liquid dielectrics and its dependence on oxidation of the electrodes

By R. Hancox, Ph.D.,* Queen Mary College, University of London

[*Paper received* 16 *July*, 1957]

The dependence of the impulse breakdown strength of a liquid dielectric on the natural oxide layer on the electrodes used for the test is considered. It is shown that an electric field may exist in the oxide layer owing to the chemisorption of oxygen, and that this would be expected to reduce the probability of electron emission from the cathode and thus increase the recorded breakdown strength. Results are given of experiments on the breakdown of pretreated transformer oil using stainless steel, brass, and aluminium electrodes which support this conclusion.

The impulse breakdown strength of a pure liquid is not an intrinsic property of the liquid but is also dependent upon the electrodes used for the test. In general, electrodes of metals with a high work-function give a high breakdown strength,[1] and this is interpreted as showing that the breakdown is initiated by electron emission from the cathode. Tests with carefully prepared samples of transformer oil often show the same dependence[2] and in these cases it appears that the breakdown mechanism is similar to that which is operative in pure liquids.[3] If the breakdown is initiated by the emission of electrons from the cathode, then the strength should not only depend on the metal of the electrodes but also, with a given metal, upon the factors which influence the surface of the electrodes. It is intended in the present paper to discuss the effect of a thin oxide layer on the emission of electrons from a metal, and to support the conclusions reached by reference to the results of tests on the impulse breakdown of transformer oil.

Llewellyn-Jones has shown that the breakdown voltage of an air gap under pulsed conditions may be reduced when oxidized electrodes are used. In these experiments breakdowns occurred at the rate of fifty per second and it was suggested that positive ions resulting from one discharge influenced the next. Thus, positive ions remaining in the gap from a previous discharge and attracted to the cathode could form a layer of positive charge on an oxide layer which would not be immediately neutralized, causing enhanced emission and lowering the applied voltage required for breakdown.[4] It has been suggested that the same process is applicable to liquid breakdown. In this case, however, since it is not practical to use such a high rate of testing owing to decomposition of the liquid by the discharges, sufficient time would elapse between each breakdown to allow dispersion of positive ions in the gap and neutralization of the positive layer of charge on the electrodes. Under these conditions, therefore, the mechanism of electron emission proposed by Llewellyn-Jones would not be expected to apply, but rather the oxide layer would be expected to reduce the probability of emission for a given applied field.

* Now at Atomic Energy Research Establishment, Harwell, Berks.

Under certain conditions the d.c. breakdown of pure liquids is also found to be electrode-dependent.[5] The argument which is advanced in the following sections is not necessarily valid in these cases, since it has been suggested by Green[6] that positive ions originating from dissociation of impurities in the liquid may be attracted to the cathode, and form there a layer of positive charge which will enhance emission in the same manner as proposed by Llewellyn-Jones. The conditions under which the results predicted in this paper would be expected are, therefore, tests in which the purity of the liquid is such as to necessitate electron emission from the cathode to initiate breakdown, but in which the time between breakdowns is sufficiently long and the time of application of the voltage sufficiently short to prevent the formation of a positive ion layer on the cathode. In practice most tests with filtered and degassed liquids using microsecond duration impulse voltages come within these limits.

THEORY

All metals, with the exception of gold, and all alloys form a natural oxide layer in air at room temperature. This layer grows to a thickness of up to 30 Å in a few hours on a clean surface after which growth is very slow. For any given metal the rate of growth during this initial period is dependent only upon the temperature and, in some cases, the partial pressure of oxygen. The theory of the growth of such a layer originally proposed by Mott[7] is generally accepted as being correct in principle although the details have been strongly criticized.

In order that an oxide layer may grow, either metal ions must diffuse through the layer to the oxide/gas interface and there react with oxygen, or oxygen ions must diffuse to the oxide/metal interface. Owing to the comparatively large size of the oxygen atom the former is the most likely process. This may be accomplished by the movement of interstitial cations in the case of *n*-type semiconducting oxides such as aluminium oxide, or by the movement of cation defects in *p*-type semiconducting oxides such as cuprous oxide.

At room temperature the rate at which the oxide layer may grow is limited by the rate at which metal ions may break away from the metal lattice and pass into the oxide. Normally the probability of this occurring is negligible, but with thin layers such a transfer of ions is aided by a strong electrical field in the oxide owing to the presence of chemisorbed oxygen ions at the oxide/gas interface. According to Mott the necessary electrons for the adsorption of this oxygen originate from the metal and pass through the oxide by thermal emission or quantum-mechanical tunnelling until a quasi-steady state is obtained with equal numbers of electrons passing in both directions. Under these conditions there will be a constant potential difference across the oxide layer, independent of its thickness. As the layer grows the field gradient will fall, reducing the rate at which metal ions may enter the oxide, until the field reaches a critical value at which the oxide practically ceases to grow owing to the very small probability of ions breaking away from the metal lattice. The critical field for aluminium has been calculated by Cabrera and Mott[8] and found to be of the order of 10^7 V/cm.

Serious criticism of Mott's theory has been made by Grimley and Trapnell[9] in connexion with the chemisorption of oxygen at the oxide/gas interface. Mott supposes that there will be reversible adsorption such that the potential across the layer is constant, thus implying that the amount of oxygen chemisorbed decreases as the layer grows. The high values of the heat of adsorption of oxygen on such layers suggests, however, that a complete monolayer of oxygen will be present at all times. Another assumption is that the electrons necessary for the chemisorption of the oxygen originate from the metal. In some cases this may not be entirely correct. Adsorption on cuprous oxide, for example, may result in a change of valency of the surface copper ions, in which case the adsorption would not contribute to the field in the oxide layer. In this particular example there is probably a transition, the proportion of oxygen ions adsorbed by valency changes increasing as the layer grows. If this is correct the field in the oxide layer will still decrease as the layer grows, but not linearly as predicted by Mott. With other metals similar complications may arise, such as the chemisorption without dissociation of oxygen molecules which cannot be built into the oxide. In all these instances, however, it appears that the field in the oxide will diminish as the thickness increases, and that the general picture of oxidation given by Mott still holds although the details may vary considerably.

If the chemisorption of oxygen is prevented by some means, such as the adsorption of an inert monolayer of liquid molecules or by placing the metal in a degassed liquid before the oxide layer has grown to its limiting thickness, metal ions will continue to pass into the oxide and diffuse towards the oxide/gas interface, thus reducing the field in the layer. This process will continue until the field falls to the critical value when ions may no longer pass into the oxide and equilibrium conditions are attained. Under these conditions, therefore, there will always be the same critical field in the oxide, dependent on the metal and the temperature but independent of the thickness. This corresponds to an electrical double layer, the potential difference across which is proportional to the thickness of the layer, the negative charge being furthest from the metal. Such a double layer will reduce the probability of electron emission from the metal, and will have an increasing effect as the thickness of the layer increases. The effect on the thermal emission barrier is illustrated in Fig. 1.

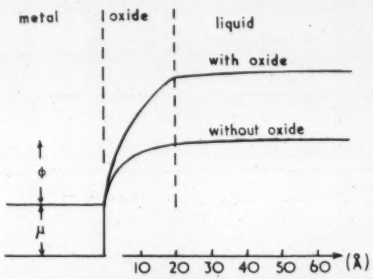

Fig. 1. Electron emission barrier with and without an oxide layer

A secondary effect of the oxide layer will be a reduction of the image force on an electron leaving the metal, due to the dielectric constant of the oxide. The refractive index of an oxide layer of 30 Å thickness on steel was found by Tronstad[10] to be 3·0. The effect of this may not be calculated exactly since the concept of a dielectric constant is not strictly applicable on an atomic scale, but an approximate calculation for

such a layer shows that the image barrier would be reduced by about 0·4 V when emission occurred into a liquid of dielectric constant 2·5. The double layer due to the field in the oxide under these conditions would increase the barrier by about 2·0 V, and is therefore the more important effect.

Emission into a liquid will be influenced by the adsorbed layers at the oxide/liquid interface, which will probably increase the emission barrier. If the adsorbed layer contains polar molecules which are physically adsorbed then the potential of the surface double layer will be dependent on

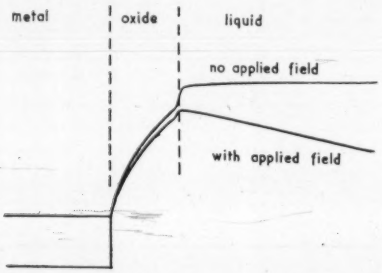

Fig. 2. Electron emission barrier for oxidized metal surface with and without an applied field

the field in the oxide and on the applied field. The complete emission barrier, with and without applied fields, is illustrated in Fig. 2.

EXPERIMENTAL PROCEDURE

The impulse breakdown strength of filtered and degassed transformer oil was measured in a test cell constructed from lengths of Pyrex glass pipe-line. The test cell consisted of two sections, the actual test chamber which was of 9 in. internal diameter and 18 in. high and a high voltage bushing which enabled voltages of up to 600 kV to be used for the tests. The test chamber could be evacuated to a pressure of 0·01 mm of mercury. The electrodes, which consisted of 2·5 cm diameter hemispherically-ended rods, were mounted so that the gap setting could be adjusted and measured by means of an external micrometer. A gap of 2·0 to 2·5 mm was normally employed.

The impulse voltage was derived from a six-stage Marx–Goodlet generator of 0·003 μF output capacitance, a nominal 1/50 μs impulse waveform being used for all the tests. The breakdown voltage was found by applying a series of impulses increasing in steps of 1% of the expected breakdown voltage until breakdown occurred. New electrodes were specially prepared for each breakdown measurement.

The test cell was connected to a circulatory cleaning system in which the oil could be filtered and degassed before each test. This was accomplished by heating the oil and passing it into a vacuum through a sintered glass filter of 10 μ pore diameter. One sample of oil was used for all the tests described, and by keeping it under vacuum between tests and filtering before each test consistent results were obtained.

Electrodes of stainless steel, brass, and aluminium were used for the breakdown measurements, and were polished before use. This could normally have been accomplished by chemical or electro-chemical polishing, but, since in the present work it was required to study the effect of oxidation of the metal surface, it was vital that after polishing there should be no adsorbed layers on the surface. Mechanical polishing was employed, using a buffing mop and cutting composition, after which the electrodes were degreased in hexane and buffed on a clean swansdown mop. Such a technique causes very high local temperatures on the surface and frees it from adsorbed layers without badly affecting the polish. After this treatment the electrodes were examined for scratches or other surface imperfections under a metallurgical microscope and then placed in a desiccator containing a drying agent. After a certain time the electrodes were transferred to the test cell which was evacuated to a pressure of 0·01 mm of mercury. After a further interval the test cell was filled with oil and the breakdown strength measured at atmospheric pressure.

EXPERIMENTAL RESULTS

Stainless steel electrodes were used for the first tests. The breakdown strength of the oil was found to vary with the time for which the electrodes were stored in the desiccator before being placed in the test cell, and this variation is shown in Fig. 3. Any particular point on the curve could be reproduced with a coefficient of variation of 3%. A few tests were carried out without any drying agent in the desiccator in order to see whether this influenced the measured strength, but the same results were obtained. It was also found that the results were independent of the time for which the electrodes were kept in the evacuated test cell before the test when this was varied between 2 and 60 h. Variation of the pressure during this period between 0·01 and 1 mm of mercury did not affect the results.

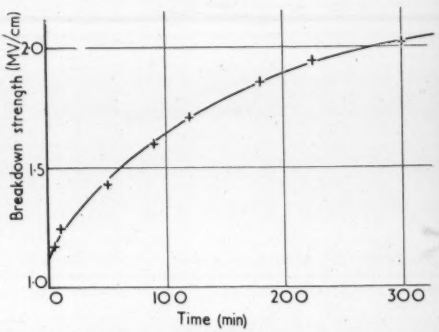

Fig. 3. Variation of the breakdown strength with the time for which the electrodes are stored in the desiccator, using stainless steel electrodes

In a few cases the electrodes were washed in hexane before being placed in the desiccator. When this was done no time-dependent variation in strength was observed, but a strength of 1100 kV/cm was obtained in every case. From Fig. 3 it appears that this point corresponds to the strength which would have been obtained if the electrodes had been placed in the test cell immediately after the final buffing, a condition which could not be realized in practice.

The change in breakdown strength with electrode preparation suggested a very simple means of determining whether the anode or the cathode played the most important part in the breakdown process. In some tests a freshly prepared anode was used with a cathode which had been kept in the desiccator for several hours, or *vice versa*. In every case the result depended only upon the preparation of the cathode.

During some of the tests time lag records were taken, and these showed that breakdown occurred on, or just after, the peak of the voltage waveform, the maximum time lag recorded being 6 μs from the peak of the impulse.

Similar breakdown measurements were made with brass electrodes but all attempts to obtain consistent results failed. For electrodes placed in the test cell within 3 min of their final polishing the strength varied between 1040 and 1230 kV/cm. With electrodes which had been kept in the desiccator for 100 min, strengths between 1250 and 1430 kVcm were obtained.

Aluminium electrodes gave consistent results, shown in Fig. 4. In this case washing the electrodes in hexane after the final buffing did not prevent the time-dependent results from being obtained, but the strength obtained with electrodes which were kept immersed in hexane until placed in the test cell did correspond with the strength which would have been expected from electrodes placed in the test cell immediately after buffing, i.e. 890 kV/cm.

DISCUSSION OF RESULTS

From the results quoted above it is obvious that the cathode underwent some change during the time between polishing and its being placed in the test cell. At the high electrical stresses used in the experiments breakdown is initiated by electron emission from the cathode, and therefore the variation in strength gives evidence of a change in the conditions on the surface of the electrode. Breakdown may be dependent in some cases on the formation of gas bubbles on the surface of the cathode, but previous work has shown that under the conditions of the present tests such bubbles were not present.[11] It therefore appears that some chemical change occurred whilst the electrodes were kept in the desiccator prior to their transfer to the test cell. Furthermore, this change was not associated with the drying agent in the desiccator and did not continue whilst the electrodes were stored in the evacuated test cell.

Of the surface reactions which might occur oxidation is the most probable. In this connexion it is interesting to consider the state of the electrode surface immediately after the final buffing. Normally the metal has a crystalline structure, but polishing results in the formation of an amorphous or micro-crystalline layer which is some 50 Å or more thick. This change in structure has been shown to be due to the fact that the surface of the metal is heated locally to such high temperatures during polishing that it becomes molten.[12] In some cases, e.g. copper, this high surface temperature leads to very rapid oxidation of the metal during the polishing process, with the result that the newly-formed surface contains crystals of oxide and is rapidly covered with a complete oxide layer. In other cases an oxide-free surface is obtained which, owing to the heating of the surface, will be free from surface contamination if a clean mop is used.

After polishing, the clean metal surface will immediately begin to oxidize if left in an atmosphere containing even small quantities of oxygen, and it is suggested that this is, in fact, the cause of the change in strength observed in the experiments. If this is so it should be possible to correlate roughly the variation of the breakdown strength observed with the rate of growth of the oxide. The growth of the oxide layer on stainless steel at room temperature has been studied by Winterbottom[13] and it was found to behave in a manner similar to iron during the first few hours. The thickness of the layer increased to its maximum value over a period of approximately 10 h, which is consistent with the results shown in Fig. 3. In the case of aluminium the rate of growth of the oxide layer becomes negligible after about 15 min exposure of the clean metal surface. This was demonstrated by results quoted by Cabrera and Mott[9] obtained at a pressure of 10^{-2} to 10^{-4} mm of mercury, and since the oxidation of aluminium is independent of pressure the results should be the same at atmospheric pressure. A similar result was obtained by Gulbranson and Wysong[14] with undegassed aluminium at a pressure of 76 mm of mercury, and it may be seen that this corresponds closely to the variation of breakdown strength with time shown in Fig. 4. The

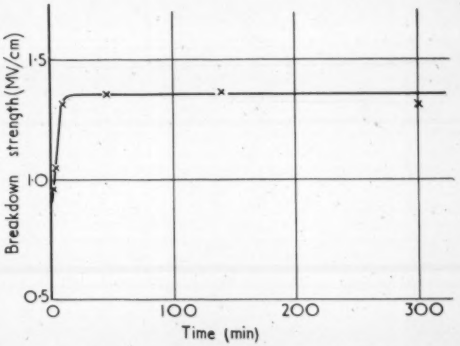

Fig. 4. Variation of the breakdown strength with the time for which the electrodes are stored in the desiccator, using aluminium electrodes

study of the oxidation of brass is complicated by the fact that the rate of oxidation of copper, one of its constituents, is very temperature-dependent. Thus when brass surfaces are mechanically polished an oxide layer of varying thickness may be observed immediately after polishing,[15] and it is probably because of this that a very large scatter was found in the experiments with brass electrodes.

If a stable adsorbed layer, other than one of oxygen or oxide, is formed on the surface of the metal then oxidation will cease. It is considered that this in fact occurred when the electrodes were placed in the test cell owing to adsorption of various components of the oil.

In view of the results quoted above it appears reasonable to suggest that the impulse breakdown strength of the oil tested was, in fact, influenced by the growth of an oxide layer on the freshly prepared electrodes, and it is therefore natural to seek evidence for the effect of such a layer on electron emission from previous work. Although no useful results are available for emission into liquids, several workers have investigated emission into gases at room temperature. Fiand and Lange[16] have measured the variation in work

function of many metal surfaces after they had been abraded in vacuum. A very rapid decrease, due to chemisorption of the first monolayer of oxygen, was followed by a slower increase which may be attributed to the formation of an oxide layer.

Recently, a number of workers have studied the emission of electrons from abraded metal surfaces by means of Geiger counters, and have shown that electrons are emitted from such surfaces even when no electrical field is applied. This effect was first fully reported by Kramer[17] who showed that the rate of emission decreased and died away in a few hours. Later work has connected this decrease with the formation of an oxide layer on the metal,[18] and Grunberg and Wright[19] suggest that the electrons originate from crystal faults in the oxide. In view of this anomalous emission from freshly prepared metal surfaces, it might be supposed that the results of the present investigation on the breakdown of liquids could be attributed to the same cause. The work on abraded surfaces, however, was performed with negligible applied fields and the first application of a high voltage impulse would almost certainly remove all the available electrons and fatigue the surface. Any further electrons would then be emitted by the metal through the oxide as previously suggested.

CONCLUSION

The dependence of the impulse breakdown strength of liquid dielectrics on the natural oxide layer on the electrodes used for the measurement has been considered. It has been shown that such an oxide layer would be expected to result in the formation of an electrical double layer, which would hinder electron emission from the cathode and hence increase the recorded breakdown strength. Experimental results have been reported which support this conclusion. When stainless steel or aluminium electrodes were used variations in the breakdown strength with the time for which the electrodes were allowed to oxidize were obtained which were consistent with published curves for the growth of the oxide layer. When brass electrodes were used scattered results were obtained, which was probably due to the method of preparation of the electrodes.

ACKNOWLEDGEMENTS

The author wishes to thank Prof. John, lately Dean of the Faculty of Engineering at Queen Mary College, for the use of the facilities of the Dept. of Electrical Engineering, and Dr. H. Tropper, Senior Lecturer in the Dept. of Electrical Engineering, for his supervision of the work reported here and for his continual encouragement. The author also wishes to acknowledge the receipt of a maintenance grant from the Department of Scientific and Industrial Research which enabled the work to be undertaken.

REFERENCES

(1) Goodwin, D. W., and Macfadyen, K. A. *Proc. Phys. Soc.* [*London*] *B*, **66**, p. 85 (1953).

(2) Watson, P. K., and Higham, J. B. *Proc. Instn Elect. Engrs*, II(A), **100**, p. 168 (1953).

(3) Crowe, R. W., Bragg, J. K., and Sharaugh, A. H. *J. Appl. Phys.*, **25**, p. 392 (1954).

(4) Llewellyn Jones, F., and Morgan, C. G. *Proc. Roy. Soc. A*, **218**, p. 88 (1953).

(5) Salvage, B. *Proc. Instn Elect. Engrs*, IV, **98**, p. 15 (1951)

(6) Green, W. B. *J. Appl. Phys.*, **26**, p. 1257 (1955).

(7) Mott, N. F. *Trans Faraday Soc.*, **43**, p. 429 (1947).

(8) Cabrera, N., and Mott, N. F. *Rep. Progr. Phys.*, **12**, p. 163 (1949).

(9) Grimley, T. B., and Trapnell, B. M. *Proc. Roy. Soc. A*, **234**, p. 405 (1956).

(10) Tronstad, L. *Nature* [*London*], **127**, p. 127 (1931).

(11) Hancox, R., and Tropper, H. *Proc. Instn Elect. Engrs.* To be published.

(12) Bowden, F. P., and Hughes, T. P. *Nature* [*London*], **139**, p. 152 (1937).

(13) Winterbottom, A. B. *J. Iron Steel Inst.*, **165**, p. 9 (1950).

(14) Gulbransen, A. E., and Wysong, W. S. *J. Phys. Chem.*, **51**, p. 1087 (1947).

(15) Preston, G. D., and Bircumshaw, L. L. *Phil. Mag.*, **20**, p. 706 (1935).

(16) Fiand, F., and Lange, E. *Z. Elektrochem.*, **55**, p. 237 (1951).

(17) Kramer, J. *Der Metallische Zustand* (Göttingen: Vandenhoeck u. Ruprecht, 1950).

(18) Rubinek, F., and Seidl, R. *Czech. J. Phys.*, **2**, p. 84 (1953).

(19) Grunberg, L., and Wright, K. H. R. *Proc. Roy. Soc. A*, **232**, p. 403 (1955).

Spectral response and linearity of photomultipliers

By H. EDELS, B.Sc.Tech., Ph.D., A.M.I.E.E., and W. A. GAMBLING, B.Sc.(Eng.), Ph.D., A.M.I.E.E.,*
Department of Electrical Engineering, The University of Liverpool

[*Paper first received* 7 *June, and in final form* 2 *August*, 1957]

The spatial variations of the spectral response of type RCA931A photomultiplier tubes have been measured by two different methods. The results, in agreement with earlier work, show that the spatial form of the response varies widely with wavelength. It is shown that for experiments utilizing only a restricted portion of the cathode surface errors up to 10% may be made in relative intensity measurements if the calibration and experimental sources do not illuminate the same portion of the cathode area. Other experiments show that the multiplier output varies linearly with input intensity for output currents up to at least 10 μA, if the electrical circuit is suitably designed.

It is well known that the response of photomultiplier cathodes varies widely with the frequency of the incident radiation. Thus for the determination of relative intensities, the multiplier must be calibrated for each of the wavelengths under observation. This can be achieved easily by using, for example, a calibrating source, a spectroscope and a step filter. If the response is linear at each wavelength, then the relative intensities at λ_1 and λ_2 for the source under observation is given by

$$\frac{I_{\lambda 1}}{I_{\lambda 2}} = \frac{R_{\lambda 1}}{R_{\lambda 2}} \cdot \frac{S_{\lambda 2}}{S_{\lambda 1}} \qquad (1)$$

where $R_{\lambda 1}$ and $R_{\lambda 2}$ are the responses and $S_{\lambda 1}$ and $S_{\lambda 2}$ are the slopes of the response curves. This formulation assumes that the same response curves are obtained for both the calibration and experimental sources. However it has been shown[1, 2] that the surface is markedly non-uniform in spectral response. Thus, if the sources illuminate different cathode areas, the simple formulation above will hold only if the spatial variation of the response has the same form for different wavelengths and if the linearity condition holds at all points on the surface. Thus assuming linearity is maintained, if calibration is made at a point A, and the experimental source illuminates a point B, then

$$\frac{I_{\lambda 1}}{I_{\lambda 2}} = \left(\frac{R_{\lambda 1}}{R_{\lambda 2}}\right)_B \cdot \left(\frac{S_{\lambda 2}}{S_{\lambda 1}}\right)_A \qquad (2)$$

if the same percentage change occurs in the responses of both λ_1 and λ_2 when moving from A to B.

In order to determine whether equation (2) held, we investigated the spatial-spectral response of type RCA931A multipliers (by the Radio Corporation of America) and our results, given in an earlier paper,[3] indicated that the equation was not valid. Thus we concluded that for experiments in which only a portion of the cathode surface is illuminated, accurate relative intensity measurements can be achieved only if the calibration and experimental sources are closely aligned, so as to illuminate the same cathode area. If maximum sensitivity is not required, the effects of the variations in spatial form of spectral response can be overcome by uniformly illuminating the whole of the cathode surface. However, Keohane and Metcalf[4] have criticized our method and, using a similar type of tube (type I.P. 21), obtain results which are in agreement with equation (2). It is most desirable that the situation be clarified, since serious errors can result if it is wrongly assumed that the spatial variations are of the same form at different wavelengths. We have therefore repeated our earlier measurements and confirmed them by a different and more accurate method. We found, in fact, that not only are our first measurements correct, but that the effect is more marked than was at first thought.

SPATIAL VARIATION OF SPECTRAL RESPONSE

Repeating our earlier experiments, the spatial variations in response were determined using a standard tungsten filament lamp maintained at a temperature of 2848° K by a high-stability 12 V accumulator. In view of the criticisms of Keohane and Metcalf, the experimental details, which were not given previously, are described here. The voltage across the lamp was maintained constant to $\pm 0{\cdot}25\%$ during each series of tests. The filament, of cross-section 5 mm × 1 mm, was mounted, with the long dimension vertical, at a distance of 150 cm from the photomultiplier. A vertical slit, 0·1 mm wide, was placed 5 cm in front of the multiplier cathode, so that the incident beam on the cathode was only fractionally greater than the slit width. The radiation of the standard lamp was filtered to produce wavelength bands of 4300 ± 200 Å, 5300 ± 150 Å and 6800 ± 200 Å. By lateral movement of the slit, the spatial variation of the response to these bands was obtained. We found that the results were closely similar to those given earlier.[3] Keohane and Metcalf[4] suggest that it is difficult to produce a uniform patch of light in front of the multiplier and that hence our method is not permissible. However, considering the dimensions of our light source and the spacing between lamp and slit it is extremely unlikely that any appreciable variation in intensity exists over the 10 mm moved by the slit. This view is confirmed since we obtain similar results by the following second method, in which the slit is kept stationary and the multiplier moved.

In our second method an ultra-violet monochromator (by Hilger and Watts Ltd.) was used to produce the restricted wavelength bands. The standard filament lamp was mounted vertically 150 cm from the entrance slit and the output beam from the spectroscope was used to excite the photomultiplier cathode. In order to obtain the spatial variation the multiplier was mounted on a travelling microscope carriage so that the tube could be accurately moved in steps of $\frac{1}{4}$ mm. Since the beam from the spectroscope is widely divergent, an auxiliary slit was placed between the spectroscope slit and the multiplier, and in this way the beam width on the multiplier cathode was restricted in all our experiments to 1 mm. By adjustment of the spectroscope, the following wavebands were obtained: 6500 ± 50 Å, 6000 ± 50 Å, 5500 ± 50 Å, 5000 ± 25 Å, 4500 ± 25 Å. The variations in the response across the cathode surface to these bands were determined

* Now at the University of British Columbia, Vancouver, Canada.

and are given in Fig. 1. These results are similar to those we obtained earlier and show the marked change in the form of the response with wavelength. In particular it will be seen that the position of the response peak moves gradually across the cathode surface as the wavelength is changed, so that the slope of the spatial curves changes sign. The anomalous edge peaks which were noted earlier are again observed. The results show that these peaks gradually attenuate with decrease in wavelength. The central portion of the response curves have been normalized about the 6 mm position and are shown in Fig. 2. These curves show very clearly the differences in spatial response forms at different wavelengths. If the cathode is calibrated at the 6 mm position the error in assuming the validity of equation (2) is simply equal to the ratio of the responses at any other position. Thus, for example, an increment of ± 1 mm gives errors of $+10\%$ and -9% in the intensity ratio of 6500/4500 Å. These are in marked contrast to the errors of $\simeq 0{\cdot}3\%$ given by Keohane and Metcalf, and emphasize the importance, if a restricted cathode area is to be used, of correctly determining the spatial response curves or ensuring that the same cathode area is illuminated by both the calibration and experimental sources.

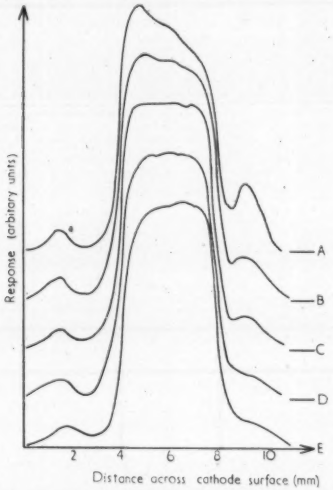

Fig. 1. Variation in response across cathode surface to following wavebands

A, 6500 ± 50 Å; *B*, 6000 ± 50 Å; *C*, 5500 ± 50 Å; *D*, 5000 ± 25 Å; *E*, 4500 ± 25 Å.

Arbitary zeros indicated by horizontal lines.

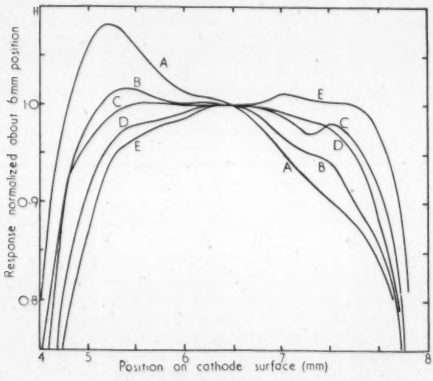

Fig. 2. Response curves of Fig. 1 normalized about 6 mm position

A, 6500 ± 50 Å; *B*, 6000 ± 50 Å; *C*, 5500 ± 50 Å; *D*, 5000 ± 25 Å; *E*, 4500 ± 25 Å.

MULTIPLIER LINEARITY

As indicated by equation (1), intensity measurements are simplified if the multiplier output varies linearly with the input intensity. The existence of such a linearity has been questioned by Kortum and Maier[5] who estimate that a 10% deviation from linearity may exist for commercial multipliers. Using a step filter and spectroscope we have therefore determined the input-output characteristics of the type RCA931A multipliers at different surface positions at current outputs from 0 to 10 μA and at wavelengths from 4000 to 6500 Å. We found in all cases that, within our measurement accuracy, no measurable deviation from linearity occurred. This is in accordance with the previous investigations of Engstrom[6] and of Keohane and Metcalf.[4] However, non-linearity can easily be produced at high current outputs due to the formation of a space charge sufficient to modify the current flow. Thus if too high a resistance is placed in the collector circuit, the space charge between dynode 9 and the collector can produce this result. With a low resistor in the output circuit non-linearity first occurs due to the space charge between dynodes 8 and 9. Non-linearity is also commonly caused by poor voltage regulation on the potentiometer chain supplying the dynodes. In our arrangement a chain current of 20 mA was used so that no appreciable voltage changes occur for collector currents up to 10 μA. It is also important to ensure that the dynodes are supplied from a high stability source, for the rate of change of multiplier gain with stage voltage is $\simeq 7\%$ per volt per stage at the optimum stage voltage of 100 V. Hence in order to keep the gain constant to better than 1% the supply voltage must not vary by more than $\pm 0{\cdot}1\%$. In our case the dynode voltages were obtained from a 1000 V battery-stabilized power pack which gave an output voltage constant to $\pm 0{\cdot}01\%$.

REFERENCES

(1) Morton, G. A., and Mitchell, J. A. *R.C.A. Rev.*, **9**, p. 363 (1948).

(2) Smyth, M. J. *Monthly Not. Roy. Astron. Soc.*, **112**, p. 88 (1952).

(3) Edels, H., and Gambling, W. A. *J. Sci. Instrum.*, **31**, p. 121 (1954).

(4) Keohane, K. W., and Metcalf, W. K. *J. Sci. Instrum.*, **32**, p. 259 (1955).

(5) Kortum, G., and Maier, H. *Z. Naturforsch.*, **8a**, p. 235 (1953).

(6) Engstrom, R. W. *J. Opt. Soc. Amer.*, **37**, p. 420 (1947).

Summarized proceedings of the eleventh annual conference of the Stress Analysis Group—Leicester, April 1957

By A. F. C. Brown

See pages 467–470

[Reproduced from *Philosophical Magazine*]

Fig. 1. Trace left by movement of dislocation in aluminium crystal showing occurrence of cross-slip (×45 000)

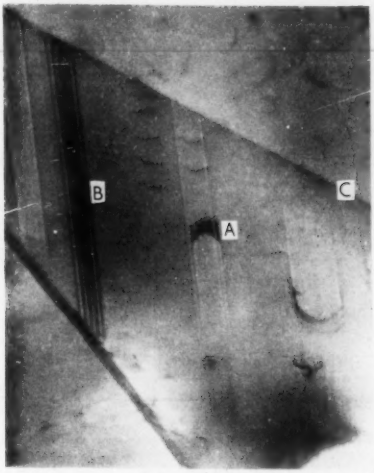

[Reproduced from *Proceedings of the Royal Society of London*]

Fig. 2. Traces of partial dislocations in stainless steel (×20 000)

Fig. 3. Deformation in alpha phase of alpha-beta brass (×500)

Fig. 4. Slip bands in pure aluminium after fatigue loading (×1500)

***

Fig. 5. Extrusion from slip bands of aluminium 4% copper alloy after fatigue loading (×1500)

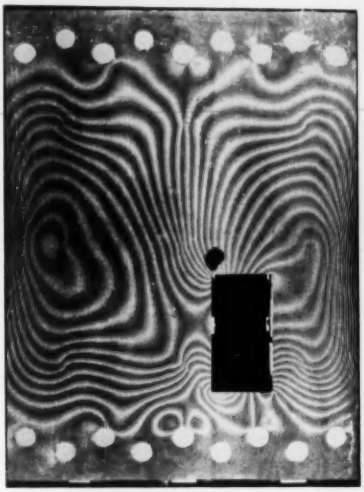

Fig. 7. *Moiré* fringes for plate clamped at its edges with rectangular hole, under uniform loading

CORRESPONDENCE

Some carbon replica techniques for the electron microscopy of small specimens and fibres

From B. J. Spit

See page 493

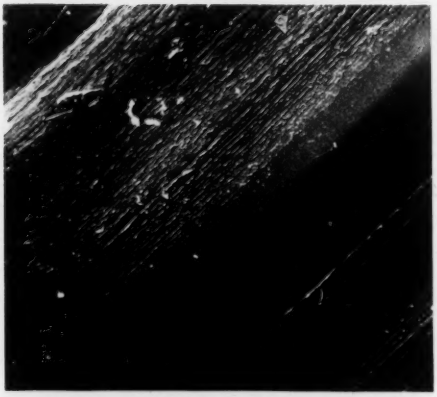

Fig. 1. Replica of a cord rayon fibre using the Dlugosz method, ×16000

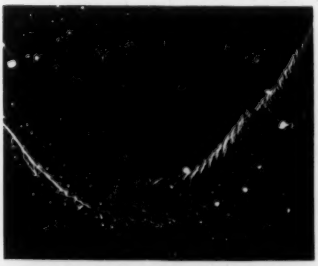

Fig. 2. Replica of the spiral body of a bull spermatozoid. Dlugosz method, ×12000

Fig. 3. Replica of a diatom surface with pores of about 500 Å. Dlugosz method, × 20000

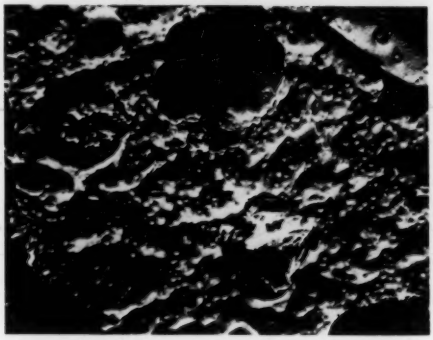

Fig. 4. Replica of a pollen grain *althea rosea nigra*. Dlugosz method, × 5000

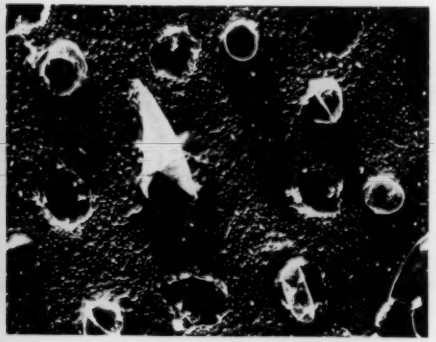

Fig. 5. Replica of an acetolysed pollen grain of *althea rosea nigra*. Dlugosz method, × 5000

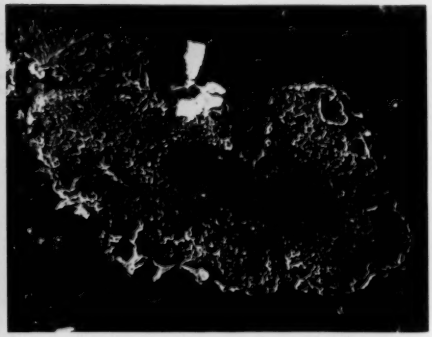

Fig. 7. Preshadowed carbon replica of a "milky" rayon fibre section. Section was joined with albumin on glass, × 2500

Fig. 6. Preshadowed carbon replica of an asparagus section, treated with ethanol amine, × 40000

See pages 488–9

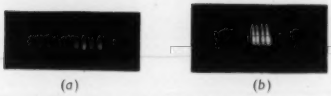

Fig. 2. Preference records without significant repetitions obtained with exposures of 15 × 30s, *f*/5·6

Fig. 4. Comparison of preference records for successive photographs I(*a*) and I(*b*)

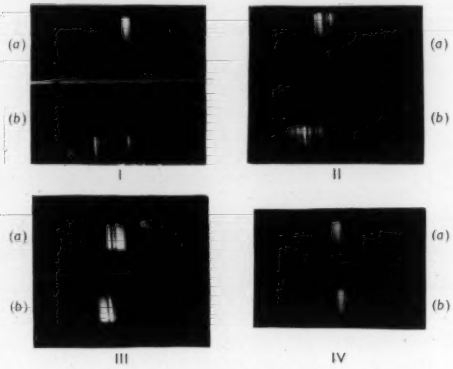

Fig. 3. Preference records with significant repetitions I(*a*, *b*), 15 × 30 s, *f*/5·6; II(*a*, *b*), 30 × 20 s, *f*/5·6; III(*a*, *b*), 30 × 120 s, *f*/5·6; IV(*a*, *b*), 20 × 30 s, *f*/5·6.

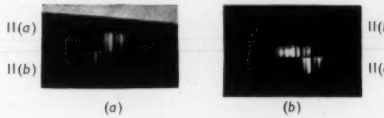

Fig. 5. Comparison of preference records for successive photographs II(*a*) and II(*b*)

Fig. 6. Comparison of preference records for successive photographs III(*a*) and III(*b*)

Fig. 7. Comparison of preference records for successive photographs IV(*a*) and IV(*b*)

Valve instability with cathode standing waves of cylindrical symmetry

By W. W. H. CLARKE, Ph.D., A.M.I.E.E., A.Inst.P.,* Defence Research Board, Ottawa, Ontario, Canada

[*Paper first received* 12 *February, and in final form* 1 *April*, 1957]

Experiments demonstrating the existence of preferred emission levels in thermionic valves, due to standing waves in the virtual cathode plasma, have been extended to the case of a very small circular cathode. This case is distinctive in that standing waves in the radial direction only are expected, so that a simpler pattern of preferences may be obtained, with greater spacing of preferred currents due to the small size of the cathode. Because this cathode is much smaller than those previously investigated, the change in wavelength from one supposedly boundary-satisfying standing wave pattern to the next is substantially greater. This and the (probable) absence of changes in an orthogonal standing wave structure allow significance to be attached to repeatability of the emission current preference pattern. Significant repeatability is demonstrated by experimental results, providing an important confirmation of the existence of preferred (boundary satisfying) standing wave patterns and associated preferred emission current characteristics.

The existence of cathode standing waves was first reported by Klemperer,[1] for rectangular cathodes supporting waves of Cartesian symmetry, and subsequently by Clarke and Jacob[2, 3] for small circular cathodes supporting standing waves of cylindrical symmetry. In a recent paper,[4] experiments were described which showed that preferred emission levels occur in thermionic valves, in accordance with predictions based on standing wave patterns. Preferences for particular values of cathode current, under static conditions of applied potentials, were demonstrated in the form of time anomalies in the current variation. However, description of the current as a function of applied potential and the wavelengths of two orthogonal standing wave patterns, did not allow significance to be attached to the repeatability of the complicated preference patterns.

Comparable experiments have now been carried out with a small circular cathode, assumed to support circular standing waves.[2, 3] The preference pattern is presumed to be simpler since only one wavelength is concerned, and the smaller cathode size provides that the change of wavelength, between

* Now at Cossor (Canada) Ltd., Halifax, Nova Scotia, Canada.

successive patterns satisfying the boundary conditions, is greater. Hence the spacing of the preference pattern should be wider as a fraction of the current.

The results show significant repeatability of some of the preference lines, and simpler preference patterns, which have been obtained with a modified experimental procedure.

THE STANDING WAVE MECHANISM

It is proposed here to review the mechanism of generation of standing waves and their significance as a factor in valve instability. In an explanation which is consistent with the experiments of Klemperer,[1] and Clarke and Jacob,[2, 3] neglecting end effects, q or $q + \frac{1}{2}$ wavelengths, where q is an integer, are required to occupy the length between the boundaries of the cathode space; the waves are propagated by the Coulomb interaction[5] and the wavelength lies between that given by the Debye length (λ_D), and that given by the velocity of light and the plasma frequency (ω_p). The Debye length is a measure of the range of the Coulomb interaction:

$$\lambda_D^2 = \left(\frac{KT}{4\pi ne^2}\right) = \tfrac{1}{3}\left\{[(v_i^2)_{Av}]/\omega_p^2\right\} \qquad (1)$$

with the notation of Bohm and Pines.[5] The plasma frequency (ω_p) is given in the same notation, by:

$$\omega_p = (4\pi ne^2/m)^{\frac{1}{2}} \qquad (2)$$

At high space charge densities, such as are encountered near the cathode in practical valves, the wavelength approaches the Debye length, though it must be realized that when the pattern becomes intense, and the electrons are precipitated[6] at nodes, the foregoing statistical concepts do not provide an accurate physical model.

It has been assumed[4] that the standing wave pattern is an organized distribution of charge, through which the current removed from the cathode is filtered; changes of the statistics of the cathode emission are supposed to undergo a feedback effect similar to space charge limitation, until the change in electron feed to the standing wave is sufficiently large for another pattern to be preferred. When a new pattern is formed, a new value of the emission current occurs. More generally for the rectangular cathode symmetry previously considered:

$$i(n, m, V_A) = \phi(n, m)V_A^{3/2} = \text{a.b. } P(n/b)Q(m/a) \,.\, V_A^{3/2} \qquad (3)$$

where P and Q are polynomials, a, b are the cathode dimensions, V_A is the anode potential, and n, m are the (whole) numbers of wavelengths across and along the cathode.

The range of possible values of the product of the polynomials formed an interleaved pattern of characteristics, for example,

$$\begin{array}{lllll}
\ldots I(n-2, m-2), & I(n-2, m-1), & I(n-2, m), & I(n-2, m+1), & I(n-2, m+2) \ldots \\
\ldots I(n-1, m-2), & I(n-1, m-1), & I(n-1, m), & I(n-1, m+1), & I(n-1, m+2 \ldots \\
\ldots I(n, m-2), & I(n, m-1), & I(n, m), & I(n, m+1), & I(n, m+2) \ldots \\
\ldots I(n+1, m-2), & I(n+1, m-1), & I(n+1, m), & I(n+1, m+1), & I(n+1, m+2) \ldots \\
\ldots I(n+2, m-2), & I(n+2, m-1), & I(m+2, m), & I(n+2, m+1), & I(n+2, m+2) \ldots
\end{array}$$

For such multiple possibilities, no significance could be attached to repeatability of a "preference line" at any one current. For the cathode of circular symmetry, however, simpler conditions apply:

$$i = i(n, V_A) = r \,.\, P(n/r)V_A^{3/2} \qquad (4)$$

where r is the radius of the cathode, or more generally the radius of the space charge containing cylinder, and n becomes the number of wavelengths in this radius. Hence repeatability of preference lines becomes significant and expected.

The evidence for the occurrence of standing waves of circular symmetry,[3] showed conclusively that pattern changes could be detected by a set of collecting electrodes without analysing "pinholes" as used by Klemperer.[1] This may be explained by the mutual repulsion of the low energy dense beam used, which prevented intermingling of the various "sheaths" of the beam. This work indicated that there is only one established standing wave at a time, and that Klemperer's alternative suggestion[1] of all the possible waves being simultaneously excited at different distances from the cathode was not tenable. The recent work of Dolder and Klemperer[6] has now established this by direct experiment, and made an important contribution to the understanding of the plasma behaviour and boundary conditions.

It has been suggested that a saddle-back field is necessary to produce a region wherein transverse plasma oscillations may be contained, and it is indeed likely that any system with a single aperture modulator (rather than a wire mesh grid) would satisfy this requirement. The electrons emitted from the periphery of the cathode could not be subject (except for positive modulator potentials) to as great an accelerating field as those nearer the centre of the cathode; hence a higher charge density will build up around the cathode, providing suitable conditions for reflecting electrons which approach transversely.

From a qualitative point of view, where a cathode is very small so that only one or two wavelengths of the plasma oscillation extend right across the cathode, lack of containing (saddle-back) field would remove electrons contributing to the wave and thus damp it out. However, if a substantial number of wavelengths occur across the cathode, the loss of electrons at the periphery may not prevent a standing wave from occurring. For maintenance of a standing wave it is necessary only that the waves suffer reflexions at the cathode boundaries. This condition may be satisfied both in the presence of an applied positive or negative radial (or transverse in the general case) potential gradient, because the change in plasma statistics at the cathode boundary implies a change in the medium supporting the wave, from which wave reflexions must occur. The two cases (positive and negative potential gradient) may be likened to "short-circuited" and "open-circuited" transmission lines. Whether the applied potentials impose an overall saddle-back field or not, the initiation of a standing wave introduces bunching of charge

in particular regions, which must be associated with a multiple self-generating saddle-back field. The waves will, in general, occupy a space where the potential can become so depressed that electrons may fall to very low energies.

Patches of different work function, which vary in size and location, still remain the basic instigators of flicker noise and instability, but the values of current which may be drawn become subject to a striated preference pattern, corresponding with the different boundary-satisfying patterns. The plasma above a patch has different propagation characteristics and the space charge wave therefore suffers reflexion at its boundaries which will, in general, be favourable to some patterns and destructive to others. Thus a pattern is expected to be instantaneously compatible with the total effect of the patches, and to be forced to change (by steps) in conformity with the changes in total patch effect.

EXPERIMENTAL PROCEDURE

Results have been obtained by using a galvanometer to indicate the variations of valve current. An integration of the time spent by the galvanometer spot in different parts of the scale has been produced photographically. The galvanometer spot was reduced to a slit as before,[4] and a Polaroid camera utilized, mounted on a light-tight box containing the galvanometer and an uncalibrated paper "scale." A backing-off circuit was used for the galvanometer as shown in Fig. 1. The grid modulator potential was derived from a decade potentiometer, and all supplies were derived from batteries.

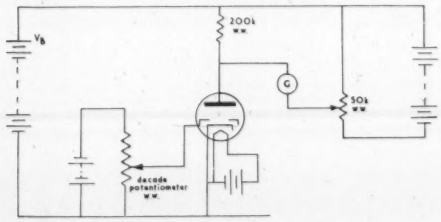

Fig. 1. Backing-off circuit used for the galvanometer

Checks on the stability of the system, apart from the valve instability, were carried out. These were similar to those described in an earlier paper[4] and they are not treated in detail here.

There is no simple means, with photographic integration of time spent at a given spot, for discriminating between bright lines built up by one long exposure and those built up by numerous occurrences of that galvanometer current. The method first adopted[4] of recording a galvanometer reading visually every few seconds could, however, discriminate, and an interval of eight seconds between readings was chosen so that the build-up of "preferred levels" should not be too greatly influenced by continued steady readings occurring for a number of (eight second) intervals. The circular cathode here examined showed a somewhat greater tendency to come to rest for significant intervals of time. For this reason a modified experimental procedure was devised to encourage the plasma in the virtual cathode to change pattern.

The decade potentiometer was employed as a convenient means of stepping the grid bias precisely. With the galvanometer spot near its mid-scale position, the bias could be switched to make the spot swing just off-scale (to the left or right), and then return exactly to its original position, when the galvanometer settled fairly quickly to a steady indication. It was checked in a potentiometer circuit, without any valve, that the galvanometer returned to its exact original position after such a step and return (to and from left or right). This checked against any deleterious mechanical factors, and also against the possible occurrence of different values of contact potential in the modulator bias circuit. Use was then made of this procedure in obtaining valve current preference data. The integrating camera shutter was opened with the galvanometer spot at a fairly stable position, and an exposure of, for example, thirty seconds taken. Then, with the shutter closed, a voltage step to the "left" was applied for some five seconds and returned to the "zero" position; after approximately twenty-five seconds a second exposure was taken again of thirty seconds, followed by a voltage step to the right, and then another exposure, and so forth. Notation employed defined a photographic integration record by the number of exposures, the time of each exposure and the f number (in every case nearly thirty seconds was allowed for recovery, an adequate time according to the check that was made). Thus (30×30 s, $f/5{\cdot}6$) meant that thirty exposures were taken, each of thirty seconds, using an aperture of $f/5{\cdot}6$.

Attention was given to the repeatability of the preference pattern, and a simple method of alining the patterns obtained in successive photographs was adopted. Analysis of the photographic records was facilitated by the use of a microphotometer.

EXPERIMENTAL RESULTS

Results are presented for one valve with a moderate standing cathode current. These are believed to be representative of what may be obtained with other valves both with the same ($V_B = 135$ V, $I = 55\ \mu$A), and with different standing currents, though only three valves were studied. The previous results[4] with a rectangular cathode are taken to justify this limitation.

The results are given both as photographic records and as intensity plots from the microphotometer analysis. In using the microphotometer (the record of which is not by any means a linear measure of "time on the spot") it was found helpful to plot the intensity pattern at several levels on the records; thus very intense lines might be resolved at the expense of losing weak ones. Hence, more than one intensity plot is presented for some photographic records.

Fig. 2 (p. 486) shows two records obtained with exposures of 15×30 seconds, $f/5{\cdot}6$. They are not concerned with repeatability, but demonstrate the clarity of the record obtainable. Fig. 2*a*, has fourteen separate lines, the spacing of which is significant; the lines are apparently spaced by either one or two units of the same magnitude which is indicative of a regular pattern. The inequality of line intensity denies the assumption that each line corresponds with a separate camera exposure. There was rigorous control of the timing which would have secured equal intensities if the lines had individually corresponded with the exposures. Fig. 2(*b*) shows two weak lines and four strong lines which are well defined and equispaced.

Repeatability of preferred levels is demonstrated by four pairs of successive photographic records, shown in Fig. 3 (p. 486), and denoted by I(*a*), and (*b*); II(*a*), and (*b*), etc. Splitting the records horizontally and setting the lower half of an (*a*) record against the upper half of the corresponding (*b*) record demonstrates the character of the repetitions occurring.

The alinement procedure used involved accurate registration of the edge of the exposed film, assuming the camera and galvanometer remain fixed in moving the film up to the next exposure. Figs. 4, 5, 6 and 7 (p. 486) are devoted to such paired comparisons, which reveal some of the repetitions clearly, but do not do full justice to them all owing to the wide range of exposures compared. A better idea of the significance of these results is obtained from the paired intensity plots shown in Figs. 8, 9, 10 and 11.

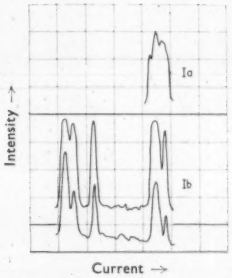

Fig. 8. Comparison by microphotometer analysis of successive preference records I(*a*) and I(*b*)

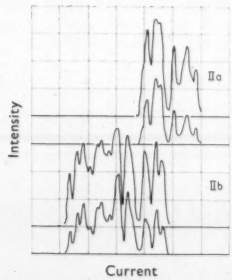

Fig. 9. Comparison by microphotometer analysis of successive preference records II(*a*) and II(*b*)

All the records presented are to the same scale, and the sensitivity is most easily defined by the record II(*b*) in Fig. 3—this record is approximately 10^{-7} A (valve current) in total extent.

DISCUSSION

In experiments designed to reveal certain essential characteristics of phenomena which are otherwise random, it is desirable that conclusions shall be based upon sufficient evidence to make spurious support of the supposed characteristics extremely unlikely. The present data relates to four pairs of consecutive exposures selected from some thirty pairs, of which about twenty were inadequately exposed for use. Since the number of pattern lines which will be occupied during a given exposure is a quantity with widely varying statistics, the intensities of individual lines are arbitrary; interest has been focused on fairly stable conditions, so that a number of under-exposed records have had to be rejected. Of ten exposure-pairs, eight exhibited overlapped records and the four selected were those with overlap and coincidence of lines. The four rejected pairs did not, however, contain overlap regions with fine structure of a contradictory nature, they merely contained, for example, two bunches of lines with a large gap for one record, and, for the other, one bunch of lines corresponding with the large gap. Thus the four record pairs represent all cases obtained with bunches of lines in the same region, and exhibit coincidence of: two

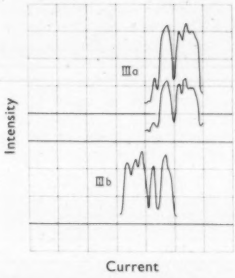

Fig. 10. Comparison by microphotometer analysis of successive preference records III(*a*) and III(*b*)

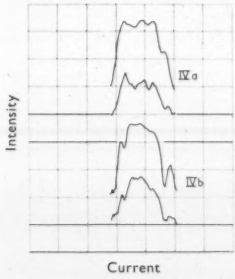

Fig. 11. Comparison by microphotometer analysis of successive preference records IV(*a*) and IV(*b*)

maxima and three minima, three maxima and four minima, two maxima and three minima, and finally entire coincidence of two records, with regard to their limits, but with a fine structure which does not coincide in all its detail.

A great deal of experimental work would be required to obtain data of a more extensive order than that presented here—greater numbers of overlapping consecutive records, records at various values of applied potentials, and a study of a large number of similar valves. But at any level of quantity, the interpretation difficulty would remain. The formal accuracy of computing cross correlation coefficients between two curves is not justified because of the non-linearities of the photographic records and of the subsequent microphotometer analysis; hence the importance of a qualitative evaluation of the results. Since the basic supposition is that the cathode plasma prefers to support a standing wave satisfying boundary conditions, and contains no suggestions of any distribution of preference on a time basis between

the preferred states, it seems likely that the magnitude, in any record, of the time ordinate at one preferred state has indefinite significance. This is not to suggest that cathode temperature is ineffective; temperature naturally controls the plasma statistics and therefore indirectly the preferred wavelength of standing wave pattern. Thus a widely varying temperature would undermine the basis of experiments; but the substantially constant temperature in use should only have changed the plasma enough to encourage small pattern changes. However, since any given pattern line probably has a natural width definable by a probability distribution, the apparent width photographically should increase in proportion to the time ordinate (exposure of the line). This could account for small displacements of the minima between preferred states.

The foregoing argument supports a case for examining results qualitatively on a "yes or no" basis and for attaching no significance to non-overlap regions. In Figs. 8, 9, 10, there are seven maxima and ten minima which coincide and there are no maxima apparently coincident with significant minima; thus on the "yes or no" basis, seventeen "yes" conditions occurred and the probability that these coincidences occurred fortuitously becomes $(\frac{1}{2})^{17} = 1/131\,072$. If it is desired to admit only maxima then the probability of fortuitous coincidence is 1/128.

The present work demonstrates the occurrence of a repetitive preference pattern in the current characteristic of a valve with a circular cathode. The preferences are supposed to be associated with transverse standing waves in the plasma, which satisfy the cathode boundary conditions, there being only one degree of freedom in the circular cathode case. The repeatable patterns found for this case are of great significance in establishing the validity of the standing wave interpretation.

ACKNOWLEDGEMENTS

The author wishes to thank Dr. L. Jacob for helpful criticism of his previous paper[4] and of the interpretation and presentation of the present material. He also wishes to thank Mr. E. A. Walker for helpful discussions and suggestions regarding the experimental procedure. He is indebted to the Defence Research Board of Canada for their permission to publish this paper.

REFERENCES

(1) KLEMPERER, O. *Proc. Roy. Soc. A*, **190**, p. 376 (1947).
(2) CLARKE, W. W. H., and JACOB, L. *Nature [London]*, **168**, p. 1120 (1951).
(3) CLARKE, W. W. H., and JACOB, L. *Proc. Phys. Soc. [London] B*, **68**, p. 805 (1955).
(4) CLARKE, W. W. H. *Brit. J. Appl. Phys.*, **6**, p. 433 (1955).
(5) BOHM, D., and PINES, D. *Phys. Rev.*, **82**, p. 625 (1951); **85**, p. 338 (1952); **92**, p. 609 (1953).
(6) DOLDER, K. T., and KLEMPERER, O. *J. Electronics*, **1**, p. 601 (1956).

Spectral sensitivity of neon discharge tubes

By T. J. DILLON, M.Sc., F.Inst.P., Queen Elizabeth College (University of London), Campden Hill Road, London

[*Paper first received* 16 *May, and in final form* 27 *June*, 1957]

The relative photoresponse of certain types of neon discharge tubes to irradiation at different wavelengths has been investigated by spectrophotometric methods. The experimental results, using a large number of discharge tubes, are expressed graphically as relative photoresponse for equal energy of incident radiation plotted against wavelength. The curves show that the discharge tubes act like photoemissive cells with caesium alloy cathodes. It is suggested that the photosensitivity is due to the positive Joshi effect as well as to the presence of ceasium on the tube electrodes.

INTRODUCTION

An investigation into the photosensitive properties of certain types of neon discharge tubes in relaxation oscillation circuits and a comparison of the effects of irradiation upon them with those of photoemissive cells led to a study of their spectral sensitivity. When it was originally found that these tubes exhibited marked photoelectric properties, presumably due both to the layer of caesium on the electrodes and to the positive Joshi effect, investigations were carried out to see if they could be put to practical use for photoelectric purposes. It was established that they are suitable for comparative measurements of high illuminations, and they have the advantage of small size, low striking voltage and low cost. Previous papers[1,2] have outlined their performance under both static and dynamic conditions.

In the case of neon discharge tubes which are being operated under oscillating conditions at audio-frequencies, the discharge is in the region of negative characteristic, and a decrease in striking voltage produced by irradiation is accompanied by an increase of frequency and corresponding increase of current through the tube. The photoelectric response can therefore be measured in terms of any of these quantities. The change of current was selected as being the most suitable variable for these spectral investigations mainly because the photosensitivity of the discharge tubes is small and a higher degree of accuracy could be attained by means of a sensitive galvanometer than by the measurement of frequency changes or by photographic recording of voltage variations.

A usual method of measuring the spectral sensitivity curve of any light sensitive device such as a photoelectric cell is to find the photocurrent at each wavelength when the same energy is incident on the cell through the spectrum. Using a source of known spectral energy distribution and with a means of isolating comparatively narrow bands, the corresponding photocurrent is plotted against the mean wavelength.

The first approximate investigations on these neon discharge tubes were made using a set of filters of known spectral transmission. This was followed by a spectrophotometer arrangement using a movable slit of adjustable width together with a source of known spectral energy distribution. Finally a prism spectrophometer, designed by W. Harrison[3] with eight slits on a disk, was modified and calibrated by U. Andrewes as a 15 slit instrument, each slit covering approximately 20 mμ throughout the visible spectrum.

APPARATUS AND METHODS OF MEASUREMENT

The tubes were of the L 7A and L 10 type of neon indicators of Siemens-Ediswan Ltd., and also V.I. 132 of British Thomson-Houston Co. Ltd. The base metal of the electrodes is iron on which is painted a layer of a mixture of caesium azides and barium in an aqueous solution. During exhaust the azides are heated in a vacuum and reduced to metallic barium and caesium with the evolution of nitrogen. The weight of activation on the electrodes is of the order of 1×10^{-4} g of which 10% is caesium. The tubes are filled with neon at a pressure of about 10 mm of mercury. The tubes can therefore be considered as gas-filled photocells of an alloy-surface type, with caesium as one of the components of the alloy, as originally suggested by Goerlich[4] and a certain degree of sensitivity through the visible spectrum would be expected.

The electrodes of the neon discharge tube are concentric with a central disk anode mounted above an annular cathode of radius about 0·5 cm. As the photoelectric effect depends on the area of cathode exposed to irradiation it was necessary, for comparative spectral measurements, to keep the exposed area constant. The circuit components were chosen so that when the frequency of oscillations in the discharge tube circuit was of the order of 400 c/s, the mean current through the tubes was about 25 μA.

It has been shown previously[5] that the average photosensitivity to "white light" for tubes of this type under these conditions is of the order of 20 μA/lm. The low illumination levels of under 10 lm/ft² produced current changes of only from 0·1 to 1%, so that in order to measure the correspondingly small photoelectric effects a galvanometer of sensitivity 110 cm/μA was used and the current through it was balanced by a subsidiary circuit.

EXPERIMENTAL DETAILS AND RESULTS

(*a*) *Spectrum filters.* For the preliminary experiments using filters, the discharge tubes were placed in a blackened box directly behind a slotted window into which the filters could be fitted and the irradiating source was a 500 W tungsten filament lamp assumed to be operating at a colour temperature of 2850° K. This was placed at a distance of about 1 ft from the window. A set of Ilford spectrum filters Nos 601–608 were used and the current changes in the discharge tube were measured as the electrodes were irradiated by light transmitted through each filter in turn. The total transmission values of the filters for the light source as observed by the photopic eye were calculated and hence the relative energies in each of the eight wave bands were determined. The curve given in Fig. 1(*a*) represents an average of sets of readings for nine selected tubes. The relative response is plotted against the maximum value of the wavelength in each waveband as given in the spectral transmission data for the filters.

(*b*) *A six-slit spectrophotometer.* A six-slit spectrophotometer arrangement was set up using a curved slit and the 500 W lamp as source. A spectrum of 3×2 cm² was formed, and a slit mechanism of razor blades mounted on a vernier scale was arranged to move across the spectrum plane. The spectrum was calibrated using helium and mercury cadmium discharge lamps. A neon discharge tube was then placed

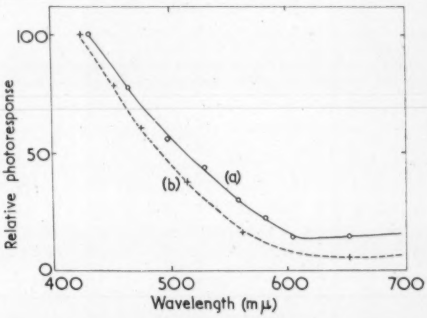

Fig. 1. Average spectral response curves for neon discharge tubes using (*a*) spectrum filters, and (*b*) a six slit spectrophotometer

with electrodes opposite the slit so that the light in the selected waveband fell normally on the cathode. The change of current in the tube circuit was recorded as the slit and tube were moved through distances of 5 mm through the spectrum.

From the calibration curve and the energy distribution curve of the source the relative spectral sensitivities in the slit regions were determined. The table gives typical sets of results for selected tubes showing that they vary considerably in sensitivity, which would be expected as they are produced commercially and vary in shape and in the thickness of the caesium layer on the electrodes. Fig. 1(*b*) gives the average of sets of results of four tubes by this method and are in fair agreement with those obtained by the filter method.

Slit position	*λ-range (mμ)*	*Relative current change per unit energy of irradiation*				
1	414–434	100	100	100	100	100
2	434–460	80	85	92	79	87
3	460–490	57	51	70	56	54
4	490–534	45	29	43	39	33
5	534–600	11·6	14·5	20	22	12
6	600–700	1·9	4	4	6	1·3

(*c*) *Spectral band photometer with rotatable disk.* A more accurate investigation was carried out using a spectral band photometer with a rotatable disk in the image plane for bringing the slits in turn into different positions throughout the spectrum and to allow the light to fall on a photovoltaic cell placed behind the slit. The instrument was modified by U. Andrewes into a 15 slit spectrophotometer. The slits with razor blade edges were mounted on the disk and were of suitable width to allow for approximately a 20 mμ waveband in each part of the spectrum. The instrument was calibrated as before using the spectral lines of discharge lamps and the

values of the relative energy for each slit were calculated from the spectral response curve of a photovaltaic cell which had been calibrated by the National Physical Laboratory.

The neon discharge tubes were mounted on a stand that could be moved into a central position in front of a slit to receive the light through each slit in turn. To avoid the complications due to the different widths of the slits, a cylindrical lens focused an image of each slit in turn on to the

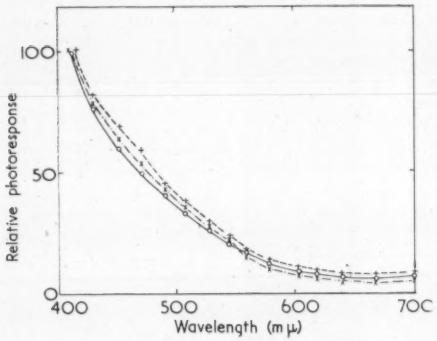

Fig. 2. Spectral response curves for three neon discharge tubes using a 15 slit spectrophotometer

cathode. A 1000 W lamp of the same type was substituted for the 500 W lamp, and care was taken to avoid the effects of stray light. The final spectral response curves for three selected tubes are given in Fig. 2.

CONCLUSION

The general shape of the spectral response curves of these discharge tubes suggest that they behave like photoemissive cells probably of the commercial type with caesium-antimony or caesium-magnesium alloy cathodes, which have decreasing sensitivity from the blue to the red.

It would appear that in the discharge tubes with a neon filling the positive Joshi effect (or the influence of light on the mechanism of a gaseous discharge), is present, and this has also been observed in tubes which have no caesium coating. In addition, the caesium coating on the electrodes considerably increases the photoelectric effect.

Work on neon discharge tubes by Om Prakash[6] had shown that the lowering of striking voltage on irradiation was greater for blue than for yellow light, and Arnikar[7] showed that the voltage variation depended on the frequency of the light. Mohanty[8] used coloured glass filters in similar investigations on the Joshi effect in gases other than neon, and, more recently,[9] he published further work on the frequency dependence of the effect.

As the general photosensitive properties of these commercial tubes had been established it seemed to be of interest to investigate their spectral sensitive properties by the methods outlined, and the results obtained are in general agreement with those that would be expected from their electrode configuration, treatment of surface and gas filling.

ACKNOWLEDGEMENTS

The author expresses thanks to her colleague, Dr. U. Andrewes, for the construction and careful calibration of the 15 slit disk and for helpful discussions, and to members of the research staff of Siemens-Ediswan Ltd. for kindly supplying neon discharge tubes and relevant information.

REFERENCES

(1) Dillon, T. J. *Brit. J. Appl. Phys.*, **4**, p. 245 (1953).
(2) Dillon, T. J. *Brit. J. Appl. Phys.*, **6**, p. 138 (1955).
(3) Harrison, W. *Siemens Eng. Bull.*, **231**, p. 1 (1947).
(4) Goerlich, P. *J. Opt. Soc. Amer.*, **31**, p. 504 (1941).
(5) Dillon, T. J. *Proc. Phys. Soc.* [*London*] *B*, **65**, p. 236 (1952).
(6) Om Prakash. *Curr. Sci.*, **18**, p. 370 (1955).
(7) Arnikar, H. J. *Curr. Sci.*, **19**, p. 47 (1950).
(8) Mohanty, S. R., and Kamath, *J. Ind. Chem. Soc.*, **25**, pp. 10, 467 (1948).
(9) Mohanty, S. R. *Z. Phys.*, **140**, p. 370 (1955).

Correspondence

Some carbon replica techniques for the electron microscopy of small specimens and fibres

Bradley discussed in his article, published on p. 150 of the April issue of this *Journal*, three methods for the preparation of replicas. It seems justified to make some remarks on each of his techniques.

For some years we have been studying replica techniques suited for fibres. We have also started with softening Perspex by heat and softening celluloid by methyl ethyl ketone to make impressions of fibres. Both methods yielded unsatisfactory imprints of the fibre surface. The replica technique for fibres described by Bradley has no advantage over the technique used by Dlugosz[1] which we have been using since early 1956.

The embedding is greatly facilitated by the fact that the wet gelatin plate suitably adjusts the height of protrusion. Replication by evaporating a thick silver layer on the embedded fibres (Fig. 1, p. 484) gives more detail than an impression in a softened material, as we concluded from our first experiments. Bradley's Fig. 1 does not illustrate the claimed fibrils of 100–200 Å. Another advantage of the Dlugosz technique is the possibility of making more replicas from the same embedding plate. Last, but not least, shadowing the embedded fibres with aluminium and covering them with the embedding material and a cover glass gives a beautiful specimen for optical microscopy.

The second technique given by Bradley is for small specimens. Bradley states in his discussion "The technique for small specimens is particularly important since such objects are continually being encountered and, hitherto, there has not been any effective way of studying them. Though the method is complicated, it is unlikely that any simple technique could be devised for such objects."

In this connexion we want to point out that we also applied the replica technique of Dlugosz to small biological specimens. Diatoms, bull spermatozoids and pollen grains were easily replicated by this technique, as shown in Figs. 2–5 (pp. 484–5). In the case of Fig. 5 the pollen grains were acetolysed and small pieces of the exine were placed on the gelatin plate. The great advantage of the Dlugosz method is that the specimen itself need not be dissolved so that, even though the polymerization of the resin takes some fifteen hours, the total time does not exceed that taken by Bradley. Only routine operations are required.

Although specimens may exist which can be replicated better by the method described by Bradley, these are not illustrated in the given pictures and we believe that there is little ground for the remark "it is unlikely that any simple technique could be devised for such objects."

Bradley's third method for biological specimens is clearly a modification and, in some ways, an improvement of the method described by König,[2] Dalitz,[3] and Mühletahler.[4] We usually use 400 Å carbon replicas, which we consider easily thin enough for resolution better than 50 Å. Making 150 Å replicas only increases preparation difficulties as backing layers will not withstand reagents such as chromic acid. In making replicas of asparagus sections,[5] by preshadowing and evaporating a carbon layer about 400 Å thick, it is possible to strip the film together with the section and to dissolve the latter in chromic acid. The dimensions of the sections were $2 \times 0{\cdot}2$ mm and of $2\,\mu$ thickness. Fibrils 100–200 Å in size can be seen in Fig. 6 (p. 485).

The same technique was applied to a fibre section. These sections were studied by Hermans[6] several years ago. Fig. 7 (p. 485) gives a result.

I am grateful to Dr. P. H. Hermans of the Institute for Cellulose Research of the A.K.U. for providing the sections of the fibre.

Technisch Physische Dienst T.N.O. en T.H., Delft, Netherlands. B. J. SPIT
[1 June, 1957]

REFERENCES

(1) DLUGOSZ, J. *Proc. Electron Microscopy Conf.*, p. 283 (Stockholm: Almqvist and Wiksell, 1956).
(2) KÖNIG, H., and HELWIG, G. *Z. Phys.*, **129**, p. 491 (1951).
(3) DALITZ, V. CH. *Z. Wiss. Mikr.*, **61**, p. 292 (1953).
(4) MÜHLETAHLER, K. *Planta*, **46**, p. 1 (1955).
(5) STERLING, C., and SPIT, B. J. *Am. J. Botany*. To be published.
(6) HERMANS, P. H. *Text. Res. J.*, **20**, p. 105 (1950).

An electron microscopist who needs to use replicas will decide on techniques to suit his own particular problems, as has been the case in this Laboratory. It was felt that the methods we have used might be of value to other workers, and they were therefore published. The paper concerned was not intended to replace the work of Dlugosz.

Associated Electrical Industries Ltd., Aldermaston, Berks. D. E. BRADLEY
[18 July, 1957]

The application of the centripetal effect in air to the design of a pump

In a letter published on p. 452 of the December, 1956, issue of this *Journal* we described an instrument by which the centripetal effect in air can be demonstrated. It is regretted that the figure which accompanied this letter did not represent the instrument as actually built. We thought that the design could be improved, and incorporated this intended improvement in the drawing. However, when changing the instrument in accordance with this supposed improvement, it turned out to make the instrument less workable. When we demonstrated the pump at the Brussels Congress of Applied Mechanics in September 1956 it was as originally built, and it therefore worked well. Sir Geoffrey Taylor in his paper, *Effects of compressibility at low Reynolds numbers*, presented at the Annual Meeting of the Institute of the Aeronautical Sciences held in New York in January 1957, showed a drawing of an apparatus "after Reiner" which did not include the feature described below. His apparatus evidently also worked well. However, we know that a number of workers in different parts of the world, some of whom saw the pump at Brussels, are trying to repeat the experiment, and a letter has been received from one of them (from Holland) complaining that he "tried to reproduce (the)

experiment with negative results, notwithstanding the fact that the apparatus was constructed with the utmost care." Therefore we beg permission to explain this essential feature.

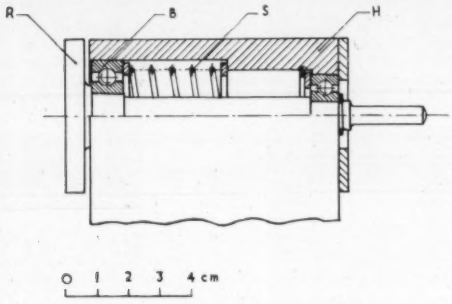

Fig. 1. Rotor as in original instrument

The problem was to enable the rotor to rotate with the smallest amplitude of longitudinal vibrations when the rotor-stator gap is extremely small and the speed is high.

A $\frac{1}{15}$ h.p. motor was mounted on the frame of the pump. The isolation of the motor vibration was achieved by means of a felt and leather packing between the motor and the pump mounting, and the vibrations were reduced by attaching a 4 kg mass to the rotor.

A spring *S* between housing *H* and the ball race *B* near the rotor *R* was provided in order to diminish the play of both ball bearings (see Fig. 1). The "centripetal effect" develops a pressure in the gap between rotor and stator, and therefore an axial thrust. Whenever an excessive pressure is developed in the gap or when the stator inadvertently comes into contact with the rotor the spring yields to the thrust. It therefore serves as a safety device to prevent any damage. However, it was desired to know exactly the size of the gap and to measure it by means of a micrometer screw. This was not possible when the spring was in the position shown in Fig. 1. Therefore the spring *S* was re-positioned at the other end of the rotor shaft housing, as shown in the figure of our original communication.

At the same time a larger motor, $\frac{1}{2}$ h.p., was mounted on the frame, the small rotor used in the earlier experiments having proved to be inadequate as it stalled prior to a constant pressure at the centre being achieved.

After these modifications were completed, there were repeated failures of the coupling between the rotor shaft and the motor, whenever the gap was set to less than 5 μ, which had not occurred with the first arrangement.

It was assumed that this was due to the stator and rotor coming into contact, because their surfaces were not exactly parallel. A self-aligning rotor was therefore constructed as shown in Fig. 2. It was assumed that the air pressure developed in the gap would bring about parallelism. However, this device did not work, and again failure of the coupling occurred. It seems that this failure is due to an unstable gyroscopic effect. Accordingly, the two alterations described require further thinking out and trials before they can work as desired.

The theory of the centripetal pump effect in air is contained in a paper by one of us, which appeared after the publication of our original letter.*

Israel Institute of Technology, Haifa, Israel.

B. POPPER
M. REINER

[29 July, 1957]

* REINER, M. *Proc. Roy. Soc. A*, **240**, pp. 173–189 (1957).

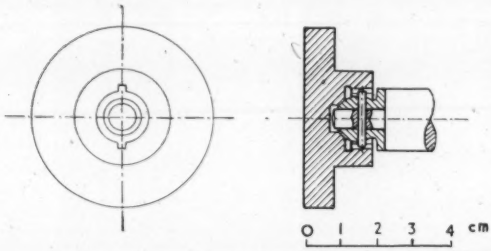

Fig. 2. Self-aligning rotor

The flow of gas at very low pressure

In the recent paper by Mr. C. W. Oatley[1] on "The flow of gas through composite systems at very low pressures" it is stated that the conventional method of calculating gas flow through composite systems is based on an untenable assumption and leads to incorrect results.

I believe this is misleading because in this laboratory and presumably in many others a slightly different though equally conventional approach is usually used which avoids the incorrect result referred to and in fact leads to the same formulae deduced by Mr. Oatley. The purpose of this note is to correct the view that calculations to date on the conductance of composite vacuum systems have generally been greatly in error.

P. Clausing in his various papers has solved the problem of flow through tubes of finite lengths and in Mr. Oatley's paper it is shown how the Clausing correction should be applied to obtain correct results for composite systems. This is carried out from the Clausing point of view in which the probability of molecules entering a tube and passing through without returning plays the fundamental role. This concept is a very sound one and there is a lot to be said for it when deducing some of the fundamental relations. It is, however, implicit in the Clausing derivation that the probability of molecules entering a tube end *from free space* (large vessel) is considered, and any attempt to allot a Clausing "con-

ductance" to a tube having its mouth connected to the tail of another tube obviously involves inherent inaccuracies. The common alternative procedure generally adopted by technicians working out conductance of practical pumping systems is as follows. The conductance of a tube connecting two large vessels is split up into an entrance-aperture conductance and a tube conductance and this procedure completely overcomes the apparent difficulties so that the correct application of these concepts leads to the identical results obtained from a different point of view by Mr. Oatley.

For a detailed discussion of the method of entrance-aperture see, for example, the chapter by R. Loevinger,[2] but the same idea already occurs in early papers by M. Knudsen and S. Dushman. This method may be used to illustrate its application to some of the examples in Mr. Oatley's paper as follows.

A tube connects two large vessels filled with gas at very low pressure then the effective conductance F_{eff} may be split up into an aperture and tube conductance.

$$\frac{1}{F_{eff}} = \frac{1}{F_{ap}} + \frac{1}{F_{tube}} \tag{1}$$

The usual argument is that the gas must find the aperture before it can flow through the tube.

If there is an aperture of area A within a tube of area A_0 one easily shows that the conductance of the aperture is modified to:

$$F_A \cdot \frac{A_0}{A_0 - A} \tag{2}$$

where F_A is the equivalent conductance of such an aperture in a very large vessel. These two concepts serve to calculate the conductance for any of the usual composite tube systems.

In the case of two tubes of equal cross-sectional area joined end to end as in Fig. 1 of Oatley's paper, we have in effect only to consider the single aperture at the entrance. This is also seen from (2) where we have in this case $F = \infty$ for the aperture at the junction of the two tubes. Hence for this case of two tubes of conductances F_{T_1} and F_{T_2}, we have:

$$\frac{1}{F} = \frac{1}{F_{ap}} + \frac{1}{F_{T_1}} + \frac{1}{F_{T_2}} \tag{3}$$

If one takes this in terms of the Clausing coefficients one must remember that the Clausing method takes the tube and aperture together, i.e. in the combination $1/\alpha_1 + 1/\alpha_2$ the aperture conductance has been taken twice and according to (3) the value of $1/\alpha$ for one aperture must be subtracted and so the result:

$$\frac{1}{\alpha} = \frac{1}{\alpha_1} + \frac{1}{\alpha_2} - 1$$

is also obtained. Again, in the other example of two tubes of the same radius separated by a large reservoir we must now consider two apertures, so that $1/\alpha_1 + 1/\alpha_2$ is in order. One could of course avoid the confusion by splitting up the Clausing factor α into an entrance-aperture 1 and tube conductance factor α_T:

$$\frac{1}{\alpha} = \frac{1}{\alpha_T} + 1; \text{ or } \alpha_T = \frac{\alpha}{1 - \alpha} \tag{4}$$

For large values of L/r, for cylindrical tubes, $\alpha_T \to 8/3\ r/L$ as in the Knudsen formula and in many practical cases it is sufficiently accurate to take one of the well-known approximations to the Clausing factor.

The use of the entrance-aperture and tube conductance factors α_T can be further illustrated by the example of a vapour trap discussed in Oatley's paper (Fig. 4). It is assumed that the trap is connected between two large vessels and then the entrance-aperture of the first baffle has a conductance factor $\alpha = \frac{1}{2}$ ($\alpha = 1$ for the full tube diameter). For the next half length of tube the modified Clausing tube conductance factor is α_T. The next baffle is situated in a tube so that the conductance factor is modified as in equation (2) above and the equivalent α is therefore $\frac{1}{2} \cdot 1/(1 - \frac{1}{2}) = 1$. The same holds for the next half section of tube and the 3rd baffle. Altogether the total equivalent conductance factor is therefore given by:

$$\frac{1}{\alpha} = \frac{1}{\frac{1}{2}} + \frac{1}{\alpha_T} + 1 + \frac{1}{\alpha_T} + 1 = 4 + \frac{2}{\alpha_T} \tag{5}$$

To show that (5) is equivalent to equation (13) in Oatley's paper it is only necessary to substitute $1/\alpha_1 - 1$ for $1/\alpha_T$ from (4) above.

Edwards High Vacuum Ltd.,
Crawley, Sussex.

W. STECKELMACHER
[25 February, 1957]

REFERENCES

(1) OATLEY, C. W. *Brit. J. Appl. Phys.*, **8**, p. 15 (1957).
(2) GUTHRIE and WAKERLING. *Vacuum Equipment and Techniques*, p. 21 (New York: McGraw-Hill Book Co. Inc., 1949).

I was very interested in Mr. Steckelmacher's defence of the method of calculating the flow of gas in composite vacuum systems by splitting the conductance of a tube into an aperture conductance and a tube conductance. This procedure was used as early as 1920 by Dushman[1] to obtain an approximate value for the conductance of a cylindrical tube of finite length, but I think Mr. Steckelmacher may be overstating his case when he says that the unlimited extension of the method which he advocates is "generally adopted by technicians." Of three fairly recent and authoritative textbooks on vacuum technique which I have consulted, that edited by Guthrie and Wakerling[2] derives Mr. Steckelmacher's equation (2) for a single aperture in a tube, but does not consider any extension of the method to more complicated systems, Dushman[3] quotes the same equation, but ". . . has been unable to find details of the derivation," and does not take the matter further, while Reimann[4] suggests that it will usually be sufficiently accurate to neglect end corrections when considering composite systems. I believe I am right in saying that neither of these books derives equation (14) of my paper, for the effective speed of a vacuum pump plus connecting tube.

Turning to the "aperture method" itself, I hesitate to make dogmatic statements about its applicability because I have no experience in trying to use it, but it is not immediately obvious to me how the method would be used to deal with the problem illustrated in Fig. 2(*a*) of my paper, where gas is flowing from a tube of small diameter into a tube of larger diameter. However, my real objection to the method is that I believe it to lack any sound theoretical justification. Mr. Steckelmacher's equation (1)

$$\frac{1}{F_{eff}} = \frac{1}{F_{ap}} + \frac{1}{F_{tube}}$$

is usually justified by an appeal to the analogy with electric circuits. In an attempt to establish this analogy, Loevinger,[2]

referring to a closed circuit in a vacuum system, says "The pressure will change as we go around the circuit but is continuous and single-valued, and hence it plays the same role as potential in the electrical case." A little thought will show, however, that the pressure is *not* single-valued. If it were measured at any point of a system, through which a molecular flow of gas was taking place, by means of a manometer with directional properties (e.g. an ionization gauge enclosed in a tube with a small hole in one side), the reading obtained would depend on the direction in which the gauge was pointing. Surely Kirchhoff's laws would not be valid if the reading obtained with a voltmeter depended on the direction in which the connecting wires approached the circuit under investigation!

The "aperture method" may, in some cases, give the correct result, but I believe this to be somewhat fortuitous. Until a more logical proof of its validity can be given, I think it must be regarded with suspicion.

Department of Engineering,
University of Cambridge.

C. W. OATLEY
[19 March, 1957]

REFERENCES

(1) DUSHMAN, S. *Gen. Elect. Rev.*, **23**, p. 493 (1920).
(2) GUTHRIE and WAKERLING. *Vacuum Equipment and Techniques* (New York: McGraw-Hill Book Co. Inc., 1949).
(3) DUSHMAN, S. *Scientific Foundations of Vacuum Technique*, (New York: John Wiley & Sons Inc., 1949).
(4) REIMANN, A. L. *Vacuum Technique* (London: Chapman and Hall Ltd., 1952).

New books

American Institute of Physics handbook. Edited by DWIGHT E. GRAY. (New York: McGraw-Hill Book Co.; London: McGraw-Hill Publishing Co. Ltd., 1957.) Pp. 1200. Price 112*s*. 6*d*.

This handbook, devoted specifically to physics and sponsored by the American Institute of Physics, is the first in this field to be compiled in America and is notable for the comprehensive range and detail of information included between its covers. With Dr. Gray, National Science Foundation, as co-ordinating editor and the eight editors responsible for the main sections into which the handbook is divided for logical presentation of the data, there is an impressive list of 105 specialist contributors. The sections and the editors are: mathematical aids to computation (Dr. Albert A. Bennett); mechanics (Dr. R. Bruce Lindsay); acoustics (Dr. Floyd A. Firestone); heat (Dr. Mark W. Zemansky); electricity and magnetism (Dr. D. F. Bleil); optics (Dr. Bruce H. Billings); atomic and molecular physics (Dr. G. H. Dieke); and nuclear physics (Dr. F. N. D. Kurie).

Apart from the short section of five pages on mathematical aids to computation, mainly devoted to listing the standard mathematical handbooks of tables available from international sources, the general organization of material in the sections is typified by the following list of contents for acoustics (179 pages): acoustical definitions; letter symbols and conversion factors for acoustical quantities; propagation of sound in fluids; acoustic properties of gases, liquids and solids; properties of transducer materials; frequencies of simple vibrators; musical scales; radiation of sound; architectural acoustics; speech and hearing; classical electro-dyanmical analogies; the mobility and classical impedance analogies; and selected references on acoustics. As examples of the tremendous scope of the new handbook the following topics in other sections may be mentioned: geophysical data, including subsections on geodesy, seismology, oceanography and meteorology; rheological data; cavitation in flowing liquids; laminar and turbulent flow of gases; shock waves in fluids; properties of paramagnetic salts, with data relating to very low temperatures; high pressure effects on solids and liquids; electric and magnetic properties of the Earth and stars; radiation detection, thermal and quantum; spectroscopic data; radio-astronomy; general atomic constants (as evaluated at Johns Hopkins University in 1954); nuclear reaction cross-sections; fission-product chains and yields; health physics; particle accelerators (with a table of the locations and principal characteristics of operational machines throughout the world); and a catalogue of available information on nuclear reactors.

The sources of information are legion, but among those frequently quoted are the International Critical Tables (1926), the Smithsonian Physical Tables (9th revised edition, 1954) and Circulars and other data published by the National Bureau of Standards. An important key to such a storehouse of knowledge is the index, which in this case runs to 48 pages and appears, on a few spot tests, to fulfil its function reasonably well. The text, tabulated data, diagrams, graphs and charts are well presented and the type, though small, is clear. It is difficult for any single reviewer to criticize comprehensively and to suggest improvements for future editions. The ice point on the thermodynamic temperature scale is given as 273·16° K (instead of 273·15° K) and no mention is made of the new definition of the second (ephemeris time) based on the tropical year 1900·0, but both changes are the result of international decisions made in 1954 or later.

This handbook constitutes an invaluable reference work and is strongly recommended to the attention of all physicists, both pure and applied, as well as engineers.

H. BARRELL

An introduction to junction transistor theory. By R. D. MIDDLEBROOK. (New York: John Wiley and Sons Inc.; London: Chapman and Hall Ltd., 1957.) Pp. xxiv + 296. Price 68*s*.

The principal aim of the volume is to characterize the properties of junction transistors in terms of equivalent circuits and then to relate the equivalent components to the geometrical and physical parameters of the transistor unit. It pre-supposes no specialized knowledge on the part of the reader and, indeed, about one-third of the book is devoted to introductory chapters on semiconductor theory. While providing a useful background for the understanding of later

chapters, this part could not, in its present form, stand on its own as an adequate general introduction to the subject. In contrast, the chapters dealing specifically with the structure of equivalent circuits seem much superior. The distinctions between the performance of grown and fused junctions are well analysed and explained, as are high frequency effects and the complications which arise from the varying thickness of the collector barrier. It is perhaps surprising that treatments based on one-dimensional models can achieve a great measure of practical success, even when the base regions of the transistors are very thin. As always, the equivalent circuits which represent the transistor behaviour most accurately are highly complex. In the last part the author discusses simplifying transformations which render them more suitable for use by the circuit engineer. H. K. HENISCH

Anleitung zum praktischen Gebrauch der Laplace-transformation. By GUSTAV DOETSCH. (Munich: R. Oldenbourg Verlag, 1956.) Pp. 198. Price DM. 22.00.

With this volume the author has added to his several monumental monographs and textbooks on Laplace transforms a practical guide for experimental physicists and engineers. The theory is briefly given, the emphasis being on applications and not on mathematical rigour. The eight chapters deal respectively with the definition of the Laplace transforms, rules for their use, their application to ordinary differential equations, to difference equations, to partial differential equations, to integral equations, the determination of a function whose transform is known, and asymptotic behaviour and stability. The volume contains extensive tables.

As Laplace transforms are extensively used, and are fast becoming a standard method for the solution of many problems, the appearance of this volume is most welcome.

D. TER HAAR

Théorie et technique de la radiocristallographie. By A. GUINIER. (Paris: Dunod, 1956.) Pp. xviii + 736 + XVI. Price 9500 fr.

This book is, in origin, a second edition of *Radiocristallographie*, which appeared in 1945, and was written without much knowledge of non-French work later than 1940. An English translation, with some revision, was issued in 1952 (reviewed in the *British Journal of Applied Physics*, **4**, p. 62).

The new book is about twice the size of the old, and the great development of the subject since 1945 has made it necessary to rewrite all but a few paragraphs. The scope is limited in the same fashion; the determination of crystal structures is barely mentioned (nine pages out of over 700), but apparatus, techniques, and the theory of scattering are treated in considerable detail. "We have had in view the needs of other users of X-rays in the laboratories, not only [laboratories] of crystallography, but of physics of solids, of chemistry, of metallography, etc. . . . One is working, then, with crystals whose structure is known or deliberately left undetermined. The problems presenting themselves are, for example, phase identification, quantitative analysis of a solid, mode of crystallization, imperfections of structure, etc. . . ." The chief technical advance recorded is the application of counter methods. The chief theoretical advance is in the interpretation of diffraction by imperfect crystals. The latter has led to the abandonment of the elementary mathematical level of the first edition; much use is made of Fourier transforms, and an appendix (25 pages) is devoted to them.

The book is divided into five parts: General properties of X-rays, Elements of crystallography and diffraction theory, Experimental methods, Applications, Diffraction by imperfect crystals and amorphous bodies. The last part contains much theory, most of it more recent than 1945. Each chapter (not each part) is followed by a bibliography, and there is a further bibliography of general works. The book ends with about 30 pages of tables. The indexes are more extensive than is usual in French books.

The nearest English equivalent is, perhaps, *X-ray Diffraction by Polycrystalline Materials*, but there are significant differences. Guinier devotes some 50 pages to single-crystal techniques (deliberately excluded from the English book), and one page to high- and low-temperature cameras (36 pages in the English book). As would be expected, the treatment of low-angle scattering is very thorough. Such differences in emphasis make the books complementary rather than competitive.

The treatment is always lucid; the figures clear, the accuracy high. The book can be criticized seriously only on the ground of price (nearly £10), and perhaps weight (over 3 lb, which means that it cannot be read comfortably in an armchair, but only at a desk). One minor idiosyncrasy: the figures are numbered consecutively throughout each chapter in the form Fig. V–1, Fig. V–2, etc., but referred to in the text as 5.1, 5.2, etc. A. J. C. WILSON

Elements of pulse circuits. By F. J. M. FARLEY. (London: Methuen and Co. Ltd., 1956.) Pp. viii + 143. Price 8*s*. 6*d*.

The excellent series of monographs on physical subjects is further enhanced by this introduction to pulse circuits. The author has a clear style and builds up the picture in a lucid manner and by easy stages. He does not waste valuable space on descriptions of valves and their characteristics but concentrates on the several unit circuits, employing thermionic valves, which are used in this class of work.

Starting with a description of typical transient waveforms, explaining how these may be differentiated and integrated, progress is then through several basic valve circuits to build up such devices as square-wave generators, time-base generators, trigger circuits and pulse amplifiers. The final chapter gives a few selected applications drawn from the television, radar and nuclear physics fields.

Circuits built around cold-cathode valves of various types are not included but then one must not expect too much in such a limited space. A. J. MADDOCK

Analysis of deformation. Vol. 3. Fluidity. By K. SWAINGER. (London: Chapman and Hall Ltd., 1956.) Pp. xxvii + 266. Price 65*s*.

The fundamental equation of fluid kinematics, as presented by "classical" writers, is:

$$dV/dt = (\partial V/\partial t) + V \,.\, \nabla V$$

and is based on the notion that the velocity of any particle in the fluid stream is a function of both time and position. Dr. Swainger cites cases of simple fluid accelerations for which the above theory appears not to apply, and suggests that the correct equation is the simpler and, incidentally, the altogether linear form:

$$\frac{dV}{dt} = \frac{\partial V}{\partial t}$$

Since the notion of fluid acceleration is basic to the logical

structure of hydrodynamics, plasticity and the theory of turbulence, many of the famous theorems (e.g. Navier–Stokes Equation, Bernoulli's Theorem) are rendered invalid if the suggested new form is substituted for the "classical" one. In particular, it is concluded that Bernoulli's theorem is "a necessary mathematical condition but it is not sufficient." Also, using the linear form for acceleration does away with the need for boundary layer theory.

This book reviews the classical theories of deformation and strain velocity very critically and demands a high degree of concentration from its reader. It is a scholarly essay which develops the mathematics of flow problems from first principles and which highlights the issues on which there has been controversy in the past and which are still likely to lead to confusion of thought. To some extent it is a budget of paradoxes, the analyses of which lead the author to suggest breaking with the traditional idea of "convective acceleration."

The mathematics is carried out by vector and tensor methods, with a notation similar in style to that of Weatherburne's textbook. There are difficulties in following the argument in places, particularly where the author develops the "classical" theory in his own way and takes "classical" authors to task for their views. Thus an important collection of results on p. 101 for the purpose of comparing classical fundamental equations of fluidity and elasticity has notes indicating that some expressions are ignored in the classical theory!

I. I. BERENBLUT

The atomic nucleus. By R. D. EVANS. (London: McGraw-Hill Publishing Co. Ltd., 1955.) Pp. xv + 972. Price £5 9*s*.

To quote the author—"This text is an experimentalist's approach to the understanding of nuclear phenomena." Physical concepts are discussed at length while mathematical details of the theory are frequently omitted and the results quoted. Extensive references are made, however, to the original work and some of the basic theoretical analyses have been appended.

The early chapters of the book deal with the fundamental properties of nuclei: size, mass, magnetic and electric moments, parity and statistics. Chapters 8 to 17 consider the systematics of stable nuclei, binding energy of nuclei, internucleon forces, various nuclear models, nuclear reactions, radioactive series decay, alpha spectra and beta decay. Chapters 18 to 25 discuss the various processes which occur during the passage of charged particles and photons through matter. The last three chapters discuss statistical fluctuations and the estimation of errors. Problems are offered for solution at the end of many sections.

The author has adopted the procedure of giving a satisfactory account of a nuclear phenomenon at the point in the text where it is introduced. For example, in Chapter 2 on the radius of nuclei, the reader is introduced to the wave-mechanical penetration of a potential barrier so that he can understand how nuclear radii are inferred from alpha decay half-lives. And, since it is not assumed that the reader has a prior knowledge of wave mechanics, the necessary mathematical and conceptual portions of this subject are developed from first principles. (A more detailed discussion of the wave-mechanical treatment of various kinds of barrier problems is given as an Appendix.) Although this method leads occasionally to duplication the varied reiteration of basic ideas is in itself instructive. The early chapters of the book consequently give an exceptionally comprehensible introduction to the nature of the nucleus. One feels that under certain topics covered by subsequent chapters (for example, electromagnetic transitions in the n–p system), more mathematical formulation of the theory would have been justified for the sake of improved clarity. And, while there is understandably a necessity for selection of subject-matter to be included in a book covering such a broad field, the absence of more than a brief mention of collective nuclear motion and the unified model seems unfortunate. The chapters on statistical fluctuations and the estimation of errors enhance the value of this text for the experimental nuclear physicist, especially since special applications of Poisson statistics to data taken with various types of instruments commonly used in experimental nuclear physics are considered. Throughout the book nuclear phenomena have been introduced with a thorough historical review of the important experiments and the manner in which the theory evolved as a result of them. This historical treatment makes the reader aware of the various experimental evidence in support of the present theory.

In general the subject-matter is comprehensible on a level appropriate to the final year of an undergraduate course in physics. And, because of the amount of detail afforded by the sheer size of the book, it is valuable as a reference text for more advanced students.

H. M. SKARSGARD

Quantum chemistry: an introduction. By WALTER KAUZMANN. (New York: Academic Press Inc.; London: Academic Books Ltd., 1957.) Pp. xii + 744. Price 96*s*.

This is an up-to-date and very valuable book with a refreshing tendency to approach old topics in new ways. For this reason it will be particularly valuable to teachers who wish to put new life into the usual treatments and to find alternative ways of looking at well-known topics, but it should also appeal to research students in experimental subjects whose mathematical equipment does not reach the Honours degree standard and who want to find out what can be done by theory. The arrangement is logical and the book is exceptionally readable; it can literally be read from cover to cover and the student who does this will learn a lot of interesting physics on the way. The maximum of applicable mathematics is given in a most palatable form, with repeated emphasis on physical application and meaning; classical treatments are invariably given before quantum treatments so that the student can appreciate that there is very little additional difficulty in the latter. This is a most important point because in the reviewer's opinion many of the difficulties encountered by students of quantum mechanics arise not from the inherent difficulty of the subject but from the fact that they have not been properly grounded in classical mechanics. Undergraduates who have read, say, Coulson's *Valence* and are prepared to think about the subject should find the book very helpful.

In a book of this size, containing a great deal of mathematics, some misprints are inevitable, but they are not numerous nor likely to mislead. The typography, although not particularly attractive, is clear, but some of the diagrams are difficult to decipher. British textbooks on the subject are more numerous and useful than would appear from the bibliography. Useful problems are given throughout the text, and an improvement worthy of consideration for future editions is a set of answers to them, since the book will undoubtedly be used by many for private study.

E. G. COX

Jets, wakes and cavities. By G. BIRKHOFF and E. H. ZARANTONELLO. Applied Mathematics and Mechanics: Vol. 2. (New York: Academic Press Inc.; London: Academic Books Ltd., 1957.) Pp. xii + 353. Price 80*s*.

Books written by mathematicians of such versatility as the senior author here should always be taken seriously, the more so as specialism continues to increase, and this one is no exception.

The first chapter entitled "background and prospectus" as well as fulfilling its promise contains surprisingly enough an account, admittedly brief, of the theory of shaped and lined hollow charges. The main part of the book, Chaps. II–XI, some 230 pages, is concerned with inviscid flows with free boundaries, "i.e. liquid flows bounded by a liquid-gas interface." The authors state quite frankly that the major part of the book has been devoted to these applications "not because of their greater practical importance but because more can be said about them theoretically." Certainly in your reviewer's opinion with this as objective it can be said that in these chapters the book measures up to its task. Chapter VII deserves special mention. Apart from the last chapter which contains miscellaneous experimental facts the remainder of the book Chaps. XII–XIV, some fifty pages, deals with laminar viscous, periodic and turbulent jets and wakes. Here one feels that the emphasis is too heavily weighted by what can be mathematically proven, and the treatment scarcely as balanced as one would wish.

Although there are extensive footnotes and a bibliography there is regrettably no index of names. The subject index is scanty and the price to British eyes excessive.

L. HOWARTH

Plant and process dynamic characteristics. By THE SOCIETY OF INSTRUMENT TECHNOLOGY. (London: Butterworth's Scientific Publications, 1957.) Pp. xii + 246. Price 50*s*.

Twenty-three years ago Ivanhoff published a paper "Theoretical Foundations of the Automatic Regulation of Temperature" describing for the first time the frequency response analysis of process plant. Being somewhat before its time it did not promote the interest in quantitative design of process control systems based on a knowledge of the dynamic characteristics of processes and plants that might have been expected. The Proceedings of the Conference arranged last Spring by the Society of Instrument Technology show that nowadays process control engineers are alive to modern industrial requirements and that considerable progress is being made in the development of calculating process and plant characteristics from their design data. The papers now published are heterogeneous in subject-matter and quality of treatment, but have provided a stimulating basis for discussion and thought which promotes the hope that, in the not too distant future, the designer of "unit operations" plant will be able to use automatic control with full advantage, thereby promoting efficiency and reduction of operating costs. After another five years the basic work on the design of control systems for the physical processes should be substantially complete, and the more difficult field of development of techniques for application to chemical processes, with the help of the digital computer, may be more rapid than could have been predicted a few years ago.

The Conference was designed for those actually working in the field and the Proceedings reflect this. The Society of Instrument Technology has performed a very useful service in arranging the Conference and in publishing the papers and discussions.

J. TAYLOR

The theory of networks in electrical communication and other fields. By F. E. ROGERS. (London: Macdonald and Co. Ltd., 1957.) Pp. xx + 560. Price 65*s*.

Circuits used in power and particularly in telecommunication technics are nowadays often so complex that they must be resolved and simplified before they can be understood and evaluated numerically. The author, a lecturer at the Polytechnic, London, has set himself the task of presenting the most important principles of network theory in a way that should meet the requirements of students of final-year Engineering Degree or Diploma standard. He starts thus from the foundations of electrical circuitry and builds up to four-terminal and filter networks; Laplace transformation and matrices are, however, omitted.

The book is divided into 12 chapters: Introduction, foundation of network theory, multi-mesh networks, network theorems, fundamental networks, network equivalences, two-terminal networks, uniform lines and cables, four-terminal networks, insertion loss and impedance matching, filter networks, measurements on linear networks. Nearly all chapters are concluded by illustrative examples and a short list of references. Being mainly a textbook, the volume cannot contain much original work. It bears, however, constant witness to the teaching experience of the author, giving useful hints or stating explicitly conclusions which although obvious, may seem improbable to the reader. For this reason it will be particularly useful to external students.

The volume is well produced, with large diagrams clearly drawn. One may question, however, the inclusion in a book of this type, of so many illustrations showing the external appearance of measuring equipment. Data on dimensions and weight of such apparatus would be more useful than, for example, a picture showing that a push-button attenuator is a box with a row of push-buttons.

H. R. J. KLEWE

Voltage stabilized supplies. By F. A. BENSON. [London: Macdonald & Co. (Publishers) Ltd., 1957.] Pp. 370. Price 50*s*.

Up to 1950 there appeared to be no books dealing with voltage stabilizers, but in that year the present author wrote a monograph on the subject: other books have followed since and now the author has written a much longer work covering rather a wider field than in his original monograph and adding much more detail in certain sections. He still gives no description of stabilizers used on power supply systems though his title might well be taken as indicating that he was making a comprehensive survey.

This book will form a valuable work of reference and is best regarded as such and it is obvious that the author has made a thorough search of the literature: there are, in fact, over one thousand references given. It is stated that the book will be suitable for University and other students, but in the opinion of the reviewer it is too indigestible for this purpose: for them more emphasis on principles would be more appropriate. In fact a more critical discussion of the relatively few basic principles of stabilizers would have been of benefit for all readers.

There is considerable unbalance in the treatment of the different forms of stabilizer making certain types appear more important than they really are. Thus, one-third of the complete text is devoted to glow-discharge tubes and one-quarter to miscellaneous circuits. Thermionic valve stabilizers receive their fair treatment but, curiously, half the information and analysis of such circuits is diverted to a chapter on supplies for microwave oscillators, an anomalous heading

for a chapter in relation to the other main divisions. Electromechanical stabilizers receive scant attention, a mere two pages or so, which leaves much unsaid about several types that could well have figured here. A. J. MADDOCK

Switchgear principles. By P. G. H. CRANE. (London: Cleaver-Hume Press Ltd., 1957.) Pp. vii + 238. Price 25*s*.

The Electrical Research Association has played an important part in switchgear research and development, and Mr. Crane, a member of the E.R.A. staff who also has some manufacturing experience, is in a good position to present the principles of circuit-breaking.

The necessary background information to the main theme is provided by the first four chapters on, the supply and control of electricity; causes and effects of short-circuits and overvoltages; system protection; and electrical discharges. The principles of d.c. and a.c. circuit-breaking are then discussed, and the second half of the book deals with oil and air circuit-breakers; switchgear components and accommodation; and finally, tests and specifications. A list of references for further study is included.

The text is clearly written and well illustrated, although the reviewer would have been tempted to include some photographs of 400 kV switchgear to show the size and complexity of modern high-voltage equipment, and to inspire someone to try to invent less impressive, and less expensive, means of circuit control.

However, the book adequately fulfils the author's aim, namely, to cater for the needs of the student and the non-specialist user of switchgear. It should also provide a useful general introduction for physicists working on discharge and contact phenomena. J. S. FORREST

Rubber in engineering. (London: The Natural Rubber Development Board, 1957.) Pp. v + 160. Gratis.

This record of the proceedings of a recent conference on rubber in engineering contains five papers on diverse subjects connected with the application of rubber to engineering problems. The inclusion of the discussion, with all the usual conference chatter, *verbatim*, and the absence of any coherent relation between the papers, tend to obscure the real merit of some of the individual contributions. One cannot help feeling that it would have been better if the papers had been submitted separately to the appropriate scientific journals.

L. R. G. TRELOAR

The electrical production of music. By ALAN DOUGLAS. (London: Macdonald and Co. Ltd., 1957.) Pp. 223. Price 28*s*.

The volume commences with an excellent survey of the physics of musical instruments, musical scales and intervals, noise and starting transients. There follows a description of the various types of sound generators, including magnetic, electrostatic, oscillatory and photocell. This naturally leads to the production of tone colour from synthetic wave forms and its subsequent control, through rate of attack, vibrato and reverberation. The loud speaker being the physical instrument of expression of all forms of electrical sound production, stress is rightly laid on its most apt positioning, together with room acoustics. Horn and diaphragm types are discussed. The sad fact remains that modern amplifiers generally far exceed the capabilities of the loud speaker.

The final chapter on "future trends" gives a lucid description of the Cologne broadcasting mixer which incorporates the Bode melochord and the double generator trautonium. The book is written by an expert in a clear style and is well illustrated with diagrams, circuits and half-tone blocks.

R. W. JUKES

Progress in biophysics and biophysical chemistry. Vol. 7. Edited by J. A. V. BUTLER and B. KATZ. (London: Pergamon Press Ltd., 1957.) Pp. viii + 362. Price 70*s*.

This latest volume of the series, which is somewhat larger than its immediate predecessors, includes articles on a wide variety of topics; in general, however, the different chapters should be interesting and comprehensible to the specialist and non-specialist alike, and ideas and descriptions of techniques are presented in an assimilable form. The mechanism of discharge of electric organs in relation to general and comparative physiology is described in considerable detail by Grundfest in an article which includes an extensive bibliography. A thermodynamic study of the isohaemagglutinins given by Wurmser and Filitti: Wurmser shows how quantitative data—for instance the heat of reaction and the entropy change—involved in the fixation of isohaemagglutinins by red cells may be obtained, and how this data reveals some unexpected facts, particularly concerning specificity, about the reaction. The use of labelled plasma proteins in the study of nutritional problems is described by McFarlane, and the use of isotopes in the study of intermediate metabolism by Arnstein and Grant, in articles where emphasis is laid on the details of the techniques involved, and on the avoidance of pitfalls in the interpretation of the results. An article by Clark and Iball describes the application of X-ray diffraction analysis to the study of bone and explains the various types of information that can be obtained by this technique. Muscle structure and theories of contraction are considered by A. F. Huxley in a chapter which will be of particular interest to the specialist in this field, for it contains much unpublished material. It is shown how on at least two occasions in the past, the overthrow of sound experimentally-based conclusions on theoretical grounds has impeded progress; and a hypothesis is put forward, concerning the details of the actin-myosin interaction in the "sliding filament" model, which is consistent with other contemporary experimental results, and from which, by appropriate but reasonable choice of numerical constants, the observed mechanical and thermal properties of striated muscle can be fairly successfully predicted. Although it is not easy from the present account to assess the extent to which this success confirms the hypothesis made, it is a great and stimulating advance to have a theory which, in the main, can predict the right results. The volume concludes with a lucid account of photosynthetic mechanisms in chloroplasts, and their relation to structure, by Whittingham.

H. E. HUXLEY

Spheroidal wave functions. By CARSON FLAMMER. (London: Oxford University Press, 1957.) Pp. ix + 220. Price 68*s*.

In recent years, the wave equation has become of increasing practical importance, particularly in connexion with diffraction by circular disks and apertures, in electromagnetic problems concerning antennas of various shapes and in

quantum mechanics. One method of obtaining solutions of the wave equation in a particular co-ordinate system is to reduce it to a number of ordinary differential equations, one for each co-ordinate, and to solve these latter equations. Such solutions have already been tabulated for plane, cylindrical, spherical and elliptic-cylindrical waves. The present monograph presents both formulae and tabulated values for prolate and oblate spheroidal co-ordinates, together with a discussion of some of their properties. The tables include values of spheroidal eigen values, expansion coefficients and the spheroidal functions themselves, gleaned from various sources but with some errors corrected after recalculation by the author.

The author is aware of the scanty nature of his tables and makes the inevitable comparison with an earlier and more comprehensive book of the same title by Stratton, Morse, Chu, Little and Corbató. However, not all readers will be able to afford the fuller version nor wish to carry it around. For many, the present volume, which contains a wealth of information at a reasonable price, will be highly acceptable.

J. CRANK

The calculation of atomic structures. By D. R. HARTREE. (New York: John Wiley and Sons Inc.; London: Chapman and Hall Ltd., 1957.) Pp. xiii + 181. Price 40*s*.

In order to be able to calculate the electronic structures of atoms, i.e. to evaluate the wave functions representing their possible quantum states, one has in practically all cases to use approximation methods and numerical computations. In the early stages of the development of the quantum theory of the atom the comparison between the results of such calculations and the observations of atomic spectra provided the most important material for the verification of the theory. It was mainly for this purpose that the most powerful method for the calculation of atomic structures, generally known as the "method of the self-consistent field," was developed by Professor Hartree and his school.

In recent years the interest in this method has been revived as detailed knowledge of atomic structures is required for the study of transition probabilities, mainly for applications to astrophysics, of molecular and solid state properties, and of X-ray and neutron scattering. Also the great advances made in automatic digital computation now makes many numerical calculations possible which were quite intractable before.

The present book is mainly written for the benefit of research workers actively engaged in the determination of atomic structures. It not only presents the essentials of the theory but also gives detailed instruction for obtaining the best approximations, illustrated by suitable examples. Other approximation methods, like the Thomas–Fermi method, are also briefly mentioned.

R. FÜRTH

The hypercircle in mathematical physics. By J. L. SYNGE. (London: Cambridge University Press, 1957.) Pp. xii + 424. Price 70*s*.

The method of the hypercircle, first introduced by J. L. Synge and W. Prager in 1947, has been used extensively by Synge and his collaborators to obtain the approximate solutions of a wide class of boundary value problems in mathematical physics. The method has the double advantage of giving a simple geometrical form to complex problems and of providing solutions with rigorously controlled error.

In the present book Professor Synge gives a full account of the method and its applications. The major part of the book (pp. 1–367) is concerned with the geometry of a function-space with a positive definite metric and the application of the hypercircle method to the solution of a variety of problems in mathematical physics—the Dirichlet problem for a finite region, the torsion problem, flow problems, mixed boundary value problems, elastic equilibrium. The rest of the book is given over to a discussion of function-space with indefinite metric which is the type which arises in the geometrization of problems of forced vibrations, mechanical and electromagnetic.

The book is most attractively written ("on the assumption that appeal to geometrical intuition, not for proof but for suggestion, will please the reader as much as it pleases the author") and contains a good deal of the details of the calculations so that it provides an authoritative and readable account of a powerful technique.

I. N. SNEDDON

The detection and measurement of infra-red radiation. By R. A. SMITH, F. E. JONES and R. P. CHASMAR. (Oxford: Clarendon Press; London: Oxford University Press, 1957.) Pp. xiii + 458. Price 70*s*.

This book aims at giving "an account of modern practice in infra-red techniques." In this aim it is largely successful; the components of infra-red instruments are described in detail, and copious references are provided. A large part of the book is devoted to detectors. Thermocouples and bolometers are treated in sixty pages, and the Golay detector in three. Fifty pages are devoted mainly to photocells; a further sixty pages describe the limitations of the detectors. There is a comprehensive account of optical materials for the infra-red. The most uneven part of the book is the chapter on infra-red spectrometers. Perhaps in the next edition of the book this chapter may be broadened to become more catholic. However, the authors are not greatly concerned with infra-red spectroscopy as such, but rather with the behaviour of individual constituents of a spectrometer. The book is a mine of information.

A. C. MENZIES

Theories of nuclear moments. By R. J. BLIN-STOYLE. (London: Oxford University Press, 1957.) Pp. 86 + vi. Price 8*s*. 6*d*.

After a brief outline of the theoretical origins of the moments, the author gives a very brief but clear account of experimental methods. The measured (and listed) values of the various electric and magnetic moments are then discussed in terms of the values predicted by the individual particle model of the nucleus and the collective model, as well as the one-particle picture. This book contains a brief but excellent account of nuclear moments, well documented for those who demand more detail. The author and the publishers are to be congratulated on the first volume in this library. A series of small monographs on limited subjects may be difficult to produce, but it is likely to be popular and to have as wide a reading public amongst physicists as the series of Cambridge Tracts has amongst mathematicians.

G. J. KYNCH

Notes and comments

Publications of the British Standards Institution

The *British Standards Annual Report* has recently been published price 7*s*. 6*d*. Among the achievements it records are sales of more than a million British Standards, and new issues bringing the total number of standards to over 3000. The report contains 270 pages and shows developments over the whole range of industry giving a detailed review of the standards projects completed and in hand for the sixty major industries served. In the comprehensive reports of standards progress in the main industrial divisions of B.S.I. a new system has been introduced into the Report by which readers can see immediately what stage has been reached in the preparation of any particular standard.

Two new British Standards have also recently been published which are: *Memorandum on Therapeutic X-ray equipment* (B.S. 2849: 1957), and *Precise conversion of inch and metric sizes on engineering drawings* (B.S. 2856: 1957). The standards are priced at 4*s*. and 3*s*. 6*d*. respectively. Copies of the publications may be obtained from the British Standards Institution, Sales Branch, 2 Park Street, London, W.1.

Translation of Russian journals

The Pergamon Institute has commenced the translation into English of a number of Russian medical and biological journals. Issues received are as follows: *Journal of Microbiology, Epidemiology and Immunobiology*, Vol. 28, No. 1; *Biophysics*, Vol. 2, No. 1; *Problems of Hematology and Blood Transfusion*, Vol. 2, No. 1; *Problems of Virology*, Vol. 2, No. 1. The Pergamon Institute, a non-profit-making organization, has recently been formed in New York, and is in the course of formation in London, for the purpose of making available to English-speaking scientists, doctors and engineers from all countries that are members of the United Nations, the results of scientific, technological and medical research and development in the Soviet Union and other countries in the Soviet orbit. Further details may be obtained from the Institute, 4–5 Fitzroy Square, London, W.1.

Semiconductor Electronics

A new periodical has been announced which is devoted exclusively to the theory, production, and use of semiconductor material and devices. Entitled *Semiconductor Electronics*, the first issue appeared in January this year. At present, the periodical consists mainly of a monthly survey of the published literature in the field indicated by its title, but its scope will no doubt be enlarged at a later date. Items are classified in such a way as to enable anyone to organize the abstracts into a logical sequence. Further details may be obtained from the publishers, Semiconductor Information Service, Box 407, Cambridge 39, Massachusetts, U.S.A.

The Physics of Fluids

In January 1958, the American Institute of Physics will publish the first issue of a new journal, entitled *The Physics of Fluids*. The journal will be devoted to original contributions to the physics of fluids covering kinetic theory, statistical mechanics, structure and general physics of fluids bordering geophysics, astrophysics, biophysics and other fields of science. The scope of these fields of physics includes: magneto-fluid dynamics, ionized fluid and plasma physics, shock and detonation wave phenomena, hypersonic physics, rarefied gases and upper atmosphere phenomena, physical aeronomy, transport phenomena, hydrodynamics, dynamics of compressible fluids, boundary layer and turbulence phenomena, liquid state physics and superfluidity.

The journal will consider appropriate for publication original papers containing sufficiently significant results not published in any other recognized publication. It will start as a bi-monthly publication and will be published monthly as soon as it appears desirable.

Correspondence on editorial matters should be addressed to: F. N. Frenkiel, Editor, *The Physics of Fluids*, Applied Physics Laboratory, The Johns Hopkins University, Silver Spring, Maryland, U.S.A. Subscription information can be obtained from the American Institute of Physics, 335 East 45th St., New York 17, New York, U.S.A.

Conference on nuclear fuel cycles

The Institute of Physics has arranged a three-day conference on Nuclear Fuel Cycles to be held at the Institution of Civil Engineers, London, on 15, 16, 17 January, 1958. Full details may be obtained from The Deputy Secretary, The Institute of Physics, 47 Belgrave Square, London, S.W.1.

Journal of Scientific Instruments

Contents of the December issue

SPECIAL ARTICLE

Solid state image amplifiers. By G. F. J. Garlick.

ORIGINAL CONTRIBUTIONS

Papers

The Hall-effect compass. By I. M. Ross, E. W. Saker and N. A. C. Thompson.

Experiments using a simple thermal comparator for measurement of thermal conductivity, surface roughness and thickness of foils or of surface deposits. By R. W. Powell.

A tunable infra-red interference filter. By S. D. Smith and O. S. Heavens.

The application of vacuum ultra-violet techniques to the continuous monitoring of trace concentrations of water in several gases. By W. R. S. Garton, M. S. W. Webb and P. C. Wildy.

An automatic adiabatic bomb calorimeter. By W. F. Raymond, R. J. Canaway and C. E. Harris.

A lateral extensometer for the determination of Poisson's ratio of rock. By E. R. Leeman and C. Grobbelaar.

A water-wave measuring apparatus. By A. Brebner.

A two-camera technique for measuring fall velocities. By R. H. Magarvey.

Laboratory and workshop notes

Simple greaseless valves. By E. Raats, J. Harley and V. Pretorius.

An extension to the range of the McLeod gauge. By J. A. Barnard.

A simple specimen holder and apparatus for measurement of conductivity and Hall voltage over a temperature range. By A. A. Brooker, R. A. Clay and A. S. Young.

The cleaving of mica in water. By A. Aharoni and E. H. Frei.

A simple and inexpensive emission regulator for ionization gauges. By M. P. Reece.

A re-entrant cavity for magnetic measurements. By E. A. Faulkner.

A current regulator to facilitate resistance measurements at low temperature. By M. W. Thompson.

NOTES AND NEWS

New instruments, materials and tools

New books

Notes and comments

THIS JOURNAL is produced monthly by The Institute of Physics, in London. It deals with all branches of applied physics (including theory and technique).

All rights reserved. Responsibility for the statements contained herein attaches only to the writers.

EDITORIAL MATTER. Communications concerning editorial matter should be addressed to the Editor, The Institute of Physics, 47 Belgrave Square, London, S.W.1. (*Telephone:* Belgravia 6111.) Prospective authors are invited to prepare their scripts in accordance with the *Notes on the preparation of contributions*. (Price 2*s*. 6*d*. including postage.)

REPRODUCTION. The Institute of Physics is a signatory to The Royal Society's Fair Copying Declaration. Details may be obtained upon application from The Royal Society, London, W.1.

ADVERTISEMENTS. Communications concerning advertisements should be addressed to the agents, Messrs. Walter Judd Ltd., 47 Gresham Street, London, E.C.2. (*Telephone:* Monarch 7644.)

CLAIMS FOR MISSING JOURNALS. Claims from regular subscribers to this *Journal* for missing numbers will only be considered if received within 60 days of the date of mailing plus normal outward time of transit and time for lodging the claim. Losses attributable to failure to notify a change of address or to similar omissions will not be considered.

SUBSCRIPTION RATES. A new volume commences each January. The charge is £5 per volume ($14.25 U.S.A.), including index (post paid), payable in advance. Single parts, so far as available, may be purchased at 10*s*. each ($1.50 U.S.A.), post paid, cash with order. Orders should be sent to The Institute of Physics, 47 Belgrave Square, London, S.W.1, or to any bookseller.